# NUCLEAR PHYSICS

JOURNAL DEVOTED TO THE EXPERIMENTAL AND THEORETICAL STUDY OF THE FUNDAMENTAL CONSTITUENTS OF MATTER AND THEIR INTERACTIONS

EDITOR: L. ROSENFELD - COPENHAGEN
ASSOCIATE EDITOR: O. NATHAN - COPENHAGEN

## VOLUME VI

NORTH-HOLLAND PUBLISHING COMPANY - AMSTERDAM

# NUCLEAR PHYSICS

## EDITORIAL BOARD


| | |
|---|---|
| AUSTRIA: | B. Karlik (Vienna), H. Thirring (Vienna) |
| BELGIUM: | M. de Hemptinne (Louvain), J. Verhaeghe (Ghent) |
| CANADA: | G. Volkoff (Vancouver) |
| DENMARK: | C. Møller (Copenhagen), S. Rozental (Copenhagen) |
| EGYPT & ARAB COUNTRIES: | F. El Bedewi (Alexandria), M. G. Nooh (Cairo) |
| FINLAND: | L. Simons (Helsinki) |
| FRANCE: | A. Berthelot (Saclay), S. Gorodetzky (Strasbourg), F. Joliot (Paris) |
| GERMANY (FED. REP.): | W. Gentner (Freiburg i. B.), J. H. D. Jensen (Heidelberg) |
| GERMANY (DEM. REP.): | G. Hertz (Leipzig) |
| GREAT BRITAIN: | S. Devons (Manchester), T. H. R. Skyrme (Harwell) |
| HUNGARY: | L. Janossy (Budapest) |
| INDIA: | H. Bhabha (Bombay), B. Peters (Bombay), R. Ramanna (Trombay) |
| IRISH REPUBLIC: | J. McConnell (Maynooth) |
| ISRAEL: | G. Racah (Jerusalem) |
| ITALY: | E. Amaldi (Rome) |
| JAPAN: | S. Kikuchi (Tokyo), S. Tomonaga (Tokyo) |
| NETHERLANDS: | H. Brinkman (Groningen), S. R. de Groot (Leiden) |
| NORWAY: | E. Hylleraas (Oslo), A. Lundby (Oslo), H. Wergeland (Trondheim) |
| POLAND: | L. Infeld (Warsaw) |
| PORTUGAL: | J. M. Araújo (Porto), J. R. de Almeida Santos (Coimbra) |
| SOUTH AMERICA: | G. Beck (Saõ Paulo), J. Leite Lopes (Rio de Janeiro) |
| SPAIN: | J. M. Otero (Madrid), C. Sanchez del Rio (Madrid) |
| SWEDEN: | O. Klein (Stockholm), K. Siegbahn (Uppsala), I. Waller (Uppsala) |
| SWITZERLAND: | P. Huber (Basel), P. Scherrer (Zürich) |
| U.S.S.R.: | M. A. Markov (Moscow), I. S. Shapiro (Moscow), D. V. Skobeltzyn (Moscow) |
| YUGOSLAVIA: | I. Supek (Zagreb) |
| U.S.A. & MEXICO: | V. Weisskopf (Cambridge, Mass.) |
| AUSTRALIA & NEW ZEALAND: | H. Messel (Sydney), M. L. Oliphant (Canberra) |

# NUCLEAR PHYSICS

MONTHLY JOURNAL DEVOTED TO THE EXPERIMENTAL AND THEORETICAL STUDY OF ATOMIC NUCLEI, NUCLEAR FIELDS AND THE FUNDAMENTAL ASPECTS OF COSMIC RADIATION

EDITOR: L. ROSENFELD - MANCHESTER

VOLUME VI

MARCH 1958—MAY 1958

NORTH-HOLLAND PUBLISHING COMPANY - AMSTERDAM

PRINTED IN THE NETHERLANDS

*Nuclear Physics* **6** (1958) 1—9; © *North-Holland Publishing Co., Amsterdam*

Not to be reproduced by photoprint or microfilm without written permission from the publisher

# DEPENDENCE OF μ-MESON AND ELECTRON POLARIZATION ON CORRELATION PARAMETERS IN $K_{\mu 3}$ AND $K_{e3}$ DECAYS

J. WERLE

*Institute for Nuclear Research, Warsaw*

Received 11 September 1957

**Abstract:** The polarization of the $\mu$-mesons and electrons emitted in $K_{\mu 3}$ and $K_{e3}$ decays is investigated on the basis of the two-component theory of the neutrino field. A quite general form of the transition matrix is used under the only assumption that the corresponding K-mesons have no spin. It is shown that for pure couplings the form of the functional dependence of the polarization vector on the correlation parameters $E$ and $\theta$ is uniquely determined by the type of coupling and does not involve the unknown coupling factors $C_i(E, \theta)$. A combined correlation and polarization experiment can, therefore, provide the best tool for the investigation of the actual form of the coupling responsible for the $K_{\mu 3}$ and $K_{e3}$ decays.

## 1. Introduction

The longitudinal polarization of the $\mu$-mesons and electrons emitted in the K-meson decays of types

$$K \to \pi + \nu + \mu(e) \tag{1}$$

has been calculated in a recent paper [1]) under the assumption that the corresponding K-mesons have no spin. The calculation has been performed on the basis of the two-component theory of the neutrino field [2]) which implies that a neutrino is always completely polarized in the direction of its motion. Since we do not know anything about the interaction responsible for (1) a transition matrix containing four different couplings

$$\Phi(P')\varphi^*(P)\bar{\psi}(p)\left\{C_S + \frac{1}{M}(C_V P_\alpha + C'_V P'_\alpha)\gamma_\alpha + \frac{1}{2M^2} C_T P_\alpha P'_\beta(\gamma_\alpha\gamma_\beta - \gamma_\beta\gamma_\alpha)\right\}\psi_\nu(q) \tag{2}$$

has been used †. The symbols $P'_\alpha$, $P_\alpha$, $p_\alpha$, $q_\alpha$ and $\Phi(P')$, $\varphi(P)$, $\psi(p)$, $\psi_\nu(q)$ denote here the four-momenta and the quantised wave functions of the K-meson, $\pi$-meson, $\mu$-meson (or electron) and neutrino respectively. It has been assumed that the coupling factors $C_i$ can depend on the scalar product $P'_\alpha P_\alpha$ only. In the rest system of the K-meson $P'_\alpha P_\alpha = -M\varepsilon =$

† The second vector interaction V′ is actually not independent of the remaining three since it can be reduced to a superposition of S and V terms. Nevertheless, we have retained it in order to have more pure cases.

$= -M\sqrt{m^2+p^2+q^2+2pq\cos\theta}$ where $M$ is the mass of the K-meson, $m$ is the mass of the $\pi$-meson and $\varepsilon$ its energy in this system.

It has been shown in ref. [1]) that the polarization measurements can provide a very sensitive tool for the investigation of the actual form of the transition matrix. However, in order to calculate definite curves of longitudinal polarisation one additional simplifying assumption, turns out to be necessary even for the pure cases S, V, V′ or T. In fact, it has been assumed that the coupling factors $C_i(\varepsilon)$ can be regarded as constants. This assumption, made by other authors as well [3]), cannot be fully justified. Nevertheless we could not draw any definite conclusion about the longitudinal polarization without this simplification. The reason for this situation stems from the fact that the quantity $\varepsilon$ depends on the $\mu$-meson (or electron) energy $E$ and on the angle $\theta$ between the neutrino and $\mu$-meson (or electron) momenta, and the final formulae for the longitudinal polarization involve an integration over this angle. For pure correlations the situation is a little better because we can keep the $\pi$-meson energy fixed, studying the dependence of the correlation on the angle $\theta$ or — even more conveniently — the angle $\vartheta$ between the $\pi$-meson and $\mu$-meson (electron) momenta [4]). However, pure correlation measurements do not seem to be very suitable for the investigation of the $K_{\mu 3}$ decays [4]). On the other hand it should be remembered that the form of the transition matrix used in ref. [1, 3, 4]) is not the most general one, since it has been assumed for its deduction that the interaction between the $\mu$-meson (or electron) and $\pi$-meson can be neglected.

It is the aim of this paper to show that in principle we can get rid of all these simplifying assumptions by combining correlation and polarization measurements. In fact, the complete polarization of the neutrino implies that for fixed correlation parameters $E$ and $\theta$ the polarization of the $\mu$-meson (or electron) is also complete. The polarization vector of the $\mu$-meson (or electron) is therefore a unit vector whose dependence on the correlation parameters is uniquely determined by the form of the transition matrix. It turns out that for pure couplings the polarization vector is determined by the covariance structure of the coupling and does not involve the unknown coupling factors $C_i$ at all.

In the next section we shall outline a covariant polarization formalism which will be used in the following two sections for the calculation of the polarization vector of the $\mu$-meson (or electron) as a function of $E$ and $\theta$.

## 2. Covariant Polarization Formalism for Dirac Particles of Non-vanishing Mass

An arbitrary spinor $\psi'(p_\alpha)$ describing a free Dirac particle of definite momentum and energy $p_\alpha (p_4 = iE = i\sqrt{\mu^2+p^2})$ can be written in the form

$$\psi'(p_\alpha) = a\{\psi_+(p_\alpha)+b\psi_-(p_\alpha)\}. \tag{3}$$

$\psi_+(p_\alpha)$ and $\psi_-(p_\alpha)$ denote here the eigenfunctions of the usual (longitudinal) spin projection operators $\lambda_\pm = \frac{1}{2}\pm(\boldsymbol{\sigma}\cdot\mathbf{p}/2p)$. The symbol $\mu$ denotes the mass of the particle. Apart from the non-essential multiplying constant $a$ the state of a free Dirac particle of definite energy and momentum $p_\alpha$ is completely determined by the complex parameter $b$, i.e. by two real parameters. Evidently a one-to-one correspondence can be found between a complex parameter and a three-dimensional unit vector. From the point of view of pure mathematics the choice of the correspondence is not unique and to a large extent arbitrary. However, one can remove this arbitrariness by imposing suitable physical conditions. Several authors recently found [5]) a covariant physical form of the correspondence by demanding that the spinor $\psi'$ be an eigenfunction of the projection operator

$$\lambda(s_\alpha) = \frac{1-i\gamma_5\gamma_\alpha s_\alpha}{2} \tag{4}$$

with the pseudovector $s_\alpha$ satisfying two additional conditions:

$$s_\alpha s_\alpha = 1, \quad s_\alpha p_\alpha = 0. \tag{5}$$

$\lambda(s_\alpha)$ commutes with the usual projection operator

$$\Lambda(p_\alpha) = \frac{\mu-i\gamma_\alpha p_\alpha}{2\mu} \tag{6}$$

which distinguishes a Dirac particle from an antiparticle. $\psi'(p_\alpha) = \psi(p_\alpha, s_\alpha)$ is, therefore, a simultaneous eigenfunction of $\Lambda(p_\alpha)$ and $\lambda(s_\alpha)$:

$$\Lambda(p_\alpha)\lambda(s_\alpha)\psi' = \lambda(s_\alpha)\Lambda(p_\alpha)\psi' = \psi', \tag{7}$$

provided that a suitable $s_\alpha(b)$ satisfying the relations (5) is taken. It can easily be shown that the operator $\lambda(s_\alpha)$ when occurring in the product $\lambda\Lambda$ can be replaced by the operator

$$\lambda'(\boldsymbol{\zeta}) = \tfrac{1}{2}(1+\boldsymbol{\sigma}\cdot\mathbf{n}+\gamma_4\boldsymbol{\sigma}\cdot\mathbf{t}) \tag{8}$$

where $\mathbf{n}$ and $\mathbf{t}$ respectively denote the parallel and transverse part of the unit vector $\boldsymbol{\zeta}$, i.e.

$$\boldsymbol{\zeta} = \mathbf{n}+\mathbf{t}, \quad \zeta^2 = n^2+t^2 = 1, \quad \mathbf{p}\cdot\mathbf{t} = 0, \quad \mathbf{p}\cdot\mathbf{n} = pn, \quad n = \eta\sqrt{1-t^2}, \quad \eta = \pm 1. \tag{9}$$

$\lambda'(\boldsymbol{\zeta})$ commutes not only with $\Lambda(p_\alpha)$ but also with the free particle Hamiltonian $H(p) = \gamma_5\boldsymbol{\sigma}\cdot\mathbf{p}+\gamma_4\mu$:

$$\Lambda\lambda = \Lambda\lambda' = \lambda'\Lambda, \quad H\lambda' = \lambda' H. \tag{10}$$

The unit vector $\boldsymbol{\zeta}$ has a simple physical meaning: $\boldsymbol{\zeta}$ coincides with the four-vector $s_\alpha$ transformed to the rest system of the particle and gives

the direction of the spin of the particle in this system. In other words: if we transform the particle to its rest system, and then measure the spin, its direction will be given by the unit vector $\boldsymbol{\zeta}$. We shall call $\boldsymbol{\zeta}$ a polarization vector. In the following the more convenient operator $\lambda'(\boldsymbol{\zeta})$ will be used for determining the state of a free Dirac particle with non-vanishing mass.

### 3. General Consideration of the Transition Probability

Let us now consider the K-meson decays of the type (1) assuming that an antineutrino is always emitted with a negative $\mu$-meson or electron. The position in space of the plane of reaction and the direction of one of the momenta are of course irrelevant. We shall take the plane of decay of a K-meson at rest as $(x, y)$ plane with the vector $\mathbf{p}$ pointing in the direction of the $x$-axis. Since the vectors $\mathbf{P}$, $\mathbf{p}$, $\mathbf{q}$ have to satisfy the conservation equations

$$\mathbf{P}+\mathbf{p}+\mathbf{q} = 0, \quad \varepsilon+E+q = M, \tag{11}$$

it follows that only two momentum parameters are left arbitrary on the plane of decay. For the sake of convenience we take the $\mu$-meson (or electron) energy $E = \sqrt{\mu^2+p^2}$ and the angle $\theta$ between the $\mu$-meson (or electron) and neutrino momenta as the two independent parameters which determine completely the geometry of the decay. E.g. the angle $\vartheta$ between the $\mu$-meson (or electron) and $\pi$-meson momenta, the absolute magnitudes $P$ and $q$ etc. can all be expressed as functions of $E$ and $\theta$.

Let us now confine our attention to those $K_{\mu 3}$ and $K_{e3}$ decays in which a negative $\mu$-meson (or electron) is emitted. The corresponding transition matrix has the following quite general form

$$\Phi(P')\varphi^*(P)\psi^*(p)\Gamma\psi_\nu(q) \tag{12}$$

where $\Gamma$ is constructed from the $\gamma_\alpha$'s and from the momentum vectors $P'_\alpha$, $P_\alpha$, $p_\alpha$, $q_\alpha$ in such a way that the expression (12) is an invariant under proper Lorentz transformations. The density of probability for finding the particles $\pi$, $\mu^-(e^-)$, $\bar{\nu}$ in a correlation given by $E$ and $\theta$ and the $\mu$-meson in a state of definite polarization $\boldsymbol{\zeta}$ has the form

$$W(E, \theta, \boldsymbol{\zeta}) = \frac{N}{\varepsilon E q}\operatorname{tr}\{(1+\boldsymbol{\sigma}\cdot\mathbf{n}+\gamma_4\boldsymbol{\sigma}\cdot\mathbf{t})(E+\gamma_5\boldsymbol{\sigma}\cdot\mathbf{p}+\mu\gamma_4)\Gamma(1+\gamma_5)(q+\gamma_5\boldsymbol{\sigma}\cdot\mathbf{q})\Gamma^*\} \tag{13}$$

where we have applied the two-component theory of the neutrino field [2]); $N$ is a constant which is irrelevant for the present considerations. Because of (9) we can insert

$$\mathbf{n} = n\frac{\mathbf{p}}{|p|}, \quad n = \eta\sqrt{1-t^2}, \quad \eta = \frac{\mathbf{p}\cdot\mathbf{n}}{|pn|}. \tag{14}$$

It can now easily be seen that in the coordinate system defined above the function $W$ has in general the following form:

$$W(E, \theta, \zeta) = \tfrac{1}{2}(A + B\eta\sqrt{1-t^2} + Yt_y + Zt_z) \tag{15}$$

where the quantities $A$, $B$, $Y$, $Z$ depend only on $E$ and $\theta$.

$\zeta$ is a dichotomic variable. Therefore the sum of the probabilities of finding the $\mu$-meson (or electron) in two states of opposite polarizations gives the total probability of finding the particles in a correlation determined by $E$ and $\theta$:

$$W(E, \theta, \zeta) + W(E, \theta, -\zeta) = W(E, \theta) = A(E, \theta). \tag{16}$$

It follows that always

$$A(E, \theta) \geqq 0. \tag{17}$$

So far the vector $\zeta$ was completely arbitrary. We shall call $\zeta'$ a polarization vector of the $\mu$-meson (or electron) if the function $W(E, \theta, \zeta)$ has for $\zeta = \zeta'$ the maximum possible value $A(E, \theta)$ or, in other words, if $W(E, \theta, -\zeta') = 0$. Let us now calculate $\zeta'$. The usual conditions for an extremum

$$\begin{aligned} \frac{\partial W(E, \theta, \zeta)}{\partial t_y} &= \tfrac{1}{2}\left(\eta B \frac{-t_y}{\sqrt{1-t^2}} + Y\right) = 0, \\ \frac{\partial W(E, \theta, \zeta)}{\partial t_z} &= \tfrac{1}{2}\left(\eta B \frac{-t_z}{\sqrt{1-t^2}} + Z\right) = 0 \end{aligned} \tag{18}$$

lead to the following result:

$$(t_y)_{ex} = Y\frac{B}{|B|}\eta(B^2+Y^2+Z^2)^{-\frac{1}{2}}, \quad (t_z)_{ex} = Z\eta\frac{B}{|B|}(B^2+Y^2+Z^2)^{-\frac{1}{2}},$$
$$n_{ex} = \eta|B|(B^2+Y^2+Z^2)^{-\frac{1}{2}}. \tag{19}$$

Inserting (19) into (15) we find

$$W(E, \theta, \zeta_{ex}) = \tfrac{1}{2}(A + \eta\frac{B}{|B|}(B^2+Y^2+Z^2)^{+\frac{1}{2}}). \tag{20}$$

For $\eta B/|B| = +1$ we have a maximum

$$W_{max} = W(E, \theta, \zeta_m) = \tfrac{1}{2}(A + (B^2+Y^2+Z^2)^{+\frac{1}{2}}). \tag{21}$$

For $\eta B/|B| = -1$ we have a minimum

$$W_{min} = W(E, \theta, -\zeta_m) = \tfrac{1}{2}(A - (B^2+Y^2+Z^2)^{+\frac{1}{2}}), \tag{22}$$

with $\zeta_m$ obtained from (19) by putting $\eta B/|B| = +1$. Since both $W_{max}$ and $W_{min}$ are non-negative we must have

$$A^2 \geqq B^2+Y^2+Z^2. \tag{23}$$

Now we shall show that actually $W_{min} = W(E, \theta, -\zeta_m) = 0$. We find from the condition

$$W(E,\ \theta,\ -\zeta') = \tfrac{1}{2}(A - \eta' B\sqrt{1-t'^2} - Yat' - Zbt') = 0 \qquad (24)$$

that

$$t' = \frac{A(aY+bZ) \pm \sqrt{B^2(B^2+(aY+bZ)^2-A^2)}}{(aY+bZ)^2+B^2} \qquad (25)$$

where we have put $t_y = at$, $t_z = bt$, $a^2+b^2 = 1$. The condition of reality of the expression (25) leads to the inequality

$$A^2 \leqq B^2+(aY+bZ)^2. \qquad (26)$$

On the other hand we have always

$$(aY+bZ)^2 \leqq Y^2+Z^2. \qquad (27)$$

The inequalities (23), (26) and (27) are only compatible if

$$a = \frac{Y}{\sqrt{Y^2+Z^2}},\ b = \frac{Z}{\sqrt{Y^2+Z^2}},\ (aY+bZ)^2 = Y^2+Z^2,\ A^2 = B^2+Y^2+Z^2. \qquad (28)$$

We now find from (28) and (22) that in fact $W_{\min} = 0$ and that the vector $\zeta_m = \zeta'$ is the actual polarization vector of the $\mu$-meson (or electron). Its components are

$$\zeta'_x = n' = \frac{B}{A},\ \zeta'_y = t'_y = \frac{Y}{A},\ \zeta'_z = t'_z = \frac{Z}{A} \text{ with } A^2 = B^2+Y^2+Z^2. \qquad (29)$$

The last equation (29) can be regarded as a coherence condition which must be satisfied by any transition matrix. It should be stressed that $\zeta_z$ is different from zero only if $Z$, which is proportional to $(\mathbf{p} \wedge \mathbf{q})$, does not vanish. The problem of vanishing or non-vanishing $Z$ is closely connected with the problem of invariance of the transition matrix under time reversal. We shall see that for all pure couplings considered in the next section $Z = 0$ and consequently the polarization vector lies in the plane of reaction.

## 4. Calculation of $\zeta$ for Pure Couplings

Let us now consider the form of the operator $\Gamma$ which occurs in the transition matrix (12). It can easily be seen that we can write $\Gamma$ in the following quite general form:

$$\Gamma = \sum_i C_i R_i \qquad (30)$$

where the $R_i$'s are known scalar or pseudoscalar forms constructed from the $\gamma_\alpha$'s and from the vectors $P'_\alpha$, $P_\alpha$, $p_\alpha$, $q_\alpha$ in such a way that no scalar products between any two momentum vectors occur. On the other hand the $C_i$'s are unknown scalar functions constructed from the momentum vectors only. Because of the Dirac equations which must be satisfied by $\psi$ and $\psi_\nu$ and because of the conservation equations, some of the $R_i$'s can be com-

pletely equivalent in spite of the apparently different forms. E.g. $R_1 = \gamma_4$ and $R_2 = \gamma_4\gamma_\alpha p_\alpha$ are completely equivalent and can be represented by only one of them. We shall call the case when all the $C_j = 0$ $(j \neq i)$ but one $C_i \neq 0$ a pure coupling case. It can easily be seen that for a pure coupling the ratios $B/A, Y/A, Z/A$ which determine uniquely the polarization vector $\zeta$ do not depend on the unknown coupling factors $C_i$. That means that for pure couplings the functional dependence of the polarization vector on the correlation parameters $E$ and $\theta$ can be calculated exactly without any simplifying assumptions. In particular the results of the calculation are completely independent of the simplifying assumption made usually that the momenta $p_\alpha$ and $q_\alpha$ can occur in $\Gamma$ only in the form of the sum $(p_\alpha+q_\alpha)$ and consequently the $C_i$'s depend only $P'_\alpha P_\alpha$. Thus we see that a combined correlation and polarization measurement can become a very powerful tool for the investigation of the actual form of the transition matrix. It is obvious that in order to have good comparison possibilities with the future experiments we should have a rather numerous set of different pure couplings even without paying attention to their linear independence.

We shall now list the results of the calculations for a few pure cases. We find for the couplings S, V, V', T defined by the expression (2):

$$\text{(S)} \qquad n' = \frac{(E\cos\theta - p)}{E - p\cos\theta}, \quad t'_y = \frac{\mu\sin\theta}{E - p\cos\theta}; \tag{31}$$

$$\text{(V)} \qquad n' = \frac{(M^2+\mu^2)E\cos\theta + (M^2-\mu^2)p - 2M\mu^2\cos\theta}{(M^2+\mu^2)E + (M^2-\mu^2)p\cos\theta - 2M\mu^2},$$
$$t'_y = \frac{(M^2+\mu^2-2ME)\mu\sin\theta}{(M^2+\mu^2)E + (M^2-\mu^2)p\cos\theta - 2M\mu^2}; \tag{32}$$

$$\text{(V')} \qquad n' = \frac{E\cos\theta + p}{E + p\cos\theta}, \quad t'_y = \frac{\mu\sin\theta}{E + p\cos\theta}; \tag{33}$$

$$\text{(T)} \quad n' = \frac{(2pq + (p^2+q^2)\cos\theta)E - (p^2+q^2+2pq\cos\theta)p}{(p^2+q^2+2pq\cos\theta)E - (2pq + (p^2+q^2)\cos\theta)p},$$
$$t'_y = \frac{\mu(q^2-p^2)\sin\theta}{(p^2+q^2+2pq\cos\theta)E - (2pq + (p^2+q^2)\cos\theta)p}, \tag{34}$$

with

$$q = \frac{M^2+\mu^2-m^2-2EM}{2(M - E + p\cos\theta)}; \tag{35}$$

$t'_z = 0$ for all four cases.

It may be more convenient for the experimental physicist to have the vector $\zeta$ expressed as a function of $E$ and $\vartheta$ instead of $\theta$. This can be done by means of the relation

$$\tan \vartheta = \frac{-q \sin \theta}{p + q \cos \theta}. \tag{36}$$

The expressions (31—34) are valid for all the $K_{\mu 3}$ and $K_{e3}$ decays in which an antineutrino is emitted. We can obtain the corresponding expressions for those $K_{\mu 3}$ and $K_{e3}$ decays in which a neutrino is emitted multiplying (31—34) simply by $-1$.

Since we have dropped the simplifying assumption that the lepton momenta occur in $\Gamma$ only in the sum $(p_\alpha + q_\alpha)$ the number of possible pure couplings will be much greater than four. A more comprehensive list of the vectors $\zeta'$ calculated for various pure couplings will be given in a subsequent paper.

## 5. Discussion

It can easily be seen from (31—34) that in the non-relativistic limit $p \to 0$ all four couplings lead to the same value $n^0 = \cos\theta$, $t_y^0 = \sin\theta$ if an antineutrino is emitted, and $n^0 = -\cos\theta$, $t_y^0 = -\sin\theta$ if a neutrino is emitted. That means that in the non-relativistic limit the spin of the $\mu$-meson or electron is always antiparallel to the spin of the neutrino or antineutrino. Thus we see that the region of very small energies $(p \ll \mu)$ is rather unsuitable for the application of the proposed method. The same is partly true for the highly relativistic region $(p \gg \mu)$ where the transverse components of the polarization vector corresponding to a pure coupling are very small and practically only the sign of the longitudinal component depends on the type of coupling. The most suitable is the region of intermediate energies $(p \approx \mu)$ where the differences between the vectors $\zeta'$ calculated for various pure couplings are rather big. E.g. for $p = \mu$ and $\theta = 45°$ we have for the scalar coupling $n' = 0$, $t'_y = 1$, whereas for the second vector coupling V′ we find $n = 0.942$, $t_y = 0.333$. In the case of $K_{\mu 3}$ decays the highest possible value of the $\mu$-meson momentum is roughly $\approx 2\mu$, whereas in $K_{e3}$ decays the highest possible value of the electron momentum is roughly $\approx 440\mu$. An overwhelming majority of the electrons emitted in $K_{e3}$ decays has, therefore, highly relativistic energies at which the polarization vectors $\zeta'$ corresponding to different couplings differ only in sign. In the case of $K_{\mu 3}$ decays most of the $\mu$-mesons have just the most suitable energies at which the polarization vectors depend in a more sensitive manner on the type of coupling. Another reason why the $K_{\mu 3}$ decays seem to be more suitable from the experimental point of view lies in the fact that the polarization of the $\mu$-meson can be studied from the asymmetries in the electron distribution in the subsequent decay of the $\mu$-meson. However, the possibility of different depolarization rates for the longitudinal and transversal components of the polarization vector during the slowing down process should be taken into account.

## References

1) J. Werle, Nuclear Physics **4** (1957) 171, 693
2) A. Salam, Nuovo Cimento **5** (1957) 229; L. D. Landau, Nuclear Physics **3** (1957) 127; T. D. Lee and C. N. Yang, Phys. Rev. **105** (1957) 1671
3) S. Furuichi, T. Kodama, Y. Suguhara, A. Wakasa and M. Yonezawa, Progress Theor. Phys. **16** (1956) 64
4) A. Pais and S. B. Treiman, Phys. Rev. **105** (1957) 1616
5) L. Michel and A. S. Wightman, Phys. Rev. **98** (1955) 1190; H. P. Stapp, Phys. Rev. **103** (1956) 425; B. Stech, Z. Physik **144** (1956) 214

*Nuclear Physics* **6** (1958) 10—19; © *North-Holland Publishing Co., Amsterdam*
Not to be reproduced by photoprint or microfilm without written permission from the publisher

# SPINS AND PARITIES OF THE $_{\Lambda}H^4$ HYPERFRAGMENT AND K-MESON

CHOU KUANG-CHAO and M. I. SHIROKOV
*Joint Institute of Nuclear Research, Laboratory of Theoretical Physics, Dubna, U.S.S.R.*

Received 24 July 1957

**Abstract:** If K-mesons, hyperfragments or hyperons are created in the $\pi^-+He^4$ reaction near the threshold or in the $K^-+He^4$ reaction at low $K^-$-particle energies (but without mesic atom formation), the spins of these unstable particles (and in some cases their parities) can be determined from the correlations between the directions of the momenta of the particles involved in these reactions and the directions of emission of decay products of the unstable particles. Qualitative changes in the correlation formulae for the cascade $K^-+He^4 \to {}_{\Lambda}H^4+\pi^0$, ${}_{\Lambda}H^4 \to He^4+\pi^-$ are indicated which arise if one rejects the assumption that the K-meson spin is zero. The helium experiments together with the previously suggested hydrogen experiments (e.g. $\pi^-+p \to \Sigma+K$ or $K^-+p \to \Sigma+\pi$) are the only ones which are of practical use for the determination of new particle spins from angular correlations.

## 1. Introduction

The method employed in the present paper for the determination of the spins of unstable particles consists in the following. The cascade $a+b \to c+d$, $c \to e+f$ is studied. The products of the first cascade reaction (particles c and d) are in general polarized in some definite way. The angular distribution of the decay products of a particle depends on the magnitude of its spin and on the nature of its polarization, that is, on the wave function of its spin state. Under suitable conditions this function may be known and then for each spin value of particle c a particular distribution will exist. If the experiment is carried out under prescribed experimental conditions the particle spin can be established by comparing these theoretical distributions with the experimental one.

By correlation we understand the angular distribution of the decay products of c (and/or d) which depends on its spin state; the latter in turn may depend on the angle of emission of the created particle as a parameter. If only particle c is considered and the beam a and target b are unpolarized (or possess zero spins) the correlation parameters and arguments in the general case are three vectors: the direction of the incident beam a, direction of emission of the reaction product c, and the direction of emission of its decay products. In view of the invariance of all processes under three-dimensional rotations the correlation will in fact depend only on the

relative position of these three vectors which can be specified by three angles (see below).

Dalitz [1]) earlier mentioned that measurement of the correlation for $K^-+He^4 \to {}_\Lambda H^4+\pi^0$, ${}_\Lambda H^4 \to He^4+\pi^-$ should yield information not only on the spin of the hyperfragment but also on the parities of the new particles. The hyperfragment spin may give information on the $\Lambda^0$ spin and on the nature of the interaction between $\Lambda^0$ and nucleon. The $\theta$ correlations for spins 0 and 1 of the ${}_\Lambda H^4$ are presented in ref. [2]) for various parities on the assumption that the K-meson spin is zero.

## 2. Correlation for the $\pi+He^4$ Cascade

### 2.1. GENERAL METHOD

General formulae for the angular distribution of the decay products of an unstable particle and for the spin state of particle c and/or d produced in a reaction of the $a+b \to c+d$ type have been obtained, for example, in ref. [3]). We shall now obtain the correlation for the simple case of the cascade $\pi^-+He^4 \to {}_\Lambda H^4+K$, ${}_\Lambda H^4 \to He^4+\pi^-$ and thus illustrate the general arguments presented above (and also the method used in ref. [3])).

The wave function $\psi^f$ for the products of the reaction $\pi^-+He^4 \to {}_\Lambda H^4+K$ can be written in the form

$$\Psi^f = \hat{S}(T, -T)\Psi^0. \tag{1}$$

Of course this does not make $\psi^f$ a better known function; so far only the dependence of $\psi^f$ on the dynamics of the problem (i.e., on the $S$-matrix of the problem) has been formally singled out and in addition it has been emphasized that $\psi^f$ depends on $\psi^0$ (initial condition at time $-T$).

Since the total momentum $\mathbf{P}$ of an isolated system is conserved, we get that $\mathbf{P}_f = 0$ if $\mathbf{P}_0 = 0$. The state of the system of particles ${}_\Lambda H^4$, K or $\pi^-$, $He^4$ can therefore be described in their relative momentum $\mathbf{p}$ and spin projection $m$ representation (in the c.m.s.). Rewriting (1) in Dirac's notation [4]) we obtain the following expression for the probability amplitude that after the reaction ${}_\Lambda H^4$ and K will possess a momentum $\mathbf{p}_f$ and spin projections $m_i$ and $m_k$

$$\begin{aligned}(\mathbf{p}_f;\ m_i,\ m_k|f) &= (\mathbf{p}_f;\ m_i,\ m_k|S|\mathbf{p})(\mathbf{p}|\mathbf{p}_0) \\ &= (\mathbf{p}_f;\ m_i,\ m_k|S|\mathbf{p}_0).\end{aligned} \tag{2}$$

The symbol $(\mathbf{p}|\mathbf{p}_0)$ signifies that prior to the reaction $\pi^-$ and $He^4$ had a definite momentum $\mathbf{p}_0$. Integration over $\mathbf{p}$ is implied.

Note that we have employed the law of conservation of total momentum. We shall now make use of the law of conservation of total angular momentum (a.m.) $\mathbf{J}$. Rewriting (1) for the case when the initial state $\psi^0$ is characterized by definite values of the total a.m. quantum number $J_0$ and

its projection $M_0$, we see that in order for $\psi^f$ to describe a state with the same definite $J$ and $M$ the $S$-matrix must be diagonal in $J$ and $M$:

$$(\ldots J'M'|S|\ldots JM)=(\ldots|S^J|\ldots)\cdot\delta_{J'J}\cdot\delta_{M'M}. \tag{3}$$

(It can be proved that elements that are diagonal with respect to $M$ do not depend on $M$.)

We now express the elements $(\mathbf{p}_f;\ m_i,\ m_k|S|\mathbf{p}_0)$ in (2) in terms of the elements of (3):

$$\begin{aligned}(\vartheta_f\varphi_f p_f;\ m_i,\ m_k|S|\mathbf{p}_0) &= C(p_0)\cdot\sum(\vartheta_f\varphi_f|l'\mu')(ikm_im_k|iks'm')\\ &\cdot(s'l'm'\mu'|s'l'J'M')(s'l'J'M'p_f|S|JMp_0)(JM|\vartheta_0\varphi_0).\end{aligned} \tag{4}$$

The unitary transformation function for transition from the representation in variables $\mathbf{p}_f$, $m_i$, $m_k$ to the representation involving $J$ and $M$ is obtained as the product of familiar transformation functions: 1) the wave function of a state with definite orbital a.m. $l'$ and its projection $\mu'$ in the representation in spherical angles $\vartheta_f$, $\varphi_f$ of the vector $\mathbf{p}_f$, that is, the spherical function $Y_{l'\mu'}(\vartheta_f,\ \varphi_f)\equiv(\vartheta_f\varphi_f|l'\mu')$; 2) the wave function of a state with a definite total spin $s'$ and its projection $m'$ in the representation in variables $m_i$ and $m_k$, i.e., the so-called Clebsch-Gordan coefficient $(ikm_im_k|iks'm')$[5]; and 3) the coefficient $(s'l'm'\mu'|s'l'J'M')$.

$C(p_0)$ is a normalization factor which is of no importance for the following exposition; $i$ and $k$ are the spins of particles ${}_\Lambda H^4$, and K. $\sum$ denotes the sum over $l'$, $\mu'$, $s'$, $m'$, $J'$, $M'$, $J$ and $M$.

Employing (3), orienting the $z$-axis parallel to $\mathbf{p}_0$ and taking into account that in this case

$$Y_{JM}(0,\ \varphi_0)=[2J+1/4\pi]^{\frac{1}{2}}\cdot\delta_{M,0},$$

we obtain the following final expression for the wave function of the reaction products:

$$\begin{aligned}(\mathbf{p}_f;\ m_i,\ m_k|\mathrm{f}) &= C'(p_0)\cdot\sum_{l'\mu's'm'}(\vartheta_f\varphi_f|l'\mu')(ikm_im_k|iks'm')\\ &\cdot(s'l'm'\mu'|s'l'l0)(s'l'|S^l|l)(2l+1)^{\frac{1}{2}}.\end{aligned} \tag{5}$$

The symbol $J$ has been replaced by $l$ which is the orbital angular momentum of particles $\pi^-$ and $He^4$ (and is equal to the total a.m. before the reaction).

The law of conservation of total parity (a consequence of the invariance of interactions under space reflection) is expressed by the equality of the total parities before and after the reaction. Thus $l$ and $l'$ should be such that $\Pi_\pi\cdot\Pi_{\mathrm{He}}(-1)^l=\Pi_{\mathrm{H}}\cdot\Pi_{\mathrm{K}}(-1)^{l'}$ or $\Pi(-1)^{l+l'}=+1$ where $\Pi$ is the product of intrinsic parities of all four particles participating in the reaction.

In a similar manner the angular distribution of the decay products of a polarized particle of spin $i$ at rest can be obtained if the particle decays into two zero spin particles

$$\mathcal{F}(\vartheta, \varphi) = |\sum_m Y_{im}(\vartheta, \varphi)\psi_m|^2; \tag{6}$$

$\psi_m$ is the spin wave function of the particle.

### 2.2. K-MESON SPIN ZERO AND LOW $\pi$-MESON ENERGY

Let us temporarily assume that the K-meson spin is zero; then $s' = i$. Suppose the reaction $\pi^- + \mathrm{He}^4 \to {}_\Lambda\mathrm{H}^4 + \mathrm{K}$ is being studied near the threshold, that is, at $\pi$-meson kinetic energies of 620—640 MeV in the laboratory system. ($\pi$-mesons of such energies can be obtained with the Birmingham proton synchrotron.) We assume that the forces between ${}_\Lambda\mathrm{H}^4$ and K are of the short range type (that is, these particles are created in a certain finite volume and do not interact after escaping from this volume). Since we know nothing more about these forces it will be most natural to assume that slow (in c.m.s.) ${}_\Lambda\mathrm{H}^4$ and K-particles are created predominantly in the s-state ($l' = 0$)†. Disregarding all matrix elements $(il'|S^l|l)$ with $l' = 1, 2 \ldots$ compared with $(i0|S^l|l)$ we find that $l$ can assume only a single value $l = i$. However, this value can be forbidden by the law of conservation of parity if $\Pi(-1)^i = -1$.

In the case when $\Pi = (-1)^i$, (5) takes the form

$$(m_i|\mathrm{f}) = \delta_{m_i,0} \cdot C'' \cdot (i0|S_i|i)(2i+1)^{\frac{1}{2}}. \tag{7}$$

Inserting (7) in (6) and denoting $\vartheta$ by $\gamma$ we get

$$\mathcal{F}_i(\gamma) \propto [P_i(\cos\gamma)]^2 \tag{8}$$

where $P_i(x)$ is an unnormalized Legendre polynomial (see ref. [6])) and $\gamma$ is the angle between the direction of emission of the hyperfragment decay products (in its c.m.s.) and the chosen $z$-axis (that is, the direction of the incident $\pi$-mesons). The correlations for spin values $i = 1$ and 2 are presented in table 1.

TABLE 1

| Parity \ Spin | $i = 1$ | $i = 2$ |
|---|---|---|
| $\Pi = (-1)^i$ | $3\cos^2\gamma$ | $\frac{5}{4}(1 - 6\cos^2\gamma + 9\cos^4\gamma)$ |
| $\Pi = -(-1)^i$ | $\frac{3}{2}(1 - \cos^2\gamma)$ | $\frac{15}{2}(\cos^2\gamma - \cos^4\gamma)$ |

If $\Pi = -(-1)^i$ the value $l' = 0$ will be forbidden, because in this case $l = i$ and $\Pi \cdot (-1)^i = -1$. Assuming that ${}_\Lambda\mathrm{H}^4$ and K are chiefly formed in the p-state ($l$ can again then assume only one value $l = i$) we obtain

† Of course it is always possible to imagine an interaction for which this will not be true (even if $l' = 0$ is not forbidden by the parity conservation law; see below). However the correlations derived below are valid for arbitrary short range forces although the angular ($\vartheta_l$) range in which the correlations are valid may be smaller (see section 3).

$$(\mathbf{p}_t;\ m_i|\mathrm{f}) \propto Y_{1,-m_i}(\vartheta_t,\ \varphi_t)(1i-m_i m_i|1ii0). \tag{9}$$

Besides $\gamma$, the correlation depends on two other angles ($\vartheta_t$ and $\varphi_t-\varphi$). Integrating over them we can obtain the correlation

$$I_i(\gamma) \propto \sum_{m=1}^{i} [Y_{im}(\gamma,\ 0)(1i-mm|1ii0)]^2$$

(see table 1).

## 3. Correlation for Restricted Directions of Emission

### 3.1. K-MESON SPIN ZERO AND HIGHER $\pi$-MESON ENERGIES

Adair [7]) has indicated another approach to the problem of determining the spin from correlations. Mathematically this method is based on the formula $Y_{l,\mu}(0,\ \varphi) = [2l+1/4\pi]^{\frac{1}{2}} \cdot \delta_{\mu,0}$ (the quantal expression of the perpendicularity of the angular momentum to the corresponding momentum.) We shall again assume that the K-meson spin is zero but shall not impose the restriction that the $\pi$-meson energy is close to the threshold value. We shall consider the decays of only those hyperfragments which are emitted at angles $\vartheta_t \approx 0$ or $\vartheta_t \approx \pi$, i.e., along the axis $z\|\mathbf{p}_0$. From (5) it immediately follows that $(0,\ \varphi_t;\ m_i|\mathrm{f}) \propto \delta_{m_i,0}$, i.e., the spin wave function of these hyperfragments is the same as (7)†. Thus the correlation formulae are the same as those near the threshold for the parity case $\Pi = (-1)^i$.

What is the angular range of $\vartheta_t$ in which these formulae are valid? From the deduction it follows that in this interval we should be able to neglect spherical functions $Y_{l',\mu'}(\vartheta_t,\ \varphi_t)$ with $\mu' \neq 0$ compared with $Y_{l',0}(\vartheta_t,\ \varphi_t)$. A calculation shows that for $l' = 1$ one tenth compared to unity is neglected in the $\vartheta_t$ interval ($0^0-20^0$). This interval should decrease with increasing $l'$. A consequence of this is that one is obliged to assume that the forces are of short range and that the threshold should not be considerably exceeded in the experiments. For each given energy the maximum essential value of $l'$ should be found by assuming some range of forces (usually $\approx 10^{-13}$ cm) and the permissible angular range should be estimated.

At the threshold and for $\Pi = (-1)^i$ formula (7) is valid over the whole sphere of directions of emission of the hyperfragment (for all angles $\vartheta_t$).

† This result can easily be explained in a descriptive manner. The projection of the total a.m. on the axis $z\|\mathbf{p}_0$ is zero before the reaction as the $\pi^-$ and $He^4$ spins are zero and the projection of the orbital a.m. on the momentum itself is zero. Thus after the reaction the sum of the projection of the ${}_\Lambda H^4$ spin and the orbital a.m. $l'$ should vanish. For hyperfragments ejected along the $z$-axis $\mu'$ is again the projection of the a.m. on the momentum and must therefore vanish. Therefore for such hyperfragments $m_i$ can assume only one value: $m_i = 0$. It can be seen that it is sufficient to use only conservation of the projection of the total a.m. providing that $m_i = 0$ and emission in the direction of the $z$-axis is not forbidden by the laws of conservation of the total a.m. and parity. (This prohibition just occurs near the threshold for $\Pi = -(-1)^i$; see below).

As the $\pi$-meson energy is increased, the region of applicability contracts towards the poles. When $\Pi = -(-1)^i$ the angular distribution as well as the spin wave-function of hyperfragments emitted along the $z$-axis vanish at the threshold (see (9); $(\mathbf{p}_t;\ 0|f) = 0$, as $(1i00|1ii0) = 0$). This means that in this case and near the threshold no region exists in which (7) is valid. As the energy increases, hyperfragments begin to appear also at the poles and correlation (8) is valid for them.

### 3.2. K-MESON SPIN NOT ZERO

The assumption that the K-meson spin is zero may be abandoned if one applies Adair's method (although, admittedly, the statistics are impaired in this case). If $k \neq 0$ the most general correlation will be a function of five angles (a function of the relative position of four vectors) $\mathscr{F}(\vartheta_t;\ \vartheta,\ \varphi;\ \vartheta_K,\ \varphi_K)$ where $\vartheta_K$, $\varphi_K$ are the angles of emission of the $K \to \pi+\pi$ decay products in the K-meson rest system; these angles, as well as $\vartheta$ and $\varphi$, are measured in a coordinate system whose axis is $z||\mathbf{p}_0$ †.

Let us construct the correlation $\mathscr{F}(0;\ \vartheta,\ \varphi;\ 0,\ \varphi_K)$, i.e., construct the angular distribution for decay products from the following ensemble of hyperfragments: first of all hyperfragments (and K-mesons) those emitted along the $z$-axis are chosen; after this from these events we choose those in which the decay $\pi$-mesons from $K \to \pi+\pi$ are emitted parallel to the $z$-axis. Formula (6) for the $K \to \pi+\pi$ decay shows that only the components $(0,\ \varphi_t,\ p_t;\ m_i,\ 0|f)$ of the wave-function $(\vartheta_t,\ \varphi_t,\ p_t;\ m_i,\ m_k|f)$ are required for this correlation. From (5) we then deduce that $(0, \varphi_t, p_t; m_i, 0|f) \propto \delta_{m_i,0}$, that is, the correlation $\mathscr{F}(0;\ \vartheta,\ \varphi;\ 0,\ \varphi_K)$ is identical to (8). The correlation $\mathscr{F}(0,\ 0,\ \varphi,\ \vartheta_K,\ \varphi_K)$ has also the same form and permits one to determine the K-meson spin. It should be noted that in the cascade $\pi+p \to \Sigma+K$, $\Sigma \to N+\pi$, $K \to \pi+\pi$ this correlation can yield a spin value $k$ or $k-1$ and hence the measured value of the K-meson spin may turn out to be smaller than the true value [7]).

In conclusion it should be stressed that the parity can be determined experimentally only in the vicinity of the threshold and only if the K-meson spin is zero. If the $\pi^-$-meson and helium parities are known it should be possible to determine the product of the K-meson and hyperfragment parities. It may be mentioned that the law of conservation of strangeness (not mentioning the laws of conservation of electric charge and number of baryons) does not permit one to determine separately the parity of each new particle.

† The so-called polarization correlation of ${}_\Lambda H^4$ and K is used. In this connection it should be mentioned that formula (1.5) in ref. [3]), p. 1033, and the corresponding paragraph are wrong.

## 4. Correlation for the $K^-+He^4$ Cascade

The $K^-+He^4 \to {}_\Lambda H^4+\pi^0$ reaction is of the same type as that discussed above (if $k=0$ it is symbolically written as $0+0 \to i+0$) but it is accompanied by release of energy.

The most frequent events are those involving electromagnetic capture of $K^-$ mesons on one of the helium atom orbits (formation of a mesic atom) and subsequent (non-electromagnetic) interaction with the helium nucleus. However, this subsequent capture may proceed from the s-orbit ($l=0$) as well as from the p-orbit ($l=1$); according to theoretical estimates[8]) the probabilities for each of these events are approximately the same. The presence of $l=1$ in the initial state is explained by the fact that a system (mesic atom) with a.m. equal to 0, 1, 2 etc., is initially formed by the long range electromagnetic forces. The probability for mesic atom formation rapidly decreases with increase of K-meson energy[9]). At an energy $\approx 0.1$ MeV the cross section for mesic atom formation is approximately a million times smaller than the nuclear geometric cross section, i.e. $\approx 10^{-4}$ mb. Moreover the mesic atom is predominantly produced in the s-state when the K-meson energy exceeds the ionization energy of the mesic atom ($\approx 0.01$ MeV). Thus if it is ascertained in some way that the reaction takes place "in flight" †, that is, without mesic atom formation (or mesic atom formation in the s-state) the effect of long range electromagnetic forces will be negligible. Employing the generally accepted concept of a finite K-meson-nucleon interaction range it seems most natural to consider the element $(s'l'|S^0|0)$ in (5) to be larger than all other elements ($l \neq 0$) providing that the energy of the incident K-meson does not exceed 20 MeV (the interaction range in this case should be assumed to be of the order of the helium nucleus, i.e., $1.6\times10^{-13}$ cm). For $\Pi=(-1)^i$ and $k=0$ we then obtain from (5) for the hyperfragment wave function $(m_i|\mathrm{f}) \propto Y^*_{i,m_i}(\vartheta_t, \varphi_t)$ and for the angular distribution of the hyperfragment decay products

$$\mathcal{F}(\vartheta_t,\ \varphi_t;\ \vartheta,\ \varphi) \propto \left|\sum_m Y_{im}(\vartheta,\ \varphi)Y^*_{im}(\vartheta_t,\ \varphi_t)\right|^2 \propto [P_i\ (\cos\theta)]^2 \qquad (10)$$

where $\theta$ is the angle between the directions $\vartheta_t$, $\varphi_t$ and $\vartheta$, $\varphi$. The correlation is the same as that described by (8) but refers to a different angle.

Suppose now that comparison of experiment with theory indicates that the parity is $\Pi=-(-1)^i$. The statistics can then be expanded by considering events involving mesic atom formation, since capture from the s-orbit is forbidden. The same correlation formulae as those in the second line in table 1 are obtained if capture from the d-orbit is neglected. (It should

† For example the reaction $K^-+He^4$ occurs before the K-meson track becomes perceptibly curved or the reaction products in the laboratory system are observed to emerge in directions which do not differ by exactly 180°.

be noted that if the hyperfragment and K-meson spins are zero the reactions $\pi^-+He^4 \to {}_\Lambda H^4+K$ and $K^-+He^4 \to {}_\Lambda H^4+\pi^0$ will in general be forbidden for $\Pi = -(-1)^0 = -1$.)

At low K-meson energies ($l = 0$) and $\Pi = (-1)^i$ Adair's procedure for the reaction under consideration is identical with that presented above (indeed for $l = 0$ the $z$-axis can be chosen parallel to $\mathbf{p}_f$ and from (4) and (3) it then follows that for the projection on this axis $(m_i|f) \propto \delta_{m_i 0}$ and (10) is immediately obtained); for $\Pi = -(-1)^i$ it does not have any region of applicability.

At higher energies Adair's procedure should be slightly modified: the $z$-axis is chosen parallel to $\mathbf{p}_f$ (instead of $z||\mathbf{p}_0$) and the region of applicability of (10) is then restricted by the largest significant value of $l$ which is the orbital angular momentum *before the reaction*: those events should be chosen in which the angle between the incident K-mesons and the axis $z||\mathbf{p}_f$ is small in the c.m.s., or, what is the same, in which the hyperfragments are emitted at small angles with respect to $\mathbf{p}_0$.

It should be noted that the statistics obtained for the $\pi^-+He^4 \to {}_\Lambda H^4+K_0$ and $K^-+He^4 \to {}_\Lambda H^4+\pi^0$ reactions can be plotted on a single graph (if $k = 0$).

The possibility $k \neq 0$ can be accounted for only qualitatively for the cascade $K^-+He^4 \to {}_\Lambda H^4+\pi^0$, ${}_\Lambda H^4 \to He^4+\pi^-$ (one additional assumption being made.) If $k \neq 0$ one obtains $l' = |i-k|, |i-k|+1, \ldots i+k$ (see eq. (5).)

Since the energy release in the reaction $K^-+He^4 \to {}_\Lambda H^4+\pi^0$ is not very large ($\approx$ 150 MeV) we shall assume that of all these values of $l'$ only the lowest value occurs, that is $l' = |i-k|$ (or $l' = |i-k|+1$ in the other parity

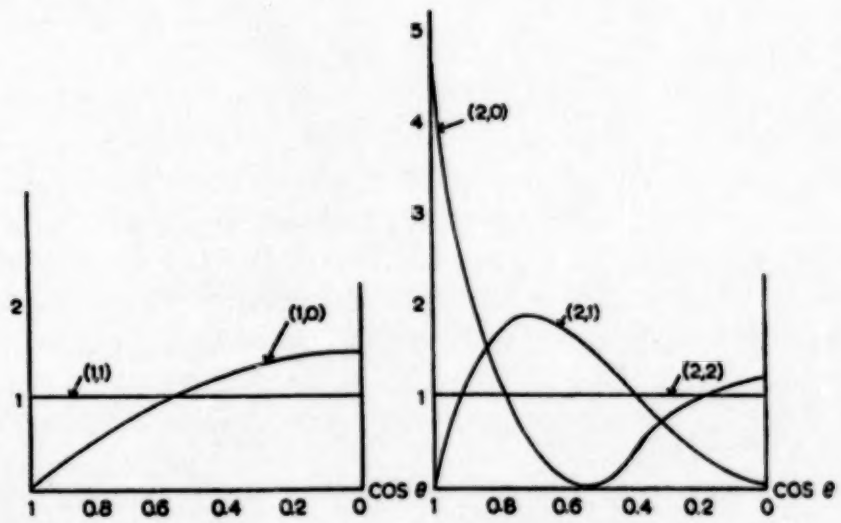


Fig. 1. Correlation in $K^-+He^4 \to {}_\Lambda H^4+\pi$, ${}_\Lambda H^4 \to He^4+\pi^-$ cascade for various cases $(i, k)$ of the spin values of the hyperfragment and K-meson (the product of their parities being $-1$.)

case.) Clearly, the larger $|i-k|$ is, the better founded this assumption is. The calculations are now more complicated (the K-meson beam is assumed to be unpolarized.) A summary of the angular ($\theta$) distribution for various spin values of the hyperfragment and K-meson is presented in fig. 1. (The product of their parities is $-1$, which corresponds to $\Pi = +1$. It should be noted that in table 1 the method of classification with respect to parity is different; thus the cases $i = 1, \Pi = -1$ and $i = 2, \Pi = +1$ are united in the same row.) Qualitatively the effect of $k \neq 0$ can be expressed as follows: $|i-k|$ or $|i-k|+1$ can be determined from the correlation. Thus $k \neq 0$ smoothes out the correlation (10) for hyperfragments (and hence lowers the measured spin value). The same conclusion can be drawn for the cascade $K^- + p \to \Sigma + K$, $\Sigma \to N + \pi$. Thus even if the $\theta$ correlation is set up for Alvarez events [10]) "in flight", isotropy, strictly speaking, would merely indicate that the hyperon and K-meson spin values are approximately equal.

## 5. Other Reactions

Besides the reactions discussed above, two other reactions of the $0+0 \to i+0$ type exist: the interaction of $\pi$ and K-mesons with helium accompanied by formation of a ${}_{\Lambda}He^4$ hyperfragment. However at present no two-particle ${}_{\Lambda}He^4$ decays are known.

Other modes of interaction of $\pi$ and K-mesons with helium are possible, such as $K^- + He^4 \to {}_{\Lambda}H^3 + n$, ${}_{\Lambda}H^3 \to He^3 + \pi^-$, and $K^- + He^4 \to \Sigma^0(\Lambda^0) + H^3$ or $K^- + He^4 \to \Sigma^- + He^3$, followed by $\Sigma \to N + \pi$. The correlation formulae for such reactions (of the $0+0 \to j+\frac{1}{2}$, $j \to \frac{1}{2}+0$ type) turn out to be the same as those for the $K^- + p \to \Sigma^- + \pi^+$ reaction [11]) so that, for example, cases of the $K^- + He^4 \to \Sigma^- + He^3$ reaction can be easily plotted on the $\theta$ correlation graph of the $K^- + p \to \Sigma^- + \pi^+$ reaction.

Besides the reactions (of the $0+0 \to i+0$, $i \to 0+0$ and $0+0 \to j+\frac{1}{2}$, $j \to \frac{1}{2}+0$ types) analyzed above and those of the $0+\frac{1}{2} \to j+0$ type † previously suggested [7, 8, 11]), no other reactions exist which are suitable for the determination of the spins of new unstable particles produced by bombarding hydrogen, deuterium, $H^3$, $He^3$ or $He^4$ targets with $\pi$ mesons, K-mesons or nucleons. For other types of reactions (e.g. $K^- + D \to \Sigma + p$) the correlation formulae inevitably contain unknown parameters. In some cases certain assumptions regarding these parameters can be introduced which are similar to that made in section 4. However, in this case the

† Examples of such reactions are $\pi^{\mp} + p \to Y + K$ where Y is a $\Sigma$ or $\Lambda^0$ particle; $K^- + p \to \overset{\circ}{\Sigma}{}^- + \overset{\circ}{K}{}^+$, $\pi^- + He^3 \to {}_{\Lambda}H^3 + K^0$; and in general reactions of the type $\pi$ + nucleus (spin $\frac{1}{2}$) → hyperfragment + K, hyperfragment → $\frac{1}{2}+0$.) Reactions involving energy release: $K^- + p \to Y + \pi$, $K^- + H^3 \to {}_{\Lambda}H^3 + \pi^-$, $\tilde{p} + He^4 \to {}_{\Lambda}H^3 + K^0$ ($\tilde{p}$ is an antiproton.)

correlation formulae cannot be expected to yield more than qualitative results and the respective reactions cannot be a reliable means of determination of the spins of new particles, although they may yield a non-trivial ($> \frac{1}{2}$) lower limit for the spin.

The authors express their appreciation to Prof. M. A. Markov for interest in this work and discussions.

*Note added in the proof:* After the present paper was sent to print we learned that an identical result regarding the determination of the K-meson spin by Adair's method has been obtained by J. J. Sakurai (Phys. Rev. **107** (1957) 1119). From a point of view different from ours, Dr. Sakurai also emphasized the importance of the $\pi + He^4 \rightarrow {}_{\Lambda}H^4 + K$ reaction.

## References

1) K. Dalitz, Proceedings of the Rochester Conference (1956)
2) M. Gell-Mann, Phys. Rev. **106** (1957) 1298
3) M. I. Shirokov, JETP **32** (1957) 1022
4) P. A. M. Dirac, The Principles of Quantum Mechanics
5) A. Simon, Numerical Table of the Clebsch-Gordan Coefficients (ORNL-1718)
6) E. Jahnke and F. Emde, Tables of Functions
7) R. K. Adair, Phys. Rev. **100** (1955) 1540
8) R. Gatto, Nuovo Cimento **3** (1956) 1142
9) M. I. Podgoretsky, Ups. Fiz. Nauk **51** (1953) 253
10) L. W. Alvarez *et al.*, Nuovo Cimento **5** (1957) 1026
11) S. B. Treiman, Phys. Rev. **101** (1956) 1216

*Nuclear Physics* **6** (1958) 20—33; © *North-Holland Publishing Co., Amsterdam*

Not to be reproduced by photoprint or microfilm without written permission from the publisher

# DIRECT AND COMPOUND PROCESSES IN NUCLEAR REACTIONS

M. SANO and S. YOSHIDA

*Institute for Nuclear Study, University of Tokyo*

and

T. TERASAWA

*Institute of Science and Technology, University of Tokyo*

Received 16 September 1957

**Abstract:** The elastic and inelastic scattering of nucleons by nuclei are investigated taking account of the direct and compound processes. First, we choose a few channels which are strongly coupled to the entrance channel and introduce a potential matrix, which describes the interaction among chosen channels and the distortion of the wave in each channel. Then the transition matrix element is written as a sum of two contributions, one from the direct process and the other from the compound process. The average cross section is also divided into two parts, and the interference term vanishes by a suitable choice of the potential matrix. The cross section of the direct process has a stronger energy dependence than the single particle resonance behaviour. The compound cross section, which is the contribution from nearby levels and can be calculated if the potential matrix is known, is shown to have the form of the conventional statistical model with a modified definition of the transmission factor.

## 1. Introduction

The elastic scattering of a nucleon by nuclei has been investigated by many authors, and the optical model was found to give good agreement with experiment [1]). However, this model can predict only the gross structure of the cross sections, that is, an average of the total and elastic cross sections over a rather wide range of energy. On the other hand, the inelastic scattering or nuclear reactions have been analyzed so far mostly in terms of the statistical theory. Although the statistical theory was successful in explaining some phenomena, there remained many cases in which the theory failed to give a good agreement. In particular when the residual nucleus is left in a low excited state we often find an asymmetry of the angular distribution about 90° and large cross sections which are not compatible with the statistical theory. These difficulties are expected to be removed by the introduction of direct interactions or modification of the statistical theory.

The direct interaction has been investigated by many authors assuming single particle excitation [2]) or collective excitation [3]). But most of them used the distorted wave approximation which cannot be applied to the energy region of the single particle resonances. Besides, the distorted wave approximation has the other defect that it can only predict the gross

structure. One of the present authors (S. Y) tried to overcome the former defect by solving the problem by the Tamm-Dancoff method in a special case [4]) and further proposed an approximation method for the general case [5]). For the energy dependence of the cross section we have some data which seem difficult to explain by single particle or compound resonances [6]).

The purpose of this paper is to give a formulation which describes both the direct and the compound process from a unified point of view. This formulation is considered as an extension of the optical model and the direct interaction model. The transition matrix element is divided into three parts: The first is the contribution from the direct process which is calculated exactly taking account of a few chosen channels connected strongly with the entrance channel in the presence of the interaction potentials. The second part gives the contribution from the direct interaction which is not contained in the first part. The third part represents the contribution from the resonance levels and has a sharp energy dependence at low energy in contrast to the first two parts (§ 2).

The average cross section is calculated in § 3. The potential is chosen so that the energy average of the second and third terms of the transition matrix element may vanish. Then the cross section is written in two parts, the contribution from the direct interaction and the energy average of the contribution from the compound process. The former cross section comes mainly from far resonances, and the latter is the contribution from the nearby resonance levels which may be calculated by the statistical theory.

The choice of the potential is discussed in § 4 and it will be shown that the distorting potential is different from the usual optical potential. In § 5 the behaviour of the direct interaction process is discussed and it will be shown that the direct interaction in our theory may predict the energy dependence of the cross section which may be called "the intermediate structure" in contrast with the single particle or the compound resonances.

## 2. The Transition Matrix Element

We consider the nucleon scattering by nuclei at low and intermediate energies. The exchange effect of the incident nucleon with the nucleons in the target nucleus will be neglected to simplify the treatment, and reactions other than the elastic and inelastic scattering of nucleons will not be taken into account.

The Hamiltonian of our system is written as

$$H = H_0 + V, \tag{1}$$

where $H_0$ represents the sum of the Hamiltonian of the target nucleus and the kinetic energy of the incident nucleon and $V$ is the interaction between

the incident nucleon and the target nucleus. The wave function $\Psi_s^{(+)}$ with one entrance channel s satisfies the following integral equation

$$\Psi_s^{(+)} = \Phi_s + \frac{1}{E+i\varepsilon-H_0} V\Psi_s^{(+)}, \tag{2}$$

where $\varepsilon$ is a small positive number to insure the outgoing wave character of $\Psi_s^{(+)}$. $\Phi_s$ is a free wave function satisfying

$$(H_0-E)\Phi_s = 0, \tag{3}$$

which contains only one partial wave specified by the channel index s;

$$\Phi_s = \frac{2}{i} k_s r j_{l_s}(k_s r)\chi_s(\xi). \tag{4}$$

In the above equation $j_{l_s}(k_s r)$ is the spherical Bessel function of order $l_s$, the orbital angular momentum of the channel s, and the argument is a product of the wave number in the channel s and the radial coordinate $r$ of the incident nucleon.

$\chi_s(\xi)$ is the channel wave function, and $\xi$ represents all variables but $r$. However, because of the normalization of (4), $\chi_s(\xi)$ contains factor $1/r$. The channel indices s, t, . . . are used to represent the states of the target nucleus, channel spin, orbital angular momentum of the incident nucleon and also the total angular momentum of the whole system.

We now choose a few channels which are strongly coupled to the entrance channel. The chosen channel is not necessarily an open channel, it may be a closed channel. We introduce the interaction $U(r, \xi)$ from which the matrix element with respect to the states of the target nucleus $U_{st}(r)$ is derived:

$$U_{st}(r) = \int \chi_s^*(\xi)U(r, \xi)\chi_t(\xi)\mathrm{d}\xi; \tag{5}$$

this will hereafter be called "potential matrix". This potential matrix $U_{st}(r)$ has non-diagonal elements only between chosen channels whereas the diagonal elements are the distorting potentials defined for all channels. The interaction $U$ or potential matrix $U_{st}(r)$ should be chosen to get a good approximation and to make the calculation easy: this will be discussed later. This potential matrix is a generalization of the optical potential.

If the wave function described by the Hamiltonian $H_0+U$ is denoted by $\varphi_s^{(+)}$ then

$$\varphi_s^{(+)} = \Phi_s + \frac{1}{E+i\varepsilon-H_0} U\varphi_s^{(+)}, \tag{6}$$

where the channel index s is written to specify the entrance channel. The integral equation (6) may be rewritten in the form of coupled equations for the wave amplitudes of the chosen channels.

The transition matrix element $T_{ts}$ may be obtained from (2) and (6) as

$$T_{ts}=\frac{iM}{\hbar^2\sqrt{k_s k_t}}\Big[\langle\Phi_t|U|\varphi_s^{(+)}\rangle+\langle\varphi_t^{(-)}|V-U|\varphi_s^{(+)}\rangle + \langle\varphi_t^{(-)}|(V-U)\frac{1}{E+i\varepsilon-H}(V-U)|\varphi_s^{(+)}\Big] \quad (7)$$

by the usual procedure employed by Gell-Mann and Goldberger [7]), Hayakawa [7]), and Ui [2]). In the equation (7) the factor $iM/\hbar^2\sqrt{k_s k_t}$ is introduced for the normalization and $M$ is the reduced mass of the incident nucleon.

For later convenience we define three transition matrices which correspond to each term of (7), so (7) is expressed by

$$T_{ts}=T_{ts}^{(1)}+T_{ts}^{(2)}+T_{ts}^{(3)}. \quad (8)$$

In the last equation the first term has non-vanishing non-diagonal matrix elements only between the chosen channels and represents the contribution from the direct interaction, while the diagonal elements pertaining to other channels represent the contribution from the optical potential. If the equation (6) is solved without approximation then $T_{ts}^{(1)}$ is the exact transition matrix element for the direct interaction $U(r, \xi)$.

The second term of (8) will be discussed in the next section. The third term represents the contribution from the compound nucleus and exhibits a resonance behaviour. To show this we introduce the eigenfunctions for the compound states $X_\lambda$ according to Kapur and Peierls [8]). The eigenfunction $X_\lambda$ satisfies the equation

$$(H-W_\lambda)X_\lambda=0 \quad (9)$$

in the internal region of the configuration space and the boundary condition

$$R\cdot\int\chi_s^*\cdot\operatorname{grad}X_\lambda\,\mathrm{dS}=(S_s+iP_s)\int\chi_s^*\cdot X_\lambda\,\mathrm{dS}, \quad (10)$$

where $W_\lambda$ is the complex energy eigenvalue, $R$ is the nuclear radius, $S_s$ and $P_s$ are the real and imaginary part of the logarithmic derivative of the outgoing wave of wave number $k_s$ evaluated at $r=R$, and dS denotes a surface element of the boundary of the internal region. The eigenfunction is normalized by †

$$\int X_\lambda X_{\lambda'}\,\mathrm{d}\tau=\delta_{\lambda\lambda'} \quad (11)$$

and satisfies the following completeness condition

$$\sum_\lambda X_\lambda X_\lambda=1. \quad (12)$$

† This normalization differs from the original one used by Kapur and Peierls [8]). Cf. G. E. Brown and C. T. DeDominicis [3]).

By using $X_\lambda$, $T_{ts}^{(3)}$ is written as

$$T_{ts}^{(3)} = \frac{iM}{\hbar^2\sqrt{k_s k_t}} \sum_\lambda \langle \varphi_t^{(-)}|V-U|X_\lambda\rangle \frac{1}{E-W_\lambda} \langle X_\lambda^*|V-U|\varphi_s^{(+)}\rangle. \quad (13)$$

We shall express the last equation in a more familiar form. From the Schrödinger equation for $X_\lambda$ and $\varphi_s^{(+)}$ we have

$$\langle X_\lambda^*|V-U|\varphi_s^{(+)}\rangle = \langle X_\lambda^*|H_0|\varphi_s^{(+)}\rangle - \langle \varphi_s^{*(+)}|H_0|X_\lambda\rangle + (W_\lambda - E)\langle X_\lambda^*|\varphi_s^{(+)}\rangle. \quad (14)$$

The first term may be expressed in the following form by Green's theorem:

$$\langle X_\lambda^*|H_0|\varphi_s^{(+)}\rangle - \langle \varphi_s^{*(+)}|H_0|X_\lambda\rangle = -\frac{\hbar^2}{2M}\int_s \{X_\lambda \cdot \mathrm{grad}_n\, \varphi_s^{(+)} - \mathrm{grad}_n\, X_\lambda \cdot \varphi_s^{(+)}\}\, \mathrm{dS}.$$

To evaluate the right hand side of the last equation, we decompose the eigenfunction $X_\lambda$ into single particle states according to Lane, Thomas and Wigner [9]):

$$X_\lambda = \sum_{s,\,p} C_{\lambda sp}\chi_s(\xi)\hat{u}_{sp}(r), \quad (15)$$

where $\hat{u}_{sp}(r)$ is the radial wave function of the single particle state sp for the potential $U_{ss}(r)$ which is normalized by

$$\int_0^R (\hat{u}_{sp}(r))^2\, \mathrm{d}r = 1 \quad (16)$$

and satisfies the following boundary condition:

$$R \cdot \left[\frac{\mathrm{d}\hat{u}_{sp}}{\mathrm{d}r}/\hat{u}_{sp}\right]_{r=R} = S_s + iP_s. \quad (17)$$

The coefficient $C_{\lambda sp}$ is the amplitude of the single particle state sp in the compound state $\lambda$ and gives the reduced width $\gamma_{\lambda s}$ together with $\hat{u}_{sp}(R)$

$$\gamma_{\lambda s} = \sqrt{\frac{\hbar^2}{2MR}} \sum_p C_{\lambda sp}\, \hat{u}_{sp}(R). \quad (18)$$

This definition of the reduced width follows Thomas [10]). The wave function for the direct interaction is also decomposed as

$$\varphi_s^{(+)} = \sum_t \chi_t(\xi) u_t^s(r), \quad (19)$$

where $u_t^s(r)$ is the amplitude of the direct interaction wave function in the t channel when the entrance channel is s. The asymptotic form is given by

$$u_t^s(r) = \delta_{st} u_t^{(-)}(r) - \sqrt{\frac{k_s}{k_t}} S_{ts}^{(1)} u_t^{(+)}(r). \quad (20)$$

The wave function $u_t^{(\pm)}(r)$ is the outgoing (incoming) wave defined by Blatt and Weisskopf [11]), and

$$S_{ts}^{(1)} = \delta_{ts} + T_{ts}^{(1)} \quad (21)$$

is the collision matrix for the direct interaction. The outgoing wave $u_t^{(+)}$ evaluated at $r = R$ is expressed by using $P_t$ as

$$u_t^{(+)} = G_t + iF_t = e^{i\phi_t}\sqrt{\frac{x_t}{P_t}}, \tag{22}$$

where $x_t$ represents $k_tR$, $F_t$ and $G_t$ are the regular and irregular solution evaluated at $r = R$ which are defined by Blatt and Weisskopf [11]), and

$$\tan\phi_t = F_t/G_t. \tag{23}$$

By using these relations we obtain

$$\langle X_\lambda^*|H_0|\varphi_s^{(+)}\rangle - \langle\varphi_s^{*(+)}|H_0|X_\lambda\rangle = \sqrt{\frac{\hbar^2 k_s}{2M}}\,2ie^{-i\phi_s}\sqrt{P_s}\sqrt{\frac{\hbar^2}{2MR}}\sum_p C_{\lambda sp}\,\hat{u}_{sp}(R). \tag{24}$$

The evaluation of the third term of (14) is more involved. Instead of decomposing the eigenfunction $X_\lambda$ into single particle states directly, we introduce the eigenfunction for the direct interaction $\psi_a$:

$$(H_0 + U - W_a)\psi_a = 0. \tag{25}$$

$W_a$ is the complex eigenvalue and the boundary condition for $\psi_a$ is the same as $X_\lambda$. Then we have expansions

$$X_\lambda = \sum_a a_{\lambda a}\,\psi_a, \tag{26a}$$

$$\psi_a = \sum_{sp} a_{asp}\,\chi_s\,\hat{u}_{sp}(r). \tag{26b}$$

Comparing with (15), the following relation is obtained:

$$\sum_a a_{\lambda a}\,a_{asp} = C_{\lambda sp}. \tag{27}$$

By using these expansion coefficients, the third term of (14) may be written as

$$(W_\lambda - E)\int X_\lambda\,\varphi_s^{(+)}\,d\tau = \sum_a \left(\frac{W_\lambda - E}{E - W_a}\right) a_{\lambda a}\int \psi_a(E - W_a)\varphi_s^{(+)}\,d\tau. \tag{28}$$

From the Schrödinger equation for $\psi_a$ and $\varphi_s^{(+)}$ we obtain

$$\int \psi_a(E - W_a)\varphi_s^{(+)}\,d\tau = -\frac{\hbar^2}{2M}\int_S [\psi_a \cdot \mathrm{grad}_n\,\varphi_s^{(+)} - \varphi_s^{(+)}\,\mathrm{grad}_n\,\psi_a]\,dS,$$

which is in turn expressed using the expansion (26b) as

$$\sqrt{\frac{\hbar^2 k_s}{2M}}\,2ie^{-i\phi_s}\sqrt{P_s}\sqrt{\frac{\hbar^2}{2MR}}\sum_p a_{asp}\,\hat{u}_{sp}(R).$$

By putting the above expression into the equation (28)

$$(W_\lambda - E)\int X_\lambda \cdot \varphi_s^{(+)}\,d\tau = \sqrt{\frac{\hbar^2 k_s}{2M}}\,2ie^{-i\phi_s}\sqrt{P_s}\sqrt{\frac{\hbar^2}{2MR}}\sum_{ap}\left(\frac{W_\lambda - E}{E - W_a}\right) a_{\lambda a}\,a_{asp}\,\hat{u}_{sp}(R) \tag{29}$$

is obtained. Here we introduce the modified reduced width

$$\tilde{\gamma}_{\lambda s} = \sqrt{\frac{\hbar^2}{2MR}} \sum_{ap} \left( \frac{W_\lambda - W_a}{E - W_a} \right) a_{\lambda a} a_{asp} \hat{u}_{sp}(R) \tag{30}$$

and we finally obtain

$$\langle X_\lambda^* | V - U | \varphi_s^{(+)} \rangle = \sqrt{\frac{\hbar^2 k_s}{2M}} 2i e^{-i\phi_s} \sqrt{P_s} \tilde{\gamma}_{\lambda s}. \tag{31}$$

In a similar way we get

$$\langle \varphi_t^{(-)} | V - U | X_\lambda \rangle = \sqrt{\frac{\hbar^2 k_t}{2M}} 2i e^{-i\phi_t} \sqrt{P_t} \tilde{\gamma}_{\lambda t}. \tag{32}$$

Thus we can express $T_{ts}^{(3)}$ as

$$T_{ts}^{(3)} = 2ie^{-i\phi_t} \sqrt{P_t} \sum_\lambda \frac{\tilde{\gamma}_{\lambda t} \tilde{\gamma}_{\lambda s}}{E - W_\lambda} \sqrt{P_s} e^{-i\phi_s}. \tag{33}$$

It is noted that the modified reduced width $\tilde{\gamma}_{\lambda s}$ approaches the usual reduced width $\gamma_{\lambda s}$ if

$$\left| \frac{W_\lambda - E}{E - W_a} \right| \ll 1,$$

by eqs. (18) and (27). From eq. (33) it is seen that $T_{ts}^{(3)}$ has a sharp resonance behaviour and the resonance energy is $W_\lambda$.

The cross section for the transition from the channel s to the channel t is given (apart from the statistical factor) by

$$\sigma_{ts} = \frac{\pi}{k_s^2} |T_{ts}|^2 = \frac{\pi}{k_s^2} |T_{ts}^{(1)} + T_{ts}^{(2)} + T_{ts}^{(3)}|^2. \tag{34}$$

The angular distribution may be calculated by using the formula of Blatt and Biedenharn [12]).

## 3. Average Cross Section

We now calculate the average cross section over an energy interval $\delta$ which is small compared to the level distance of the single particle resonances and large compared to the level distance for the compound resonances $D$. Since the transition matrix elements $T_{ts}^{(1)}$ and $T_{ts}^{(2)}$ are slowly varying functions of $E$, they can be considered to be constant over the interval $\delta$. Thus we obtain

$$\bar{T}_{ts}^{(1)} = T_{ts}^{(1)}, \quad \bar{T}_{ts}^{(2)} = T_{ts}^{(2)}, \tag{35}$$

where the bar indicates the energy average over $\delta$. The average of the cross section (34) is written as

$$\bar{\sigma}_{ts} = \frac{\pi}{k_s^2}\left[|T_{ts}^{(1)}|^2 + 2\ \mathrm{Re}\ T_{ts}^{(1)*}(T_{ts}^{(2)} + \bar{T}_{ts}^{(3)}) + \overline{|T_{ts}^{(2)} + T_{ts}^{(3)}|^2}\right]. \quad (36)$$

We assume that the potential matrix may be chosen in such a way that

$$\bar{T}_{ts}^{(2)} + \bar{T}_{ts}^{(3)} = 0, \quad (37)$$

where s and t are chosen channels if they are different. So the interference term in eq. (36) is dropped. The requirement (37) is not unreasonable because the life time of the compound nucleus may be considered to be long compared to the life time of the compound state induced by the direct interaction, so both contributions are expected to be incoherent. Thus we obtain

$$\begin{aligned}\bar{\sigma}_{ts} &= \frac{\pi}{k_s^2}\left[|T_{ts}^{(1)}|^2 + \overline{|T_{ts}^{(3)} - \bar{T}_{ts}^{(3)}|^2}\right] = \frac{\pi}{k_s^2}\left[|T_{ts}^{(1)}|^2 + (\overline{|T_{ts}^{(3)}|^2} - |\bar{T}_{ts}^{(3)}|^2)\right] \\ &\equiv \sigma_{ts}^{(1)} + \bar{\sigma}_{ts}^{(3)}\end{aligned} \quad (38)$$

where $\sigma_{ts}^{(1)}$ corresponds to the term containing $T_{ts}^{(1)}$ and $\bar{\sigma}_{ts}^{(3)}$ to the term $T_{ts}^{(3)}$.

$\bar{\sigma}_{ts}^{(3)}$ may be calculated by using (33) as

$$\bar{\sigma}_{ts}^{(3)} = \frac{\pi}{k_s^2} 4P_s P_t \frac{\pi}{\delta}\left[\sum_{\lambda,\mu} \frac{\tilde{\gamma}_{\lambda s}\tilde{\gamma}_{\mu s}^{*}\tilde{\gamma}_{\lambda t}\tilde{\gamma}_{\mu t}^{*}(\Gamma_\mu + \Gamma_\lambda)}{(E_\lambda - E_\mu)^2 + \frac{1}{4}(\Gamma_\mu + \Gamma_\lambda)^2} - \frac{\pi}{\delta}\sum_{\lambda,\mu}\tilde{\gamma}_{\lambda s}\tilde{\gamma}_{\mu s}^{*}\tilde{\gamma}_{\lambda t}\tilde{\gamma}_{\mu t}^{*}\right], \quad (39)$$

where $E_\lambda$ and $\Gamma_\lambda$ are real and imaginary part of $W_\lambda$ respectively. The sum over $\lambda$ is restricted to those $E_\lambda$'s which belong to the energy interval $\delta$. In evaluating the last equation the modified reduced width was assumed to be a slowly varying function of $E$ in the energy interval $\delta$ compared to the energy denominator $E - W_\lambda$; this assumption seems plausible from the definition (30). In the summation over $\lambda$ and $\mu$ in the first term of (39), the cross terms with $\mu \neq \lambda$ may be neglected by the same argument as that of Thomas [10]). That is, for each level in the $\lambda$ sum there will be about $\Gamma_\lambda/D$ levels contributing from the $\mu$ sum owing to the denominator and about $\delta\Gamma_\lambda/D^2$ pairs altogether. In view of the random nature of $\tilde{\gamma}_{\lambda s}$ signs, the contribution from the term $\lambda \neq \mu$ will be proportional to the square root of this number of pairs in contrast with the number $\delta/D$ contributing from the positive definite terms with $\lambda = \mu$. The second term of eq. (39) is also evaluated neglecting the cross-terms $\lambda \neq \mu$. If we denote the average of $\Gamma_\mu$ over the energy interval $\delta$ by $\Gamma$, and the modified width $\tilde{\Gamma}_s$ averaged over $\delta$ by

$$\tilde{\Gamma}_s = 2P_s \cdot |\tilde{\gamma}_s|^2, \quad (40)$$

where $|\tilde{\gamma}_s|^2$ is the average of $|\tilde{\gamma}_{\lambda s}|^2$ over $\delta$, we obtain

$$\bar{\sigma}_{ts}^{(3)} = \frac{\pi}{k_s^2}\frac{\pi}{D}\left(\frac{2}{\Gamma} - \frac{\pi}{\delta}\right)\tilde{\Gamma}_s\tilde{\Gamma}_t. \quad (41)$$

The second term on the right hand side of the last equation depend on $\delta$, but it is of same order of magnitude as neglected terms in the first sum of (39) and negligible compared to the first term. This average compound cross section coincides with the result of the conventional statistical theory when $\delta \gg \Gamma$ and $\tilde{\Gamma}_s = \Gamma_s$. The first condition was necessary to derive (41) while the second condition is expressed by the equation (30) as

$$|(W_\lambda - E)/(W_a - E)| \ll 1. \tag{42}$$

The eigenvalue $W_\lambda$ is limited in the energy interval $\delta$ centred at $E$, so $|W_\lambda - E| < \delta/2$ because $\delta \gg \Gamma$. The denominator $|W_a - E|$ is large compared to $\delta$ if $E$ is far form the direct interaction resonance, whose level distance may be considered of the order of the single particle resonance distance $\Delta$ divided by $N$, the number of states of the target nucleus taken into account in the direct interaction. In this case the second condition is considered to be satisfied if $N$ is not too large. But if $E$ is near $W_a$ then the denominator $|W_a - E|$ becomes of the order of the imaginary part of the distorting potential $U^{\mathrm{Im}}$. Thus in this case it is necessary that

$$\delta/U^{\mathrm{Im}} \ll 1.$$

We now show that the cross section $\bar{\sigma}_{ts}^{(3)}$ can be evaluated even if $\tilde{\Gamma}_s$ is different from $\Gamma_s$ provided $T_{ts}^{(1)}$ is known. The collision matrix is given by

$$S_{ts} = S_{ts}^{(1)} + T_{ts}^{(2)} + T_{ts}^{(3)} \tag{43}$$

using the relation (21). From eq. (43) the following energy average of the absolute square of the collision matrix is obtained:

$$\overline{|S_{ts}|^2} = |S_{ts}^{(1)}|^2 + \overline{|T_{ts}^{(3)}|^2} - |\bar{T}_{ts}^{(3)}|^2 \tag{44}$$

where the relation $S_{ts}^{(1)} = \bar{S}_{ts}^{(1)}$ is used. From the unitarity and symmetry properties of the collision matrix we obtain

$$1 = \sum_t |S_{ts}|^2 = \sum_t \overline{|S_{ts}|^2} = \sum_t (|S_{ts}^{(1)}|^2 + \overline{|T_{ts}^{(3)}|^2} - |\bar{T}_{ts}^{(3)}|^2), \tag{45}$$

from which

$$T_t \equiv 1 - \sum_t |S_{ts}^{(1)}|^2 = \sum_t (\overline{|T_{ts}^{(3)}|^2} - |\bar{T}_{ts}^{(3)}|^2) \tag{46}$$

is obtained. In the last equation the transmission factor [11] $T_s$ is introduced, which gives the cross section for the compound nucleus formation from the channel s, $\sigma_s^{(c)}$ as

$$\sigma_s^{(c)} = \frac{\pi}{k_s^2} T_s. \tag{47}$$

On the other hand, (41) may be written as follows:

$$\overline{|T_{ts}^{(3)}|^2} - |\bar{T}_{ts}^{(3)}|^2 = C \tilde{\Gamma}_t \tilde{\Gamma}_s, \tag{48}$$

where $C$ is a constant independent of the channel index. By summing both sides of (48) over the channel s

$$T_t = C\tilde{\Gamma}_t \cdot \sum_s \tilde{\Gamma}_s$$

and further summing over t we obtain

$$\sum_t T_t = C\,(\sum_s \tilde{\Gamma}_s)^2.$$

From the last two equations

$$\tilde{\Gamma}_t = \frac{T_t}{\sqrt{C \sum_s T_s}}. \tag{49}$$

By putting (49) into (48) we can express the cross section $\bar{\sigma}_{ts}^{(3)}$ in terms of the transmission factor:

$$\bar{\sigma}_{ts}^{(3)} = \frac{\pi}{k_s^2} \frac{T_t T_s}{\sum_t T_t}. \tag{50}$$

This result is that of the conventional statistical theory [11]) with the modified definition of the transmission factor $T_s$. The angular distribution may be calculated using the formula of Blatt and Biederharn [12]) along the same lines as given in ref. [3]). We can now calculate the average cross section contributed by the compound nucleus, if the direct interaction cross section is calculated by assuming the potential matrix. In the next section we shall discuss the potential matrix.

## 4. The Potential Matrix

In the last section it was assumed that the potential matrix can be obtained so as to satisfy the equation (37), i.e.,

$$\langle \varphi_t^{(-)}|V-U|\varphi_s^{(+)}\rangle + \langle \varphi_t^{(-)}|(V-U)\,\frac{1}{E+i\varepsilon-H}\,(V-U)|\varphi_s^{(+)}\rangle = 0. \tag{51}$$

By using the eigenfunction for the compound state $X_\lambda$, (51) becomes

$$\langle \varphi_t^{(-)}|V-U|\varphi_s^{(+)}\rangle - \frac{i\pi}{\delta} \sum_\lambda \langle \varphi_t^{(-)}|V-U|X_\lambda\rangle\langle X_\lambda^*|V-U|\varphi_s^{(+)}\rangle = 0, \tag{52}$$

where the summation over $\lambda$ is limited to those $\lambda$ whose $E_\lambda$ belongs to the energy interval $\delta$. The potential matrix would be obtained in a self-consistent way so as to satisfy the condition (52), if the eigenfunction $X_\lambda$ were known. However it is practically impossible to obtain $X_\lambda$, so a phenomenological method was employed to obtain the potential matrix in the previous paper [3]). First assuming that

$$U_{st}(r) = \int \chi_s^*(\xi) V(\xi, r) \chi_t(\xi)\, d\xi \tag{53}$$

for the non-diagonal elements, the diagonal elements were chosen so that the calculated elastic scattering cross section in presence of the direct interaction may well reproduce the experiments. This method is of practical use also in our case, but we shall seek the qualitative difference of the diagonal matrix element of $U$ from the usual optical potential in a simple case.

To simplify the argument we now assume that the non-diagonal element of the potential (53) is small and the diagonal element of the potential is well described by the average potential; that is

$$U_{ss}(r) = \int \chi_s^*(\xi) V(\xi, r) \chi_s(\xi)\, d\xi + \Delta U_s, \tag{54}$$

where $\Delta U_s$ is a small constant inside of the nucleus and vanishes outside. In this case the wave function $\varphi_s^{(+)}$ is not so different from the solution when the potential is given by the first term on the right hand side of the equation (54). If the normalized wave function for $r < R$ is denoted by $\hat{\varphi}_s^{(+)}$ then eq. (52) leads to

$$\Delta U_s = -\frac{i\pi}{\delta} \sum_{\lambda} \langle \hat{\varphi}_s^{(-)} | V - U | X_\lambda \rangle \langle X_\lambda^* | V - U | \hat{\varphi}_s^{(+)} \rangle. \tag{55}$$

The sum $\sum_\lambda$ should be taken over those $E_\lambda$ which belong to the interval $\delta$. Further the expansion (15) is applied to $X_\lambda$. Eq. (55) becomes

$$\begin{aligned} \Delta U_s = -\frac{i\pi}{\delta} \Big[ & \sum_{u,v,p,q}{}' \langle \varphi_s^{(-)} | V | \chi_u \hat{u}_{up} \rangle \langle \chi_v^* \hat{u}_{vq}^* | V | \hat{\varphi}_s^{(+)} \rangle \sum_\lambda C_{\lambda up} C_{\lambda vq} \\ & - \sum_{u,p,q}{}' \langle \hat{\varphi}_s^{(-)} | V | \chi_u \hat{u}_{up} \rangle \langle \chi_s^* \hat{u}_{sq}^* | \Delta U_s | \hat{\varphi}_s^{(+)} \rangle \sum_\lambda C_{\lambda up} C_{\lambda sq} \\ & - \sum_{v,p,q}{}' \langle \hat{\varphi}_s^{(-)} | \Delta U_s | \chi_s \hat{u}_{sp} \rangle \langle \chi_v^* \hat{u}_{vq}^* | V | \hat{\varphi}_s^{(+)} \rangle \sum_\lambda C_{\lambda sp} C_{\lambda vq} \\ & + \sum_{p,q}{}' \langle \hat{\varphi}_s^{(-)} | \Delta U_s | \chi_s \hat{u}_{sp} \rangle \langle \chi_s^* \hat{u}_{sq}^* | \Delta U_s | \hat{\varphi}_s^{(+)} \rangle \sum_\lambda C_{\lambda sp} C_{\lambda sq} \Big], \end{aligned} \tag{56}$$

where the notation $\sum'$ means the exclusion of the chosen channels from the sum over u and v. The random sign of $C_{\lambda up}$ makes the following approximation possible:

$$\sum_\lambda C_{\lambda up} C_{\lambda vq} = \delta_{uv} \delta_{pq} \cdot \frac{\delta}{D} \overline{C_{\lambda up}^2}. \tag{57}$$

By means of the last relation we finally obtain from (56)

$$\Delta U_s = -\frac{i\pi}{D} \Big[ \sum_{u,p}{}' \langle \hat{\varphi}_s^{(-)} | V | \chi_u \hat{u}_{up} \rangle^2 \cdot \overline{C_{\lambda up}^2} + \sum_p \langle \varphi_s^{(-)} | \Delta U_s | \chi_s \hat{u}_{sp} \rangle^2 \cdot \overline{C_{\lambda sp}^2} \Big]. \tag{58}$$

The second term on the right hand side of the above equation is much

smaller than the first term if the incident energy is far from resonances, because the second term contains $\overline{C^2_{\lambda sp}}$ which is small. We see from the last equation that the deviation of the distorting potential has a real and an imaginary part and the imaginary part comes mainly from the first term of the right hand side of (58) if $\Delta U_s$ is small.

Let us now compare the imaginary part of $\Delta U_s$ with that of the usual optical potential which was discussed by Bowcock [13]), Brown and De Dominicis [2]). The corresponding equation to (58) for the optical potential is given by

$$\Delta U_s = -\frac{i\pi}{D}\Big[\sum_{u\neq s,p}\langle\hat{\varphi}_s^{(-)}|V|\chi_u\hat{u}_{up}\rangle^2\cdot\overline{C^2_{\lambda up}}\cdot\sum_p\langle\hat{\varphi}_s^{(-)}|\Delta U_s|\chi_s\hat{u}_{sp}\rangle^2\cdot\overline{C^2_{\lambda sp}}\Big].$$

The main difference is the sum in the first term. Again assuming that the imaginary part is small, we see that the imaginary part of the distorting potential $U_{ss}$ is smaller than that of the usual optical potential by the contribution from the chosen channels in the sum in the first term.

## 5. Discussion

In the preceding sections it became clear that the present theory can treat the direct process and compound process from a unified point of view, and further both contributions may be calculated if a suitable potential matrix is chosen. The determination of the potential matrix from the nuclear interaction is difficult but the phenomenological method will be used in practical cases.

We now consider the contribution from the direct interaction and study the energy dependence of the cross section. To simplify the argument, the elastic scattering is considered and a few excited states of the target nucleus are chosen to which the ground state is more strongly coupled than to other states. First it is assumed that the non-diagonal elements of the interaction vanish. Then we shall observe the single particle resonances, that is the gross structure. If the non-diagonal interaction is taken into account and the equation for the direct interaction (6) is solved, the single particle level splits into a few levels whose number is equal to the number of chosen channels. This situation is similar to that of the configuration mixing in the nuclear spectroscopy. We shall call this energy dependence of the cross section the intermediate structure. If other small matrix elements are further introduced we shall observe a fine structure, but a suitable energy average of the cross section leads again to the intermediate structure. A similar argument is expected to apply to the inelastic scattering. The energy level occurring in the intermediate coupling model of Lane [14]) is considered as a special example of this type of level. We can expect that this intermediate structure will be useful in analyzing some nuclear reactions.

The angular distribution of the cross section will also be affected by the resonances in the intermediate structure. The closed channels may also play an important role in some cases. In fact, it was found that in the calculation of the neutron scattering by $Mg^{24}$ the angular distribution at low energy varies rapidly with energy by the effect of the second excited state of $Mg^{24}$ (this forms a closed channel) [5].

The usual distorted wave approximation can be obtained if the diagonal potential is used for the potential matrix $U$ [15]. Then the first term of the transition matrix element $T_{ts}$ in eq. (7) represents the transition matrix for the usual optical model, the second term represents that of the usual distorted wave approximation, and the third term represents the contribution from the compound process. Since $U$ is diagonal the first term has only diagonal matrix elements. The average cross section can be calculated in a similar way to that given in § 4. However, this approximation fails at a single particle resonance because at that energy the second and higher order contributions of the transitions between chosen channels will be large; these contributions are contained in the third term and then the assumption of the random phases of the modified reduced widths $\tilde{\gamma}_{\lambda s}$ will not hold. On the contrary, in our theory these contributions are contained in the first term exactly, so the compound process will not suffer from the breakdown of the randomness of the phases of $\tilde{\gamma}_{\lambda s}$.

Our approximation is rather different from the treatment by the optical model, which is applied to the inelastic scattering by Ui [16]. In the latter treatment the interaction between the two particles is taken into account exactly not only for the chosen channels but also the other channels, in contrast to our treatment in which the two body interaction is taken into account only for the chosen channels. However, the effect of the successive scattering of the incident nucleon by the different nucleons in the nucleus is taken into account for the chosen channels in our treatment, whereas this is neglected in the optical model. Further, our approximation has the advantage that it can be applied also to interactions like the collective interactions which cannot easily be expressed in terms of the two particle interactions.

The authors would like to express their sincere thanks to Professors T. Muto and G. Takeda and Messrs. M. Kawai and H. Ui for interesting discussions and valuable advices for the manuscript.

## References

1) H. Feshbach, C. E. Porter and V. F. Weisskopf, Phys. Rev. **96** (1954) 448; F. L. Friedman and V. F. Weisskopf, in Niels Bohr and the development of physics (Pergamon Press, London 1955)
2) Kajikawa, Watari and Sasakawa, Prog. Theor. Phys. **16** (1956) 152;

R. Kajikawa and W. Watari, Prog. Theor. Phys. **18** (1957) 103;
J. A. Lamarsh and H. Feshbach, Phys. Rev. **104** (1956) 1633;
S. T. Butler, Phys. Rev. **106** (1957) 272;
H. Ui, Prog. Theor. Phys. **18** (1957) 163;
G. E. Brown and C. T. DeDominicis, Proc. Phys. Soc. A **70** (1957) 668, 686
3) S. Hayakawa and S. Yoshida, Prog. Theor. Phys. **14** (1955) 1;
D. M. Brink, Proc. Phys. Soc. A **68** (1955) 994
4) S. Yoshida, Proc. Phys. Soc. A **69** (1956) 668
5) S. Yoshida, to be published in Prog. Theor. Phys.
6) R. M. Eisberg and N. M. Hintz, Phys. Rev. **103** (1956) 645;
G. W. Greenlees, B. C. Haywood, L. G. Kuo and M. Petrović, Proc. Phys. Soc. A **70** (1957) 331
7) M. Gell-Mann and M. L. Goldberger, Phys. Rev. **91** (1953) 398;
S. Hayakawa, Transactions of the Bose Research Institute **20** (1955) 21
8) P. L. Kapur and R. E. Peierls, Proc. Roy. Soc. A **166** (1938) 277
9) A. M. Lane, R. G. Thomas and E. P. Wigner, Phys. Rev. **98** (1955) 693
10) R. G. Thomas, Phys. Rev. **97** (1955) 224
11) J. M. Blatt and V. F. Weisskopf, Theoretical Nuclear Physics, (John Wiley & Sons, 1952)
12) J. M. Blatt and L. C. Biedenharn, Rev. Mod. Phys. **24** (1952) 258
13) J. Bowcock, Proc. Phys. Soc. A **70** (1957) 515
14) A. M. Lane, Proc. Phys. Soc. A **66** (1953) 65
15) G. E. Brown, private communication
16) H. Ui, Prog. Theor. Phys. **14** (1955) 75

*Nuclear Physics* **6** (1958) 34—49; © *North-Holland Publishing Co., Amsterdam*
Not to be reproduced by photoprint or microfilm without written permission from the publisher

# THE ELECTRON-NEUTRINO ANGULAR CORRELATION IN DECAY OF $Ne^{23}$

B. W. RIDLEY
*Atomic Energy Research Establishment, Harwell, Didcot, Berks*

Received 18 November 1957

**Abstract:** The electron-neutrino angular correlation in decay of $Ne^{23}$ has been determined by measuring the distribution of electron energies and recoil momenta without selection of angle. The angular correlation parameter $\alpha$ was found to be $-0.05 \pm 0.10$. This implies a ratio of coupling strengths of the axial vector and tensor parts of the Gamow-Teller interaction within the limits $0.85 \leqq |C_A|/|C_T| \leqq 1.62$.

## 1. Introduction

Evidence about the composition of the beta decay interaction has in the past been drawn mainly from beta spectrum shapes, K-capture to positon emission ratios and electron-neutrino angular correlations in allowed transitions. It was believed that the Fermi and Gamow-Teller interactions were each composed of an essentially pure invariant on grounds of continued failure to observe Fierz interference effects [1, 2, 3, 4]). Measurements of electron-neutrino angular correlations in recoil experiments then aimed to show more or less qualitatively whether the Gamow-Teller interaction was T or A and the Fermi interaction S or V.

The discovery of parity violation in $\beta$-processes has required a reexamination of this procedure for indentifying the component invariants. Jackson *et al.* [5]) have calculated distributions for allowed $\beta$-decay generalized to permit violation of parity and time reversal. For the energy spectrum and electron-neutrino angular correlation, their expression reduces to

$$P_{\pm}(E,\theta)\cdot \mathrm{d}E\mathrm{d}\Omega_\theta = F(Z,E)\cdot pE(E_0-E)^2\cdot\xi\cdot\left\{1+(\alpha_0\pm\alpha_t)\frac{v}{c}\cos\theta\pm\frac{b}{E}\right\}\cdot \mathrm{d}E\mathrm{d}\Omega_\theta, \quad (1)$$

where $E$ is the electron energy and $\theta$ the angle between the electron and neutrino rays,

$$\xi = [|C_S|^2+|C'_S|^2+|C_V|^2+|C'_V|^2]\cdot|M_F|^2 + [|C_T|^2+|C'_T|^2+|C_A|^2+|C'_A|^2]\cdot|M_{GT}|^2, \quad (2)$$

$$\alpha_0\cdot\xi = [-|C_S|^2-|C'_S|^2+|C_V|^2+|C'_V|^2]\cdot|M_F|^2 + \tfrac{1}{3}[|C_T|^2+|C'_T|^2-|C_A|^2-|C'_A|^2]\cdot|M_{GT}|^2, \quad (3)$$

$$\alpha_t \cdot \xi = \frac{\alpha Z}{p} \cdot 2\,\mathrm{Im}\,[(C_S C_V^* + C'_S C'^*_V)|M_F|^2 + \tfrac{1}{3}(C_T C_A^* + C'_T C'^*_A)|M_{GT}|^2], \quad (4)$$

$$b \cdot \xi = (1-\alpha^2 Z^2)^{\frac{1}{2}} \cdot 2\,\mathrm{Re}\,[(C_S C_V^* + C'_S C'^*_V)|M_F|^2 + (C_T C_A^* + C'_T C'^*_A|M_{GT}|^2]. \quad (5)$$

The coupling constants $C$, $C'$ refer to the parity conserving and violating parts of the interaction respectively. These constants are complex if time reversal is violated. The angular correlation coefficient $\alpha_0$ remains essentially the same as in the old parity conserving $\beta$-decay theory. If time reversal is violated, however, an additional momentum dependent correction $\alpha_t$ may arise due to Coulomb interactions, but will be unimportant in the high energy low $Z$ emitters hitherto studied. A striking feature of expression (5) is that a zero value for the Fierz term $b$ no longer ensures purity of the Fermi and G.T. interactions unless certain special relations are assumed between the $C$ and $C'$ for each interaction. One set of such relations is provided by the two component neutrino theory of Lee and Yang [6]), from which it follows that for each invariant $C' = \mp C$ for negaton emission and $C' = \pm C$ for positon emission. If no such assumptions are made, then knowledge of the angular correlation parameter alone can determine uniquely the relative strengths of these basic interactions.

Individual angular correlations can be interpreted uniquely only when either Fermi or G.T. nuclear matrix elements are eliminated by selection rules. In the pure G.T. decay of $He^6$, Rustad and Ruby [7]) found that $\alpha = +0.36 \pm 0.10$ and $+0.31 \pm 0.14$ in two measurements, implying a predominantly T interaction. Pure Fermi emitters are comparatively rare and so far none has been found suitable for recoil experiments. However, mixed transitions (occurring when $\Delta J = 0$, not $0 \to 0$) can yield information about the Fermi interaction if the ratio of Fermi to G.T. matrix elements is known and the nature of the G.T. interaction assumed. Recoil experiments on two such decays, those of the free neutron (Robson [8])) and $Ne^{19}$ (Maxson *et al.* [9]), Good and Lauer [10]) and Alford and Hamilton [11])) gave values of $\alpha$ clustering around zero, showing that the Fermi interaction is mainly S if the G.T. interaction is assumed to be T. In view of the importance of Rustad and Ruby's $He^6$ experiment in identifying both the Fermi and G.T. interactions, we felt is desirable to check their result by experiments on another essentially pure G.T. emitter, $Ne^{23}$. Interest in such a measurement has been further enhanced by recent evidence from decay of $A^{35}$ that the Fermi interaction is not S after all, but mainly V [12]).

## 2. Principle of the Experiment

$Ne^{23}$ decays with a half-life of $37.6 \pm 0.1$ sec. The decay scheme with spin assignments suggested by Penning and Schmidt [13]) is shown in fig. 1. Transitions occur to the ground and first and second excited states of $Na^{23}$

with end point energies and branching ratios of 4.39±0.05 MeV (67±3 %), 3.95±0.05 MeV (32±3 %) and 2.4±0.1 MeV (1.0±0.15 %) respectively. In decay to the ground state, a spin change 5/2 → 3/2 (no) ensures that the effective interactions are G.T. In decay to the first excited state, a spin change 5/2 → 5/2 (no) might permit an additional contribution from Fermi interactions. However, this contribution should be very small since a change of isobaric spin 3/2 → 1/2 is involved. Elliott [14]) estimates that in the first excited state of $Na^{23}$, the admixture of configurations with $T = 3/2$ that would form a large Fermi matrix element with the ground state of $Ne^{23}$ is most unlikely to be greater than $10^{-4}$ in intensity. For these reasons, we have assumed that both transitions are pure G.T. and exhibit identical electron-neutrino angular correlations.

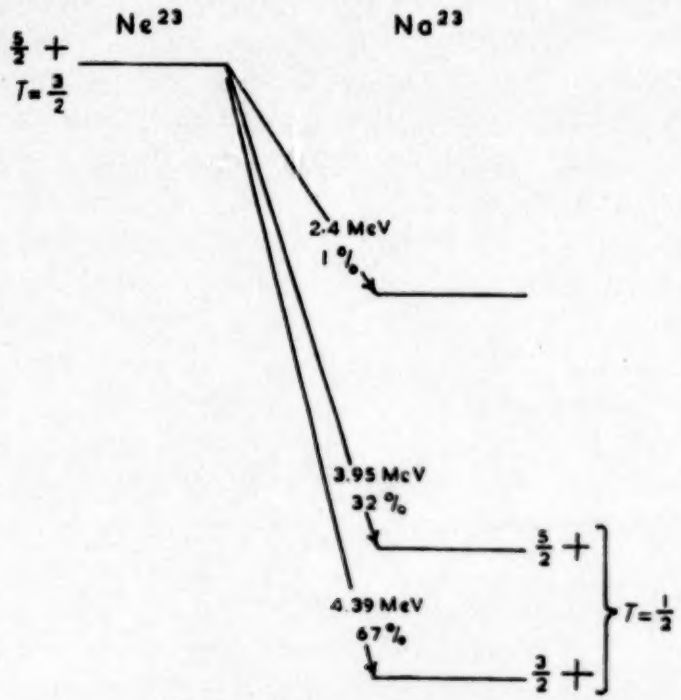


Fig. 1. Decay scheme for $Ne^{23}$.

The problem of determining electron-neutrino correlations from distributions of observable quantities has been considered by Kofoed-Hansen [15]). In this experiment we chose to measure the distribution of electron energies and recoil momenta without selection of angle. When no $\gamma$-ray is emitted, these quantities suffice to determine the momentum vector diagram for the decay and thus, in principle, the angle between the beta and neutrino rays. For allowed transitions, this distribution has the form

$$P_{\pm}(E, r) \cdot \mathrm{d}r\mathrm{d}E = F(Z, E) \cdot \xi \cdot \left[ q(E \pm b) + \frac{\alpha}{2} (r^2 - p^2 - q^2) \right] r \cdot \mathrm{d}r\mathrm{d}E \qquad (6)$$

where $r$ is the momentum of the recoiling nucleus and $p$ and $q$ those of the electron and neutrino respectively. When a $\gamma$-ray is also emitted, the recoil momentum distribution will be smeared by isotropic emission of photons relative to the beta rays. In decay to the first excited state of $Na^{23}$ the smearing due to the 0.44 MeV $\gamma$-ray, though not a substantial effect, must be taken into account. Distortion of the momentum diagram by surface and molecular binding effects does not occur since Ne is a monatomic gas. Of course, the gas pressure in the apparatus must be low enough to avoid collisions of the recoil ions.

Electron energies were measured using a scintillation counter with an effectively "$4\pi$" geometrical efficiency. The radioactive $Ne^{23}$ was fed into a cavity within the phosphor which served to define the source volume. Recoil ions which escaped through an open mouth of the cavity were detected at a known distance from the source and their velocities measured by time of flight. Both the electron energy and recoil flight time were recorded for each observed event, enabling information to be collected economically and eliminating problems of normalisation. No attempt was made to distinguish between events arising from the 3.95 and 4.39 MeV transitions. Contributions from the weak 1 % 2.4 MeV transition were neglected since these would be well submerged within the available statistics from the two dominant transitions.

## 3. Description of Apparatus

### 3.1. THE DETECTORS

The arrangement of detectors is illustrated in fig. 2. The source cavity is defined by a cylindrical hole drilled into the 1 inch cube sodium iodide

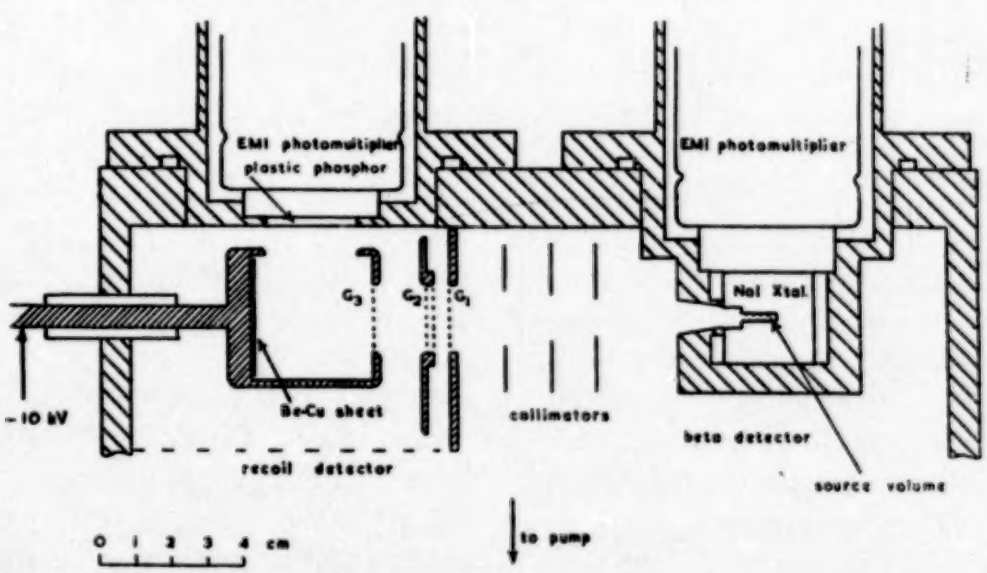


Fig. 2. Arrangement of beta and recoil detectors.

crystal used for detecting $\beta$-particles. The radioactive gas is fed into the rear of the source volume through another hole 1 mm diameter drilled at right angles to it (out of the plane of the diagram). The length of the source is 1 cm and its diameter 0.2 cm. The hole is lined with a 1 mg/cm$^2$ aluminium foil containing an internal helical rib in its surface of pitch 1 mm and height 0.2 mm. The foil serves to maintain the source volume at earth potential. The inward projecting rib prevents escape of scattered recoils in the direction of the recoil detector. The phosphor is surrounded by brass shielding so that only $\beta$-particles originating from decays within the cavity can be detected. The small aperture through which recoils escape admits few $\beta$-particles from outside.

Sodium iodide was chosen as scintillator for the reason of its high stopping power for $\beta$-particles. This enables the geometry of the source volume to be scaled down, giving better definition of the length of flight path. The usual objection to sodium iodide for $\beta$-spectrometry on grounds of strong back scattering does not apply in the present case of an internal source. However, difficulties do arise from the emission of undetected bremsstrahlung photons, especially by the higher energy electrons, and substantial corrections must be made to the electron energy distribution near the upper limit of the spectrum. The energy response of the $\beta$-detector was calibrated by irradiation with $\gamma$-rays from $Cs^{137}$ (0.661 MeV), radiothorium (2.615 MeV and escape peaks at 2.104 and 1.593 MeV) and $C^{12}$ from a Po-Be neutron source (4.43 MeV and escape peaks at 3.92 and 3.41 MeV). The width at half height of the $Cs^{137}$ photo peak was 11 %.

The recoil detector consists essentially of a hybrid of an electron multiplier and scintillation counter. Recoils entering the aperture of the earthed grid $G_2$ are accelerated by 10 kilovolts through grid $G_3$ onto a sheet sensitised beryllium-copper lining the rear face of a cubical box. The resulting shower of secondary electrons is accelerated back to earth through an aperture in the top of the box and detected with a thin plastic phosphor and photomultiplier. The surface of the phosphor is thinly aluminized to provide the earthed attracting electrode. The phosphor thickness was so chosen that the energy dissipated in it by traversal of a fast $\beta$-particle would be at least four times the 60 keV or so carried in by the secondary electron shower. Pulse height selection could then be used to discriminate against the rather strong background of fast $\beta$-particles.

The additional grid $G_2$ is fitted to enable an electrostatic retarding field to be applied to the recoils in subsidiary experiments. $G_1$ is always earthed. $G_2$ is also earthed during normal runs. When required the retarding field is applied by taking up $G_2$ to the required potential.

The effective aperture of the recoil detector is that of the grid $G_3$, which is circular of diameter 2 cm. The recoil flight path, defined essentially by

the distance from the back of the source volume to $G_2$, is 9.8 cm. The distribution of activity within the source volume leads to an uncertainty of 1 cm, or about 10 %, in the flight path. Collimators limit the field of view of the detector to the cone of recoils emerging from the source, and so reduce background from residual gaseous activity in the detector housing.

The detector characteristics were investigated with an artificial source of sodium ions. With the output biassed to limit the noise rate to 2 counts per sec, a detection efficiency of about 90 % was achieved. The efficiency varied by less than 1 % for ion energies ranging from 50 to 700 eV and was uniform over the entire aperture of $G_2$.

The detector assembly is mounted in a vacuum chamber immediately above a 6 inch mercury diffusion pump protected by a liquid air trap. The relative speed of the pump and conductance of the source cavity ensure that the mean gaseous activity per unit volume inside the source region is about $10^4$ times that in the rest of the detector housing.

### 3.2. SOURCE PRODUCTION AND PUMPING SYSTEM

$Ne^{23}$ was produced in the $Na^{23}$(n, p) reaction using neutrons of about 10 MeV energy obtained from a $Be^9$ (d, n) reaction in the Cavendish cyclotron at the University of Cambridge. The target consisted of 200 g of an artificial ion exchange zeolite, "Decalso Y" (produced by the Permutit Co.), ground to a grain size of 5 to 15 microns. This had previously been dehydrated at a temperature of 350° C, leaving the material in a highly emanating form.

The gas pumping system is shown schematically in fig. 3. The zeolite

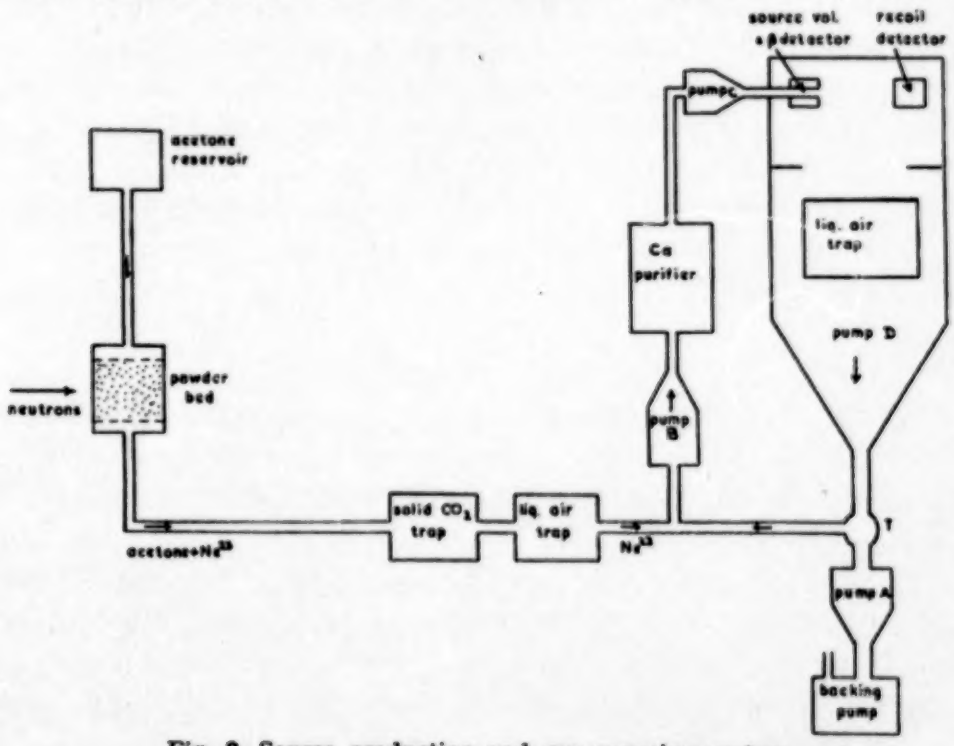


Fig. 3. Source production and gas pumping system.

powder is packed between porous sintered bronze plates. The $Ne^{23}$ is swept away by a stream of acetone vapour from a reservoir at a pressure of 5 cm Hg. This then passes through a pipe line 100 ft long to the site of the detecting equipment, where the bulk of the acetone is liquefied in a solid $CO_2$ cooled trap and the final traces frozen out in a liquid air trap. $Ne^{23}$ emerging from the acetone traps now enters an almost closed circuit vacuum system associated with the detectors. After being pumped through a purifier containing calcium metal at a temperature of 500° C, the gas is delivered into the source cavity by a specially designed pump C. Undecayed gas which is lost through the open mouth of the source volume is quickly collected by the large pump D and delivered into the next cycle. The three-way tap T bleeds off a fraction of the circulating gas, which is evacuated to the atmosphere. The continuous bleeding is necessary to prevent accumulation of impurities not held by the calcium. During a normal run the bleeding was adjusted to maintain a pressure of $10^{-3}$ mm Hg at the rear of the source volume, when the pressure in the detector chamber was $6 \times 10^{-7}$ mm Hg. Under these conditions the enhancement of useful source strength due to recirculation was about 160 : 1. The system delivered $10^6$ atoms of $Ne^{23}$ per sec into the recoil apparatus, giving a counting rate in the $\beta$-particle detector of 500 per sec.

To test the radiochemical purity of the $Ne^{23}$, the sodium iodide detector was replaced by one with a plastic phosphor containing a closed cavity into which the gas was fed by pump C. In lifetime and $\beta$-energy measurements, no evidence was found for the presence of any contaminating activity. A single half life of $39 \pm 1$ sec was observed in a decay curve taken over an interval of 130 sec. The pulse height distribution was consistent with the summed spectra with energies of 4.39 MeV and 3.95 MeV obtained by Penning and Schmidt [13]). The observed end point energy was $4.50 \pm 0.18$ MeV. The $\gamma$-ray spectrum, measured with a separate sodium iodide scintillation counter showed a prominent line at $0.44 \pm 0.01$ MeV, attributable to de-excitation of the first excited level of $Na^{23}$.

### 3.3. ELECTRONIC AND RECORDING EQUIPMENT

For each "event", both the amplitude of the $\beta$-pulse and the interval between the $\beta$ and recoil pulses are recorded photographically from a cathode ray tube. A delay to pulse height converter operated by fast signals from the detectors produces an X-deflection proportional to the recoil flight time. The $\beta$-pulse height is displayed as a Y-deflection. The beam is normally biassed off and the recording film continuously exposed. When a $\beta$-pulse is followed within 5 $\mu$sec by a recoil pulse, the resulting deflections are held constant for 30 $\mu$sec while the beam is switched on by the output from a coincidence unit, enabling the datum to be recorded as a spot on the film.

This equipment was calibrated with the aid of a double pulse generator whose output signals were made to simulate precisely those from the $\beta$ and recoil detectors. The generator time scale was itself calibrated by visual comparison with a synchronized 5 Mc/sec crystal oscillator on an oscillograph. The simulated $\beta$-pulse amplitude was calibrated against photopeaks produced by irradiating the $\beta$-detector with $\gamma$-rays of known energy. By injecting pulses from the generator into the electronic and recording equipment, a matrix of spots was produced on the recording film from which a grid could be drawn up for use in analysing the experimental spot distribution. In this calibration the only residual uncertainties in the recoil time of flight scale arise from different transit times in the two photomultipliers and ion transit times in the recoil detector. The former were eliminated by adjusting dynode potentials to give simultaneous output pulses when both photomultipliers were looking at the same piece of phosphor. The ion transit times were calculated.

The time-of-flight calibration points obtained before and after each experimental run were found to be reproducible to $\pm 0.02$ $\mu$sec. This is only 1.7 % of the time-of-flight of the fastest recoils and errors from this cause will be negligible compared with those arising from the 10 % uncertaintity in length of the flight path.

## 4. Experimental Data

### 4.1. INTEGRAL RECOIL ENERGY SPECTRUM

This was measured primarily to confirm that the upper limit of recoil energies was consistent with the known decay energy and mass of $Ne^{23}$. An electrostatic retarding field between grids $G_1$ and $G_2$ was applied to recoils entering the detector and the counting rate coincident with $\beta$-particles (resolving time 5 $\mu$sec) measured as a function of the potential of grid $G_2$. The maximum energy of recoils was found in this way to be $525 \pm 25$ eV, consistent with a value of 556 eV calculated from the $\beta$-decay energy of 4.39 MeV.

### 4.2. ELECTRON ENERGY AND RECOIL FLIGHT TIME DISTRIBUTION

This distribution was measured with grids $G_1$ and $G_2$ at earth potential. The pressure at the rear of the source cavity was $10^{-3}$ mm Hg, and should fall approximately linearly to less than $10^{-6}$ mm at the mouth 1 cm away. Photographic records taken by the method described in § 3.3 were analysed into time-of-flight distributions within bands of $\beta$-energy 1 $mc^2$ wide. Typical histograms are shown in figs. 4 and 5.

It is important to ensure that the recoil momentum spectrum is not appreciably distorted by scattering either from the walls of the source volume or by gas molecules. Precautions to eliminate the effects of wall

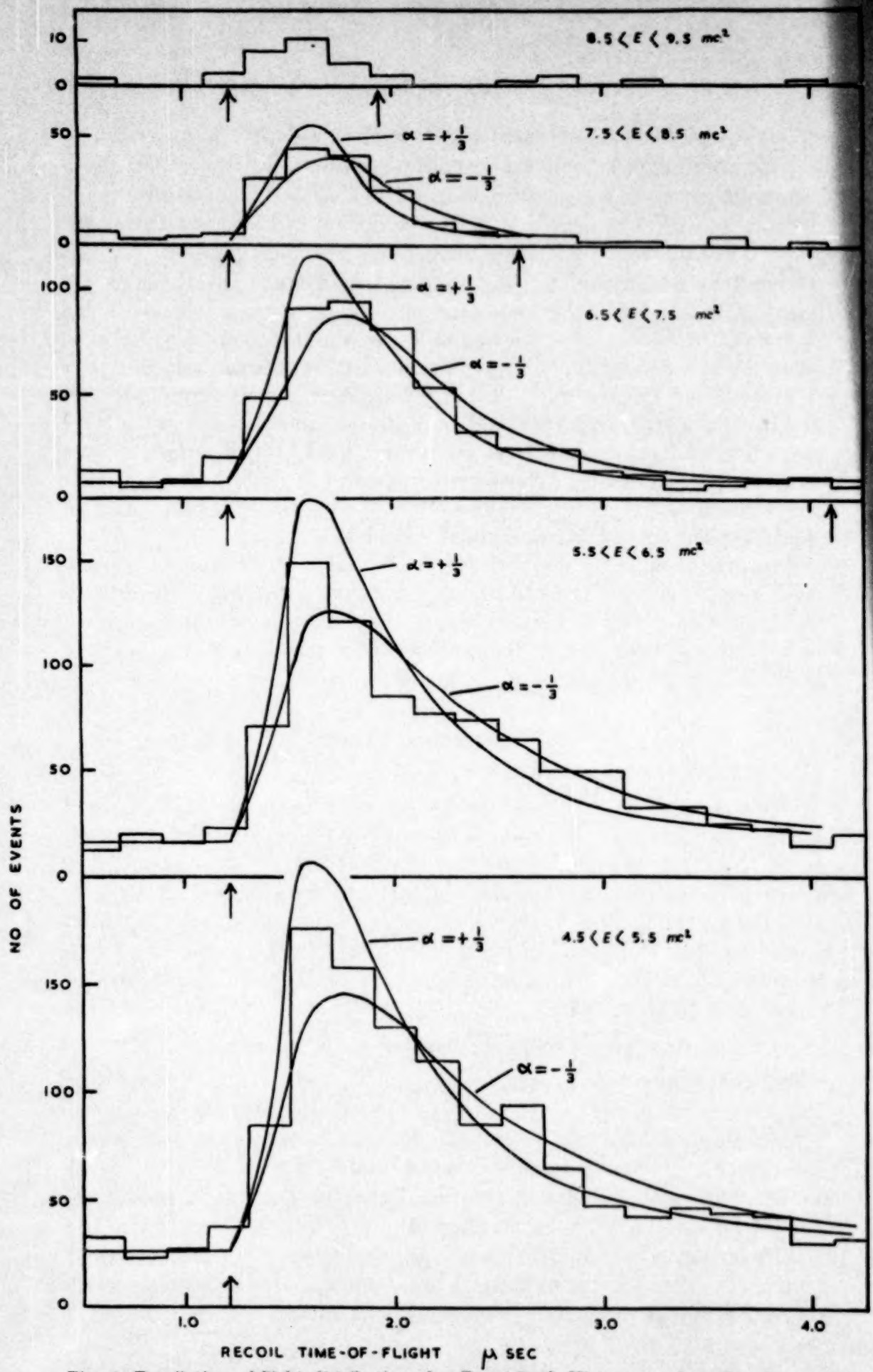


Fig. 4. Recoil time-of-flight distributions for $E > 4.5mc^2$. Histograms show the observed distributions taken at source volume pressure of $10^{-3}$ mm Hg. Smooth curves show the

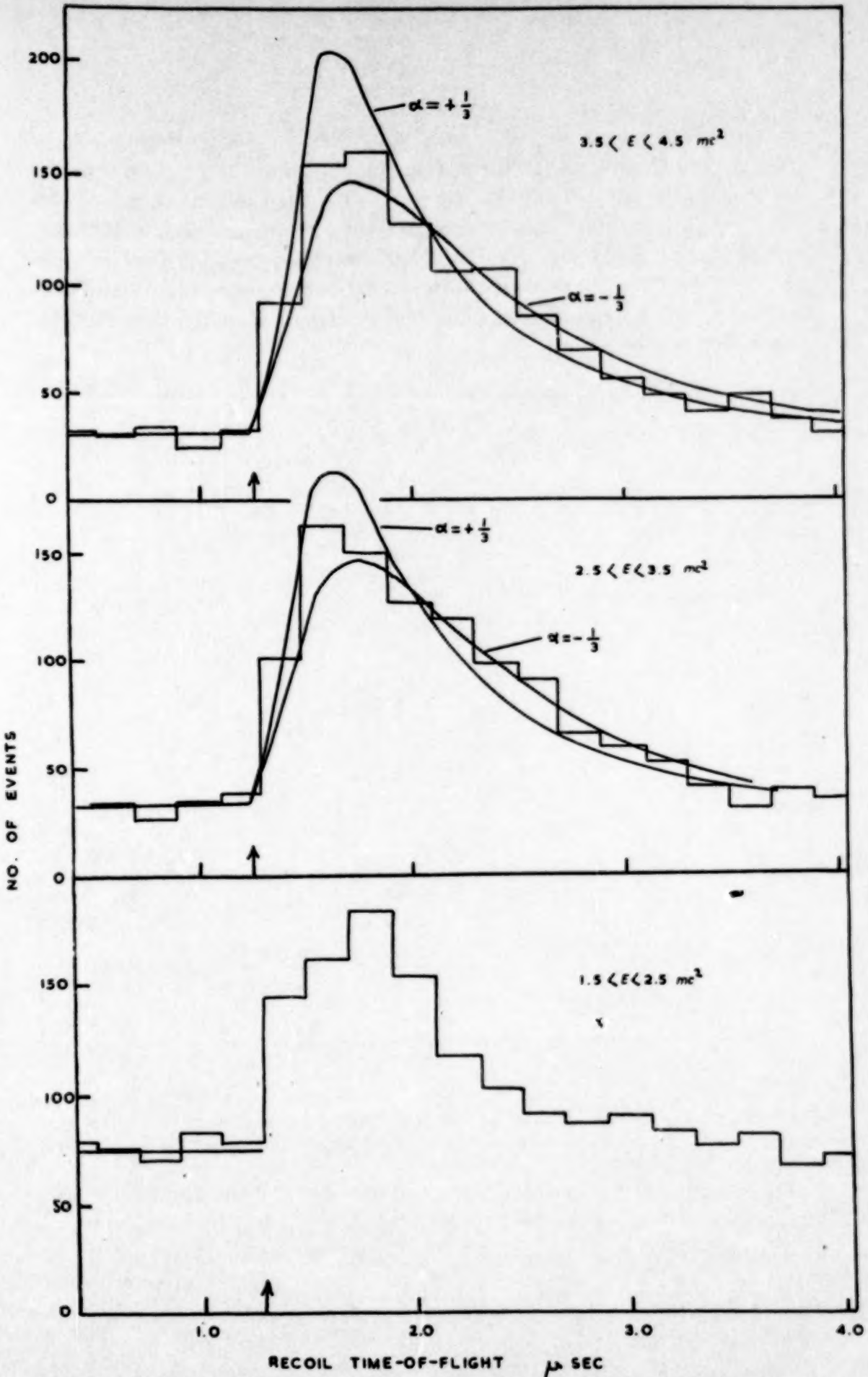


Fig. 5. Recoil time-of-flight distributions for $1.5\ mc^2 < E < 4.5mc^2$. Histograms show the observed distributions taken at source volume pressure of $10^{-3}$ mm Hg. Smooth curves show the predicted distributions for $\alpha = +1/3$ and $-1/3$, together with expected background. Only the expected background is shown for $1.5mc^2 < E < 2.5mc^2$.

scattering have been described in § 3.1. Possible gas scattering will be restricted to the interior of the source volume, since the pressure over the external flight path is only $6\times10^{-7}$ mm. To test the importance of this effect, the distribution was remeasured with a pressure of $2 \times 10^{-3}$ mm at the rear of the source volume. Recoil spectra integrated over energies greater than 2.5 $mc^2$ are shown in fig. 6 for both pressures. No significant difference was found between these two spectra and we conclude that gas scattering can be neglected.

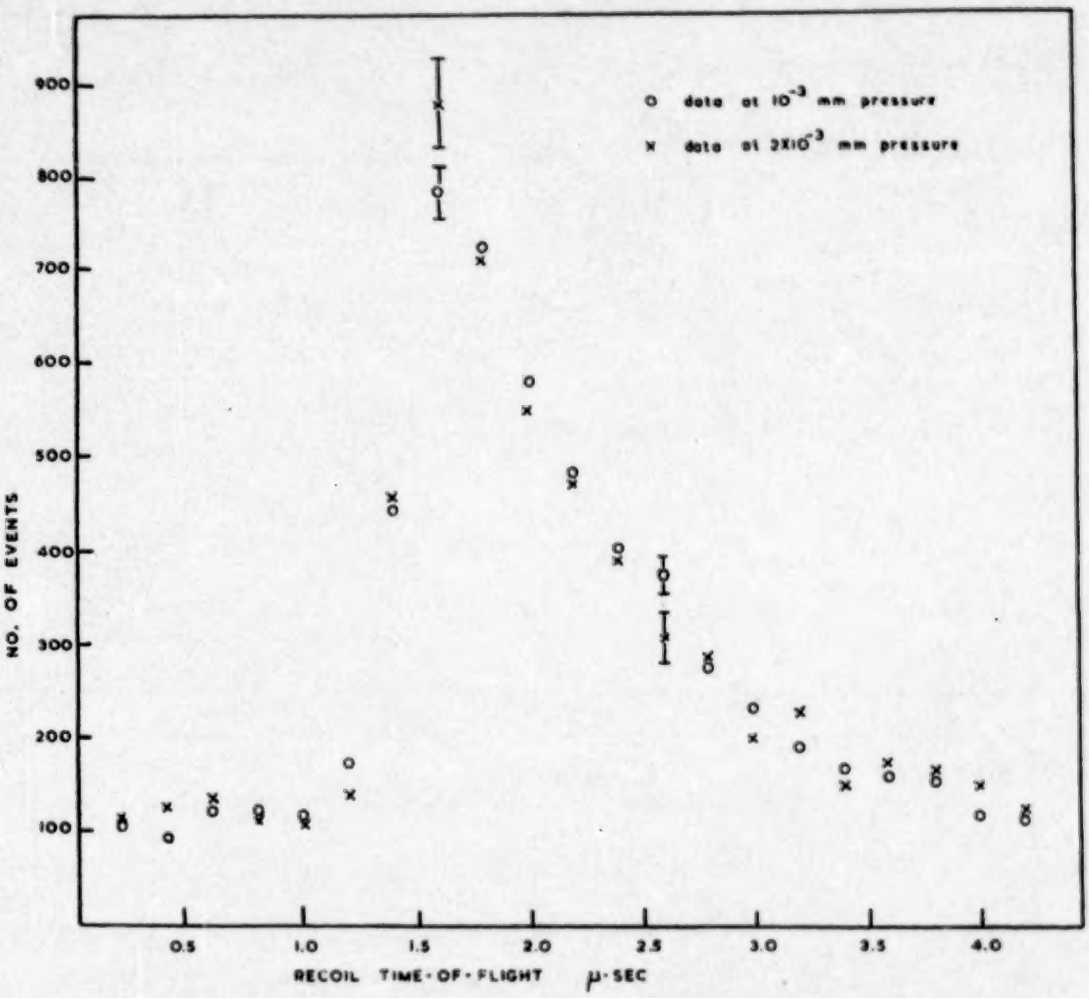


Fig. 6. Recoil time-of-flight distributions for $E < 2.5mc^2$ taken at source volume pressures of $10^{-3}$ and $2 \times 10^{-3}$ mm Hg. Data at $2 \times 10^{-3}$ mm are normalised to those at $10^{-3}$ mm.

The recoil momentum distribution $r$ at any given $\beta$-energy is restricted by conservation of momentum to the range $p+q \geqq r \geqq |p-q|$ if no $\gamma$-ray is emitted. When a $\gamma$-ray of momentum $g$ is also emitted, the permitted range is $p+q+g \geqq r \geqq ||p-q|-g|$. The corresponding limits on recoil time-of--flight are shown by arrows in figs. 4 and 5 when these lie within the observed range. We see that the observed distributions of events above

a flat background do indeed lie within the permitted ranges. The background itself is attributed to accidental coincidences and agrees in strength with an estimate from detector counting rates. As a test for effects of scattering, the recoil distributions at higher $\beta$-energies suggest that this is not serious to within the available statistics. Unfortunately, at intermediate $\beta$-energies

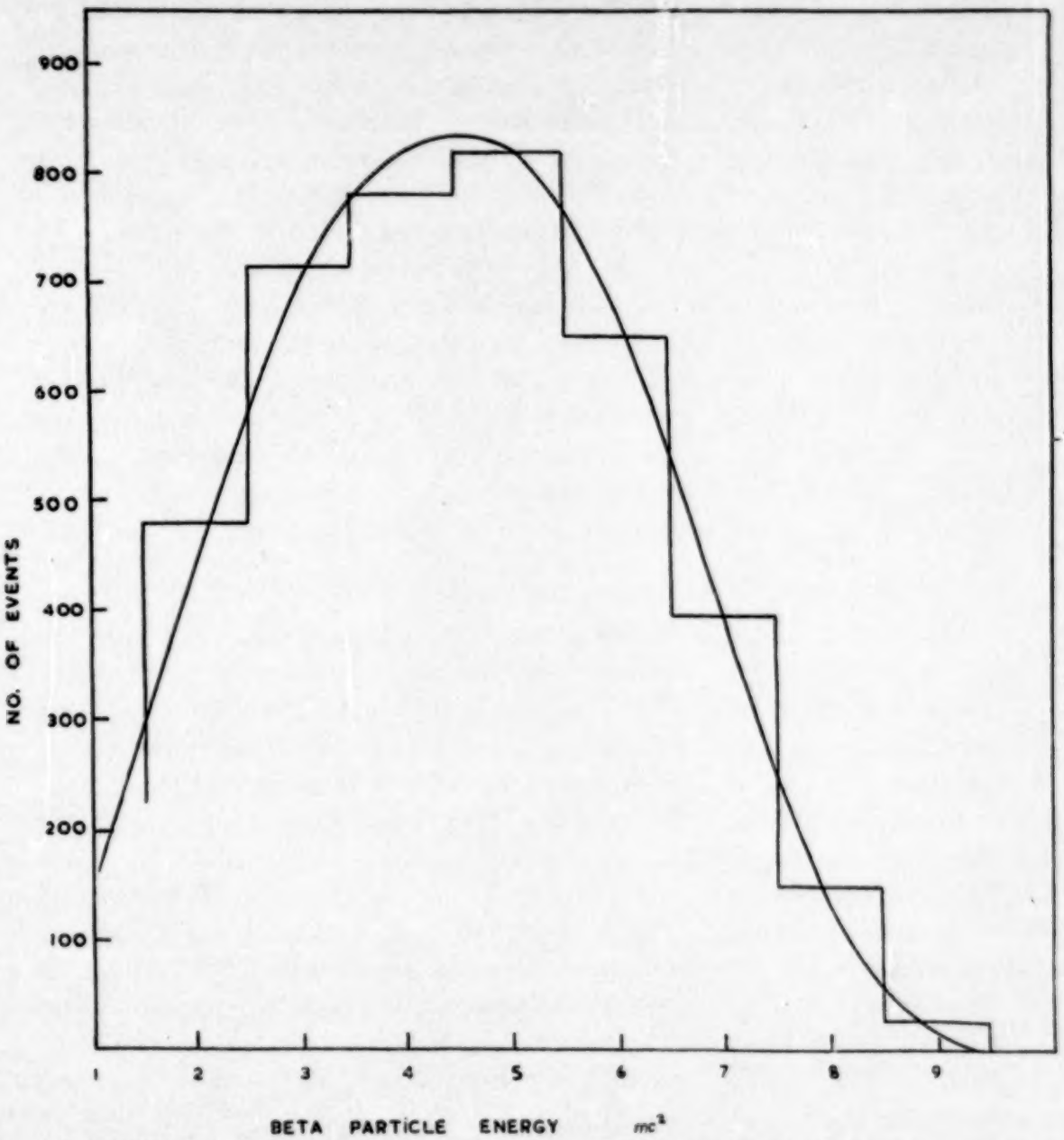


Fig. 7. Histogram showing $\beta$-spectrum after subtraction of background and integration over recoil flight times up to 4.5 $\mu$sec. The continuous curve shows the predicted spectrum.

where the statistics are better, the long tail of the time-of-flight distribution precludes a direct test of this kind.

Distortion of the observed recoil spectrum might occur through a possible dependence of the recoil ion charge on its momentum if the detector

sensitivity varies with charge. However, this is unlikely to be significant since the maximum recoil velocity is only of the order of 1/50 of the velocities of the atomic electrons in $Na^+$.

The $\beta$-energy spectrum, after subtraction of background and integration over recoil flight times up to 4.5 $\mu$sec is shown by the histogram in fig. 7. The continuous curve shows the summed theoretical Fermi spectra for the 3.95 and 4.39 MeV transitions. These have been corrected for the emission of undetected bremsstrahlung photons in the sodium iodide, for stopping of 0.44 MeV $\gamma$-rays following the 3.95 MeV transition, and for the low recoil momentum cut-off imposed by the maximum accepted flight-time of 4.5 $\mu$sec. The latter correction is slightly sensitive to the value of the angular correlation coefficient $\alpha$: this was taken to be $-0.05$. In the region of forbidden flight times, the pulse height spectrum from the $\beta$-particle detector was very different, showing a marked excess of pulses below 0.5 MeV in energy, and closely resembled the "singles" spectrum. The large number of low energy pulses is probably due to stopping of 0.44 MeV $\gamma$-rays from disintegrations occurring in the detector vacuum chamber. The different $\beta$-spectrum shapes within and outside the permitted region suggests that the background arises from accidental coincidences whereas the excess within the permitted region is due to the detection of genuine events.

## 5. Evaluation of the Angular Correlation Coefficient

In the evaluation of $\alpha$, the decay energies and log $ft$ values were taken to be those found by Penning and Schmidt [13]). These are 4.39 MeV (log $ft = 5.25$) and 3.95 MeV (log $ft = 5.38$). In addition the Fierz coefficient $b$ was assumed to be zero. The theoretical expression (6) for the $(E, r)$ distribution was transformed into one of $\beta$-energy and recoil time-of-flight, $N(E, t)$, and the various instrumental effects folded in. In the distribution for the 3.95 MeV transition, an additional correction was made for recoil due to emission of the 0.44 MeV $\gamma$-ray photons. These were assumed to be emitted isotropically with respect to $\beta$-particles. Instrumental effects considered in the $\beta$-detector were emission of undetected bremsstrahlung photons and capture of $\gamma$-rays following the 3.95 MeV transition. Instrumental line width was neglected since this is small compared with the $\beta$-energy band width chosen. In the time-of-flight measurement, account was taken of the ion transit time in the recoil detector and uncertainty in length of flight path due to the distribution of activity within the source volume. Here it was assumed that the source strength fell linearly to zero at the mouth. A reduction in solid angle for escape of recoils from the rear of the source volume was also considered.

For each transition, the $(E, t)$ distribution can be expressed in the form

$$N(E, t) = A(E, t) + \alpha B(E, t).$$

The $A$ and $B$ are numerical functions of $E$ and $t$ and are, of course, different for the 4.39 and 3.95 MeV transitions. These were multiplied by factors inversely proportional to the appropriate $ft$ values and added, assuming $\alpha$ to be the same for both transitions. The resulting sum was then integrated over the same bands of $\beta$-energy as the observed distributions and normalised to the total number of observed events after subtraction of background. The theoretical distributions for $\alpha = +1/3$ and $\alpha = -1/3$ superimposed on the calculated background are shown by the smooth curves in figs. 4 and 5.

Values of $\alpha$ obtained from recoil spectra in the different bands of $\beta$-energy are listed in table 1.

TABLE 1

| $E/mc^2$ | $\alpha$ |
|---|---|
| 2.5 to 3.5 | $-0.04 \pm 0.13$ |
| 3.5 to 4.5 | $-0.11 \pm 0.11$ |
| 4.5 to 5.5 | $+0.03 \pm 0.11$ |
| 5.5 to 6.5 | $-0.14 \pm 0.12$ |
| 6.5 to 7.5 | $+0.02 \pm 0.16$ |

As a test of goodness of fit for the overall $(E, t)$ distribution a $\chi^2$ fit was made to the recoil distributions for all $\beta$-energy bands with $E > 2.5\ mc^2$ simultaneously. This gave a value

$$\alpha = -0.05 \pm 0.10.$$

For $\alpha = -0.05$ the probability that a random sample gives no better fit than the observed distribution is 35 %. The error limits correspond to a 10 % level.

Separate estimates of $\alpha$ for the two transitions could not be obtained because of inadequate statistics and the closeness of their end point energies.

## 6. The Beta Decay Interaction

For convenience in the following discussion we shall use $X$ to denote the ratio of axial vector to tensor coupling strengths in the G.T. interaction, where

$$X^2 = \frac{|C_A|^2 + |C'_A|^2}{|C_T|^2 + |C'_T|^2}.$$

If we assume that both the major transitions from $Ne^{23}$ are pure G.T., then the value $\alpha = -0.05 \pm 0.10$ implies that $0.86 \leqq X \leqq 1.62$. This appears to be in serious disagreement with the result $-0.5 \leqq X \leqq +0.3$ quoted by Rustad and Ruby [7]) for another pure G.T. emitter, $He^6$. The $He^6$ result, however, was evaluated on the basis of the old parity conserving beta decay theory in which an admixture of T and A interactions necessarily

implies the existence of a Fierz interference term. If the Fierz term is assumed to be zero, as required by experiments on allowed spectrum shapes and K-capture to positon emission ratios, the $He^6$ results imply that $X < 0.6$ and $X < 0.4$ for the two values of $\alpha$ quoted.

Though the discrepancy is reduced, it can hardly be ignored. If we force an agreement between the $He^6$ and $Ne^{23}$ data by supposing that the almost certainly pure G.T. ground state transition from $Ne^{23}$ is dominated by the T interaction, then we find that for the 3.95 MeV transition of $Ne^{23}$,

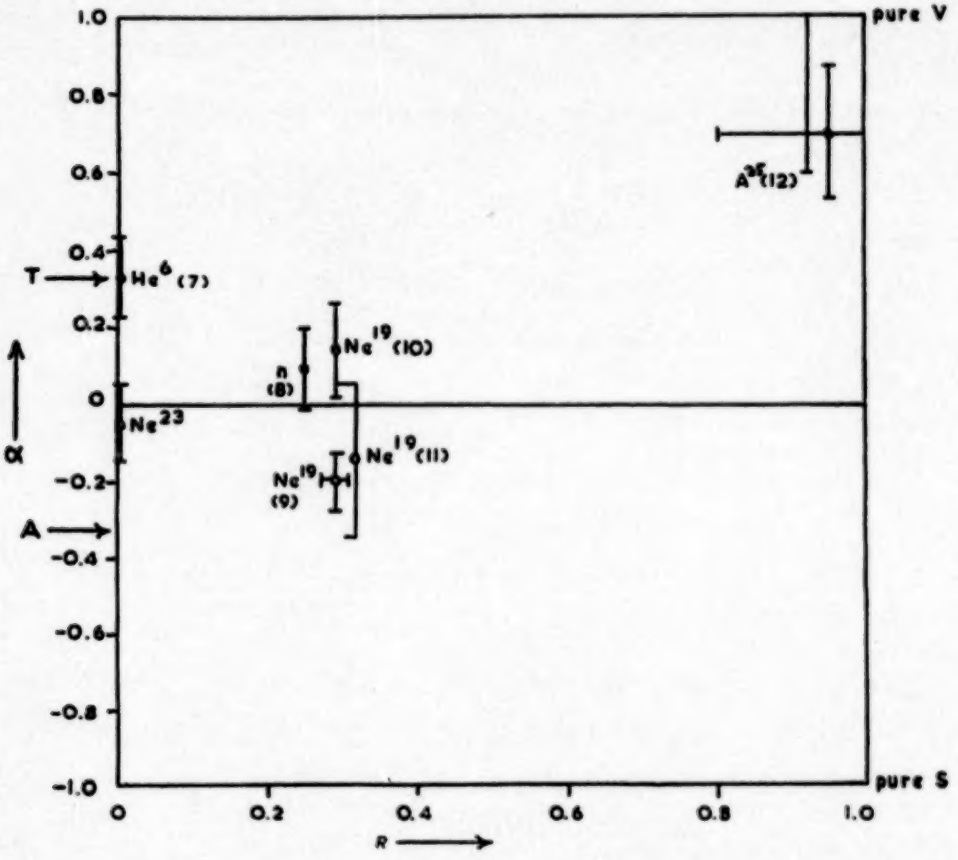


Fig. 8. Plot of $\alpha$ against $R$ for existing electron-neutrino correlation results. Figures in brackets indicate the reference.

$\alpha = -0.85 \pm 0.3$. This would require the latter transition to be substantially a Fermi one, dominated by an S interaction. This is in contradiction both with Elliott's [14]) conclusions on the effective magnitude of the Fermi matrix element and with evidence from decay of $A^{35}$ that the Fermi interaction is mainly V [12]).

Scott [16]) has pointed out that the expression (3) for a mixed Fermi – G.T. decay may be rewritten in the form

$$\alpha = \alpha_F R + \alpha_{GT}(1-R)$$

where $\alpha_F$ and $\alpha_{GT}$ are the angular correlation coefficients for pure Fermi and G.T. interactions respectively and $R = C_F^2|M_F|^2/[C_F^2|M_F|^2+C_{GT}^2|M_{GT}|^2]$. If $\alpha$ is plotted against $R$ for a variety of different allowed decays, all points should lie on a straight line. The intercepts $\alpha_{GT}$ and $\alpha_F$ at $R = 0$ and 1 respectively determine the combination of invariants in the G.T. and Fermi interactions. Angular correlation data measured up to date are presented in this way in fig. 8. A straight line through the existing points is clearly out of the question. The diagram is, however, highly suggestive in the direction of a (V, T, A) or (V, A) combination.

I am indebted to the United Kingdom Atomic Energy Authority for a research fellowship at Harwell, during the tenure of which this work was performed. My thanks are also due to Professors N.F. Mott and O. R. Frisch for allowing me to use the Cavendish cyclotron at Cambridge over long periods and to Mr. E. G. T. Morley for operating the machine. Many persons have contributed to the work, but especially I should like to thank Professor O. R. Frisch and Dr. P. E. Cavanagh for their interest, advice and criticism and Dr. C. W. McCutchen for his help and stimulating company during long night runs. The sensitised Be-Cu for the recoil detector was prepared by Mr. R. B. Owen. Finally I must express a debt of gratitude to my wife who performed much of the heavy computation involved in the analysis of results.

## References

1) R. Sherr and R. H. Miller, Phys. Rev. **93** (1954) 1076
2) R. W. P. Drever, A. Moljk and J. Scobie, Phil. Mag. **1** (1956) 942
3) A. V. Pohm, R. C. Waddell and E. N. Jensen, Phys. Rev. **101** (1956) 1315
4) J. Scobie and G. M. Lewis, Phil. Mag. **2** (1957) 1089
5) J. D. Jackson, S. B. Trieman and H. W. Wyld, Nuclear Physics **4** (1957) 206
6) T. D. Lee and C. N. Yang, Phys. Rev. **105** (1957) 1671
7) B. M. Rustad and S. L. Ruby, Phys. Rev. **97** (1955) 991
8) J. M. Robson, Phys. Rev. **100** (1955) 933
9) D. R. Maxson, J. S. Allen and W. K. Jentschke, Phys. Rev. **97** (1955) 109
10) M. L. Good and E. J. Lauer, Phys. Rev. **105** (1957) 213
11) W. P. Alford and D. R. Hamilton, Phys. Rev. **105** (1957) 673
12) W. B. Herrmannsfeldt, D. R. Maxson, P. Stähelin and J. S. Allen, Phys. Rev. **107** (1957) 641
13) J. R. Penning and F. H. Schmidt, Phys. Rev. **105** (1957) 647
14) J. P. Elliott, private communication
15) O. Kofoed-Hansen, Mat. Fys. Medd. Dan. Vid. Selsk. **28** (1954) no. 9
16) J. M. C. Scott, private communication

*Nuclear Physics* 6 (1958) 50—54; © *North-Holland Publishing Co., Amsterdam*
Not to be reproduced by photoprint or microfilm without written permission from the publisher

# ZUR STREUUNG VON K⁻-MESONEN AN KOMPLEXEN KERNEN

P. MITTELSTAEDT
*Max-Planck-Institut für Physik, Göttingen*

Eingegangen am 11. November 1957

**Abstract:** The investigations of the K⁻-meson-nucleus scattering by means of the optical model have shown that the imaginary part of the optical potential is very large while the real part almost vanishes. Here it is shown that the vanishing of the real part of the optical potential results from the strong absorption of K⁻-mesons in the K⁻-nucleon scattering process.

## 1. Einleitung

Die Streuung von K⁻-Mesonen an komplexen Kernen wurde experimentell in dem Energiebereich von 40 bis 140 MeV untersucht [1, 2]). Die gemessene Winkelverteiling der elastischen Streuung und die Energieverteilung der inelastischen Streuung lässt sich phänomenologisch in guter Näherung durch ein optisches Kernmodell beschreiben [3]). Neben dem bekannten Coulombpotential des Kernes tritt dabei noch ein komplexes Potential $V = V_1 + iV_2$ auf, dessen Parameterwerte durch Anpassung an die oben genannten Experimente gewonnen wurden. Es ergab sich bei einer Energie von 60 MeV: $V_1 = 0$ MeV, $V_2 = -10 \pm 2$ MeV [3]). Auch die bei 100 MeV durchgeführten Experimente scheinen zu denselben Daten für $V_1$ und $V_2$ zu führen [2, 3]). Die Ortsabhängigkeit der Potentiale wurde in diesen Untersuchungen als kastenförmig vorausgesetzt.

Vergleicht man diese Werte mit den Parametern, die man etwa bei der K⁺-Mesonenstreuung für die optischen Potentiale erhalten hat ($V_1 = +25$ MeV, $V_2 = -5.6$ MeV) [4]), so fällt neben der stärkeren Absorption bei K⁻-Mesonen (kleinerer $V_2$-Wert) insbesondere das verschwindende Realpotential $V_1$ auf. Auch bei der Untersuchung der Nukleonen-Streuung an Kernen sind bisher keine verschwindenden Realpotentiale gefunden worden.

Dieses zunächst unverständliche Verhalten der K⁻-Mesonen bei der Kernstreuung lässt sich jedoch in einfacher Weise aus der K⁻-Meson-Nukleon-Streuung verständlich machen. Im Gegensatz zu K⁺-Mesonen gibt es bei den K⁻-Mesonen neben der elastischen Streuung

$$K^- + P \rightarrow K^- + P \qquad \text{(I)}$$

und dem Ladungsaustausch

$$K^- + P \rightarrow K^0 + N \qquad \text{(II)}$$

noch die Umwandlung in Hyperonen

$$K^- + P \rightarrow Y^{\pm}_{0} + \pi^{\mp}_{0} \qquad \text{(III)}$$

wobei der durch die Reaktionen (II) und (III) bewirkte Reaktionsquerschnitt $\sigma_r$ etwa ebensoviel zum totalen Querschnitt $\sigma_t$ ($\sigma_t \approx 100$ mb bei $E = 60$ MeV) beiträgt wie der elastische Querschnitt $\sigma_e$ ($\sigma_e \approx 50$mb bei $E = 60$ MeV) [1]). Für die K⁻-Neutron-Streuung sind die Zahlenwerte für $\sigma_e$ und $\sigma_r$ nach den bisher vorliegenden Experimenten etwa dieselben wie bei der K⁻-Proton-Streuung [1, 5]).

Es soll im Folgenden an einem einfachen Modell für die K⁻-Nukleon-Wechselwirkung gezeigt werden, daß der verhältnismäßig grosse Reaktionsquerschnitt $\sigma_r$ der K⁻-Nukleon-Streuung die Ursache für das Verschwinden des Realteils des optischen Potentials ist.

## 2. K⁻-Meson-Nukleon-Streuung

Die Streuung eines K⁻-Mesons an einem Nukleon soll im Folgenden in der s-Streuung behandelt werden. Dies wird möglich sein, wenn man etwa annimmt, daß sich der Streuprozess im Schwerpunktsystem durch die Streuung an einer Kugel beschreiben lässt, außerhalb deren keinerlei Wechselwirkung zwischen den beiden Teilchen mehr stattfindet, und deren Radius im Verhältnis zur Wellenlänge der Teilchen so klein ist, daß die p-Streuung keine wesentliche Rolle mehr spielt. Über die Wechselwirkung im Inneren der Kugel sollen keine Annahmen gemacht werden.

Wir untersuchen hier die Streuung bei einer Energie $E = 60$ MeV im Laborsystem für die K⁻-Mesonen, da für diesen Energiewert die genauesten Querschnittsmessungen sowohl für den Einzelstoß als auch für die Streuung an komplexen Kernen vorliegen. Ist $m_1$ die Masse des K⁻-Mesons, $m_2$ die Masse des Nukleons, so ist im Schwerpunktsystem die Wellenlänge

$$\lambda\!\!\!^{-} = \frac{1}{k} = \frac{m_1 + m_2}{m_2} \frac{1}{\sqrt{2 m_1 E}} = 1.225 \times 10^{-13} \text{ cm}.$$

Bei der Wahl des Radius $R$ des Wechselwirkungsgebietes gehen wir von der Tatsache aus, daß die Wechselwirkung zwischen einem K⁻-Meson und einem Nukleon vermutlich durch Hyperonen vermittelt wird [6]). Es ist daher naheliegend, den Bereich, innerhalb dessen Wechselwirkung besteht, durch die De Broglie-Wellenlänge eines Nukleons, $\lambda\!\!\!^{-}_N = 0.21 \times 10^{-13}$ cm abzugrenzen. Bei der hier untersuchten Energie ist dann $x = kR = 0.169$. Dies bedeutet, daß bei der Berechnung der Wirkungsquerschnitte hier die s-Streuung allein ausreichen wird, da die p-Streuung nur etwa 1 % der s-Streuung ausmacht. Selbst bei einer Vergrösserung des Radius $R$ auf $R = 0.4 \times 10^{-13}$ cm würde der durch Vernachlässigung der p-Streuung

entstandene Fehler nur etwa 10 % ausmachen. In Hinblick auf die Ungenauigkeit der Experimente, die dieser Arbeit zugrundeliegen, ist ein Fehler von 10 % in den Querschnittsberechnungen jedoch nicht wesentlich. Im übrigen werden die im folgenden hergeleiteten Ergebnisse nicht von dem Radius $R$ abhängig sein. Nur die Tatsache, daß die s-Streuung eine gute Näherung ist, ist natürlich von der Größe von $R$ abhängig.

Zur Berechnung des totalen Querschnittes $\sigma_t$ und des Reaktionsquerschnittes $\sigma_r$ benötigt man außer der Größe $\lambda\!\!\!^{-}$ noch das Diagonalelement $\eta$ des $S$-Matrix. In der hier diskutierten s-Streuung ist dann

$$\sigma_t = 2\pi\lambda\!\!\!^{-2}(1-\mathrm{Re}\,\eta), \tag{1}$$

$$\sigma_r = \pi\lambda\!\!\!^{-2}[1-(\mathrm{Re}\,\eta)^2-(\mathrm{Im}\,\eta)^2]. \tag{2}$$

Nach den Experimenten ist nun

$$\sigma_t \approx 2\pi\lambda\!\!\!^{-2} = 96\ \mathrm{mb}. \tag{3}$$

Aus dieser Tatsache folgt wegen (1), daß

$$\mathrm{Re}\,\eta = 0 \tag{3a}$$

ist. Weiterhin gilt experimentell

$$\sigma_r \approx \pi\lambda\!\!\!^{-2} = 48\ \mathrm{mb} \tag{4}$$

woraus wegen (2) und (3a) folgt

$$\mathrm{Im}\,\eta = 0. \tag{4a}$$

Um den physikalischen Inhalt der so gewonnenen Glgn. (3a) und (4a) etwas zu verdeutlichen, ist es nützlich, die logarithmische Ableitung $f$ der Wellenfunktion an der Stelle $r = R$ genauer zu untersuchen. Der Zusammenhang zwischen $\eta$ und $f$ ist durch

$$\eta = \mathrm{e}^{-2ikR}\frac{f+ikR}{f-ikR} \tag{5}$$

gegeben. Da nun wegen (3a) und (4a) $\eta = 0$ ist, so folgt aus (5), daß

$$f = -ikR \tag{6}$$

rein imaginär ist. Diese in der Kernphysik als Kontinuumtheorie bezeichnete [7]) Beziehung (6) besagt, daß sämtliche in das Gebiet $r \leqq R$ eindringenden Teilchen zum Reaktionsquerschnitt beitragen, im vorliegenden Falle also zu Ladungsaustausch und Hyperonenerzeugung führen. Schreibt man etwas allgemeiner $f = -ik'R$, und meint mit $k'$ die Wellenzahl des eindringenden Teilchens im Gebiet $r \leqq R$, jedenfalls in der Nähe von $r = R$, so besagt (6), daß $k = k'$ ist, die Wellenzahl im Inneren und Äußeren des Wechselwirkungsgebietes also dieselbe ist.

## 3. Die optischen Potentiale

Für die weiteren Untersuchungen ist es nützlich, die Streuamplitude $F(\vartheta)$ einzuführen, die jedoch im Falle der hier untersuchten s-Streuung nicht von $\vartheta$ abhängig ist. Es ist

$$F(\vartheta) = \frac{1}{2k} \operatorname{Im} \eta + \frac{i}{2k} (1 - \operatorname{Re} \eta). \tag{7}$$

Aus $F(\vartheta)$ berechnet sich der differentielle Streuquerschnitt durch

$$\frac{\mathrm{d}\sigma}{\mathrm{d}\Omega} = |F(\vartheta)|^2.$$

Das optische Potential eines komplexen Kernes steht nun einem sehr engen Zusammenhang mit der eben eingeführten Streuamplitude an der Stelle $\vartheta = 0$. Es ist [8])

$$V_1 + iV_2 = -\varrho \frac{2\pi\hbar^2}{\mu} F(0), \tag{8}$$

wobei $\varrho$ die Dichte der Nukleonen im Kern ist, und $\mu$ die reduzierte Masse von Nukleon und K⁻-Meson. Der hier besonders interessierende reelle Teil des Potentials $V_1$ ist dann wegen (7) und (8)

$$V_1 = -\varrho \frac{2\pi\hbar^2}{\mu} \frac{\operatorname{Im} \eta}{2k}. \tag{9}$$

Nun ist aber nach (4) der experimentelle Reaktionsquerschnitt

$$\sigma_r \approx \pi\lambda\!\!\!^{-2} = 48 \text{ mb}.$$

Da wegen (3) $\operatorname{Re} \eta = 0$ ist, so folgt, wie oben gezeigt wurden, aus (4) daß auch $\operatorname{Im} \eta = 0$ ist. Das bedeutet aber, daß nach (9) der Realteil $V_1$ des optischen Potentials verschwindet. Umgekehrt folgt aus dem Verschwinden von $V_1$, daß $\sigma_r = \pi\lambda\!\!\!^{-2}$ ist.

Diese Überlegungen zeigen also, daß bei s-Streuung unter der Voraussetzung, $\sigma_t = 2\pi\lambda\!\!\!^{-2}$ die Aussage, daß $\sigma_r = \pi\lambda\!\!\!^{-2}$ ist, und die Aussage, daß der reelle Teil des optischen Potentials verschwindet, einander äquivalent sind.

Damit ist gezeigt, daß das zunächst unverständliche Phänomen eines rein imaginären optischen Kernpotentials für die K⁻-Kernstreuung durch die besonders starke Absorption bei der K⁻-Nukleon-Streuung verständlich gemacht werden kann.

Herrn Prof. W. Heisenberg und Herrn Dr. G. Lüders danke ich für wertvolle Diskusionen.

## Literatur

1) W. Alles, N. N. Biswas, M. Ceccarelli und J. Crussard, Nuovo Cimento **6** (1957) 571
2) E. Lohrmann, M. Nikolić, M. Schneeberger, P. Waloschek und H. Winzeler, Preprint Bern (1957)
3) P. Mittelstaedt, Zeitschr. f. Naturf. (im Druck)
4) G. Costa und G. Patergnani, Nuovo Cimento (1957) 448;
P. Mittelstaedt, Nuovo Cimento **5** (1957) 1480
5) Goldhaber, International Conference on Mesons and recently discovered Particles (Venice, 1957)
6) M. Gell-Mann, Phys. Rev. **106** (1957) 1296
7) Blatt and Weisskopf, Theoretical Nuclear Physics (New York, 1952)
8) W. Brenig, Nuclear Physics **4** (1957) 363

*Nuclear Physics* **6** (1958) 55—61; © *North-Holland Publishing Co., Amsterdam*
Not to be reproduced by photoprint or microfilm without written permission from the publisher

# ANGULAR DISTRIBUTIONS OF ELASTICALLY AND INELASTICALLY SCATTERED DEUTERONS FROM NEON

I. J. VAN HEERDEN

*Nuclear Physics Division of the National Physical Research Laboratory, C.S.I.R.*
*Pretoria, South Africa*

Received 25 September 1957

**Abstract:** The elastic and inelastic differential scattering cross sections of deuterons from $Ne^{20}$ have been measured using nuclear emulsions. The angular distribution of the deuterons inelastically scattered from the 1.63 MeV level, has been compared with the predictions of the nuclear and electrical interaction theories of deuteron scattering.

## 1. Introduction

The first excited state of $Ne^{20}$ is at 1.63 MeV, and the log *ft* value of the $\beta$-radiation from $F^{20}$ shows that it has even parity [1, 2]). Empirically, the first excited states of even nuclei favour a spin of two [3]), and from the angular correlation of the $\alpha$- and $\gamma$-rays from the $Na^{23}$ (p, $\alpha\gamma$)$Ne^{20}$ reaction, Seed [4]) has in fact shown that this is the case for the 1.63 MeV level of $Ne^{20}$. However, from the angular distribution of inelastically scattered deuterons determined by Middleton and Tai [5]), it would appear to have a spin of 1 or 2, and odd parity. Their measurements on elastically and inelastically scattered deuterons from $Ne^{20}$ have therefore been repeated and extended to more angles, and are reported in this paper; in an attempt to resolve the above discrepancy, the (d, d') angular distribution has been compared with the nuclear and electrical interaction theories.

## 2. Experimental Procedure

The 'scattering camera' used has been described in detail by Burrows, Powell and Rotblat [6]). The chamber was filled with spectroscopic pure neon gas of normal isotopic composition at a pressure of 19.7 cm Hg, and exposed to the 8 MeV deuteron beam of the Liverpool cyclotron. Particles scattered over an angular range of 10° to 165° were detected in Ilford C2 emulsions, 100$\mu$ thick. The exposure was made as part of the collaboration between the Universities of Bristol and Liverpool.

The projected ranges of the scattered proton and deuteron tracks were determined at thirty-one angles between 10° and 155°. A total of 1000 to

3000 tracks contained in an area of about 0.1 cm² was measured at each angle; their true ranges were deduced by applying an overall correction corresponding to their angle of dip in the emulsion. The loss of energy suffered by the particles whilst traversing the gas was calculated from values of the stopping power of neon given by Brolley and Ribe [7]). All the particle

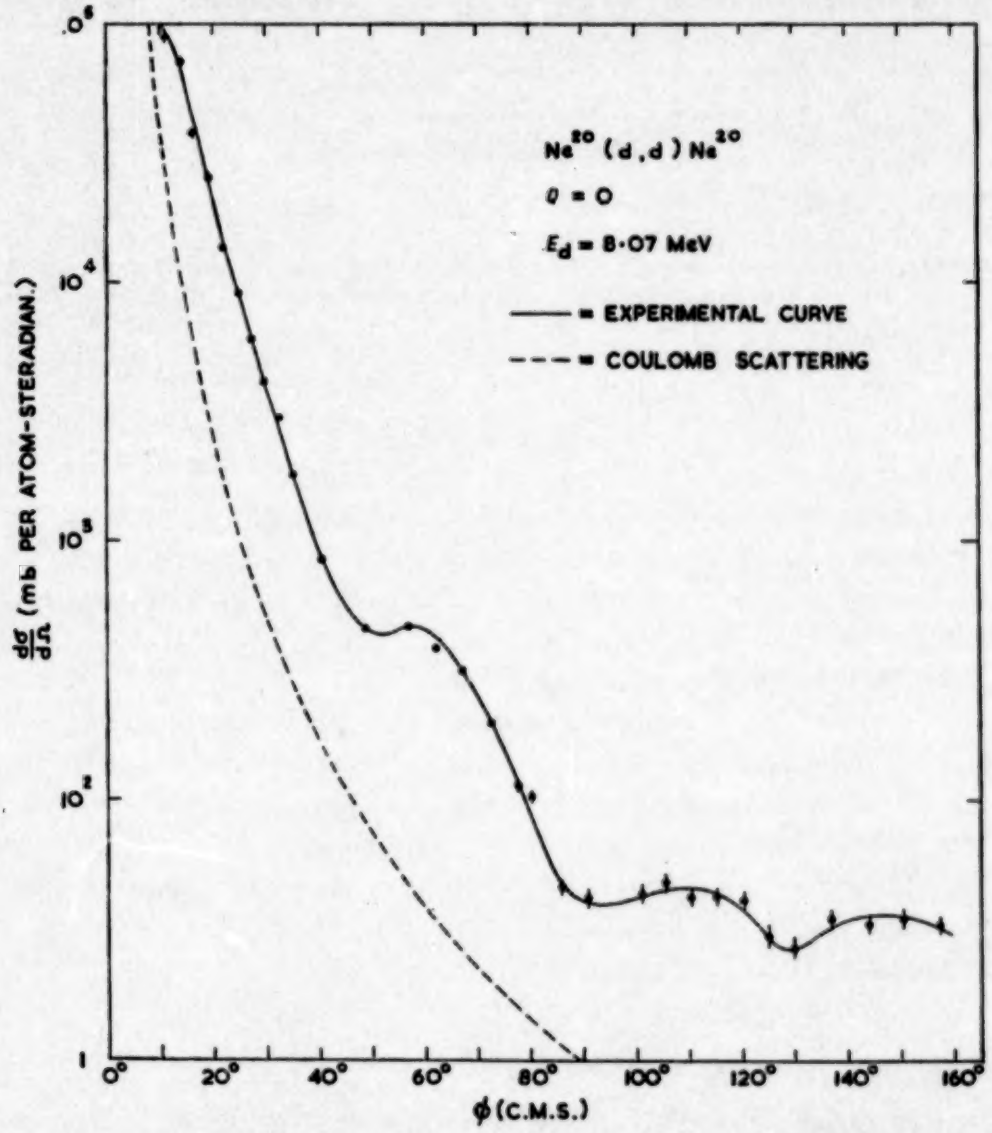


Fig. 1. Angular distribution of deuterons elastically scattered from $Ne^{20}$. The dashed line is the Coulomb scattering curve.

groups appearing in the histograms of measured ranges were assigned to known energy levels in $Ne^{20}$ [8]) and in $Ne^{21}$ which have recently been determined with great accuracy by Burrows, Green, Hinds and Middleton [9]), using a magnetic analyser. At most of the angles where measurements were made, those deuteron groups due to the ground state and 1.63 MeV level in $Ne^{20}$ were entirely resolved; otherwise, the number of tracks in a particular group

was determined by fitting a Gaussian distribution to the group. To obtain the number of deuterons elastically scattered from $Ne^{20}$, the contribution of 9 % $Ne^{22}$ had to be subtracted. This was done on the assumption that the deuteron scattering cross section was the same for both isotopes.

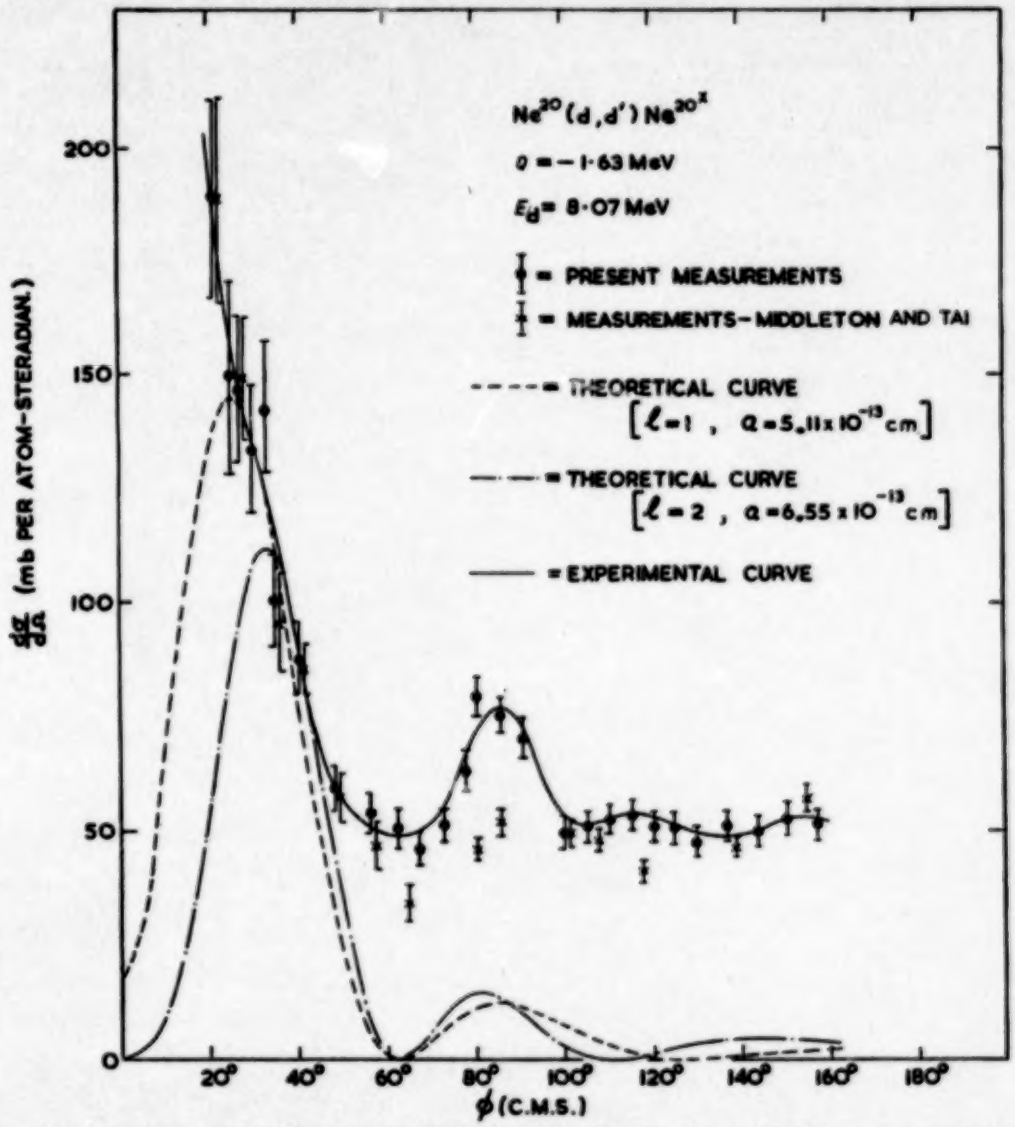


Fig. 2. Comparison of the $Ne^{20}$ (d, d')$Ne^{20*}$ angular distribution with the nuclear interaction theory.

From the ranges of the elastically scattered deuterons a value of $8.07 \pm 0.07$ MeV was obtained for the energy of the incident deuteron beam. In all these calculations the range-energy relation of Gibson, Prowse and Rotblat [10]) was used.

## 3. Results and Discussion

Fig. 1 shows the angular distribution in the centre-of-mass system for the elastic scattering of deuterons by $Ne^{20}$. The differential cross sections are given in millibarns per atom-steradian, and have been calculated using

the formula and calibration constant given by Burrows, Gibson and Rotblat[11]). The general behaviour of this distribution is very similar to that obtained by Middleton and Tai, but it would appear, however, that even at an angle of 10° the elastic scattering does not agree with pure Coulomb scattering. In fig. 2 the angular distribution of deuterons inelastically scattered from

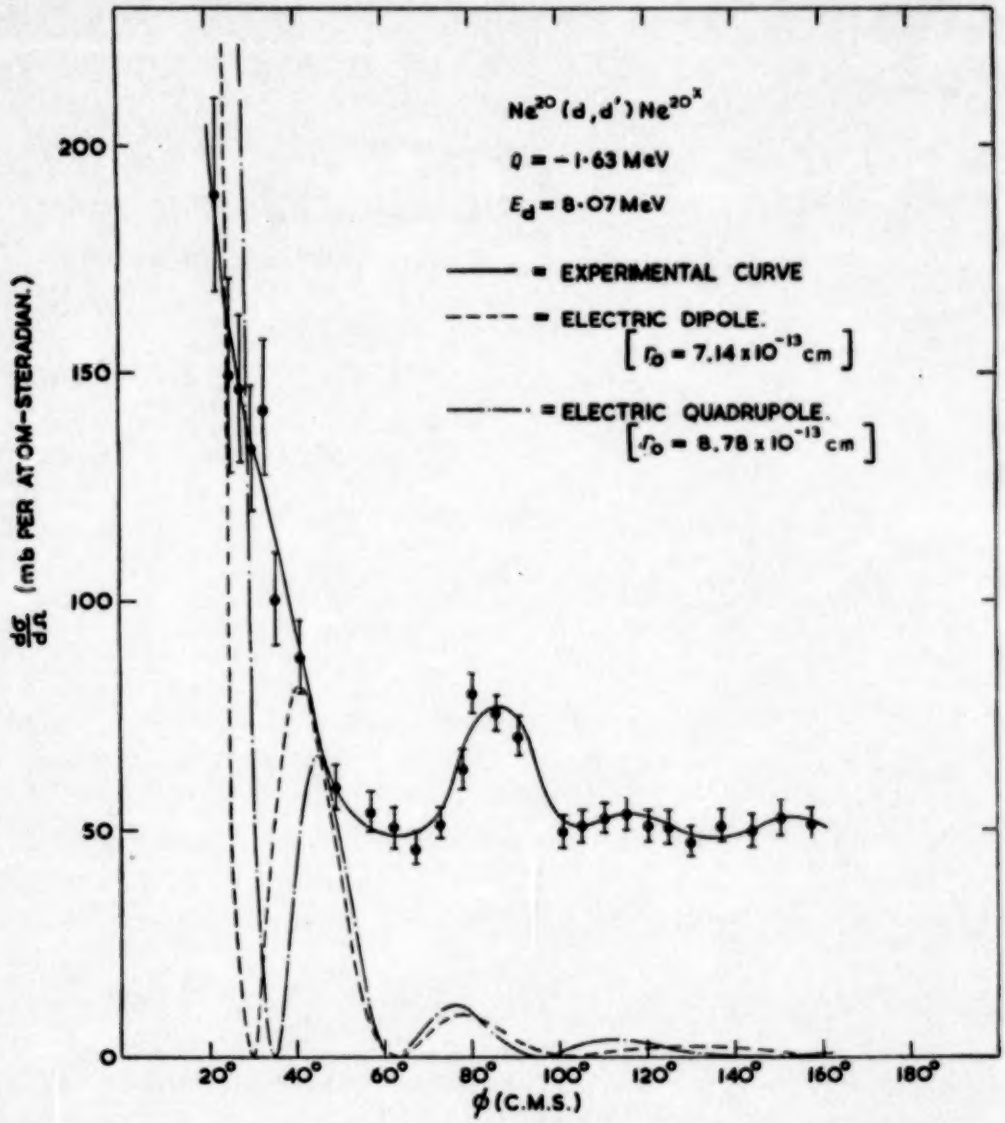


Fig. 3. Comparison of the $Ne^{20}$ (d, d')$Ne^{20*}$ angular distribution with the electrical interaction theory.

the 1.63 MeV level of $Ne^{20}$ is compared with the nuclear interaction theory of Huby and Newns [12]), and in fig. 3 with the electrical interaction theory of Mullin and Guth [13]). The errors shown are of a statistical nature only. The differential cross sections obtained by Middleton and Tai are also shown in fig. 2, and although they are much lower than the present measurements at $\phi = 64.5°$, 80.5°, 86.0° and 118.0°, the positions of the maxima and

minima of the angular distribution are nearly the same for the two sets of data.

The nuclear interaction theory is very similar to the stripping theory, and assumes that the neutron is the only constituent of the deuteron taking part in the interaction with the nucleus, the proton remaining outside the range of the nuclear forces. During the interaction the neutron excites the nucleus, and then re-combines with the proton, the deuteron thus being inelastically scattered. The differential cross section is derived in Born approximation and given by

$$\frac{\mathrm{d}\sigma}{\mathrm{d}\Omega}(\phi) = \sum_{l=0}^{\infty} \left\{ |A_l| \left[ \frac{4\alpha}{k} \tan^{-1} \frac{k}{4\alpha} \right] j_l(ka) \right\}^2 \qquad (1)$$

where

$\alpha = (1/\hbar) \cdot (M_p \times \text{deuteron binding energy})^{\frac{1}{2}} = 0.23 \times 10^{13}$ cm$^{-1}$,

$k = (k_1^2 + k_f^2 - 2k_1k_f \cos\phi)^{\frac{1}{2}}$, $\mathbf{k}_1$ and $\mathbf{k}_f$ being the wave numbers of the incident and scattered deuteron plane wave functions,

$a$ = radius of interaction sphere outside of which the nuclear force field is assumed zero,

$j_l$ = spherical Bessel function of order $l$.

The $A_l$'s are unknown constants; $l$ is the value of the orbital angular momentum transferred by the incident deuteron to the target nucleus. If $l$ is even, there is no change of parity in the nucleus; $l$ odd indicates a parity change.

To compare the data with the nuclear interaction theory, the first minimum at $\phi = 62.25°$ has been fitted to the first minimum of each of the theoretical curves. From this one can derive a value of the interaction radius, $a$, for each value of $l$. The $a$-values have to be compared with the interaction radius for $Ne^{20}$, $5.01 \times 10^{-13}$ cm, following from neutron scattering [14]). All values ot $l$ give unreasonable values for $a$, except $l = 1,2$ which yield $a_1 = 5.11 \times 10^{-13}$ cm and $a_2 = 6.55 \times 10^{-13}$ cm, respectively. On the basis of this comparison $l = 1$ would be favoured. However, the maxima and minima of the theoretical curve for $l = 2$ appear to fit the data better than those for $l = 1$. The 1.63 MeV level of $Ne^{20}$ must then have spin 1, 2 or 3 and even parity, which is consistent with the value 2+ obtained from other experiments. It seems to be a general feature of existing theories based on the Born approximation, that the values of the interaction radius required for a consistent comparison with measured (d, p) and (d, n) angular distributions [15]), always turn out greater than those given by the empirical formula. This is also borne out by the results of Hafner [16]) on inelastically scattered deuterons.

According to the electrical interaction theory, energy is transferred to the target nucleus by the electromagnetic field of the incident deuteron. The

scattering cross section for $2^l$-pole excitation of the nucleus is obtained in Born approximation and is given by

$$\frac{d\sigma}{d\Omega}(\phi) = 4\gamma^2 \cdot \frac{k_1 k_f}{2j_A+1} \cdot \frac{M_{AB}^2}{r_0^{2(l-2)}} \cdot \left[\frac{j_{l-1}(kr_0)}{kr_0}\right]^2 \tag{2}$$

where

$\gamma = e^2/\hbar v_1$, $v_1$ being the velocity of the incident deuteron in the c.m.s. system,

$j_A$ = spin of initial state A of target nucleus,

$M_{AB}$ = multipole matrix element for transition of the nucleus to final state B,

$r_0$ = radius of sphere outside of which the electric field is arbitrarily assumed zero.

In the comparison of the data with the electrical interaction theory, the first minimum at $\phi = 62.25°$ has been fitted to the second minimum of each of the theoretical curves. The values of $M_{AB}$ required to make the absolute values of the differential cross sections at $\phi = 42.75°$ for $l = 1$ and at $\phi = 47.5°$ for $l = 2$ agree with theory, are given in table 1 and compared with the expected values calculated from the formula [17])

$$M = \frac{3}{l+3} \cdot \frac{1}{\sqrt{4\pi}} \cdot R^l. \tag{3}$$

TABLE 1

| Value of $l$ | $r_0$ in cm | Multipole moment $M_{AB}$ required | Multipole moment expected theoretically |
|---|---|---|---|
| 1 | $7.14 \times 10^{-13}$ | $6.079 \times 10^{-12}$ cm | $8.042 \times 10^{-14}$ cm |
| 2 | $8.78 \times 10^{-13}$ | $6.754 \times 10^{-24}$ cm$^2$ | $2.444 \times 10^{-28}$ cm$^2$ |

It is noticeable that the multipole moments required to make the electrical interaction theory account for inelastic deuteron scattering are about two orders of magnitude greater than the theoretically expected values. For all the theoretical curves, the values of $r_0$ required to fit the data turn out much too large. This seems to be generally the case in comparisons of measured (d, d') angular distributions with the electrical interaction theory [16]).

The author would like to thank Dr. S. J. du Toit, head of the Nuclear Physics Division, for his interest in this work; Dr. W. E. Frahn for many informative discussions, Miss G. Daum and Mr. L. P. Reyburn for their co-operation with the microscope work and the South African Council for Scientific and Industrial Research for permission to publish this paper. Finally, he is very much indebted to Dr. D. J. Prowse of the University of Bristol for making available the developed plates for this work.

## References


1) D. E. Alburger, Phys. Rev. **88** (1952) 1257
2) D. A. Bromley, J. A. Bruner and H. W. Fulbright, Phys. Rev. **89** (1953) 396
3) G. Scharff-Goldhaber, Phys. Rev. **90** (1953) 587
4) J. Seed, Phil. Mag. **44** (1953) 921
5) R. Middleton and C. T. Tai, Proc. Phys. Soc. A **65** (1952) 752
6) H. B. Burrows, C. F. Powell and J. Rotblat, Proc. Roy. Soc. A **209** (1951) 461
7) J. E. Brolley and F. L. Ribe, Phys. Rev. **98** (1955) 1112
8) R. Middleton and C. T. Tai, Proc. Phys. Soc. A **64** (1951) 801
9) H. B. Burrows, T. S. Green, S. Hinds and R. Middleton, Proc. Phys. Soc. A **69** (1956) 310
10) W. M. Gibson, D. J. Prowse and J. Rotblat, Nature **173** (1954) 1180
11) H. B. Burrows, W. M. Gibson and J. Rotblat, Proc. Roy. Soc. A **209** (1951) 489
12) R. Huby and H. C. Newns, Phil. Mag. **42** (1951) 1442
13) C. J. Mullin and E. Guth, Phys. Rev. **82** (1951) 141
14) G. Gamov and G. L. Critchfield, Atomic Nucleus and Nuclear Energy Sources (Clarendon Press, Oxford, 1949)
15) A. B. Bhatia, K. Huang, R. Huby and H. C. Newns, Phil Mag. **43** (1952) 485
16) J. W. Hafner, Phys. Rev. **103** (1956) 1398
17) J. M. Blatt and V. F. Weisskopf, Theoretical Nuclear Physics (John Wiley and Sons, New York, 1952)

*Nuclear Physics* **6** (1958) 62—81; © *North-Holland Publishing Co., Amsterdam*
Not to be reproduced by photoprint or microfilm without written permission from the publisher

# ON THE LEVEL DENSITY OF DEFORMED NUCLEI

TORLEIF ERICSON

*Institute for Theoretical Physics, University of Copenhagen, Denmark*

and

*Institute for Theoretical Physics, University of Lund, Sweden*†

Received 30 October 1957

**Abstract:** A simplified unified model is applied to a statistical calculation of the level densities of deformed nuclei. Configurations of nucleons of the same kind and in the same orbit are favoured by a pairing energy. With increasing energy more and more pairs are broken and the spin and parity of the levels are entirely determined by the unpaired nucleons and the collective modes of excitation. The validity of the model at higher excitation is discussed. The parameters entering the final expression for the level density are known in principle.

## 1. Introduction

At low excitation the nuclear levels are well defined, and it is possible, at least in principle, to determine their properties both experimentally and theoretically. However, when the excitation energy of a heavy nucleus increases, the levels rapidly become so numerous that we soon lose all possibility of describing each level individually. It is therefore to be expected that some kind of statistical description has to be used. This can be accomplished, if a particular nuclear model is specified, either by applying the methods of statistical thermodynamics or by an explicit count of the levels on the basis of the model. The simplest approach is to assume the nucleons to move freely in a spherical box as a Fermi gas [1–5]). This model has the advantage of being very simple, but is ot course very crude. In the more recent of the papers just quoted attempts have therefore been made to include e.g. odd-even effects and shell structure. The other extreme of very strong nuclear interactions led to the picture of the nucleus as a liquid drop [6]). This point of view stresses particularly the collective features of the excitations.

In the last few years the unified model [7, 8]), which includes both particle and collective features, has been very successful in describing the low energy spectra of deformed, rotating nuclei. The intrinsic states of these nuclei are characterized by the projection of the particle angular momentum along the nuclear symmetry axis, and each intrinsic state is the parent of a rotational band. The intrinsic states are twofold degenerate, since a change

† Present address: NORDITA (Nordisk Institut for teoretisk Atomfysik), Copenhagen, Denmark.

of sign of the projection only corresponds to a change of the direction of the motion about the nuclear axis. It has been found that the nuclear forces favour the pairing of two nucleons in the same orbit and that this tendency can be expressed in terms of a pairing energy [9]), defined as the energy necessary to break a pair †.

The aim of this paper is to apply these ideas to a region of higher excitation. Thus, we shall assume the nucleons to move independently in a deformed potential [11]) with the nucleon interaction introduced only as a pairing energy and the average potential. With increasing excitation the energy is used partly to break pairs and to form different intrinsic states from the possible configurations of paired and unpaired particles and partly to excite the nucleus collectively. The spin and parity of the state are determined by the unpaired particles and the collective modes.

One of the most interesting quantities at higher excitation is the nuclear level density. Its amount as a function of the excitation energy and its dependence on the spin will be determined both by statistical methods and by explicit counting based on the model. The parameters entering the final expressions for the level density are roughly determined by low energy data.

## 2. Density of Intrinsic States

The calculations of this and the following sections assume that the nucleus can be described as consisting of nucleons moving independently of each other as two gases, one of neutrons, the other of protons, in a non-spherical average potential well [11]). The remaining nucleon interaction is taken into account in terms of a pairing energy between nucleons of the same kind and in the same orbit. In order to simplify the calculations the pairing energy $\Delta$ has been taken to be a constant; this is not expected to affect the result seriously (for a discussion of the influence on the result of this and other assumptions, see section 5). The number of unpaired particles $\nu$ in a configuration has a decisive influence on the spin and parity of the state (see section 3), and it is, therefore, convenient to divide the states into groups according to their number of unpaired neutrons $n$ and unpaired protons $z$. This has the further advantage that the number of broken pairs $\mu$ within each of these groups is known ††.

We can now reduce the problem of calculating the level density of this system to a free particle problem as follows: the total level density at excitation $U$, $\varrho(U)$, is by definition the number of levels per unit energy. Similarly, we define level densities $\varrho_1(U, n, z)$ as the number of levels per

† For pairing energy in the shell model, see ref. [10]).

†† $\mu$ is related to $n$ and $z$ and is equal to $\frac{1}{2}(n+z)$ for even nuclei, $\frac{1}{2}(n+z-1)$ for odd mass nuclei and $\frac{1}{2}(n+z-2)$ for odd nuclei. As will be seen later, we introduce the intrinsic difference between even, odd and odd mass nuclei at this point.

unit energy with $n$ unpaired neutrons and $z$ unpaired protons when there is no pairing energy, as well as $\varrho(U, n, z)$ when the pairing energy is $\Delta$. The number of broken pairs is, however, entirely determined by $n$ and $z$. $\varrho(U, n, z)$ and $\varrho_1(U, n, z)$ thus differ only by the zero point for the energy: as we first use an energy $\mu\Delta$ to break pairs so as to give the correct values of $n$ and $z$, and then the remaining energy $U-\mu\Delta$ to excite the nucleons as free, we obtain the relation

$$\varrho(U, n, z) = \varrho_1(U-\mu\Delta, n, z). \tag{2.1}$$

The total level density is by definition the sum of the partial level densities:

$$\varrho(U) = \sum_{n,z}{}' \varrho(U, n, z) = \sum_{n,z}{}' \varrho_1(U-\mu\Delta, n, z), \tag{2.2}$$

where the $'$ on the sums indicates that the summation should be taken only over those $n$ and $z$ which can arise from the nucleus under consideration. In $\varrho_1(U, n, z)$ are still included effects due to the different possible couplings of the particle angular momenta and the dependence on spin and parity. We will first solve the simpler problem which does not include these effects, thus determining a level density $P(U, n, z)$ in terms of which $\varrho_1(U, n, z)$ will be expressed.

We start from a system consisting of non-interacting neutrons and protons with single particle levels of energies $a_s$ and $b_s$, $n_s$ and $z_s$ being the corresponding occupation numbers, which can take the values 0, 1 and 2, as the levels are doubly degenerate. Let $E$ be the total energy of the nucleus, $N$ and $Z$ the total number of neutrons and protons. According to the preceding the neutron and proton gases are subject to the following restrictions:

$$\begin{aligned} E &= \sum_s n_s a_s + \sum_s z_s b_s, \\ N &= \sum n_s, \qquad Z = \sum_s z_s, \\ n &= \sum_s \delta_{n_s 1}, \qquad z = \sum_s \delta_{z_s 1}, \end{aligned} \tag{2.3}$$

where the $\delta_{n_s 1}$ and $\delta_{z_s 1}$ are Kronecker $\delta$-symbols.

In the appendix $P(U, n, z)$ is calculated both by using the methods of statistical thermodynamics and by recursion techniques. We have assumed the neutron and proton single particle spacing to be equidistant, which is justified in the regions of deformed nuclei and at not too high excitations [11]). The statistical calculation gives eq. (A. 10)

$$P(U, n, z) = \frac{g_1^{n-\frac{1}{2}} g_2^{z-\frac{1}{2}} \pi^{\nu-3/2} U_1^{\nu-2} \exp 2\left\{\frac{\pi^2}{6} g U_1 + \left(\frac{\nu-1}{2}\right)^2\right\}^{\frac{1}{2}}}{n!\, z!\, 2^{\nu+1}\left[\left(\frac{\pi^2}{6} g U_1 + \left(\frac{\nu-1}{2}\right)^2\right)^{\frac{1}{2}} + \frac{\nu-1}{2}\right]^{\nu-2}\left(\frac{\pi^2}{6} g U_1 + \left(\frac{\nu-1}{2}\right)^2\right)^{1/4}}. \tag{2.4}$$

Here $g_1$ and $g_2$ are the neutron and proton single particle level densities. $U_1$, $g$ and $\nu$ are abbreviations for

$$U_1 = U - \frac{1}{\pi^2}\left[\frac{n(n-1)}{g_1} + \frac{z(z-1)}{g_2}\right], \tag{2.5}$$

$$g = \frac{g_1+g_2}{2}, \qquad \nu = n+z.$$

For further details we refer to the appendix.

## 3. Intrinsic Spin and Parity

According to the unified model the single particle states are characterized by the projection of the particle angular momentum $\Omega_p$ along the nuclear symmetry axis, when the particle is strongly coupled to the nuclear surface. In the same way a configuration of several particles is characterized [8, 12]) by a quantum number $\Omega$, which is the sum of the individual $\Omega_p$'s. The particle states are degenerate in $\pm\Omega_p$ and there is a preference for the particles to fill pairwise into states of opposite $\Omega_p$. $\Omega$ is thus obtained by summing only over the unpaired particles. As the individual nucleon states are degenerate in $\pm\Omega_p$, $\Omega$ is degenerate for changes of the signs of the $\Omega_p$ in $\Omega = \sum_p \Omega_p$. If there are $\nu$ unpaired particles, this degeneracy will therefore be $2^\nu$-fold; it is not included in eq. (2.4).

The distribution of the intrinsic states among the different $\Omega$ can be determined, if the probability distributions for the individual $\Omega_p$'s are known, as $\Omega$ can be regarded as obtained from a random distribution of $\nu$ quantities $\Omega_p$. The probability distribution of the $\Omega_p$ is obtained with

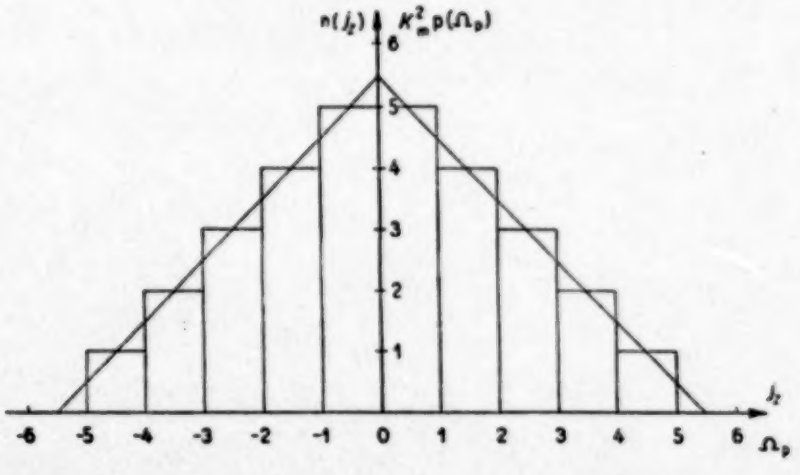


Fig. 1. Example of the number of levels for each $j_z$ in a three-dimensional harmonic oscillator. The area of the rectangles in the histogram correspond to the number of levels $n(j_z)$. The two straight lines $K_m^2 p(\Omega_p)$ correspond to eq. (3.1).

sufficient accuracy if taken to be the same as that of $j_z$ in a three-dimensional harmonic oscillator and is thus given by

$$p(\Omega_p) = \frac{1}{K_m}\left[1 - \frac{|\Omega_p|}{K_m}\right]; \quad |\Omega_p| \leqq K_m \tag{3.1}$$

where $K_m$ is the maximum $\Omega_p$ of the shell plus 1 (see fig. 1). $K_m$ can be obtained from the level scheme of Nilsson[11]), from which eq. (3.1) also can be derived approximately. The mean value of $\Omega_p$ for each nucleon is zero, the variance $\sigma^2$ is $\frac{1}{6}K_m^2$. A well-known theorem of statistics (the central limit theorem) gives then the variance $\nu\sigma^2$ for the distribution of levels over $\Omega$ with $\Omega = \sum_p \Omega_p$, if there are $\nu$ unpaired nucleons distributed at random among the $\Omega_p$. The probability for a certain $\Omega$ is thus approximately given by the Gaussian

$$\frac{1}{K_m}\sqrt{\frac{3}{\pi\nu}}\exp\left\{-\frac{3\Omega^2}{\nu K_m^2}\right\}. \tag{3.2}$$

The convergence of this expression to the exact one for the model is very rapid with increasing $\nu$, for the single particle distributions have already a form which is close to a Gaussian (see fig. 1).

From symmetry considerations it can be shown that both signs of $\Omega$ will appear in the wave function of the system and that only a certain combination of them is possible. A level is, therefore, characterized already [8]) by the positive value of $\Omega$. Thus, only $\Omega \geqq 0$ should be used in (3.2), as otherwise the same state would be counted twice.

The parity can be accounted for in a similar way. Two nucleons which are paired together, have always positive parity regardless of the parity of the particle level. The parity is entirely determined by the unpaired particles and the collective modes of excitation. For the particle states there is a probability for both parities and already a rather small possibility for both parities is sufficient to make both parities about equally probable even when the number of unpaired nucleons is small. It is possible to account roughly for the parity effect by dividing by 2, which gives finally as the density of intrinsic states of given intrinsic spin $\Omega$ and parity $\Pi$, from eqs. (2.4), (3.2) and the remarks of this section,

$$P(U, n, z, \Omega, \Pi) = \frac{g_1^{n-\frac{1}{2}} g_2^{z-\frac{1}{2}}}{n!\, z!\, 4K_m}\left(\frac{3}{\nu}\right)^{\frac{1}{2}}\left[\frac{\pi U_1}{\left(\frac{\pi^2}{6}gU_1 + \left(\frac{\nu-1}{2}\right)^2\right)^{\frac{1}{2}} + \frac{\nu-1}{2}}\right]^{\nu-2}$$
$$\times \frac{\exp 2\left(\frac{\pi^2}{6}gU_1 + \left(\frac{\nu-1}{2}\right)^2\right)^{\frac{1}{2}}}{\left(\frac{\pi^2}{6}gU_1 + \left(\frac{\nu-1}{2}\right)^2\right)^{1/4}} \exp\left\{-\frac{3\Omega^2}{\nu K_m^2}\right\}. \tag{3.3}$$

## 4. Rotational Levels

When the distribution of intrinsic states over the intrinsic spin $\Omega$ is known, the rotational states can easily be included. The coupling of the nucleonic motion to the deformed core and the splitting of levels due to this coupling have already been taken into account to a large extent by the use of the Nilsson level scheme. It is therefore to be expected that the terms which should be used in the rotational law are those due to collective effects. As a matter of fact the detailed structure of this law will not affect the result strongly for low spin values. Each intrinsic state $E_\Omega^{(i)}$ will be the parent of a rotational band with a spectrum

$$U = E_\Omega^{(i)} + \frac{\hbar^2}{2\mathscr{I}_3}(K-\Omega)^2 + \frac{\hbar^2}{2\mathscr{I}}(I(I+1)-K^2). \tag{4.1}$$

Here $K$ denotes the projection of the total angular momentum of the system on the nuclear symmetry axis, $\mathscr{I}_3$ and $\mathscr{I}$ are the moments of intertia with regard to this axis and an axis perpendicular to it, and $I$ is the total spin. In the strong coupling region $K$ will be a good quantum number. The low energy data indicate that states with $K \neq \Omega$ are very hard to excite, which means that $\mathscr{I}_3 \ll \mathscr{I}$. The contribution of these states will then be small even at higher excitation and we have therefore made the approximation $K = \Omega$ in (4.1), which then transforms into

$$U = E_K^{(i)} + \frac{\hbar^2}{2\mathscr{I}}(I(I+1)-K^2), \tag{4.2}$$

$$I = K,\ K+1, \ldots \text{ (same parity as } E_K^{(i)}).$$

The low energy spectra show that the parity restriction should not be expected to be of much importance for nuclei with several unpaired nucleons excited. We will therefore assume that all $I \geqq K$ can appear. According to (3.3) and (4.2) the density of states of given $K$ and $I$ can then be written as

$$\varrho(U,I,K,n,z,\Pi) = P(U-\frac{\hbar^2}{2\mathscr{I}}(I(I+1)-K^2),n,z,0,\Pi)\exp\left\{-\frac{3K^2}{\nu K_m^2}\right\}. \tag{4.3}$$

The total spin of the excited nucleus will be a good quantum number, but at higher excitations already weak remaining particle interactions will cause an intermixing of states with the same $I$ and different $K$ due to the very close spacing of the levels. Levels of the same total spin and parity are thus expected to share their properties to a large extent and the interesting level density will in most cases be the sum of (4.3) over $K$ rather than (4.3) itself, as the sum will give the total level density with given $I$ and $\Pi$. Thus,

$$\varrho(U,I,n,z,\Pi) = \sum_{K\leq I}\varrho(U,I,K,n,z,\Pi) \approx \int_0^{I+\frac{1}{2}}\varrho(U,I,K,n,z,\Pi)\mathrm{d}K. \tag{4.4}$$

The integral of (4.4) can be evaluated approximately by exploiting the fact that $P(U, n, z, 0, \Pi)$ can be written to a good approximation as $P_0 \exp(U/T)$ where $P_0$ and $T$ are slowly varying functions of $U$. Introducing (4.3) into (4.4) and expanding the exponent in a power series, an integration and some rewriting of the expressions yield

$$\varrho(U, I, n, z, \Pi) = P_0\left(U - \frac{\hbar^2}{2\mathscr{I}} I(I+1)\right)\int_0^{I+\frac{1}{2}} \exp\left\{\frac{\hbar^2}{2\mathscr{I}}\frac{K^2}{T} - \frac{3K^2}{\nu K_m{}^2}\right\} dK$$

$$= (I+\tfrac{1}{2})P\left(U - \frac{\hbar^2}{2\mathscr{I}} I(I+1), n, z, 0, \Pi\right)\left\{1 + \left(\frac{\hbar^2}{\mathscr{I}T} - \frac{3}{\nu K_m{}^2}\right)\frac{(I+\frac{1}{2})^2}{3} + \ldots\right\} \quad (4.5)$$

$$= (I+\tfrac{1}{2})P\left(U - \frac{(I+\frac{1}{2})^2}{3}\left(\frac{\hbar^2}{\mathscr{I}} + \frac{3T}{\nu K_m{}^2}\right),\ n,\ z,\ 0,\ \Pi\right).$$

As is seen from (4.5) the level density obeys the well-known $(2I+1)$-law for low spin values, but there will be deviations for higher spins. These deviations will depend rather strongly on $\hbar^2/2\mathscr{I}$ and on the exact validity (on the average) of (4.2). As an example the spin dependence of (4.5) has been compared to the $(2I+1)$-law in fig. 2 for a nucleus in the actinide region at

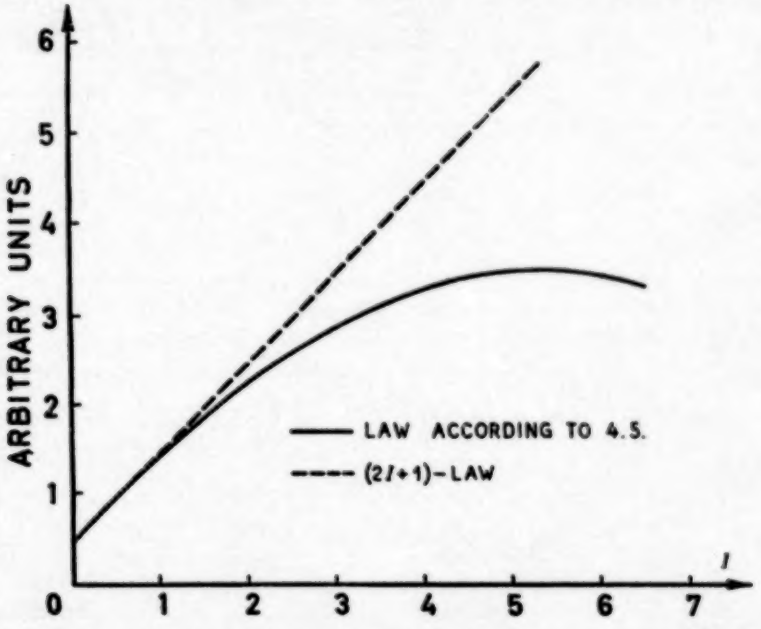


Fig. 2. Comparison of the spin law of eq. (4.5) and the $(2I+1)$-law for a nucleus in the actinide region at 5 MeV excitation energy. $T = 0.5$ MeV, $\hbar^2/2\mathscr{I} = 7.5$ keV, $K_m = 7$, $\nu = 4$. The deviations depend fairly strongly on the parameters for higher spins.

neutron binding energy. The deviation becomes appreciable for a spin $\approx 3$ and at a spin $\approx 5$ the function even starts decreasing. The experimental material available in the regions of application has not sufficed to decide which of the laws should be preferred.

The $(2I+1)$-law and the law (4.5) yield much the same general shape of curve. The first is usually obtained by calculating the number of levels

with $z$-component of the angular momentum $M$. This number is proportional to $\exp(-aM^2)$, where $a$ is a small number [1]). The number of states with angular momentum $I$ is then the difference of the number of states with $M = I$ and $M = I+1$, i.e. proportional to

$$\exp(-aI^2) - \exp(-a(I+1)^2) \approx a(2I+1).$$

This result is thus obtained essentially by a differentiation. It is, therefore, interesting to note that a law which resembles it can be obtained from an entirely different point of view and by an integration.

## 5. Discussion of the Model

The calculations of the preceding sections have been based on a model of the nucleus which is essentially the unified model, though simplified to a certain extent. This model has been applied to a region of fairly high excitation, i.e. to a region where the model might break down. It is therefore necessary to discuss the validity of the assumptions and investigate their influence on the result.

The main assumptions are

1. the existence of $K$ as a good quantum number and of a rotational law of the type (4.1),
2. the neglect of the vibrational states,
3. equidistant single particle level spacing,
4. constant pairing energy,
5. the averaging over the equilibrium deformations of the nucleus corresponding to the different nucleonic states,
6. the excitation of pairs without extra cost of energy,
7. the influence of the intrinsic difference between even, odd and odd mass nuclei.

In the following discussion it should be kept in mind that we are not interested in the individual properties of the states, but in the average properties of a large number of levels, so that it is sufficient that the assumptions hold on the average. With increasing excitation the levels will come very close to each other, and already very weak perturbations will therefore cause a strong mixing of states of different $K$ but same spin and parity. At the same time the perturbations will shift the positions of the levels, pushing some to a higher energy, others to a lower one, but they will not change the spin or the parity, nor will they create or destroy levels. The effect on the level density should, therefore, be expected to be of the second order, if there is no preference for either direction. The perturbations will also tend to destroy the rotational law (4.1), but on the basis of the above argument the average density should still be reproduced. In this context we want to point out that the variation of the level density with

the spin does not depend strongly on the validity of (4.1) for small spin values, as the integrand of (4.4) for small $K$ is nearly a constant; it is essentially this fact that has been exploited.

The neglect of the vibrational states is to a certain extent justified by their expected large spacing, as they are built on intrinsic states at a considerably lower energy. Because of the rapid variation of the level density with energy the number of these parent states is so much lower that also the relative contribution of the vibrational states to the level density should be small.

The approximation of a constant single particle level spacing should be expected to be good in the regions of deformed nuclei, $150 < A < 190$, $A > 225$, as is shown by the calculations of Nilsson [11]). Also, as no systematic variation of the single particle spacing exists in these regions, there will be a smoothing out of the uncorrelated irregularities of the spacing, making the approximation even more justified. It is mainly the limitation on the validity of this assumption which prevents us from applying the calculations to nuclei outside the strong coupling region.

The pairing energy has been taken to be constant in this investigation, though it is known to increase with increasing angular momentum. The reason is that the nucleonic states appropriate to a strongly deformed field are mixtures of different $l$-states and, what is even more important, we have several pairs broken, so there will be a strong tendency to averaging. The uncertainty of this approximation should, therefore, be expected to be small.

The total energy of an intrinsic state is a function of the nuclear deformation and the energy minimum corresponds to the actually observed nuclear state. Thus, due to an adjustment of the deformation the actual state will usually be obtained at a lower energy than that which obtains if the state is calculated with a fixed deformation of the nucleus. Of the individual nucleons some will lose and some will gain energy by this process. It therefore seems plausible that the average effect for a large number of levels would be only a slight increase in the excitation energy, though it is possible that for certain nuclei special effects might occur.

Inherently it has been assumed that pairs can be excited without extra cost of energy, as e.g. something similar to the pairing energy. It is not impossible that such effects exist and we have therefore investigated the extreme case when the remaining interaction is so strong that no pairs can be excited. With the same parameters as in the following section it is found that at an excitation of 6 MeV the level density is decreased about 25 times. To obtain the same level density as before the single particle spacing has to be decreased to about half its preceding value, if treated as an adjustable parameter. This decrease is so large that it seems to exclude at least the limiting case.

We have also made a special investigation of the odd-even effect, which has partly an intrinsic source, and is partly due to the pairing energy. In the appendix the intrinsic effect is found to give 25 % more levels in an odd nucleus than in an even one for the same number of unpaired particles. This is negligible in comparison to the other effect which is due to the fact that we have to break one more pair in an even nucleus than in an odd one to get the same number of unpaired particles. This gives the following rule for referring all level densities to those of odd nuclei: for even nuclei, subtract the average pairing energy, for odd mass nuclei, half the average pairing energy, from the total excitation energy.

## 6. Comparison with Experiments

The present experimental information on level densities comes mainly from slow neutron capture cross sections and from energy spectra of particles evaporated from highly excited nuclei. The capture cross sections furnish the value of the level density only for a particular energy, the neutron binding energy, but the data are very reliable, and good data exist for a large number of isotopes. When a slow neutron is captured by a nucleus of spin $I_0$, only states with spin $|I_0 \pm \frac{1}{2}|$ and the same parity as the parent nucleus are excited, as the neutron has $l = 0$. These experiments will thus, at least in principle, permit a test of the spin dependence, but for an accurate comparison with the theoretical predictions it is necessary to know the neutron binding energy with good accuracy. The unfortunate fact is that there are very few binding energies known for odd nuclei in the rare earth region and that the errors of the measured energies in most regions are too large to permit a more detailed conclusion on the spin dependence. The measured energies in the rare earth region indicate that the mass formula is a good approximation in this region, and we have therefore used this to derive unknown binding energies. The spectra of evaporated particles give the variation of the level density with energy. Due to difficulties of separating direct processes from that part of the reaction which proceeds through the nuclear compound state and of obtaining accurate results from the tail of an energy distribution the data cannot be considered completely reliable for lower energies. Experiments for deformed nuclei are also lacking. The existing data show definitely that the variation with energy is exponential, as predicted by all theories, and the level density can then be written as $\exp(U/T)$, where $T$ is called the nuclear temperature and is a slowly varying function of $U$. Below 10 MeV there is some evidence [1]) that $T$ varies more slowly than $\sqrt{U}$, and by some authors it is even claimed to be constant in this region [13, 14]). A third possibility is to analyse the (n, $\gamma$)-cross sections of heavy even nuclei [15]), which will give the spin

dependence and the temperature somewhat above the neutron binding energy. The experimental material is still very scarce.

The regions for comparison with experiments are $152 \leqq A \leqq 187$, $A \geqq 233$, where the level density is known for 23 isotopes. The parameters entering the final expression for the level density are $g_1$, $g_2$, $\Delta$, $\hbar^2/2\mathcal{I}$, $K_m$, $U$ and $I_0$, all of which are known in principle. $U$ and $I_0$ are varying from nucleus to nucleus and can be directly determined; the others with the exception of $K_m$ can be measured, but enter as averages and have therefore been given average values for each of the regions; finally, $K_m$ has been taken from the calculations of Nilsson [11]. We have put $g_1 = g_2 = g$ and computed $g$ from the experimental spacing of intrinsic states of odd mass-nuclei at low energy on the assumption that particle and hole configurations are equally probable, giving $g^{-1} = 360$ keV in the rare earth and 300 keV in the actinide region. These values should be expected to be somewhat high on account of some levels not being populated owing to selection rules; $g$ has, therefore, been used as a free parameter and the predicted level densities have been listed for $g^{-1} = 300$ and 333 keV in the rare earth and for $g^{-1} = 225$ and 250 keV in the actinide region. For the average pairing energy $\Delta$ the values 1.2 and 0.8 MeV, respectively, have been used for the two regions. The remaining parameters $K_m$ and $\hbar^2/2\mathcal{I}$ enter only in correction terms for small spin values and the result is not very sensitive to their exact values; $K_m$ is obtained as 7 and 8 respectively, $\hbar^2/2\mathcal{I}$ is taken to be a constant equal to 7.5 keV for both regions.

When the neutron binding energy in the rare earth region is not known, it has been calculated from the mass formula used by Metropolis and Reitwiesner [16], which gives the neutron binding energy as

$$B_n(A,Z) = 0.931\left[15.04+14\left\{(A-1)^{2/3}-A^{2/3}\right\}+83\left[\frac{\{\frac{1}{2}(A-1)-Z\}^2}{A-1}-\frac{(\frac{1}{2}A-Z)^2}{A}\right]+0.627Z^2\{(A-1)^{-1/3}-A^{-1/3}\}+\delta\right]\text{MeV}; \tag{6.1}$$

$\delta = \mp 36(A-1)^{-3/4}$ for $A$ odd, $\begin{cases} Z \text{ even}, \\ Z \text{ odd} \end{cases}$; $\delta = \mp 36A^{-3/4}$ for $A$ even, $\begin{cases} Z \text{ even} \\ Z \text{ odd} \end{cases}$.

In view of other uncertainties no attempt has been made to include shell effects in the values so obtained. The binding energy has otherwise principally been obtained from the measurements of Johnson and Nier [17] and Johnson and Bhanot [18]) for the rare earths and from the compilation of Huizenga [19]) for the actinides.

Tables 1 and 2 contain a comparison between the theoretical predictions of this paper and experimental results obtained from slow neutron capture. When isotopes with only 1 or 2 known resonances in a limited interval are left out, the available material consists of 13 rare earth and 10 actinide

TABLE 1

| Isotope | $I_0$ | $B'_n$ MeV | $B_n$ MeV | Type $Z$ $N$ | $D$ eV | $D_0$ eV | $D_{op}$ eV | | Remarks |
|---|---|---|---|---|---|---|---|---|---|
| | | | | | | | $g^{-1}$ = 300 keV | $g^{-1}$ = 333 keV | |
| $Eu^{152}$ | 5/2 | 6.60 | 6.5 [17]) | O–O | 0.85 | 4.6 | 8.5 | 19 | A |
| $Eu^{154}$ | 5/2 | 6.26 | | O–O | 1.0 | 5.4 | 12 | 25 | A |
| $Tb^{160}$ | 3/2 | 6.12 | | O–O | 5.3 | 20 | 14 | 30 | A |
| $Ho^{166}$ | 7/2 | 5.99 | | O–O | 5.6 | 34 | 17 | 36 | A |
| $Tm^{170}$ | 1/2 | 6.20 | | O–O | 7.0 | 14 | 13 | 28 | A |
| $Lu^{176}$ | 7/2 | 6.08 | | O–O | 5.4 | 32 | 15 | 32 | B |
| $Lu^{177}$ | ≈8 | 7.33 | | O–E | 1.4 | 9.5 | 6.9 | 16 | B† |
| $Hf^{178}$ | 7/2 | 7.56 | 7.55 [18]) | E–E | 3.0 | 18 | 13 | 28 | A |
| $Hf^{180}$ | 9/2 | 7.26 | 7.32 [18]) | E–E | 4.0 | 26 | 19 | 42 | A |
| $Ta^{182}$ | 7/2 | 5.98 | 6.07 [21]) | O–O | 4.5 | 27 | 15 | 33 | A |
| $W^{183}$ | 0 | 6.22 | 6.29 [18]) | E–O | ≈50 | ≈50 | 16 | 36 | C |
| $W^{184}$ | 1/2 | 7.42 | 7.45 [18]) | E–E | 15 | 30 | 15 | 34 | B |
| $W^{186}$ | 0 | 5.67 | 6.4 [22]) | E–O | ≈75 | ≈75 | 29 | 58 | C |

† Sensitive to $\hbar^2/2\mathcal{I}$.

In the columns are listed: resulting isotope, spin of target isotope [20]) $I_0$, neutron binding energy from mass formula $B'_n$, measured neutron binding energy $B_n$, type of the resulting nucleus (O for odd, E for even), measured level spacing [20]) $D$, same corrected for spin $D_0$, predicted $D_0$ for two values of the single particle spacing ($D_{op}$). The letters in the last column indicate the reliability of the experimental spacing (A good measurement, B few levels and/or uncertain isotope assignment, C one or two levels only). $g^{-1}$ is the single particle spacing. The predicted $D_0$ has been calculated using $B_n$ when known. $\Delta = 1.2$ MeV, $K_m = 7$.

TABLE 2

| Isotope | $I_0$ | $B_n$ MeV [19]) | Type $Z$ $N$ | $D$ eV | $D_0$ eV | $D_{op}$ eV | | Remarks |
|---|---|---|---|---|---|---|---|---|
| | | | | | | $g^{-1}$ = 225 keV | $g^{-1}$ = 250 keV | |
| $Th^{232}$ | 0 | 5.09 | E–O | 18 | 18 | 8.99 | 18.5 | A |
| $U^{234}$ | 5/2 | 6.81 | E–E | 0.73 | 4.0 | 0.87 | 2.32 | A |
| $U^{235}$ | 0 | 5.18 | E–O | 13 | 13 | 7.55 | 15.1 | A |
| $U^{236}$ | 7/2 | 6.42 | E–E | 0.65 | 4.4 | 1.79 | 4.39 | A |
| $U^{237}$ | 0 | 5.42 | E–O | 16 | 16 | 4.75 | 8.93 | A |
| $U^{239}$ | 0 | 4.70 | E–O | 18 | 18 | 19.1 | 43.6 | A |
| $Np^{238}$ | 5/2 | 5.43 | O–O | 0.66 | 3 | 2.07 | 4.84 | C |
| $Pu^{240}$ | 1/2 | 6.41 | E–E | 2.5 | 5.0 | 1.82 | 4.47 | A |
| $Pu^{241}$ | 0 | 5.53 | E–O | 19 | 19 | 3.84 | 7.01 | B |
| $Pu^{242}$ | 5/2 | 6.22 | E–E | 1.7 | 9 | 2.59 | 6.12 | A |

Columns labelled as in table 1, with the exception that column $B'_n$ has been left out. $\Delta = 0.8$ MeV, $K_m = 8$.

isotopes. The agreement between the experimental and predicted values must be considered satisfactory in view of the sensitivity of the predicted values to the binding energy, which will prevent an accurate agreement; a change of this energy by 0.2 MeV in the actinide region, for instance, will change the predicted value by a factor of 1.4. The uncertainty of the binding energies in this region is 0.15 MeV or more. Furthermore an additional uncertainty of the binding energy might be introduced as it is obtained by forming mass differences of different α-series. A few nuclei seem to deviate from the predicted values. These are the two europiums and $U^{239}$ which have too large a predicted spacing. It should be noted, however, that the same discrepancy will arise if a similar comparison is based on other current models.

The comparison shows that the best value for the single particle spacing is between 300 and 333 keV for the rare earths and about 250 keV for the actinides. In table 3 the predicted spin independent spacing is listed for

TABLE 3

Spin-independent spacing as a function of energy in the rare earth region for two values of the single particle spacing

| Type of nucleus \ $U$ MeV | | 5.5 | 6.0 | 6.5 | 7.0 | 7.5 |
|---|---|---|---|---|---|---|
| $g^{-1} = 300$ keV | even | 263 | 126 | 58.1 | 27.8 | 14.0 |
| | odd mass | 92.3 | 45.1 | 21.6 | 10.7 | 5.51 |
| | odd | 32.9 | 17.3 | 8.45 | 4.28 | 2.24 |
| $g^{-1} = 333$ keV | even | 4.87 | 252 | 119 | 59.0 | 30.1 |
| | odd mass | 188 | 92.6 | 46.5 | 23.9 | 12.5 |
| | odd | 70.9 | 36.0 | 18.7 | 9.79 | 5.23 |

$\Delta = 1.2$ MeV, $K_m = 7$.

application to isotopes in the rare earth region for the parameter values $\Delta = 1.2$ MeV, $g^{-1} = 300$ and 333 keV.

The recent analysis of the (n, $\gamma$)-cross sections of $Th^{232}$ and $U^{238}$ by Lane and Lynn [15]) give a nuclear temperature for these nuclei of about 0.5 MeV and a spin dependence which does not deviate strongly from the $(2I+1)$-law below spin 3. This is in good agreement with the predicted temperature of 0.55 MeV for these nuclei at the same energy and with eq. (4.5). Similar experimental results for the rare earth region are lacking, but the predicted temperature is 0.7 MeV.

The predicted variation of the level density with energy is shown in fig. 3, as well as the way in which the total level density is built up from the partial level densities, according to eq. (2.2). The nuclear temperature is predicted to have a variation with energy between that of the $\sqrt{U}$-law

and that of a constant. There is unfortunately no experimental material to test this prediction for nuclei in these regions.

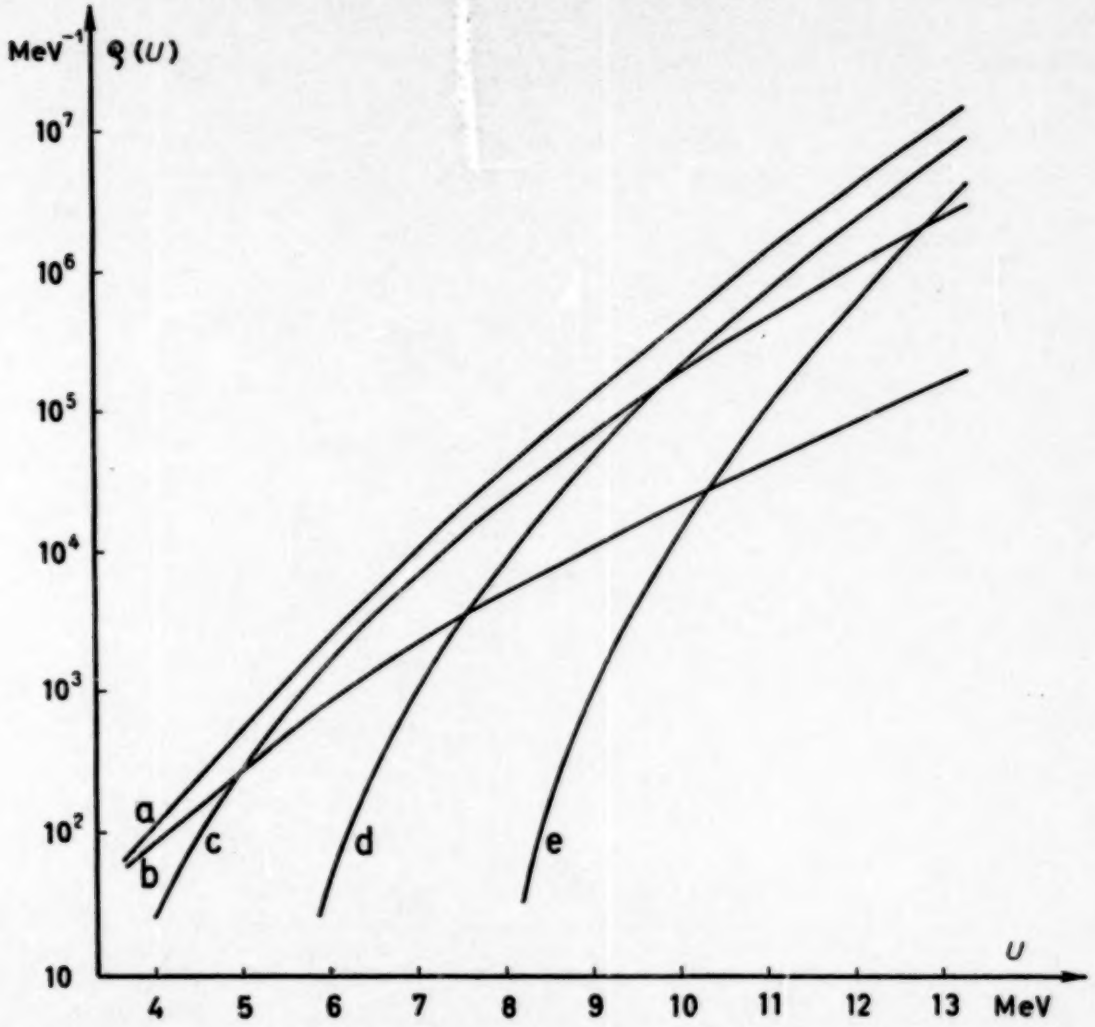


Fig. 3. The total spin independent level density $\varrho(U)$ for an even nucleus as a function of energy and its formation according to eq. (2.2) from partial densities with a definite number of pairs broken.

Parameters: $g^{-1} = 0.33$ MeV, $\Delta = 1.33$ MeV, $K_m = 7$.

The curves represent

(a) total density,
(b) partial density with 1 pair broken,
(c) partial density with 2 pairs broken,
(d) partial density with 3 pairs broken,
(e) partial density with 4 pairs broken.

To investigate the dependence of the result on the parameters we have varied the pairing energy, keeping the single particle spacing fixed. The result is shown in fig. 4. It should be kept in mind, however, that a simultaneous adjustment of the pairing energy and the single particle spacing

will produce curves which have very similar slopes and ordinates and that these two parameters therefore should be considered jointly.

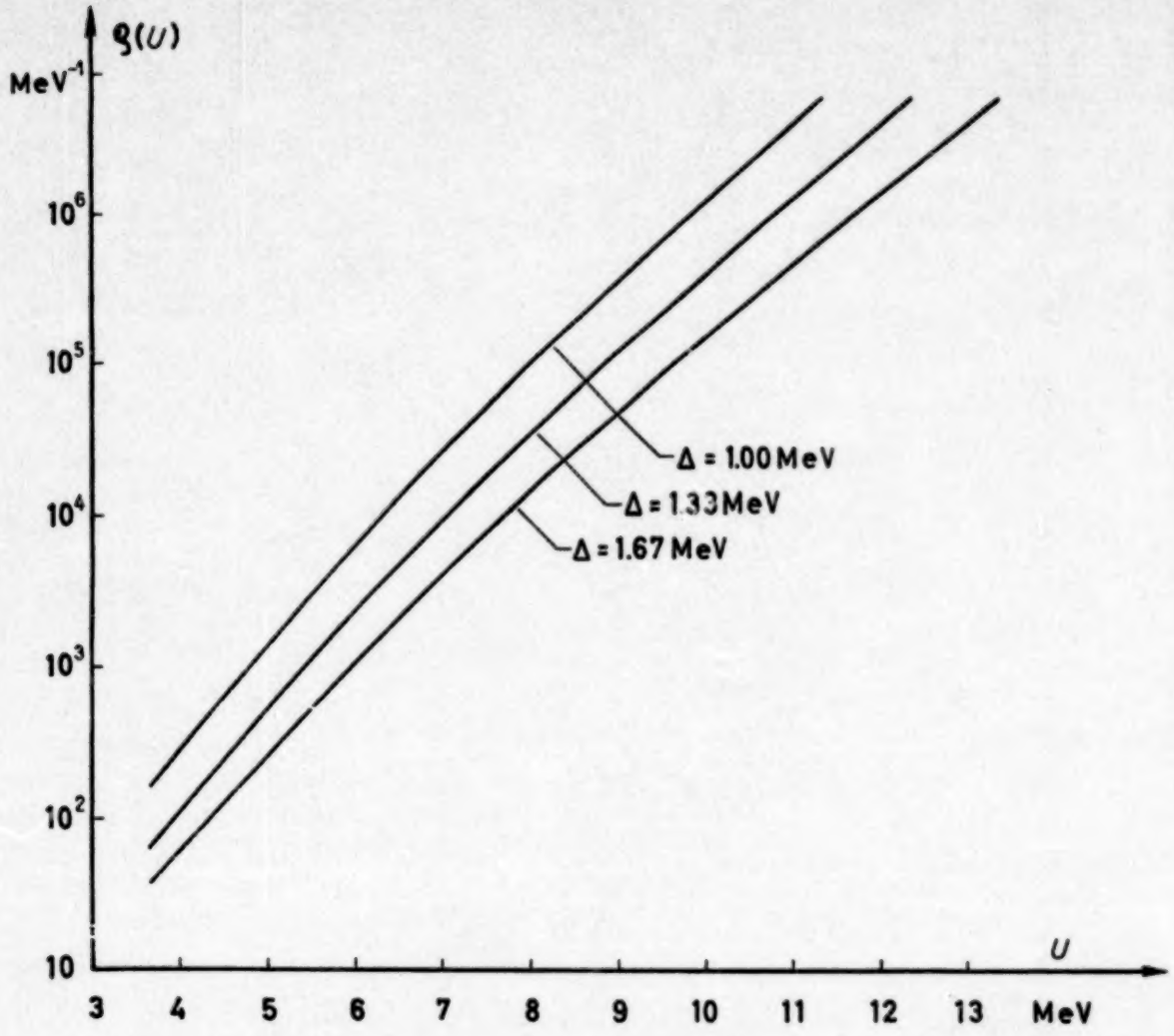


Fig. 4. Variation of the total spin independent level density for an even nucleus with the pairing energy $\Delta$ (expressed in MeV).
Parameters: $g^{-1} = 0.33$ MeV, $K_m = 7$.

On the basis of the preceding comparison we conclude that the unified model will describe the levels of highly excited deformed nuclei correctly when applied to calculations of level densities, i.e. that it will give the number of levels, its variation with energy, its distribution over spin and its dependence on the nuclear type correctly for reasonable values of the parameters. Nearly all the deviations are within the experimental errors. The region of validity for heavy nuclei is expected to be up to approximately 10 MeV.

I wish to express my sincere gratitude to Professor A. Bohr and Dr. B. R. Mottelson for suggesting this problem and for their valuable help and criticism, to Professor T. Gustafson for his kind interest and support and

to various members of the Institutes for Theoretical Physics in Copenhagen and Lund for stimulating discussions. The financial support of the Swedish Atomic Committee is gratefully acknowledged.

## Appendix

CALCULATION OF $P(U, n, z)$

This appendix contains a derivation of $P(U, n, z)$ first by statistical mechanics, then by an exact count of the levels with the help of recursion formulae, and finally a comparison of the results of the two methods in order to check the validity of the approximations used in the first one.

The neutrons and protons are assumed to move freely but are subjected to the restrictions of § 2:

$$\begin{aligned} E &= \sum_s n_s a_s + \sum_s z_s b_s, \\ N &= \sum_s n_s, \qquad Z = \sum_s z_s, \\ n &= \sum_s \delta_{n_s 1}, \qquad z = \sum_s \delta_{z_s 1}, \end{aligned} \tag{A.1}$$

where the notation is the same as before. We define an auxiliary function $Z(\xi, \zeta, \eta, \theta, \beta)$, the partition function of statistical thermodynamics, as

$$\begin{aligned} &Z(\xi, \zeta, \eta, \theta, \beta) \\ &= \sum \xi^{\Sigma n_s} \zeta^{\Sigma z_s} \eta^{\Sigma \delta_{n_s 1}} \theta^{\Sigma \delta_{z_s 1}} \mathrm{e}^{-\beta \Sigma (a_s n_s + b_s z_s)} \\ &= \sum \xi^{N'} \zeta^{Z'} \eta^{n'} \theta^{z'} \mathrm{e}^{-\beta E'} = \sum_{N', Z', n', z'} \xi^{N'} \zeta^{Z'} \eta^{n'} \theta^{z'} \int P(E', N', Z', n', z') \mathrm{e}^{-\beta E'} \mathrm{d}E', \end{aligned} \tag{A.2}$$

where the summation extends over every allowed combination of $n_s$ and $z_s$. The allowed values of $n_s$ and $z_s$ are 0, 1 and 2, and we can therefore write $Z(\xi, \zeta, \eta, \theta, \beta)$ as

$$Z = \prod_s (1 + \xi\eta \mathrm{e}^{-\beta a_s} + \xi^2 \mathrm{e}^{-2\beta a_s})(1 + \zeta\theta \mathrm{e}^{-\beta b_s} + \zeta^2 \mathrm{e}^{-2\beta b_s}). \tag{A.3}$$

Our aim is now to invert (A.2). This can be accomplished by calculating the residues of

$$\xi^{-(N+1)} \zeta^{-(Z+1)} \eta^{-(n+1)} \theta^{-(z+1)} Z(\xi, \zeta, \eta, \theta, \beta)$$

and applying a Laplace transformation in $\beta$. To exploit this formal expression for $P(E, N, Z, n, z)$ we evaluate $Z$ from (A.3) on the basis of the model and put this $Z$ into the above expression.

To evaluate (A.3) take the logarithm and write the sums as integrals:

$$\begin{aligned} \log Z(\xi, \zeta, \eta, \theta, \beta) = &\int_0^\infty g_1(\varepsilon) \log(1 + \xi\eta \mathrm{e}^{-\beta\varepsilon} + \xi^2 \mathrm{e}^{-2\beta\varepsilon}) \mathrm{d}\varepsilon \\ &+ \int_0^\infty g_2(\varepsilon) \log(1 + \zeta\theta \mathrm{e}^{-\beta\varepsilon} + \zeta^2 \mathrm{e}^{-2\beta\varepsilon}) \mathrm{d}\varepsilon, \end{aligned} \tag{A.4}$$

where $g_1(\varepsilon)$ and $g_2(\varepsilon)$ are the single particle level densities for neutrons and protons, which have been taken to be constants in the model.

After the substitutions $t = \xi e^{-\beta\varepsilon}$ and $t = \zeta e^{-\beta\varepsilon}$ in the two integrals, (A.4) transforms into

$$\log Z = \frac{g_1}{\beta}\int_0^{\xi} \frac{\log(1+\eta t+t^2)}{t}\,dt + \frac{g_2}{\beta}\int_0^{\zeta} \frac{\log(1+\theta t+t^2)}{t}\,dt. \qquad (A.5)$$

We now make the further assumption that $N$ and $Z$ are very large and that $n$ and $z$ are much smaller than $N$ and $Z$. As is easily seen, these assumptions do not introduce anything new, as for moderate excitation energies we only excite nucleons on the top of the energy distribution.

From (A.5) we now obtain the partition function $Z$ with the given values of $N$, $Z$, $n$ and $z$ by the theorem of residues. As $N$ and $Z$ are large, the residues in $\xi$ and $\zeta$ will be calculated by the method of steepest descent, which makes $\xi$ and $\zeta$ large at the saddle point. $n$ and $z$ are small and we will therefore evaluate the residues in $\eta$ and $\theta$ exactly. This is accomplished by expanding the $Z$ of (A.5) in a power series of $\eta$ and $\theta$, neglecting terms proportional to $\xi^{-1}$, $\zeta^{-1}$ and $\beta^2$. This gives

$$Z(\xi, \zeta, \beta) = \sum_{N', Z'} \xi^{N'}\zeta^{Z'} \int P(E', N', Z', n, z)\, e^{-\beta E'}\,dE', \qquad (A.6)$$

where it should be noted that only those values of $N'$ and $Z'$ which are compatible with the given $n$ and $z$ can appear in the sum, as $n$ and $N'$ (as well as $z$ and $Z'$) are even and odd at the same time. We get

$$\begin{aligned}&\int dE'\, P(E', N, Z, n, z)\exp(-\beta E') \\ &\quad = \frac{\beta}{\pi}\frac{g_1^{n-\frac{1}{2}} g_2^{z-\frac{1}{2}}}{n!\,z!}\left(\frac{\pi}{2\beta}\right)^{n+z}\left[1-\frac{\beta}{\pi^2}\left(\frac{n(n-1)}{g_1}+\frac{z(z-1)}{g_2}\right)\right] \\ &\quad \times \exp\left(\frac{\pi^2}{12\beta}(g_1+g_2)-\frac{\beta N^2}{4g_1}-\frac{\beta Z^2}{4g_2}\right),\end{aligned} \qquad (A.7)$$

where an extra factor 4 comes from the restriction above. We want to express $P$ as a function of the excitation energy

$$U = E - \int_0^{N/2g_1} 2g_1\varepsilon\,d\varepsilon - \int_0^{Z/2g_2} 2g_2\varepsilon\,d\varepsilon = E - \frac{N^2}{4g_1} - \frac{Z^2}{4g_2}. \qquad (A.8)$$

Writing the right hand side of (A.7) as an exponential and expanding the exponent in powers of $\beta$, there will remain a linear term in $\beta$, even when $U$ has been introduced on the left hand side and common factors are cancelled. To make this disappear we introduce instead the formal excitation energy

$$U_1 = U - \frac{1}{\pi^2}\left[\frac{n(n-1)}{g_1}+\frac{z(z-1)}{g_2}\right]. \qquad (A.9)$$

Eq. (A.7) is then inverted by a Laplace transformation and the path

integral is evaluated by the method of steepest descent, giving

$$P(U, n, z) = \frac{g_1^{n-\frac{1}{2}} g_2^{z-\frac{1}{2}} \pi^{\nu-3/2} U_1^{\nu-2} \exp 2\left\{\frac{\pi^2}{6} gU_1 + \left(\frac{\nu-1}{2}\right)^2\right\}^{\frac{1}{2}}}{n!z!\, 2^{\nu+1}\left[\left(\frac{\pi^2}{6} gU_1 + \left(\frac{\nu-1}{2}\right)^2\right)^{\frac{1}{2}} + \frac{\nu-1}{2}\right]^{\nu-2}\left(\frac{\pi^2}{6} gU_1 + \left(\frac{\nu-1}{2}\right)^2\right)^{1/4}}, \quad \text{(A.10)}$$

where the non-relevant parameters $N$ and $Z$ have been dropped in $P$, and $2g = g_1 + g_2$, $\nu = n + z$.

The expression (A.10) is an asymptotic formula for $P(U, n, z)$ and should be expected to be a good approximation for large values of $U$. At small values for $U$ there might be deviations, particularly because terms proportional to $\beta^2$ have been neglected in the exponent at the saddle point and $\beta$ is increasing at this point with decreasing $U$. It is possible, however, to obtain a check on the validity of the approximations by calculating the level density exactly from the same model in the special case when the single particle level spacing is equal to the unit energy for both neutrons and protons, i.e. when $g_1 = g_2 = 1$. In this case the excited states are always obtained at integer

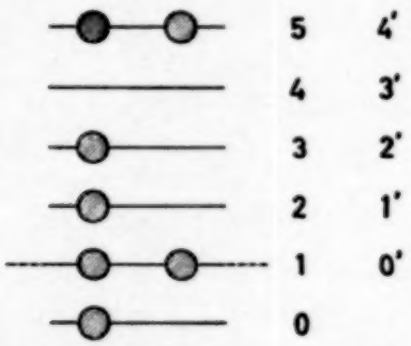


Fig. 5. Illustration of a configuration expressed in relation to the lowest and next lowest particle level. The numbers denote the single particle energy counted from the lowest level if unprimed, from the next lowest if primed. Originally the state has $N = 17$, $m = 2$ and $n = 3$, but when it is expressed with respect to the next lowest level, it has $N = 11$, $m = 2$ and $n = 2$.

values of the energy, and the level density is a discontinuous function which has to be suitably averaged over an energy interval. In practice this can be done for nearly all values of $n$ and $z$ by taking the level density at the integer points to be the number of states there. The points so obtained are then joined to a curve to give the value in points between the integers. This curve will be fairly smooth. The actual calculation is done as follows.

Consider first a nucleus consisting of only one kind of independent particles and with equidistant single particle spacing. Further we prescribe that there are $2m$ paired and $n$ unpaired particles, and we denote the

total energy of the nucleus by $N$ ($N$ integer). The number of different ways to arrange $m$ pairs and $n$ unpaired particles at energy $N$ is denoted by $A(N, m, n)$. The lowest level is now taken away (see fig. 5) and the total energy is re-expressed in relation to the next lowest level, which now will be the lowest, and the number of ways into which the particles can be arranged is again counted. Three mutually exclusive cases are possible:

(1) The lowest level is empty. Every particle has its energy decreased by one unit and the number of states is $A(N-2m-n, m, n)$.

(2) An unpaired particle in the lowest level. There is one unpaired particle less, the remaining particles have their energy decreased by one unit. Hence, the number of states is $A(N-2m-(n-1), m, n-1)$.

(3) A pair in the lowest level. There is one pair less and in the same way as above we get the number of states as $A(N-2(m-1)-n, m-1, n)$.

The possibilities are now exhausted and we obtain immediately

$$A(N, m, n) = A(N-2m-n, m, n)+A(N-2m-(n-1), m, n-1) \\ +A(N-2(m-1)-n, m-1, n). \tag{A.11}$$

As states with negative values of $N$, $m$ or $n$ have no physical meaning, $A(N, m, n)$ is defined to be 0 for these. When $N = m = n = 0$, we have the void 'configuration', which can be realized only once, as no rearrangement of the particles is possible: $A(0, 0, 0)$ is therefore defined to be 1. By the use of these initial values and the recursion formula (A.11) $A(N, m, n)$ can be calculated. However, it is the number of states as a function of the excitation energy $N^+$ that is wanted. If the ground state total energy of the $(2m+n)$ particles is denoted by $N_0$, we have

$$N^+ = N-N_0,$$

$$N_0 = \left(m+\frac{n-1}{2}\right)^2 - \tfrac{1}{4} \text{ for even } n; \quad N_0 = \left(m+\frac{n-1}{2}\right)^2 \text{ for odd } n. \tag{A.12}$$

Defining $B(N^+, m, n)$ as the number of ways to arrange $m$ pairs and $n$ unpaired particles at an excitation energy $N^+$ we have

$$B(N^+, m, n) = A(N^+ + N_0, m, n), \tag{A.13}$$

which together with (A.11) and (A.12) gives

$$B(N^+, m, n) = B(N^+-2m-n, m, n) \\ + B\left(N^+-m-\frac{n-1}{2}-\delta, m, n-1\right)+B(N^+, m-1, n), \tag{A.14}$$

where $\delta$ is $\frac{1}{2}$ for even $n$, 0 for odd $n$.

We are particularly interested in the case when the number of pairs is not restricted, i.e. in $\lim_{m\to\infty} B(N^+, m, n)$. This limit is obtained e.g. if we take $m > \frac{1}{2}N^+$.

The number of possible configurations for two gases at a total excitation energy $N^+$ and $\nu$ unpaired nucleons is then

$$C(N^+, \nu) = \sum_{n+z=\nu}{}' \sum_{N'^+=0}^{N^+} B(N'^+, \infty, n) B(N^+ - N'^+, \infty, z), \qquad \text{(A.15)}$$

where the prime on the first sum indicates that only those values of $n$ and $z$ should be taken that are compatible with the nucleus under consideration. The computation of $C(N^+, \nu)$ for values $N^+ \leqq 50$, $\nu \leqq 10$ has been performed on the electronic computer SMIL at Lund.

Eq. (A.15) has been compared to the asymptotic expression (A.10) with $g_1 = g_2 = 1$ and summed over $n$ and $z$ as above. The agreement is very good even for small values of $N^+$. For $10 \leqq N^+ \leqq 35$, which is the important region for the applications in this paper, the approximations in the derivation of (A.10) give 10—20 % too many levels in even nuclei, 5—10 % too few in odd nuclei and nearly the correct number of levels in odd mass nuclei. The agreement might be made even better by a slight shift of the zero-point of the energy for the different groups, but there has been no justification for this procedure. Throughout this paper the exact evaluation has been used.

There is an intrinsic difference in the number of configurations in even and odd nuclei, when the number of unpaired particles and the excitation energy are the same. This effect gives about 20—30 % more states in the odd nuclei in the region $10 \leqq N^+ \leqq 50$. This is discussed in section 5.

## References


1) H. Bethe, Revs. Mod. Phys. **9** (1937) 69
2) F. C. Auluck and D. S. Kothari, Proc. Cambr. Phil. Soc. **42** (1946) 272
3) J. M. Lang and K. J. Le Couteur, Proc. Phys. Soc. A **67** (1954) 585
4) T. D. Newton, Can. J. Phys. **34** (1956) 804
5) N. Rosenzweig, Phys. Rev. **105** (1957) 950
6) N. Bohr and F. Kalckar, Mat. Fys. Medd. Dan. Vid. Selsk. **14** (1937) no. 10
7) A. Bohr, Mat. Fys. Medd. Dan. Vid. Selsk. **26** (1952) no. 14
8) A. Bohr and B. R. Mottelson, Mat. Fys. Medd. Dan. Vid. Selsk. **27** (1953) no. 16
9) A. Bohr and B. Mottelson, Mat. Fys. Medd. Dan. Vid. Selsk. **30** (1955) no. 1
10) M. G. Mayer and J. H. D. Jensen, Elementary theory of nuclear shell structure (Wiley, New York, 1955)
11) S. G. Nilsson, Mat. Fys. Medd. Dan. Vid. Selsk. **29** (1955) no. 16
12) K. W. Ford, Phys. Rev. **90** (1953) 29
13) D. L. Livesey, Can. J. Phys. **33** (1955) 391
14) L. E. H. Trainor and W. R. Dixon, Can. J. Phys. **34** (1956) 229
15) A. M. Lane and J. E. Lynn, Proc. Phys. Soc. A **70** (1957) 557
16) N. Metropolis and G. Reitwiesner, NP-1980 (1950)
17) W. H. Johnson Jr. and A. O. Nier, Phys. Rev. **105** (1957) 1014
18) W. H. Johnson Jr. and V. B. Bhanot, in the press
19) J. R. Huizenga, Physica **21** (1955) 410
20) D. J. Hughes and J. A. Harvey, BNL 325 (1955); Supplement (1957)
21) J. A. Harvey, Phys. Rev. **81** (1951) 353
22) A. H. Wapstra, Physica **21** (1955) 385

*Nuclear Physics* **6** (1958) 82—86; © *North-Holland Publishing Co., Amsterdam*
Not to be reproduced by photoprint or microfilm without written permission from the publisher

# INELASTIC SCATTERING OF 185 MeV PROTONS ON LITHIUM, BERYLLIUM, BORON AND NITROGEN

H. TYRÉN and TH. A. J. MARIS†

*The Gustaf Werner Institute for Nuclear Chemistry, University of Uppsala, Sweden*

Received 11 November 1957

The measurements of the energy spectra of protons inelastically scattered on light nuclei have been continued. The experimental set-up and its parameters were the same as in ref. [1, 2]). The average scattering energy was about 182 MeV. Only targets consisting of natural isotopic mixture have been used. A selection of the measured spectra is shown in the figs. 1 and 2. Prominent maxima are listed in table 1 and some angular distributions have been plotted in fig. 3. For a discussion of the errors see ref. [2]).

In figs. 1 and 2 typical statistical errors are indicated. The total error in $d^2\sigma/d\Omega dE$ is thought to be less than 15 %. The cross sections in fig. 3 may have errors of 20 % or more dependent on the separability of the peak under consideration from the background of unresolved levels. The dashed curves in fig. 3 could be wrong by 40 %. However, it is felt that the angular distributions are at least qualitatively correct.

The only sharp peak in the lithium spectrum is attributed to $Li^7$ (abundance 92.5 %). Its energy is $4.4 \pm 0.2$ MeV and the angular distribution (fig. 3) has a forward minimum. The cross section at small angles is, however, still considerable. This fact and the small angle at which the maximum of the angular distribution for this light nucleus appears suggest an orbital angular momentum change not larger than one.

In nearly all of the nuclei hitherto investigated [1, 2]) there is a group of levels excited in the energy region of the well known giant $\gamma$-resonances. We think these levels to be at least partly identical with the giant $\gamma$-resonance levels [3]). Their differential cross section is limited to small angles, in agreement with the small angular momentum change of these dipole excitations. Experimentally the angular distributions are even forward peaked. This may be a result of Coulomb excitation or because the impulse approximation is not sufficiently good in this case.

The giant $\gamma$-resonance maxima are not clearly visible in the spectra of the lightest nuclei. The reason could be a splitting-up of the levels by strong deformations of these nuclei [4]). For lithium other observations too indicate

† Present address: Institute for theoretical Physics, Copenhagen.

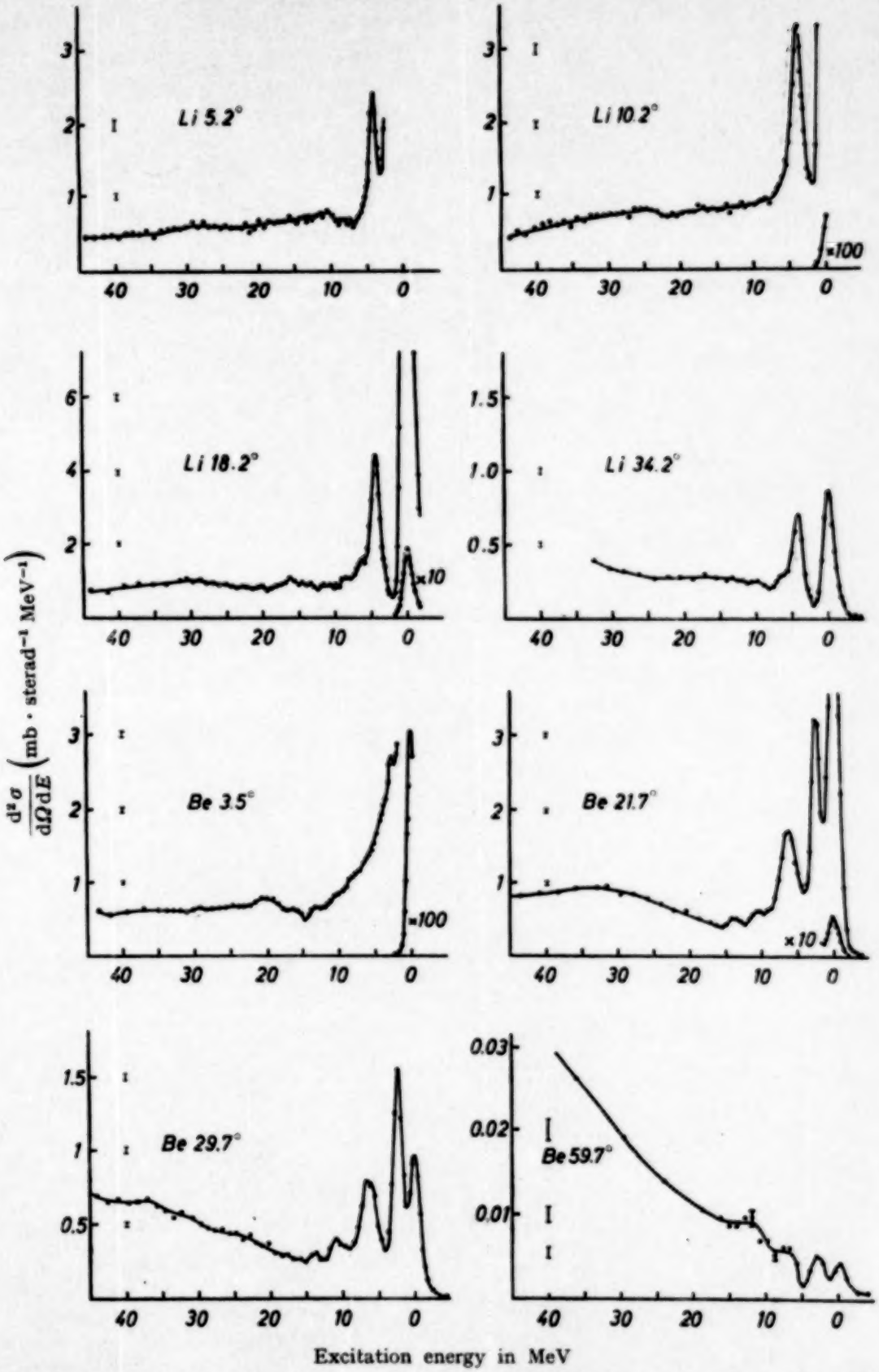


Fig. 1. Energy spectra for inelastic scattering of 182 MeV protons on natural Li and Be. Typical statistical errors for the ordinates are shown near the left margin of the figures.

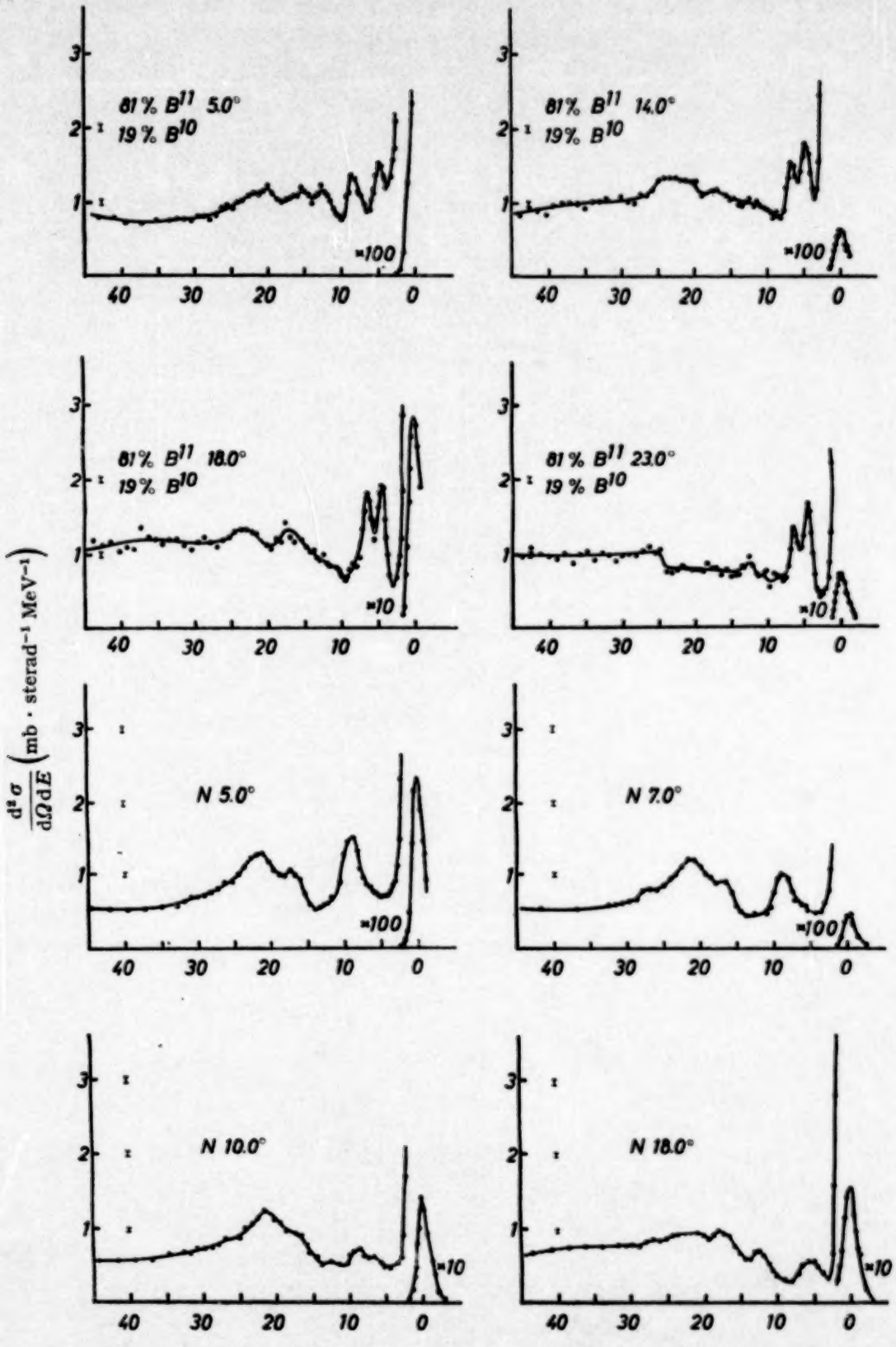


Fig. 2. Energy spectra for inelastic scattering of 182 MeV protons on natural B and N.

that the giant $\gamma$-resonance levels are spread out over a large energy region between 10 and 20 MeV [5]).

In beryllium two strong excitations appear at $2.3\pm0.2$ MeV and at about 6 MeV. Both angular distributions have a forward minimum. The suspicion of Benveniste *et al.* [6]), based on inelastic scattering of 31 MeV protons, that there may exist more levels around 6 MeV is clearly confirmed. The energy of the maximum of this peak varies from 5.7 to 6.7 MeV for an angular change from 15 to 45 degrees. At 21.7 and 25.7 degrees the width of the peak is 1.5 times the width of the elastic one. An estimate of the 6 MeV cross section from the spectra is rather uncertain and therefore the angular distribution is not plotted in fig. 3.

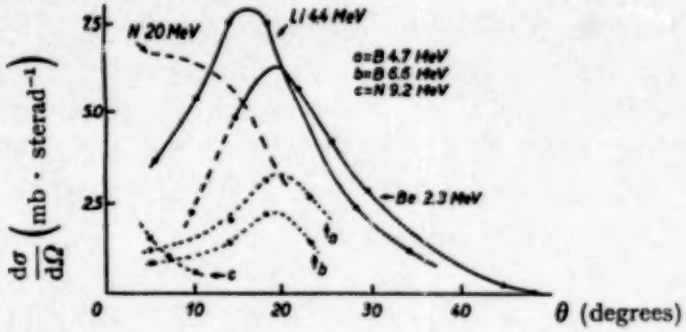


Fig. 3. Differential cross sections for some strongly excited levels in Li, Be, B and N. The errors in the full and dashed curves are thought to be not larger than 20 % and 40 % respectively.

TABLE 1

| Element | Level (MeV) |
|---|---|
| Li | $4.4\pm0.2$ |
| Be | $2.3\pm0.2$ |
| Be | $\approx 6$ |
| B | $4.7\pm0.2$ |
| B | $6.6\pm0.2$ |
| B | $8.5\pm0.4$ |
| N | $9.2\pm0.4$ |
| N | $\approx 20$ |

At small angles there are indications of a smeared-out level structure in the giant $\gamma$-resonance region.

In the spectra of boron (81 % $B^{11}$ and 19 % $B^{10}$) the cross sections belonging to $B^{11}$ and to $B^{10}$ should be multiplied with factors 1.24 and 5.3 respectively. Comparing the magnitude of the observed cross sections with those of other nuclei, it seems likely that the clearly visible peaks, with the possible exception of the 8.5 MeV maximum at 5 degrees, come from $B^{11}$.

The spectra show three relatively large peaks at $4.7\pm0.2$ MeV, $6.6\pm0.2$ MeV and $8.5\pm0.4$ MeV. The first two are forward dipped. It is difficult to

estimate the contribution of the unresolved neighbouring levels and therefore these cross sections in fig. 4 are uncertain, although the angular dependence should be roughly correct. Comparing the spectra with the level scheme [5]) of $B^{11}$ it is clear that the main contribution to the 4.7 MeV maximum does not come from the 5.03 MeV level, except perhaps at 5 degrees scattering angle. The $8.5\pm0.4$ MeV peak is interesting. It shows a strongly forward peaked cross section similar to that of the 15 MeV level in carbon [2]) and we therefore also attribute it to a spin flip of a target nucleon, possibly by magnetic interaction. From this follows the assignment $J = \frac{1}{2}-$, 3/2− or 5/2−.

The rise and the shape of the spectrum at 5 degrees between 10 and 25 MeV are probably due to a broad giant resonance structure. The form of the spectrum in this energy region changes going from 5 to 18 degrees. A similar observation may be made in the carbon and oxygen spectra. At the larger angles the cross sections for single particle excitations between adjoining shells resulting in angular momentum changes larger than one can become predominant over the dipole excitations of the giant resonance levels, which have a rather narrow forward peaked angular distribution.

In the nitrogen spectrum no strong excitations appear at large angles. At 12.8 MeV a small peak is visible. The maximum at 6 MeV in the 14 and 18 degree spectra may be due to a small oxygen contamination of the liquid target.

The small angle spectra show the giant resonance structure with maxima at 17 and 21.5 MeV. There is a strongly forward peaked excitation at $9.2\pm0.4$ MeV with an angular distribution comparable with those of the 15.0 MeV level in carbon and the 8.5 MeV level in boron. In this case the peak is somewhat broadened.

We are grateful to Prof. T. Svedberg for his support. We are indebted to Dr. Peter Hillman for stimulating discussions and for his instructions for the building of the cryostat. We thank Mr Å. Svanheden and his cyclotron crew for their cooperation, Mr P. Isacsson and C. A. Ståhlbrandt for technical assistance and Miss M. Rooth for help with the spectrum transformations.

## References

1) H. Tyrén and Th. A. J. Maris, Nuclear Physics **3** (1957) 52
2) H. Tyrén and Th. A. J. Maris, Nuclear Physics **4** (1957) 637
3) Th. A. J. Maris and H. Tyrén, Nuclear Physics **4** (1957) 662
4) S. G. Nilsson, Mat. Fys. Medd. Dan. Vid. Selsk. **29** (1955) no. 16
5) F. Ajzenberg and T. Lauritsen, Revs. Mod. Phys. **27** (1955) 77
6) J. Benveniste, R. G. Finke and E. A. Martinelli, Phys. Rev. **101** (1956) 655

*Nuclear Physics* **6** (1958) 87—99; © *North-Holland Publishing Co., Amsterdam*
Not to be reproduced by photoprint or microfilm without written permission from the publisher

# MESONIC EFFECTS IN BETA-DECAY

J. S. BELL
*Atomic Energy Research Establishment, Harwell, Nr. Didcot, Berks.*
and
R. J. BLIN-STOYLE
*Clarendon Laboratory, Oxford*

Received 22 November 1957

**Abstract:** It is found impossible to give a consistent account of mirror transitions involving nuclei with *LS*-closed cores plus or minus one particle in terms of conventional beta-decay theory and using shell model wave functions. Possible explanations of the discrepancies are discussed and it is concluded that there is some evidence for mesonic effects of an exchange character.

## 1. Introduction

The object of this paper is to discuss whether there is at present any indication of mesonic effects in the beta-decay of nuclei. Such effects have already been treated in the case of isolated nucleons by various authors [1–4]) and the indications are that, because of the interaction between the nucleon and pion fields, the effective beta decay interaction for a real nucleon differs from that for a bare nucleon. This effect is analogous to that which obtains in the case of the electromagnetic field and which, for example, accounts for the discrepancy between the magnetic moments of real nucleons and the values given by the Dirac theory.

Taking the analogy a step further, it is believed that the difference between the magnetic moments of $H^3$ and $He^3$ from those predicted by any reasonable theoretical picture (i.e. predominantly $^2S_{\frac{1}{2}}$ state) of these nuclei is due to meson exchange currents [5]). That is, the effective magnetic moment operator for these nuclei is not just a sum of single particle operators but contains also two and three body terms. In the same way it might be expected that similar terms (we shall refer to them as exchange terms) will occur in the effective beta-decay interaction. If such terms do occur then they will invalidate those attempts (e.g. ref. [6])) which have been made to deduce a beta-decay interaction from consideration of the life-times of various particularly simple nuclei, since such attempts are based on the assumption that no exchange terms appear in the beta-decay Hamiltonian.

In section 2 we discuss the relevant experimental data and the discrepancies that they seem to imply. Possible explanations of these discrepancies, other than mesonic, are considered in sections 3 and 4, whilst the form and magnitude of mesonic corrections are discussed in section 5.

## 2. Experimental Data

On the conventional theory of beta-decay (i.e. not including exchange terms), the $ft$ value associated with the allowed decay of a nucleus can be written as follows [7]):

$$(ft)^{-1} = \alpha\left(1 \pm b_F \left\langle \frac{1}{E} \right\rangle_{av}\right)|M_F|^2 + \beta\left(1 \pm b_{GT}\left\langle \frac{1}{E}\right\rangle_{av}\right)|M_{GT}|^2 \qquad (1)$$

where

$$\begin{aligned}
\alpha &= \frac{1}{2\pi^3 \ln 2}\{|G_S|^2+|G_V|^2+|G'_S|^2+|G'_V|^2\} \\
\beta &= \frac{1}{2\pi^3 \ln 2}\{|G_T|^2+|G_A|^2+|G'_T|^2+|G'_A|^2\} \\
b_F &= 2\gamma \,\mathrm{Re}\,\{G_S G_V^* + G'_S G'^*_V\}/\{|G_S|^2+|G_V|^2+|G'_S|^2+|G'_V|^2\} \\
b_{GT} &= 2\gamma \,\mathrm{Re}\,\{G_T G_A^* + G'_T G'^*_A\}/\{|G_T|^2+|G_A|^2+|G'_T|^2+|G'_A|^2\}
\end{aligned}$$

and $\gamma = [1-(Z/137)^2]^{\frac{1}{2}}$. The $G$ and $G'$ are the parity conserving and parity non-conserving coupling constants for the S, V, A and T interactions. $\langle 1/E\rangle_{av}$ is the average of $1/E$ for the transition with units $m = c = \hbar = 1$. In the above formulae the upper sign refers to negaton and the lower to positon decay. The Fermi and Gamow-Teller matrix elements are given by

$$\begin{aligned}
|M_F|^2 &= |(\psi_f, \sum_j \tau_y^{(j)} \psi_i)|^2 \\
|M_{GT}|^2 &= \sum_{M_f} |(\psi_f, \sum_j \tau_y^{(j)} \sigma^{(j)} \psi_i)|^2
\end{aligned} \qquad (2)$$

where the summation $M_f$ is over all spin orientations of the final nucleus and the summation $j$ is over all nucleons. $\tau_y^{(j)}$ is the $y$-component of the isobaric spin operator for the $j^{\text{th}}$ nucleon and $\sigma$ the usual Pauli spin operator.

There are experimental indications (q.v.) that the Fierz interference terms $b_F$ and $b_{GT}$ are small, and for the moment we do not consider them. It therefore follows that a plot of $y = (ft)|M_F|^2$ against $x = (ft)|M_{GT}|^2$ for allowed transitions should be a straight line whose slope is given by

$$-\frac{\alpha}{\beta} = -\frac{|G_S|^2+|G_V|^2+|G'_S|^2+|G'_V|^2}{|G_T|^2+|G_A|^2+|G'_T|^2+|G'_A|^2}$$

and measures the relative strengths of the Fermi and Gamow-Teller inter-

actions. The uncertainty in the values of $|M_F|^2$ and $|M_{GT}|^2$ precludes the use ot any but the most simple nuclei if any significant results are to be obtained from such a plot. We therefore consider only the decays listed in table 1. Apart from $O^{14} \rightarrow N^{14}$ and $Al^{26} \rightarrow Mg^{26}$ these are all mirror

TABLE 1

| Decay | $ft$ | $\|M_F\|^2$ | $\|M_{GT}\|^2$ | $ft\|M_F\|^2 \times 10^{-3}$ | $ft\|M_{GT}\|^2 \times 10^{-3}$ |
|---|---|---|---|---|---|
| $n \rightarrow p$ | $1220 \pm 150$ | 1 | 3 | $1.22 \pm 0.15$ | $3.66 \pm 0.45$ |
| $H^3 \rightarrow He^3$ | $1060 \pm 40$ | 1 | 3 | $1.06 \pm 0.04$ | $3.18 \pm 0.12$ |
| $O^{14} \rightarrow N^{14}$ | $3300 \pm 75$ | 2 | 0 | $6.60 \pm 0.15$ | 0 |
| $O^{15} \rightarrow N^{15}$ | $4400 \pm 100$ | 1 | 1/3 | $4.40 \pm 0.10$ | $1.47 \pm 0.03$ |
| $F^{17} \rightarrow O^{17}$ | $2330 \pm 80$ | 1 | 7/5 | $2.33 \pm 0.08$ | $3.26 \pm 0.11$ |
| $Al^{26} \rightarrow Mg^{26}$ | $3080 \pm 80$ | 2 | 0 | $6.16 \pm 0.16$ | 0 |
| $Ca^{39} \rightarrow K^{39}$ | $4650 \pm 300$ | 1 | 3/5 | $4.65 \pm 0.30$ | $2.79 \pm 0.18$ |
| $Sc^{41} \rightarrow Ca^{41}$ | $2560 \pm 160$ | 1 | 9/7 | $2.56 \pm 0.16$ | $3.29 \pm 0.21$ |

transitions between nuclei having a single particle or hole in the presence of a doubly closed $LS$ core and for such decays it is reasonable to use the values for $|M_F|^2$ and $|M_{GT}|^2$ predicted by the simple $jj$ shell model (see e.g. ref. [8])). These values are given in table 1. The $O^{14} \rightarrow N^{14}$ and $Al^{26} \rightarrow Mg^{26}$ decays are $0^+ \rightarrow 0^+$ so that only $|M_F|^2$ contributes and its value is determined to be 2 purely on the assumption of the charge independence of nuclear forces.

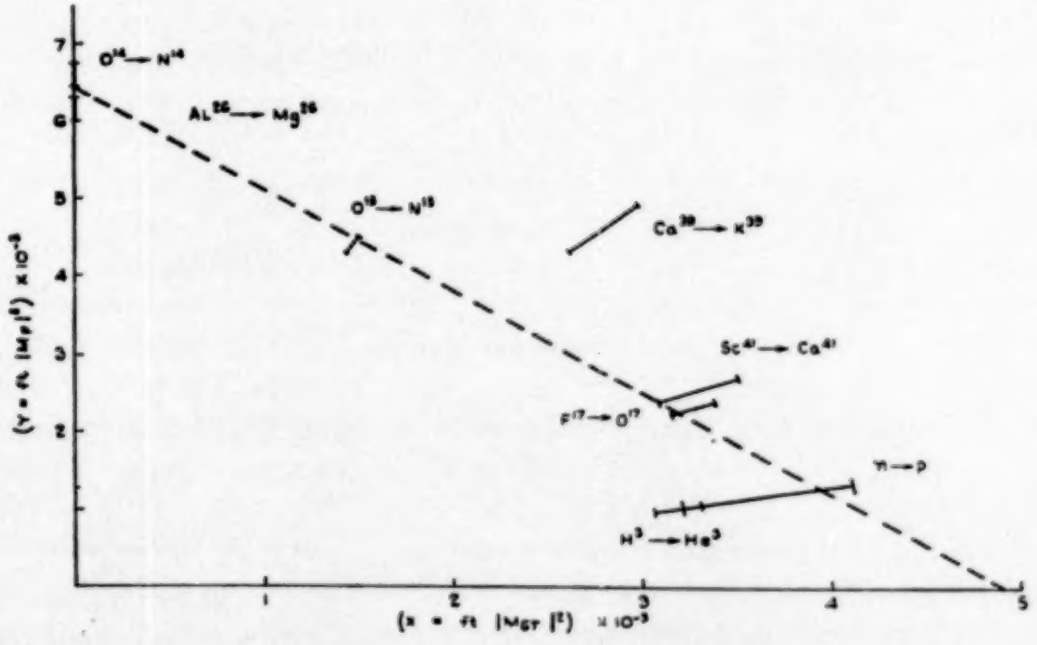


Fig. 1. Plot of $y = ft\,|M_F|^2 \times 10^{-3}$ against $x = ft|M_{GT}|^2 \times 10^{-3}$ for the beta-decay of various simple nuclei. The experimental data are taken from Kofoed-Hansen and Winther [6]).

In fig. 1 $y$ is plotted against $x$ for each of the decays, the extension of the line for each decay representing the spread due to experimental error. From inspection it is clear that, while it is possible to draw a straight line through most of the points as shown, with the rather poor neutron data not definitely off it, the $H^3 \rightarrow He^3$ and $Ca^{39} \rightarrow K^{39}$ points are considerably displaced.

These discrepancies could be due to inaccuracy in the shell model estimates of the matrix elements (2) or to deficiencies in the theory leading to (1). These possibilities are examined in turn.

## 3. Improvement of the Matrix Elements

In plotting the experimental points in fig. 1 it has been assumed that the values to be used for $|M_{GT}|^2$ are those given by the simple shell model. There is justification for this in so far as other dynamic properties (e.g. magnetic moments) of these nuclei are in general well accounted for on this extreme picture. However there is always the possibility that configurational mixing may take place and so modify the value of $|M_{GT}|^2$. $|M_F|^2$ is, of course, determined solely on the assumption of charge independence of nuclear forces and so its value is much more reliable.

Of the nuclei with which we are concerned $H^3$ and $He^3$ are the simplest and have the most reliable wave functions. Blatt [9]) has considered the possibility of configurational mixing in some detail for these nuclei and concludes that $|M_{GT}|^2 = 3$ is probably an upper limit and that configurational mixing might decrease it by a few percent. It could then be supposed that the $n \rightarrow p$ $ft$ value coincides with that of $H^3 \rightarrow He^3$ (which is not definitely incompaitlbe with the experimental data) and that in the heavier nuclei the shell model overestimates $|M_{GT}|^2$ by from 15 % (in $O^{15} \rightarrow N^{15}$) to 60 % (in $Ca^{39} \rightarrow K^{39}$). Since these heavier nuclei are all of the type "doubly $LS$-closed core plus or minus one particle", configurational mixing effects cannot occur in first order. A second order calculation using shell model wave functions is prohibitive, but Bell [10]) has estimated the magnitude of the effect for a simple Fermi gas model. He finds that in this case $|M_{GT}|^2$ is reduced by less than 4 %. This is the right direction but far too small to resolve the discrepancies. However, it is not impossible that larger effects would appear with a better model, and/or the explicit consideration of tensor forces.

An alternative approach to this problem has been used by Kofoed-Hansen and Winther [6]), in which the deviation of the magnetic moment from the Schmidt value is used to estimate the correction to $|M_{GT}|^2$ assuming that both effects are due to a rather restricted form of configurational mixing. They quote the following formula:

$$|M_{GT}|^2 = 4\frac{I+1}{I}\frac{\mu - g_l I}{g_s - g_l} \tag{3}$$

where $I$ is the nuclear spin, $g_l$ and $g_s$ the orbital and spin gyromagnetic ratios for the odd particle, and $\mu$ the measured magnetic moment. This formula is valid on the weak coupling collective model for the nucleus in which impurities of shell model states are attributed to the excitation of surface oscillations, and it is also valid if the impurities are due to certain restricted mixtures of odd particle states (see ref. [8]), p. 114). There is a possibility that it might account for the particularly large discrepancy of the $Ca^{39} \rightarrow K^{39}$ decay, since for this nucleus a weak collective description might be reasonable. In fact using (3) one obtains $ft\,|M_{GT}|^2 = (1.81 \pm 0.11) \times 10^{+3}$ instead of $(2.79 \pm 0.18) \times 10^{+3}$. This brings the decay into much better alignment with the other nuclei. However this agreeable result is somewhat invalidated by the fact that deviations from the Schmidt lines may be due not only to configurational mixing, but also to exchange magnetic moments; an estimate by Bell [11]) gives a space exchange contribution in $K^{39}$ which is itself roughly equal to the total deviation. Again for $H^3$ and $He^3$ the use of the semi-empirical formula is inadmissable in so far as the magnetic moment deviations of these nuclei are also substantially due to exchange effects [5]) which are ignored in the derivation of eq. (3). In fact if the estimated spin exchange correction is subtracted before eq. (3) is applied, the correction to $|M_{GT}|^2$ changes sign and is then in better agreement with Blatt's discussion of configurational mixing in these nuclei [9]).

Coulomb effects could reduce both Fermi and Gamow-Teller matrix elements in the heavier nuclei, by reducing the overlap of the odd particle wave functions. A simple estimate (appendix A) using harmonic oscillator wave functions suggests that in the worst case ($Sc^{41} \rightarrow Ca^{41}$) the effect is about one percent in the squared matrix elements. While this is no doubt an underestimate, it seems unlikely that the real effect can be as large as those with which we are concerned.

## 4. Improvement of the Theory (non-mesonic)

Possible deficiencies, other than mesonic, in the theory underlying (1) can be listed as follows: (4.1) the assumption of no Fierz interference, (4.2) the approximate treatment of the lepton wave functions, and (4.3) the neglect of relativistic effects of nucleon motion. Each of these is now discussed.

### 4.1. FIERZ INTERFERENCE TERMS

If the Fierz interference terms cannot be neglected then we see that they have the effect of changing the magnitudes of $x$ and $y$ by $b_{GT}\langle 1/E\rangle_{av} \times 100\%$

and $b_F \langle 1/E_{av} \rangle \times 100\ \%$ respectively. Now Kofoed-Hansen and Winther [6]) found that after using the semi-empirical formula (3) for $|M_{GT}|^2$, the coherence of the data could be further improved by the hypothesis of considerable interference in the Fermi part ($b_F = 0.29$, $b_{GT} = 0$). However, experiments on the ratio of K-capture to positon emission now suggest [12]) that $b_F < 0.1$ and $b_{GT} < 0.01$. Further $\langle 1/E \rangle_{av}$ is of the order 1 for the triton decay and less than $\frac{1}{2}$ for the others. Thus the maximum changes in $x$ and $y$ are of the order 2 % and 10 % respectively for $H^3 \to He^3$ and less than 1 % and 5 % for the other decays. Such changes are much too small to bring the experimental data into line even with the most liberal interpretations of the errors and most favourable choice of sign for the $b$'s.

### 4.2. LEPTON WAVE FUNCTIONS

The approximations normally used with the lepton wave functions also seem adequate. In the absence of Coulomb effects the error would be to ignore terms other than the first in the expansion

$$\exp\,[i(\mathbf{k}_e+\mathbf{k}_\nu)\cdot\mathbf{r}] = 1+i(\mathbf{k}_e+\mathbf{k}_\nu)\cdot\mathbf{r}-\tfrac{1}{2}[(\mathbf{k}_e+\mathbf{k}_\nu)\cdot\mathbf{r}]^2+\ldots.$$

The second term cannot contribute for transitions with no change of nuclear parity. To estimate the third, we replace $|\mathbf{k}_\nu+\mathbf{k}_e|$ by $E/\hbar c$ where $E$ is the energy released in the decay (which is certainly an overestimate), and $r$ by the nuclear radius $R = 1.2\,A^{1/3}\times 10^{-13}$ cm, giving

$$\tfrac{1}{2}[(\mathbf{k}_e+\mathbf{k}_\nu)\cdot\mathbf{r}]^2 \approx \tfrac{1}{2}\left(\frac{ER}{\hbar c}\right)^2 = \tfrac{1}{2}\left(\frac{E}{mc^2}\,\frac{A^{1/3}}{320}\right)^2 \qquad (4)$$

where $m$ is the electron mass. This is largest for $Ca^{39} \to K^{39}$, where the numerical value is about 0.008. From this source therefore we would expect corrections to the squared matrix elements of less than 2 %. Of course the influence of the Coulomb field on the charged lepton is not in fact small. Intuitively we would expect proper allowance for this to reduce further the variation of the positon wave function over the nucleus (and apart from $n \to p$ and $H^3 \to He^3$ we are only concerned with positon emission), for the positon does not have the full final momentum until well clear of the nucleus. The Coulomb field of the finite nucleus is not usually considered accurately, but is replaced by that of a point nucleus and the lepton wave functions evaluated at the nuclear surface. The work of Rose and Holmes [13]) suggests that this also causes negligible error for these light nuclei.

### 4.3. RELATIVISTIC EFFECTS

Relativistic effects may be estimated by a method already used for magnetic moments [14, 15]), which is to evaluate the nuclear matrix elements between the Dirac wave functions of the odd particle moving in an external

field due to the core. This is carried out in appendix B for the corrections of lowest order. If terms depending on the assumed transformation properties of the nuclear field are set aside and matrix elements taken using Pauli wave functions for the odd particle then the results can be expressed as follows. We denote the beta-decay matrix element in the non-relativistic limit by $M_0$ and the relativistically corrected matrix elements by $M$, the relation between them being

$$|M|^2 = |M_0|^2[1+Y\langle \mathbf{p}^2/m^2c^2\rangle] \tag{5}$$

where $Y$ is given by table 2, $\mathbf{p}$ is the nucleon momentum, and $\langle\ \ \rangle$ denotes

TABLE 2

| | Scalar | Polar Vector | Tensor | Axial Vector |
|---|---|---|---|---|
| $j = l+\frac{1}{2}$ | $-1$ | $0$ | $-\frac{1}{2}(j+1)$ | $-(2j+1)/(2j+2)$ |
| $j = l-\frac{1}{2}$ | $-1$ | $0$ | $\frac{1}{2}j$ | $-(2j+1)/2j$ |

an average over the appropriate one-particle state. Taking oscillator wave functions,

$$\langle \mathbf{p}^2/m^2c^2\rangle = (n+\tfrac{3}{2})\hbar\omega/mc^2 \approx 0.44(n+\tfrac{3}{2})A^{-1/3}$$

where $n$ is the principal quantum number and the approximate formula

$$\hbar\omega \approx 42A^{-1/3}\ \text{MeV}$$

of Levinger [16]) has been used.

The combination of interactions which actually occurs is not now known. To obtain the largest relativistic effects we would choose S and A. Then $|M_F|^2$ would be reduced by from 4.5 % to 6 % (greatest for $F^{17} \to O^{17}$) and $|M_{GT}|^2$ by from 3 % to 9 % (greatest for $O^{15} \to N^{15}$). Even if relativistic effects in $H^3 \to He^3$ were ignored, these reductions would be insufficient to overcome the discrepancy between this case and the others, an effect of more like 20 % in each matrix element being required. In any case it is unlikely that nucleon kinetic energies in $H^3$ and $He^3$ are down by a factor of more than two as compared with heavier nuclei [17]). For all of the interactions, S, V, T and A, the relativistic interactions reduce the matrix elements for $H^3 \to He^3$, so bringing this decay into more definite disagreement with that of the neutron.

## 5. Mesonic Effects

There remains the possibility of substantial mesonic effects. The states $\psi_i$ and $\psi_f$ in (2) should in principle contain not only the nucleon variables but also those of the meson field. When the latter are eliminated by canon-

ical transformation, the primitive operators of allowed decay, $\sum_j \tau_y^{(j)}$ and $\sum_j \tau_y^{(j)} \boldsymbol{\sigma}^{(j)}$, are replaced by effective operators. For an isolated nucleon[1–4]) these new operators are just multiples of the originals, but in the presence of several particles there may be expected to appear in addition terms of many body character. This situation is familiar in connection with magnetic moments, where the no-recoil PS—PV theory has been used by Villars [5]) to obtain the two-body exchange moments in second order perturbation theory. For beta-decay, with the same meson theory, the calculation has now been performed by Blin-Stoyle, Gupta and Primakoff; this work will be reported in detail later. In second order no many body effects arise, but in fourth order the expected two- and three-body contributions do appear.

As in the magnetic moment case [18]) the general form of the result can be anticipated on symmetry grounds. Thus the effective operators can be assumed to transform under rotation in isobaric spin space, rotation and inversion in ordinary space, and under time reversal [19]), as do the primitive operators $\sum_j \tau_y^{(j)}$ and $\sum_j \tau_y^{(j)} \boldsymbol{\sigma}^{(j)}$. With no-recoil meson theory the effective operators will be velocity independent, although it is problematic to what extent this will be so for more realistic theories. As in conventional treatments of nuclear forces and of exchange moments we consider here only the two-body contributions. With the assumptions mentioned, and of course the requirement of symmetry between all the particles, the following expressions are readily obtained for the effective beta-decay exchange operators for the Fermi and Gamow-Teller parts:

$$
\begin{aligned}
H_{\mathrm{F}} &= \sum_{i \neq j} [f_{\mathrm{I}} + f_{\mathrm{II}} \boldsymbol{\sigma}^{(i)} \cdot \boldsymbol{\sigma}^{(j)} + f_{\mathrm{III}} S_{ij}] [\tau_y^{(i)} + \tau_y^{(j)}], \\
H_{\mathrm{GT}} &= \sum_{i \neq j} \left[ g_{\mathrm{I}} \boldsymbol{\sigma}^{(i)} \wedge \boldsymbol{\sigma}^{(j)} + g_{\mathrm{II}} \frac{\mathbf{r}_{ij} \mathbf{r}_{ij} \cdot (\boldsymbol{\sigma}^{(i)} \wedge \boldsymbol{\sigma}^{(j)})}{r_{ij}^2} \right] [\boldsymbol{\tau}^{(i)} \wedge \boldsymbol{\tau}^{(j)}]_y \\
&\quad + \sum_{i \neq j} \left[ h_{\mathrm{I}} (\boldsymbol{\sigma}^{(i)} - \boldsymbol{\sigma}^{(j)}) + h_{\mathrm{II}} \frac{\mathbf{r}_{ij} \mathbf{r}_{ij} \cdot (\boldsymbol{\sigma}^{(i)} - \boldsymbol{\sigma}^{(j)})}{r_{ij}^2} \right] [\tau_y^{(i)} - \tau_y^{(j)}] \\
&\quad + \sum_{i \neq j} \left[ j_{\mathrm{I}} (\boldsymbol{\sigma}^{(i)} + \boldsymbol{\sigma}^{(j)}) + j_{\mathrm{II}} \frac{\mathbf{r}_{ij} \mathbf{r}_{ij} \cdot (\boldsymbol{\sigma}^{(i)} + \boldsymbol{\sigma}^{(j)})}{r_{ij}^2} \right] [\tau_y^{(i)} + \tau_y^{(j)}]
\end{aligned}
\tag{6}
$$

where $f_{\mathrm{I}}$, $f_{\mathrm{II}}$, etc. are arbitrary functions of the internucleon distance $r_{ij}$, and

$$S_{ij} = 3[(\boldsymbol{\sigma}^{(i)} \cdot \mathbf{r}_{ij})(\boldsymbol{\sigma}^{(j)} \cdot \mathbf{r}_{ij})/r_{ij}^2 - \boldsymbol{\sigma}^{(i)} \cdot \boldsymbol{\sigma}^{(j)}].$$

The effect of the above exchange terms on the $H^3 \rightarrow He^3$ decay is being evaluated using the coefficients given by the perturbation theory. The results promise to explain how this decay can proceed more rapidly than that of the neutron, whereas all the other effects considered tend in the opposite direction.

No detailed application has yet been made to the heavier nuclei, but some general features can be anticipated. For nuclei with doubly $LS$-closed cores plus one particle (and equivalent results are obtained with a hole) the operators (6) can be integrated over the shell model core wave function to give an effective single-body operator acting on the odd particle. This process is particularly simple in the limit of extreme short range for the functions $f_{\mathrm{I}}$ etc., when, for example, the space exchange operator $P^{r}_{ij}$ (which occurs in the factor $(1-P^{r}_{ij}P^{\sigma}_{ij}P^{\tau}_{ij})$ by which each term of (6) must be multiplied to allow for antisymmetry) can be replaced by unity. Moreover this approximation is reasonable here, for arising as they do only in fourth order the two-body operators have only half the Yukawa range. The resultant effective single-body operators are readily found to be

$$\begin{aligned} H'_{\mathrm{F}} &= \tau_{\nu}[\tfrac{1}{2}F_{\mathrm{I}}-\tfrac{3}{2}F_{\mathrm{II}}]\varrho(r), \\ H'_{\mathrm{GT}} &= \tau_{\nu}\boldsymbol{\sigma}[G_{\mathrm{I}}+\tfrac{1}{3}G_{\mathrm{II}}+H_{\mathrm{I}}+\tfrac{1}{3}H_{\mathrm{II}}]\varrho(r) \end{aligned} \tag{7}$$

where $\varrho(r)$ is the density of the core nucleons at the position of the odd particle, and

$$F_{\mathrm{I}} = \int f_{\mathrm{I}}(r_{ij})\mathrm{d}\mathbf{r}_{ij}, \text{ etc.}$$

When the expressions (7) are integrated over the radial wave function we have again just multiples of the primitive operators. The radial integrals should not vary much from nucleus to nucleus. Thus in the diagram the heavier nuclei might be expected to lie on a straight line from which the $\mathrm{n} \rightarrow \mathrm{p}$ datum (when more accurately known) and that of $\mathrm{H}^3 \rightarrow \mathrm{He}^3$ for which the short range approximation might be poor) would be displaced. Only the apparently extreme behaviour of $\mathrm{Ca}^{39}$ is in obvious disagreement with this picture.

## 6. Conclusions

The work presented in this paper has, of course, been only exploratory and any conclusions are quite tentative. Various non-mesonic effects have been considered in an attempt to resolve the discrepancies which appear to exist between the experimental data on particularly simple nuclei and the conventional theory of beta-decay. Individually none of the effects seems capable of enabling a consistent account of the beta-decays of these nuclei to be given. At the same time the possibility cannot be ruled out that in combination a resolution of the discrepancies might be achieved. However, this would require a most liberal interpretation of the orders of magnitude and signs of the effects. On the other hand it seems quite likely that the major part of the discrepancies might be interpreted in terms of mesonic exchange effects as described in section 5. A more quantitative estimate

of the magnitude of these effects will be given in a subsequent paper. Our aim at this stage has been to point out the existing inconsistencies and to emphasize that until this problem has been cleared up, care has to be taken in attempting to deduce a beta-decay interaction of the conventional type (i.e. excluding exchange effects) by comparing the *ft*-values for the various simple decays considered. Finally we would like to stress the importance of an accurate determination of the *ft*-value for the $n \to p$ decay and also our interest in a remeasurement of the *ft*-value for the $Ca^{39} \to K^{39}$ decay whose apparently extreme behaviour still remains a puzzle.

The authors are indebted to Dr. T. H. R. Skyrme for helpful comments on this work.

## Appendix A

COULOMB EFFECT

We here consider the neutrons and protons to move in central single-particle potential wells, that for the latter differing from that for the former by the classical Coulomb potential of the nuclear charge distribution. This ignores exchange contributions from the Coulomb forces. With *LS*-closed cores plus or minus one particle the decay matrix elements are given by the appropriate operators, $\tau_\nu$ or $\tau_\nu \sigma$, evaluated between the initial and final single particle states involved in the transition. Considered as a perturbation on the initial proton wave function, the effect of the Coulomb field is to mix in states of different radial quantum number. In lowest order the squared matrix elements are thereby reduced by a fraction

$$X = \sum_{i \neq 0} \left| \frac{\langle i|C|0\rangle}{E_1 - E_0} \right|^2 \tag{A1}$$

where $|0\rangle$ is the unperturbed initial single particle state, $|i\rangle$ the complete set of such states, $E_i$ the single particle energies, and $C$ the Coulomb potential. Denoting by $(\Delta E)^{-2}$ the average value of $(E_1 - E_0)^{-2}$,

$$X = (\Delta E)^{-2}(\langle C^2\rangle - \langle C\rangle^2) \tag{A2}$$

where $\langle\ \rangle$ denotes an expectation value in the state $|0\rangle$.

To estimate this we follow MacDonald [20]) in using oscillator wave functions and energies, and in representing the Coulomb field by that of a uniformly charged sphere of radius $R$:

$$C = \frac{Ze^2}{2R}\left[3 - \left(\frac{r}{R}\right)^2\right], \quad r < R \tag{A3}$$

$$= \frac{Ze^2}{r}, \qquad r > R \tag{A4}$$

where the coefficients $A, \ldots, \mathbf{H}$, which represent the average effect of other nucleons, are functions of position $\mathbf{r}$ and momentum $\mathbf{p}$. Lorentz invariance would impose transformation relations between, for example, $A$ and $\mathbf{E}$, but this need not concern us here. Assuming as usual that the single particle potentials are symmetric under rotation and reflection, $C$ and $D$ are zero (for no preudoscalar can be constructed from the two vectors $\mathbf{r}$ and $\mathbf{p}$) but all the remaining terms might be present. To obtain the equivalent 2-spinor description, following Foldy and Wouthuysen [22]), large and small components are decoupled by a series of canonical transformations,

$$H \to \mathrm{e}^{iS_1} H \mathrm{e}^{-iS_1} \to \mathrm{e}^{iS_2}\mathrm{e}^{iS_1} H \mathrm{e}^{-iS_1}\mathrm{e}^{-iS_2} \text{ etc.}, \tag{B2}$$

where $S_1$, $S_2$, etc., are of successively higher order in $m^{-1}$. The effective 2-component decay operators are obtained by subjecting the 4-component forms to the same series of transformations, and finally dropping parts referring to the small components.

For allowed decay we need consider only those operators which involve no change of parity; thus we have the following forms:

| | |
|---|---|
| scalar | $\beta$ |
| vector | $\mathbf{1}$ |
| tensor | $\beta\boldsymbol{\sigma}$ |
| axial vector | $\boldsymbol{\sigma}$. |

(B3)

To order $m^{-2}$, each of these transforms is

$$O \to O + [iS_1, O] + [iS_2, O] + \tfrac{1}{2}\{(iS_1)^2, O\} - iS_1 O i S_1. \tag{B4}$$

Because we are finally interested only in the large component parts, the second and third terms can be ignored; for the matrices (B3) have no elements connecting large and small components, while the matrices $S_1$ and $S_2$ have no others; so we need only $iS_1$ which is

$$iS_1 = (2m)^{-1}\beta(\boldsymbol{\alpha}\cdot\mathbf{p} + \boldsymbol{\alpha}\cdot\mathbf{E} + i\beta\boldsymbol{\alpha}\cdot\mathbf{F}). \tag{B5}$$

In the absence of information about $\mathbf{E}$ and $\mathbf{F}$ we now ignore these quantities. Then with the lowest order corrections the following effective 2-component operators are obtained:

| | |
|---|---|
| scalar | $1 - \mathbf{p}^2/2m^2$ |
| vector | $\mathbf{1}$ |
| tensor | $\boldsymbol{\sigma} - \boldsymbol{\sigma}\cdot\mathbf{pp}/2m^2$ |
| axial vector | $\boldsymbol{\sigma}(1 - \mathbf{p}^2/2m^2) + \boldsymbol{\sigma}\cdot\mathbf{pp}/2m^2$. |

Finally, to order $m^{-2}$ the non-relativistic squared matrix elements are found to be corrected according to (5).

It is of course regrettable that the validity of these results depends on $\mathbf{E}$ and $\mathbf{F}$ being sufficiently small, a point on which we have no information.

where $Z$ is the charge number of the final nucleus. MacDonald shows that there is not much error in using (A3) for all values of $r$. There are then selection rules such that

$$E_1 - E_0 = \pm 2\hbar\omega$$

whence $\Delta E = 2\hbar\omega$, and with matrix elements provided by Shaeffer [21]) the result is

$$X = \left(\frac{Z}{41}\right)^2 \left(\frac{R}{r_e}\right)^2 \left(\frac{b}{R}\right)^8 \tfrac{1}{2}(n^2 - l^2 + 3n - l + 3) \qquad \text{(A5)}$$

where $r_e$ is the classical electron radius, $b$ the scale factor of the oscillator wave functions (which contain a factor $\exp(-r^2/2b^2)$), $n$ the principal quantum number (so that $E_0 = (n+\frac{3}{2})\hbar\omega$), and $l$ the azimuthal quantum number. To determine $(b/R)$ we take

$$r_{av}^2 = \tfrac{3}{5}R^2 \qquad \text{(A6)}$$

where $r_{av}^2$ is the mean square radius of the nucleus as given by the oscillator functions; $R$ is assumed to be $1.2A^{1/3} \times 10^{-13}$ cm.

For $Sc^{41}$ we find $X = 0.004$, implying a reduction of less than half of one percent. For $Ca^{39}$ $X$ is slightly less than this, and for $O^{15}$ and $F^{17}$ it is down by a factor of about four.

As a partial check on the above method we can use it to calculate the Coulomb energy release in the transition, obtaining

$$\frac{Ze^2}{2R}\left\{3 - \left(\frac{b}{R}\right)^2 (n+\tfrac{3}{2})\right\}. \qquad \text{(A7)}$$

For $Sc^{41}$ this gives 7.3 MeV as compared with the experimental 6.2 MeV. The agreement could be improved by an increase of either $R$ or $(b/R)$. The latter adjustment would be the more serious for $X$, which would increase by a factor of about three.

It would be of interest to have the results of such calculations with wells of finite depth, where the odd proton might be expected to be more easily perturbed by the Coulomb field, with correspondingly enhanced reductions of the matrix elements.

## Appendix B

### RELATIVISTIC EFFECT

We now consider determinantal wave functions in which each component wave function is determined by a single particle Dirac equation instead of the usual Schrödinger equation. The most general Dirac equation is $E\psi = H\psi$ with

$$H = m\beta + \boldsymbol{\alpha}\cdot\mathbf{p} + A + \beta B + \gamma_5 C + i\gamma_5\beta D + \boldsymbol{\alpha}\cdot\mathbf{E} + i\beta\boldsymbol{\alpha}\cdot\mathbf{F} + \boldsymbol{\sigma}\cdot\mathbf{G} + \beta\boldsymbol{\sigma}\cdot\mathbf{H} \qquad \text{(B1)}$$

However it might be expected that the dominant terms in (B1) would be those involving the scalars $A$ and $B$; it is very satisfactory that the results do not depend on these — unlike the results of the corresponding discussion of magnetic moments.

## References


1) R. J. Finkelstein and S. A. Moszkowski, Phys. Rev. **95** (1954) 1695
2) S. S. Gerschtein and Ia. B. Zel'dovich, Soviet Physics (JETP) **2** (1956) 576
3) B. Stech, Z. Physik, **145** (1956) 319
4) M. Ross, Phys. Rev. **104** (1956) 1736
5) F. Villars, Helv. Phys. Acta **20** (1947) 476
6) O. Kofoed-Hansen and A. Winther, Mat. Fys. Medd. Dan. Vid. Selsk. **30** (1956) no. 20
7) J. D. Jackson, S. B. Treimann and H. W. Wyld, Nuclear Physics **4** (1957) 206
8) E. Feenberg, Shell Theory of the Nucleus (Princeton University Press, 1955)
9) J. M. Blatt, Phys. Rev. **89** (1953) 86
10) J. S. Bell, Nuclear Physics **5** (1958) 167
11) J. S. Bell, Nuclear Physics **4** (1957) 295
12) J. Scobie and G. M. Lewis, Phil. Mag. **2** (1957) 1089
13) M. E. Rose and D. K. Holmes, Phys. Rev. **83** (1951) 190
14) G. Breit, Phys. Rev. **71** (1947) 400
15) R. G. Sachs, Phys. Rev. **72** (1947) 91
16) J. S. Levinger, Phys. Rev. **97** (1955) 123
17) J. M. Blatt and V. F. Weisskopf, Theoretical Nuclear Physics (John Wiley and Sons, 1952)
18) R. K. Osborne and L. L. Foldy, Phys. Rev. **79** (1950) 795
19) G. J. Kynch, Phys. Rev. **81** (1951) 1060
20) M. MacDonald, Princeton thesis and U.C.R.L. Report 2746 (1954)
21) W. Shaeffer, Revs. Mod. Phys. **16** (1944) 245
22) L. L. Foldy and S. A. Wouthuysen, Phys. Rev. **78** (1950) 29

*Nuclear Physics* **6** (1958) 100—101; © *North-Holland Publishing Co., Amsterdam*
Not to be reproduced by photoprint or microfilm without written permission from the publisher

# CORE EFFECTS IN LIGHT NUCLEI

G. BARTON
*Clarendon Laboratory, Oxford*

Received 22 November 1957

In the $O^{17}$ nucleus collective effects must be invoked for the ground state quadrupole moment and for the reduced matrix element of the first excited to ground state quadrupole transition ($\langle 2s_{\frac{1}{2}}||E2||1d_{5/2}\rangle$ on the oscillator shell model). Both have been calculated [1, 2]), by applying closure to a complete first order perturbation expansion, using a Gaussian nucleon-nucleon potential $-B\Sigma_{i>j}\exp[-(r_{ij}/a)^2]$ with oscillator wave-functions. Application of closure introduces one parameter which is treated as adjustable, namely $B/\bar{E}$, with $\bar{E}$, loosely speaking, a certain mean excitation of the core; both quantities are fitted with $B/\bar{E} \approx 3$. They can also be accounted for on the weak surface coupling collective model if one is willing to apply it to such a light nucleus [3]).

Using the same methods and parameters as Amado [1]) the corresponding reduced matrix element has been calculated for the $2s_{\frac{1}{2}} \rightarrow 1d_{5/2}$ transition in the mirror nucleus $F^{17}$, since there is now some possibility of its being measured. On the collective model the effects of the cores in these two nuclei are of course identical. It is interesting therefore that using the same value for $B/\bar{E}$ one finds in $F^{17}$ a core contribution very nearly twice as great as that in $O^{17}$. The difference is due to the anti-symmetrisation of the odd proton with those of the core, which the collective model necessarily ignores. The "stiffness" constant $\bar{E}$ is to an excellent approximation a property of the core. Taking it therefore from the $O^{17}$ data the reduced matrix element in $F^{17}$ is increased in magnitude from its single-particle value of $-3.95\times10^{-26}$ cm$^2$ to $-8.95\times10^{-26}$ cm$^2$, entailing an increase of the transition width by a factor or 4.2, which can be regarded as defining an effective charge $e\sqrt{4.2}$ for the odd nucleon *in this particular transition.* Were the core contribution the same as in $O^{17}$ one would get an effective charge of only $e\sqrt{2}$. Hence a measurement of this transition width would give unambiguous information on the applicability of the weak coupling collective model to this region of the periodic table.

A similar calculation has been performed for a hypothetical nucleus consisting of a $He^4$ core plus an odd particle, with the following in mind. If one may assume that core contributions to 1p shell quadrupole transition

widths can be represented by an increased effective charge of each p-shell nucleon independently of the behaviour of the others, then this increase can be evaluated, again with a single adjustable parameter $B/\bar{E}$. Kurath [4]) has discussed these transitions for intermediate coupling of the 1p nucleons with each other, and even overestimating the nuclear radii finds evidence for collective effects. The calculated core contributions are of the right order of magnitude to account for these with $B/\bar{E} \approx 1$. Here again the effect is very nearly twice as great for protons as it is for neutrons. The great increase in $\bar{E}$ for the $He^4$ core compared with the $O^{16}$ core is also intuitively satisfactory.

I am grateful to Dr. R. J. Blin-Stoyle who suggested this problem and who has given much valuable advice in the course of its solution.

*Note added in proof:* The $F^{17}$ lifetime has now been measured [5]) as $(2.5\pm0.7)\times10^{-10}$ sec. This establishes the ratio

$$\frac{\langle\|E2\|\rangle_T}{\langle\|E2\|\rangle_0} = \varrho \approx 4\pm1$$

(the probable error is indicated).

The collective model gives $\varrho \approx 2.5$ and configuration mixing $\varrho \approx 3.5$.

## References

1) R. D. Amado, Oxford Thesis (unpublished) (1957)
2) R. J. Blin-Stoyle, Proc. Phys. Soc. A **70** (1957) 532; and ref. [1])
3) B. J. Raz, Phys. Rev. **107** (1957) 1201
4) D. Kurath, Phys. Rev. **106** (1957) 975
5) Lehmann *et al.*, private communication.

*Nuclear Physics* **6** (1958) 102—106; © *North-Holland Publishing Co., Amsterdam*
Not to be reproduced by photoprint or microfilm without written permission from the publisher

# ROTATIONAL CHARACTER OF THE TRANSITION FROM THE 473 keV LEVEL IN $Tm^{169}$

O. NATHAN and I. MARKLUND†

*Institute for Theoretical Physics, University of Copenhagen*

Received 14 November 1957

**Abstract:** The lifetime of the 473 keV state of $Tm^{169}$ is investigated by means of a $\beta$-ray spectrometer operated in coincidence with a NaI scintillation detector. An upper limit of $\approx 5\times 10^{-8}$ sec is obtained for the halflife, which is consistent with a rotational interpretation of this state.

## 1. Introduction

The extensive material available on the electron capture decay of $Yb^{169}$ to levels in $Tm^{169}$ [1–4]) has allowed a detailed comparison with the unified model of nuclear structure [4]). In fig. 1 the decay scheme is shown as constructed by Hatch *et al.* [4]) on the basis of their high resolution $\beta$- and $\gamma$-ray spectroscopy. The levels B to D have been interpreted as a rotational band associated with the $K = \frac{1}{2}$ ground state, while the states E(7/2+) and F (7/2−) most likely can be classified as single particle excitations. The appearance of these levels in $Tm^{169}$ is in good agreement with the predictions of Mottelson and Nilsson [5]) if one assumes that $Tm^{169}$ has a deformation parameter $\delta \approx 0.28$.

However, a serious difficulty exists in the interpretation of level G. The Pasadena group [4]) characterized this state as a rotational state built on level F. This classification was based on the M1+E2 multipolarity of the 94 keV transition GF and on the observed branching ratio of electron capture transitions to levels F and G. On the other hand, Mihelich *et al.* [3]) studied the lifetime of level G by $\gamma$—$\gamma$ coincidence techniques and found a halflife of 0.4 $\mu$sec, from which they conclude that the level must be interpreted as an intrinsic excitation. In the case of a rotational transition, the lifetime would have been of the order of $10^{-10}$ sec.

The present note is concerned with an attempt to put an upper limit on the lifetime of level G by means of a $\beta$-ray spectrometer operated in coincidence with a NaI $\gamma$-ray scintillation detector. This technique makes it possible to remove some of the ambiguities, which are connected with delayed coincidence work based exclusively on scintillation crystals.

† Permanent address: Institute of Physics, Uppsala, Sweden.

The 473 keV level in $Tm^{169}$ presents an especially complicated problem, since the de-excitation takes place by the 94 keV transition GF followed by the 63 keV transition FE, and these two photons appear in the NaI spectrum unresolved from the neighbouring radiations at 110 keV and 50 keV (transitions CB and K X-rays, respectively). The halflife of level E is 0.64 $\mu$sec; it seems, therefore, that any attempt to measure the halflife

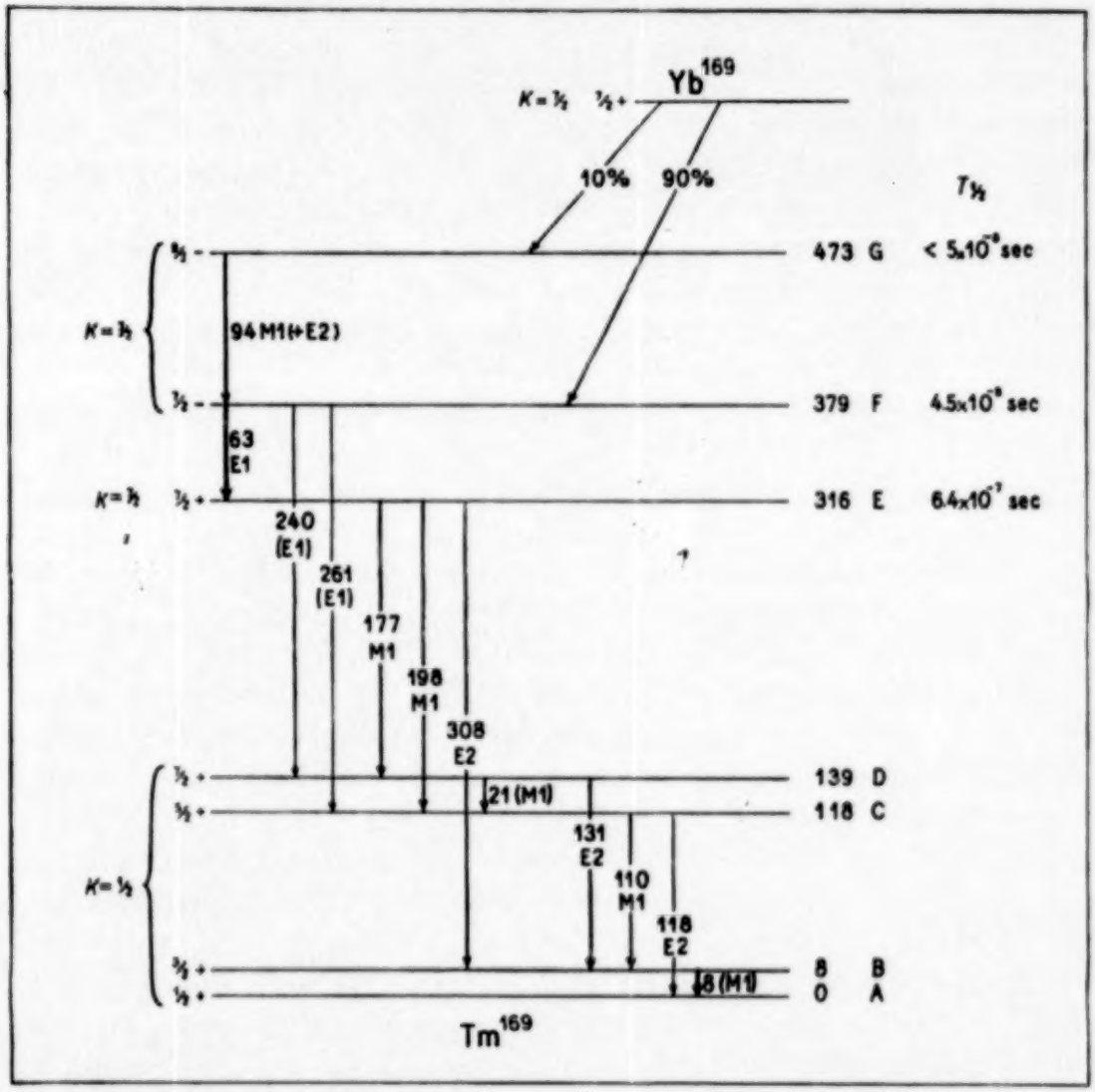


Fig. 1. The $Yb^{169} \rightarrow Tm^{169}$ decay scheme as proposed by Hatch *et al.* [4]). The halflives quoted for levels E and F are taken from the work of Mihelich *et al.* [3]). The upper limit given for the halflife of level G is based on our work.

of level G by taking coincidences between the K X-rays and the 63 keV transition may be masked by the presence of internal conversion X-rays from transitions below the 0.64 $\mu$sec state, which are in delayed coincidence with electron capture X-rays and with 63 keV photons.

## 2. Results and Discussion

A sample of natural $Yb_2O_3$ was irradiated for four weeks in the Saclay reactor, stored for two months to reduce the relative content of $Yb^{175}$ and vacuum evaporated on a 2.5 mg/cm² aluminium foil. The source was inserted in the small six-gap $\beta$-ray spectrometer and for detection of coincident radiation, a $1\frac{1}{2}'' \times 1\frac{1}{2}''$ NaI crystal was placed immediately behind the active sample.

Information on the lifetime of the level G can conveniently be obtained from the coincidence behaviour of the L conversion electrons from the 94 keV transition GF. The corresponding line can easily be resolved in the $\beta$-ray spectrometer and is situated in the vicinity of the 110 keV L line which is delayed with a known halflife of 0.64 $\mu$sec with respect to capture X-rays. The pertinent part of the conversion spectrum is shown in fig. 2. Curve A presents the normal spectrum, while curve B shows the spectrum obtained in coincidence with the K X-rays in the NaI detector, using a resolving time of $2\tau \approx 5 \times 10^{-8}$ sec. When a 0.2 $\mu$sec delay is introduced in the X-ray side, the coincidence spectrum of fig. 2 C results.

Due to the uncertainty in the amount of 63 keV $\gamma$-rays contained in the selected X-ray channel, and to the poor statistics and background conditions in the coincidence spectra, we shall not attempt a detailed quantitative analysis of the curves presented in fig. 2. However, from the above data we can immediately conclude that the halflife of level G must be considerably shorter than 0.4 $\mu$sec. The 94 keV transition is only preceded by capture X-rays, and the L line of this transition is found to be almost absent in the coincidence spectrum, when delaying 0.2 $\mu$sec in the X-ray side. Moreover, if one compares the intensities of the 110 keV and 94 keV L lines in the normal spectrum and in the undelayed coincidence spectrum, it appears that the former line is reduced by a factor of $\approx 2.5$ in the coincidence spectrum. From a consideration of the transition intensities and internal conversion coefficients given by Hatch *et al.* [4]) it follows that this fact can be explained only on the assumption that most of the coincidences between capture X-rays and 94 keV L electrons were recorded by the coincidence circuit, which indicates an upper limit of $\approx 5 \times 10^{-8}$ sec for the lifetime of level G.

It may thus be concluded that the rotational interpretation of level G is consistent with the result of the present investigation. It is interesting to note that this interpretation is in good agreement with the analysis of Mottelson and Nilsson [2]), which does not predict the presence of a single particle state of the 9/2— type in $Tm^{169}$ at a deformation parameter $\delta \approx 0.28$.

We wish to thank Professor Niels Bohr for the ideal working conditions at the Institute for Theoretical Physics. One of us (I.M.) is further indebted to the Institute for financial support during his stay in Copenhagen.

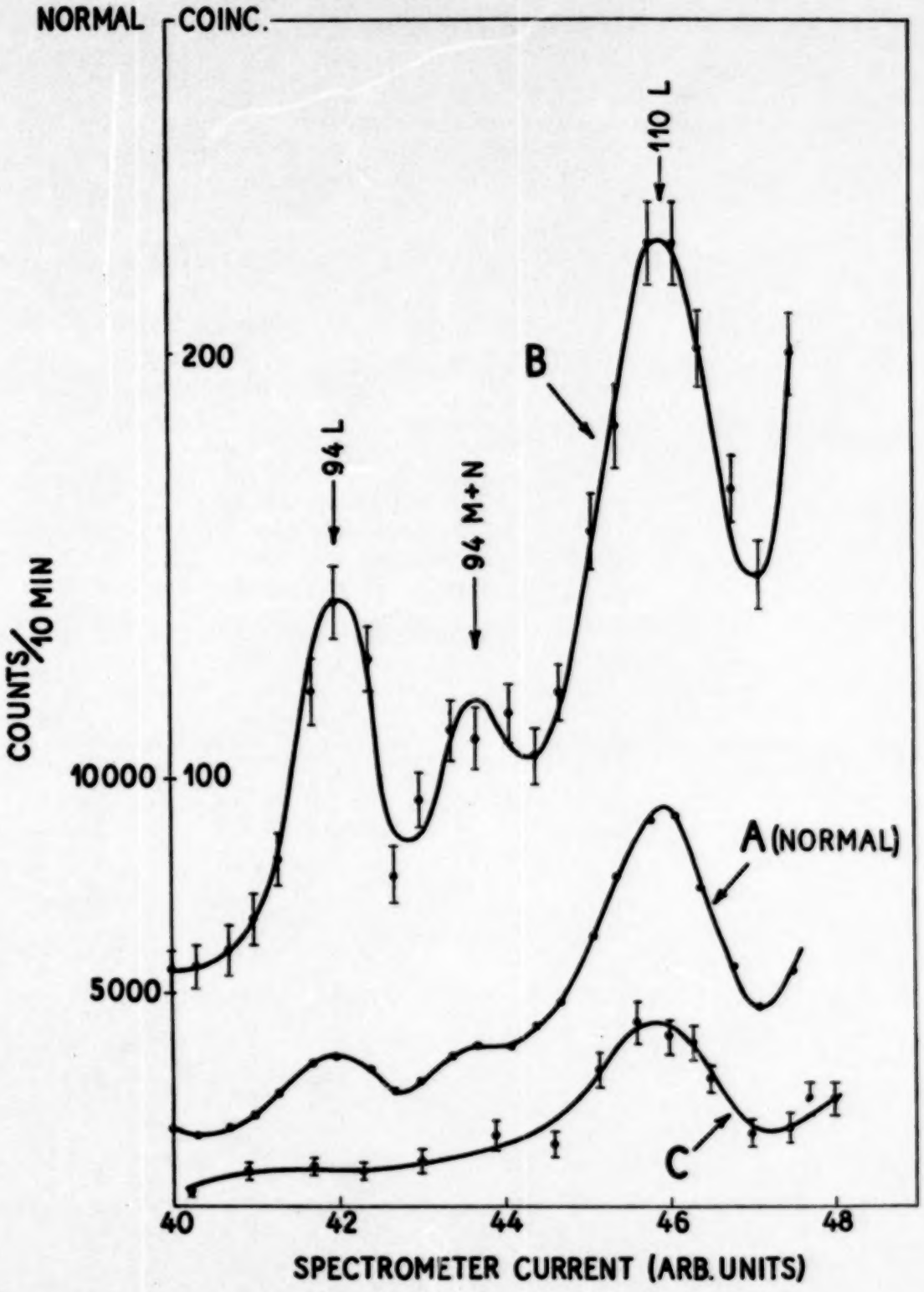


Fig. 2. Part of the internal conversion spectrum of $Yb^{169}$.
A. The normal spectrum.
B. The spectrum in coincidence with K X-rays. No delay.
C. The spectrum in delayed coincidence with K X-rays 0.2 $\mu$sec delay introduced in the X-ray side.

## References

1) S. A. E. Johansson, Phys. Rev. **100** (1955) 835
2) Cork, Brice, Martin, Schmid and Helmer, Phys. Rev. **101** (1956) 1042
3) Mihelich, Ward and Jacob, Phys. Rev. **103** (1956) 1285
4) Hatch, Boehm, Marmier and DuMond, Phys. Rev. **104** (1956) 745
5) B. R. Mottelson and S. G. Nilsson, Phys. Rev. **99** (1955) 1615

*Nuclear Physics* **6** (1958) 107—113; © *North-Holland Publishing Co., Amsterdam*

Not to be reproduced by photoprint or microfilm without written permission from the publisher

# INVESTIGATION OF THE $B^{10}(n, \alpha)Li^7$ REACTION BY THE PHOTOEMULSION METHOD

E. BUJDOSÓ

*Institute of Nuclear Research of the Hungarian Academy of Sciences, Debrecen* †

Received 11 November 1957

**Abstract:** Nuclear emulsion Agfa K3 (loaded with boron) was exposed to slow neutrons. By measuring the range $R(\alpha+Li^7)$, we obtained $Q^* = 2.29 \pm 0.09$ MeV and $Q = 2.76 \pm 0.17$ MeV for the energy of the reaction. The ratio of decays leading to the ground and excited states of the $Li^7$ nucleus is

$$\frac{\sigma[B^{10}(n, \alpha)Li^7]}{\sigma[B^{10}(n, \alpha)Li^{7*}]} = 0.086 \pm 0.009.$$

## 1. Introduction

The excitation energy of the $Li^7$ nucleus is known with an accuracy of a keV [1]. The published values are in good agreement. We cannot say the same of the $Q$ values of the reaction. Values of various authors widely differ [2–21]). This caused us to make new investigations of the $B^{10}(n, \alpha)Li^7$ reaction effected by thermal neutrons, using the nuclear emulsion method. We have determined the $Q$ values of the $B^{10}(n, \alpha)Li^{7*}$, $Li^7$ reactions, as well as the ratio of these transitions.

## 2. Methods of Measurement

We used Agfa K3 emulsion of 100 $\mu$ thickness loaded with boron (natural isotope mixture). The boron concentration of the emulsion was 63 mg/cm$^3$ [22]). The exposure was effected by a 100 mC Ra-Be neutron source in a paraffin block. The distance from the source was 15 cm, the time of exposure 23 hours. The slow neutron flux at the plates was 690 sec$^{-1}$ cm$^{-2}$. The plates were protected from $\gamma$-rays by a lead shield of 7.5 cm thickness.

We used amidol developer for the plates [23]). The tracks were measured with a C. Zeiss LgOG microscope, with a Leitz Ks 100 × objective. The magnification was 1800×. One division of the scale in the ocular corresponded to 0.719 $\mu$. The shrinkage factor was directly determined by measuring the thickness. Its value was $S = 2.73 \pm 0.22$.

We measured the total length of the $\alpha+Li^7$ tracks. The tracks are extremely short, thus in evaluating the results, for the sake of greater accuracy

† Now at the Hungarian Research Institute for Non-Ferrous Metals, Budapest.

we used only those with a dip smaller than $h \leqq 1\mu$ after the usual correction for shrinkage.

Results of our measurements are shown in fig. 1. The area under the curve corresponds to 1 230 tracks measured. Two definite peaks may be

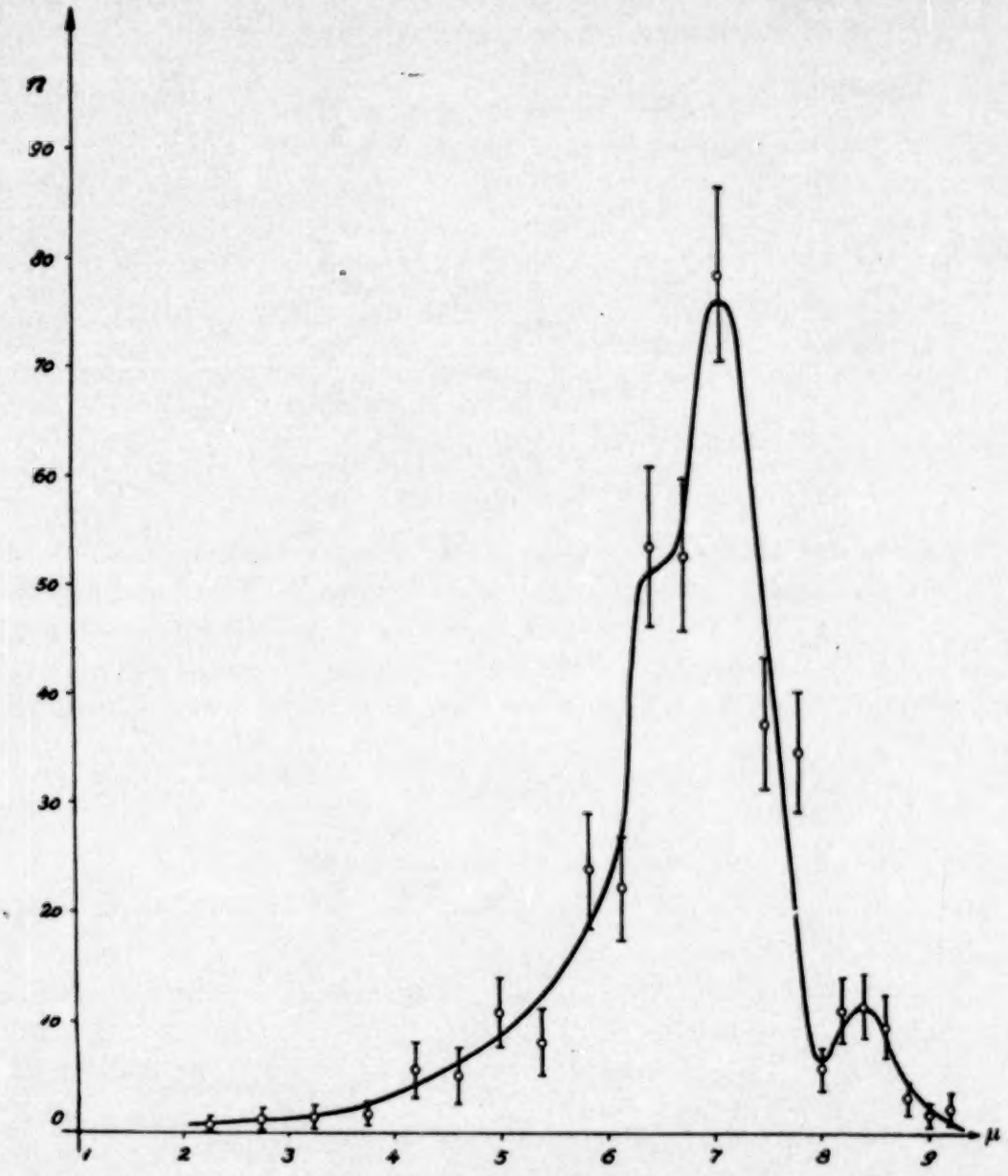


Fig. 1. Distribution of the range of $\alpha+Li^7$ tracks arising from $B^{10}(n, \alpha)Li^7$ reactions.

discerned, corresponding to the excited and the ground states of the $Li^7$ nucleus. The peaks may be found at

$$R(\alpha+Li^7)^* = 7.1\pm0.1\mu$$

$$R(\alpha+Li^7) = 8.4\pm0.3\mu$$

ranges, measured in the emulsion. The errors were determined by calculation.

## 3. Discussion of the results.

In order to determine the energy of the particle in the emulsion, we have to know the range-energy relation. For α-particles in Agfa K2 emulsion K. Lanius [24]) determined the range-energy relation, but we could not use his

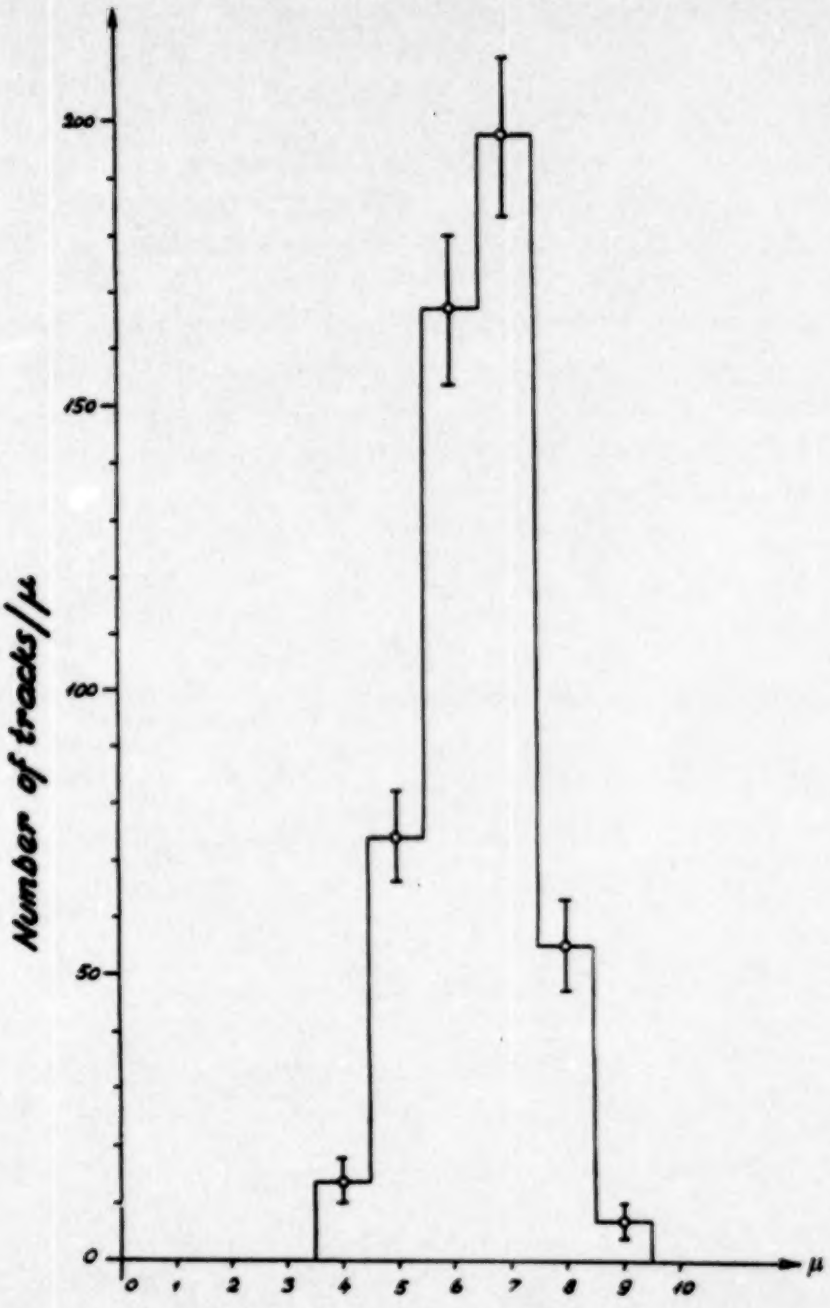


Fig. 2. Distribution of the range of $_{62}Sm^{147}$ α-tracks.

results for low energies, as his curve has no points below 5 MeV, further the stopping power of the K2 emulsion is not the same as that of K3 loaded with boron.

To determine the range-energy relation of our emulsion we used Sm α-particles in our experiments. We loaded the K3 emulsion with samarium nitrate and exposed it for 30 days. Processing and measuring techniques were the same as described above. The results based on measurements of 515 tracks are shown in fig. 2. The $_{62}Sm^{147}$ isotope is an α-emitter [25]), its energy $E_\alpha = 2.12 \pm 0.03$ MeV [26]). For the mean range of α-particles we obtained

$$R_{Sm\alpha} = 6.9 \pm 0.3\mu.$$

This result is in good agreement [27]) with the exact range-energy relation obtained by H. Faraggi for low α-energies [28]). In our investigations we used this relation for Agfa K3 emulsions. It gives somewhat lower values than the range-energy curve for α-particles of the K2 emulsion [24]).

In dealing with reactions of light nuclei, we may not neglect the track of the recoil nucleus. We have to deduct this from the total $R(\alpha+Li^7)$ range. According to Faraggi's measurements $R_{Li^{7*}} = 2.2 \pm 0.2\mu$ and $R_{Li^7} = 2.6 \pm 0.4\mu$. Based on these values, the range for transitions into the excited state is

$$R_\alpha^* = 4.9 \pm 0.2\mu,$$

that for transitions into the ground state

$$R_\alpha = 5.8 \pm 0.4\mu.$$

By using the range-energy relation, we get

$$E_\alpha^* = 1.46 \pm 0.06 \text{ MeV},$$
$$E_\alpha = 1.76 \pm 0.17 \text{ MeV}.$$

The energy released in the $B^{10}(n, \alpha)Li^{7*}$ and $B^{10}(n, \alpha)Li^7$ reactions is given by

$$Q = \frac{11}{7} E_\alpha,$$

which yields

$$Q^* = 2.29 \pm 0.09 \text{ MeV},$$
$$Q = 2.76 \pm 0.17 \text{ MeV}.$$

It follows that the energy of the excited level

$$Q - Q^* = 0.47 \text{ MeV}$$

in good agreement with measurements [1]) for the emitted radiation.

From our measurements we can determine the ratio of α-decays for thermal neutrons leading to the ground or excited state of $Li^7$ nucleus. Besides the $B^{10}(n, \alpha)Li^7$ reaction, slow neutrons effect also $N^{14}(n, p)C^{14}$ reactions in the emulsion. The energy of the ejected proton is $E_p = 0.58$ MeV. Taking into account the recoiling $N^{14}$ nucleus this corresponds to a

track of 6.4 $\mu$ length [28]). If the tracks are so short, we cannot distinguish protons from $\alpha$-particles; we must therefore deduct the number of these tracks from the first maximum (their presence is conspicuous in fig. 1). The relative frequency of the $N^{14}(n, p)C^{14}$ reaction is

$$K = \frac{\sigma_{N^{14}(n, p)} \cdot N_{N^{14}}}{\sigma_{B^{10}(n, \alpha)} \cdot N_{B^{10}}};$$

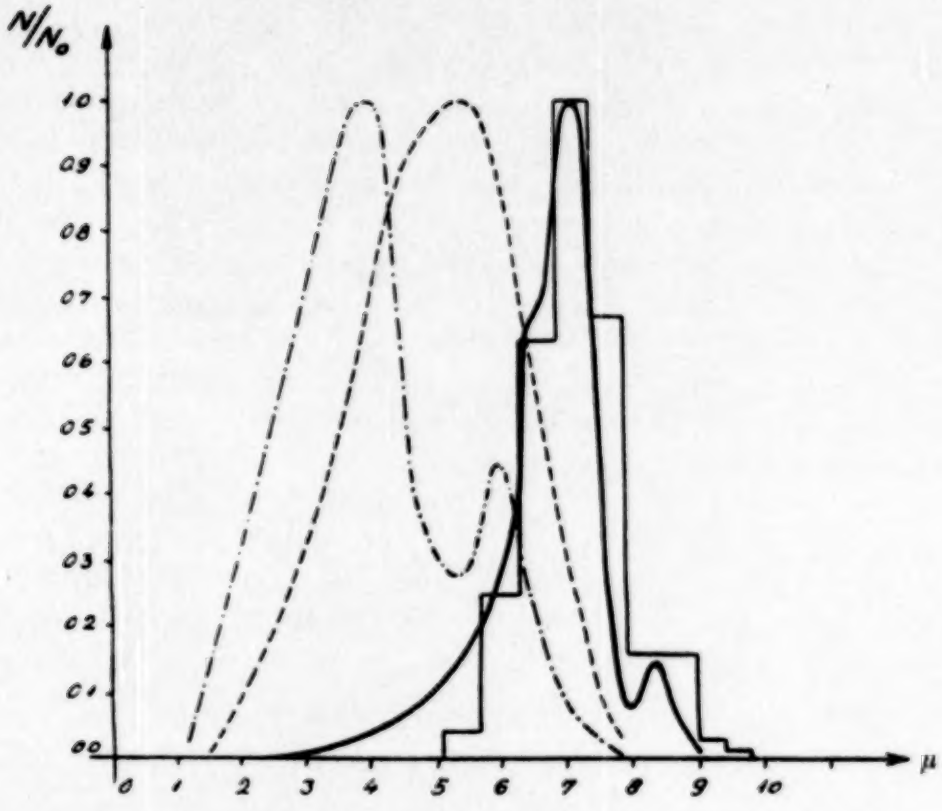


Fig. 3. Comparison of the range distribution given in fig. 1 with some published results.
-·-·-·- Allred, Phillips, Rosen and Tallmadge (1950) [15])
——— Faraggi (1951) [29])
- - - - - Taschaschel and Lohman (1955) [30])
——— Result of the author (1957)

$\sigma_{N^{14}}$ and $\sigma_{B^{10}}$ are the capture cross sections for thermal neutrons, $N_{N^{14}}$ and $N_{B^{10}}$ the numbers of $N^{14}$ and $B^{10}$ atoms per unit volume of the emulsion. Taking $\sigma_{N^{14}} = 1.75$ barn, $\sigma_{B^{10}} = 4010$ barn [29]) and $N_N = 0.07$ g/cm$^3$ [24]), $N_B = 0.063$ g/cm$^3$ [22]), we get $K = 0.46$ %. Taking into account the geometrical correction [27]) we get for the ratio of the cross sections of the two transitions

$$\frac{\sigma[B^{10}(n, \alpha)Li^7]}{\sigma[B^{10}(n, \alpha)Li^{7*}]} = 0.086 \pm 0.009.$$

Thus we conclude that only in $8.6 \pm 0.9$ % of the cases the $Li^7$ nucleus gets into the ground state over the decay of an intermediate $B^{11}$ nucleus.

Our results are in good agreement with those of C. W. Gilbert [10]). Various authors obtained different values for the ratio of decays leading to ground and excited states of the $Li^7$ nucleus. This may be attributed to strong dependence on the energy of bombarding neutrons [20]), further to the fact that irradiation was not always effected with slow neutrons.

Some published results for the range. obtained by the photoemulsion method, are shown in fig. 3. To facilitate the comparison the maxima of measurements are normalized to unity. Tracks of the longer range group differ only by 0.47 MeV energy from the main group. They constitute only a few percent, which makes the measurements more difficult. In demonstrating them we reach the limit of the resolving power of the emulsion technique, as the precision of range measurement is about 4—5 % for such small energies. Results might be expected from further refinement of the emulsion technique. The positions of maxima vary considerably in the results of different authors. This may be explained by the use of different emulsions and probably different procedures. The distribution of the measured ranges coincides very nearly with H. Faraggi's histogram [28]).

I am much indebted to Prof. A. Szalay for the interest he has taken in this work and to Mr. L. Medveczky for his constant help and support, further to Miss F. Jost, Mrs. E. Medveczky and Mrs. I. Perczel for making the microscopic measurements. Special thanks are due to Mr. A. Neszmélyi who exposed the plates and measured the neutron flux.

## References

1) A. B. Brown, C. W. Snyder, W. A. Fowler and C. C. Lauritsen, Phys. Rev. **82** (1951) 159
2) O. Haxel, Zs. f. Physik **104** (1937) 540
3) M. S. Livingston and J. G. Hoffman, Phys. Rev. **53** (1938) 227
4) J. C. Bower, E. Bretscher and C. W. Gilbert, Proc. Camb. Phil. Soc. **34** (1938) 290
5) C. O'Ceallaigh and W. T. Davies, Proc. Roy. Soc. **167** (1938) 81
6) W. Maurer and J. K. Fisk, Zs. f. Physik **112** (1939) 436
7) R. S. Wilson, Proc. Roy. Soc. **177** (1941) 382
8) S. D. Chatterjee, Indian J. Phys. **18** (1944) 269
9) J. K. Bøggild, Mat. Fys. Medd. Dan. Vid. Selsk. **23** (1945) no. 4
10) C. W. Gilbert, Proc. Camb. Phil. Soc. **44** (1948) 447
11) A. Stebler, P. Huber and H. Bichsel, Helv. Phys. Acta **22** (1949) 362
12) C. Y. Chao, C. C. Lauritsen and A. V. Tollestrup, Phys. Rev. **76** (1949) 586
13) W. E. Burcham and J. M. Freeman, Phil. Mag. **41** (1950) 337
14) G. C. Hanna, Phys. Rev. **80** (1950) 530
15) J. C. Allred, A. N. Phillips, L. Rosen and F. K. Tallmadge, Rev. Sci. Instr. **21** (1950) 225
16) H. Fränz and H. Westmeyer, Zs. f. Physik **128** (1950) 617
17) W. P. Jesse, H. Forstat and J. Sadauskis, Phys. Rev. **77** (1950) 782
18) P. Cüer and J. P. Lonchamp, Compt. Rend. **232** (1951) 1824

19) J. Rhodes, W. Franzen and W. E. Stephens, Phys. Rev. **87** (1952) 141
20) H. Bichsel, W. Hälg, P. Huber and A. Stebler, Helv. Phys. Acta **25** (1952) 119
21) V. H. Hauser, Zs. f. Naturforsch. **7a** (1952) 781
22) VEB Agfa Wolfen, private communication
23) E. Bujdosó and L. Medveczky, Acta Physica Hungarica **7** (1957) 135
24) K. Lanius, Eigenschaften einer neuen Kernspur-Emulsion der Agfa K2 Platte (Diplomarbeit Berlin, 1952); Zs. f. wiss. Phot. **48** (1953) 243
25) B. Weaver, Phys. Rev. **80** (1950) 301
26) D. Szteinsznaider, Journ. Phys. Rad. **14** (1953) 465
27) Bujdosó Ernő, Magyar Fizikai Folyóirat, in publication
28) H. Faraggi, Ann. de Phys. **6** (1951) 325
29) D. J. Hughes and J. A. Harvey, Neutron cross sections (McGraw-Hill Book Co. 1955)
30) R. Tzschaschel and W. Lohman, Zs. f. wiss. Phot. **50** (1956) 451

*Nuclear Physics* **6** (1958) 114—124; © *North-Holland Publishing Co., Amsterdam*
Not to be reproduced by photoprint or microfilm without written permission from the publisher

# DECAY INTERACTION OF THE PI-MESON

S. KAMEFUCHI †
*Institute for Theoretical Physics, University, Copenhagen*
and
S. ONEDA ††
*Department of Theoretical Physics, University, Manchester*

Received 5 October 1957

**Abstract:** It is pointed out that the question of the elementarity of the decay interaction of the $\pi$-meson could be settled by considering its radiative decay. For this purpose, the energy spectrum and the angular correlation function of daughter particles are calculated without using any approximation for strong interactions. These functions also serve to determine the concrete form of the decay interaction.

## 1. Introduction

As is well-known, there are two possible ways of explaining the decay of the $\pi$-meson. One way is to assume phenomenologically an elementary interaction linear in $\pi$-meson ($\pi$), $\mu$-meson ($\mu$), and neutrino ($\nu$) field, respectively (I), and the other is to regard the process as a secondary effect of other elementary interactions (II).

From the standpoint (I), $\mu$-capture by nucleons may be interpreted as an indirect effect of the elementary $\pi \to \mu+\nu$ interaction, whereas, from the standpoint (II), the decay of the $\pi$-meson is usually assumed to occur through the intermediary of the weak Fermi type interactions comprising $\mu$ and $\nu$ fields such as, for instance, $\mu^- + \mathrm{P} \to \mathrm{N} + \nu$. The very scarcity of the $\mathrm{e}+\nu$-decay mode of the $\pi$-meson and K-meson would suggest that the weak interactions containing $\mu$, $\nu$ and e, $\nu$ have different properties. Schwinger [1]), for instance, conjectured that the $\mu$, $\nu$ and e, $\nu$ fields will be associated with different types of interactions, the $\mu$-meson being coupled to bosons (such as $\pi \to \mu+\nu$ and $\mathrm{K} \to \mu+\nu$) and the electron to fermions ($\beta$-decay and $\Lambda \to \mathrm{N}+\mathrm{e}+\nu$, etc.).

On the other hand, in the so-called universal Fermi interaction model, the above peculiar behaviour of electron decay might indicate that the coupling types will have certain asymmetries between $\mu$, $\nu$ and e, $\nu$ fields. Therefore, the study of the $\mu$, $\nu$ and e, $\nu$ vertices would be one of the important problems in the present day particle physics.

† On leave of absence from Institute of Theoretical Physics, Nagoya University.
†† On leave of absence from Institute of Theoretical Physics, Kanazawa University.

The purpose of this paper is to suggest a method to settle the choice of the alternatives (I) or (II). We also hope to get some conclusions on the coupling types of $\mu$, $\nu$ fields if the standpoint (II) turned out to be true. We propose to show that information in this respect could be obtained from observing the decay of the $\pi$-meson accompanied by the emission of a gamma-ray †. That is, if only the first alternative (I) is responsible for the decay, then the energy spectrum of the gamma-ray and the angular correlation between decay products would take unique forms. On the contrary, if experiments show a behaviour different from these unique forms, then it would necessarily mean that some contributions come from the second mechanism (II) and that therefore some other particles intervene virtually our decay processes.

Suppose, for the moment, that the latter be the case. Then, we may get some information about the net effect of interactions between ($\mu$, $\nu$) pair fields and those virtual particles which intervene in the process, such as nucleons. On the other hand, detailed information on the interaction $\mu^- + \mathrm{P} \rightarrow \mathrm{N} + \nu$ could be supplied by measuring, say, the angular correlation between the $\mu$-meson spin and the recoil nucleon. Combining these results it might also be possible to know something about the interaction between the $\mu$-meson and other particles than nucleons, such as $\Xi$, which may contribute to the process.

On the contrary, if the mechanism (I) happened, that is, if the $\pi \rightarrow \mu + \nu$ interaction were elementary, then we should have a possibility of describing the $\mu$-capture by nucleons in terms of the secondary effects of the $\pi$-nucleon and $\pi \rightarrow \mu + \nu$ interactions. This could also be checked by observing interaction forms of these capture processes, because in this case the interaction type is restricted to the P(seudo-scalar) type only, while otherwise all the five types of covariance are possible. (The proof of this statement will be given in appendix A.)

In the following all the calculations are made without any approximation for strong interactions, while the lowest-order perturbation method is used for electromagnetic and weak interactions. This seems to be a fairly good approximation.

## 2. Matrix Elements

We shall begin with the general discussion on the second alternative. In our approximation, defined in the previous section, the matrix element for the decay of a $\pi$-meson into a $\mu$-meson, and a neutrino with the emission of a photon comes from processes as shown in fig. 1. The black box contains all the complicated diagrams coming from the strong interactions, while

† The radiative decay of the $\pi$-meson has been discussed by many authors [2, 3, 4].

for the electromagnetic and weak interactions only the lowest-order terms have been retained, in which therefore $\mu$, $\nu$ pairs are emitted at single points.

Now, it is quite easy to write down the possible effective matrix elements from the familiar arguments of relativistic and gauge invariance. For the sake of simplicity, let us consider the rest system of the $\pi$-meson and,

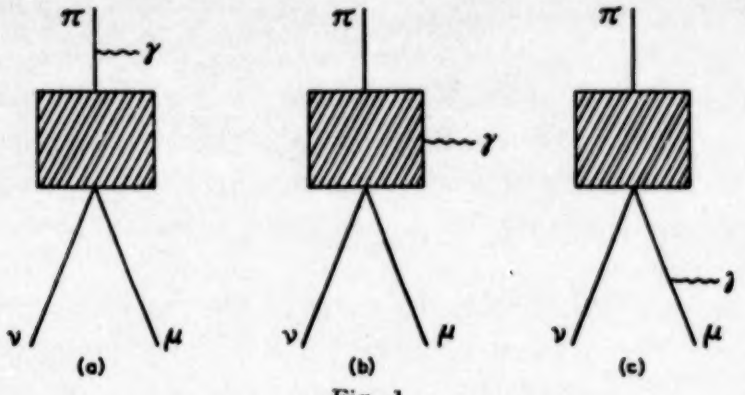


Fig. 1

moreover, choose a special gauge such that $(P\varepsilon) = 0$, where $P_\mu$ and $\varepsilon_\mu$ are the energy momentum 4-vector of the $\pi$-meson and the polarization vector of the photon, respectively, and ( ) means the 4-dimensional scalar product. Then, the contributions from diagram (a) of fig. 1 become zero †.

In the following we shall call the terms S, V, T, A and P, according to their respective covariant forms of the pair of two spinor fields $\psi$ and $\varphi$ of $\mu$-meson and neutrino and denote the matrix elements by $\mathcal{M}_S, \ldots, \mathcal{M}_A$, respectively. Now, we can easily see (i) that $\mathcal{M}_S = 0$, (ii) that $\mathcal{M}_V$ or $\mathcal{M}_T$ comes from the diagram (b) only, (iii) that $\mathcal{M}_P$ from diagram (c) only and (iv) that $\mathcal{M}_A$ from both the diagrams (b) and (c). After some calculations their explicit forms become as follows:

$$
\begin{aligned}
\mathcal{M}_V &= \frac{g_V}{M^3}\bar{\psi}\{(k\gamma)(\varepsilon\gamma)(p\gamma)+(pk)(\varepsilon\gamma)\}\gamma_5\varphi, \\
\mathcal{M}_T &= \frac{2g_T}{M^2}\bar{\psi}(\varepsilon\gamma)(k\gamma)\gamma_5\varphi, + \frac{2g'_T}{M^4}\bar{\psi}(pk)(\varepsilon\gamma)(p\gamma)\gamma_5\varphi, \\
\mathcal{M}_P &= \frac{g_P}{2(qk)}\bar{\psi}\{2(q\varepsilon)+(\varepsilon\gamma)(k\gamma)\}\gamma_5\varphi, \\
\mathcal{M}_A &= \frac{g_A}{M}\bar{\psi}\left\{(\varepsilon\gamma)\left(1+f+\frac{im(k\gamma)}{2(qk)}\right)+\frac{im(q\varepsilon)}{(qk)}\right\}\gamma_5\varphi \text{ ††}.
\end{aligned}
\tag{1}
$$

† Higher-order corrections to the electromagnetic vertex of (a) in fig. 1 merely reduce to the renormalization of electric charge, and the matrix element is always proportional to $(P\varepsilon)$.

†† The use of the condition imposed by gauge invariance does not simplify the term $\mathcal{M}_A$ any more. This is due to the circumstance that, for the general gauge, $\mathcal{M}_A$ involves four undetermined functions in all and the above condition gives merely two independent relations between them.

Here, $k$ and $q$ are the energy-momentum 4-vectors of the photon and the $\mu$-meson and $M$ and $m$ the masses of the $\pi$-meson and the $\mu$-meson, respectively. Among factors $g$'s, which represent the contribution of the black box and have all the same dimension, $g_P$ and $g_A$ are functions of $M$ and masses of possible virtual particles and thus are constant, whereas $g_V$, $g_T$ and $g'_T$ are scalar functions of masses and $(pk)$ or $|k|$. In $\mathcal{M}_A$, $g_A$ and $g_A f$ represent the contributions of the black box corresponding to the diagrams (c) and (b) respectively, and the dimensionless constant $f$ is again a function of masses and $(pk)$. In the above calculations, we have omitted terms which violate parity conservation, because for our present purpose these terms give just the same contributions as the corresponding parity conserving ones.

If our decay process takes place through the mechanism (I), i.e., if the interaction $\pi \to \mu + \nu$ is elementary, then the matrix element becomes just the same as $\mathcal{M}_P$ in (1), but with a numerical factor possibly different from $g_P$. This is evident for the direct $\pi \to \mu + \nu$ interaction and we can show that the gradient interaction also leads to the same result, except for a constant factor, as the direct one (equivalence theorem).

In concluding this section, we wish to add some remarks about restrictions, imposed by charge conjugation and time reversal. In our present case, we are only concerned with the parity conserving terms for the reason already mentioned above; therefore, from the invariance requirement for both transformations we get identical conditions on the functions $g$'s and $f$. These are stated as follows: In general, functions $g$'s and $f$ are divided into two groups, $(g_T, g'_T, g_P)$ and $(g_V, g_A, f)$ and the relative phase between two functions, each belonging to the same (different) group is real (imaginary).

## 3. Angular Correlation and Energy Spectrum

In this section, we give the expressions for angular correlation and energy spectrum of daughter particles. The calculations are straightforwardly carried out in the standard way.

First, let us consider the correlation functions. For the sake of simplicity of calculation, we shall give here the angular correlation between the photon and the neutrino. Since the exact expressions are rather involved and moreover the low-energy region of the photons, like $\approx 5$ MeV, may be preferable for the experiment, we give below the approximate results valid for this energy region (exact expressions will be found in appendix B).

Let $W(x, \theta)\mathrm{d}k\mathrm{d}(\cos\theta)$ be the probability distribution, $\theta$ be the angle between the photon and the neutrino and $x$ and $y$ be the quantities defined in terms of the photon energy $k$, $m$ and $M$ by $x \equiv k/(M-k)$ and $y \equiv m/(M-k)$, respectively. Then, neglecting $x$ as compared with 1,

we obtain the correlation function for a given photon energy

$$F(x,\theta) \equiv (1+x\cos\theta)^2(1+x)W(x,y,\theta)/x(1-x^2-y^2)$$

as follows:

$$F_V(x,\theta) = |g_V|^2 x^2(1-y^2)\left(1-\frac{1-y^2}{2}\sin^2\theta\right),$$

$$F_T(x,\theta) = 4x^2(1-y^2)\{|g_T|^2[(1-y^2)\sin^2\theta+2y^2(1-\cos\theta)]$$
$$+|g'_T|^2[2-(1-y^2)(1+\cos^2\theta)]-\mathrm{Re}\,(g_T g'^*_T)[\sin^2\theta+y^2(1-\cos\theta)^2]\},$$

$$F_P(x,\theta) = |g_P|^2\frac{(1-y^2)^3\sin^2\theta}{2x^2[(1+\cos\theta)+y^2(1-\cos\theta)]^2}, \tag{2}$$

$$F_A(x,\theta) = \frac{|g_A|^2}{|g_P|^2}y^2F_P(x,\theta)+|g_A|^2\frac{1-y^2}{2x^2}\left\{|f|^2x^2[2-(1-y^2)\sin^2\theta]\right.$$
$$\left.-2\,\mathrm{Re}\,(f)\frac{xy^2(1-y^2)\sin^2\theta}{[(1+\cos\theta)+y^2(1-\cos\theta)]}\right\},$$

and the cross terms (henceforth assuming $g'_T = 0$) are given by

$$F_{VT}(x,\theta) = \mathrm{Im}\,(g_V g_T^*)4x^2y(1-y^2)(1-\cos\theta),$$

$$F_{VP}(x,\theta) = -\mathrm{Im}\,(g_V g_P^*)\frac{2xy(1-y^2)}{(1+\cos\theta)+y^2(1-\cos\theta)}(1-\cos\theta),$$

$$F_{TP}(x,\theta) = -\,\mathrm{Re}\,(g_T g_P^*)\frac{2(1-y^2)^2}{(1+\cos\theta)+y^2(1-\cos\theta)}\sin^2\theta,$$

$$F_{VA}(x,\theta) = -2x(1-y^2)\{\mathrm{Re}\,(g_V g_A^*)\frac{y^2(1-\cos\theta)}{(1+\cos\theta)+y^2(1-\cos\theta)} \tag{3}$$
$$+\mathrm{Re}\,[g_V g_A^*(1+f^*)]\cos\theta+\mathrm{Re}\,(g_V g_A^* f^*)x\},$$

$$F_{TA}(x,\theta) = 2y(1-y^2)(1-\cos\theta)\,[\mathrm{Im}\,(g_T g_A^*)\frac{(1-y^2)(1+\cos\theta)}{(1+\cos\theta)+y^2(1-\cos\theta)}$$
$$-2\,\mathrm{Im}\,(g_T g_A^* f^*)x],$$

$$F_{PA}(x,\theta) = -\frac{y(1-y^2)^2\sin^2\theta}{x^2[(1+\cos\theta)+y^2(1-\cos\theta)]}$$
$$\cdot[\mathrm{Im}\,(g_P g_A^*)\frac{1-y^2}{(1+\cos\theta)+y^2(1-\cos\theta)}-\mathrm{Im}\,(g_P g_A^* f^*)x],$$

where we have omitted a common constant factor. It is to be remarked here that, in our approximation, terms such as $fx$ or $(fx)^2$ could usually be neglected except for the peculiar case that the order of magnitude of $f$ itself is exceedingly large as compared with other factors $g$'s, because $f$ is free from the singularity like $1/x$.

We have tentatively put $g'_T = 0$, for otherwise the expressions become too lengthy. The $g'_T$-term, in contrast to the others, does not appear in

the lowest order approximation of $\mathcal{M}_T$ in the case of the usual pseudo-scaler interaction of pion and nucleon. On the other hand, it appears in the case of pseudo-vector interaction, which, however, is not renormalizable. Calculationc of cross terms comprising $g'_T$ can be carried out in the same manner as for the others. The behaviour of the photon energy spectrum $W'_{T'}(k)$ due to $g'_T$ is similar to those of $W_V(k)$ and $W_T(k)$ below.

If we require the $S$-matrix to be invariant under charge conjugation and time reversal, then we must take, say, $g_V$, $g_A$ and $f$ as real and $g_T$, $g'_T$ and $g_P$ as imaginary, respectively. Therefore, even if we add the above restrictions, all the cross terms still survive.

In order to obtain the energy spectrum of the photon we have only to integrate over the angle $\theta$ the expression given by (B1) and (B2). Results thus obtained are rather lengthy and here we give the pure coupling terms only. Apart from a common constant factor they read as follows:

$$\begin{aligned}
W_V(k)\mathrm{d}k &= \frac{2|g_V|^2}{3} I_1 \,\mathrm{d}k, \\
W_T(k)\mathrm{d}k &= \frac{16|g_T|^2}{3} I_2 \,\mathrm{d}k, \\
W_P(k)\mathrm{d}k &= |g_P|^2 I_3 \,\mathrm{d}k, \\
W_A(k)\mathrm{d}k &= |g_A|^2 \left[\frac{y^2}{(1+x)^2} I_3 + \frac{2|f'|^2}{3} I_2 - 2\,\mathrm{Re}\,(f') I_4\right] \mathrm{d}k,
\end{aligned} \tag{4}$$

where

$$\begin{aligned}
I_1 &\equiv \frac{x^3(1-x^2-y^2)^2(2-2x^2+y^2)}{(1+x)^7(1-x)^2}, \\
I_2 &\equiv \frac{x^3(1-x^2-y^2)(1-x^2+2y^2)}{(1+x)^6(1-x)^3}, \\
I_3 &\equiv \frac{1}{x(1+x)^3}\left\{\frac{2(1-x^2-y^2)[(1-x)y^2-(1+x)]}{1-x}\right. \\
&\qquad \left. +[(1+x^2)(1+x)^2+2x(1+x)y^2-y^4]\log\frac{1-x^2}{y^2}\right\}, \\
I_4 &\equiv \frac{xy^2}{(1+x)^5}\left[\frac{(1-x^2-y^2)(1-2x-3x^2+y^2)}{1-x^2} - 2(y^2-x-x^2)\log\frac{1-x^2}{y^2}\right].
\end{aligned} \tag{5}$$

Here, we have introduced a new function $f'$, and between $f$ and $f'$ there exists a relation which is required from the gauge invariance, that is, $1+f = f'k/M$.

As already mentioned in the previous section, $g_T$, $g_V$ and $f$ (or $f'$) are still functions of $k$; thus, among the above results, $W_P$ alone gives the explicit final expression for the energy spectrum. The only point we can

definitely say about the behaviour of $g_T$, $g_V$ and $f$ is that they must be regular throughout our energy region including zero energy.

## 4. Discussion

From the theoretical viewpoint it may be desirable first to measure the energy spectrum of the photon (or of the $\mu$-meson). Although we do not know the detailed properties of functions $g_V$, $g_T$ and $f'$ which appear in (4) and (5), we can derive at least the following conclusions concerning the energy spectrum: (i) In the case of the elementary $\pi \to \mu + \nu$ interaction (I) or of the P-type term of the mechanism (II), the energy spectrum is just given by $I_3$, because of $g_P$ being constant; (ii) The spectral functions $I_1$ and $I_2$ for the V- and T-type terms vanish at both zero and the maximum energies, since $g_V$ and $g_T$ must not be singular at these points; (iii) The function $I_4$ appearing in the A-type term vanishes at the maximum energy, whereas it only vanishes at zero energy when the function $f'$ is regular there; (iv) The energy spectrum must necessarily contain the function $I_3$, which shows the infra-red behaviour. This is because at least one of the elementary $\pi \to \mu + \nu$ interaction (I), the P- and A-type term of (II) must exist to allow the usual non-radiative decay.

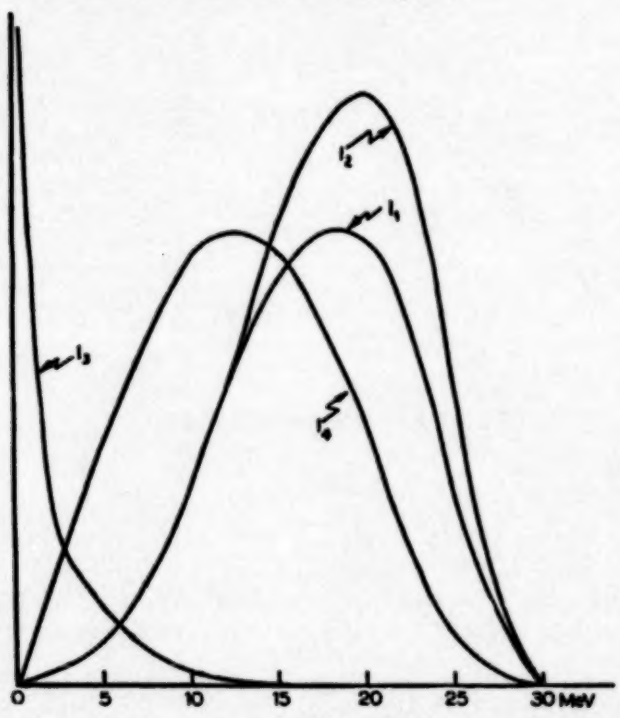


Fig. 2

In fig. 2 we present graphs of the functions $I$'s (in arbitrary scale). If it is justified to regard the functions $g_V$, $g_T$ and $f$ (or $f'$) as constant throughout our energy region, then these curves will directly give the information about the spectrum.

In connection with the energy spectrum it is most interesting to see whether the spectrum experimentally obtained deviates from the curve $I_3$ or not. This is so because the deviation, if any, will necessarily mean that it comes from the mechanism (II) and, therefore, that the elementary $\pi \to \mu + \nu$ interaction alone is not sufficient to explain our decay process.

If some deviations really were found experimentally, then more detailed information would be provided by measuring the angular correlation (or the energy correlation) between the photon and the $\mu$-meson. This is due to the fact that in contrast to the energy spectrum we know theoretically unambiguous expressions for the correlation functions and also to the fact that the correlation functions show rather different behaviours according to the coupling types as seen from fig. 3, where we have plotted in an arbitrary

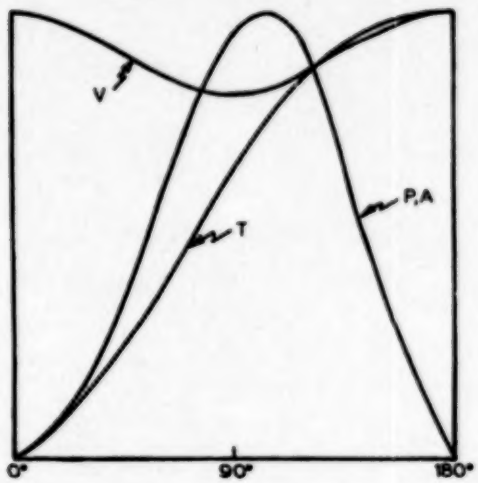


Fig. 3

scale equations (2) valid in the low-energy region (about 5 MeV), assuming that terms like $xf$ and $g'_T$ are negligible. Although we cannot definitely say, at present, at which energy the deviation, if any, would be detectable, it would be expected to appear at 15—20 MeV, provided that $g_V$, $g_T$ and $f'$ are slowly varying functions. In any case, in order to ascertain the existence of V- and T-types terms in addition to A- or P-type terms or both, the correlation experiment would be most effectively carried out at this energy. Thus, the selection of this energy region is hoped to be done in the first place.

We should like to express our thanks to Professor Niels Bohr and the Institute for Theoretical Physics, Copenhagen, for the hospitality extended to us. We are also indebted to Professor L. Rosenfeld and Dr. B. Hyams for stimulating discussions.

## Appendix A

Here, from the assumption that the interaction $\pi \to \mu+\nu$ is elementary we shall derive the general form of interaction for the $\mu$-capture by nucleons. In this case the process takes place through two stages as shown in fig. 4. The main contributions to the black box come from the strong interactions which are invariant under space reflection and also are charge-independent. Thus, the form of the contributions from this part is

$$M_1(\not{p},\ \not{q})\bar{\psi}_{\mathrm{P}}(p)\gamma_5\psi_{\mathrm{N}}(q)\varphi_\pi(p-q), \tag{A1}$$

where $\not{p}_\mu$ and $\not{q}_\mu$ are energy-momentum 4-vectors of proton and neutron,

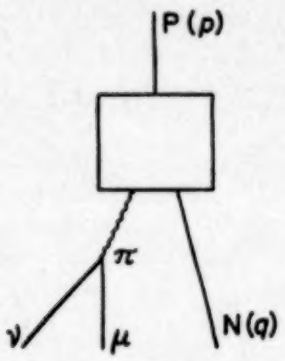


Fig. 4

respectively, and $M(\not{p}, \not{q})$ is a scalar function of $p^2 = -M_{\mathrm{P}}{}^2$, $q^2 = -M_{\mathrm{N}}{}^2$ and $\not{p}_\mu \not{q}_\mu$.

It should be noted that the contributions like $\mathrm{K} \to \mu+\nu$ are completely negligible, because we cannot have strong interactions of the form $\mathrm{P} \to \mathrm{N}+\mathrm{K}$, etc., and only bosons which have strangeness quantum number zero can contribute to our process.

Now, within the framework of the local theory, the possible elementary interactions leading to $\pi \to \mu+\nu$ are given by

$$g\bar{\psi}(1+a\gamma_5)\varphi\phi_\pi, \tag{A2}$$

$$g'\bar{\psi}(1+a\gamma_5)\gamma_\alpha\varphi\partial_\alpha\phi_\pi, \tag{A3}$$

where we have included terms of parity violation. Since in our aproximation we have only to consider the first-order term as regards this interaction, we can always reduce the interaction form (A3) to (A2) by using equations of motion for the $\mu$-meson and neutrino. Therefore, the general form of the interaction $\mu^-+\mathrm{P} \to \mathrm{N}+\nu$ reduces simply to

$$M_2(\not{p},\ \not{q})\bar{\psi}(1+a\gamma_5)\varphi\bar{\psi}_{\mathrm{P}}\gamma_5\psi_{\mathrm{N}}. \tag{A4}$$

Here, $\not{p}\not{q} = -M_{\mathrm{P}}E_{\mathrm{N}}$, with neutron energy $E_{\mathrm{N}}$ (in the rest system of the proton). In the case of $\mu^-+\mathrm{P} \to \mathrm{N}+\nu$, the recoil kinetic energy of neutrons

is only 6 MeV and we may thus put $(pq) = -M_P N_N = \text{const}$. Hence, in effect, (A4) can be regarded as a local interaction of the form

$$f\bar{\psi}(1+a\gamma_5)\varphi \cdot \bar{\psi}_P \gamma_5 \psi_N . \tag{A5}$$

On the contrary, if the process $\mu^- + P \to N + \nu$ is a direct Fermi interaction, then it could have, in principle, the usual five covariant forms $\psi(1+a\gamma_5)O_j\varphi \cdot \bar{\psi}_P O_j \cdot \psi_N$ with $O_j$ $(j = 1, \ldots, 5)$. Thus, if we could find other covariances than (A5), this would give us the proof of the existence of the direct Fermi interaction.

## Appendix B

Exact expressions for the correlation functions $F(x, \theta)$ defined in § 3 are as follows:

$$F_V(x, \theta) = |g_V|^2 \frac{x^2(1-x^2-y^2)}{(1+x)^4(1+x\cos\theta)}\left[(1+x\cos\theta) - \frac{1-x^2-y^2}{2(1+x\cos\theta)}\sin^2\theta\right],$$

$$\begin{aligned} F_T(x,\theta) = \frac{4x^2(1-x^2-y^2)}{(1+x)^4(1+x\cos\theta)^2}\{&|g_T|^2(1-\cos\theta)[(1+x)^2(1+\cos\theta)+y^2(1-\cos\theta)] \\ &+ |g'_T|^2[2(1-x^2\cos^2\theta)-(1-x^2-y^2)(1+\cos^2\theta)] \\ &+ \mathrm{Re}\,(g_T g'^*_T)(1-\cos\theta)[(1-x^2-y^2)(1-\cos\theta)-2(1+x)(1+x\cos\theta)]\}, \end{aligned}$$

$$\begin{aligned} F_P(x, \theta) = |g_P|^2 &\frac{(1-x^2-y^2)(1-\cos\theta)}{x^2[(1+x)^2(1+\cos\theta)+y^2(1-\cos\theta)]^2} \\ &\cdot\left[\frac{(1+x)^2(1+x^2-y^2)-y^2(1-x^2-y^2)}{2}(1+\cos\theta)+x^2\,y^2(1-\cos\theta)\right], \end{aligned} \tag{B1}$$

$$\begin{aligned} F_A(x, \theta) = \frac{|g_A|^2}{|g_P|^2}\frac{y^2}{(1+x)^2}F_P(x, \theta) + |g_A|^2 &\frac{(1-x^2-y^2)}{2(1+x)^2(1+x\cos\theta)} \\ &\cdot\{-|1+f|^2\left[\frac{1-x^2-y^2}{1+x\cos\theta}\sin^2\theta - 2(1+x\cos\theta)\right] \\ &-2[1+\mathrm{Re}\,(f)]\frac{y^2(1-\cos\theta)}{x[(1+x)^2(1+\cos\theta)+y^2(1-\cos\theta)]} \\ &\cdot[(1-x^2-y^2)(1+\cos\theta)+2x(1+x\cos\theta)]\}, \end{aligned}$$

and the cross terms (for $g'_T = 0$) are

$$F_{VT}(x, \theta) = \mathrm{Im}\,(g_V g_T^*)\frac{4x^2\,y(1-x^2-y^2)}{(1+x)^4(1+x\cos\theta)}(1-\cos\theta),$$

$$F_{VP}(x, \theta) = -\mathrm{Im}\,(g_V g_P^*)\frac{2xy(1-x^2-y^2)}{(1+x)^2[(1+x)^2(1+\cos\theta)+y^2(1-\cos\theta)]}(1-\cos\theta),$$

$$F_{TP}(x,\theta)=-\operatorname{Re}(g_T g_P^*)\frac{2(1-x^2-y^2)}{(1+x)^2[(1+x)^2(1+\cos\theta)+y^2(1-\cos\theta)]}$$
$$\cdot\frac{1-\cos\theta}{1+x\cos\theta}\{[(1+x)^3-y^2(1+x)](1+\cos\theta)+2xy^2(1-\cos\theta)\}, \tag{B2}$$

$$F_{VA}(x,\theta)=-\frac{2x(1-x^2-y^2)}{(1+x)^3(1+x\cos\theta)}\{\operatorname{Re}(g_V g_A^*)\frac{y^2(1-\cos\theta)(1+x\cos\theta)}{(1+x)^2(1+\cos\theta)+y^2(1-\cos\theta)}$$
$$+\operatorname{Re}[g_V g_A^*(1+f^*)](x+\cos\theta)\},$$

$$F_{TA}(x,\theta)=\frac{2y(1-x^2-y^2)(1-\cos\theta)}{(1+x)^3(1+x\cos\theta)}$$
$$\cdot\left[\operatorname{Im}(g_T g_A^*)\frac{(1+x)(1-x^2-y^2)(1+\cos\theta)}{(1+x)^2(1+\cos\theta)+y^2(1-\cos\theta)}-2\operatorname{Im}(g_T g_A^* f^*)x\right],$$

$$F_{PA}(x,\theta)=-\frac{y(1-x^2-y^2)(1-\cos\theta)}{x(1+x)(1+x\cos\theta)[(1+x)^2(1+\cos\theta)+y^2(1-\cos\theta)]} \tag{B2}$$
$$\cdot\{\operatorname{Im}(g_P g_A^*)\frac{(1-x^2-y^2)^2(1+x)(1+\cos\theta)}{x[(1+x)^2(1+\cos\theta)+y^2(1-\cos\theta)]}$$
$$-\operatorname{Im}(g_P g_A^* f^*)[2x+(1-y^2)(1+\cos\theta)-x^2(1-\cos\theta)]\}.$$

## References

1) J. Schwinger, Phys. Rev. **104** (1956) 1164
2) H. Primakoff, Phys. Rev. **84** (1951) 1255
3) T. Eguchi, Phys. Rev. **85** (1952) 943
4) T. Nakano, J. Nishimura and Y. Yamaguchi, Prog. Theor. Phys. **6** (1952) 1028

*Nuclear Physics* **6** (1958) 125—131; © *North-Holland Publishing Co., Amsterdam*
Not to be reproduced by photoprint or microfilm without written permission from the publisher

# THE CIRCULAR POLARIZATION OF INTERNAL AND EXTERNAL BREMSSTRAHLUNG

H. SCHOPPER † and S. GALSTER
*Physikalisches Institut, Universität Erlangen, Germany*

Received 20 January 1958

**Abstract:** The circular polarization of internal and external bremsstrahlung was measured as a function of photon energy for the decay of $Sr^{90}+Y^{90}$. The experimental results are in general agreement with theoretical predictions assuming maximum violation of parity and ST- or VA-interaction.

## 1. Introduction

The suggestion of Lee and Yang [1]) that parity is not conserved in weak interactions has been verified by several experiments [2–5]). One of the consequences of non-conservation of parity is the longitudinal polarization of $\beta$-particles. These $\beta$-particles give rise to a circularly polarized *external* bremsstrahlung. This has been confirmed by Goldhaber *et al.* [6]), Boehm and Wapstra [7]) and Cohen *et al.* [8]). From the measurement of the circular polarization of the external bremsstrahlung the same information about the $\beta$-interaction can be obtained as from a direct determination of the electron polarization. But also the *internal* bremsstrahlung accompanying the emission of $\beta$-particles is expected to be circularly polarized if parity is not conserved ††. While the experiments reported here were under way more detailed calculations were published by Ford [9]), Cutkosky [10]) and Pytte [11]). The circular polarization of internal bremsstrahlung experimentally determined as a function of photon energy is in general agreement with these calculations assuming ST- or VA-interaction and maximum violation of parity conservation and with the measurements of electron polarization †††.

## 2. Experimental procedures

The circular polarization of $\gamma$-rays can be detected by Compton-scattering with oriented electrons available in magnetized iron [12]). If the $\gamma$-radiation is circularly polarized the number of scattered quanta changes on reversing the magnetization. As the bremsstrahlung yield is low a scattering magnet as shown in fig. 1 was used instead of a cylindrical one [5, 7]). The cross section

† Now at the Institut für Kernphysik, Universität Mainz.

†† The suggestion for such an experiment arose in a discussion between L. Spruch and one of the authors (H.S.).

††† Preliminary results were communicated at the International Conference on Nuclear Structure, Rehovoth, September 1957.

of the magnet is an approximation to a semicircular shape giving roughly the same scattering angle ($\theta \approx 59°-67°$) for all directions of incident $\gamma$-rays. In this way it is possible to use a large solid angle without being too far off the optimal scattering angle.

The direct radiation was absorbed by a lead absorber. The scattered quanta were detected by a NaI(Tl)-scintillation crystal which was surrounded by lead in order to reduce the background. The output of the multiplier was fed into a single channel pulse height discriminator permitting the selection of different photon energies. In order to reduce the influence of the magnetic stray field on the multiplier a mu-metal shield and a compensation coil was used. The current in the compensation coil was reversed together with the magnet current. The change of the counting rate due to the stray field was smaller than 0.2 %. The counting time for a preset number of counts could be printed and a great part of the measurements was registered automatically reversing the magnetization approximately every 3 minutes. If we define $N_+$ as the counting rate with the magnetization pointing toward the source and $N_-$ as the counting rate with the opposite magnetization we can compute the polarization effect $E = 2(N_+-N_-)/(N_++N_--2N_0)$ where the background $N_0$ has been taken into account. $N_0$ was determined experimentally and includes the quanta penetrating the central lead absorber. For 100 % circularly polarized photons $E$ was computed as a function of photon energy from the known Compton cross sections, the magnet geometry and the fraction of oriented electrons per iron atom at saturation ($\approx 8$ %). The results are the broken curves in figs. 3 and 4. Details of these calculations will be published elsewhere [16]). The $Sr^{90}+Y^{90}$-source used in these measurements was spread on a plastic foil ($\approx 1$ mg/cm$^2$). The source thickness was approximately 1 mg/cm$^2$, the source strength about 5 mC.

## 3. The Intensity of Internal and External Bremsstrahlung

An absorber must be placed between source and scattering magnet in order to prevent the $\beta$-particles to be stopped in the magnet. There they would produce bremsstrahlung which could get into the counter without being scattered on magnetized iron. By using absorbers with different $Z$ the ratio of the intensities of internal (IB) and external bremsstrahlung (EB) can be changed as the production of EB is roughly proportional to $Z$ whereas the intensity of IB is constant. In order to measure the circular polarization of IB a paraffin absorber was used (see fig. 1). For the investigation of the EB an additional lead absorber (not shown in fig. 1) was placed between source and paraffin absorber.

However, even for this low (resp. high) value of $Z$ there is still some

contamination of EB (resp. IB). In order to determine its magnitude a method first described by Wu [13]) can be used. In fig. 2 the measured in-

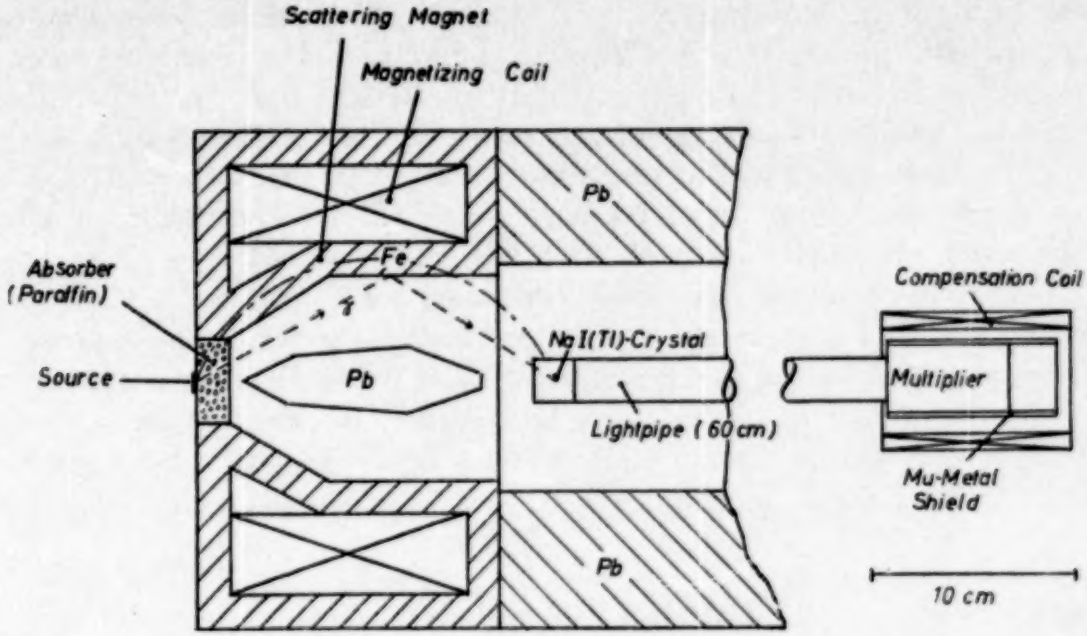


Fig. 1. Scheme of the experimental arrangement for the measurement of the circular polarization of external and internal bremsstrahlung.

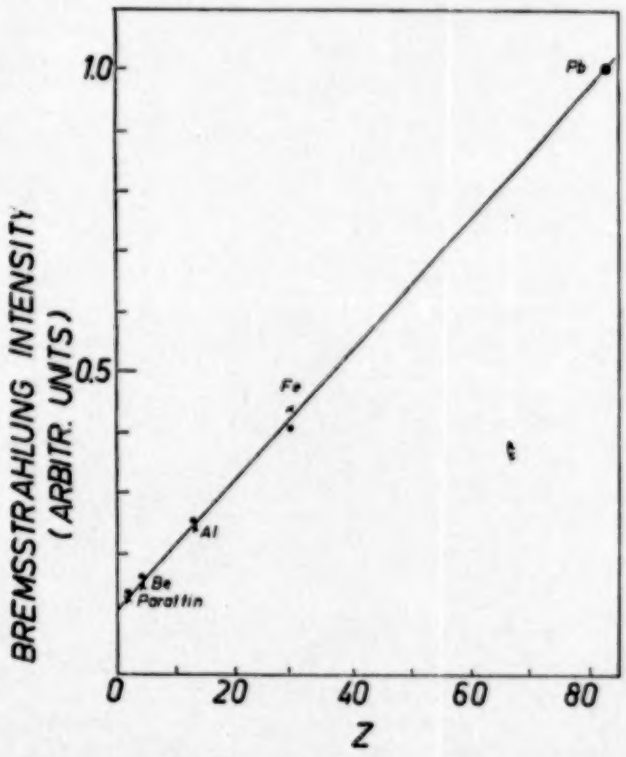


Fig. 2. Total intensity of EB and IB (background subtracted) as a function of the nuclear charge $Z$ of the absorber. The radiation at $Z = 0$ is due to IB alone. Measurements for photon energies between 0.6 to 1 MeV (×) and for 1 to 1.4 MeV (○) (normalized at $Z = 82$).

tensity of bremsstrahlung excited in different absorbers thick enough to stop all $\beta$-particles is plotted as a function of $Z$. It is easy to extrapolate this nearly linear function down to $Z = 0$. The radiation (background subtracted) still present at $Z = 0$ gives the intensity of IB. (The EB excited in the source itself can be neglected.) It can be seen that with a paraffin absorber one gets a mixture of approximately 80 % IB and 20 % EB. On the other hand, with a lead absorber one has about 90 % EB and 10 % IB. The percentage of IB in this case will even be smaller as the absorption of the photons in the lead has been neglected.

Such measurements have been performed for two ranges of photon energies. If they are normalized at $Z = 82$ there is practically no difference. This is to be expected as the shapes of the EB and IB spectra are very similar [14]). From fig. 2 it may also be seen that the absolute intensity of IB is much lower than that of EB. All these results are in good agreement with theoretical estimates.

## 4. Results and discussion

The circular polarization of EB and IB was measured for $Sr^{90}+Y^{90}$ as a function of photon energy. To check the experimental set-up a few measure-

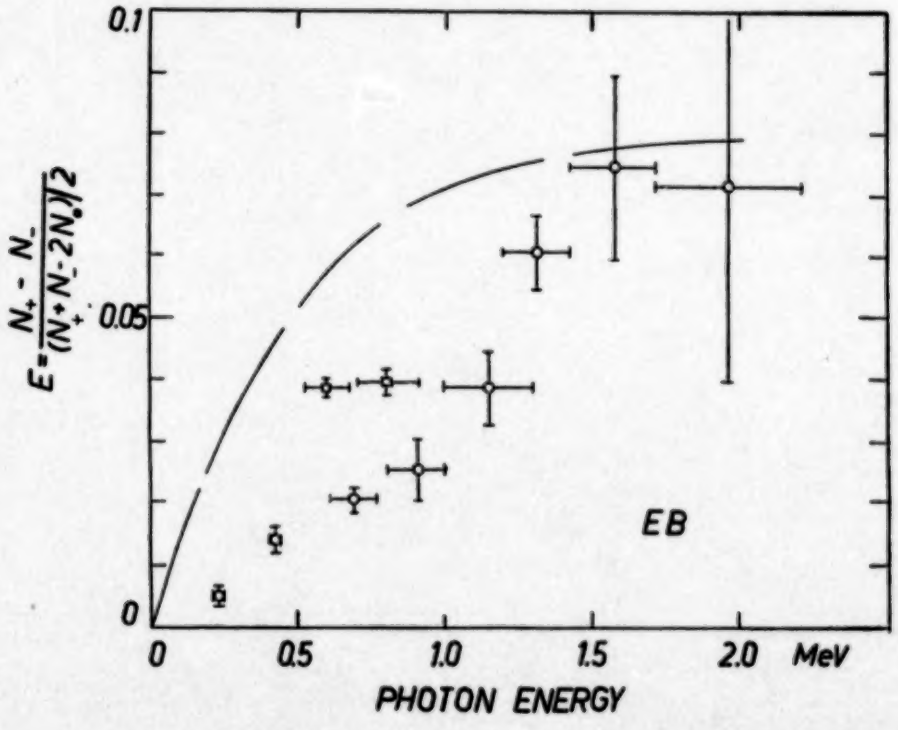


Fig. 3. External bremsstrahlung: Experimental results for $E$ for $Sr^{90}+Y^{90}$ (○) and $Tm^{170}$ (□). The vertical bars indicate the statistical errors, the horizontal bars the position of the discriminator window. The broken line is the calculated magnet response for 100 % circular polarization.

ments of the circular polarization of EB were performed with thick $Tm^{170}$ and $Tl^{204}$ sources.

The results for EB are plotted in fig. 3 and for IB in fig. 4. In both cases the polarization is small at low energies and approaches 100 % at high energies. The vertical bars give the mean statistical errors and the horizontal bars indicate the position and width of the discriminator window. No

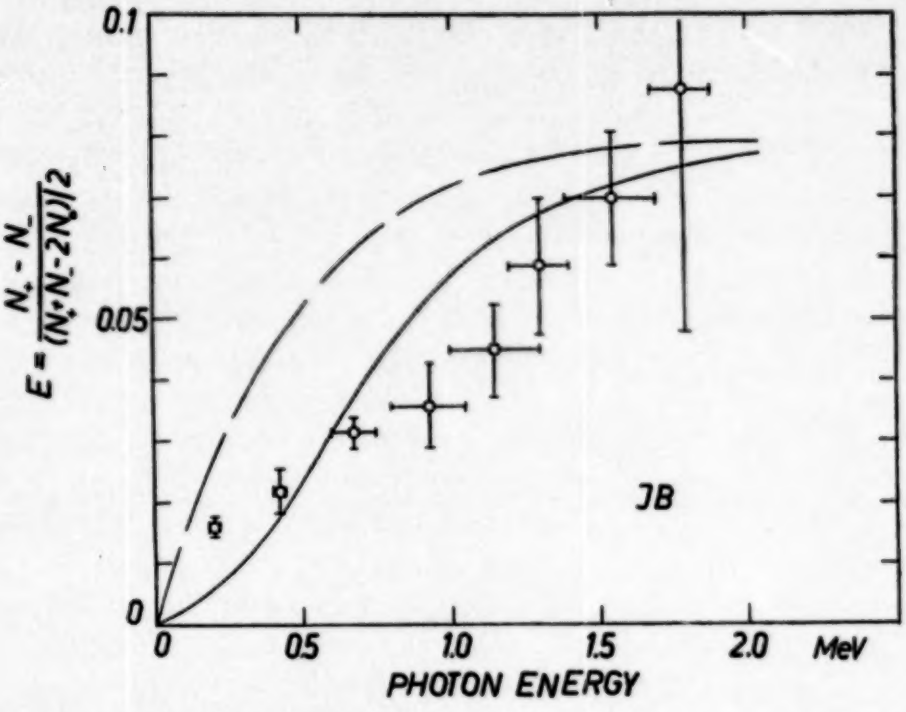


Fig. 4. Internal bremsstrahlung: Experimental values of $E$ for $Sr^{90}+Y^{90}$ and the theoretical prediction according to Ford [9]) (full line). Further explanations see fig. 3.

corrections were made for the admixture of IB in the case of EB and vice versa. As these admixtures are small (see section 3) and the polarizations are very similar these corrections are much smaller than the statistical errors.

The results for EB are in agreement with previous measurements [6, 7, 8]). However, a detailed comparison with theory is very complicated. The circular polarization of EB excited by completely polarized monoenergetic electrons in a thin target was calculated by McVoy [15])†. In order to apply these calculations to $\beta$-decay one has to average over the $\beta$-spectrum taking into account the energy dependence of bremsstrahlung yield and of the longitudinal polarization of the $\beta$-particles. Furthermore one has to integrate over the penetration depth of the electrons in the thick target.

† Only the case of exact forward emission was considered. Racah, at the International Conference on Nuclear Structure at Rehovoth, pointed out that this case might not be representative.

Also the scattering of the electrons before the emission of EB may be of some influence †. Such calculations have not yet been performed. However, the qualitative behaviour of the circular polarization of EB is that to be expected. Especially from the fact that the circular polarization is nearly complete for high quantum energies it can be inferred that the electron polarization is close to $v/c$ in agreement with direct measurements.

In the case of IB comparison between experiment and theory is much easier. Ford [9]) and Pytte [11]) have computed the circular polarization for different photon energies for allowed decays (integrated over the spectrum). $Sr^{90}$ and $Y^{90}$ are, however, unique first forbidden transitions. On the other hand the process of IB production seems to be very insensitive to the type of $\beta$-transition. Neither the total yield and the spectral shape nor the angular correlation show a pronounced dependence of the degree of forbiddenness. Therefore it was thought that the experimental results obtained with $Sr^{90}+Y^{90}$ could be compared with the calculations for allowed transitions. The polarization $P$ was computed using the formula of Ford [9]) with $W_0 = 5.3$ and $b = 0$, $d = -1$. The full line in fig. 4 was obtained by multiplying $P$ with the magnet response for 100 % polarization (broken line). The agreement between experiment and theory seems to be satisfactory ††, thus proving the assumption of maximum parity violation and ST- or VA-interaction.

It is to be expected that also the inner bremsstrahlung accompanying K-capture is circularly polarized. One could think that the detection of this polarization should even be easier as there are no electrons producing unwanted EB. However, the yield of IB following K-capture is still lower ($\lesssim 10^{-4}$ $\gamma$ per $\beta$) and therefore even small contaminations of the source mask the effect. Preliminary measurements with a $Cr^{51}$-source gave at first an effect which disappeared after two months. This is proably due to a small contamination with a long half life. An indication of such a contamination was indeed found in the $\gamma$-spectrum. The sign of this polarization was opposite to that found for the IB following $\beta$-decay in agreement with the theoretical prediction [10]). No quantitative results can yet be presented owing to the above mentioned contamination. Experiments with better sources in are preparation.

The authors are indebted to Prof. Fleischmann for his continued interest. We would like to thank Mr. G. Hartwig for his assistance in some of the

† These effects also permit to explain the difference between the $Sr^{90}+Y^{90}$ and the $Tm^{99}$ measurements.

†† No corrections for the Compton-recoil electrons in the NaI-crystal were made. This might explain that the polarization for low photon energies is somewhat too high, as owing to this effect quanta with higher energies, and therefore higher polarization as well, are registered as low energy photons.

computations and measurements. This work was supported by the Deutsche Forschungsgemeinschaft. Finally we are obliged to the firm Frieseke und Hoepfner G.m.b.H., Erlangen for lending us radioactive sources and electronic equipment.

## References

1) T. D. Lee and C. N. Yang, Phys. Rev. **104** (1956) 254
2) C. S. Wu, E. Ambler, R. W. Hayward, D. D. Hoppes and R. P. Hudson, Phys. Rev. **105** (1957) 1413
3) R. L. Garwin, L. M. Lederman and U. M. Weinrich, Phys. Rev. **105** (1957) 1415
4) H. Frauenfelder, R. Bobone, E. von Goerler, N. Levine, H. R. Lewis, R. N. Peacock, A. Rossi and G. de Pasquali, Phys. Rev. **106** (1957) 386
5) H. Schopper, Phil. Mag. **2** (1957) 710
6) M. Goldhaber, L. Grodzins and A. W. Sunyar, Phys. Rev. **106** (1957) 826
7) F. Boehm and A. H. Wapstra, Phys. Rev. **106** (1957) 1364; and preprints
8) S. G. Cohen *et al.*, report at the International Conference on Nuclear Structure, Rehovoth
9) G. W. Ford, Phys. Rev. **107** (1957) 321
10) R. E. Cutkosky, Phys. Rev. **107** (1957) 330
11) A. Pytte, Phys. Rev. **107** (1957) 1681
12) See H. A. Tolhoek, Revs. Mod. Phys. **28** (1956) 277
13) C. S. Wu, Phys. Rev. **59** (1941) 481
14) M. Goodrich, J. S. Levinger and W. Payne, Phys. Rev. **91** (1953) 1225
15) K. W. McVoy, Phys. Rev. **106** (1957) 828 and preprint
16) H. Schopper, Nuclear Instruments, to be published

*Nuclear Physics* **6** (1958) 132—134; © *North-Holland Publishing Co., Amsterdam*
Not to be reproduced by photoprint or microfilm without written permission from the publisher

# BETA-NEUTRINO-GAMMA ANGULAR CORRELATION

M. MORITA†
*Department of Physics, Columbia University, New York*

Received 23 December 1957

There are three important remaining questions on the interactions in beta decay. These questions are:

1. Is the beta interaction of the Fermi transitions S or V? Similarly, is that of the GT-transitions T or A? If there are mixtures, what are the mixing ratios $|C_S|^2/|C_V|^2$ and $|C_T|^2/|C_A|^2$?

2. Are the interactions for negaton decay the same as those for positon decay?

3. Are the coupling constants real? i.e., are beta interactions invariant under time-reversal?

We have deduced the electron-neutrino-gamma angular correlation which may help to answer these questions. This angular correlation is deduced from the combined calculations of the electron-neutrino angular correlation [1]) and the beta-gamma angular correlation [2]). The decay scheme is assumed to be $j(\beta)j_1(\gamma)j_2$. The gamma ray is a mixture of $2^{L_1}$, $2^{L'_1}$, .... If $\mathbf{p}$, $\mathbf{q}$ and $\mathbf{k}$ denote the momenta of the negaton (positon) and antineutrino (neutrino), and the unit vector of the momentum of the gamma ray, respectively, the result for allowed beta transitions is

$$
\begin{aligned}
&W(\mathbf{p},\ \mathbf{q},\ \mathbf{k},\ E)\,\mathrm{d}E\,\mathrm{d}\Omega_e\,\mathrm{d}\Omega_\nu\,\mathrm{d}\Omega_\gamma \\
&\quad = F(Z,\ E)\,pq^2\,E\mathrm{d}E\,\mathrm{d}\Omega_e\,\mathrm{d}\Omega_\nu\,\mathrm{d}\Omega_\gamma \\
&\quad \times \xi\left(\left[1+a\frac{\mathbf{p}\cdot\mathbf{q}}{Eq}+b\frac{m}{E}\right]\left[\sum_{L_1}(j_1\|L_1\|j_2)^2\right]\right. \\
&\quad + \left[-\left(A_1\frac{\mathbf{p}\cdot\mathbf{k}}{E}+B_1\frac{\mathbf{q}\cdot\mathbf{k}}{q}\right)\{12(j_1+1)\}^{-\frac{1}{2}}\{2+j_1(j_1+1)-j(j+1)\}\right. \\
&\quad \left.\left.+\left(A_2\frac{\mathbf{p}\cdot\mathbf{k}}{E}+B_2\frac{\mathbf{q}\cdot\mathbf{k}}{q}+D\frac{\mathbf{p}\cdot(\mathbf{q}\times\mathbf{k})}{Eq}\right)\delta_{j_1 j}(3)^{-\frac{1}{2}}\right]\right. \\
&\quad + P\left[\sum_{L_1,\,L'_1}(-)^{L_1+L'_1}(j_1\|L_1\|j_2)(j_1\|L'_1\|j_2)F_1(L_1L'_1j_2j_1)\right] \\
&\quad + c\left\{3\frac{(\mathbf{p}\cdot\mathbf{k})(\mathbf{q}\cdot\mathbf{k})}{Eq}-\frac{\mathbf{p}\cdot\mathbf{q}}{Eq}\right\}(-)^{j_1-j+1}\{2(2j_1+1)/3\}^{\frac{1}{2}}W(j_1j_1\,11;\ 2j) \\
&\quad \left.\times\left[\sum_{L_1,\,L'_1}(-)^{L_1+L'_1}(j_1\|L_1\|j_2)(j_1\|L'_1\|j_2)F_2(L_1L'_1j_2j_1)\right]\right),
\end{aligned}
\tag{1}
$$

† On leave from Kobayasi Institute of Physical Research, Kokubunzi, Tokyo, Japan. Formerly Fellow of the Nishina Memorial Foundation, Japan, now Ernest Kempton Adams Fellow of the Columbia University.

with the condition $\delta+\delta'+L_1+L'_1 =$ even and

$$F_n(L_1L'_1j_2j_1)$$
$$=(-)^{j_2-j_1+1}\{(2j_1+1)(2L_1+1)(2L'_1+1)\}^{\frac{1}{2}}(L_1L'_11-1|n0)W(j_1j_1L_1L'_1;\ nj_2).$$

Here, $\xi$, $a$, $b$, $c$, $A$, $B$ and $D$ are the symbols defined in ref. [3]), $\Lambda_{J'J}$, $\lambda_{J'J}$ and $\delta_{J'J}\{J/(J+1)\}^{\frac{1}{2}}$ being replaced by unity in our case. The subscripts 1 and 2 of $A$ and $B$ denote the parts of $A$ and $B$ referring to GT-interaction and to cross-product of GT and F-interaction, respectively. $P=+1$ $(-1)$ for a left (right) circulary polarized gamma ray. $\delta=0$ $(+1)$ for magnetic (electric) radiation. $(j_1j_2m_1m_2|jm)$ and $W(abcd;\ ef)$ are the Clebsch-Gordan and Racah coefficients, respectively. $(j_1||L_1||j_2)$ is the nuclear matrix element of the gamma ray.

Now, let us restrict our considerations to the case of the pure GT transitions. In this case, all the experimental data [4]) support the assumption of a linear combination of T and A with $C_T=-C'_T$ and $C_A=C'_A$; but the ratio $|C_T|^2/|C_A|^2$ is not yet known. Now, the terms $a$, $c$ and $B_1$ in eq. (1) have a dependence on $(|C_A|^2-|C_T|^2)$, from which we can determine the value of $|C_T|^2/|C_A|^2$, thus answering question 1. Since this experiment is applicable to both the negaton and positon decays, we also obtain an answer to question 2.

Similarly, we may get knowledge about the Fermi part of the beta interaction by using a $\Delta j=0$ beta transition.

The question of the invariance property of the beta interactions under time-reversal (question 3) will be answered by measuring the term $\mathbf{p}\cdot(\mathbf{q}\times\mathbf{k})$. Only beta decays with $\Delta j=0$ (except $0\to 0$) can be used for this experiment if they are allowed transitions. The measurement of $\mathbf{p}\cdot(\mathbf{q}\times\mathbf{k})$ is rather difficult, because we can only observe the recoil of the nucleus with spin $j_2$ instead of that of the nucleus with spin $j_1$. The observed recoil should thus be corrected for the effect of the gamma ray. Such a correction was once introduced by M. E. Rose [5]) in the case of the beta decay of $O^{14}$.

In the case of K-capture †, the angular correlation of the neutrino and gamma ray is very similar to that of eq. (1). Further investigation of the recoil-gamma correlation is being made ††.

The author would like to express his sincere thanks to Professor C. S. Wu for suggesting this problem, to Professor W. W. Havens, Jr., for his hospitality, and to the Columbia University for a fellowship. He is also deeply indebted to Drs. L. Lidofsky and A. Schwarzschild for valuable discussions.

† Since this work has been completed, a preprint by H. Frauenfelder, J. D. Jackson and H. W. Wyld (to be published) has been brought to our attention, in which the calculation is given for the case of K-capture.

†† *Note added in proof:* We have now [6]) proposed more than 30 different kinds of possible experiments using direct measurement of recoil nucleus and nuclear resonance fluorescence.

## References

1) See e.g. M. Morita, Progr. Theoret. Phys. **9** (1953) 345
2) See e.g. M. Yamada and M. Morita, Progr. Theoret. Phys. **8** (1952) 431
3) J. D. Jackson, S. B. Treiman and H. W. Wyld, Jr., Phys. Rev. **106** (1957) 517; Nuclear Physics **4** (1957) 206
4) C. S. Wu, Proceedings Rehovoth Conference on Nuclear Structure (North Holland Publishing Company, Amsterdam)
5) M. E. Rose, Phys. Rev. **90** (1953) 1123
6) M. Morita, Phys. Rev.

*Nuclear Physics* **6** (1958) 135—136; © *North-Holland Publishing Co., Amsterdam*

# BOOK REVIEWS

G. W. SERIES, *Spectrum of atomic hydrogen* (Oxford University Press 1957. viii-87 pages. 8s.6d. in U.K. only).

This is the second tract of the 'Oxford Library of the Physical Sciences' (cf. this journal **4** (1957) 491), the aim of which is to provide the post-graduate student with a cheap collection of monographs on topical problems of physics. It seems to me that the present essay — in spite of its real merit — does not quite strike the right note. It starts, hopefully, with a broad historical survey of the spectroscopy of atomic hydrogen and ionised helium, which is indeed of great didactic value; but it ends as a rather crowded 'report on recent progress' of the usual type, too sketchy to be really educative for the inexperienced student. The specialist, on the other hand (who will skip the first half of the booklet) will find just this report of help to him as a skilful outline and guide to the bibliography of the subject.

Apart from this unfortunate lack of unity, the exposition is generally clear and competent, though not entirely flawless. The account of the correspondence principle and of the introduction of quantum mechanics shows that the author has not breathed the pure air of the Sound. And it does not help matters to refer the reader, for further details, to the second volume of Whittaker's *History of Aether and Electricity*, which (in sharp contrast to the first volume, a true masterpiece) is about the most uncritical and unbalanced exposition of the growth of modern physics one can find. Likewise, sentences like "The magnetic moment of a free electron has not yet been measured directly", or "A virtual process is one in which energy is not conserved", are calculated to corrupt the youth rather than to enlighten it.

It is a pity that the important correction to the fourth-order term of the anomalous magnetic moment of the electron could not be properly discussed in the text. It is all the more regrettable that the only allusion to it, in a footnote, quotes only Sommerfield's results and ignores the paper by A. Petermann, *Nuclear Physics* **3** (1957) 689, in which attention was first drawn to the error in Karplus and Kroll's pioneering computation of the effect.

This being said, it should be stressed that we have here a monograph which should be specially recommended to the serious student's meditations. It treats a problem of great simplicity, yet involving a number of fundamental points of quantum theory, which it illustrates in a most instructive way. It will invite the student to look back upon the deeplying difficulties which gave rise to the elaboration of quantum theory, and confront him with some of those which are now hampering its further development.

L. R.

A. I. AKHIEZER and V. B. BERESTETSKY, *Quantum electrodynamics* [Moscow 1953] (Consultants Bureau, Inc., New York 1957. 549 pages. $ 35.00)

Those Western physicists who have been wise enough to learn Russian know already that the best textbook on quantum electrodynamics is the one which is now made accessible to all by an English translation. This book bears the distinctive mark of the Landau school, and derives a special interest from the fact that Prof. Akhiezer, as a long-standing authority on the subject, is able to place the new methods of invariant formulation in their true perspective, without neglecting the valuable aspects of older work. One might say that the treatise under review combines the outstanding qualities of Heitler's *Theory of radiation* and Jauch and Rohrlich's *Theory of photons and electrons*, with the advantage of a more unified and better balanced exposition. Moreover, it gives a fuller treatment of the most important applications than is found in the other textbooks of similar scope: in particular, the discussion of multipole radiation and internal conversion is carried out in considerable detail, and

includes the consideration of nuclear size effects. A welcome feature is the incorporation into the text of the methods and results developed by Russian physicists (among whom the authors are prominent in this field), which are still much too neglected in the West.

The treatise of Akhiezer and Berestetsky is widely used in the Soviet Union as an advanced textbook, and there is no reason why (apart from its value as a reference work) it should not be adopted for the same purpose in the West. This brings me to the examination of the way in which it is presented to the Western reader. The translation is very competently done, although it lacks some minor refinements: for instance, it is ridiculous to quote such classics as Mott and Massey as edited by the 'Foreign Literature Press'; on the other hand, references to Russian textbooks, like Blokhintzev's *Quantum Mechanics*, are of little help to the Western student, and ought to be replaced by references to equivalent textbooks current in the West. Then, the Russians are unfortunately still using the clumsy German notation in vector analysis, which is now generally abandoned in favour of the system due to Gibbs: the translator, while lavishly indulging in the bad habits of American physicists in the way of terminology and notation ('electron-positron', 'quantum mechanical', Mev instead of MeV), has been too timid, apparently, to avail himself of the one American contribution to the improvement of usage in this respect.

More serious, however, are the drawbacks of the publication form adopted for this translation. It is not printed, but typewritten, and looks like a very bulky preprint, within flimsy paper covers. The typing is well-done, and even the complicated formulae are quite legible; but for some reason different types are used for the same symbols in the text and in the displayed formulae (e.g. $\underline{k}$ and $k$), which does not make for clarity. Obviously, this kind of thing is not good enough for a textbook of this importance, and the price charged by the translators for their "service" will in any case put the book out of the reach of those who need it most. It would be unduly harsh, nevertheless, to heap reproach upon the firm responsible for producing the translation. They rather deserve congratulations for their enterprising spirit, the judicious choice of the book to translate and the care and competence with which the translation has been executed. But, one may well ask, why on earth not print the translation as a fine, neatly bound book and sell it for a small fraction of present price?

L. R.

D. J. DePaul (editor), *Corrosion and wear handbook for water-cooled reactors* (McGraw-Hill Book Company, New York, Toronto, London, 1957. ix—293 pages. $ 6, 45 s.).

The central section of this handbook consists of tabulated information on the corrosion behaviour of a range of ferrous and non ferrous metals and alloys in high purity water at 500°F or 600°F under static and flow conditions. There are also tables relating to the wear behaviour of pairs of materials operating without lubrication under similar conditions. This information was obtained on behalf of the U.S. Atomic Energy Commission in connection with the preliminary development of pressurized water reactors of the *Nautilus* prototype and represents a considerable body of experimental evidence on a hitherto little known topic. The tables are presented in the hope that they will be of assistance to design engineers engaged on the design of high pressure, high temperature high purity water systems and are preceded by a series of chapters explaining the test procedures used in obtaining the tabulated information.

The last portion of the book is of particular interest in that certain special aspects of corrosion are dealt with in greater detail than is possible in a collection of tables. The topics discussed are crevice corrosion, stress corrosion, intergranular corrosion, the problem of corrosion products in a recirculation system, a discussion of the tabulated information on wear and a discussion of corrosion and wear in relation to manufacturing procedures. There are some excellent photographs of corrosion effects and the general standard of production is good.

P. J. Axon

*Nuclear Physics* **6** (1958) 137—140; © *North-Holland Publishing Co., Amsterdam*

# NEWS ITEMS

## NORDIC INSTITUTE FOR THEORETICAL ATOMIC PHYSICS

## (NORDITA)

The five Nordic countries (Denmark, Finland, Iceland, Norway and Sweden) have set up an Organization with the purpose of strengthening scientific co-operation in the field of atomic physics. One of the main objects of the Organization is the establishment of the Nordisk Institut for Teoretisk Atomfysik (Nordic Institute for Theoretical Atomic Physics) in Copenhagen in a building which will be erected by the Danish Government in connection with the existing premises of the Institute for Theoretical Physics of the University of Copenhagen. Further activities envisaged are exchange of Nordic scientists, organization of symposia, and visits of scientists from other countries to Nordic physical institutions.

Research work and educational activities will be the task of the staff of the Nordic Institute. Facilities will be provided for a number of younger physicists from the member states to receive advanced training in the field of theoretical atomic physics. In addition, the Institute will serve as a gathering place for physicists from the Nordic countries and have possibilities to invite scientists from other places to lecture and take part in the discussions.

The whole Organization is governed by a Board composed of theoretical physicists delegated by the five countries. Professor Niels Bohr has been elected the first Chairman of the Board.

Until a formal agreement has been established by the participating governments, the Organization works on an interim basis, and the Nordic Institute, which will be known as NORDITA, has started its activities on October 1st, 1957, using facilities put at its disposal by the Copenhagen Institute for Theoretical Physics. For the interim period C. Møller has been appointed Director of the Institute, and is assisted by G. Källén, B. Mottelson and S. Rozental. From February 1st, 1958, L. Rosenfeld has permanently joined the staff of the Institute.

# NUCLEAR SIZES AND DENSITY DISTRIBUTIONS

## REPORT ON THE STANFORD CONFERENCE

## (Stanford University, 17-19 December, 1957)

A conference on Nuclear Sizes and Density Distributions was held at Stanford University on December 17—19, 1957. Among the more than 250 physicists who attended, there were representatives from Australia, Canada, Denmark, France, Germany, Israel, Italy, Soviet Union, Switzerland and United Kingdom. As a rule, the conference proceeded at a very pleasant and unusually leisurely pace and it was found unnecessary to have parallel sessions. The April issue of the Reviews of Modern Physics is scheduled to contain the papers delivered at the conference.

One of the chief problems which was discussed was the radial distribution of the charge density, that is the proton density, in nuclei. The more accurate of present-day experiments can measure at most one or two parameters of these distributions; these are the rms radius $\bar{r}$, and the fall-off distance at the edge of the nucleus. Five diverse types of experiments are all in essential agreement, that to within a few percent the value of $\bar{r}$ is $1.20\,A^{1/3}\times 10^{-13}$ cm.

Probably the most accurate of these experiments is the one on electron-nuclear scattering which in addition to the value of $\bar{r}$ above also yields a fall-off distance of $2.4 \times 10^{-13}$ cm independent of $A$. The analysis of the low-lying levels of mu-mesic atoms as well as the Coulomb repulsion terms in the semi-empirical mass formula are in very reasonable agreement with this value for $\bar{r}$. Dr. O. Kofoed-Hansen reported that the value for $\bar{r}$ obtained from the Coulomb repulsion in mirror nuclei is now, despite its previously larger value, also in accord with the other experiments. Lastly, the analysis of the experiments of X-ray fine structure, as reported by Dr. R. L. Shacklett, albeit yielding a slightly smaller value of $\bar{r}$, are also no longer considered to be in serious conflict with the others. This parameter of the radial distribution of protons in nuclei thus seems fairly well settled.

With regard to the distribution of neutrons in nuclei the situation was not too clear. High-energy experiments on scattering of pions on nuclei seem to indicate that the neutrons have a smaller value for $\bar{r}$ than protons. On the other hand, experiments on scattering of nucleons nuclei seem to indicate the opposite. The quoted uncertainties in the above results were of such a nature as not to preclude the possibility that the distributions of neutrons and protons in nuclei have about the same radius. In any event, it is clear that nuclei do not have a very thick shell of neutrons on the outside.

Perhaps the greatest interest at the conference was aroused by Dr. Hofstadter's report on the measurements of the nucleon charge and magnetic moment form factors. For protons the evidence points to the fact that the charge and magnetic moment distributions both have an rms radius of $0.8 \times 10^{-13}$ cm and seem to be best represented by exponential shapes. The magnetic moment form factor for the neutron, although subject to greater uncertainties because it is measured in deuterium, seems to be roughly the same as that of the proton. On the other hand, the deuteron experiments support the low-energy neutron-electron scattering experiments in requiring the charge radius of the neutron to be very small. Dispersion relations calculations by Chew, Goldberger, and collaborators which were reported at the conference are not yet sufficiently developed to shed light on this seeming fundamental asymmetry between neutrons and protons.

S. Gartenhaus

## INTERNATIONAL CONGRESS ON NUCLEAR PHYSICS

### (Paris, 7-12 July, 1958)

At a time when the development of research in Nuclear Physics in France is gaining new impetus with the implementation of modern installations, in particular those of the new Orsay laboratories, it seems fitting, in accordance with tradition, to organize an International Congress on Nuclear Physics. This Congress is to be held in Paris and its vicinity, including among others the Centres of Orsay (University of Paris) and of Saclay (Atomic Energy Commission), with the participation of provincial Centres.

The Congress is sponsored by the International Union of Physics and by UNESCO. Its aim is to survey all the recent experimental and theoretical results, which may help to understand nuclear structure and more generally nuclear interactions.

Problems of high energy nuclear physics will be excluded, a separate Conference on this subject being already organized by the European Centre for Nuclear Research (CERN).

General reviews of each topic will be given before the opening of discussions. In order to facilitate the selection of contributions, participants are requested to refrain from presenting results of only documentary value and without any attempt at interpretation.

In principle the number of papers presented should be sufficiently limited to leave room for an ample discussion. Papers gathering results from several teams will be particularly appreciated. As far as possible arrangements will be made to absorb the content of short communications within the general papers.

The languages in which the papers should be given and the discussion conducted will be French, English and Russian.

The Congress will be held at the "Maison de la Chimie", 28, rue Saint-Dominique, Paris (7e).

A special effort will be made to publish the proceedings at an early date.

Those interested in taking part in this Congress are requested to apply as soon as possible for further information. Every suggestion concerning the organization of the Congress will be welcomed.

The general secretary of the Congress is F. Netter.

All communications should be addressed to the Comité d'organisation du Congrès international de Physique nucléaire (C.I.P.N.), Institut du Radium, 11, rue Pierre Curie, Paris (5e).

## NINTH SESSION OF COUNCIL OF CERN

At its Ninth Session in Geneva on December 19, 1957, the Council of CERN, the European Organization for Nuclear Research, elected M. François de Rose (France) as its President for 1958.

In compliance with the terms of the Convention, which limits tenure of office to three successive years, M. de Rose succeeds Sir Ben Lockspeiser who has presided over the governing body of CERN since October 1954.

M. J. Willems (Belgium) and Prof. W. Heisenberg (Germany) have been elected Vice-Presidents. They succeed M. F. de Rose and Prof. Holtsmark (Norway).

Prof. E. Amaldi (Italy) assumed the Chairmanship of the Scientific Policy Committee, succeeding Prof. W. Heisenberg. Chairmanship of the Finance Committee was taken over by M. J. H. Bannier (the Netherlands) in succession to M. J. Willems.

The Council approved total contributions from the Member States for 1958 of 36 000 000 Swiss francs. At the same time the Council agreed that the contributions for the two years 1958 and 1959 should be fixed at a ceiling of 100 000 000 Swiss francs.

Whilst 1957 was the year of peak building activity, 1958 will see European scientists launch a nuclear research programme with the first of CERN's two big accelerators, the 600 MeV Synchrocyclotron. A long-term programme of research will be carried out.

Assembly of the accelerator components in the recently completed buildings of the 25 GeV Proton Synchrotron — known as the "Eurotron" — will start early next year.

The Proton Sychrotron is expected to come into operation in 1960. Experimental physicists, in collaboration with CERN's Theoretical Division, have started preliminary work on the preparation of a suitable research programme.

A special section comprised of both experimental and theoretical physicists has recently been set up to investigate new principles of high energy particle acceleration.

CERN will again play host to nuclear physicists of all nations in 1958, when the Eighth Annual Conference on High Energy Nuclear Physics will be held in Geneva as a continuation of the well known international conferences held for seven years in succession at the University of Rochester in the United States. Invitation to the CERN Conference will shortly be sent out to physicists of CERN Member States and others, including the United States and the Soviet Union.

During 1957 the entire staff of CERN moved into its permanent headquarters at Meyrin near Geneva. The total number of personnel is now 598 of which about two-thirds are scientific and technical.

### *The New President*

M. François de Rose was born in 1910 and is a career diplomat.

He was first appointed, before the war, to the French Embassy in London and subsequently served in Rome, New York and Madrid.

Since 1946 he has participated in the study of nuclear problems, first at the United Nations Committee for the International Control of Atomic Energy and later on in France, where he is a member of the Atomic Energy Committee and Head of the Atomic Energy Office as well as Head of the NATO Office at the Ministry of Foreign Affairs.

After taking an active part in the negotiations and studies which preceded the creation of CERN, he was chairman of the first conference held in 1952, which, under the auspices of UNESCO, laid the foundations of the Organization. He has been Vice-President of the CERN Council since 1956.

M. de Rose holds the "Croix de Guerre" and is a member of the "Légion d'honneur".

*Nuclear Physics* **6** (1958) 141—150; © *North-Holland Publishing Co., Amsterdam*
Not to be reproduced by photoprint or microfilm without written permission from the publisher

# POLARIZATION MEASUREMENTS ON D+D AND T+D NEUTRONS GENERATED BY LOW ENERGY DEUTERONS

P. J. PASMA

*Natuurkundig Laboratorium der Rijksuniversiteit, Groningen*

Received 4 December 1957

**Abstract:** The polarization of D+D and T+D neutrons has been determined from the left-right asymmetry induced by elastic scattering through $^4$He. A gas scintillator with helium served as the scatterer. The scattered neutrons were detected in coincidence with the helium recoil nuclei. The D+D neutron polarization was found to increase from 6 % at 200 keV to about 9.5 % at 500 keV deuteron bombarding energy. Neutrons from the T+D reaction appeared to be nearly unpolarized for deuteron energies below 300 keV.

## 1. Introduction

In all experiments recently reported on the polarization of neutrons from the $^2$H (d, n) $^3$He reaction, the polarization was derived from the left-right asymmetry in the elastic scattering of the neutrons by a spin zero nucleus involving spin-orbit coupling. Elastic scattering by $^{12}$C was employed by Meier, Scherrer and Trumpy [1]) in thin target measurements at $E_D = 600$ keV, and by McCormac *et al.* [2]) who used a thick target at deuteron energies between 500 and 700 keV. In order to avoid background difficulties Levintov *et al.* [3]) detected the recoil nuclei in a $^4$He filled proportional counter with directional properties, instead of observing the scattered neutrons. The work of the latter authors comprises both thin and thick target investigations for deuteron energies ranging from 600 to 1 800 keV.

In the present experiments $^4$He was used as a polarization analyzer. We recorded the scattered neutrons in coincidence with the helium recoil nuclei. For this purpose a helium gas scintillation counter was developed [4]), in which the light pulses accompanying the recoil $\alpha$-particles are detected by a quartz photomultiplier. In the case of the D+D neutrons we used thin heavy ice targets at deuteron energies from 200 to 500 keV. For the reaction $^3$H (d, n)$^4$He the incident deuteron energy was varied from 100 to 300 keV; no earlier polarization measurements have been published on T+D neutrons.

## 2. Definitions and Method

The differential cross section for the scattering of a neutron beam with a polarization $\mathbf{P}_n(\theta)$ is given by the well-known formula [5])



March (3) 1958

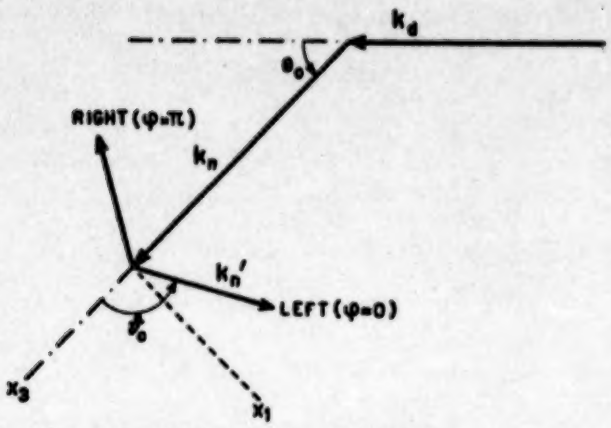


Fig. 1. Diagram of the wave vectors in connection with the sign convention adopted in the text.

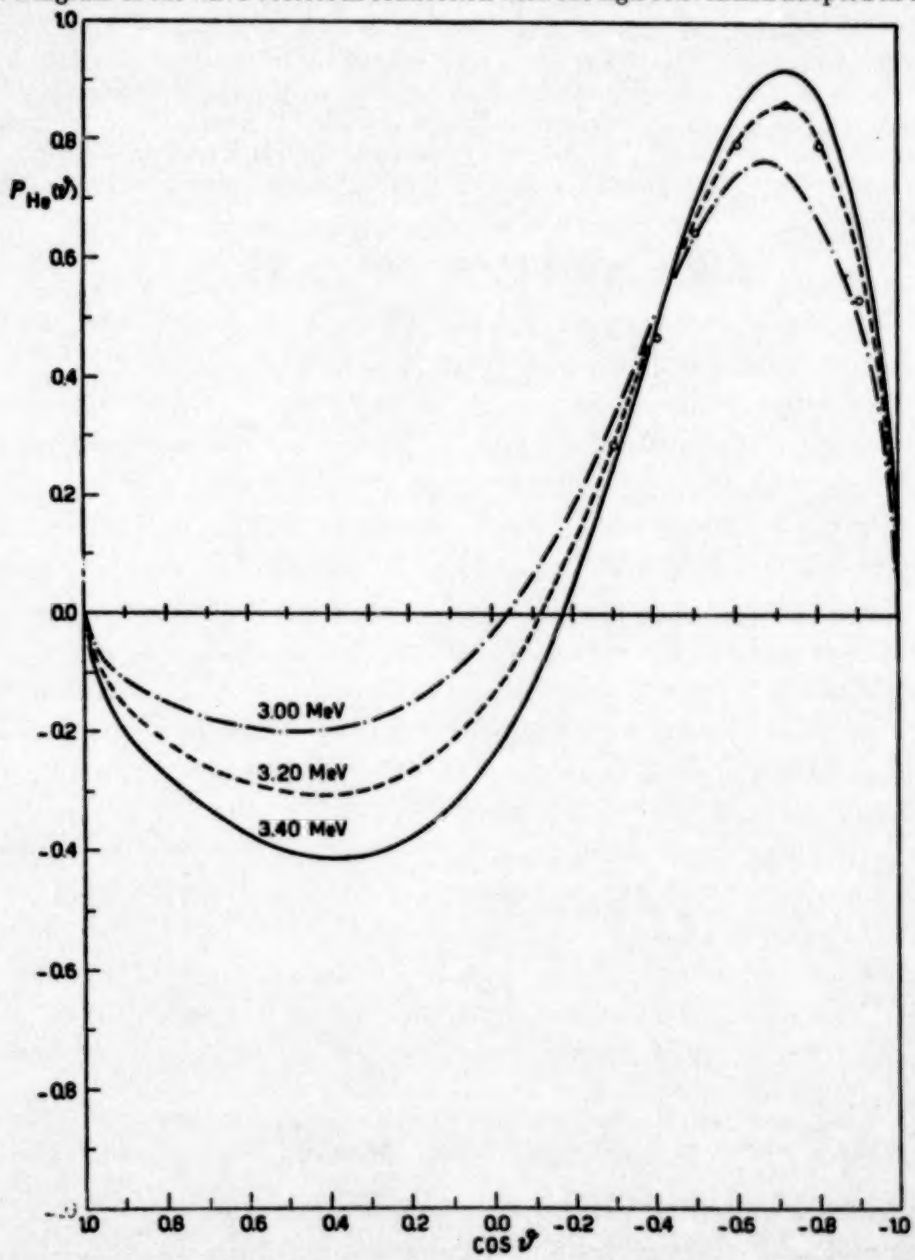


Fig. 2. Polarization efficiency $P_{He}(\vartheta)$ for the indicated neutron energies, according to Van Wageningen [6]). Open circles correspond to a $\sin^2 2\vartheta$ approximation of the curve for 3.2 MeV in the neighbourhood of $\cos\vartheta = -0.7$.

$$\sigma(\vartheta, \varphi) = \sigma_u(\vartheta)\{1+\mathbf{P}_n(\theta)\cdot\mathbf{P}_{He}(\vartheta)\}, \quad (1)$$

where $\sigma_u(\vartheta)$ is the differential cross section for an unpolarized beam, and $\mathbf{P}_{He}(\vartheta)$ is the polarization efficiency of the helium scatterer, the polarization generated by scattering an originally unpolarized beam through a c.m. angle $\vartheta$. The directions of $\mathbf{P}_n(\theta)$ and $\mathbf{P}_{He}(\vartheta)$ are fixed by the vectors $\mathbf{n}_1$ and $\mathbf{n}_2$ according to (fig. 1)

$$\mathbf{P}_n(\theta) = \mathbf{n}_1 P_n(\theta), \qquad \mathbf{n}_1 = \mathbf{k}_d\times\mathbf{k}_n/|\mathbf{k}_d\times\mathbf{k}_n|; \quad (2)$$

$$\mathbf{P}_{He}(\vartheta) = \mathbf{n}_2 P_{He}(\vartheta), \qquad \mathbf{n}_2 = \mathbf{k}_n\times\mathbf{k}'_n/|\mathbf{k}_n\times\mathbf{k}'_n|. \quad (3)$$

Here the $\mathbf{k}$'s are the wave vectors of the deuteron, the neutron and the scattered neutron respectively.

Taking the scattering plane the same as the plane of the (d, n) reaction, the left-right asymmetry is here defined as

$$\varepsilon = \frac{\sigma(\vartheta, 0)-\sigma(\vartheta, \pi)}{\sigma(\vartheta, 0)+\sigma(\vartheta, \pi)}. \quad (4)$$

From the equations (1), (2) and (3) we have

$$\varepsilon = P_n(\theta)P_{He}(\vartheta). \quad (5)$$

The helium polarization efficiency was derived by Van Wageningen[6]) from the measurements of Seagrave[7]) and $P_{He}(\vartheta)$ curves are given in fig. 2 for neutron energies 3.4, 3.2 and 3.0 MeV. In the experiments the angle $\vartheta$ was chosen so as to make $\varepsilon$ as large as possible, that is to say, $\cos\vartheta = -0.7$, at which angle $P_{He}(\vartheta)$ exhibits a maximum for these neutron energies. Then with the aid of eq. (5) $P_n(\theta)$ can be calculated from the measured asymmetry $\varepsilon$.

## 3. Experimental Details

The experimental arrangement is shown in fig. 3. Deuterons from a h.f. ion source are accelerated by means of a cascade generator. After magnetic analysis a 100 $\mu$A beam is allowed to hit a heavy ice target, with an estimated stopping power of 50 keV. The target was the same as described by Sikkema[8]). Notwithstanding the coincidence technique it turned out to be favourable to shield the neutron counters with lead bricks and wooden boxes filled with a mixture of paraffin and boric acid. The neutron beam striking the helium scatterer was collimated within 3.5°.

The helium was contained in a cylindrical stainless steel cup with a diameter of 5 cm and a length of 7 cm. The inside was coated with a layer of magnesium oxide and the cell was closed with a 1 cm thick quartz plate; through this plate the scintillations were viewed by a photomultiplier with quartz envelope, type E.M.I. 6255B. The filling of the gas scintillator was a mixture of 90 % helium and 10 % xenon[9]), to a total pressure of 17

atmospheres. We performed preliminary investigations with several other colour shifters, both solid and gaseous, but for our experiments xenon turned out to be the most suitable colour shifter. Alpha particles from a Po test source inside the cell produced maximum pulse heights exceeding the average noise level by a factor of 30. The neutron detectors I and III were provided with liquid scintillators (p-terphenyl in xylene), enclosed in glass cylinders with a diameter of 36 mm and a height of 26 mm. These counters were mounted together with the gas scintillation counter II on

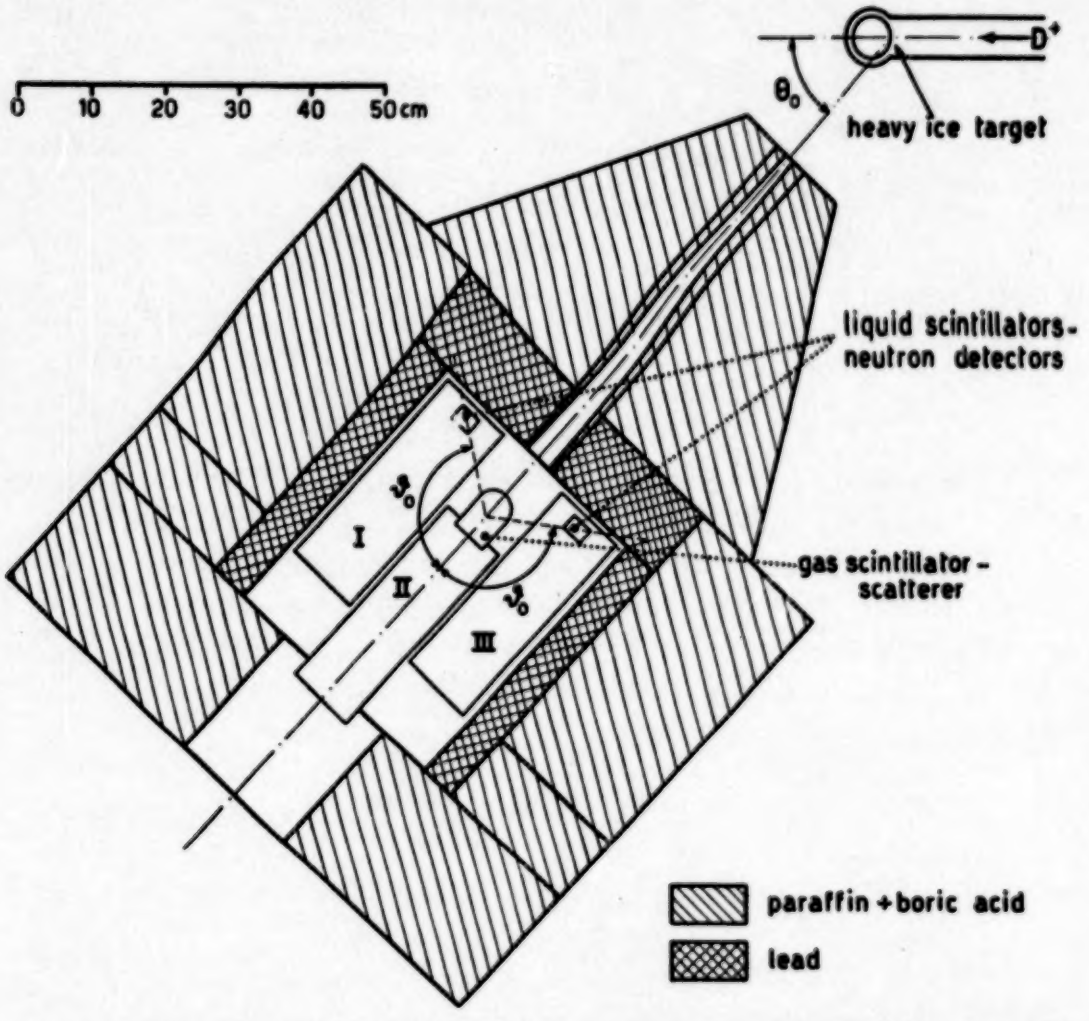


Fig. 3. Experimental arrangement used in the D+D neutron polarization measurements, showing the position of the counters inside the neutron and gamma shielding.

an iron frame work, which as a whole could be rotated about the axis of the collimator tube without removing anything of the shielding arrangement. In this way intensities left and right for the same counter could be compared. The counting rates of the detectors were normalized by the counting rate of the gas scintillation counter, acting as a monitor.

The resolving time of the coincidence circuits was 0.2 $\mu$sec and a (small) correction for the number of chance coincidences was applied.

## 4. Corrections

Corrections to be made on the measured quantities have been treated in some detail by the authors mentioned in ref. [1, 2]). Multiple scattering and asymmetry due to the variation of the neutron intensity over the angle subtended by the scatterer, were considered negligible in our case. For the evaluation of the geometrical correction, arising from the finite sizes of scatterer and detectors we followed a method outlined by McCormac *et al.* [2]). Their geometrical arrangement is quite similar to ours, except for the orientation of the scatterer with respect to the incoming neutron beam. In the course of the computation we used in the neighbourhood of $\cos\vartheta = -0.7$ an approximation $P_{\mathrm{He}}(\vartheta) = P_{\mathrm{He\text{-}max}} \sin^2 2\vartheta$, where $P_{\mathrm{He\text{-}max}}$ is the maximum value of $P_{\mathrm{He}}(\vartheta)$. This approximation for $E_{\mathrm{n}} = 3.2$ MeV is indicated by the open circles in fig. 2. Following the procedure of McCormac *et al.* the counting rate of the scattered neutrons can be written as a function of the direction cosines $\lambda_i$ of the vector $\boldsymbol{\xi}$ connecting scatterer centre and detector centre:

$$C(\lambda_i) \propto \beta_1(\lambda_i) + \beta_2(\lambda_i) P_{\mathrm{n}} P_{\mathrm{He\text{-}max}}. \tag{6}$$

For our geometry and the $\sin^2 2\vartheta$ approximation, $\beta_1(\lambda_i)$ and $\beta_2(\lambda_i)$ are rather complicated expressions, containing $\sigma_{\mathrm{u}}$, $\sigma'_{\mathrm{u}}$, $\sigma''_{\mathrm{u}}$ (the derivatives of $\sigma_{\mathrm{u}}(\cos\vartheta)$ evaluated at $\cos\vartheta = \lambda_3$) and constants $A$ and $B$ given by

$$A = (1/2\xi^2)(M_{11} + M'_{11}) = (1/2\xi^2)(M_{22} + M'_{22})$$
$$B = (1/2\xi^2)(M_{33} + M'_{33}).$$

Here the $M$'s are the moments of the scatterer and detectors (cf. ref. [2])).

From eq. (6) and (4) the left-right asymmetry takes the form

$$\varepsilon = \frac{\beta_2(\lambda_i)}{\beta_1(\lambda_i)} P_{\mathrm{n}} P_{\mathrm{He\text{-}max}}.$$

Thus

$$P_{\mathrm{n}} = \gamma \cdot \frac{\varepsilon}{P_{\mathrm{He\text{-}max}}} \text{ with } \gamma = \frac{\beta_1(\lambda_i)}{\beta_2(\lambda_i)}.$$

In the calculation of the factor $\gamma$ for the actual experiment values for $\sigma_{\mathrm{u}}$ and its derivatives were derived from the data of Seagrave [7]), yielding $\gamma = 1.12$, independently of the deuteron energies used in our experiments.

In order to ascertain the absence of possible asymmetries in the apparatus we performed a number of test measurements. No asymmetry should be present in the forward direction and under 90° (c.m.) with the deuteron beam, $P_{\mathrm{n}}$ being zero in these directions. A second check is found in taking the scattering plane perpendicular to the D+D reaction plane, again making $\varepsilon = 0$. Finally the asymmetry can be caused to disappear by choosing $\vartheta$ so as to make $P_{\mathrm{He}}(\vartheta) = 0$, which happens at $\vartheta$ (c.m.) $\approx 96°$

for $E_n = 3.2$ MeV. In all checks we found no asymmetry outside the limits of the statistical accuracy.

## 5. Results

The final data for D+D neutrons, obtained from experiments at deuteron energies between 200 and 500 keV are summarized in table 1. The neutron emission angle $\theta_0$ was 47° (lab. system), the scattering angle at the analyzer was fixed at 135° (c.m.) (= 123° lab.system).

TABLE 1

Data for D+D neutron polarization

| $E_D$ (keV) | asymmetry | polarization (%) |
|---|---|---|
| 200 | $-0.038 \pm 0.016$ | $-5.8 \pm 2.5$ |
| 300 | $-0.062 \pm 0.016$ | $-9.0 \pm 2.3$ |
| 350 | $-0.058 \pm 0.017$ | $-8.2 \pm 2.4$ |
| 400 | $-0.062 \pm 0.008$ | $-8.6 \pm 1.1$ |
| 450 | $-0.071 \pm 0.010$ | $-9.5 \pm 1.3$ |
| 500 | $-0.070 \pm 0.006$ | $-9.2 \pm 0.8$ |

The errors listed are merely statistical. Besides, in fig. 4 is shown the dependence of the polarization on deuteron energy, including results of

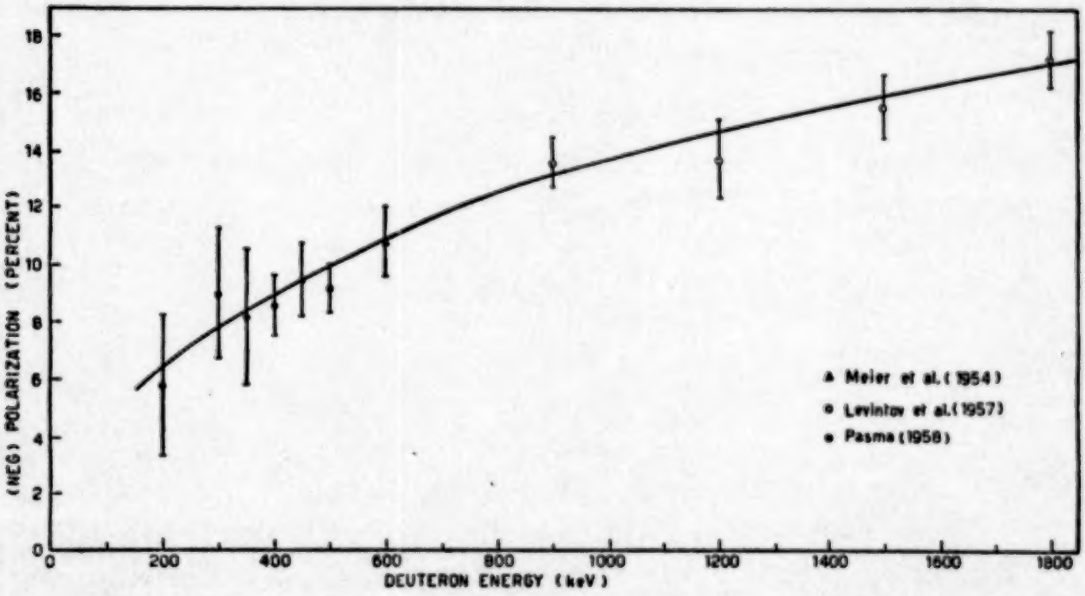


Fig. 4. Thin target D+D neutron polarization data for $\theta_0 = 47° - 49°$ *vs.* deuteron energy.

Meier *et al.* [1]) and Levintov *et al.* [3]) obtained at nearly the same neutron emission angle. The line is drawn somewhat arbitrarily through the experimental points.

Theoretically the polarization of D+D neutrons (and protons) was studied by several authors [10, 11, 12, 13]). For low deuteron energies, when

only incoming S and P waves need be considered, Blin-Stoyle [10]) gives the polarization in dependence of the deuteron energy $E$ and the angle $\theta$ (c.m.) as

$$P(E, \theta) = C\frac{A(E)\sin\theta\cos\theta}{1+A(E)\cos^2\theta}, \tag{8}$$

where $C$ is a constant involving matrix element that cannot be calculated without assuming some theory of nuclear forces, and $A(E)$ is the factor occurring in the expression for the angular distribution as the coefficient of $\cos^2\theta$. For a fixed value of $E$, the polarization reaches a maximum at $\cos\theta_{max} = (A(E)+2)^{-\frac{1}{2}}$.

Under certain assumptions Blin-Stoyle [11]) found a maximum possible polarization of 7 % at $E_D = 300$ keV, and Cini [12]) calculated maxima of 6 % at $E_D = 200$ keV and 9 % at $E_D = 500$ keV.

In fig. 5 are shown together theoretically and experimentally determined values for the maximum polarization at low deuteron energies. Strictly

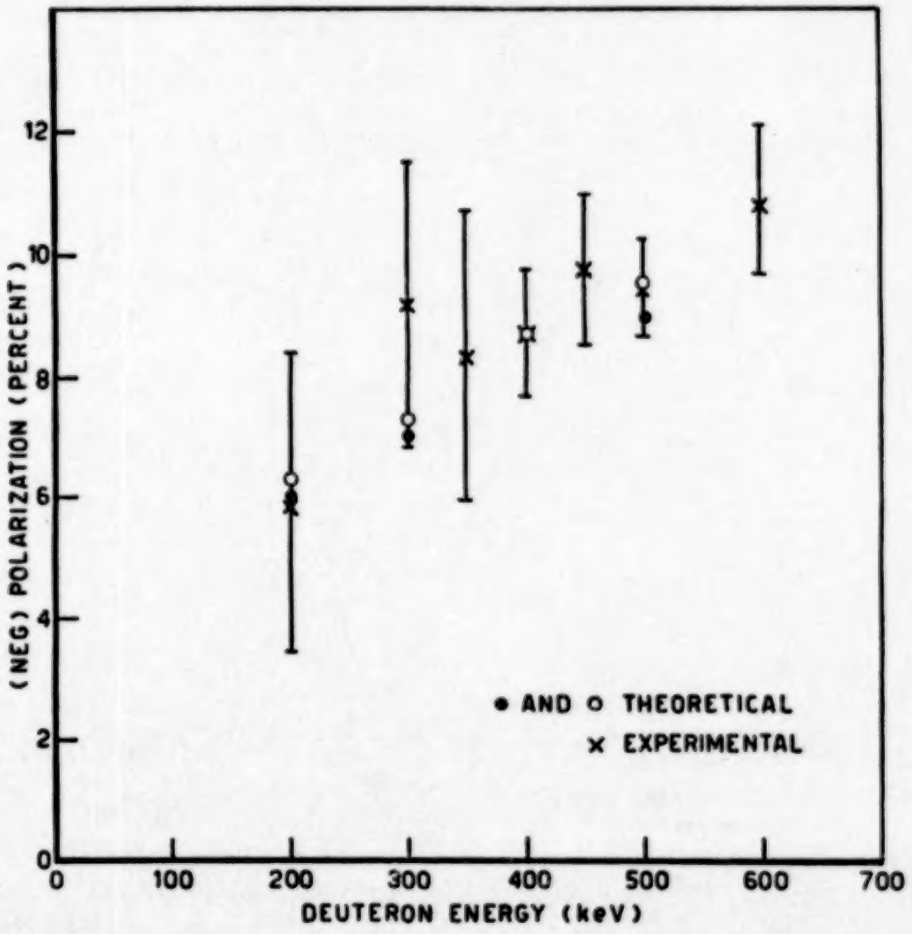


Fig. 5. Comparison of theoretical and experimental D+D neutron polarization data at low deuteron energy (at $\theta_{max}$ ).

speaking, the experimental values were for a part not taken, at the angle $\theta_{max}$. Therefore we calculated, in those cases, what would have been found at $\theta_{max}$ and these data are plotted in fig. 5. The closed circles are the calculated values of Blin-Stoyle and Cini. The open circles were obtained from

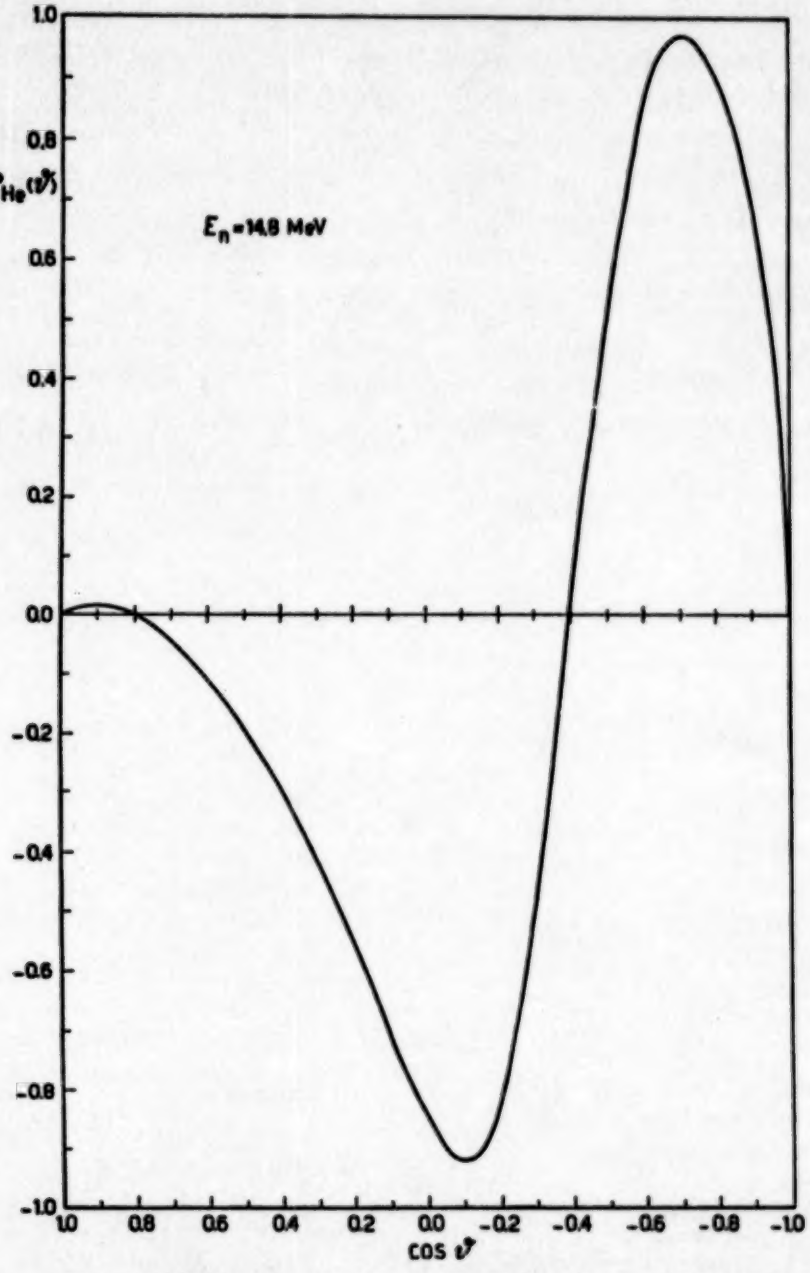


Fig. 6. Polarization efficiency $P_{He}(\vartheta)$ for $E_n = 14.8$ MeV.

eq. (8), taking the coefficients $A(E)$ from recent angular distribution measurements [14, 17]) and using for $C$ a value of $-0.180$ so as to make the point at 400 keV coincide with the experimental one. The agreement between theoretical and experimental points turns out to be fairly good. This may

be an indication that the theoretical assumptions are valid in this energy region. However, it must be pointed out, that for low deuteron energy the results of polarization measurements on protons of the accompanying $^2$H(d, p)$^3$H reaction are not in agreement with theory. See for instance ref. [15]).

The experiments with the fast neutrons of the $^3$H(d, n)$^4$He reaction were carried out in a similar manner. Here the shielding of the neutron counters consisted only of lead interposed on the lines connecting the tritium loaded zirconium target and the liquid scintillators.

Fig. 6 shows the helium polarization efficiency for 14.8 MeV neutrons, calculated again from the phase shift analysis of Seagrave [7]). From this curve it appears that the scattering angle $\vartheta$ can be chosen most favourably corresponding to $\cos\vartheta = -0.1$ or $\cos\vartheta = -0.7$ (c.m.). At both angles we performed a number of measurements on neutrons emitted under 45° (lab.system) for incident deuteron energies between 100 and 300 keV. A few of the results are summarized in table 2.

TABLE 2

Left-right asymmetries obtained for T+D neutrons

| $E_D$ (keV) | asymmetry |
|---|---|
| 100 | $+0.02\pm0.02$ |
| 200 | $+0.01\pm0.03$ |
| 300 | $-0.02\pm0.03$ |

The measured asymmetries do not differ significantly from zero; the polarization (if any) will be very small. Combined with the isotropy of the angular distribution in the c.m. system [16]), the absence of polarization may be an indication that at these low deuteron energies no P-waves take part in the reaction.

A more detailed report of the measurements described is given elsewhere [4]).

The author wishes to express his thanks to Professor H. Brinkman, the director of this laboratory, for his continuous interest and encouraging support. Further he is indebted to Dr C. P. Sikkema and Dr H. Nauta for cooperation in several parts of the work, to Mr E. Houtman for his aid in taking the data and to Dr R. van Wageningen for many helpful discussions and the computation of the $P_{He}(\vartheta)$ curves. The work was part of the research program of the „Stichting voor Fundamenteel Onderzoek der Materie" (F.O.M.), financially supported by the Netherlands Organization for Pure Scientific Research (Z.W.O.).

## References

1) R. W. Meier, P. Scherrer and G. Trumpy, Helv. Phys. Acta **27** (1954) 577
2) B. M. McCormac, M. F. Steuer, C. D. Bond and F. L. Hereford, Phys. Rev. **104** (1956) 718
3) I. I. Levintov, A. V. Miller and V. N. Shamshev, Nuclear Physics **3** (1957) 221;
I. I. Levintov, A. V. Miller, E. Z. Tarumov and V. N. Shamshev, Nuclear Physics **3** (1957) 237
4) P. J. Pasma, Thesis, (Groningen, 1958)
5) J. V. Lepore, Phys. Rev. **79** (1950) 137
6) R. van Wageningen, Intern Rapport Natuurkundig Laboratorium IR 15 (Groningen, 1954)
7) J. D. Seagrave, Phys. Rev. **92** (1953) 1222
8) C. P. Sikkema, Nuclear Physics **3** (1957) 375
9) J. A. Northrop and R. Nobles, Nucleonics **14**, no. 4 (1956) 36
10) R. J. Blin-Stoyle, Proc. Phys. Soc. A **64** (1951) 700
11) R. J. Blin-Stoyle, Proc. Phys. Soc. A **65** (1952) 949
12) M. Cini, Nuovo Cimento **8** (1951) 1007
13) M. Fiertz, Helv. Phys. Acta **25** (1952) 629
14) P. R. Chagnon and G. E. Owen, Phys. Rev. **101** (1956) 1798
15) R. E. Segel and S. S. Hanna, Phys. Rev. **106** (1957) 536
16) H. V. Argo, R. F. Taschek, H. M. Agnew, A. Hemmendinger and W. T. Leland, Phys. Rev. **87** (1952) 612
17) J. C. Fuller, W. E. Dance and D. C. Ralph, Phys. Rev. **108** (1957) 91

*Nuclear Physics* 6 (1958) 151—156; © *North-Holland Publishing Co., Amsterdam*
Not to be reproduced by photoprint or microfilm without written permission from the publisher

# SMALL ANGLE SCATTERING OF 1.33 MeV AND 1.17 MeV GAMMA RAYS

A. STORRUSTE and P. O. TJÓM
*Institute of Physics, University of Oslo, Blindern*

Received 18 December 1957

**Abstract:** The differential scattering cross section for gamma rays of energy of 1.33 MeV and 1.17 MeV scattered by lead and copper at angles varying from 1° to 8° has been measured. The result is in fair agreement with the elastic scattering cross section calculated by the form factor method and the Hartree electron distribution.

## 1. Introduction

During the last few years much work has been done on the elastic scattering of gamma rays, but relatively little on the small angle scattering. The experiments described here were set up to measure the scattering at angles as small as possible.

Only the experimental method and the results obtained will be reported here. A discussion of the various types of scattering involved can be found in the papers referred to below.

## 2. Apparatus

When measuring at small angles, earlier investigators have not employed shielding for the detector or the source [1]). Here a different method was adopted and thick shields of lead were placed around both the scintillation counter and the source as shown in fig. 1.

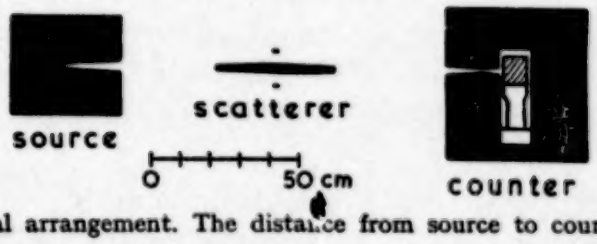


Fig. 1. Experimental arrangement. The distance from source to counter is not to scale.

The 50 mC $Co^{60}$ source was a 6 mm diameter rod enclosed in a thin aluminium can. The gamma rays escaped through a cone-shaped opening in the shield which was 18 cm deep. The counter shield was 18 cm thick. The throat of the double cone-shaped opening had a diameter of 1 cm. A 40-cm copper rod slightly conical towards both ends prevented the direct

beam from reaching the counter. When the scattering at the smallest angles was measured, the copper rod had a diameter of 1.6 cm and the full opening angle of the cones in the lead shields was 4°. For larger angles the diameter of the copper rod was 2.5 cm and the full opening angle of the cones was 7.5°.

The scintillation counter consisted of a 3″ NaI(Tl) crystal mounted on a 3″ DuMont photomultiplier tube. Its resolution can be seen in curve C, fig. 2. Observations were taken with a pulse-height analyzer of the Hutchinson-Scarrot design using 80 channels.

The distance between the source and the throat of the cone in the counter shield was 298 cm. The scattering angle was varied by choosing ring scatterers of different diameters. The rings of lead and of copper had cross sections

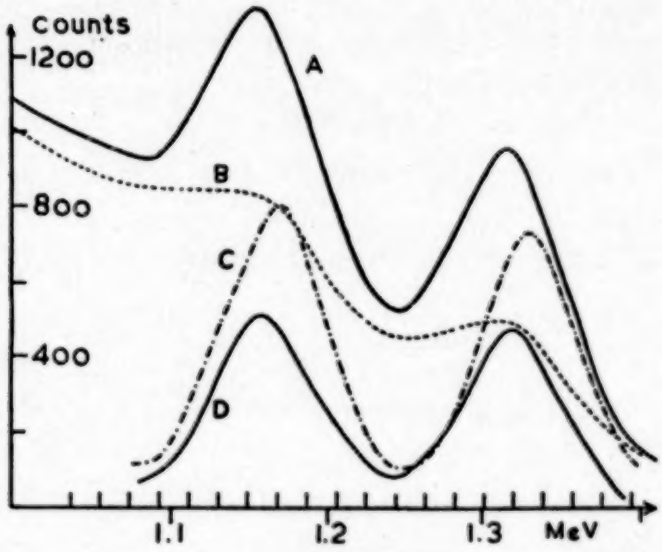


Fig. 2. Pulse height distributions. Curve A: scatterer in place. Curve B: scatterer removed. Curve C: direct beam from a small source. Curve D: the difference between curves A and B.

of 1 cm × 1.6 cm and 1 cm × 2.3 cm respectively. The three smallest lead rings had cross sections of about 0.5 cm × 1.6 cm. The copper rods and the rings were suspended by strings halfway between the source and the counter. By a special screw arrangement the rod and the ring could be accurately centered on the horizontal line through the source and the scintillator.

The scintillation counter together with the shield was placed on a heavy steel turntable so that the cone could be directed through a window. To find the strength of the source, thus, the counting rate could be measured when the source was 51.8 m away.

## 3. Measurements

Fig. 2 shows the result of a series of observations. Curve A corresponds to a 30 min run with a lead scatterer in place, curve B to a 30 min run with

the scatterer removed and curve C to a 3 min run with a small source at a fixed distance.

To find the counts due to the scattered rays, curve B was subtracted from curve A. The difference, curve D, has almost the same shape as curve C which was produced by unscattered rays. It was noticed, however, that the photo peaks of curve D were slightly displaced to the left upon increasing the scattering angle. In order to find this displacement, and also to control the counter, curve C was repeated for each measurement. The background curve B was repeated a few times every day, even though the counter turned out to be stable enough to allow the use of the same background curve for all the runs.

The energy difference between corresponding peaks of curves D and C as well as the halfwidths of curve D compared to that of curve C depend on the ratio of Compton-scattered to elastically scattered rays. It turned out, however, that the curves could not be used for a quantitative calculation of the above ratio using this method, because the differences in energies and the halfwidths were so small and because the counter was not perfectly stable.

When comparing the various difference curves D, 4 channels covering about one halfwidth of the photo peak were used. This was done since the small energy difference between Compton and elastically scattered rays prevented the use of the peak heights in this comparison, and an integration over the whole peak gave a smaller ratio of counts to background. With the lead scatterer the 4 channels of curve D gave a total of about 2 000 counts. The measurements were repeated 7 times for each of the lead scatterers and 4 times for each of the copper scatterers. There was no substantial variation from one measurement to the other, the largest difference observed between a single measurement and the average of the 7 measurements for one ring being 13 percent.

## 4. Corrections

The comparison of the scattered rays with the incident beam from the source was straightforward since the counter arrangement was not changed. To compensate for absorption in the ring scatterer, 1.6 cm of lead was inserted in front of the counter. For 1.17 MeV and 1.33 MeV gamma rays correction factors of 1.430 and 1.395 were used for the absorption in the 48.8 m longer distance of air.

The smallest ring scatterer will absorb some of the rays scattered at small angles in the air and in the lead shields. To find a correction for this, two methods were applied. At scattering angles of 1° and 1.78° the ring scatterers were replaced by copper tubes which had corresponding diameters but were

8 cm long. By appropriate use of the corresponding curves observed, the correction could be found. The other method was to ensure that the ratio of peak to valley for the 1.33 MeV photo peak should be the same in curves C and D. This ratio may be smaller for the 1.17 MeV photo peak in curve D due to bremsstrahlung, although the experimental results show that the contribution of the bremsstrahlung to the 1.17 MeV peak must be small. The final correction factor $x$ which was observed is given in table 1.

To find the variation of counter efficiency with scattering angle a small source was placed at different points on a line perpendicular to the copper rod. The observed decrease from the copper rod determined a corresponding correction factor $y$ which is given in table 1.

TABLE 1

Correction factors applied when using rings of lead

| Angle in degrees | 1.0 | 1.15 | 1.37 | 1.78 | 2.87 | 3.80 | 4.80 | 5.75 | 6.80 | 7.80 |
|---|---|---|---|---|---|---|---|---|---|---|
| $x$ (1.33 MeV) | 1.42 | 1.34 | 1.30 | 1.13 | 1.07 | 1.03 | 1.02 | 1.00 | 1.00 | 1.00 |
| $x$ (1.17 MeV) | 1.44 | 1.35 | 1.31 | 1.14 | 1.08 | 1.04 | 1.02 | 1.00 | 1.00 | 1.00 |
| $y$ | 1.00 | 1.00 | 1.00 | 1.00 | 1.01 | 1.03 | 1.05 | 1.08 | 1.12 | 1.22 |

## 5. Results

The corrected total cross sections are given in table 2 and plotted in figs. 3 and 4. The Compton scattering cross sections plotted in the figures are calculated from curves given by Nelms [2]).

To find the contribution of the elastic scattering to the total cross section observed, the Compton scattering cross section must be subtracted. At the largest angles and with copper as the scatterer, this difference is less than the experimental error. This is to be expected since it confirms the correctness of the Klein-Nishina formula. In fact, copper was used mainly to control the measurements. A few observations were, however, taken at the smallest angles. Before plotting the curves, the observed counting rates were corrected in a manner similar to that described above, where rings of lead were used.

The measurements with lead gave good quantitative results for the elastic scattering. The observed elastic scattering cross section is comparable to or even larger than the Compton scattering cross section, and reasonable accuracy is obtained at medium and smaller size angles. At the largest angle the observed difference between the total and the Compton scattering is only about twice the overall uncertainty. For the smallest scattering angle,

TABLE 2

Observed total scattering cross sections $S$ in barns per sterad

| Angle in degrees | 1.0 | 1.15 | 1.37 | 1.78 | 2.87 | 3.80 | 4.80 | 5.75 | 6.80 | 7.80 |
|---|---|---|---|---|---|---|---|---|---|---|
| $S$ (1.17 MeV) | 100 | 75.9 | 51.4 | 30.5 | 16.0 | 10.5 | 8.05 | 7.10 | 6.97 | 6.95 |
| $S$ (1.33 MeV) | 88.1 | 65.5 | 45.0 | 28.1 | 14.4 | 9.45 | 7.27 | 6.70 | 6.40 | 6.19 |

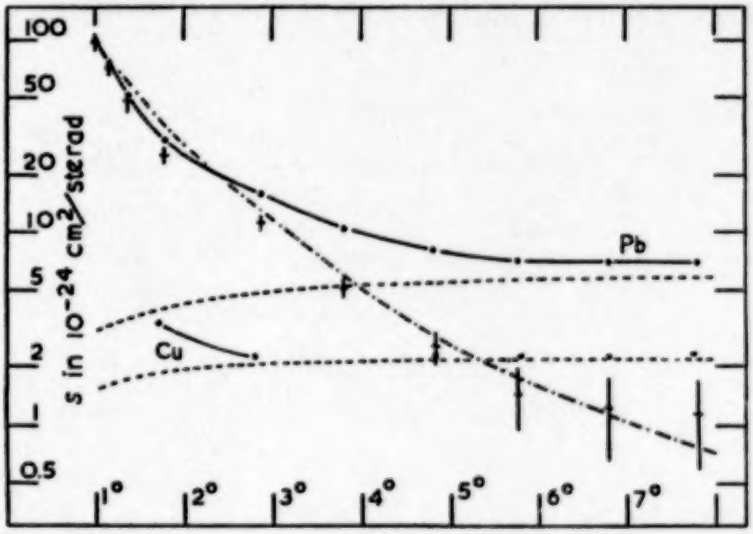


Fig. 3. The cross sections per unit solid angle for scattering at small angles of 1.17 MeV gamma rays by lead and copper. ·——·—— Observed total scattering cross sections. – – – – – – Calculated Compton scattering cross sections. . — . — . — . Calculated Rayleigh scattering cross sections. † Observed elastic scattering cross sections.

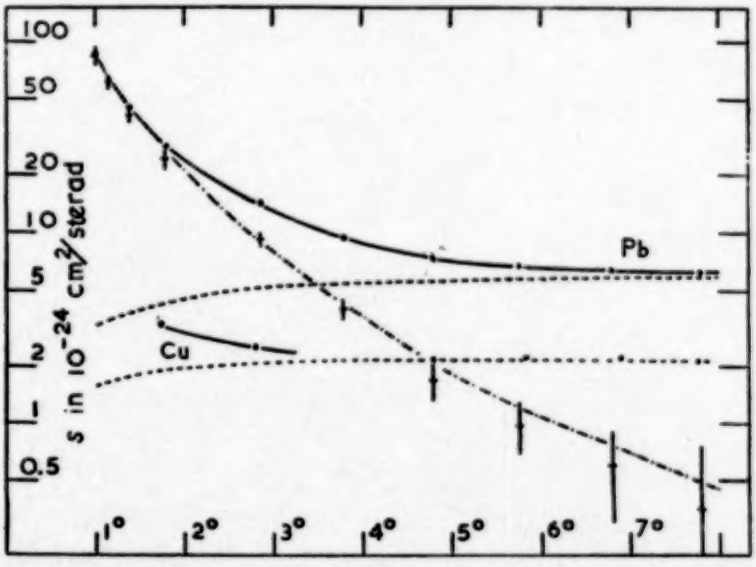


Fig. 4. The cross sections per unit solid angle for scattering at small angles of 1.33 MeV gamma rays by lead and copper.

the largest error is probably due to uncertainties in the correction factor $x$. An estimated probable error is indicated in figs. 3 and 4, assuming the calculated Compton cross section to be correct.

For comparison the elastic scattering cross section calculated from the curves given by Nelms and Oppenheim [3]) is plotted in figs. 3 and 4. The calculations of Brown and Mayers [4]) may be more correct, but these calculations have not been extended to small enough angles. The result is that there must be a large contribution from scattering by L-electrons, and the experiment shows fair agreement with calculations based on the form factor method using the Hartree electron distribution.

## References

1) H. Schopper, Zeits. f. Physik **147** (1957) 253
2) A. T. Nelms, Nat. Bur. Stand. Circ. 524 (1953)
3) A. T. Nelms and I. Oppenheim, Nat. Bur. Stand. **55** (1955) 53
4) G. E. Brown and D. F. Mayers, Proc. Roy. Soc. A **242** (1957) 89

*Nuclear Physics* **6** (1958) 157—160; © *North-Holland Publishing Co., Amsterdam*
Not to be reproduced by photoprint or microfilm without written permission from the publisher

# MOMENTUM DEPENDENCE OF THE NUCLEAR SHELL MODEL POTENTIAL

R. B. HALL
*Kings College, Cambridge*
and
R. J. EDEN
*Clare College, Cambridge*†

Received 4 December 1957

**Abstract:** The momentum dependence of the shell model potential near the edge of the $O^{16}$ nucleus is investigated by taking the average of an assumed form of pseudo-potential acting between pairs of nucleons. The reduced mass approximation is used and the variation of $m^*$ is calculated as a function of nuclear density.

## 1. Introduction

It has been pointed out by several authors [1, 2, 3]) that the single particle potential of the shell model should depend on both the momentum and the coordinates of the particle. In this paper we describe a preliminary investigation into the form of this dependence near the surface of a nucleus where the nuclear density is changing rapidly.

According to Brueckner's theory [4, 5, 6]) the shell model potential can be derived by a self-consistent procedure which ultimately gives the potential as a Hartree-Fock average of an effective two-body potential (the $t$-matrix). The difficult nature of this self-consistent procedure for a finite sized nucleus will necessitate approximations, particularly near the nuclear edge. It is hoped that the results of this paper will give some guidance in choosing these approximations. We proceed here by assuming a simple form for the effective two-body potential and compare the momentum dependence of the resulting average single particle potential with the momentum dependence which is obtained by an extrapolation from average potentials in infinite nuclear matter. The reduced mass approximation has been used throughout. This approximation represents a nucleon as moving in a static potential but with a mass $m^*$ which is less than its actual mass $m$. For nuclear matter the value of $m^*$ necessary to provide a binding energy of 14 MeV and a separation energy of 14 MeV at a density corresponding to $r_0 = 1.2\times10^{-13}$ cm is 0.41 $m$ [3]).

† This work was commenced at the Department of theoretical Physics, Manchester University.

In a full calculation using the $t$-matrix the momentum dependence of the single particle potential will arise from several sources including (1) exchange forces, (2) antisymmetrisation of the wave function, (3) direct momentum dependence in the $t$-matrix arising from centre of mass effects, many-body effects and restrictions on intermediate states in the integral equation for the $t$-matrix. Our assumed form of the effective potential includes (1) and (2) but not (3); this limitation was adopted because exchange and antisymmetrisation effects are certainly of importance in the present context and there is less doubt about how to introduce them into an assumed effective potential than terms of type (3). It should be noted also that we have not made our calculation self-consistent partly because it is unlikely that such a refinement would change the character of our results and partly because it seems more important to express our results at an actual nuclear density rather than at a self-consistent density. A calculation directed at self-consistency rather than at a study of momentum dependence has been carried our recently [7]) but not in a manner which yields the correct separation energy.

## 2. Momentum Dependence near the Nuclear Surface

The calculation was performed for the nucleus of $O^{16}$ using harmonic oscillator wave-functions and an inter-nucleon potential

$$v(r_{ij}) = (WP^{W}+MP^{M}+HP^{H}+BP^{B})V_0 \exp(-r_{ij}^2/a^2). \tag{2.1}$$

The average field for one nucleon is then

$$\begin{aligned} V_i(r_1) = &\sum_j \left[\int \psi_j^*(\mathbf{r}_2)\psi_i^*(\mathbf{r}_1)v(r_{12})\psi_j(\mathbf{r}_2)\psi_i(\mathbf{r}_1)d\tau_2\right]/|\psi_i(\mathbf{r}_1)|^2 \\ &- \sum_j \left[\int \psi_j^*(\mathbf{r}_2)\psi_i^*(\mathbf{r}_1)v(r_{12})\psi_i(\mathbf{r}_2)\psi_j(\mathbf{r}_1)d\tau_2\right]/|\psi_i(\mathbf{r}_1)|^2. \end{aligned} \tag{2.2}$$

After summing over spin and isobaric spin this becomes

$$\begin{aligned} V_i(r_1) = &\sum_j (4W+2B-M-2H)V_0 \int \phi_j^*(\mathbf{r}_2) \exp(-r_{12}^2/a^2)\phi_j(\mathbf{r}_2)d\mathbf{r}_2 \\ &+ \sum_j (4M+2H-2B-W)V_0 \\ &\qquad \frac{\int \phi_j^*(\mathbf{r}_2)\phi_i^*(\mathbf{r}_1)\exp(-r_{12}^2/a^2)\phi_i(\mathbf{r}_2)\phi_j(\mathbf{r}_1)d\mathbf{r}_2}{\phi_i(\mathbf{r}_1)|^2}. \end{aligned} \tag{2.3}$$

This gives two forms for the single particle potential $V_i(r)$, depending on whether $i$ denotes a 1s or a 1p state. A similar procedure for the kinetic energy $(-\hbar^2/2m)\nabla^2$ leads to two values $T_i(r)$ for this operator acting on the 1s or 1p wave function at the point $\mathbf{r}$. (Using harmonic oscillator wave functions the difference of these two values is independent of $\mathbf{r}$.) We define the nucleon reduced mass at the point $\mathbf{r}$ as the value $m^*$ of the mass which

will absorb the whole change in $V_i(r)$ into the kinetic energy terms. Thus with a kinetic energy operator $(-\hbar^2/2m^*)\nabla^2$, the potential energy can be regarded as independent of momentum.

The parameters in the wave function were chosen to give an r.m.s. of $2.65\times10^{-13}$ cm to the density distribution. The exchange parameters $W$, $M$, $H$ and $B$ occur only in the combinations shown in eq. (2.3); these were chosen to give for $O^{16}$ a binding energy of 127.2 MeV and a separation energy of 14 MeV. The required choice was

$$\begin{aligned} W &= \alpha & M &= 4-\alpha \\ B &= 11/2-(5/4)\alpha & H &= (5/4)\alpha-17/2 \end{aligned} \tag{2.5}$$

where $\alpha$ is an arbitrary parameter.

In fig. 1 the density $\varrho$, the single particle potentials $V_i(r)$ and the reduced

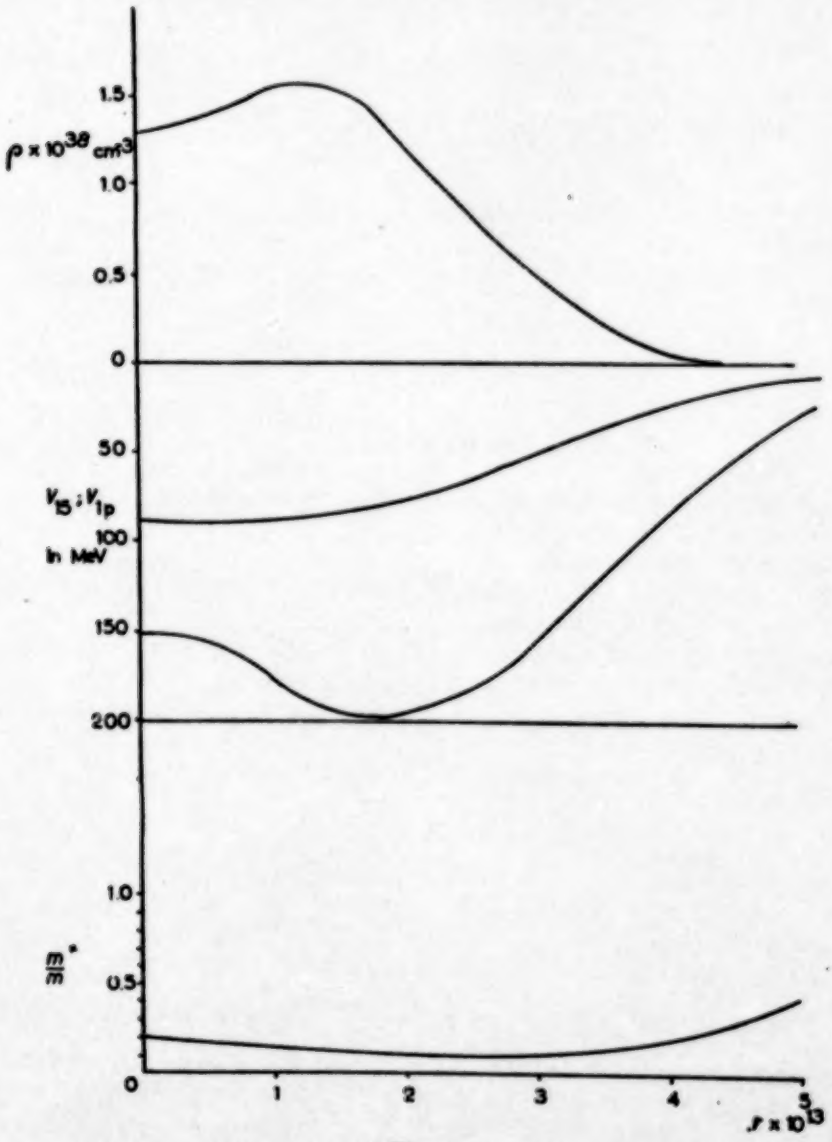


Fig. 1

mass $m^*$ are plotted as functions of $r$. In fig. 2 $m^*$ is plotted as a function of $\varrho$. For comparison we have also plotted $m^*_\infty(\varrho)$ which is the value which $m^*$ would have in infinite nuclear matter at uniform density $\varrho$, and $m_0^*(\varrho)$ defined by $m_0^*=m/(1+k\varrho)$. This last function is the nearest comparison we can make with the phenomenological potential used by several authors [8, 9, 10]. From fig. 2 it can be seen that the reduced mass required is very small, being only one tenth of the true mass, and that this small value holds out to very low densities of nuclear matter.

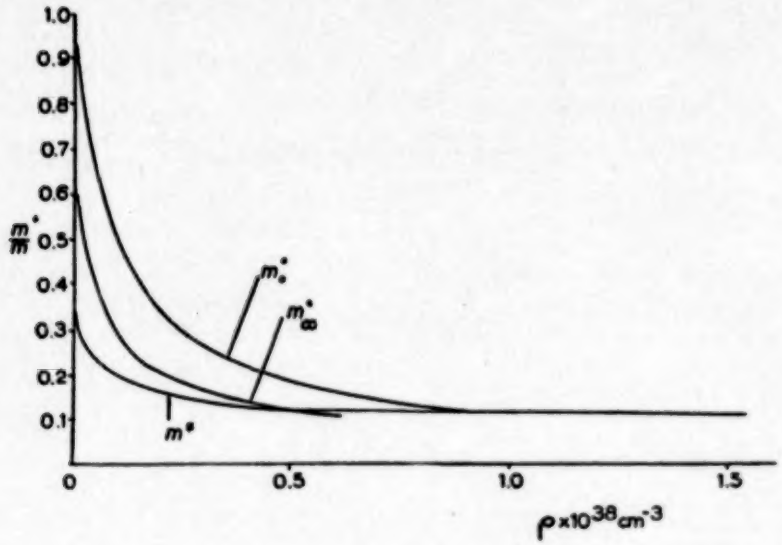


Fig. 2

## References

1) M. H. Johnson and E. Teller, Phys. Rev. **98** (1955) 783
2) K. A. Brueckner, Phys. Rev. **97** (1955) 1353
3) V. F. Weisskopf, Nuclear Physics **3** (1957) 423
4) K. A. Brueckner and C. A. Levinson, Phys. Rev. **97** (1955) 1344
5) H. A. Bethe, Phys. Rev. **103** (1956) 1353
6) R. J. Eden, Nuclear Reactions, Vol. I (North Holland, Publ. Co., 1958) in press
7) G. E. Tauber and T. Y. Wu, Phys. Rev. **105** (1957) 1772
8) A. A. Ross, R. D. Lawson and H. Mark, Phys. Rev. **104** (1956) 401
9) W. E. Frahn, Nuovo Cimento **4** (1956) 313
10) W. E. Frahn and R. H. Lemmer, Nuovo Cimento **5** (1957) 523, 1564

*Nuclear Physics* **6** (1958) 161—174; © *North-Holland Publishing Co., Amsterdam*
Not to be reproduced by photoprint or microfilm without written permission from the publisher

# APPROXIMATE OPTICAL MODEL EXPRESSIONS FOR THE ELASTIC SCATTERING AND POLARIZATION OF FAST PROTONS BY NUCLEI IN THE FORWARD SCATTERING PEAK

H. S. KÖHLER
CERN, *Geneva* †

Received 2 December 1957

**Abstract:** It is pointed out that in the forward peak the elastic differential cross-sections and polarization of fast protons or neutrons scattered from nuclei, when calculated from the usual nuclear optical model interaction, are not sensitive to the shape of the central well. On these grounds expressions have been derived that should represent the scattering from any plausible well shape and with which it is practically possible to obtain optical model parameters by handmachine-calculation. The formulae may be of some guidance when electronic machine calculations are made. They are applied to a few cases.

## 1. Introduction

Several optical model calculations on the scattering and polarization of nucleons have been published[1–5]). In these a real spin-orbit coupling of the type suggested by Fermi has mostly been assumed. Reasonably good agreement has been obtained, at least for small angles. It has also been suggested (e.g. ref. [4])) that the spin-orbit coupling may be complex. As there is no a priori information as to its magnitude, that assumption will introduce one more parameter into the calculations which will now become more complicated and difficult to interpret. It has therefore been felt that it should be of value to have some formula for the polarization, in which the nuclear parameters appear explicitly, and from which one could see how these affect the scattering and polarization without getting involved in too much computation.

It has been shown in previous papers [1, 5]) that for neutrons (if the electromagnetic spin-orbit interaction is neglected and the Thomas form is used for the nuclear spin-orbit interaction) the Born approximation result for the polarization is better than the Born approximation for the scattering amplitudes alone would lead one to expect ††. One thus finds that the polariza-

† The main part of this work was done while the author was at the Institute for Theoretical Physics, University of Uppsala.

†† This result has also been obtained by I. I. Levintov [6]).

tion of neutrons, if calculated from the assumed interaction and with the usual high energy W.K.B. approximation for the phase shifts, is (if one restricts oneself to the angular region of forward scattered particles or at least avoids the diffraction minima) very closely also given by a simple explicit formula. With the potential defined by eq. (2) below, one obtains in the same way as in ref. [1])

$$P(\theta) = \frac{\alpha(\gamma+\beta)k^2 \sin\theta}{1+\beta^2+\frac{1}{4}\alpha^2 k^4(1+\gamma^2)\sin^2\theta}; \tag{1}$$

$k$ is the wave number and $\theta$ the scattering angle. This formula also says that the polarization of neutrons is not very sensitive to the form of the central well.

In the forward scattering peak, however, one does not expect the *scattering amplitudes* (for neutrons or for protons) to depend much on the form of the central well, provided that the other well-parameters are suitably adjusted. That is, if one fixes the amplitudes, central and spin-orbit, at one angle, then the difference in angular dependence of these amplitudes for different central wells is not large for angles in the forward peak.

With these facts in mind we have derived in this paper expressions that give differential cross-sections and polarization (with inclusion of the electromagnetic spin-orbit coupling) of neutrons and protons in the forward scattering peak in good agreement with much more complicated calculations.

Besides showing in a relatively simple way how the nuclear parameters affect the results, these formulae may serve as a rough guide when electronic machine calculations are made.

## 2. Derivation of Formula

We assume the interaction of the high energy nucleon with a spherical nucleus to be given by a potential

$$V = V(r)(1+i\beta)+\alpha(1-i\gamma)\frac{V'(r)}{r}\mathbf{l}\cdot\mathbf{s}, \qquad \alpha = \alpha_1\frac{\hbar^2}{2M^2c^2}, \tag{2}$$

where $\mathbf{s}$ and $\mathbf{l}$ are the spin and orbital angular momenta; $M$ is the nucleon mass. Previous calculations with $\gamma = 0$ have given $\alpha_1 \approx 30$. To the nuclear potential the electromagnetic interaction † should be added

$$V_{el} = e\phi T_- + C\frac{e\phi'}{r}\mathbf{l}\cdot\mathbf{s}, \quad C = (g_s - T_-)\frac{\hbar^2}{2M^2c^2}, \tag{3}$$

† The spin-orbit term has been shown by T. Eriksson [3]) and W. Heckrotte [4]) to give a contribution to the polarization for small angles.

where $g_s$ denotes the Landé factor $2\mu_n$ or $2\mu_p$ for the nucleon ($2\mu_p = 5.59$; $2\mu_n = -3.82$); $T_-$ is the isobaric spin operator that has eigenvalues $+1$ and 0 for a proton and neutron respectively; $\phi$ is the potential due to the charged nucleus.

A phase-shift analysis will give neutron scattering amplitudes

$$\begin{aligned} A(\theta) &= \sum [(l+1)\exp(2i\delta_{l+\frac{1}{2}}) + l\exp(2i\delta_{l-\frac{1}{2}}) - (2l+1)]\, P_l(\cos\theta) \\ B(\theta) &= \sum [\exp(2i\delta_{l+\frac{1}{2}}) - \exp(2i\delta_{l-\frac{1}{2}})]\, P_l^1(\cos\theta). \end{aligned} \tag{4}$$

The proton amplitudes are formally different [7]). The phases are determined from the potentials according to the scheme

$$\delta_{l+\frac{1}{2}} \text{ from } V_c + \frac{l}{2} V_{so},$$

$$\delta_{l-\frac{1}{2}} \text{ from } V_c - \frac{l+1}{2} V_{so},$$

with $V_c$ and $V_{so}$ denoting the sums of the nuclear and electromagnetic central and spin-orbit potentials respectively. For the differential cross-section, polarization †, total and absorption cross-sections one obtains, respectively,

$$\begin{aligned} \sigma(\theta) &= \frac{1}{4k^2}(|A(\theta)|^2 + |B(\theta)|^2, \quad P(\theta) = \frac{2\,\mathrm{Im}\, AB^*}{|A|^2 + |B|^2}, \\ \sigma_t &= \mathrm{Im}\frac{2\pi}{ik^2} A(0), \\ \sigma_a &= \frac{\pi}{k^2} \sum [(2l+1) - (l+1)\,|\exp(2i\delta_{l+\frac{1}{2}})| - l\,|\exp(2i\delta_{l-\frac{1}{2}})|]. \end{aligned} \tag{5}$$

So far no approximations are made. Calculation of the phases in the usual high-energy approximation †† will give

$$\begin{aligned} \delta_l[U(r)] &= -\frac{1}{2E}\int_0^\infty U(r)\mathrm{d}z, \quad z = (k^2 r^2 - \nu^2)^{\frac{1}{2}}, \\ \nu &= \begin{cases} 0 & (l = 0) \\ l + \frac{1}{2} & (l \neq 0); \end{cases} \end{aligned} \tag{6}$$

$E$ is the energy of the incident particle. One should note that the phase is linear in the potential. For later use we introduce the notations

† In previous papers [1, 5, 7]) the expression for the polarization (but not the calculated values) has been given the opposite sign from the conventional one adopted here.

†† Most authors call this the W.K.B. approximation, while in previous papers we have preferred to call it the Born approximation. One should remember that it is not exactly either.

$$\begin{aligned}
\delta_l\,[V(r)(1+i\beta)] &= \delta_l \\
\delta_l[e\phi] &= \delta_l^{\,c} \\
\delta_l\left[\alpha_1 \frac{V'(r)}{r}\right] &= \delta_l^{\,s} \equiv \frac{-2K}{l+\frac{1}{2}} \frac{\mathrm{d}}{\mathrm{d}l}\delta_l \\
\delta_l\left[C\frac{e\phi'}{r}\right] &= \delta_l^{\,c,s} \equiv \frac{2K_c}{l+\frac{1}{2}} \frac{\mathrm{d}}{\mathrm{d}l}\delta_l^{\,c}
\end{aligned} \tag{7}$$

where

$$2K = \frac{\alpha(1-i\gamma)}{1+i\beta}k^2, \quad 2K_c = Ck^2.$$

The spin-orbit phase-shifts are related to the central phase-shifts as in ref. [1, 5]). For $l+\frac{1}{2} > kR_p$, where $R_p$ is the radius of the proton charge distribution in the nucleus, one will have

$$\delta_l^{\,c} \equiv \eta_l = n \ln (l+\tfrac{1}{2}) \text{ with } n = \frac{Ze^2}{\hbar v};$$

$v$ is the velocity of the incident particle and $Z$ the charge of the nucleus.

We will now introduce further approximations by first treating the spin-orbit phase-shifts as small. In the neutron case this (and the neglect of the electromagnetic spin-orbit interaction) led to the simple expression (1) for the polarization. For protons the scattering amplitudes will be

$$\begin{aligned}
A(\theta) &= f_c(\theta)\cdot 2ik + \sum (2l+1)\,[\exp 2i(\delta_l+\delta_l^{\,c}) - \exp(2i\eta_l)]\,P_l(\cos\theta) \\
B(\theta) &= 2K \exp(2i\eta) \sum \exp(2i\delta_l) \frac{\mathrm{d}}{\mathrm{d}l}(2i\delta_l) P_l^{\,1}(\cos\theta) \\
&\quad + 2K_c \sum \exp 2i(\delta_l+\delta_l^{\,c}) \frac{\mathrm{d}}{\mathrm{d}l}(2i\delta_l^{\,c}) P_l^{\,1}(\cos\theta);
\end{aligned} \tag{8}$$

$f_c(\theta)$ is the Coulomb amplitude for scattering on a point charge, $\eta$ is some mean phase that is a function of the set $\delta_l$ and $\theta$. For every usual well that is almost constant in depth up to some radius and then goes to zero in the surface region the phases $\delta_l^{\,s}$ are largest for $l$ close to $L = kR$. Therefore the orbital angular momenta close to $L$ will give the main contribution to the sum $B(\theta)$. Further, the phases $\delta_l^{\,c}$ vary only slowly with $l$ (especially for light nuclei) so that it will always be a fairly good approximation to put $\eta = \eta_L$; this will later be done when a special set $\delta_l$ has been chosen.

To simplify further we should now like to be able to sum over the phases $\delta_l$. It was already stated in the introduction that in the forward direction the scattering does not depend much on the form of the well, that is on the set $\delta_l$. A simple choice is

$$\begin{aligned}
\delta_l &= \delta \quad \text{for} \quad l \leqq L, \\
\delta_l &= 0 \quad \text{for} \quad l > L.
\end{aligned} \tag{9}$$

It was just said that the $\delta_l^s$ would be treated as small. However, according to (7) they will now become infinite for $l = L$. We will therefore treat (9) as the limit of another set in which $\delta_l$ goes gradually to zero. The well corresponding to (9) will be one that is deepest at the edges of the nucleus. This is not how one imagines a real nucleus with a diffuse surface. The procedure should therefore be considered as purely mathematical.

By the same procedure as used in ref. [1]) to derive (1) the first term in $B(\theta)$ of (8) is replaced by a summation over the $P_l$. Then going to the limit (9) the second term can also be rewritten. Noting that

$$\sum_0^L (2l+1)P_l(\cos\theta) = \frac{1}{\sin\theta}(P_L^1 + P_{L+1}^1) \equiv (L+1)^2 g_L(\theta),$$

where $g_L(\theta) = 1$ for $\theta = 0$ and decreases continually for increasing $\theta$ in the forward scattering peak, one obtains

$$A(\theta) = f_c(\theta)2ik - \sum_0^L (2l+1)\exp(2i\eta_l)P_l(\cos\theta) + e^{2i\delta}\sum_0^L (2l+1)\exp(2i\delta_l^c)P_l(\cos\theta), \qquad (10)$$

$$B(\theta) = -K_c A(\theta)\sin\theta + (K+K_c)\exp(2i\eta_L)[\exp(2i\delta)-1](L+1)^2 g_L(\theta)\sin\theta.$$

In these formulae one can also insert approximations for the sums over the Coulomb phase-shifts. Especially for light nuclei these are readily obtained, since the Coulomb-phases are small and vary only slowly with $l$, and it has some sense to speak of a "mean phase". In the first sum we determine this mean phase at zero degree and we get

$$\sum_0^L (2l+1)\exp(2i\eta_l)P_l(\cos\theta) \approx \frac{1}{1+in} e^{2in\ln(L+1)}(L+1)^2 g_L(\theta).$$

The second sum depends on what is assumed about the charge distribution in the nucleus. The phases $\delta_l^c$, however, vary less with $l$ than the $\eta_l$; the absolute value will be less decreased than in the first sum where it is reduced by the factor $(1+n^2)^{-\frac{1}{2}}$. It has been found to be a pretty good approximation to take a mean phase $\exp(2i\eta_{L'})$ with $L' = kR_p$, where $R_p$ is the radius of the charge distribution. Thus,

$$\sum_0^L (2l+1)\exp(2i\delta_l^c)P_l(\cos\theta) = \exp(2i\eta_L)(L+1)^2 g_L(\theta).$$

For very rough estimates or discussion it will sometimes be enough (for light nuclei) to put both "mean phases" equal to $\eta_L$. In this case one obtains some expressions that are still simpler to handle than (10):

$$A(\theta) = f_c(\theta)2ik + \exp(2i\eta_L)[\exp(2i\delta)-1](L+1)^2 g_L(\theta),$$
$$B(\theta) = -K_c f_c(\theta)2ik\sin\theta + K\exp(2i\eta_L)[\exp(2i\delta)-1](L+1)^2 g_L(\theta)\sin\theta. \qquad (11)$$

If these last formulae are applied, it should be remembered, however, that the errors in them are rather much larger than in (10), and the extra amount of labour necessary to do the actual summations in (10) will mostly be worth while.

For neutrons one obtains, similarly to (10),

$$A(\theta) = [\exp(2i\delta)-1]\,(L+1)^2 g_L(\theta),$$

$$B(\theta) = KA(\theta)\sin\theta + i\exp(2i\delta)\sum_0^L (2l+1)\delta_l^{c,s} P_l^1 + 4iK_c n \frac{P_L(\cos\theta)}{\theta}. \quad (12)$$

To obtain the last term in $B(\theta)$ one has to perform the summation

$$\sum_L^\infty \frac{P_L^1(\cos\theta)}{l+\frac{1}{2}}.$$

To do this we used the known relation

$$P_l^1(\cos\theta) \to l\left(\frac{\theta}{\sin\theta}\right)^{\frac{1}{2}} J_1[(l+\tfrac{1}{2})\theta]$$

which gives

$$\sum_L^\infty \frac{P_l^1(\cos\theta)}{l+\frac{1}{2}} \approx \left(\frac{\theta}{\sin\theta}\right)^{\frac{1}{2}} \int_L^\infty J_1[(l+\tfrac{1}{2})\theta]\,dl = \frac{1}{\theta}\left(\frac{\theta}{\sin\theta}\right)^{\frac{1}{2}} J[l+\tfrac{1}{2})\theta] \to \frac{P_L(\cos\theta)}{\theta}.$$

The second term in $B(\theta)$ is small and can often be neglected.

In the formula for the scattering amplitudes thus obtained the nuclear central interaction parameters are contained in $\delta$ and $L$. The polarization is mainly determined by the complex quantity $K$.

The main limitation in these amplitudes is that they are obtained from the set of phases (9). It is known, however [1]), that in the case of neutrons the polarization is independent of the central well shape. In the angular region where the influence of the Coulomb field is small we therefore expect the formulae (10) to be good, that is to represent the polarization from a more physical well than the set (9) corresponds to, although that particular set was chosen for the calculation. We expect the Coulomb field to be important in the vicinity of the forward direction and for angles larger than or around the first diffraction minimum. But the $\delta$ in formulae (10) is best determined from the differential cross-section in the forward Coulomb interference region †. This procedure gives us the correct amplitude $A(\theta)$ for these small angles. When this amplitude is fixed the amplitude $B(\theta)$ is very insensitive to changes in the shape of the central well. For angles above the diffraction minimum, finally, the applicability of the high energy W.K.B. approximation for the phases already becomes uncertain.

We have thus found that the formulae (10) should be good for the cal-

† $L$ is adjusted to give the experimental width of the forward scattering peak.

culation of polarization for two reasons. First, in the forward Coulomb interference region, because there we quite naturally fix the amplitudes by the requirement of reproducing differential cross-sections; and secondly, for larger angles, because then the neutron formula tends to be valid, and this is independent of the well-shape. The formulae should be most useful for light nuclei because the forward scattering peak is broadest in that case. Also in this case the Coulomb field is important around the forward direction mainly.

A straightforward way to see how good the formulae are, is, we believe, to make a comparison with the results from an usual W.K.B. calculation. Such a comparison is shown in figs. 1—2. The full curves were obtained

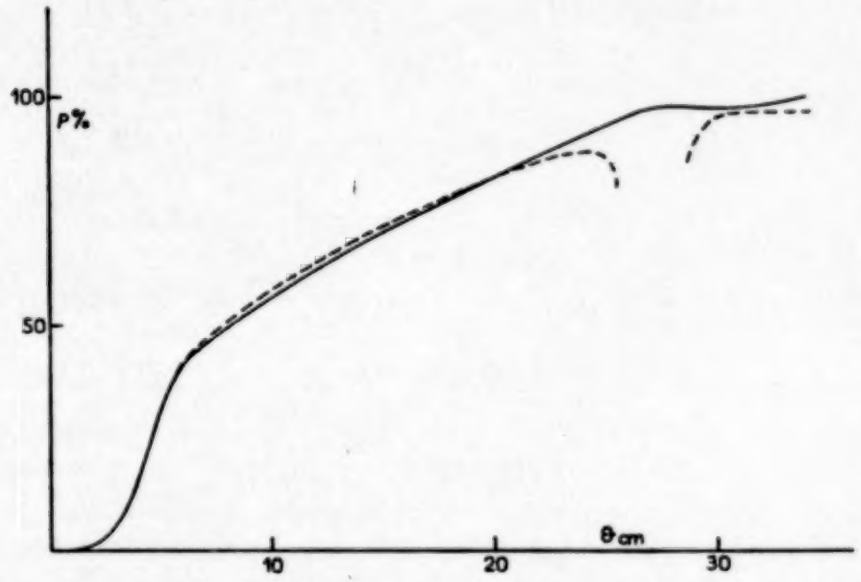


Fig. 1. Comparison between polarization from eq. (10) and "exact" calculation for C at 135 MeV. Oscillator well parameters: $V = 24$, $\beta = 0.79$, $r_0 = 1.8$, $\gamma = 0.79$, $\alpha_1 = 25$. Parameters of the "well" (9): $2\delta = 0.810\ (1+0.71i)$, $r_0 = 1.48$, $\gamma = 0.88$, $\alpha_1 = 23$.

with an oscillator central potential 1. The dotted lines were obtained from (10). When making the comparison, $A(\theta)$ in (10) was made to agree with the "exact" $A(\theta)$ at one angle. Then $L$ was adjusted to give the best fit at a larger angle. The value of $K$ used in the "exact" formula was put in.

The nucleus surface is about $2 \times 10^{-13}$ cm thick [8]). The oscillator potential is always too diffuse and the set [9]) corresponds to too sharp a potential; one might expect calculations based on a more realistic potential to give a polarization curve somewhere between these two. In fig. 2 it may even lie closer to the dotted line, as in this case the oscillator is certainly much too diffuse a potential.

We conclude that the formulae (10) do represent the scattering well within the forward scattering peak, insofar as the W.K.B. approximation

is good. Calculation by means of the formulae (10) requires relatively little work and they contain the nuclear parameters in a way that shows how they affect the results and in a way that really makes it practically possible

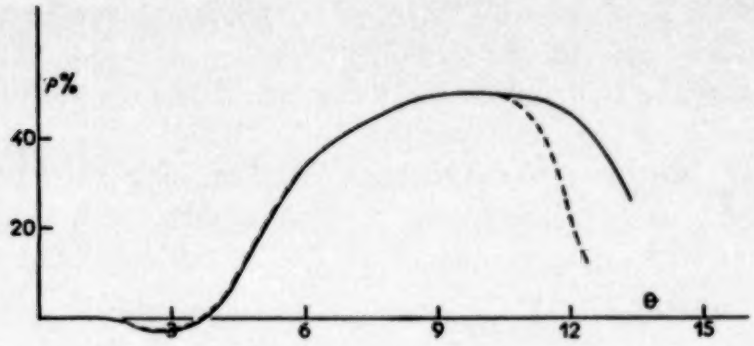


Fig. 2. Comparison between polarization from eq. (10) and "exact" calculation for Ag at 135 MeV. Oscillator well parameters: $\beta = 0.81$, $\gamma = 0.40$, $\alpha_1 = 30$. Parameters of the "well" (9): $2\delta = 1.53\,(1+0.69i)$, $r_0 = 1.29$, $\gamma = 0.50$, $\alpha_1 = 27$.

to adjust them by hand-calculation to agree with the experiments. So we can apply the formulae to investigate if the nuclear interaction (2) does describe the experiments and if the parameters can be determined.

## 3. Applications

An application of the formula to an analysis of differential cross-sections and polarization data is suitably made by first adjusting $\delta$ to give the observed differential cross-sections at two angles in the forward Coulomb interference region. At this stage one has to estimate $|B(\theta)|$ approximately and $L$ is treated as a variable †, and afterwards determined from the observed differential cross-section at some larger angle so that the experimental width of the forward peak is reproduced. Then the complex quantity $K \equiv \alpha' \exp i\varphi$ is varied to get the best fit to the observed polarization. It should at this point be observed that for the scattering of *protons* changes in $\varphi$ or in $\alpha'$ in general affect the polarization differently in the Coulomb interference region. It will thus often be possible to determine these quantities separately from small angle data alone. This is not so for *neutrons*. The reason is that the polarization is proportional to the sine of the angle between the amplitudes $A(\theta)$ and $B(\theta)$ in the complex plane. This angle is for neutrons (in the approximation leading to eq. (1)) a constant equal to $\varphi$. For protons this angle is changing rapidly in the interference region and there will be a change of the proton polarization relative to the neutron,

† It is convenient to let $L$ vary continuously, and one has to interpolate in the sums over the $P_l$ with discrete $l$-values. One can of course also replace the Legendre polynomials by Bessel functions, as is often done if the latter are more easily obtainable. The sums are then replaced by integrals and $L$ is treated as a continuous variable.

if the Coulomb field is switched on, and this change will in general depend on the value of $\varphi$. In both cases however the polarization will increase with $\alpha'$.

Some experiments were analysed by the above method (figs. 3—8).

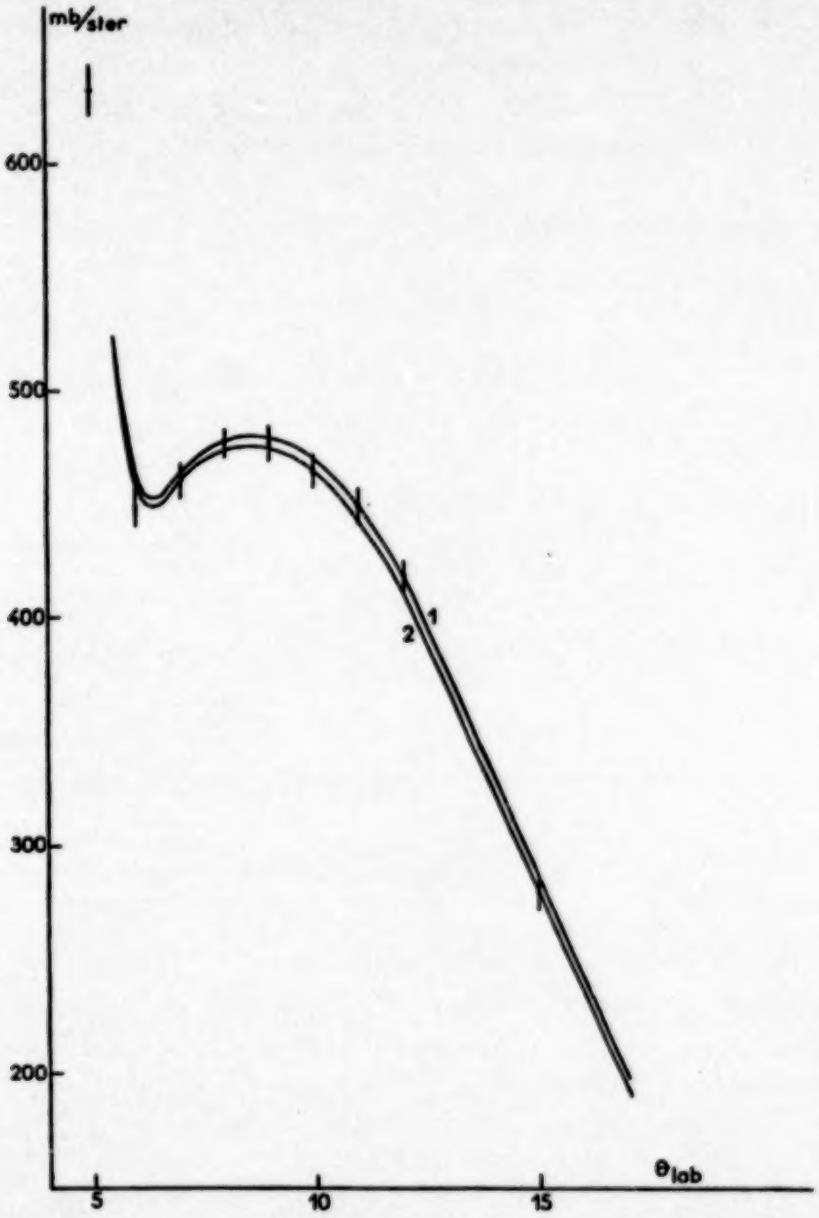


Fig. 3. Differential cross-section versus angle for C at 97 MeV fitted at 8.3, 11.1 and 13.8° (lab) to get $2\delta = 0.802\,(1+0.562i)$, $r_0 = 1.50$ and $\sigma_s = 0.15$, $\sigma_t = 0.48$ barn. Exp.: $\sigma_s = 0.23$, $\sigma_t = 0.50$ barn. For the other parameters see text under fig. 4.
Experimental points from Harwell [9]).

In this analysis no correction was made for the finite angular resolution of the experiments. It should also be pointed out that only the small angle data of the experiments have been plotted as it is with these that this investigation is concerned. The values of $r_0 = (L+\frac{1}{2})kA^{1/3}$ ($k$ is the wave-

number and $A$ the mass number), $2\delta$ and $\beta$ were obtained in the case of C at 135 and 97 MeV from a fit with experimental differential cross-sections (figs. 3—5) in the way described above. In the case of Ag and Ca no such data were available at the time. For the Ag parameters we therefore took the values obtained by the comparison made in section 2 with the calculation based on an oscillator well. For Ca we took some interpolated values using the law that $2\delta$ should be proportional to the radius. It should be pointed out that the polarization is rather insensitive to the central well parameters.

It may not seem so surprising that the differential cross-sections in figs. 3

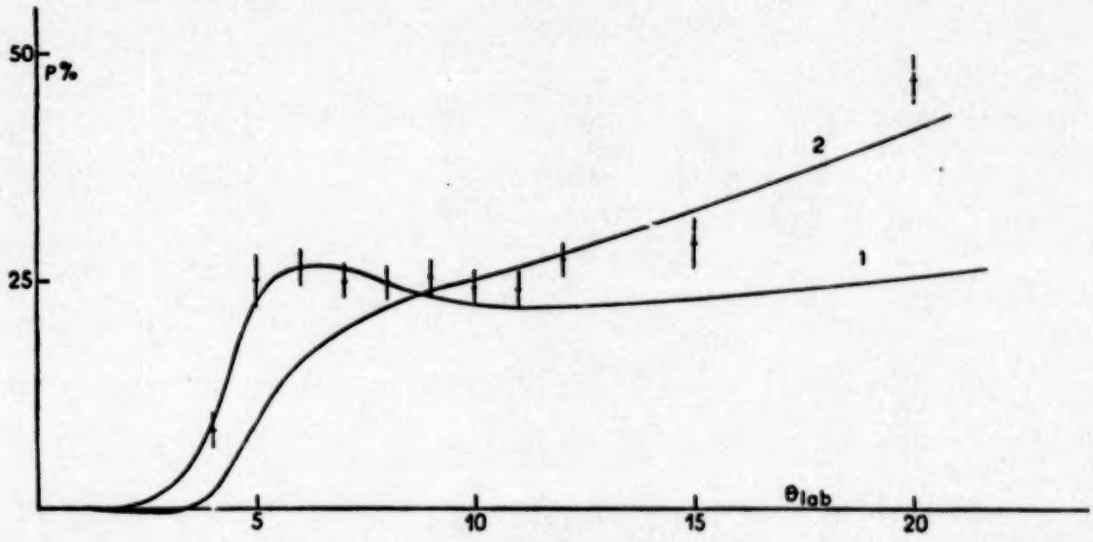


Fig. 4. Polarization versus angle for C at 97 MeV. Curve 1: $\alpha_1 = 17.0, \gamma = 0$. Curve 2: $\alpha_1 = 7.73$, $\gamma = 1.78$. For the other parameters see text under fig. 3.
Experimental points from Harwell [9]).

and 5 are rather well reproduced as they are made to fit at three angles by adjusting the parameters. Of these $r_0$, however, should be a constant (or increase for the light nuclei [12])), and the potential depths, here represented by $\delta$, depend on energy only, in order to give an optical model. In figs. 3 and 5 we are only concerned with the first requirement, which we see is fulfilled.

We have also calculated the total and absorption cross-sections (neglecting the spin-orbit phases) and these are found in the captions to the figures together with experimental values [13, 14]), The total cross-sections agree well with experiments. This just shows, by the optical theorem, that the imaginary part of the forward nuclear scattering obtained in the analysis agrees with experiment as it should when one has fitted the forward differential cross-section. The absorption cross-sections are too low by 30—40 %. This can also be understood. Assume that the forward nuclear amplitude is correctly obtained by our previous analysis. This amplitude consists of

two sums $\sum_0^L (2l+1)$ and $\sum_0^L (2l+1) \exp 2i\delta_l$. To get the absorption cross-section we have to take the absolute value of each term in the last sum and subtract this from the first. If one makes a plot of these sums in the complex plane, one sees that it is plausible that the absorption increases if one makes the well diffuse at the edge as then more $l$-values are brought into the sum and the large $l$-values give the largest contribution to the sum.

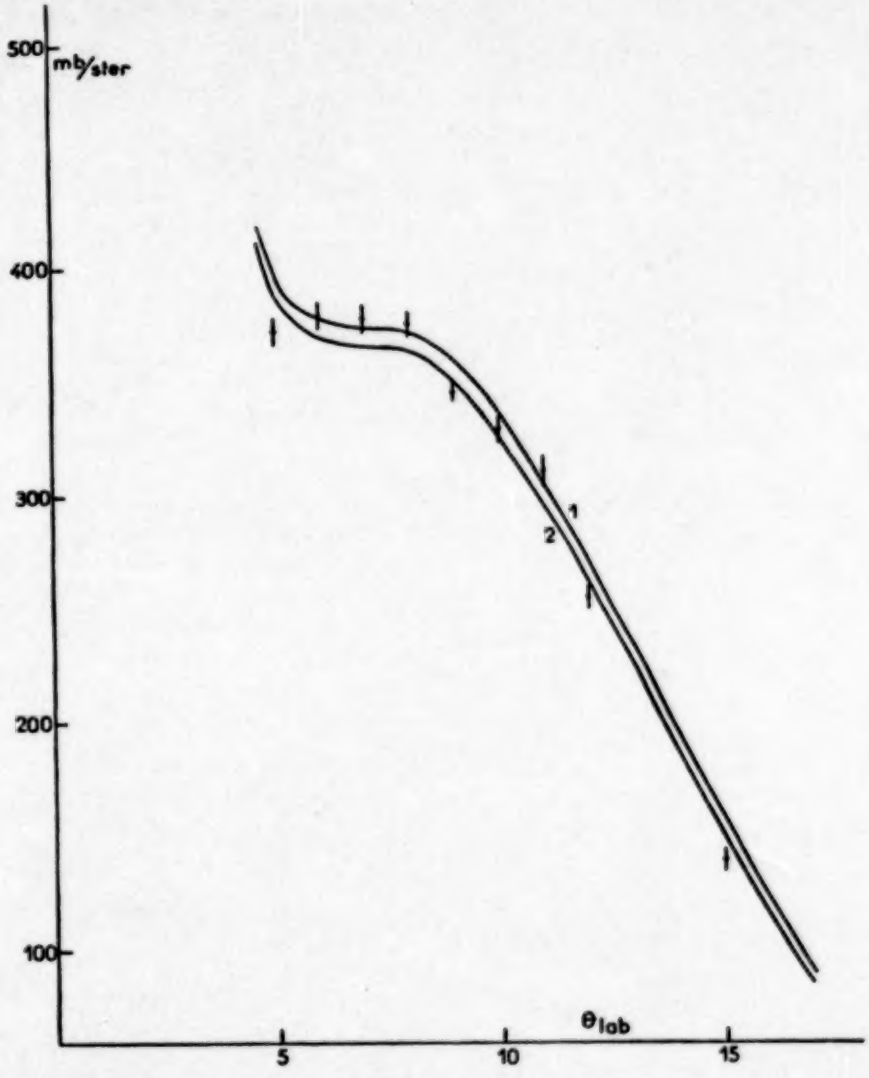


Fig. 5. Differential cross-section versus angle for C at 135 MeV fitted at 5.6°, 8.3° and 13.8° (lab) to get $2\delta = 0.531\ (1+0.798i)$, $r_0 = 1.48$ and $\sigma_s = 0.14$, $\sigma_t = 0.36$ barn. Exp.: $\sigma_s = 0.23$, $\sigma_t = 0.37$ barn. For the other parameters see text under fig. 6.
Experimental points from Harwell [9]).

In this connection we also note that it would in principle be possible to get information on the well-diffuseness if we first deduce the forward scattering amplitude e.g. by an analysis of the differential cross-section in the Coulomb interference region as done above and then vary the well-shape (at the same time changing the radius so as to keep constant the width of the for-

ward peak, and the depth of the potential so as to keep constant the forward amplitude until the absorption cross-section is reproduced.

As regards the polarization, it is seen that, in the angular region investigated here, good fits can be obtained for Ca and Ag; for Ag with

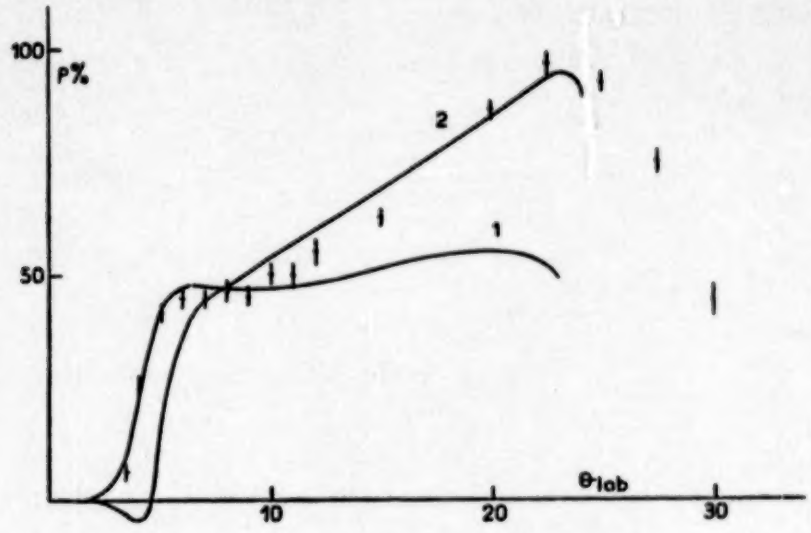


Fig. 6. Polarization versus angle for C at 135 MeV. Curve 1: $\alpha_1 = 30$, $\gamma = 0$. Curve 2: $\alpha_1 = 17$, $\gamma = 1.25$. For the other parameters see text under fig. 5.
Experimental points from Harwell [9]).

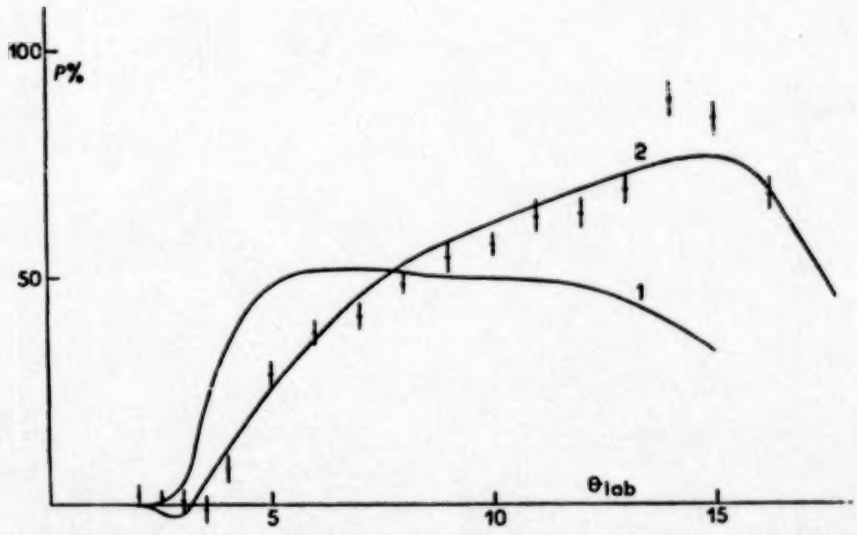


Fig. 7. Polarization versus angle for Ca at 155 MeV. Both curves with $2\delta = 0.829\ (1+0.800i)$, $r_0 = 1.37$, that gives $\sigma_s = 0.36$, $\sigma_t = 0.97$ barn. Exp.: $\sigma_s = 0.57$, $\sigma_t = 0.92$ barn. Curve 1: $\alpha_1 = 30$, $\gamma = 0$. Curve 2: $\alpha_1 = 14$, $\gamma = 1.25$.
Experimental points from Uppsala [10]).

$\gamma = 0.28$, $\alpha_1 = 27$ and for Ca with $\gamma = 1.25$, $\alpha_1 = 14$. The energies are rather close, so one should be able to compare these numbers directly. For C at 135 or 97 MeV, however, it is not possible to obtain good fits for all

angles. From small angles ($< 10°$) one deduces $\gamma = 0$, but from the larger ones $\gamma > 1$. It could be that the optical model in the form (2) is good for angles up to some 10 or 15 degrees only. Then one would still be in trouble, however, as one wants the parameters to be dependent on energy only, and not on mass number. A value $\gamma = 0$ (or slightly larger) is in pretty good agreement with both the C and Ag experiments up to around 10°. For, Ca, $\gamma$ is definitely not zero. It was pointed out before that $\gamma$ is not uniquely determined from the curves but depends on the value of $\beta$, that in the case of Ca has been put equal to 0.80. The curve 2 is obtained for all values of $\beta$ and $\gamma$ that fulfil $\beta\gamma = 1$ (if $\beta$ does not deviate so much from 0.80 that the differential cross-section is changed considerably). Thus a

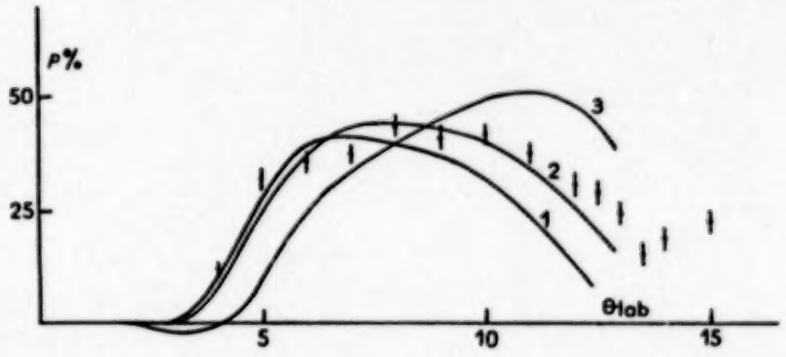


Fig. 8. Polarization versus angle for Ag at 135 MeV. All curves with $2\delta = 1.525\ (1+0.685i)$, $r_0 = 1.29$ that gives $\sigma_s = 0.82$, $\sigma_t = 2.48$ barn. Exp.: $\sigma_s = 1.16$, $\sigma_t = 2.40$ barn. Curve 1: $\alpha_1 = 29$, $\gamma = 0$. Curve 2: $\alpha_1 = 27$, $\gamma = 0.28$. Curve 3: $\alpha_1 = 15$, $\gamma = 1.46$. Experimental points from Harwell [11]).

small $\gamma$ would give a very large $\beta$. It should be pointed out that the measurements at 155 MeV on C and O in Uppsala [10]) seem to agree with $\gamma \approx 0$ up to $\approx 10$ degrees.

We also wish to report that the calculations in ref [1]) with $\gamma = 0$ on Ag and Bi agree very well with the experiments [11]) even beyond the diffraction minimum and up to $\approx 18$ degrees. For this comparison a correction was made for the finite angular resolution of the apparatus [11]).

The final answer to the inconsistencies found above may wait until further experiments are available and the extensive calculations by electronic computers undertaken at several places are completed. For these the investigation described here may be of some help.

I wish to express my gratitude to Professor Ivar Waller for his kind interest in this work and to Dr. L. Wolfenstein for a discussion of the paper in manuscript. Dr. J. M. Dickson at Harwell, and R. Alphonce, A. Johansson and G. Tibell at The Gustaf Werner Institute in Uppsala have communicated experimental results before publication, for which I am very grateful.

## References

1) H. S. Köhler, Nuclear Physics **1** (1956) 430
2) T. Eriksson, Nuclear Physics **2** (1956/57) 91
3) Ref. in L. Wolfenstein, Annual Review of Nuclear Science **6** (1956) 43
4) W. Heckrotte, Phys. Rev. **101** (1956) 1406
5) H. S. Köhler, Nuovo Cimento **2** (1955) 907
6) I. I. Levintov, Dokl. Akad. Nauk. U.S.S.R. **107** (1956) 240
7) A. Sjölander and H. S. Köhler, Arkiv för Fysik **8** (1954) 521
8) Melkanoff, Nodvik and Saxon, Phys. Rev. **106** (1957) 793
9) J. M. Dickson and D. C. Salter, Nuovo Cimento **6** (1957) 235
10) Private communication
11) Private communication from J. M. Dickson
12) L. Rosenfeld, Nuclear Physics **2** (1956/57) 450
13) V. A Nedzel, Phys. Rev. **94** (1954) 174
14) G. P. Millburn *et al.*, Phys. Rev. **95** (1954) 1268

*Nuclear Physics* **6** (1958) 175—176; © *North-Holland Publishing Co., Amsterdam*
Not to be reproduced by photoprint or microfilm without written permission from the publisher

# TEMPERATURE DEPENDENCE OF THE DIFFUSION COEFFICIENT AND THE DIFFUSION LENGTH OF THERMAL NEUTRONS IN WATER

W. H. DIO and E. SCHOPPER
*Institut für Kernphysik der Universität Frankfurt/M.*

Received 9 December 1957

Measurements of the diffusion coefficient $D$ and the mean life time $\theta$ of thermal neutrons were made in water at different temperatures, using a pulsed neutron source. The diffusion length $L$ was calculated from the relation

$$L = \sqrt{\theta \cdot D}.$$

The values of $D$ and $L$ are given below, as obtained by us at three temperatures:

| Temperature | $D$(cm$^2 \cdot$ s$^{-1}$) | $L$ (cm) |
|---|---|---|
| 19° C | 35 050± 600 | 2.70±0.05 |
| 49° C | 38 550±1000 | 2.85±0.07 |
| 75° C | 42 250±1000 | 3.00±0.07 |

The temperature dependence of the diffusion coefficient $D$ following from our measurements is smaller than that estimated by Antonov *et al.* [1]) from their values of $D$ at 23° C and 80° C. A very good agreement with the values of $D$ measured by us is obtained by computing the values at 40° C and at 75° C from the value of $D$ at 19° C, assuming a $1/v$ dependence of the transport cross section [2]).

We obtain the following expression for the temperature dependence of $D$ in the range 19°—75° C in linear approximation:

$$D = 35\,050 + (T - 19)\ (130 \pm 30)\ \text{cm}^2 \cdot \text{s}^{-1}$$

where $T$ is the temperature in °C. Our temperature coefficient of

$$(3.7 \pm 0.9) \times 10^{-3} \text{ per °C}$$

is somewhat higher than the value of

$$(2.4 \pm 0.4) \times 10^{-3} \text{ per °C}$$

reported by Von Dardel and Sjöstrand [3]) over the temperature range 10°—35° C.

The values of the diffusion length $L$ agree very well with the expression for the temperature dependence of $L$ deduced by Deutsch [2]):

$$L = \frac{2.719}{\varrho}\left[\frac{T+273.1}{295.1}\right]^{\frac{1}{2}}\left[\frac{1.0614}{1+0.0614\left[\frac{T+273.1}{295.1}\right]^{\frac{1}{2}}}\right]^{\frac{1}{2}}$$

where $\varrho$ is the water density and $T$ the temperature in °C.

For the temperature dependence of the diffusion length in the 19°—75° C temperature interval we obtain in linear approximation

$$L = 2.70+(T-19)\ (0.0054\pm 0.0022)\ \text{cm},$$

where $T$ is the temperature in °C. Our temperature coefficient

$$0.0054\ \text{cm/°C}$$

is in good agreement with the value

$$0.0061\ \text{cm/°C}$$

given by Fermi [4]), which is based on an unpublished work by Wilson, Bragdon and Kanner. The results of Antonov *et al.* [1]) fit in well with our expression above. The measurements of Von Dardel and Sjöstrand [4]) yield a temperature coefficient of the diffusion length of 0.003 cm/°C in the temperature range 10°—35° C, which is somewhat smaller than our value.

The work was supported by means of the Deutsche Forschungsgemeinschaft; the experimental part of this work was performed at the Hochspannungslaboratorium Hechingen (Max Planck-Gesellschaft).

## References

1) A. V. Antonov, A. I. Isakoff, I. D. Murin, B. A. Neupocoyev, I. M. Frank, E. L. Shapiro and I. V. Shtranich, Geneva Conference Paper No. 661 (1955)
2) R. W. Deutsch, Nuclear Science and Engineering **1** (1956) 252
3) G. F. Von Dardel and N. G. Sjöstrand, Phys. Rev. **96** (1954) 1245
4) E. Fermi, lecture notes on Neutron Physics (1945), see AECD 2664, p. 74, cited by R. W. Deutsch [2])

*Nuclear Physics* **6** (1958) 177—187; © *North-Holland Publishing Co., Amsterdam*
Not to be reproduced by photoprint or microfilm without written permission from the publisher

# POLARIZATION OF NEUTRONS SCATTERED BY INTERMEDIATE AND HEAVY NUCLEI

J. D. CLEMENT†, F. BORELI††, S. E. DARDEN†††, W. HAEBERLI and H. R. STRIEBEL*
*University of Wisconsin, Madison, Wisconsin***

Received 22 November 1957

**Abstract:** Measurements of the polarization produced in the scattering of neutrons from heavy nuclei have been carried out at neutron energies of 380 keV and 980 keV. The $Li^7$ (p, n) $Be^7$ reaction was used as a source of polarized neutrons. Right-left asymmetries in scattering of these neutrons from several elements ranging in atomic weight from 55 to 238 were measured at scattering angles of 55°, 90° and 130°. With few exceptions the observed polarizations vary smoothly with atomic weight. Measured values of the polarization range from —0.10 to +0.15 at 380 keV, and from —0.17 to +0.20 at 980 keV. The results at 380-keV neutron energy are compared with values predicted by the complex square well potential modified by a surface spin-orbit interaction. Using several sets of well parameters it has not been possible to reproduce the experimental results.

## 1. Introduction

Experiments on the scattering of polarized neutrons from nuclei provide a straightforward method for investigating spin-orbit forces in the neutron-nucleus interaction. If such forces are present, the scattered neutron flux exhibits a right-left asymmetry in the scattering plane which is chosen perpendicular to the direction of polarization of the incident neutrons. This asymmetry depends on the polarization of the incident neutrons and on the quantity $P(\theta)$, denoting the polarization which would be produced in an unpolarized beam upon being scattered through the angle $\theta$. The quantity $P(\theta)$ depends on the strength of the spin-orbit interaction.

Adair [1]) and Okazaki [2]) have used 380-keV polarized neutrons from the $Li^7$(p, n)$Be^7$ reaction to investigate polarization effects in scattering from intermediate and heavy nuclei for a scattering angle of 90°. Data obtained for a number of elements indicated that $P(\theta)$ varies fairly smoothly with atomic weight. These results were compared with polarizations calculated assuming a complex square well potential modified by a spin-orbit inter-

† Now at Westinghouse Atomic Power Division, Pittsburgh, Pennsylvania.
†† Now at Institute Boris Kidrich, Belgrade, Yugoslavia.
††† Now at Notre Dame University, Notre Dame, Indiana.
* On leave from the University of Basel, Switzerland.
** Work supported by the U.S. Atomic Energy Commission and by the Graduate School from funds supplied by the Wisconsin Alumni Research Foundation.

action. Qualitative agreement between computed and measured polarizations was found for nuclei in the atomic weight region of the giant P-wave resonance observed in the total cross sections at this energy. Polarization experiments involving heavy nuclei have also been carried out at a neutron bombarding energy of 3.2 MeV [3, 4]) as well as at energies in the 100-MeV region †.

The present experiments continue the previous work [1, 2]) at 380-keV neutron energy and extend the measurements to scattering angles of 55° and 130°, where one would expect the effect of a D-wave splitting on the polarization to be more prominent. In addition, measurements were carried out at a neutron energy of 980 keV for scattering angles of 55°, 90° and 125°.

## 2. Experimental Procedure

The experimental arrangement used for measuring the right-left asymmetries was similar to that employed by Adair [1]) and Okazaki [2]) and is shown in fig. 1. Neutrons were produced by bombarding an evaporated

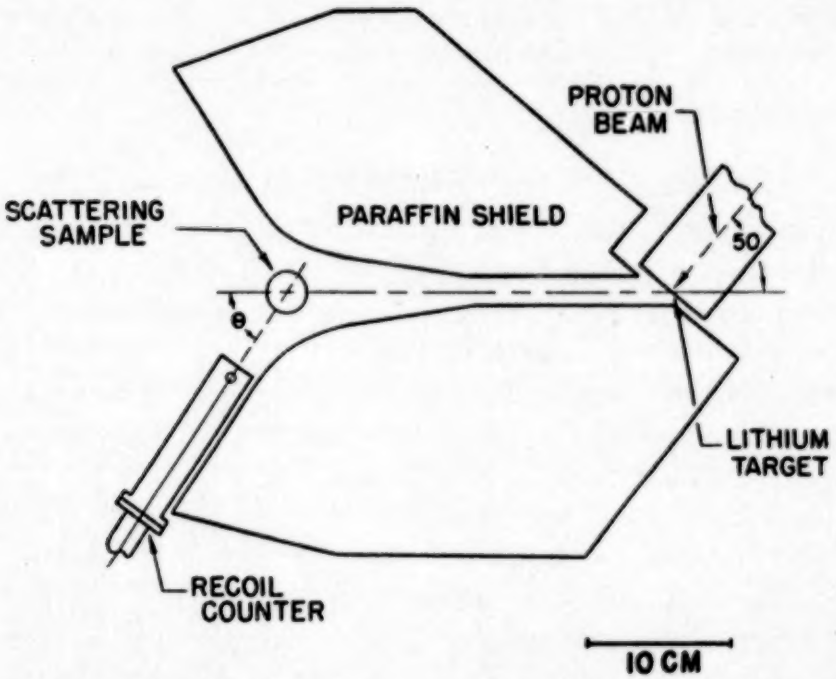


Fig. 1. Top view of the experimental arrangement used for a scattering angle of 55°.

metallic lithium target with protons from an electrostatic generator. The target chamber was connected to the generator beam tube by a metal bellows, which allowed the chamber to be rotated around the beam direction during bombardment. This together with air cooling of the target permitted a 6-$\mu$A proton beam to be used over a period of a few hundred hours before

† A summary of high energy measurements is given in ref. [5]).

deterioration of the target set in. Neutrons emitted at a laboratory angle of 50° with respect to the proton beam were collimated by a paraffin shield. The collimator hole was tapered such that the direct neutron beam could not strike any part of the collimator surface exposed to the counter. The energy spread of the neutrons was inferred from the target thickness which was determined by the rise method [6]) and from a measurement of the apparent width of the 620-keV resonance in the total cross section of Be. The two values reduced to a proton bombarding energy of 2.3 MeV were 80 keV and 92 keV.

The scattering samples were in the form of right circular cylinders, most of which had lengths of 6 cm and diameters between 1.5 and 2.5 cm. Three of the rare earth samples † had lengths of 4 cm and the U sample was 8.5 cm long. The liquid Br and Hg as well as the powdered Mn and V were contained in thin-wall stainless steel cylinders. Scatterers were aligned with axes perpendicular to the scattering plane. The collimated neutron beam irradiated all samples except the uranium sample over their entire lengths.

Neutrons scattered through the angle $\theta$ were detected with a cylindrical proportional counter. The counter was filled with five atmospheres of hydrogen for the 380-keV measurements and with 15 atmospheres of helium for the 980-keV measurements. The counter pulses were recorded on two scalers having different discriminator settings. For the lower energy experiment the discriminator levels corresponded to recoil energies of 200 keV and 150 keV respectively. For the measurements at the higher energy the corresponding figures are 800 keV and 570 keV.

The counter was mounted upon a movable support which could be rotated around the axis of the sample. The intensity of neutrons scattered through a given angle was determined by measuring the number of counts obtained with the sample in position for a run during which a fixed charge was collected on the target and by subtracting from this number the counts obtained during a corresponding run with the sample removed. Right-left intensity ratios were obtained by alternately carrying out this procedure for right and left scatterings. Background counts averaged 20 to 40 % of the sample-in counts at the forward scattering angles, and 50 to 60 % at the back angle.

In order to avoid false asymmetries, an accurate determination of the counter position corresponding to a scattering angle of 0° is necessary, particularly in cases for which the differential cross section varies rapidly with angle. For this purpose the transmission of a sample was measured as a function of the angular position of the counter for scattering angles near 0°. The setting about which the transmission curve is symmetric

† The authors wish to thank F. H. Spedding of the Ames Laboratory of the U. S. Atomic Energy Commission for granting the loan of the rare earths Sm, Nd and Er.

could be determined within $\pm 0.25°$ and was taken to be the 0° setting. This procedure was repeated several times during the experiments. In order to check other aspects of the alignment, such as the constancy of the distance from the sample axis to the counter, the right-left asymmetries of neutrons scattered from carbon was measured for scattering angles of $\theta = 55°$, 90° and 130° at the lower neutron energy. No appreciable asymmetry is expected at this energy since the contribution to the scattering by neutrons with angular momenta larger than zero is negligible. No asymmetry was observed within the statistical uncertainties of the measurements (see table 1).

## 3. Polarization of the $Li^7(p, n)Be^7$ Neutrons

Since the right-left asymmetry in the scattering of polarized neutrons from nuclei depends on the polarization of the neutrons being scattered [1]), the polarization $P_1$ of the $Li^7(p, n)Be^7$ neutrons must be determined in a separate experiment. Measurements of the polarization of 980-keV neutrons are reported in the following paper. Previous measurements [1, 2]) at 380 keV have been repeated. A value of $P_1 = -0.38 \pm 0.045$ † was found for neutrons emitted at a laboratory angle of 50° with respect to the proton beam direction. This value is consistent with Okazaki's result of $-0.41 \pm 0.02$. At the higher energy a value of $P_1 = -0.30 \pm 0.02$ was used. The quoted error limits include in addition to the usual statistical uncertainties, uncertainties in the calculation of $P(\theta)$ of the oxygen analyzer, errors in the determination of the target thickness, and uncertainties in the multiple scattering corrections. At both energies it was assumed that $P_1$ does not vary with energy over the energy spectrum of the neutrons. Since at the lower energy previous measurements suggest that $P_1$ may vary rapidly with energy this assumption introduces an additional uncertainty in $P_1$ of 6 % of its value.

## 4. Results and Discussion

Right-left ratios measured for the intermediate and heavy elements are summarized in tables 1 and 2. Since no significant differences between the results obtained at the two bias settings were found, the values used are those having the smaller statistical uncertainty. These ratios were then corrected for the variation of the neutron flux across the sample and for the effect of neutrons scattered more than once before leaving the sample. The correction for flux variation increased the measured ratios by about 1 %. The procedure followed in correcting for multiple scattering is similar

† The positive direction of the polarization is in the direction of the vector $\mathbf{n} = \mathbf{k} \times \mathbf{k}_0$, where $\mathbf{k}$ and $\mathbf{k}_0$ are the propagation vectors of the outgoing and incident beams respectively.

TABLE 1

Summary of experimental results for $E_n = 380$ keV

| Element | $A$ | Measured $R/L$ | | | $P_1$ | | |
|---|---|---|---|---|---|---|---|
| | | 55° | 90° | 130° | 55° | 90° | 130° |
| C | 12.0 | 0.995±0.004 | 0.997±0.006 | 1.000±0.009 | −0.004±0.006 | −0.009±0.008 | −0.010±0.016 |
| Cu | 63.5 | 1.020±0.011 | 1.024±0.009 | 1.026±0.018 | −0.043±0.018 | −0.048±0.015 | −0.050±0.030 |
| Zn | 65.4 | 1.001±0.014 | 1.014±0.010 | 1.018±0.017 | −0.009±0.021 | −0.031±0.016 | −0.036±0.029 |
| Ge | 72.6 | 0.996±0.009 | 1.020±0.015 | 1.008±0.019 | 0.000±0.012 | −0.039±0.024 | −0.018±0.018 |
| Se | 79.0 | 0.990±0.012 | 1.005±0.011 | | 0.003±0.018 | −0.020±0.017 | |
| Br | 79.9 | 0.991±0.014 | 1.024±0.016 | | 0.001±0.014 | −0.047±0.023 | |
| Zr | 91.2 | 0.965±0.010 | 0.973±0.009 | 1.040±0.018 | 0.054±0.017 | 0.040±0.017 | −0.074±0.032 |
| Nb | 92.9 | 0.954±0.008 | 0.924±0.013 | 0.957±0.015 | 0.076±0.019 | 0.131±0.027 | 0.072±0.029 |
| Mo | 96.0 | 0.929±0.010 | 0.914±0.005 | 0.984±0.013 | 0.126±0.023 | 0.152±0.019 | 0.025±0.024 |
| Ag | 107.9 | 0.941±0.013 | 0.938±0.012 | 0.983±0.018 | 0.088±0.023 | 0.096±0.022 | 0.023±0.031 |
| Cd | 112.4 | 0.948±0.008 | 0.935±0.013 | 0.986±0.019 | 0.083±0.018 | 0.105±0.026 | 0.017±0.033 |
| In | 114.8 | 0.963±0.013 | 0.956±0.012 | 0.982±0.022 | 0.052±0.022 | 0.065±0.021 | 0.021±0.036 |
| Sn | 118.7 | 0.963±0.008 | 0.975±0.010 | 0.980±0.014 | 0.054±0.014 | 0.033±0.016 | 0.040±0.023 |
| Sb | 121.8 | 0.979±0.012 | 0.963±0.011 | 0.979±0.020 | 0.024±0.018 | 0.051±0.020 | 0.025±0.033 |
| Te | 127.6 | 0.968±0.009 | 0.965±0.010 | 1.000±0.022 | 0.039±0.015 | 0.043±0.016 | −0.013±0.036 |
| Ce | 140.1 | 0.976±0.007 | 0.972±0.011 | 1.022±0.020 | 0.029±0.012 | 0.032±0.018 | −0.043±0.031 |
| Nd | 144.3 | 0.999±0.012 | 0.996±0.015 | | −0.004±0.016 | 0.000±0.020 | |
| Sm | 150.4 | 0.980±0.011 | 0.986±0.013 | | 0.024±0.015 | 0.017±0.018 | |
| Er | 167.2 | 1.025±0.007 | 1.036±0.008 | 0.984±0.027 | −0.045±0.012 | −0.062±0.013 | 0.020±0.042 |
| Ta | 180.9 | 1.000±0.009 | 1.041±0.013 | 1.051±0.015 | −0.003±0.014 | −0.068±0.020 | −0.083±0.025 |
| W | 183.9 | 1.021±0.012 | 1.043±0.012 | 1.055±0.033 | −0.038±0.019 | −0.073±0.016 | −0.090±0.054 |
| Hg | 200.6 | 0.983±0.009 | 1.004±0.009 | 1.033±0.015 | 0.018±0.015 | −0.014±0.014 | −0.061±0.025 |
| Bi | 209.0 | 1.065±0.011 | 1.026±0.011 | 0.982±0.018 | −0.104±0.018 | −0.048±0.016 | 0.021±0.031 |
| U | 238.1 | 1.051±0.015 | 1.023±0.011 | 0.994±0.014 | −0.079±0.023 | −0.036±0.017 | 0.008±0.022 |

TABLE 2

Summary of experimental results for $E_n = 980$ keV

| Element | $A$ | Measured $R/L$ | | | $P_2$ | | |
|---|---|---|---|---|---|---|---|
| | | 55° | 90° | 125° | 55° | 90° | 125° |
| V | 51.0 | 0.997±0.017 | | | −0.022±0.037 | | |
| Mn | 54.9 | 0.992±0.017 | 0.975±0.017 | 1.021±0.018 | 0.000±0.033 | 0.034±0.040 | −0.063±0.037 |
| Co | 59.0 | 0.950±0.015 | | | 0.093±0.034 | | |
| Cu | 63.5 | 1.050±0.006 | 1.016±0.008 | | −0.115±0.017 | −0.052±0.018 | |
| Zn | 65.4 | 1.036±0.010 | | | −0.088±0.022 | | |
| Ge | 72.6 | 1.052±0.017 | 0.964±0.015 | | −0.107±0.034 | 0.058±0.033 | |
| Se | 79.0 | 1.003±0.014 | 0.912±0.010 | 0.940±0.017 | −0.025±0.027 | 0.173±0.027 | 0.117±0.041 |
| Mo | 96.0 | 0.997±0.015 | 0.932±0.010 | | −0.060±0.033 | 0.150±0.026 | |
| Ag | 107.9 | 0.979±0.012 | 0.907±0.016 | | 0.027±0.023 | 0.207±0.042 | |
| Cd | 112.4 | 1.003±0.010 | 0.920±0.016 | 0.987±0.028 | −0.023±0.020 | 0.177±0.044 | 0.016±0.055 |
| Sn | 118.7 | 0.984±0.018 | | | 0.017±0.037 | | |
| Sb | 121.8 | 0.966±0.010 | | | 0.050±0.020 | | |
| Te | 127.6 | 0.978±0.008 | 0.948±0.013 | | 0.023±0.017 | 0.103±0.034 | |
| Ce | 140.1 | 0.967±0.007 | 0.975±0.015 | | 0.050±0.018 | 0.046±0.043 | |
| Er | 167.2 | 1.037±0.018 | | | −0.080±0.034 | | |
| Ta | 180.9 | 1.048±0.010 | | | −0.103±0.022 | | |
| W | 183.9 | 1.040±0.016 | 1.011±0.018 | 0.975±0.021 | −0.090±0.034 | −0.043±0.043 | 0.041±0.045 |
| Hg | 200.6 | 1.021±0.008 | 1.026±0.016 | | −0.060±0.018 | −0.073±0.033 | |
| Tl | 204.4 | 1.057±0.011 | 1.017±0.017 | | −0.127±0.025 | −0.047±0.037 | |
| Bi | 209.0 | 1.085±0.017 | 1.078±0.009 | 1.004±0.019 | −0.173±0.036 | −0.157±0.025 | −0.023±0.037 |
| U | 238.1 | 1.061±0.010 | 1.013±0.016 | 0.962±0.027 | −0.120±0.023 | −0.037±0.030 | 0.065±0.053 |

to that used by Walt and Barschall [7]). In making this correction it was assumed that the multiply scattered neutrons exhibit no right-left asymmetry. Consequently the corrections have the effect of increasing the magnitude of the measured polarizations. At 400-keV neutron energy the average value of this correction is about 25 % of the value of the polarization. At the higher neutron energy the average corrections amount to 16 %, 23 % and 30 % of the value of the polarization at scattering angles of 55°, 90° and 125° respectively. Corrected values of $P_2$ are given in the last three columns of tables 1 and 2.

The assumption that the multiply scattered neutrons exhibit no ap-

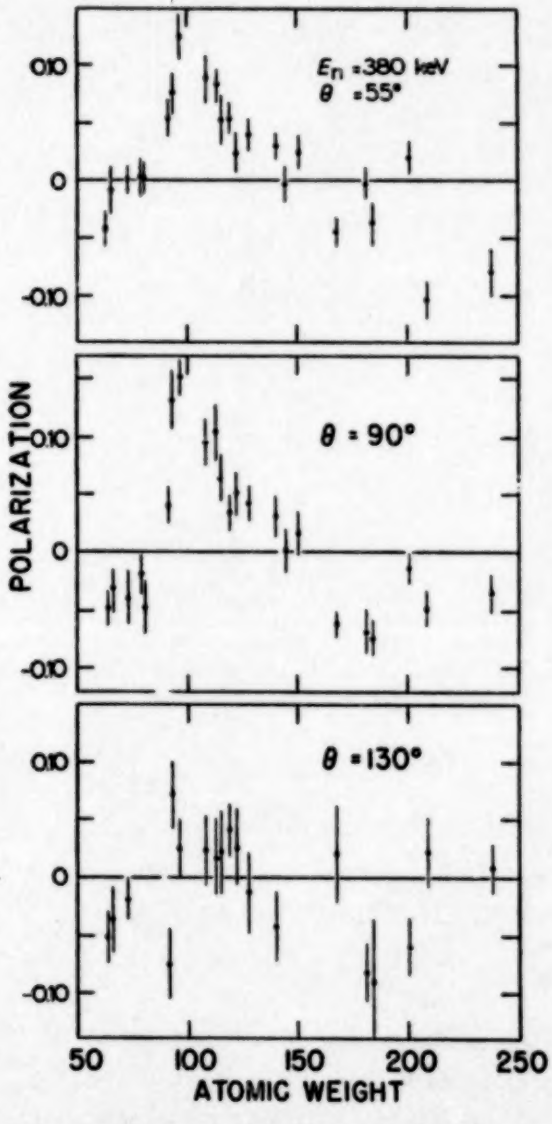


Fig. 2. Measured polarizations as a function of atomic weight for a neutron energy of 380 keV. The scattering angle is indicated in the upper right hand corner of the graphs.

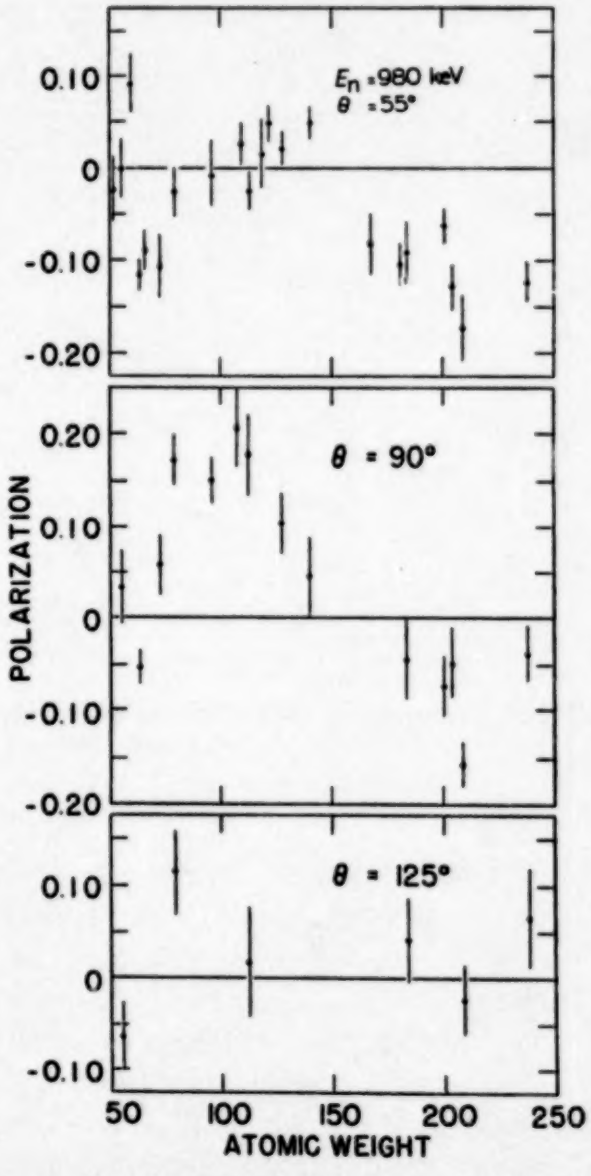


Fig. 3. Measured polarizations as a function of atomic weight for a neutron energy of 980 keV. The scattering angle is indicated in the upper right hand corner of the graphs.

preciable right-left asymmetry requires some justification. It was tested by a numerical calculation of the number of doubly scattered neutrons in Bi. The results of this calculation indicated that if the singly scattered neutrons exhibit a right-left ratio of 1.11 for a scattering angle of 90°, the doubly scattered neutrons will exhibit a ratio of 1.04 for the same angle. This number varies from element to element. Bi was chosen for the numerical calculation, since qualitative considerations indicated that for other elements this ratio is closer to unity. In this particular case, the

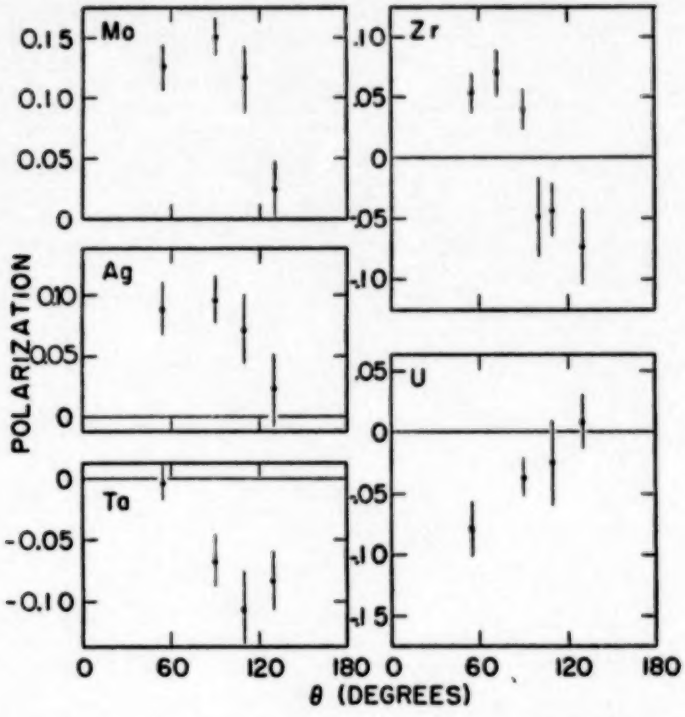


Fig. 4. Polarization versus scattering angle for Zr, Mo, Ag, Ta and U. The data are for a neutron energy of 380 keV.

assumption that the multiply scattered neutrons exhibit no right-left asymmetry introduces an error in the multiple scattering correction of 1/3 of its value. Since the average value of the multiple scattering correction was 25 %, an error of 8 % has been included in the uncertainties given in tables 1 and 2.

The measured polarizations are plotted as a function of atomic weight in figs. 2 and 3. For the lower neutron energy, measurements of the angular dependence of the polarizations are shown in fig. 4 for a number of elements. With few exceptions, the polarization varies smoothly with atomic weight. No dependence on the spin of the target nucleus is evident. At the lower neutron energy the polarizations are small, having a maximum value of 0.15. The most prominent feature of these data is the peak in the atomic weight

region of 100 for scattering angles of 55° and 90°. Negative polarizations are observed in the vicinity of $A = 75$ for 90° and 135° and in the region of the heavier elements for all angles. The 90° data are in fair agreement with the results of Adair [1]) and of Okazaki [2]). The small negative polarizations in the neighborhood of $A = 75$ and $A = 175$ do not appear in Okazaki's data. At the higher neutron energy the polarizations are similar in magnitude to those observed at 380 keV. However, at the higher energy there is a more pronounced change in the polarization in going from the scattering angle of 55° to the angle of 90°.

Measurements [3, 4]) have been performed at a neutron energy of 3.2 MeV. At this energy polarizations in excess of 0.5 have been reported, and in addition the data seem to exhibit a more complex angular dependence.

The energy spread of the neutron beam used in the present experiments is large compared to the level spacing of the compound nucleus for most of the elements studied. Consequently the measured polarizations are averages over many levels, and theories of the average properties of the neutron-nucleus interaction might be expected to reproduce the general features of the observed polarizations, since other features of the neutron-nucleus interaction have been reproduced using such theories [8]). Naturally the potential used must be modified to include spin-orbit coupling in order to account for the observed polarizations.

Calculations † were available for a potential of the form

$$V(r) = \begin{cases} -V_0(1+i\zeta) - \dfrac{q\hbar^2}{RM}\,\delta(r-R)\mathbf{L}\cdot\mathbf{S} & r \leqq R \\ 0 & r > R \end{cases} \qquad (1)$$

where $M$ is the neutron mass. The target nucleus was assumed to have zero spin. $q$ is a measure of strength of the spin-orbit coupling. The nuclear radius $R$ was taken to be $R = 1.45\ A^{1/3} \times 10^{-13}$ cm and a value $V_0 = 42$ MeV was assumed for the well depth. Total cross sections, calculated on the basis of this model have been compared [9]) with the observed total cross sections as a function of atomic weight for a neutron energy of 380 keV. Qualitative agreement between the measured and calculated values was found. However, the agreement becomes appreciably poorer as the absorption parameter $\zeta$ is increased from 0.03 to 0.1 and/or as a significant amount of spin-orbit coupling is added. The polarizations predicted by the model have been compared with the results of the present experiment, using values of the parameter $q$ between 0.5 and 6.0 and values of $\zeta$ of 0.03 and 0.10. For all the values of $q$ and $\zeta$ tried, the calculated curves exhibit in the atomic weight region near $A = 100$ structure which is associated with the splitting of the giant P-wave resonance in this region.

† These calculations were performed by the late R. G. Thomas.

This feature is evident in the 55° and 90° data. Some of the calculated curves are shown in fig. 5 for a scattering angle of 90°. It can be seen that with the smaller value of $\zeta$, which is indicated by the measured total cross sections, the correct amount of polarization at the $A = 100$ peak is obtained. However, the peak is much too narrow and the negative polarizations below $A = 100$ are too large in magnitude. The peak can be widened by increasing the spin-orbit coupling, in which case, however, the polarizations are too large in magnitude. The magnitude of the predicted polarizations may be reduced without strongly affecting the width of the peak by increasing the absorption parameter to 0.1, but this drastically reduces the P-wave peak in the total cross section. The behaviour at the other scattering angles is similar, except

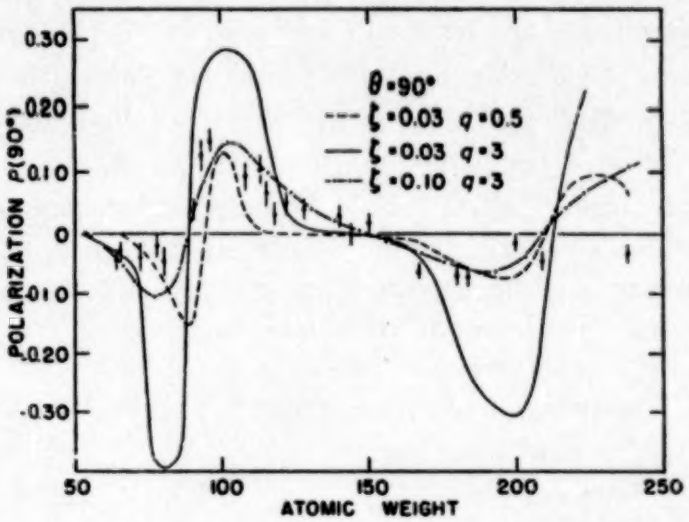


Fig. 5. Calculated values of the polarization produced in shape elastic scattering for a scattering angle of 90° and a neutron energy of 380 keV. The curves were computed from the potential (1), using the parameters given in the figure. The experimental data are also shown.

that at 130° the calculated polarizations for $q = 3$ are larger than the measured ones by an order of magnitude, even with $\zeta = 0.1$.

The comparison between theory and experiment is complicated by the fact that the model predicts only the polarization of the shape elastically scattered neutrons. The effect of compound elastically scattered neutrons may be taken into account by assuming that they are on the average unpolarized [1]) and that their angular distribution is isotropic. This will have the effect of reducing the predicted polarizations in the atomic weight region near $A = 100$ by as much as 20 %, 30 % and 50 % for the scattering angles of 55°, 90° and 135° respectively. The amount of this reduction depends upon the fraction of absorbed neutrons which are re-emitted elastically. At a neutron energy of 400 keV the amount of reduction quoted above would be expected to hold since at this energy inelastic scattering is relatively unimportant.

It is not surprising that calculations based on a square well potential fail to reproduce the measured polarization since this model has already been shown to be unsatisfactory. The introduction of rounded wells has considerably improved the agreement between the calculated and the measured differential cross sections [8]). However, parameters obtained from such comparisons are uncertain to the extent that the effect of spin-orbit coupling has not been considered in such potentials. Calculations [10]) for a complex potential with rounded edges including a spin-orbit coupling are in progress.

The authors wish to thank Prof. H. H. Barschall for suggesting the experiment and for his continued interest in this work.

## References

1) R. K. Adair, S. E. Darden and R. E. Fields, Phys. Rev. **96** (1954) 503
2) A. Okazaki, Phys. Rev. **99** (1955) 55
3) A. E. Remund, Helv. Phys. Acta **29** (1956) 545
4) B. M. McCormac, M. F. Steuer, C. D. Bond and F. L. Hereford, Phys. Rev. **108** (1957) 116
5) L. Wolfenstein, Ann. Rev. Nucl. Sci. **6** (1956) 43
6) R. Taschek and A. Hemmendinger, Phys. Rev. **74** (1948) 373
7) M. Walt and H. H. Barschall, Phys. Rev. **93** (1954) 1062
8) See, for instance, J. R. Beyster, M. Walt and E. W. Salmi, Phys. Rev. **104** (1956) 1319
9) M. S. Zucker, Phys. Rev. **104** (1956) 1025
10) R. F. Bjorklund, private communication

*Nuclear Physics* **6** (1958) 188—195; © *North-Holland Publishing Co., Amsterdam*

Not to be reproduced by photoprint or microfilm without written permission from the publisher

# POLARIZATION OF $Li^7(p, n)Be^7$ NEUTRONS

H. R. STRIEBEL†, S. E. DARDEN†† and W. HAEBERLI
*University of Wisconsin, Madison, Wisconsin*†††

Received 22 November 1957

**Abstract:** The polarization of neutrons emitted from the $Li^7(p, n)Be^7$ reaction at an angle of 50° was measured for neutron energies between 0.7 and 1.5 MeV. The polarization was deduced from the right-left asymmetry in the scattering of these neutrons from liquid oxygen. The results indicate that the polarization is close to —0.3, independent of bombarding energy. One measurement for neutrons emitted at 30° yields a polarization only slightly smaller than for neutrons emitted at 50° for the same proton energy. The total neutron cross section of oxygen was remeasured for neutron energies between 0.7 MeV and 1.4 MeV.

## 1. Introduction

Neutrons emitted in nuclear reactions are in general expected to be polarized [1]). Measurements of the degree of polarization contribute to the study of the reaction mechanism and are also of interest since polarized neutrons are useful for the study of spin-orbit effects in the neutron-nucleus interaction. Reactions which have been investigated to date include the $Li^7(p, n)Be^7$ [2–5]), the $D^2(d, n)He^3$ [6–9]) and the $C^{12}(d, n)N^{13}$ [10]) reactions. In all of these cases the procedure followed to determine the polarization has been to measure the right-left asymmetry in the scattering of the neutrons from a suitable nucleus. Provided the neutron scattering phase shifts for this nucleus are known, the polarization of the incident neutrons can be calculated from the observed right-left asymmetry.

Adair [2]), Okazaki [5]) and Willard [3]) have investigated the polarization of $Li^7(p, n)Be^7$ neutrons emitted at laboratory angles of 50° [2, 5]) and 42° [3]) and ranging in energy from 270 keV to 600 keV. The polarization was determined from measurements of the asymmetry in the scattering by oxygen. In this energy region polarization values * of the order of −0.40 were found.

In the present experiment the same procedure has been used to extend the previous measurements to neutron energies between 700 keV and

† On leave from the University of Basel, Switzerland.

†† Now at University of Notre Dame, South Bend, Indiana.

††† Work supported by the U. S. Atomic Energy Commission and by the Graduate School from funds supplied by the Wisconsin Alumni Research Foundation.

* The positive direction of the polarization is chosen in the direction of the vector $\mathbf{k} \times \mathbf{k}_0$, where $\mathbf{k}$ and $\mathbf{k}_0$ are the propagation vectors of the outgoing and incident beams respectively.

1.5 MeV. An analysis of the total cross section and angular distribution data for oxygen provides sufficiently accurate values of the phase shifts to allow a calculation of the polarizing power of the oxygen scatterer.

## 2. Polarization of Neutrons Scattered from Oxygen

In order to calculate the polarizing power of oxygen, *i.e.*, the polarization which would result in the scattering of an initially unpolarized beam, the scattering phase shifts must be known over the energy interval of interest. In general the phase shifts can be obtained from the measured total and differential cross sections. In the present experiment the phase shifts were obtained from the oxygen total cross section. For neutron energies below 1.4 MeV the total cross section of oxygen has been measured [11]) using $Li^7(p, n)Be^7$ neutrons and an energy insensitive neutron detector. Since in the meantime a low energy group of neutrons due to the $Li^7(p, n)Be^{7*}$

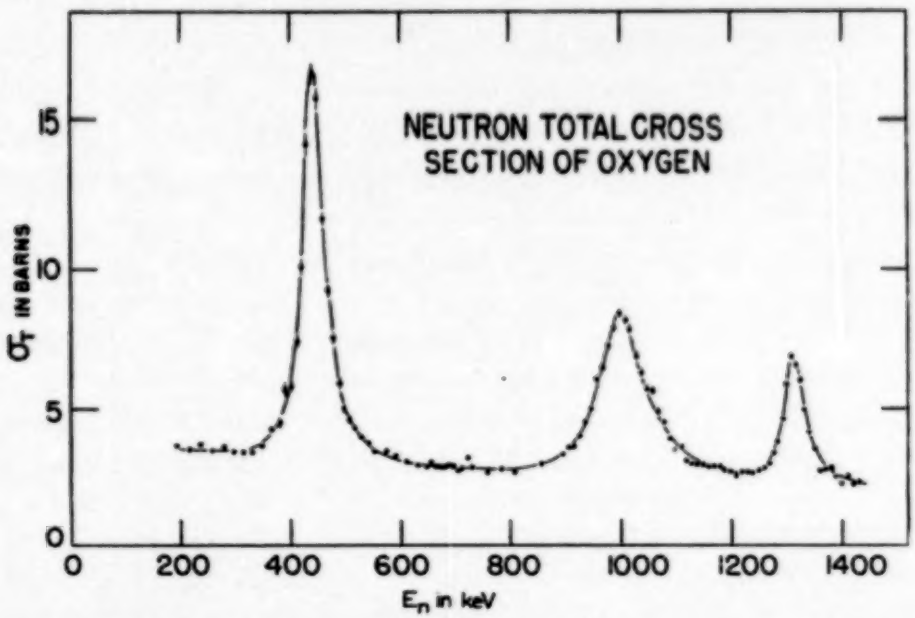


Fig. 1. Total neutron cross section of oxygen. The statistical uncertainties are indicated, where larger than the dots. The data below $E_n = 700$ keV are those of Okazaki [5]).

reaction has been found, these measurements may be inaccurate. The total cross section was remeasured by the transmission method, using $SnO_2$ and Sn scattering samples. Again the $Li^7(p, n)Be^7$ reaction served as a neutron source, but the low energy neutrons were discriminated against by using a propane filled recoil counter and by accepting only the largest counter pulses. The neutron energy spread was 8 keV. It was determined from the apparent width of the 585-keV resonance in sulfur. Measured values of the cross sections for neutron energies between 0.7 and 1.4 MeV are plotted in fig. 1. Also included in fig. 1 are the data of Okazaki [5])

below 0.7 MeV. An inscattering correction was applied to the data. The magnitude of the correction varied between 1.5 % and 3 % depending on neutron energy. The statistical uncertainties are indicated in the figure. Where no error bars are shown the uncertainties are less than the diameter of the dots.

At most energies the cross sections agree with the older measurements [11]) within about 10 %. Resonances occur at 442 keV, 1 000 keV, and 1 312 keV with widths at resonance of 48 keV, 100 keV and 44 keV. The total angular momenta and parities of the corresponding levels in $O^{17}$ are known to be $3/2^-$, $3/2^+$ and $3/2^-$ respectively [12]).

In analyzing the total cross section, the S-wave potential phase shift was first obtained for two neutron energies, one below and one above the energy interval of interest here. For a neutron energy of 2.3 MeV the S-wave potential phase shift was determined from the shape of the S-wave resonance at this energy. From angular distribution experiments of neutrons scattered from oxygen [5]) it is known that orbital angular momenta larger than zero make negligible contributions to the total cross section at 0.2 MeV energy. Therefore the S-wave potential phase shift at 0.2 MeV may be obtained directly from the total cross section. The phase shifts at 2.3 MeV and at 0.2 MeV so obtained require a hard sphere radius of $5.60 \times 10^{-13}$ cm. For the energy interval between these two points, the potential S-wave phase shift was calculated using the above radius. The assumption of a constant radius is not unreasonable, since the spacing of the S-wave size resonances is large compared to the energy interval considered here. Indeed calculations based on a square well [13]) yield S-wave phase shifts practically identical to the ones used here. The total cross section between resonances is well reproduced by using these S-wave phase shifts and the tails of the P- and D-wave resonances. This indicates that the potential P- and D-wave phase shifts must be small. The addition of either a $3/2^-$ or a $3/2^+$ potential phase shift of $-2°$ causes, in disagreement with the experiment, a perceptible decrease of the calculated cross section in the energy region below and an increase above the corresponding resonances. Since it is impossible to remove such a disagreement without introducing an inflection point into the curve of the S-wave phase shift versus energy, the potential P- and D-wave phase shifts were taken to be zero. For the calculation of the resonance phase shifts a Breit-Wigner single-level formula [14]) was used. A radius of $5.5 \times 10^{-13}$ cm was chosen for the calculation of the penetrabilities. The tangent of the $3/2^-$-phase shift was taken to be the sum of the tangents of the phase shifts from the two $3/2^-$ resonances.

Total cross sections calculated from the phase shifts discussed above are shown by the solid curve in fig. 1. Fowler and Cohn [13]) have measured angular distributions of neutrons scattered from oxygen. From their data

they obtained phase shifts essentially identical to the phase shifts used in the present investigation except at a neutron energy of 730 keV, where a $3/2^+$-phase shift of $-5°$ was required to fit their data. This discrepancy will be discussed later.

Values of the polarizing power $P_2(\theta)$ calculated from the phase shifts [15]) discussed above are shown in fig. 2 as a function of neutron energy for a centre-of-mass scattering angle of $\theta = 60°$. In table 1 are listed polarizations $P_2(\theta)$ at those energies and angles for which asymmetry measurements were performed. Since the neutrons used had an estimated energy spread of 80 keV, the $P_2$ given are values of $\overline{\sigma(\theta) \cdot P_2(\theta)}/\overline{\sigma(\theta)}$, where the average is taken over the energy spread. Though of no practical importance it should be mentioned that the above calculations were carried out for $\theta = 60°$, 90° and 130° while in the experiment scattering angle $\theta_{c.m.} = 58°$, 90° and 128° were used.

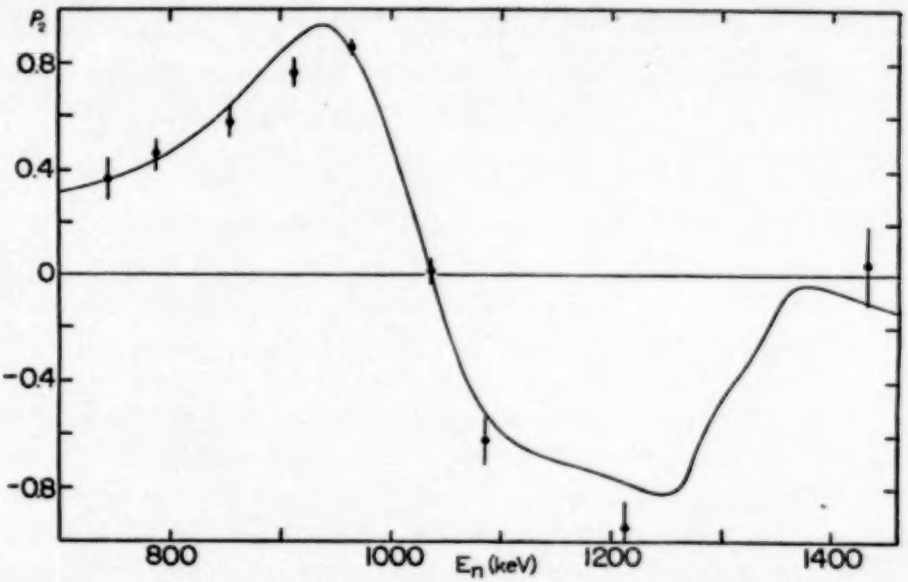


Fig. 2. $P_2$ of oxygen for a scattering angle of 60° averaged over 80 keV. The experimental points represent the measured values of $P_1P_2$ (58°) divided by a fixed value of $P_1 = -0.3$.

In order to estimate uncertainties of $P_2$, variations in the phase shifts were introduced. In particular the effect of possible $1/2^-$ and $3/2^-$ potential phase shifts was studied. Since practically no information can be obtained about the $1/2^-$-phase shift from the total cross section alone, the angular distributions [13]) were also considered. While it is difficult to make reliable statements about the uncertainty in $P_2(\theta)$, it is estimated that the $P(60°)$ as shown in fig. 2 have a maximum error of $\pm 0.1$ near 700-keV neutron energy and of $\pm 0.15$ near 1.2 MeV and probable errors somewhat less than half as large. The uncertainties in $P_2(\theta)$ become appreciably smaller near 950-keV neutron energy, but somewhat larger for energies above 1.4 MeV.

## 3. Experimental Procedure

The experimental arrangement and procedure used to measure the right-left asymmetry of scattered neutrons were essentially the same as used in earlier work [4, 5]). Some details are given in the preceding paper. Neutrons emitted at an angle of 50° from a metallic Li target were scattered from a sample of liquid oxygen. The liquid oxygen was contained in a thin-walled (0.2 mm) can 2 cm in diameter and 13 cm high. Surrounding the can was a styrofoam jacket of 0.7 cm thickness. The collimated neutron beam irradiated the sample only over a length of 6 cm, so that the exposed part of the container was filled for the entire duration of each run. The proportional counter was filled with 2.4 atmospheres of propane and biased sufficiently high to discriminate against the low energy group of target neutrons. Background measurements were taken with the empty can in position. The number of background counts ranged from 48 % to 67 % of the counts obtained with the filled container.

## 4. Results and Discussion

The measured right-left ratios $R/L$ are listed in table 1. This ratio is related to the polarizing power $P_2(\theta)$ of oxygen and to the polarization $P_1$ of the $Li^7$(p, n) $Be^7$ neutrons by the equation

$$P_1 P_2(\theta) = \left(\frac{R}{L}(\theta) - 1\right)\left(\frac{R}{L}(\theta) + 1\right)^{-1}. \qquad (1)$$

Values of $P_1P_2(\theta)$ obtained from the measured right-left ratios using eq. (1) were corrected for multiple scattering and for the variation of the neutron flux across the sample. In most cases the multiple scattering corrections amounted to about 10 % of the values of $P_1P_2(\theta)$, except at a neutron energy of 965 keV, where the correction was 20 %. The multiple scattering corrections were calculated in the manner described in the preceding paper, but here the effect of the energy loss of the neutrons in the first collision was taken into account in calculating the fraction of neutrons scattered more than once. Corrected values of $P_1P_2$ are given in column 6 of table 1.

At a neutron energy of 965 keV $P_1P_2(\theta)$ was determined for centre-of-mass scattering angles of 58°, 90° and 128°. The results confirm the assignment of $J^\pi = 3/2^+$ to the level corresponding to the 1.0-MeV resonance. As expected $P_1P_2(\theta)$ changes sign between $\theta = 58°$ and $\theta = 128°$ and is close to zero for $\theta = 90°$. Similarly, a value of $P_1P_2$ close to zero at a neutron energy of 1430 keV confirms the assignment $J^\pi = 3/2^-$ to the level corresponding to the 1312-keV resonance, since this assignment predicts a value close to zero for $P_2$ at this energy.

Values of $P_1$, the polarization of the $Li^7(p, n)Be^7$-neutrons, are presented in the last column of table 1. They were obtained by dividing the corrected values of $P_1P_2(\theta)$ by the calculated oxygen polarizations $P_2(\theta)$. In cases for which $P_2(\theta)$ is so small that no meaningful value of $P_1$ can be obtained,

TABLE 1

Summary of experimental results

| $\overline{E_p}$ (MeV) | $\overline{E_n}$ (MeV) | Angle of neutron emission (degrees, lab. system) | Neutron scattering angle $\theta$ (degrees c.m.) | $R/L$ | Corrected $P_1P_2$ | $P_2$ | $P_1$ |
|---|---|---|---|---|---|---|---|
| 2.618 | 0.744 | 50 | 58 | 0.813±0.040 | −0.110±0.024 | +0.362 | −0.304±0.066 |
| 2.667 | 0.788 | 50 | 58 | 0.771±0.032 | −0.139±0.020 | +0.442 | −0.314±0.045 |
| 2.739 | 0.855 | 50 | 58 | 0.723±0.027 | −0.174±0.017 | +0.640 | −0.272±0.027 |
| 2.798 | 0.912 | 50 | 58 | 0.655±0.025 | −0.228±0.016 | +0.892 | −0.256±0.018 |
| 2.857 | 0.965 | 50 | 58 | 0.630±0.011 | −0.258±0.008 | +0.849 | −0.304±0.009 |
| 2.857 | 0.965 | 50 | 90 | 1.035±0.029 | +0.023±0.015 | +0.020 | |
| 2.857 | 0.965 | 50 | 128 | 1.405±0.063 | +0.193±0.029 | −0.605 | −0.319±0.048 |
| 2.935 | 1.036 | 50 | 58 | 0.986±0.028 | −0.004±0.016 | +0.013 | |
| 2.990 | 1.086 | 50 | 58 | 1.333±0.051 | +0.186±0.027 | −0.524 | −0.355±0.052 |
| 3.127 | 1.213 | 50 | 58 | 1.645±0.072 | +0.283±0.030 | −0.773 | −0.366±0.039 |
| 3.284 | 1.357 | 50 | 90 | 0.751±0.036 | −0.154±0.024 | +0.635 | −0.243±0.033 |
| 3.366 | 1.432 | 50 | 58 | 0.966±0.082 | −0.014±0.045 | −0.090 | |
| 2.722 | 0.948 | 30 | 58 | 0.622±0.022 | −0.222±0.017 | +0.923 | −0.240±0.018 |

no value is given. The uncertainties of table 1 indicate the statistical uncertainties only. Uncertainties of $P_2$ and the multiple scattering correction are discussed in section 2 and in the previous paper respectively. The dependence of the polarization $P_1$ on energy is shown in fig. 3. For proton energies below 2.50 MeV the results are those of Okazaki [5]). It can be seen from the figure that $P_1$ does not vary appreciably over the energy range covered by the present experiment. Most points are consistent with a polarization of $P_1 = -0.30$. The measurement at 1 357-keV neutron energy for $\theta_2 = 90°$ has been omitted from fig. 3 because this point is less reliable than the others since $P_2$ is most uncertain in the 1 400-keV neuron energy region and varies very rapidly with energy. That the polarization of the neutrons remains fairly constant is, for the present data, also illustrated in fig. 2. The points indicated are the measured values of $P_1P_2(58°)$ divided by an assumed constant polarization $P_1 = -0.30$. The points lie quite close to the calculated $P_2(60°)$ which demonstrates that the observed variation of $P_1P_2(\theta)$ can be attributed essentially to the variation of $P_2(\theta)$.

The use of a $-5°$ $3/2^+$-phase shift at 730-keV neutron energy as indicated by the angular distribution data [11]) results in a calculated $P_2(60°)$ which passes through zero at an energy around 800 keV. This is in disagree-

ment with the measured values of $P_1P_2(\theta)$ which do not change sign in this energy region.

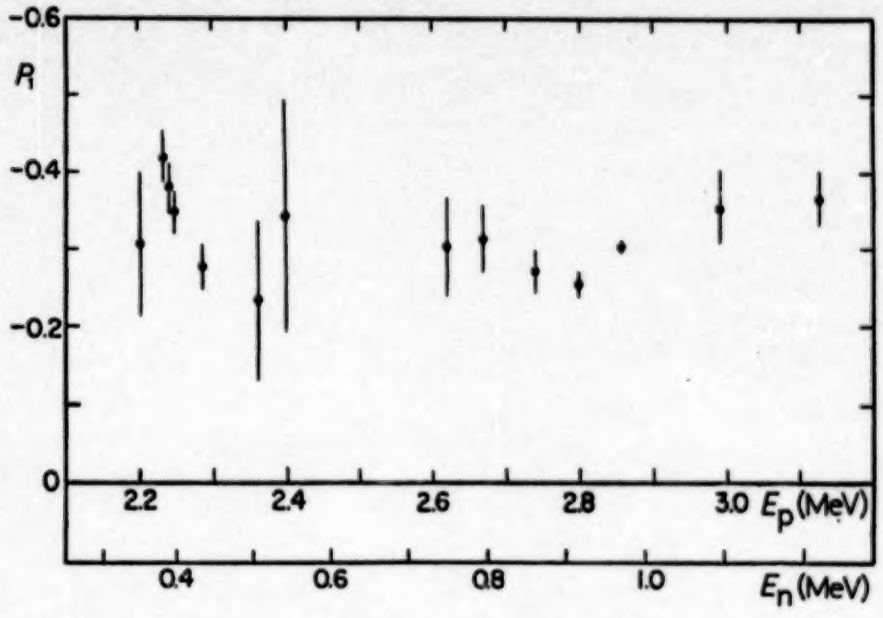


Fig. 3. Polarization of $Li^7$(p, n)$Be^7$ neutrons as a function of proton and neutron energy for a neutron emission angle of 50° in the laboratory system.

In fig. 2 the calculated $P_2$ passes through zero at a neutron energy of 1 030 keV. Since the measured $P_1P_2$ must pass through zero at the same energy, this point was used as a reference point for the neutron energy scale. If the neutron energies are calculated from the proton bombarding energies, neglecting the finite thickness of the lithium target, the experimental points in fig. 2 are displaced by 40 keV to higher energies with respect to the calculated curve. This difference is reasonably attributed to the finite thickness of the target, and indicates an 80-keV energy spread of the neutrons. A determination of the target thickness by the rise method [16]) indicated a thickness corresponding to only 50 keV energy spread. This discrepancy is not surprising in view of the uncertainties associated with the rise method. As long as the energy scale is fixed by the reference point mentioned above, results are insensitive to the energy spread assumed.

The results of the present investigation indicate that the polarization of $Li^7$(p, n)$Be^7$ neutrons emitted at 50° with respect to the proton beam is approximately $-0.30$ over the range of proton bombarding energies from 2.6 to 3.4 MeV. A polarization value of $-0.240\pm0.018$ was measured at 2.72 MeV proton energy for an emission angle of 30°. This is to be compared to a value of $-0.272\pm0.027$ for an emission angle of 50° at essentially the same proton bombarding energy. Polarizations of the same sign and similar magnitude were found at lower proton bombarding energies by Willard *et al.* [3]) and by Okazaki [5]). There is some evidence in these data [3, 5])

for a variation of $P_1$ with energy, although the two measurements do not entirely agree with each other. Such a variation has been predicted by Adair [4]) who has assumed that the well known resonance in the $Li^7(p, n)$ $Be^7$ reaction at a proton bombarding energy of 2.25 MeV is due to a $J^\pi = 3^+$ state in $Be^8$. The background reaction intensity was assumed to arise predominantly from $1^-$ and $2^-$ states, *i.e.*, by incident protons of zero angular momentum.

According to Adair's calculations, the polarization should decrease appreciably in magnitude as the proton bombarding energy is varied away from the region of the resonance energy. This is in diasgreement with the experimental results which suggest that the background reaction intensity may involve orbital angular momenta greater than zero, since S-wave interaction alone would not produce any polarization of the outgoing neutrons. Although a strong resonance has been observed in the $Li^7(p, \alpha)$ cross section[17]) at a proton energy of 3.0 MeV, no corresponding variation is evident in either the polarization or the forward yield of the Li(p, n) reaction [18]). It is possible that the Li(p, n) reaction may be interpreted more easily in terms of a direct interaction mechanism [19]).

We wish to thank Professor Barschall for his stimulating interest in this work.

## References

1) A. Simon and T. A. Welton, Phys. Rev. **90** (1953) 1036
2) R. K. Adair, S. E. Darden and R. E. Fields, Phys. Rev. **96** (1954) 503
3) H. B. Willard, J. K. Bair and J. D. Kington, Phys. Rev. **95** (1954) 1359
4) R. K. Adair, Phys. Rev. **96** (1954) 709
5) A. Okazaki, Phys. Rev. **99** (1955) 55
6) E. Baumgartner and P. Huber, Helv. Phys. Acta **26** (1953) 545
7) R. W. Meier, P. Scherrer and G. Trumpy, Helv. Phys. Acta **27** (1954) 577
8) B. M. McCormac, M. F. Steuer, C. D. Bond and F. L. Hereford, Phys. Rev. **104** (1956) 718
9) I. I. Levintov, A. V. Miller and V. N. Shamshev, Nuclear Physics **3** (1957) 221
10) W. Haeberli, to be published
11) C. K. Bockelman, Phys. Rev. **80** (1950) 1011
12) R. K. Adair, Phys. Rev. **92** (1953) 1491
13) Fowler and Cohn, Phys. Rev., to be published
14) R. K. Adair, Phys. Rev. **86** (1952) 155
15) L. Wolfenstein, Ann. Rev. Nucl. Science **6** (1956) 43
16) R. Taschek and A. Hemmendinger, Phys. Rev. **74** (1948) 373
17) N. P. Heydenburg, C. M. Hudson, D. R. Inglis and W. D. Whitehead, Phys. Rev. **74** (1948) 405
18) J. K. Bair, H. B. Willard, C. W. Snyder, T. M. Hahn, J. D. Kington and F. P. Green, Phys. Rev. **85** (1952) 946
19) J. Sawicki, Phys. Rev. **104** (1956) 1441

*Nuclear Physics* **6** (1958) 196—202; © *North-Holland Publishing Co., Amsterdam*

Not to be reproduced by photoprint or microfilm without written permission from the publisher

# HALF-LIVES OF THE POSITON EMITTING MIRROR NUCLEIDES

S. E. ARNELL, J. DUBOIS and O. ALMÉN

*Department of Physics Chalmers University of Technology, Gothenburg*

Received 30 June 1957

**Abstract:** The half-lives of the positon emitters $C^{11}$, $N^{13}$, $F^{17}$, $Na^{21}$, $Al^{25}$ and $Al^{26}$, $P^{30}$ have been determined. The decay spectrum of $Al^{25}$ has been investigated. No evidence for $\gamma$-rays indicating a complex decay was found.

A plot of log $T_{\frac{1}{2}}$ against log $A^{3/8}$ is discussed in terms of shell effects. It is shown that individual lines can be drawn through the points belonging to successive proton subshells. The value for $Ne^{19}$ falls below the line representing the $d_{5/2}$-subshell, which somewhat favours the proposal that the ground states of $Ne^{19}$ and $F^{19}$ are $2s_{\frac{1}{2}}$-states.

From a plot of the $\beta^+$-energies the pairing energy difference seems to have a value of about 0.1 MeV in the $d_{5/2}$-subshell.

## 1. Introduction

Because of the simplicity of their decay the mirror nucleides have been given considerable attention. If the specific nuclear forces are considered to be approximately charge independent, the energy difference between the members of such pairs of adjacent isobars consists only of the difference in the Coulomb energy of parent and daughter nucleus, which difference is roughly proportional to $A^{2/3}$, and of the mass excess of a neutron over a proton. A plot of the Coulomb energy differences against $A^{2/3}$ gives also a rather straight line.

However, it has been pointed out by Kofoed-Hansen in a recently published paper [1]) that the increasing accuracy in the experimentally determined energy differences makes it possible to observe effects from the nuclear shell structure. He shows that a better fit to the experimental points is obtained by drawing individual lines containing the data from nucleides between successive double closed main shells. Breaks occur consequently in the straight line at $A = 4$, 16, 40.

According to Fermi's theory, the dependence of the half-lives on the $\beta$-decay end point energy $E$ is given by

$$T_{\frac{1}{2}} = \frac{\text{const.}}{f(Z, E)\,|M|^2}.$$

For the positon decay of light nucleides the Fermi integral function $f(Z, E)$

is approximately proportional to $E^5$ in the higher energy region. In the mirror transitions the wave functions for the initial and final states are expected to be almost identical as the transforming proton in the last proton orbital goes over into an identical neutron orbital. This gives a good overlap between the wave functions of the two states and consequently large matrix elements $M$. For the positon emitting mirror transitions these quantities, as given by the experimental log $ft$-values, constitute a homogeneous group with a mean value of about 3.6. The transition $Ne^{19}$ $(\beta^+)F^{19}$, however, has a somewhat lower log $ft$-value.

The half-life is thus very sensitive to the Coulomb energy difference and a plot of log $T_{\frac{1}{2}}$ against log $A^{2/3}$ may show the shell effects more clearly for the positon emitting members of the mirror nucleides.

In the following we have tried to determine some of the half-lives of the mirror nucleides accurately. The result, combined with other measurements, is used to discuss the shell effects mentioned above.

## 2. Experimental Arrangements and Half-Life Calculation

The radioactive isotopes were produced by resonance capture of protons, accelerated by the Van de Graaff-generator at this Institute. After activation the proton beam was switched off and the target turned to measuring position. A scintillation counter detected the positon radiation. The decay was measured using a ten channel ringscaler, which recorded the counts during successive equal intervals, the length of which could be chosen to suit the experiment.

The switching from one channel to the next is effected by an electronic switch, driven by an accurately calibrated crystal oscillator. The frequency of the oscillator is scaled down by binary circuits and dekatron tubes. The pulses thus obtained are used to drive a ten-way-selector tube, GS10C. From the cathodes of this tube pulses are fed to ten bi-stable flip-flop circuits in such a way that when a pulse triggers one flip-flop, the next pulse brings it back and at the same time triggers a second flip-flop and so on. One of the anodes of each flip-flop is connected via a high ohm resistor to the cathode of a diode. Detector pulses are fed to the anodes of all the diodes and when a flip-flop is triggered, the cathode potential of the corresponding diode is lowered and detector pulses can pass through it to the input of a scaler during the preset time.

The length of the intervals was chosen to be less than one half of a half-life but long enough to accumulate a significant number of counts. The period of time chosen for the calculation of the half-lives was of the order of 4—6 half-lives. When the optimum durations, according to Peierls [2, 3]), were calculated, we often found the number of intervals to be slightly excessive, owing to the straggling of the last points. It is natural that the

optimum durations so obtained are a little too long, as Peierls considers pure statistical fluctuations only. In a practical half-life determination, other small fluctuations may also be of influence. In order to reduce such fluctuations, the stability of the detector system has received special attention. Photomultiplier-tubes with AgMg-dynodes are possibly not quite suitable, because the pulse-height may decrease with decreasing counting rate [4]). However, in the present experiments no significant difference was found between a tube with AgMg-dynodes and a tube with SbCsO-dynode material.

Each measurement was corrected for the finite resolving time of the scalers and for the background. If precision measurements are to be made, these corrections must be very well known. To get an accurate resolving time correction, a discriminator with a constant paralysis time of 20 $\mu$s was used, and to be sure that no long lived activity disturbed the measurements, the decay was followed into the background.

The half-lives were calculated by the method of least squares from the logarithms of the corrected activities. A plot of the residuals showed to be very sensitive to the activities of impurities and other errors.

## 3. Measured Half-Lives

Mirror nucleides:

| $C^{11}$ | $N^{13}$ | $F^{17}$ |
|---|---|---|
| 20.11±0.13 min | 597.6±1.8 sec | 66.6±0.5 sec |
| $Na^{21}$ | $Al^{25}$ | |
| 23.0±0.2 sec | 7.15±0.12 sec | |

Other nucleides:

| $Al^{26}$ | $P^{30}$ |
|---|---|
| 6.45±0.10 sec | 150.8±1.0 sec. |

The quoted uncertainties represent mean square errors. Each of these values is the result of several determinations with different targets and values found are within the limits of error quoted above.

For $N^{13}$ the half-life was also calculated using Peierls' mean-life determination, which gives slightly too high values due to the finite length of the intervals. In this case we used intervals of 100 and 200 seconds and when the half-life calculated by the method of least squares was compared to the values obtained by Peierls' method, the latter were found to be 0.33 % and 1.3 % higher, respectively, in good agreement with Peierls' predictions.

Separated targets of $B^{10}$, $Ne^{20}$, $Mg^{24}$, $Mg^{25}$ were used to get $C^{11}$, $Na^{21}$, $Al^{25}$, $Al^{26}$. The $B^{10}$ target was supplied by A.E.R.E., Harwell, England,

the other three were prepared with the electromagnetic isotope separator [13]) of this Institute by one of us (O.A.).

## 4. Discussion

A plot of log $T_{\frac{1}{2}}$ against log $A^{2/3}$ is shown in fig. 1. The plot was constructed using the data given in table 1.

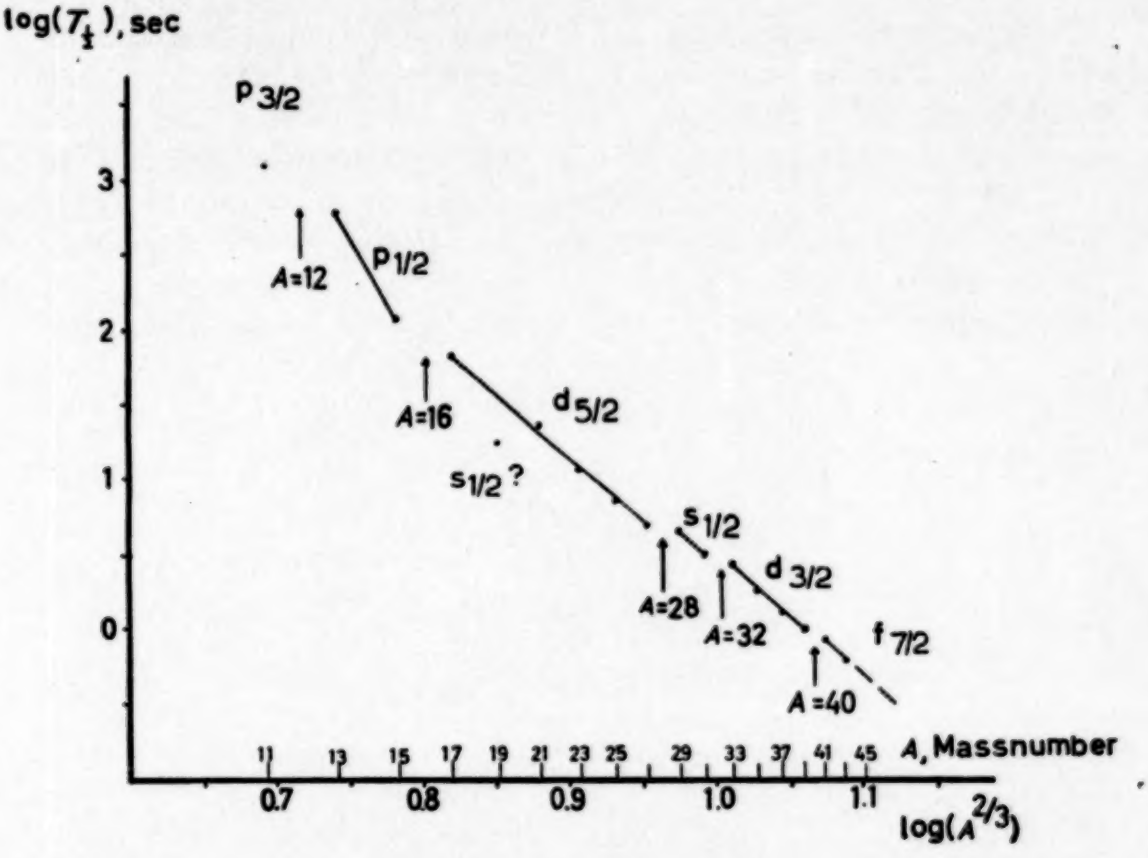


Fig. 1

Plot of the logarithm of the half-lives against log $A^{2/3}$ for all positon emitting mirror nucleides. The notations $p_{3/2}$ etc. show the filling of the respective proton shells.

From the plot it is apparent that a good fit to the experimental points is obtained if individual lines are drawn through the points belonging to successive proton subshells. Breaks occur consequently at $A = 12$, 16, 28, 32, 40, which shows that shell effects are revealed by the half-lives.

Relatively longer half-lives appear where the $\beta^+$-transforming proton in the parent nucleus is just outside a closed proton shell. This may be visualized, if it is assumed that the new proton orbital to be filled has a weaker coupling to the Coulomb field arising from the rest of the nucleus and consequently the change in Coulomb energy is less than expected from a model in which the charge is uniformly distributed.

The individual lines † seem to be nearly parallel from $A = 16$. For small $A$-values the approximation $E^5$ for the Fermi integral function is rather rough due to the low $\beta^+$-energies.

The logarithm of the half-life of the transition $Ne^{19}$ $(\beta^+)F^{19}$ falls below the line between $A = 17$ and $A = 27$. However, there are suggestions that the ground state configurations of these nucleides are complex. The log $ft$-value for this transition is somewhat smaller than for the rest of the mirror nucleides.

If all the breaks in fig. 1 are due to breaks in the Coulomb energy difference they should also be evident in a plot of the $\beta^+$-decay end point energy against $A^{2/3}$. Such a plot is shown in fig. 2. The $\beta^+$-energies are taken from ref. [1]) and some other references [5, 6]). The possibility of small breaks at $A = 12$, 28 and 32 besides the breaks at 16 and 40 cannot be excluded. The measuring accuracy from $A = 31$ on, however, is not very good as regards the $\beta^+$-energies.

Superimposed on the shell effects in the Coulomb energies there is another

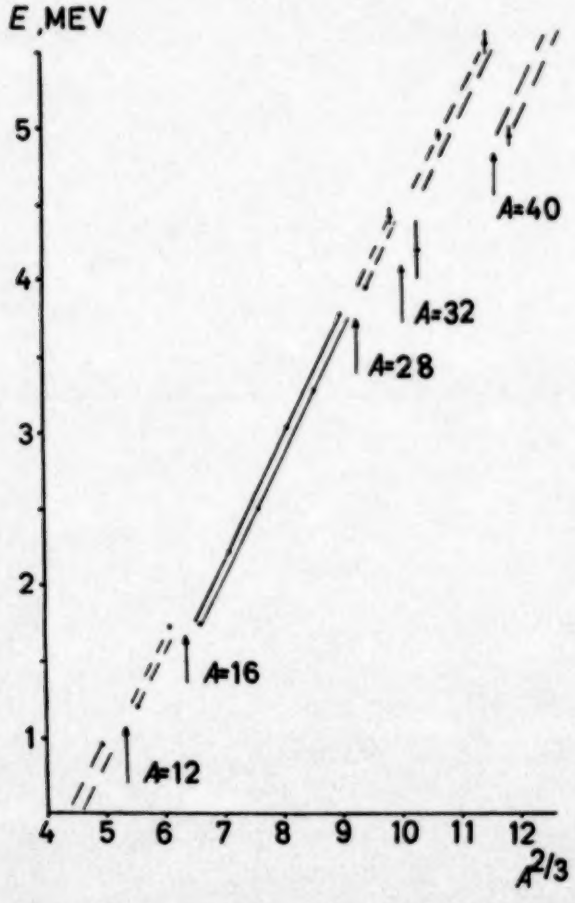


Fig. 2. Plot of the end-point energy $E$ against $A^{2/3}$ for the positon emitting mirror nucleides.

† From the line for the $f_{7/2}$-shell one can extrapolate the half-lives 0.40 sec for the transition $V^{45}$ $(\beta^+)Ti^{45}$, 0.28 sec for $Cr^{47}$ $(\beta^+)V^{47}$ and 0.20 sec for $Mn^{49}$ $(\beta^+)Cr^{49}$.

effect present due to a difference between the proton pairing energy and the neutron pairing energy [7]). Compare, in fig. 2, the decays in which an odd proton is transformed to an odd neutron to those in which a neutron pair is formed at the expense of a proton pair. The pairing energy difference seems to have a value of about 0.1 MeV in the $d_{5/2}$ subshell.

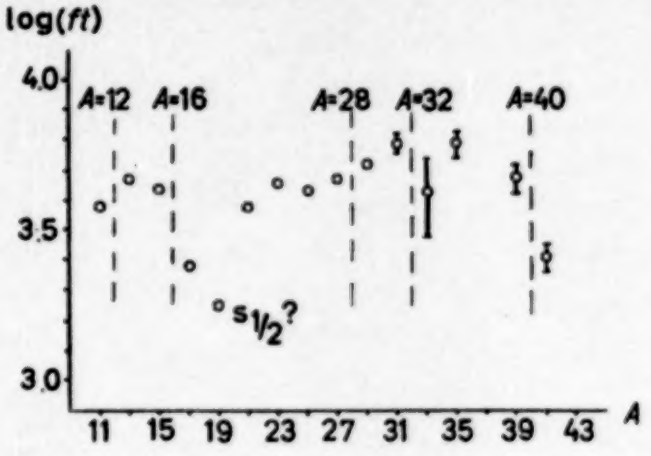


Fig. 3. Plot of the experimental log *ft*-values against *A* for the positon emitting mirror nucleides.

In fig. 1 fluctuations in the matrix elements have also some influence. A plot of the experimental matrix elements, as given by the log *ft*-values, is shown in fig. 3. The Fermi integral function was calculated using the

TABLE 1

| Transition | Half-life, sec | Reference |
|---|---|---|
| $C^{11} - B^{11}$ | 1207 ±8 | This work |
| $N^{13} - C^{13}$ | 597.6 ±1.8 | This work |
| $O^{15} - N^{15}$ | 123.95±0.5 | Penning and Schmidt, Phys. Rev. **105** (1957) 647 |
| $F^{17} - O^{17}$ | 66.6 ±0.5 | This work |
| $Ne^{19} - F^{19}$ | 17.7 ±0.1 | Penning and Schmidt, Phys. Rev. **105** (1957) 647 |
| $Na^{21} - Ne^{21}$ | 23.0 ±0.2 | This work |
| $Mg^{23} - Na^{23}$ | 11.9 ±0.3 | Huber *et al.*, Helv. Phys. Acta **16** (1943) 33 |
| $Al^{25} - Mg^{25}$ | 7.15±0.12 | This work |
| $Si^{27} - Al^{27}$ | 4.7 ±0.15 | Blaser *et al.*, Helv. Phys. Acta **24** (1951) 465 |
| $P^{29} - Si^{29}$ | 4.45±0.05 | Roderick *et al.*, Phys. Rev. **97** (1955) 97 |
| $S^{31} - P^{31}$ | 3.18±0.04 | Elliot and King, Phys. Rev. **60** (1941) 489 |
| $Cl^{33} - S^{33}$ | 2.8 | Hoag, Phys. Rev. **57** (1940) 937 |
| $A^{35} - Cl^{35}$ | 1.83±0.03 | Kistner *et al.*, Phys. Rev. **104** (1956) 154 |
| $K^{37} - A^{37}$ | 1.3 ±0.1 | Langmuir, Phys. Rev. **74** (1948) 1559 (A) |
| $Ca^{39} - K^{39}$ | 0.90±0.01 | Kline and Zaffarano, Phys. Rev. **96** (1954) 1620 |
| $Sc^{41} - Ca^{41}$ | 0.87±0.03 | Elliot and King, Phys. Rev. **60** (1941) 489 |
| $Ti^{43} - Sc^{43}$ | 0.58±0.04 | Schelberg *et al.*, Rev. Sci. Instr. **19** (1948) 458 |

tables of Moszkowski and Jantzen [8]) and with due consideration to complex decay where that was known [6, 9, 10]). There is a rather good agreement between these experimental values and the semi-empirical matrix elements calculated by O. Kofoed-Hansen and A. Winther [11, 12]).

More precise experimental investigations should be of interest as regards the $\beta^+$-energies as well as the shorter half-lives; also the possibility of complex decays requires closer investigation.

We wish to express our sincere gratitude to Professor N. Ryde for his kind interest in this work and to Dr. O. Kofoed-Hansen for a valuable discussion. The Swedish Atomic Energy Commission has financially supported the investigation.

## References

1) O. Kofoed-Hansen, Nuclear Physics **2** (1956/57) 441
2) R. Peierls, Proc. Roy Soc. A **149** (1935) 467
3) R. Evans, The Atomic Nucleus (McGraw Hill Company, Inc. New York, 1955) p. 812
4) K. Siegbahn, Beta- and Gamma-Ray Spectroscopy (North-Holland Publishing Company, Amsterdam, 1955) p. 147
5) O. Kistner, A. Schwarzschild and B. Rustad, Phys. Rev. **105** (1957) 1339
6) O. Kistner, A. Schwarzschild and B. Rustad, Phys. Rev. **104** (1956) 154
7) B. C. Carlson and I. Talmi, Phys. Rev. **96** (1954) 436
8) S. A. Moszkowski and K. M. Jantzen, Ucla Technical Report, no. 10-26-55
9) H. Roderick, O. Lönsjö and W. Meyerhof, Phys. Rev. **97** (1955) 97
10) W. Meyerhof and G. Lindström, Phys. Rev. **93** (1954) 949
11) O. Kofoed-Hansen and A. Winther, Mat. Fys. Medd. Dan. Vid. Selsk. **27** (1953) no. 14
12) O. Kofoed-Hansen and A. Winther, Mat. Fys. Medd. Dan. Vid. Selsk. **30** (1956) no. 20
13) O. Almén, G. Bruce and A. Lundén, Nuclear Instruments (in press)

*Nuclear Physics* **6** (1958) 203—209; © *North-Holland Publishing Co., Amsterdam*
Not to be reproduced by photoprint or microfilm without written permission from the publisher

# THE ELASTIC SCATTERING OF 30.5 MeV ALPHA-PARTICLES FROM Ni, Cu and Au

L. WAYNE SWENSON, ULRICH SCHINDEWOLF† and N. S. WALL

*Laboratory for Nuclear Science and Physics Department, Massachusetts Institute of Technology, Cambridge (Mass.)*††

Received 8 November 1957

**Abstract:** The angular distributions of 30 MeV alpha particles elastically scattered from Au, Cu, and Ni have been measured and compared to pure Coulomb scattering. A sensitive comparison of the Cu and Ni data was made by comparing the ratio of Cu to Ni from experiment to that which would be expected if diffraction scattering were the only contributing process. An absence of a significant compound elastic contribution is concluded.

## 1. Introduction

Experiments performed over the past few years with protons of energy up to about 40 MeV [1–8]) have shown that by and large the interactions of these protons with complex nuclei can be interpreted on the basis of a complex-potential well representation [9–11]). There have, however, been some experiments in the 5 MeV range on Cu and Ni [5]) as well as the experiments at about 9 MeV on Mg [12]), which have raised some questions as to the validity of such an interpretation. In particular we wish to examine the elements Ni and Cu to see if they can in fact be represented by a potential well which differs, primarily, only in the effective radius of such a well.

Even keeping to a complex potential well representation differences between Ni and Cu may arise. There are three rather straightforward factors which might explain such differences. First of all there could be a nuclear spin-dependent term in the interaction Hamiltonian. Secondly, there could be fluctuations in the level density of the compound nucleus pertinent to each target which would manifest itself in somewhat different complex-potential well parameters for each element. Finally there could be a difference in the low-lying levels of the target (residual) nucleus which affects the compound-elastic contribution to the elastic scattering. In a previous paper by one of the authors [6]) it is shown that this latter contribution yields the most reasonable explanation for the differences in the

† Now at University of Michigan.

†† This work was supported in part by a joint program of ONR and AEC.

elastic proton angular distributions. In that paper it was suggested that the observation of moderately high energy elastic alpha particle scattering might tend to substantiate the conclusions reached there concerning the proton angular distribution. The reasons that $\alpha$-particles are particularly appropriate for these observations are first of all there can be no spin-dependence; secondly, the high energy means that both compound nuclei should be similar; and finally the high energy available means that differences in the level structure near the ground state should not influence the elastic scattering.

From previous experiments on high energy alpha particle scattering [13]) we know that the locations of the characteristic maxima and minima are those given by a simple diffraction formula. The usual explanation of this formula makes use of the fact that $\alpha$-particles seem to be strongly absorbed (i.e., have a short mean free path) in nuclear matter [14, 15]). Therefore, one expects the nuclei to appear as opaque spheres. We have made use of the diffraction character to display our data in a manner which will "magnify" any differences in the scattering process from nearby nuclei. The result of this is that we then have essentially a "more sensitive" technique for comparing various nuclei to each other. Essentially this same concept was used by Hahn [16]) in an analysis of high energy electron scattering from two Ni isotopes and $Fe^{56}$.

## 2. Experimental Procedure

The 30.5 MeV alpha particle beam and the scattering chamber apparatus [17]) at the M.I.T. Cyclotron were used in this experiment. A NaI(Tl) scintillation spectrometer was used to detect the scattered particles in conjunction with conventional electronic equipment and a twenty-channel pulseheight analyzer. The instrumentation as well as the comparison method of data accumulation and analysis has been previously described by Waldorf and Wall [6]).

A representative spectrum of the counts registered by the spectrometer counter is given in fig. 1 for a counter angle of 84° and a Cu target. The background is due to the presence of inelastic scattering and a contribution probably from ($\alpha$, p) reactions in the target. The subtractions of background introduces an error in each count of about 10—15 percent at this angle. The accuracy at smaller angles is substantially better and becomes increasingly poorer at larger angles because of the ability to make a correct background subtraction.

The Cu and Ni data were compared to Au to obtain a measure of the absolute cross section.

In analyzing the Au data for a given monitor count the number of

counts in the elastic group of the spectrum registered by the spectrometer counter was summed for each angle $\theta$ between 6° and 90°. The sum was then multiplied by $\sin^4 \frac{1}{2}\theta$ at each angle $\theta$ to obtain something proportional to $(d\sigma/d\Omega)/(d\sigma/d\Omega)_{Coul}$ the ratio to pure Coulomb scattering. This was found to approach a constant value at small angles ($\lesssim 30°$). At small angles, that is for classical apsidal distances large compared to the nuclear radius, the scattering would be expected to be pure Coulomb and therefore $(d\sigma/d\Omega)/(d\sigma/d\Omega)_{Coul}$ for Au was normalized to unity at these angles.

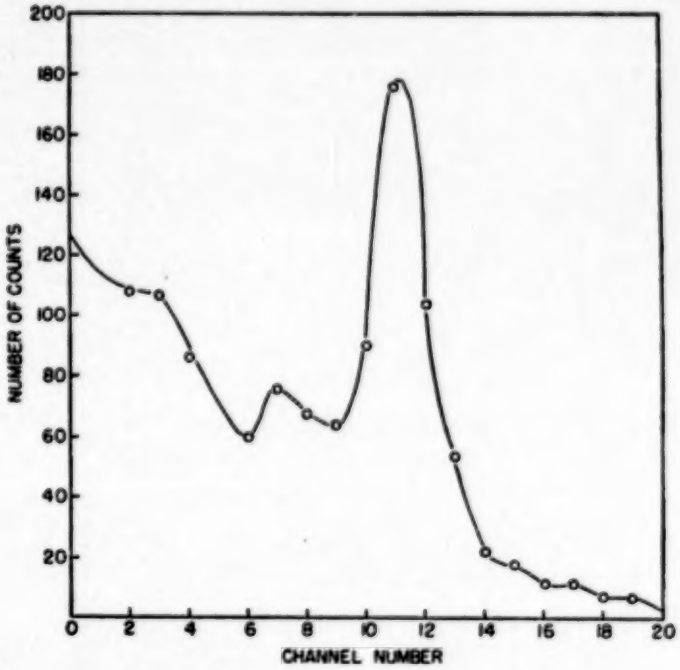


**Fig. 1. Spectrum of 30.5 MeV alpha particles scattered from Cu at 84° Lab. Angle. The elastic group is in channels 10–12.**

The Ni and Cu data were recorded as the ratio to Au, which was then readily transformed to the ratio to Coulomb. The transformation was accomplished by multiplying by the factor $(d\sigma/d\Omega)/(d\sigma/d\Omega)_{Coul}$ for Au which we shall call $R$ and the factor $(Z_{Au}/Z)^2$ where $Z_{Au}$ is the atomic number of Au and $Z$ that of Cu or Ni. The ratio of Cu or Ni to Au multiplied by $R(Z_{Au}/Z)^2$ would yield $(d\sigma/d\Omega)/(d\sigma/d\Omega)_{Coul}$ directly for Cu and Ni if the scattering process were pure Coulomb at the angle at which the monitor counter was situated. This, however, was not the case as Cu and Ni differ from pure Coulomb at all measured angles. A separate normalization was required to enable us to measure $(d\sigma/d\Omega)/(d\sigma/d\Omega)_{Coul}$ for the Cu and Ni data. This normalization was accomplished in a separate experiment with targets of known thickness by a direct comparison of the cross sections of Au, Cu and Ni at 27° where Au is pure Coulomb. The normalization is accurate to about 20 percent.

## 3. Results and Discussions

The angular distributions, along with typical statistical errors are shown in fig. 2. The general character of the Au distributions is similar to those previously observed for heavy elements in this general energy range [18, 19, 20]). The Cu and Ni angular distributions show the typical oscillatory behaviour seen in light nuclei [13]). The pronounced drop-off in the Au distribution as

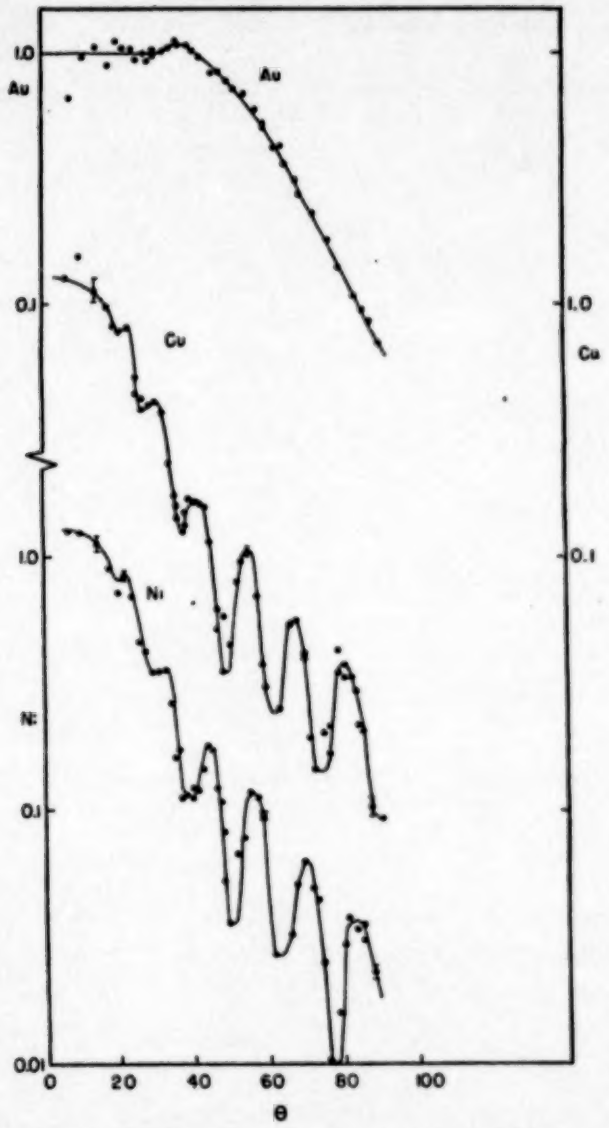


Fig. 2. Angular distribution of 30.5 MeV alpha particles elastically scattered from Au, Cu and Ni. The ratio of the differential cross section to pure Coulomb scattering is plotted against the scattering angle $\theta$. The errors indicate statistical fluctuations.

well as the drop-off with a superimposed oscillatory behaviour in Ni and Cu is characteristic of the absorption phenomenon which gives rise to a large imaginary part of the phenomenological potentials which have been found [14, 15]). To the extent that, because of this absorption, the scattering

nuclei can be represented by an opaque charged sphere, the differential cross-section ($d\sigma/d\Omega$) can be written as [21])

$$\frac{d\sigma}{d\Omega} = k^2 R^4 \left[ \frac{J_1\left(2kR \sin \frac{\theta}{2}\right)}{2kR \sin \frac{\theta}{2}} \right]^2 . \tag{1}$$

In this expression $R$ is the interaction radius, $k$ the wave number of the incident particle, $\theta$ the angle of scattering and $J_1(x)$ the ordinary Bessel function of the first order. The general range of validity of this expression is $\alpha/kR \ll \theta \ll 1$ where $\alpha$ is the Coulomb parameter $Zze^2/h\nu$. For 30 MeV $\alpha$ particles on $Z = 29$ $\alpha$ has a value $\approx 3$. Using the relationship $R = r_0 A^{1/3}$ with $r_0 = 1.4 \times 10^{-13}$ cm then gives as our range of validity for this equation $13° \leqq \theta \leqq 57°$. We also have assumed that $\alpha \approx 3$ can be considered very much greater than unity [21]).

In order to display the diffraction pattern most effectively as well as magnify any small differences, other than the effective size of the scattering centre we have plotted our data in a somewhat unusual manner. We have taken the data shown in fig. 2 and from the diffraction maxima and minima we have derived an effective nuclear interaction radius. For Ni and Cu these values turn out to be 6.56 and 6.80 in units of $10^{-13}$ cm respectively. Using these values for the parameter $R$ in the above differential cross-section formula we have computed the ratio of the differential cross-sections for Ni and Cu and compared this to the observed experimental ratios. As can be seen in fig. 3 over the range of from 40° to 85° the experimental curve agrees quite nicely with the theoretical curve expected on the basis of the diffraction analysis. The sharp discontinuities in the theoretical curve arise from the fact that the arguments of the Bessel function for the slightly different radius parameter reach the zeros of the Bessel function for the slightly different angles. The fact that the experimental curves do not swing through the same extremes only indicates that the assumption of a sharp angular momentum cut-off made in the derivation of eq. (1) is not quite valid and by the uncertainty relationship we expect such a "washing out" of sharp features.

Several other points should be noted from fig. 3. First of all the angular range where agreement is obtained actually occurs at angles large compared to those expected on the basis of the above criteria. This may arise because of our use of $2kR \sin \frac{1}{2}\theta$ rather than $kR\theta$ for the argument of the Bessel function. One also sees that as we get to smaller angles the agreement actually becomes poorer. This is as expected because of our neglect of the Coulomb scattering, as can be seen from the fact that eq. (1) is just what one expects for fast neutron scattering.

The fact that at larger angles the scattering from both Ni and Cu seems to be mainly diffraction scattering is consistent with our hypothesis that for high energy alpha particles the scattering from these two elements should be similar because in both cases the compound elastic contribution

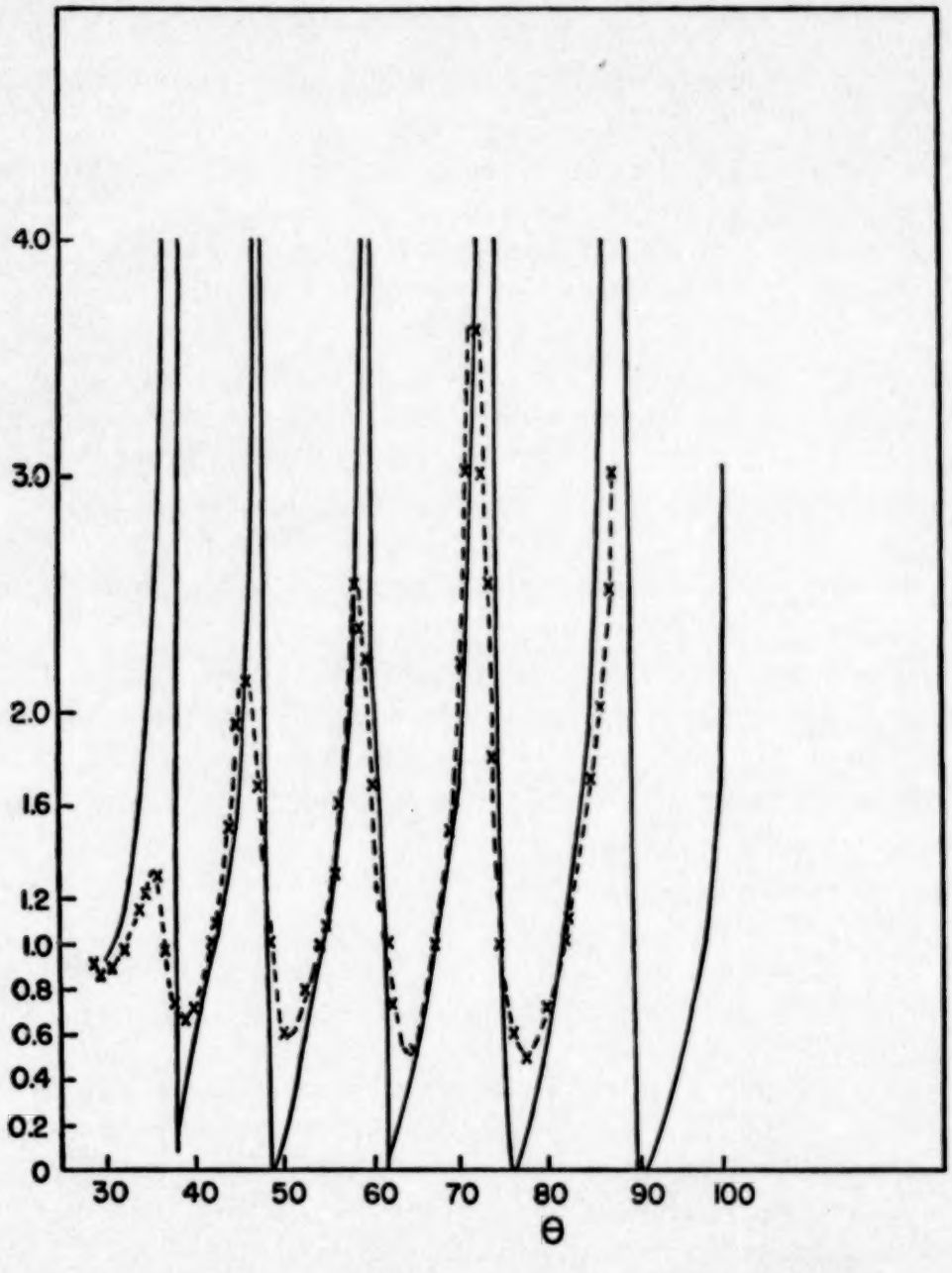


Fig. 3. A comparison of the ratio of the experimental angular distributions to the ratio of $J_1^2(2kR \sin \frac{1}{2}\theta)$ for Ni and Cu.

is negligible. One therefore feels that we have a consistent picture with the low energy elastic proton data if we take into account in this latter case the compound elastic contribution.

## References


1) N. Hintz, Phys. Rev. **100** (1955) 1794
2) B. B. Kinsey and T. Stone, Phys. Rev. **103** (1956) 975
3) B. Dayton and S. Schrank, Phys. Rev. **101** (1956) 1358
4) Greenlees *et al.*, to be published
5) D. A. Bromley and N. S. Wall, Phys. Rev. **102** (1956) 1560
6) W. F. Waldorf and N. S. Wall, Phys. Rev. **107** (1957) 1602
7) Kliucharev, Bolotin and Lutsik, JETP **30** (1956) 573
8) Takedan Michiya, Kato, Hu, Nakasima and Yamable, Journal Phys. Soc. of Japan **12** (1957) 6
9) H. Feshbach, D. E. Porter and V. F. Weisskopf, Phys. Rev. **96** (1954) 448
10) D. A. Saxon and M. A. Melkanoff, Phys. Rev. **101** (1956) 507
11) A. E. Glassgold and Cheston, Phys. Rev. **106** (1957) 1215
12) Greenlees *et al.*, Proc. Phys. Soc. A **70** (1957) 331
13) Igo, Wegner and Eisberg, Phys. Rev. **101** (1956) 1508
14) Glassgold and Cheston, Phys. Rev. **106** (1957) 1215
15) G. Igo and R. M. Thaler, Phys. Rev. **106** (1957) 126
16) Hahn, Hafstadter and Ravenhall, Phvs. Rev. **105** (1957) 1353
17) H. J. Watters, Phys. Rev. **103** (1956) 1763
18) Wall, Rees and Ford, Phys. Rev. **97** (1955) 726
19) Wegner, Eisberg and Igo, Phys. Rev. **99** (1955) 825
20) H. Gove, Phys. Rev. **99** (1955) 1353
21) A. Akhieser and I. Pomeranchuk, J. Phys. (U.S.S.R.) **9** (1945) 471

*Nuclear Physics* **6** (1958) 210—218; © *North-Holland Publishing Co., Amsterdam*
Not to be reproduced by photoprint or microfilm without written permission from the publisher

# ANGULAR DISTRIBUTION OF ELASTICALLY SCATTERED 14.7 MeV NEUTRONS

S. BERKO†, W. D. WHITEHEAD and B. C. GROSECLOSE
*Department of Physics University of Virginia, Charlottesville, Virginia, U.S.A.*††

Received 10 December 1957

**Abstract:** The differential elastic scattering cross sections of 14.7 MeV neutrons have been obtained for Mg, Al, Ni, Cu, Pb and Bi. The neutrons from the (d, t) reaction were scattered from cylindrical scatterers and were counted by a time of flight setup measuring n—α coincidences with $2.5 \times 10^{-9}$ sec resolving time. The angular distributions thus obtained are compared with recent theoretical distributions from Livermore employing a potential which has a rounded real part, a surface imaginary part and a real spin-orbit coupling term.

## 1. Introduction

The theoretical attempts to understand the success of the "cloudy crystal ball" model from basic nucleon-nucleon interactions ††† have brought about, in the last few years, an increased interest in the exact shape and parameters of the complex potential needed in such a model. Measurements of the elastic differential scattering cross section of medium energy protons and neutrons have been used to determine these parameters.

The investigation to be reported in this paper was undertaken to measure the differential elastic scattering cross section of 14.7 MeV neutrons for various elements, and was started at a time when the available data at this energy were very scarce [2]). Subsequent reports [3]) from other laboratories have made these data more complete, allowing for a more careful theoretical fitting of the cross section [4]). We have chosen 14.7 MeV neutrons not only for the practical aspects of the T(d, n)α reaction, but also because at these energies the relatively small contribution of the compound elastic channel permits a more favourable comparison with the complex potential predictions.

† A. P. Sloan Research Fellow 1957—58.

†† Jointly supported by U.S. Atomic Energy Commission and the Office of Ordnance Research.

A report on this work was presented at the International Conference on the Neutron Interactions with the Nucleus, held at Columbia University, September 1957.

††† See ref. [1]) and papers quoted therein.

## 2. Experimental Procedure

In order to partially circumvent the experimental difficulties encountered in high energy neutron experiments, a time of flight setup was built similar to that of Cross and Jarvis [2]). The mechanical setup is shown in fig. 1.

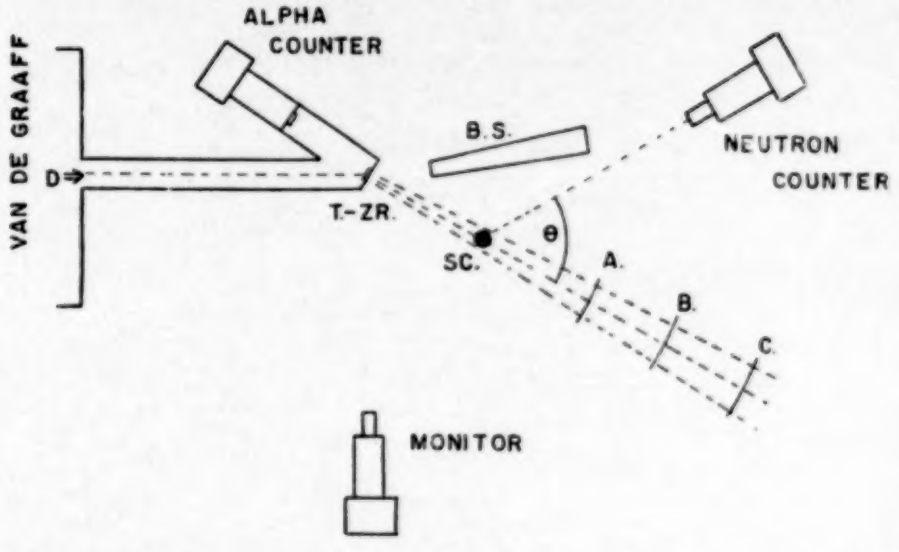


Fig. 1. Mechanical setup. Drawings not on scale. T.—ZR. = tritium-zirconium target; B.S. = Brass shield; SC. = Scatterer. Positions A, B and C were used to test time of flight efficiency and to draw the curves of fig. 4.

The α-counter was a 2 × 1 cm plastic phosphor 0.002 to 0.004 in. thick, mounted on the face of an RCA 6342 phototube which served simultaneously as a vacuum seal. This counter viewed the thin tritium-zirconium target at an angle of 145° from the deuteron beam. The α-counter in coincidence with the neutron counter thus defined a rectangularly shaped beam of 14.7 MeV neutrons. The neutron counter was a 2 × 4 × 5 cm plastic scintillator mounted with the 2 cm side horizontal on an RCA 6342 tube, which was mounted on an arm that could be pivoted either about the target or about the scatterers. The various scatterers were cylinders, 2.5 cm in diameter, 5 cm high and could be placed in the neutron beam on a light lucite platform.

The block diagram of the coincidence circuit is shown in fig. 2. Pulses from the plates of RCA 6342 photomultiplier tubes (H.V. 1750V) were sent through cathode followers, and were amplified by Hewlett-Packard 460-A wide band amplifiers before cutting off the Western Electric 404A sharp cutoff pentodes that terminated the H-P amplifiers. The shaped pulses were fed into a Bell and Graham coincidence diode set to accept only double pulses. The pre-amplifiers had a second cathode follower sending pulses from one of the last dynodes into linear amplifiers (AID, Oak Ridge). After pulse height discrimination, the pulses were fed into a slow triple

coincidence circuit of $10^{-6}$ sec resolving time, which was used to mix the pulse height information with the fast-time resoltion. In actual practice it was found that due to the very fast counting rate of the α-crystal it was hard to stabilize the α side-channel. This then was discarded, thereby

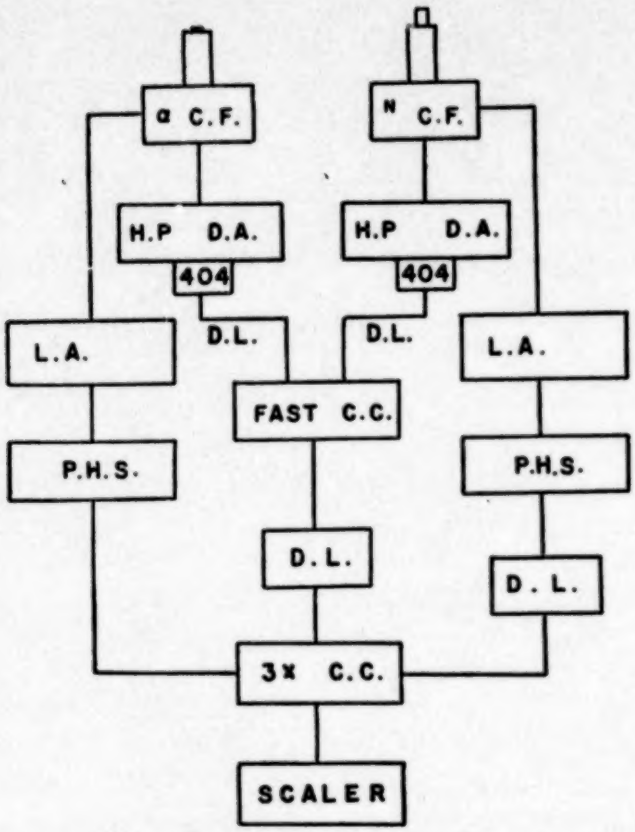


Fig. 2. Block diagram of electronic circuitry. C.F. = cathode followers; H.P.D.A. = Hewlett-Packard distributed amplifiers; 404 = Western Electric 404A pentodes; L.A. = linear amplifiers; D.L. = delay lines; P.H.S. = pulse height discriminators; Fast C.C. = $2.5\times10^{-9}$ sec coincidence circuit; 3 × C.C = $10^{-6}$ sec triple coincidence circuit.

sacrificing some decrease in background in favor of more stability. In such a setup the pulse height discriminator of the neutron side fed two sides of the slow triple coincidence circuit.

In order to test the apparatus the following runs were made:

1. To test the angular collimination efficiency, the neutron counter was set to swing in an arc of 40 cm radius with the axis of rotation through the tritium target. The counting rate *vs.* angle is plotted in fig. 3, showing a collimated beam of 6° width at half maximum. The width, of course, could be varied at will with the size of the α-counter. A similar test was made along the vertical direction to ascertain the rectangular shape of the neutron beam thus collimated. Background to peak ratios of 5 000 to 1 could be obtained.

2. To test the time of flight feature, the neutron counter was set at

the angle which gave the highest coincidence counting rate (position A) and a delay cable *vs.* coincidence counting rate curve was plotted. The width

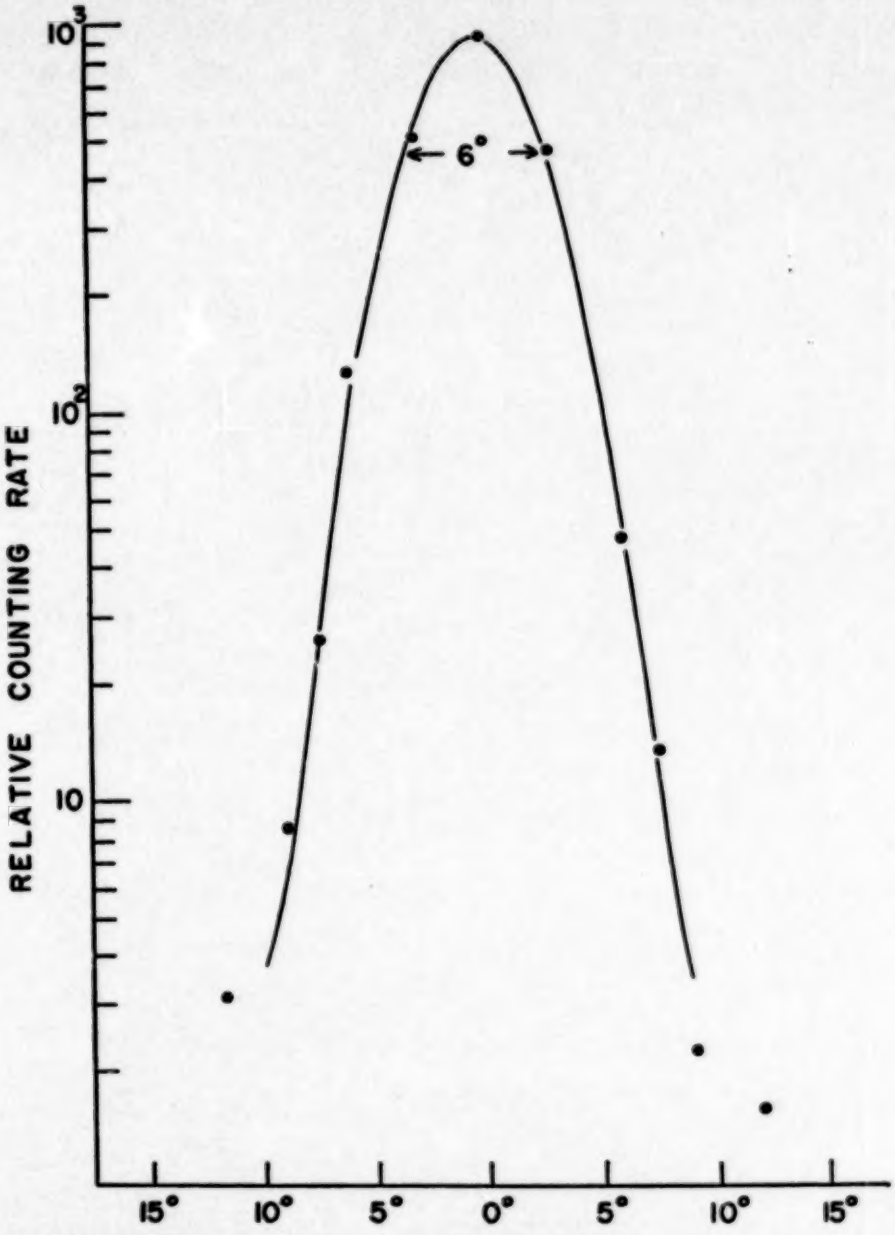


Fig. 3. Angular collimation curve. Obtained by pivoting the neutron counter about the T—Zr target and plotting n—α coincidences against angle. No brass shield was used for this curve.

of the resolution curve was about $2.5 \times 10^{-9}$ sec. Then keeping the angle fixed, the target to neutron counter distance was increased 15 cm (position B) and then 30 cm (position C) and delay curves were taken at each distance. Fig. 4 shows the resulting delay curves, after curves B and C were normalized for the inverse square correction. From these curves it is obvious that the efficiency of the circuit is high, and that room scattered neutrons and gamma

rays are adequately rejected. For the distances used, however, the time of flight feature was not sufficient to reject inelastic groups from low excited states. We therefore used an integral discriminator on the neutron side-channel.

In order to determine the angular distributions, the scatterers were placed

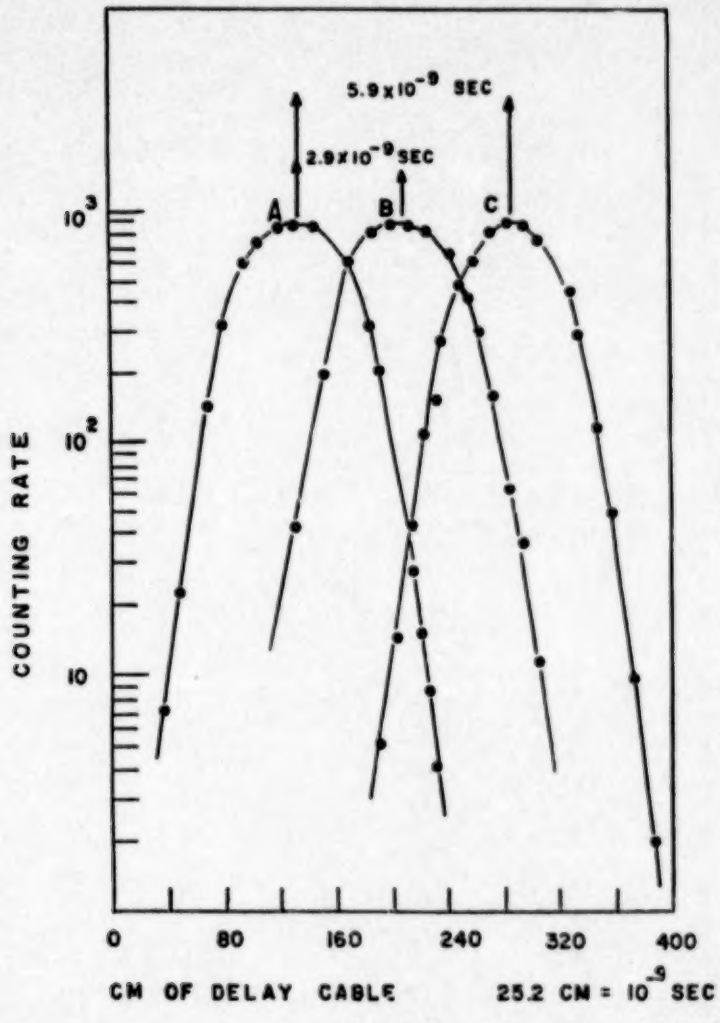


Fig. 4. Delay curves; n—α coincidences plotted against variable delay on the α-side of the fast coincidence circuit at three positions of the neutron counter. The neutron flight path between positions A and B and B and C was 15 cm.

in the neutron beam 20 cm for the T-Zr target, and the arm supporting the neutron counter was pivoted about an axis through the center of the scatterer. The distance from the scatterer to the face of the neutron counter was generally 20 cm; the neutron counter was biased at 10—11 MeV. The counting rate when the neutron counter was out of the beam and the scatterer removed seemed to be due entirely to accidental coincidences and could be greatly reduced by placing a brass absorbing cone between the neutron counter and the target. The data were normalized against a neutron

counter placed at a fixed position on the floor, and biased to count neutrons above 10 MeV. The ratio of the counting rate with scatterer in, to the counting rate with the scatterer out, depended on the angle and on the scatterer, and varied from 15 : 1 to 2 : 1.

## 3. Experimental Results

The true counting rate (actual counts — background) was corrected for finite geometry and for attenuation in the scatterer by a method very

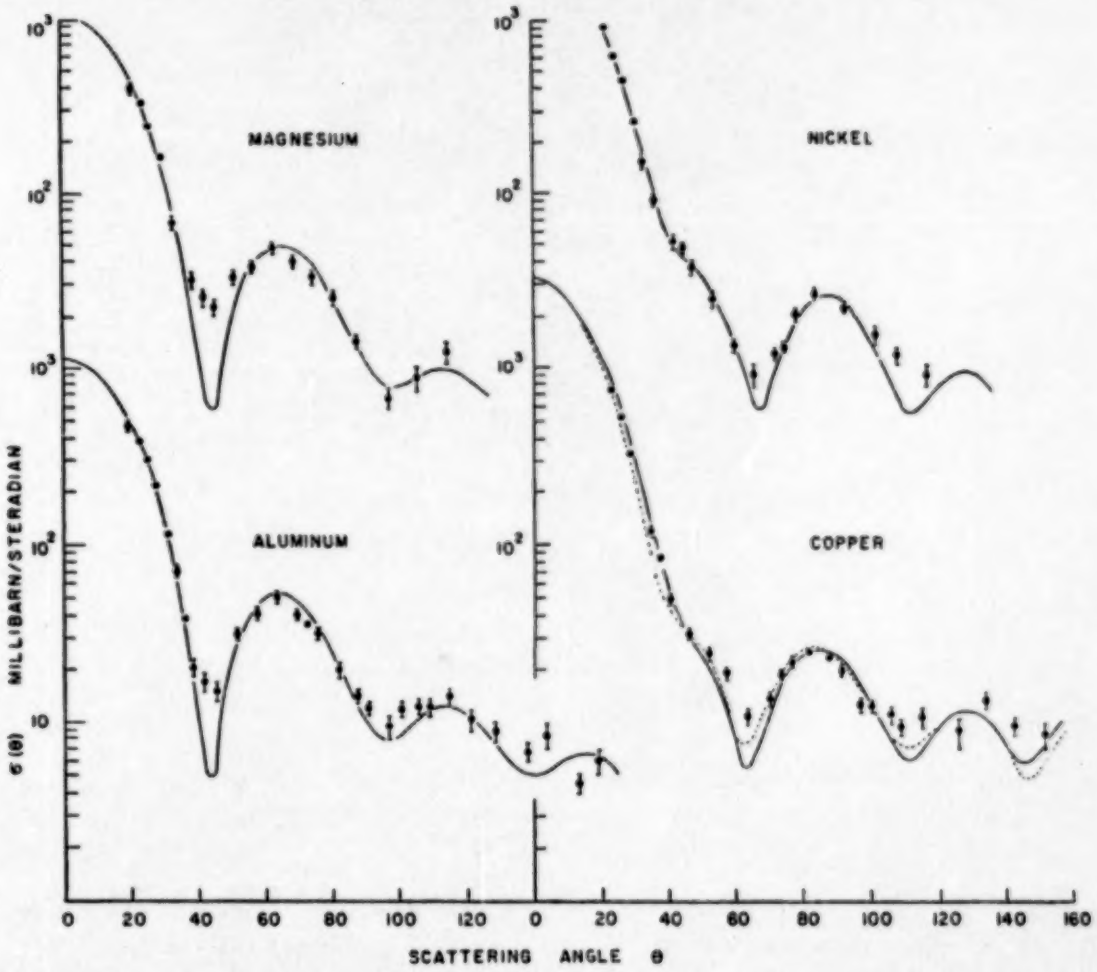


Fig. 5. Differential elastic scattering cross sections for Mg, Al, Ni and Cu. The solid (14 MeV) and dashed (15 MeV) curves are the theoretical differential cross sections discussed in the text.

similar to that described by Meier *et al.* [5]). The attenuation in the scatterer has two effects: it changes the absolute value of the cross section and the "effective scattering angle" by shifting the "effective scattering center." These effects were computed by numerical integration for each scatterer used. To correct for the finite geometry the cross section was expanded in a Taylor series in $\theta$ and the differential equation obtained for $\sigma(\theta)$ by keeping terms through the second order was solved by a first order iteration process.

This procedure corrected, of course, only partially for the finite geometry. No corrections for multiple scattering have been made on the angular distributions. The differential cross sections are strongly peaked in the forward direction, making the multiple scattering corrections on angular distributions rather small at this energy, except at narrow minima. It is hoped that more data will be taken at these angles with smaller size scatterers so as to experimentally minimize multiple scattering contributions.

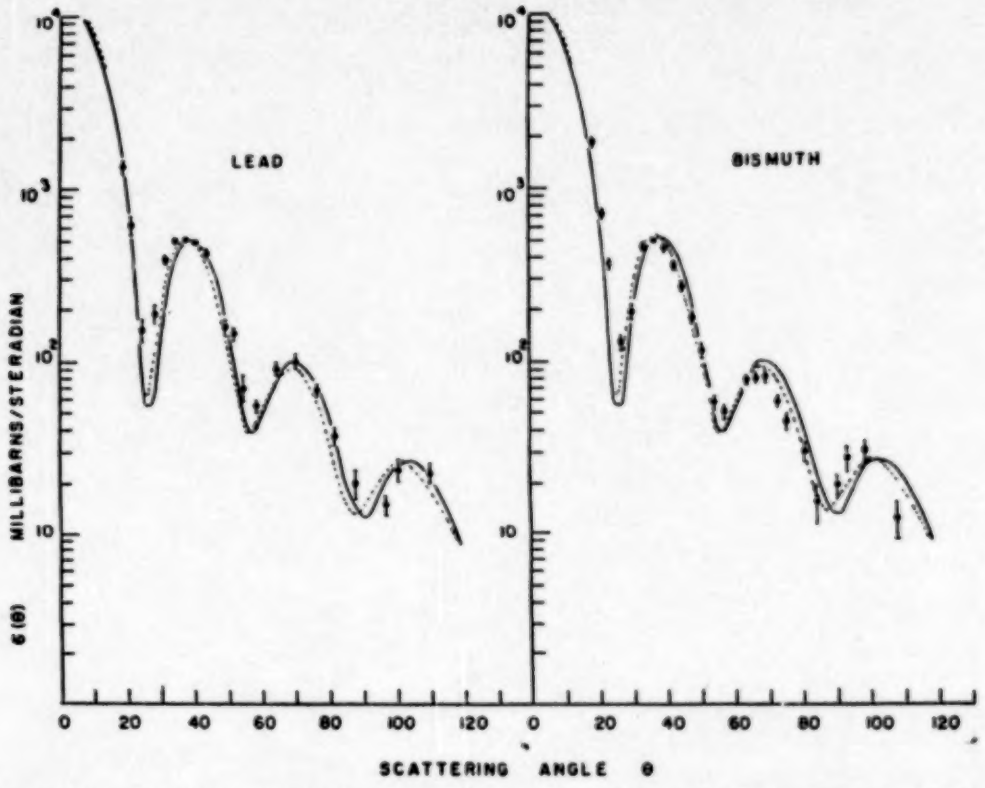


Fig. 6. Differential elastic scattering cross sections for Pb and Bi. The solid (14 MeV) and dashed (15 MeV) curves are the theoretical differential cross sections discussed in the text.

The corrected data for magnesium, aluminium, nickel and copper are plotted in fig. 5, and for lead and bismuth in fig. 6. Since the main corrections influence the absolute, but not the relative angular distributions, we have plotted our experimental results corrected for geometry and absorption in figs. 5 and 6 as relative cross sections, normalizing them to the theoretical curves at one angle. In each case, however, the absolute differential cross section, determined from the corrected angular distributions and the counting rates at 0° with the scatterer removed, came within 20 % of the theoretically predicted values at the point of normalization.

The theoretical curves in figs. 5 and 6 will be discussed in the next section. In fig. 6 we have actually used smaller diameter scatterers at the first minima, in order to minimize multiple scattering effects and improve the

geometry. The errors are mainly due to counting rate statistics. The fairly large errors for the backward angles are due to the low absolute counting rate and to the increase in accidental rate due to the approach of the neutron counter to the Tritium source. The low coincidence counting rate was governed by the limitation in the counting rate of the $\alpha$ crystal due to its 100 % efficiency. This, at the moment, is the main drawback of the setup for large angle scattering.

## 4. Discussion

The theoretical curves of figs. 5 and 6 are the most recent results of F. Bjorklund and S. Fernbach [6]) from Livermore. The solid lines represent curves for 14 MeV neutrons. Where available, 15 MeV neutron distributions are drawn in by the dashed lines. They correspond to exact phase shift calculations carried out on the UNIVAC, using the following potential:

$$V = V_{CR}\, p(r) + iV_{CI}\, q(r) + V_{SR}\left(\frac{\hbar}{\mu c}\right)^2 \frac{1}{r}\frac{dp(r)}{dr}\,\sigma\cdot\mathbf{l}$$

where

$$p(r) = 1/[1+\exp\,(r-R_0)/a],$$

$$q(r) = \exp\,[-(r-R_0)^2/b^2], \quad R_0 = r_0 A^{1/3}.$$

The notation is the same as that used by Riesenfeld and Watson [7]). Table 1 shows the parameters selected to fit the available data best at

TABLE 1

Parameters adopted by Bjorklund and Fernbach [6]) as giving the best fit to the neutron scattering experimental data at 4.1, 7 and 14 MeV

| $E$ (MeV) | $V_{CR}$ (MeV) | $V_{CI}$ (MeV) | $V_{SR}$ (MeV) | $a$ ($10^{-13}$ cm) | $b$ ($10^{-13}$ cm) | $r_0$ ($10^{-13}$ cm) |
|---|---|---|---|---|---|---|
| 4.1 | 50 | 7 | 9.5 | 0.65 | 0.98 | 1.25 |
| 7 | 45.5 | 9.5 | 8.6 | 0.65 | 0.98 | 1.25 |
| 14 | 44 | 11 | 8.3 | 0.65 | 0.98 | 1.25 |

various energies. As can be seen, the spin-orbit term corresponds in magnitude to the one required by the shell model. It is obvious from our data that more accuracy will be needed in order to be able to state whether or not the experimental data require a surface imaginary potential. Since our experiments have been performed, more data from other laboratories have become available, particularly at the large angles [8]). All these data indicate that there are no large minima in the backward hemisphere. Bjorklund and Fernbach state that the inclusion of the spin-orbit term has made the theory fit the experimentally observed curves much better, particularly

as far as their damping in the backward direction is concerned. The only real test for the existence of such a spin-orbit term would be, of course, polarization experiments via double scattering measurements. Such experiments are presently under consideration in our laboratory. Our setup, in avoiding ring geometry, would be ideally suited for such experiments.

We are grateful to Dr. F. E. Bjorklund for sending us the theoretical angular distribution curves prior to publication. One of us (S.B.) would like to thank Dr. W. G. Cross of Chalk River for valuable information regarding the time of flight technique. We thank P. J. Dolan, H. A. Fincher and P. J. Kenny for building parts of the original time of flight apparatus, and for cooperating in the early stages of this work.

## References

1) H. A. Bethe, Phys. Rev. **103** (1956) 1353
2) J. H. Coon and R. W. Davis, Phys. Rev. **94** (1954) 785A; W. G. Cross and R. G. Jarvis, Phys. Rev. **99** (1955) 621A
3) J. O. Elliot, Phys. Rev. **101** (1956) 684; H. Nauta, Nuclear Physics **2** (1956) 124
4) G. Culler, S. Fernbach and N. Sherman, Phys. Rev. **101** (1956) 1047; F. E. Bjorklund, S. Fernbach and N. Sherman, Phys. Rev. **101** (1956) 1832L
5) R. W. Meier, P. Scherrer and G. Trumpy, Helv. Phys. Acta **27** (1954) 577
6) Private communication. To be published in Phys. Rev.
7) W. B. Riesenfeld and K. M. Watson, Phys. Rev. **102** (1956) 1157
8) J. H. Coon *et al.*, Bull. Am. Phys. Soc. **2** (1957) 233; C. Wong *et al.*, Bull. Am. Phys. Soc. **1** (1956) 388

*Nuclear Physics* **6** (1958) 219—221; © *North-Holland Publishing Co., Amsterdam*
Not to be reproduced by photoprint or microfilm without written permission from the publisher

# DERIVATION OF THE $\Lambda^0$—$\alpha$ POTENTIAL FROM THE $^5He_\Lambda$ AND $^9Be_\Lambda$ HYPERFRAGMENT BINDING ENERGIES

H. WILHELMSSON †
NORDITA (*Nordisk Institut for Teoretisk Atomfysik*), *Copenhagen*
and
P. ZIELINSKI
*Instytut Badan Jadrowych Polskiej Akademii Nauk, Warszawa*

Received 27 November 1957

The scanty experimental information concerning hyperfragments and $\Lambda^0$ particles makes a quantitative description of the hyperfragment properties rather difficult. As a rough approximation the "$\Lambda^0$+core" model of the hyperfragment may be assumed [1]). In order to avoid many specific assumptions let us consider the simplest hyperfragments. From the point of view of the above model the $^5He_\Lambda$ hyperfragment is particularly simple. The $\alpha$ core is very tightly bound and one may expect negligible deformation of the core due to the interaction with the $\Lambda^0$ particle. Assuming an s state for the $\Lambda^0$ particle (which is here admitted by the Pauli principle in contrast to the case of $He^5$) and taking zero spin for the $\alpha$ core some information about the $\Lambda^0$—$\alpha$ potential can be obtained.

Since the wave function of the $\Lambda^0$ particle extends appreciably outside the region of the $\alpha$ core, only the depth $V_0$ and range $a$ of the potential are important. Taking the value of the binding energy of the $\Lambda^0$ in $^5He_\Lambda$ from experiment we obtain a relation between the two parameters.

Let us further consider the $^9Be_\Lambda$ hyperfragment according to an "$\alpha+\Lambda^0+\alpha$" model. Using some information about the $\alpha$—$\alpha$ interaction and taking the value of the binding energy of the $\Lambda^0$ in $^9Be_\Lambda$ from experiment, we find a second relation between the depth $V_0$ and range $a$ of the potential. This relation together with that obtained from $^5He_\Lambda$ determines the values of the parameters $V_0$ and $a$.

The simple calculation was made assuming a Gaussian form for the $\Lambda^0$—$\alpha$ potential as well as for the wave function †† of the $^5He_\Lambda$ hyperfragment. We obtain the formulae

† On leave from the Institute for Theoretical Physics, Lund.
†† This form of the wave function is better than the exponential one as appears from a variational treatment.

$$V_0 = \frac{\hbar^2}{2ma^2}\sqrt{1+\frac{1}{a}}\,(1+\alpha)^2,$$

$$\alpha(\alpha-\tfrac{1}{2})\frac{\hbar^2}{2ma^2} = B_\Lambda(^5\mathrm{He}_\Lambda)$$

($m$ denotes the reduced mass, $\alpha$ defines the extension of the wave function), from which, by eliminating $\alpha$, the first relation between $V_0$ and $a$ follows.

Treating the $^9\mathrm{Be}_\Lambda$ structure according to the assumed model, we use a variational procedure indicated by Bethe and Bacher [2]†. For the $\alpha$—$\alpha$ potential we take only the Coulomb term, which gives a lower limit for the range $a$. (The error caused by using trial wave functions acts in the same direction.) We should not expect a considerable change of the final results if we use a more adequate $\alpha$—$\alpha$ potential [4]. In fact the ground state of $Be^8$ has been determined to be a virtual state at an energy of approximately 90 keV above that for an inifinite separation of two $\alpha$ particles [5].

Obtaining in this way a second relation between $V_0$ and $a$ from the $^9\mathrm{Be}_\Lambda$ hyperfragment and inserting the experimental value for $B_\Lambda(^5\mathrm{He}_\Lambda) = 2.56\pm0.3$ MeV as given by Levi Setti, Slater and Telegdi [6], we find for the range and depth as a function of the binding energy of the $\Lambda^0$ in $^9\mathrm{Be}_\Lambda$ the results of the accompanying table. The experimental value for the binding energy of $\Lambda^0$ in $^9\mathrm{Be}_\Lambda$ is $6.13\pm0.3$ MeV [6].

| $a$ ($10^{-13}$ cm) | $V_0$ (MeV) | $B_\Lambda(^9\mathrm{Be}_\Lambda)$ (MeV) |
|---|---|---|
| 1.6 | 44 | 6.6 |
| 1.7 | 40 | 6.1 |
| 1.8 | 37 | 5.6 |

The information obtained about the $\Lambda^0$—$\alpha$ potential, after treating the $^9\mathrm{Be}_\Lambda$ hyperfragment by other methods for comparison, may be used as a basis for an investigation of the $\Lambda^0$-nucleon potential, which could yield some indication of its range and thus of the agent of the $\Lambda^0$-nucleon force [7].

The work upon which this note is based was mainly performed during our stay at the Summer School for Theoretical Physics of the University of Grenoble at Les Houches, France, 1957. We are greatly obliged to many colleagues especially to Dr J. Reignier for valuable discussions. We also wish to acknowledge a stimulating correspondence with Dr. R. Gatto.

† This procedure was used in the treatment of the $^3\mathrm{H}_\Lambda$ hyperfragment by F. Duimio [3].

## References

1) R. H. Dalitz, Reports on Progress in Physics **20** (1957) 163
2) H. A. Bethe and R. F. Bacher, Revs. Mod. Phys. **8** (1936) 134
3) F. Duimio, Nuovo Cimento **1** (1955) 688
4) A. Herzenberg, Nuclear Physics **3** (1957) 1
5) A. V. Tollestrup, W. A. Fowler and C. C. Lauritsen, Phys. Rev. **76** (1949) 428
6) R. Levi Setti, W. Slater and V. L. Telegdi, Report of the 7th Annual Rochester Conference (1957)
7) D. Lichtenberg and M. Ross, Phys. Rev. **103** (1956) 1131; N. Dallaporta and F. Ferrari, N. Cimento **5** (1957) 111; M. Gell-Mann, Phys. Rev. **106** (1957) 1296

*Nuclear Physics* **6** (1958) 222—251; © *North-Holland Publishing Co., Amsterdam*

Not to be reproduced by photoprint or microfilm without written permission from the publisher

# ON THE THEORY OF SCATTERING MEASUREMENTS IN NUCLEAR EMULSION

## II. THE ESTIMATION OF TRUE SCATTERING IN THE PRESENCE OF DISTORTION

N. SOLNTSEFF

*The F.B.S. Falkiner Nuclear Research and Adolph Basser Computing Laboratories, School of Physics, The University of Sydney* †

Received 22 October 1957

**Abstract:** The effect of distortion on the scattering measurements in nuclear emulsion is here evaluated theoretically. The Molière-d'Espagnat method for estimating true scattering in the presence of experimental errors is extended to the case when third or fourth differences of the coordinates are used. The expressions for the relative standard error of the estimates of scattering from third and fourth differences are derived. The distortion is assumed to be of second order but the treatment can be easily extended to any regular type of distortion.

It is found that an unbiassed estimate can also be obtained for a distorted track by Fowler's method of eliminating distortion, in which the algebraic mean second difference is subtracted from each of the $D_i$. However, the relative standard error of such an estimate will in general be larger than the error of an estimate obtained from third and fourth differences. In the measurement of particles with $pv$ greater than 1 GeV the bias introduced by distortion can be appreciable and third or fourth differences should be used.

An imaginary estimate of noise is sometimes obtained. This will happen whenever the standard deviation of the $D_i$ due to noise only is less than $\approx \overline{D_d}$, where $\overline{D_d}$ is the mean second difference due to distortion.

The estimation equations recommended for practical use are given at the end of the article in section 4.

## CONTENTS

**1. Introduction** . . . . . 223

**2. An Outline of the Estimation Theory** . . . . . 224

2.1. THE GENERAL THEORY OF ESTIMATION
2.2. THE MAXIMUM LIKELIHOOD METHOD APPLIED TO SCATTERING
2.3. THE MOLIÈRE-D'ESPAGNAT METHOD
2.4. THE ESTIMATION EQUATIONS

**3. The Estimation of Scattering when Distortion is Present** 232

3.1. LINEAR AND CURVATURE DISTORTION
3.2. THE EFFECT OF DISTORTION ON THE COORDINATES $y_i$
3.3. THE COMBINED EFFECT OF SCATTERING AND DISTORTION
3.4. THE ESTIMATION OF SCATTERING PARAMETERS
3.5. THE MEASUREMENT OF VERY HIGH MOMENTA

**4. Summary and Conclusions** . . . . . 248

† Also supported by the Nuclear Research Foundation within the University of Sydney.

## 1. Introduction

This paper deals with the problem of estimating true scattering from the results of scattering measurements made in the presence of experimental errors, particularly in the case when distortion is present. The aim of the treatment of measurements in the presence of distortion is to give an account of the theory underlying the methods that are used in practice.

We will only treat the case of measurements made on high-energy particles, i.e. those that do not lose an appreciable amount of energy as they traverse the emulsion, in which case the track is divided into equal cells. For each cell we measure a quantity that depends on the multiple scattering of the particle. Such quantities, which we have called "characteristics" in Part I of this investigation [1]) (in the following referred to as I), can be the angles between tangents drawn to the track, the angles between chords or any order of differences of the coordinates. In the following we will only deal with coordinate differences.

In I we derived the distribution functions of the $r^{\text{th}}$ differences. We denote the $r^{\text{th}}$ difference obtained for the $i^{\text{th}}$ cell by $D_i$. The Joint Probability Function (JPF), which is the probability that $D_i$ lies between $D_i$ and $D_i+\mathrm{d}D_i$, $i = 1, 2, \ldots, n$, is the distribution function used in the theory of estimation. In I we obtained an expression for the JPF of the observed $D_i$ which arise both from true scattering and experimental errors.

The errors can be classified as follows:

1) *Random Errors.* Errors which are independent of the cell length used or of position along the track and do not affect the algebraic mean of the $D_i$ †, but increase the spread of the distribution of the $D_i$ are called random errors.

2) *Systematic Errors.* Errors which affect the algebraic mean of the $D_i$ are called systematic errors.

The contribution of random errors to the standard deviation of the observed $D_i$ is called "noise" in I. This definition is slightly different from that used by some other authors in that, by definition, noise is here taken to be independent of the cell length. In I, for the purpose of deriving the JPF, all the sources of noise, i.e. grain, reading and stage errors, were treated collectively and we assumed that the coordinates $y_i$, due to the random errors alone, are independent normal variates with a standard deviation $\sigma_N$.

The contribution of systematic errors can be subdivided into distortion and spurious scattering. In the following, as in I, we use the term distortion for both stage and emulsion distortion because both will have similar effects on the $D_i$. We will not consider the methods of eliminating spurious

† The algebraic mean is defined as $\overline{D_i} = \Sigma_i D_i/n$.

scattering from the results of measurement since the only way of estimating its magnitude is by measuring the scattering of particles of known energy. With the exception of section 3.5 we assume that spurious scattering is negligible.

If we assume that there is no spurious scattering, each of the observed $D_i$ can be considered to be the sum of contributions $D_{si}$ arising from true scattering, $D_{ei}$ from noise and $D_{di}$ from distortion. If we denote the standard deviation of the $D_{si}$ by $\sigma_s$, the aim of the theory of estimation can be stated to be the obtaining of information about the value of $\sigma_s$ from the set of the observed $D_i$. The problem is one of sampling and has been treated by several authors [1–5]). Moyal [2]) was the first to apply the statistical theory of estimation to scattering measurements. Molière [3]) derived an approximate method of simultaneously estimating scattering and noise for the second differences of the coordinates, and this method was then developed by d'Espagnat [4]). These authors used the normal approximation to the JPF. Huybrechts [5]) has thoroughly investigated the theory of estimation, particularly the consequences of using the normal approximation.

In section 2 of this paper we outline the theory of estimating scattering and noise when there is no distortion present. The Molière-d'Espagnat method is extended to the third and fourth differences of the coordinates, using the normal approximation.

In section 3 the effect of distortion on scattering measurements is described. The distortion is assumed to be of second order, i.e. a straight track is distorted into a second-order curve, but the theory can be easily extended to distortion of any order. It is shown that the method proposed by Fowler [6]), in which the algebraic mean of the second differences is subtracted from each of the $D_i$, will lead to an unbiassed estimate of $\sigma_s$, but the use of third and fourth differences will give a smaller standard error of $\sigma_s$ if the distortion-to-signal ratio $\delta \gtrapprox 0.3$. Finally, the effect of distortion on the measurement of very high momenta is discussed. The upper limit to the momenta that can be measured is calculated as a function of the magnitude of the distortion vector and the angle of dip of the track. An approximate correction for spurious scattering can be made by subtracting the spurious-scattering contribution from the total scattering observed [7]). An expression for the standard error of $\sigma_s$ is derived also for this case.

## 2. An Outline of the Estimation Theory

### 2.1. THE GENERAL THEORY OF ESTIMATION

The problem that we have to deal with is to obtain a value of a parameter $\alpha$, whose true value is unknown, from $n$ determinations of the quantity $x$ which is distributed according to some Frequency Function (FF) $f(x \mid \alpha)$.

The theory of estimating $\alpha$ from a sample of size $n$ when the JPF $f(\mathbf{x} \mid \alpha)$ is known has been treated extensively [5]). We denote the estimate of $\alpha$ by $\alpha^*$. $\alpha^*$ is a statistical variable with a distribution function $f(\alpha^* \mid \alpha)$ whose mean will be denoted by $E(\alpha^*)$ and the standard deviation by $\sigma(\alpha^*)$. If $E(\alpha^*) = \alpha$ we say that the estimate is unbiassed.

When $n$ is small the estimation theory is complicated and although in principle it is possible to correct $\alpha^*$ for bias, in practice very often this is impossible. We will therefore restrict ourselves to the case when $n \gg 1$. For the treatment in sections 2.3 and 2.4 to give reliable results $n$ must be greater than approximately 25 [5]).

The aim of the theory of estimation is to determine an estimate of the parameter $\alpha$ which is unbiassed and which gives the most information about $\alpha$ from the sample. To estimate $\alpha$ we can use any function of $\alpha$ and we will call such a function the "estimator" of $\alpha$ and the particular value taken to be the estimate the "value estimated" or simply the estimate. This nomenclature was introduced by Pitman [9]). If the parameter $\alpha$ is estimated in a number of different ways and we denote the estimators by $\alpha_i^*$, then $\sigma^2(\alpha_k^*)$, the variance of the distribution of the estimator used in the $k^{\text{th}}$ method, will be a measure of the spread of the repeated estimations of $\alpha$ using the $k^{\text{th}}$ method. It can be shown [8]) that, subject to certain mathematical restrictions which are usually met in practice, there exists an estimator $\alpha^*$ such that

$$\sigma^2(\alpha^*) \leqq \sigma^2(\alpha_i^*) \tag{2.1}$$

and that $\sigma^2(\alpha^*)$ is the smallest variance of any estimator that we can use. The efficiency of an estimator $e(\alpha_i^*)$ is defined by

$$e(\alpha_i^*) = \sigma^2(\alpha^*)/\sigma^2(\alpha_i^*) \tag{2.2}$$

and has a value between 0 and 1. If as $n \to \infty$, $e(\alpha^*) \to 1$ we say that $\alpha_i^*$ is asymptotically efficient.

The most important general method of estimation so far known is the Maximum Likelihood Method (MLM). It was first introduced by R. A. Fisher [10]). The MLM consists of maximizing the logarithm of the JPF $f(\mathbf{x} \mid \alpha)$ with respect to the parameter we wish to estimate. The MLM estimate of $\alpha$ is then a solution of the equation

$$\frac{\partial}{\partial \alpha} \ln f(\mathbf{x} \mid \alpha) = 0. \tag{2.3}$$

Eq. (2.3) is usually called the likelihood equation.

The importance of the MLM is due to the following propositions which are proved by Cramér [8]).

1) If an efficient estimate $\alpha^*$ of $\alpha$ exists then the likelihood equation will have a unique solution equal to $\alpha^*$.

2) Subject to certain general conditions on the differentiability and integrability of $\ln f$, the solution of the likelihood equation converges to the true value of $\alpha$ as $n \to \infty$, i.e. $\alpha^*$ is unbiassed.

3) The solution of the likelihood equation is an asymptotically efficient estimate of $\alpha$, and the distribution of $\alpha^*$ tends to normality as $n \to \infty$. The variance of this estimate approaches the value

$$\sigma^2(\alpha^*) = \frac{1}{E\left\{\left(\frac{\partial \ln f}{\partial \alpha}\right)^2\right\}}. \tag{2.4}$$

4) If $\alpha^*$ and $\beta^*$ are joint MLM estimators of $\alpha$ and $\beta$, i.e. simultaneous solutions of $\partial \ln f/\partial\alpha = 0$ and $\partial \ln f/\partial\beta = 0$, then it is impossible to find a better estimator of $\alpha$ than $\alpha^*$ and of $\beta$ than $\beta^*$ and both estimates are asymptotically efficient.

### 2.2. THE MAXIMUM LIKELIHOOD METHOD APPLIED TO SCATTERING

The aim of an estimation theory is to obtain the contribution of true scattering to the observed value of some function of the observed coordinate differences. We shall choose as the estimator $\sigma_s$, the standard deviation of the coordinate differences due to true scattering. We denote the standard deviation of the observed differences by $\sigma_0$ and the standard deviation arising from noise by $\sigma_\epsilon$. For the time being we assume that there is no distortion or spurious scattering present, so that the algebraic mean of the $D_i$ is zero.

Let $D_i = D_{si} + D_{\epsilon i}$ be the observed $i^{\text{th}}$ difference where $D_{si}$ is the contribution from true scattering and $D_{\epsilon i}$ from noise. The JPF of the $D_i$ is given by eq. (5.7) of I. We can rewrite it in a more convenient form by introducing the quantity $\mu$, defined by

$$\mu = \sigma_\epsilon^2/\sigma_s^2, \tag{2.5}$$

which is the square of the signal-to-noise ratio in the normal approximation. Then

$$f(\mathbf{D}|\sigma_s, \mu) = \{(2\pi\sigma_s^2)^n |a^{(s)} + \mu a^{(\epsilon)}|\}^{-\frac{1}{2}} \cdot \exp\{-\mathbf{D}^{\mathrm{T}}(\mathbf{a}^{(s)} + \mu\mathbf{a}^{(\epsilon)})^{-1}\mathbf{D}/2\sigma_s^2\}, \tag{2.6}$$

where we have used the matrix notation for the set $D_i$, and $\mathbf{D}^{\mathrm{T}}$ is the transpose of the single-column matrix $\mathbf{D}$. The matrices $\mathbf{a}^{(s)}$ and $\mathbf{a}^{(\epsilon)}$ are the matrices of the correlation coefficients of the $D_{si}$ and $D_{\epsilon i}$. The values of the matrices are given in I. The matrix of the correlation coefficients of the observed differences is given in terms of $\mathbf{a}^{(s)}$ and $\mathbf{a}^{(\epsilon)}$ by the equation

$$\mathbf{a} = (\mathbf{a}^{(s)} + \mu\,\mathbf{a}^{(\epsilon)})/(1+\mu). \tag{2.7}$$

The logarithm of the JPF can then be written as

$$\ln f = -\frac{n}{2}\ln 2\pi - n\ln\sigma_s - \tfrac{1}{2}\ln|a^{(s)}+\mu a^{(e)}| - \tfrac{1}{2}\sigma_s^{-2}Q, \tag{2.8}$$

where $Q$ is the quadratic form

$$Q = \mathbf{D}^{\mathrm{T}}(\mathbf{a}^{(s)}+\mu\,\mathbf{a}^{(e)})^{-1}\mathbf{D}. \tag{2.9}$$

We wish to extimate $\sigma_s$ and $\sigma_e$, so that the likelihood equations become

$$-\frac{n}{\sigma_s}+\frac{Q}{\sigma_s^3}=0 \tag{2.10}$$

and

$$\frac{\partial}{\partial\mu}\ln|a^{(s)}+\mu a^{(e)}|+\sigma_s^{-2}\frac{\partial}{\partial\mu}Q=0. \tag{2.11}$$

Eqs. (2.10) and (2.11) have to be solved simultaneously to obtain estimates of $\sigma_s$ and $\mu$. It can be seen that the differentiation of $\ln|a^{(s)}+\mu a^{(e)}|$ and $Q$ with respect to $\mu$ is unmanageable. Even if performed, the resulting equations for the estimate of $\mu$ would be extremely complicated so that an exact solution is impossible. However, if $\mu$ is known, i.e. if $\sigma_s$ and $\sigma_e$ have been determined by some other method, we can obtain a second approximation to $\sigma_s$ from eq. (2.10). The MLM estimate of $\sigma_s$ when $\mu$ is known is

$$\sigma_s^{*2} = Q/n. \tag{2.12}$$

The estimate of the variance of $\sigma_s^*$ can be found from eq. (2.4) as

$$S^2(\sigma_s^*) = Q/2n^2 = \sigma_s^{*2}/2n \tag{2.13}$$

and the relative standard deviation of $\sigma_s^*$ therefore is given by

$$S(\sigma_s^*) = 1/\sqrt{2n}. \tag{2.14}$$

The quadratic form $Q$ can be expressed in the following way

$$Q = q_{ii}D_i^2+q_{i,i+1}D_iD_{i+1}+q_{i,i+1}D_iD_{i+2}+\ldots, \tag{2.15}$$

where the quantities $q_{ij}$ depend on $\mu$. To determine the $q_{ij}$ we have to invert the $n\times n$ matrix $\mathbf{a}^{(s)}+\mu\mathbf{a}^{(e)}$ where in general there are $r$ independent elements where $r$ is the order of differences used. Molière [3]), using an approximate method of inversion, has derived these coefficients for the case of the second differences for several values of $\mu$.

The quantity $E\{(\partial\ln f/\partial\sigma_s)^2\}$ will depend on the exact shape of the JPF $f(\mathbf{D}|\sigma_s)$, so that the expression for the standard error of $\sigma_s^*$ (eq. 2.13) is only correct for the normal approximation. The correction to $S(\sigma_s^*)$, to take into account the non-normal character of the JPF, can be made using the method developed by Huybrechts [5]). As we have seen in I, the matrix of the correlation coefficients of the $D_i$ is the same whatever the shape of the distribution function, therefore eq. (2.12) will give an estimate of $\sigma_s$ which is independent of the shape of the FF of the $D_i$.

## 2.3. THE MOLIÈRE-D'ESPAGNAT METHOD

In the preceding section we have seen that the MLM estimate of $\sigma_s$ when $\mu$ is known is

$$\sigma_s^* = (Q/n)^{\frac{1}{2}}, \tag{2.12}$$

where $Q$ is the quadratic form

$$Q = \sum_{j,k} q_{jk} D_j D_k. \tag{2.15}$$

If we take a quadratic form $R = \sum b_{jk} D_j D_k$, in which for the time being we leave the matrix $\mathbf{b}$ arbitrary, as an approximation to $Q$, we see that the quantity $(R/n)^{\frac{1}{2}}$ will be equal to the MLM estimate of $\sigma_s$ when $\mathbf{b} = \mathbf{q}$. This suggests that we can use $R$ to make an approximate estimate of $\sigma_s$; in particular the estimate will be of the form $(R/n)^{\frac{1}{2}}$.

To derive equations to be used for estimating $\sigma_s$ and $\sigma_c$ we proceed as follows. For a large number of tracks left by particles of the same energy the mean of $R$ is given by

$$E(R) = \sum_{j,k} b_{jk} E(D_j D_k). \tag{2.16}$$

$E(D_j D_k)$ can be found using eq. (3.8) of I, together with the Fourier Transform $g(\boldsymbol{\eta})$ of the JPF of the $D_i$ which, in the normal approximation, can be written as

$$g(\boldsymbol{\eta}) = \exp\left(\tfrac{1}{2}\boldsymbol{\eta}^{\mathrm{T}} \boldsymbol{\lambda} \boldsymbol{\eta}\right), \tag{2.17}$$

where $\boldsymbol{\lambda}$ is the moment matrix of the $D_i$. If $\boldsymbol{\lambda}^{(s)}$ and $\boldsymbol{\lambda}^{(c)}$ are the moment matrices of the $D_{si}$ and $D_{ck}$ then

$$\boldsymbol{\lambda} = \boldsymbol{\lambda}^{(s)} + \boldsymbol{\lambda}^{(c)}. \tag{2.18}$$

If there is no distortion or spurious scattering we have

$$E(D_j D_k) = \lambda_{jk} = \boldsymbol{\lambda}_{jk}^{(s)} + \boldsymbol{\lambda}_{jk}^{(c)}. \tag{2.19}$$

Eq. (2.19) holds whatever the distribution function of the $D_i$.

Substituting eq. (2.19) into (2.16) we get

$$E(R) = \mathrm{Tr}(\mathbf{b}\boldsymbol{\lambda}) = \mathrm{Tr}\,(\mathbf{b}\boldsymbol{\lambda}^{(s)}) + \mathrm{Tr}\,(\mathbf{b}\boldsymbol{\lambda}^{(c)}), \tag{2.20}$$

where Tr $\mathbf{a}$ is the trace of the matrix $\mathbf{a}$ or the sum of its diagonal elements. We can now choose a particular value for the matrix $\mathbf{b}$. Let $\mathbf{b}^{(s)}$ be the matrix such that

$$\mathrm{Tr}\,(\mathbf{b}^{(s)} \boldsymbol{\lambda}^{(c)}) = 0. \tag{2.21}$$

Then, since $\boldsymbol{\lambda}^{(s)} = \sigma_s^2 \mathbf{a}^{(s)}$, we can write eq. (2.20) as

$$\sigma_s^2 = E(R_s)/\mathrm{Tr}\,(\mathbf{b}^{(s)} \mathbf{a}^{(s)}), \tag{2.22}$$

where

$$R_s = \sum b_{jk}^{(s)} D_j D_k. \tag{2.23}$$

We obtain a similar expression for $\sigma_c^2$ if we use $\mathbf{b}^{(c)}$ instead of $\mathbf{b}^{(s)}$, where

$\mathbf{b}^{(\varepsilon)}$ is defined so that

$$\mathrm{Tr}\,(\mathbf{b}^{(\varepsilon)}\boldsymbol{\lambda}^{(s)}) = 0. \tag{2.24}$$

We can now derive the estimation equations as follows. If we have a large number of tracks all of the same energy, each track will have associated with it a parameter $R_s$ describing scattering. If an observer measures these tracks with the same noise level there will also be a parameter $R_\varepsilon$ associated with each track. The relation between $\sigma_s$ and $E(R_s)$ is given by eq. (2.22) with a similar equation giving the relation between $R_\varepsilon$ and $\sigma_s$. What the observer can obtain by measurement, however, is not $E(R_\varepsilon)$, which is the population mean of $R_s$, but $\bar{R}_s$, the sample mean for a large number of tracks. Further, from the measurements on one track we usually want to estimate $\sigma_s$ for that track only. We assume in this case, that the set of $D_i$ obtained is a sample from an infinite population. As an estimate of $E(R_s)$ and $E(R_\varepsilon)$ we take

$$R_s^* = \sum_{j,k} b_{jk}^{(s)} D_j D_k \tag{2.25}$$

and

$$R_\varepsilon^* = \sum_{j,k} b_{jk}^{(\varepsilon)} D_j D_k. \tag{2.26}$$

Then substituting $R_s^*$ for $E(R_s)$ in eq. (2.22), and similarly with $R_\varepsilon^*$, we obtain $\sigma_s^*$ and $\sigma_\varepsilon^*$ the estimates of $\sigma_s$ and $\sigma_\varepsilon$.

The estimates of the variances of $\sigma_s^*$ and $\sigma_\varepsilon^*$ can be found from the variance of $R_s$ and $R_\varepsilon$, since

$$S^2(\sigma_s^*)/\sigma_s^* = \tfrac{1}{2} S^2(R_s^*)/R_s^*, \tag{2.27}$$

with a similar expression for the variance of $\sigma_\varepsilon^*$ with the subscript s replaced by $\varepsilon$. $S^2(R_s)$ can be found from the JPF of the $D_i$ by the method used for finding $E(R)$. After some calculation we find

$$\begin{aligned} S^2(R_s) &= 2\,\mathrm{Tr}\,(\mathbf{b}^{(s)}\boldsymbol{\lambda}\mathbf{b}^{(s)}\boldsymbol{\lambda}) \\ &= 2\,\mathrm{Tr}(\mathbf{b}^{(s)}\boldsymbol{\lambda}^{(s)}\mathbf{b}^{(s)}\boldsymbol{\lambda}^{(s)}) + 4\mathrm{Tr}(\mathbf{b}^{(s)}\boldsymbol{\lambda}^{(s)}\mathbf{b}^{(s)}\boldsymbol{\lambda}^{(\varepsilon)}) + 2\mathrm{Tr}(\mathbf{b}^{(s)}\boldsymbol{\lambda}^{(\varepsilon)}\mathbf{b}^{(s)}\boldsymbol{\lambda}^{(\varepsilon)}). \end{aligned} \tag{2.28}$$

Finally combining equations (2.22), (2.27) and (2.28) the expression for the relative standard error of $\sigma_s^*$ becomes

$$\begin{aligned} \frac{S(\sigma_s^*)}{\sigma_s^*} = &- \frac{1}{\sqrt{2}\,\mathrm{Tr}\,(\mathbf{b}^{(s)}\mathbf{a}^{(s)})} \{\mathrm{Tr}\,(\mathbf{b}^{(s)}\mathbf{a}^{(s)}\mathbf{b}^{(s)}\mathbf{a}^{(s)}) \\ &+ 2\mu\,\mathrm{Tr}\,(\mathbf{b}^{(s)}\mathbf{a}^{(s)}\mathbf{b}^{(s)}\mathbf{a}^{(\varepsilon)}) + \mu^2\,\mathrm{Tr}\,(\mathbf{b}^{(s)}\mathbf{a}^{(\varepsilon)}\mathbf{b}^{(s)}\mathbf{a}^{(\varepsilon)})\}^{\frac{1}{2}}, \end{aligned} \tag{2.29}$$

where $\mu = \sigma_\varepsilon^2/\sigma_s^2$. The expression for $S(\sigma_\varepsilon^*)/\sigma_\varepsilon^*$ is similar to (2.29) but with $(\varepsilon)$ in place of the superscript (s) and $1/\mu$ in place of $\mu$.

The final choice of the matrices $\mathbf{b}^{(s)}$ and $\mathbf{b}^{(\varepsilon)}$ has still to be made. The conditions imposed by eqs. (2.21) and (2.24) are not strict and can be satisfied by a large number of possible matrices. We chose $\mathbf{b}^{(s)}$ and $\mathbf{b}^{(\varepsilon)}$

as simple as possible:

$$\mathbf{b} = \begin{bmatrix} 1 & b & 0 & . & \\ b & 1 & b & . & 0 \\ 0 & b & 1 & . & \\ . & . & . & . & . \\ & & 0 & b & 1 \end{bmatrix}. \tag{2.30}$$

The quadratic form $R$ can now be written:

$$R = \sum_i D_i^2 + 2b \sum_i D_i D_{i+1}. \tag{2.31}$$

If we compare (2.31) and (2.15) which gives an expression for the quadratic form $Q$ which occurs in the MLM, we see that by using $R$ instead of $Q$ we are making use of the correlations between the $D_i$ and $D_{i+1}$ only, the correlations between $D_i$ and $D_{i+k}$, with $k \geqq 2$, being neglected.

From eqs. (2.21) and (2.24) we can find the off-diagonal elements of the matrices $\mathbf{b}^{(s)}$ and $\mathbf{b}^{(e)}$. They are

$$b^{(s)} = -\frac{n}{n-1}\frac{1}{2a_{12}^{(e)}} \tag{2.32}$$

and

$$b^{(e)} = -\frac{n}{n-1}\frac{1}{2a_{12}^{(s)}} \tag{2.33}$$

where $n$ is the number of $r^{\text{th}}$ differences obtained. Finally, the equations for estimating $\sigma_s^*$ are obtained by combining eqs. (2.22), (2.31) and (2.32). Similarly we obtain the estimation equations for $\sigma_e^*$. These equations are

$$\sigma_s^{*2} = (a_{12}^{(e)}\overline{D_i^2} - \overline{D_i D_{i+1}})/(a_{12}^{(e)} - a_{12}^{(s)}) \tag{2.34}$$

$$\sigma_e^{*2} = (-a_{12}^{(s)}\overline{D_i^2} + \overline{D_i D_{i+1}})/(a_{12}^{(e)} - a_{12}^{(s)}). \tag{2.35}$$

The elements of the matrices $\mathbf{a}^{(s)} = \mathbf{A}^{(s)}/A_{11}^{(s)}$ and $\mathbf{a}^{(e)} = \mathbf{A}^{(e)}/A_{11}^{(e)}$, where the matrices $\mathbf{A}^{(s)}$ and $\mathbf{A}^{(e)}$ are defined in I, can be found from tables 1 and 2 of I for second, third and fourth differences of the coordinates. The expressions for the standard errors of $\sigma_s^*$ and $\sigma_e^*$ can be found from eq. (2.29). In calculating the traces we have taken $n \gg 1$, which is equivalent to neglecting the changes in the correlation of the $D_i$ very near to the ends of the track. The estimation equations are given below.

The eqs. for $\sigma_s^{*2}$ and $\sigma_e^{*2}$ are independent of the exact shape of the distribution of the $D_{si}$ and $D_{ei}$[1]). On the other hand the expressions for the relative standard errors are only valid for the normal approximation. Huybrechts [5, 11]) has calculated a correction factor for $S(\sigma_s^*)/\sigma_s^*$ to take into account the non-normal character of the distribution functions of the $D_{si}$. The correction factors have been denoted below by $R_c$. For example, in the case of second differences the correction factor is 1.32 when $|D_i|$

greater than $4|\overline{D_i}|$ are rejected [11]). Thus the relative standard errors given by eqs. (2.36–2.38) without the factor $R_c$ are an underestimate of the spread of the $\sigma_s^*$.

## 2.4. THE ESTIMATION EQUATIONS

Second differences:

$$\sigma_s^{*2} = \tfrac{12}{11}[\tfrac{2}{3}\overline{D_i^2}+\overline{D_i D_{i+1}}],$$
$$\sigma_e^{*2} = \tfrac{12}{11}[\tfrac{1}{4}\overline{D_i^2}-\overline{D_i D_{i+1}}],$$
$$S(\sigma_s^*)/\sigma_s^* = \frac{R_c}{\sqrt{2n}}\{2.10+0.31\,\mu_2+0.18\,\mu_2^2\}^{\frac{1}{2}}, \tag{2.36}$$
$$S(\sigma_e^*)/\sigma_e^* = \frac{R_c}{\sqrt{2n}}\left\{2.69+1.35\frac{1}{\mu_2}+0.49\frac{1}{\mu_2^2}\right\}^{\frac{1}{2}}.$$

Third differences:

$$\sigma_s^{*2} = \tfrac{12}{5}[\tfrac{3}{4}\overline{D_i^2}+\overline{D_i D_{i+1}}],$$
$$\sigma_e^{*2} = \tfrac{12}{5}[-\tfrac{1}{3}\overline{D_i^2}-\overline{D_i D_{i+1}}],$$
$$S(\sigma_s^*)/\sigma_s^* = \frac{R_c}{\sqrt{2n}}\{2.38+1.30\,\mu_3+0.59\,\mu_3^2\}^{\frac{1}{2}}, \tag{2.37}$$
$$S(\sigma_e^*)/\sigma_e^* = \frac{R_c}{\sqrt{2n}}\left\{4.09+4.10\frac{1}{\mu_3}+1.72\frac{1}{\mu_3^2}\right\}^{\frac{1}{2}}.$$

Fourth differences:

$$\sigma_s^{*2} = \tfrac{80}{19}[\tfrac{8}{10}\overline{D_i^2}+\overline{D_i D_{i+1}}],$$
$$\sigma_e^{*2} = \tfrac{80}{19}[-\tfrac{9}{16}\overline{D_i^2}-\overline{D_i D_{i+1}}],$$
$$S(\sigma_s^*)/\sigma_s^* = \frac{R_c}{\sqrt{2n}}\{3.43+2.98\,\mu_4+1.35\,\mu_4^2\}^{\frac{1}{2}}, \tag{2.38}$$
$$S(\sigma_e^*)/\sigma_e^* = \frac{R_c}{\sqrt{2n}}\left\{5.94+7.63\frac{1}{\mu_4}+3.53\frac{1}{\mu_4^2}\right\}^{\frac{1}{2}}.$$

In the above equations $\mu_r$ is the square of the noise-to-signal ratio for $r^{\text{th}}$ differences,

$$\overline{D_i^2} = (\sum_i D_i^2)/n \text{ and } \overline{D_i D_{i+1}} = (\sum_i D_i D_{i+1})/(n-1),$$

where $n$ is the number of $r^{\text{th}}$ differences obtained.

The quantity that we are finally interested in is $pv$, which is given in terms of the arithmetic mean $r^{\text{th}}$ difference by the equation

$$pv = \frac{K\,s^{3/2}}{E(|D_r|)}, \tag{2.39}$$

where $K$ is the scattering constant. The reason for using the arithmetic mean, instead of the standard deviation $\sigma_s$, was discussed in I. Because of the assumptions used in deriving the JPF, and in particular because the

effect of the finite size of the nucleus was ignored, which introduces a cut off for large $D_i$, the standard deviation of the $D_i$ calculated from the Molière distribution function diverges. Eqs. (2.36)—(2.38) are still valid, however, since in deriving them we have only used the correlation matrices $\mathbf{a}^{(s)}$, which as shown in I, are independent of the exact shape of the distribution functions.

To be able to use the published values of the scattering constant [12]), which are all calculated for the arithmetic mean, the estimation equations have to be expressed in terms of $|\overline{D_r^*}|$ and not $\sigma_s^*$. To do this we assume that the distribution functions of the $D_i$ are sufficiently gaussian so that we can write $|\overline{D_r^*}| = \sqrt{(2/\pi)}\,\sigma_s^*$. The value of the ratio $\sqrt{(2/\pi)}|\overline{D_i^2}|/|\overline{D_i}|$ has been experimentally determined [13]) for the case when a replacement cut off is used for the large $D_i$. The value obtained was $0.993 \pm 0.003$, so that putting $|\overline{D_r^*}| = \sqrt{(2/\pi)}\,\sigma_s^*$ will not introduce a serious error.

## 3. The Estimation of Scattering when Distortion is Present

### 3.1. LINEAR AND CURVATURE DISTORTION

During processing of glass-mounted nuclear emulsion the gelatin swells and becomes deformable. If the emulsion layers move with respect to the glass a track that is originally straight will be distorted into some kind of a curve. If the deformations are large the plate will, in general, be useless for measurements. In the case where distortion does not make scattering measurements completely impossible we have to take into account the contributions to the mean value of the $r^{\text{th}}$ difference arising from distortion.

When distortion is present, a point at a depth $z$ from the glass-emulsion interface, which will be called the G surface, will be displaced from its original position in a plane parallel to the G surface. We will denote the displacement by a vector $\mathbf{\Delta}$ which lies in a plane parallel to the G surface. We can express $\mathbf{\Delta}$ as a power series in $z/T$ where $T$ is the processed emulsion thickness, and we have

$$\mathbf{\Delta} = \mathbf{K}_1 \frac{z}{T} + \mathbf{K}_2 \left(\frac{z}{T}\right)^2 + \mathbf{K}_3 \left(\frac{z}{T}\right)^3 + \ldots . \tag{3.1}$$

The term $\mathbf{K}_1 z/T$ describes a linear displacement which is zero at the G surface and has the value $\mathbf{K}_1$ at the emulsion-air interface, which will be called the A surface. This type of distortion is called linear distortion.

The term $\mathbf{K}_2(z/T)^2$ will produce a second-order curvature in a track which was originally straight and will be called quadratic distortion. The displacement produced by quadratic distortion is zero at the G surface and has the value $\mathbf{K}_2$ at the A surface.

The term $\mathbf{K}_3(z/T)^3$ describes third-order curvature and will be called third-order distortion.

The magnitudes of $\mathbf{K}_1$, $\mathbf{K}_2$ and so on, will depend on the thickness of the emulsion. Unless otherwise stated, the units of the distortion vectors $\mathbf{K}$ will be microns and the thickness of the unprocessed emulsion will be taken to be 600 $\mu$. In the case of quadratic distortion the magnitude of the distortion vector is generally expressed in Covans [14]) where the magnitude of the distortion vector $k_2$ in Covans is defined by

$$k_2 = K_2/t^2 \tag{3.2}$$

where $K_2$ is in microns and $t$ is the unprocessed emulsion thickness in mm. The quadratic distortion vector is therefore normalized to a plate of unprocessed thickness 1 mm.

The shear stress producing distortion must be zero at the A surface and the direction of the track at this surface must be the same as the original direction.

Also, at the A surface the rate of change of displacement $\mathrm{d}\boldsymbol{\Delta}/\mathrm{d}z$ must be zero, therefore

$$\left[\frac{\mathrm{d}\boldsymbol{\Delta}}{\mathrm{d}z}\right]_{z=T} = \frac{\mathbf{K}_1}{T} + \frac{2\mathbf{K}_2}{T} + \frac{3\mathbf{K}_3}{T} + \ldots = 0. \tag{3.3}$$

If $\mathbf{K}_3$, $\mathbf{K}_4$, ..., are small compared with $\mathbf{K}_1$ and $\mathbf{K}_2$ we see that approximately

$$\mathbf{K}_1 = -2\mathbf{K}_2. \tag{3.4}$$

Apostolakis and Major [15]) have determined experimentally the ratio $|K_1/K_2|$. They find $|K_1/K_2| = (2.03 \pm 0.03)$, so that the magnitude of $\mathbf{K}_3$ and the higher-order distortion vectors is less than two per cent of that of $\mathbf{K}_2$. In the treatment of the scattering measurements in the presence of distortion that follows we shall therefore assume there is only linear and quadratic emulsion distortion present.

### 3.2. THE EFFECT OF DISTORTION ON THE COORDINATES $y_i$

In this section we derive the equations for the lateral displacement $y$ of the track due to distortion. Knowing $y$ will enable us to calculate the contribution of distortion to the mean $r^{\text{th}}$ difference. We assume that the distortion is of second order, so that $\mathbf{K}_3 = \mathbf{K}_4 = \ldots = 0$. First order distortion will not affect the measurements. From the preceding section we see that the assumption that emulsion distortion is of second order is in agreement with experimental results. Stage and temperature distortions, however, will vary from one microscope to another, and have to be investigated before any measurements are made. If the distortions are of third order or higher the treatment given below can be easily extended to cover the required case.

Any point such as P on the distorted track (fig. 1) will be displaced by an amount $\Delta$ from its original position at D. Since the displacement will take

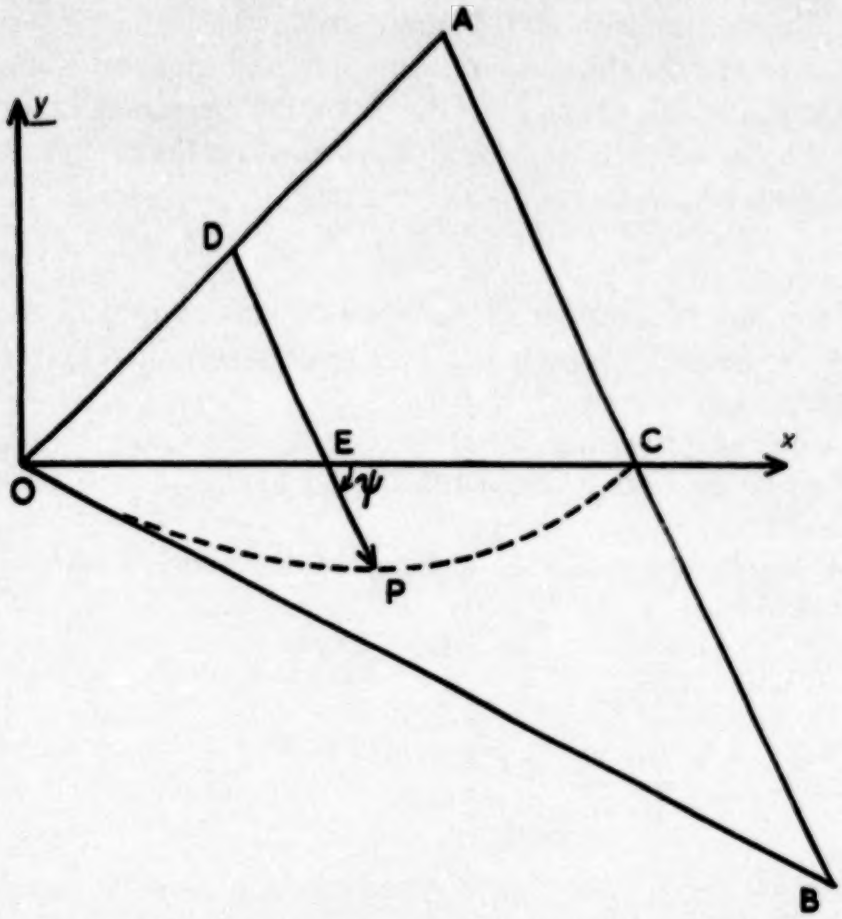


Fig. 1. The projection of a distorted track in the plane of the emulsion which is taken as the $(x, y)$ plane. The $z$ axis is vertically upward from the plane of the paper. OA is the projection of the undistorted track, OB that after linear distortion and OPC is the final projection. The $x$ axis is taken to pass through the points O and C, the projection of the points where the track intersects the G and A surfaces. $AB = K_1$ and $BC = K_2$.

place in a plane parallel to the G surface, the height of P above the G surface can be written as

$$z = x \tan \beta \tag{3.5}$$

where $x$ is the distance OE (not the $x$ coordinate of P) and $\beta$ is the angle between the $x$ axis, as shown, and the line joining the glass and air intersections of the track in the processed emulsion. $\beta$ is approximately the dip angle of the track in the processed emulsion. The two angles would be equal if there were no distortion.

Then, in the case of second-order distortion, from eqs. (3.1) and (3.4) we have

$$\Delta = -2K_2 \frac{x}{T} \tan \beta + K_2 \left(\frac{x}{T}\right)^2 \tan^2 \beta. \tag{3.6}$$

We want to determine the magnitude of the coordinate $y$ as a function of $x$. If we denote the vector EP by $\delta$, then, neglecting second-order effects,

$$y = \delta \sin \psi, \tag{3.7}$$

where $\psi$ is the angle between the vector $\delta$ and the $x$ axis. The following convention is adopted in measuring the angle $\psi$. The angle is measured

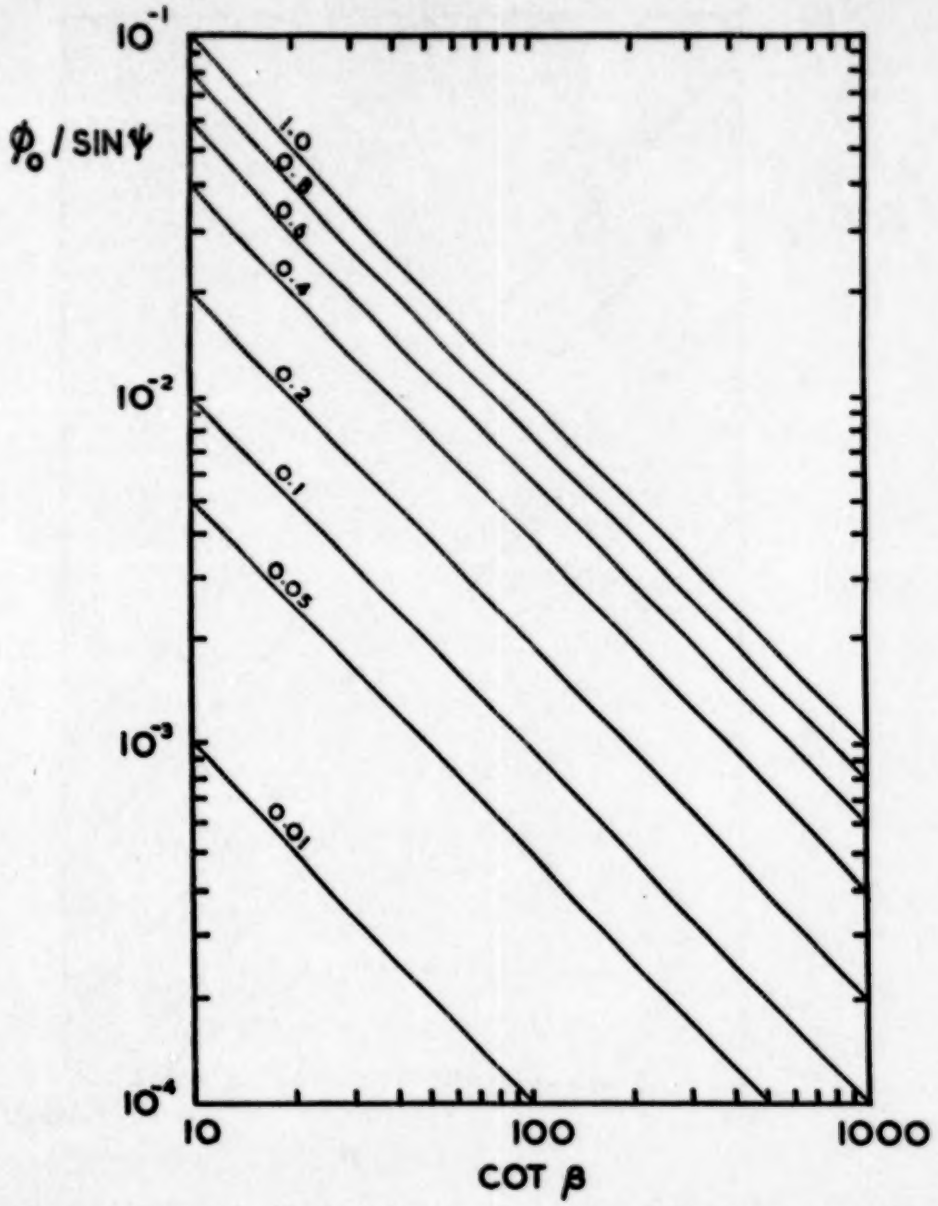


Fig. 2. $\varphi_0/\sin\psi$ as a function of cot $\beta$ for several values of $K_s/T$. $\beta$ is the dip angle in the processed emulsion, and $T$ is the processed thickness.

from the $x$-axis, as shown in fig. 1, and positive angles are measured in the anticlockwise direction. It can be shown that the error in the value of $y$ introduced through the use of eq. (3.7) is generally of the order of one per cent.

$\delta$ is the displacement of P from the point E, i.e. $\delta = \Delta - DE$, and therefore

$$y = -K_2 \frac{x}{T} \tan \beta \sin \psi + K_2 \left(\frac{x}{T}\right)^2 \tan^2 \beta \sin \psi. \tag{3.8}$$

From eq. (3.8) we see that in the small-angle approximation

$$\varphi_0 = K_2 \tan \beta \sin \psi / T \tag{3.9}$$

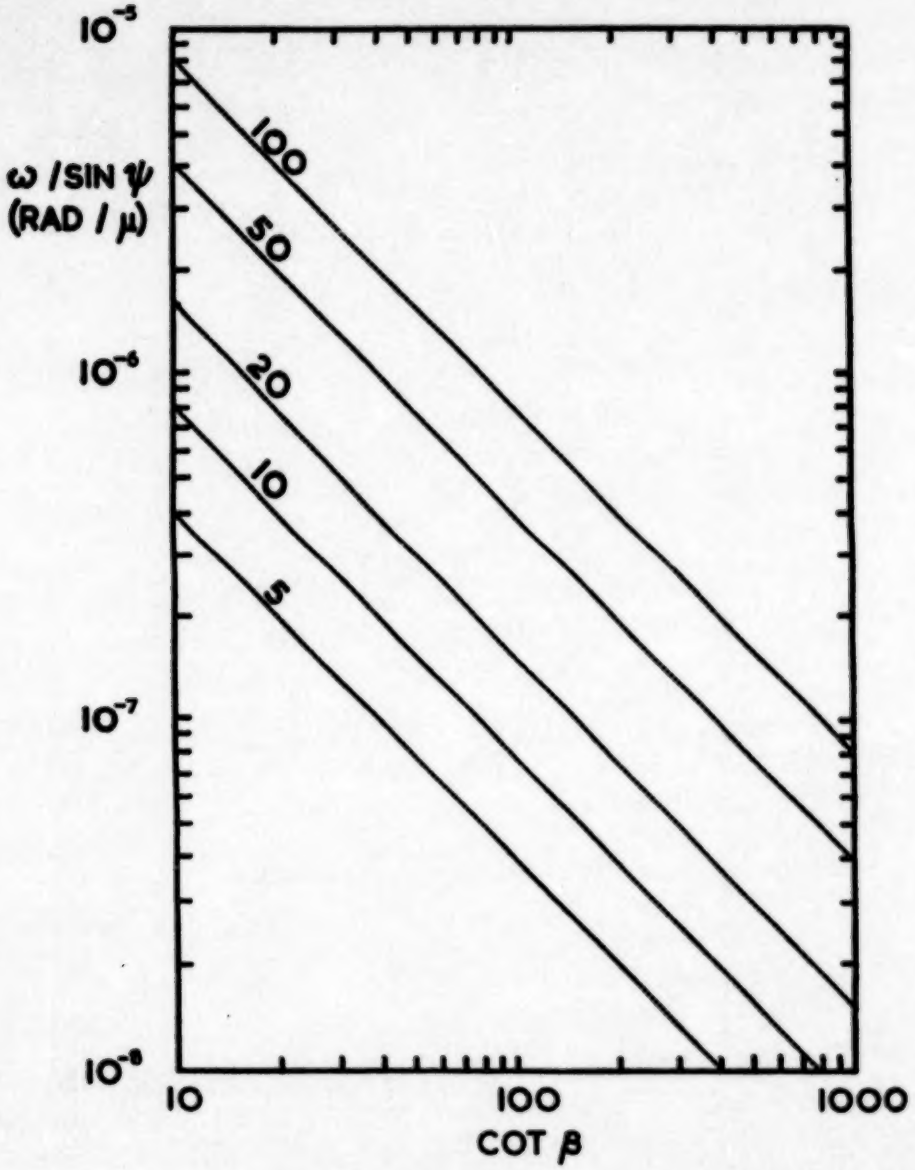


Fig. 3. $\omega/\sin\psi$ as a function of $\cot\beta$ for several values of $k_2$, the magnitude of the distortion vector in Covans.

is the angle between $x$ axis and the tangent to the track at the point O. The small-angle approximation is valid because, as we shall see later in this section, the magnitude of $\varphi_0$ is usually less than 5°.

If $\varphi$ is the angle between the $x$ axis and the tangent to the track at any point, the change in $\varphi$ or the angular deviation per unit distance along the

$x$ axis is given by

$$\omega = -2\frac{K_2}{T^2}\sin\psi\tan^2\beta. \tag{3.1}$$

The minus sign is introduced in eq. (3.10) so that $y$ is of the appropriate sign when the convention for $\psi$ given above is used.

The magnitude of $\varphi_0/\sin\psi$ as a function of $\cot\beta$ is given in fig. 2 for several values of $K_2/T$. Fig. 3 gives $\omega/\sin\psi$ as a function of $\cot\beta$ for several values of $k_2$ (Cov). The angle $\beta$ when distortion is not too high is approximately equal to the angle of dip in the processed emulsion.

The equation of the distorted track can now be written as

$$y = \varphi_0 x - \tfrac{1}{2}\omega x^2. \tag{3.11}$$

We take OC as the reference line for scattering measurements. This does not entail any loss of generality because even if the reference line is inclined at a small angle $\alpha$ to OC, the $r^{\text{th}}$ differences will be independent of $\alpha$. We divide OC into $m$ equal cells of length $s$ microns and measure the coordinates at the beginning of each cell, then $y_i$ the coordinate measured at the $i^{\text{th}}$ point will be

$$y_i = \varphi_0 x_i - \tfrac{1}{2}\omega x_i^2 \tag{3.12}$$

and the mean $y_i$ due to distortion will be, if $m \gg 1$,

$$\bar{y}_i = \frac{1}{m+1}\sum_{i=0}^{m+1} y_i = \tfrac{1}{2}\varphi_0 ms - \tfrac{1}{6}\omega m^2 s^2. \tag{3.13}$$

The second difference $D_i$ due to distortion can be found from eq. (3.12),

$$D_i = \omega s^2 \tag{3.14}$$

so that the mean, $\overline{D_i}$, is equal to $\omega s^2$. From eq. (3.14) we see that the third and fourth differences are zero when distortion is of second order, as was to be expected.

### 3.3. THE COMBINED EFFECT OF SCATTERING AND DISTORTION

The coordinate $y_i$ when both distortion and true scattering are present is the sum of a contribution $y_{si}$ due to scattering and $y_{di}$ due to distortion. When experimental errors which give rise to noise are also present, there will be a contribution $y_{ei}$ to the observed value of $y_i$. We assume that spurious scattering is negligible, so that we have

$$y_i = y_{si} + y_{ei} + y_{di}. \tag{3.15}$$

In eq. (3.15) $y_{si}$ is the scattering contribution from the portion of the track of length $l_i$ where $l_i$ is the along-the-track or arc length in the unprocessed emulsion. Eq. (3.12) giving $y_{di}$ is in terms of $x_i$, the distance measured along the reference line which is approximately parallel to the

projection of the track in the plane of the emulsion. In making scattering measurements the cell lengths are measured along $Ox$ and not along the track in the unprocessed emulsion.

If there is no distortion

$$l_i = x_i \sec\theta \tag{3.16}$$

where $\theta$ is the angle of dip of the track in the unprocessed emulsion. Hence, the cell length $s$ corresponds to a cell length $s_0$ in the unprocessed emulsion, given by $s_0 = s \sec\theta$.

When distortion is moderate, for tracks that are long enough to be measured, e.g. those that are longer than 2 mm, we have $\varphi_0/\sin\varphi_0 \approx 1$ and so the projected arc length is approximately equal to the projected chord length. When $\varphi_0/\sin\varphi_0 \approx 1$ it can be shown that

$$s_0 \approx s \sec\theta \left(1 - \frac{K_2}{x_T} \cos\psi\right), \tag{3.17}$$

where $x_T$ is approximately equal to the total projected track length. Hence, the error introduced in neglecting the effect of distortion on the cell length $s$ will be of the order of $K_2/x_T$. For a track longer than 5 mm in a plate 600 $\mu$ thick for which $K_2 = 50$ $\mu$, if we take $s_0 = s \sec\theta$ the error will be less than one per cent. The error is appreciable only for steep tracks for which $x_T \approx K_2$.

In this section we wish to determine the contribution of distortion to the variances and covariances of the $r^{\text{th}}$ differences $D_i$. The $r^{\text{th}}$ difference $D_i$ can be expressed as

$$D_i = \sum_j C_{ij} y_j. \tag{3.18}$$

The statistical expectation of $D_i$ is then

$$E(D_i) = \sum_j C_{ij} E(y_j). \tag{3.19}$$

In section 3.2 we have seen that $E(D_i) = \omega s^2$ for second differences and is zero for third and higher-order differences. If the distortion is of higher order than the second, in general, $E(D_i)$ will not be zero.

The variance of the $D_i$ is given by

$$E(D_i^2) = \sum_j C_{ij}^2 E(y_j^2) \tag{3.20}$$

and since the contributions of scattering, noise and distortion are independent, we have

$$E(D_i^2) = E(D_{si}^2) + E(D_{ei}^2) + E(D_{di}^2). \tag{3.21}$$

From eqs. (3.9) and (4.24a) of I we have

$$E(D_{si}^2) = \sigma_s^2 \tag{3.22}$$

and

$$E(D_{si}^2) = \sigma_s^2, \tag{3.23}$$

where $\sigma_s$ is the standard deviation of the $D_{si}$, which is finite if we take into account the finite size of the nucleus or the experimental cut off, and $\sigma_e$ is the standard deviation of the $D_{ei}$. From eq. (3.14) we have in the case of second differences

$$E(D_{di}^2) = \omega^2 s^4, \tag{3.24}$$

so that eq. (3.21) becomes, in the case of second differences,

$$E(D_i^2) = \omega^2 s^4 + \sigma_s^2 + \sigma_e^2. \tag{3.25}$$

Similarly, we can find that for second differences

$$E(D_i D_{i+1}) = \omega^2 s^4 + \tfrac{1}{4}\sigma_s^2 - \tfrac{2}{3}\sigma_e^2, \tag{3.26}$$

$$E(D_i D_{i+2}) = \omega^2 s^4 + \tfrac{1}{6}\sigma_e^2 \tag{3.27}$$

and

$$E(D_i D_{i+k}) = \omega^2 s^4 \text{ for } k \geqq 3. \tag{3.28}$$

For third and fourth differences we find that in the case of quadratic distortion $E(D_i D_j)$ is independent of $\omega$ and the expressions given in I are correct:

$$E(D_i D_j) = a_{ij}^{(s)} \sigma_s^2 + a_{ij}^{(e)} \sigma_e^2. \tag{3.29}$$

The JPF of the $r^{\text{th}}$ differences can now be conveniently expressed as follows. Let $\mathbf{z}$ be the single-column matrix of the quantities $D_i - E(D_i)$ and $\boldsymbol{\lambda}$ be the moment matrix of the $D_i$,

$$\lambda_{ij} = E(z_i z_j), \tag{3.30}$$

then the JPF can be written as [8])

$$f(\mathbf{z})\mathrm{d}z_1\,\mathrm{d}z_2 \ldots \mathrm{d}z_2 \ldots \mathrm{d}z_n = [(2\pi)^n |\boldsymbol{\lambda}|]^{-\frac{1}{2}} \exp\,(-\mathbf{z}^{\mathrm{T}} \boldsymbol{\lambda}^{-1} \mathbf{z})\, \mathrm{d}z_1 \mathrm{d}z_2 \ldots \mathrm{d}z_n, \tag{3.31}$$

where $\mathbf{z}^{\mathrm{T}}$ is the transpose of the matrix $\mathbf{z}$. Finally, the Fourier Transform of $f(\mathbf{z})$ is given by

$$g(\boldsymbol{\eta}) = \exp\,(-\tfrac{1}{2}\boldsymbol{\eta}^{\mathrm{T}} \boldsymbol{\lambda} \boldsymbol{\eta}).$$

### 3.4. THE ESTIMATION OF SCATTERING PARAMETERS

The elimination equations which give us an estimate of $\sigma_s$ and $\sigma_e$ when distortion is negligible were derived in section 2.2. If we substitute the values of $E(D_i^2)$ and $E(D_i D_{i+1})$ obtained above into eqs. (2.36) we find that when the distortion is of second order the third and fourth differences will give an unbiassed estimate of $\sigma_s^2$ because the $E(D_i D_j)$ are independent of $\omega$. However for second differences we have

$$\sigma_s^{*2} = \sigma_s^2 \left\{1 + \frac{20}{11} \frac{\omega^2 s^4}{\sigma_s^2}\right\}. \tag{3.32}$$

The bias introduced through distortion is therefore $1.82\ \omega^2 s^4/\sigma_s^2$.

From eq. (3.32) we can establish a criterion which can be easily used in practice, for seeing whether the effect of second-or higher-order distortion can be neglected. Since $\overline{D_i} = \overline{D_i D_{i+3}} = \omega s^2$, for $\sigma_s^*$ to be biassed by less than $1\,\%$ we must have

$$\overline{D_i} \lessapprox 0.13\ |\overline{D_2^*}|, \qquad \overline{D_i D_{i+3}} \lessapprox 0.13\ |\overline{D_2^*}|, \tag{3.33}$$

where $|\overline{D_2^*}|$ is the estimated arithmetic mean second difference due to true scattering only.

In the case of the estimate of noise we have

$$\sigma_\varepsilon^{*2} = \sigma_\varepsilon^2 \left\{1 - \frac{9}{11}\frac{\omega^2 s^4}{\sigma^2}\right\}. \tag{3.34}$$

In practice it is occasionally found that when noise is estimated using eq. (2.36), the estimate $\sigma_\varepsilon^*$ obtained is imaginary. From eq. (3.34) we see that this can occur because of distortion, since, if $\sigma_\varepsilon^2 \lessapprox 0.82\ \omega^2 s^4$ the estimated value $\sigma_\varepsilon^{*2}$ will be negative.

We can correct the estimate $\sigma_s^{*2}$ obtained using second differences when distortion is present in the following way. The expectation value of the quadratic form $R_s$ (defined in section 2.2) is given as before (eq. 2.16):

$$E(R_s) = \sum_{j,k} b_{jk}^{(s)} E(D_j D_k), \tag{3.35}$$

where the matrix $\mathbf{b}^{(s)}$ is defined by eq. (2.21). If we substitute the values of $E(D_j D_k)$ for second differences (eqs. (3.25)–(3.28)) into eq. (3.35), we obtain

$$E(R_s) = \mathrm{Tr}\ (\mathbf{b}^{(s)}\boldsymbol{\zeta}), \tag{3.36}$$

where we have used the abbreviation $\boldsymbol{\zeta}$ for the matrix of the quantities

$$\zeta_{ij} = \lambda_{ij} + E(D_i)E(D_j). \tag{3.37}$$

We denote the quantities $E(D_i)E(D_j)$ by the symbol $M_{ij}$ in what follows.

Eq. (3.36) can now be written as

$$E(R_s) = \mathrm{Tr}\ (\mathbf{b}^{(s)}\boldsymbol{\lambda}^{(s)}) + \mathrm{Tr}\ (\mathbf{b}^{(s)}\mathbf{M}), \tag{3.38}$$

where $\boldsymbol{\lambda}^{(s)}$ is defined by eq. (2.18) and $\mathbf{M}$ is the matrix of the $M_{ij}$. In eq. (3.38) the term $\mathrm{Tr}\ (\mathbf{b}^{(s)}\mathbf{M})$ is the contribution from distortion. From (3.38) we thus obtain

$$\sigma_s^2 = \frac{E(R_s) - \mathrm{Tr}\ (\mathbf{b}^{(s)}\mathbf{M})}{\mathrm{Tr}\ (\mathbf{b}^{(s)}\mathbf{a}^{(s)})}. \tag{3.39}$$

If we now take $R_s^* = \sum b_{jk} D_j D_k$ to be an estimate of $E(R_s)$, we get as before an expression for $\sigma_s^{*2}$, the estimate of $\sigma_s^2$:

$$\sigma_s^{*2} = \frac{R_s^* - \mathrm{Tr}\ (\mathbf{b}^{(s)}\mathbf{M})}{\mathrm{Tr}\ (\mathbf{b}^{(s)}\mathbf{a}^{(s)})}. \tag{3.40}$$

This estimate is corrected for distortion since we have subtracted a term Tr $(\mathbf{b}^{(s)}\mathbf{M})$, the distortion contribution. Expanding eq. (3.40) as before, we get

$$\sigma_s^{*2} = \frac{1}{a_{12}^{(e)} - a_{12}^{(s)}} \{a_{12}^{(e)} (\overline{D_i^2} - m^2) - (\overline{D_i D_{i+1}} - m^2)\}, \tag{3.41}$$

where $m = (1/n)\sum D_i$ is the algebraic mean of the $D_i$. Eq. (3.41) shows that by subtracting $m$ from each of the $D_i$ or, alternatively, subtracting $m^2$ from $\overline{D_i^2}$ and $\overline{D_i D_{i+1}}$ we can obtain an unbiassed estimate of $\sigma_s$ using second differences when distortion is present. This procedure is just that which was proposed by Fowler [6].

The standard error of the estimate $\sigma_s^*$ obtained using second differences can be found in exactly the same way as in section 2.2. The relative standard error is given by

$$\frac{S(\sigma_s^*)}{\sigma_s^*} = \frac{1}{2} \frac{S(R_s^*)}{R_s^* - \mathrm{Tr}\,(\mathbf{b}^{(s)}\mathbf{M})}. \tag{3.42}$$

Taking $S^2(R_s^*)$ to be an estimate of the variance of $R_s$, which is defined as

$$\mathrm{Var}\,(R_s) = E(R_s^2) - [E(R_s)]^2, \tag{3.43}$$

we find, using the same method as in section 2.2,

$$S(R_s^*) = [2\mathrm{Tr}\,(\mathbf{b}^{(s)}\boldsymbol{\lambda}\mathbf{b}^{(s)}\boldsymbol{\lambda}) + 4\mathrm{Tr}\,(\mathbf{b}^{(s)}\boldsymbol{\lambda}\mathbf{b}^{(s)}\mathbf{M})]^{\frac{1}{2}} \tag{3.44}$$

and, since

$$E(R_s) - \mathrm{Tr}(\mathbf{b}^{(s)}\mathbf{M}) = \mathrm{Tr}(\mathbf{b}^{(s)}\boldsymbol{\lambda}), \tag{3.45}$$

the denominator of eq. (3.42) is equal to Tr $(\mathbf{b}^{(s)}\boldsymbol{\lambda})$.

Thus we get

$$\frac{S(\sigma_s^*)}{\sigma_s^*} = \frac{1}{2} \frac{[\mathrm{Tr}(\mathbf{b}^{(s)}\boldsymbol{\lambda}\mathbf{b}^{(s)}\boldsymbol{\lambda}) + 2\,\mathrm{Tr}(\mathbf{b}^{(s)}\boldsymbol{\lambda}\mathbf{b}^{(s)}\mathbf{M})]^{\frac{1}{2}}}{\mathrm{Tr}(\mathbf{b}^{(s)}\boldsymbol{\lambda})}. \tag{3.46}$$

The first term of eq. (3.46) is just the expression for the standard error when there is no distortion and is given by eq. (2.36). The second term, evaluated for the case $n \gg 1$ is

$$9.92\, m^2/\sigma_s^2, \tag{3.47}$$

so that, if we denote $m^2/\sigma_s^2$ by $\delta^2$, we finally get

$$\frac{S(\sigma_s^*)}{\sigma_s^*} = \frac{R_c}{\sqrt{2n}} \{2.10 + 0.31\,\mu_2 + 0.18\,\mu_2^2 + 9.92\,\delta^2\}^{\frac{1}{2}}, \tag{3.48}$$

where $n$ is the number of second differences obtained, $R_c$ is the Huybrechts correction factor [5], $\mu$ is the square of the noise-to-signal ratio and $\delta$ can be called the distortion-to-signal ratio.

The reason for the increase of the relative standard error of $\sigma_s^*$ with $\delta$, even if $\sigma_s^*$ is corrected for distortion, can be seen from the following con-

siderations. Because of scattering fluctations the angular deviation per unit track length at a given point on the track will be different from $\omega$, the deviation due to distortion only. Because of these fluctuations $\overline{D_i}$, the algebraic mean of the $D_i$, will be distributed in some way about the mean which is $\omega s^2$. The correction applied, which entails the subtraction of $(\overline{D_i})^2$ from $\overline{D_i^2}$ and $\overline{D_i D_{i+1}}$, will therefore be an average correction, and for any particular track there will be an increase in the spread of $\sigma_s^*$.

The standard error of an estimate $\sigma_s^*$ can be found from fig. 4 for any value of the distortion-to-signal ratio $\delta$. Fig. 4 gives the ratio of the relative standard error when distortion is present to the relative standard error when there is no distortion. As can be seen from fig. 4 noise makes very little difference to this ratio, the difference between the cases $\mu_2 = 0$ and $\mu_2 = 1$ is less than 10 %, so that only the ratios for $\mu_2 = 0$ and $\mu_2 = 1$ are given.

The relative standard error of $\sigma_s^*$, obtained from second differences, when $\delta = 0$, 0.5 and 1.0 is given in table 1 for three typical values of the noise-to-signal ratio $\mu_2$. The errors are given in per cent assuming that the number of $r^{\text{th}}$ differences obtained is 100. From the table it is seen that the error increases with $\delta$. In the same table the relative standard error is given when $\sigma_s^*$ is obtained from third and fourth differences. Since $\mu_r$ increases with the order of the differences $r$, we have taken $\mu_2$ to be fixed. We also

TABLE 1

Relative standard error of $\sigma_s^*$ per cent

| | | $\mu_2 = 0.01$ | $\mu_2 = 0.1$ | $\mu_2 = 0.5$ |
|---|---|---|---|---|
| Second Differences (Corrected for distortion) | $\delta = 0$ | 10.3 | 10.3 | 10.7 |
| | $\delta = 0.5$ | 15.1 | 15.2 | 15.5 |
| | $\delta = 1.0$ | 24.5 | 24.6 | 24.7 |
| Third Differences | | 11.0 | 11.6 | 14.9 |
| Fourth Differences | | 11.8 | 14.8 | 22.5 |

assume that the distortion is of second order. If the distortion is of higher order, the errors for the third and fourth differences will be higher than shown in the table. In this case the errors can be calculated in exactly the same way as done above for second-order distortion.

From table 1 it can be seen that when $\delta$ is large for low values of noise the error of $\sigma_s^*$ obtained from corrected second differences is much higher than that of $\sigma_s^*$ obtained from third and fourth differences. For high values of noise the improvement obtained using third and fourth differences is not so marked, but from fig. 4 and table 1 we see that the error of $\sigma_s^*$ using second differences is equal to that using third differences if $\delta \geqq 0.3$ when $\mu = 0.5$. Therefore, if $\delta \geqq 0.3$ third differences should be used.

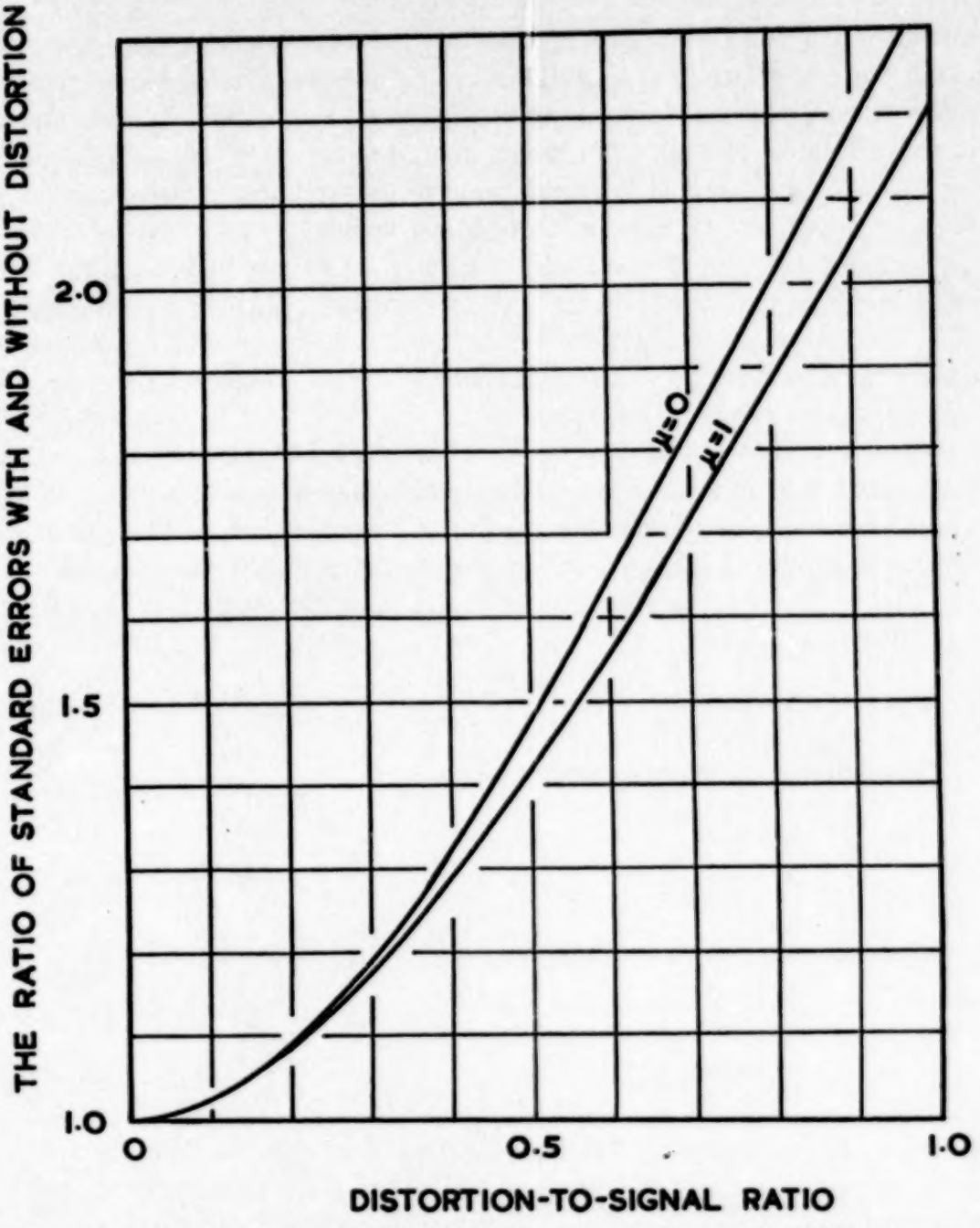


Fig. 4. Standard error of the estimated second difference after correction for distortion. The quantity plotted along the ordinate is the ratio

$$\left[\frac{S(\sigma_s^*)}{\sigma_s^*}\right]_{\text{distortion}} \Big/ \left[\frac{S(\sigma_s^*)}{\sigma_s^*}\right]_{\text{no distortion}}.$$

### 3.5. THE MEASUREMENT OF VERY-HIGH MOMENTA

In this section we will discuss some of the consequences of the presence of second-order distortion in the case of measurements of very high momenta, such as are encountered in cosmic-ray work. When scattering measurements are made the cell length $s$ is usually chosen so that $\sigma_0$, the total scattering

observed, is equal to four times the noise $\sigma_\varepsilon$ [16]). As the momentum to be measured increases, the cell length to be used increases and, since the bias in $\sigma_s^*$ due to distortion is proportional to $s^2$ in the case of uncorrected second differences, the bias introduced can become large. To illustrate the magnitude of this effect we can calculate the estimated value of $pv$, which we denote by $pv^*$, as a function of the true value of $pv$ for uncorrected second differences when second-order distortion is present.

Since $\omega$ depends on $\beta$, the angle of dip in the processed emulsion, we will calculate $pv^*$ for several regions of $\beta$, or since most authors give the value of $\theta$, the dip angle in the unprocessed emulsion, for several regions of $\theta$. $\theta$ is given in terms of $\beta$ by the relation $\cot\theta = \frac{1}{2}\cot\beta$, where we have taken the shrinkage factor to be equal to 2.0.

We assume that the angle $\psi$ between the track and the distortion vector **K** and that the dip angle $\theta$ are randomly distributed in the interval 0—90°. This assumption will not be true for emulsion exposed to a beam of particles artificially produced, but for cosmic-ray work this restriction is not important. The mean value of $\omega$ averaged over the value of the angle $\psi$ is then from eq. (3.10)

$$\bar{\omega} = \frac{4}{\pi}\frac{K_2}{T^2}\tan^2\beta. \tag{3.49}$$

We take the following intervals of $\cot\theta$:

1) $5 < \cot\theta < 10$,
2) $10 < \cot\theta < 20$,
3) $20 < \cot\theta < 30$,
4) $30 < \cot\theta$.

The mean values of $\omega$ for these intervals of $\cot\theta$ are

1) $\bar{\omega}_1 = 8.31\times10^{-8}\ K_2$,
2) $\bar{\omega}_2 = 2.06\times10^{-8}\ K_2$,
3) $\bar{\omega}_3 = 6.23\times10^{-9}\ K_2$,
4) $\bar{\omega}_4 = 1.32\times10^{-9}\ K_2$,

where $K_2$ is in microns and the unprocessed emulsion thickness has been taken to be 600 $\mu$ with a shrinkage factor of 2.0. For a well-developed plate of unprocessed thickness 600 $\mu$ the order of magnitude of $K_2$ is 20 $\mu$. We have adopted this value of $K_2$ in the following.

In practice, when a track is measured, the value of the cell length $s$ is adjusted so that the observed mean $r^{\text{th}}$ difference $|\overline{D_0}|$, or the observed standard deviation $\sigma_0$, is equal to four times the contribution due to noise. This adjustment can be made, for example, by a trial measurement with a cell length, say of 100 $\mu$ and then obtaining $|\overline{D_0}|$ for values of $s$ which are multiples of 100 $\mu$. The cell length finally adopted will be such that

$$\sigma_0^2 = \sigma_s^2 + \sigma_\varepsilon^2 + \omega^2 s^4 = 16\sigma_\varepsilon^2. \tag{3.50}$$

To evaluate theoretically the cell length that would be obtained by the above procedure in the case of a track with a definite, although unknown, value of $pv$ we calculate $\sigma_0^2$ for a given value of $\sigma_\varepsilon^2$ and $\omega$ and plot it as a function of $s$ for several values of $pv$. The value of $s$ for which $\sigma_0^2 = 16\,\sigma_\varepsilon^2$ is then obtained graphically. Table 2 gives a typical set of values of $s$ as a function of $pv$ for very flat tracks ($\cot\theta > 30$). We have used eq. (6.4) of I and the scattering constant of Gottstein *et al.* [12]) to determine $\sigma_s$. $\sigma_\varepsilon$ is taken to be 0.2 $\mu$.

TABLE 2

| $pv$ (GeV) | 1 | 5 | 10 | 50 | 100 |
|---|---|---|---|---|---|
| Cell length (microns) | 560 | 1600 | 2500 | 5000 | 5000 |

$pv^*$, the estimate of $pv$, can now be obtained from eq. (3.32) together with eq. (6.4) of I in the form

$$\frac{1}{(pv^*)^2} = \frac{1}{(pv)^2} + \frac{20}{11}\,\frac{2}{\pi}\,\frac{\omega^2 s}{K^2} \tag{3.51}$$

where $K$ is the scattering constant. Substituting the values of $\omega$ and $s$ into eq. (3.51) and using the value of $K$ appropriate to the value of the particle velocity and of $s$ taken we can calculate $pv^*$ as a function of $pv$. The results of this calculation are given in fig. 5.

From fig. 5 we see that for tracks with $5 < \cot\theta < 10$ the limit for accurate measurement of $pv$ is $pv_{\text{lim}} \approx 1$ GeV. For tracks with $10 > \cot\theta < 20$ the limit is $pv_{\text{lim}} \approx 3$ GeV, for $20 < \cot\theta < 30$ $pv_{\text{lim}} \approx 7$ GeV and finally for very flat tracks $pv_{\text{lim}} \approx 20$ GeV. From eq. (3.51) we can find an expression for $pv_{\text{lim}}$, for a given value of $\omega$, $K$ and $s$, such that using uncorrected second differences there is a bias of $\xi$ per cent in $pv^*$ due to distortion. We have approximately

$$pv_{\text{lim}} = 1.05\,K\xi/\omega\sqrt{s}. \tag{3.52}$$

In view of this limit, which is only due to distortion, it is essential that the estimation of very high momenta is done using third or fourth differences, or alternatively, second differences are corrected by Fowler's method.

In the above we have assumed that the distortion is of second order. To check on the validity of this assumption we can use the values of the algebraic mean $\overline{D_i}$ and $\overline{D_i D_{i+4}}$ for third differences. For third-order distortion to be negligible $\overline{D_i}$ and $\overline{D_i D_{i+4}}$ should be $\lessapprox 0.09|\overline{D_3^*}|$. Similarly, if in the case of fourth differences $\overline{D_i}$ and $\overline{D_i D_{i+5}}$ are $\lessapprox 0.06\,|\overline{D_4^*}|$, then fourth-order distortion is negligible. If the distortion is of higher order than the second, the method of taking distortion into account developed above can be used to calculate the bias introduced in the estimate of $\sigma_s$ using un-

corrected third or fourth differences and also to obtain expressions for the standard error of $\sigma_s$*.

It is now known that there is another source of error in the measurement

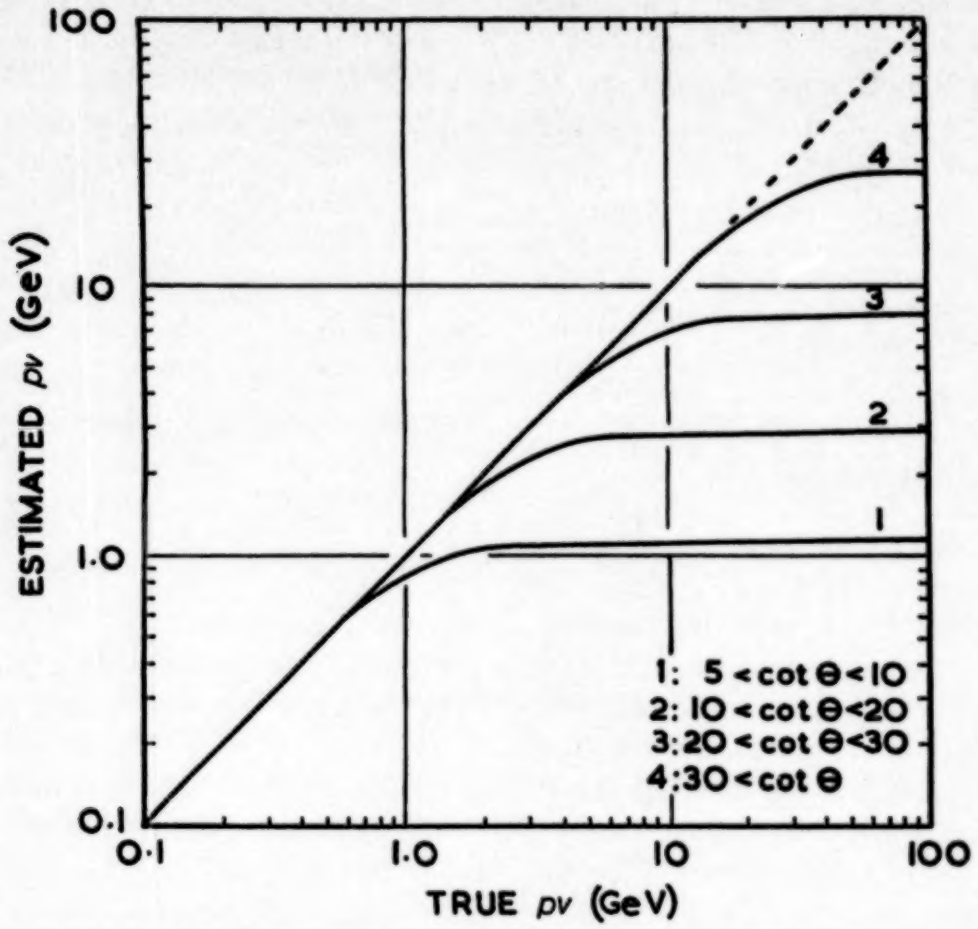


Fig. 5. Estimated $pv$ from uncorrected second differences when distortion is present ($K_s = 20\,\mu$) as a function of the true value of $pv$ for several regions of track dip. $\theta$ is the dip angle in the unprocessed emulsion.

of very high momenta, namely spurious scattering, which we have neglected in the preceding discussion [7, 17, 18, 19, 20]). Spurious scattering arises from small-scale dislocations of the emulsion which occur in regions whose extent is comparable to the cell length used. The direction in which the track is displaced due to spurious scattering remains constant over large distances but the magnitude of the displacement changes irregularly along the track. Emulsion distortion, on the other hand, is caused by a regular displacement of the track over a region large compared to the cell length. The mean second difference due to distortion can be expressed as

$$\overline{D_{ss}} = a\, s^b \text{ microns}, \tag{3.53}$$

where $a$ and $b$ are approximately constant and $s$ is in microns. From the published results the value of $a$ lies between 2 and $4 \times 10^{-4}$ microns and

$b$ is approximately equal to 1. Since spurious scattering and distortion are both produced by faults of the emulsion, in the case where $\overline{D_{ss}} \approx \overline{D_d}$ the separation of the effects of distortion and spurious scattering may not be possible and distortion can be neglected in comparison to spurious scattering, particularly for very flat tracks. This can be the case in practice, since to obtain a sufficiently large number of $r^{\text{th}}$ differences using cell lengths of the order of a mm long track lengths per plate are required.

If eqs. (2.36), (2.37) and (2.38) are applied to estimate $\sigma_s$ in the presence of spurious scattering, the estimate $\sigma_s^*$ will include a contribution from spurious scattering. We can calculate the effect of spurious scattering on the estimated value of $pv$ in the same way as for the case of distortion given above. We take the case of a track 5 mm long per plate and take the quantity $a$ in eq. (3.53) to be $2.2\times10^{-4}$ $\mu$. We assume that $k_2 = 20$ Cov. To calculate the relative standard error of $\sigma_s^*$ in this case we assume that, in the first approximation, the correlation matrix $\mathbf{a}^{(ss)}$ due to spurious scattering is the same as $\mathbf{a}^{(s)}$ due to scattering, because spurious scattering is almost indistinguishable from true scattering. Further, we assume that the distribution of the $D_i$ due to spurious scattering is approximately gaussian, as is experimentally observed [19, 20]. Therefore, to calculate the relative standard error of $\sigma_s^*$, where now $\sigma_s^{*2} = \sigma_s^2 + \sigma_{ss}^2$, we can repeat the treatment given in section (2.3). The expression for $S(\sigma_s^*)/\sigma_s^*$ in this case is the same as eq. (3.48).

Fig. 6 gives the estimated $pv^*$, after correction for distortion, as a function of the true value of $pv$. In the figure the dashed curves give the limits of error of $pv^*$ calculated from eq. (3.48). From fig. 6 we see that for $pv \lessapprox 5$ GeV the bias due to spurious scattering is less than 10 %.

Apostolakis *et al.* [7]) have shown that an approximate correction for spurious scattering can be made if we know the average value of $\sigma_{ss}$ for a region of the plate in which we are making measurements. The contribution of spurious scattering to the quantity $E(R_s)$, defined in section 2.2, can be expressed as $\mathrm{Tr}\,(\mathbf{b}^{(s)}\boldsymbol{\lambda}^{(ss)})$, where $\boldsymbol{\lambda}^{(ss)}$ is the moment matrix of the $r^{\text{th}}$ differences due to spurious scattering. The standard error of $R_s$ will now be

$$S(R_s) = 2\mathrm{Tr}[\mathbf{b}^{(s)}(\boldsymbol{\lambda}^{(ss)}+\boldsymbol{\lambda})\mathbf{b}^{(s)}(\boldsymbol{\lambda}^{(ss)}+\boldsymbol{\lambda})], \tag{3.54}$$

where $\boldsymbol{\lambda}$, as before, is the moment matrix for both true scattering and noise.

The correction to $E(R_s)$, arising from the presence of spurious scattering, can be written as

$$\mathrm{Tr}\,(\mathbf{b}^{(s)}\boldsymbol{\lambda}^{(ss)}) = \sigma_{ss}^2\,\mathrm{Tr}(\mathbf{b}^{(s)}\mathbf{a}^{(ss)}), \tag{3.55}$$

where $\mathbf{a}^{(ss)}$ is the matrix of correlation coefficients of the $r^{\text{th}}$ differences due to spurious scattering only. Taking $\mathbf{a}^{(s)} = \mathbf{a}^{(ss)}$, as above, we repeat the calculation of $S(\sigma_s^*)/\sigma_s^*$ as in section 2.2. Putting

$$\nu = \sigma_{ss}^2/\sigma_s^2, \tag{3.56}$$

where $\nu$ is the square of the ratio of spurious scattering to true scattering,

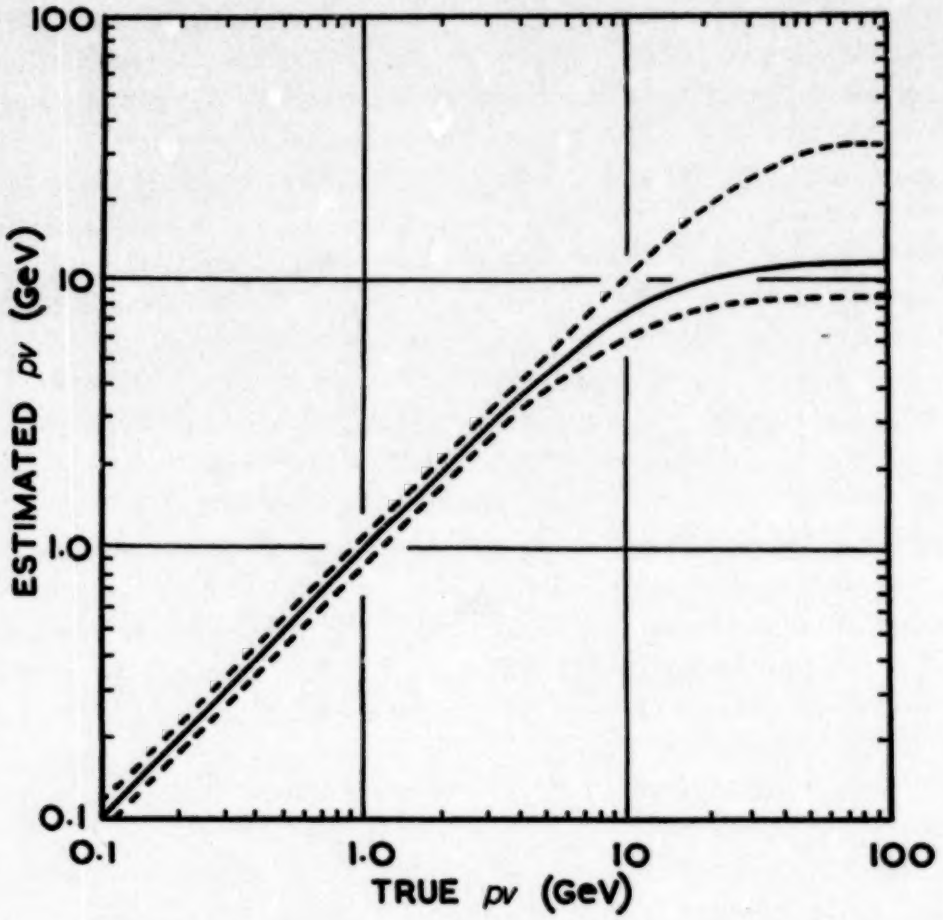


Fig. 6. The value of $pv$, corrected for distortion estimated in the presence of spurious scattering as a function of the true value of $pv$, for a track 5 mm long per plate. The value of the spurious scattering is taken from Brisbout *et al* [20]). The dashed curves give the linits of error, calculated from eq. (3.48) assuming that the magnitude of the distortion vector $h_3$ is 20 Cov.

we finally get the following expression for the standard error of $\sigma_s^*$, the estimate of $\sigma_s$ after correction for spurious scattering:

$$\frac{S(\sigma_s^*)}{\sigma_s^*} = \frac{R_c}{\sqrt{2n}} \{(1+\nu)^2 A + (1+\nu) B\, \mu_r + C\mu_r^2\}^{\frac{1}{2}}. \tag{3.57}$$

In eq. (3.57) the numerical coefficients $A$, $B$ and $C$ are the same as those in eqs. (2.36—2.38). If second-order distortion is not negligible, eq. (3.57) will also contain the term (3.47) in the case of second differences.

## 4. Summary and Conclusions

The Molière-d'Espagnat method has been extended to the estimation of true scattering in the presence of second-order distortion. The treatment

can be easily adapted to deal with third- or higher-order distortion.

The criteria that can be used to decide whether distortion is of second or higher orders are the following:

1. If $\overline{D_i}$, the algebraic mean second difference, and $\overline{D_i D_{i+3}}$, the algebraic mean of the product $D_i D_{i+3}$ of second differences, is $\lessapprox 0.13\ |\overline{D_2^*}|$, where $|\overline{D_2^*}|$ is the estimated arithmetic mean second difference due to true scattering only, then second- and higher-order distortion is negligible, i.e. the effect of distortion can be neglected altogether.

2. If for third differences $\overline{D_i}$ and $\overline{D_i D_{i+4}} \lessapprox 0.09\ |\overline{D_3^*}|$, then third-and higher-order distortion is negligible.

The equations giving the estimate $\overline{D_r^*}$ and $\varepsilon_r$, the arithmetic mean noise, for $r^{\text{th}}$ differences are given below. We have assumed $E(|D_r|)=\sqrt{(2/\pi)}\sigma_s$, where $\sigma_s$ is the standard deviation of the $r^{\text{th}}$ differences due to true scattering only, so that the values of the scattering constant given in the literature [12]) can be used directly.

Third differences:

$$|\overline{D_3^*}|^2 = \frac{2}{\pi}\,\frac{12}{5}\,[\tfrac{3}{4}\overline{D_i^2}+\overline{D_i D_{i+1}}], \tag{4.1}$$

$$\varepsilon_3^{*2} = \frac{2}{\pi}\,\frac{12}{5}\,[-\tfrac{1}{3}\overline{D_i^2}-\overline{D_i D_{i+1}}]. \tag{4.2}$$

The relative standard error of $\overline{D_3^*}$ is given by:

$$S(|\overline{D_3^*}|)/|\overline{D_3^*}| = \frac{R_c}{\sqrt{2n}}\,\{2.38+1.30\,\mu_3+0.59\,\mu_3^2\}^{\frac{1}{2}}. \tag{4.3}$$

Fourth differences:

$$|\overline{D_4^*}|^2 = \frac{2}{\pi}\,\frac{80}{19}\,[\tfrac{8}{10}\overline{D_i^2}+\overline{D_i D_{i+1}}], \tag{4.4}$$

$$\varepsilon_4^{*2} = \frac{2}{\pi}\,\frac{80}{19}\,[-\tfrac{9}{16}\overline{D_i^2}-\overline{D_i D_{i+1}}] \tag{4.5}$$

and the relative standard error of $|\overline{D_4^*}|$ is given by

$$S(|\overline{D_4^*}|)/|\overline{D_4^*}| = \frac{R_c}{\sqrt{2n}}\,\{3.43+2.98\,\mu_4+1.35\,\mu_4^2\}^{\frac{1}{2}}. \tag{4.6}$$

In the above equations $R_c$ is the Huybrechts correction factor [5]), $\mu_r$ the square of the noise-to-signal ratio for $r^{\text{th}}$ differences, $\overline{D_i^2} = \sum_i D_i^2/n$ and $\overline{D_i D_{i+1}} = (\sum_i D_i D_{i+1})/(n-1)$, where $n$ is the number of $r^{\text{th}}$ differences obtained. Since in practice $\sigma_c^2$ and $\sigma_s^2$ are unknown, $\mu_r$ has to be estimated from the relation

$$\mu_r = (\varepsilon_r^*/|\overline{D_r^*}|)^2. \tag{4.7}$$

True scattering can also be estimated from second differences by subtracting the algebraic mean second difference from each of the $D_i$. Alternatively, we can subtract $\overline{D_i}^2$ from $\overline{D_i^2}$ and $\overline{D_i D_{i+1}}$ and the estimation equation to be used in this case is

$$|\overline{D_2^*}|^2 = \frac{2}{\pi}\frac{12}{11}[\tfrac{2}{3}(\overline{D_i^2}-\overline{D_i}^2)+(\overline{D_i D_{i+1}}-\overline{D_i}^2)]. \tag{4.8}$$

The relative standard error of such an estimate is

$$S(|\overline{D_2^*}|)/|\overline{D_2^*}| = \frac{R_c}{\sqrt{2n}}\{2.10+0.31\,\mu_2+0.18\,\mu_2^2+9.92\,\delta^2\}^{\frac{1}{2}} \tag{4.8}$$

where $\delta$, the distortion-to-signal ratio, can be estimated from the equation

$$\delta = \frac{\pi}{2}\frac{\omega s^2}{|\overline{D_2^*}|}, \tag{4.10}$$

in which $\omega$ is the "curvature" of the track per unit length due to second-order distortion. $\omega$ can be obtained from

$$\omega = -2\frac{K_2}{T^2}\sin\psi\tan^2\beta, \tag{4.11}$$

where $K_2$ (microns) is the magnitude of the quadratic distortion vector, $T$ (microns) is the processed thickness of the emulsion, $\beta$ is approximately the dip-angle in the processed emulsion and $\psi$ is the angle shown in fig. 1.

In practice it is sometimes found that the estimate of noise obtained is imaginary. This can happen because of distortion; whenever $\sigma_\varepsilon \lessapprox \overline{D_d}$, where $\overline{D_d}$ is the algebraic mean $r^{\text{th}}$ difference due to distortion, the estimated value of $\varepsilon_r^{*2}$ will come out negative.

If $\delta \gtrapprox 0.3$, the relative standard error given by eq. (4.9) is larger than the error of $|\overline{D_r^*}|$ obtained using third or fourth differences (eq. (4.3) and (4.6)). Therefore, in this case third or fourth differences should be used in preference to correcting the second differences.

For $pv \gtrapprox 1$ GeV, where the effect of spurious scattering is important, an approximate correction can sometimes be made by subtracting the contribution of spurious scattering, if known for the region of the plate in which measurements are made, from the estimate obtained using the above equations [7]). The relative standard error of such an estimate, corrected for spurious scattering, is given by

$$\frac{S(|\overline{D^*_{\text{corr.}}}|)}{|\overline{D^*_{\text{corr.}}}|} = \frac{R_c}{\sqrt{2n}}\{(1+\nu)^2 A+(1+\nu)B\mu_r+C\mu_r^2\}^{\frac{1}{2}} \tag{4.12}$$

where the values appropriate to the order of differences used have to be taken for the numerical coefficients $A$, $B$ and $C$,

$$\nu = (|\overline{D^*_{\text{sp.sc.}}}|/|\overline{D^*_{\text{corr.}}}|)^2 \tag{4.13}$$

and

$$\mu_r = (\varepsilon_2^*/|\overline{D^*_{\text{corr.}}}|)^2. \tag{4.14}$$

If second order distortion is not negligible, eq. (4.12) will contain an additional term

$$9.92\delta^2 = 9.92\,\frac{\pi}{2}\,\omega^2 s^4/|\overline{D^*_{\text{corr.}}}|^2. \tag{4.15}$$

I wish to acknowledge the helpful discussions I have had with Dr. A. J. Herz. I should like to express my appreciation to Professor Messel for making it possible for me to work under excellent conditions. I am also indebted to the Research Committee of the University of Sydney for a Research Studentship.

## References

1) N. Solntseff, Nuclear Physics **4** (1957) 337
2) J. E. Moyal, Phil. Mag. **41** (1950) 1058
3) G. Molière, privately circulated preprint (1950); Zeits. für Naturf. **10a** (1955) 177
4) B. d'Espagnat, Comptes Rendus **232** (1951) 800; Journ. Phys. **13** (1952) 74
5) M. Huybrechts, Bul. Centre de Phys. Nuc. Univ. Lib. Brux. No. 41 (1956)
6) P. H. Fowler, Phil. Mag. **41** (1950) 169
7) A. J. Apostolakis, J. O. Clarke and J. V. Major, Nuovo Cimento **5** (1956) 337
8) H. Cramér, Mathematical Methods of Statistics (Princeton University Press, 1954)
9) E. J. G. Pitman, Proc. Camb. Phil. Soc. **32** (1936) 567
10) R. A. Fisher, Phil. Trans. Roy. Soc. A **222** (1921) 309; Proc. Camb. Phil. Soc. **22** (1925) 700; Proc. Roy. Soc. A **144** (1934) 285
11) M. Huybrechts, Nuovo Cimento Suppl. **4** (1956) 903
12) K. Gottstein, M. G. K. Menon, J. H. Mulvey, C. O'Ceallaigh and O. Rochat, Phil. Mag. **42** (1951) 708; L. Voyvodic and E. Pickup, Phys. Rev. **85** (1952) 91
13) R. H. W. Johnston, Nuovo Cimento Suppl. **4** (1956) 456
14) L. Voyvodic, Prog. in Cosmic Ray Physics **2** (1954) 217
15) A. J. Apostolakis and J. V. Major (1956) to be published
16) Committee for the Standardization of Measurements in Photographic Emulsions, Nuovo Cimento Suppl. **12** (1954) 474
17) S. Biswas, B. Peters and Rama, Proc. Ind. Acad. Sci. **41** (1951) 154
18) H. Fay, Zeits. für Naturf. **10a** (1955) 572
19) E. Lohrman and M. Teucher, Nuovo Cimento **3** (1956) 59
20) F. A. Brisbout, C. Dahanayake, A. Engler, P. H. Fowler and P. B. Jones, Nuovo Cimento **3** (1956) 1400

*Nuclear Physics* **6** (1958) 252—259; © *North-Holland Publishing Co., Amsterdam*
Not to be reproduced by photoprint or microfilm without written permission from the publisher

# EXCITED LEVELS OF $^{155}$Gd

A. BISI and L. ZAPPA
*Istituto di Fisica Sperimentale del Politecnico, Milano*

Received 12 December 1957

**Abstract:** The decay of $^{155}$Eu was investigated by means of a scintillation spectrometer, proportional counter spectrometer and coincidence technique.
A level scheme of $^{155}$Gd is proposed.

Pursuing our program of studying the low-lying levels of odd-mass rare earth nuclei, produced in radioactive decays, the levels of $^{155}$Gd were investigated.

$^{155}$Eu decays by beta emission to the levels of $^{155}$Gd with a half-life of 1.7 y. The transition energy to the ground level of $^{155}$Gd is known to be 0.248 MeV[1,2,3]). Several $\gamma$-rays accompanying the decay were reported[1,2,3]). Dubey, Mandeville and Rothman [4]) and Bohem and Hatch [5]) have proposed decay schemes, but among these schemes there is lack of agreement. Although conversion electron spectrum has been extensively investigated by various authors [1]), accurate $\gamma-\gamma$ coincidence measurements are lacking.

The Coulomb excitation with $\alpha$-particles and with protons of rotational levels of $^{155}$Gd employing enriched isotopes was observed respectively by Heydenburg and Temmer [6]) and by Bjerregaard and Meyer-Berkhout [7]). The first and the second rotational levels were found to occur at 0.060 MeV and 0.145 MeV.

The present paper reports the results of an investigation of the $\gamma$- and X-radiations from $^{155}$Eu.

The sample of $^{155}$Eu was obtained as a daughter of $^{155}$Sm ($T_{\frac{1}{2}} = 23.5$ min) by neutron irradiation of spectroscopically pure samarium oxide in the Harwell pile (BEPO). The investigation was started 4 months after the irradiation when the short-lived activity of $^{153}$Sm ($T_{\frac{1}{2}} = 1.96$ d) had practically disappeared.

The $\gamma$- and X-radiations were investigated by means of a single crystal scintillation spectrometer (NaI, Tl activated, cylindrical in shape, 1″ × 1.5″ optically coupled to a Dumont 6292 tube) and a proportional counter spectrometer [8]). $\gamma-\gamma$ and X$-\gamma$ coincidence techniques were employed both between the proportional counter and the scintillation spectrometer and between two identical scintillation spectrometers. Only the LX-rays

detected in the proportional counter and the pulses belonging to the core of the photopeak at the output of the scintillation spectrometer were

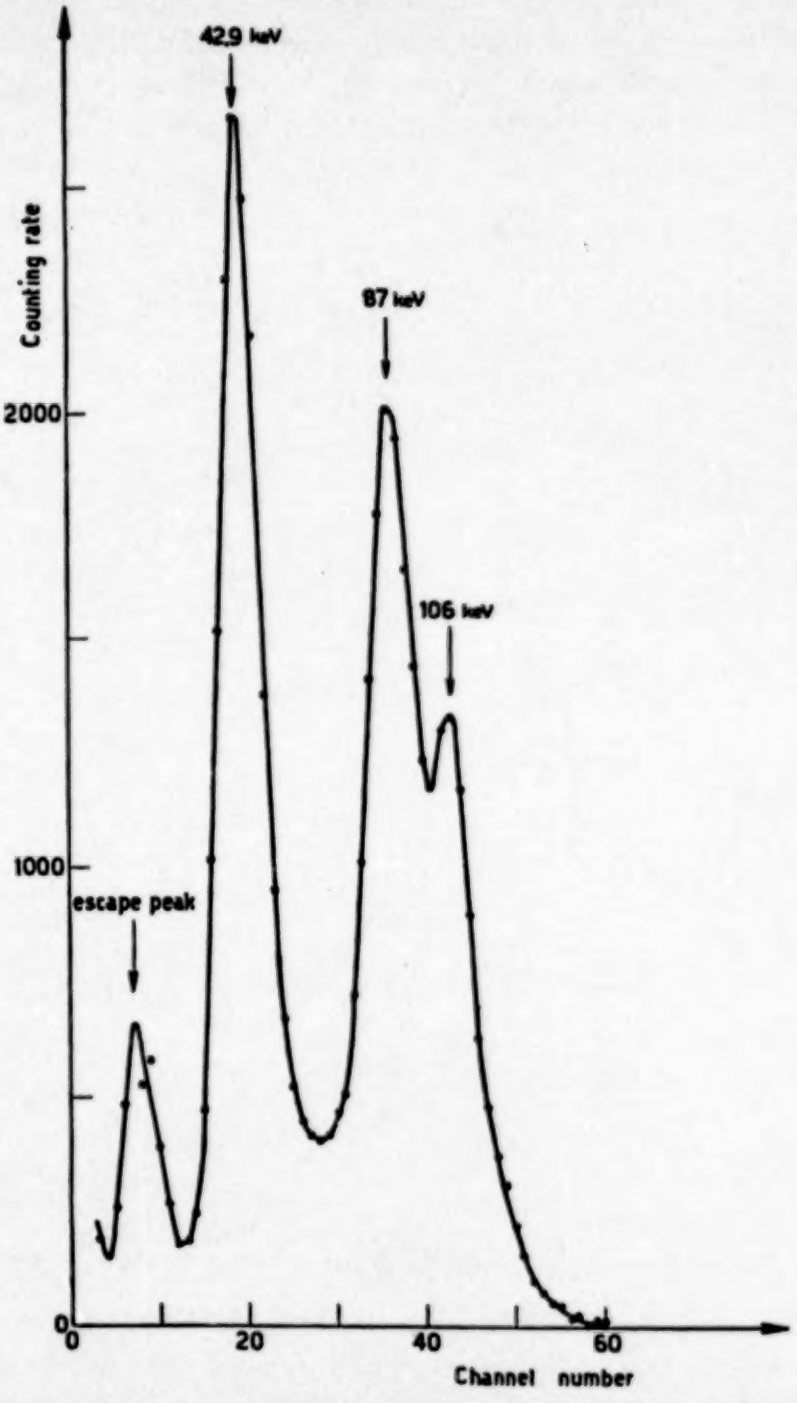


Fig. 1. $\gamma$-spectrum from $^{155}$Eu taken with the scintillation spectrometer.

used to trigger the coincidence circuit (resolving time $\approx$ 1.5 $\mu$sec). The pulse sizes were measured by means of a ten-channel electronic pulse analyzer [9]).

The $\gamma$-spectrum is shown in fig. 1. Two intense $\gamma$-rays, whose photopeaks are only partially resolved occur at 87 and 105 keV. The peak at 42.9 keV is interpreted as mainly due to KX-rays of gadolinium ($K_\alpha$ X-rays energy = 42.7 keV). Very weak peaks were found in the energy range between 0.200 and 1.2 MeV: the value of their energy suggests that they arise from the decays of the long-lived even isotopes $^{152}$Eu and $^{154}$Eu present as impurities in the sample. In the proportional counter spectrometer LX-rays and KX-

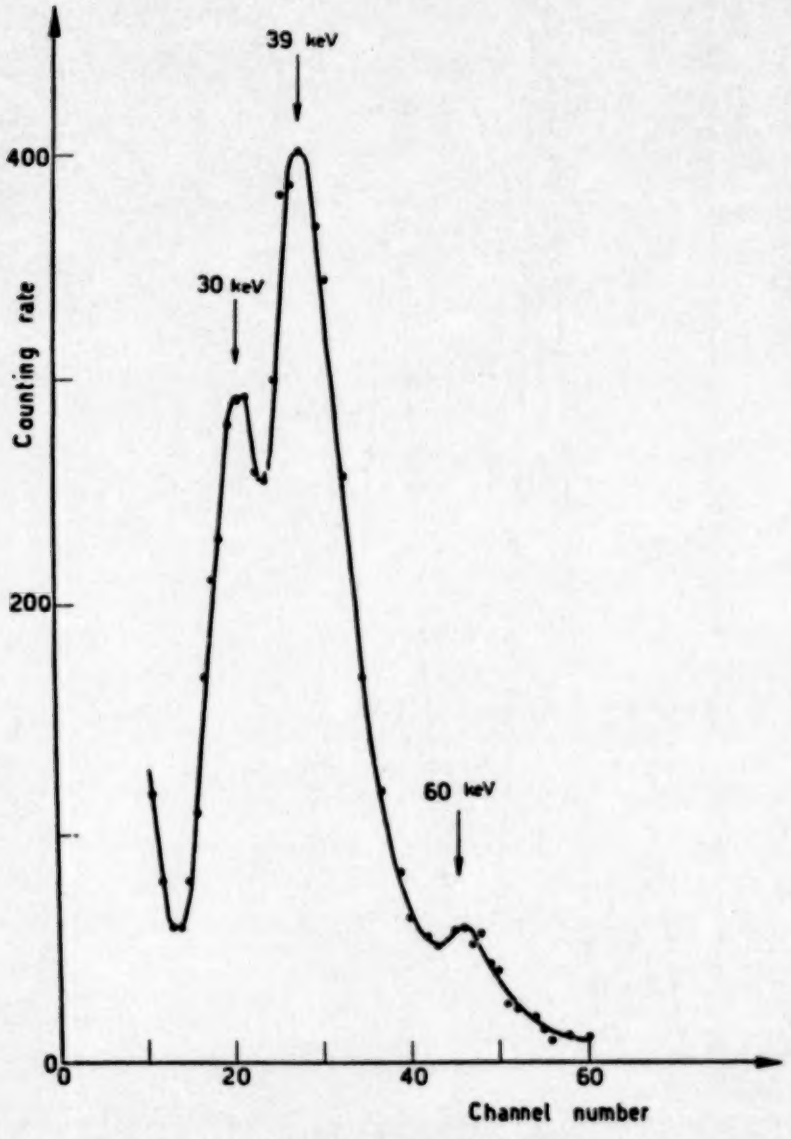


Fig. 2. Spectrum of $\gamma$-rays time-coincident with the pulses belonging to the 42.9 keV peak.

rays were easily detected; no other low-energy $\gamma$-rays were observed. In particular, the 18 keV $\gamma$-ray reported by previous authors [1, 5]), if present, occur with an intensity lower than $5 \times 10^{-3}$ relative to the KX-rays. Table 1 gives the relative intensities of the observed radiations.

TABLE 1

| Radiation energy | Intensity |
|---|---|
| 42.9 | 100 |
| 87 | 77 |
| 105 | 46 |
| LX-rays | 25 |

In the coincidence measurements, very weak $\gamma$-rays were detected at 30, 39 and 60 keV energy. The $\gamma$-spectra time coincident with the pulses belonging to the 42.9 keV, 87 keV, 105 keV and LX-rays peaks are shown respectively in fig. 2, 3, 4, 5. Table 2 summarizes the results obtained.

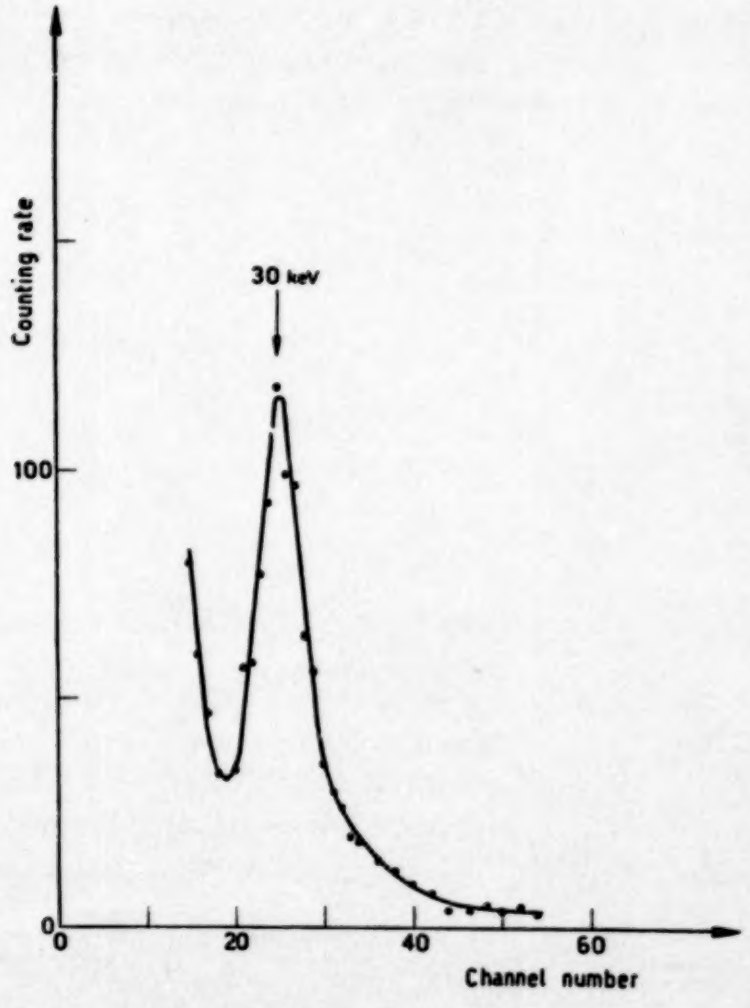


Fig. 3. Spectrum of $\gamma$-rays time-coincident with the 87 keV $\gamma$-ray.

TABLE 2

| Triggering peak (keV) | Time coincident $\gamma$-ray energy (keV) | Coincidence intensity |
|---|---|---|
| | | Intensity of triggering peak |
| 42.9 | 30 | 0.027 |
| | 39 | 0.119 |
| | 60 | very weak |
| 87 | 30 | 0.016 |
| 105 | 39 | 0.08 |
| LX-rays | 42.9 | |
| | 87 | |

The 30 and 39 keV peaks were not reported by previous authors [1]). The energy of this last peak was carefully checked by calibrating the spectrometer with known KX-rays and particularly with the KX-rays characteristic of Eu arising from the disintegration of $^{153}$Gd. Therefore it was interpreted as a $\gamma$-ray and not as KX-rays characteristic of Gd. As

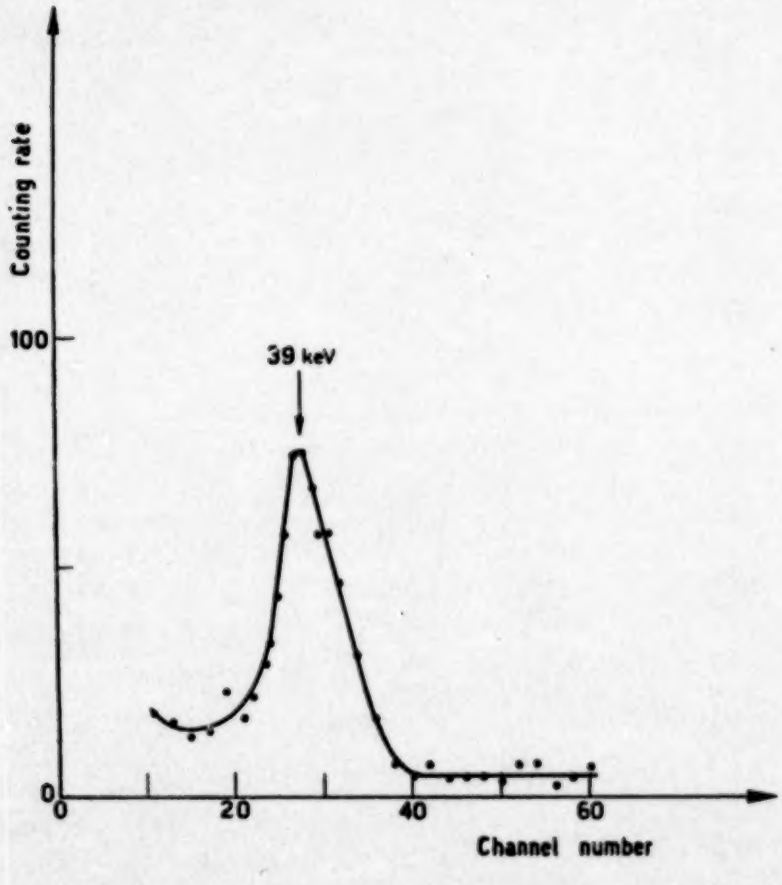


Fig. 4. Spectrum of $\gamma$-rays time-coincident with the 105 keV $\gamma$-ray.

this ray is coincident with the 105 keV $\gamma$-ray we assumed that the 39 keV—105 keV $\gamma$-cascade arised from the deexcitation of the second rotational level of $^{155}$Gd at 144 keV.

As far as concerns the coincidence spectrum triggered by the 42.9 keV peak, we can observe that to the triggering peak belong pulses due to

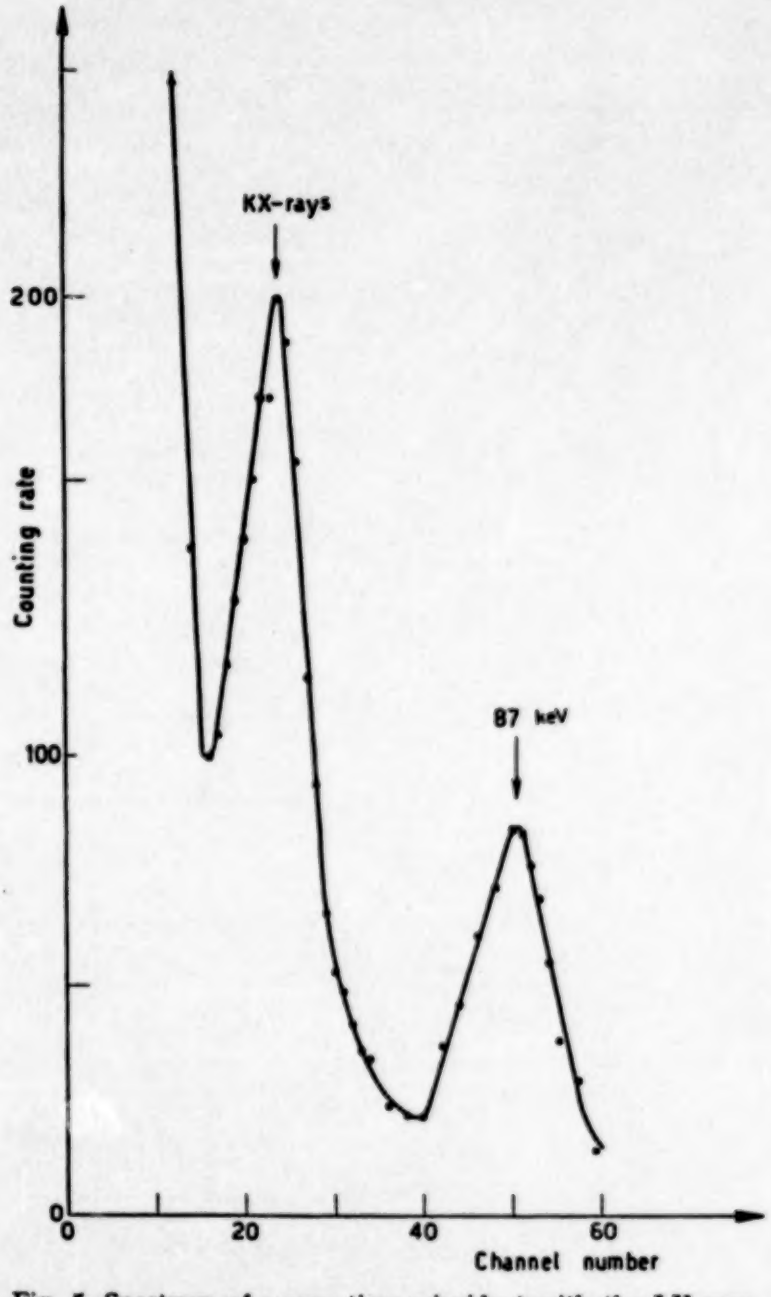


Fig. 5. Spectrum of $\gamma$-rays time-coincident with the LX-rays.

KX-rays and to weak $\gamma$-rays having about the same energy, owing to the following facts:

a) the $\gamma$-rays at 30 and 39 keV energy present in the coincidence spectrum

are triggered by KX-rays due to K-conversion of the 87 keV and 105 keV $\gamma$-rays. In effect the same $\gamma$-rays are emitted in cascade respectively with the 87 keV and 105 keV $\gamma$-rays (figs. 3 and 4).

b) the presence of the very weak $\gamma$-ray at 60 keV energy that we interprete as due to the deexcitation of the first rotational level of $^{155}$Gd can be

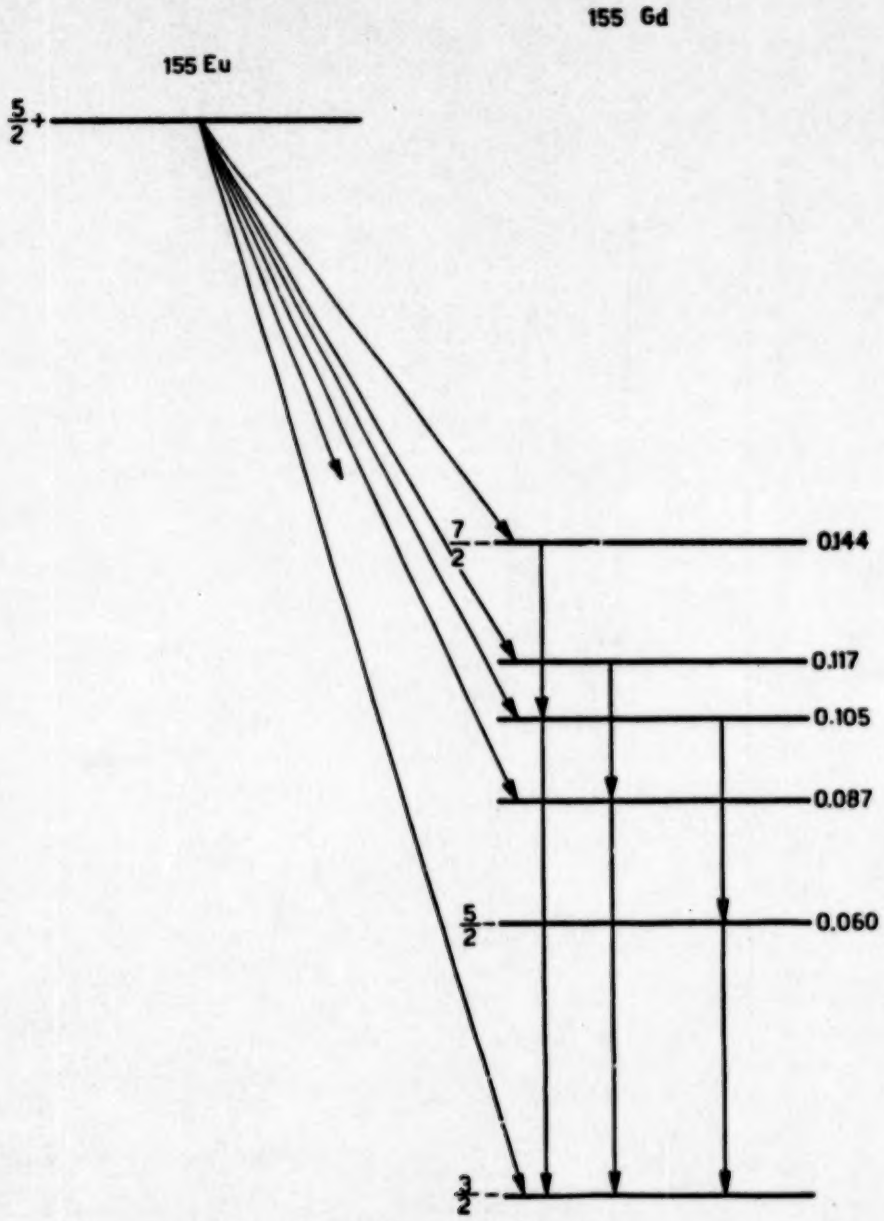


Fig. 6. Proposed level scheme of $^{155}$Gd.

accounted for by assuming the existence of a $\gamma$-ray at 45 keV from the 105 keV level or of a $\gamma$-ray from higher levels strongly converted in the K-shell and therefore having a higher energy than the critical KX-ray absorption energy of Gd (50.23 keV). As a $\gamma$-ray at 45 keV has been observed

by Bohem and Hatch [5]) we prefer the first interpretation, although the presence of other weak $\gamma$-rays cannot be excluded.

The level scheme given in fig. 6 is consequently proposed. This scheme accounts satisfactorily also for the observed radiations in coincidence with the LX-rays.

Finally if we compare the results of our measurements with those of previous authors, we observe that there is a good agreement as far as concerns the intense $\gamma$-rays; the agreement is not so close for the other weak $\gamma$-rays. Nevertheless our level scheme is nearly like that proposed by Bohem and Hatch; only two more levels were inserted by us at 117 and 144 keV, the latter having already been observed in Coulomb excitation measurements [6, 7])

Thanks are due to prof. G. Bolla for his kind interest in this work.

## References

1) D. Strominger, J. M. Hollander and G. T. Seaborg, Table of isotopes, to be published
2) Nuclear Data Cards, C. L. McGinnis editor, Washington
3) A. H. Sullivan, Trilinear chart of nuclides, USAEC 1957
4) V. S. Dubey, C. E. Mandeville and M. A. Rothman, Phys. Rev. **103** (1956) 1430
5) F. Bohem and E. N. Hatch, Bull. Am. Phys. Soc. **2** (1957) 231 W 3
6) N. P. Heydenburg and G. M. Temmer, Phys. Rev. **104** (1956) 981
7) J. H. Bjerregaard and U. Meyer-Berkhout, Z. Naturforsch. **11a** (1956) 273
8) A. Bisi, E. Germagnoli and L. Zappa, Nuovo Cimento **4** (1956) 764
9) E. Gatti, Nuovo Cimento **11** (1954) 163

*Nuclear Physics* 6 (1958) 260—270; © *North-Holland Publishing Co., Amsterdam*
Not to be reproduced by photoprint or microfilm without written permission from the publisher

# SECTIONS EFFICACES TOTALES POUR DES NEUTRONS D'ÉNERGIE VOISINE DE 14 MeV

J. F. VERVIER† et A. MARTEGANI
*Centre de Physique Nucléaire de l'Université de Louvain*

Reçu le 9 décembre 1957

**Abstract:** The total cross section of C, Mg, Al, Fe, Cu, Pb and U has been measured for neutron energies near 14 MeV by transmission experiments with good geometry. The agreement with previous measurements is satisfactory; the general form of total cross section curves is the same for elements with neighbouring $A$-values; giant resonances have been found for C, Mg and Al. The "strong coupling model" is not valid in this energy region, but the results agree qualitatively with the "intermediate coupling model".

## 1. Introduction

Le „modèle du couplage fort" ou „théorie continue" de Feshbach et Weisskopf [1, 2]) prédit que la moyenne sur les résonances de la section efficace totale pour neutrons rapides $\sigma$ diminue lorsque l'énergie $E_n$ des neutrons augmente et que la forme générale des courbes $\sigma(E_n)$ est la même pour tous les noyaux; cette conclusion est en désaccord avec les résultats expérimentaux [3, 4]). L'existence de résonances géantes dans les courbes $\sigma(E_n)$ a amené Feshbach, Porter et Weisskopf [5]) à développer le „modèle du couplage intermédiaire" ou „modèle optique", dans lequel l'interaction entre le neutron et le noyau est représentée par un potentiel complexe $V = -V_0(1+i\zeta)$. Jusqu'à présent, cette théorie a surtout été appliquée avec succès à des neutrons d'énergie inférieure à environ 10 MeV, elle permet de prévoir la forme générale des courbes $\sigma(E_n)$ ainsi que la distribution angulaire des neutrons diffusés élastiquement. Diverses expériences, notamment sur le carbone [6, 14]), l'argent et le plomb [7]) et d'autres éléments [3, 4]) montrent qu'aux environs de 14 MeV la section efficace totale de certains noyaux augmente avec l'énergie, ou atteint un maximum, ce qui semble indiquer l'existence de résonances géantes dans cette région d'énergie et même au delà: le „modèle du couplage fort" ne serait donc pas valable non plus aux environs de 14 MeV.

Pour confirmer ces résultats, nous avons mesuré la section efficace totale de quelques éléments pour des neutrons d'énergie voisine de 14 MeV. Dans cette région, la distance entre les niveaux d'énergie du noyau composé est

† Boursier du S.E.E.N.

du même ordre de grandeur que leur largeur, et les résonances sont indiscernables; la résolution en énergie de notre expérience est d'ailleurs trop faible pour pouvoir les séparer si cela était possible. Nos résultats ne nous donnent donc que la moyenne sur les résonances de la section efficace totale: le sens général de sa variation donne des indications sur l'existence de résonances géantes dans cette région d'énergie. Des résultats préliminaires ont déjà été publiés [14]).

## 2. Description de l'Appareillage

### 2.1. SOURCE DE NEUTRONS

Comme source de neutrons, nous utilisons la réaction $T^3(d, n) He^4$. La cible est une plaquette T—Zr ou T—Ti de 2.5 cm de diamètre, fournie par l'A.E.R.E. Les deutérons sont accélérés à 400 keV par la machine de Van de Graaf du Centre de Physique Nucléaire de Louvain; comme le faisceau n'est pas analysé et que la cible est épaisse, l'énergie $E_D$ des deutérons qui réagissent est comprise entre 0 et 400 keV. L'intensité du faisceau est de l'ordre de 100 $\mu$A.

Une table de l'énergie $E_n$ des neutrons émis lors de la réaction T—D, en fonction de l'angle $\theta$ entre la direction d'émission et le faisceau de deutérons, a été publiée récemment pour diverses valeurs de $E_D$ [8]). En utilisant cette table ainsi que la variation avec $E_D$ de la section efficace totale pour la réaction T—D [8]), nous avons calculé le spectre d'énergie des neutrons émis dans une direction donnée dans les hypothèses suivantes:

1) L'énergie $E_D$ des deutérons qui réagissent est répartie uniformément entre 0 et 400 keV; cette hypothèse est la plus simple en l'absence d'indications précises sur la répartition de tritium dans la cible, sur le spectre d'énergie des deutérons incidents et sur leur ralentissement dans le zirconium ou le titane de la cible.

2) Le nombre de neutrons émis dans une direction donnée est proportionnel à la section efficace totale pour la réaction T—D, le facteur de proportionnalité étant indépendant de $E_D$; ceci suppose que la distribution angulaire des neutrons émis lors de la réaction T—D ne change pas de forme si $E_D$ varie, ce qui est approximativement réalisé pour $E_D \leqq 400$ keV [8]).

3) La direction des deutérons reste à peu près constante, c'est à dire qu'ils subissent peu de déviation au cours de leur ralentissement dans la cible T—Zr ou T—Ti. On peut tenir compte de ces diffusions [9]) mais les calculs sont compliqués, et la forme du spectre diffère peu de celle que l'on obtient en utilisant la présente hypothèse.

La détermination du spectre d'énergie des neutrons émis dans une direction donnée nous a permis de calculer leur énergie moyenne et leur dispersion. Les résultats sont repris à la table 1: pour des angles multiples

TABLE 1

Énergie $E_n$ des neutrons émis dans une direction $\theta$ par rapport au faisceau de deutérons dans la réaction T–D.

| $\theta$(°) | 0 | 5 | 10 | 15 | 20 | 25 | 30 | 35 | 40 | 45 | 50 |
|---|---|---|---|---|---|---|---|---|---|---|---|
| $E_n$ (MeV) | 14.84 ±0.25 | 14.84 ±0.25 | 14.83 ±0.25 | 14.81 ±0.25 | 14.78 ±0.24 | 14.76 ±0.23 | 14.73 ±0.22 | 14.70 ±0.21 | 14.65 ±0.20 | 14.61 ±0.19 | 14.56 ±0.17 |

| $\theta$(°) | 55 | 60 | 65 | 70 | 75 | 80 | 85 | 90 | 95 | 100 | 105 |
|---|---|---|---|---|---|---|---|---|---|---|---|
| $E_n$ (MeV) | 14.50 ±0.16 | 14.45 ±0.14 | 14.39 ±0.13 | 14.33 ±0.11 | 14.27 ±0.09 | 14.20 ±0.07 | 14.14 ±0.05 | 14.08 ±0.04 | 14.01 ±0.02 | 13.95 ±0.01 | 13.89 ±0.02 |

| $\theta$(°) | 110 | 115 | 120 | 125 | 130 | 135 | 140 | 145 | 150 | 155 | 160 |
|---|---|---|---|---|---|---|---|---|---|---|---|
| $E_n$ (MeV) | 13.82 ±0.05 | 13.77 ±0.06 | 13.70 ±0.08 | 13.66 ±0.09 | 13.60 ±0.10 | 13.55 ±0.11 | 13.52 ±0.12 | 13.48 ±0.13 | 13.45 ±0.14 | 13.42 ±0.15 | 13.40 ±0.16 |

Les calculs sont effectués conformément aux hypothèses énoncées au § 2.1.

de 10°, nous avons utilisé la table 5 de la réf. [8]); les données aux angles intermédiaires sont calculées par interpolation. Pour obtenir des neutrons de diverses énergies aux environs de 14 MeV sans changer la tension de l'accélérateur, il suffit de placer le compteur à neutrons à différents angles par rapport au faisceau de deutérons.

### 2.2. DÉTECTEUR ET MONITEUR DE NEUTRONS

Le détecteur de neutrons est, soit un scintillateur liquide, soit un scintillateur plastique. Le scintillateur liquide est composé d'un xylène, de p-terphényl (5g/l) et de diphénylhexatriène (10 mg/l); il est contenu dans un récipient en lucite (fig. 1). Le scintillateur plastique, du type NE 101 †,

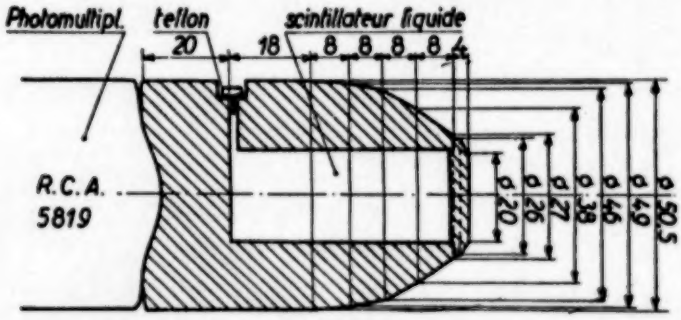


Fig. 1. Récipient en lucite du scintillateur liquide utilisé comme détecteur de neutrons.

a la forme d'un cylindre de 2 cm de diamètre et 5 cm de long, entouré d'un réflecteur en aluminium et monté directement sur le photomultiplicateur; le couplage optique entre le récipient en lucite du scintillateur liquide ou

† Fourni par Nuclear Enterprise Ltd, Bankhead Medway, Sighthill, Edinburgh 11.

le scintillateur plastique et le photomultiplicateur est assuré par de la graisse au silicone Si 200.

Le photomultiplicateur, type RCA 5819, est entouré d'une protection magnétique en $\mu$-métal. Le scintillateur et son phototube sont protégés de la lumière par un capuchon en aluminium maintenu par des ressorts. Les impulsions sortant du photomultiplicateur passent par un préamplificateur "cathode follower", un amplificateur linéaire avec discriminateur et un scaler. Le moniteur de neutrons est un long-compteur du type Hanson-McKibben [10]); il est placé à 90° par rapport au faisceau de deutérons, à 1.20 m de la cible.

### 2.3. SUPPORT DU DÉTECTEUR ET DES ÉCHANTILLONS

Le support du détecteur et des échantillons permet de changer l'angle entre la direction des neutrons détectés et le faisceau de deutérons; on aligne la source de neutrons, l'échantillon et le détecteur par une méthode optique. Le détecteur se trouve à 60 cm de la cible, et les échantillons à mi-distance. Le diamètre des échantillons est de 2.5 cm; leur épaisseur est choisie pour obtenir une transmission de 50 % environ.

## 3. Méthode Expérimentale

Les sections efficaces totales $\sigma$ sont mesurées par une méthode de transmission: on détermine le taux de comptage sans échantillon ($I_0$), avec échantillon ($I_E$) et avec une barre en cuivre de 2.5 cm de diamètre et 40 cm de long, ce qui donne le bruit de fond des neutrons diffusés par les murs du laboratoire ($I_{BG}$).

Le seuil du discriminateur qui suit l'amplificateur linéaire du détecteur de neutrons a été choisi pour éliminer du comptage les $\gamma$ et les neutrons parasites, ainsi d'ailleurs que les impulsions provenant de l'interaction des neutrons de 14 MeV avec le récipient en lucite du scintillateur liquide (fig. 1).

Pour déterminer approximativement cette valeur du seuil, nous avons mesuré la variation, avec le seuil du discriminateur, de la section efficace totale $\sigma$ de l'aluminium pour des neutrons de 14.12 MeV. Nous avons obtenu la courbe de la fig. 2: $\sigma$ augmente avec le seuil et tend vers la valeur $\sigma = 1.75$ barn obtenue par Coon *et al.* [11]) pour des neutrons de cette énergie; la courbe atteint cette limite pour un seuil de 80 V, valeur adoptée pour les mesures ultérieures. Comme la hauteur des impulsions varie avec le temps, à longue échéance, par suite de la fatigue du phototube et des fluctuations dans l'amplification, nous avons repris plusieurs fois, au cours de nos mesures, cette détermination de la valeur du seuil à adopter; nous avons toujours obtenu des courbes du même genre que celle de la fig. 2.

Pour éliminer l'influence sur les résultats de fluctuations possibles dans

le détecteur de neutrons, nous avons pour chaque angle $\theta$, donc chaque énergie de neutrons, réalisé une série de 20 mesures alternées de $I_0$ et $I_E$, normalisées chacune à un comptage de 10 000 au moniteur; le flux de

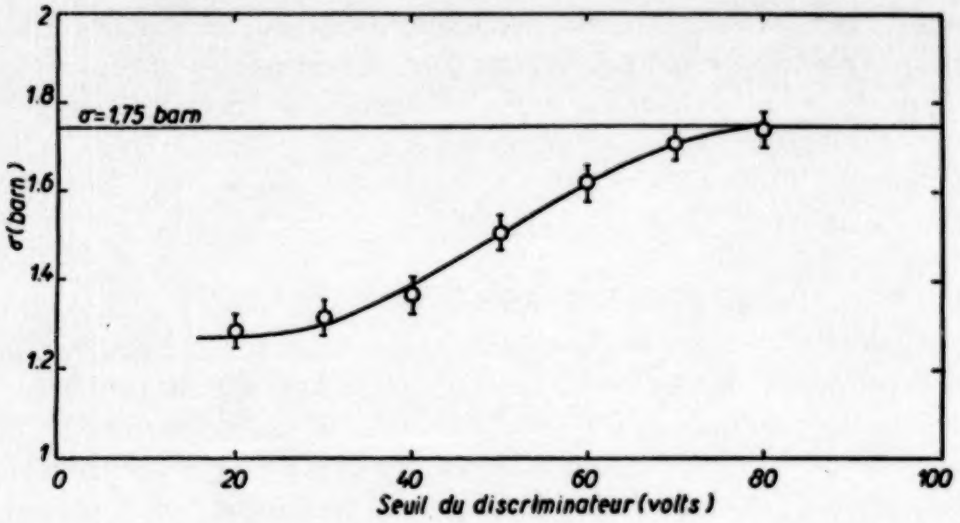


Fig. 2. Variation, avec le seuil du discriminateur, de la section efficace totale de l'aluminium pour des neutrons de 14.12 MeV.

neutrons est maintenu aussi constant que possible. Avec la valeur adoptée pour le seuil du discriminateur, le bruit de fond $I_{BG}$ est de l'ordre de 2 % de $I_0$. La précision statistique des résultats est d'environ 2 à 5 %. Certaines mesures ont été reprises plusieurs fois, à des mois d'intervalle et avec des détecteurs de neutrons différents: les résultats concordent aux erreurs statistiques près.

Les corrections de diffusion ont été calculées suivant une méthode exposée d'autre part [12]): elles sont inférieures aux erreurs statistiques, à cause de la bonne géométrie de notre expérience, et n'ont pas été appliquées. Nous avons d'ailleurs mesuré la section efficace totale de l'aluminium pour des neutrons de 14.12 MeV avec des échantillons de 2.5 cm et 4 cm de diamètre, présentant donc au faisceau de neutrons des surfaces différentes: nous avons obtenu le même résultat à la précision statistique près; cela confirme le fait que les corrections de diffusion sont effectivement négligeables[12])

## 4. Résultats Expérimentaux

Les résultats obtenus sont repris à la table 2 et aux figs. 3 à 9; la signification des symboles utilisés est donnée à la fig. 3. Les épaisseurs des échantillons de C, Mg, Al, Fe, Cu, Pb et U sont respectivement de 5, 9, 6, 3, 3, 4 et 2.5 cm; dans le cas de Al, Fe, Cu et Pb, ils sont extraits de blocs métalliques courants. Le Mg est pur à 99 %; les échantillons de C et U proviennent de

TABLE 2

Sections efficaces totales (en barns) pour des neutrons d'énergie voisine de 14 MeV

| $\theta$(°) | 130 | 125 | 120 | 115 | 110 | 105 | 100 | 95 | 90 | 85 | 80 |
|---|---|---|---|---|---|---|---|---|---|---|---|
| $E_n$ (MeV) | 13.60 | 13.66 | 13.70 | 13.77 | 13.82 | 13.89 | 13.95 | 14.01 | 14.08 | 14.14 | 14.20 |
| C | – | – | – | 1.32 ±0.06 | 1.32 ±0.06 | 1.30 ±0.06 | 1.28 ±0.05 | 1.32 ±0.05 | 1.28 ±0.05 | 1.30 ±0.06 | 1.37 ±0.06 |
| Mg | – | – | – | 1.65 ±0.04 | 1.70 ±0.04 | 1.74 ±0.04 | 1.72 ±0.04 | 1.78 ±0.04 | 1.76 ±0.04 | 1.78 ±0.04 | 1.83 ±0.04 |
| Al | – | – | 1.75 ±0.04 | 1.76 ±0.04 | 1.70 ±0.04 | 1.78 ±0.04 | 1.79 ±0.04 | 1.73 ±0.04 | 1.81 ±0.04 | 1.78 ±0.04 | 1.81 ±0.04 |
| Fe | – | – | – | 2.52 ±0.06 | 2.59 ±0.06 | 2.59 ±0.06 | 2.61 ±0.06 | 2.52 ±0.06 | 2.52 ±0.05 | 2.52 ±0.05 | 2.45 ±0.05 |
| Cu | – | – | 2.96 ±0.06 | 2.92 ±0.06 | 2.94 ±0.06 | 2.94 ±0.06 | 2.88 ±0.06 | 2.90 ±0.06 | 2.90 ±0.06 | 2.84 ±0.06 | 2.87 ±0.06 |
| Pb | – | – | – | 5.33 ±0.11 | 5.40 ±0.11 | 5.48 ±0.10 | 5.33 ±0.10 | 5.55 ±0.10 | 5.49 ±0.10 | 5.47 ±0.10 | 5.53 ±0.10 |
| U | 5.39 ±0.18 | 5.39 ±0.18 | 5.47 ±0.18 | 5.52 ±0.18 | 5.52 ±0.18 | 5.57 ±0.18 | 5.43 ±0.18 | 5.61 ±0.18 | 5.65 ±0.18 | 5.78 ±0.18 | 5.94 ±0.18 |

| $\theta$(°) | 75 | 70 | 65 | 60 | 55 | 50 | 45 | 40 | 35 | 30 | 25 |
|---|---|---|---|---|---|---|---|---|---|---|---|
| $E_n$ (MeV) | 14.27 | 14.33 | 14.39 | 14.45 | 14.50 | 14.56 | 14.61 | 14.65 | 14.70 | 14.73 | 14.76 |
| C | 1.32 ±0.06 | 1.31 ±0.07 | 1.34 ±0.07 | 1.39 ±0.07 | 1.35 ±0.07 | 1.41 ±0.07 | 1.47 ±0.07 | 1.48 ±0.07 | 1.47 ±0.07 | 1.50 ±0.09 | 1.44 ±0.07 |
| Mg | 1.83 ±0.04 | 1.83 ±0.04 | 1.84 ±0.04 | 1.83 ±0.04 | 1.78 ±0.04 | 1.89 ±0.04 | 1.78 ±0.03 | 1.74 ±0.03 | 1.71 ±0.03 | 1.71 ±0.03 | 1.69 ±0.03 |
| Al | 1.75 ±0.04 | 1.78 ±0.04 | 1.75 ±0.04 | 1.78 ±0.04 | 1.73 ±0.04 | 1.72 ±0.04 | 1.74 ±0.04 | 1.72 ±0.04 | 1.66 ±0.04 | 1.69 ±0.04 | 1.66 ±0.04 |
| Fe | 2.46 ±0.05 | 2.48 ±0.05 | 2.46 ±0.05 | 2.45 ±0.05 | 2.44 ±0.05 | 2.44 ±0.05 | 2.53 ±0.06 | 2.43 ±0.06 | 2.44 ±0.06 | 2.46 ±0.06 | 2.50 ±0.06 |
| Cu | 2.98 ±0.06 | 2.90 ±0.06 | 2.92 ±0.06 | 2.84 ±0.06 | 2.79 ±0.06 | 2.90 ±0.06 | 2.77 ±0.08 | 2.84 ±0.08 | 2.79 ±0.08 | 2.75 ±0.08 | 2.74 ±0.08 |
| Pb | 5.54 ±0.10 | 5.51 ±0.10 | 5.43 ±0.10 | 5.49 ±0.10 | 5.51 ±0.10 | 5.49 ±0.11 | 5.47 ±0.11 | 5.55 ±0.11 | 5.35 ±0.14 | 5.40 ±0.14 | 5.55 ±0.16 |
| U | 5.90 ±0.18 | 5.73 ±0.18 | 5.90 ±0.18 | 5.73 ±0.18 | 5.71 ±0.18 | 5.71 ±0.16 | 5.57 ±0.17 | 5.69 ±0.15 | 5.70 ±0.17 | 5.75 ±0.16 | 5.65 ±0.16 |

blocs de graphite et de barres d'uranium utilisés pour le réacteur BRI de Mol (Belgique) et sont donc très purs. Les figs. 3 à 9 montrent que nos résultats sont en bon accord avec ceux d'autres expérimentateurs; les formes générales des variations de la section efficace totale avec l'énergie, aux environs de 14 MeV, se raccordent de façon très satisfaisante aux courbes $\sigma(E_n)$ obtenues par Nereson et Darden [3]) en dessous de 13.2 MeV.

4.1. CARBONE (fig. 3)

Comme la densité du graphite varie d'un échantillon à l'autre et n'est pas constante à l'intérieur même d'un échantillon, nous avons normalisé

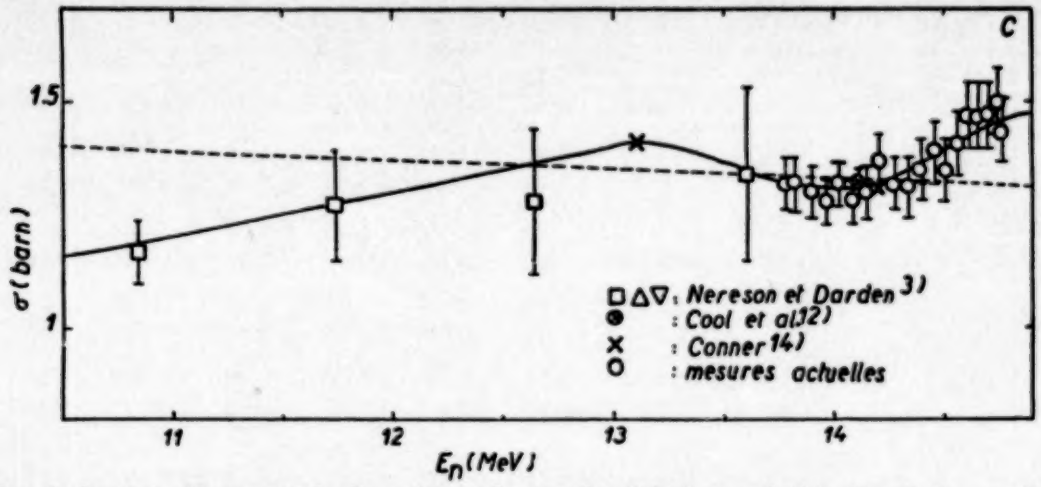


Fig. 3. Section efficace totale du carbone. La courbe théorique calculée d'après le „modèle du couplage fort" [1, 2]) est en trait interrompu.

nos résultats de telle sorte que la section efficace à 14.08 MeV soit 1.28 barn, valeur qui a été mesurée avec grande précision par Poss *et al.* [9]). La section efficace totale du carbone entre 13.1 et 15.6 MeV a été déterminée récemment par Conner [13]) en utilisant une méthode semblable à la nôtre: partant de 1.41 barn à 13.1 MeV, $\sigma$ passe par un minimum de 1.31 barn à 14.2 MeV et remonte jusque 1.49 barn à 15.6 MeV. On voit, sur la fig. 3, que nos résultats concordent avec ceux de Conner de façon très satisfaisante.

4.2. MAGNÉSIUM (fig. 4) ET ALUMINIUM (fig. 5)

La courbe de la fig. 4 indique nettement l'existence d'une résonance géante dans la section efficace totale du magnésium aux environs de 14 MeV: la décroissance de $\sigma$ au delà de 14.4 MeV a été vérifiée à plusieurs reprises et la fig. 4 donne la moyenne des divers résultats.

La section efficace totale de l'aluminium aux environs de 14 MeV présente, elle aussi, une résonance géante, moins nette cependant que pour le magné-

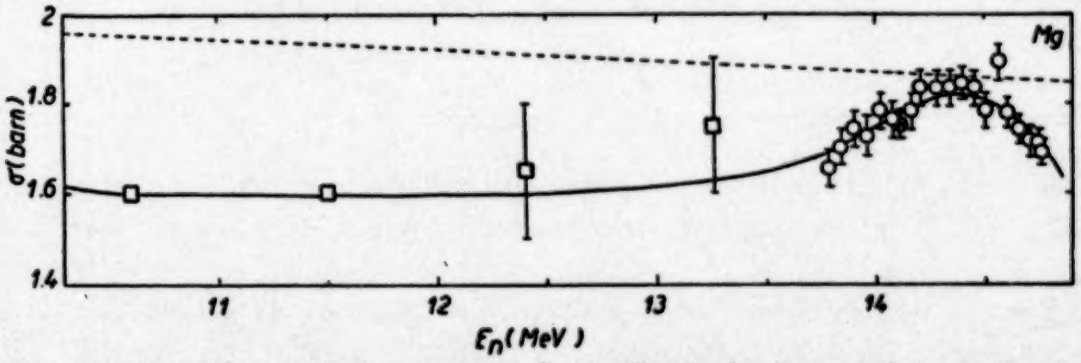


Fig. 4. Section efficace totale du magnésium. La signification des divers symboles est donnée à la fig. 3.

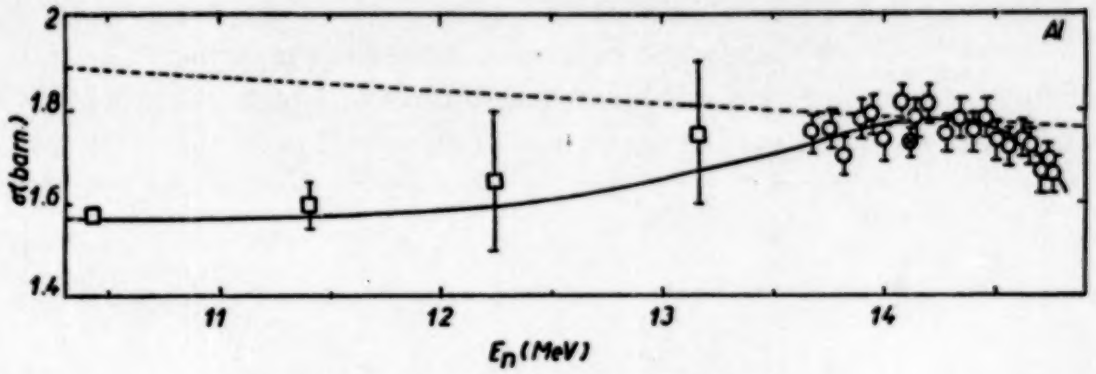


Fig. 5. Section efficace totale de l'aluminium.

sium; la décroissance de la courbe $\sigma(E_n)$ au delà de 14.4 MeV a également été vérifiée plusieurs fois.

4.3. FER (fig. 6) ET CUIVRE (fig. 7)

La section efficace totale décroît lorsque l'énergie des neutrons augmente, entre 13.7 et 14.8 MeV.

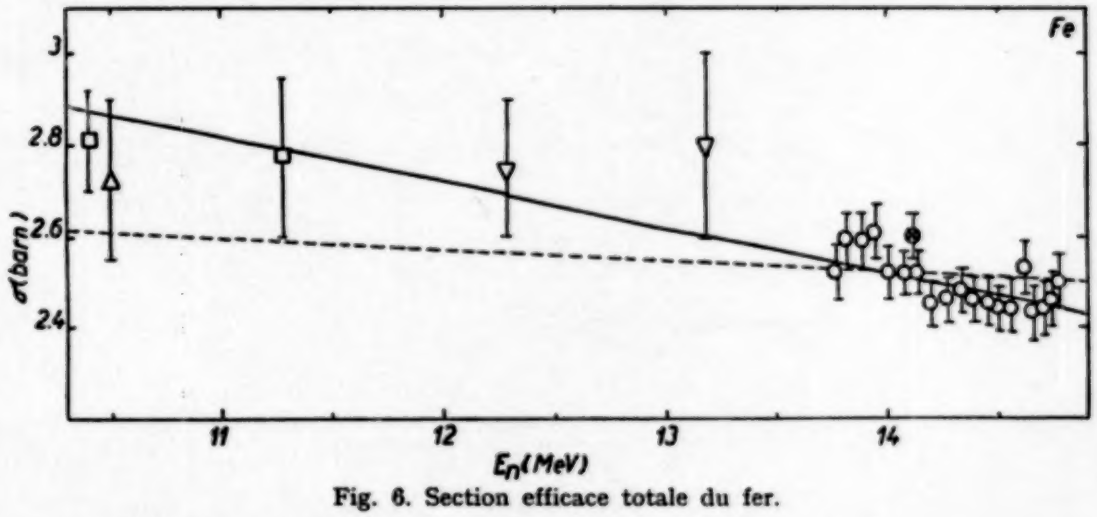


Fig. 6. Section efficace totale du fer.

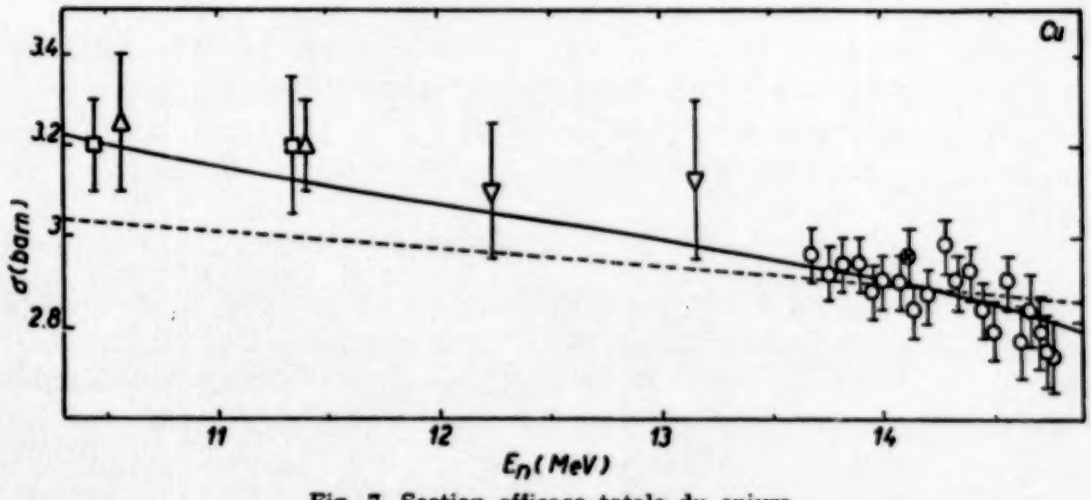


Fig. 7. Section efficace totale du cuivre.

4.4. PLOMB (fig. 8) ET URANIUM (fig. 9)

Comme l'échantillon de plomb contient une certaine proportion (2 à 5 %) d'impuretés (zinc, argent . . .) dont la nature et la quantité ne sont pas connues exactement, nous avons normalisé nos résultats de telle sorte que

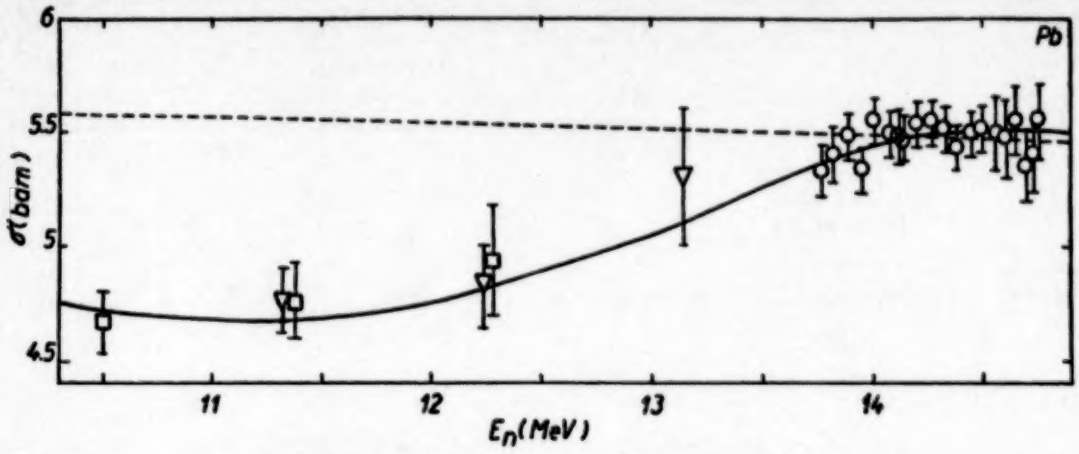


Fig. 8. Section efficace totale du plomb.

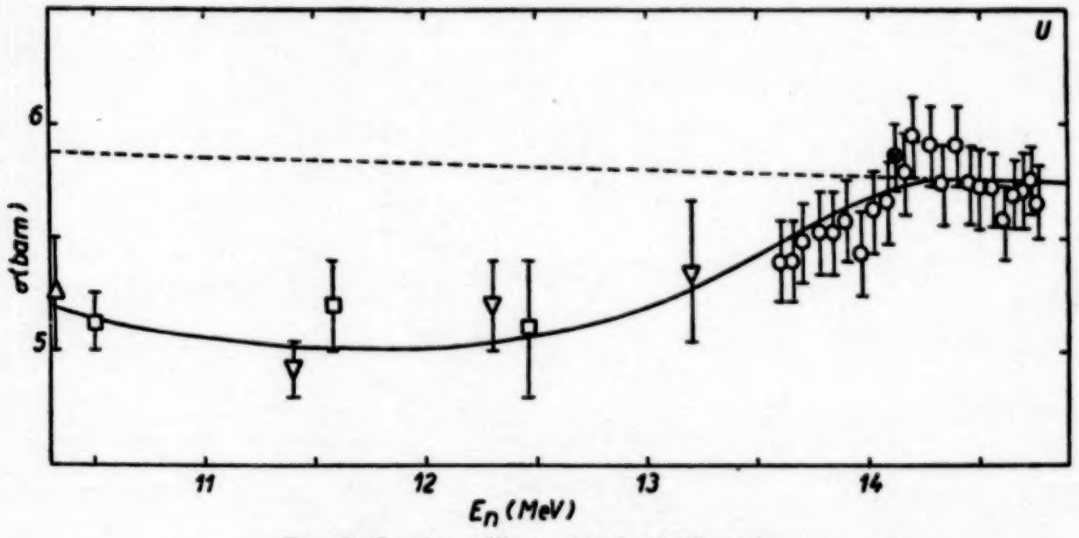


Fig. 9. Section efficace totale de l'uranium.

la section efficace à 14.12 MeV soit 5.48 barn, valeur obtenue par Coon *et al.* [11]). Les figs. 8 et 9 montrent que la section efficace du plomb et de l'uranium augmente légèrement jusque 14.1 MeV puis garde une valeur constante jusque 14.8 MeV.

## 5. Discussion

Dans les figs. 3 à 9, sont représentées, en trait interrompu, les courbes théoriques $\sigma(E_n)$ calculées d'après le „modèle du couplage fort" de Feshbach et Weisskopf [1, 2]). Le rayon $R$ du noyau qui intervient dans ce modèle n'est pas connu avec précision; aussi, seule la forme générale des courbes théoriques des figs. 3 à 9 a-t-elle un sens, et non les valeurs absolues: ces

courbes sont pratiquement des droites dont la pente est peu sensible à la valeur de $R$ et peut donc être déterminée par le modèle. On voit que nos résultats expérimentaux ne concordent pas avec les prévisions théoriques du „modèle du couplage fort", sauf peut-être pour Fe et Cu.

Nos résultats et ceux de Conner [13]) indiquent l'existence de résonances géantes dans la section efficace de C aux environs de 14 MeV; il en existe d'ailleurs d'autres dans des régions d'énergie plus élevées [4]). Les autres éléments que nous avons étudiés se répartissent en 3 classes: deux éléments légers, Mg ($A \approx 24$) et Al ($A \approx 27$), deux éléments intermédiaires, Fe($A \approx 56$) et Cu ($A \approx 63$) et deux éléments lourds, Pb($A \approx 207$) et U ($A \approx 238$). Dans chaque classe, les deux éléments ont des nombres de masse voisins et la forme générale des courbes $\sigma(E_n)$ est la même aux environs de 14 MeV; une telle similitude se retrouve d'ailleurs dans d'autres régions d'énergie [3, 4]). Pour Mg et Al, une résonance géante apparaît nettement aux environs de 14 MeV; elle est cependant moins marquée et plus étroite que celles obtenues par Nereson et Darden [3]) dans d'autres régions d'énergie et pour d'autres éléments. Les courbes expérimentales de Pb et U semblent se raccorder asymptotiquement aux courbes théoriques du „modèle du couplage fort" aux environs de 14 MeV.

D'après le „modèle du couplage intermédiaire" de Feshbach, Porter et Weisskopf [5]), la forme générale des courbes $\sigma(E_n)$ change progressivement avec le nombre de masse $A$ et doit être la même pour des noyaux de $A$ voisins; nos résultats concordent donc, sur ce point, avec les prévisions du modèle. Les courbes théoriques $\sigma(E_n)$ ont été calculées par Feshbach, Porter et Weisskopf [5]) pour diverses valeurs des paramètres du modèle, $V_0$ et $\zeta$, et pour des énergies $E_n$ (en MeV) comprises entre 0 et $x^2 = [A^{1/3} \cdot A/10\,(A+1)] \cdot E_n = 9$; sauf pour C, ces calculs ne couvrent pas la région d'énergie que nous avons étudiée, et ne peuvent donc être comparés directement avec nos résultats. On remarque cependant [5]) que la position des résonances géantes se déplace systématiquement vers les basses énergies $E_n$ si $A$ augmente; la forme générale des courbes théoriques $\sigma(E_n)$ aux environs de $x^2 = 9$, pour des noyaux dont le nombre de masse $A$ est légèrement supérieur à celui de l'élément étudié, donne donc des indications sur la courbe $\sigma(E_n)$ dans la région d'énergie où elle n'a pas été calculée.

C'est ainsi que le „modèle du couplage intermédiaire" prévoit [5]) une résonance F au delà de 10 MeV pour $A \approx 15$, donc pour C, et une résonance G, étroite et relativement peu marquée, aux environs et même au delà de 10 MeV, pour $A \approx 25$, donc pour Mg et Al; nos résultats concordent donc avec les prévisions théoriques. Celles-ci sont obtenues aussi bien pour $\zeta = 0.05$ que pour $\zeta = 0.03$ [5]) mais, dans le deuxième cas, la résonance G semble devoir être plus étroite et située à une énergie supérieure

à 10 MeV, pour $A \approx 25$, ce qui correspond mieux à nos résultats. Pour $A \approx 60$, donc pour Fe et Cu, le modèle prévoit une décroissance de la courbe $\sigma(E_n)$ aux énergies élevées, en accord avec les figs. 6 et 7. Les calculs théoriques sont trop fragmentaires pour pouvoir être comparés à nos résultats pour $A \approx 200$ à 240, c.à.d. pour Pb et U.

## 6. Conclusion

Nous avons mesuré la section efficace totale $\sigma$ de 7 éléments, C, Mg, Al, Fe, Cu, Pb et U, pour des neutrons d'énergie $E_n$ voisine de 14 MeV, par une méthode de transmission avec une bonne géométrie. Les résultats ne concordent pas avec le „modèle du couplage fort". La forme générale des courbes $\sigma(E_n)$, pour des éléments de nombres de masse $A$ voisins, est la même, conformément au „modèle du couplage intermédiaire"; celui-ci prévoit correctement la forme de ces courbes, notamment pour C, Mg et Al où de nouvelles résonances géantes ont été trouvées.

L'interaction entre un neutron de 14 MeV et un noyau n'est donc pas aussi forte qu'on le croyait jusqu'à présent: l'absorption du neutron à son entrée dans le noyau n'est pas complète et l'onde neutronique subit, en plus d'une diffraction à la surface du noyau et d'une absorption à l'intérieur, une réfraction sans formation du noyau composé [15]).

Nous remercions MM. les professeurs M. de Hemptinne et J. M. Delfosse pour leurs encouragements et leurs conseils au cours de ce travail, ainsi que Melle C. Trussart et Mr G. Deconninck pour leur aide précieuse au cours des mesures.

## Bibliographie

1) H. Feshbach et V. F. Weisskopf, Phys. Rev. **76** (1949) 1550
2) J. M. Blatt et V. F. Weisskopf, Theoretical Nuclear Physics (J. Wiley and Sons, 1952)
3) N. Nereson et S. E. Darden, Phys. Rev. **89** (1952) 775; **94** (1954) 1678
4) D. J. Hughes et J. A. Harvey, Neutron Cross Sections, BNL 325 (1955)
5) H. Feshbach, C. E. Porter et V. F. Weisskopf, Phys. Rev. **96** (1954) 448
6) C. F. Cook et T. W. Bonner, Phys. Rev. **94** (1954) 651
7) T. W. Bonner, F. Alba, A. Fernandez et M. Mazari, Phys. Rev. **97** (1955) 985
8) J. L. Fowler et J. E. Brolley, Revs. Mod. Phys. **28** (1956) 103
9) H. D. Poss, E. O. Salant, G. A. Snow et L. C. Yuan, Phys. Rev. **87** (1952) 11
10) A. O. Hanson et J. L. Mc Kibben, Phys. Rev. **72** (1947) 673
11) Coon, Graves et Barschall, Phys. Rev. **88** (1952) 562
12) J. F. Vervier, Nuclear Instruments (à paraître)
13) J. P. Conner, Bull. Am. Phys. Soc. **2** (1957) 267
14) J. F. Vervier et A. Martegani, Phys. Rev. (à paraître)
15) M. Walt et H. H. Barschall, Phys. Rev. **93** (1954) 1062

*Nuclear Physics* **6** (1958) 271—281; © *North-Holland Publishing Co., Amsterdam*
Not to be reproduced by photoprint or microfilm without written permission from the publisher

# TABLES OF AVERAGE NUMBERS FOR ELECTRON-PHOTON SHOWERS AT SMALL DEPTHS OF ABSORBER

J. C. BUTCHER, B. A. CHARTRES and H. MESSEL

*The F. B. S. Falkiner Nuclear Research and Adolph Basser Computing Laboratories, School of Physics, The University of Sydney*†

Received 25 November 1957

**Abstract:** Accurate numerical results for the average numbers of electrons and photons at small depths of absorber, in an electron-photon shower, have not hitherto been available. Results are now presented for the average numbers in approximation A, for small depths. The calculations were performed using the digital computer Silliac.

## 1. Introduction

Numerical results for the average number of electrons and photons in a shower, with energies greater than some given amount, at various depths of absorber have been given in many papers and review articles since the original work by Bhabha and Heitler [1]) on this subject appeared twenty years ago. See for instance Rossi and Greisen [2]), Rossi [3]) or Janossy and Messel [4]).

In order to make the shower equations for the average numbers tractable, approximations must be made to the actual cross-sections describing the various phenomena making up a shower. In the so-called approximation A one uses the asymptotic forms of the Bethe-Heitler cross-sections for radiation phenomena and pair production with complete screening; collision processes and Compton effect are neglected. In approximation B one includes, in addition to the processes considered in approximation A, the energy loss suffered by electrons in the production of ionisation in the absorbing medium.

Solutions of the average number equations in both approximation A and B are usually obtained (see ref. [3])) using Laplace and Mellin transform techniques and are presented in the form of a single or double complex integral. The evaluation of the integrals is by no means a straightforward task unless a number of further assumptions are made in regard to the depth of absorber and energy of the particles considered. The saddle point method (see ref. [3, 4])) is usually used for the evaluation of the integrals concerned and this method, in the case of average numbers, is thought to

† Also supported by the Nuclear Research Foundation within the University of Sydney.

be only valid when the primary energy $W_0$ of the initiating particle is substantially greater than the energy $W$ of the secondary particles under consideration. Even in this case it has been difficult hitherto to assess the accuracy of the results. In addition the use of the saddle point method does not allow one to obtain numerical results which can be treated with much confidence, for small depths of absorber. For this reason no reliable tables have appeared for the average numbers under approximation A, at small depths.

Bhabha and Heitler [1]) and Arley [5]) in their early work used a method of successive collisions and obtained results for $W_0 > W$ and for small depths. However, only super-simplified cross-sections [2]) for bremsstrahlung and pair production were used, hence the accuracy of these results has been hitherto unknown.

The advent of fast electronic digital computers has made it possible to calculate accurately the average number both at large and small depths and for all values of $W_0/W$ under approximation A. We present the numerical results of such a calculation carried out on our computer Silliac.

## 2. Formulae for the Average Numbers

Under approximation A, the average numbers of particles at a given depth and of energy greater than $W$ in a shower initiated by a single particle of energy $W_0$ may be found by performing an inverse Mellin transform. Thus,

$$Q_{i,j}(W_0, W; \zeta) = \frac{1}{2\pi i}\int_{b-i\infty}^{b+i\infty}\left(\frac{W_0}{W}\right)^{z-1}\phi_{i,j}(z,\zeta)\mathrm{d}z, \tag{1}$$

where $Q_{i,j}$ is the average number of electrons ($i = 1$) or photons ($i = 2$) at a depth $\zeta$, with energies greater than $W$, due to a primary election ($j = 1$) or photon ($j = 2$), of energy $W_0$. $\phi_{i,j}$ represents the set of four functions

$$\begin{aligned}
\phi_{1,1} &= \frac{1}{z-1}\left\{\frac{D-\lambda_1}{\lambda_2-\lambda_1}\mathrm{e}^{-\lambda_1\zeta} + \frac{D-\lambda_2}{\lambda_1-\lambda_2}\mathrm{e}^{-\lambda_2\zeta}\right\}\\
\phi_{1,2} &= \frac{1}{z-1}\left\{\frac{B}{\lambda_2-\lambda_1}\mathrm{e}^{-\lambda_1\zeta} + \frac{B}{\lambda_1-\lambda_2}\mathrm{e}^{-\lambda_2\zeta}\right\}\\
\phi_{2,1} &= \frac{1}{z-1}\left\{\frac{C}{\lambda_2-\lambda_1}\mathrm{e}^{-\lambda_1\zeta} + \frac{C}{\lambda_1-\lambda_2}\mathrm{e}^{-\lambda_2\zeta}\right\}\\
\phi_{2,2} &= \frac{1}{z-1}\left\{\frac{\lambda_2-D}{\lambda_2-\lambda_1}\mathrm{e}^{-\lambda_1\zeta} + \frac{\lambda_1-D}{\lambda_1-\lambda_2}\mathrm{e}^{-\lambda_2\zeta}\right\},
\end{aligned} \tag{2}$$

where $\lambda_1$ and $\lambda_2$ are the roots of the equation

$$\lambda^2-(A+D)\lambda+(AD-BC) = 0, \tag{3}$$

hence

$$\lambda_1 = \tfrac{1}{2}(A+D)-\tfrac{1}{2}\{(A-D)^2+4BC\}^{\frac{1}{2}}$$
$$\lambda_2 = \tfrac{1}{2}(A+D)+\tfrac{1}{2}\{(A-D)^2+4BC\}^{\frac{1}{2}}, \tag{4}$$

and $A$, $B$, $C$ and $D$ are given by

$$A = (\tfrac{4}{3}+\alpha)\{\psi(z)-\psi(1)\}+\tfrac{1}{2}-\frac{1}{z(z+1)} \text{ where } \psi(z) = \frac{\mathrm{d}}{\mathrm{d}z}\log(z!),$$
$$B = 2\left\{\frac{1}{z}-(\tfrac{4}{3}+\alpha)\frac{1}{(z+1)(z+2)}\right\}, \tag{5}$$
$$C = \frac{1}{z+1}+(\tfrac{4}{3}+\alpha)\frac{1}{z(z-1)}, \quad D = \tfrac{7}{9}-\tfrac{1}{6}\alpha;$$

$\alpha$ is a constant depending on the medium. We take its value as 0.0246 which is an average value for media of low atomic number.

The integrations (1) are to be performed along a line parallel to the imaginary axis and which cuts the real axis at the point $b$, where $b > 1$.

## 3. Evaluation of the Formulae

As mentioned in the introduction, calculations of the functions $Q_{i,s}$ have been based on the saddle point approximation, which is unsuitable in case when $\zeta$ is small.

Under certain conditions, which the functions $\phi_{i,s}$ satisfy (see appendix) the integrals in (1) may be evaluated by integration along a parabolic contour of the form

$$y^2 = 4a(b-x), \quad a > 0 \tag{6}$$

instead of along the line Re $(z) = b$. This throws the integral into a convenient form for computation which converges very quickly. It was found possible to design a Silliac subroutine to perform such integrations for any given function $\phi(z)$ satisfying the required conditions. This subroutine was used with $\phi(z) = \phi_{i,s}$ to evaluate the functions $Q_{i,s}$.

The form of the integral used in the actual computation is obtained by expressing the parabola in parametric coordinates:

$$y = 2at, \; x = b-at^2, \tag{7}$$

and observing that $Q_{i,s}$ is real. In addition we note that since

$$\phi(z) = X+iY \tag{8}$$

is real for real $z$,

$$\phi(\bar{z}) = \overline{\phi(z)} = X-iY. \tag{9}$$

Setting $(W_0/W) = \exp m$, and for convenience dropping the suffixes, we obtain the following expression for $Q$:

$$Q = \frac{1}{2\pi i}\int_{b-i\infty}^{b+i\infty} e^{m(z-1)}\phi(z)\,dz. \tag{10}$$

Writing

$$\begin{aligned} G(t) &= e^{-mat^2}\cos 2mat, \\ S(t) &= e^{-mat^2}\sin 2mat, \end{aligned} \tag{11}$$

we get

$$Q = \frac{2a\,e^{m(b-1)}}{\pi}\int_0^{\infty} [X(G-tS)-Y(S+tG)]\,dt. \tag{12}$$

Let $\delta t$ be the interval of integration and let $G_n$, $S_n$ be the values of the functions $G$, $S$ at the points $t = n\delta t$. Then if we write

$$\begin{aligned} g_n &= e^{-2mat\delta t - ma\delta t^2}\cos 2ma\delta t, \\ s_n &= e^{-2mat\delta t - ma\delta t^2}\sin 2ma\delta t, \end{aligned} \tag{13}$$

$G_n$, $S_n$, $g_n$ and $s_n$ may be generated by the formulae

$$\begin{aligned} G_{n+1} &= G_n g_n - S_n s_n, & G_0 &= 1; \\ S_{n+1} &= S_n g_n + G_n s_n, & S_0 &= 0; \\ g_{n+1} &= g_n\, e^{-2ma\delta t^2}, & g_0 &= e^{-ma\delta t^2}\cos 2ma\delta t; \\ s_{n+1} &= s_n\, e^{-2ma\delta t^2}, & s_0 &= e^{-ma\delta t^2}\sin 2ma\delta t. \end{aligned} \tag{14}$$

We have performed the calculations for $Q_{i,j}$ for various values of $\zeta$ using eqs. (10)–(14). We choose $a = 1$ and $b = 1.6$; however, other values with $b > 1$, $a > 0$ could be used with no difference in the final result. Each integral was performed with two different intervals of integration and where necessary the truncation error involved in the numerical integration was estimated and removed. In no case did this affect a result by more than one unit in the third decimal of $\log_{10} Q_{i,j}$. The numerical results may thus be taken as correct to three decimals.

In addition to performing our calculations for small values of $\zeta$ for which no previous accurate values existed, we also obtained results for $Q_{i,j}$ for a range of values of depth and energy for which numerical results had been obtained using the saddle point method [4]). This allows one to make a check upon the accuracy of the saddle point method in shower calculations.

## 4. Results

In table 1–4 we have presented the numerical results for the average number of particles with energies greater than $W$ at a depth $\zeta$ measured in radiation lengths, due to an initial primary particle of energy $W_0$. It is convenient to present the results for $\log_{10} Q_{i,j}(W_0, W_1, \zeta)$ tabulated against $\zeta$ and $\varepsilon = \log_{10}(W_0/W)$.

TABLE 1

Integral average numbers of electrons produced by an electron

$\log_{10} Q_{1,1}(W_0, W; \zeta)$

| Depth $\zeta$ (rad. lengths) | $\varepsilon = \log_{10}(W_0/W)$ | | | | | | | | | |
|---|---|---|---|---|---|---|---|---|---|---|
| | 1 | 2 | 3 | 4 | 5 | 6 | 7 | 8 | 9 | 10 |
| 0.1 | −0.001 | 0.012 | 0.022 | 0.032 | 0.041 | 0.051 | 0.060 | 0.069 | 0.078 | 0.087 |
| 0.2 | 0.004 | 0.045 | 0.080 | 0.113 | 0.144 | 0.174 | 0.202 | 0.228 | 0.254 | 0.278 |
| 0.3 | 0.013 | 0.091 | 0.159 | 0.219 | 0.274 | 0.324 | 0.371 | 0.414 | 0.454 | 0.493 |
| 0.4 | 0.024 | 0.145 | 0.246 | 0.333 | 0.409 | 0.478 | 0.540 | 0.597 | 0.650 | 0.700 |
| 0.5 | 0.035 | 0.201 | 0.334 | 0.445 | 0.541 | 0.626 | 0.701 | 0.771 | 0.834 | 0.894 |
| 0.6 | 0.052 | 0.252 | 0.423 | 0.552 | 0.667 | 0.765 | 0.853 | 0.933 | 1.007 | 1.076 |
| 0.7 | 0.058 | 0.307 | 0.504 | 0.654 | 0.784 | 0.896 | 0.995 | 1.086 | 1.169 | 1.246 |
| 0.8 | 0.064 | 0.360 | 0.581 | 0.750 | 0.895 | 1.019 | 1.130 | 1.231 | 1.323 | 1.408 |
| 0.9 | 0.068 | 0.409 | 0.653 | 0.841 | 0.999 | 1.136 | 1.258 | 1.368 | 1.469 | 1.562 |
| 1.0 | 0.072 | 0.455 | 0.721 | 0.926 | 1.098 | 1.247 | 1.379 | 1.498 | 1.608 | 1.709 |
| 1.1 | 0.074 | 0.497 | 0.784 | 1.007 | 1.192 | 1.352 | 1.495 | 1.623 | 1.741 | 1.850 |
| 1.2 | 0.075 | 0.536 | 0.844 | 1.083 | 1.282 | 1.453 | 1.606 | 1.743 | 1.869 | 1.986 |
| 1.3 | 0.074 | 0.572 | 0.901 | 1.156 | 1.367 | 1.550 | 1.712 | 1.858 | 1.993 | 2.117 |
| 1.4 | 0.072 | 0.605 | 0.954 | 1.224 | 1.449 | 1.642 | 1.814 | 1.969 | 2.111 | 2.243 |
| 1.5 | 0.069 | 0.635 | 1.004 | 1.290 | 1.527 | 1.732 | 1.913 | 2.076 | 2.226 | 2.365 |
| 1.6 | 0.064 | 0.663 | 1.052 | 1.353 | 1.602 | 1.817 | 2.008 | 2.180 | 2.337 | 2.483 |
| 1.7 | 0.058 | 0.688 | 1.097 | 1.413 | 1.674 | 1.900 | 2.100 | 2.280 | 2.445 | 2.597 |
| 1.8 | 0.052 | 0.711 | 1.140 | 1.470 | 1.744 | 1.980 | 2.189 | 2.377 | 2.549 | 2.708 |
| 1.9 | 0.041 | 0.732 | 1.180 | 1.525 | 1.811 | 2.057 | 2.275 | 2.471 | 2.651 | 2.816 |
| 2.0 | 0.030 | 0.751 | 1.218 | 1.578 | 1.875 | 2.131 | 2.358 | 2.562 | 2.749 | 2.921 |
| 2.1 | 0.017 | 0.769 | 1.254 | 1.628 | | | | | | |
| 2.2 | 0.003 | 0.785 | 1.289 | 1.676 | | | | | | |
| 2.3 | −0.012 | 0.799 | 1.321 | 1.723 | | | | | | |
| 2.4 | −0.028 | 0.812 | 1.352 | 1.768 | | | | | | |
| 2.5 | −0.044 | 0.823 | 1.381 | 1.811 | | | | | | |
| 2.6 | −0.062 | 0.833 | 1.409 | 1.852 | | | | | | |
| 2.7 | −0.080 | 0.842 | 1.435 | 1.891 | | | | | | |
| 2.8 | −0.099 | 0.850 | 1.460 | 1.930 | | | | | | |
| 2.9 | −0.118 | 0.856 | 1.484 | 1.966 | | | | | | |
| 3.0 | −0.140 | 0.861 | 1.506 | 2.002 | | | | | | |
| 3.2 | −0.184 | 0.868 | 1.547 | 2.068 | | | | | | |
| 3.4 | −0.230 | 0.871 | 1.584 | 2.130 | | | | | | |
| 3.6 | −0.278 | 0.871 | 1.616 | 2.187 | | | | | | |
| 3.8 | −0.327 | 0.868 | 1.644 | 2.240 | | | | | | |
| 4.0 | −0.378 | 0.861 | 1.669 | 2.289 | | | | | | |
| 4.2 | −0.429 | 0.852 | 1.690 | 2.334 | | | | | | |
| 4.4 | −0.482 | 0.840 | 1.709 | 2.375 | | | | | | |
| 4.6 | −0.536 | 0.826 | 1.724 | 2.414 | | | | | | |
| 4.8 | −0.589 | 0.810 | 1.736 | 2.449 | | | | | | |
| 5.0 | −0.643 | 0.791 | 1.746 | 2.481 | | | | | | |

TABLE 2

Integral average numbers of electrons produced by a photon

$\log_{10} Q_{1,2}(W_0, W; \zeta)$

| Depth $\zeta$ (rad. lengths) | $\varepsilon = \log_{10}(W_0/W)$ | | | | | | | | | |
|---|---|---|---|---|---|---|---|---|---|---|
| | 1 | 2 | 3 | 4 | 5 | 6 | 7 | 8 | 9 | 10 |
| 0.1 | −0.890 | −0.831 | −0.822 | −0.818 | −0.814 | −0.811 | −0.807 | −0.804 | −0.800 | −0.797 |
| 0.2 | −0.612 | −0.539 | −0.519 | −0.505 | −0.492 | −0.480 | −0.467 | −0.455 | −0.443 | −0.431 |
| 0.3 | −0.458 | −0.367 | −0.332 | −0.303 | −0.277 | −0.251 | −0.226 | −0.202 | −0.179 | −0.156 |
| 0.4 | −0.355 | −0.242 | −0.188 | −0.141 | −0.098 | −0.058 | −0.020 | 0.017 | 0.052 | 0.085 |
| 0.5 | −0.278 | −0.142 | −0.065 | 0.000 | 0.060 | 0.116 | 0.167 | 0.216 | 0.262 | 0.305 |
| 0.6 | −0.208 | −0.068 | 0.050 | 0.125 | 0.207 | 0.276 | 0.340 | 0.401 | 0.456 | 0.510 |
| 0.7 | −0.165 | 0.010 | 0.148 | 0.245 | 0.342 | 0.425 | 0.501 | 0.573 | 0.638 | 0.701 |
| 0.8 | −0.130 | 0.080 | 0.238 | 0.357 | 0.468 | 0.565 | 0.653 | 0.735 | 0.809 | 0.880 |
| 0.9 | −0.101 | 0.142 | 0.323 | 0.461 | 0.588 | 0.697 | 0.796 | 0.887 | 0.971 | 1.050 |
| 1.0 | −0.077 | 0.200 | 0.402 | 0.560 | 0.700 | 0.822 | 0.932 | 1.032 | 1.125 | 1.212 |
| 1.1 | −0.057 | 0.253 | 0.476 | 0.653 | 0.806 | 0.940 | 1.060 | 1.170 | 1.271 | 1.366 |
| 1.2 | −0.041 | 0.302 | 0.547 | 0.740 | 0.907 | 1.053 | 1.183 | 1.302 | 1.411 | 1.513 |
| 1.3 | −0.028 | 0.347 | 0.613 | 0.824 | 1.004 | 1.160 | 1.300 | 1.428 | 1.546 | 1.655 |
| 1.4 | −0.017 | 0.389 | 0.676 | 0.903 | 1.096 | 1.263 | 1.413 | 1.549 | 1.675 | 1.791 |
| 1.5 | −0.008 | 0.428 | 0.735 | 0.978 | 1.183 | 1.362 | 1.521 | 1.666 | 1.799 | 1.922 |
| 1.6 | −0.002 | 0.465 | 0.792 | 1.050 | 1.267 | 1.456 | 1.625 | 1.778 | 1.919 | 2.049 |
| 1.7 | 0.003 | 0.499 | 0.845 | 1.118 | 1.348 | 1.547 | 1.725 | 1.887 | 2.035 | 2.172 |
| 1.8 | 0.004 | 0.530 | 0.896 | 1.184 | 1.425 | 1.635 | 1.822 | 1.991 | 2.147 | 2.291 |
| 1.9 | 0.005 | 0.559 | 0.944 | 1.246 | 1.500 | 1.720 | 1.915 | 2.093 | 2.256 | 2.407 |
| 2.0 | 0.004 | 0.587 | 0.989 | 1.306 | 1.571 | 1.801 | 2.006 | 2.191 | 2.361 | 2.519 |
| 2.1 | 0.002 | 0.612 | 1.033 | 1.364 | | | | | | |
| 2.2 | −0.002 | 0.635 | 1.074 | 1.419 | | | | | | |
| 2.3 | −0.006 | 0.657 | 1.114 | 1.472 | | | | | | |
| 2.4 | −0.012 | 0.677 | 1.151 | 1.523 | | | | | | |
| 2.5 | −0.019 | 0.695 | 1.187 | 1.572 | | | | | | |
| 2.6 | −0.026 | 0.712 | 1.221 | 1.619 | | | | | | |
| 2.7 | −0.035 | 0.728 | 1.253 | 1.664 | | | | | | |
| 2.8 | −0.045 | 0.742 | 1.284 | 1.708 | | | | | | |
| 2.9 | −0.053 | 0.755 | 1.313 | 1.750 | | | | | | |
| 3.0 | −0.064 | 0.767 | 1.341 | 1.791 | | | | | | |
| 3.2 | −0.090 | 0.787 | 1.393 | 1.867 | | | | | | |
| 3.4 | −0.117 | 0.803 | 1.440 | 1.939 | | | | | | |
| 3.6 | −0.148 | 0.815 | 1.482 | 2.005 | | | | | | |
| 3.8 | −0.180 | 0.823 | 1.520 | 2.067 | | | | | | |
| 4.0 | −0.214 | 0.828 | 1.555 | 2.124 | | | | | | |
| 4.2 | −0.248 | 0.830 | 1.585 | 2.177 | | | | | | |
| 4.4 | −0.286 | 0.829 | 1.612 | 2.227 | | | | | | |
| 4.6 | −0.325 | 0.826 | 1.636 | 2.273 | | | | | | |
| 4.8 | −0.365 | 0.820 | 1.657 | 2.315 | | | | | | |
| 5.0 | −0.405 | 0.812 | 1.675 | 2.355 | | | | | | |

TABLE 3

Integral average numbers of photons produced by an electron

$\log_{10} Q_{2,1}(W_0, W; \zeta)$

| Depth $\zeta$ (rad. lengths) | $\varepsilon = \log_{10}(W_0/W)$ | | | | | | | | | |
|---|---|---|---|---|---|---|---|---|---|---|
| | 1 | 2 | 3 | 4 | 5 | 6 | 7 | 8 | 9 | 10 |
| 0.1 | −0.652 | −0.291 | −0.089 | 0.050 | 0.156 | 0.241 | 0.313 | 0.375 | 0.430 | 0.479 |
| 0.2 | −0.383 | −0.011 | 0.198 | 0.343 | 0.455 | 0.545 | 0.623 | 0.690 | 0.750 | 0.804 |
| 0.3 | −0.238 | 0.147 | 0.366 | 0.519 | 0.639 | 0.738 | 0.823 | 0.897 | 0.964 | 1.025 |
| 0.4 | −0.143 | 0.256 | 0.487 | 0.651 | 0.781 | 0.890 | 0.984 | 1.068 | 1.143 | 1.212 |
| 0.5 | −0.076 | 0.339 | 0.584 | 0.761 | 0.902 | 1.022 | 1.127 | 1.220 | 1.305 | 1.382 |
| 0.6 | −0.033 | 0.406 | 0.667 | 0.857 | 1.012 | 1.143 | 1.258 | 1.362 | 1.456 | 1.542 |
| 0.7 | 0.005 | 0.463 | 0.740 | 0.945 | 1.113 | 1.256 | 1.382 | 1.495 | 1.599 | 1.694 |
| 0.8 | 0.033 | 0.512 | 0.806 | 1.026 | 1.208 | 1.363 | 1.500 | 1.623 | 1.735 | 1.838 |
| 0.9 | 0.056 | 0.555 | 0.867 | 1.103 | 1.298 | 1.465 | 1.612 | 1.745 | 1.866 | 1.977 |
| 1.0 | 0.073 | 0.594 | 0.924 | 1.175 | 1.384 | 1.562 | 1.720 | 1.862 | 1.991 | 2.111 |
| 1.1 | 0.085 | 0.629 | 0.977 | 1.244 | 1.466 | 1.656 | 1.824 | 1.975 | 2.112 | 2.239 |
| 1.2 | 0.095 | 0.661 | 1.027 | 1.310 | 1.544 | 1.746 | 1.923 | 2.083 | 2.229 | 2.363 |
| 1.3 | 0.101 | 0.690 | 1.075 | 1.373 | 1.620 | 1.832 | 2.020 | 2.188 | 2.342 | 2.483 |
| 1.4 | 0.105 | 0.717 | 1.120 | 1.433 | 1.692 | 1.915 | 2.112 | 2.289 | 2.451 | 2.599 |
| 1.5 | 0.106 | 0.742 | 1.163 | 1.491 | 1.762 | 1.996 | 2.202 | 2.387 | 2.556 | 2.712 |
| 1.6 | 0.106 | 0.764 | 1.204 | 1.546 | 1.830 | 2.073 | 2.289 | 2.482 | 2.659 | 2.821 |
| 1.7 | 0.103 | 0.785 | 1.243 | 1.599 | 1.894 | 2.149 | 2.373 | 2.574 | 2.758 | 2.927 |
| 1.8 | 0.099 | 0.805 | 1.280 | 1.650 | 1.957 | 2.221 | 2.454 | 2.664 | 2.855 | 3.031 |
| 1.9 | 0.093 | 0.822 | 1.315 | 1.699 | 2.018 | 2.291 | 2.533 | 2.751 | 2.949 | 3.131 |
| 2.0 | 0.086 | 0.839 | 1.349 | 1.746 | 2.076 | 2.360 | 2.610 | 2.835 | 3.040 | 3.230 |
| 2.1 | 0.078 | 0.854 | 1.381 | 1.792 | | | | | | |
| 2.2 | 0.069 | 0.867 | 1.411 | 1.835 | | | | | | |
| 2.3 | 0.059 | 0.880 | 1.440 | 1.877 | | | | | | |
| 2.4 | 0.048 | 0.891 | 1.468 | 1.918 | | | | | | |
| 2.5 | 0.037 | 0.901 | 1.494 | 1.957 | | | | | | |
| 2.6 | 0.024 | 0.910 | 1.519 | 1.994 | | | | | | |
| 2.7 | 0.011 | 0.918 | 1.543 | 2.031 | | | | | | |
| 2.8 | −0.003 | 0.925 | 1.565 | 2.066 | | | | | | |
| 2.9 | −0.017 | 0.931 | 1.587 | 2.099 | | | | | | |
| 3.0 | −0.032 | 0.936 | 1.607 | 2.132 | | | | | | |
| 3.2 | −0.065 | 0.944 | 1.645 | 2.193 | | | | | | |
| 3.4 | −0.100 | 0.948 | 1.678 | 2.250 | | | | | | |
| 3.6 | −0.136 | 0.949 | 1.708 | 2.303 | | | | | | |
| 3.8 | −0.174 | 0.948 | 1.735 | 2.352 | | | | | | |
| 4.0 | −0.214 | 0.944 | 1.758 | 2.398 | | | | | | |
| 4.2 | −0.254 | 0.938 | 1.779 | 2.440 | | | | | | |
| 4.4 | −0.296 | 0.929 | 1.797 | 2.479 | | | | | | |
| 4.6 | −0.339 | 0.918 | 1.812 | 2.515 | | | | | | |
| 4.8 | −0.383 | 0.906 | 1.824 | 2.548 | | | | | | |
| 5.0 | −0.427 | 0.891 | 1.834 | 2.579 | | | | | | |

TABLE 4

Integral average numbers of photons produced by a photon

$\log_{10} Q_{2,2}(W_0, W; \zeta)$

| Depth $\zeta$ (rad. lengths) | $\varepsilon = \log_{10}(W_0/W)$ | | | | | | | | | |
|---|---|---|---|---|---|---|---|---|---|---|
| | 1 | 2 | 3 | 4 | 5 | 6 | 7 | 8 | 9 | 10 |
| 0.1 | −0.029 | −0.020 | −0.010 | 0.000 | 0.010 | 0.020 | 0.030 | 0.039 | 0.048 | 0.057 |
| 0.2 | −0.049 | −0.015 | 0.023 | 0.058 | 0.092 | 0.123 | 0.153 | 0.181 | 0.208 | 0.234 |
| 0.3 | −0.061 | 0.011 | 0.084 | 0.151 | 0.210 | 0.264 | 0.313 | 0.359 | 0.402 | 0.442 |
| 0.4 | −0.067 | 0.051 | 0.162 | 0.257 | 0.340 | 0.413 | 0.478 | 0.539 | 0.594 | 0.646 |
| 0.5 | −0.067 | 0.099 | 0.245 | 0.366 | 0.468 | 0.557 | 0.637 | 0.709 | 0.775 | 0.837 |
| 0.6 | −0.039 | 0.150 | 0.327 | 0.473 | 0.589 | 0.695 | 0.786 | 0.869 | 0.945 | 1.016 |
| 0.7 | −0.035 | 0.203 | 0.408 | 0.573 | 0.706 | 0.823 | 0.926 | 1.020 | 1.105 | 1.184 |
| 0.8 | −0.029 | 0.255 | 0.486 | 0.667 | 0.815 | 0.945 | 1.059 | 1.162 | 1.257 | 1.344 |
| 0.9 | −0.021 | 0.305 | 0.558 | 0.757 | 0.918 | 1.060 | 1.184 | 1.297 | 1.401 | 1.496 |
| 1.0 | −0.013 | 0.352 | 0.627 | 0.841 | 1.016 | 1.169 | 1.304 | 1.426 | 1.538 | 1.642 |
| 1.1 | −0.005 | 0.397 | 0.692 | 0.921 | 1.110 | 1.273 | 1.419 | 1.550 | 1.670 | 1.781 |
| 1.2 | 0.004 | 0.438 | 0.753 | 0.997 | 1.198 | 1.373 | 1.528 | 1.668 | 1.797 | 1.915 |
| 1.3 | 0.011 | 0.478 | 0.810 | 1.069 | 1.283 | 1.469 | 1.634 | 1.783 | 1.919 | 2.045 |
| 1.4 | 0.018 | 0.514 | 0.865 | 1.138 | 1.364 | 1.561 | 1.735 | 1.893 | 2.037 | 2.170 |
| 1.5 | 0.025 | 0.548 | 0.916 | 1.204 | 1.442 | 1.649 | 1.833 | 1.999 | 2.151 | 2.291 |
| 1.6 | 0.030 | 0.580 | 0.965 | 1.267 | 1.517 | 1.735 | 1.927 | 2.101 | 2.261 | 2.408 |
| 1.7 | 0.034 | 0.609 | 1.012 | 1.327 | 1.589 | 1.817 | 2.019 | 2.201 | 2.368 | 2.522 |
| 1.8 | 0.044 | 0.636 | 1.056 | 1.385 | 1.659 | 1.896 | 2.107 | 2.297 | 2.471 | 2.632 |
| 1.9 | 0.046 | 0.662 | 1.099 | 1.440 | 1.726 | 1.973 | 2.193 | 2.391 | 2.572 | 2.739 |
| 2.0 | 0.047 | 0.686 | 1.139 | 1.494 | 1.791 | 2.048 | 2.276 | 2.482 | 2.670 | 2.844 |
| 2.1 | 0.047 | 0.708 | 1.177 | 1.545 | | | | | | |
| 2.2 | 0.046 | 0.729 | 1.214 | 1.595 | | | | | | |
| 2.3 | 0.043 | 0.748 | 1.249 | 1.643 | | | | | | |
| 2.4 | 0.041 | 0.766 | 1.282 | 1.689 | | | | | | |
| 2.5 | 0.037 | 0.783 | 1.314 | 1.733 | | | | | | |
| 2.6 | 0.032 | 0.798 | 1.344 | 1.776 | | | | | | |
| 2.7 | 0.027 | 0.813 | 1.373 | 1.817 | | | | | | |
| 2.8 | 0.021 | 0.826 | 1.401 | 1.857 | | | | | | |
| 2.9 | 0.010 | 0.838 | 1.428 | 1.895 | | | | | | |
| 3.0 | 0.002 | 0.849 | 1.453 | 1.932 | | | | | | |
| 3.2 | −0.015 | 0.868 | 1.500 | 2.003 | | | | | | |
| 3.4 | −0.034 | 0.883 | 1.543 | 2.069 | | | | | | |
| 3.6 | −0.056 | 0.895 | 1.582 | 2.130 | | | | | | |
| 3.8 | −0.079 | 0.904 | 1.618 | 2.187 | | | | | | |
| 4.0 | −0.105 | 0.910 | 1.650 | 2.241 | | | | | | |
| 4.2 | −0.133 | 0.913 | 1.679 | 2.291 | | | | | | |
| 4.4 | −0.162 | 0.914 | 1.704 | 2.337 | | | | | | |
| 4.6 | −0.193 | 0.913 | 1.727 | 2.380 | | | | | | |
| 4.8 | −0.225 | 0.909 | 1.747 | 2.420 | | | | | | |
| 5.0 | −0.258 | 0.903 | 1.765 | 2.458 | | | | | | |

Our results for $Q_{i,j}$ for small $\zeta$ are straightforward and need no further comment.

One cannot compare directly the results in tables 1—4 with those given by Arley [5]) for small $\zeta$, for he has measured depth in units of 0.693 of a cascade unit. We therefore had Silliac carry out a series of calculations using this unit of depth. We find that Arley's calculations are inaccurate by an amount varying from 2 to 15 percent, which is not surprising considering that he used only super-simplified cross-sections.

For higher values of $\zeta$ our results for $Q_{i,j}$ using direct numerical integ a-tions may be compared with the results obtained by Janossy and Messel [4]) and other authors. As could be predicted, one finds that for small $\zeta$ and low $\varepsilon$ the saddle point calculations are in many cases inaccurate by 10 percent. The extent of the inaccuracy depends critically upon the $Q_{i,j}$ considered.

The results presented here are at least as accurate as is justified by the use of the approximation A idealization of cascade theory. Thus when high energies are being considered the assumptions of approximation A are almost realized and the figures given here are valid.

It is clear, however, that the method used is applicable to a wide range of problems which involve the evaluation of an inverse Mellin or Laplace transform.

As methods such as that used here are of little value in solving shower problems of a general nature, we have devised methods of solving many such problems using a Monte Carlo technique. By the nature of the method, no approximations need be made in the cross-sections and the phenomena ignored in the approximation A formulation may be included.

In particular the number fluctuations and the angular and radial distributions will first be calculated using this method. It is hoped that these results will be available during 1958.

## Appendix

It is necessary to establish a set of conditions on a function $\phi(z)$ such that for $m > 0$ the integrals

$$\frac{e^{-m}}{2\pi i}\int_{b-i\infty}^{b+i\infty} e^{mz}\phi(z)dz \tag{A1}$$

and

$$\frac{e^{-m}}{2\pi i}\int_{\Gamma} e^{mz}\phi(z)dz \tag{A2}$$

are equal. We have set $W_0/W = \exp m$, and $\Gamma$ is the contour consisting of the parabola $y^2 = 4a(b-x)$, $a > 0$.

The conditions are that there is a positive number $k$ such that $|z^k\phi(z)|$ is bounded in the region S between the parabola and the line, and that $\phi(z)$ is analytic in this region.

As in fig. 1, let CC'D be part of a circle with centre O and radius $R$.

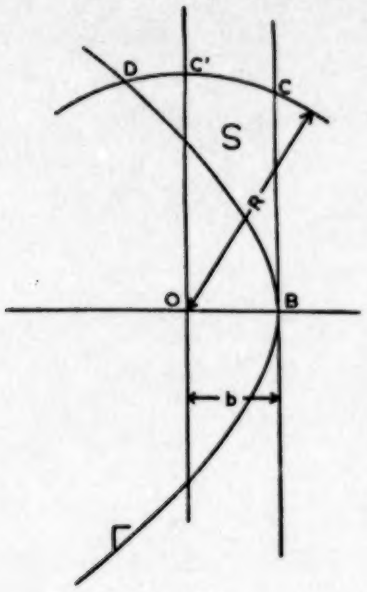


Fig. 1

We need only show that the integral:

$$\int_{CD} e^{mz}\phi(z)dz$$

tends to zero as $R \to \infty$.

Write

$$\int_{CD} e^{mz}\phi(z)dz = \int_{CC'} e^{mz}\phi(z)dz + \int_{C'D} e^{mz}\phi(z)dz = I_1 + I_2. \tag{A3}$$

Since length of arc $CC' < \frac{1}{2}\pi b$, and $\phi(z) < AR^{-k}$ for some $A$ we have

$$\begin{aligned} |I_1| &\leqq AR^{-k}\left|\int_{CC'} e^{mz}\,dz\right| \\ &< AR^{-k}\, e^{mb}\,\tfrac{1}{2}\pi b \to 0 \text{ as } R \to \infty. \end{aligned} \tag{A4}$$

Consider the integral $I_2$, and write

$$z = R\{\cos(\theta+\tfrac{1}{2}\pi) + i\sin(\theta+\tfrac{1}{2}\pi)\}.$$

We then have

$$\begin{aligned} |I_2| &\leqq AR^{-k+1}\int_0^{\frac{1}{2}\pi} |\exp[mR(\cos(\theta+\pi/2)+i\sin(\theta+\pi/2))] \\ &\quad \cdot\{-\sin(\theta+\pi/2)+i\cos(\theta+\pi/2)\}|d\theta \\ &= AR^{-k+1}\int_0^{\pi/2} e^{-mR\sin\theta}\,d\theta < AR^{-k+1}\int_0^{\pi/2} e^{-mR\frac{2\theta}{\pi}}\,d\theta \\ &= \frac{\pi A}{2m}R^{-k}(1-e^{-mR}) \to 0 \text{ as } R \to \infty, \end{aligned} \tag{A5}$$

and since $\phi(z)$ has no poles in the region S, we have the required result.

It is now necessary to show that the functions $\phi_{i,j}$ in (2) satisfy these conditions with $b > 1$. Consider the expressions (4) and (5); as $|z| \to \infty$ in the region S, $B, C \to 0$ and Re $(A) \to +\infty$,

$$\lambda_1 = \tfrac{1}{2}(A+D) - \left\{\tfrac{1}{2}(A-D) + \mathrm{O}\left(\frac{BC}{A-D}\right)\right\} = D + \mathrm{O}\left(\frac{BC}{A-D}\right), \quad \text{(A6)}$$

$$\lambda_2 = \tfrac{1}{2}(A+D) + \left\{\tfrac{1}{2}(A-D) + \mathrm{O}\left(\frac{BC}{A-D}\right)\right\} = A + \mathrm{O}\left(\frac{BC}{A-D}\right). \quad \text{(A7)}$$

From (2), (A6) and (A7) it is clear that for $\phi(z) = \phi_{i,j}$ and $|z|$ sufficiently large, $|z\phi(z)|$ is bounded. This establishes our first condition with $k = 1$.

We must now show that the $\phi_{i,j}$ are analytic in the region S. The functions $A$, $B$, $C$ are analytic except at certain points on the real axis to the left of Re $(z) = b$. The only possible poles in S are therefore the zeros of $\lambda_2 - \lambda_1$. However, each of the $\phi_{i,j}$ can be so written that $(\lambda_2 - \lambda_1)^{-1}$ only occurs multiplied by $\mathrm{e}^{-\lambda_1 \zeta} - \mathrm{e}^{-\lambda_2 \zeta}$. Writing $\mu = \zeta(\lambda_2 - \lambda_1)$ we have

$$\frac{\mathrm{e}^{-\lambda_1 \zeta} - \mathrm{e}^{-\lambda_2 \zeta}}{\lambda_2 - \lambda_1} = \zeta\, \mathrm{e}^{-\lambda_2 \zeta} \cdot \frac{\mathrm{e}^{\mu} - 1}{\mu}.$$

The fact that $(\mathrm{e}^{\mu} - 1)/\mu$ is analytic at $\mu = 0$ establishes the result that the $\phi_{i,j}$ are analytic at the zeros of $\lambda_2 - \lambda_1$.

## References


1) H. S. Bhabha and W. Heitler, Proc. Roy. Soc. A **159** (1937) 432
2) B. Rossi and K. Greisen, Revs. Mod. Phys. **13** (1941) 240
3) B. Rossi (Prentice Hall Incorporated, New York, 1951)
4) Leonie Janossy and H. Messel, Proc. Roy. Irish Acad. A **54** (1952) 217
5) N. Arley, Proc. Roy. Soc. A **168** (1938) 519

*Nuclear Physics* **6** (1958) 282—286; © *North-Holland Publishing Co., Amsterdam*
Not to be reproduced by photoprint or microfilm without written permission from the publisher

# ON THE "NEUTRINO CHARGE" IN WEAK AND STRONG INTERACTIONS

M. KONUMA, S. NAKAMURA and H. UMEZAWA
*Department of Physics, University of Tokyo*

Received 18 December 1957

**Abstract:** It is proposed here to extend the idea of the neutrino charge of the leptons to all the elementary particles. No experiments have been found to contradict the assumption that parity is conserved when the neutrino charge is and that the neutrino charge changes by a constant in any process due to the weak interactions in which the conservation of the parity is violated. It is likely that the neutrino charges of the baryons and mesons can be assigned to be the same as their hypercharges.

## 1. Introduction

It is a remarkable feature of the weak interactions that the neutrino appears only in the eigenstates of its polarization. This leads us to the attractive hypothesis that each lepton chooses a neutrino of a specific type as its partner.

This has been formulated in terms of the generalized gauge transformation [1–4])

$$\begin{aligned} \psi'_\nu &= e^{i\frac{\alpha}{2}\gamma_5}\psi_\nu, \\ \psi'_a &= e^{-in(a)\alpha}\psi_a, \end{aligned} \tag{1}$$

where $\psi_a$ stands for the wave functions of the particles besides the neutrino and the latter's wave function is denoted by $\psi_\nu$. The constant $n(a)$ is called the neutrino charge of the a-particle†. The neutrino charge is $+\frac{1}{2}$ and $-\frac{1}{2}$ for the neutrino in the right (d–) and left (l–) handed states respectively. The neutrino charge of a particle and that of its antiparticle differ from each other only by their sign. The neutrino charge is conserved in the processes due to interactions which are invariant under the generalized gauge transformation. We call the set of particles involved in the transformation (1) the *neutrino charge set.*

The validity of the conservation law can be tested by observing the longitudinal polarization of the $\mu$-meson in $\pi-\mu$ decay and that of the electron in $\mu-e$ decay. It was shown in our previous reports that the former and latter polarizations should be different from each other provided that the neutrino charges are conserved in the lepton processes [3, 4]).

† The neutrino charges defined here correspond to half of those in the previous articles [2–4]).

In the previous papers we discussed the weak interactions by assuming the conservation of the neutrino charge. We shall here take a different standpoint for the neutrino charge.

## 2. Neutrino Charge and Lepton Processes

It has been recently reported that the parity is not conserved in the $\Lambda$-decay process [5]), in which no lepton is involved. To understand the situation, we shall assume that the parity is conserved only when the neutrino charge is conserved. This forces us to include heavy particles in the neutrino charge set; any particle has its intrinsic neutrino charge.

There is no room for a phase transformation of the wave function of the neutral $\pi$-meson which is real. Thus, its neutrino charge is zero: $n(\pi^0) = 0$. So is the neutrino charge of the photon, $n(\gamma) = 0$. Taking into account the charge independence of the $\pi$-nucleon interaction, we see that the neutrino charge of the charged $\pi$-meson is also zero: $n(\pi^{\pm}) = 0$.

Let us further assume that the neutrino charge changes in any process due to weak interactions by $\Delta n$. We shall show that this assumption, with $\Delta n = \pm 1$, is consistent with the known phenomena. The assumption leaves us four possible cases for the lepton processes:

$$\text{(I)} \quad \begin{cases} \pi^+ \to \mu^+ + (\text{d-neutrino}) \\ \mu^+ \to e^+ + \nu(\text{d}) + \tilde{\nu}(\text{d}) \\ n \to p + e^- + (\text{l-neutrino}) \end{cases}$$

$$\text{(II)} \quad \begin{cases} \pi^+ \to \mu^+ + (\text{l-neutrino}) \\ \mu^+ \to e^+ + (\text{d-neutrino}) + (\text{l-neutrino}) \\ n \to p + e^- + (\text{l-neutrino}) \end{cases}$$

$$\text{(III)} \quad \begin{cases} \pi^+ \to \mu^+ + (\text{l-neutrino}) \\ \mu^+ \to e^+ + \nu(\text{l}) + \tilde{\nu}(\text{l}) \\ n \to p + e^- + (\text{d-neutrino}) \end{cases}$$

$$\text{(IV)} \quad \begin{cases} \pi^+ \to \mu^+ + (\text{d-neutrino}) \\ \mu^+ \to e^+ + (\text{l-neutrino}) + (\text{d-neutrino}) \\ n \to p + e^- + (\text{d-neutrino}), \end{cases}$$

where $\nu(\text{d})$ $[\tilde{\nu}(\text{d})]$ is the neutrino [antineutrino] in the right-handed state and (d-neutrino) means $\nu(\text{d})$ or $\tilde{\nu}(\text{d})$. Here we have taken into account the experimental results on the angular distribution of positons in the $\mu$—e decay, Michel's $\varrho$ value ($\neq 0$) and the angular distribution of negatons in the beta decay of the polarized $Co^{60}$. If we take into account the recent result that the polarization of the positons in the $\mu$—e decay is predominantly right-handed, the cases (III) and (IV) will be ruled out [6]).

The experiments on the longitudinal polarization of the electrons in beta decay show that the main part of the beta interactions should be of S.T.(P.) [V.A.] types in the cases (I) and (II) [(III) and (IV)].

The two component theory of the neutrino cannot apply to cases (I) and (III). This is true also in cases (II) and (IV) when we require the conservation of the lepton number†. The $\mu^-$ should be the particle (not the antiparticle) in the cases (I) or (III) when we assume the conservation of the lepton number.

The neutrino charges of the leptons in these four cases are shown in the table 1.

TABLE 1

| neutrino charge | $-\frac{1}{2}$ | $+\frac{1}{2}$ |
|---|---|---|
| I | $\mu^-e^-$ | $\mu^+e^+$ |
| II | $\mu^+e^-$ | $\mu^-e^+$ |
| III | $\mu^+e^+$ | $\mu^-e^-$ |
| IV | $\mu^-e^+$ | $\mu^+e^-$ |
| | $\nu$(l), $\tilde{\nu}$ (l) | $\nu$(d), $\tilde{\nu}$ (d) |

## 3. Neutrino Charge of Heavy Mesons and Hyperons

Let us now discuss the other weak interactions. The processes

$$K \to 2\pi \text{ and } K \to 3\pi$$

show that

$$n(K) = +1 \text{ or } -1.$$

Then, we have

$K^+ \to \mu^+ + (\text{l-neutrino})$ for the cases (I), (IV);

$K^+ \to \mu^+ + (\text{d-neutrino})$ for the cases (II), (III).

Further, we have

$K^+ \to e^+ + \pi^0 + (\text{l-neutrino})$ for the cases (I), (II);

$K^+ \to e^+ + \pi^0 + (\text{d-neutrino})$ for the cases (III), (IV).

† On the other hand, assuming $\Delta n = 0$, we have two cases:

(II′)
$$\begin{cases} \pi^+ \to \mu^+ + (\text{l-neutrino}) \\ \mu^+ \to e^+ + (\text{d-neutrino}) + (\text{l-neutrino}) \\ n \to p + e^- + (\text{d-neutrino}), \end{cases}$$

where the Fermi interactions are of the V. A. types;

(IV′)
$$\begin{cases} \pi^+ \to \mu^+ + (\text{d-neutrino}) \\ \mu^+ \to e^+ + (\text{l-neutrino}) + (\text{d-neutrino}) \\ n \to p + e^- + (\text{l-neutrino}), \end{cases}$$

where the Fermi interactions are of the S.T.(P.) types. The two component theory of the neutrino together with the conservation of the lepton number can apply to these cases. The assumption $\Delta n = 0$ has been discussed in detail in ref. [3, 4]).

It is interesting to see that the magnitudes $|n|$ of the neutrino charges of K and $\pi$ are equal to twice the charge centre [7]) or Schwinger's hypercharge $Y$ (i.e. strangeness + nucleon number) [8]).

The conservation of the neutrino charge in the processes due to the strong interactions leads us to assign to the hyperons neutrino charges equal to their hypercharges: +1 for nucleons, 0 for $\Lambda$, etc. This is a situation similar to that of the attribute in the Sachs theory [9]) †. Thus, it might be that the neutrino charge may pave the way to a deeper understanding of the strangeness.

It is remarkable that all the interactions can be classified in terms of the neutrino charge by the assumption that $\Delta n = 0$ *for the strong interactions and* $\Delta n = \pm 1$ *for all the weak interactions* in which the conservation of the parity is always violated.

## 4. Forbidden Processes

Let us now briefly discuss the unobserved processes like

$$\mu^- + p \to p + e^- \qquad (2a)$$
$$\mu^\pm \to e^\pm + e^+ + e^-,$$

$$K^0 \to e^\pm + \mu^\mp \qquad (2b)$$
$$K^0 \to e^\pm + \mu^\mp + (\pi^0 \text{ or } \gamma),$$

$$K^+ \to \mu^+ + e^+ + \pi^-, \qquad (2c)$$

$$K^0 \to 2\nu, \qquad (2d)$$

$$\pi^\pm \to e^\pm + \nu \qquad (2e)$$
$$K^\pm \to e^\pm + \nu.$$

The rule $\Delta n = \pm 1$ forbids the processes (2a) and (2c) in the cases (I) and (III), the processes (2b) in the cases (II) and (IV) and the process (2d) in the case where K is a spinless particle. This is because both of the neutrinos in (2d) should appear in a same polarization state. By the conservation law of the lepton number the processes (2a) and (2b) can be forbidden if we can assume $\mu^-$ to be the antiparticle, i.e., in the cases (II) and (IV), and the process (2c) can be forbidden if we can assign $\mu^-$ to be the particle. No way can be found to forbid the processes (2e) so far as we use only the rule $\Delta n = \pm 1$ together with the conservation of the lepton numbers.

† The Sachs attribute leads us to selection rules slightly different from ours. Indeed, assuming $\Delta n = 0$ for both the lepton processes (cf. refs. [3, 4]) and the strong interactions and assuming $\Delta n = \pm 1$ for the weak interactions not associated with leptons, we are also led to neutrino charges of the baryons and heavy mesons just equal to the hypercharge. These selection rules are the same as those of the attribute [9]).

## 5. Neutrino Charge and "Screw"

The situation regarding the neutrino charge may be intuitively understood in terms of the "screw". Let us introduce two sorts of screws; one couples with the left handed neutrino and the other with the right-handed one. They are called the l- and d-screw respectively. The screws of the same type can couple with each other. When no screw is left open, the interactions are strong and invariant under space inversion. The more screws are left open, the weaker the interactions are. The interactions are not invariant when there are some screws open, because the screw concept is not invariant under space inversion. Indeed, to keep the generalized gauge transformation invariant, we need to change the sign of all the neutrino charges under space inversion.

If any important role of the neutrino charge would be established in future, the screw-model might suggest something concerning the structure of the elementary particles. It may be also argued that the law of conservation (violation) of the neutrino charge in the strong (weak) interaction may serve as a clue to the deeper understanding of the phenomenological theory[10]) for parity violation.

*Note added in proof:* There have appeared several experiments which are not inconsistent with the selection rule $\Delta n = 0$ for the lepton interactions. Even if $\Delta n = 0$ should be required for the lepton interactions, the screw-model would hold with a slight modification (cf. footnotes in sections 2 and 3).

## References

1) W. Pauli, Nuovo Cimento **6** (1957) 204
2) H. Umezawa and A. Visconti, Nuclear Physics **4** (1957) 224
3) M. Konuma, Nuclear Physics **5** (1958) 504
4) M. Konuma, S. Nakamura and H. Umezawa, Phys. Rev.
5) F. S. Crawford *et al.*, Phys. Rev. **108** (1957) 1102;
F. Eisler *et al.*, Phys. Rev. **108** (1957) 1353
6) G. Culligan, S. G. F. Frank, J. R. Holt, J. C. Kluyver and T. Massam, Nature **180** (1957) 751
7) H. Umezawa, Quantum Field Theory (North Holland Publishing Co., Amsterdam, 1956) Ch. VII § 3
8) J. Schwinger, Phys. Rev. **104** (1956) 1164
9) R. G. Sachs, Phys. Rev. **99** (1955) 1573
10) T. D. Lee and C. N. Yang, Phys. Rev. **104** (1956) 254;
L. Landau, Nuclear Physics **3** (1957) 127

*Nuclear Physics* **6** (1958) 287—294; © *North-Holland Publishing Co., Amsterdam*
Not to be reproduced by photoprint or microfilm without written permission from the publisher

# A THEOREM ON POTENTIALS WITH HARD CORES

G. H. DERRICK
*The F. B. S. Falkiner Nuclear Research and Adolph Basser Computing Laboratories, School of Physics, University of Sydney*†

Received 5 November 1957

**Abstract:** It is shown for quite general systems of particles that a potential with a hard core gives the same binding energy in the limit of vanishing core radius as the corresponding potential with no hard core at all.

## 1. Introduction

Consider the motion of a single particle subject to a potential $V(r-r_0)$ which is a function of $r-r_0$, where $r$ is the radial distance and $r_0$ a "hard core radius". The potential is supposed so strongly repulsive for $r<r_0$ that the wave function vanishes here. The wave equation is then

$$\frac{-\hbar^2}{2m}\left(\frac{\mathrm{d}^2}{\mathrm{d}r^2}+\frac{2}{r}\frac{\mathrm{d}}{\mathrm{d}r}\right)\psi(r)+V(r-r_0)\psi(r)=E\,\psi(r) \qquad (r>r_0) \quad (1)$$

$$\lim_{r\to r_0}\psi(r)=0.$$

The solution of eq. (1) is

$$\psi(r)=[1-(r_0/r)]\varphi(r-r_0) \qquad (r>r_0) \quad (2)$$

where $\varphi(r)$ is the wave function when the hard core is absent, i.e. $\varphi(r)$ is the eigenfunction of

$$\frac{-\hbar^2}{2m}\left(\frac{\mathrm{d}^2}{\mathrm{d}r^2}+\frac{2}{r}\frac{\mathrm{d}}{\mathrm{d}r}\right)\varphi(r)+V(r)\varphi(r)=E\varphi(r) \qquad (r>0). \quad (3)$$

Since in general $\varphi(0)\neq 0$, eq. (3) is *not* the limiting case of eq. (1) as $r_0\to 0$. In fact eq. (2) shows that the wave function $\psi(r)$ with a very small core radius and the wave function $\varphi(r)$ with no core behave quite differently near the origin. For $r\approx r_0$ $\mathrm{d}\psi(r)/\mathrm{d}r$ varies very rapidly and becomes large like $1/r_0$ as $r_0\to 0$, while $\mathrm{d}\varphi(r)/\mathrm{d}r$ will in general be finite at the origin.

Despite this different behaviour of $\psi(r)$ and $\varphi(r)$ both functions lead to the same kinetic and potential energies. This is proved by changing the variable of integration from $r$ to $r-r_0$ in the relevant integrals.

However, what of more general systems of particles than the simple one above? In a system with more than two particles the volume of con-

† Also supported by the Nuclear Research Foundation within the University of Sydney.

figuration space excluded by the hard core is infinite, in contrast to the finite volume $\frac{4}{3}\pi r_0^3$ excluded in the single particle system just considered. Might not the rapid variation of the wave function as interparticle distances $\to r_0$ lead to a contribution to the kinetic energy which does not vanish as $r_0 \to 0$?

The object of this paper is to show that the result obtained above for the one-particle system holds quite generally:

*a potential with a hard core gives the same binding energy in the limit of vanishing core radius as the "corresponding" potential with no hard core at all.*

A more precise statement of this result will now be given.

## 2. Definition of the Problem

Consider a system of $N$ particles subject to a potential $V(\mathbf{r}_{\lambda\mu}, r_0) = V(\mathbf{r}_{12}, \mathbf{r}_{13}, \ldots \mathbf{r}_{1N}, r_0)$ which is a *continuous function of* $r_0$, *and is defined and bounded for all* $r_{\lambda\mu} \geqq r_0 \geqq 0$. $\mathbf{r}_{\lambda\mu}$ is the vector separation of the particles numbered $\lambda$ and $\mu$ ($\lambda, \mu = 1, 2, \ldots N$), and $r_{\lambda\mu}$ its magnitude. $V(\mathbf{r}_{\lambda\mu}, r_0)$ is defined only when *all* $r_{\lambda\mu} \geqq r_0$. Since $\mathbf{r}_{\lambda\mu} = \mathbf{r}_{1\mu} - \mathbf{r}_{1\lambda}$ we may take as our independent variables the $3(N-1)$ relative co-ordinates $\mathbf{r}_{12}, \mathbf{r}_{13}, \ldots \mathbf{r}_{1N}$. Let $D$ be the domain of all real values of these co-ordinates, and $D(r_0)$ that subspace of $D$ for which all interparticle distances $r_{\lambda\mu} > r_0$.

We must now define what we mean by the "energy with no hard core", and the "energy with a hard core of radius $r_0$". These energies will be denoted by $E$ and $E(r_0)$ respectively.

### 2.1. NO HARD CORE

Let us define $E$ as the (greatest) lower bound of

$$E[\varphi(\mathbf{r}_{\lambda\mu})] = \frac{\int_D \varphi^\dagger(\mathbf{r}_{\lambda\mu})[T + V(\mathbf{r}_{\lambda\mu}, 0)]\varphi(\mathbf{r}_{\lambda\mu})\mathrm{d}\tau}{\int_D |\varphi(\mathbf{r}_{\lambda\mu})|^2 \mathrm{d}\tau} \tag{4}$$

for the set $\mathfrak{S}$ of all functions $\varphi(\mathbf{r}_{\lambda\mu}) = \varphi(\mathbf{r}_{12}, \mathbf{r}_{13}, \ldots \mathbf{r}_{1N})$ for which

(i) all second derivatives with respect to the $\mathbf{r}_{1\varkappa}$ are continuous in $D$,

(ii) all the integrals of (4) separately converge,

(iii) $$\int_D \varphi^\dagger(\mathbf{r}_{\lambda\mu}) \nabla_\varkappa^2 \varphi(\mathbf{r}_{\lambda\mu}) \mathrm{d}\tau = -\int_D |\boldsymbol{\nabla}_\varkappa \varphi(\mathbf{r}_{\lambda\mu})|^2 \mathrm{d}\tau$$

where $\mathrm{d}\tau = \mathrm{d}^3\mathbf{r}_{12}\mathrm{d}^3\mathbf{r}_{13} \ldots \mathrm{d}^3\mathbf{r}_{1N}$ and

$$T = -\sum_{\varkappa=1}^{N} \frac{\hbar^2}{2M_\varkappa} \nabla_\varkappa^2$$

$M_\varkappa$ being the mass of particle number $\varkappa$.

The energy is defined by this variation method rather than as the lowest eigenvalue of a differential equation since for many potentials there is no

wave function satisfying the Schrödinger equation at all points. In those cases where there is an element of $\mathfrak{S}$ satisfying the Schrödinger equation everywhere the two definitions of the energy are equivalent. $E$ defined as above must always exist since

$$E[\varphi(\mathbf{r}_{\lambda\mu})]=\frac{\int_D \sum_{\kappa=1}^{N} \frac{\hbar^2}{2M_\kappa} |\nabla_\kappa \varphi(\mathbf{r}_{\lambda\mu})|^2 \mathrm{d}\tau + \int_D V(\mathbf{r}_{\lambda\mu}, 0)|\varphi(\mathbf{r}_{\lambda\mu})|^2 \mathrm{d}\tau}{\int_D |\varphi(\mathbf{r}_{\lambda\mu})|^2 \mathrm{d}\tau} \geqq -M,$$

where $M$ is the upper bound of $|V(\mathbf{r}_{\lambda\mu}, r_0)|$.

### 2.2. WITH A HARD CORE

Let us define $E(r_0)$ as the (greatest) lower bound of

$$E[r_0, \varphi(\mathbf{r}_{\lambda\mu}, r_0)] = \frac{\int_{D(r_0)} \varphi^\dagger(\mathbf{r}_{\lambda\mu}, r_0)[T+V(\mathbf{r}_{\lambda\mu}, r_0)]\varphi(\mathbf{r}_{\lambda\mu}, r_0)\mathrm{d}\tau}{\int_{D(r_0)} |\varphi(\mathbf{r}_{\lambda\mu}, r_0)|^2 \mathrm{d}\tau} \tag{5}$$

for the set $\mathfrak{S}(r_0)$ of all functions $\varphi(\mathbf{r}_{\lambda\mu}, r_0)=\varphi(\mathbf{r}_{12}, \mathbf{r}_{13} \ldots \mathbf{r}_{1N}, r_0)$ for which

(i) all second derivatives with respect to the $\mathbf{r}_{1\kappa}$ are continuous in $D(r_0)$ and as any $r_{\lambda\mu} \to r_0$,

(ii) all the integrals of (5) separately converge,

(iii) $\int_{D(r_0)} \varphi^\dagger(\mathbf{r}_{\lambda\mu}, r_0)\nabla_\kappa^2 \varphi(\mathbf{r}_{\lambda\mu}, r_0)\mathrm{d}\tau = -\int_{D(r_0)} |\nabla_\kappa \varphi(\mathbf{r}_{\lambda\mu}, r_0)|^2 \mathrm{d}\tau$,

(iv) $\varphi(\mathbf{r}_{\lambda\mu}, r_0) \to 0$ as any $r_{\lambda\mu} \to r_0$.

*It should be noted that the functions $\varphi(\mathbf{r}_{\lambda\mu})$ in $\mathfrak{S}$ have no restriction imposed on them corresponding to (iv).* It is just this condition (iv) which makes the problem non-trivial.

$E(r_0)$ must exist for all $r_0 \geqq 0$ since $E[r_0, \varphi(\mathbf{r}_{\lambda\mu}, r_0)] \geqq -M$ as before. Our problem, then, is to show that $\lim_{r_0 \to 0} E(r_0)$ exists, and equals $E$.

## 3. Proof that $\lim_{r_0 \to 0} E(r_0) = E$

The proof is in three main parts:

(1) A preliminary theorem which enables the "wave functions" to be cut off at finite distances. This removes convergence difficulties.

(2) An upper limit to $E - E(r_0)$ is obtained using the "wave function" *with* a hard core in the variation principle (4) for $E$. This "wave function" must first be extrapolated and smoothed as described below.

(3) A lower limit to $E-E(r_0)$ is obtained using the "wave function" *without* a hard core in the variation principle (5) for $E(r_0)$. As in part (2), this "wave function" must be somewhat modified first.

Both the upper and the lower limit to $E-E(r_0)$ obtained in this way approach zero with $r_0$. Hence our result follows.

The term "wave function" is used loosely here for any *sequence* of functions in $\mathfrak{S}$ (or $\mathfrak{S}(r_0)$) whose expectation values (4) (or (5)) have $E$ (or $E(r_0)$) as their limit. Nowhere do we assume that $E$ or $E(r_0)$ is actually attained for a member of $\mathfrak{S}$ or $\mathfrak{S}(r_0)$.

### 3.1. PRELIMINARY THEOREM

Given any positive number $\varepsilon$, we can find a function $\varphi_S(\mathbf{r}_{\lambda\mu})$ in $\mathfrak{S}$ and a positive number $S$ such that

$$\begin{aligned} &E \leqq E[\varphi_S(\mathbf{r}_{\lambda\mu})] < E+\varepsilon \\ &\text{and } \varphi_S(\mathbf{r}_{\lambda\mu}) = 0 \quad \text{when} \quad R \geqq S \end{aligned} \tag{6}$$

where $R^2 = \sum_{\iota<\kappa} r_{\iota\kappa}^2$.

To prove the theorem, let a function $u(\mathbf{r}_{\lambda\mu})$ in $\mathfrak{S}$ be chosen such that $E \leqq E[u(\mathbf{r}_{\lambda\mu})] < E+\frac{1}{2}\varepsilon$. Define

$$\begin{aligned} \varphi_S(\mathbf{r}_{\lambda\mu}) &= u(\mathbf{r}_{\lambda\mu}) && R \leqq \tfrac{1}{2}S \\ &= 0 && R \geqq S \\ &= F(R/S)u(\mathbf{r}_{\lambda\mu}) && \tfrac{1}{2}S < R < S \end{aligned} \tag{7}$$

where

$$F(t) = \exp\left\{-\frac{e^{\frac{1}{t-1}}}{1-t}\right\}.$$

Now $F(t) \to 1$ as $t \to \frac{1}{2}+$, and $\to 0$ as $t \to 1-$, while all its derivatives are continuous for $\frac{1}{2} < t < 1$ and approach zero at both ends of the interval. Also all derivatives of $R$ with respect to the $\mathbf{r}_{1\kappa}$ are continuous for $R \neq 0$ and bounded as $R \to \infty$. Hence $\varphi_S(\mathbf{r}_{\lambda\mu})$ is an element of $\mathfrak{S}$ and $E \leqq E[\varphi_S(\mathbf{r}_{\lambda\mu})]$.

It is shown in appendix 1 that

$$\lim_{S\to\infty} E[\varphi_S(\mathbf{r}_{\lambda\mu})] = E[u(\mathbf{r}_{\lambda\mu})]. \tag{8}$$

Let us choose $S$ sufficiently large that

$$|E[\varphi_S(\mathbf{r}_{\lambda\mu})] - E[u(\mathbf{r}_{\lambda\mu})]| < \tfrac{1}{2}\varepsilon.$$

Then

$$\begin{aligned} E[\varphi_S(\mathbf{r}_{\lambda\mu})] &< E[u(\mathbf{r}_{\lambda\mu})]+\tfrac{1}{2}\varepsilon \\ &< E+\varepsilon \end{aligned}$$

which proves the theorem (6).

A similar result holds for $E(r_0)$.

### 3.2. UPPER LIMIT TO $E-E(r_0)$

Let $\varepsilon$ be any positive number. Choose "wave functions" $\psi(\mathbf{r}_{\lambda\mu})$ in $\mathfrak{S}$ and $\psi(\mathbf{r}_{\lambda\mu}, r_0)$ in $\mathfrak{S}(r_0)$, and a positive number $S$ such that

$$\begin{aligned} E &\leqq E[\psi(\mathbf{r}_{\lambda\mu})] < E+\tfrac{1}{2}\varepsilon \\ E(r_0) &\leqq E[r_0,\ \psi(\mathbf{r}_{\lambda\mu},\ r_0)] < E(r_0)+\tfrac{1}{2}\varepsilon \end{aligned} \tag{9}$$

and $\psi(\mathbf{r}_{\lambda\mu})$ and $\psi(\mathbf{r}_{\lambda\mu},\ r_0) = 0$ when $R \geqq S$.

We now wish to take $\psi(\mathbf{r}_{\lambda\mu},\ r_0)$ as trial function in the variation principle (4) for $E$. However $\psi(\mathbf{r}_{\lambda\mu},\ r_0)$ is not an element of $\mathfrak{S}$, and must first be extrapolated and then "rounded off" as follows. Denote by $\Delta(r_0)$ the (finite) region

$$\chi \equiv \prod_{\lambda<\mu}\left(\frac{r_{\lambda\mu}-r_0}{r_0}\right) < 1, \text{ all } r_{\lambda\mu} > r_0 \text{ and } R < S.$$

Let

$$\begin{aligned} \varphi(\mathbf{r}_{\lambda\mu}) &= 0 \quad \text{if any } r_{\lambda\mu} \leqq r_0, \\ &= \psi(\mathbf{r}_{\lambda\mu},\ r_0) \quad \text{in} \quad D(r_0)-\Delta(r_0), \\ &= \psi(\mathbf{r}_{\lambda\mu},\ r_0)\ \exp\left\{-\frac{e^{\frac{1}{\chi-1}}}{\chi}\right\} \text{ in } \Delta(r_0). \end{aligned} \tag{10}$$

Then $\varphi(\mathbf{r}_{\lambda\mu})$ has continuous second derivatives everywhere in $D$, and is an element of $\mathfrak{S}$. Hence $E \leqq E[\varphi(\mathbf{r}_{\lambda\mu})]$.

In appendix 2 it is shown that

$$\lim_{r_0 \to 0} |E[\varphi(\mathbf{r}_{\lambda\mu})]-E[r_0,\ \psi(\mathbf{r}_{\lambda\mu},\ r_0)]| = 0. \tag{11}$$

Let us choose $r_0$ so small that

$$|E[\varphi(\mathbf{r}_{\lambda\mu})]-E[r_0,\ \psi(\mathbf{r}_{\lambda\mu},\ r_0)]| < \tfrac{1}{2}\varepsilon.$$

Then, using (9) and this result,

$$E-E(r_0) < \varepsilon. \tag{12}$$

### 3.3. LOWER LIMIT TO $E-E(r_0)$

The function $\psi(\mathbf{r}_{\lambda\mu})$ defined at the beginning of § 3.2 cannot be used directly in the variation principle (5) for $E(r_0)$, since it does not vanish as the $r_{\lambda\mu} \to r_0$. From $\psi(\mathbf{r}_{\lambda\mu})$ we construct a function $\varphi(\mathbf{r}_{\lambda\mu},\ r_0)$ in $D(r_0)$ as follows:

$$\begin{aligned} \varphi(\mathbf{r}_{\lambda\mu},\ r_0) &= \psi(\mathbf{r}_{\lambda\mu}) \qquad\qquad \text{in } D(r_0)-\Delta(r_0), \\ &= \psi(\mathbf{r}_{\lambda\mu})\ \exp\left\{-\frac{e^{\frac{1}{\chi-1}}}{\chi}\right\} \text{ in } \Delta(r_0), \end{aligned}$$

where $\Delta(r_0)$ and $\chi$ have the same meaning as in § 3.2. Then $\varphi(\mathbf{r}_{\lambda\mu},\ r_0)$ is an element of $\mathfrak{S}(r_0)$ and $E(r_0) \leqq E[r_0,\ \varphi(\mathbf{r}_{\lambda\mu},\ r_0)]$. By methods similar to those used in appendix 2 to prove (11), it can be shown that $\lim_{r_0 \to 0} E[r_0,\ \varphi(\mathbf{r}_{\lambda\mu}, r_0)] = E[\psi(\mathbf{r}_{\lambda\mu})]$. We may therefore choose $r_0$ sufficiently small that

$$|E[r_0,\ \varphi(\mathbf{r}_{\lambda\mu},\ r_0)]-E[\psi(\mathbf{r}_{\lambda\mu})]| < \tfrac{1}{2}\varepsilon.$$

Then, using (9) and the above result,

$$E-E(r_0) > -\varepsilon. \tag{13}$$

Combining (12) and (13), given any positive number $\varepsilon$, then for all sufficiently small $r_0$

$$|E-E(r_0)| < \varepsilon.$$

Hence $\lim_{r_0\to 0} E(r_0)$ exists and equals $E$.

The author is indebted to Dr. J. M. Blatt and to Dr. M. R. Schafroth for suggesting the problem, and for their valuable comments. In addition, he is grateful for a research grant from the Australian Atomic Energy Commission. Finally, he would like to thank Professor H. Messel for the excellent research facilities afforded him in the Sydney School of Physics.

## Appendix 1

PROOF OF EQ. (8)

Let us consider the behaviour as $S \to \infty$ of each of the integrals involved in $E[\varphi_S(\mathbf{r}_{\lambda\mu})]$, where $\varphi_S(\mathbf{r}_{\lambda\mu})$ is given by (7). In the first place,

$$\left|\int_D \{|\varphi_S(\mathbf{r}_{\lambda\mu})|^2-|u(\mathbf{r}_{\lambda\mu})|^2\}\,d\tau\right| = \left|\int_{R>S/2} \{|\varphi_S(\mathbf{r}_{\lambda\mu})|^2-|u(\mathbf{r}_{\lambda\mu})|^2\}\,d\tau\right|$$
$$< \int_{R>S/2} |u(\mathbf{r}_{\lambda\mu})|^2\,d\tau \to 0 \text{ as } S\to\infty$$

since $\int|u(\mathbf{r}_{\lambda\mu})|^2\,d\tau$ converges over $D$. Similarly,

$$\left|\int_D \{|\varphi_S(\mathbf{r}_{\lambda\mu})|^2-|u(\mathbf{r}_{\lambda\mu})|^2\}V(\mathbf{r}_{\lambda\mu},\ 0)\,d\tau\right| < M\int_{R>S/2}|u(\mathbf{r}_{\lambda\mu})|^2\,d\tau \to 0 \text{ as } S\to\infty;$$

$M$ is the upper bound of $|V(\mathbf{r}_{\lambda\mu}, r_0)|$. Further,

$$\left|\int_D \{|\nabla_\kappa\varphi_S(\mathbf{r}_{\lambda\mu})|^2-|\nabla_\kappa u(\mathbf{r}_{\lambda\mu})|^2\}\,d\tau\right|$$
$$\leqq \int_{S>R>S/2}|\nabla_\kappa\varphi_S(\mathbf{r}_{\lambda\mu})|^2\,d\tau+\int_{R>S/2}|\nabla_\kappa u(\mathbf{r}_{\lambda\mu})|^2\,d\tau.$$

As before the second integral $\to 0$ as $S\to\infty$ since $\int_D|\nabla_\kappa u(\mathbf{r}_{\lambda\mu})|^2\,d\tau$ converges. Now, for $S > R > \frac{1}{2}S$, eq. (7) yields

$$\nabla_\kappa\varphi_S(\mathbf{r}_{\lambda\mu}) = F(R/S)\nabla_\kappa u(\mathbf{r}_{\lambda\mu})+\frac{F'(R/S)}{S}u(\mathbf{r}_{\lambda\mu})\nabla_\kappa R; \tag{14}$$
$$\therefore |\nabla_\kappa\varphi_S(\mathbf{r}_{\lambda\mu})| < |\nabla_\kappa u(\mathbf{r}_{\lambda\mu})|+K/S|u(\mathbf{r}_{\lambda\mu})|$$

where $K$ is some positive number independent of $S$.

$$\therefore \int_{S>R>S/2}|\nabla_\kappa\varphi_S(\mathbf{r}_{\lambda\mu})|^2\,d\tau$$
$$< \int_{S>R>S/2}\{|\nabla_\kappa u(\mathbf{r}_{\lambda\mu})|+K/S|u(\mathbf{r}_{\lambda\mu})|\}^2\,d\tau < (B+KA/S)^2,$$

using Minkowski's inequality, where

$$A^2 = \int_{S>R>S/2} |u(\mathbf{r}_{\lambda\mu})|^2 \mathrm{d}\tau$$

$$B^2 = \int_{S>R>S/2} |\nabla_\kappa u(\mathbf{r}_{\lambda\mu})|^2 \mathrm{d}\tau.$$

Both $A$ and $B \to 0$ as $S \to \infty$ because of the convergence of $\int_D |u(\mathbf{r}_{\lambda\mu})|^2 \mathrm{d}\tau$ and $\int_D |\nabla_\kappa u(\mathbf{r}_{\lambda\mu})|^2 \mathrm{d}\tau$.

$$\therefore \lim_{S\to\infty} \int_D \{|\nabla_\kappa \varphi_S(\mathbf{r}_{\lambda\mu})|^2 - |\nabla_\kappa u(\mathbf{r}_{\lambda\mu})|^2\} \mathrm{d}\tau = 0.$$

Hence, combining our limiting results for the normalization, potential and kinetic energy integrals,

$$\lim_{S\to\infty} E[\varphi_S(\mathbf{r}_{\lambda\mu})] = E[u(\mathbf{r}_{\lambda\mu})].$$

## Appendix 2

PROOF OF EQ. (11)

$$\Delta(r_0) \subset \left\{ \begin{matrix} \text{all } r_{\lambda\mu} > r_0 \\ \text{at least one } r_{\lambda\mu} < 2r_0 \\ R < S \end{matrix} \right\} \qquad (\lambda, \mu = 1, 2, \ldots N;\ \lambda \neq \mu)$$

$$\subset \sum_{\iota<\kappa} \left\{ \begin{matrix} S > \text{all } r_{\lambda\mu} > r_0 \\ r_{\iota\kappa} < 2r_0 \end{matrix} \right\}$$

$$\subset \sum_{\iota<\kappa} \left\{ \begin{matrix} S > \text{all } r_{\iota\mu} > r_0 \\ r_{\iota\kappa} < 2r_0 \end{matrix} \right\} \qquad (\mu = 1, 2, \ldots, N;\ \mu \neq \iota)$$

where $\subset$ denotes "is a subspace of".

$$\therefore \int_{\Delta(r_0)} \mathrm{d}\tau < \frac{N(N-1)}{2} (4\pi)^{N-1} \int_{r_0}^{2r_0} r_{12}^2 \mathrm{d}r_{12} \int_{r_0}^{S} r_{13}^2 \mathrm{d}r_{13} \ldots \int_{r_0}^{S} r_{1N}^2 \mathrm{d}r_{1N}$$

$$< \frac{N(N-1)}{2} \left(\frac{4\pi}{3}\right)^{N-1} 7 r_0^3 (S^3 - r_0^3)^{N-2} \qquad (15)$$

$$\therefore \lim_{r_0\to 0} \frac{1}{r_0^2} \int_{\Delta(r_0)} \mathrm{d}\tau = 0.$$

We now consider the behaviour as $r_0 \to 0$ of the integrals involved in $E[\varphi(\mathbf{r}_{\lambda\mu})]$ and $E[r_0, \psi(\mathbf{r}_{\lambda\mu}, r_0)]$. Firstly,

$$\int_D |\varphi(\mathbf{r}_{\lambda\mu})|^2 \mathrm{d}\tau - \int_{D(r_0)} |\psi(\mathbf{r}_{\lambda\mu}, r_0)|^2 \mathrm{d}\tau = \int_{\Delta(r_0)} \{|\varphi(\mathbf{r}_{\lambda\mu})|^2 - |\psi(\mathbf{r}_{\lambda\mu}, r_0)|^2\} \mathrm{d}\tau$$

$$\to 0 \text{ as } r_0 \to 0$$

since the integrand is bounded, and $\lim_{r_0\to 0} \int_{\Delta(r_0)} \mathrm{d}\tau = 0$ by (15). Secondly,

$$\left|\int_D |\varphi(\mathbf{r}_{\lambda\mu})|^2 V(\mathbf{r}_{\lambda\mu}, 0)\,d\tau - \int_{D(r_0)} |\psi(\mathbf{r}_{\lambda\mu}, r_0)|^2 V(\mathbf{r}_{\lambda\mu}, r_0)\,d\tau\right|$$
$$< \int_{D(r_0)} |\psi(\mathbf{r}_{\lambda\mu}, r_0)|^2 |V(\mathbf{r}_{\lambda\mu}, r_0) - V(\mathbf{r}_{\lambda\mu}, 0)|\,d\tau$$
$$+ \int_{\Delta(r_0)} \left||\varphi(\mathbf{r}_{\lambda\mu})|^2 - |\psi(\mathbf{r}_{\lambda\mu}, r_0)|^2\right| \cdot |V(\mathbf{r}_{\lambda\mu}, r_0)|\,d\tau.$$

Since $V(\mathbf{r}_{\lambda\mu}, r_0)$ is continuous in $r_0$ for $r_0 \geqq 0$, given any positive number $\nu$ we can find a positive number $\zeta$ *independent of* $\mathbf{r}_{\lambda\mu}$ for $R < S$ such that

$$|V(\mathbf{r}_{\lambda\mu}, r_0) - V(\mathbf{r}_{\lambda\mu}, 0)| < \nu \text{ for all } r_0 < \zeta.$$

The first integral on the right therefore $\to 0$ as $r_0 \to 0$, while the second $\to 0$ with $r_0$ because the integrand is bounded.

Corresponding to eq. (14) in appendix 1, we obtain from (10), for all points in $\Delta(r_0)$,

$$|\nabla_\kappa \varphi(\mathbf{r}_{\lambda\mu})| < |\nabla_\kappa \psi(\mathbf{r}_{\lambda\mu}, r_0)| + \frac{L}{r_0} |\psi(\mathbf{r}_{\lambda\mu}, r_0)|$$

where $L$ is some positive number independent of $r_0$. Then,

$$\left|\int_D |\nabla_\kappa \varphi(\mathbf{r}_{\lambda\mu})|^2 d\tau - \int_{D(r_0)} |\nabla_\kappa \psi(\mathbf{r}_{\lambda\mu}, r_0)|^2 d\tau\right|$$
$$= \left|\int_{\Delta(r_0)} \{|\nabla_\kappa \varphi(\mathbf{r}_{\lambda\mu})|^2 - |\nabla_\kappa \psi(\mathbf{r}_{\lambda\mu}, r_0)|^2\} d\tau\right|$$
$$< \int_{\Delta(r_0)} \{|\nabla_\kappa \psi(\mathbf{r}_{\lambda\mu}, r_0)| + \frac{L}{r_0} |\psi(\mathbf{r}_{\lambda\mu}, r_0)|\}^2 d\tau + \int_{\Delta(r_0)} |\nabla_\kappa \psi(\mathbf{r}_{\lambda\mu}, r_0)|^2 d\tau$$
$$\to 0 \text{ as } r_0 \to 0$$

since $|\psi(\mathbf{r}_{\lambda\mu}, r_0)|$ and $|\nabla_\kappa \psi(\mathbf{r}_{\lambda\mu}, r_0)|$ are bounded and $\lim_{r_0 \to 0} 1/r_0^2 \int_{\Delta(r_0)} d\tau = 0$ by (15).

Combining our limiting results for the normalization, potential and kinetic energy integrals we obtain eq. (11).

*Nuclear Physics* **6** (1958) 295—304; © *North-Holland Publishing Co., Amsterdam*
Not to be reproduced by photoprint or microfilm without written permission from the publisher

# OPTICAL MODEL CALCULATION OF THE INTERACTION OF SLOW NEUTRONS WITH PROLATE NUCLEI

V. V. VLADIMIRSKY and I. L. ILYINA
*USSR Academy of Sciences, Moscow*

Received 9 August 1957

**Abstract:** The cross sections for absorption and scattering of slow neutrons by non-spherical ellipsoidal nuclei are calculated on the basis of the optical model. Diffuseness of the nuclear boundary and rotation of the nucleus are neglected. The results obtained allow us to explain the great width of the giant resonance in the region $A = 150$. It is shown that in the case of prolate nuclei the main resonances are accompanied by additional maxima.

## 1. Introduction

The simple optical model [1]) of neutron-nucleus interaction provides a qualitative explanation of the irregular trend of the average neutron cross sections as a function of the nuclear mass. In particular, it allows us easily to explain the sharp increase in neutron absorption near $A = 60$ and $A = 150$, connecting it with the giant resonance of the neutron wave function. On the assumption that the path length of the neutron in the nuclear matter considerably exceeds the dimensions of the nucleus it is possible to compute the width and height of the giant resonances and by comparison with the experimental data to estimate the path length, or, in other words, the magnitude of the complex part of the optical potential. For a quantitative comparison, however, it is necessary to elucidate some points of the elementary theory based on the optical model. Two simple possible causes of the increase in the height and width of the giant resonances may be indicated: the diffuse boundary of the nuclear potential and the non-spherical form of a considerable number of nuclei.

As has been shown by Nemirovsky [2]), if the potential jump on the boundary of the nucleus is replaced by a smooth trend of the potential, the giant resonances at large neutron energies become highly diffuse as a result of the strong decrease in neutron reflection at the boundary. At small energies the effect of diffuseness of the boundary is considerably less, since the wave length of the neutron outside the nucleus is great. However, even in this case the effect is appreciable. In the appendix are given estimates for a potential which falls off according to the exponential law

$$\begin{aligned} U &= -U_0 && 0 < r < r_0 \\ U &= -U_0 e^{\frac{r_0 - r}{a}} && r_0 < r < \infty. \end{aligned} \tag{1}$$

It is shown that the difference between this case and that of a sharp boundary practically reduces to replacing the well-known expression

$$P = \frac{4k_e}{k_1} \tag{2}$$

for the penetrability of the nuclear surface in the case of an abrupt potential jump by the formula

$$P = \frac{4k_e}{k_1} \frac{1}{J_0^2 + J_1^2} \tag{3}$$

where $J_0(x)$ and $J_1(x)$ are Bessel functions of the argument $x = 2ak_1$; $k_1$ and $k_e$ are the wave numbers of the neutron inside and outside the nucleus with $k_e \ll k_1$. The penetrability of the nuclear surface may increase by a factor 1.5—2, remaining nevertheless very small. As a result, for small neutron energies the giant resonances are only slightly affected by the diffuseness of the nuclear boundary and one may with good approximation utilize the simpler sharp boundary model and then correct for the effect of the diffuse boundary.

Similar results were recently obtained by Gribov [3]) and Nemirovsky [4]).

## 2. Computations for a Prolate Spheroid

The calculations for non-spherical nuclei were made on the following assumption. Inside the prolate ellipsoid of revolution

$$\frac{x^2}{b^2} + \frac{y^2}{b^2} + \frac{z^2}{a^2} = 0 \tag{4}$$

the potential is equal to the constant complex quantity

$$U = -U_0(1+i\zeta), \tag{5}$$

the imaginary part of which is small in comparison with the real part. Outside the nucleus the potential is equal to zero. The energy of the neutrons is assumed to be small. The wave function satisfies the equation

$$\nabla^2 u + k^2 u = 0. \tag{6}$$

Inside the nucleus

$$k_1^2 = \frac{2m}{\hbar^2} [E + U_0(1+i\zeta)]. \tag{7}$$

Outside the nucleus

$$k_e^2 = \frac{2mE}{\hbar^2}. \tag{8}$$

In utilizing the simple wave equation (6) we neglect the rotation of the nucleus; this is permissible if the moment of inertia of the nucleus is much greater than $ma^2$ for the neutron. $k_e$ satisfies the inequalities

$$k_e a \ll 1, \quad k_e \ll |k_1|. \tag{9}$$

Since the dimensions of the nucleus are small compared to the wavelength of the neutron outside the nucleus, it is possible to solve the internal problem on the assumption $E = k_e = 0$, and then in the region of intermediate distances from the centre of the nucleus $a \ll r \ll \lambda_e$ to connect the solution obtained with the well-known solution

$$u = \frac{B \cos k_e r + \sin k_e r}{k_e r} \tag{9a}$$

of the external problem for the s-wave by means of the approximation

$$u \approx \frac{B}{k_e r} + 1 \tag{10}$$

for $k_e r \ll 1$. Expression (10) should be put equal to the solution of the internal problem at $r \gg a$; the absence of terms which increase as $r \to \infty$ is a natural boundary condition of the internal problem.

The internal problem was solved in elliptical coordinates

$$\begin{aligned} x &= c\sqrt{(\xi^2-1)(1-\eta^2)}\cos\varphi \\ y &= c\sqrt{(\xi^2-1)(1-\eta^2)}\sin\varphi \\ z &= c\xi\eta. \end{aligned} \tag{11}$$

Only those solutions were considered which are independent of the azimuth $\varphi$. The boundary of the nucleus corresponds to the coordinate surface $\xi = \xi_1$, where

$$\xi_1 = \frac{a}{c}, \quad c = \sqrt{a^2-b^2}. \tag{12}$$

The general solution of Laplace's equation for $\xi > \xi_1$ has the following form

$$u(\xi, \eta) = \sum_l [a_l P_l(\xi) + b_l Q_l(\xi)] P_l(\eta) \tag{13}$$

where $P_l$ is a Legendre polynomial, and $Q_l(\xi)$ are associated Legendre functions, so defined that $Q_l(\xi)$ is real along the real axis at $|\xi| > 1$:

$$Q_0(\xi) = \tfrac{1}{2} \ln \frac{\xi+1}{\xi-1}, \text{ etc.} \tag{14}$$

Comparing (13) and (10) for $\xi \to \infty$ we obtain

$$\begin{aligned} a_0 &= 1, \quad b_0 = \frac{B}{k_e c}, \\ a_l &= 0 \quad \text{for} \quad l \geqq 1. \end{aligned} \tag{15}$$

The solution inside the nucleus may be represented in the form

$$u(\xi, \eta) = \sum_l \chi_l(\xi) P_l(\eta) \tag{16}$$

The function $\chi_l(\xi)$ satisfies the system of equations

$$\frac{d}{d\xi}\left[(\xi^2-1)\frac{d\chi_l}{d\xi}\right]-l(l+1)\chi_l+k_1^2c^2\left\{\xi^2\chi_l - \frac{(l-1)l}{(2l-3)(2l-1)}\chi_{l-2}-\frac{2l^2+2l-1}{(2l-1)(2l+3)}\chi_l-\frac{(l+1)(l+2)}{(2l+3)(2l+5)}\chi_{l+2}\right\}=0 \tag{17}$$

with the boundary conditions at $\xi=\xi_1$

$$\chi_0=1+b_0Q_0(\xi_1);\quad \frac{d\chi_0}{d\xi}=b_0Q'_0(\xi_1);$$
$$\frac{\chi'_l}{\chi_l}=\frac{Q'_l}{Q_l}\ \text{for}\ l\geqq 1. \tag{18}$$

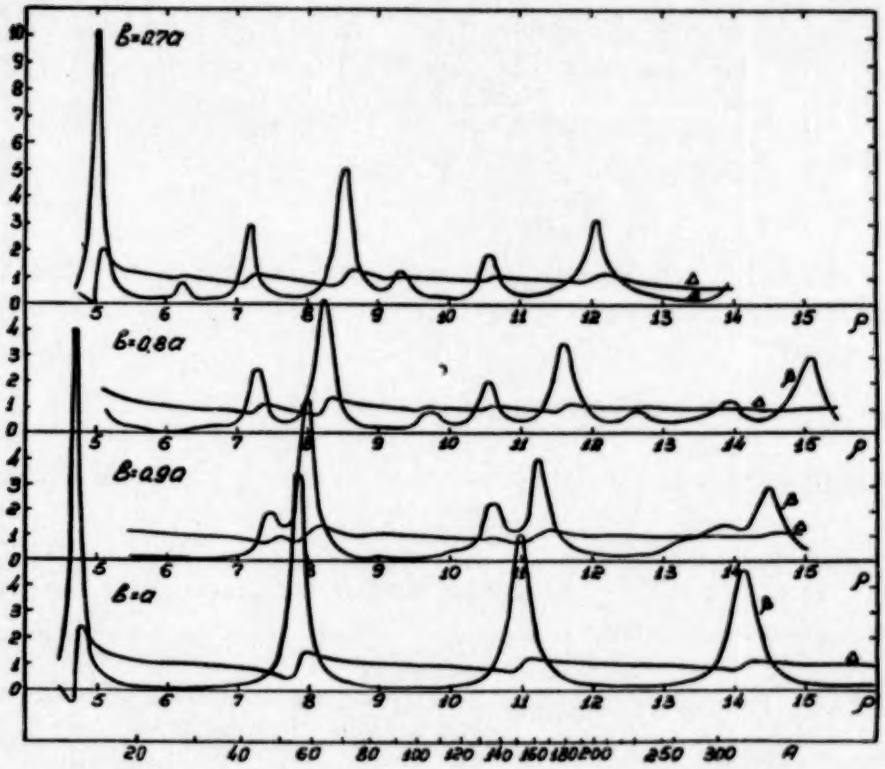


Fig. 1. Parameters $\Delta$ and $\beta$ characterizing the real and imaginary part of the scattered wave amplitude as functions of $\varrho\approx 2.06A^{1/3}$ for prolateness ratios $b/a=0.7,\ 0.8,\ 0.9,\ 1$.

At $\xi=1$ the equations have a singular point. Regularity at $\xi=1$ is an additional boundary condition. The functions $\chi_l(\xi)$ were expanded in the power series

$$\chi_l(\xi)=\sum\alpha_{kl}(\xi-1)^k. \tag{19}$$

The coefficients $\alpha_{kl}$ up to $k\approx 30$ were obtained by the recursion formula

$$\alpha_{n+1,l} = \frac{k_1^2 c^2}{2(n+1)^2}\alpha_{n-2,l} - \frac{k_1^2 c^2}{(n+1)^2}\alpha_{n-1,l}$$
$$- \frac{1}{2(n+1)^2}\left[n(n+1) - l(l+1) + k_1^2 c^2\left(1 - \frac{2l^2+2l-1}{(2l-1)(2l+3)}\right)\right]\alpha_{nl}$$
$$+ \frac{(l-1)lk_1^2 c^2}{(2l-3)(2l-1)2(n+1)^2}\alpha_{n,l-2} + \frac{(l+1)(l+2)k_1^2 c^2}{2(n+1)^2(2l+3)(2l+5)}\alpha_{n,l+2}.$$

The system of simultaneous algebraic linear equations for the coefficients $\alpha_{nl}$ was truncated at $l = 14$.

## 3. Results

Calculations were carried out on a small electronic computer, assuming the following values for the nuclear parameters:

$$U_0 = 42 \text{ MeV}, \qquad \zeta = 0.03,$$
$$\bar{R} = 1.45 \times 10^{-13} A^{1/3} \text{ cm}, \tag{20}$$

where $\bar{R}$ is the radius of the sphere having the same volume as the nucleus, and three different values of the prolateness ratio

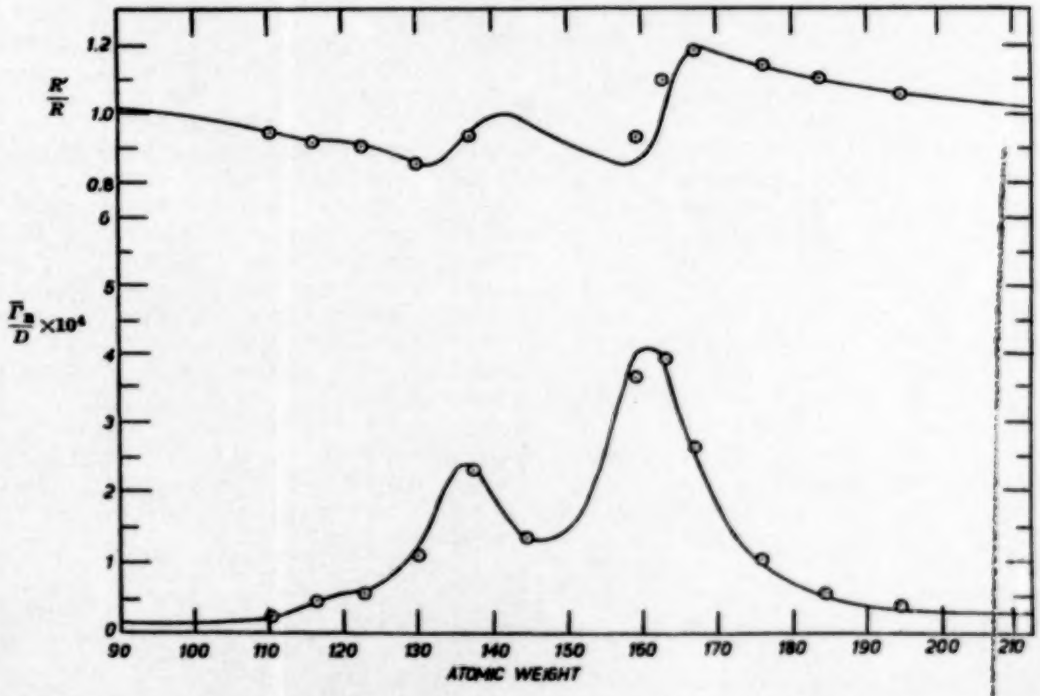


Fig. 2. Ratio $\Delta$ of scattering length $R'$ to equivalent nuclear radius $\bar{R}$ (upper part of fig.), and ratio of average neutron width $\bar{\Gamma}_n$ to level distance $D$ (lower part of fig.), as functions of $A$ for prolateness $b/a = 0.9$.
⊙ = present calculation; continuous line = calculation of ref. [7]).

$$\frac{b}{a} = 0.9,\ 0.8,\ 0.7. \tag{21}$$

Data for spherical nuclei were also computed according to the formulae of ref. [1]).

The results of the calculations of the real and imaginary part of the amplitude of the scattered wave

$$B = \frac{k_0}{|k_1|}[i\beta - \varrho\Delta]$$

are presented in the tables and fig. 1. For convenience in comparing the curves we chose as independent variable the quantity

$$\varrho = |k_1|(ab^2)^{1/3} = |k_1|\bar{R} \tag{22}$$

which, with the parameter values (20), is simply related to the nuclear mass:

$$\varrho \approx 2.06A^{1/3}. \tag{23}$$

TABLE 1

Scattered wave amplitude for $b/a = 0.7$

| $a$ | $\varrho$ | $\beta$ | $\Delta$ | $a$ | $\varrho$ | $\beta$ | $\Delta$ | $a$ | $\varrho$ | $\beta$ | $\Delta$ |
|---|---|---|---|---|---|---|---|---|---|---|---|
| 6.000 | 4.730 | 0.596 | 0.567 | 9.800 | 7.726 | 0.284 | 0.991 | 14.800 | 11.668 | 1.332 | 0.92 |
| 6.200 | 4.888 | 2.170 | 0.194 | 10.000 | 7.884 | 0.298 | 0.944 | 15.200 | 11.983 | 2.811 | 0.94 |
| 6.300 | 4.967 | 5.979 | 0.021 | 10.200 | 8.041 | 0.405 | 0.892 | 15.297 | 12.060 | 3.200 | 1.03 |
| 6.350 | 5.006 | 9.314 | 0.456 | 10.600 | 8.357 | 1.900 | 0.725 | 15.348 | 12.100 | 3.047 | 1.07 |
| 6.380 | 5.030 | 10.243 | 1.044 | 10.800 | 8.514 | 5.036 | 0.935 | 15.400 | 12.141 | 2.683 | 1.11 |
| 6.400 | 5.046 | 9.822 | 1.440 | 10.832 | 8.540 | 5.144 | 1.045 | 15.600 | 12.299 | 1.359 | 1.11 |
| 6.469 | 5.100 | 5.585 | 2.012 | 10.908 | 8.600 | 4.144 | 1.246 | | | | |
| 6.600 | 5.203 | 1.763 | 1.724 | 11.000 | 8.672 | 2.522 | 1.291 | 16.200 | 12.772 | 0.652 | 0.68 |
| 6.800 | 5.361 | 0.612 | 1.406 | 11.200 | 8.830 | 0.984 | 1.193 | 16.600 | 13.087 | 0.266 | 0.66 |
| 7.000 | 5.519 | 0.330 | 1.256 | 11.400 | 8.987 | 0.610 | 1.112 | 16.800 | 13.245 | 0.226 | 0.65 |
| 7.400 | 5.834 | 0.190 | 1.104 | 11.600 | 9.145 | 0.640 | 1.054 | 17.000 | 13.402 | 0.229 | 0.64 |
| 7.600 | 5.992 | 0.213 | 1.049 | 11.800 | 9.303 | 1.247 | 1.076 | 17.200 | 13.560 | 0.264 | 0.63 |
| 7.800 | 6.149 | 0.469 | 0.994 | 12.000 | 9.460 | 0.836 | 1.105 | 17.400 | 13.718 | 0.370 | 0.62 |
| 7.900 | 6.228 | 0.801 | 1.018 | 12.200 | 9.618 | 0.409 | 1.073 | 17.600 | 13.875 | 0.646 | 0.61 |
| 8.000 | 6.307 | 0.588 | 1.071 | 12.600 | 9.934 | 0.263 | 1.014 | | | | |
| 8.200 | 6.465 | 0.238 | 1.027 | 12.800 | 10.091 | 0.297 | 0.988 | | | | |
| 8.400 | 6.622 | 0.206 | 0.981 | 13.000 | 10.249 | 0.430 | 0.959 | | | | |
| 8.600 | 6.780 | 0.260 | 0.932 | 13.200 | 10.406 | 0.852 | 0.928 | | | | |
| 8.800 | 6.938 | 0.495 | 0.868 | 13.400 | 10.564 | 1.876 | 0.971 | | | | |
| 9.000 | 7.095 | 1.588 | 0.803 | 13.500 | 10.643 | 1.841 | 1.044 | | | | |
| 9.082 | 7.160 | 2.711 | 0.882 | 13.600 | 10.722 | 1.301 | 1.071 | | | | |
| 9.133 | 7.200 | 2.968 | 1.016 | 14.200 | 11.195 | 0.397 | 0.986 | | | | |
| 9.200 | 7.253 | 2.333 | 1.152 | 14.400 | 11.353 | 0.488 | 0.956 | | | | |
| 9.400 | 7.411 | 0.705 | 1.117 | | | | | | | | |
| 9.600 | 7.568 | 0.363 | 1.043 | | | | | | | | |

The cross-section for neutron absorption averaged over the resonance levels of the nucleus is related to the amplitude of the scattered wave by the formula

$$\bar{\sigma}_a = 2\pi^2 \lambda_e^2 \frac{\Gamma_n}{D} \approx 4\pi\lambda_e^2 \operatorname{Im} B,$$
$$\frac{\Gamma_n}{D} \approx \frac{2}{\pi} \operatorname{Im} B = \frac{2}{\pi} \frac{k_e}{|k_1|} \beta, \tag{24}$$

while the cross section for potential scattering

$$\bar{\sigma}_s \approx 4\pi\lambda_e^2 (\operatorname{Re} B)^2 = 4\pi \bar{R}^2 \Delta^2 = 4\pi R'^2 \tag{25}$$

where $R' = \lambda_1 \varrho \Delta$ is the scattering length. For strongly absorbing nuclei the quantities $\beta$ and $\Delta = R'/\bar{R}$ are close to unity. Typical results are shown in fig. 2.

TABLE 2

Scattered wave amplitude for $b/a = 0.8$

| $a$ | $\varrho$ | $\beta$ | $\Delta$ | $a$ | $\varrho$ | $\beta$ | $\Delta$ | $a$ | $\varrho$ | $\beta$ | $\Delta$ |
|---|---|---|---|---|---|---|---|---|---|---|---|
| 6.000 | 5.171 | 0.778 | 1.512 | 10.800 | 9.307 | 0.248 | 1.012 | 15.800 | 13.616 | 0.809 | 0.984 |
| 6.200 | 5.343 | 0.360 | 1.310 | 11.000 | 9.480 | 0.347 | 0.981 | 16.000 | 13.788 | 1.075 | 0.975 |
| 6.600 | 5.688 | 0.162 | 1.138 | 11.200 | 9.652 | 0.766 | 0.962 | 16.200 | 13.961 | 1.283 | 1.010 |
| 6.800 | 5.860 | 0.133 | 1.087 | 11.400 | 9.824 | 0.800 | 1.016 | 16.400 | 14.133 | 0.814 | 1.016 |
| 7.000 | 6.032 | 0.120 | 1.046 | 11.600 | 9.997 | 0.438 | 0.993 | 16.600 | 14.305 | 0.810 | 0.992 |
| 7.400 | 6.377 | 0.163 | 0.972 | 11.800 | 10.169 | 0.450 | 0.955 | 16.800 | 14.478 | 0.862 | 0.966 |
| 7.600 | 6.550 | 0.229 | 0.902 | 12.000 | 10.341 | 0.806 | 0.916 | 17.000 | 14.650 | 0.999 | 0.940 |
| 7.800 | 6.722 | 0.256 | 0.944 | 12.200 | 10.514 | 1.903 | 0.948 | | | | |
| 8.000 | 6.894 | 0.284 | 0.890 | 12.230 | 10.540 | 1.996 | 0.960 | | | | |
| 8.200 | 7.067 | 0.600 | 0.815 | 12.400 | 10.686 | 1.295 | 1.056 | | | | |
| 8.400 | 7.239 | 2.339 | 0.788 | 12.600 | 10.858 | 0.588 | 1.019 | | | | |
| 8.600 | 7.411 | 1.522 | 1.114 | 12.800 | 11.031 | 0.533 | 0.975 | | | | |
| 8.800 | 7.584 | 0.586 | 1.014 | 13.000 | 11.203 | 0.679 | 0.931 | | | | |
| 9.000 | 7.756 | 0.488 | 0.925 | 13.200 | 11.375 | 1.346 | 0.882 | | | | |
| 9.100 | 7.842 | 0.595 | 0.888 | 13.400 | 11.548 | 3.152 | 0.926 | | | | |
| 9.200 | 7.928 | 0.822 | 0.829 | 13.483 | 11.620 | 3.503 | 1.024 | | | | |
| 9.400 | 8.101 | 2.420 | 0.709 | 13.600 | 11.720 | 2.579 | 1.136 | | | | |
| 9.500 | 8.187 | 4.406 | 0.773 | 13.800 | 11.893 | 1.151 | 1.124 | | | | |
| 9.600 | 8.273 | 5.138 | 1.189 | 14.000 | 12.065 | 0.648 | 1.080 | | | | |
| 9.800 | 8.445 | 1.576 | 1.292 | 14.200 | 12.237 | 0.494 | 1.045 | | | | |
| 10.000 | 8.618 | 0.648 | 1.182 | 14.400 | 12.410 | 0.550 | 1.017 | | | | |
| 10.200 | 8.790 | 0.384 | 1.116 | 14.600 | 12.582 | 0.876 | 1.010 | | | | |
| 10.400 | 8.962 | 0.301 | 1.073 | 14.800 | 12.754 | 0.811 | 1.036 | | | | |
| 10.600 | 9.135 | 0.248 | 1.042 | 15.000 | 12.927 | 0.499 | 1.023 | | | | |

A comparison of the results for nuclei with different degrees of prolateness shows that the giant resonances of spherical nuclei shift in the direction of greater nuclear dimensions with increasing prolateness. This gives a qualitative explanation of the great width of the giant resonance in the region $A = 150$, since at $A = 150$ lies the boundary between the highly prolate nuclei and the lighter, more spherical nuclei [5]). A more detailed comparison with the experimental data will be given in ref. [6]). In prolate nuclei the main resonances are accompanied by additional maxima,

connected with the higher terms $l = 2$ and $l = 4$. The comparatively large value of the maxima corresponding to the d-wave, even for slightly prolate nuclei, is evidently to be explained by the fact that the limiting values of the eigenvalues of the d-wave for a sphere are very close to those of the s-wave. With increasing prolateness of the nuclei the secondary maxima shift towards smaller nuclear dimensions. The presence of these maxima indicates that in slow neutron capture in prolate nuclei the motion of the neutron inside the nucleus is very far from being spherically symmetrical and in a number of cases may approach forms which correspond to $l = 2$ or even $l = 4$, according to spectroscopic classification.

TABLE 3

Scattered wave amplitude for $b/a = 0.9$

| $a$ | $\varrho$ | $\beta$ | $\Delta$ | $a$ | $\varrho$ | $\beta$ | $\Delta$ |
|---|---|---|---|---|---|---|---|
| 6.000 | 5.593 | 0.160 | 1.151 | 11.200 | 10.440 | 1.091 | 0.851 |
| 6.200 | 5.780 | 0.125 | 1.097 | 11.400 | 10.627 | 2.288 | 0.936 |
| 6.400 | 5.966 | 0.107 | 1.056 | 11.586 | 10.800 | 1.407 | 0.983 |
| 6.600 | 6.152 | 0.099 | 1.021 | 12.000 | 11.186 | 3.631 | 0.936 |
| 6.800 | 6.339 | 0.092 | 0.990 | 12.101 | 11.280 | 3.887 | 1.104 |
| 7.000 | 6.525 | 0.108 | 0.960 | 12.200 | 11.373 | 2.652 | 1.190 |
| 7.200 | 6.712 | 0.118 | 0.960 | 12.400 | 11.559 | 1.037 | 1.153 |
| 7.600 | 7.085 | 0.283 | 0.842 | 12.600 | 11.745 | 0.543 | 1.102 |
| 7.800 | 7.271 | 0.664 | 0.759 | 12.800 | 11.932 | 0.356 | 1.068 |
| 7.938 | 7.400 | 1.741 | 0.708 | 13.000 | 12.118 | 0.272 | 1.043 |
| 8.200 | 7.644 | 1.394 | 0.910 | 13.200 | 12.305 | 0.233 | 1.023 |
| 8.400 | 7.830 | 2.190 | 0.720 | 13.400 | 12.491 | 0.226 | 1.006 |
| 8.600 | 8.017 | 6.204 | 1.134 | 13.600 | 12.678 | 0.244 | 0.989 |
| 8.800 | 8.203 | 1.802 | 1.357 | | | | |
| 9.000 | 8.390 | 0.690 | 1.221 | 14.200 | 13.237 | 0.802 | 0.947 |
| 9.200 | 8.576 | 0.371 | 1.142 | 14.600 | 13.610 | 1.114 | 0.931 |
| 9.400 | 8.762 | 0.133 | 0.998 | 14.800 | 13.796 | 1.430 | 0.964 |
| 9.600 | 8.949 | 0.194 | 1.061 | 15.000 | 13.983 | 1.380 | 0.996 |
| 9.800 | 9.135 | 0.166 | 1.034 | 15.200 | 14.169 | 1.301 | 0.962 |
| 10.200 | 9.508 | 0.160 | 0.990 | 15.400 | 14.355 | 2.249 | 0.951 |
| 10.400 | 9.695 | 0.184 | 0.967 | 15.600 | 14.542 | 2.793 | 1.067 |
| 10.600 | 9.881 | 0.253 | 0.943 | 15.800 | 14.728 | 1.440 | 1.105 |
| 10.800 | 10.067 | 0.464 | 0.917 | 16.000 | 14.915 | 0.750 | 1.078 |
| 11.000 | 10.254 | 0.593 | 0.904 | | | | |

In a recent paper by Margolis and Troubetzkoy [7]) similar calculations are carried out for slightly prolate nuclei. Their results are in good agreement with our curve for $b/a = 0.9$ (fig. 2).

The authors express their deep gratitude to the corresponding member of the Academy I. S. Bruk for his kind permission to use the small electronic computer. The authors thank A. S. Kronrod for advice on computing technique and K. A. Ter-Martirosyan for discussion of the results of this work.

## Appendix

### SPHERICAL NUCLEUS WITH DIFFUSE BOUNDARY

The model of a spherical nucleus with a diffuse boundary can easily be computed on the assumption of a potential decreasing according to an exponential law

$$\begin{aligned} U(r) &= -U_0 \qquad 0<r<r_0, \\ U(r) &= -U_0 e^{\frac{r_0-r}{a}} \qquad r_0<r<\infty. \end{aligned} \tag{A.1}$$

In the equation

$$\frac{d^2(ru)}{dr^2}+\frac{2m}{\hbar^2}[E-U(r)]ru=0 \tag{A.2}$$

for the s-wave at $E=0$, $r>r_0$ it is convenient to make the substitution

$$ru=v, \qquad r=r_0-2a\ln t, \tag{A.3}$$

which leads to the equation for the Bessel function

$$\frac{d^2v}{dt^2}+\frac{1}{t}\frac{dv}{dt}+4a^2k_1^2v=0 \tag{A.4}$$

where $k_1^2=(2m/\hbar^2)U_0$. The solution $v=Z_0(2ak_1t)$ at $t=0$ should be connected with the asymptotic form of the wave function at $r\to\infty$; while at $t=1$, $r=r_0$ it should be combined with the solution

$$u(r)=\frac{\sin k_1 r}{k_1 r} \tag{A.5}$$

for the inner region. With the notation (10) we obtain

$$B=\frac{k_e}{k_1}\left[\frac{\pi x}{2}\frac{\sin\varrho\, Y_1(x)-\cos\varrho Y_0(x)}{\sin\varrho J_1(x)-\cos\varrho J_0(x)}-\varrho-x\ln\frac{\gamma x}{2}\right] \tag{A.6}$$

where

$$\varrho=k_1r, \qquad x=2ak_1t.$$

The maxima of the cross section are at

$$\operatorname{ctg}|\varrho|=\frac{J_1(|x|)}{J_0(|x|)}. \tag{A.7}$$

The cross section at the maximum is given by the expression

$$\beta_{\max}\approx\frac{2}{[|\varrho+x|(J_1^2+J_0^2)-J_0J_1]\zeta} \tag{A.8}$$

which for $a\to 0$ becomes $\beta_{\max}\approx 2/|\varrho|\xi$ for the model with a sharply defined boundary. The minima of the cross section are at $\operatorname{ctg}|\varrho|=Y_1/Y_0$ and are equal correspondingly to

$$\beta_{\min} \approx \frac{\pi^2}{8} x^2 \zeta[|\varrho+x|(Y_1^2+Y_0^2)-Y_0 Y_1]+\tfrac{1}{2}x\zeta. \tag{A.9}$$

The limiting value equals $\beta_{\min} \approx |\varrho|\zeta/2$ for a sharp boundary. At $a=0.5\times 10^{-13}$cm, $|x|=1.45$ the values of $\beta$ increase 1.5—2-fold both at the maximum and at the minimum.

The approximation to strong coupling can be easily computed by assuming for the inner region $r < r_0$ a purely convergent wave $v = A\exp(-ik_1 r)$. Instead of (A.6) we obtain

$$B = \frac{k_e}{k_1}\left[\frac{\pi x}{2}\frac{Y_0+iY_1}{J_0+iJ_1} - x\ln\frac{\gamma x}{2} - \varrho\right]. \tag{A.10}$$

The imaginary part of this expression gives (3).

## References

1) H. Feshbach, C. E. Porter and V. F. Weisskopf, Phys. Rev. **96** (1954) 448
2) P. E. Nemirovsky, International Conference on the Peaceful Uses of Atomic Energy (P/**654**) (1955)
3) V. N. Gribov, JETP **32** (1957) 647
4) P. E. Nemirovsky, JETP **32** (1957) 1143
5) K. Alder, A. Bohr, T. Huus, B. Mottelson and A. Winter, Rev. Mod. Phys. **28** (1956) 432
6) V. V. Vladimirsky, A. A. Panov, I. A. Radkevich and V. V. Sokolovsky, Atomic Energy **3** (1957) 444
7) B. Margolis and E. S. Troubetzkoy, Phys. Rev. **106** (1957) 105

*Nuclear Physics* **6** (1958) 305—309; © *North-Holland Publishing Co., Amsterdam*
Not to be reproduced by photoprint or microfilm without written permission from the publisher

# CALCULATION OF SOME RELATIVISTIC CORRECTIONS TO THE ALLOWED AND *l*-FORBIDDEN BETA TRANSITIONS

G. ALAGA, L. ŠIPS and D. TADIĆ
*Institute Rudjer Bošković and University of Zagreb, Zagreb, Yugoslavia*

Received 13 September 1957

**Abstract:** Making use of the non-relativistic form of the relativistic operators, we have computed the corrections to the allowed $\beta$-transitions. The main contributions are of the order of magnitude $M^{-1}(\alpha Z/r_0)$, $p/M$ and $q/M$. This may affect the spectra, angular correlations, $K/\beta^+$ ratios and half lives to the extent of a few per cent. It seems that these effects in some cases are within the precision of present day experimental technique and may provide additional information on $\beta$-coupling constants. In a following paper we intend to give an analysis of some experiments.

## 1. Fermi Transitions

The interaction Hamiltonian for Fermi transitions can be written in the form [1])

$$H'_\beta = -g_1 L_1 + g_2 L_2 - g_2 \boldsymbol{\alpha} \cdot \mathbf{L}_2 + g_3 \beta \boldsymbol{\alpha} \cdot \mathbf{L}'_3; \tag{1}$$

$g_1$, $g_2$ and $g_3$ are the relative scalar, vector and tensor coupling constants, respectively. They are assumed to be real. $L_1$, $L_2$, $\mathbf{L}_2$ and $\mathbf{L}'_3$ are the corresponding lepton covariants. For the relativistic coupling we use [2])

$$\begin{pmatrix} \boldsymbol{\alpha} \cdot \mathbf{L}_2 \\ \beta \boldsymbol{\alpha} \cdot \mathbf{L}'_3 \end{pmatrix} = \frac{i}{2M} \nabla \cdot \begin{pmatrix} \mathbf{L}_2 \\ \mathbf{L}'_3 \end{pmatrix}. \tag{2}$$

A simple calculation gives the result for angular correlations and spectrum as follows:

$$A_F = g_1^2 + g_2^2 \pm 2 g_1 g_2 \frac{1}{W} + \frac{1}{M}\left[ g_2(g_1+g_3)\frac{q}{W} \mp (g_1 g_3 - g_2^2)\frac{p^2}{W} \pm (g_1 g_3 + g_2^2) q \right]$$
$$+ \left\{ \frac{g_2^2 - g_1^2}{W} + \frac{1}{M}\left[ \frac{g_2(g_1+g_3) \mp (g_1 g_3 - g_2^2) q}{W} \pm (g_1 g_3 + g_2^2) \right] \right\} p \cos\theta \tag{3}$$

$$C_F = (g_1^2 + g_2^2) L_0 \pm g_1 g_2 2 P_0$$
$$+ \frac{1}{M}\{ (U P_0 - L_0) g_2 (g_1 - g_3) \mp (U L_0 - P_0)(g_1 g_3 - g_2^2) + 2q(\pm L_0 g_2 + P_0 g_1) g_2 \}. \tag{4}$$

The upper and lower signs refer to the negaton and positon emission

respectively. The meaning of the symbols is the following: $W$ and $p$ are the energy and momentum of the negaton; $q$ is the momentum of the neutrino; $\theta$ is the angle between the two emitted particles; $M$ is the nucleon mass; $L_0$ and $P_0$ are usual [3]) abbrevations for radial wave functions; $U = W - V_c - q$ where $V_c = \mp(\alpha Z/r_0)$ is the Coulomb energy of the emtitted particle taken at the position $r_0$.

## 2. Gamow-Teller Transitions

The interaction Hamiltonian for Gamow-Teller transitions is of the form [1])

$$H'_\beta = -g_2\boldsymbol{\alpha}\cdot\mathbf{L}_2 - g_3\boldsymbol{\sigma}\cdot\mathbf{L}_3 + g_3\beta\boldsymbol{\alpha}\cdot\mathbf{L}'_3 + g_4\boldsymbol{\sigma}\cdot\mathbf{L}_4 - g_4\gamma_5 L_4 + g_5\beta\gamma_5 L_5 . \tag{5}$$

Besides the symbols already explained there are the pseudovector and pseudoscalar coupling constants $g_4$ and $g_5$, respectively, with the corresponding lepton covariants $L_4$, $\mathbf{L}_4$ and $L_5$.

For the relativistic coupling we use [2])

$$\begin{pmatrix}\boldsymbol{\alpha}\cdot\mathbf{L}_2\\ \beta\boldsymbol{\alpha}\cdot\mathbf{L}'_3\end{pmatrix} = -\frac{1}{2M}(\boldsymbol{\sigma}\wedge\boldsymbol{\nabla})\cdot\begin{pmatrix}\mathbf{L}_2\\ \mathbf{L}'_3\end{pmatrix} = \frac{i}{2M}(\boldsymbol{\sigma}\wedge(\mathbf{p}+\mathbf{q}))\cdot a_e^*\begin{pmatrix}1\\ \beta\end{pmatrix}\alpha b_\nu, \tag{6}$$

$$\begin{pmatrix}\gamma_5 L_4\\ \beta\gamma_5 L_5\end{pmatrix} = \frac{i}{2M}\boldsymbol{\sigma}\cdot\boldsymbol{\nabla}\begin{pmatrix}L_4\\ L_5\end{pmatrix} = \frac{1}{2M}\boldsymbol{\sigma}\cdot(\mathbf{p}+\mathbf{q})a_e^*\begin{pmatrix}1\\ \beta\end{pmatrix}\gamma_5 b_\nu; \tag{7}$$

$a_e^*$ and $b_\nu$ are the spin functions of the free negaton and antineutrino.

The angular correlation and the spectrum are

$$\begin{aligned}A_{GT} = {} & g_3^2+g_4^2 \pm g_3 g_4\frac{2}{W} + \frac{1}{3M}\left[\pm(g_3 g_5+2g_2 g_4)\left(q-\frac{p^2}{W}\right)\right.\\ & \left.\pm(g_4^2+2g_3^2)\left(q+\frac{p^2}{W}\right)+(3g_3 g_4+g_4 g_5+2g_2 g_3)\frac{q}{W}\right]\\ & +\left\{(g_3^2-g_4^2)\frac{p}{W}+\frac{1}{M}\left[\pm(g_3 g_5+2g_2 g_4)\left(1-\frac{q}{W}\right)p\right.\right.\\ & \left.\left.\pm(g_4^2+2g_3^2)\left(1+\frac{q}{W}\right)p+(3g_3 g_4+g_4 g_5+2g_2 g_3)\frac{p}{W}\right]\right\}\frac{\cos\theta}{3},\end{aligned} \tag{8}$$

$$\begin{aligned}C_{GT} = {} & (g_3^2+g_4^2)L_0 \pm 2g_3 g_4 P_0 + \frac{1}{3M}[\pm(2g_3^2-2g_2 g_4-g_3 g_5+g_4^2)(UL_0-P_0)\\ & +(3g_3 g_4-2g_2 g_3-g_4 g_5)(UP_0-L_0)\pm(2g_3^2+g_4^2)2qL_0+6g_3 g_4 q P_0].\end{aligned} \tag{9}$$

As in the case of Fermi transitions the upper and lower signs correspond to the negaton and positon transitions, respectively.

### 3. *l*-Forbidden Transitions

Those Gamow-Teller transitions in which the orbital angular momentum change is $\Delta l = \pm 2$ and have large $ft$ values ($\log ft \approx 7.5$) are called the allowed $l$-forbidden transitions [4]). The correction factor is of the form

$$C_{GT_1} = \frac{1}{(2M)^2}\frac{2}{9}|\langle||r^2 T_{12}(\mathbf{r}, \boldsymbol{\sigma})||\rangle_\beta|^2 \frac{1}{r_0^4}\Big\{[g_2^2+g_3^2+g_4^2+g_5^2 - 2(g_2g_4+g_3g_5)]\{[(W-V_c)^2+1]L_0+(6N_0-2P_0)(W-V_c)-6R_0+9M_0\} \pm 2[g_2g_5+g_3g_4-(g_2g_3+g_4g_5)]\{[(W-V_c)^2+1]P_0 + (6R_0-2L_0)(W-V_c)-6N_0-9Q_0\}\Big\}; \quad (10)$$

$T$ is a tensor operator defined by

$$T^{\mu}_{1\Lambda}(\mathbf{r}, \boldsymbol{\sigma}) = \sum_{mm'} (1m'\Lambda m|1\Lambda I\mu) Y_\Lambda{}^m \sigma_1{}^{m'}, \quad (11)$$

where $Y_\Lambda{}^m$ denote the spherical harmonics with the phases as in TAS; $(1m'\Lambda m|1\Lambda I\mu)$ is the Clebsch-Gordan vector addition coefficient, also with the phases as in TAS. $N_0$, $R_0$, $Q_0$ and $M_0$ are abbreviations for linear combinations of the radial functions [3]).

The wave functions of the initial and final nuclear states usually contain some admixtures of $l' = l \pm 2$, so that the transitions with $\Delta l = 0$ [eq. (9)] slowed down with a certain amplitude will compete with the transitions resulting from the correction factor (10). Because of the large $ft$ values the corrections due to the variation of the lepton wave function over the nucleus may also be important [5]).

### 4. Mixed Fermi and Gamow-Teller Transitions

For the allowed transition which is a mixture of Fermi and Gamow-Teller transition we get for the angular correlation and the spectrum the following expressions:

$$N\mathrm{d}W \sin\theta\, \mathrm{d}\theta = \frac{g_\beta^2}{4\pi^3} F(\pm Z, W) pW(W_0-W)^2[A_F|M_F|^2 + A_{GT}|M_{GT}|^2]\, \mathrm{d}W \sin\theta\, \mathrm{d}\theta, \quad (12)$$

$$N\mathrm{d}W = \frac{g_\beta^2}{2\pi^3} F(\pm Z, W) pW(W_0-W)^2[C_F|M_F|^2+C_{GT}|M_{GT}|^2]\, \mathrm{d}W. \quad (13)$$

The mean life or the corrected $ft$ value is obtained by integrating expression (13) over the energy. $F(\pm Z, W)$ is the well known Fermi function. The upper and lower sign of $Z$ refers to the negaton and positon emission respectively. $M_F$ and $M_{GT}$ are the reduced matrix elements defined in the

usual manner. In the case of $l$-forbidden transitions the amplitude of the admixed state has to be taken into account in the second term of the square bracket and the term (10) has to be added.

## 5. Concluding Remarks

From the formulae (3), (4), (8), (9) and (10) it can be seen that the corrections may have some influence on the estimate of the magnitude of the Fierz interference terms [2, 6]) and may provide some additional information on the pseudoscalar coupling constant [7]). Part of the possible deviations of the $l$-forbidden spectrum shapes from the allowed shape [8]) may be perhaps also understood by means of the additional terms (10).

A calculation of the effects of the additional terms on the angular distribution of the electrons from polarized nuclei and an analysis of the experimental material is in preparation [9]). The effect of parity non-conservation on the allowed and some forbidden $\beta$-transitions has recently been studied by several authors [10]) but so far they have neglected the contributions of the relativistic terms to the allowed and $l$-forbidden transitions.

A full account of this work is submitted for publication to the Glasnik Matematičko Fizički i Astronomski.

We would like to acknowlede many helpful and illuminating discussions with Drs V. Glaser and B. Jakšić.

*Note added in proof.*

There is interference between the allowed and $l$-forbidden Gamow-Teller transitions. The cross-terms to be added to the expression (9) for $C_{GT}$ are

$$\frac{2\pi\sqrt{2}}{3M}\left[\langle||T_{10}||\rangle\langle||r^2 T_{12}||\rangle^* + \text{c.c.}\right]\frac{1}{r_0^2}$$
$$\times\Big\{(2g_3g_4 - g_4g_5 - g_3g_2)[(W-V_c)P_0 - L_0 + 3R_0] \qquad (9a)$$
$$\pm(g_4^2 + g_3^2 - g_2g_4 - g_3g_5)[(W-V_c)L_0 - P_0 + 3N_0]\Big\}.$$

The contribution from the other couplings [11]) seem to be smaller, compared to the terms (9) and (9a), by a factor of about $r_0^2/M$.

## References

1) S. R. de Groot and M. A. Tolhoek, Physica **16** (1950) 456;
M. Fierz, Zs. f. Phys. **104** (1937) 553
2) M. E. Rose and R. K. Osborn, Phys. Rev. **93** (1954) 1315;
R. F. Herbst, Phys. Rev. **96** (1954) 372;
H. Takebe, Progr. Theor. Phys. **12** (1954) 561; also ref. [5])

3) J. E. Konopinski and G. E. Uhlenbeck, Phys. Rev. **60** (1941) 308;
M. E. Rose, C. L. Perry amd N. M. Dismuke, ORNL report 1459 (1953);
B. S. Dželepov and L. N. Zerianova, Vlianie electritsheskogo polia atoma na beta-raspad (Akademia Nauk SSSR, Moskva—Leningrad, 1956)
4) L. W. Nordheim, Revs. Mod. Phys. **23** (1951) 322;
M. Brysk, Phys. Rev. **94** (1954) 1794
5) G. Alaga and B. Jakšić, Glasnik Matematičko Fizički i Astronomski **12** (1957) 31
6) O. Kofoed-Hansen and A. Winther, Mat. Fys. Medd. Dan. Vid. Selsk. **27** (1953) no. 14;
H. M. Mahmoud and E. J. Konopinski, Phys. Rev. **88** (1952) 1266;
O. Kofoed-Hansen and A. Winther (preprint 1956)
7) G. Alaga, O. Kofoed-Hansen and A. Winther, Mat. Fys. Medd. Dan. Vid. Selsk. **28** (1953) no. 3;
J. Fujita and M. Yamada, Progr. Theor. Phys. **10** (1953) 518;
G. Alaga and B. Jakšić, Phys. Rev. **103** (1956) 1441;
L. N. Zarianova, Izvestia Akademii Nauk SSSR **20** (1956) 1399;
M. J. Laubitz, Proc. Phys. Soc. A **69** (1956) 789;
G. Alaga, L. Šips and D. Tadić, Glasnik Matematičko Fizički i Astronomski (in the press)
8) F. T. Porter, F. Wagner, Jr. and M. S. Freedman, Bul. Am. Phys. Soc. **2** (1957) 229
9) G. Alaga, L. Šips and D. Tadić (in preparation)
10) L. Landau, Nuclear Physics **3** (1957) 127;
T. D. Lee and C. N. Yang, Phys. Rev. **105** (1957) 1671;
J. D. Jacksson, S. B. Treiman and H. W. Wyld Jr., Nuclear Physics **4** (1957) 206;
M. E. Ebel and G. Feldman, Nuclear Physics **4** (1957) 213;
K. Alder, S. Stech and A. Winther, Phys. Rev. **107** (1957) 728
11) B. C. Carlson and G. B. Heuton, Bull. Am. Phys. Soc. **7** (1957) 358

*Nuclear Physics* **6** (1958) 310—319; © *North-Holland Publishing Co., Amsterdam*
Not to be reproduced by photoprint or microfilm without written permission from the publisher

# ON THE ELASTIC SCATTERING OF PIONS BY DEUTERONS

B. H. BRANSDEN and R. G. MOORHOUSE

*Department of Natural Philosophy, Glasgow University*

Received 28 November 1957

**Abstract:** The elastic scattering of pions by deuterons is calculated for incident pion energies from 85 to 378 MeV. A variational method is employed which includes the effects of multiple scattering. Satisfactory agreement is obtained with experiment. For the pion-deuteron system the multiple scattering corrections turn out to be small but it is suggested that the method presented may be particularly suitable for future applications when multiple scattering effects are not small.

## 1. Introduction

In most calculations of the scattering of pions by deuterons the impulse approximation is taken as a starting point. Fernbach, Green and Watson [1]) formulate the impulse approximation for $\pi$—D scattering; the scattering amplitude is expressed as a linear superposition of free nucleon scattering amplitudes, given in terms of the experimentally determined free nucleon phase shifts. This involves neglecting multiple scattering, the inter-nucleon potential during the scattering, and the fact that the pion-nucleon matrix element in $\pi$—D scattering is off the energy shell of pion-free nucleon scattering. Brueckner [2]) considers the corrections due to multiple scattering and finds a considerable reduction ($\approx$ 50% at 30° and 135 MeV) from the impulse approximation; however his calculation neglects off the-energy-shell parts of pion-nucleon scattering matrix elements. Rockmore [3]) calculates $\pi$—D scattering with the pure impulse approximation, with the inclusion of Coulomb scattering and obtains excellent agreement with the experimental results of Rogers and Lederman [4]) at 85 MeV. Though the pure impulse approximation is in good agreement with experiment Rockmore considers the corrections due to multiple scattering and the internucleon potential. He shows that Brueckner's [2]) neglect of the off-the-energy shell matrix elements in multiple scattering is certainly invalid, but he does not evaluate the multiple scattering correction. From a perturbation calculation the correction due to the inter-nucleon potential is given by Rockmore as $\approx$ 10 % and the contribution of an absorption effect is also discussed.

It is of interest to start from a point of view which is not that of the impulse approximation. Such a starting point is provided by the Schwinger variational method, and the formulation that follows includes effects of

multiple scattering, but not the effects of the inter-nucleon potential during the scattering process (although these effects may be easily calculated by a perturbation procedure, if required; cf. Rockmore [3]). The results are similar to those obtained from the impulse approximation (except in the lower energy region, where the s-state pion-nucleon interaction is comparable with the p-state interaction) and in satisfactory agreement with experiment. In particular in the present paper it is shown explicitly that multiple scattering effects are small and may be neglected. As the multiple scattering effects are evaluated with some simplicity in the present formalism, further applications of the method to processes for which this correction is thought to be large, such as pion-alpha scattering, are intended.

## 2. Formulation of the Method

Experiments on pion-nucleon scattering indicate that the 33 phase shift is large and the other p-wave phase shifts small in the region from 80 MeV to 400 MeV incident pion energy. This being the case, and forgetting for the moment the s-state interaction, it is permissible to take the pion-nucleon interaction as being due to a potential operating on the 3/2, 3/2 state only and still obtain good agreement with experiment. With this assumption the pion-deuteron scattering equation is

$$\left(E-\omega(k)+\frac{1}{2M}\nabla_1^2+\frac{1}{2M}\nabla_2^2-V(\mathbf{r}_1-\mathbf{r}_2)\right)\Psi(\mathbf{r}_1\mathbf{r}_2;\ i\mathbf{k}) = \int\frac{\mathrm{d}^3k'}{(2\pi)^3}H(\mathbf{r}_1\mathbf{r}_2;\ i\mathbf{k};\ i'\mathbf{k}')\,\Psi(\mathbf{r}_1\mathbf{r}_2;\ i'\mathbf{k}') \quad (2.1)$$

where

$$H(\mathbf{r}_1\mathbf{r}_2;\ i\mathbf{k};\ i'\mathbf{k}') = K_{33}(\mathbf{r}_1;\ i\mathbf{k};\ i'\mathbf{k}')+K_{33}(\mathbf{r}_2;\ i\mathbf{k};\ i'\mathbf{k}'). \quad (2.2)$$

In (2.1), (2.2) $E$ is the total energy of the system; $\omega(k) = \sqrt{(1+k^2)}$ is the energy of the pion; $M$ is the nucleon mass; $V(\mathbf{r}_1-\mathbf{r}_2)$ is the inter-nucleon potential; $\mathbf{r}_1$, $\mathbf{r}_2$ are the positions of the two nucleons; $i(=1, 2, 3)$ is the isobaric spin variable of the pion; $\mathbf{k}$ is the momentum of the pion (the spin and isobaric spin variables for the nucleons are not mentioned explicitly). $K_{33}(\mathbf{r}_1;\ i\mathbf{k};\ i'\mathbf{k}')$, for example, is the scattering kernel for the pion being scattered by nucleon 1 at position $\mathbf{r}_1$, the $_{33}$ suffix indicating that this kernel only operates while the pion is in a 3/2, 3/2 state with respect to nucleon 1. The particular form of $K_{33}$ will be given later, but some of the physical significance of eqs. (2.1), (2.2) may readily be seen. Thus pion-deuteron scattering is taken to be due to successive scatterings on the single nucleons, with respect to which the pion is in a 3/2, 3/2 state. So the processes shown in fig. (1a), (b) are taken account of, but not that of fig. 1(c).

Eq. (2.1) is of the form of the familiar scattering equation

$$(E-H_0)\Psi = H'\Psi \tag{2.3}$$

with

$$H_0 = \omega - \frac{1}{2M}\nabla_1^2 - \frac{1}{2M}\nabla_2^2 + V(\mathbf{r}_1-\mathbf{r}_2).$$

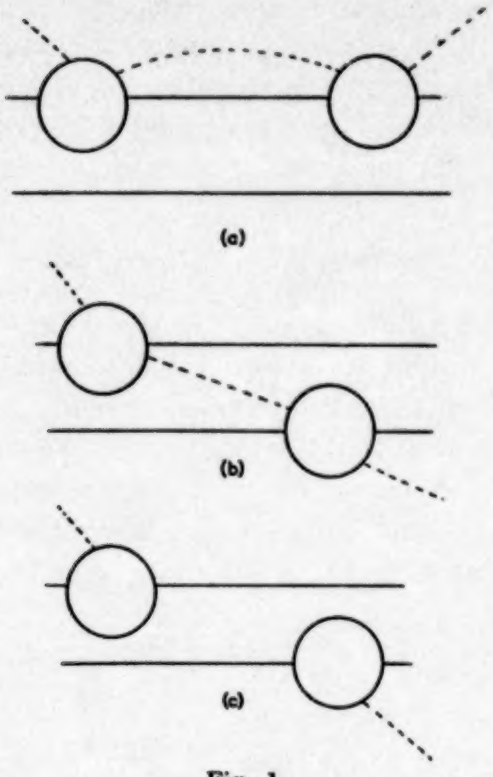


Fig. 1.

A scattering solution of (2.3) is

$$\Psi_a^+ = \phi_a + \frac{1}{E-H_0+i\varepsilon}H'\Psi_a^+ \tag{2.4}$$

where

$$E = E_a \quad \text{and} \quad (E_a-H_0)\phi_a = 0.$$

In the Schwinger variational expression [5, 6] for the transition matrix

$$T_{ba} = \frac{(\Psi_b^{-\prime} H' \phi_a)(\phi_b H' \Psi_a^{+\prime})}{(\Psi_b^{-\prime} H' \Psi_a^{+\prime}) - \left(\Psi_b^{-\prime} H' \frac{1}{E-H_0+i\varepsilon} H' \Psi_a^{+\prime}\right)} \tag{2.5}$$

where $E = E_a = E_b$ and $\Psi_b^{-\prime}$, $\Psi_a^{+\prime}$ are trial functions, we will take $\Psi_b^{-\prime} = \phi_b$, $\Psi_a^{+\prime} = \phi_a$. This simple form of 'trial function' was suggested by Chew [6] for use in the variational expression for the $K$-matrix.

Particularizing to elastic scattering of pions by deuterons (with the pion

making a transition from a state of momentum $\mathbf{k}$, isobaric spin $i$ to one of momentum $\mathbf{k}'$, isobaric spin $i'$, and the deuteron a transition from $z$-component of spin $M$ to $z$-component of spin $M'$) eq. (2.5) becomes with the aforesaid trial functions and neglecting the deuteron recoil

$$T_{\mathbf{k}M,i'\mathbf{k}'M'} = \frac{L^2_{\mathbf{k}M,i'\mathbf{k}'M}}{L_{\mathbf{k}M,i'\mathbf{k}'M'} - N_{\mathbf{k}M,i'\mathbf{k}'M'}} \tag{2.6}$$

where

$$L_{\mathbf{k}M,i'\mathbf{k}'M'} = \int \mathrm{d}^3\mathbf{r}\,\phi_{\mathrm{D}}^*(\mathbf{r}) u_M^+ H(\mathbf{r}_1\mathbf{r}_2; i\mathbf{k}; i'\mathbf{k}') u_{M'}\phi_{\mathrm{D}}(\mathbf{r}), \tag{2.7}$$

$$N_{\mathbf{k}M,i'\mathbf{k}'M'} = \int \frac{\mathrm{d}^3k''}{(2\pi)^3} \int \mathrm{d}^3\mathbf{r}\phi_{\mathrm{D}}^*(\mathbf{r}) u_M^+ H(\mathbf{r}_1\mathbf{r}_2; i\mathbf{k}; i''\mathbf{k}'')$$
$$\left(E + \frac{1}{M}\nabla_r^2 - \omega(k'') - V(r) + i\varepsilon\right)^{-1} H(\mathbf{r}_1\mathbf{r}_2; i''\mathbf{k}''; i'\mathbf{k}') u_{M'}\phi_{\mathrm{D}}(\mathbf{r}). \tag{2.8}$$

In eqs. (2.6)—(2.8) a factor $\delta$ (total momentum) has been omitted as it disappears in the final evaluation of the cross-section. $\mathbf{r} = \mathbf{r}_1 - \mathbf{r}_2$, $\phi_{\mathrm{D}}(\mathbf{r})$ is the configuration space part of the deuteron wave function and $u_M$ is the spin-isobaric spin part of the deuteron wave function.

The eqs. (2.6)—(2.8) are indefinite until an explicit form for $H$ or its components $K_{33}$ has been fixed. In the fixed source pseudoscalar meson theory the first Tamm-Dancoff equation for the scattering of a pion by a nucleon situated at $\mathbf{r}_1$ is

$$\left(E - \omega(k) + \frac{1}{2M}\nabla_1^2\right)\Psi(\mathbf{r}_1 i\mathbf{k})$$
$$= 4\pi f^2 \int^{k_m} \frac{\mathrm{d}^3k'}{(2\pi)^3 2\sqrt{\omega(k)\omega(k')}} \left[\frac{(\boldsymbol{\sigma}_1\cdot\mathbf{k}')(\boldsymbol{\sigma}_1\cdot\mathbf{k})\tau_{1i'}\tau_{1i}}{E - \omega(k) - \omega(k')}\right. \tag{2.9}$$
$$\left. + \frac{(\boldsymbol{\sigma}_1\cdot\mathbf{k})(\boldsymbol{\sigma}_1\cdot\mathbf{k}')\tau_{1i}\tau_{1i'}}{E} \mathrm{e}^{i(\mathbf{k}'-\mathbf{k})\cdot\mathbf{r}_1}\right]\Psi(\mathbf{r}_1, i'\mathbf{k}')$$

where the source function has a square cut-off in momentum space at momentum $|\mathbf{k}| = k_{\mathrm{m}}$ and the nucleon energy has been neglected in the energy denominators on the right hand side. Since the scattering in the energy range 80—400 MeV is predominantly in the 3/2, 3/2 state it is permissible to replace the kernel on the right hand side in eq. (2.9) by that part of it which only operates when the pion is in a 3/2, 3/2 state with respect to the nucleon situated at $\mathbf{r}_1$. The only part of (2.9) that contributes is the first, or cross-over, term in the square brackets. Eq. (2.9) is replaced by

$$\left(E - \omega(k) + \frac{1}{2M}\nabla_1^2\right)\Psi(\mathbf{r}_1, i\mathbf{k}) = \int^{k_m} \frac{\mathrm{d}^3k'}{(2\pi)^3} K_{33}(\mathbf{r}_1; i\mathbf{k}; i'\mathbf{k}')\Psi(\mathbf{r}_1, i'\mathbf{k}') \tag{2.10}$$

and it is found that $K_{33}$ is given by

$$K_{33}(\mathbf{r}_1;\ i\mathbf{k};\ i'\mathbf{k}')$$
$$=\sum_{i''}\int\frac{\mathrm{d}(\cos\Theta'')\mathrm{d}\Phi''}{2\sqrt{\omega(k)\omega(k')}}\left(\frac{(\boldsymbol{\sigma}_1\cdot\mathbf{k}'')(\boldsymbol{\sigma}_1\cdot\mathbf{k})\tau_{1i''}\tau_{1i}}{E-\omega(k)-\omega(k')}\right)P(\Theta''\Phi'',\Theta'\Phi')Q(i'',i')\mathrm{e}^{i(\mathbf{k}''-\mathbf{k})\cdot\mathbf{r}_1} \tag{2.11}$$

where $\mathbf{k}'=(k',\ \Theta',\ \Phi')$, $\mathbf{k}''=(k',\ \Theta'',\ \Phi'')$, and $P$, $Q$ are projection operators given by

$$P=\frac{1}{k'^2}\,\frac{3}{4\pi}\,(\mathbf{k}''\cdot\mathbf{k}'-\tfrac{1}{3}(\boldsymbol{\sigma}'\cdot\mathbf{k}'')(\boldsymbol{\sigma}\cdot\mathbf{k}'))$$
$$Q=(\delta_{i''i'}-\tfrac{1}{3}\tau_{i''}\tau_{i'}).$$

With $K_{33}$ defined by (2.11) one might proceed to solve the pion-nucleon scattering eq. (2.10) by the usual method of splitting $\Psi$ into partial waves. All phase shifts except the 3/2, 3/2 one are zero and the 3/2, 3/2 phase shift can be found by taking the Schwinger variational expression for the $K$-matrix in pion-nucleon scattering that corresponds to the expression (2.5) for the $T$-matrix. This then gives complete equivalence to the variational method of Cini and Fubini [7]) as applied by Sartori and Wataghin [8]) to the p-wave scattering. Instead of doing this the expression (2.5) is taken for the $T$-matrix in pion-nucleon scattering with the scattering eq. (2.10), and then the cross section is written down from the $T$-matrix. We found that a small change in the values of the coupling constant and the cut-off (from the values got using the Cini-Fubini $K$-matrix method) gave the correct position and height of the resonance. The values of cut-off and coupling constant found are

$$\omega_{\mathrm{m}}=\sqrt{(1+k_{\mathrm{m}}^2)}=6.8,\quad f^2=0.09.$$

With these values the kernel $K_{33}$ given by (2.11) is substituted in the pion-deuteron scattering eq. (2.1), (2.2). The transition matrix for elastic pion-deuteron scattering can then be found from eqs. (2.6)—(2.8). The results are given in the next section.

## 3. Evaluation and Results

We consider the elastic scattering of $\pi^+$ pions by deuterons as recent experimental results [4]) exist for this case. The $\pi^-$scattering is the same except for the Coulomb interference term. We take the incoming pions along the $z$-axis and consider the scattering into an angle $\Theta'$, $\Phi'$. Thus $\mathbf{k}=(k,\ 0,\ 0)$, $\mathbf{k}'=(k,\ \Theta',\ \Phi')$ (neglecting deuteron recoil) and eq. (2.6) can be written

$$T_{M,M'}(\Theta'\Phi')=\frac{L^2_{M,M'}(\Theta'\Phi')}{L_{M,M'}(\Theta'\Phi')-N_{MM'}(\Theta'\Phi')} \tag{3.1}$$

with

$$L_{MM'}(\Theta'\Phi')$$
$$= -\frac{32\pi f^2 k^2}{9\,\omega^2(k)}\phi_D{}^2\left(\frac{\mathbf{k}'-\mathbf{k}}{2}\right)Y_{1,M'-M}(\Theta'\Phi')(1+\delta_{MM'})\sqrt{\frac{4\pi}{3}} \quad \text{for} |M-M'|\leqq 1 \quad (3.2)$$
$$L_{MM'}(\Theta',\ \Phi') = 0 \qquad \text{for} |M-M'| = 2,$$

$$N_{MM'}(\Theta'\Phi') = -\frac{4f^2\omega(k)}{3\pi}I(\mathbf{k})L_{MM'}(\Theta'\Phi')$$
$$+\frac{f^4k^2}{\omega(k)}\frac{128}{243}\sqrt{\frac{4\pi}{3}}\Big[Y_{1,M'-M}(\Theta'\Phi')(1-\delta_{MM'})(I_2(\mathbf{k})-I_0(\mathbf{k}))$$
$$+\delta_{M0}\delta_{M'0}\left\{Y_{1,0}(\Theta'\Phi')(I_0(\mathbf{k})-\tfrac{1}{4}I_2(\mathbf{k}))+\tfrac{3}{4}\sqrt{\frac{3}{4\pi}}I_2(\mathbf{k})\right\}\Big] \text{ for } |M-M'|\leqq 1 \quad (3.3)$$
$$N_{MM'}(\Theta'\Phi') = \frac{f^4k^2}{\omega(k)}\frac{64}{81}(1+\cos\Theta')e^{(M'-M)i\Phi'}I_2(\mathbf{k}) \qquad \text{for } |M-M'|=2.$$

In these expressions

$$\phi_D{}^2\left(\frac{\mathbf{k}'-\mathbf{k}}{2}\right) = 4\pi\int r^2\,dr\,\phi_D{}^2(\mathbf{r})\,e^{i\frac{\mathbf{k}'-\mathbf{k}}{2}\cdot\mathbf{r}}$$

$$I(\mathbf{k}) = \int_0^{k_m}\frac{p^4\,dp}{\omega^3(p)(\omega(k)-\omega(p))}$$

$$I_l(\mathbf{k}) = 4\pi\int_0^{k_m}dp\int_0^{\infty}dr\,\frac{j_l\left(\left|\frac{\mathbf{k}+\mathbf{k}'}{2}\right|r\right)j_l(pr)p^4\phi_D{}^2(\mathbf{r})r^2}{\omega^3(p)(\omega(k)-\omega(p))} \qquad (l=0,\ 2).$$

The deuteron wave function is taken to be

$$\phi_D(\mathbf{r}) = N\frac{e^{-\alpha r}-e^{-\beta r}}{r} \quad (3.4)$$

where $N$ is a normalization constant and [9]) $\alpha = 0.237 \cdot 10^{13}$ cm$^{-1}$, $\beta = 1.55\times 10^{13}$ cm$^{-1}$. $L_{MM'}$ in eq. (3.1) comes from a single scattering process by the kernel or potential $K_{33}$, $N_{MM'}$ in the same equation comes from a repeated scattering; the first term on the right hand side of (3.3) corresponds to the process shown in fig. 1(a), a double scattering on the same nucleon; all the other terms in $N_{MM'}$ correspond to fig. 1(b) and thus represent an effect of multiple scattering. Evaluation of the integrals $I_0(\mathbf{k})$, $I_2(\mathbf{k})$ shows that inclusion of these terms alters the cross section by less than 5 % even at the most favourable angles and energies in the energy range considered. The smallness of the multiple scattering terms compared with those involving one nucleon only is due to the high momentum tail of the deuteron wave function (3.4). (If one were considering the scattering by helium where the high momentum tail is probably not present, multiple

scattering might contribute appreciably at backward angles.) The smallness of the multiple scattering terms is a justification of the impulse approximation assumption that they can be neglected. Evaluating (3.1) without them we get

$$T_{MM'}(\Theta'\Phi') = L_{MM'}(\Theta'\Phi')\left[1+\frac{4f^2}{3\pi}\omega(k)I(k)\right]^{-1}.$$

The differential cross section is

$$\frac{\mathrm{d}\sigma}{\mathrm{d}\Omega'} = \tfrac{1}{3}\sum_{MM'}|T_{MM'}(\Theta'\Phi')|^2\frac{\omega^2(k)}{4\pi^2\left(1+\dfrac{\omega(k)}{2M}\right)^2}.$$

In table 1 is given the resultant differential cross section in millibarns per steradian at various pion energies in the laboratory system. The figure in brackets in the 30° column is the differential cross section including the Coulomb correction; for higher angles the Coulomb correction is negligible.

TABLE 1

| Pion energy (MeV) \ Angle | 0° | 30° | 60° | 90° | 120° | 150° | 180° |
|---|---|---|---|---|---|---|---|
| 85 | 8.48 | 5.22(4.31) | 1.41 | 0.35 | 0.50 | 0.79 | 0.90 |
| 146 | 18.63 | 9.33(8.90) | 1.73 | 0.33 | 0.39 | 0.55 | 0.61 |
| 221 | 16.65 | 6.02(5.95) | 0.78 | 0.11 | 0.10 | 0.14 | 0.15 |
| 298 | 10.44 | 2.72(2.72) | 0.25 | 0.03 | 0.02 | 0.03 | 0.03 |
| 378 | 6.77 | 1.24(1.24) | 0.08 | 0 | 0 | 0 | 0 |

These calculated values are in agreement with the $\pi^+$ experimental results of Rogers and Lederman [4]) at 85 MeV and also with the earlier $\pi^-$ experiment of Arase *et al.* [10]) at 140 MeV. In a calculation for 85 MeV pion energy using the impulse approximation Rockmore [3]) gets agreement with the experimental results; however in an earlier impulse approximation calculation for 140 MeV pion energy Green [11]) obtains a markedly too large cross section to give agreement with experiment.

## 4. Inclusion of the s-State Interaction

So far we have ignored the fact that a pion interacts with a nucleon when the two are in a mutual s-state as well as when they are in a p-state. This neglect of the s-state interaction appears reasonable in the energy region 80—400 MeV incident pion energy for which our calculations have been done; in this region pion-nucleon scattering data indicate that the $p_{3/2,\,3/2}$ interaction is dominant. We have verified that our neglect of s-state interaction in pion-deuteron scattering was justified by the calculation

outlined below. This calculation was explicitly performed for 85 MeV pion energy. Above this energy we should expect our result on the unimportance of s-waves to be true *a fortiori* but below it, as the magnitude of the p-wave interaction decreases fast, we should expect that s-state interaction is important.

In pion-nucleon s-wave scattering the (unknown) interaction Hamiltarian is sometimes simulated by the static non-local interaction

$$H_s = g\int \varrho(x)\varrho(x')\boldsymbol{\phi}(x)\cdot\boldsymbol{\phi}(x')\mathrm{d}x\,\mathrm{d}x' + \lambda\int \varrho(x)\varrho(x')\,\boldsymbol{\tau}\cdot(\boldsymbol{\phi}(x)\times\boldsymbol{\pi}(x'))\mathrm{d}x\,\mathrm{d}x' \tag{4.1}$$

where bold type denotes a vector in isobaric spin space and $\varrho(x)$ is a source function. Lomon [12]) has given an exact solution for this theory.

We consider s-wave pion-nucleon scattering by writing down the first Tamm-Dancoff from the interaction (4.1) (with the source function corresponding to a square cut-off in momentum space at $\omega_m = 6.8$ as in § 2) and solve using the variational expression (2.5). This enables us to fit $g$, $\lambda$ to the s-phase shifts at 85 MeV as given by Orear [13]). The results are $g = -0.268$, $\lambda = 0.192$. It can be shown [14]) that for these coupling constants this method of solution gives a very good approximation to the exact solution.

With these coupling constants we add the kernel of the s-wave Tamm-Dancoff equation to the p-wave kernel $K_{33}$ in the pion-deuteron scattering equation. The resultant pion-deuteron scattering equation was solved using the variational expression (2.5) as usual. It was found that the contribution of s-wave scattering at 85 MeV is $< 10\,\%$, and thus has no significant effect on the comparison with experiment.

## 5. Conclusion

For this calculation of pion-deuteron scattering the coupling constants and cut-off for the 3/2, 3/2 pion-nucleon interaction have been chosen using a variational expression for the solution of the scattering equation. With the pion-nucleon interaction thus fixed and put in the pion-deuteron scattering equation, a calculation with the same variational expression gives agreement with the experimental results on elastic scattering of negative pions at 85 MeV and 140 MeV. Impulse approximation methods have formerly gained agreement with experiment at 85 MeV [3]) but disagreement at 140 MeV [11]). However we have shown that multiple scattering can be neglected (disagreeing with a result of Brueckner [3])) and this being the case our calculation is formally identical to an impulse approximation calculation in which the transition matrix for pion-nucleon scattering is calculated

using (2.5), with the pion-nucleon interaction taking place in the 3/2, 3/2 state only.

With the introduction of s-state pion-nucleon interaction any formal identity with an impulse approximation calculation is destroyed. At 85 MeV, and *a fortiori* above, the s-state interaction contributes $< 10\,\%$ to elastic pion-deuteron scattering. Below 80 MeV it should be important, and moreover the method of this paper will give a significant difference from any impulse approximation result. However at such small energies our assumption that the 3/2, 3/2 part of the p-state interaction is dominant is in great doubt. Calculations using the full p-state interaction and the above formulation (using a suitable renormalization procedure) have indicated that the trial functions employed are inadequate for an accurate solution. In the energy region (below $\approx$ 80 MeV) where it is important to use the full interaction, it may be possible to improve the trial functions, or alternatively direct approximate numerical solutions of the scattering eqs. (2.2) may be attempted. The latter approach is difficult for pion-deuteron scattering as different partial waves are coupled, but it is intended to explore this method for pion-alpha scattering where the angular momentum of the incident pion is a constant of motion and equations for different $l$ are uncoupled.

## References

1) S. Fernbach, T. A. Green and K. M. Watson, Phys. Rev. **84** (1951) 1084
2) K. A. Brueckner, Phys. Rev. **89** (1953) 834; **90** (1953) 715
3) R. M. Rockmore, Phys. Rev. **105** (1957) 256
4) K. C. Rogers and L. M. Lederman, Phys. Rev. **105** (1957) 247
5) B. A. Lippmann and J. Schwinger, Phys. Rev. **79** (1950) 469
6) G. F. Chew, Phys. Rev. **93** (1954) 341
7) M. Cini and S. Fubini, Nuovo Cimento **11** (1954) 142
8) L. Sartori and V. Wataghin, Nuovo Cimento **12** (1954) 145
9) G. F. Chew and M. L. Goldberger, Phys. Rev. **77** (1950) 474
10) E. Arase, G. Goldhaber and S. Goldhaber, Phys. Rev. **90** (1953) 160
11) T. A. Green, Phys. Rev. **90** (1953) 161
12) E. L. Lomon, Nuovo Cimento **4** (1956) 106
13) J. Orear, Nuovo Cimento **4** (1956) 856
14) B. H. Bransden and R. G. Moorhouse, Nuovo Cimento **6** (1957) 693

*Nuclear Physics* **6** (1958) 319—322; © *North-Holland Publishing Co., Amsterdam*
Not to be reproduced by photoprint or microfilm without written permission from the publisher

# POLARIZATION OF THE RECOIL NUCLEUS IN $\mu^-$-CAPTURE

THOMAS FULTON
*The Johns Hopkins University, Baltimore, Maryland* †

Received 6 January 1958

**Abstract:** The complete expression is calculated for the allowed, non-relativistic transition rate of $\mu^-$-capture from the atomic K-shell. It is used to obtain the expression for the polarization of the recoil nucleus. As is well known, the polarization term governs the asymmetry in the subsequent beta decay. If the incident $\mu$ are unpolarized, the polarization of the recoil following $\mu$-capture in a Gamow-Teller transition can in principle distinguish between the coupling constants suggested by Lee and Yang [7]) and by Feynman and Gell-Mann [8]).

Suggestions have recently been made [1, 2]) †† for using the capture process $\mu^- + C^{12} \rightarrow B^{12} + \nu$ and the subsequent beta decay of $B^{12}$ to study the coupling types involved in $\mu^-$-capture. Some of the experimental difficulties connected with the problem, such as the depolarization of the $\mu^-$ and of the recoil $B^{12}$ and the possibility of capture from and transitions to excited states have also been discussed [1]). Suffice it to say here that these problems make the experiment difficult but not impossible to perform. The short half life ($\approx 0.025$ sec) and high beta end point (13.4 MeV) of $B^{12}$ somewhat alleviate these difficulties.

Different terms in the recoil distribution, as well as the polarization of the recoil have been calculated by various authors [1, 2, 3, 4]). The aim of this note is to present a complete calculation and explore some conclusions to be drawn from the expressions obtained.

The distribution of the recoil nucleus for a specific final spin orientation, and an allowed, non-relativistic, transition is given by †††

$$w \approx (2\pi)^{-2} M M^\dagger p^2 m (p+m)^{-1} \mathrm{d}\Omega, \tag{1}$$

where

$$MM^\dagger = \tfrac{1}{4}(\mu\alpha)^3\{\mathscr{A} + \mathscr{B}\langle\boldsymbol{\sigma}\rangle\cdot\hat{\mathbf{p}} + \mathscr{C}\mathbf{J}\cdot\hat{\mathbf{p}} + \mathscr{D}\mathbf{J}\cdot\langle\boldsymbol{\sigma}\rangle + \mathscr{E}\hat{\mathbf{p}}\cdot(\langle\boldsymbol{\sigma}\rangle\times\mathbf{J}) + \mathscr{F}[(\hat{\mathbf{j}}\cdot\langle\boldsymbol{\sigma}\rangle)(\hat{\mathbf{j}}\cdot\hat{\mathbf{p}}) - \tfrac{1}{3}(\langle\boldsymbol{\sigma}\rangle\cdot\hat{\mathbf{p}})][J(J+1) - 3(\mathbf{J}\cdot\hat{\mathbf{j}})^2]\}. \tag{2}$$

† Supported in part by the U.S. Air Force through the Air Force Office of Scientific Research of the Air Research and Development Command under Contract No. AF 18(603)—143.

†† The latter work was called to the author's attention after completion of the present calculation.

††† The notation used below is similar to, but not identical with that used in ref. [4]).

In the above expression, we set $\hbar = c = 1$. The symbol $\alpha$ is the fine structure constant, $\mu$ the effective mass of the meson in the initial nucleus, $p$ and $m$ respectively the magnitudes of the momentum and mass of the recoil nucleus, $\langle \sigma \rangle$ the polarization of the mu meson, **J** the spin vector of the outgoing nucleus, $\hat{\mathbf{j}}$ a unit vector in the direction $\langle \mathbf{J} \rangle$ and $\hat{\mathbf{p}}$ a unit vector in the direction of the recoil nucleus.

We define the auxiliary quantities

$$\gamma_{JJ'} = \begin{cases} [(J+1)(2J+3)]^{-1} & J+1 \to J \\ -[J(J+1)]^{-1} & J \to J \\ [J(2J-1)]^{-1} & J-1 \to J, \end{cases} \tag{3}$$

$$\varkappa_{JJ'} = \begin{cases} -[J+1]^{-1} & J+1 \to J \\ [J(J+1)]^{-1} & J \to J \\ J^{-1} & J-1 \to J, \end{cases} \tag{4}$$

and

$$\varepsilon = \delta_{JJ'} |M_{\mathrm{F}}| \, |M_{\mathrm{GT}}| / \sqrt{J(J+1)}, \tag{5}$$

where $J$ is the spin of the nucleus after mu capture and $J'$ is the spin of the initial nucleus. The constants $\mathscr{A}, \ldots, \mathscr{F}$ can now be expressed as functions of the mu decay coupling constants $G$ and of the auxiliary quantities $\gamma$, $\varkappa$ and $\varepsilon$:

$$\mathscr{A} = |M_{\mathrm{F}}|^2 (|G_{\mathrm{S}}+G_{\mathrm{V}}|^2 + |G'_{\mathrm{S}}+G'_{\mathrm{V}}|^2) + |M_{\mathrm{GT}}|^2 (|G_{\mathrm{T}}+G_{\mathrm{A}}|^2 + |G'_{\mathrm{T}}+G'_{\mathrm{A}}|^2), \tag{6a}$$

$$\mathscr{B} = 2 \,\mathrm{Re}\, \{|M_{\mathrm{F}}|^2 (G_{\mathrm{S}}+G_{\mathrm{V}})(G'_{\mathrm{S}}+G'_{\mathrm{V}})^* - \tfrac{1}{3} |M_{\mathrm{GT}}|^2 (G_{\mathrm{T}}+G_{\mathrm{A}})(G'_{\mathrm{T}}+G'_{\mathrm{A}})^*\}, \tag{6b}$$

$$\mathscr{C} = 2 \,\mathrm{Re}\, \{\varepsilon [(G_{\mathrm{S}}+G_{\mathrm{V}})(G'_{\mathrm{A}}+G'_{\mathrm{T}})^* + (G'_{\mathrm{S}}+G'_{\mathrm{V}})(G_{\mathrm{T}}+G_{\mathrm{A}})^*] - \varkappa_{JJ'} |M_{\mathrm{GT}}|^2 (G_{\mathrm{T}}+G_{\mathrm{A}})(G'_{\mathrm{T}}+G'_{\mathrm{A}})^*\}, \tag{6c}$$

$$\mathscr{D} = 2\varepsilon \,\mathrm{Re}\, \{(G_{\mathrm{S}}+G_{\mathrm{V}})(G_{\mathrm{T}}+G_{\mathrm{A}})^* + (G'_{\mathrm{S}}+G'_{\mathrm{V}})(G'_{\mathrm{T}}+G'_{\mathrm{A}})^*\} + \varkappa_{JJ'} |M_{\mathrm{GT}}|^2 (|G_{\mathrm{T}}+G_{\mathrm{A}}|^2 + |G'_{\mathrm{T}}+G'_{\mathrm{A}}|^2), \tag{6d}$$

$$\mathscr{E} = 2\varepsilon \,\mathrm{Im}\, \{(G_{\mathrm{S}}+G_{\mathrm{V}})(G'_{\mathrm{T}}+G'_{\mathrm{A}})^* + (G'_{\mathrm{S}}+G'_{\mathrm{V}})(G_{\mathrm{T}}+G_{\mathrm{A}})^*\}, \tag{6e}$$

$$\mathscr{F} = 2 \, |M_{\mathrm{GT}}|^2 \gamma_{JJ'} \,\mathrm{Re}\, \{(G_{\mathrm{T}}+G_{\mathrm{A}})(G'_{\mathrm{T}}+G'_{\mathrm{A}})^*\}. \tag{6f}$$

We have also calculated relativistic corrections for the special case of mu absorption by the proton. Their effect is to add terms bilinear in the coupling constants and proportional to $p(m+E)^{-1}$ ($\approx 10\,\%$) to all the coefficients $\mathscr{A}$ to $\mathscr{E}$ ($\mathscr{F}$ vanishes for the process $\mu^- + \mathrm{p} \to \mathrm{n} + \nu$). In addition, there is a term bilinear in the coupling constants which is proportional to $p(m+E)^{-1} (\hat{\mathbf{p}} \cdot \langle \sigma \rangle)(\hat{\mathbf{p}} \cdot \mathbf{J})$.

The magnitude of relativistic corrections is quite small even for light nuclei and is of the order of 1 % of the contributions to be expected from matrix elements from forbidden transitions †.

The recoil distribution, eq. (2), can be used to obtain the expectation

† Due to the large recoil momenta involved, the definition of what is meant by a forbidden transition becomes somewhat ambiguous. This problem is briefly discussed in ref. [1]).

value of the recoil spin:

$$\langle \mathbf{J} \rangle = \frac{\mathrm{tr}\, MM^{\dagger}\, \mathbf{J}}{\mathrm{tr}\, MM^{\dagger}} = \tfrac{1}{3}J(J+1)\, \frac{\mathscr{C}\hat{\mathbf{p}} + \mathscr{D}\langle \boldsymbol{\sigma} \rangle + \mathscr{E}(\hat{\mathbf{p}} \times \langle \boldsymbol{\sigma} \rangle)}{\mathscr{A} + \mathscr{B}\langle \boldsymbol{\sigma} \rangle \cdot \hat{\mathbf{p}}} \tag{7}$$

The angular distribution of electrons arising from the decay of the recoil nucleus has the well known form [6, 5])

$$I(\theta)\mathrm{d}\theta = \mathrm{const}\, [1 + \chi \langle \mathbf{J} \rangle \cdot (\mathbf{q}/E_e)] \sin\theta\, \mathrm{d}\theta, \tag{8}$$

where $\theta$ is the angle between the direction of polarization of the recoil nucleus (i.e. the nucleus which subsequently beta decays) and the outgoing electron. $\chi$ is defined by the equation

$$\chi = A[1 + b(m_e/E_e)]^{-1}. \tag{9}$$

$A$ and $b$ above are defined in ref [5]) and $q$, $m_e$ and $E_e$ are respectively the momentum, mass and energy of the electron.

One can observe that only for unpolarized incident $\mu$—s is the direction of polarization of the recoil in the direction of recoil momentum. In the more general case, it is neither in the direction of the recoil nor in the direction of mu polarization. This difference in the direction of the axis of symmetry of the electron distribution for the case of unpolarized and polarized incident mu mesons, if detectable, is perhaps an experimentally convenient characteristic of the mu capture process.

If the incident mu meson is unpolarized and only a Gamow-Teller transition is allowed by the selection rules, the $\langle \mathbf{J} \rangle$ of the recoil after mu capture is given by

$$\langle \mathbf{J} \rangle = \mp \tfrac{1}{3}J\hat{\mathbf{p}} \qquad \text{for } J+1 \to J, \tag{10}$$

and

$$\langle \mathbf{J} \rangle = \pm \tfrac{1}{3}(J+1)\hat{\mathbf{p}} \qquad \text{for } J-1 \to J.$$

The upper signs arise from the choice of coupling constants [7]) $G_T = -G'_T$, $G_A = G'_A = 0$, and the lower signs from the choice [8]) $G_T = G'_T = 0$, $G_A = G'_A$.

Finally if the same set of couplings and relative signs (but not necessarily magnitudes) are chosen for the beta coupling as for the mu coupling, the angular distribution of electrons for the above described case is given by

$$I(\theta)\mathrm{d}\theta \propto (1 + \alpha \cos\theta) \sin\theta\, \mathrm{d}\theta,$$

where

$$\alpha = \mp \tfrac{1}{3}[(J+1)/J](q/E_e) \text{ for } J-1 \to J \to J-1,$$

and

$$\alpha = \mp \tfrac{1}{3}[J/(J+1)](q/E_e) \text{ for } J+1 \to J \to J+1.$$

The author would like to thank G. Feldman and L. Madansky for helpful discussions.

## References

1) J. D. Jackson, S. B. Treiman and H. W. Wyld, Jr., Phys. Rev. **107** (1957) 327
2) S. B. Treiman, to be published
3) K. Huang, C. N. Yang and T. D. Lee, to be published
4) I. S. Shapiro, E. I. Dolinsky and L.D. Blokhintsev, Nuclear Physics **4** (1957) 273
5) M. E. Ebel and G. Feldman, Nuclear Physics **4** (1957) 213; J. D. Jackson, S. B. Treiman and H. W. Wyld, Jr., Nuclear Physics **4** (1957) 206
6) T. D. Lee and C. N. Yang, Phys. Rev. **104** (1956) 254
7) T. D. Lee and C. N. Yang, Phys. Rev. **105** (1957) 1671
8) R. Feynman and M. Gell-Mann, Phys. Rev. **109** (1958) 193

*Nuclear Physics* **6** (1958) 323—324; © *North-Holland Publishing Co., Amsterdam*

# BOOK REVIEWS

O. R. FRISCH (Editor), *Progress in nuclear physics*, volume 6 (Pergamon Press, London &c. 1957. vii—297 pages. 84 s.)

The present volume of this well-known series maintains the high standard set by the preceding ones. The editor has made a happy choice of the topics presenting the greatest novelty or usefulness at the moment, and secured the collaboration of some of the best specialists for the preparation of the survey articles which compose the volume. For some reason he has not extended his attention to the actual arrangement of the articles, which follow each other in a perfectly haphazard sequence. Here they are:

T. F. Johns (Harwell) on isotope separation
R. J. Eden (Cambridge) on nuclear models
K. F. Smith (Cambridge) on nuclear moments and spins
M. B. Stearns (Pittsburgh) on mesic atoms
H. E. Duckworth (Hamilton) on nuclear masses $> 40$
M. L. Smith (Harwell) on isotope enrichment
G. N. Walton (Harwell) on fission recoil
J. Mattauch and F. Everling (Mainz) on nuclear masses $< 40$
O. R. Frisch (Cambridge) and T. H. R. Skyrme (Harwell) on parity non-conservation.

The articles, while packed with data and references, are rather intended for quick orientation; they do not duplicate the more ponderous expositions of the same topics appearing, for instance, in the Encyclopedia of Physics or in special treatises such as Kopfermann's *Kernmomente*. There *is*, however, some duplication with articles of much the same scope and style published in other collections: Annual Reviews of Nuclear Science, Reports on progress in physics, Reviews of modern physics, to mention only a few written in English. To these must be added the published proceedings of numerous specialized conferences, which often contain excellent up-to-date reports of topical problems. Moreover, the two newly started series of monographs, Interscience Tracts and Oxford Library of the Physical Sciences, are providing again other surveys of similar character in what I think is a better form: the isolated, handy monograph. One has the uneasy feeling that the production of survey articles is approaching a state of chaos: a great amount of able, but unco-ordinated effort is being wasted in the name of I don't know what "freedom", a freedom which looks too much like anarchy.

L. R.

H. HINTENBERGER (Editor), *Nuclear masses and their determination* (Pergamon Press, London &c. 1957. ix-267 pages. 84 s.)

This book contains the full proceedings (text of contributions and main points of discussions) of the Conference on nuclear masses held at Mainz in July 1956. With regard to the contents, it will suffice to refer the reader to the report of this conference written by H. A. Wapstra for this journal (**2**(1956/57)286). Although the contributions now collected in book form are highly technical and do not aim (except one or two) at surveying the field, the book will be very useful (and presumably remain so for some time, in spite of the rapid rate of progress) to all workers in nuclear physics. It is true that one looks in vain for the nice table of nuclear masses which one would naively expect from such an array of experts; we are only told how difficult it is to make one. But in the various articles many comparative

data about binding energies, $Q$ values, etc. are disseminated, which it would not be easy to find elsewhere. Since the presence of these tables or graphs is not always apparent from the titles of the articles, an index would have been convenient. It is also to be regretted that the legibility of many graphs is impaired by excessive reduction. Apart from such minor points, the reader is well served — but at what a price!

L. R.

*Nuclear Physics* **6** (1958) 325—328; © *North-Holland Publishing Co., Amsterdam*

# NEWS ITEMS

## THE 1958 ANNUAL INTERNATIONAL CONFERENCE ON HIGH ENERGY PHYSICS AT CERN

### (Geneva, June 30-July 5, 1958)

1. *Introduction*

Following the invitation issued at the Seventh Annual Conference (Rochester 1957) and the deliberations at the June (1957) Session of the CERN Council, the next "Rochester" Conference (Eighth Annual) will be held in Geneva during the period June 30—July 5, 1958. The Organization Committee set up at CERN and responsible for organizing the Conference, consists of Bakker (Chairman); Bernardini, Ferretti, Gentner, Kowarski, Tièche, Weisskopf (members); Prentki (scientific secretary).

Advice has been obtained from a European Advisory Committee (membership: the CERN Scientific Policy Committee, Amaldi, Butler, Levy, Peierls), from a U.S. Advisory Committee (membership: Alvarez, Marshak, Panofsky, Oppenheimer, Sachs, Wick) and from prominent USSR scientists (Tamm, Veksler).

2. *Outline of the Organization*

For the 1958 Annual Conference, we propose a somewhat different procedure for presenting the material, since the previous conferences have often suffered from an unorganized array of short communications.

As the enclosed programme shows, the field is divided into ten subdivisions, each of which should be treated in one half day session. All contributions in a given field should be presented by one person: the Rapporteur. It is he who introduces the subject, presents and explains the work of the contributors who have submitted their contributions to the conference. We assume there will also be some contributions from contributors who will not participate in the conference. The talk of the Rapporteur will take up half the session. An equal period of time will be allotted to the discussion and, if necessary, the Chairman will give the contributors, or their representatives, the opportunity of criticizing the presentation and conclusions, or of drawing attention to major points that may have been omitted. For some sessions two Rapporteurs have been proposed, each reporting one quarter of a session, followed by an equal period of discussion.

With such a procedure a great responsibility rests upon the Rapporteur and the Chairman. The Rapporteur must be familiar with every detail, not only of the field in general, but also with the newest contributions brought to the conference and he must be able to present them in an objective and understandable fashion. The Chairman must try to lead the discussion in such a way that it supplements the talk of the Rapporteur. Points that may have remained unclear should be clarified. Questions from the audience should be turned into fruitful and informative discussions. Facts and viewpoints which may have been neglected by the Rapporteur should be brought out. The contributors should also have the possibility of adding important points to the discussion. However, the Chairman must see to it that the discussion does not degenerate into a second presentation of the contributions by their authors, or into a presentation of unimportant details which the Rapporteur has justifiably omitted.

We believe in the superiority of this system, because it makes it easier for the participants to absorb the material if it is presented in an orderly fashion. A unified presentation of a field of research by a well selected individual is usually far better than a collection of original contributions. Furthermore, it cannot be denied that an intelligent expert is often better able to present a new development in which he has not himself directly participated, than are the actual authors themselves who are often too close to the subject. There are evidently exceptions

to this rule and it will be up to the Chairman, or even up to the Planning Committee (consisting of all Chairmen and Rapporteurs) to decide whether, in some cases, the presentation could better be made by the author himself.

This system can only be successful if ample time is reserved for a thorough contact between Rapporteur and Chairman, on the one hand, and the contributors on the other. Firstly, the contributors' papers should be in the hands of the Rapporteurs and Chairmen at the latest by June 1, so that they have time to study them. In addition, it is planned that two days before the official opening of the Conference, i.e. June 27 and 28, shall be given up to intimate and thorough discussions between the members of the "team" for each session, comprising the Rapporteur, Chairman and contributors, or their representatives. Each team will have a room with secretary, blackboard, etc. available for these two days for discussions and preparation of the session. In addition to this, all Chairmen and Rapporteurs will meet after these two days, on Sunday June 29, for a final planning conference.

We would like to emphasize that this system should not be understood as calling for the elimination of original contributions to the conference. On the contrary, such contributions are, of course, the backbone of the conference. The contributed papers will appear in full in the Proceedings if the authors so desire, and subject to the final decision of the CERN Organization Committee. Our innovation concerns only the method of presentation at the actual sessions.

### 3. *Advance Information for Participants*

It is felt that it would add to the success of the conference if all participants could have the opportunity of acquainting themselves beforehand with the information already existing on the various subjects to be discussed at the conference. With this in view, all Rapporteurs are invited to give their advice as regards the literature and, in particular, any review articles, the study of which could usefully serve as an introduction to their own reports. Such a procedure will have the additional advantage of enabling Rapporteurs to make a short introduction only to their subject and to devote the major part of the time alloted to them to the presentation of new contributions to the field. If, by way of additional information to the literature suggested for study, the Rapporteur cares to write himself a short introduction to his report, he should be encouraged to do so. In any case and whatever their preferences in this respect, the Rapporteurss should forward to CERN, at latest by April 1, 1958, a list of the literature, articles, etc. which they suggest should be studied together with any introductory paper of their own. Observance of this dead-line of April 1 is essential to allow time for the preprinting and mailing of the information by CERN and its study by future participants.

Contributors will be asked to send their contributions to the Rapporteurs as soon as possible and, at latest, before June 1. The final list of Rapporteurs will be communicated at the earliest possible date in Bulletin No. 2. Contributors will be asked to send a copy of their contributions to CERN at the same time as to the Rapporteurs.

### 4. *Reports and Papers*

The final texts of the contributors' papers should be made available to CERN during the conference. The Rapporteurs' reports and the texts of the discussions should be communicated to CERN shortly afterwards. Tape recording will be provided and, if the Rapporteur so desires and providing it is possible, the recording of his report will be made available to him in typewritten form for correction. Worked-out tape recordings of the discussion should be checked by the Chairman of the session.

### 5. *Place of Conference and Participation*

The conference proper will be held in the big Auditorium of the Physics Institute of the University of Geneva, 24, Quai de l'École de Médecine, Geneva.

The organizing sessions on June 27 and 28 will be held in the CERN laboratories in Meyrin, Geneva.

Participation in the conference will be exclusively by invitation. CERN regrets that, apart from a few exceptional cases, the Organization is not in a position to contribute towards

the expenses of participants unable to obtain grants from their own national authorities. Any requests for financial aid from CERN should reach the Organization at latest by April 1, 1958.

6. *Language*

The official language of the conference will be English.

7. *Bulletin No. 2*

Bulletin No. 2 will be issued on March 1, or shortly afterwards.

8. *Correspondence*

All correspondence related to the conference should be addressed as follows: CERN Conference Secretariat, Geneva, 23, CERN, Switzerland.

## Programme

| | | *Rapporteurs Invited* | *Chairmen Invited* |
|---|---|---|---|
| *Monday, June 30* | *Plenary Session I* | | |
| morning | "Nucleon structure" | | |
| | Experimental | W. K. H. Panofsky, Stanford | E. I. Tamm, USSR. |
| | Theoretical | L. L. Foldy, Case Inst. | E. I. Tamm, USSR. |
| | *Plenary Session II* | | |
| afternoon | "Nucleon and its interaction with pions, photons, nucleons and anti-nucleons" | | |
| | Experimental | | |
| | To 3/2, 3/2 resonance | G. Puppi, Bologna | S. Ia. Nikitin, USSR. |
| | Above 3/2, 3/2 resonance | O. Piccioni, Brookhaven | S. Ia. Nikitin, USSR. |
| *Tuesday, July 1* | *Plenary Session III* | | |
| morning | "Nucleon and its interaction with pions, photons, nucleons and anti-nucleons" | | |
| | Theoretical | G. F. Chew, Berkeley | R. E. Peierls, Birmingham |
| | *Plenary Session IV* | | |
| afternoon | "Fundamental theoretical ideas" | F. Dyson, Inst. for Adv. Study, Princeton<br>W. Heisenberg, Göttingen | W. Pauli, Zürich |
| *Wednesday, July 2* | Free Day | | |
| *Thursday, July 3* | *Plenary Session V* | | |
| morning | "Strange particle production" | | |
| | Experimental | J. Steinberger, Columbia | C. C. Butler, Imp. Coll., London |
| | Theoretical | M. Gell-Mann, Cal. Tech. | C. C. Butler, Imp. Coll., London |
| | *Plenary Session VI* | | |
| afternoon | "Strange particle interaction" | | |
| | Experimental | M. F. Kaplon, Rochester | Ia. A. Smorodinsky, USSR. |
| | Theoretical | R. H. Dalitz, Chicago | Ia. A. Smorodinsky, USSR. |
| *Friday, July 4* | *Plenary Session VII* | | |
| morning | "Invariance principles and selection rules" | C. N., Yang Inst. for Adv. Study, Princeton<br>L. D. Landau, USSR. | H. Lehmann, Hamburg |

| | *Plenary Session VIII* | *Rapporteurs Invited* | *Chairmen Invited* |
|---|---|---|---|
| afternoon | "Weak interactions: leptonic modes" | | |
| | Experimental | M. Goldhaber, Brookhaven | L. Michel, Lille |
| | Theoretical | A. Salam, Imp. Coll. London | L. Michel, Lille |
| *Saturday, July 5* | *Plenary Session IX* | | |
| morning | "Weak interactions: other modes" | | |
| | Experimental | D. A. Glaser, Michigan | R. E. Marshak, Rochester |
| | Theoretical | S. B. Treiman, Princeton | R. E. Marshak, Rochester |
| | *Plenary Session X* | | |
| afternoon | Concluding remarks | J. R. Oppenheimer, Inst. for Adv. Study, Princeton | C. J. Bakker, CERN |

## ELECTRON MICROSCOPE SOCIETY OF AMERICA

The Annual Meeting of the Electron Microscope Society of America will be held in Los Angeles on August 7, 8 and 9, 1958. Please note that this is a change from the earlier date announced. The meeting location has not been changed.

The Local Chairman for this meeting will be Dr. Henry C. Froula, Department of Engineering, University of California, Los Angeles 24, California.

The Program Chairman is Dr. Charles M. Schwartz, Battelle Memorial Institute, 505 King Avenue, Columbus 1, Ohio.

The officers of the Electron Microscope Society of America for 1958 are:

President: Dr. Max Swerdlow, Solid State Sciences Division, Air Force Office of Scientific Research (ARDC), Washington 25, D. C.

Secretary: Dr. D. Maxwell Teague, Chrysler Corporation, P. O. Box 1118, Detroit 31, Michigan.

Treasurer: Dr. Robert V. Rice.

*Nuclear Physics* **6** (1958) 329—347; © *North-Holland Publishing Co., Amsterdam*
Not to be reproduced by photoprint or microfilm without written permission from the publisher

# SUR LA THÉORIE DES PERTURBATIONS DES ÉTATS LIÉS

CLAUDE BLOCH
*Centre d'Études Nucléaires de Saclay, Gif-sur-Yvette (S. & O.)*

Reçu le 16 décembre 1957

**Abstract:** Two methods leading to general prescriptions for the construction of the time independent perturbation expansions for bound states to all orders are discussed. The two methods differ by the choice of the zeroth-order wave functions. In both cases, the expansions are simplified by the use of non-orthonormalized zeroth-order wave functions. The terms of the expansions are described by means of diagrams. The accuracy of the expansions is tested by a calculation of two eigen-values of the Mathieu equation.

## 1. Introduction

Dans les présentations habituelles de la théorie des perturbations des spectres discrets les termes d'ordre $n$ dans les développements des valeurs propres et des fonctions propres sont soit donnés par des relations de récurrence permettant de les déterminer à partir des termes d'ordre inférieur [1]), soit donnés par des équations implicites qu'il faut résoudre par approximations successives [2]). On peut naturellement, en effectuant un nombre d'opérations algébriques fini, mais d'autant plus grand qu'on pousse les développements plus loin, arriver à des développements *explicites* en puissances de la perturbation. Dans le cas des systèmes comprenant un grand nombre de particules en interaction par des forces à courte portée, Brueckner [3]) et Goldstone [4]) ont montré que le développement explicite final de l'énergie de liaison comprenait seulement des termes proportionnels au volume dans le cas limite d'un volume très grand. Au contraire les développements plus ou moins implicites tirés des formulations habituelles de la théorie des perturbations font apparaître des termes proportionnels à des puissances du volume supérieures à l'unité qui disparaissent quand on pousse le calcul jusqu'au bout. Ce fait montre l'avantage des développements explicites dans l'étude des systèmes comprenant un grand nombre de particules.

La méthode suivie par Goldstone, directement inspirée de l'élimination des fluctuations du vide dans la théorie des champs, est très liée à la nature particulière du problème qu'il a considéré, et en particulier au fait que l'état fondamental du système non perturbé est non dégénéré. Nous nous proposons ici de montrer qu'on peut, en se plaçant dans le cas le plus

général de la théorie des perturbations des spectres discrets, établir directement la forme des termes d'ordre quelconque dans le développement explicite des valeurs propres et des fonctions propres.

Nous considérerons un système dont l'Hamiltonien s'écrit

$$H = H_0+V, \tag{1}$$

où $H_0$ est l'Hamiltonien non perturbé et $V$ la perturbation. Soit $E_0$ la valeur propre de $H_0$ qui nous intéresse. Ce ne sera pas forcément l'état fondamental, mais $E_0$ devra appartenir au spectre discret de $H_0$. La valeur propre $E_0$ pourra être dégénérée d'ordre $g$ et nous appellerons $\Omega_0$ l'espace à $g$ dimensions défini par les fonctions propres appartenant à $E_0$.

Supposons maintenant qu'on introduise la perturbation d'une manière continue en faisant croître $\lambda$ d'une manière continue de 0 à 1 dans l'Hamiltonien d'interpolation $H_0+\lambda V$. La valeur propre $E_0$ va se transformer en $g$ valeurs propres généralement distinctes que nous désignerons par $E_0+E_\alpha$ $(\alpha = 1, 2, \ldots g)$, et nous aurons, en appelant $|\alpha\rangle$ les fonctions propres orthonormalisées correspondantes,

$$H|\alpha\rangle = (E_0+E_\alpha)|\alpha\rangle \qquad (\alpha = 1, 2, \ldots g). \tag{2}$$

Nous supposerons pour simplifier les raisonnements que la perturbation lève entièrement la dégénérescence. Cette restriction n'a aucun caractère essentiel et l'adaptation des résultats établis dans ce qui suit aux autres cas est immédiate. Nous appellerons $\Omega$ l'espace à $g$ dimensions défini par les fonctions d'onde $|\alpha\rangle$.

L'objet de la théorie des perturbations est alors, d'une part, de former un problème de valeurs propres de dimension $g$ défini par exemple dans l'espace $\Omega_0$, et dont les $g$ racines soient les valeurs propres $E_\alpha$. Nous appellerons les fonctions propres correspondant à ces racines et qui appartiennent à l'espace $\Omega_0$ les *„bonnes fonctions" non perturbées* et nous les désignerons par $|\alpha\rangle_{np}$. La théorie doit d'autre part permettre de construire un opérateur $\mathcal{O}$ qui appliqué aux bonnes fonctions non perturbées donne les fonctions propres de $H$:

$$|\alpha\rangle = \mathcal{O}|\alpha\rangle_{np}. \tag{3}$$

Le problème ainsi posé comprend un grand degré d'arbitraire. De toute solution du problème, on peut en effet déduire une autre solution par la transformation

$$|\alpha\rangle_{np} \to T\,|\alpha\rangle_{np},$$
$$\mathcal{O}\,\mathcal{O}\,T^{-1}; \to$$

où $T$ est une transformation linéaire quelconque possédant un inverse. On peut, en fait, se donner comme bonnes fonctions non perturbées un système arbitraire de $g$ fonctions d'onde appartenant à $\Omega_0$, à condition seulement qu'elles soient linéairement indépendantes.

Dans la théorie habituelle des perturbations, on tente de restreindre l'arbitraire des $|\alpha\rangle_{np}$ en leur imposant de former un système orthonormal. En réalité, cette condition produit l'effet inverse car il est clair d'un point de vue géométrique qu'il est impossible en général de trouver dans $\Omega_0$ un système de fonctions d'ondes orthonormales qui soit lié d'une façon naturelle aux fonctions $|\alpha\rangle$. Il suffit pour le voir de se représenter dans l'espace ordinaire à trois dimensions deux plans $\Omega$ et $\Omega_0$ non parallèles, et un système d'axes orthogonaux dans $\Omega$. Aucun des systèmes d'axes orthogonaux de $\Omega_0$ n'est lié naturellement aux axes de $\Omega$.

Au contraire, si on renonce à la condition d'orthonormalité des bonnes fonctions, deux systèmes de fonctions s'associent tout naturellement aux fonctions $|\alpha\rangle$ (fig. 1):

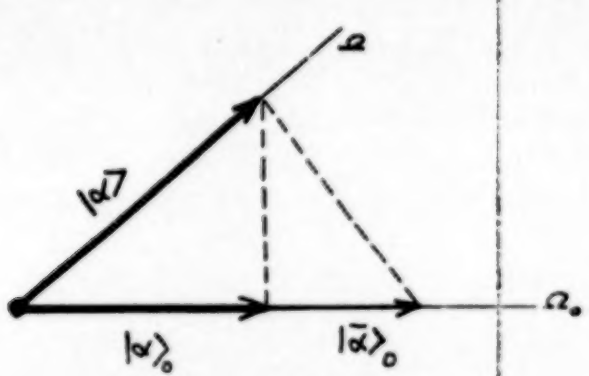


Fig. 1. Les vecteurs de base.

1° Les projections (auxquelles nous réserverons dans ce qui suit la notation $|\alpha\rangle_0$) des fonctions $|\alpha\rangle$ sur l'espace $\Omega_0$;

2° Les fonctions (que nous désignerons dans ce qui suit par $|\bar{\alpha}\rangle_0$) dont les projections sur $\Omega$ sont les fonctions $|\alpha\rangle$.

Ni les fonctions $|\alpha\rangle_0$, ni les fonctions $|\bar{\alpha}\rangle_0$ ne constituent un système orthonormal, mais nous verrons au paragraphe suivant que les deux systèmes de fonctions pris ensemble forment un système biorthogonal.

Nous décrirons ici deux méthodes basées sur l'emploi soit des fonctions $|\alpha\rangle_0$, soit des fonctions $|\bar{\alpha}\rangle_0$ comme bonnes fonctions non perturbées. L'usage des fonctions $|\bar{\alpha}\rangle_0$ conduit essentiellement à la méthode de Kato [5]) qui sera rappelée au § 3. Toutefois on verra que les résultats les plus simples sont obtenus lorsque les bonnes fonctions sont les $|\alpha\rangle_0$. Nous désignerons par $\mathscr{P}$ l'opérateur $\mathscr{O}$ de la relation (3) permettant de passer des bonnes fonctions non perturbées $|\bar{\alpha}\rangle_0$ aux fonctions propres $|\alpha\rangle$ et par $\mathscr{U}$ l'opérateur permettant de passer des $|\alpha\rangle_0$ aux $|\alpha\rangle$. La construction de $\mathscr{P}$ jouera donc le rôle essentiel dans la méthode de Kato alors que la seconde méthode sera centrée sur la construction de $\mathscr{U}$.

Dans le cas d'un problème non-dégénéré, la fonction $|\bar{\alpha}\rangle_0$ ne diffère de $|\bar{\alpha}\rangle_0$ que par un facteur numérique, mais les deux méthodes restent cependant

distinctes. L'utilisation de $|\alpha\rangle_0$ conduit en effet pour les fonctions propres comme pour les valeurs propres à des développements en séries de puissances du potentiel, alors que $|\bar{\alpha}\rangle_0$ conduit plus naturellement à mettre ces quantités sous la forme de quotients de deux séries.

## 2. Définition et Propriétés des Opérateurs $\mathscr{Q}$ et $\mathscr{P}$

### 2.1. LES VECTEURS DE BASE

Dans ce qui suit, nous désignerons par $P_0$ et $P$ les opérateurs de projection sur les espaces $\Omega_0$ et $\Omega$. On a donc

$$H_0 P_0 = P_0 H_0 = E_0 P_0, \qquad P = \sum_\alpha |\alpha\rangle \langle\alpha|. \tag{4}$$

Nous désignerons par $Q_0$ et $Q$ les opérateurs de projection complémentaires

$$Q_0 = 1 - P_0, \qquad Q = 1 - P. \tag{5}$$

Nous supposerons toujours que les espaces $\Omega$ et $\Omega_0$ sont *non-orthogonaux* au sens suivant: il n'existe aucun vecteur de $\Omega$ qui soit orthogonal à tous les vecteurs de $\Omega_0$. Cette propriété entraîne qu'inversement il n'existe aucun vecteur de $\Omega$ qui soit orthogonal à tous les vecteurs de $\Omega_0$. Cette condition sera satisfaite si la perturbation n'est pas trop grande.

Les fonctions $|\alpha\rangle_0$ sont par définition les projections des $|\alpha\rangle$ sur $\Omega_0$:

$$|\alpha\rangle_0 = P_0 |\alpha\rangle. \tag{6}$$

Les fonctions $|\alpha\rangle_0$ sous-tendent tout l'espace $\Omega_0$. En effet, s'il existait dans $\Omega_0$ un vecteur $|\rangle_0$ orthogonal à tous les $|\alpha\rangle_0$ on aurait

$$0 = {}_0\langle\, |\alpha\rangle_0 = {}_0\langle |P_0|\alpha\rangle = {}_0\langle |\alpha\rangle \qquad (\alpha = 1, 2, \ldots g),$$

car ${}_0\langle |P_0 = {}_0\langle|$. Autrement dit, $|\rangle_0$ serait un vecteur de $\Omega_0$ orthogonal à tous les vecteurs de $\Omega$; ce qui est exclu par la condition de non-orthogonalité de $\Omega$ et $\Omega_0$. La dimension de l'espace $\Omega_0$ étant égale au nombre des vecteurs $|\alpha\rangle_0$, ceux-ci sont forcément linéairement indépendants. Il en résulte qu'on peut déterminer des vecteurs $|\bar{\alpha}\rangle_0$ linéairement indépendants qui associés aux $|\alpha\rangle_0$ forment un système biorthogonal, c'est-à-dire tels que

$${}_0\langle\alpha|\bar{\beta}\rangle_0 = \delta_{\alpha\beta}. \tag{7}$$

Les $|\bar{\alpha}\rangle_0$ sont les vecteurs dont les projections sur $\Omega$ sont les fonctions $|\alpha\rangle$, c'est-à-dire que

$$P\,|\bar{\alpha}\rangle_0 = |\alpha\rangle. \tag{8}$$

En effet, d'après (4) et (7),

$$P|\bar{\alpha}\rangle_0 = \sum_\beta |\beta\rangle \langle\beta|\bar{\alpha}\rangle_0 = \sum_\beta |\beta\rangle\, {}_0\langle\beta|\bar{\alpha}\rangle_0 = \sum_\beta |\beta\rangle\delta_{\alpha\beta} = |\alpha\rangle.$$

Enfin, on peut montrer facilement que le projecteur $P_0$ s'écrit

$$P_0 = \sum_\alpha |\alpha\rangle_0\, {}_0\langle\bar{\alpha}| = \sum_\alpha |\bar{\alpha}\rangle_0\, {}_0\langle\alpha|. \tag{9}$$

### 2.2. LES OPÉRATEURS $\mathscr{U}$ ET $\mathscr{P}$

Par définition, $\mathscr{U}$ et $\mathscr{P}$ sont *les opérateurs qui transforment les bonnes fonctions non perturbées* $|\alpha\rangle_0$ *et* $|\tilde{\alpha}\rangle_0$ *dans les fonctions propres* $|\alpha\rangle$:

$$\mathscr{U}|\alpha\rangle_0 = |\alpha\rangle, \qquad P\,|\tilde{\alpha}\rangle_0 = |\alpha\rangle. \tag{10}$$

Pour compléter la définition de $\mathscr{U}$ et $\mathscr{P}$ nous ajouterons que $\mathscr{U}$ et $\mathscr{P}$ donnent zéro lorsqu'on les applique à des vecteurs orthogonaux à $\Omega_0$:

$$\mathscr{U}|\rangle = \mathscr{P}\,|\rangle = 0, \qquad \text{si } P_0\,|\rangle = 0. \tag{11}$$

Ces conditions définissent entièrement $\mathscr{U}$ et $\mathscr{P}$, et on voit tout de suite que ces opérateurs peuvent se mettre sous la forme

$$\mathscr{U} = \sum_\alpha |\alpha\rangle\,{}_0\langle\tilde{\alpha}|, \qquad \mathscr{P} = \sum_\alpha |\alpha\rangle\,{}_0\langle\tilde{\alpha}| = PP_0. \tag{12}$$

### 2.3. CALCUL DES VALEURS PROPRES ET DES FONCTIONS PROPRES

Supposons pour l'instant qu'on ait réussi à calculer $\mathscr{U}$ et $\mathscr{P}$ et cherchons comment à partir de ces opérateurs on peut déterminer les $E_\alpha$ et les bonnes fonctions non perturbées $|\alpha\rangle_0$ ou $|\tilde{\alpha}\rangle_0$.

Avec $\mathscr{U}$ on formera l'opérateur

$$\boxed{\mathscr{A} = P_0 V \mathscr{U}}. \tag{13}$$

C'est un *opérateur de l'espace* $\Omega_0$ qui sera par conséquent représenté par une *matrice de dimension* $g$ dans une base quelconque introduite dans $\Omega_0$. D'après (1), (2) et (12) on a

$$P_0 V \mathscr{U} = P_0(H-H_0)\sum_\alpha |\alpha\rangle\,{}_0\langle\tilde{\alpha}| = P_0 \sum_\alpha |\alpha\rangle\, E_\alpha\, {}_0\langle\tilde{\alpha}|,$$

et par conséquent $\mathscr{A}$ peut se mettre sous la forme

$$\mathscr{A} = \sum_\alpha |\alpha\rangle_0\, E_\alpha\, {}_0\langle\tilde{\alpha}|. \tag{14}$$

Sous cette forme on vérifie immédiatement que

$$(\mathscr{A}-E_\alpha)\,|\alpha\rangle_0 = 0, \tag{15}$$

c'est-à-dire *les valeurs propres de* $\mathscr{A}$ *sont les* $E_\alpha$ *et ses fonctions propres sont les bonnes fonctions non perturbées.* En effet,

$$(\mathscr{A}-E_\alpha)|\alpha\rangle_0 = (\mathscr{A}-E_\alpha P_0)|\alpha\rangle_0 = \sum_\beta |\beta\rangle_0 (E_\beta - E_\alpha)_0\langle\bar{\beta}|\alpha\rangle_0$$

$$= \sum |\beta\rangle_0 (E_\beta - E_\alpha)\delta_{\alpha\beta} = 0.$$

Avec $\mathscr{P}$ on formera les deux opérateurs† de l'espace $\Omega_0$

$$A = P_0 V \mathscr{P} = P_0 V P P_0, \qquad B = P_0 \mathscr{P} = P_0 P P_0. \tag{16}$$

Ces deux opérateurs peuvent se mettre sous la forme

$$A = \sum_\alpha |\alpha\rangle_0\, E_\alpha\, {}_0\langle\alpha|, \qquad B = \sum_\alpha |\alpha\rangle_0\, {}_0\langle\alpha|. \tag{17}$$

† Dans le cas de $\mathscr{U}$ l'équivalent de $B$ est simplement égal à $P_0$ car $P_0\,\mathscr{U} = P_0$.

*Les $E_\alpha$ et les bonnes fonctions non perturbées $|\tilde{\alpha}\rangle_0$ sont alors données par le problème de valeurs propres*

$$(A-BE_\alpha)\,|\tilde{\alpha}\rangle_0 = 0. \tag{18}$$

En effet

$$(A-BE_\alpha)|\tilde{\alpha}\rangle_0 = \sum_\beta |\beta\rangle_0 (E_\beta - E_\alpha)_0\langle\beta|\tilde{\alpha}\rangle_0$$
$$= \sum_\beta |\beta\rangle_0 (E_\beta - E_\alpha)\delta_{\alpha\beta} = 0.$$

Les opérateurs $\mathscr{A}$ et $A$ sont visiblement très proches l'un de l'autre. On passe de $\mathscr{A}$ à $A$ en remplaçant les $\langle\tilde{\alpha}|$ par les ${}_0\langle\alpha|$. En fait, $B$ est l'opérateur qui transforme les $|\tilde{\alpha}\rangle_0$ en $|\alpha\rangle_0$. En effet, d'après (7) et (17),

$$B\,|\tilde{\alpha}\rangle_0 = |\alpha\rangle_0.$$

Il en résulte que considéré comme un opérateur agissant seulement à l'intérieur de $\Omega_0$, $B$ possède un inverse tel que

$$B^{-1}\,|\alpha\rangle_0 = |\tilde{\alpha}\rangle_0.$$

On vérifie d'ailleurs immédiatement que $B^{-1}$ peut s'écrire sous la forme

$$B^{-1} = \sum_\alpha |\tilde{\alpha}\rangle_0\,{}_0\langle\tilde{\alpha}|.$$

Cet opérateur permet d'exprimer la relation entre $\mathscr{A}$ et $A$ sous la forme

$$\mathscr{A} = AB^{-1}.$$

Notons enfin que $\mathscr{A}$ n'est pas un opérateur hermitique dans $\Omega_0$. C'est pourquoi, s'il est vrai que ses valeurs propres sont réelles, ses fonctions propres ne sont pas deux à deux orthogonales. Au contraire, les opérateurs $A$ et $B$ sont hermitiques, mais ils ne commutent pas l'un avec l'autre.

## 3. Première Méthode: Calcul de $P$

### 3.1. LE DÉVELOPPEMENT DE KATO

D'après la seconde relation (12), le calcul de $\mathscr{P}$ se ramène essentiellement à celui de $P$.

Pour calculer $P$, nous partirons suivant Kato [5]) de la formule

$$P = \frac{1}{2\pi i}\int_C \frac{d\varepsilon}{\varepsilon - H}; \tag{19}$$

où C est un contour dans le plan complexe des énergies entourant $E_0$ et toutes les valeurs propres $E_\alpha$ mais aucune autre valeur propre de $H$. Pour calculer (19) nous utiliserons le développement habituel

$$\frac{1}{\varepsilon-H} = \frac{1}{\varepsilon-H_0} + \frac{1}{\varepsilon-H_0}V\frac{1}{\varepsilon-H_0} + \frac{1}{\varepsilon-H_0}V\frac{1}{\varepsilon-H_0}V\frac{1}{\varepsilon-H_0} + \ldots \tag{20}$$

En écrivant

$$\frac{1}{\varepsilon-H_0} = P_0\frac{1}{\varepsilon-H_0} + Q_0\frac{1}{\varepsilon-H_0}, \tag{21}$$

on notera que

$$P_0 \frac{1}{\varepsilon - H_0} = \frac{P_0}{\varepsilon - E_0},$$

tandis que le terme en $Q_0$, ne présentant aucune singularité au voisinage de $\varepsilon = E_0$, peut être développé en série de Taylor autour de ce point:

$$Q_0 \frac{1}{\varepsilon - H_0} = Q_0 \frac{1}{a + \varepsilon - E_0} = \sum_{k=1}^{\infty} (-)^{k-1} (\varepsilon - E_0)^{k-1} \frac{Q_0}{a^k}.$$

Ici nous avons introduit la notation suivante qui sera conservée dans la suite:

$$\boxed{a = E_0 - H_0}.$$

Ceci permet d'écrire (21) sous la forme

$$\frac{1}{\varepsilon - H_0} = \frac{P_0}{\varepsilon - E_0} + \sum_{k=1}^{\infty} (-)^{k-1} (\varepsilon - E_0)^{k-1} \frac{Q_0}{a^k}.$$

Pour rendre ce développement plus symétrique nous introduirons la notation $S^k (k \geqq 0)$ définie par

$$\boxed{S^0 = -P_0, \qquad S^k = \frac{Q_0}{a^k}} \quad (k \geqq 1).$$

Nous pouvons alors écrire

$$\frac{1}{\varepsilon - H_0} = \sum_{k=0}^{\infty} (-)^{k-1} (\varepsilon - E_0)^{k-1} S^k.$$

Il suffit maintenant pour déterminer $P$ de substituer cette expression dans (20) et de chercher le coefficient de $(\varepsilon - E_0)^{-1}$ dans le développement obtenu. Ceci donne

$$P = -\sum S^{k_1} V S^{k_2} V \ldots V S^{k_{n+1}}; \tag{22}$$

où la sommation est étendue à *toutes les combinaisons* de nombres entiers $k_1, k_2, \ldots k_{n+1}$, tels que

$$\begin{aligned} &k_i \geqq 0 \qquad (i = 1, 2, \ldots n+1), \\ &k_1 + k_2 + \ldots + k_{n+1} = n \geqq 0. \end{aligned} \tag{23}$$

Ainsi jusqu'au second ordre le développement de $P$ s'écrit

$$\begin{aligned} P = P_0 &+ P_0 V \frac{Q_0}{a} + \frac{Q_0}{a} V P_0 \\ &+ \frac{Q_0}{a} V \frac{Q_0}{a} V P_0 + \frac{Q_0}{a} V P_0 V \frac{Q_0}{a} + P_0 V \frac{Q_0}{a} V \frac{Q_0}{a} \\ &- \frac{Q_0}{a^2} V P_0 V P_0 - P_0 V \frac{Q_0}{a^2} V P_0 - P_0 V P_0 V \frac{Q_0}{a^2} + \ldots, \end{aligned} \tag{24}$$

et la règle générale de formation des termes est facile à voir.

Pour obtenir le développement de $\mathscr{P}$ il suffit de sélectionner dans ce développement les termes tels que

$$k_{n+1} = 0.$$

Ainsi le développement de $\mathscr{P}$ jusqu'au second ordre s'écrit

$$\mathscr{P} = P_0 + \frac{Q_0}{a} V P_0 + \frac{Q_0}{a} V \frac{Q_0}{a} V P_0 - \frac{Q_0}{a^2} V P_0 V P_0 - P_0 V \frac{Q_0}{a^2} V P_0 + \ldots.$$

### 3.2. LES DIAGRAMMES ASSOCIÉS AUX TERMES DU DÉVELOPPEMENT

Chaque terme du développement de $P$ est caractérisé par les nombres entiers $k_1, k_2, \ldots k_{n+1}$. Il sera commode pour la suite d'avoir une représentation graphique de ces nombres obtenue comme l'indique la fig. 2. Chaque

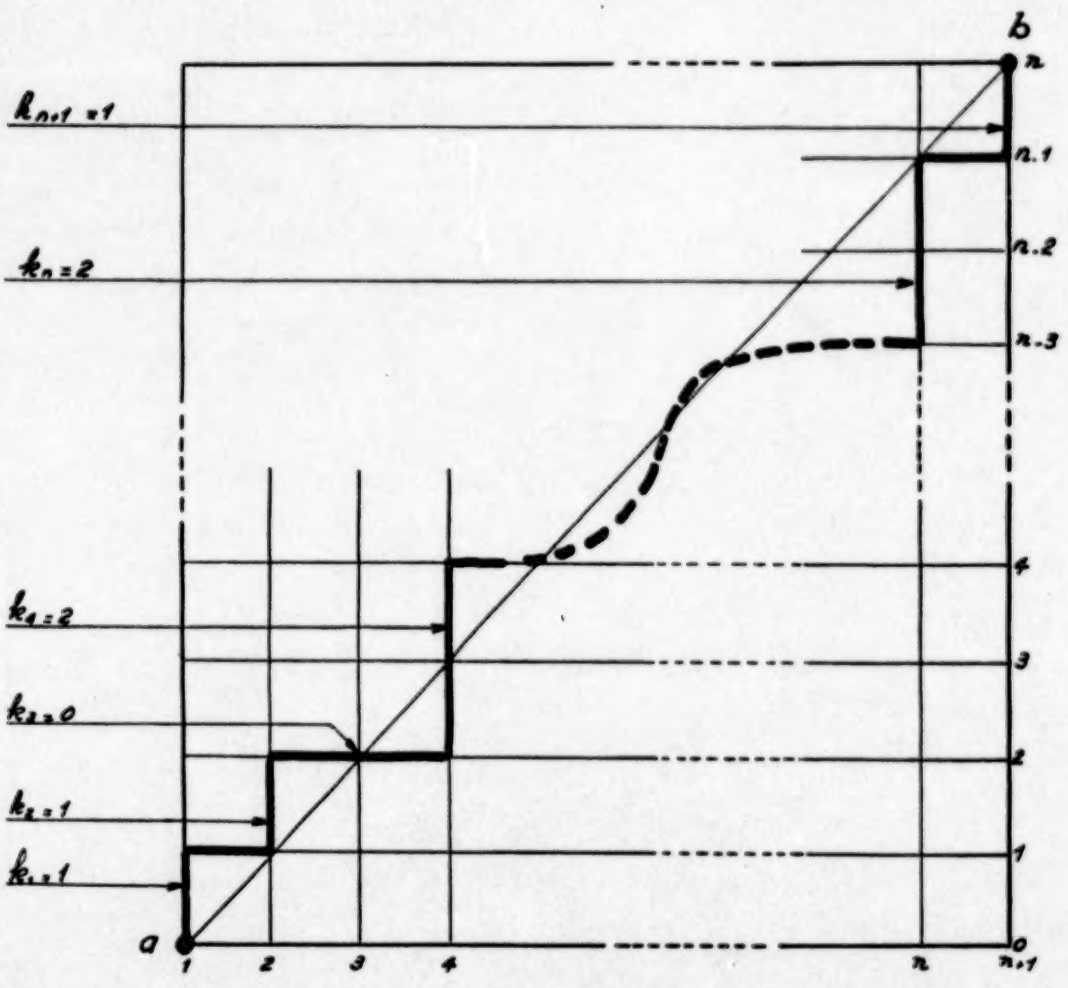


Fig. 2. Le diagramme d'un terme.

terme d'ordre $n$ en $V$ est représenté par une ligne en escalier joignant les deux extrémités $a$ et $b$ d'une diagonale d'un carré de côté égal à $n$. Cette ligne est formée de $n$ segments horizontaux de longueur unité et de $n+1$

segments verticaux de longueurs égales à $k_1, k_2, \ldots k_{n+1}$. Les conditions que la ligne joigne $a$ et $b$ et que les marches de l'escalier soient toutes des marches montantes équivalent exactement aux conditions (23) imposées aux nombres $k_1, \ldots k_{n+1}$.

Pour former le développement de $P$, il faut donc tracer *tous les escaliers* du type indiqué. A titre d'exemple, la fig. 3 donne tous les diagrammes d'ordre $n = 2$. Les nombres $k_1, k_2, k_3$ sont indiqués sous les diagrammes et les termes correspondants du développement sont, dans l'ordre, ceux des deux dernières lignes de (24).

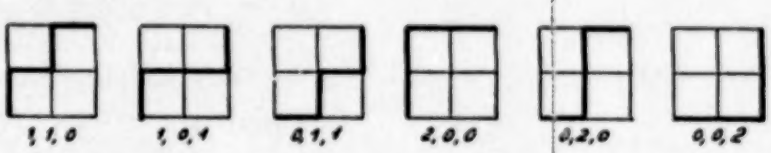


Fig. 3. Les diagrammes du second ordre pour le développement de $P$.

## 4. Deuxième Méthode: Calcul de $\mathscr{U}$

### 4.1. L'ÉQUATION SATISFAITE PAR $\mathscr{U}$

La méthode de calcul de $P$ indiquée au paragraphe précédent reposait essentiellement sur la possibilité d'exprimer $P$ comme une fonction de $H$. Cette possibilité résulte du fait que $P$ commute avec $H$. Une méthode de ce genre ne s'applique pas au calcul de $\mathscr{U}$ qui ne commute pas avec $H$. Par contre, nous allons voir que $\mathscr{U}$ satisfait une équation relativement simple qui permettra le calcul de cet opérateur.

Nous allons commencer par montrer qu'on peut utiliser l'opérateur $\mathscr{U}$ pour éliminer $E_\alpha$ de l'équation de Schrödinger

$$(H-E_0)|\alpha\rangle = E_\alpha|\alpha\rangle; \tag{25}$$

c'est-à-dire pour établir une équation satisfaite par $|\alpha\rangle$ mais ne contenant plus la valeur propre inconnue $E_\alpha$. En multipliant (25) à gauche par $P_0$ nous obtenons

$$P_0V\,|\alpha\rangle = E_\alpha\,|\alpha\rangle_0, \tag{26}$$

car

$$P_0(H-E_0) = P_0(H_0-E_0+V) = P_0V.$$

En multipliant (26) à gauche par $\mathscr{U}$ il vient

$$\mathscr{U}V\,|\alpha\rangle = E_\alpha\,|\alpha\rangle, \tag{27}$$

car $\mathscr{U}P_0 = \mathscr{U}$. En retranchant (27) de (25) nous obtenons l'équation cherchée pour $|\alpha\rangle$:

$$(H-E_0-\mathscr{U}V)\,|\alpha\rangle = 0. \tag{28}$$

Multiplions maintenant (28) à droite par ${}_0\langle\bar{\alpha}|$ et sommons sur $\alpha$ de 1 à $g$, de façon à reformer l'opérateur $\mathscr{U}$ (voir la relation (12)). Nous obtenons

alors l'équation suivante satisfaite par $\mathcal{U}$:

$$(H-E_0-\mathcal{U}V)\mathcal{U}=0.$$

Cette équation s'écrit aussi

$$(E_0-H_0)\mathcal{U}=V\mathcal{U}-\mathcal{U}V\mathcal{U}. \tag{29}$$

On a d'autre part évidemment

$$\mathcal{U}=P_0\mathcal{U}+Q_c\mathcal{U}, \tag{30}$$

et d'après la définition (12) de $\mathcal{U}$ et la relation (9)

$$P_0\mathcal{U}=P_0.$$

En substituant (30) dans le premier membre de (29) on obtient

$$(E_0-H_0)Q_0\mathcal{U}=V\mathcal{U}-\mathcal{U}V\mathcal{U},$$

car $(E_0-H_0)P_0=0$. Dans l'espace des vecteurs orthogonaux à $\Omega_0$, l'opérateur $E_0-H_0$ a un inverse bien défini et on peut écrire

$$Q_0\mathcal{U}=\frac{Q_0}{a}(V\mathcal{U}-\mathcal{U}V\mathcal{U}).$$

En reportant cette expression dans (30) on obtient finalement l'équation cherchée satisfaite par $\mathcal{U}$:

$$\boxed{\mathcal{U}=P_0+\frac{Q_0}{a}(V\mathcal{U}-\mathcal{U}V\mathcal{U})}. \tag{31}$$

### 4.2. LE DÉVELOPPEMENT DE $\mathcal{U}$

L'éq. (31) se prête particulièrement bien au calcul du développement de $\mathcal{U}$ en série de puissances de la perturbation $V$. Posons en effet

$$\mathcal{U}=\mathcal{U}^{(0)}+\mathcal{U}^{(1)}+\mathcal{U}^{(2)}+\ldots;$$

où $\mathcal{U}^{(n)}$ est d'ordre $n$ en $V$. En substituant ce développement dans (31) et en identifiant dans les deux membres les termes de même ordre en $V$ on obtient les relations de récurrence suivantes:

$$\mathcal{U}^{(0)}=P_0,$$

$$\mathcal{U}^{(n)}=\frac{Q_0}{a}\left[V\mathcal{U}^{(n-1)}-\sum_{p=1}^{n-1}\mathcal{U}^{(p)}V\mathcal{U}^{(n-p-1)}\right], \tag{32}$$

qui permettent, en principe de calculer les $\mathcal{U}^{(n)}$ de proche en proche. On notera dans ces relations l'absence du terme $p=0$ due à ce que $\mathcal{U}^{(0)}=P_0$ et au fait que

$$\frac{Q_0}{a}P_0=0.$$

Les premiers termes du développement sont faciles à obtenir. Ainsi le développement de $\mathscr{U}$ jusqu'au troisième ordre s'écrit

$$\mathscr{U} = P_0 + \frac{Q_0}{a} V P_0 + \frac{Q_0}{a} V \frac{Q_0}{a} V P_0 - \frac{Q_0}{a^2} V P_0 V P_0$$
$$+ \frac{Q_0}{a} V \frac{Q_0}{a} V \frac{Q_0}{a} V P_0 - \frac{Q_0}{a} V \frac{Q_0}{a^2} V P_0 V P_0 - \frac{Q_0}{a^2} V \frac{Q_0}{a} V P_0 V P_0$$
$$- \frac{Q_0}{a^2} V P_0 V \frac{Q_0}{a} V P_0 + \frac{Q_0}{a^3} V P_0 V P_0 V P_0 + \dots$$

La comparaison de ce développement avec celui de $\mathscr{P}$ montre que les deux développements sont formés de termes identiques. Jusqu'au premier ordre les développements sont exactement les mêmes. Au second ordre le développement de $\mathscr{U}$ est égal à celui de $\mathscr{P}$ où un terme a été supprimé. Les termes du troisième ordre de $\mathscr{P}$ n'ont pas été écrits parce qu'ils sont très nombreux, mais on voit immédiatement que tous les termes du troisième ordre de $\mathscr{U}$ font partie du développement de $\mathscr{P}$; la réciproque n'étant pas vraie. Ceci suggère que le développement de $\mathscr{U}$ peut s'écrire avec les notations du paragraphe précédent

$$\boxed{\mathscr{U} = \sum' S^{k_1} V S^{k_2} V \dots S^{k_n} V P_0} \; ; \tag{33}$$

où les nombres $k_1, k_2, \dots k_n$ sont tels que

$$k_i \geqq 0 \qquad (i = 1, 2, \dots n),$$
$$k_1 + k_2 + \dots k_n = n \geqq 0. \tag{34}$$

Nous avons ici introduit explicitement la restriction

$$k_{n+1} = 0, \qquad S^{k_{n+1}} = -P_0,$$

qui est visiblement satisfaite par les premiers termes du développement. Le signe $\sum'$ signifie que la sommation est *étendue seulement à certaines combinaisons de nombres satisfaisant les relations* (34).

Il est facile de vérifier que si les termes de $\mathscr{U}$ ont la forme indiquée dans (33) jusqu'à l'ordre $n-1$, les relations de récurrence (32) entraînent la même propriété à l'ordre $n$.

Il reste toutefois à déterminer quelles sont les combinaisons de nombres qui entrent dans la sommation $\sum'$.

### 4.3. LES DIAGRAMMES DES TERMES DE $\mathscr{U}$

La fig. 4 représente les diagrammes définis au § 3.2 relatifs aux termes du troisième ordre de $\mathscr{U}$. On remarque que

1° tous ces diagrammes sont entièrement situés au-dessus de la diagonale *ab*,

2°. tous les diagrammes d'ordre 3 entièrement situés au-dessus de la diagonale *ab* correspondent effectivement à des termes de $\mathscr{U}$.

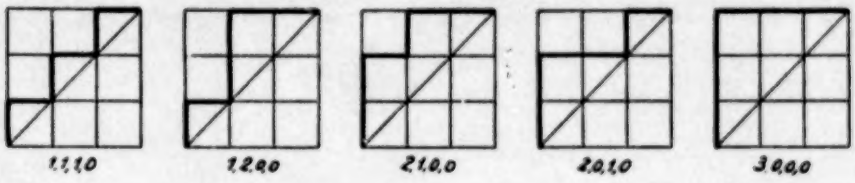


Fig. 4. Les diagrammes du troisième ordre pour le développement de $\mathscr{U}$.

Nous allons démontrer que cette propriété est générale, c'est-à-dire que *dans le développement de* $\mathscr{U}$, *la sommation doit être étendue à tous les systèmes de nombres* $k_1, k_2, \ldots k_n$ *correspondant à des diagrammes entièrement situés au-dessus de la diagonale ab.*

A défaut d'un terme meilleur, nous appellerons *convexes* les diagrammes entièrement situés au-dessus de la diagonale *ab.*

La démonstration repose sur l'étude de la manière dont les diagrammes convexes d'ordre $n$ peuvent être construits à partir de diagrammes convexes d'ordre inférieur.

Soit donc un diagramme convexe quelconque d'ordre $n$. On a obligatoirement $k_1 \geqq 1$, sinon le diagramme partirait de $a$ en s'engageant sous la diagonale. Nous allons distinguer les cas où $k_1 = 1$ et où $k_1 > 1$.

($\alpha$) Supposons que $k_1 = 1$ (fig. 5$\alpha$). La première marche du diagramme a une hauteur égale à 1. Elle aboutit au point $c$ de la diagonale. Le reste du

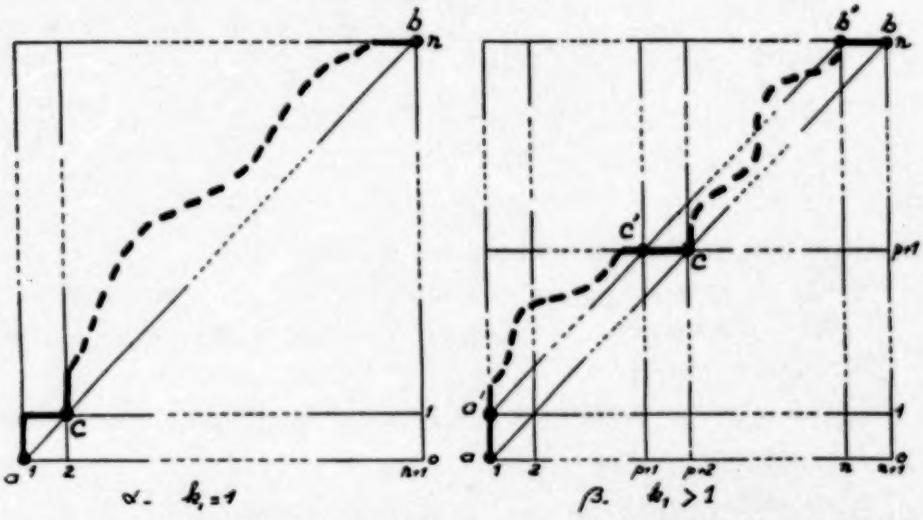


Fig. 5. Décomposition des diagrammes convexes d'ordre $n$ en diagrammes convexes d'ordre plus bas.

diagramme allant de $c$ à $b$ est alors un diagramme convexe d'ordre $n-1$. Par conséquent tout diagramme convexe d'ordre $n$ tel que $k_1 = 1$ s'obtient en ajoutant une marche unité au début d'un diagramme convexe d'ordre

$n-1$. Inversement en ajoutant une marche unité au début d'un diagramme convexe quelconque d'ordre $n-1$ on obtient bien un diagramme convexe d'ordre $n$ tel que $k_1 = 1$.

($\beta$) Supposons que $k_1 > 1$ (fig. 5$\beta$). Traçons la parallèle à la diagonale $a'b'$ telle que

$$aa' = bb' = 1.$$

Le diagramme s'engage au-dessus de cette ligne en $a'$ puisque $k_1 > 1$. Comme le diagramme doit aboutir au point $b$ situé au-dessous de $a'b'$ il recoupe certainement cette ligne en au moins un autre point. Il peut même recouper plusieurs fois $a'b'$, mais nous désignerons par $c'$ le point d'intersection *le plus proche* de $a'$. La définition du point $c'$ est donc unique pour un diagramme donné. Eventuellement, le point $c'$ peut se trouver rejeté en $b'$. Si on suit le diagramme de $a$ vers $b$, au point $c'$ la courbe passe obligatoirement de la région supérieure délimitée par $a'b'$ à la région inférieure. On voit alors que la portion du diagramme allant de $a'$ à $c'$ est un diagramme convexe d'ordre $p (1 \leqq p \leqq n-1)$ si $p$ est la dimension du carré de diagonale $a'c'$, et que la portion du diagramme allant de $c$ à $b$ est un diagramme convexe d'ordre $n-p-1$ pouvant se réduire au seul point $b$ si $p = n-1$.

Nous avons donc décomposé d'une manière unique un diagramme convexe quelconque d'ordre $n$ tel que $k_1 > 1$ en un diagramme convexe d'ordre $p$ et un diagramme convexe d'ordre $n-p-1$. Inversement, partant d'un diagramme convexe quelconque d'ordre $p (1 \leqq p \leqq n-1)$ et d'un diagramme convexe quelconque d'ordre $n-p-1$, la construction de la fig. 5 $\beta$ conduit à un diagramme convexe d'ordre $n$ tel que $k_1 > 1$.

Supposons maintenant que jusqu'à l'ordre $n-1$ tous les termes du développement de $\mathcal{U}$ soient obtenus à partir de tous les diagrammes convexes. La relation de récurrence (32) nous permet de construire les termes d'ordre $n$.

Considérons un terme de $\mathcal{U}^{(n-1)}$ caractérisé par les nombres

$$k_1, k_2, \ldots k_n.$$

Le terme obtenu en multipliant celui-ci à gauche par $(Q_0/a)V$ sera caractérisé par les nombres

$$1, k_1, k_2, \ldots k_n.$$

La relation entre les diagrammes correspondants est celle du cas ($\alpha$) décrit plus haut.

Considérons ensuite deux termes de $\mathcal{U}^{(p)}$ et $\mathcal{U}^{(n-p-1)}$ caractérisés par les nombres

$$k_1, k_2, \ldots k_{p+1} \text{ et } k'_1, k'_2, \ldots k'_{n-p}.$$

En formant le produit

$$-\frac{Q_0}{a}\mathcal{U}^{(p)} V \mathcal{U}^{(n-p-1)}$$

ces deux termes conduiront à un terme caractérisé par les nombres

$$k_1+1,\ k_2, \ldots k_{p+1},\ k'_1,\ k'_2, \ldots k'_{n-p},$$

et la relation entre les diagrammes correspondants sera celle du cas ($\beta$).

Comme nous avons vu que les constructions ($\alpha$) et ($\beta$) conduisaient à l'ensemble des diagrammes convexes d'ordre $n$, la propriété à démontrer est établie pour les termes d'ordre $n$. Elle est donc vraie à tous les ordres.

## 5. Relation entre les deux Méthodes. Seconde Démonstration du Développement de $\mathscr{U}$

Nous allons montrer qu'on peut déduire le développement de $\mathscr{U}$ du développement de $\mathscr{P}$ établi au § 3. Pour cela nous partirons des relations

$$\mathscr{P} = \mathscr{U}B, \qquad \mathscr{U}Q_0 = 0, \tag{35}$$

qui résultent immédiatement de (7), (12) et (17). Inversement, les relations (35) peuvent servir de définition à l'opérateur $\mathscr{U}$.

Nous savons d'après le § 3 que $\mathscr{P}$ est donné par le développement

$$\mathscr{P} = \sum S^{k_1} V S^{k_2} V \ldots S^{k_n} V P_0,$$

où la sommation est étendue à tous les diagrammes, et que $B$ est donné par le même développement avec la restriction

$$k_1 = 0.$$

Autrement dit, les diagrammes de $B$ s'engagent sous la diagonale au départ en $a$.

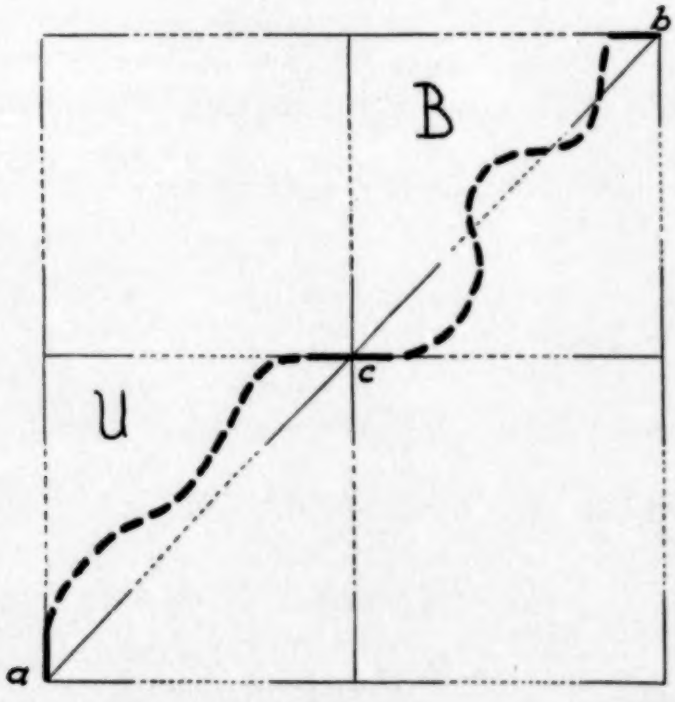


Fig. 6. Décomposition d'un diagramme de $\mathscr{P}$ en un diagramme de $\mathscr{U}$ et un diagramme de $B$.

Soit maintenant un diagramme quelconque de $\mathscr{P}$ (fig. 6). Appelons $c$ le point le plus proche de $a$ où le diagramme passe du demi-plan situé au-dessus de la diagonale au demi-plan situé au-dessous. Si le diagramme s'engage sous la diagonale au départ en $a$, nous dirons que $c$ est en $a$. Si le diagramme est entièrement au-dessus de la diagonale nous dirons que $c$ est en $b$. On voit alors que la partie $ac$ du diagramme est un diagramme convexe (pouvant se réduire à un point) et que la partie $cb$ est un diagramme de $B$ (pouvant également se réduire à un point). Tout diagramme de $\mathscr{P}$ peut être ainsi divisé d'une manière unique en un diagramme convexe suivi d'un diagramme de $B$, et inversement en mettant bout à bout un diagramme convexe et un diagramme de $B$ on obtient un diagramme unique de $\mathscr{P}$. Il en résulte que la somme (33) des termes correspondant aux diagrammes convexes satisfait bien les relations (35). Elle est donc égale à $\mathscr{U}$.

## 6. Dénombrement des Termes. Convergence

Il est intéressant de connaître le nombre des termes de degré donné dans les développements que nous avons considérés.

Le nombre $N_n(P)$ des termes de degré $n$ dans le développement (22) de $P$ est le coefficient de $x^n$ dans le développement en série de

$$(1+x+x^2+\ldots)^{n+1} = \frac{1}{(1-x)^{n+1}}.$$

D'où

$$N_n(P) = \frac{2n!}{(n!)^2} \approx \frac{2^{2n}}{\sqrt{\pi n}}.$$

Pour le développement de $\mathscr{P}$, le nombre $N_n(\mathscr{P})$ est le coefficient de $x^n$ dans le développement de $1/(1-x)^n$. On trouve

$$N_n(\mathscr{P}) = \tfrac{1}{2}N_n(P) = \frac{(2n-1)!}{n!(n-1)!}.$$

Par des raisonnements analogues on trouve que

$$N_n(A) = N_{n-1}(\mathscr{P}) = \frac{(2n-3)!}{(n-1)!(n-2)!},$$

$$N_n(B) = \frac{(2n-2)!}{n!(n-2)!}.$$

En ce qui concerne le développement de $\mathscr{U}$, les relations de récurrence (32) entraînent

$$N_0(\mathscr{U}) = 1,$$

$$N_n(\mathscr{U}) = \sum_{p=0}^{n-1} N_p(\mathscr{U}) N_{n-p-1}(\mathscr{U}).$$

Ces relations montrent que la fonction génératrice

$$f(x) = \sum_{n=0}^{\infty} x^n N_n(\mathscr{U})$$

satisfait à l'équation

$$xf^2 - f + 1 = 0.$$

D'où, en prenant la racine de cette équation du second degré qui reste finie lorsque $x \to 0$,

$$f(x) = \frac{1}{2x}[1 - \sqrt{1-4x}];$$

et en développement la racine carrée on obtient

$$N_n(\mathscr{U}) = \frac{(2n)!}{n!(n+1)!} = \frac{2}{n+1} N_n(\mathscr{P}).$$

On voit que le développement de $\mathscr{U}$ comprend notablement moins de termes que celui de $\mathscr{P}$. Enfin on a évidemment

$$N_n(\mathscr{A}) = N_{n-1}(\mathscr{U}) = \frac{(2n-2)!}{n!(n-1)!} = \frac{2}{n} N_n(A).$$

Si on suppose que $V$ est un opérateur borné on peut indiquer des conditions suffisantes de convergence des développements. La norme de chacun des termes d'ordre $n$ de $P, \mathscr{P}$ ou $\mathscr{U}$ est en effet inférieure ou égale à $(||V||/d)^n$; où $||V||$ est la norme de $V$ et $d$ la *distance d'isolement* de $E_0$ dans le spectre de $H_0$, c'est-à-dire la distance de $E_0$ à la valeur propre la plus proche. D'autre part

$$\lim_{n\to\infty} \frac{N_{n+1}(P)}{N_n(P)} = \lim_{n\to\infty} \frac{N_{n+1}(\mathscr{P})}{N_n(\mathscr{P})} = \lim_{n\to\infty} \frac{N_{n+1}(\mathscr{U})}{N(\mathscr{U})} = 4.$$

Nous obtenons alors pour les trois développements 'a condition suffisante de convergence

$$\frac{||V||}{d} < \frac{1}{4}.$$

Cette condition de convergence est sans doute très pessimiste et en fait Kato [5]) a pu montrer que le développement de $P$ et par conséquent celui de $\mathscr{P}$ convergent pour

$$\frac{||V||}{d} < \frac{1}{2}.$$

## 7. Un Exemple Simple: L'Équation de Mathieu

Il est intéressant d'essayer les développements qui viennent d'être indiqués sur l'exemple très simple de l'équation de Mathieu pour laquelle il existe des tables de valeurs propres exactes.

L'équation de Mathieu s'écrit

$$\left[-\frac{d^2}{d\theta^2}+s\cos^2\theta\right]\psi(\theta)=E\psi(\theta),$$

et on cherche les solutions $\psi(\theta)$ périodiques:

$$\psi(\theta+2\pi)=\psi(\theta).$$

On pose

$$H_0=-\frac{d^2}{d\theta^2}, \qquad V=s\cos^2\theta.$$

Les valeurs propres et les fonctions propres normalisées non perturbées peuvent se mettre sous la forme

$$E_0^{(n)}=n^2, \quad \varphi_0^{+}=\frac{1}{\sqrt{2\pi}}, \quad \varphi_n^{\pm}=\frac{1}{\sqrt{\pi}}\begin{matrix}\cos\\ \sin\end{matrix} n\theta \,(n>0);$$

où le signe + se rapporte aux fonctions cos et le signe − aux fonctions sin. Les fonctions propres non perturbées ainsi définies se divisent en quatre groupes

$$\varphi_{2n}^{+}; \quad \varphi_{2n+1}^{+}; \quad \varphi_{2n+2}^{-}; \quad \varphi_{2n+1}^{-} \quad (n=0,1,2,\ldots),$$

qui ne sont pas mélangés par la perturbation $V$ et qui peuvent par conséquent être traités indépendamment les uns des autres. Nous considérerons le premier groupe seulement ici. Les seuls éléments de matrice non nuls de $V$ entre fonctions de ce groupe sont

$$\langle n|V|n\rangle=\frac{s}{2} \qquad (n=0,2,4,\ldots),$$

$$\langle 0|V|2\rangle=\langle 2|V|0\rangle=\frac{s}{\sqrt{8}},$$

$$\langle n|V|n+2\rangle=\langle n+2|V|n\rangle=\frac{s}{4} \qquad (n=2,4,6,\ldots).$$

Jusqu'au 3ème ordre les développements de $A$, $B$ et $\mathscr{A}$ s'écrivent

$$A=P_0VP_0+P_0V\frac{Q_0}{a}VP_0+P_0V\frac{Q_0}{a}V\frac{Q_0}{a}VP_0-P_0V\frac{Q_0}{a^2}VP_0VP_0$$
$$-P_0VP_0V\frac{Q_0}{a^2}VP_0+\ldots \qquad (36)$$

$$B=P_0-P_0V\frac{Q_0}{a^2}VP_0+\ldots$$

$$\mathscr{A}=P_0VP_0+P_0V\frac{Q_0}{a}VP_0+P_0V\frac{Q_0}{a}V\frac{Q_0}{a}VP_0-P_0V\frac{Q_0}{a^2}VP_0VP_0+\ldots.$$

Le problème considéré étant non dégénéré, ces quantités sont égales à l'opérateur $P_0$ multiplié par des nombres purs. Dans ce qui suit nous

omettrons le facteur $P_0$ et nous désignerons par $A$, $B$ et $\mathscr{A}$ les nombres purs qui multiplient $P_0$ dans les expressions (36). Les valeurs propres de l'équation de Mathieu sont alors données par

$$E_0+\frac{A}{B} \text{ ou } E_0+\mathscr{A}$$

suivant qu'on utilise le développement $\mathscr{P}$ ou le développement $\mathscr{U}$.

Considérons d'abord l'état fondamental $E_0^{(0)}=0$. On trouve jusqu'au 4ème ordre les expressions suivantes:

$$A=\frac{s}{2}-\frac{1}{2}\left(\frac{s}{4}\right)^2-\frac{1}{4}\left(\frac{s}{4}\right)^3+\frac{15}{128}\left(\frac{s}{4}\right)^4+O(s^5),$$

$$B=1-\frac{1}{8}\left(\frac{s}{4}\right)^2+O(s^4),$$

$$\mathscr{A}=\frac{s}{2}-\frac{1}{2}\left(\frac{s}{4}\right)^2+\frac{7}{128}\left(\frac{s}{4}\right)^4+O(s^5).$$

Le tableau suivant indique pour $s=2$ et $s=4$ les valeurs aux 2ème, 3ème et 4ème ordres données par $A/B$, $\mathscr{A}$ et par la méthode de perturbation-itération (P.I.) décrite par Morse et Feshbach [2]), ainsi que les valeurs exactes:

$s=2$

$\frac{\|V\|}{d}=\frac{1}{2}$

| Ordres | 2 | 3 | 4 | Exact |
|---|---|---|---|---|
| $A/B$ | 0.8750 | 0.8710 | 0.8785 | 0.8782 |
| $\mathscr{A}$ | 0.8750 | 0.8750 | 0.8784 | |
| P.I. | 0.8333 | 0.8920 | 0.8737 | |

$s=4$

$\frac{\|V\|}{d}=1$

| Ordres | 2 | 3 | 4 | Exact |
|---|---|---|---|---|
| $A/B$ | 1.5 | 1.4286 | 1.5625 | 1.5448 |
| $\mathscr{A}$ | 1.5 | 1.5 | 1.5547 | |
| P.I. | 1 | 1.7778 | 1.1541 | |

Considérons ensuite l'état excité $E_0^{(6)}=36$. On trouve en se limitant au 3ème ordre:

$$A=\frac{s}{2}+\frac{1}{10}\left(\frac{s}{4}\right)^2-\frac{37}{4900}\left(\frac{s}{4}\right)^3+O(s^4),$$

$$B=1-\frac{37}{9800}\left(\frac{s}{4}\right)^2+O(s^3),$$

$$\mathscr{A}=\frac{s}{2}+\frac{1}{70}\left(\frac{s}{4}\right)^2+O(s^4).$$

Les valeurs numériques pour $s = 2$ et $s = 30$ sont données ci-dessous

$s = 2$

$\frac{||V||}{d} = \frac{1}{10}$

| Ordres | 1 | 2 | Exact |
|---|---|---|---|
| $A/B$ | 1 | 1.00357 | 1.00357 |
| $\mathscr{A}$ | 1 | 1.00357 | |
| P.I. | 1 | 1.00356 | |

$s = 30$

$\frac{||V||}{d} = \frac{3}{2}$

| Ordres | 1 | 2 | 3 | Exact |
|---|---|---|---|---|
| $A/B$ | 15 | 15.804 | 16.020 | 15.829 |
| $\mathscr{A}$ | 15 | 15.804 | 15.804 | |
| P.I. | 15 | 12.280 | 17.285 | |

On voit que dans l'exemple traité la méthode basée sur $\mathscr{U}$ est nettement meilleure que la méthode de perturbation-itération et qu'elle est légèrement meilleure que la méthode basée sur $\mathscr{P}$. C'est également la méthode $\mathscr{U}$ qui fait intervenir les développements comprenant le plus petit nombre de termes.

Les trois méthodes indiquées ont évidemment d'étroites relations. Ainsi le développement de la méthode P.I. arrêté à l'ordre $n$ fournit une équation algébrique qu'il faut résoudre pour obtenir la valeur propre. Au lieu de résoudre numériquement cette équation par itération, par exemple, on peut exprimer sa solution sous la forme d'un développement en puissances de la perturbation. Ce développement arrêté à l'ordre $n$ sera alors identique au développement de $\mathscr{A}$ jusqu'à l'ordre $n$. Il est remarquable que cette méthode approchée de résolution de l'équation fournie par la méthode P.I. donne un résultat plus exact pour les valeurs propres de l'équation de Mathieu que la résolution exacte de l'équation.

De même si on développe le quotient $A/B$ en puissances de la perturbation on obtient le développement de $\mathscr{A}$. A nouveau il est remarquable que le développement de $\mathscr{A}$ donne de meilleurs résultats que le quotient $A/B$ calculé exactement.

L'auteur tient à remercier M. J. Horowitz pour plusieurs discussions stimulantes sur ce problème.

## Bibliographie

1) L. I. Schiff, Quantum Mechanics (Mc Graw-Hill, New-York 1949) § 25
2) P. M. Morse et H. Feshbach, Methods of Theoretical Physics (McGraw-Hill, New-York, 1953) § 9.1
3) K. A. Brueckner, Phys. Rev. **100** (1955) 36
4) J. Goldstone, Proc. Roy. Soc. A **239** (1957) 267
5) T. Kato, Prog. Teor. Phys. **4** (1949) 514; **5** (1950) 95, 207

*Nuclear Physics* **6** (1958) 348—358; © *North-Holland Publishing Co., Amsterdam*
Not to be reproduced by photoprint or microfilm without written permission from the publisher

# DEUTERON CROSS SECTIONS FOR HIGH ENERGY PROJECTILES

JOHN S. BLAIR†
*University of Washington, Seattle, Washington*††

Received 23 December 1957

**Abstract:** The absorption cross section of a deuteron for high energy particles is computed in a semi-classical model in which the elementary neutron and proton cross sections are represented by classical black disks and the impulse approximation describes the collision. Computations have been carried out for Hulthén and Gartenhaus wave functions and results are presented in graphical or tabular form. Approximate formulas and the sensitivity of the calculations to deuteron wave function are discussed. Recent antiproton experiments imply that the shadow corrections are a large fraction of the antiproton-nucleon cross sections.

## 1. Introduction

It has been pointed out by Glauber [1]) that because of the eclipse of one nucleon in the deuteron by the other, the cross section of a deuteron for a high energy projectile may be less than the sum of the corresponding free neutron and proton cross sections. This shadow effect was illustrated by quantitative consideration of a simple semi-classical model in which (1) the elementary proton and neutron cross sections are represented by classical black absorbing disks and (2) the impulse approximation is used to describe the interaction between the deuteron and the high energy particle; in Glauber's calculations, the proton and neutron cross sections are taken to be equal. It is the primary purpose of this note to present plots (for a variety of proton cross sections) of the difference between true and apparent neutron cross sections versus apparent neutron cross section as given by the above semi-classical model with representative deuteron wave functions; we believe that this model will provide a good approximation for many high energy interactions and that the graphs will be of assistance to experimenters wishing to estimate true elementary cross sections from observed deuteron cross sections.

The present calculations have been motivated by recent experiments with antiproton beams [2]) which have yielded large antiproton-proton total cross sections (minus small angle scattering) and annihilation cross sections.

† Presently on leave at Princeton University.
†† Supported in part by the U. S. Atomic Energy Commission.

Apparent antiproton-neutron cross sections, obtained by subtraction of the proton from corresponding deuteron cross sections, are also found to be large although smaller than the free proton cross sections. Because of the shadow effect and the magnitude of the elementary cross sections, the true neutron cross sections are considerably larger than the apparent values; we shall see that for recent values of proton and deuteron cross sections the semi-classical model gives true neutron cross sections of the order of the corresponding proton-antiproton cross sections.

The semi-classical model appears particularly appropriate for the interaction of antiprotons with deuterons. The black disk assumption seems promising because (1) the wavelength corresponding to the relative motion of the antiproton and a nucleon is much smaller than the black disk radius appropriate to observed proton cross sections (for 457 MeV antiprotons, the relative antiproton-nucleon wavelength $\approx 3\times 10^{-14}$ cm while the black disk radius $\approx 1.8\times 10^{-13}$ cm) and (2) the range of antinucleon-nucleon forces implied with a completely absorbing disk is already incredibly large; it is thus plausible that any region of transparency will be confined to a ring whose width is small compared to the disk radius. The impulse approximation should be trustworthy if (1) the time of interaction between antiproton and nucleons is short compared to the "period" of the deuteron [3]) and (2) the proximity of the nucleons in the deuteron does not modify their elementary interactions with the antiproton, an assumption whose validity we are unable to assess at present.

## 2. Calculations

It has proved convenient to formulate the semi-classical calculation in the following elementary manner. Let the radii of the proton and neutron

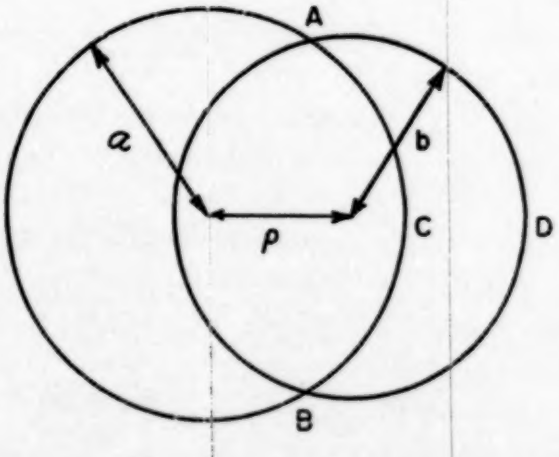


Fig. 1. Deuteron cross section in semi-classical model when $\varrho$, the projection of neutron-proton separation on a plane perpendicular to the beam, lies between $a-b$ and $a+b$.

black disks be denoted $a$ and $b$, respectively; as a matter of convention, let $a > b$. The deuteron absorption cross section, $\sigma_D$, depends strongly on $\varrho$, the projection of neutron-proton relative distance on a plane perpendicular to the beam. When $\varrho < a-b$, $\sigma_D = \pi a^2$ since the neutron cross section is completely eclipsed by the proton cross section. When $\varrho > a+b$, $\sigma_D = \pi(a^2+b^2)$. In the intermediate case $a-b < \varrho < a+b$, $\sigma_D = \pi a^2 + A(\varrho)$ where $A(\varrho)$ is the crescent moon which the neutron presents; in fig. 1, $A(\varrho)$ is the area ACBDA which is simply evaluated with the help of some formulas from plane geometry. With the notation $c = b/a$,

$$A(\varrho) = a^2\left\{c^2 \arccos\left[\frac{a}{2\varrho c}(1-c^2) - \frac{\varrho}{2ac}\right] - \arccos\left[\frac{a}{2\varrho}(1-c^2)+\frac{\varrho}{2a}\right]\right\} + \varrho a\sqrt{1-\left[\frac{a}{2\varrho}(1-c^2)+\frac{\varrho}{2a}\right]^2}. \tag{1}$$

The probability that $\varrho$ lies in the range $d\varrho$ is [4])

$$P(\varrho)d\varrho = 4\pi\varrho d\varrho \int_\varrho^\infty |\psi_D|^2 \frac{r dr}{\sqrt{r^2-\varrho^2}}. \tag{2}$$

The deuteron absorption cross section averaged over $\varrho$ is then

$$\sigma_D = \pi a^2 + \pi b^2 \int_{a-b}^\infty P(\varrho)d\varrho - \int_{a-b}^{a+b} (\pi b^2 - A(\varrho))P(\varrho)d\varrho. \tag{3}$$

In the case $a = b$, eq. (3) simplifies to

$$\sigma_D = 2\pi a^2 - 4a^3 \int_0^1 (\arccos \varrho' - \varrho'\sqrt{1-\varrho'^2})P(2a\varrho')d\varrho'. \tag{4}$$

This cross section for $a = b$ is equivalent to what is obtained from multiplication of Glauber's eqs. (29) and (30) [1]) by the deuteron wave function and subsequent numerical integration of the product over $r$.

Eqs. (3) and (4) have been evaluated with the following choices of deuteron wave function:

(a) Hulthén wave function (which approximates the solution for a Yukawa potential),

$$\psi_D = \left[\frac{\alpha}{2\pi}\frac{\beta(\alpha+\beta)}{(\alpha-\beta)^2}\right]^{\frac{1}{2}} \frac{(e^{-\alpha r}-e^{-\beta r})}{r} \tag{5}$$

with $\beta = 6\alpha$ corresponding to triplet effective range [5]), $\varrho_t(-\varepsilon, -\varepsilon) =$

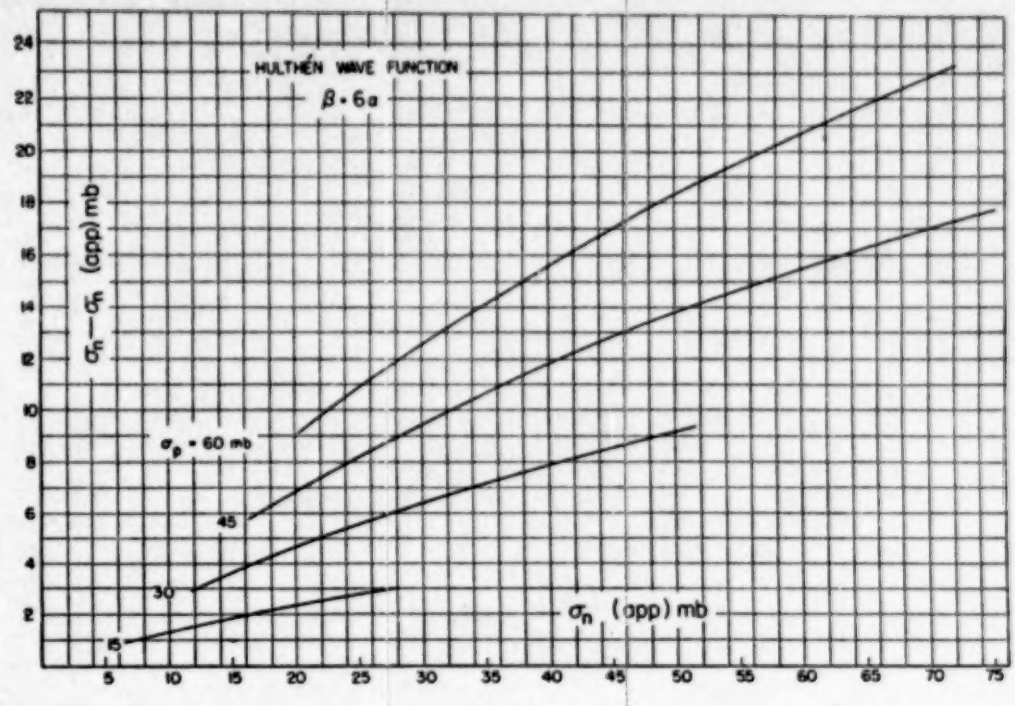


Fig. 2. Difference between true and apparent neutron cross sections versus apparent neutron cross section for proton cross sections equal to 15, 30, 45, and 60 mb. The deuteron is described by a Hulthén wave function with $\beta = 6\alpha$.

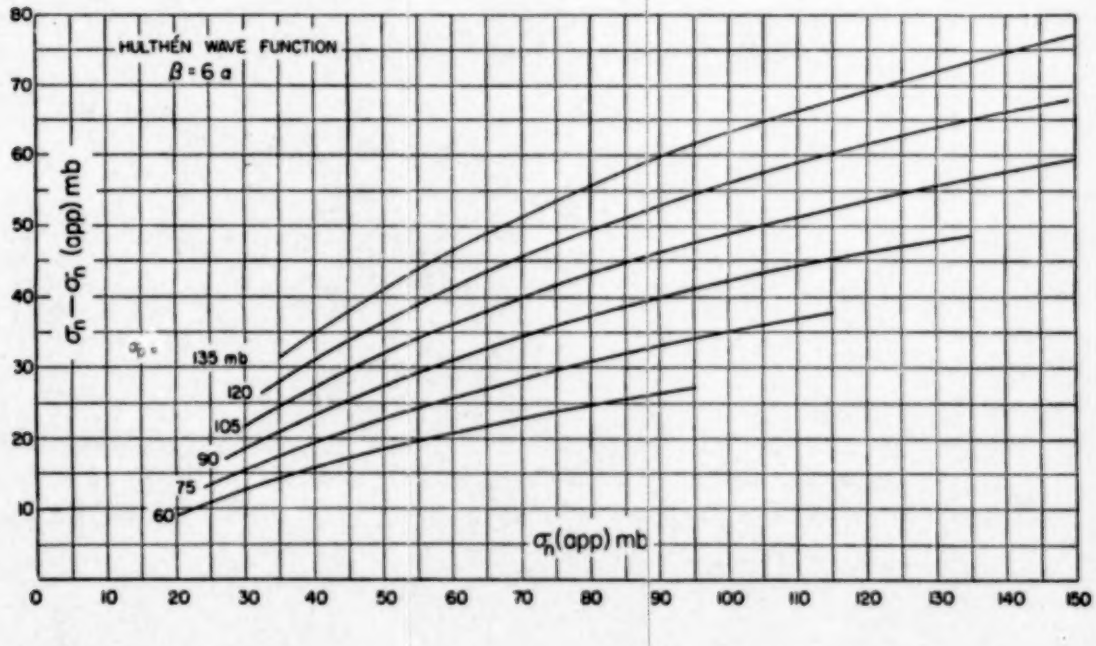


Fig. 3. Difference between true and apparent neutron cross sections versus apparent neutron cross section for proton cross sections equal to 60—135 mb. The deuteron is described by a Hulthén wave function with $\beta = 6\alpha$.

$1.75 \times 10^{-13}$ cm; the difference between true neutron and apparent neutron absorption cross sections,

$$\sigma_n - \sigma_n(\text{app}) = \sigma_n + \sigma_p - \sigma_D,$$

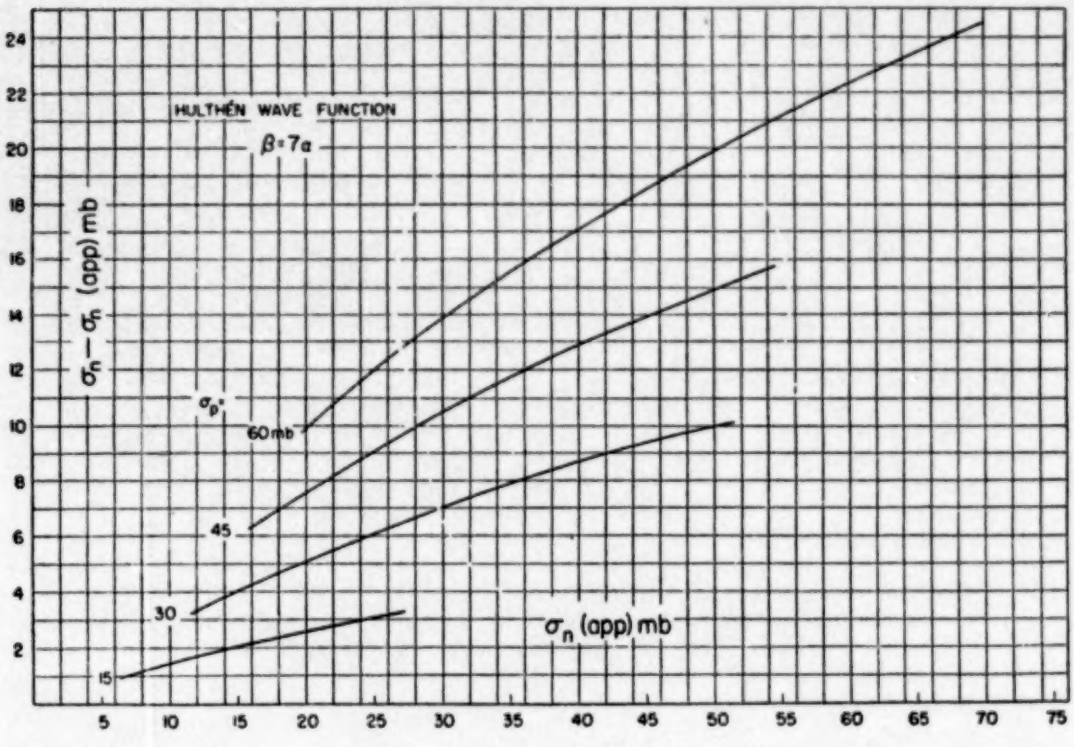


Fig. 4. Difference between true and apparent neutron cross sections versus apparent neutron cross section for proton cross sections equal to 15, 30, 45, and 60 mb. The deuteron is described by a Hulthén wave function with $\beta = 7\alpha$.

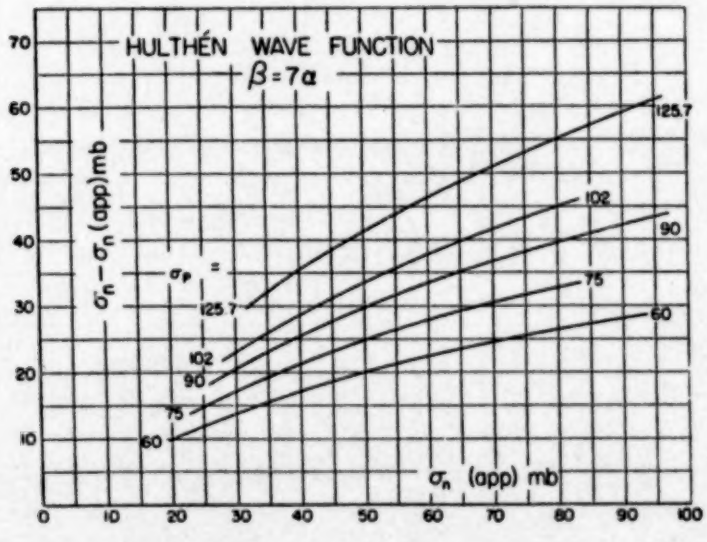


Fig. 5. Difference between true and apparent neutron cross sections versus apparent neutron cross section for proton cross sections equal to 60, 75, 90, 102, and 125.7 mb. The deuteron is described by a Hulthén wave function with $\beta = 7\alpha$.

is plotted versus apparent neutron cross section in figs. 2 and 3 for $\sigma_p$ varied from 15 millibarns to 135 millibarns in steps of 15 millibarns.

(b) Hulthén wave function, $\beta = 7\alpha$, corresponding to $\varrho_t(-\varepsilon, -\varepsilon) = 1.54\times10^{-13}$ cm. The results are shown in figs. 4 and 5.

(c) Gartenhaus wave function [6]), which is the solution of a potential obtained from the Yukawa meson theory with cut-off; this potential has the characteristic that the central contribution becomes extremely repulsive at very small distances while the tensor contribution goes to zero; the corresponding triplet effective range, $\varrho_t(-\varepsilon, -\varepsilon) = 1.76\times10^{-13}$ cm which is essentially equal to $\varrho_t(0, -\varepsilon) = 1.75\times10^{-13}$ cm [6]) determined for this potential.

Results for the case $a = b$ are given in table 1 for the Gartenhaus wave-function as well as the Hulthén wave function with $\beta = 6\alpha$. The probability, $P(\varrho)$, is shown in fig. 6 for all three wave functions.

TABLE 1

The difference $\sigma_n - \sigma_n$ (app) as a function of $\sigma_n$ for Hulthén ($\beta = 6\alpha$) and Gartenhaus wave functions in the case $\sigma_p = \sigma_n$

| $\sigma_n$ | $\sigma_n - \sigma_n$(app) Hulthén ($\beta = 6\alpha$) | $\sigma_n - \sigma_n$ (app) Gartenhaus |
|---|---|---|
| 15 | 1.66 | 1.17 |
| 30 | 5.46 | 4.32 |
| 45 | 10.53 | 8.96 |
| 60 | 16.6 | 14.5 |
| 75 | 23.6 | 21.0 |
| 90 | 30.8 | 27.8 |
| 105 | 38.6 | 35.5 |
| 120 | 46.9 | 43.3 |
| 135 | 55.8 | 51.8 |

The best experimental values for triplet effective range are

$$\varrho_t(0, -\varepsilon) = (1.70\pm0.03)\times10^{-13} \text{ cm } [7]),$$
$$\varrho_t(-\varepsilon, -\varepsilon) = (1.79\pm0.09)\times10^{-13} \text{ cm } [8]),$$

which are in good agreement if account is taken of the energy dependence of the range should the potential be of the Yukawa type [8]). The computations with the Hulthén potential for the case $\beta = 6\alpha$ are thus to be preferred over those with $\beta = 7\alpha$.

It is observed that the computed values of true minus apparent cross section are about 10 % higher for $\beta = 7\alpha$ than for $\beta = 6\alpha$; it is reasonable that the eclipsing corrections should be larger for the more compact wave function. Similarly, it is seen that the values computed with the Gartenhaus potential lie only about 10 % under those for Hulthén $\beta = 6\alpha$ except at

very small $\sigma_p$; the smaller value of $\sigma_n - \sigma_n(\text{app})$ for the Gartenhaus potential is attributable to the repulsive core. We shall comment on the larger percentage difference between these deuteron models observed at small $\sigma_p$ in the following section.

The general agreement in results as computed with the three different wave functions suggests that errors arising through use of an approximate rather than the unknown true deuteron wave function are probably small compared to other errors inherent to the semi-classical model.

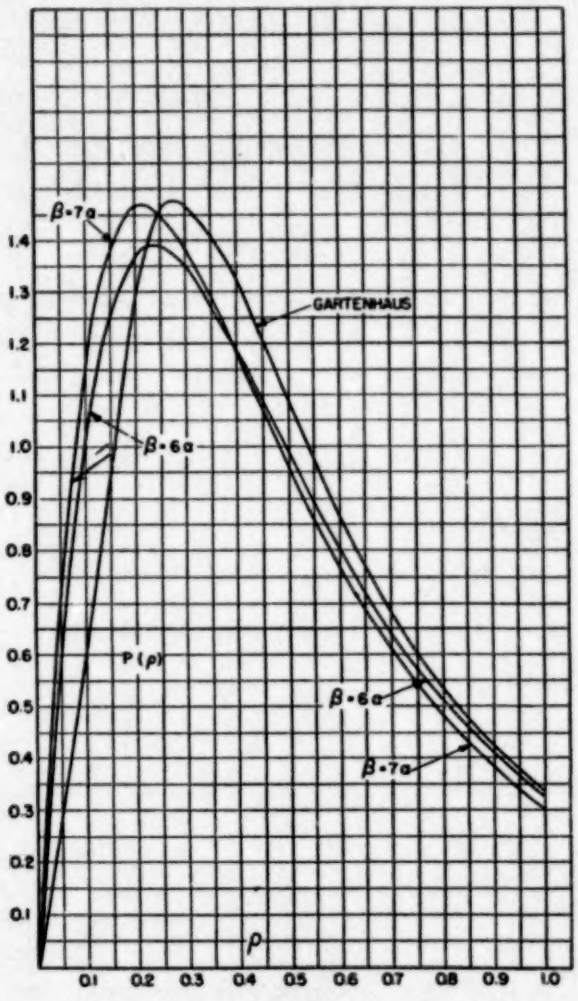


Fig. 6. The probability $P(\varrho)$ for the three wave functions: Hulthén $\beta = 6\alpha$, Hulthén $\beta = 7\alpha$, and Gartenhaus. $\varrho$ in units $1/\alpha$.

## 3. Discussion

An elementary geometrical argument has been given by Glauber [1]) to derive the following approximate formula for the difference between apparent and true neutron absorption cross sections,

$$\sigma_n - \sigma_n(\text{app}) = (\sigma_p \sigma_n / 2\pi)\langle 1/r^2 \rangle_D \qquad (6)$$

where $\langle 1/r^2 \rangle_D$ is the average value of the inverse radius squared of the deuteron. The constant $2C = (1/2\pi)\langle 1/r^2 \rangle_D$ has been estimated from high energy nucleon collisions to be $7.32 \times 10^{-3}$ mb$^{-1}$ [9]).

Inspection of figs. 2 and 4 shows indeed that for small cross sections, the graphs have the linear dependence predicted by eq. (6). We note, however, three difficulties which limit the usefulness of eq. (6):

(a) For large cross sections, the plots of $\sigma_n - \sigma_n$ (app) versus $\sigma_n$ (app) are not well approximated by straight lines passing through the origin.

(b) A value of $C$ appropriate to small cross sections ($\sigma_p \approx 15$—$30$ mb) is in bad disagreement with the magnitude of the eclipsing correction for

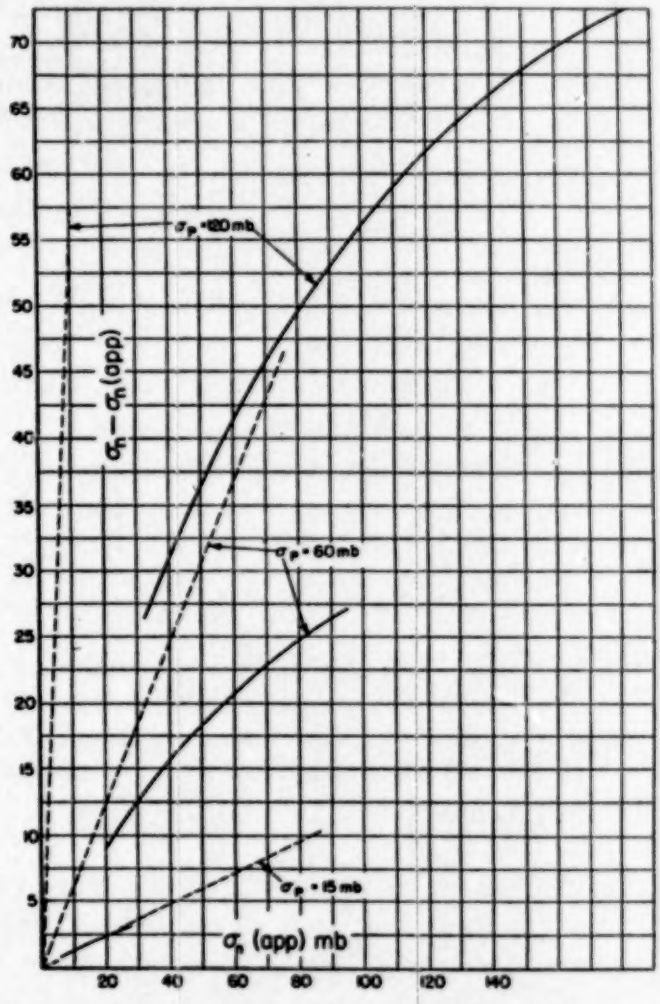


Fig. 7. Difference between true and apparent neutron cross sections versus apparent cross section for $\sigma_p = 15$, 60, and 120 mb as computed for Hulthén wave function with $\beta = 6\alpha$, as well as the linear dependence resulting from eq. (6) when $2C = 7.1 \times 10^{-3}$ mb$^{-1}$ to match the $\sigma_p = 15$ mb curve.

large cross sections ($\sigma_p \geqq 60$ mb). This is illustrated in fig. 7 where we have plotted $\sigma_n - \sigma_n$ (app) versus $\sigma_n$ (app) for 15, 60 and 120 mb as well as the

linear dependence resulting from eq. (6) when $2C = 7.1\times10^{-3}$ mb$^{-1}$ to match the $\sigma_p = 15$ mb curve.

(c) Even for small cross sections, the value of $C$ determined by approximately matching the computed curves is a function of $\sigma_p$. In the case of the Hulthén wave function $\beta = 6\alpha$, we find $2C = 7.1$, 6.2, and $5.2\times10^{-3}$ mb$^{-1}$, respectively, for $\sigma_p = 15$, 30, and 45 mb. The dependence is less marked for the Gartenhaus wave function where the corresponding values of $2C$ are 5.2, 4.8, and $4.4\times10^{-3}$ mb$^{-1}$.

The physical reason [1]) for discrepancies between eq. (6) and the numerical calculations is simply that eq. (6) was derived in the approximation that the black disk radii be small compared to the deuteron separation. To understand more quantitatively the region of validity of this equation, let us consider possible approximations to eq. (4). When $2a < \varrho_{max}$, the value of $\varrho$ at which $P(\varrho)$ is a maximum, inspection of fig. 6 suggests that it is reasonable to represent $P(2a\varrho')$ in eq. (4) by $2\varrho' P(a)$. Then eq. (4) becomes

$$\sigma_n - \sigma_n(\text{app}) \approx \sigma_n \sigma_p \frac{P(a)}{2\pi a}. \tag{7}$$

From fig. 6 we find that the coefficient $P(a)/2\pi a$ is $6.9\times10^{-3}$ mb$^{-1}$ for the Hulthén wave-function with $\beta = 6\alpha$, and $5.5\times10^{-3}$ mb$^{-1}$ for the Gartenhaus wave function when $\pi a^2 = 15$ mb, in good agreement with the previous values of $C$ obtained by inspection of fig. 2 and table 1. The agreement is much less satisfactory, however, for larger values of $\pi a^2$.

Should $|\psi_D|^2$ be very small for $r$ less than or of the order of $a$, we see from eq. (2) that it is justified to approximate further

$$P(a)/a \approx \langle 1/r^2\rangle_D, \tag{8}$$

a result which immediately leads to eq. (6) †. This replacement appears well justified for the Gartenhaus wave function where we compute $(1/2\pi)\langle 1/r^2\rangle_D = 4.7\times10^{-3}$ mb$^{-1}$. In the case of the Hulthén wave function eq. (8) holds only at extremely small $a$; for $\beta = 6\alpha$ we compute

$$(1/2\pi)\langle 1/r^2\rangle_D = 11.4\times10^{-3}\,\text{mb}^{-1}.$$

The above is in agreement with Glauber's similar observation that the asymptotic result, eq. (6), is a good approximation with another repulsive core wave function, proposed by Blatt and Kalos [10]), when $\pi a^2 = 22.7$ mb.

It is not clear that deuteron experiments, where both the comparable proton and neutron cross sections are known, can be used to investigate the aspect of the deuteron wave functions at small separation as suggested by eqs. (6) and (7); when there are significant percentage differences between the shadow corrections predicted by various models, the elementary cross

† Cf. a more general derivation in ref. [1]), resulting in eq. (25) of ref. [1]).

sections are so small that the classical black disk assumption is quite questionable, and further, the ratio of the shadow correction to elementary cross section approaches zero. Let us mention again that the shadow correction in the black disk approximation does not appear greatly dependent on deuteron model when the elementary cross sections are large; in these cases, the correction depends more strongly on the deuteron wave function at moderate and large separations, which is determined largely by the binding energy and effective range.

In application of these results to the antiproton experiments, the question arises, what measured cross section is the appropriate classical cross section of these formulas. If the only appreciable physical processes are annihilation and diffraction scattering, then the annihilation cross section is clearly the appropriate quantity. If, however, it is believed that a bad geometry total cross section does not include appreciable diffraction scattering but only "classical" scattering and annihilation, then such a total cross section should be used. The semi-classical calculation of the absorption cross section does not include small corrections due to the fact that the shadow of one nucleon on the other is not sharp. Proton and apparent neutron cross sections for 457 MeV antiprotons with cut-off below $14^0$ are $104\pm8$ and $70\pm8$ mb, respectively [2]); the corresponding true neutron cross section for Hulthén wave function with $\beta = 6\alpha$ equals 110 mb. Proton and apparent neutron annihilation cross sections are $89\pm7$ and $46\pm8$ mb [2]); the corresponding corrected neutron cross section is 72 mb. The small amount of diffraction scattering observed by Cork, Lambertson, Piccioni and Wenzel [11]) implies, however, that the antiproton cross sections are not well represented by sharp edged black disks. It is likely that this observation can be explained by a partially absorbing ring with width of the order $\lambda\!\!\!^{-}$ at the edge of the disk, in which case the corrected cross sections quoted above will still be fair estimates.

We wish to thank Professor Owen Chamberlain for conversations which induced us to undertake this computation, Mr. Paul Stevens for carrying out much of the tedious numerical work, and Dr. Solomon Gartenhaus for providing us with tabulated values for his deuteron wave function. We gratefully acknowledge the support provided by the U. S. Atomic Energy Commission and the Higgins Scientific Trust Fund while the author was completing this work at Princeton University.

## References

1) R. J. Glauber, Phys. Rev. **100** (1955) 242
2) Chamberlain, Keller, Mermod, Segrè, Steiner and Ypsilantis, Phys. Rev. **108** (1957) 1553

3) G. F. Chew and G. C. Wick, Phys. Rev. **85** (1952) 636
4) R. Serber, Phys. Rev. **72** (1947) 1008
5) H. A. Bethe, Phys. Rev. **76** (1949) 38
6) S. Gartenhaus, Phys. Rev. **100** (1955) 900
7) Ringo, Burgy and Hughes, Phys. Rev. **82** (1951) 344
8) D. H. Wilkinson, Phys. Rev. **86** (1952) 373
9) F. F. Chen, C. P. Leavitt and A. M. Shapiro, Phys. Rev. **103** (1956) 211, Appendix 1
10) J. M. Blatt and M. H. Kalos, Phys. Rev. **92** (1953) 1563
11) Cork, Lambertson, Piccioni and Wenzel, Phys. Rev. **107** (1957) 248

*Nuclear Physics* **6** (1958) 359—403; © *North-Holland Publishing Co., Amsterdam*
Not to be reproduced by photoprint or microfilm without written permission from the publisher

# PHENOMENOLOGICAL NEUTRON PROTON POTENTIALS

L. C. BIEDENHARN
*Rice Institute, Houston, Texas*

J. M. BLATT
*The F.B.S. Falkiner Nuclear Research and Adolph Basser Computing Laboratories, School of Physics, University of Sydney* †

and

M. H. KALOS
*Nuclear Development Associates, White Plains, N.Y.*

Received 30 September 1957

**Abstract:** This paper presents in tabular form, and discusses some of the features of a number of phenomenological neutron-proton potentials all of which fit the low energy neutron-proton data in the triplet spin state. Special attention has been paid to the influence of different well shapes for the central and tensor forces, and to the effect of an infinite repulsive core.

## 1. Introduction

In this paper we present, and discuss, a number of phenomenological neutron-proton potentials all of which fit the low energy neutron proton data in the triplet spin state. Special attention has been paid to the influence of different well shapes for the central and tensor forces, and to the effect of an infinite repulsive core. A number of representative wave functions for the ground state of the deuteron are also tabulated here.

We intend to use these potentials to analyze two-body scattering data at higher energies, and data concerning the nuclear three-body problem. Thus the present work should be considered the first step in an investigation of the phenomenology of nuclear forces, not as a set of final results. That is, although all the potentials given here do fit the low energy two-body data, most of them will not fit the high energy two-body data, or the three-body data, or both. We are publishing the present information because it forms a reasonably self-contained portion of the whole investigation, and the results may be useful to others.

In view of the mounting evidence that the high energy two-body data cannot be described by any static potential [1]) and the well-known fact that

† Also supported by the Nuclear Research Foundation within the University of Sydney. Part of this work was done while this author was visiting Professor at Princeton University.

the low-energy two-body scattering data are described very well by the effective range theory [2, 3]), one might question the value of a phenomenological investigation based on static potentials. We believe, however, that such an investigation is worth while, for the following reasons:

1) Not all the low-energy two-body data can be discussed in terms of the effective range theory. Outstanding exceptions are the quadrupole moment of the deuteron and the deviation of the deuteron magnetic moment from the sum of proton and neutron magnetic moments.

2) Although the two-body scattering data at energies around 300 MeV are very likely inconsistent with simple static potentials, it is not at all clear at present at which energy the description in terms of static potentials breaks down. It is quite possible, a priori, that static potentials can provide a reasonable fit to the intermediate energy two-body data and yet break down badly at energies in excess of 100 MeV. If this should turn out to be true, these static potentials would be a more convenient description of the intermediate energy two-body data than the effective range theory.

3) Finally, as soon as we want to use the information from the two-body data to analyze other nuclei, for example the triton, the effective range description of the two-body data fails completely, and so do all descriptions based entirely on scattering matrix quantities. Matrix elements "off the energy shell" become essential. The difficulty of solving the Schroedinger equation for the triton in the presence of non-central forces is so large that, for the present at least, it is highly desirable to describe the nuclear forces in terms of static potentials or perhaps minor modifications thereof. Suppose, for the sake of argument, that there exists a static potential which fits the two-body data to a reasonable approximation up to energies of the order of 100 MeV, but fails at higher energies. In that case this static potential cannot be the complete law of nuclear force. Nevertheless, this potential should give a reasonable approximation for the triton, because the kinetic energies in the triton ground state are predominantly below 100 MeV. Conversely, if the theoretical predictions from this hypothetical potential should fail to fit the triton data, this would be a strong indication that many-body forces are present and of importance, and one could obtain at least some information about these many-body forces.

For such a program to succeed, it is essential, however, that the potential used for the triton investigation fits the two-body data not only at very low energies, but also in the intermediate range of energies (10 to 100 MeV, say). Two different potentials both fitting the *low* energy two-body data but leading to different results for two-body scattering at intermediate energies, will in general give quite different results for the triton.

Hence the potentials given in this paper need further investigation before

being used in a study of the triton. We intend to examine the effects of these potentials for intermediate energy two-body scattering, and then use the acceptable potentials (if any) for an investigation of the triton. Unlike ref. [1]), however, we shall not require that the potentials fit the two-body data at energies around 300 MeV.

Section 2 presents the set of potentials which we have determined and discusses the reasons for their choice. In section 3 we discuss the numerical results, paying particular attention to the effects of well shape and of a repulsive core. In section 4 we present potentials which satisfy the criterion that the range and shape of the central force (but not its well depth) be the same for the singlet and triplet spin states of the neutron-proton system. Such potentials have often been used in the analysis of three-body data, especially the ones with Gaussian well shapes, and no repulsive core.

## 2. Potentials used and Numerical Results

In a phenomenological investigation such as this, it is necessary to restrict the choice of potentials to "simple" shapes. We shall restrict ourselves to potentials which have the same sign everywhere outside a "core radius" $r_0$. The wave functions are supposed to vanish at $r = r_0$, i.e., we assume an infinitely high perfectly repulsive core. Outside the core, the phenomenological well shape can either be "cut off" by the core, or "moved out" bodily beyond the core. For example, the Gaussian well shape can be written either as a "cut off" well:

$$\begin{aligned} V(r) &= +\infty && (r < r_0) \\ &= -V_0 \exp(-\alpha r^2) && (r > r_0), \end{aligned} \tag{2.1}$$

or else as a "moved out" well:

$$\begin{aligned} V(r) &= +\infty && (r < r_0) \\ &= -V_0 \exp[-\alpha(r-r_0)^2] && (r > r_0). \end{aligned} \tag{2.2}$$

We shall always use "moved out" wells. We shall see that the interpretation of the results is aided considerably by considering the potential outside the core as the quantity of main interest, the core itself acting merely as a boundary condition.

Of course, if there exists a repulsive core in nature, it must be at least somewhat "soft". However, the likely distances over which the repulsive core potential rises to substantially infinite heights (for low energy purposes) are so short that the "softness" of the core can be ignored here. A soft but very steep repulsive core can be replaced to a very good approximation by an infinitely hard repulsive core at some appropriate mean distance. This is the sense in which our assumption of an infinitely hard core should be understood.

We have used three well shapes for the potentials outside the core: the Gauss well, the exponential well, and the Yukawa well. Since we move the potential out beyond the core, *our "Yukawa" wells have an infinitely deep hole just outside the core*, unlike the "cut-off" Yukawa wells used in ref. [1]). The Gauss shape is very "concentrated", the Yukawa shape gives a very "long-tailed" and "deep-hole" well, whereas the exponential well is a reasonable intermediate shape. Thus we believe that any conclusions which are true for these three well shapes may be assumed to hold for all "simple" well shapes.

In order to make comparison between different well shapes easy, we have used the "intrinsic range" $b$ and the non-dimensional well-depth parameter $s$ to specify the range and depth of the moved-out well [4]). We recall that $s = 1$ means a (central) potential which yields a zero energy scattering resonance. The value of $s$ appropriate for the singlet state of the neutron-proton system lies between 0.9 and 1.0.

It is convenient to measure energies in units of the binding energy of the deuteron, $B = 2.226$ MeV, and lengths in units of the "radius" of the deuteron, $R = 4.315 \times 10^{-13}$ cm.

For any choice of the two well shapes (one for the central force, the other for the tensor force), there remain five adjustable parameters:

$$\begin{aligned} &r_0, \text{ the core radius,} \\ &s_c, \text{ the depth of the central force outside the core,} \\ &b_c, \text{ the range of the central force outside the core,} \\ &s_t, \text{ the depth of the tensor force outside the core,} \\ &b_t, \text{ the range of the tensor force outside the core.} \end{aligned} \tag{2.3}$$

These are reduced to two free parameters by using three experimental data:

$$\begin{aligned} &\text{the binding energy of the deuteron, } B = 2.226 \text{ MeV,} \\ &\text{the quadrupole moment of the deuteron, } Q = 2.74 \times 10^{-27} \text{ cm}^2 \\ &\text{the zero energy triplet scattering length, } a_t = 5.39 \times 10^{-13} \text{ cm.} \end{aligned} \tag{2.4}$$

This scattering length is the measured quantity from which the so-called triplet effective range is derived. Although the triplet effective range could in principle be measured directly, this has not been done as yet. For very long-tailed wells, the distinction between the scattering length and the effective range is important, but for most of the wells given here, fitting $a_t$ can be described as "fitting the triplet effective range".

The computer adjusts the tensor force well depth $s_t$ to give the right binding energy $B$ (this equals 1 in our units), and we are then left with 4 parameters to fit the 2 experimental quantities

$$\text{“}Q\text{”} = Q/R^2 = 0.0147 \qquad \text{“}a_t\text{”} = a_t/R = 1.249. \tag{2.4'}$$

We have chosen the core radius $r_0$ and the central force well depth $s_c$ as our two "free" parameters for most of this investigation. In section 4 we have used the central force range $b_c$ rather than $s_c$ as a free parameter, in order to get a central well which differs from the potential in the $^1S$ state only by a change in the well depth.

Four choices were allowed for the core radius $r_0$, namely,

$$\begin{aligned} r_0 &= 0 \\ r_0 &= 0.05\,R = 0.22\times 10^{-13}\ \text{cm} \\ r_0 &= 0.10\,R = 0.43\times 10^{-13}\ \text{cm} \\ r_0 &= 0.15\,R = 0.65\times 10^{-13}\ \text{cm}, \end{aligned} \tag{2.5}$$

and three choices were allowed for the central force depth $s_c$:

$$\begin{aligned} s_c &= 0.6 \\ s_c &= 0.9 \\ s_c &= 1.0. \end{aligned} \tag{2.6}$$

Four choices for $r_0$, three choices for $s_c$, three choices (Gaussian, exponential, and Yukawa) for the central force well shape, and three choices for the tensor force well shape, give altogether 108 combinations. We have determined suitable sets of the remaining parameters ($b_c$, $s_t$, and $b_t$) for 104 out of these 108 possibilities, and have obtained wave functions as well. Some representative wave functions are tabulated at the end of this paper. The 4 missing cases will be discussed later.

Tables 2.1, 2.2 and 2.3 of this section contain a summary of the numerical results (excluding wave functions). In addition to the quantities mentioned so far, the tables also give the D-state probability $P_D$, the "shape parameter" $P$ of the effective range formula [4]), and the partial derivatives of most quantities with respect to variations in the ranges $b_c$ and $b_t$. These derivatives were obtained from numerical results for wells which are close to the ones given in the table; the derivatives are to be understood as follows: the independent variables are the core radius $r_0$ (expressed in units of $R$), the central force well depth parameter $s_c$, the binding energy of the deuteron $B$ (= 1, in our units), and the ranges $b_c$ and $b_t$. Of these five quantities, the first three are kept constant as well as one of $b_c$ or $b_t$. Thus the derivative $\partial Q/\partial b_c$, for example, is equal to $(\partial Q/\partial b_c)_{r_0, s_c, B, b_t}$. Since a change in the binding energy of the deuteron amounts to merely a change of scale, other derivatives can be inferred from the ones given here.

The calculation was performed on the SILLIAC, the electronic computer in the Adolph Basser Computing Laboratory within the School of Physics, Sydney University. We used a code which had been developed for the

ILLIAC at the University of Illinois [5]). Some slight modifications were made, but no extensive recoding was required because the order codes of SILLIAC and ILLIAC are identical.

Although the numerical accuracy of the solution of the Schroedinger equation with the assumed potentials is adequate for our purposes, there are relativistic and meson theoretic corrections to results obtained with any static potential. It is commonly believed that these corrections are small for the quantities we have used as input data. In particular, estimates of field theoretic corrections to the quadrupole moment of the deuteron [6]) show these corrections to be small. This is as expected: the main contribution to $Q$ comes from the "exterior" region, i.e., the region in which the two nucleons are well separated and a simple static approximation should be valid. Furthermore, the quadrupole moment, as an electric moment, is less subject to mesonic corrections than magnetic moments [7]).

---

## Table Captions for Tables 2.1-2.4

These tables contain a large number of potentials which fit the low energy properties of the neutron-proton system in the triplet spin state, i.e., the binding energy of the deuteron, the quadrupole moment of the deuteron and the triplet scattering length $a_t$ (related to the triplet effective range).

The unit of length in these tables is the "radius of the deuteron", $R = 4.315\times 10^{-13}$ cm, and the unit of energy is the binding energy of the deuteron, $B = 2.226$ MeV. In these units, the quadrupole moment $Q = 0.0147$, and the triplet scattering length $a_t = 1.249$.

The first three columns define the central force; the three well shapes used are Gaussian (G), exponential (E), and Yukawa (Y). In the case of non-zero repulsive core, these are "moved out" wells, for example the "Yukawa" well shape becomes infinite at the core radius, not at $r = 0$. The central force well depth $s_c$ is defined so that $s_c = 1$ corresponds to a scattering resonance at zero energy, if there is no tensor force acting; $b_c$ is the intrinsic range of the central force, defined as in Blatt and Jackson, and measured in units of the deuteron radius. The next three columns define the shape, depth, and range of the tensor force.

Column 7 contains the D-state probability, $P_D$, column 8 the effective range $\varrho$ computed from the ground state wave functions, i.e., $\varrho(-\varepsilon, -\varepsilon)$ of Bethe [8]). Columns 9 and 10 contain two different estimates of the shape-dependent parameter $P$ of the effective range theory. These two estimates are

$$P_1 = \frac{\varrho - r_{0t}}{4(r_{0t})^3}, \qquad P_2 = [1-(a_t)^{-1}-\tfrac{1}{2}r_{0t}]\,(r_{0t})^{-2},$$

where $r_{0t}$ is the effective range determined from the zero-energy wave functions, i.e., $\varrho(0, 0)$ in the notation of Bethe.

The next 8 columns contain partial derivatives of various quantities ($s_t$, $P_D$, $Q$, and $a_t$) with respect to the two ranges $b_c$ and $b_t$. These derivatives were estimated from numerical results for potentials with neighbouring parameters, and are not very accurate. The core radius $r_0$, central force strength $s_c$, and binding energy of the deuteron ($B = 1$ in our units) are the other independent variables which are kept constant in this partial differentiation. Since a change in $B$ amounts to merely a change of the scale of lengths and energies, other partial derivatives can be inferred from the ones given here.

Table 2.1 contains results with core radius $r_0 = 0$, table 2.2 has $r_0 = 0.05\ R = 0.22\times 10^{-13}$ cm, table 2.3 has $r_0 = 0.10\ R = 0.43\times 10^{-13}$ cm, and table 2.4 has $r_0 = 0.15\ R = 0.65\times 10^{-13}$ cm.

TABLE 2.1

TABLE 2.1

Core Radius $r_0 = 0$

| Central Force | | | Tensor Force | | | $P_D$ | $\varrho$ | $P_1$ | $P_2$ | $\frac{\partial s_t}{\partial b_c}$ | $\frac{\partial s_t}{\partial b_t}$ | $\frac{\partial P_D}{\partial b_c}$ | $\frac{\partial P_D}{\partial b_t}$ | $\frac{\partial Q}{\partial b_c}$ | $\frac{\partial Q}{\partial b_t}$ | $\frac{\partial A}{\partial b_c}$ | $\frac{\partial A}{\partial b_t}$ |
|---|---|---|---|---|---|---|---|---|---|---|---|---|---|---|---|---|---|
| Shape | Depth $s_c$ | Range $b_c$ | Shape | Depth $s_t$ | Range $b_t$ | | | | | | | | | | | | |
| G | 0.6 | 0.4648 | G | 1.1993 | 0.6017 | 0.05343 | 0.3953 | —0.027 | —0.029 | | | | | | | | |
| ,, | 0.9 | 0.4241 | ,, | 0.9766 | 0.6868 | 0.04306 | 0.3957 | —0.024 | —0.025 | | | | | | | | |
| ,, | 1.0 | 0.4174 | ,, | 0.8821 | 0.7435 | 0.03782 | 0.3962 | —0.021 | —0.023 | | | | | | | | |
| ,, | 0.6 | 0.5409 | E | 1.2468 | 0.6116 | 0.04914 | 0.3966 | —0.017 | —0.017 | 0.33 | 0.40 | 0.009 | 0.068 | 0.007 | 0.032 | 0.27 | 0.38 |
| ,, | 0.9 | 0.4627 | ,, | 0.9837 | 0.7291 | 0.03918 | 0.3968 | —0.017 | —0.018 | 0.42 | 0.47 | 0.025 | 0.047 | 0.012 | 0.025 | 0.30 | 0.16 |
| ,, | 1.0 | 0.4489 | ,, | 0.8908 | 0.7968 | 0.03491 | 0.3973 | —0.013 | —0.014 | 0.48 | 0.48 | 0.038 | 0.038 | 0.016 | 0.022 | 0.34 | 0.14 |
| ,, | 0.6 | 0.6076 | Y | 1.3413 | 0.6186 | 0.04447 | 0.3990 | 0.001 | 0.000 | 0.45 | 0.25 | 0.011 | 0.054 | 0.007 | 0.027 | 0.18 | 0.18 |
| ,, | 0.9 | 0.4940 | ,, | 1.0388 | 0.7730 | 0.03532 | 0.3988 | —0.002 | —0.004 | 0.66 | 0.26 | 0.030 | 0.033 | 0.014 | 0.019 | 0.31 | 0.11 |
| ,, | 1.0 | 0.4748 | ,, | 0.9333 | 0.8676 | 0.03147 | 0.3997 | 0.005 | 0.002 | 0.77 | 0.26 | 0.039 | 0.025 | 0.018 | 0.016 | 0.36 | 0.08 |
| E | 0.6 | 0.4840 | G | 1.2109 | 0.6009 | 0.05343 | 0.3967 | —0.016 | —0.017 | 0.05 | 0.71 | 0.001 | 0.086 | 0.003 | 0.038 | 0.14 | 0.32 |
| ,, | 0.9 | 0.4390 | ,, | 0.9787 | 0.6899 | 0.04245 | 0.3973 | —0.011 | —0.012 | 0.15 | 0.72 | 0.014 | 0.065 | 0.007 | 0.033 | 0.24 | 0.24 |
| ,, | 1.0 | 0.4340 | ,, | 0.8896 | 0.7421 | 0.03757 | 0.3979 | —0.007 | —0.008 | 0.27 | 0.69 | 0.027 | 0.055 | 0.011 | 0.030 | 0.27 | 0.21 |
| ,, | — | — | E | — | — | — | — | — | — | — | — | — | — | — | — | — | — |
| ,, | 0.6 | 0.5903 | ,, | 1.2470 | 0.6138 | 0.04890 | 0.4000 | 0.008 | 0.007 | 0.23 | 0.45 | 0.007 | 0.069 | 0.005 | 0.032 | 0.14 | 0.24 |
| ,, | 0.9 | 0.4907 | ,, | 0.9874 | 0.7304 | 0.03885 | 0.3993 | 0.004 | 0.002 | 0.33 | 0.51 | 0.020 | 0.048 | 0.009 | 0.026 | 0.25 | 0.17 |
| ,, | 1.0 | 0.4748 | ,, | 0.8936 | 0.7985 | 0.03451 | 0.3999 | 0.007 | 0.006 | 0.41 | 0.48 | 0.030 | 0.040 | 0.013 | 0.023 | 0.32 | 0.17 |
| ,, | 0.6 | 0.6943 | Y | 1.3322 | 0.6231 | 0.04410 | 0.4054 | 0.051 | 0.047 | 0.39 | 0.30 | 0.001 | 0.053 | 0.004 | 0.027 | 0.12 | 0.19 |
| ,, | 0.9 | 0.5345 | ,, | 1.0297 | 0.7830 | 0.03475 | 0.4025 | 0.028 | 0.026 | 0.52 | 0.30 | 0.023 | 0.033 | 0.011 | 0.019 | 0.25 | 0.11 |
| ,, | 1.0 | 0.5105 | ,, | 0.9250 | 0.8803 | 0.03084 | 0.4033 | 0.034 | 0.031 | 0.63 | 0.29 | 0.032 | 0.026 | 0.015 | 0.016 | 0.31 | 0.08 |
| Y | 0.6 | 0.5210 | G | 1.2288 | 0.5977 | 0.05368 | 0.3997 | 0.006 | 0.004 | 0.00 | 0.72 | 0.000 | 0.088 | 0.002 | 0.039 | 0.09 | 0.33 |
| ,, | 0.9 | 0.4677 | ,, | 0.9939 | 0.6851 | 0.04256 | 0.4005 | 0.012 | 0.010 | 0.08 | 0.77 | 0.008 | 0.069 | 0.005 | 0.034 | 0.19 | 0.24 |
| ,, | 1.0 | 0.4659 | ,, | 0.8989 | 0.7389 | 0.03741 | 0.4016 | 0.021 | 0.019 | 0.24 | 0.68 | 0.021 | 0.059 | 0.009 | 0.031 | 0.22 | 0.20 |
| ,, | 0.6 | 0.7224 | E | 1.2595 | 0.6094 | 0.04876 | 0.4106 | 0.083 | 0.066 | 0.14 | 0.48 | 0.004 | 0.070 | 0.003 | 0.034 | 0.07 | 0.32 |
| ,, | 0.9 | 0.5460 | ,, | 0.9973 | 0.7264 | 0.03870 | 0.4052 | 0.047 | 0.041 | 0.22 | 0.54 | 0.012 | 0.052 | 0.010 | 0.026 | 0.23 | 0.17 |
| ,, | 1.0 | 0.5257 | ,, | 0.8998 | 0.7955 | 0.03420 | 0.4056 | 0.051 | 0.046 | 0.36 | 0.50 | 0.022 | 0.045 | 0.010 | 0.025 | 0.22 | 0.19 |
| ,, | — | — | Y | — | — | — | — | — | — | — | — | — | — | — | — | — | — |
| ,, | 0.9 | 0.6262 | ,, | 1.0282 | 0.7829 | 0.03425 | 0.4123 | 0.105 | 0.094 | 0.36 | 0.32 | 0.016 | 0.033 | 0.008 | 0.019 | 0.15 | 0.09 |
| ,, | 1.0 | 0.5869 | ,, | 0.9210 | 0.8835 | 0.03025 | 0.4121 | 0.105 | 0.095 | 0.49 | 0.28 | 0.024 | 0.026 | 0.011 | 0.017 | 0.22 | 0.06 |

TABLE 2.2

Core Radius $r_0 = 0.05$

| Central Force | | | Tensor Force | | | $P_D$ | $\varrho$ | $P_1$ | $P_2$ | $\frac{\partial s_t}{\partial b_c}$ | $\frac{\partial s_t}{\partial b_t}$ | $\frac{\partial P_D}{\partial b_c}$ | $\frac{\partial P_D}{\partial b_t}$ | $\frac{\partial Q}{\partial b_c}$ | $\frac{\partial Q}{\partial b_t}$ | $\frac{\partial A}{\partial b_c}$ | $\frac{\partial A}{\partial b_t}$ |
|---|---|---|---|---|---|---|---|---|---|---|---|---|---|---|---|---|---|
| Shape | Depth $s_c$ | Range $b_c$ | Shape | Depth $s_t$ | Range $b_t$ | | | | | | | | | | | | |
| G | 0.6 | 0.3336 | G | 1.0052 | 0.5479 | 0.05803 | 0.3943 | —0.035 | —0.035 | —0.05 | 0.89 | —0.005 | 0.085 | 0.004 | 0.038 | 0.18 | 0.30 |
| ,, | 0.9 | 0.3116 | ,, | 0.8051 | 0.6501 | 0.04454 | 0.3948 | —0.031 | —0.032 | 0.02 | 0.83 | 0.014 | 0.063 | 0.008 | 0.032 | 0.28 | 0.23 |
| ,, | 1.0 | 0.3093 | ,, | 0.7275 | 0.7160 | 0.03815 | 0.3953 | —0.027 | —0.028 | 0.24 | 0.76 | 0.036 | 0.051 | 0.013 | 0.029 | 0.35 | 0.19 |
| ,, | 0.6 | 0.3980 | E | 0.9961 | 0.5747 | 0.05379 | 0.3949 | —0.030 | —0.031 | 0.27 | 0.64 | 0.006 | 0.068 | 0.007 | 0.031 | 0.21 | 0.22 |
| ,, | 0.9 | 0.3461 | ,, | 0.7837 | 0.7110 | 0.04126 | 0.3955 | —0.026 | —0.028 | 0.36 | 0.58 | 0.026 | 0.045 | 0.013 | 0.025 | 0.32 | 0.16 |
| ,, | 1.0 | 0.3367 | ,, | 0.7067 | 0.7990 | 0.03549 | 0.3962 | —0.021 | —0.023 | 0.50 | 0.53 | 0.043 | 0.036 | 0.017 | 0.022 | 0.38 | 0.13 |
| ,, | 0.6 | 0.4532 | Y | 0.9979 | 0.6227 | 0.04841 | 0.3964 | —0.019 | —0.021 | 0.44 | 0.46 | 0.012 | 0.049 | 0.009 | 0.025 | 0.22 | 0.16 |
| ,, | 0.9 | 0.3745 | ,, | 0.7750 | 0.8222 | 0.03676 | 0.3975 | —0.012 | —0.015 | 0.65 | 0.35 | 0.035 | 0.027 | 0.017 | 0.016 | 0.35 | 0.09 |
| ,, | 1.0 | 0.3611 | ,, | 0.6967 | 0.9619 | 0.03158 | 0.3991 | —0.001 | —0.005 | 0.79 | 0.31 | 0.050 | 0.020 | 0.023 | 0.013 | 0.41 | 0.06 |
| E | 0.6 | 0.3372 | G | 1.0166 | 0.5458 | 0.05820 | 0.3947 | —0.031 | —0.032 | —0.12 | 0.93 | —0.009 | 0.087 | 0.002 | 0.039 | 0.15 | 0.32 |
| ,, | 0.9 | 0.3164 | ,, | 0.8138 | 0.6469 | 0.04457 | 0.3954 | —0.026 | —0.027 | 0.01 | 0.84 | 0.009 | 0.065 | 0.007 | 0.033 | 0.25 | 0.24 |
| ,, | 1.0 | 0.3160 | ,, | 0.7321 | 0.7146 | 0.03794 | 0.3960 | —0.022 | —0.023 | 0.23 | 0.77 | 0.031 | 0.053 | 0.012 | 0.030 | 0.32 | 0.20 |
| ,, | 0.3 | 0.6357 | E | 1.2011 | 0.5072 | 0.06271 | 0.3986 | —0.003 | —0.005 | 0.13 | 0.73 | 0.002 | 0.087 | 0.002 | 0.037 | 0.06 | 0.25 |
| ,, | 0.6 | 0.4175 | ,, | 0.9970 | 0.5767 | 0.05366 | 0.3961 | —0.021 | —0.022 | 0.18 | 0.69 | 0.002 | 0.069 | 0.005 | 0.032 | 0.18 | 0.23 |
| ,, | 0.9 | 0.3580 | ,, | 0.7867 | 0.7118 | 0.04101 | 0.3965 | —0.018 | —0.020 | 0.28 | 0.61 | 0.020 | 0.047 | 0.011 | 0.025 | 0.28 | 0.16 |
| ,, | 1.0 | 0.3485 | ,, | 0.7080 | 0.8015 | 0.03510 | 0.3973 | —0.013 | —0.015 | 0.43 | 0.55 | 0.037 | 0.037 | 0.015 | 0.022 | 0.34 | 0.13 |
| ,, | 0.6 | 0.4909 | Y | 0.9851 | 0.6324 | 0.04801 | 0.3987 | —0.002 | —0.004 | 0.34 | 0.49 | 0.010 | 0.049 | 0.007 | 0.025 | 0.18 | 0.16 |
| ,, | 0.9 | 0.3950 | ,, | 0.7653 | 0.8396 | 0.03612 | 0.3992 | 0.001 | —0.002 | 0.53 | 0.37 | 0.029 | 0.027 | 0.015 | 0.016 | 0.31 | 0.09 |
| ,, | 1.0 | 0.3797 | ,, | 0.6880 | 0.9867 | 0.03084 | 0.4010 | 0.013 | 0.009 | 0.68 | 0.32 | 0.044 | 0.020 | 0.020 | 0.013 | 0.36 | 0.06 |
| Y | 0.6 | 0.3418 | G | 1.0342 | 0.5413 | 0.05877 | 0.3955 | —0.026 | —0.026 | —0.15 | 0.96 | —0.013 | 0.090 | 0.001 | 0.040 | 0.12 | 0.33 |
| ,, | 0.9 | 0.3242 | ,, | 0.8266 | 0.6411 | 0.04488 | 0.3965 | —0.018 | —0.019 | —0.02 | 0.86 | 0.003 | 0.067 | 0.005 | 0.034 | 0.21 | 0.25 |
| ,, | 1.0 | 0.3279 | ,, | 0.7376 | 0.7126 | 0.03777 | 0.3974 | —0.012 | —0.013 | 0.21 | 0.78 | 0.026 | 0.054 | 0.010 | 0.030 | 0.28 | 0.21 |
| ,, | 0.6 | 0.4507 | E | 1.0043 | 0.5753 | 0.05377 | 0.3985 | —0.005 | —0.007 | 0.09 | 0.75 | —0.001 | 0.072 | 0.003 | 0.033 | 0.13 | 0.25 |
| ,, | 0.9 | 0.3782 | ,, | 0.7936 | 0.7091 | 0.04098 | 0.3985 | —0.004 | —0.006 | 0.19 | 0.65 | 0.013 | 0.049 | 0.008 | 0.026 | 0.23 | 0.17 |
| ,, | 1.0 | 0.3687 | ,, | 0.7105 | 0.8025 | 0.03473 | 0.3993 | 0.003 | 0.001 | 0.36 | 0.58 | 0.030 | 0.038 | 0.013 | 0.022 | 0.29 | 0.14 |
| ,, | 0.6 | 0.5730 | Y | 0.9742 | 0.6404 | 0.04756 | 0.4047 | 0.036 | 0.030 | 0.22 | 0.53 | 0.006 | 0.049 | 0.005 | 0.025 | 0.12 | 0.17 |
| ,, | 0.9 | 0.4325 | ,, | 0.7552 | 0.8578 | 0.03512 | 0.4028 | 0.029 | 0.025 | 0.40 | 0.40 | 0.022 | 0.028 | 0.011 | 0.017 | 0.24 | 0.09 |
| ,, | 1.0 | 0.4137 | ,, | 0.6776 | 1.0168 | 0.02993 | 0.4046 | 0.043 | 0.039 | 0.55 | 0.33 | 0.035 | 0.019 | 0.016 | 0.013 | 0.30 | 0.06 |

TABLE 2.3

Core Radius $r_0 = 0.10$

| Central Force | | | Tensor Force | | | $P_D$ | $\varrho$ | $P_1$ | $P_2$ | $\frac{\partial s_t}{\partial b_c}$ | $\frac{\partial s_t}{\partial b_t}$ | $\frac{\partial P_D}{\partial b_c}$ | $\frac{\partial P_D}{\partial b_t}$ | $\frac{\partial Q}{\partial b_c}$ | $\frac{\partial Q}{\partial b_t}$ | $\frac{\partial A}{\partial b_c}$ | $\frac{\partial A}{\partial b_t}$ |
|---|---|---|---|---|---|---|---|---|---|---|---|---|---|---|---|---|---|
| Shape | Depth $s_c$ | Range $b_c$ | Shape | Depth $s_t$ | Range $b_t$ | | | | | | | | | | | | |
| G | 0.6 | 0.2109 | G | 0.8492 | 0.4813 | 0.06512 | 0.3938 | —0.038 | —0.039 | —0.34 | 1.11 | —0.030 | 0.088 | 0.001 | 0.039 | 0.15 | 0.32 |
| ,, | 0.9 | 0.2045 | ,, | 0.6721 | 0.5959 | 0.04796 | 0.3943 | —0.035 | —0.036 | —0.26 | 0.94 | —0.007 | 0.065 | 0.004 | 0.033 | 0.25 | 0.24 |
| ,, | 1.0 | 0.2053 | ,, | 0.5987 | 0.6860 | 0.03858 | 0.3949 | —0.030 | —0.031 | 0.16 | 0.80 | 0.039 | 0.050 | 0.013 | 0.029 | 0.35 | 0.19 |
| ,, | 0.6 | 0.2701 | E | 0.8031 | 0.5206 | 0.06067 | 0.3940 | —0.037 | —0.038 | 0.12 | 0.77 | —0.010 | 0.067 | 0.006 | 0.031 | 0.22 | 0.22 |
| ,, | 0.9 | 0.2369 | ,, | 0.6276 | 0.6776 | 0.04465 | 0.3947 | —0.032 | —0.034 | 0.23 | 0.57 | 0.019 | 0.040 | 0.012 | 0.023 | 0.33 | 0.14 |
| ,, | 1.0 | 0.2304 | ,, | 0.5624 | 0.7987 | 0.03624 | 0.3956 | —0.026 | —0.028 | 0.46 | 0.58 | 0.050 | 0.033 | 0.019 | 0.021 | 0.40 | 0.10 |
| ,, | 0.6 | 0.3129 | Y | 0.7733 | 0.5879 | 0.05527 | 0.3948 | —0.032 | —0.033 | 0.44 | 0.47 | —0.013 | 0.044 | 0.007 | 0.023 | 0.26 | 0.14 |
| ,, | 0.9 | 0.2620 | ,, | 0.5919 | 0.8470 | 0.03992 | 0.3965 | —0.020 | —0.023 | 0.63 | 0.34 | 0.039 | 0.023 | 0.021 | 0.015 | 0.40 | 0.07 |
| ,, | 1.0 | 0.2534 | ,, | 0.5314 | 1.0682 | 0.03232 | 0.3991 | —0.002 | —0.007 | 0.85 | 0.28 | 0.064 | 0.015 | 0.029 | 0.011 | 0.46 | 0.05 |
| E | 0.6 | 0.2067 | G | 0.8606 | 0.4775 | 0.06566 | 0.3939 | —0.037 | —0.038 | —0.45 | 1.11 | —0.038 | 0.089 | —0.001 | 0.040 | 0.12 | 0.33 |
| ,, | 0.9 | 0.2040 | ,, | 0.6789 | 0.5912 | 0.04828 | 0.3944 | —0.034 | —0.034 | 0.28 | 0.94 | —0.013 | 0.067 | 0.003 | 0.034 | 0.23 | 0.24 |
| ,, | 1.0 | 0.2070 | ,, | 0.6008 | 0.6849 | 0.03844 | 0.8951 | —0.029 | —0.030 | 0.18 | 0.80 | 0.036 | 0.051 | 0.014 | 0.029 | 0.35 | 0.19 |
| ,, | 0.3 | 0.3752 | E | 0.9721 | 0.4496 | 0.07068 | 0.3946 | —0.032 | —0.033 | 0.07 | 0.85 | —0.004 | 0.080 | 0.002 | 0.037 | 0.09 | 0.29 |
| ,, | 0.6 | 0.2753 | ,, | 0.8062 | 0.5205 | 0.06081 | 0.3943 | —0.034 | —0.035 | 0.03 | 0.80 | —0.014 | 0.069 | 0.004 | 0.032 | 0.19 | 0.23 |
| ,, | 0.9 | 0.2404 | ,, | 0.6307 | 0.6761 | 0.04466 | 0.3950 | —0.030 | —0.032 | 0.13 | 0.66 | 0.009 | 0.046 | 0.010 | 0.025 | 0.30 | 0.16 |
| ,, | 1.0 | 0.2345 | ,, | 0.5631 | 0.8008 | 0.03594 | 0.3960 | —0.023 | —0.025 | 0.41 | 0.57 | 0.045 | 0.034 | 0.018 | 0.021 | 0.38 | 0.13 |
| ,, | 0.6 | 0.3281 | Y | 0.7635 | 0.5977 | 0.05504 | 0.3955 | —0.026 | —0.028 | 0.33 | 0.50 | 0.003 | 0.045 | 0.009 | 0.023 | 0.22 | 0.14 |
| ,, | 0.9 | 0.2708 | ,, | 0.5852 | 0.8665 | 0.03944 | 0.3972 | —0.015 | —0.018 | 0.53 | 0.35 | 0.030 | 0.023 | 0.018 | 0.015 | 0.36 | 0.07 |
| ,, | 1.0 | 0.2620 | ,, | 0.5257 | 1.1026 | 0.03162 | 0.4001 | 0.006 | 0.001 | 0.77 | 0.28 | 0.057 | 0.014 | 0.026 | 0.011 | 0.43 | 0.04 |
| Y | 0.6 | 0.2003 | G | 0.8784 | 0.4712 | 0.06669 | 0.3940 | —0.036 | —0.037 | —0.46 | 1.13 | —0.040 | 0.091 | —0.004 | 0.041 | 0.09 | 0.35 |
| ,, | 0.9 | 0.2031 | ,, | 0.6903 | 0.5831 | 0.04905 | 0.3947 | —0.032 | —0.033 | —0.31 | 0.96 | —0.020 | 0.069 | 0.001 | 0.034 | 0.20 | 0.25 |
| ,, | 1.0 | 0.2100 | ,, | 0.6038 | 0.6830 | 0.03836 | 0.3955 | —0.026 | —0.027 | 0.15 | 0.81 | 0.031 | 0.052 | 0.012 | 0.029 | 0.32 | 0.20 |
| ,, | 0.6 | 0.2826 | E | 0.8148 | 0.5173 | 0.06133 | 0.3949 | —0.030 | —0.031 | —0.02 | 0.74 | —0.016 | 0.061 | 0.003 | 0.032 | 0.16 | 0.24 |
| ,, | 0.9 | 0.2458 | ,, | 0.6371 | 0.6705 | 0.04500 | 0.3956 | —0.026 | —0.028 | 0.08 | 0.68 | 0.002 | 0.048 | 0.007 | 0.026 | 0.27 | 0.16 |
| ,, | 1.0 | 0.2412 | ,, | 0.5644 | 0.8020 | 0.03566 | 0.3967 | —0.018 | —0.020 | 0.36 | 0.57 | 0.038 | 0.036 | 0.016 | 0.022 | 0.35 | 0.14 |
| ,, | 0.6 | 0.3538 | Y | 0.7543 | 0.6076 | 0.05494 | 0.3969 | —0.016 | —0.018 | 0.22 | 0.53 | —0.001 | 0.045 | 0.006 | 0.023 | 0.18 | 0.14 |
| ,, | 0.9 | 0.2853 | ,, | 0.5780 | 0.8887 | 0.03898 | 0.3984 | —0.006 | —0.009 | 0.41 | 0.37 | 0.020 | 0.023 | 0.014 | 0.014 | 0.31 | 0.07 |
| ,, | 1.0 | 0.2764 | ,, | 0.5185 | 1.1498 | 0.03074 | 0.4018 | 0.020 | 0.014 | 0.57 | 0.28 | 0.031 | 0.012 | 0.013 | 0.009 | 0.31 | 0.04 |

TABLE 2.4

Core Radius $r_0 = 0.15$.

| Central Force | | | Tensor Force | | | $P_D$ | $\varrho$ | $P_1$ | $P_2$ | $\frac{\partial s_t}{\partial b_c}$ | $\frac{\partial s_t}{\partial b_t}$ | $\frac{\partial P_D}{\partial b_c}$ | $\frac{\partial P_D}{\partial b_t}$ | $\frac{\partial Q}{\partial b_c}$ | $\frac{\partial Q}{\partial b_t}$ | $\frac{\partial A}{\partial b_c}$ | $\frac{\partial A}{\partial b_t}$ |
|---|---|---|---|---|---|---|---|---|---|---|---|---|---|---|---|---|---|
| Shape | Depth $s_c$ | Range $b_c$ | Shape | Depth $s_t$ | Range $b_t$ | | | | | | | | | | | | |
| G | — | — | G | — | — | — | — | — | — | — | — | — | — | — | — | — | — |
| ,, | 0.9 | 0.0985 | ,, | 0.5734 | 0.5099 | 0.05582 | 0.3939 | —0.037 | —0.038 | —0.90 | 1.01 | —0.084 | 0.067 | —0.009 | 0.035 | 0.13 | 0.26 |
| ,, | 1.0 | 0.1036 | ,, | 0.4915 | 0.6519 | 0.03907 | 0.3948 | —0.031 | —0.033 | 0.09 | 0.80 | 0.040 | 0.049 | 0.013 | 0.028 | 0.36 | 0.18 |
| ,, | 0.6 | 0.1533 | E | 0.6564 | 0.4422 | 0.07097 | 0.3936 | —0.040 | —0.041 | —0.19 | 1.17 | —0.054 | 0.082 | 0.002 | 0.037 | 0.20 | 0.30 |
| ,, | 0.9 | 0.1341 | ,, | 0.5063 | 0.6139 | 0.05084 | 0.3941 | —0.036 | —0.038 | 0.02 | 0.78 | —0.011 | 0.059 | 0.009 | 0.028 | 0.32 | 0.16 |
| ,, | 1.0 | 0.1283 | ,, | 0.4483 | 0.7960 | 0.03696 | 0.3954 | —0.028 | —0.030 | 0.40 | 0.55 | 0.057 | 0.031 | 0.021 | 0.020 | 0.43 | 0.11 |
| ,, | 0.6 | 0.1902 | Y | 0.6062 | 0.5181 | 0.06510 | 0.3939 | —0.038 | —0.040 | 0.19 | 0.22 | —0.047 | 0.020 | 0.007 | 0.021 | 0.25 | 0.11 |
| ,, | 0.9 | 0.1584 | ,, | 0.4526 | 0.8404 | 0.04527 | 0.3955 | —0.027 | —0.030 | 0.53 | 0.32 | 0.008 | 0.018 | 0.020 | 0.013 | 0.42 | 0.06 |
| ,, | 1.0 | 0.1529 | ,, | 0.4086 | 1.2308 | 0.03299 | 0.3999 | 0.004 | —0.002 | 1.04 | 0.23 | 0.078 | 0.010 | 0.034 | 0.008 | 0.47 | 0.03 |
| E | — | — | G | — | — | — | — | — | — | — | — | — | — | — | — | — | — |
| ,, | 0.9 | 0.0967 | ,, | 0.5795 | 0.5039 | 0.05666 | 0.3940 | —0.037 | —0.038 | | | | | —0.006 | 0.036 | 0.17 | 0.27 |
| ,, | 1.0 | 0.1036 | ,, | 0.4919 | 0.6519 | 0.03898 | 0.3948 | —0.031 | —0.032 | 0.10 | 0.81 | 0.040 | 0.050 | 0.013 | 0.030 | 0.36 | 0.17 |
| ,, | 0.3 | 0.1858 | E | 0.8010 | 0.3736 | 0.08103 | 0.3936 | —0.040 | —0.040 | —0.11 | 0.97 | —0.029 | 0.079 | 0.001 | 0.037 | 0.09 | 0.30 |
| ,, | 0.6 | 0.1523 | ,, | 0.6621 | 0.4392 | 0.07148 | 0.3936 | —0.039 | —0.040 | —0.36 | 0.98 | —0.063 | 0.078 | —0.001 | 0.034 | 0.16 | 0.24 |
| ,, | 0.9 | 0.1341 | ,, | 0.5098 | 0.6084 | 0.05133 | 0.3941 | —0.036 | —0.038 | —0.29 | 0.71 | —0.047 | 0.048 | 0.003 | 0.026 | 0.28 | 0.17 |
| ,, | 1.0 | 0.1290 | ,, | 0.4486 | 0.7973 | 0.03680 | 0.3954 | —0.027 | —0.029 | 0.39 | 0.55 | 0.054 | 0.032 | 0.020 | 0.020 | 0.41 | 0.11 |
| ,, | 0.6 | 0.1948 | Y | 0.6010 | 0.5237 | 0.06517 | 0.3940 | —0.037 | —0.038 | 0.26 | 0.50 | —0.024 | 0.040 | 0.007 | 0.023 | 0.25 | 0.14 |
| ,, | 0.9 | 0.1613 | ,, | 0.4492 | 0.8541 | 0.04514 | 0.3958 | —0.026 | —0.029 | 0.49 | 0.32 | 0.009 | 0.020 | 0.017 | 0.013 | 0.39 | 0.06 |
| ,, | 1.0 | 0.1563 | ,, | 0.4062 | 1.2714 | 0.03245 | 0.4007 | 0.009 | 0.002 | 1.06 | 0.20 | 0.087 | 0.008 | 0.040 | 0.007 | 0.53 | 0.02 |
| Y | — | — | G | — | — | — | — | — | — | — | — | — | — | — | — | — | — |
| ,, | 0.9 | 0.0934 | ,, | 0.5921 | 0.4910 | 0.05852 | 0.3939 | —0.037 | —0.038 | —1.42 | 1.11 | —0.149 | 0.078 | —0.018 | 0.037 | 0.03 | 0.29 |
| ,, | 1.0 | 0.1033 | ,, | 0.4950 | 0.6453 | 0.03946 | 0.3948 | —0.031 | —0.032 | —0.02 | 0.84 | 0.021 | 0.053 | 0.010 | 0.030 | 0.33 | 0.20 |
| ,, | 0.6 | 0.1503 | E | 0.6734 | 0.4328 | 0.07249 | 0.3937 | —0.039 | —0.040 | | 0.92 | | 0.069 | 0.007 | 0.035 | 0.22 | 0.26 |
| ,, | 0.9 | 0.1341 | ,, | 0.5167 | 0.5967 | 0.05245 | 0.3942 | —0.036 | —0.037 | —0.42 | 0.74 | —0.065 | 0.048 | 0.000 | 0.027 | 0.23 | 0.17 |
| ,, | 1.0 | 0.1301 | ,, | 0.4499 | 0.7937 | 0.03691 | 0.3955 | —0.027 | —0.029 | 0.28 | 0.57 | 0.040 | 0.033 | 0.017 | 0.021 | 0.39 | 0.12 |
| ,, | 0.6 | 0.2016 | Y | 0.5979 | 0.5274 | 0.06555 | 0.3943 | —0.035 | —0.036 | 0.12 | 0.53 | —0.028 | 0.043 | 0.006 | 0.023 | 0.21 | 0.14 |
| ,, | 0.9 | 0.1656 | ,, | 0.4465 | 0.8654 | 0.04534 | 0.3961 | —0.023 | —0.026 | 0.38 | 0.33 | —0.004 | 0.022 | 0.012 | 0.014 | 0.36 | 0.06 |
| ,, | 1.0 | 0.1616 | ,, | 0.4037 | 1.3241 | 0.03187 | 0.4018 | 0.016 | 0.009 | | | | | 0.033 | 0.008 | 0.48 | 0.03 |

The magnetic moment of the deuteron, on the other hand, is subject to much larger corrections which are at present rather uncertain. The most recent estimate of these corrections [8]) is based on the Tamm-Dancoff approximation. Unfortunately, this approximation becomes doubtful in the very region (close approach of the two nucleons) which contributes a major share of the effect. Since the D-state probability $P_D$ is inferred from the magnetic dipole moment of the deuteron, we have not used $P_D$ to limit our choice of potentials. The value of $P_D$ obtained from the simple phenomenological theory without any corrections is 4 percent. All our potentials give values between 3 and 7 percent.

Still another approach to the study of the deuteron wave function is the scattering of high energy electrons on deuterons [9])†. Since the deBroglie wave length associated with the momentum transfer of the electrons is comparable to the dimensions of the deuteron, details of the deuteron structure can be observed by this method, at least in principle. The simplest assumption would be that the neutron does not interact with electrons at all, the proton interacts purely as a point charge, and that conventional quantum electrodynamics is valid to describe this interaction. In that case the experimentally measured form factor is a transform of the radial probability distribution $u^2(r)+w^2(r)$ of the deuteron, and can be compared directly with wave functions such as the ones given in this paper.

Unfortunately, the experiments are grossly at variance with this simple interpretation. In view of the fact that the electron-proton scattering measurements are inconsistent with this same interpretation (i.e., indicate either a rather large proton size or a breakdown of electrodynamics, or both), this is not surprising. The situation is discussed in detail in the review article of Yennie, Levy, and Ravenhall [10]), and we have nothing to add to their excellent summary of the present situation, beyond the obvious remark that until and unless the data on electron scattering by single nucleons are well understood, electron scattering by more complex systems such as the deuteron cannot be used to get any except gross information about the internal structure of these complex systems.

We intend to alter our code so as to make the machine calculate, in addition to the wave functions, the trivial form factors (point nucleons, conventional electrodynamics) for the deuteron. These calculations will be published later, and we hope they will eventually prove useful in eliminating at least some of the many potentials we have found here.

† We would like to thank Dr. McIntyre for helpful correspondence and discussions, as well as for sending us data prior to publication.

## 3. Discussion of the Numerical Results

### 3.1. RADIAL WAVE FUNCTIONS AND TENSOR POTENTIAL

In fig. 3.1 we have plotted the S-state radial wave function $u(r)$ and the D-state radial wave function $w(r)$ for two different potentials, one without repulsive core, the other with a repulsive core radius $r_0 = 0.10$ in units of the radius of the deuteron $R = 4.31 \times 10^{-13}$ cm. Although the wave functions are quite different at small separations $r$, they agree closely for $r \gtrapprox 0.6$, in the "exterior" region. This behaviour is typical of all the wave functions found here, and is a direct consequence of the fact that we have

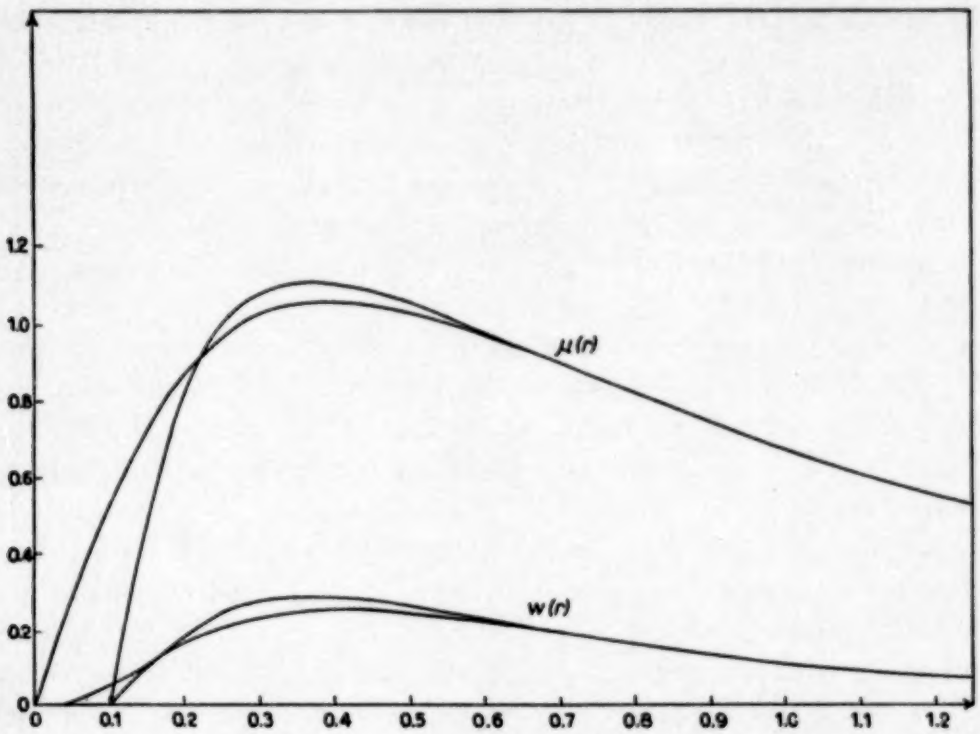


Fig. 3.1. The radial wave functions $u(r)$ ($^3S_1$ state) and $w(r)$ ($^3D_1$ state) for the ground state of the deuteron. Two sets of curves are given, the first resulting from a potential without a repulsive core, the second from a repulsive core potential. Although these wave functions differ considerably in the "interior" region, say $r \lessapprox 0.4\ R = 1.73 \times 10^{-13}$ cm, they are very close to each other in the "exterior" region.

fitted the binding energy of the deuteron, the quadrupole moment, and the triplet scattering length (triplet effective range). Although the argument is well-known [2]) we repeat it here quickly for the convenience of the reader.

Outside the range of the forces, the wave functions assume the asymptotic forms

$$u(r) = N \exp(-r) \tag{3.1}$$

$$w(r) = N' \left(1 + \frac{3}{r} + \frac{3}{r^2}\right) \exp(-r). \tag{3.2}$$

The radial dependences are determined by the binding energy, only the constants $N$ and $N'$ are unknown.

The effective range computed from the ground state wave function is given by [11] †

$$\varrho_{0t} = 2\int_0^\infty \left[\exp(-2r) - \frac{u^2(r)+w^2(r)}{N^2+N'^2}\right] dr. \tag{3.3}$$

We use the normalization integral

$$\int_0^\infty [u^2(r)+w^2(r)]dr = 1 \tag{3.4}$$

to obtain

$$N^2+N'^2 = \frac{2}{1-\varrho_{0t}}. \tag{3.5}$$

In the expression for the quadrupole moment,

$$Q = (50)^{-\frac{1}{2}}\int_0^\infty r^2 uw dr - (20)^{-1}\int_0^\infty r^2 w^2 dr, \tag{3.6}$$

it is a reasonable (perhaps 10 percent) approximation to neglect the second integral and to replace $u$ and $w$ in the first integral by their asymptotic forms (3.1) and (3.2). This gives

$$NN' \approx 8^{\frac{1}{2}} Q. \tag{3.7}$$

Equations (3.5) and (3.7) determine both $N$ and $N'$.

Although this conventional argument is essentially correct as it stands, and does lead to the desired conclusion, (3.2) is *not* an accurate form for the wave function except quite far out, for $r \gg 1$, for practically all cases studied here. We shall now discuss the reason for this, thereby also developing an improved approximation for $w(r)$.

The differential equations satisfied by $u$ and $w$ are

$$-d^2u/dr^2+(1+V_c)u = -8^{\frac{1}{2}}V_t w, \tag{3.8a}$$

$$-d^2w/dr^2+\left(\frac{6}{r^2}+1+V_c-2V_t\right)w = -8^{\frac{1}{2}}V_t u. \tag{3.8b}$$

The asymptotic forms (3.1) and (3.2) are obtained by setting $V_c = V_t = 0$. However, by looking at the tables of section 2, we see that the range $b_t$ of the tensor force is generally quite appreciable. For zero core radius, $b_t$ varies between 0.6 and 0.9. Similar values are obtained from the other tables if the core radius $r_0$ is added to the range $b_t$ of the "moved out" well, as it should be for this purpose. Thus the approximation $V_t = 0$ is hardly very good.

An alternative, and much better, approximation can be obtained by noticing that the centrifugal force term $6/r^2$ dominates the coefficient of

† This is the quantity $\varrho(-\varepsilon, -\varepsilon)$ of Bethe, ref. [3]).

$w(r)$ in (3.8b) over practically the entire interesting region. For example, at $r = 0.1$, the centrifugal term is 600 in our units, i.e. $600B = 1335$ MeV. At $r = 0.5$ it is 24, or 53.5 MeV, and at $r = 1$ it is 6, or 13.4 MeV. These numbers are much larger than the combination $1+V_c-2V_t$ for most of the potentials used here, except perhaps very close to the core radius itself, in a very narrow interval of $r$. This suggests the approximation of replacing the differential equation (3.8b) by the approximate differential equation

$$-\mathrm{d}^2w/\mathrm{d}r^2+6w/r^2 = -8^{\frac{1}{2}}V_t\,u \tag{3.9}$$

with the solution

$$w(r) = -8^{\frac{1}{2}}\int_0^\infty G(r,\,r')V_t\,(r')u(r')\mathrm{d}r' \tag{3.10}$$

where the Green's function $G(r, r')$ is given by †

$$\begin{aligned} G(r,\,r') &= 0 \quad \text{if} \quad r < r_0 \text{ or } r' < r_0 \text{ or both,} \\ &= [r_<^3-(r_0^5/r_<^2)]/5r_>^2 \text{ otherwise.} \end{aligned} \tag{3.11}$$

In the special case $r_0 = 0$ this simplifies to

$$G(r,\,r') = r_<^3/5r_>^2 \text{ for zero core radius.} \tag{3.12}$$

For the potentials used here, $u(r)$ varies slowly over most of the interesting region of $r$, and the scale of $u$ is given essentially by the normalization integral (3.4). Thus (3.10) shows that $w(r)$ is determined directly by the tensor potential $V_t(r)$. Conversely, information about $w(r)$, such as the value of the quadrupole moment $Q$, imposes severe restrictions on the possible values of $V_t(r)$ in the region of $r$ which makes the main contribution to the quadrupole moment, say $0.4 < r < 1$. Thus *the long range tensor forces characteristic of this study are not accidental, but are demanded by the data on the deuteron.*

To illustrate this, we have drawn, in fig. 3.2, several tensor potentials found here, with different core radii and different central forces. All of them agree reasonably well in the region of $r$ under discussion.

Equations (3.6) and (3.10) to (3.12) show that the region near the core is unimportant for the determination of $Q$. Since this "interior" region is weighted quite heavily in the specification of the tensor potential $V_t$ in terms of its intrinsic depth $s_t$ and intrinsic range $b_t$, this specification is not nearly as useful for the tensor force as it is for the central force. It is apparent from the tables of section 2 that $s_t$ and $b_t$ vary much more strongly between different tensor well shapes than the actual values of $V_t(r)$ in the "exterior" region of $r$. Although a more appropriate "intrinsic" specification of tensor wells could be developed fairly easily, based on the approximation (3.10), we have retained the less appropriate specification for the sake of uniformity and simplicity.

† We use the notation $r_< = \mathrm{Min}\,(r, r')$ and $r_> = \mathrm{Max}\,(r, r')$.

Substitution of (3:10) into (3.8a) yields an equation for $u(r)$ alone, of the form

$$-\mathrm{d}^2u/\mathrm{d}r^2+V_{\mathrm{eff}}u=-u \tag{3.13}$$

where the "effective potential" $V_{\mathrm{eff}}$ is the operator

$$V_{\mathrm{eff}}u=V_{\mathrm{c}}(r)u(r)-8V_{\mathrm{t}}(r)\int_0^\infty G(r,\,r')V_{\mathrm{t}}(r')u(r')\mathrm{d}r'. \tag{3.14}$$

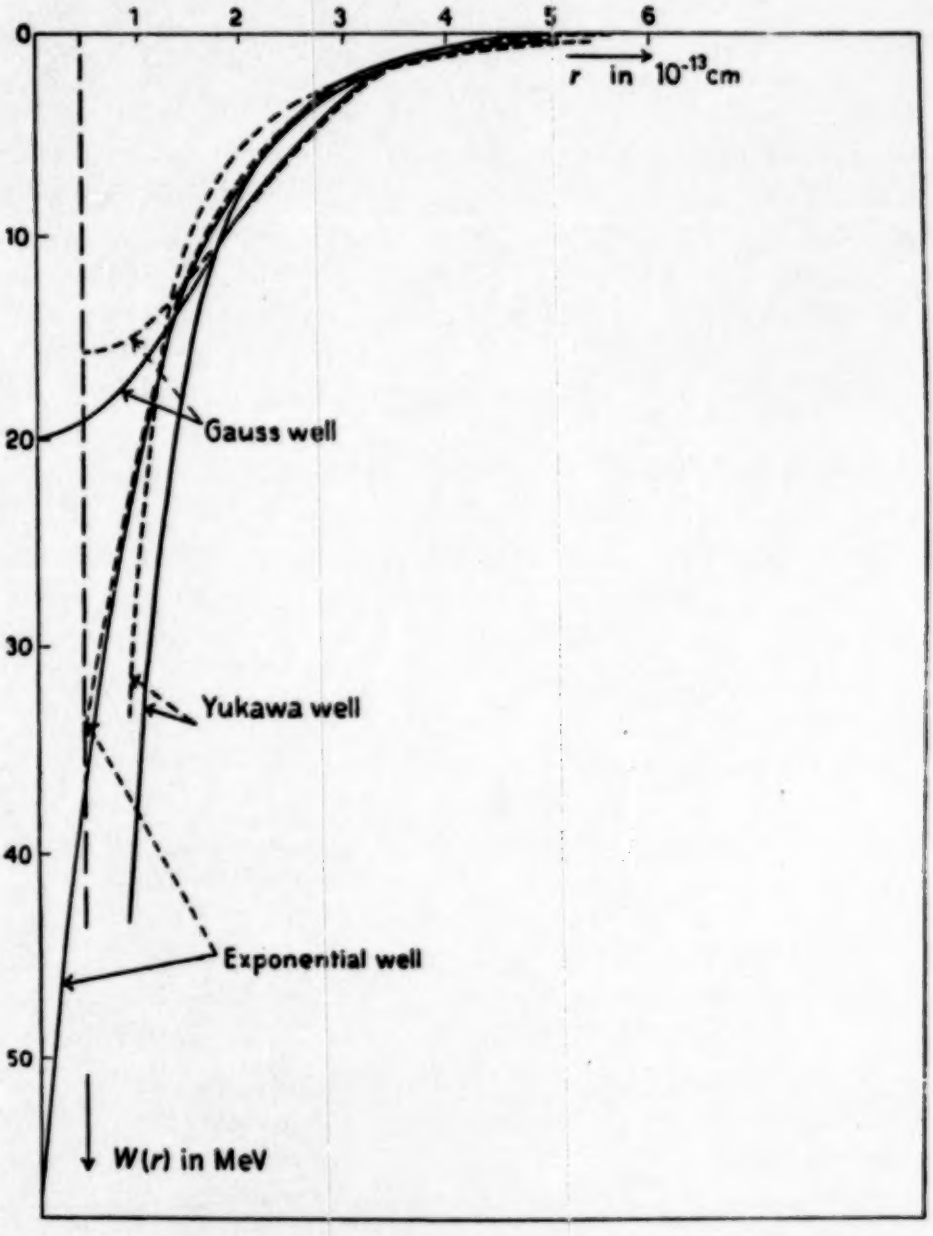


Fig. 3.2. Various tensor potentials, with or without repulsive core; note that these potentials agree well with each other in the "exterior" region.

This shows an interesting and important property of the tensor force: changing the sign of $V_{\mathrm{t}}$ makes very little difference (no difference at all

in approximation (3.13)) to the behaviour of $u(r)$, and hence to the binding energy and effective range. In its effect on both, the tensor force acts like an attractive potential of a strength proportional to the square of its actual strength. Changing the sign of $V_t$ leaves $u(r)$ unchanged, and replaces $w(r)$ by $-w(r)$, in this approximation †.

### 3.2. INFLUENCE OF SPIN-ORBIT COUPLING

This same approximation can be used to demonstrate that a spin-orbit coupling term of type

$$V_{LS}(r)\mathbf{L}\cdot\mathbf{S} \tag{3.15}$$

has very little effect on the properties of the deuteron and low energy scattering. The operator $\mathbf{L}\cdot\mathbf{S}$ commutes with $J^2$ and $L^2$; hence, unlike the tensor force, such a term gives no coupling between $^3S_1$ and $^3D_1$ states. Furthermore, the operator $\mathbf{L}\cdot\mathbf{S}$ vanishes in the $^3S_1$ state. Hence equation (3.8a) is unchanged, and equation (3.8b) is altered to

$$-\mathrm{d}^2w/\mathrm{d}r^2+\left(\frac{6}{r^2}+1+V_c-2V_t-3V_{LS}\right)w=-8\tfrac{1}{2}V_t u. \tag{3.16}$$

The centrifugal term $6/r^2$ dominates the coefficient of $w$ in (3.16) everywhere except very far out and perhaps very close to the core radius itself. The changes far out are unimportant qualitatively, and since $w$ is small close to the core radius anyway, changes very close to the core radius have very little effect on the solution of (3.16) in the intermediate region of $r$. In approximation (3.14) equations (3.8b) and (3.16) are completely equivalent, i.e., the $\mathbf{L}\cdot\mathbf{S}$ force produces no change at all in low energy properties of the nucleon-nucleon system. Thus the potentials given in this paper, in which we have not introduced $\mathbf{L}\cdot\mathbf{S}$ forces, are qualitatively, and to a good first approximation even quantitatively, unaffected by the introduction of such a force.

### 3.3. THE CENTRAL POTENTIAL

Having understood the main features of the tensor potential, let us now discuss the central potential $V_c(r)$. In fig. 3.3 we have plotted the intrinsic range $b_c$ of this potential against the core radius $r_0$. This figure includes all potentials with $s_c = 0.9$. The figure shows that $b_c$ decreases rapidly with increasing core radius. For $r_0 \geqq 0.10$, the intrinsic range of the central force is nearly independent of the central force well shape. Furthermore,

† The fact that the tensor force always increases the binding energy can be seen more simply: the expectation value of the tensor operator $S_{12}$ in the $^3S_1$ state vanishes. Hence a pure $^3S_1$ function used as a trial function in a variational calculation gives an upper bound to the energy, which contains no contribution from the tensor force. The tensor force then adds to the binding by coupling in the $^3D_1$ state. The statements above are however more specific.

the parameters of the tensor potential (given its shape) are then also independent of the well shape of the central force. To show the striking accuracy with which these statements hold, we produce in table 3.1 an excerpt from the tables of section 2, namely the values of $b_c$, $s_t$, and $b_t$ for $s_c = 0.9$ and a tensor force of exponential shape.

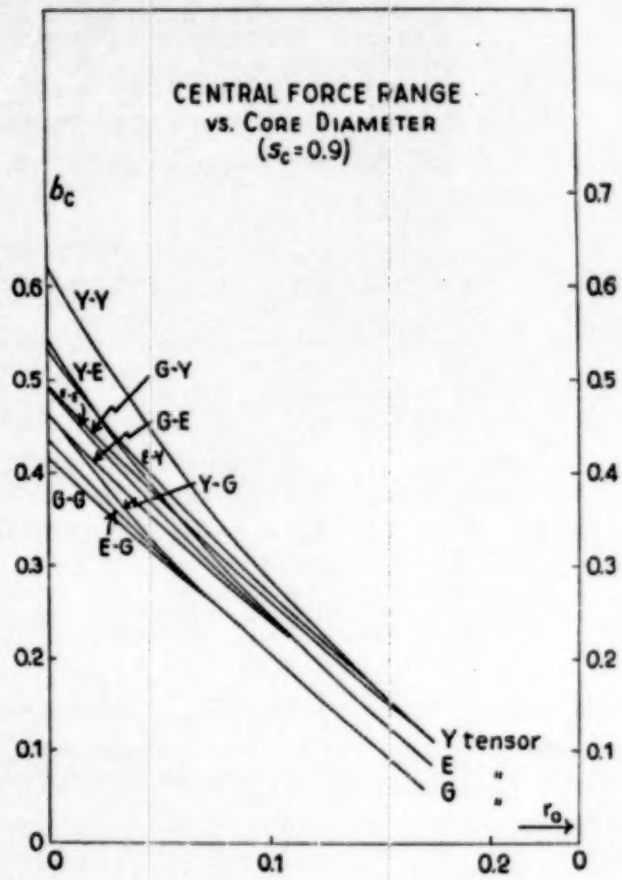


Fig. 3.3. The intrinsic range of the central potential outside the core, *vs.* core radius. All combinations of well shapes (G = Gaussian, E = exponential, Y = Yukawa) are included, but the strength parameter $s_c$ of the central force equals 0.9 for all potentials used for this figure. Note that the range $b_c$ decreases rapidly with increasing core radius, i.e., the central potential becomes more concentrated as the core radius increases.

The range of the tensor force is determined by the quadrupole moment, and is necessarily rather large. If the central force had a long range also, the overall effective range would exceed the experimental value. For appreciable well depths $s_c$ we can make a very simple estimate of the necessary range of $V_c(r)$ outside the core radius. Consider a square well of range b and intrinsic depth $s = 1$ (i.e., a scattering resonance at zero energy) moved out beyond a core of radius $r_0$. A straightforward calculation then yields the following value for the effective range:

$$r_{eff} = b + 2r_0. \tag{3.17}$$

This crude estimate is surprisingly useful. The actual effective range in the

triplet state is about 0.4, so that (3.17) gives $b_c = 0.2$ for $r_0 = 0.1$, and $b_c = 0.1$ for $r_0 = 0.15$. These numbers are practically precise for a tensor force of Gaussian well shape (see fig. 3.3). For other tensor well shapes they give the correct dependence on $r_0$, i.e., $b_c + 2r_0$ is nearly independent of $r_0$ for all tensor well shapes.

Once we have understood the short intrinsic range $b_c$ of the central force in the presence of a repulsive core, the shape independence follows automatically, since the parametrization in terms of $s_c$ and $b_c$ was chosen in just such a way that the shape of a short range central well is unimportant †. This then provides the qualitative explanation of table 3.1.

TABLE 3.1

Values of $b_c$, $s_t$, and $b_t$ for various core radii $r_0$ and various central force well shapes. The tensor force has exponential well shape throughout, and the central force has strength $s_c = 0.9$ throughout.

| $r_0$ | Central Well Shape | $b_c$ | $s_t$ | $b_t$ |
|---|---|---|---|---|
| 0 | Gauss | 0.4627 | 0.9837 | 0.7291 |
| | Exponential | 0.4907 | 0.9874 | 0.7304 |
| | Yukawa | 0.5460 | 0.9973 | 0.7264 |
| 0.05 | Gauss | 0.3461 | 0.7837 | 0.7110 |
| | Exponential | 0.3580 | 0.7867 | 0.7118 |
| | Yukawa | 0.3782 | 0.7936 | 0.7091 |
| 0.10 | Gauss | 0.2369 | 0.6276 | 0.6776 |
| | Exponential | 0.2404 | 0.6307 | 0.6761 |
| | Yukawa | 0.2458 | 0.6371 | 0.6705 |
| 0.15 | Gauss | 0.1341 | 0.5063 | 0.6139 |
| | Exponential | 0.1341 | 0.5098 | 0.6084 |
| | Yukawa | 0.1341 | 0.5167 | 0.5967 |

## 3.4. INFLUENCE OF CORE RADIUS

It is clear from fig. 3.3 as well as from these estimates that there exists a maximum core radius $r_0$ beyond which it is impossible to fit both the scattering length and the quadrupole moment. From the information we have so far, it appears that a core radius $r_0 = 0.15$ is close to this limit for a tensor force of Gaussian well shape and a central force with $s_c = 0.9$ (and any well shape); decreasing the central well depth to $s_c = 0.6$ puts us beyond that limit ††. This is the reason for the missing entries in table 2.3.

† Table 3.1 and the associated arguments depend crucially on our choice of "moved out" rather than "cut off" wells. The very striking regularities observed here would have been concealed completely by "cutting off" wells of different shapes.

†† A central force with $s_c \leqq 1$ and vanishing range is equivalent to no force at all in its effect on the wave function. Thus decreasing the depth of the central force make it necessary to allow a larger central force range $b_c$, which is then in contradiction to the observed effective range.

The shortening of the range of the central force with increasing core radius is an effect of major qualitative importance to the overall behaviour of the nuclear force. For a given intrinsic well depth $s_c$, the actual well depth $V_{0c}$ of the central force is inversely proportional to $b_c^2$, since $s$ is proportional to $V_0 b^2$. Thus shortening the range makes the force very much stronger within its range of action. In fig. 3.4 we have plotted the central

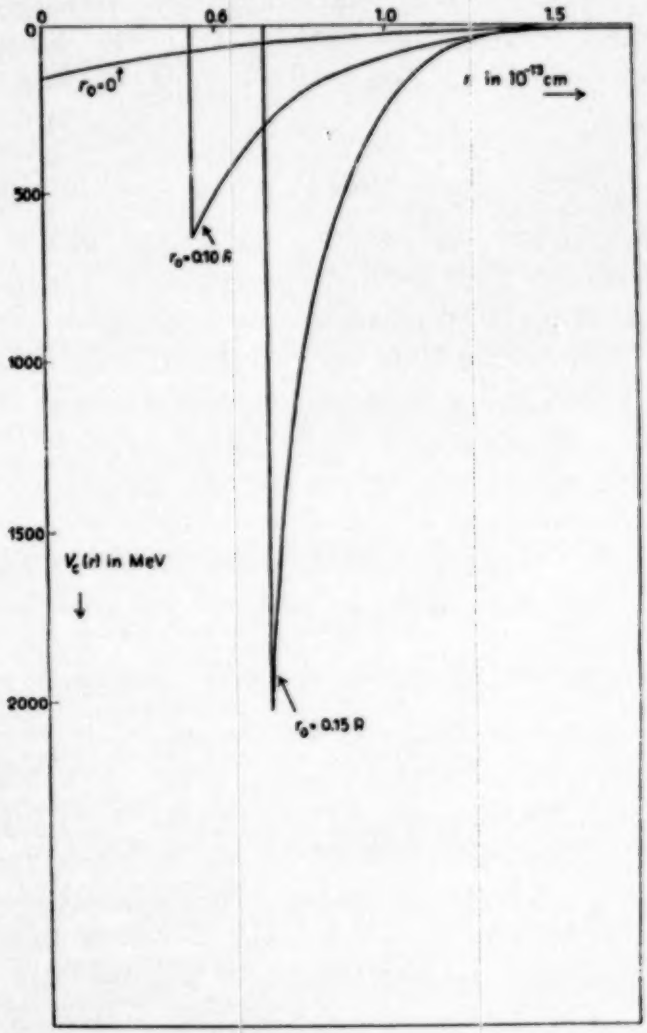


Fig. 3.4. Central potentials for three different core radii. Note the rapid increase in the value of $V(r)$ as the core radius increases. Such deep dan narrow potentials are phenomenologically equivalent to a "sticky core" boundary condition on the wave function.

potentials for three different core radii. The well shapes are exponential for both forces, and the intrinsic depth $s_c$ equals 0.9 in all three cases. Although the values of the tensor force do not differ very much (we have seen this before), the central force is drastically dependent on the core radius. For zero core radius the well depths of the central and tensor forces are comparable in magnitude, $V_{0c}$ being roughly twice as large as $V_{0t}$.

But for a core radius $r_0 = 0.10\ R = 0.43 \times 10^{-13}$ cm, $V_{0c}$ is 630 MeV, more than 10 times as large as $V_{0t}$. This qualitative change to a very deep, short-range central force as a result of the introduction of repulsive core is independent of the well shapes chosen, and may therefore be considered significant. The only exceptions are provided by potentials with very weak central forces, so weak that the properties of the $^3S_1+^3D_1$ state at low energies are determined almost exclusively by the tensor potential.

A very short-ranged and deep central force is practically equivalent to a "sticky core" boundary condition on the wave function, of type

$$\left[\frac{u}{r(du/dr)}\right]_{r=r_1} = g; \tag{3.18}$$

$g = 0$ means a perfectly repulsive core, $g > 0$ means a "sticky core". It is perhaps significant that, starting from the assumption of a repulsive core, we have come to the conclusion that the required central potential is such that we can replace it by a "sticky core" boundary condition.

Of course, the low energy data alone cannot determine whether a repulsive core is necessary. What we have shown is that, *if* a repulsive core is required by other (high energy) data, *then* the low energy data lead to a central force which is essentially equivalent to a change from a "repulsive core" to a "sticky core" boundary condition. Additional longer-range central forces may be present, but would be of much less importance.

### 3.5. REGION OF SMALL CENTRAL FORCES

Since most of this investigation has been concerned with central forces of appreciable strength ($s_c \gtrapprox 0.6$), we have made some additional calculations to investigate the region of very small central forces It is useful to consider the case of no central force at all outside the repulsive core. Since the tensor force depth $s_t$ is adjusted to fit the binding energy of the deuteron, this leaves two parameters free, the tensor force range $b_t$ and the core radius $r_0$. Table 3.2 contains the results for the following combinations:

$$r_0 = 0,\quad 0.05,\quad 0.10,\quad 0.15,$$
$$b_t = 0.3,\quad 0.5,\quad 0.7,$$

tensor well shape = Gaussian, exponential, Yukawa.

These results are shown graphically for zero core radius in fig. 3.5, and for $r_0 = 0.10\ R$ in fig. 3.6. Both figures give curves of triplet scattering length $a_t$ *vs.* quadrupole moment $Q$, with $b_t$ varying along each curve. The experimental point, $a_t = 1.249$ and $Q = 0.0147$, is also shown on each figure.

First of all, we note that the curves for different well shapes are rather similar. Since the Gaussian and (moved-out) Yukawa shapes are already

TABLE 3.2

No central force

| Core Radius | Tensor Force | | | Ground State Quantities | | | Zero Energy Quantities | | |
|---|---|---|---|---|---|---|---|---|---|
| | Well Shape | Strength $s_t$ | Range $b_t$ | $P_D$ | $Q$ | $\varrho$ | $a_t$ | $r_{et}$ | $P_1$ |
| 0 | G | 1.4635 | 0.3 | 0.0430 | 0.00567 | 0.2263 | 1.1279 | 0.2270 | —0.016 |
| | ,, | 1.5924 | 0.5 | 0.0666 | 0.01340 | 0.3544 | 1.2172 | 0.3599 | —0.030 |
| | ,, | 1.7298 | 0.7 | 0.0865 | 0.02280 | 0.4652 | 1.3092 | 0.4799 | —0.033 |
| | E | 1.5258 | 0.3 | 0.0407 | 0.00590 | 0.2110 | 1.1181 | 0.2115 | —0.012 |
| | ,, | 1.6423 | 0.5 | 0.0619 | 0.01311 | 0.3292 | 1.1978 | 0.3316 | —0.016 |
| | ,, | 1.7635 | 0.7 | 0.0793 | 0.02120 | 0.4310 | 1.2769 | 0.4372 | —0.018 |
| | Y | 1.6089 | 0.3 | 0.0377 | 0.00613 | 0.1964 | 1.1087 | 0.1956 | 0.027 |
| | ,, | 1.7097 | 0.5 | 0.0559 | 0.01268 | 0.3033 | 1.1782 | 0.3015 | |
| | ,, | 1.8110 | 0.7 | 0.0701 | 0.01938 | 0.3937 | 1.2428 | 0.3887 | 0.021 |
| 0.05 | G | 1.1939 | 0.3 | 0.0573 | 0.00778 | 0.2809 | 1.1644 | 0.2839 | —0.033 |
| | ,, | 1.3957 | 0.5 | 0.0789 | 0.01621 | 0.3995 | 1.2534 | 0.4094 | —0.036 |
| | ,, | 1.5694 | 0.7 | 0.0973 | 0.02612 | 0.5025 | 1.3451 | 0.5245 | —0.038 |
| | E | 1.1720 | 0.3 | 0.0548 | 0.00761 | 0.2607 | 1.1506 | 0.2628 | —0.029 |
| | ,, | 1.3757 | 0.5 | 0.0739 | 0.01526 | 0.3694 | 1.2287 | 0.3754 | —0.029 |
| | ,, | 1.5425 | 0.7 | 0.0898 | 0.02368 | 0.4641 | 1.3070 | 0.4763 | —0.028 |
| | Y | 1.0923 | 0.3 | 0.0499 | 0.00704 | 0.2320 | 1.1315 | 0.2329 | —0.017 |
| | ,, | 1.2886 | 0.5 | 0.0652 | 0.01347 | 0.3253 | 1.1945 | 0.3264 | —0.008 |
| | ,, | 1.4450 | 0.7 | 0.0778 | 0.02005 | 0.4077 | 1.2555 | 0.4072 | 0.002 |
| 0.10 | G | 1.0414 | 0.3 | 0.0725 | 0.01049 | 0.3357 | 1.2038 | 0.3417 | —0.038 |
| | ,, | 1.2585 | 0.5 | 0.0919 | 0.01952 | 0.4442 | 1.2918 | 0.4597 | —0.040 |
| | ,, | 1.4461 | 0.7 | 0.1086 | 0.02990 | 0.5391 | 1.3830 | 0.5697 | —0.041 |
| | E | 1.0026 | 0.3 | 0.0706 | 0.01012 | 0.3163 | 1.1895 | 0.3211 | —0.036 |
| | ,, | 1.2110 | 0.5 | 0.0875 | 0.01815 | 0.4139 | 1.2652 | 0.4248 | —0.036 |
| | ,, | 1.3878 | 0.7 | 0.1016 | 0.02682 | 0.5002 | 1.3419 | 0.5200 | —0.035 |
| | Y | 0.9206 | 0.3 | 0.0666 | 0.00933 | 0.2902 | 1.1708 | 0.2934 | —0.032 |
| | ,, | 1.0983 | 0.5 | 0.0797 | 0.01582 | 0.3701 | 1.2290 | 0.3756 | —0.026 |
| | ,, | 1.2486 | 0.7 | 0.0904 | 0.02232 | 0.4418 | 1.2856 | 0.4480 | —0.017 |
| 0.15 | G | 0.9481 | 0.3 | 0.0871 | 0.01373 | 0.3887 | 1.2451 | 0.3989 | —0.040 |
| | ,, | 1.1613 | 0.5 | 0.1048 | 0.02332 | 0.4877 | 1.3321 | 0.5101 | —0.042 |
| | ,, | 1.3514 | 0.7 | 0.1199 | 0.03412 | 0.5746 | 1.4227 | 0.6152 | —0.044 |
| | E | 0.9081 | 0.3 | 0.0858 | 0.01325 | 0.3713 | 1.2312 | 0.3799 | —0.039 |
| | ,, | 1.1048 | 0.5 | 0.1011 | 0.02167 | 0.4593 | 1.3052 | 0.4765 | —0.040 |
| | ,, | 1.2785 | 0.7 | 0.1137 | 0.03059 | 0.5375 | 1.3805 | 0.5664 | —0.040 |
| | Y | 0.8362 | 0.3 | 0.0825 | 0.01235 | 0.3487 | 1.2136 | 0.3555 | —0.038 |
| | ,, | 0.9944 | 0.5 | 0.0945 | 0.01907 | 0.4196 | 1.2698 | 0.4309 | —0.035 |
| | ,, | 1.1330 | 0.7 | 0.1039 | 0.02563 | 0.4828 | 1.3240 | 0.4975 | —0.030 |

rather extreme shapes, we see that there is, for pure tensor forces, a fairly strong correlation between the quadrupole moment and the scattering length (triplet effective range), only weakly dependent on the well shape of the tensor force and on the core radius.

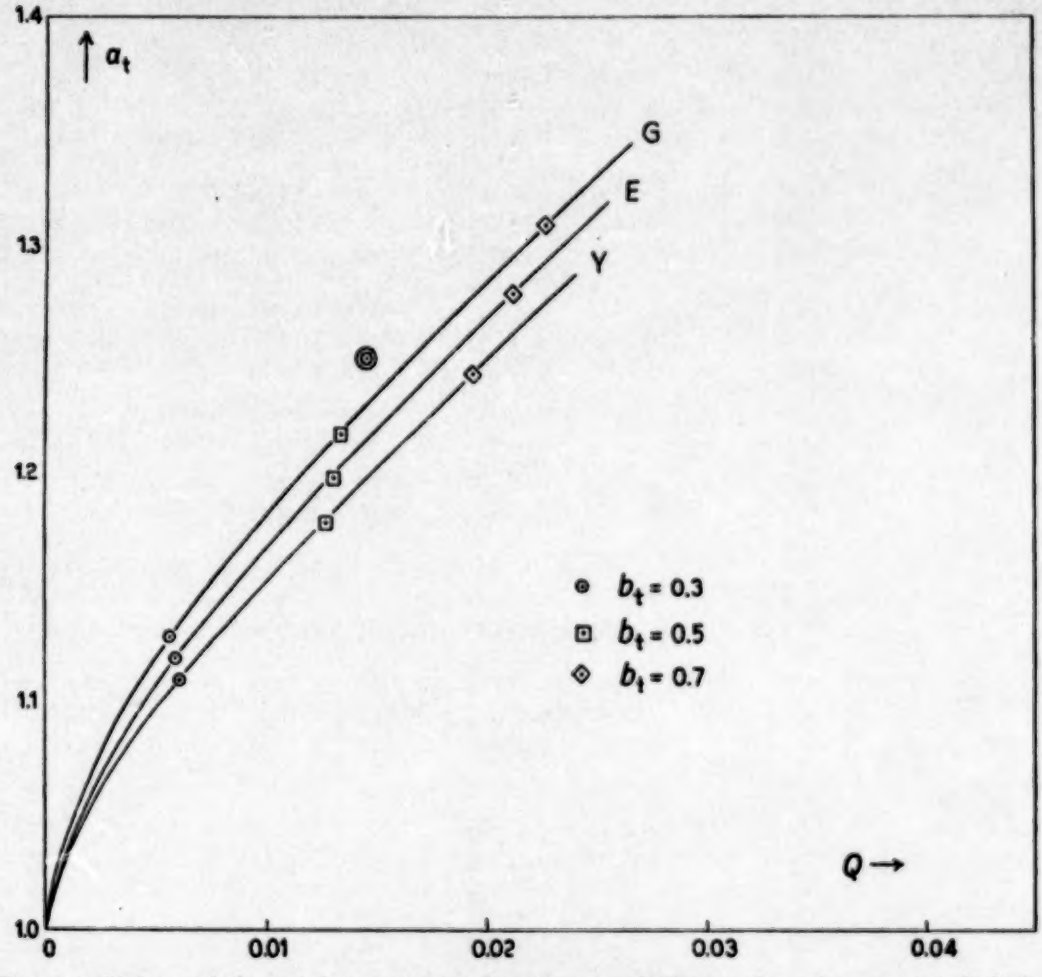


Fig. 3.5. Values of the triplet scattering length $a_t$ and the quadrupole moment $Q$ derived from a pure tensor force. The curves marked G, E and Y refer to tensor forces of Gaussian, exponential, and Yukawa shapes respectively. The parameter varied was the range $b_t$ of the tensor force; the tensor force depth $s_t$ was always adjusted to give the correct binding energy of the deuteron. The experimental values of $a_t$ and $Q$ are indicated by the point with the double circle around it. No repulsive core was assumed in this figure.

Second, we note that the experimental point does not lie far from these curves; an increase in the repulsive core radius brings these curves closer to the experimental point, so much so that for $r_0 = 0.10\ R$ a pure tensor force of Gaussian shape, with no central force at all, provides a good fit to the low energy triplet state data.

It is interesting to note that the lowest (second) order potential in the meson theory of nuclear forces [14]) is such that the tensor force is dominant throughout. Higher order potentials have a shorter range than the second-order potential, and therefore have a comparatively minor effect on the

quadrupole moment and the scattering length (effective range). Indeed, the potentials which we have found in this paper from a purely phenomenological point of view are qualitatively rather similar to the potential of meson theory, i.e., a long range tensor force together with either a very

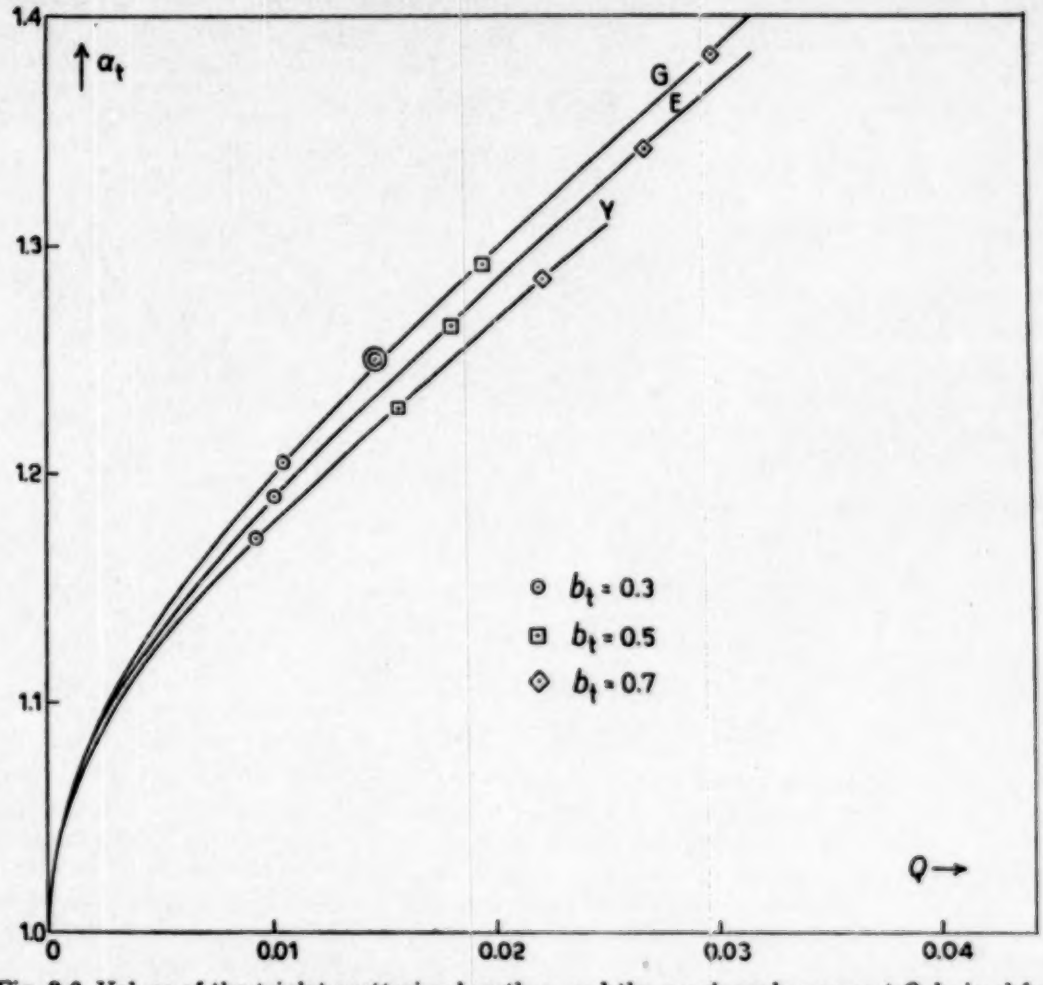


Fig. 3.6. Values of the triplet scattering length $a_t$ and the quadrupole moment $Q$ derived from a pure tensor force. The curves marked G, E and Y refer to tensor forces of Gaussian, exponential, and Yukawa shapes respectively. The parameter varied was the range $b_t$ of the tensor force; the tensor force depth $s_t$ was always adjusted to give the correct binding energy of the deuteron. The experimental values of $a_t$ and $Q$ are indicated by the point with the double circle around it. A repulsive core of $r_0 = 0.10\ R = 0.43 \times 10^{-13}$ cm was assumed in this figure.

weak central force, or a central force of appreciable strength but quite small range outside the core. Only for zero core radius do our potentials differ qualitatively from those of meson theory.

Having determined the effect of pure tensor forces, we now add small amounts of central forces. Clearly the quadrupole moment should then decrease, together with the tensor force strength $s_t$ necessary to give the correct binding energy of the deuteron. As for the effective range, it may either increase or decrease depending upon the range of the central force

which is being introduced. If the range of the central force is larger than the effective range of the wave function without any central forces, then the introduction of the central force may be expected to increase the overall effective range. Conversely, if we add a central force of range less than the effective range without central forces, the overall effective range is expected to decrease.

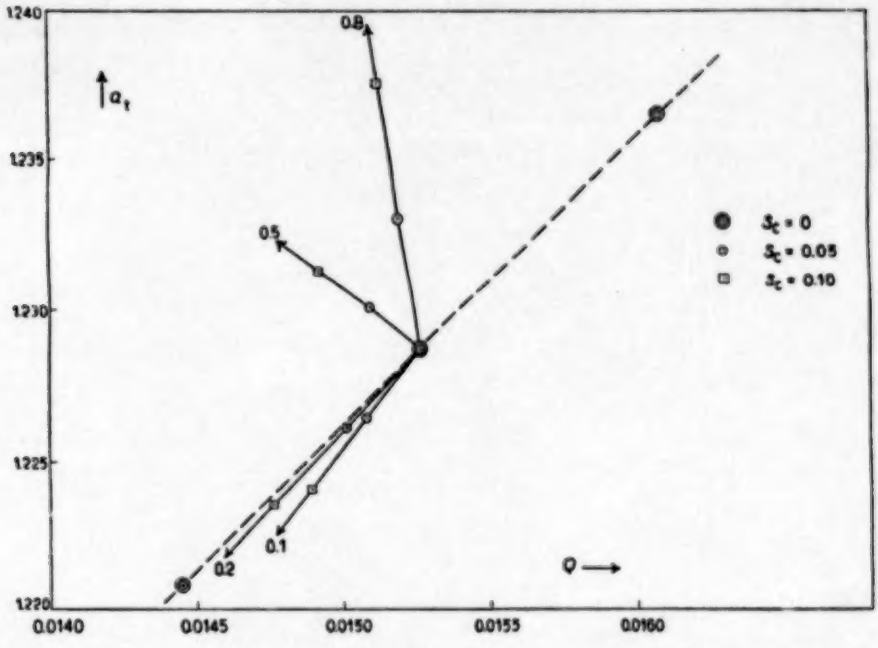


Fig. 3.7. This figure shows the effect of adding a very small amount of central force to a large tensor force. The triplet scattering length, $a_t$, is plotted against the quadrupole moment, $Q$. The doubly circled points come from pure tensor forces of exponential shape, the point in the middle of the figure deriving from a tensor force range $b_t = 0.50$, and strength $s_t$ adjusted to give the correct binding energy of the deuteron. We then add central forces, also of exponential well shape, but of various ranges $b_c$ and depths $s_c$. In each case the tensor force depth $s_t$ is readjusted to maintain the binding energy of the deuteron.

As expected, the introduction of an attractive central force always decreases the quadrupole moment $Q$, simply because it decreases the tensor force strength $s_t$ necessary to give the deuteron binding energy. The triplet scattering length $a_t$ (correlated with the triplet effective range) may be either increased or decreased, depending upon the range $b_c$ of the added central force.

Throughout this figure, a core radius of $r_0 = 0.05$ was assumed. The central force range $b_c$ is indicated by the numbers next to the arrows.

In fig. 3.7 we show the effect of adding central forces of exponential well shape, depths $s_c = 0.05$ and 0.10, and ranges $b_c = 0.1$, 0.2, 0.5, and 0.8, to a tensor force of exponential well shape and range $b_t = 0.5$, in the presence of a repulsive core of radius $r_0 = 0.05$. The effective range in the absence of any central force is 0.37, and we see that the expectations of the preceding paragraph are borne out by these calculations.

Except for extremely short central ranges ($b_c \lessapprox 0.2$)the points for an added (attractive) central force fall *above* the (dotted) curve obtained from

a pure tensor force by changing the tensor force range $b_t$. Since the experimental point lies *above* the curves for pure tensor forces, we conclude that the additional central force needed to fit the experimental data is either attractive, or amounts to merely an enlargement of the repulsive core. *A repulsive central force of appreciable range outside the core cannot fit the data*, for core radii less than 0.10.

Since the curves for pure tensor forces (figs. 3.5 and 3.6) do not in general pass through the experimental point, some non-zero central force must be present in order to fit the data. Conversely, if the strength $s_c$ of the central force is too weak, we may not be able to fit the three experimental data ($B$, $Q$, $a_t$) in spite of the fact that we have three parameters ($b_c$, $s_t$, $b_t$) at our disposal. This situation does in fact occur twice in table 2.1; with both central and tensor forces of Yukawa shape, $s_c = 0.6$ is too weak a central force to allow a fit to the data; with both forces of exponential shape, $s_c = 0.3$ is too weak, but $s_c = 0.6$ is still all right. This is as expected from fig. 3.5: the curve for a pure tensor force of Yukawa shape is farther away from the experimental point than the curve for a pure tensor force of exponential shape.

## 4. Potentials with Spin-Independent Central Range

A considerable body of theoretical investigation concerning the triton and heavier nuclei has been based upon potentials of the type

$$V = (V_W + V_M P^M + V_H P^H + V_B P^B) f_c(r) + (V_{TW} + V_{TM} P^M) S_{12} f_t(r) \quad (4.1)$$

where $V_W$ etc. are constants, $P^M$ is the Majorana exchange operator, $P^H$ and $P^B$ the Heisenberg and Bartlett exchange operators, $f_c(r)$ defines the shape and range of the central potential and $f_t(r)$ defines the shape and range of the tensor potential [2]).

Because of the considerable difficulties involved in the integrations for three-body and more complex nuclei, the functions $f_c(r)$ and $f_t(r)$ are often chosen to be Gaussian in shape, without any repulsive core.

From the point of view adopted here, the limitation imposed by the choice (4.1) is simply that the *central* force must have a range which (after suitable adjustment of the well depth) can fit the scattering data in the $^1S_0$ state. This is the only restriction imposed by the low-energy data.

We have allowed three well shapes (Gaussian, exponential, and Yukawa) for $f_c(r)$, three well shapes for $f_t(r)$; the range $b_c$ was chosen to fit the low energy $^1S_0$ effective range; and the central force well depth $s_c$, the tensor well depth $s_t$, and range $b_t$ were adjusted to fit the three experimental triplet state quantities $B$, $Q$, and $a_t$. The results are given in table 4.1.

We note that $s_c$ is generally less than the value required to fit the singlet

state. That is, if (4.1) is to hold, the central force in the triplet state is *weaker* than in the singlet state; the extra binding energy in the triplet state is due entirely to the tensor force. The only exception to this is the case where both wells have the Yukawa shape; there the central force strength, as well as the range, is nearly spin-independent; this was noted earlier by Feshbach and Schwinger [15]). Table 4.1 shows that this property is true *only* of the Yukawa well shape. Furthermore, it is true only in the absence of a repulsive core.

TABLE 4.1

Wells with zero core radius and spin-independent central range which fit the low energy data.

| Central force | | | Tensor force | | | $P_D$ | $P$ |
|---|---|---|---|---|---|---|---|
| Shape | $s_c$ | $b_c$ | Shape | $s_t$ | $b_t$ | | |
| G | 0.3083 | 0.592 | G | 1.4146 | 0.5516 | 0.061 | −0.024 |
| ,, | 0.4999 | 0.592 | E | 1.3333 | 0.5863 | 0.052 | −0.014 |
| ,, | 0.6261 | 0.592 | Y | 1.3155 | 0.6279 | 0.044 | −0.001 |
| E | 0.3799 | 0.582 | G | 1.3666 | 0.5625 | 0.059 | −0.012 |
| ,, | 0.6153 | 0.582 | E | 1.2341 | 0.6181 | 0.048 | +0.007 |
| ,, | 0.7684 | 0.582 | Y | 1.1631 | 0.6975 | 0.039 | +0.028 |
| Y | 0.4896 | 0.573 | G | 1.3045 | 0.5777 | 0.057 | +0.006 |
| ,, | 0.8137 | 0.573 | E | 1.0757 | 0.6836 | 0.042 | +0.044 |
| ,, | 1.0536 | 0.573 | Y | 0.8614 | 0.9599 | 0.028 | +0.103 |

If there were no reason to suspect the presence of a repulsive core in the true nucleon-nucleon interaction, the potentials presented in this section would form a reasonable starting point for investigation of the triton. Actually, however, it is doubtful whether results for the triton obtained with any of the potentials in table 4.1 should be taken seriously. The triton problem is more sensitive to the presence of a repulsive core than the low energy two-body problem; hence a potential without a core can fit the two-body low energy data quite well and may still give grossly incorrect results for the triton. We have investigated potentials of this type and zero core radius primarily for the sake of completeness, and as a service to investigators who prefer to use a simple analytic form such as (4.1).

We are indebted to Professors V. F. Weisskopf, H. Feshbach, S. Treiman, S. T. Butler, M. R. Schafroth, and J. McIntyre for very helpful discussions on the subject of this paper. We would like to thank the staff of the Adolph Basser Computing Laboratory, School of Physics, Sydney University, for their help and cooperation in running these calculations on the SILLIAC. In particular, we are grateful to Mrs. Margaret Grouse for supervising the daily progress of the computation, and carrying out the necessary interpolations with skill and despatch.

## References


1) J. L. Gammel, R. S. Christian and R. M. Thaler, Phys. Rev. **105** (1957) 311
2) J. M. Blatt and V. F. Weisskopf, Theoretical Nuclear Physics (John Wiley and Sons, New York, 1952)
3) H. A. Bethe, Phys. Rev. **76** (1948) 38
4) J. M. Blatt and J. D. Jackson, Phys. Rev. **76** (1949) 18
5) M. H. Kalos and J. M. Blatt, Internal Report No. 50 (Digital Computer Laboratory, University of Illinois, 1953)
6) J. Bernstein and A. Klein, Phys. Rev. **99** (1955) 966;
   A. M. Sessler, Phys. Rev. **96** (1954) 793
7) A. J. F. Siegert, Phys. Rev. **52** (1937) 787
8) M. Sugawara, Phys. Rev. **99** (1955) 1601
9) J. McIntyre, Phys. Rev. **103** (1956) 1464
10) Yennie, Levy and Ravenhall, Revs. Mod. Phys. **29** (1957) 144
11) L. C. Biedenharn, Ph. D. thesis (M.I.T., 1949)
12) G. Breit and W. G. Bouricius, Phys. Rev. **75** (1949) 1029
13) H. Feshbach and F. Lomon, Phys. Rev. **102** (1956) 891
14) Taketani *et al.*, Suppl. Prog. Theor. Phys. **8** (1956)
15) H. Feshbach and J. Schwinger, Phys. Rev **84** (1951) 194


## Appendix

### TABLES OF WAVE FUNCTIONS

The tables each give three sets of wave functions $u(x)$ and $w(x)$, normalized according to eq. (3.4). The internucleon distance $x$ is measured in units of the "radius of the deuteron" $R=4.315\times10^{-13}$ cm. These wave functions all give the correct quadrupole moment of the deuteron and the correct triplet scattering length (triplet effective range). The parameters defining the potentials used are contained in tables 2.1 to 2.4 of the paper; the caption of each table in this appendix contains the information necessary to locate the corresponding entry in tables 2.1 and 2.4. The potentials for table A.9 are defined in table 4.1.

TABLE A.1

Zero core radius, both well shapes exponential;
$s_0 = 0.6$, 0.9, and 1.0

| X | U | W | U | W | U | W |
|---|---|---|---|---|---|---|
| 0.0000 | 0.000000 | 0.000000 | 0.000000 | 0.000000 | 0.000000 | 0.000000 |
| 0.0034 | 0.017468 | 0.000023 | 0.019324 | 0.000015 | 0.020212 | 0.000012 |
| 0.0068 | 0.034931 | 0.000146 | 0.038634 | 0.000096 | 0.040407 | 0.000078 |
| 0.0101 | 0.052381 | 0.000422 | 0.057915 | 0.000279 | 0.060566 | 0.000228 |
| 0.0135 | 0.069814 | 0.000882 | 0.077156 | 0.000588 | 0.080675 | 0.000482 |
| 0.0169 | 0.087223 | 0.001548 | 0.096342 | 0.001039 | 0.100716 | 0.000855 |
| 0.0203 | 0.104602 | 0.002432 | 0.115463 | 0.001642 | 0.120677 | 0.001354 |
| 0.0237 | 0.121944 | 0.003544 | 0.134506 | 0.002406 | 0.140543 | 0.001989 |
| 0.0271 | 0.139245 | 0.004885 | 0.153460 | 0.003334 | 0.160300 | 0.002762 |
| 0.0304 | 0.156496 | 0.006457 | 0.172315 | 0.004428 | 0.179936 | 0.003677 |
| 0.0338 | 0.173693 | 0.008258 | 0.191061 | 0.005690 | 0.199440 | 0.004733 |
| 0.0372 | 0.190827 | 0.010283 | 0.209688 | 0.007117 | 0.218800 | 0.005932 |
| 0.0406 | 0.207893 | 0.012528 | 0.228187 | 0.008708 | 0.238006 | 0.007271 |
| 0.0440 | 0.224884 | 0.014985 | 0.246548 | 0.010459 | 0.257047 | 0.008747 |
| 0.0474 | 0.241793 | 0.017648 | 0.264764 | 0.012366 | 0.275916 | 0.010359 |
| 0.0507 | 0.258614 | 0.020507 | 0.282827 | 0.014424 | 0.294602 | 0.012103 |
| 0.0541 | 0.275339 | 0.023554 | 0.300729 | 0.016628 | 0.313097 | 0.013974 |
| 0.0575 | 0.291964 | 0.026779 | 0.318463 | 0.018972 | 0.331395 | 0.015968 |
| 0.0609 | 0.308480 | 0.030174 | 0.336022 | 0.021450 | 0.349487 | 0.018080 |
| 0.0643 | 0.324882 | 0.033727 | 0.353400 | 0.024056 | 0.367368 | 0.020305 |
| 0.0677 | 0.341164 | 0.037430 | 0.370591 | 0.026783 | 0.385031 | 0.022638 |
| 0.0710 | 0.357319 | 0.041271 | 0.387588 | 0.029624 | 0.402471 | 0.025073 |
| 0.0744 | 0.373342 | 0.045242 | 0.404388 | 0.032574 | 0.419682 | 0.027605 |
| 0.0778 | 0.389227 | 0.049333 | 0.420984 | 0.035624 | 0.436660 | 0.030229 |
| 0.0812 | 0.404967 | 0.053533 | 0.437373 | 0.038769 | 0.453400 | 0.032938 |
| 0.0947 | 0.466384 | 0.071241 | 0.500769 | 0.052158 | 0.517911 | 0.044523 |
| 0.1083 | 0.525099 | 0.089974 | 0.560557 | 0.066534 | 0.578375 | 0.057040 |
| 0.1218 | 0.580848 | 0.109214 | 0.616588 | 0.081512 | 0.634685 | 0.070164 |
| 0.1353 | 0.633428 | 0.128517 | 0.668776 | 0.096751 | 0.686808 | 0.083599 |
| 0.1488 | 0.682691 | 0.147510 | 0.717096 | 0.111958 | 0.734770 | 0.097087 |
| 0.1624 | 0.728542 | 0.165887 | 0.761568 | 0.126884 | 0.778642 | 0.110410 |
| 0.1759 | 0.770937 | 0.183409 | 0.802253 | 0.141327 | 0.818536 | 0.123386 |
| 0.1894 | 0.809876 | 0.199891 | 0.839246 | 0.155127 | 0.854591 | 0.135869 |
| 0.2030 | 0.845398 | 0.215201 | 0.872665 | 0.168161 | 0.886967 | 0.147742 |
| 0.2165 | 0.877572 | 0.229247 | 0.902653 | 0.180336 | 0.915841 | 0.158921 |
| 0.2300 | 0.906497 | 0.241977 | 0.929362 | 0.191592 | 0.941400 | 0.169342 |
| 0.2436 | 0.932291 | 0.253366 | 0.952960 | 0.201890 | 0.963835 | 0.178966 |
| 0.2571 | 0.955089 | 0.263418 | 0.973616 | 0.211213 | 0.983338 | 0.187768 |
| 0.2706 | 0.975036 | 0.272153 | 0.991507 | 0.219559 | 1.000103 | 0.195742 |
| 0.2842 | 0.992289 | 0.279611 | 1.006807 | 0.226942 | 1.014319 | 0.202891 |
| 0.2977 | 1.007005 | 0.285841 | 1.019690 | 0.233384 | 1.026169 | 0.209230 |
| 0.3112 | 1.019346 | 0.290903 | 1.030325 | 0.238918 | 1.035830 | 0.214781 |
| 0.3248 | 1.029471 | 0.294862 | 1.038877 | 0.243582 | 1.043473 | 0.219572 |
| 0.3383 | 1.037538 | 0.297788 | 1.045505 | 0.247418 | 1.049258 | 0.223635 |
| 0.3518 | 1.043701 | 0.299754 | 1.050360 | 0.250473 | 1.053339 | 0.227007 |
| 0.3654 | 1.048108 | 0.300832 | 1.053586 | 0.252795 | 1.055860 | 0.229725 |
| 0.3789 | 1.050901 | 0.301093 | 1.055321 | 0.254432 | 1.056957 | 0.231828 |
| 0 3924 | 1.052216 | 0.300610 | 1.055693 | 0.255434 | 1.056756 | 0.233356 |
| 0.4059 | 1.052180 | 0.299451 | 1.054824 | 0.255848 | 1.055376 | 0.234349 |

| X | U | W | U | W | U | W |
|---|---|---|---|---|---|---|
| 0.4601 | 1.040844 | 0.289332 | 1.041081 | 0.252552 | 1.040146 | 0.233731 |
| 0.5142 | 1.016268 | 0.273084 | 1.015222 | 0.243315 | 1.013509 | 0.227452 |
| 0.5683 | 0.983310 | 0.253510 | 0.981697 | 0.230337 | 0.979687 | 0.217411 |
| 0.6225 | 0.945423 | 0.232591 | 0.943660 | 0.215274 | 0.941651 | 0.205082 |
| 0.6766 | 0.904987 | 0.211653 | 0.903297 | 0.199317 | 0.901452 | 0.191556 |
| 0.7307 | 0.863605 | 0.191521 | 0.862089 | 0.183282 | 0.860483 | 0.177611 |
| 0.7848 | 0.822331 | 0.172673 | 0.821021 | 0.167707 | 0.819675 | 0.163781 |
| 0.8390 | 0.781839 | 0.155341 | 0.780731 | 0.152922 | 0.779635 | 0.150420 |
| 0.8931 | 0.742547 | 0.139602 | 0.741621 | 0.139113 | 0.740748 | 0.137746 |
| 0.9472 | 0.704699 | 0.125432 | 0.703928 | 0.126365 | 0.703247 | 0.125885 |
| 1.0013 | 0.668426 | 0.112748 | 0.667785 | 0.114694 | 0.667263 | 0.114890 |
| 1.0555 | 0.633784 | 0.101438 | 0.633248 | 0.104075 | 0.632854 | 0.104774 |
| 1.1096 | 0.600778 | 0.091376 | 0.600327 | 0.094455 | 0.600036 | 0.095516 |
| 1.1637 | 0.569385 | 0.082434 | 0.569002 | 0.085767 | 0.568791 | 0.087077 |
| 1.2178 | 0.539562 | 0.074488 | 0.539232 | 0.077936 | 0.539084 | 0.079407 |
| 1.2720 | 0.511252 | 0.067424 | 0.510966 | 0.070885 | 0.510865 | 0.072449 |
| 1.3261 | 0.484395 | 0.061139 | 0.484145 | 0.064540 | 0.484080 | 0.066146 |
| 1.3802 | 0.458928 | 0.055539 | 0.458705 | 0.058832 | 0.458668 | 0.060440 |
| 1.4344 | 0.434785 | 0.050540 | 0.434586 | 0.053693 | 0.434568 | 0.055276 |
| 1.4885 | 0.411902 | 0.046071 | 0.411722 | 0.049065 | 0.411719 | 0.050602 |
| 1.5426 | 0.390217 | 0.042067 | 0.390058 | 0.044893 | 0.390061 | 0.046371 |
| 1.5967 | 0.369668 | 0.038474 | 0.369518 | 0.041127 | 0.369534 | 0.042538 |
| 1.6509 | 0.350199 | 0.035241 | 0.350061 | 0.037725 | 0.350082 | 0.039063 |
| 1.7050 | 0.331754 | 0.032327 | 0.331625 | 0.034646 | 0.331650 | 0.035910 |
| 1.9215 | 0.267178 | 0.023197 | 0.267079 | 0.024932 | 0.267108 | 0.025908 |
| 2.1380 | 0.215167 | 0.016947 | 0.215090 | 0.018237 | 0.215115 | 0.018975 |
| 2.3545 | 0.173280 | 0.012560 | 0.173218 | 0.013523 | 0.173240 | 0.014079 |
| 2.5710 | 0.139547 | 0.009416 | 0.139497 | 0.010140 | 0.139515 | 0.010560 |
| 1.7875 | 0.112381 | 0.007125 | 0.112341 | 0.007673 | 0.112355 | 0.007992 |
| 3.0040 | 0.090504 | 0.005432 | 0.090471 | 0.005850 | 0.090483 | 0.006093 |
| 3.2205 | 0.072885 | 0.004167 | 0.072859 | 0.004488 | 0.072868 | 0.004675 |
| 3.4370 | 0.058696 | 0.003214 | 0.058675 | 0.003462 | 0.058683 | 0.003606 |
| 3.6535 | 0.047270 | 0.002490 | 0.047253 | 0.002682 | 0.047259 | 0.002793 |
| 3.8701 | 0.038067 | 0.001936 | 0.038054 | 0.002085 | 0.038059 | 0.002172 |
| 4.0866 | 0.030657 | 0.001511 | 0.030646 | 0.001627 | 0.030650 | 0.001695 |
| 4.3031 | 0.024689 | 0.001182 | 0.024680 | 0.001273 | 0.024683 | 0.001326 |
| 4.5196 | 0.019882 | 0.000927 | 0.019875 | 0.000998 | 0.019878 | 0.001040 |
| 4.7361 | 0.016012 | 0.000729 | 0.016006 | 0.000785 | 0.016008 | 0.000817 |
| 4.9526 | 0.012895 | 0.000574 | 0.012890 | 0.000618 | 0.012892 | 0.000644 |
| 5.1691 | 0.010385 | 0.000453 | 0.010381 | 0.000487 | 0.010382 | 0.000508 |
| 5.3856 | 0.008363 | 0.000358 | 0.008360 | 0.000385 | 0.008361 | 0.000401 |
| 5.6021 | 0.006735 | 0.000283 | 0.006732 | 0.000305 | 0.006733 | 0.000317 |
| 5.8186 | 0.005424 | 0.000224 | 0.005422 | 0.000241 | 0.005423 | 0.000251 |
| 6.0351 | 0.004368 | 0.000178 | 0.004366 | 0.000191 | 0.004367 | 0.000199 |
| 6.2516 | 0.003518 | 0.000141 | 0.003516 | 0.000152 | 0.003517 | 0.000158 |
| 6.4681 | 0.002833 | 0.000112 | 0.002832 | 0.000121 | 0.002832 | 0.000126 |
| 6.6846 | 0.002281 | 0.000089 | 0.002281 | 0.000096 | 0.002281 | 0.000100 |
| 6.9011 | 0.001837 | 0.000071 | 0.001837 | 0.000076 | 0.001837 | 0.000079 |

TABLE A.2

Core radius 0.05, central force Gaussian, tensor force exponential well shape; $s_0 = 0.6$, 0.9, and 1.0

| X | U | W | U | W | U | W |
|---|---|---|---|---|---|---|
| 0.0500 | 0.000000 | 0.000000 | 0.000000 | 0.000000 | 0.000000 | 0.000000 |
| 0.0534 | 0.020636 | 0.003527 | 0.022071 | 0.002446 | 0.022884 | 0.002005 |
| 0.0568 | 0.041262 | 0.007106 | 0.044129 | 0.004930 | 0.045755 | 0.004042 |
| 0.0601 | 0.061866 | 0.010772 | 0.066162 | 0.007480 | 0.068597 | 0.006136 |
| 0.0635 | 0.082438 | 0.014549 | 0.088159 | 0.010116 | 0.091399 | 0.008303 |
| 0.0669 | 0.102968 | 0.018452 | 0.110106 | 0.012850 | 0.114146 | 0.010553 |
| 0.0703 | 0.123445 | 0.022490 | 0.131991 | 0.015691 | 0.136824 | 0.012896 |
| 0.0737 | 0.143858 | 0.026667 | 0.153803 | 0.018642 | 0.159421 | 0.015334 |
| 0.0771 | 0.164199 | 0.030984 | 0.175528 | 0.021707 | 0.181922 | 0.017871 |
| 0.0804 | 0.184455 | 0.035439 | 0.197157 | 0.024886 | 0.204315 | 0.020507 |
| 0.0838 | 0.204619 | 0.040028 | 0.218675 | 0.028177 | 0.226586 | 0.023242 |
| 0.0872 | 0.224678 | 0.044746 | 0.240073 | 0.031577 | 0.248723 | 0.026075 |
| 0.0906 | 0.244625 | 0.049586 | 0.261338 | 0.035083 | 0.270714 | 0.029001 |
| 0.0940 | 0.264449 | 0.054541 | 0.282459 | 0.038692 | 0.292545 | 0.032020 |
| 0.0974 | 0.284140 | 0.059603 | 0.303425 | 0.042397 | 0.314204 | 0.035125 |
| 0.1007 | 0.303689 | 0.064764 | 0.324226 | 0.046194 | 0.335681 | 0.038315 |
| 0.1041 | 0.323088 | 0.070014 | 0.344850 | 0.050077 | 0.356962 | 0.041584 |
| 0.1075 | 0.342327 | 0.075346 | 0.365287 | 0.054040 | 0.378038 | 0.044927 |
| 0.1109 | 0.361398 | 0.080750 | 0.385527 | 0.058077 | 0.398896 | 0.048339 |
| 0.1143 | 0.380293 | 0.086217 | 0.405561 | 0.062182 | 0.419527 | 0.051816 |
| 0.1177 | 0.399003 | 0.091739 | 0.425379 | 0.066348 | 0.439921 | 0.055352 |
| 0.1210 | 0.417520 | 0.097307 | 0.444972 | 0.070569 | 0.460066 | 0.058942 |
| 0.1244 | 0.435837 | 0.102911 | 0.464330 | 0.074838 | 0.479955 | 0.062580 |
| 0.1278 | 0.453947 | 0.108544 | 0.483446 | 0.079149 | 0.499578 | 0.066262 |
| 0.1312 | 0.471842 | 0.114197 | 0.502312 | 0.083496 | 0.518927 | 0.069981 |
| 0.1447 | 0.541153 | 0.136853 | 0.575122 | 0.101119 | 0.593418 | 0.085132 |
| 0.1583 | 0.606562 | 0.159231 | 0.643377 | 0.118834 | 0.662944 | 0.100478 |
| 0.1718 | 0.667777 | 0.180927 | 0.706747 | 0.136300 | 0.727170 | 0.115720 |
| 0.1853 | 0.724591 | 0.201608 | 0.765007 | 0.153223 | 0.785878 | 0.130596 |
| 0.1988 | 0.776873 | 0.221011 | 0.818031 | 0.169357 | 0.838962 | 0.144884 |
| 0.2124 | 0.824569 | 0.238942 | 0.865785 | 0.184508 | 0.886419 | 0.158404 |
| 0.2259 | 0.867688 | 0.255265 | 0.908322 | 0.198532 | 0.928341 | 0.171020 |
| 0.2394 | 0.906300 | 0.269896 | 0.945768 | 0.211327 | 0.964899 | 0.182632 |
| 0.2530 | 0.940524 | 0.282797 | 0.978314 | 0.222835 | 0.996329 | 0.193179 |
| 0.2665 | 0.970520 | 0.293968 | 1.006197 | 0.233029 | 1.022920 | 0.202629 |
| 0.2800 | 0.996480 | 0.303442 | 1.029695 | 0.241915 | 1.044996 | 0.210977 |
| 0.2936 | 1.018621 | 0.311272 | 1.049111 | 0.249521 | 1.062906 | 0.218242 |
| 0.3071 | 1.037178 | 0.317536 | 1.064763 | 0.255894 | 1.077010 | 0.224459 |
| 0.3206 | 1.052398 | 0.322322 | 1.076976 | 0.261096 | 1.087672 | 0.229674 |
| 0.3342 | 1.064531 | 0.325729 | 1.086075 | 0.265199 | 1.095245 | 0.233947 |
| 0.3477 | 1.073830 | 0.327862 | 1.092373 | 0.268281 | 1.100073 | 0.237339 |
| 0.3612 | 1.080541 | 0.328829 | 1.096175 | 0.270422 | 1.102478 | 0.239918 |
| 0.3748 | 1.084905 | 0.328738 | 1.097765 | 0.271706 | 1.102762 | 0.241752 |
| 0.3883 | 1.087153 | 0.327696 | 1.097408 | 0.272212 | 1.101201 | 0.242907 |
| 0.4018 | 1.087503 | 0.325804 | 1.095350 | 0.272019 | 1.098048 | 0.243447 |
| 0.4154 | 1.086162 | 0.323161 | 1.091813 | 0.271202 | 1.093527 | 0.243436 |
| 0.4289 | 1.083322 | 0.319859 | 1.086999 | 0.269830 | 1.087839 | 0.242930 |
| 0.4424 | 1.079159 | 0.315986 | 1.081088 | 0.267968 | 1.081163 | 0.241983 |
| 0.4559 | 1.073837 | 0.311620 | 1.074239 | 0.265677 | 1.073654 | 0.240645 |

| X | U | W | U | W | U | W |
|---|---|---|---|---|---|---|
| 0.5101 | 1.043724 | 0.290620 | 1.040036 | 0.253241 | 1.037716 | 0.232231 |
| 0.5642 | 1.004625 | 0.266552 | 0.999358 | 0.237491 | 0.996389 | 0.220505 |
| 0.6183 | 0.961251 | 0.241818 | 0.955912 | 0.220236 | 0.952934 | 0.206988 |
| 0.6725 | 0.916408 | 0.217841 | 0.911719 | 0.202623 | 0.909051 | 0.192677 |
| 0.7266 | 0.871695 | 0.195390 | 0.867892 | 0.185364 | 0.865655 | 0.178233 |
| 0.7807 | 0.827994 | 0.174824 | 0.825061 | 0.168894 | 0.823270 | 0.164093 |
| 0.8348 | 0.785773 | 0.156253 | 0.783590 | 0.153459 | 0.782210 | 0.150542 |
| 0.8890 | 0.745265 | 0.139641 | 0.743688 | 0.139183 | 0.742660 | 0.137755 |
| 0.9431 | 0.706569 | 0.124873 | 0.705462 | 0.126103 | 0.704724 | 0.125825 |
| 0.9972 | 0.669707 | 0.111797 | 0.668955 | 0.114203 | 0.668451 | 0.114791 |
| 1.0513 | 0.634658 | 0.100242 | 0.634168 | 0.103430 | 0.633846 | 0.104653 |
| 1.1055 | 0.601371 | 0.090042 | 0.601074 | 0.093713 | 0.600891 | 0.095384 |
| 1.1596 | 0.569784 | 0.081037 | 0.569625 | 0.084968 | 0.569549 | 0.086941 |
| 1.2137 | 0.539827 | 0.073081 | 0.539766 | 0.077111 | 0.539768 | 0.079270 |
| 1.2678 | 0.511426 | 0.066042 | 0.511434 | 0.070057 | 0.511492 | 0.072314 |
| 1.3220 | 0.484507 | 0.059803 | 0.484562 | 0.063725 | 0.484661 | 0.066014 |
| 1.3761 | 0.458997 | 0.054264 | 0.459083 | 0.058039 | 0.459210 | 0.060312 |
| 1.4302 | 0.434825 | 0.049334 | 0.434931 | 0.052931 | 0.435076 | 0.055153 |
| 1.4844 | 0.411923 | 0.044937 | 0.412041 | 0.048338 | 0.412197 | 0.050484 |
| 1.5385 | 0.390224 | 0.041006 | 0.390349 | 0.044203 | 0.390512 | 0.046258 |
| 1.5926 | 0.369667 | 0.037483 | 0.369795 | 0.040476 | 0.369959 | 0.042430 |
| 1.6467 | 0.350192 | 0.034318 | 0.350320 | 0.037112 | 0.350484 | 0.038960 |
| 1.7009 | 0.331743 | 0.031470 | 0.331869 | 0.034071 | 0.332030 | 0.035812 |
| 1.7550 | 0.314265 | 0.028899 | 0.314388 | 0.031317 | 0.314545 | 0.032952 |
| 1.9715 | 0.253087 | 0.020822 | 0.253192 | 0.022615 | 0.253327 | 0.023861 |
| 2.1880 | 0.203818 | 0.015265 | 0.203904 | 0.016594 | 0.204015 | 0.017532 |
| 2.4045 | 0.164140 | 0.011345 | 0.164210 | 0.012338 | 0.164300 | 0.013043 |
| 2.6210 | 0.132187 | 0.008525 | 0.132242 | 0.009272 | 0.132316 | 0.009804 |
| 2.8375 | 0.106453 | 0.006462 | 0.106498 | 0.007029 | 0.106557 | 0.007434 |
| 3.0540 | 0.085730 | 0.004935 | 0.085766 | 0.005368 | 0.085813 | 0.005677 |
| 3.2705 | 0.069040 | 0.003791 | 0.069070 | 0.004123 | 0.069108 | 0.004361 |
| 3.4870 | 0.055600 | 0.002927 | 0.055624 | 0.003184 | 0.055654 | 0.003367 |
| 3.7035 | 0.044776 | 0.002269 | 0.044795 | 0.002469 | 0.044820 | 0.002611 |
| 3.9201 | 0.036059 | 0.001766 | 0.036075 | 0.001921 | 0.036095 | 0.002032 |
| 4.1366 | 0.029040 | 0.001379 | 0.029052 | 0.001500 | 0.029068 | 0.001586 |
| 4.3531 | 0.023386 | 0.001079 | 0.023396 | 0.001174 | 0.023409 | 0.001242 |
| 4.5696 | 0.018834 | 0.000847 | 0.018842 | 0.000921 | 0.018852 | 0.000974 |
| 4.7861 | 0.015167 | 0.000666 | 0.015174 | 0.000724 | 0.015182 | 0.000766 |
| 5.0026 | 0.012215 | 0.000525 | 0.012220 | 0.000571 | 0.012227 | 0.000604 |
| 5.2191 | 0.009837 | 0.000414 | 0.009841 | 0.000450 | 0.009846 | 0.000476 |
| 5.4356 | 0.007922 | 0.000327 | 0.007925 | 0.000356 | 0.007930 | 0.000376 |
| 5.6521 | 0.006380 | 0.000259 | 0.006382 | 0.000282 | 0.006386 | 0.000298 |
| 5.8686 | 0.005138 | 0.000205 | 0.005140 | 0.000223 | 0.005143 | 0.000236 |
| 6.0851 | 0.004138 | 0.000163 | 0.004139 | 0.000177 | 0.004142 | 0.000187 |
| 6.3016 | 0.003332 | 0.000129 | 0.003333 | 0.000140 | 0.003335 | 0.000149 |
| 6.5181 | 0.002683 | 0.000103 | 0.002685 | 0.000112 | 0.002686 | 0.000118 |
| 6.7346 | 0.002161 | 0.000082 | 0.002162 | 0.000089 | 0.002163 | 0.000094 |
| 6.9511 | 0.001740 | 0.000065 | 0.001741 | 0.000071 | 0.001742 | 0.000075 |

TABLE A.3

Core radius 0.05, central force Gaussian, tensor force Yukawa well shape; $s_0 = 0.6$, 0,9, and 1.0

| X | U | W | U | W | U | W |
|---|---|---|---|---|---|---|
| 0.0500 | 0.000000 | 0.000000 | 0.000000 | 0.000000 | 0.000000 | 0.000000 |
| 0.0534 | 0.027853 | 0.010498 | 0.024978 | 0.006777 | 0.024603 | 0.005545 |
| 0.0568 | 0.055185 | 0.020231 | 0.049750 | 0.013123 | 0.049070 | 0.010753 |
| 0.0601 | 0.081967 | 0.029296 | 0.074295 | 0.019101 | 0.073384 | 0.015679 |
| 0.0635 | 0.108219 | 0.037833 | 0.098611 | 0.024799 | 0.097536 | 0.020392 |
| 0.0669 | 0.133960 | 0.045943 | 0.122696 | 0.030279 | 0.121520 | 0.024944 |
| 0.0703 | 0.159203 | 0.053702 | 0.146547 | 0.035587 | 0.145328 | 0.029372 |
| 0.0737 | 0.183963 | 0.061167 | 0.170159 | 0.040759 | 0.168953 | 0.033704 |
| 0.0771 | 0.208251 | 0.068382 | 0.193529 | 0.045820 | 0.192385 | 0.037960 |
| 0.0804 | 0.232078 | 0.075380 | 0.216652 | 0.050790 | 0.215617 | 0.042156 |
| 0.0838 | 0.255452 | 0.082187 | 0.239523 | 0.055681 | 0.238640 | 0.046302 |
| 0.0872 | 0.278383 | 0.088822 | 0.262137 | 0.060507 | 0.261445 | 0.050408 |
| 0.0906 | 0.300878 | 0.095301 | 0.284490 | 0.065273 | 0.284026 | 0.054479 |
| 0.0940 | 0.322943 | 0.101636 | 0.306575 | 0.069985 | 0.306373 | 0.058519 |
| 0.0974 | 0.344587 | 0.107836 | 0.328389 | 0.074648 | 0.328478 | 0.062530 |
| 0.1007 | 0.365814 | 0.113908 | 0.349926 | 0.079263 | 0.350335 | 0.066513 |
| 0.1041 | 0.386630 | 0.119857 | 0.371181 | 0.083833 | 0.371934 | 0.070471 |
| 0.1075 | 0.407042 | 0.125689 | 0.392150 | 0.088357 | 0.393268 | 0.074402 |
| 0.1109 | 0.427053 | 0.131406 | 0.412828 | 0.092836 | 0.414331 | 0.078305 |
| 0.1143 | 0.446669 | 0.137011 | 0.433210 | 0.097270 | 0.435114 | 0.082181 |
| 0.1177 | 0.465895 | 0.142506 | 0.453293 | 0.101657 | 0.455613 | 0.086027 |
| 0.1210 | 0.484735 | 0.147893 | 0.473071 | 0.105996 | 0.475819 | 0.089843 |
| 0.1244 | 0.503193 | 0.153172 | 0.492542 | 0.110286 | 0.495728 | 0.093626 |
| 0.1278 | 0.521274 | 0.158346 | 0.511701 | 0.114526 | 0.515332 | 0.097375 |
| 0.1312 | 0.538982 | 0.163413 | 0.530545 | 0.118715 | 0.534627 | 0.101088 |
| 0.1447 | 0.606162 | 0.182637 | 0.602709 | 0.134917 | 0.608614 | 0.115540 |
| 0.1583 | 0.667687 | 0.200200 | 0.669617 | 0.150161 | 0.677296 | 0.129266 |
| 0.1718 | 0.723797 | 0.216120 | 0.731168 | 0.164358 | 0.740482 | 0.142159 |
| 0.1853 | 0.774730 | 0.230424 | 0.787323 | 0.177435 | 0.798070 | 0.154132 |
| 0.1988 | 0.820724 | 0.243146 | 0.838111 | 0.189344 | 0.850040 | 0.165122 |
| 0.2124 | 0.862015 | 0.254332 | 0.883619 | 0.200059 | 0.896453 | 0.175088 |
| 0.2259 | 0.898845 | 0.264041 | 0.923986 | 0.209577 | 0.937438 | 0.184012 |
| 0.2394 | 0.931453 | 0.272336 | 0.959399 | 0.217911 | 0.973187 | 0.191896 |
| 0.2530 | 0.960080 | 0.279290 | 0.990085 | 0.225092 | 1.003940 | 0.198759 |
| 0.2665 | 0.984967 | 0.284980 | 1.016300 | 0.231165 | 1.029976 | 0.204633 |
| 0.2800 | 1.006351 | 0.289487 | 1.038324 | 0.236185 | 1.051606 | 0.209564 |
| 0.2936 | 1.024470 | 0.292892 | 1.056453 | 0.240213 | 1.069158 | 0.213605 |
| 0.3071 | 1.039554 | 0.295279 | 1.070988 | 0.243318 | 1.082969 | 0.216815 |
| 0.3206 | 1.051829 | 0.296729 | 1.082237 | 0.245572 | 1.093381 | 0.219257 |
| 0.3342 | 1.061514 | 0.297324 | 1.090501 | 0.247046 | 1.100726 | 0.220997 |
| 0.3477 | 1.068821 | 0.297143 | 1.096073 | 0.247814 | 1.105331 | 0.222098 |
| 0.3612 | 1.073952 | 0.296260 | 1.099236 | 0.247945 | 1.107504 | 0.222626 |
| 0.3748 | 1.077102 | 0.294748 | 1.100257 | 0.247507 | 1.107536 | 0.222640 |
| 0.3883 | 1.078454 | 0.292677 | 1.099387 | 0.246566 | 1.105697 | 0.222200 |
| 0.4018 | 1.078183 | 0.290110 | 1.096856 | 0.245181 | 1.102235 | 0.221359 |
| 0.4154 | 1.076451 | 0.287107 | 1.092880 | 0.243408 | 1.097375 | 0.220168 |
| 0.4289 | 1.073412 | 0.283726 | 1.087651 | 0.241299 | 1.091321 | 0.218673 |
| 0.4424 | 1.069207 | 0.280018 | 1.081345 | 0.238901 | 1.084254 | 0.216914 |
| 0.4559 | 1.063967 | 0.276030 | 1.074120 | 0.236256 | 1.076335 | 0.214931 |

| X | U | W | U | W | U | W |
|---|---|---|---|---|---|---|
| 0.5101 | 1.034944 | 0.258104 | 1.038583 | 0.223911 | 1.038692 | 0.205358 |
| 0.5642 | 0.997382 | 0.238548 | 0.996899 | 0.209999 | 0.995830 | 0.194249 |
| 0.6183 | 0.955476 | 0.218782 | 0.952842 | 0.195621 | 0.951249 | 0.182541 |
| 0.6725 | 0.911881 | 0.199652 | 0.908425 | 0.181403 | 0.906703 | 0.170768 |
| 0.7266 | 0.868195 | 0.181619 | 0.864681 | 0.167686 | 0.863044 | 0.159232 |
| 0.7807 | 0.825333 | 0.164899 | 0.822137 | 0.154656 | 0.820688 | 0.148106 |
| 0.8348 | 0.783798 | 0.149561 | 0.781062 | 0.142405 | 0.779839 | 0.137493 |
| 0.8890 | 0.743848 | 0.135590 | 0.741594 | 0.130971 | 0.740601 | 0.127450 |
| 0.9431 | 0.705601 | 0.122925 | 0.703792 | 0.120358 | 0.703017 | 0.118005 |
| 0.9972 | 0.669095 | 0.111480 | 0.667675 | 0.110548 | 0.667096 | 0.109165 |
| 1.0513 | 0.634322 | 0.101159 | 0.633229 | 0.101510 | 0.632823 | 0.100923 |
| 1.1055 | 0.601246 | 0.091864 | 0.600425 | 0.093203 | 0.600165 | 0.093262 |
| 1.1596 | 0.569818 | 0.083498 | 0.569217 | 0.085583 | 0.569081 | 0.086158 |
| 1.2137 | 0.539977 | 0.075971 | 0.539553 | 0.078602 | 0.539519 | 0.079585 |
| 1.2678 | 0.511659 | 0.069197 | 0.511377 | 0.072214 | 0.511426 | 0.073511 |
| 1.3220 | 0.484797 | 0.063098 | 0.484627 | 0.066373 | 0.484742 | 0.067906 |
| 1.3761 | 0.459325 | 0.057604 | 0.459242 | 0.061033 | 0.459410 | 0.062737 |
| 1.4302 | 0.435176 | 0.052651 | 0.435161 | 0.056153 | 0.435369 | 0.057975 |
| 1.4844 | 0.412286 | 0.048181 | 0.412323 | 0.051693 | 0.412561 | 0.053590 |
| 1.5385 | 0.390592 | 0.044142 | 0.390668 | 0.047617 | 0.390927 | 0.049552 |
| 1.5926 | 0.370033 | 0.040489 | 0.370138 | 0.043891 | 0.370413 | 0.045836 |
| 1.6467 | 0.350552 | 0.037180 | 0.350679 | 0.040482 | 0.350962 | 0.042415 |
| 1.7009 | 0.332094 | 0.034180 | 0.332235 | 0.037364 | 0.332523 | 0.039267 |
| 1.7550 | 0.314605 | 0.031456 | 0.314756 | 0.034509 | 0.315045 | 0.036368 |
| 1.9715 | 0.253376 | 0.022795 | 0.253534 | 0.025282 | 0.253805 | 0.026887 |
| 2.1880 | 0.204055 | 0.016760 | 0.204198 | 0.018716 | 0.204434 | 0.020032 |
| 2.4045 | 0.164333 | 0.012475 | 0.164454 | 0.013989 | 0.164652 | 0.015039 |
| 2.6210 | 0.132342 | 0.009380 | 0.132442 | 0.010545 | 0.132606 | 0.011371 |
| 2.8375 | 0.106579 | 0.007113 | 0.106660 | 0.008009 | 0.106794 | 0.008653 |
| 3.0540 | 0.085831 | 0.005432 | 0.085897 | 0.006122 | 0.086005 | 0.006623 |
| 3.2705 | 0.069122 | 0.004173 | 0.069175 | 0.004706 | 0.069263 | 0.005095 |
| 3.4870 | 0.055666 | 0.003222 | 0.055709 | 0.003634 | 0.055780 | 0.003937 |
| 3.7035 | 0.044829 | 0.002499 | 0.044864 | 0.002819 | 0.044921 | 0.003055 |
| 3.9201 | 0.036102 | 0.001945 | 0.036130 | 0.002194 | 0.036176 | 0.002378 |
| 4.1366 | 0.029074 | 0.001518 | 0.029096 | 0.001713 | 0.029134 | 0.001857 |
| 4.3531 | 0.023414 | 0.001188 | 0.023432 | 0.001341 | 0.023462 | 0.001454 |
| 4.5696 | 0.018856 | 0.000933 | 0.018871 | 0.001052 | 0.018895 | 0.001141 |
| 4.7861 | 0.015185 | 0.000733 | 0.015197 | 0.000827 | 0.015216 | 0.000897 |
| 5.0026 | 0.012229 | 0.000578 | 0.012239 | 0.000652 | 0.012254 | 0.000707 |
| 5.2191 | 0.009848 | 0.000456 | 0.009856 | 0.000514 | 0.009869 | 0.000558 |
| 5.4356 | 0.007931 | 0.000360 | 0.007937 | 0.000407 | 0.007947 | 0.000441 |
| 5.6521 | 0.006387 | 0.000285 | 0.006392 | 0.000322 | 0.006400 | 0.000349 |
| 5.8686 | 0.005144 | 0.000226 | 0.005148 | 0.000255 | 0.005154 | 0.000276 |
| 6.0851 | 0.004142 | 0.000179 | 0.004146 | 0.000202 | 0.004151 | 0.000219 |
| 6.3016 | 0.003336 | 0.000142 | 0.003339 | 0.000160 | 0.003343 | 0.000174 |
| 6.5181 | 0.002687 | 0.000113 | 0.002689 | 0.000127 | 0.002692 | 0.000138 |
| 6.7346 | 0.002164 | 0.000090 | 0.002165 | 0.000101 | 0.002168 | 0.000110 |
| 6.9511 | 0.001742 | 0.000072 | 0.001744 | 0.000081 | 0.001746 | 0.000087 |

TABLE A.4

Core radius 0.05; central force exponential, tensor force Gaussian well shape; $s_e = 0.6$, 0.9, and 1.0

| X | U | W | U | W | U | W |
|---|---|---|---|---|---|---|
| 0.0500 | 0.000000 | 0.000000 | 0.000000 | 0.000000 | 0.000000 | 0.000000 |
| 0.0534 | 0.021478 | 0.002373 | 0.025853 | 0.001838 | 0.027634 | 0.001530 |
| 0.0568 | 0.042932 | 0.004788 | 0.051659 | 0.003707 | 0.055213 | 0.003086 |
| 0.0601 | 0.064339 | 0.007275 | 0.077376 | 0.005632 | 0.082685 | 0.004687 |
| 0.0635 | 0.085680 | 0.009856 | 0.102963 | 0.007628 | 0.110005 | 0.006349 |
| 0.0669 | 0.106935 | 0.012548 | 0.128384 | 0.009707 | 0.137128 | 0.008079 |
| 0.0703 | 0.128085 | 0.015360 | 0.153604 | 0.011878 | 0.164014 | 0.009886 |
| 0.0737 | 0.149114 | 0.018301 | 0.178595 | 0.014146 | 0.190629 | 0.011774 |
| 0.0771 | 0.170007 | 0.021375 | 0.203327 | 0.016514 | 0.216940 | 0.013745 |
| 0.0804 | 0.190748 | 0.024584 | 0.227776 | 0.018984 | 0.242916 | 0.015801 |
| 0.0838 | 0.211325 | 0.027930 | 0.251918 | 0.021556 | 0.268533 | 0.017943 |
| 0.0872 | 0.231725 | 0.031411 | 0.275735 | 0.024230 | 0.293767 | 0.020169 |
| 0.0906 | 0.251937 | 0.035026 | 0.299207 | 0.027003 | 0.318596 | 0.022478 |
| 0.0940 | 0.271951 | 0.038772 | 0.322319 | 0.029873 | 0.343004 | 0.024869 |
| 0.0974 | 0.291758 | 0.042646 | 0.345057 | 0.032838 | 0.366974 | 0.027338 |
| 0.1007 | 0.311347 | 0.046643 | 0.367409 | 0.035895 | 0.390493 | 0.029885 |
| 0.1041 | 0.330713 | 0.050760 | 0.389365 | 0.039039 | 0.413549 | 0.032505 |
| 0.1075 | 0.349846 | 0.054990 | 0.410915 | 0.042267 | 0.436133 | 0.035195 |
| 0.1109 | 0.368741 | 0.059330 | 0.432053 | 0.045575 | 0.458237 | 0.037952 |
| 0.1143 | 0.387393 | 0.063772 | 0.452773 | 0.048958 | 0.479856 | 0.040773 |
| 0.1177 | 0.405794 | 0.068312 | 0.473070 | 0.052412 | 0.500986 | 0.043653 |
| 0.1210 | 0.423942 | 0.072943 | 0.492940 | 0.055932 | 0.521622 | 0.046590 |
| 0.1244 | 0.441832 | 0.077659 | 0.512382 | 0.059514 | 0.541763 | 0.049578 |
| 0.1278 | 0.459459 | 0.082454 | 0.531395 | 0.063153 | 0.561410 | 0.052616 |
| 0.1312 | 0.476821 | 0.087322 | 0.549977 | 0.066844 | 0.580561 | 0.055698 |
| 0.1447 | 0.543568 | 0.107393 | 0.620025 | 0.082041 | 0.652269 | 0.068400 |
| 0'1583 | 0.605912 | 0.128129 | 0.683349 | 0.097715 | 0.716334 | 0.081525 |
| 0.1718 | 0.663811 | 0.149146 | 0.740219 | 0.113598 | 0.773139 | 0.094859 |
| 0.1853 | 0.717284 | 0.170094 | 0.790987 | 0.129449 | 0.823156 | 0.108208 |
| 0.1988 | 0.766392 | 0.190659 | 0.836050 | 0.145058 | 0.866905 | 0.121403 |
| 0.2124 | 0.811231 | 0.210563 | 0.875826 | 0.160245 | 0.904919 | 0.134302 |
| 0.2259 | 0.851923 | 0.229574 | 0.910731 | 0.174860 | 0.937726 | 0.146785 |
| 0.2394 | 0.888608 | 0.247497 | 0.941169 | 0.188780 | 0.965828 | 0.158755 |
| 0.2530 | 0.921440 | 0.264177 | 0.967526 | 0.201908 | 0.989697 | 0.170134 |
| 0.2665 | 0.950585 | 0.279495 | 0.990161 | 0.214169 | 1.009769 | 0.180861 |
| 0.2800 | 0.976216 | 0.293365 | 1.009410 | 0.225508 | 1.026441 | 0.190892 |
| 0.2936 | 0.998510 | 0.305731 | 1.025578 | 0.235889 | 1.040075 | 0.200196 |
| 0.3071 | 1.017650 | 0.316566 | 1.038946 | 0.245288 | 1.050994 | 0.208750 |
| 0.3206 | 1.033820 | 0.325864 | 1.049772 | 0.253696 | 1.059486 | 0.216546 |
| 0.3342 | 1.047205 | 0.333641 | 1.058288 | 0.261117 | 1.065813 | 0.223580 |
| 0.3477 | 1.057988 | 0.339933 | 1.064706 | 0.267562 | 1.070202 | 0.229857 |
| 0.3612 | 1.066351 | 0.344787 | 1.069219 | 0.273051 | 1.072861 | 0.235387 |
| 0.3748 | 1.072475 | 0.348264 | 1.072003 | 0.277610 | 1.073970 | 0.240186 |
| 0.3883 | 1.076533 | 0.350435 | 1.073218 | 0.281272 | 1.073693 | 0.244273 |
| 0.4018 | 1.078695 | 0.351379 | 1.073010 | 0.284072 | 1.072173 | 0.247670 |
| 0.4154 | 1.079127 | 0.351178 | 1.071514 | 0.286052 | 1.069540 | 0.250403 |
| 0.4289 | 1.077984 | 0.349921 | 1.068851 | 0.287254 | 1.065909 | 0.252500 |
| 0.4424 | 1.075418 | 0.347695 | 1.065135 | 0.287722 | 1.061385 | 0.253989 |
| 0.4559 | 1.071572 | 0.344592 | 1.060470 | 0.287504 | 1.056060 | 0.254902 |

| X | U | W | U | W' | U | W |
|---|---|---|---|---|---|---|
| 0.5101 | 1.045952 | 0.325152 | 1.034108 | 0.280703 | 1.028314 | 0.253425 |
| 0.5642 | 1.009128 | 0.298305 | 0.998973 | 0.266628 | 0.993234 | 0.245282 |
| 0.6183 | 0.966346 | 0.268279 | 0.958704 | 0.247969 | 0.953788 | 0.232443 |
| 0.6725 | 0.921099 | 0.238082 | 0.915882 | 0.226960 | 0.912068 | 0.216646 |
| 0.7266 | 0.875548 | 0.209596 | 0.872278 | 0.205303 | 0.869549 | 0.199329 |
| 0.7807 | 0.830931 | 0.183808 | 0.829060 | 0.184194 | 0.827248 | 0.181604 |
| 0.8348 | 0.787896 | 0.161075 | 0.786949 | 0.164392 | 0.785844 | 0.164275 |
| 0.8890 | 0.746739 | 0.141360 | 0.746364 | 0.146305 | 0.745766 | 0.147874 |
| 0.9431 | 0.707561 | 0.124413 | 0.707518 | 0.130091 | 0.707261 | 0.132714 |
| 0.9972 | 0.670357 | 0.109896 | 0.670495 | 0.115737 | 0.670456 | 0.118940 |
| 1.0513 | 0.635071 | 0.097458 | 0.635300 | 0.103131 | 0.635393 | 0.106576 |
| 1.1055 | 0.601625 | 0.086772 | 0.601894 | 0.092105 | 0.602062 | 0.095572 |
| 1.1596 | 0.569933 | 0.077553 | 0.570215 | 0.082476 | 0.570421 | 0.085828 |
| 1.2137 | 0.539908 | 0.069563 | 0.540187 | 0.074061 | 0.540410 | 0.077223 |
| 1.2678 | 0.511462 | 0.062603 | 0.511734 | 0.066693 | 0.511960 | 0.069632 |
| 1.3220 | 0.484515 | 0.056511 | 0.484775 | 0.060224 | 0.484997 | 0.062930 |
| 1.3761 | 0.458987 | 0.051154 | 0.459235 | 0.054525 | 0.459450 | 0.057004 |
| 1.4302 | 0.434804 | 0.046422 | 0.435039 | 0.049486 | 0.435245 | 0.051753 |
| 1.4844 | 0.411895 | 0.042227 | 0.412118 | 0.045016 | 0.412314 | 0.047086 |
| 1.5385 | 0.390194 | 0.038493 | 0.390405 | 0.041037 | 0.390591 | 0.042929 |
| 1.5926 | 0.369635 | 0.035159 | 0.369835 | 0.037483 | 0.370012 | 0.039213 |
| 1.6467 | 0.350160 | 0.032172 | 0.350349 | 0.034299 | 0.350517 | 0.035883 |
| 1.7009 | 0.331710 | 0.029489 | 0.331890 | 0.031438 | 0.332049 | 0.032891 |
| 1.7550 | 0.314233 | 0.027071 | 0.314403 | 0.028861 | 0.314554 | 0.030195 |
| 1.9715 | 0.253060 | 0.019492 | 0.253197 | 0.020781 | 0.253319 | 0.021742 |
| 2.1880 | 0.203796 | 0.014287 | 0.203907 | 0.015232 | 0.204004 | 0.015936 |
| 2.4045 | 0.164123 | 0.010618 | 0.164211 | 0.011320 | 0.164290 | 0.011843 |
| 2.6210 | 0.132172 | 0.007978 | 0.132244 | 0.008506 | 0.132307 | 0.008899 |
| 2.8375 | 0.106442 | 0.006048 | 0.106499 | 0.006448 | 0.106551 | 0.006746 |
| 3.0540 | 0.085720 | 0.004618 | 0.085767 | 0.004924 | 0.085808 | 0.005151 |
| 3.2705 | 0.069033 | 0.003548 | 0.069070 | 0.003782 | 0.069103 | 0.003957 |
| 3.4870 | 0.055594 | 0.002739 | 0.055624 | 0.002920 | 0.055651 | 0.003055 |
| 3.7035 | 0.044771 | 0.002124 | 0.044796 | 0.002264 | 0.044817 | 0.002369 |
| 3.9201 | 0.036056 | 0.001653 | 0.036075 | 0.001762 | 0.036092 | 0.001844 |
| 4.1366 | 0.029037 | 0.001290 | 0.029052 | 0.001376 | 0.029066 | 0.001439 |
| 4.3531 | 0.023384 | 0.001010 | 0.023397 | 0.001077 | 0.023408 | 0.001127 |
| 4.5696 | 0.018832 | 0.000793 | 0.018842 | 0.000845 | 0.018851 | 0.000884 |
| 4.7861 | 0.015166 | 0.000623 | 0.015174 | 0.000665 | 0.015181 | 0.000695 |
| 5.0026 | 0.012213 | 0.000491 | 0.012220 | 0.000524 | 0.012226 | 0.000548 |
| 5.2191 | 0.009836 | 0.000388 | 0.009841 | 0.000413 | 0.009846 | 0.000432 |
| 5.4356 | 0.007921 | 0.000306 | 0.007925 | 0.000326 | 0.007929 | 0.000342 |
| 5.6521 | 0.006379 | 0.000242 | 0.006382 | 0.000258 | 0.006385 | 0.000270 |
| 5.8686 | 0.005137 | 0.000192 | 0.005140 | 0.000205 | 0.005142 | 0.000214 |
| 6.0851 | 0.004137 | 0.000152 | 0.004139 | 0.000162 | 0.004141 | 0.000170 |
| 6.3016 | 0.003332 | 0.000121 | 0.003334 | 0.000129 | 0.003335 | 0.000135 |
| 6.5181 | 0.002683 | 0.000096 | 0.002685 | 0.000102 | 0.002686 | 0.000107 |
| 6.7346 | 0.002161 | 0.000076 | 0.002162 | 0.000081 | 0.002163 | 0.000085 |
| 6.9511 | 0.001740 | 0.000061 | 0.001741 | 0.000065 | 0.001742 | 0.000068 |

TABLE A.5

Core radius 0.05; both well shapes exponential;
$s_c = 0.6$, 0.9, and 1.0

| X | U | W | U | W | U | W |
|---|---|---|---|---|---|---|
| 0.0500 | 0.000000 | 0.000000 | 0.000000 | 0.000000 | 0.000000 | 0.000000 |
| 0.0534 | 0.022586 | 0.003827 | 0.025544 | 0.002791 | 0.026943 | 0.002304 |
| 0.0568 | 0.045151 | 0.007709 | 0.051050 | 0.005622 | 0.053840 | 0.004643 |
| 0.0601 | 0.067672 | 0.011681 | 0.076482 | 0.008524 | 0.080650 | 0.007041 |
| 0.0635 | 0.090131 | 0.015768 | 0.101807 | 0.011514 | 0.107332 | 0.009515 |
| 0.0669 | 0.112508 | 0.019986 | 0.126994 | 0.014606 | 0.133850 | 0.012074 |
| 0.0703 | 0.134784 | 0.024341 | 0.152014 | 0.017806 | 0.160169 | 0.014727 |
| 0.0737 | 0.156944 | 0.028838 | 0.176840 | 0.021117 | 0.186260 | 0.017474 |
| 0.0771 | 0.178970 | 0.033474 | 0.201447 | 0.024540 | 0.212092 | 0.020318 |
| 0.0804 | 0.200846 | 0.038248 | 0.225813 | 0.028073 | 0.237640 | 0.023258 |
| 0.0838 | 0.222559 | 0.043152 | 0.249915 | 0.031712 | 0.262880 | 0.026290 |
| 0.0872 | 0.244093 | 0.048182 | 0.273736 | 0.035453 | 0.287790 | 0.029411 |
| 0.0906 | 0.265435 | 0.053327 | 0.297258 | 0.039291 | 0.312350 | 0.032617 |
| 0.0940 | 0.286572 | 0.058580 | 0.320463 | 0.043219 | 0.336543 | 0.035903 |
| 0.0974 | 0.307494 | 0.063931 | 0.343339 | 0.047230 | 0.360354 | 0.039263 |
| 0.1007 | 0.328188 | 0.069371 | 0.365872 | 0.051318 | 0.383767 | 0.042692 |
| 0.1041 | 0.348644 | 0.074888 | 0.388050 | 0.055475 | 0.406771 | 0.046185 |
| 0.1075 | 0.368852 | 0.080474 | 0.409863 | 0.059694 | 0.429356 | 0.049734 |
| 0.1109 | 0.388803 | 0.086118 | 0.431301 | 0.063967 | 0.451511 | 0.053334 |
| 0.1143 | 0.408488 | 0.091811 | 0.452358 | 0.068287 | 0.473230 | 0.056979 |
| 0.1177 | 0.427901 | 0.097541 | 0.473026 | 0.072648 | 0.494506 | 0.060663 |
| 0.1210 | 0.447033 | 0.103301 | 0.493299 | 0.077040 | 0.515334 | 0.064380 |
| 0.1244 | 0.465878 | 0.109080 | 0.513173 | 0.081458 | 0.535710 | 0.068123 |
| 0.1278 | 0.484429 | 0.114870 | 0.532643 | 0.085896 | 0.555630 | 0.071888 |
| 0.1312 | 0.502682 | 0.120662 | 0.551707 | 0.090345 | 0.575094 | 0.075669 |
| 0.1447 | 0.572619 | 0.143685 | 0.623865 | 0.108139 | 0.648368 | 0.090845 |
| 0.1583 | 0.637478 | 0.166133 | 0.689467 | 0.125661 | 0.714386 | 0.105882 |
| 0.1718 | 0.697149 | 0.187619 | 0.748627 | 0.142611 | 0.773364 | 0.120521 |
| 0.1853 | 0.751618 | 0.207845 | 0.801564 | 0.158752 | 0.825628 | 0.134559 |
| 0.1988 | 0.800955 | 0.226596 | 0.848571 | 0.173909 | 0.871574 | 0.147842 |
| 0.2124 | 0.845296 | 0.243726 | 0.889989 | 0.187959 | 0.911638 | 0.160260 |
| 0.2259 | 0.884826 | 0.259149 | 0.926187 | 0.200825 | 0.946274 | 0.171740 |
| 0.2394 | 0.919770 | 0.272830 | 0.957544 | 0.212466 | 0.975936 | 0.182241 |
| 0.2530 | 0.950376 | 0.284773 | 0.984443 | 0.222873 | 1.001067 | 0.191746 |
| 0.2665 | 0.976910 | 0.295015 | 1.007254 | 0.232060 | 1.022091 | 0.200260 |
| 0.2800 | 0.999647 | 0.303616 | 1.026338 | 0.240058 | 1.039408 | 0.207801 |
| 0.2936 | 1.018861 | 0.310652 | 1.042036 | 0.246912 | 1.053390 | 0.214400 |
| 0.3071 | 1.034827 | 0.316215 | 1.054667 | 0.252678 | 1.064384 | 0.220098 |
| 0.3206 | 1.047810 | 0.320402 | 1.064532 | 0.257416 | 1.072705 | 0.224939 |
| 0.3342 | 1.058066 | 0.323315 | 1.071907 | 0.261192 | 1.078641 | 0.228972 |
| 0.3477 | 1.065839 | 0.325059 | 1.077046 | 0.264074 | 1.082455 | 0.232247 |
| 0.3612 | 1.071361 | 0.325737 | 1.080185 | 0.266128 | 1.084384 | 0.234817 |
| 0.3748 | 1.074848 | 0.325448 | 1.081535 | 0.267421 | 1.084640 | 0.236732 |
| 0.3883 | 1.076501 | 0.324292 | 1.081292 | 0.268017 | 1.083417 | 0.238042 |
| 0.4018 | 1.076509 | 0.322359 | 1.079632 | 0.267980 | 1.080886 | 0.238797 |
| 0.4154 | 1.075045 | 0.319739 | 1.076714 | 0.267367 | 1.077202 | 0.239043 |
| 0.4289 | 1.072268 | 0.316512 | 1.072683 | 0.266236 | 1.072502 | 0.238825 |
| 0.4424 | 1.068323 | 0.312757 | 1.067668 | 0.264640 | 1.066911 | 0.238184 |
| 0.4559 | 1.063345 | 0.308543 | 1.061787 | 0.262628 | 1.060538 | 0.237160 |

| X | U | W | U | W | U | W |
|---|---|---|---|---|---|---|
| 0.5101 | 1.035354 | 0.288327 | 1.031548 | 0.251294 | 1.029038 | 0.229947 |
| 0.5642 | 0.998700 | 0.265069 | 0.994173 | 0.236432 | 0.991223 | 0.219170 |
| 0.6183 | 0.957444 | 0.240995 | 0.953044 | 0.219787 | 0.950145 | 0.206306 |
| 0.6725 | 0.914191 | 0.217489 | 0.910323 | 0.202551 | 0.907730 | 0.192413 |
| 0.7266 | 0.870569 | 0.195347 | 0.867371 | 0.185510 | 0.865190 | 0.178225 |
| 0.7807 | 0.827571 | 0.174969 | 0.825038 | 0.169156 | 0.823285 | 0.164240 |
| 0.8348 | 0.785782 | 0.156504 | 0.783839 | 0.153779 | 0.782484 | 0.150779 |
| 0.8890 | 0.745528 | 0.139946 | 0.744079 | 0.139524 | 0.743069 | 0.138043 |
| 0.9431 | 0.706975 | 0.125200 | 0.705921 | 0.126446 | 0.705198 | 0.126139 |
| 0.9972 | 0.670187 | 0.112126 | 0.669441 | 0.114536 | 0.668950 | 0.115116 |
| 1.0513 | 0.635170 | 0.100562 | 0.634658 | 0.103748 | 0.634350 | 0.104978 |
| 1.1055 | 0.601891 | 0.090347 | 0.601554 | 0.094012 | 0.601387 | 0.095702 |
| 1.1596 | 0.570299 | 0.081323 | 0.570091 | 0.085248 | 0.570030 | 0.087248 |
| 1.2137 | 0.540328 | 0.073347 | 0.540213 | 0.077371 | 0.540231 | 0.079564 |
| 1.2678 | 0.511908 | 0.066288 | 0.511861 | 0.070298 | 0.511936 | 0.072593 |
| 1.3220 | 0.484969 | 0.060031 | 0.484969 | 0.063947 | 0.485084 | 0.066277 |
| 1.3761 | 0.459437 | 0.054473 | 0.459470 | 0.058244 | 0.459614 | 0.060560 |
| 1.4302 | 0.435244 | 0.049527 | 0.435299 | 0.053120 | 0.435460 | 0.055385 |
| 1.4844 | 0.412320 | 0.045114 | 0.412390 | 0.048512 | 0.412562 | 0.050701 |
| 1.5385 | 0.390601 | 0.041168 | 0.390680 | 0.044363 | 0.390858 | 0.046460 |
| 1.5926 | 0.370025 | 0.037632 | 0.370109 | 0.040623 | 0.370288 | 0.042618 |
| 1.6467 | 0.350532 | 0.034456 | 0.350617 | 0.037248 | 0.350796 | 0.039135 |
| 1.7009 | 0.332065 | 0.031596 | 0.332150 | 0.034196 | 0.332326 | 0.035974 |
| 1.7550 | 0.314570 | 0.029015 | 0.314654 | 0.031433 | 0.314825 | 0.033103 |
| 1.9715 | 0.253333 | 0.020906 | 0.253407 | 0.022699 | 0.253553 | 0.023972 |
| 2.1880 | 0.204016 | 0.015326 | 0.204077 | 0.016656 | 0.204197 | 0.017615 |
| 2.4045 | 0.164300 | 0.011391 | 0.164349 | 0.012384 | 0.164447 | 0.013105 |
| 2.6210 | 0.132315 | 0.008559 | 0.132355 | 0.009307 | 0.132434 | 0.009851 |
| 2.8375 | 0.106557 | 0.006489 | 0.106589 | 0.007055 | 0.106653 | 0.007469 |
| 3.0540 | 0.085813 | 0.004955 | 0.085839 | 0.005388 | 0.085890 | 0.005704 |
| 3.2705 | 0.069107 | 0.003806 | 0.069128 | 0.004139 | 0.069170 | 0.004382 |
| 3.4870 | 0.055654 | 0.002939 | 0.055671 | 0.003195 | 0.055704 | 0.003383 |
| 3.7035 | 0.044820 | 0.002279 | 0.044833 | 0.002478 | 0.044860 | 0.002623 |
| 3.9201 | 0.036094 | 0.001773 | 0.036105 | 0.001928 | 0.036127 | 0.002042 |
| 4.1366 | 0.029068 | 0.001384 | 0.029077 | 0.001505 | 0.029094 | 0.001594 |
| 4.3531 | 0.023409 | 0.001084 | 0.023416 | 0.001178 | 0.023430 | 0.001248 |
| 4.5696 | 0.018852 | 0.000850 | 0.018858 | 0.000925 | 0.018869 | 0.000979 |
| 4.7861 | 0.015182 | p.000669 | 0.015187 | 0.000727 | 0.015196 | 0.000770 |
| 5.0026 | 0.012226 | 0.000527 | 0.012230 | 0.000573 | 0.012237 | 0.000607 |
| 5.2191 | 0.009846 | 0.000416 | 0.009849 | 0.000452 | 0.009855 | 0.000479 |
| 5.4356 | 0.007929 | 0.000329 | 0.007932 | 0.000357 | 0.007937 | 0.000378 |
| 5.6521 | 0.006386 | 0.000260 | 0.006388 | 0.000283 | 0.006392 | 0.000299 |
| 5.8686 | 0.005143 | 0.000206 | 0.005144 | 0.000224 | 0.005147 | 0.000237 |
| 6.0851 | 0.004142 | 0.000163 | 0.004143 | 0.000178 | 0.004145 | 0.000188 |
| 6.3016 | 0.003335 | 0.000130 | 0.003336 | 0.000141 | 0.003338 | 0.000149 |
| 6.5181 | 0.002686 | 0.000103 | 0.002687 | 0.000112 | 0.002688 | 0.000119 |
| 6.7346 | 0.002163 | 0.000082 | 0.002164 | 0.000089 | 0.002165 | 0.000094 |
| 6.9511 | 0.001742 | 0.000065 | 0.001743 | 0.000071 | 0.001744 | 0.000075 |

TABLE A.6

Core radius 0.05; central force exponential, tensor force Yukawa well shape; $s_0 = 0.6$, 0.9, and 1.0

| X | U | W | U | W | U | W |
|---|---|---|---|---|---|---|
| 0.0500 | 0.000000 | 0.000000 | 0.000000 | 0.000000 | 0.000000 | 0.000000 |
| 0.0534 | 0.029845 | 0.011081 | 0.028526 | 0.007573 | 0.028623 | 0.006278 |
| 0.0568 | 0.059145 | 0.021360 | 0.056806 | 0.014661 | 0.057071 | 0.012172 |
| 0.0601 | 0.087861 | 0.030936 | 0.084799 | 0.021334 | 0.085300 | 0.017740 |
| 0.0635 | 0.116008 | 0.039954 | 0.112485 | 0.027683 | 0.113281 | 0.023056 |
| 0.0669 | 0.143595 | 0.048518 | 0.139846 | 0.033776 | 0.140987 | 0.028174 |
| 0.0703 | 0.170630 | 0.056706 | 0.166864 | 0.039661 | 0.168392 | 0.033135 |
| 0.0737 | 0.197123 | 0.064577 | 0.193522 | 0.045375 | 0.195474 | 0.037967 |
| 0.0771 | 0.223080 | 0.072176 | 0.219805 | 0.050944 | 0.222210 | 0.042691 |
| 0.0804 | 0.248507 | 0.079537 | 0.245700 | 0.056388 | 0.248580 | 0.047324 |
| 0.0838 | 0.273411 | 0.086685 | 0.271195 | 0.061721 | 0.274567 | 0.051876 |
| 0.0872 | 0.297796 | 0.093640 | 0.296276 | 0.066955 | 0.300155 | 0.056355 |
| 0.0906 | 0.321668 | 0.100417 | 0.320935 | 0.072097 | 0.325328 | 0.060767 |
| 0.0940 | 0.345031 | 0.107030 | 0.345163 | 0.077153 | 0.350075 | 0.065115 |
| 0.0974 | 0.367892 | 0.113486 | 0.368951 | 0.082125 | 0.374383 | 0.069403 |
| 0.1007 | 0.390255 | 0.119793 | 0.392293 | 0.087017 | 0.398243 | 0.073632 |
| 0.1041 | 0.412125 | 0.125957 | 0.415184 | 0.091830 | 0.421646 | 0.077802 |
| 0.1075 | 0.433507 | 0.131982 | 0.437617 | 0.096565 | 0.444585 | 0.081913 |
| 0.1109 | 0.454407 | 0.137872 | 0.459591 | 0.101223 | 0.467053 | 0.085966 |
| 0.1143 | 0.474828 | 0.143628 | 0.481102 | 0.105802 | 0.489047 | 0.089958 |
| 0.1177 | 0.494778 | 0.149255 | 0.502147 | 0.110304 | 0.510562 | 0.093891 |
| 0.1210 | 0.514260 | 0.154752 | 0.522726 | 0.114726 | 0.531595 | 0.097762 |
| 0.1244 | 0.533281 | 0.160122 | 0.542839 | 0.119069 | 0.552145 | 0.101571 |
| 0.1278 | 0.551846 | 0.165366 | 0.562486 | 0.123332 | 0.572212 | 0.105316 |
| 0.1312 | 0.569960 | 0.170485 | 0.581666 | 0.127514 | 0.591794 | 0.108997 |
| 0.1447 | 0.638030 | 0.189728 | 0.653775 | 0.143421 | 0.665310 | 0.123058 |
| 0.1583 | 0.699366 | 0.207040 | 0.718653 | 0.157986 | 0.731264 | 0.136022 |
| 0.1718 | 0.754359 | 0.222480 | 0.776589 | 0.171197 | 0.789944 | 0.147861 |
| 0.1853 | 0.803411 | 0.236115 | 0.827943 | 0.183062 | 0.841730 | 0.158568 |
| 0.1988 | 0.846923 | 0.248026 | 0.873121 | 0.193610 | 0.887060 | 0.168162 |
| 0.2124 | 0.885289 | 0.258304 | 0.912557 | 0.202888 | 0.926401 | 0.176673 |
| 0.2259 | 0.918896 | 0.267044 | 0.946690 | 0.210957 | 0.960233 | 0.184149 |
| 0.2394 | 0.948117 | 0.274349 | 0.975957 | 0.217883 | 0.989031 | 0.190643 |
| 0.2530 | 0.973306 | 0.280323 | 1.000784 | 0.223741 | 1.013255 | 0.196216 |
| 0.2665 | 0.994801 | 0.285067 | 1.021575 | 0.228607 | 1.033344 | 0.200930 |
| 0.2800 | 1.012921 | 0.288683 | 1.038717 | 0.232558 | 1.049712 | 0.204850 |
| 0.2936 | 1.027965 | 0.291270 | 1.052566 | 0.235668 | 1.062743 | 0.208040 |
| 0.3071 | 1.040210 | 0.292921 | 1.063456 | 0.238012 | 1.072790 | 0.210561 |
| 0.3206 | 1.049915 | 0.293726 | 1.071693 | 0.239659 | 1.080180 | 0.212472 |
| 0.3342 | 1.057321 | 0.293769 | 1.077560 | 0.240675 | 1.085207 | 0.213830 |
| 0.3477 | 1.062647 | 0.293128 | 1.081312 | 0.241123 | 1.088140 | 0.214688 |
| 0.3612 | 1.066098 | 0.291879 | 1.083183 | 0.241060 | 1.089221 | 0.215094 |
| 0.3748 | 1.067860 | 0.290087 | 1.083383 | 0.240540 | 1.088668 | 0.215094 |
| 0.3883 | 1.068104 | 0.287817 | 1.082103 | 0.239613 | 1.086676 | 0.214731 |
| 0.4018 | 1.066987 | 0.285127 | 1.079514 | 0.238324 | 1.083419 | 0.214042 |
| 0.4154 | 1.064651 | 0.282069 | 1.075771 | 0.236715 | 1.079055 | 0.213064 |
| 0.4289 | 1.061227 | 0.278692 | 1.071012 | 0.234823 | 1.073721 | 0.211828 |
| 0.4424 | 1.056832 | 0.275039 | 1.065361 | 0.232683 | 1.067543 | 0.210364 |
| 0.4559 | 1.051574 | 0.271152 | 1.058929 | 0.230327 | 1.060629 | 0.208698 |

| X | U | W | U | W | U | W |
|---|---|---|---|---|---|---|
| 0.5101 | 1.023733 | 0.253931 | 1.027218 | 0.219264 | 1.027420 | 0.200472 |
| 0.5642 | 0.988426 | 0.235294 | 0.989266 | 0.206572 | 0.988550 | 0.190590 |
| 0.6183 | 0.948966 | 0.216426 | 0.948151 | 0.193193 | 0.946946 | 0.179869 |
| 0.6725 | 0.907538 | 0.198060 | 0.905796 | 0.179734 | 0.904396 | 0.168845 |
| 0.7266 | 0.865564 | 0.180627 | 0.863397 | 0.166578 | 0.861992 | 0.157867 |
| 0.7807 | 0.823959 | 0.164353 | 0.821690 | 0.153960 | 0.820392 | 0.147162 |
| 0.8348 | 0.783296 | 0.149336 | 0.781119 | 0.142012 | 0.779987 | 0.136871 |
| 0.8890 | 0.743925 | 0.135591 | 0.741946 | 0.130804 | 0.741004 | 0.127078 |
| 0.9431 | 0.706048 | 0.123080 | 0.704312 | 0.120360 | 0.703563 | 0.117829 |
| 0.9972 | 0.669768 | 0.111739 | 0.668286 | 0.110678 | 0.667719 | 0.109144 |
| 1.0513 | 0.635125 | 0.101485 | 0.633886 | 0.101735 | 0.633483 | 0.101025 |
| 1.1055 | 0.602116 | 0.092231 | 0.601098 | 0.093499 | 0.600839 | 0.093460 |
| 1.1596 | 0.570714 | 0.083887 | 0.569890 | 0.085930 | 0.569755 | 0.086432 |
| 1.2137 | 0.540874 | 0.076369 | 0.540216 | 0.078985 | 0.540184 | 0.079916 |
| 1.2678 | 0.512541 | 0.069595 | 0.512023 | 0.072620 | 0.512076 | 0.073885 |
| 1.3220 | 0.485654 | 0.063489 | 0.485252 | 0.066792 | 0.485374 | 0.068310 |
| 1.3761 | 0.460151 | 0.057984 | 0.459845 | 0.061457 | 0.460021 | 0.063162 |
| 1.4302 | 0.435969 | 0.053016 | 0.435740 | 0.056577 | 0.435959 | 0.058412 |
| 1.4844 | 0.413044 | 0.048530 | 0.412878 | 0.052112 | 0.413128 | 0.054032 |
| 1.5385 | 0.391314 | 0.044473 | 0.391199 | 0.048027 | 0.391472 | 0.049995 |
| 1.5926 | 0.370721 | 0.040802 | 0.370645 | 0.044288 | 0.370935 | 0.046274 |
| 1.6467 | 0.351206 | 0.037476 | 0.351162 | 0.040866 | 0.351462 | 0.042845 |
| 1.7009 | 0.332715 | 0.034458 | 0.332695 | 0.037733 | 0.333001 | 0.039686 |
| 1.7550 | 0.315195 | 0.031717 | 0.315194 | 0.034862 | 0.315501 | 0.036775 |
| 1.9715 | 0.253853 | 0.022994 | 0.253892 | 0.025569 | 0.254180 | 0.027234 |
| 2.1880 | 0.204440 | 0.016911 | 0.204488 | 0.018943 | 0.204740 | 0.020316 |
| 2.4045 | 0.164643 | 0.012589 | 0.164688 | 0.014166 | 0.164900 | 0.015265 |
| 2.6210 | 0.132592 | 0.009466 | 0.132631 | 0.010682 | 0.132807 | 0.011549 |
| 2.8375 | 0.106780 | 0.007179 | 0.106813 | 0.008115 | 0.106956 | 0.008793 |
| 3.0540 | 0.085993 | 0.005483 | 0.086020 | 0.006204 | 0.086136 | 0.006732 |
| 3.2705 | 0.069252 | 0.004212 | 0.069274 | 0.004769 | 0.069369 | 0.005180 |
| 3.4870 | 0.055771 | 0.003252 | 0.055789 | 0.003683 | 0.055865 | 0.004003 |
| 3.7035 | 0.044914 | 0.002522 | 0.044928 | 0.002857 | 0.044989 | 0.003106 |
| 3.9201 | 0.036170 | 0.001963 | 0.036182 | 0.002223 | 0.036231 | 0.002418 |
| 4.1366 | 0.029129 | 0.001532 | 0.029138 | 0.001736 | 0.029178 | 0.001888 |
| 4.3531 | 0.023458 | 0.001199 | 0.023466 | 0.001359 | 0.023498 | 0.001479 |
| 4.5696 | 0.018892 | 0.000941 | 0.018898 | 0.001066 | 0.018923 | 0.001160 |
| 4.7861 | 0.015214 | 0.000740 | 0.015219 | 0.000839 | 0.015240 | 0.000912 |
| 5.0026 | 0.012252 | 0.000583 | 0.012256 | 0.000661 | 0.012273 | 0.000719 |
| 5.2191 | 0.009867 | 0.000460 | 0.009870 | 0.000521 | 0.009884 | 0.000567 |
| 5.4356 | 0.007946 | 0.000364 | 0.007949 | 0.000412 | 0.007960 | 0.000448 |
| 5.6521 | 0.006399 | 0.000288 | 0.006401 | 0.000326 | 0.006410 | 0.000355 |
| 5.8686 | 0.005153 | 0.000228 | 0.005155 | 0.000258 | 0.005162 | 0.000281 |
| 6.0851 | 0.004150 | 0.000181 | 0.004152 | 0.000205 | 0.004157 | 0.000223 |
| 6.3016 | 0.003342 | 0.000144 | 0.003343 | 0.000163 | 0.003348 | 0.000177 |
| 6.5181 | 0.002692 | 0.000114 | 0.002692 | 0.000129 | 0.002696 | 0.000141 |
| 6.7346 | 0.002168 | 0.000091 | 0.002168 | 0.000103 | 0.002171 | 0.000112 |
| 6.9511 | 0.001746 | 0.000072 | 0.001746 | 0.000082 | 0.001749 | 0.000089 |

TABLE A.7

Core radius 0.10; both well shapes exponential;
$s_e = 0.6$, 0.9, and 1.0

| X | U | W | U | W | U | W |
|---|---|---|---|---|---|---|
| 0.1000 | 0.000000 | 0.000000 | 0.000000 | 0.000000 | 0.000000 | 0.000000 |
| 0.1034 | 0.030281 | 0.009224 | 0.036222 | 0.007303 | 0.039128 | 0.005959 |
| 0.1068 | 0.060500 | 0.018452 | 0.072328 | 0.014605 | 0.078113 | 0.011917 |
| 0.1101 | 0.090598 | 0.027685 | 0.108212 | 0.021904 | 0.116829 | 0.017872 |
| 0.1135 | 0.120521 | 0.036918 | 0.143781 | 0.029195 | 0.155160 | 0.023818 |
| 0.1169 | 0.150221 | 0.046147 | 0.178950 | 0.036471 | 0.193006 | 0.029751 |
| 0.1203 | 0.179653 | 0.055365 | 0.213644 | 0.043726 | 0.230276 | 0.035665 |
| 0.1237 | 0.208776 | 0.064561 | 0.247797 | 0.050951 | 0.266893 | 0.041553 |
| 0.1271 | 0.237553 | 0.073728 | 0.281352 | 0.058137 | 0.302790 | 0.047408 |
| 0.1304 | 0.265950 | 0.082854 | 0.314260 | 0.065276 | 0.337910 | 0.053223 |
| 0.1338 | 0.293938 | 0.091929 | 0.346478 | 0.072360 | 0.372206 | 0.058991 |
| 0.1372 | 0.321489 | 0.100942 | 0.377972 | 0.079380 | 0.405638 | 0.064706 |
| 0.1406 | 0.348580 | 0.109882 | 0.408711 | 0.086327 | 0.438175 | 0.070361 |
| 0.1440 | 0.375190 | 0.118740 | 0.438673 | 0.093194 | 0.469790 | 0.075951 |
| 0.1474 | 0.401301 | 0.127504 | 0.467839 | 0.099974 | 0.500467 | 0.081468 |
| 0.1507 | 0.426897 | 0.136165 | 0.496195 | 0.106659 | 0.530193 | 0.086909 |
| 0.1541 | 0.451965 | 0.144714 | 0.523731 | 0.113243 | 0.558959 | 0.092268 |
| 0.1575 | 0.476493 | 0.153142 | 0.550443 | 0.119721 | 0.586763 | 0.097541 |
| 0.1609 | 0.500472 | 0.161441 | 0.576326 | 0.126086 | 0.613606 | 0.102724 |
| 0.1643 | 0.523896 | 0.169603 | 0.601383 | 0.132335 | 0.639493 | 0.107812 |
| 0.1677 | 0.546758 | 0.177621 | 0.625616 | 0.138462 | 0.664431 | 0.112804 |
| 0.1710 | 0.569054 | 0.185488 | 0.649032 | 0.144463 | 0.688432 | 0.117696 |
| 0.1744 | 0.590782 | 0.193200 | 0.671638 | 0.150337 | 0.711507 | 0.122486 |
| 0.1778 | 0.611942 | 0.200749 | 0.693445 | 0.156079 | 0.733673 | 0.127172 |
| 0.1812 | 0.632532 | 0.208132 | 0.714463 | 0.161688 | 0.754946 | 0.131752 |
| 0.1947 | 0.709248 | 0.235927 | 0.790926 | 0.182752 | 0.831492 | 0.148995 |
| 0.2083 | 0.777136 | 0.260819 | 0.855973 | 0.201591 | 0.895383 | 0.164497 |
| 0.2218 | 0.836613 | 0.282741 | 0.910715 | 0.218219 | 0.948056 | 0.178283 |
| 0.2353 | 0.888207 | 0.301714 | 0.956296 | 0.232709 | 0.990939 | 0.190419 |
| 0.2488 | 0.932514 | 0.317831 | 0.993826 | 0.245171 | 1.025378 | 0.200999 |
| 0.2624 | 0.970153 | 0.331233 | 1.024337 | 0.255738 | 1.052596 | 0.210129 |
| 0.2759 | 1.001743 | 0.342091 | 1.048769 | 0.264556 | 1.073678 | 0.217923 |
| 0.2894 | 1.027886 | 0.350598 | 1.067958 | 0.271772 | 1.089571 | 0.224495 |
| 0.3030 | 1.049153 | 0.356954 | 1.082640 | 0.277531 | 1.101088 | 0.229955 |
| 0.3165 | 1.066075 | 0.361363 | 1.093457 | 0.281975 | 1.108925 | 0.234408 |
| 0.3300 | 1.079144 | 0.364022 | 1.100962 | 0.285233 | 1.113670 | 0.237950 |
| 0.3436 | 1.088809 | 0.365121 | 1.105634 | 0.287430 | 1.115819 | 0.240671 |
| 0.3571 | 1.095477 | 0.364840 | 1.107884 | 0.288679 | 1.115789 | 0.242653 |
| 0.3706 | 1.099515 | 0.363347 | 1.108061 | 0.289082 | 1.113929 | 0.243970 |
| 0.3842 | 1.101252 | 0.360797 | 1.106466 | 0.288735 | 1.110533 | 0.244689 |
| 0.3977 | 1.100980 | 0.357332 | 1.103357 | 0.287724 | 1.105844 | 0.244872 |
| 0.4112 | 1.098962 | 0.353082 | 1.098953 | 0.286126 | 1.100069 | 0.244573 |
| 0.4248 | 1.095428 | 0.348164 | 1.093441 | 0.284012 | 1.093381 | 0.243843 |
| 0.4383 | 1.090583 | 0.342684 | 1.086983 | 0.281446 | 1.085923 | 0.242727 |
| 0.4518 | 1.084608 | 0.336737 | 1.079718 | 0.278484 | 1.077817 | 0.241266 |
| 0.4654 | 1.077663 | 0.330409 | 1.071764 | 0.275180 | 1.069168 | 0.239497 |
| 0.4789 | 1.069886 | 0.323773 | 1.063224 | 0.271579 | 1.060061 | 0.237453 |
| 0.4924 | 1.061402 | 0.316898 | 1.054188 | 0.267724 | 1.050572 | 0.235166 |
| 0.5059 | 1.052319 | 0.309841 | 1.044731 | 0.263654 | 1.040763 | 0.232664 |

| X | U | W | U | W | U | W |
|---|---|---|---|---|---|---|
| 0.5601 | 1.011718 | 0.280756 | 1.003910 | 0.245853 | 0.999303 | 0.220983 |
| 0.6142 | 0.967297 | 0.251929 | 0.960400 | 0.226811 | 0.955947 | 0.207553 |
| 0.6683 | 0.921666 | 0.224709 | 0.916056 | 0.207650 | 0.912136 | 0.193307 |
| 0.7225 | 0.876320 | 0.199757 | 0.871991 | 0.189082 | 0.868740 | 0.178897 |
| 0.7766 | 0.832094 | 0.177311 | 0.828880 | 0.171529 | 0.826298 | 0.164764 |
| 0.8307 | 0.789434 | 0.157364 | 0.787123 | 0.155223 | 0.785145 | 0.151202 |
| 0.8848 | 0.748562 | 0.139775 | 0.746948 | 0.140259 | 0.745486 | 0.138390 |
| 0.9390 | 0.709564 | 0.124336 | 0.708473 | 0.126647 | 0.707432 | 0.126429 |
| 0.9931 | 0.672450 | 0.110816 | 0.671744 | 0.114345 | 0.671037 | 0.115358 |
| 1.0472 | 0.637188 | 0.098987 | 0.636759 | 0.103276 | 0.636312 | 0.105182 |
| 1.1013 | 0.603720 | 0.088634 | 0.603487 | 0.093345 | 0.603238 | 0.095873 |
| 1.1555 | 0.571976 | 0.079560 | 0.571880 | 0.084454 | 0.571780 | 0.087391 |
| 1.2096 | 0.541880 | 0.071594 | 0.541879 | 0.076500 | 0.541887 | 0.079683 |
| 1.2637 | 0.513354 | 0.064583 | 0.513417 | 0.069387 | 0.513504 | 0.072691 |
| 1.3178 | 0.486322 | 0.058398 | 0.486427 | 0.063025 | 0.486570 | 0.066358 |
| 1.3720 | 0.460709 | 0.052927 | 0.460840 | 0.057331 | 0.461021 | 0.060626 |
| 1.4261 | 0.436442 | 0.048072 | 0.436588 | 0.052230 | 0.436794 | 0.055438 |
| 1.4802 | 0.413450 | 0.043754 | 0.413605 | 0.047654 | 0.413825 | 0.050744 |
| 1.5344 | 0.391669 | 0.039901 | 0.391827 | 0.043543 | 0.392055 | 0.046494 |
| 1.5885 | 0.371034 | 0.036454 | 0.371192 | 0.039845 | 0.371422 | 0.042644 |
| 1.6426 | 0.351486 | 0.033363 | 0.351641 | 0.036512 | 0.351870 | 0.039154 |
| 1.6967 | 0.332968 | 0.030583 | 0.333118 | 0.033504 | 0.333343 | 0.035988 |
| 1.7509 | 0.315425 | 0.028077 | 0.315570 | 0.030784 | 0.315789 | 0.033113 |
| 1.8050 | 0.298806 | 0.025813 | 0.298946 | 0.028320 | 0.299157 | 0.030498 |
| 2.0215 | 0.240637 | 0.018675 | 0.240752 | 0.020518 | 0.240931 | 0.022164 |
| 2.2380 | 0.193791 | 0.013737 | 0.193885 | 0.015101 | 0.194031 | 0.016335 |
| 2.4545 | 0.156065 | 0.010237 | 0.156141 | 0.011256 | 0.156260 | 0.012184 |
| 2.6710 | 0.125683 | 0.007709 | 0.125745 | 0.008477 | 0.125840 | 0.009178 |
| 2.8875 | 0.101216 | 0.005855 | 0.101265 | 0.006438 | 0.101343 | 0.006971 |
| 3.1040 | 0.081512 | 0.004477 | 0.081552 | 0.004923 | 0.081614 | 0.005332 |
| 3.3205 | 0.065644 | 0.003444 | 0.065676 | 0.003787 | 0.065726 | 0.004101 |
| 3.5370 | 0.052865 | 0.002662 | 0.052890 | 0.002927 | 0.052931 | 0.003170 |
| 3.7535 | 0.042573 | 0.002066 | 0.042594 | 0.002271 | 0.042627 | 0.002460 |
| 3.9701 | 0.034286 | 0.001609 | 0.034302 | 0.001769 | 0.034328 | 0.001916 |
| 4.1866 | 0.027611 | 0.001257 | 0.027624 | 0.001382 | 0.027645 | 0.001497 |
| 4.4031 | 0.022236 | 0.000984 | 0.022247 | 0.001083 | 0.022264 | 0.001172 |
| 4.6196 | 0.017907 | 0.000773 | 0.017916 | 0.000850 | 0.017930 | 0.000920 |
| 4.8361 | 0.014421 | 0.000608 | 0.014428 | 0.000669 | 0.014439 | 0.000724 |
| 5.0526 | 0.011614 | 0.000479 | 0.011619 | 0.000527 | 0.011628 | 0.000571 |
| 5.2691 | 0.009353 | 0.000378 | 0.009357 | 0.000416 | 0.009365 | 0.000450 |
| 5.4856 | 0.007532 | 0.000299 | 0.007536 | 0.000329 | 0.007541 | 0.000356 |
| 5.7021 | 0.006066 | 0.000237 | 0.006069 | 0.000260 | 0.006073 | 0.000282 |
| 5.9186 | 0.004885 | 0.000188 | 0.004887 | 0.000206 | 0.004891 | 0.000223 |
| 6.1351 | 0.003934 | 0.000149 | 0.003936 | 0.000164 | 0.003939 | 0.000177 |
| 6.3516 | 0.003168 | 0.000118 | 0.003170 | 0.000130 | 0.003172 | 0.000141 |
| 6.5681 | 0.002551 | 0.000094 | 0.002553 | 0.000103 | 0.002555 | 0.000112 |
| 6.7846 | 0.002055 | 0.000075 | 0.002056 | 0.000082 | 0.002057 | 0.000089 |
| 7.0011 | 0.001655 | 0.000059 | 0.001656 | 0.000065 | 0.001657 | 0.000071 |

TABLE A.8

Core radius 0.15; both well shapes exponential;
$s_e = 0.6$, 0.9, and 1.0

| X | U | W | U | W | U | W |
|---|---|---|---|---|---|---|
| 0.1500 | 0.000000 | 0.000000 | 0.000000 | 0.000000 | 0.000000 | 0.000000 |
| 0.1534 | 0.045373 | 0.018547 | 0.060591 | 0.016729 | 0.070270 | 0.013321 |
| 0.1568 | 0.090488 | 0.036994 | 0.120601 | 0.033312 | 0.139737 | 0.026504 |
| 0.1601 | 0.135121 | 0.055253 | 0.179547 | 0.049625 | 0.207737 | 0.039436 |
| 0.1635 | 0.179083 | 0.073250 | 0.237036 | 0.065569 | 0.273745 | 0.052028 |
| 0.1669 | 0.222215 | 0.090919 | 0.292762 | 0.081064 | 0.337357 | 0.064209 |
| 0.1703 | 0.264387 | 0.108207 | 0.346490 | 0.096049 | 0.398278 | 0.075929 |
| 0.1737 | 0.305493 | 0.125069 | 0.398051 | 0.110480 | 0.456302 | 0.087151 |
| 0.1771 | 0.345451 | 0.141470 | 0.447329 | 0.124325 | 0.511299 | 0.097854 |
| 0.1804 | 0.384196 | 0.157381 | 0.494255 | 0.137564 | 0.563206 | 0.108023 |
| 0.1838 | 0.421683 | 0.172779 | 0.538797 | 0.150187 | 0.612009 | 0.117657 |
| 0.1872 | 0.457880 | 0.187649 | 0.580957 | 0.162192 | 0.657738 | 0.126759 |
| 0.1906 | 0.492769 | 0.201980 | 0.620760 | 0.173582 | 0.700455 | 0.135339 |
| 0.1940 | 0.526341 | 0.215766 | 0.658253 | 0.184367 | 0.740247 | 0.143409 |
| 0.1974 | 0.558599 | 0.229003 | 0.693498 | 0.194561 | 0.777222 | 0.150987 |
| 0.2007 | 0.589552 | 0.241693 | 0.726570 | 0.204181 | 0.811500 | 0.158093 |
| 0.2041 | 0.619216 | 0.253838 | 0.757551 | 0.213245 | 0.843209 | 0.164748 |
| 0.2075 | 0.647614 | 0.265445 | 0.786531 | 0.221775 | 0.872486 | 0.170973 |
| 0.2109 | 0.674769 | 0.276522 | 0.813603 | 0.229793 | 0.899466 | 0.176790 |
| 0.2143 | 0.700713 | 0.287078 | 0.838861 | 0.237320 | 0.924287 | 0.182223 |
| 0.2177 | 0.725476 | 0.297124 | 0.862401 | 0.244381 | 0.947084 | 0.187294 |
| 0.2210 | 0.749094 | 0.306671 | 0.884318 | 0.250997 | 0.967988 | 0.192023 |
| 0.2244 | 0.771601 | 0.315733 | 0.904702 | 0.257192 | 0.987128 | 0.196433 |
| 0.2278 | 0.793033 | 0.324323 | 0.923646 | 0.262987 | 1.004626 | 0.200544 |
| 0.2312 | 0.813429 | 0.332453 | 0.941236 | 0.268404 | 1.020598 | 0.204375 |
| 0.2447 | 0.885387 | 0.360672 | 0.999679 | 0.286691 | 1.071352 | 0.217254 |
| 0.2583 | 0.943670 | 0.382681 | 1.042474 | 0.300429 | 0.105447 | 0.226950 |
| 0.2718 | 0.990411 | 0.399342 | 1.073389 | 0.310575 | 1.127512 | 0.234245 |
| 0.2853 | 1.027480 | 0.411439 | 1.095314 | 0.317878 | 1.140947 | 0.239717 |
| 0.2988 | 1.056467 | 0.419664 | 1.110421 | 0.322916 | 1.148198 | 0.243787 |
| 0.3124 | 1.078707 | 0.424616 | 1.120323 | 0.326127 | 1.151003 | 0.246757 |
| 0.3259 | 1.095311 | 0.426810 | 1.126211 | 0.327849 | 1.150589 | 0.248846 |
| 0.3394 | 1.107198 | 0.426686 | 1.128970 | 0.328339 | 1.147820 | 0.250210 |
| 0.3530 | 1.115131 | 0.424621 | 1.129253 | 0.327801 | 1.143303 | 0.250966 |
| 0.3665 | 1.119741 | 0.420936 | 1.127553 | 0.326394 | 1.137471 | 0.251199 |
| 0.3800 | 1.121556 | 0.415909 | 1.124239 | 0.324247 | 1.130628 | 0.250975 |
| 0.3936 | 1.121014 | 0.409776 | 1.119599 | 0.321468 | 1.122996 | 0.250347 |
| 0.4071 | 1.118487 | 0.402740 | 1.113854 | 0.318145 | 1.114735 | 0.249358 |
| 0.4206 | 1.114283 | 0.394978 | 1.107181 | 0.314356 | 1.105966 | 0.248042 |
| 0.4342 | 1.108668 | 0.386641 | 1.099723 | 0.310166 | 1.096780 | 0.246432 |
| 0.4477 | 1.101864 | 0.377858 | 1.091598 | 0.305634 | 1.087245 | 0.244554 |
| 0.4612 | 1.094062 | 0.368744 | 1.082902 | 0.300812 | 1.077420 | 0.242434 |
| 0.4748 | 1.085424 | 0.359393 | 1.073720 | 0.295746 | 1.067348 | 0.240096 |
| 0.4883 | 1.076090 | 0.349889 | 1.064123 | 0.290478 | 1.057068 | 0.237561 |
| 0.5018 | 1.066178 | 0.340303 | 1.054173 | 0.285045 | 1.046613 | 0.234848 |
| 0.5154 | 1.055793 | 0.330695 | 1.043923 | 0.279481 | 1.036011 | 0.231978 |
| 0.5289 | 1.045021 | 0.321117 | 1.033422 | 0.273816 | 1.025286 | 0.228968 |
| 0.5424 | 1.033938 | 0.311612 | 1.022712 | 0.268077 | 1.014461 | 0.225834 |
| 0.5559 | 1.022610 | 0.302217 | 1.011830 | 0.262290 | 1.003556 | 0.222593 |

| X | U | W | U | W | U | W |
|---|---|---|---|---|---|---|
| 0.6101 | 0.975849 | 0.266250 | 0.967206 | 0.239061 | 0.959471 | 0.208833 |
| 0.6642 | 0.928459 | 0.233618 | 0.921954 | 0.216440 | 0.915294 | 0.194371 |
| 0.7183 | 0.881821 | 0.204711 | 0.877123 | 0.195077 | 0.871678 | 0.179798 |
| 0.7725 | 0.836655 | 0.179470 | 0.833363 | 0.175321 | 0.829074 | 0.165535 |
| 0.8266 | 0.793310 | 0.157615 | 0.791063 | 0.157316 | 0.787783 | 0.151861 |
| 0.8807 | 0.751933 | 0.138773 | 0.750436 | 0.141072 | 0.747994 | 0.138953 |
| 0.9348 | 0.712557 | 0.122554 | 0.711588 | 0.126523 | 0.709817 | 0.126908 |
| 0.9890 | 0.675152 | 0.108585 | 0.674549 | 0.113552 | 0.673303 | 0.115766 |
| 1.0431 | 0.639660 | 0.096533 | 0.639307 | 0.102024 | 0.638462 | 0.105526 |
| 1.0972 | 0.606003 | 0.086108 | 0.605819 | 0.091795 | 0.605278 | 0.096164 |
| 1.1513 | 0.574101 | 0.077060 | 0.574029 | 0.082725 | 0.573714 | 0.087636 |
| 1.2055 | 0.543869 | 0.069179 | 0.543870 | 0.074682 | 0.543721 | 0.079888 |
| 1.2596 | 0.515222 | 0.062288 | 0.515271 | 0.067544 | 0.515242 | 0.072864 |
| 1.3137 | 0.488082 | 0.056241 | 0.488160 | 0.061202 | 0.488217 | 0.066502 |
| 1.3678 | 0.462369 | 0.050913 | 0.462465 | 0.055559 | 0.462581 | 0.060746 |
| 1.4220 | 0.438010 | 0.046202 | 0.438115 | 0.050528 | 0.438271 | 0.055538 |
| 1.4761 | 0.414933 | 0.042022 | 0.415043 | 0.046035 | 0.415225 | 0.050827 |
| 1.5302 | 0.393071 | 0.038301 | 0.393183 | 0.042013 | 0.393381 | 0.046562 |
| 1.5844 | 0.372362 | 0.034977 | 0.372472 | 0.038406 | 0.372678 | 0.042701 |
| 1.6385 | 0.352743 | 0.032000 | 0.352850 | 0.035164 | 0.353060 | 0.039201 |
| 1.6926 | 0.334158 | 0.029325 | 0.334261 | 0.032245 | 0.334470 | 0.036027 |
| 1.7467 | 0.316552 | 0.026916 | 0.316651 | 0.029610 | 0.316857 | 0.033144 |
| 1.8009 | 0.299873 | 0.024741 | 0.299969 | 0.027227 | 0.300169 | 0.030524 |
| 1.8550 | 0.284074 | 0.022773 | 0.284165 | 0.025068 | 0.284358 | 0.028139 |
| 2.0715 | 0.228772 | 0.016543 | 0.228846 | 0.018220 | 0.229010 | 0.020518 |
| 2.2880 | 0.184236 | 0.012208 | 0.184296 | 0.013448 | 0.184430 | 0.015166 |
| 2.5045 | 0.148370 | 0.009122 | 0.148419 | 0.010049 | 0.148527 | 0.011340 |
| 2.7210 | 0.119487 | 0.006884 | 0.119526 | 0.007584 | 0.119613 | 0.008560 |
| 2.9375 | 0.096226 | 0.005237 | 0.096257 | 0.005769 | 0.096328 | 0.006513 |
| 3.1540 | 0.077493 | 0.004010 | 0.077518 | 0.004418 | 0.077575 | 0.004988 |
| 3.3705 | 0.062407 | 0.003088 | 0.062428 | 0.003402 | 0.062473 | 0.003841 |
| 3.5870 | 0.050258 | 0.002389 | 0.050275 | 0.002632 | 0.050311 | 0.002972 |
| 3.8035 | 0.040474 | 0.001856 | 0.040488 | 0.002045 | 0.040517 | 0.002308 |
| 4.0201 | 0.032595 | 0.001447 | 0.032606 | 0.001594 | 0.032630 | 0.001799 |
| 4.2366 | 0.026250 | 0.001131 | 0.026258 | 0.001246 | 0.026277 | 0.001406 |
| 4.4531 | 0.021140 | 0.000886 | 0.021146 | 0.000976 | 0.021162 | 0.001102 |
| 4.6696 | 0.017024 | 0.000696 | 0.017030 | 0.000767 | 0.017042 | 0.000866 |
| 4.8861 | 0.013710 | 0.000548 | 0.013715 | 0.000604 | 0.013725 | 0.000681 |
| 5.1026 | 0.011041 | 0.000432 | 0.011045 | 0.000476 | 0.011053 | 0.000537 |
| 5.3191 | 0.008892 | 0.000341 | 0.008895 | 0.000376 | 0.008901 | 0.000424 |
| 5.5356 | 0.007161 | 0.000270 | 0.007163 | 0.000297 | 0.007168 | 0.000335 |
| 5.7521 | 0.005767 | 0.000214 | 0.005769 | 0.000235 | 0.005773 | 0.000266 |
| 5.9686 | 0.004644 | 0.000169 | 0.004646 | 0.000187 | 0.004649 | 0.000211 |
| 6.1851 | 0.003740 | 0.000134 | 0.003741 | 0.000148 | 0.003744 | 0.000167 |
| 6.4016 | 0.003012 | 0.000107 | 0.003013 | 0.000118 | 0.003015 | 0.000133 |
| 6.6181 | 0.002426 | 0.000085 | 0.002426 | 0.000093 | 0.002428 | 0.000105 |
| 6.8346 | 0.001953 | 0.000067 | 0.001954 | 0.000074 | 0.001955 | 0.000084 |
| 7.0511 | 0.001573 | 0.000054 | 0.001574 | 0.000059 | 0.001575 | 0.000067 |

TABLE A.9

Zero core radius, central well of Gaussian shape and range $b_c = 0.592$; this range fits the singlet state effective range; the three sets of wave functions correspond to tensor forces of Gaussian, exponential, and Yukawa shapes, respectively. The force parameters are given in table 4.1 of the text

| X | U | W | U | W | U | W |
|---|---|---|---|---|---|---|
| 0.0000 | 0.000000 | 0.000000 | 0.000000 | 0.000000 | 0.000000 | 0.000000 |
| 0.0034 | 0.014030 | 0.000010 | 0.016197 | 0.000025 | 0.019693 | 0.000333 |
| 0.0068 | 0.028060 | 0.000067 | 0.032393 | 0.000156 | 0.039361 | 0.001225 |
| 0.0101 | 0.042088 | 0.000201 | 0.048585 | 0.000450 | 0.058982 | 0.002616 |
| 0.0135 | 0.056114 | 0.000433 | 0.064773 | 0.000939 | 0.078538 | 0.004438 |
| 0.0169 | 0.070137 | 0.000780 | 0.080954 | 0.001646 | 0.098010 | 0.006640 |
| 0.0203 | 0.084157 | 0.001257 | 0.097125 | 0.002583 | 0.117382 | 0.009177 |
| 0.0237 | 0.098171 | 0.001874 | 0.113283 | 0.003758 | 0.136641 | 0.012011 |
| 0.0271 | 0.112180 | 0.002640 | 0.129425 | 0.005174 | 0.155773 | 0.015108 |
| 0.0304 | 0.126182 | 0.003562 | 0.145546 | 0.006831 | 0.174766 | 0.018439 |
| 0.0338 | 0.140175 | 0.004645 | 0.161643 | 0.008727 | 0.193610 | 0.021976 |
| 0.0372 | 0.154159 | 0.005893 | 0.177712 | 0.010858 | 0.212294 | 0.025697 |
| 0.0406 | 0.168130 | 0.007309 | 0.193746 | 0.013217 | 0.230810 | 0.029578 |
| 0.0440 | 0.182088 | 0.008896 | 0.209743 | 0.015797 | 0.249150 | 0.033600 |
| 0.0474 | 0.196032 | 0.010653 | 0.225695 | 0.018590 | 0.267305 | 0.037745 |
| 0.0507 | 0.209957 | 0.012581 | 0.241597 | 0.021587 | 0.285270 | 0.041996 |
| 0.0541 | 0.223864 | 0.014680 | 0.257445 | 0.024779 | 0.303038 | 0.046338 |
| 0.0575 | 0.237748 | 0.016948 | 0.273233 | 0.028156 | 0.320604 | 0.050758 |
| 0.0609 | 0.251609 | 0.019383 | 0.288954 | 0.031708 | 0.337962 | 0.055241 |
| 0.0643 | 0.265443 | 0.021984 | 0.304603 | 0.035425 | 0.355108 | 0.059777 |
| 0.0677 | 0.279248 | 0.024746 | 0.320173 | 0.039296 | 0.372039 | 0.064355 |
| 0.0710 | 0.293021 | 0.027667 | 0.335660 | 0.043312 | 0.388750 | 0.068965 |
| 0.0744 | 0.306759 | 0.030744 | 0.351057 | 0.047461 | 0.405238 | 0.073597 |
| 0.0778 | 0.320460 | 0.033971 | 0.366359 | 0.051734 | 0.421501 | 0.078242 |
| 0.0812 | 0.334120 | 0.037346 | 0.381559 | 0.056121 | 0.437537 | 0.082894 |
| 0.0947 | 0.388289 | 0.052220 | 0.441235 | 0.074610 | 0.499361 | 0.101422 |
| 0.1083 | 0.441546 | 0.069047 | 0.498857 | 0.094168 | 0.557420 | 0.119554 |
| 0.1218 | 0.493667 | 0.087470 | 0.554118 | 0.114263 | 0.611683 | 0.137010 |
| 0.1353 | 0.544422 | 0.107115 | 0.606757 | 0.134437 | 0.662166 | 0.153591 |
| 0.1488 | 0.593582 | 0.127606 | 0.656562 | 0.154304 | 0.708920 | 0.169162 |
| 0.1624 | 0.640925 | 0.148581 | 0.703372 | 0.173545 | 0.752023 | 0.183631 |
| 0.1759 | 0.686243 | 0.169693 | 0.747074 | 0.191910 | 0.791574 | 0.196947 |
| 0.1894 | 0.729347 | 0.190621 | 0.787601 | 0.209200 | 0.827690 | 0.209085 |
| 0.2030 | 0.770069 | 0.211074 | 0.824928 | 0.225273 | 0.860496 | 0.220042 |
| 0.2165 | 0.808270 | 0.230794 | 0.859066 | 0.240028 | 0.890127 | 0.229835 |
| 0.2300 | 0.843838 | 0.249559 | 0.890058 | 0.253403 | 0.916725 | 0.238490 |
| 0.2436 | 0.876690 | 0.267179 | 0.917972 | 0.265366 | 0.940433 | 0.246045 |
| 0.2571 | 0.906773 | 0.283501 | 0.942902 | 0.275915 | 0.961399 | 0.252546 |
| 0.2706 | 0.934064 | 0.298407 | 0.964954 | 0.285068 | 0.979768 | 0.258042 |
| 0.2842 | 0.958567 | 0.311809 | 0.984254 | 0.292861 | 0.995687 | 0.262588 |
| 0.2977 | 0.980314 | 0.323652 | 1.000933 | 0.299342 | 1.009300 | 0.266240 |
| 0.3112 | 0.999359 | 0.333905 | 1.015132 | 0.304573 | 1.020748 | 0.269055 |
| 0.3248 | 1.015777 | 0.342565 | 1.026994 | 0.308619 | 1.030171 | 0.271090 |
| 0.3383 | 1.029663 | 0.349651 | 1.036666 | 0.311555 | 1.037701 | 0.272403 |
| 0.3518 | 1.041126 | 0.355200 | 1.044293 | 0.313456 | 1.043471 | 0.273048 |
| 0.3654 | 1.050287 | 0.359266 | 1.050018 | 0.314400 | 1.047606 | 0.273081 |
| 0.3789 | 1.057276 | 0.361915 | 1.053984 | 0.314464 | 1.050226 | 0.272553 |
| 0.3924 | 1.062232 | 0.363225 | 1.056326 | 0.313724 | 1.051448 | 0.271516 |
| 0.4059 | 1.065295 | 0.363284 | 1.057176 | 0.312257 | 1.051382 | 0.270017 |

| X | U | W | U | W | U | W |
|---|---|---|---|---|---|---|
| 0.4601 | 1.061470 | 0.352881 | 1.048088 | 0.300503 | 1.040267 | 0.260282 |
| 0.5142 | 1.038348 | 0.330072 | 1.024080 | 0.282259 | 1.016019 | 0.246362 |
| 0.5683 | 1.003251 | 0.300460 | 0.990581 | 0.260633 | 0.983216 | 0.230156 |
| 0.6225 | 0.961623 | 0.268420 | 0.951551 | 0.237814 | 0.945278 | 0.213014 |
| 0.6766 | 0.917147 | 0.236928 | 0.909752 | 0.215237 | 0.904655 | 0.195851 |
| 0.7307 | 0.872119 | 0.207730 | 0.867031 | 0.193770 | 0.863037 | 0.179248 |
| 0.7848 | 0.827868 | 0.181647 | 0.824576 | 0.173881 | 0.821545 | 0.163547 |
| 0.8390 | 0.785099 | 0.158884 | 0.783117 | 0.155771 | 0.780890 | 0.148928 |
| 0.8931 | 0.744147 | 0.139285 | 0.743076 | 0.139472 | 0.741500 | 0.135459 |
| 0.9472 | 0.705135 | 0.122522 | 0.704674 | 0.124915 | 0.703616 | 0.123140 |
| 1.0013 | 0.668073 | 0.108207 | 0.668009 | 0.111978 | 0.667355 | 0.111932 |
| 1.0555 | 0.632914 | 0.095965 | 0.633100 | 0.100514 | 0.632756 | 0.101767 |
| 1.1096 | 0.599585 | 0.085456 | 0.599923 | 0.090369 | 0.599814 | 0.092572 |
| 1.1637 | 0.568001 | 0.076394 | 0.568428 | 0.081395 | 0.568493 | 0.084264 |
| 1.2178 | 0.538078 | 0.068538 | 0.538552 | 0.073453 | 0.538743 | 0.076765 |
| 1.2720 | 0.509729 | 0.061695 | 0.510223 | 0.066416 | 0.510505 | 0.069997 |
| 1.3261 | 0.482873 | 0.055703 | 0.483371 | 0.060172 | 0.483715 | 0.063890 |
| 1.3802 | 0.457431 | 0.050432 | 0.457923 | 0.054621 | 0.458308 | 0.058376 |
| 1.4344 | 0.433330 | 0.045776 | 0.433809 | 0.049677 | 0.434219 | 0.053396 |
| 1.4885 | 0.410499 | 0.041646 | 0.410961 | 0.045263 | 0.411384 | 0.048894 |
| 1.5426 | 0.388870 | 0.037969 | 0.389314 | 0.041315 | 0.389741 | 0.044821 |
| 1.5967 | 0.368382 | 0.034685 | 0.368805 | 0.037774 | 0.369230 | 0.041132 |
| 1.6509 | 0.348972 | 0.031742 | 0.349376 | 0.034592 | 0.349793 | 0.037787 |
| 1.7050 | 0.330586 | 0.029098 | 0.330970 | 0.031726 | 0.331376 | 0.034752 |
| 1.9215 | 0.266229 | 0.020850 | 0.266541 | 0.022756 | 0.266890 | 0.025112 |
| 2.1380 | 0.214402 | 0.015226 | 0.214653 | 0.016623 | 0.214942 | 0.018414 |
| 2.3545 | 0.172663 | 0.011283 | 0.172866 | 0.012319 | 0.173101 | 0.013672 |
| 2.5710 | 0.139050 | 0.008458 | 0.139214 | 0.009235 | 0.139403 | 0.010259 |
| 2.7875 | 0.111981 | 0.006400 | 0.112112 | 0.006988 | 0.112266 | 0.007766 |
| 3.0040 | 0.090181 | 0.004879 | 0.090287 | 0.005328 | 0.090411 | 0.005922 |
| 3.2205 | 0.072625 | 0.003743 | 0.072711 | 0.004087 | 0.072810 | 0.004544 |
| 3.4370 | 0.058487 | 0.002887 | 0.058556 | 0.003152 | 0.058636 | 0.003505 |
| 3.6535 | 0.047101 | 0.002237 | 0.047157 | 0.002442 | 0.047221 | 0.002715 |
| 3.8701 | 0.037932 | 0.001739 | 0.037976 | 0.001899 | 0.038028 | 0.002111 |
| 4.0866 | 0.030548 | 0.001357 | 0.030583 | 0.001481 | 0.030625 | 0.001647 |
| 4.3031 | 0.024601 | 0.001062 | 0.024630 | 0.001159 | 0.024663 | 0.001289 |
| 4.5196 | 0.019812 | 0.000833 | 0.019835 | 0.000909 | 0.019862 | 0.001011 |
| 4.7361 | 0.015955 | 0.000654 | 0.015974 | 0.000715 | 0.015995 | 0.000794 |
| 4.9526 | 0.012849 | 0.000515 | 0.012864 | 0.000563 | 0.012882 | 0.000626 |
| 5.1691 | 0.010348 | 0.000407 | 0.010360 | 0.000444 | 0.010374 | 0.000493 |
| 5.3856 | 0.008333 | 0.000321 | 0.008343 | 0.000351 | 0.008354 | 0.000390 |
| 5.6021 | 0.006711 | 0.000254 | 0.006719 | 0.000277 | 0.006728 | 0.000308 |
| 5.8186 | 0.005404 | 0.000201 | 0.005411 | 0.000220 | 0.005418 | 0.000244 |
| 6.0351 | 0.004352 | 0.000160 | 0.004357 | 0.000174 | 0.004363 | 0.000194 |
| 6.2516 | 0.003505 | 0.000127 | 0.003509 | 0.000138 | 0.003514 | 0.000154 |
| 6.4681 | 0.002823 | 0.000101 | 0.002826 | 0.000110 | 0.002830 | 0.000122 |
| 6.6846 | 0.002273 | 0.000080 | 0.002276 | 0.000087 | 0.002279 | 0.000097 |
| 6.9011 | 0.001831 | 0.000064 | 0.001833 | 0.000069 | 0.001835 | 0.000077 |

*Nuclear Physics* **6** (1958) 404—419; © *North-Holland Publishing Co., Amsterdam*
Not to be reproduced by photoprint or microfilm without written permission from the publisher

# ROLE OF PION-PION INTERACTION IN $\tau$-DECAY

A. N. MITRA

*Department of Physics, Muslim University, Aligarh, U.P., India*

Received 9 December 1957

**Abstract:** The effect of the pion-pion interaction on the anisotropy of the decay pions in $\tau$-decay and on the $\tau'/\tau$-branching ratio is studied here, following the formalism of a recent paper by Dalitz. The $\pi-\pi$ interaction is assumed to be of the resonant Breit Wigner type in the isobaric spin states $I = 0$ and $I = 2$. It is found that the assumption of an $I = 2$ resonance can satisfactorily explain the experimental figures for the momentum distribution of the unlike pion as well as the $\tau'/\tau$-branching ratio. This result serves as a supporting evidence for a recent deduction by the author of an $I = 2$ resonance within the framework of the pseudoscalar meson theory.

## 1. Introduction

In recent years a large amount of experimental information has accumulated on (1) the energy and momentum distributions of charged pions in $\tau$-decay and (2) the branching ratio of the two alternative modes of decay of a $\tau$-meson ($\tau^+ \rightarrow 2\pi^+ + \pi^-$ or $\pi^+ + 2\pi^0$). The momentum distribution of the unlike (negative) pion in $\tau$-decay is most conveniently represented by means of points on the so-called triangular "Dalitz diagram" [1]), the perpendiculars from each point on the sides of the triangle representing the energies of the individual pions. Thus a study of the momentum distribution of the pions is reduced to that of the distribution of such points on the "Dalitz-diagram".

One of the principal objects of this study of points on the Dalitz-diagram has been to determine the spin and parity of the $\tau$-meson, since it is clear that any spin and parity assignment for the $\tau$-meson would reflect itself in the angular and momentum distributions of the decay pions. In particular, if pion-pion interaction is neglected, the assignment $0-$ for the $\tau$-meson would lead to a completely isotropic distribution in the various pion momenta, which fact would manifest itself in a uniform distribution of points on the Dalitz-diagram. Earlier studies [1, 2]) on the basis of rather inadequate data did in fact indicate a fairly uniform distribution of points over the "allowed region" (i.e. that obtained by taking account of energy-momentum conservation). However, with the availability of more and more data it was found that there was a small but definite deviation from isotropy, inasmuch as the negative pion tended to have a somewhat higher momentum than each of the like ones.

In recent times the Göttingen group [3]) has carried out an extensive investigation of the momentum and angular distributions of the unlike pion in τ-decay, with a view to determining the spin and parity of the τ-meson by means of statistical devices like the $\chi^2$-test, etc. By comparing the theoretical predictions about the angular and momentum distributions of the unlike pion (with different spin and parity assignments for the τ-meson) with the experimental results, they have found that the statistical tests are overwhelmingly in favour of the pseudoscalar hypothesis for the τ-meson, as Dalitz had predicted earlier, since the discrepancy between theoretical and experimental points happens to be much smaller for the 0− assignment than for any other value. However, they could not bridge up the small but unmistakable deviation from isotropy existing in experimental data by virtue of the unlike pion exhibiting somewhat higher momentum values than each of the like ones, presumably because of their neglect of pion-pion effects. In any case it is at least certain that the experimental deviation from isotropy cannot be explained simply by postulating any spin-parity value other than 0− for the τ-meson.

In a recent paper [4]), Dalitz investigated another aspect of the τ-decay process, viz. the question of isobaric spin change†, in the context of the two problems cited in the beginning of this paper. He found that an isobaric spin change $\Delta T = \frac{1}{2}$ was the most dominant transition, though the details of the data could be fitted only with small admixtures of matrix elements corresponding to $\Delta T = 3/2$ and $\Delta T = 5/2$, the transition amplitudes decreasing with increasing $\Delta T$. Dalitz's analysis was purely phenomenological and he deduced from the experimental data that the final 3-meson amplitude was mostly of the totally symmetrical type, with a very small deviation which he interpreted as the effect of the so-called [2, 1] symmetry class (the only only other possible symmetry class for a 3-pion system which remains after the totally symmetric part has been subtracted out). Dalitz, in his analysis, did not investigate the *origin* of the [2, 1] symmetry class, and merely deduced its percentage from experimental data. It may, however, be of considerable interest to regard this deviation from isotropy as arising from a pion-pion interaction which is expected to play an important part in the final state. The present investigation was undertaken with the purpose of determining the role of pion-pion interaction in (1) bringing about the above deviation from isotropy and (2) influencing the $\tau'/\tau$-branching ratio.

For the purpose of the present investigation the τ-meson has been assumed to be pseudoscalar, which now seems to be well-established. Now, since the total available kinetic energy in τ-decay is rather small ($\approx$ 75 MeV),

† According to the Gell-Mann assignment, a τ-meson has $T = \frac{1}{2}$, while a 3-pion system has an integral $T$, so that $T$ must change by a $\frac{1}{2}$-integer in τ-decay.

and the maximum possible kinetic energy of each pion still smaller ($\approx$ 30 MeV), it is reasonable to assume that only s-waves are effective for a pion-pion interaction which is generally supposed to have a very short range. This implies that for a 2-meson system, pion-pion interaction can occur only in the states † $I = 0$ and 2, $I = 1$ being ruled out since no p-waves are considered.

The calculations have been performed closely following the formalism of Dalitz, whose paper is referred to in the text as A. The notations used are those of A as far as possible, except for slight changes to be mentioned at the proper places. The only important feature is the introduction of resonant pion-pion interactions in Dalitz's analysis, thus bringing about a certain momentum dependence in the various transition amplitudes.

## 2. Amplitudes and Probabilities for $\tau$, $\tau'$ decay

Following Dalitz one can express the final state of 3 pions of unit total charges as a linear combination of states of $T = 1, 2, 3$. Let the momenta of the emitted pions be $\mathbf{p}_1$, $\mathbf{p}_2$, $\mathbf{p}_3$, with $p_1 \geqq p_2 \geqq p_3$. Now the required isobaric spin function can be constructed by first adding the $I$-spins of any two pions to give a sum $I = 0$, 1, or 2, and finally combining the result with the $I$-spin of the remaining pion to give the total $T$. At this stage we make a slight departure from Dalitz's procedure in that we first combine the $I$-spins of the pions $\mathbf{p}_2$ and $\mathbf{p}_3$ and finally obtain the total $T$ with the help of the remaining pion $\mathbf{p}_1$, instead of first associating the $I$-spins of $\mathbf{p}_1$ and $\mathbf{p}_2$. (The bearing of this procedure on the experimental data will be discussed in § 3.) In this way the 6 isobaric spin functions $\chi_I{}^T$ are obtained as follows:

$$\begin{aligned}
\chi_2{}^3 &= (15)^{-\frac{1}{2}}[(u_2w_3+w_2u_3+2v_2v_3)u_1+u_2u_3w_1+2(u_2v_3+v_2u_3)v_1] \\
\chi_2{}^2 &= (12)^{-\frac{1}{2}}[2u_2u_3w_1+(u_2v_3+u_3v_2)v_1-(2v_2v_3+u_2w_3+u_3w_2)u_1] \\
\chi_2{}^1 &= (60)^{-\frac{1}{2}}[(u_2w_3+u_3w_2+2v_2v_3)u_1-3(u_2v_3+u_3v_2)v_1+6u_2u_3w_1] \\
\chi_1{}^2 &= -\tfrac{1}{2}[(u_2w_3-u_3w_2)u_1+(u_2v_3-u_3v_2)v_1] \\
\chi_1{}^1 &= \tfrac{1}{2}[(u_2w_3-u_3w_2)u_1-(u_2v_3-u_3v_2)v_1] \\
\chi_0{}^1 &= (3)^{-\frac{1}{2}}[(u_2w_3+u_3w_2-v_2v_3)u_1].
\end{aligned} \tag{1}$$

The final transition amplitude (symmetrized) is then given by

$$\tfrac{1}{6}\sum_P (F_0\chi_0{}^1+F_1\chi_1{}^1+F_2\chi_2{}^1+G_1\chi_1{}^2+G_2\chi_2{}^2+H_2\chi_2{}^3). \tag{2}$$

Introducing the various symmetry classes as in A, (2) can be written in the alternative form

† The notation used is such that $I$ represents the resultant isobaric spin of a 2-meson system and $T$ that of the complete 3-meson system.

$$\tfrac{1}{6}\sum_P [\tfrac{1}{3}(\sqrt{5}\chi_2^1-2\chi_0^1)J+F_1\chi_1^1+G_1\chi_1^2+G_2\chi_2^2] \\ +\tfrac{1}{3}(\sqrt{5}\chi_0^1+2\chi_2^1)I+\chi_2^3 H, \qquad (3)$$

where

$$I=\tfrac{1}{6}\sum_P \tfrac{1}{3}(\sqrt{5}F_0+2F_2),\quad H=\tfrac{1}{6}\sum_P H_2,\quad J=\tfrac{1}{3}(\sqrt{5}F_2-2F_0). \qquad (4)$$

In this form the functions $I$ and $H$ are completely symmetrical in the indices 1, 2 and 3, as can be seen from (4), the symmetrization operation on these functions being possible because the isobaric spin functions associated with $I$ and $H$ are already symmetrical in the indices. The other functions $J$, $F_1$, $G_1$ and $G_2$ are necessarily of the [2, 1] symmetry class, being multiplied by isobaric spin functions of the [2, 1] type. Thus if any of these latter functions be denoted by $f(\mathbf{p}_1, \mathbf{p}_2, \mathbf{p}_3)$, the symmetrical part $\frac{1}{6}\sum_P f(\mathbf{p}_1, \mathbf{p}_2, \mathbf{p}_3)$ must be subtracted from each of them before they are inserted in (3).

Proceeding as in A, one now finds for the probability amplitudes of the three possible charged decay modes (according as the *negative pion* has momenta $\mathbf{p}_1$, $\mathbf{p}_2$ or $\mathbf{p}_3$), the following expressions:

$$A_1 = A(\pi^-\pi^+\pi^+) = \frac{1}{\sqrt{3}}\lambda+\sqrt{\tfrac{2}{3}}\alpha, \qquad (5a)$$

$$A_2 = A(\pi^+\pi^-\pi^+) = \frac{1}{\sqrt{3}}\lambda-\frac{1}{\sqrt{6}}\alpha+\frac{1}{\sqrt{2}}\gamma, \qquad (5b)$$

$$A_3 = A(\pi^+\pi^+\pi^-) = \frac{1}{\sqrt{3}}\lambda-\frac{1}{\sqrt{6}}\alpha-\frac{1}{\sqrt{2}}\gamma, \qquad (5c)$$

in the notation of A†.

The difference between (5) and the corresponding expression (3.8) of A arises from the departure from Dalitz's procedure of combining the $I$-spin functions of the three pions, as has been mentioned earlier in this section. Further, the total probabilities for $\tau$ and $\tau'$-decay are proportional to

$$\sigma(\tau) = |\lambda|^2+|\alpha|^2+|\gamma|^2, \qquad (6a)$$

$$\sigma(\tau') = |\varrho|^2+|\beta|^2+|\delta|^2, \qquad (6b)$$

again in the notation of A†.

At this stage we are in a position to introduce the resonant pion-pion interactions. For simplicity we shall consider the two cases $I = 0$ and 2 separately. We shall further assume that among the six functions $F_I$, $G_I$ and $H_I$, only those which correspond to the relevant $I$-state under con-

† $\lambda = (2I+H)/\sqrt{5}$ $\quad \varrho = (I-2H)/\sqrt{5}$
$\alpha = (J+G_2)/\sqrt{2}$ $\quad \beta = (J-G_2)/\sqrt{2}$
$\gamma = (F_1-G_1)/\sqrt{2}$ $\quad \delta = (F_1+G_1)/\sqrt{2}$.

sideration are large, the others being negligible. Thus for resonant interaction in $I = 0$, we shall neglect all the functions in (2) except $F_0$. Similarly, for $I = 2$, we shall retain only $F_2$, $G_2$ and $H_2$. In either case, $F_1 \approx G_1 \approx 0$, which leads to

$$\gamma \approx 0, \quad \delta \approx 0. \tag{5'}$$

The resonant pion-pion interaction in a certain $I$-state may be taken to be of the usual Breit-Wigner type, so that the functions $F_0$, $F_2$, etc. are of the form

$$F(\mathbf{p}_1, \mathbf{p}_2, \mathbf{p}_3) = CW_1 \equiv \frac{C}{\varkappa_{23}} \times \frac{\frac{1}{2}\Gamma}{(\omega_{23}-\omega_r)-\frac{1}{2}i\Gamma}. \tag{7}$$

Here it is assumed that the interaction is effective between the pions $\mathbf{p}_2$ and $\mathbf{p}_3$; $(\pm\varkappa_{23}, \omega_{23})$ are the 4-momenta of these pions in their own C.M. frame, $\omega_r = (\mu^2+r^2)^{\frac{1}{2}}$ is the "resonance" value of $\omega_{23}$, $\Gamma$ is the "resonance width" and $C$ is a constant independent of the momenta. Similar functions $W_2$ and $W_3$ can be defined by taking the combinations (1,3) and (1,2) respectively.

The various functions $\lambda$, $\alpha$, etc. introduced in (5) can now be expressed in terms of $W_1$, $W_2$ and $W_3$, remembering the symmetry classes of the former. Since for $I = 0$, only $F_0$ will survive, we have for this case

$$\begin{aligned} \lambda = 2\varrho &= \tfrac{2}{9} C_0(W_1+W_2+W_3), && \gamma \approx 0; \\ \alpha = \beta &= -\frac{\sqrt{2}}{9} C_0(2W_1-W_2-W_3), && \delta \approx 0. \end{aligned} \tag{8}$$

For the case $I = 2$, the non-zero functions (in our approximation) are $F_2$, $G_2$ and $H_2$, out of which $F_2$ is expected to be the largest since it corresponds to $\Delta T = \frac{1}{2}$; $G_2$ and $H_2$ would be smaller by at least one and two orders of magnitude respectively, on the basis of Dalitz's selection rule, since they correspond to $\Delta T = 3/2$ and $5/2$. We may therefore neglect both of them in the first approximation, regarding them essentially as small correction terms. In this way we find for $I = 2$

$$\begin{aligned} \lambda = 2\varrho &= \tfrac{4}{9}(5)^{-\frac{1}{2}} C_2(W_1+W_2+W_3), && \gamma \approx 0; \\ \alpha = \beta &= \tfrac{1}{9}(\tfrac{5}{2})^{\frac{1}{2}} C_2(2W_1-W_2-W_3), && \delta \approx 0. \end{aligned} \tag{9}$$

The over-all transition probabilities $X$, $Y$ and $Z$ of the different modes of charged decay according to which the unlike pion has the largest, intermediate or the smallest momentum respectively, can now be obtained by integrating the quantities $|A_1|^2$, $|A_2|^2$ and $|A_3|^2$ of (5) over the available phase space, subject to the condition $p_1 \geqq p_2 \geqq p_3$. Similarly the $\tau'/\tau$-branching ratio $R$ can be obtained by integrating the quantities $\sigma(\tau)$ and $\sigma(\tau')$ of (6) over the entire available phase space, with no restriction over the momenta. These integrations have been carried out under the following

approximations: (1) the pion momenta are all non-relativistic, which condition is amply fulfilled, and (2) the resonance width $\Gamma \ll (\omega_r - \mu)$, which is not an unreasonable approximation either. The method of integration is discussed in the appendix. Here we give only the results which can be expressed in terms of a dimensionless parameter $\theta$ defined by

$$r^2 = M\mu t_m\ \theta/(M+\mu), \tag{10}$$

which, according to the discussion in the appendix, lies between 0 and 1 ($t_m$ is the maximum kinetic energy of the negative pion).

$I = 0$:

$$Y = Z; \tag{11a}$$

$$X/Y = 4\,\frac{4\xi-3\eta+8\zeta_1-12\zeta_0+4\zeta_2}{\xi+15\eta+6\zeta_0+2\zeta_2-8\zeta_2} \quad (\theta \geqq \tfrac{1}{2}) \tag{11b}$$

$$= \frac{\xi+4\zeta_2-4\zeta_1}{4\xi+2\zeta_1-2\zeta_2} \quad (\theta \leqq \tfrac{1}{2}); \tag{11c}$$

$$R(\tau'/\tau) = \frac{5\xi-2\zeta_1+2\zeta_2}{8\xi+4\zeta_1-4\zeta_2}. \tag{11d}$$

$I = 2$:

$$Y = Z; \tag{12a}$$

$$X/Y = \frac{\xi+2\zeta_1-2\zeta_2+\frac{25}{16}(2\xi-2\zeta_1+2\zeta_2+I_p+2J_p)+\frac{5}{2}(I_p-J_p)}{\xi+2\zeta_1-2\zeta_2+\frac{25}{64}(2\xi-2\zeta_1+2\zeta_2+I_p+2J_p)-\frac{5}{4}(I_p-J_p)}; \tag{12b}$$

$$R(\tau'/\tau) = \frac{29\xi-17\zeta_1+17\zeta_2}{41\xi-7\zeta_1+7\zeta_2}. \tag{12c}$$

Here

$$I_p = 3\eta-\xi, \quad J_p = 2\zeta_1-3\zeta_0+\zeta_2 \quad \text{for} \quad \theta \geqq \tfrac{1}{2}; \tag{13a}$$

$$I_p = 2\xi, \quad J_p = \zeta_2-\zeta_1 \quad \text{for} \quad \theta \leqq \tfrac{1}{2}. \tag{13b}$$

TABLE 1

Calculated values of the quantities $X/Y$ and $R$ on the assumptions of $I = 0$ and $I = 2$ resonances

| $\theta$ | $X/Y$ | | $R(\tau'/\tau)$ | | $R$ (corrected) | |
|---|---|---|---|---|---|---|
| | $I=0$ | $I=2$ | $I=0$ | $I=2$ | $I=0$ | $I=2$ |
| 0.50 | −0.301 | −23.90 | 0.349 | 0.395 | – | – |
| 0.75 | +0.266 | +2.960 | 0.289 | 0.309 | – | – |
| 0.80 | +0.439 | +1.858 | 0.275 | 0.292 | 0.308 | 0.330 |
| 0.85 | +0.645 | +1.128 | 0.261 | 0.272 | 0.297 | 0.310 |

The quantities $\xi, \eta, \zeta_n$ $(n = 0, 1, 2)$ are defined in the appendix, from which it is seen that they are all proportional to the resonance width $\Gamma$, so that the ratios $X/Y$ and $R$ are *independent* of $\Gamma$ in our approximation. The numerical values of these ratios as functions of the parameter $\theta$ (i.e. the "resonance" energy) are given in Table 1 for the two cases $I=0$ and $I=2$.

## 3. Discussion

We note, first of all, that the over-all probabilities $Y$ and $Z$ are equal, as may be seen from (11) and (12). This is a direct consequence of (5) and (5′) and stems from the neglect of any amplitude which does not correspond to a resonant S-wave meson-meson interaction. If the combination of the isobaric functions of the 3 pions had been effected as in A, the above approximation would have led to $X = Y$ instead of $Y = Z$. It may be noted that the present combination fits very well the experimental situation described in A (p. 534, footnote) which lists the number of points in the regions $X$, $Y$ and $Z$ as 207, 181.5 and 176.5 respectively, showing that $Y$ and $Z$ are almost equal, and $X$ markedly larger than either of them. Even the earlier experimental data for $X$, $Y$ and $Z$ (which are listed in A as 83, 66.5 and 67.5) do show exactly similar features, so that one may expect these qualitative features of the momentum distribution of the unlike pion to be maintained by subsequent data (which are continually accumulating).

The date indicate a definite deviation from isotropy, in the sense that the experimental ratio $X/Y$ is larger than unity, lying between 1.2 and 1.3. Now table 1 shows that the ratio $X/Y$ varies with the "resonance parameter" $\theta$ in a rather sensitive manner. It is further seen from this table that the experimental ratio 1.2—1.3 can be obtained only in the case $I = 2$, for a value of $\theta$ lying between 0.80 and 0.85. The hypothesis $I = 0$ leads only to values of $X/Y$ which are much smaller than unity, in complete disagreement with the experimental findings. This result seems to be a strong argument in favour of an $I = 2$ resonance as against $I = 0$, the simple assumption of an isotropic distribution being already ruled out by earlier considerations. Physically also one would expect $I = 2$ to lead to higher momentum values for the negative pion, for the following reason. The resonance $I = 2$ is effective most of the time for the $(\pi^+-\pi^+)$ combination, with only a small projection on the $(\pi^+-\pi^-)$ combination. Thus with an $I = 2$ resonance the like pions would tend to be together most of the time, and conservation of momentum would then force the unlike pion to go in the opposite direction with a momentum significantly larger than that of each of the like ones. Hence on the average, $X/Y$ would necessarily be larger than unity. On the other hand, an $I = 0$ resonance has a

projection 1/3 on the $(\pi^+-\pi^-)$ combination and 0 on $(\pi^+-\pi^+)$, so that the momentum conservation argument would now lead to a higher value for one of the positive pions, instead of for the negative one, which would make $X/Y < 1$.

Regarding the branching ratio $R(\tau'/\tau)$ for $\tau$ and $\tau'$ decay modes, table 1 shows that unlike $X/Y$, this function is not so sensitive to variations in $\theta$, and the value of $\theta$ (lying between 0.80 and 0.85) which matches the ratio $X/Y$ seems to give a somewhat smaller value for $R$ than the experimental one of $0.33\pm0.06$ (as quoted in A), though the limits of error are wide enough to give rough agreement. It is further seen from table 1 that an $I = 2$ resonance gives a value somewhat closer to the experimental one than an $I = 0$ resonance.

Now it may be noted that in our present calculation of the branching ratio, no distinction has been made between the masses of charged and neutral pions, the primary motive being to avoid unnecessary complication in a formalism which already became involved on account of the pion-pion interaction. Dalitz, on the other hand, neglected the momentum dependence of the matrix elements completely, and the simplification thus produced enabled him to take full account of the $\pi^\pm-\pi^0$ mass difference, which made the $Q$-value for $\tau'$-decay 84 MeV in place of 75 MeV for the charged decay mode. This difference, according to Dalitz's calculations, made the *total* phase space for $\tau'$-decay 1.295 times larger than that for $\tau$-decay. This factor was enough to increase the theoretical branching ratio of 0.25 (obtained on the assumption of a totally symmetric transition amplitude coupled with the selection rule $\Delta T = \frac{1}{2}$, strictly) to 0.34, which was adequate to explain the experimental figure. It may, however, be seen from (8) and (9) that the momentum dependence of the transition amplitudes which is introduced by the pion-pion interaction brings, in the transition probability, an additional factor of the type $1/\kappa_{23}^2$, where $4\kappa_{23}^2 = M^2-2M\mu-3\mu^2-2Mt$ is a *linear* function of the kinetic energy $t$ of the unlike pion. This factor offsets the momentum dependence arising from the phase space to a considerable extent, so that the over-all probability now goes roughly *linearly* with $t_m$ (the maximum kinetic energy of the negative pion), rather than *quadratically* as obtained by Dalitz. (The exact momentum dependence is of course much more complicated on account of the "resonance factors" and their interference effects.) Thus the error introduced by neglecting the $\pi^\pm-\pi^0$ mass difference is expected to be much smaller than if the transition amplitudes were treated as constants as in A. We may however make a very rough correction to the branching ratio by multiplying our figures by the factor $(1.295)^{\frac{1}{2}}$ obtained from Dalitz's figure on the simple assumption (as stated above) that the total decay probability is proportional to $t_m$ instead of $t_m^2$. The corrected figures thus obtained for the branching ratio are also listed

in table 1. The agreement is now seen to be quite good for $\theta$ lying between 0.80 and 0.85. It is of course recognized that this *ad hoc* factor should not be taken too seriously, but it at least provides a qualitative correction in the *right* direction.

It is thus seen that the dynamical consideration of a resonant interaction gives results in fairly good agreement with the experimental findings. The minor discrepancies can easily be removed by the inclusion of small correction factors like interaction in the $I = 1$ state of two pions, amplitudes for $\Delta T > \frac{1}{2}$, etc., which are clearly necessary to make detailed agreement possible. It is further recognized that a more detailed comparison between theory and experiment is necessary, instead of the limited test that has been carried out here by integrating out the different variables like angles, momenta, etc., of the various pions. Thus, for example, the predictions of the theoretical $I = 2$ resonance must be tested against the angular distribution of the negative pion with respect to the rest frame of the $\tau^+$-meson, the angular distribution of each of the positive pions in their own C.M. frame, etc. Unfortunately, such detailed experimental figures not being available, these comparisons could not be made.

It may be mentioned in this connection that the problem of the pion-pion interaction was recently studied in the framework of the pseudoscalar meson theory by Mitra and Saxena [5]), using a Bethe-Salpeter approach to the interaction kernel. Their result indicated the existence of an $I = 2$ resonance for s-wave pions with the presently accepted value of $G^2/4\pi = 15.5$, which was found to be too high to give an $I = 0$ resonance. This result harmonizes with the present investigation which strongly favours an $I = 2$ resonance as a possible explanation of the deviation from isotropy in $\tau$-decay.

The author is indebted to Professor P. S. Gill for useful discussions.

## Appendix

We give here a derivation of eqs. (10)—(13) of the text.

The elementary phase space volume is given by

$$d\tau = (2\pi)^{-2}\delta^3(\mathbf{p}_1+\mathbf{p}_2+\mathbf{p}_3)\delta(\omega_1+\omega_2+\omega_3-M)\left(\frac{d^3p_1}{\omega_1}\right)\left(\frac{d^3p_2}{\omega_2}\right)\left(\frac{d^3p_3}{\omega_3}\right). \quad \text{(A1)}$$

The integrals encountered in the text, as may be seen from (5), (8) and (9), are

$$I_1 = \int |W_1|^2 d\tau, \quad J_1 = \mathrm{Re}\int W_2^* W_3 d\tau, \quad \text{(A2)}$$

with similar expressions for $I_2$, $I_3$, $J_2$ and $J_3$ obtained by permuting the indices in an obvious manner. The magnitudes of the energies $\omega_1$, $\omega_2$ and

$\omega_3$ in (A1) and (A2) vary from $\mu$ to the maximum value allowed by the $Q$-value $(M-3\mu)$ and the conservation conditions, viz.

$$t_m = (M-3\mu)(M+\mu)/2M. \tag{A3}$$

For charged decay, since we are interested in studying the momentum distribution of the negative pion, there is an additional restriction on the magnitudes of the momenta, viz.

$$p_1 \geqq p_2 \geqq p_3. \tag{A4}$$

No such restriction exists in connection with the branching ratio of the over-all $\tau$ and $\tau'$ decay probabilities, though for this case the mass difference between $\pi^0$ and $\pi^\pm$ should be taken into account. However, this difference is ignored in the present derivation for reasons discussed in section 3 of the text. Thus for the calculation of the over-all decay probabilities for $\tau$ and $\tau'$, the values of $I_1$, $I_2$ and $I_3$ (and similarly of $J_1$, $J_2$ and $J_3$) are all equal from symmetry. However, these quantities are all different for the calculation of the $\pi^-$ momentum distribution in $\tau^+$ decay. The procedure will now be shown separately for the two cases.

(a) OVER-ALL DECAY PROBABILITIES

The evaluation of the integrals $I_1$ and $J_1$ is most easily carried out by introducing 4-vector variables of integration $p_{2\lambda}$ and $p_{3\lambda}$ with the help of the relation

$$\int \frac{d^3p_2}{\omega_2}\frac{d^3p_3}{\omega_3} = 4\int \delta(p_2^2-\mu^2)\delta(p_3^2-\mu^2)d^4p_2\,d^4p_3, \tag{A5}$$

where, for the 4-vectors $A_\lambda = (A_0, \mathbf{A})$ and $B_\lambda$,

$$A^2 = A_0^2-\mathbf{A}\cdot\mathbf{A}; \quad A\cdot B = A_0B_0-\mathbf{A}\cdot\mathbf{B}. \tag{A6}$$

The $\delta$-functions in (A5) ensure that the usual energy-momentum relations for $p_{2\lambda}$ and $p_{3\lambda}$ are automatically satisfied, viz.

$$\omega_2^2 = p_{02}^2 = \mu^2+\mathbf{p}_2^2, \qquad \omega_3^2 = p_{03}^2 = \mu^2+\mathbf{p}_3^2. \tag{A7}$$

Next we change the variables $p_{2\mu}$, $p_{3\mu}$ to $Q_\mu$ and $R_\mu$ defined by

$$Q_\mu = p_{2\mu}+p_{3\mu}, \qquad R_\mu = p_{2\mu}-p_{3\mu}. \tag{A8}$$

Using (A1), (A5) and (A7), $\int d\tau$ reduces to

$$(2\pi)^{-2}\int \delta(Q\cdot R)\delta(R^2+Q^2-4\mu^2)\delta^4(Q_\mu-E_\mu)d^4Q\,d^4R\,\frac{d^3p_1}{\omega_1}, \tag{A9}$$

where $E_\mu$ is a 4-vector with the components $(M-\omega_1, -\mathbf{p}_1)$. (A9) shows that the $Q$-integration can be carried out at once, giving

$$Q_\mu = (M-\omega_1, \quad -\mathbf{p}_1), \tag{A10}$$

so that

$$Q^2 = M^2-2M\omega_1+\mu^2. \tag{A11}$$

The integrations over $R_\mu$ and $\mathbf{p}_1$ will, on the other hand, depend on the actual integrands. However, for the cases $I_1$ and $J_1$ that we have to consider, it will be seen below that the integrands will depend only on $R_0$ and the magnitude of $\omega_1$, so that integrations over $\mathrm{d}^3R$ and the angular distribution of $\mathbf{p}_1$ can be carried out as well, leading to the following result:

$$(2\pi)^{-2}\int f(\omega_1,\ R_0)\delta(Q_0R_0-\mathbf{Q}\cdot\mathbf{R})\delta(R_0^2+Q^2-4\mu^2-\mathbf{R}^2)\,\mathrm{d}^4R\,\frac{\mathrm{d}^3p_1}{\omega_1} = \iint f(\omega_1,\ R_0)\mathrm{d}R_0\,\mathrm{d}\omega_1, \tag{A12}$$

where we have used relation (A10) between $Q_\mu$ and $\mathbf{p}_1$. The $\delta$-functions in (A12) impose the following restriction on the magnitude of $R_0$

$$|Q_0R_0| \leqq |\mathbf{Q}|\,|\mathbf{R}|,$$

which leads to

$$|R_0| \leqq R_\mathrm{m} = (\omega_1^2-\mu^2)^{\frac{1}{2}}(Q^2-4\mu^2)^{\frac{1}{2}}(Q^2)^{-\frac{1}{2}}. \tag{A13}$$

Eq. (A13) gives an exact expression for $R_\mathrm{m}$, but it reduces in the non-relativistic limit to

$$R_\mathrm{m} = \left[\frac{M}{\mu}t(t_\mathrm{m}-t)\right]^{\frac{1}{2}}, \tag{A14}$$

where $t=\omega_1-\mu$ and $t_\mathrm{m}$ is defined in (A3).

Now, using (A11), the C.M. energy $\omega_{23}$ of $\mathbf{p}_2$ and $\mathbf{p}_3$ is given by

$$4(\mu^2+\kappa_{23}^2) = 4\omega_{23}^2 = (\omega_2+\omega_3)^2-(\mathbf{p}_2+\mathbf{p}_3)^2 = (M-\omega_1)^2-\mathbf{p}_1^2 = Q^2. \tag{A15}$$

Further, from (7) and (A15), we have

$$|W_1|^2 = \frac{\Gamma^2}{(Q-2\omega_r)^2+\Gamma^2}\,\frac{4}{Q^2-4\mu^2} \approx \frac{4\Gamma}{Q^2-4\mu^2}\,\delta(Q-2\omega_r), \tag{A16}$$

since we have assumed that $\Gamma \ll 2\omega_r$. Using (A12), (A14) and (A16), we have

$$I_1 = \int |W_1|^2\,\mathrm{d}\tau = 8\Gamma\int_0^{t_\mathrm{m}} \frac{\mathrm{d}t}{Q^2-4\mu^2}\,\delta(Q-2\omega_r)\left(\frac{M}{\mu}t(t_\mathrm{m}-t)\right)^{\frac{1}{2}}.$$

This integral is immediately evaluated because of the $\delta$-function. It vanishes unless $Q_\mathrm{m} = (2Mt_\mathrm{m}+4\mu^2)^{\frac{1}{2}} \geqq 2\omega_r$, and is then given by

$$I_1 = \frac{8\Gamma}{M}\left[\frac{\mu}{M}\left(\frac{2Mt_\mathrm{m}}{4r^2}-1\right)\right]^{\frac{1}{2}}. \tag{A17}$$

Introducing a dimensionless parameter $\theta$ according to the equation

$$r^2 = M\mu t_\mathrm{m}\theta/(M+\mu), \tag{A18}$$

one can write

$$I_1 = 2\xi, \tag{A19}$$

where

$$\xi = \frac{4\Gamma}{M}\left(\frac{M+\mu}{2M\theta} - \frac{\mu}{M}\right)^{\frac{1}{2}}. \tag{A20}$$

The integral $J_1$ is, according to (A12), given by

$$J_1 = \mathrm{Re}\iint \frac{\mathrm{d}\omega_1\,\mathrm{d}R_0}{\varkappa_{12}\,\varkappa_{13}}\left(\frac{\Gamma}{2\omega_{12}-2\omega_r+i\Gamma}\right)\left(\frac{\Gamma}{2\omega_{13}-2\omega_r-i\Gamma}\right). \tag{A21}$$

Now,

$$4\omega_{12}^2 = M^2-2M\omega_3+\mu^2 = 4\mu^2+(M\omega_1-3\mu^2+MR_0)$$

and

$$4\omega_{13}^2 = M^2-2M\omega_2+\mu^2 = 4\mu^2+(M\omega_1-3\mu^2-MR_0).$$

Therefore, the non-relativistic limit gives

$$2\omega_{12},\ 2\omega_{13} = 2\mu+\frac{1}{4\mu}(M\omega_1-3\mu^2\pm MR_0). \tag{A22}$$

Next we use the result

$$\mathrm{Re}\left(\frac{\Gamma}{a-i\Gamma}\,\frac{\Gamma}{b+i\Gamma}\right) = \tfrac{1}{2}\left[\frac{\Gamma^2}{a^2+\Gamma^2}+\frac{\Gamma^2}{b^2+\Gamma^2}-\frac{(a-b)^2\,\Gamma^2}{(a^2+\Gamma^2)(b^2+\Gamma^2)}\right] \tag{A23}$$
$$\approx \tfrac{1}{2}\Gamma(\delta(a)+\delta(b))-\tfrac{1}{2}(a-b)^2\,\delta(a)\delta(b).$$

Eq. (A23) shows that the second term vanishes in this approximation. Further, the presence of the factor $(a-b)^2$ shows that it is at least of order $\Gamma^2$, as against the first term which is of order $\Gamma$. Hence we neglect the second term for subsequent purposes. Using (A22) and (A23) one obtains after $\delta$-function integration over $R_0$

$$J_1 = (16\Gamma\mu/M)\int \mathrm{d}\omega_1(8r^2(M\omega_1-3\mu^2)-16r^4)^{-\frac{1}{2}} \tag{A21'}$$

provided

$$MR_{\mathrm{m}} \geqq |M\omega_1-3\mu^2-4r^2| \tag{A24}$$

and

$$8r^2(M\omega_1-3\mu^2)-16r^4 \geqq 0. \tag{A25}$$

(A18) and (A25) lead to the inequality

$$\theta \leqq 1. \tag{A26}$$

Further, (A14) and (A24) lead to the result $t_2 \leqq t \leqq t_1$, where $t_1$, $t_2$ are the roots of the equation

$$M^2(M+\mu)t^2+2M\mu t(M\mu-3\mu^2-4r^2)-M^3t_{\mathrm{m}}t+\mu(M\mu-3\mu^2-4r^2)^2=0. \tag{A27}$$

Writing

$$t_1 = \mu t_{\mathrm{m}}\theta_1/(M+\mu), \qquad t_2 = \mu t_{\mathrm{m}}\theta_2/(M+\mu), \tag{A28}$$

we find from (A27) that

$$\theta_1,\ \theta_2 = \frac{M}{2\mu} + \frac{2\mu(2\theta-1)}{M+\mu} \pm \left[\frac{M(M+\mu)}{4\mu^2} - \frac{M}{\mu}\left(\tfrac{1}{2} + \frac{2\mu(1-2\theta)}{M+\mu}\right)^2\right]^{\frac{1}{2}}, \quad \text{(A29)}$$

where the inequality (A26) ensures that both $\theta_1$ and $\theta_2$ are real and positive quantities. The limits of $\omega_1$-integration in (A21) are thus

$$\mu+t_2 \leqq \omega_1 \leqq \mu+t_1. \quad \text{(A29')}$$

From (A18), (A21') and (A29) we have finally

$$J_1 = 2(\zeta_1-\zeta_2), \quad \text{(A30)}$$

where

$$\zeta_n = \left(\frac{4\mu\Gamma}{M^2}\right)\left(\frac{4}{\theta} - 4 + \frac{2\theta_n}{\theta}\right)^{\frac{1}{2}} \quad (n = 1,\ 2). \quad \text{(A31)}$$

Using (A19) and (A30), we now obtain the following results

$$\begin{aligned} &\int |W_1+W_2+W_3|^2\,d\tau = 3I_1+6J_1 = 6(\xi+2\zeta_1-2\zeta_2);\\ &\int |2W_1-W_2-W_3|^2\,d\tau = 6I_1-6J_1 = 12(\xi-\zeta_1+\zeta_2); \quad \text{(A31')}\\ &\mathrm{Re}\int (W_1+W_2+W_3)^*(2W_1-W_2-W_3)d\tau = 0. \end{aligned}$$

Further, the over-all decay probabilities for $\tau$ and $\tau'$ decay are given from (6) and (5') by

$$P = \int (|\lambda|^2+|\alpha|^2)d\tau, \qquad P' = \int (|\varrho|^2+|\beta|^2)d\tau. \quad \text{(A31'')}$$

Substituting in (A31'') from (8), (9) and (A31') we can determine the $\tau'/\tau$-branching ratios for the two cases $I = 0,\ 2$ which are given in eqs. (11) and (12) of the text.

(b) CHARGED DECAY MODES

The evaluation of the integrals $I_1,\ J_1$ in this case involves the additional restriction (A4) which can be expressed in terms of the variables $Q_\mu,\ R_\mu$ of (A8) in a simple and straightforward manner. The result, after taking account of (A13), is

$$0 \leqq R_0 \leqq \mathrm{Min}\ (R_m,\ 3\omega_1-M); \quad \text{(A32)}$$

$$t_s = \tfrac{1}{3}(M-3\mu) \leqq t \leqq t_m,\ t = \omega_1-\mu. \quad \text{(A33)}$$

Since (A32) involves a comparison of the magnitudes $R_m$ and $3\omega_1-M$, we find from (A14) that $R_m \geqq 3\omega_1-M$ if

$$\mu(3\mu-M+3t)^2 \leqq Mt(t_m-t).$$

This leads to $t'' \leqq t \leqq t'$, where

$$t' = \tfrac{1}{2}(M-3\mu),\quad t'' = 2\mu(M-3\mu)/(M+9\mu). \quad \text{(A34)}$$

Taking account of the restrictions imposed by (A32)—(A34) and using (A16), we obtain

$$I_1 = 4\Gamma \int_{t_s}^{t'} \frac{\mathrm{d}t}{Q^2-4\mu^2}\,\delta(Q-2\omega_r)(3t+3\mu-M)$$
$$+4\Gamma \int_{t'}^{t_m} \frac{\mathrm{d}t}{Q^2-4\mu^2}\,\delta(Q-2\omega_r)\left(\frac{M}{\mu}t(t_m-t)\right)^{\frac{1}{2}}, \tag{A35}$$

where

$$Q^2-4\mu^2 = 2M(t_m-t).$$

Now in (A35), one of the integrals will be non-zero, and this will depend on the magnitude of $r$. Writing

$$t_r = (Mt_m-2r^2)/M, \tag{A36}$$

the conditions for the first and the second integrals to be non-zero, are respectively

$$t_s \leqq t_r \leqq t' \quad \text{and} \quad t' \leqq t_r \leqq t_m.$$

These inequalities lead respectively to the results $\frac{1}{2} \leqq \theta \leqq 1$ and $0 \leqq \theta \leqq \frac{1}{2}$.

Using these results we obtain

$$\begin{aligned} I_1 &= \xi \quad \text{if} \quad 0 \leqq \theta \leqq \tfrac{1}{2}, \\ &= \eta \quad \text{if} \quad \tfrac{1}{2} \leqq \theta \leqq 1, \end{aligned} \tag{A36}$$

where $\xi$ is defined in (A20) and

$$\eta = \frac{2\Gamma}{M}\left(\frac{M+3\mu}{M\theta} - \frac{6\mu}{M}\right). \tag{A37}$$

One can see immediately that $\xi = \eta$ when $\theta = \frac{1}{2}$.

Integrals $I_2$ and $I_3$ can be evaluated in an exactly similar manner, by making transformations of the type (A8) with obvious cyclic permutations of the indices. Only the condition (A4) will impose different limits for the corresponding quantities $R_0$ and $t$ than were used for the evaluation of $I_1$, viz. (A32)—(A34). The results are as follows:

$$\begin{aligned} I_2 &= \xi-\eta \quad \text{for} \quad \tfrac{1}{2} \leqq \theta \leqq 1, \\ &= 0 \qquad \text{for} \quad 0 \leqq \theta \leqq \tfrac{1}{2}; \end{aligned} \tag{A38}$$

$$I_3 = 0 \quad \text{for all } \theta. \tag{A39}$$

As regards $J_1$, the integration variable $t$ should satisfy not only (A33) and (A34), but also (A28) and (A29′) as was the case for the evaluation of the over-all decay probabilities.

Now an algebraic comparison of the magnitudes of $t_s$, $t_1$, $t_2$, $t'$ and $t''$ leads to the following rigorous inequalities:

$$t_2 < t'' < t_s < t' \leqq t_1 \quad (\theta \geqq \tfrac{1}{2}); \tag{A40}$$

$$t_2 < t'' < t_s < t_1 \leqq t' \quad (\theta \leqq \tfrac{1}{2}). \tag{A41}$$

From (A21)—(A23) one obtains

$$J_1 = 2\Gamma\iint \frac{\mathrm{d}\omega_1\,\mathrm{d}R_0}{((M\omega_1-3\mu^2)^2-M^2R_0^2)^{\frac{1}{2}}}\left[\delta\left(\frac{M\omega_1-3\mu^2-4r^2+MR_0}{4\mu}\right)\right.$$
$$\left.+\,\delta\left(\frac{M\omega_1-3\mu^2-4r^2-MR_0}{4\mu}\right)\right]. \qquad \text{(A42)}$$

Now since, according to (A32), $R_0$ can have only positive values, only one of the $\delta$-functions in (A42) will be operative. Further, it is easily verified that

$$M\omega_1-3\mu^2-4r^2 > 0 \quad \text{for} \quad t_s \leqq t \leqq t_1,$$

which implies that only the second $\delta$-function in (A42) will make a non-zero contribution.

Now, according to (A32) and (A34), $R_m > 3t+3\mu-M$ for $t_s \leqq t \leqq t'$, so that the condition for non-zero $J_1$ is obviously given by

$$R_0 = (M\omega_1-3\mu^2-4r^2)/M \leqq 3t+3\mu-M,$$

which leads to

$$t \geqq t_0 = \mu t_m\theta_0/(M+\mu), \qquad \text{(A43)}$$

where

$$\theta_0 = \frac{M+\mu}{\mu} - 2\theta. \qquad \text{(A44)}$$

It is easily verified that $t_1 \geqq t_0 > t_s$, for $\theta \geqq \frac{1}{2}$.

Taking account of (A40), (A43) and (A44), the final limits of $t$-integration in (A42) are $t_0 \leqq t \leqq t_1$ when $\theta \geqq \frac{1}{2}$, and $t_0 \leqq t \leqq t'$ for $\theta \leqq \frac{1}{2}$. One now finds immediately that

$$\begin{aligned} J_1 &= \zeta_1-\zeta_0 \qquad (\theta \geqq \tfrac{1}{2}), \\ &= 0 \qquad\quad\ (\theta \leqq \tfrac{1}{2}), \end{aligned} \qquad \text{(A45)}$$

where $\zeta_1$ is defined as in (A31) and $\zeta_0$ is a similar expression obtained by replacing $\theta_n$ by $\theta_0$.

Integrals $J_2$ and $J_3$ can be evaluated in an exactly similar manner and are given by

$$\begin{aligned} J_2 &= \zeta_0-\zeta_3 \qquad (\theta \geqq \tfrac{1}{2}), \\ &= \zeta_1-\zeta_3 \qquad (\theta \leqq \tfrac{1}{2}); \end{aligned} \qquad \text{(A46)}$$

$$J_3 = \zeta_3-\zeta_2. \qquad \text{(A47)}$$

Here $\zeta_3$ is an expression similar to (A31), but with $\theta_n$ replaced by $\theta_3$ which is defined by

$$\theta_3 = \theta + \frac{M-\mu}{2\mu}. \qquad \text{(A48)}$$

Now, from eqs. (8) and (9) of the text it is clear that the following integrals are necessary for the computation of the charged decay modes:

$$\int |W_1+W_2+W_3|^2 \,d\tau = I_s+2J_s,$$
$$I_s = I_1+I_2+I_3, \qquad J_s = J_1+J_2+J_3; \tag{A49}$$

$$\int |2W_1-W_2-W_3|^2 \,d\tau = 2I_s-2J_s+I_p+2J_p,$$
$$I_p = 2I_1-I_2-I_3, \qquad J_p = 2J_1-J_2-J_3; \tag{A50}$$

and

$$\mathrm{Re}\int (W_1+W_2+W_3)^*(2W_1-W_2-W_3)d\tau = I_p-J_p. \tag{A51}$$

From (A36)–(A50), we have the following results:

$$\theta \geqq \tfrac{1}{2}: \quad I_s = \xi,\ I_p = 3\eta-\xi,\quad J_s = \zeta_1-\zeta_2,\quad J_p = 2\zeta_1-3\zeta_0+\zeta_2; \tag{A52}$$

$$\theta \leqq \tfrac{1}{2}: \quad I_s = \xi,\quad I_p = 2\xi,\quad J_s = \zeta_1-\zeta_2,\quad J_p = \zeta_2-\zeta_1. \tag{A53}$$

Now the probabilities $X$, $Y$, $Z$ of charged decay in descending order of magnitude of the negative pion momentum are given by

$$X = \int |A_1|^2 \,d\tau, \quad Y = \int |A_2|^2 \,d\tau, \quad Z = \int |A_3|^2 \,d\tau, \tag{A54}$$

where $A_1$, $A_2$, $A_3$ are defined in eqs. (5) of the text. Substituting in (A54) from (8), (9) and (A49)–(A53) we obtain the various ratios $X : Y : Z$ in terms of $\xi$, $\eta$, $\zeta_n$ for the two cases $I = 0$, 2 as given in eqs. (11) and (12) of the text.

## References


1) R. H. Dalitz, Phil. Mag. **44** (1953) 1068; see also R. H. Dalitz, Proc. Phys. Soc. A **66** (1953) 710
2) R. H. Dalitz, Phys. Rev. **94** (1954) 1046
3) N. C. Varshneya, Ph. D. Thesis, Göttingen (1957) (unpublished)
4) R. H. Dalitz, Proc. Phys. Soc. A **69** (1956) 527
5) A. N. Mitra and R. P. Saxena, Phys. Rev. **108** (1957) 1083

*Nuclear Physics* **6** (1958) 420—433; © *North-Holland Publishing Co., Amsterdam*
Not to be reproduced by photoprint or microfilm without written permission from the publisher

# PROTONS AND ALPHA-PARTICLES FROM THE NITROGEN BOMBARDMENT OF ALUMINIUM

A. ZUCKER

*Oak Ridge National Laboratory*†, *Oak Ridge, Tennessee*

Received 30 December 1957

**Abstract:** Aluminium targets, about 0.36 mg/cm² thick, were bombarded with 28 MeV nitrogen ions. The compound nucleus $Ca^{41}$ is excited to 39.3 MeV and may decay by proton emission to $K^{40}$, and by alpha emission to $A^{37}$. Energy distributions for protons and alpha-particles were measured at six angles from 0° to 90°. The number of protons or alphas per unit beam, divided by the channel energy and the capture cross section, plotted as a function of the square root of the excitation energy in the residual nucleus yields a value of $a$ in the level density formula $w = C \exp[2(aE)^{\frac{1}{2}}]$. The data fit this formula well at all angles giving $a = 5.0 \pm 0.2$ for $K^{40}$, and $a = 4.1 \pm 0.3$ for $A^{37}$. Angular distributions were also measured and are reasonably isotropic for protons, whereas they show a definite forward peak for alpha-particles. An even-odd effect was found in the level density of the residual nuclei, $K^{40}$ having about 2.5 times the level density of $A^{37}$. In general, the nitrogen-aluminium reaction bears out the predictions of the statistical theory for the decay of a compound nucleus.

## 1. Introduction

One of the interesting properties of heavy-ion induced nuclear reactions stems from the fact that one may achieve highly excited compound states with a relatively slow-moving incident nucleus. Thus for example, the velocity of a 28 MeV nitrogen ion is about the same as that of a 2 MeV proton. Yet in the case of the nitrogen nucleus bombarding $Al^{27}$, the compound state is excited to 39.3 MeV. It is therefore hoped that the low velocity of the nitrogen nucleus will make direct interactions relatively unimportant and that one may thus achieve a highly excited compound nucleus in which the energy is shared among all the nucleons and that the method of formation will be of no consequence in the decay [1]). Highly excited compound nuclei of this nature may be produced in the usual proton, deuteron, or alpha-particle induced reactions where the kinetic energy of the incident particle is about 30 MeV. However, in such reactions direct processes may well mask a substantial part of the compound-nucleus reaction mechanism. Other experiments in which the sharing of energy is probably complete are limited to narrow regions of excitation energy, 6 to 8 MeV

† Operated for the United States Atomic Energy Commission by the Union Carbide Nuclear Corporation.

from slow-neutron absorption and several MeV higher than this from reactions induced by particles with a few MeV kinetic energy.

The decay of the compound nucleus by light-particle emission is its most likely mode of de-excitation. Details of this mechanism have been investigated by many workers who have compared excitation functions, total cross-sections, or energy spectra of emitted particles, with the predictions of a statistical model proposed by Weisskopf and his co-workers [2]). Several fundamental parameters enter into the statistical model, among them the nuclear radius, penetrabilities of charged particles on nuclei, and the level density with its energy dependence and angular momentum dependence. In this work, no attempt was made to see what effect variation of these parameters might have on the final interpretation of the data. Rather, the simplest model was used, mainly because it was tried first and produced as good a fit with the data as could reasonably be expected of any model.

Previously at this laboratory, the statistical model was used to interpret the nitrogen-induced reactions in sodium [3]) and the light-particle spectra [4, 5]) from the nitrogen bombardment of $Li^6$, $Li^7$ and $Be^9$. The same model was used elsewhere to interpret the results of the nitrogen and oxygen-induced nuclear reactions in copper [6]). The emission of protons and alpha-particles, from the bombardment of nuclei in emulsion with 100 MeV nitrogen ions [7]) has also been studied. It was found that, in this case, protons were emitted isotropically whereas the alpha-particles exhibited a pronounced forward peak. An excess of alpha-particles was found in this experiment.

In the experiment reported here, thin $Al^{27}$ targets were bombarded by 27.9 MeV nitrogen ions and the energy spectra of protons and alpha-particles produced by this reaction, were measured at 0°, 30°, 45°, 60°, 75° and 90°. Angular distributions were obtained for both protons and alpha-particles. The energy dependence of the level density is compared with the predictions of the statistical model of nuclear reactions, as is the relative probability of proton vs. alpha-particle emission.

## 2. Experimental Method

Aluminium foil, about 0.36 mg/cm² thick, was bombarded with 27.9 MeV nitrogen ions produced by the Oak Ridge National Laboratory heavy-particle cyclotron. The foil was in a 2.5 inch diameter cylindrical reaction chamber which had a 0.5 mil mylar exit window fastened on by Gelva resin. The incident beam was collimated by a circular aperture 3/16″ in diameter. After passing through the target, the nitrogen beam was stopped by a 10 mg/cm² nickel foil. Light reaction products such as protons, deuterons or alpha-particles passed through the window, and at 0° also through the

nickel foil, crossed a 4 cm air path and entered a proportional counter filled with a mix tureof 90 % argon, and 10 % methane. The counter was filled to 1.1 atm for proton detection and to 0.5 atm for alpha-particle detection. After crossing the proportional counter, the particles were stopped in a NaI(Tl) scintillation counter. The two counters formed a telescope which was encased in a three-layer soft iron magnetic shield necessary for the operation of the photomultiplier tube in the 1 000 oersted fringing field of the cyclotron magnet. Since the beam emerges vertically from the cyclotron, the plane of rotation of the counters was also vertical. All angles were measured from horizontal by means of a bubble protractor accurate to about 0.2 degrees.

It was important, in this experiment, to distinguish between various light reaction products and to this end a $dE/dx$ and $E$ particle identification scheme was used. In this method, the energy loss ($dE/dx$) which the particle suffers in the proportional counter, and its energy ($E$) as measured by the scintillation counter, suffice to identify it and measure its energy at the same time. The scheme used here was developed by Goodman and Need [4]) and operates as follows: both the $dE/dx$ and $E$ pulses, after passing through conventional linear preamplifiers and amplifiers, are shaped to have a flat top for a few microseconds. The $E$ pulse is then fed to the horizontal plates of an oscilloscope (Tektronix 541) and the $dE/dx$ pulse to the vertical plates. The oscilloscope is unblanked by a short intensifier pulse while both counter pulses are flat, so that the net result of a particle passing through both counters is a spot on the oscilloscope whose horizontal displacement is proportional to the energy of the particle and whose vertical displacement is proportional to the energy loss in the proportional counter. It is well-known that the product $E \cdot dE/dx$ is approximately constant for any one species of particle over the energy which concerns us here. There appear on the oscilloscope face hyperbolae of spots corresponding to alpha-particles, protons, deuterons, etc. A photograph of the scope face like the one shown in fig. 1 is then taken with a Fairchild oscilloscope camera using a Polaroid Land film. The photograph, which reproduces the oscilloscope face with unit magnification, is cut so as to provide a mask through which spots produced by only one kind of particle are visible. This mask is taped to the oscilloscope face, a multiplier photo-tube views the spots and gates a 20-channel pulse-height analyzer whenever a spot is visible through the mask. Meanwhile, the $E$ pulses are also fed separately to the 20-channel analyzer and thus an energy spectrum of any one particle species is obtained.

The aluminium target was 2.8 MeV thick for the zero degree runs. At larger angles, the target was tilted to make an angle $\frac{1}{2}\theta$ with the beam, where $\theta$ is the laboratory angle at which particles were counted. The target thickness then is 0.36 mg cm$^{-2}$/cos $\frac{1}{2}\theta$, and this was used in calculating the

mean energy of the beam in the target, as well as in calculating relative cross sections at different angles. A target should be much thinner for experiments of this sort, but the yield from the reactions was just marginal even under these circumstances. The usual beam was of the order of 0.1$\mu$A. The low yields are due to the high Coulomb barrier for nitrogen ions on aluminium.

The angular acceptance of the counter telescope was $\pm 3°$ defined by the cross section of the beam and the exit port on the proportional counter. The resolution of the scintillation counter was 2.2 % for 20 MeV protons. The proportional counter resolution varied somewhat from day to day depending on the length of time it was pumped before filling and also on the pressure in the counter. Typical resolution for the proportional counter was 12 % when filled to 1.1 atm for proton detection.

In practice, new aluminium targets were installed daily, and more frequently whenever it seemed that impurities were present, probably in the form of baked-on pump oil.

There is one aspect of this particle identification scheme which the author found very useful. Photographs of the scope face, such as illustrated in fig. 1, show immediately whether the proportional counter has sufficient resolution, whether the electronic circuits are operating properly, and an intense proton recoil peak shows excessive target impurity. Thus, after cursory examination of the photograph, it becomes obvious whether the apparatus is in working order, or if not wherein the trouble probably lies.

The $E$ channel was calibrated every few hours during a run by the 1.12 MeV $Zn^{65}$ $\gamma$-ray. A $Zn^{65}$ source was placed near the scintillation counter and the high voltage supply of the P. M. tube adjusted until the photopeak fell into a certain channel on the 20-channel analyzer. Thus, the gain of the entire system was kept constant over many weeks of running time. Additional details of the apparatus and the measurement of the NaI(Tl) response to protons and alpha-particles are described elsewhere [4]).

## 3. Results

The energy spectra of protons, at four angles, from the nitrogen bombardment of $Al^{27}$ are shown in fig. 2. The number of protons is plotted as a function of their energy after leaving the target. The ordinate is corrected for the non-linearity of the channel vs. energy relation due to absorber present between the scintillation counter and target. The curves for various angles are displaced arbitrarily to keep the experimental points from overlapping. The relative yields at various angles must be deduced from the angular distribution curves given below.

A similar plot is shown for alpha-particles in fig. 3. Complete alpha-

particle runs were taken at six angles because considerable anisotropy in the angular distribution was suspected after some preliminary runs.

Typical errors shown on these curves are statistical errors. In further analysis of the data, the spread in the incident energy makes other errors such as the finite angular acceptance and the uncertainty in the scintillation

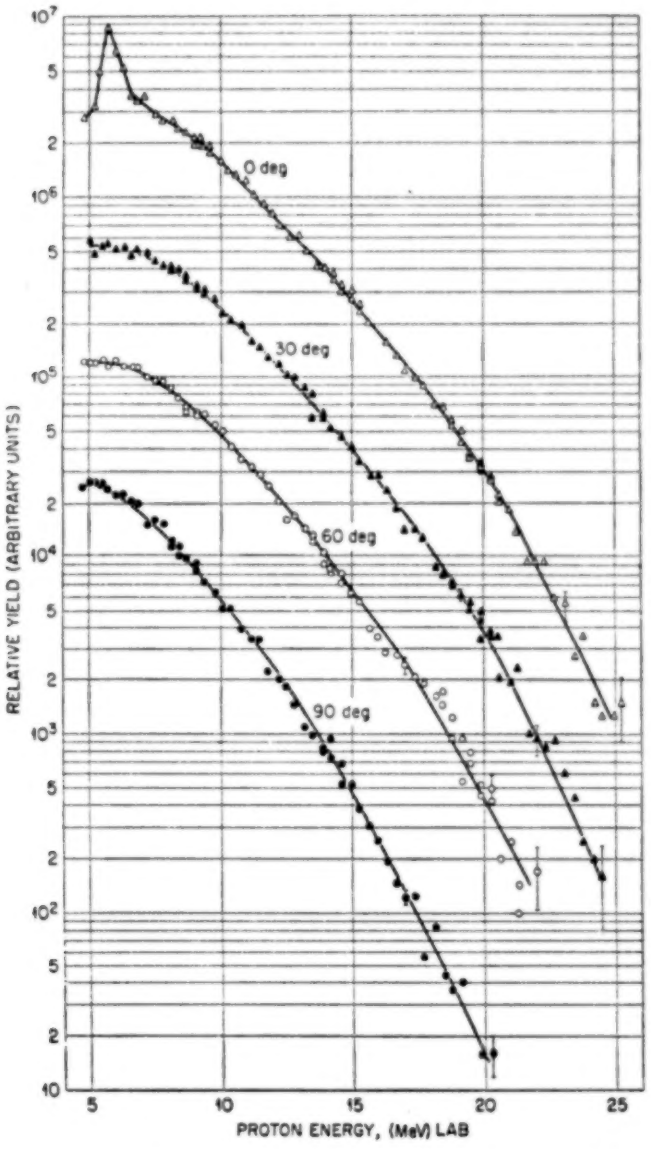


Fig. 2. Energy spectra of protons from the nitrogen bombardment of aluminium. The spectra, at various angles, are displaced from one another arbitrarily to avoid overlapping. Typical statistical errors are shown.

counter response negligible. It also makes for a smooth curve in which structure with a width of an MeV or less is not likely to be found. In fact, in the following sections, smooth lines drawn through the points in figs. 2 and 3 were used in the analysis, rather than the individual experimental

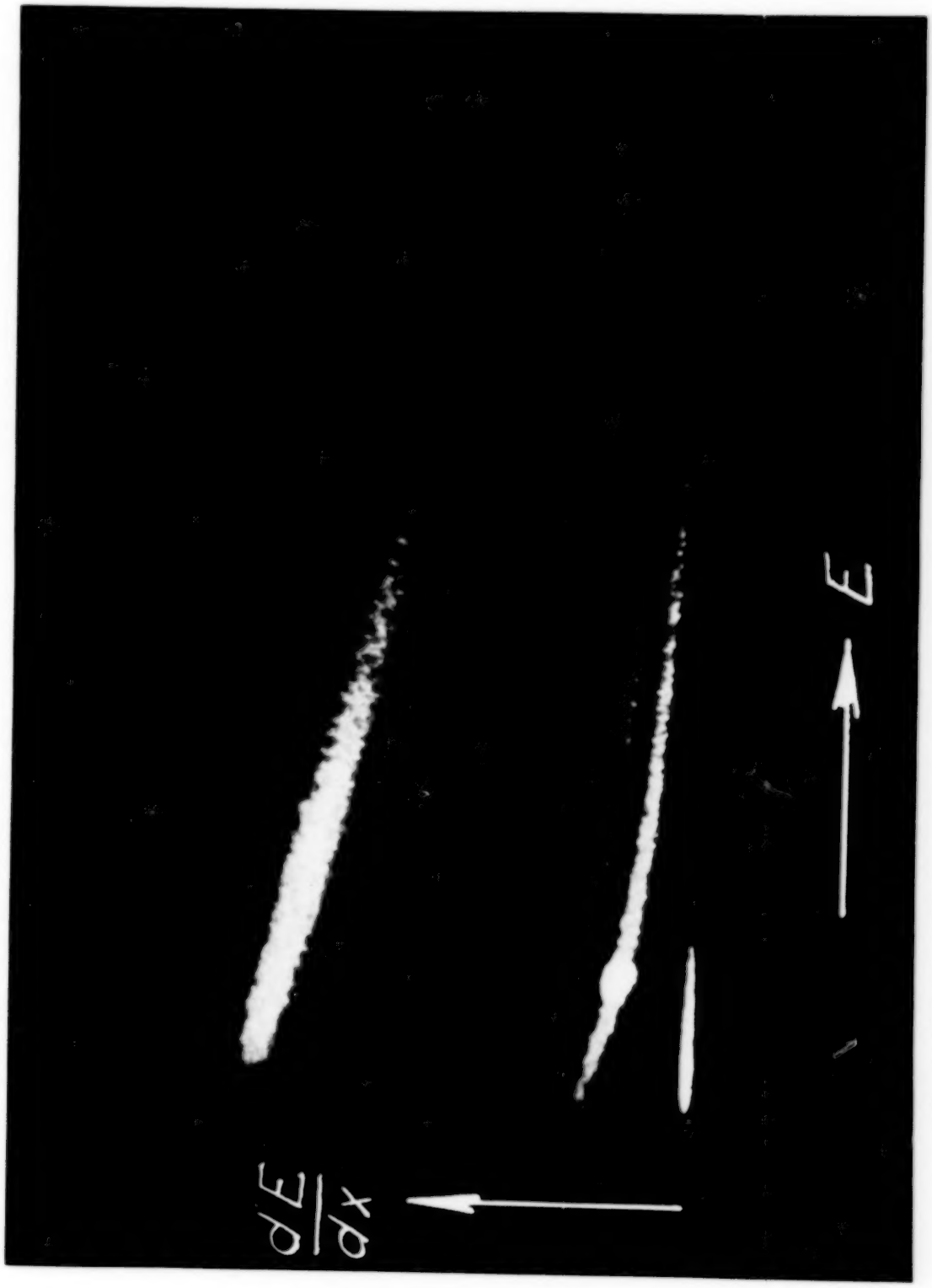


Fig. 1. Photograph of the oscilloscope face showing spots produced by protons, deuterons, tritons and alpha-particles. This photograph was obtained with a $Li^7$ target which produces deuterons and tritons more copiously than an aluminium target.

points. This procedure is justified because of the thick target, because particles corresponding to resolvable levels near the ground state of the residual nucleus were not emitted in sufficient number to be observed, and finally because only statistical aspects of the reaction were looked for so that a degree of smoothing may actually be desirable.

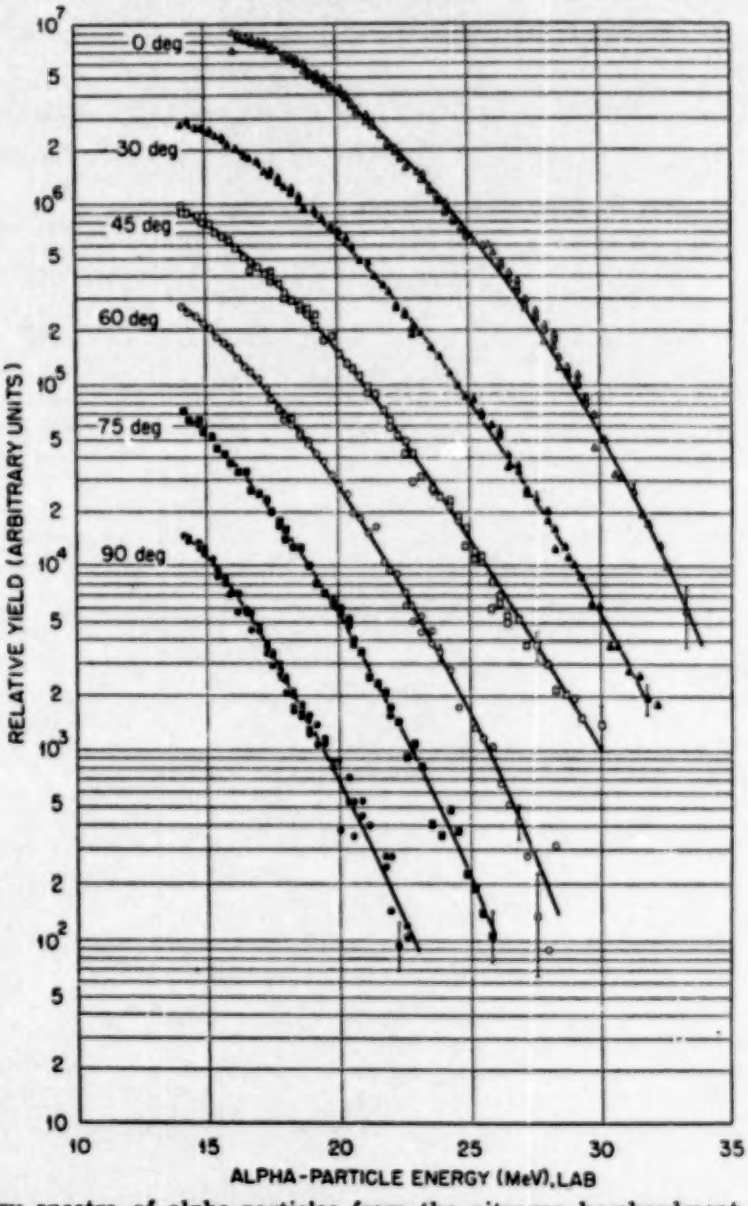


Fig. 3. Energy spectra of alpha-particles from the nitrogen bombardment of aluminium. The spectra, at various angles, are displaced from one another arbitrarily to avoid overlapping. Typical statistical errors are shown.

## 4. Discussion

### 4.1. ANGULAR DISTRIBUTIONS

Angular distributions of protons and alpha-particles were calculated from the experimental counting rates. The beam current was measured

and integrated for each run so that one had the absolute number of counts for each species of particle at each angle as a function of incident beam. To get angular distributions, we deduce from the particle laboratory energy the energy of excitation $E^*$ with which the residual nucleus is left. This conversion is, of course, different at different angles, but such kinematical manipulations are simple to carry out. The excitation energy is equivalent to the channel energy except for an additive constant. Counting rates at each $E^*$ are corrected for solid angle and for target thickness to produce angular distributions for protons and alpha-particles shown in fig. 4 and fig. 5. The errors shown at the end of each curve represent the errors for all the points on that curve. The errors here include the uncertainty and drift

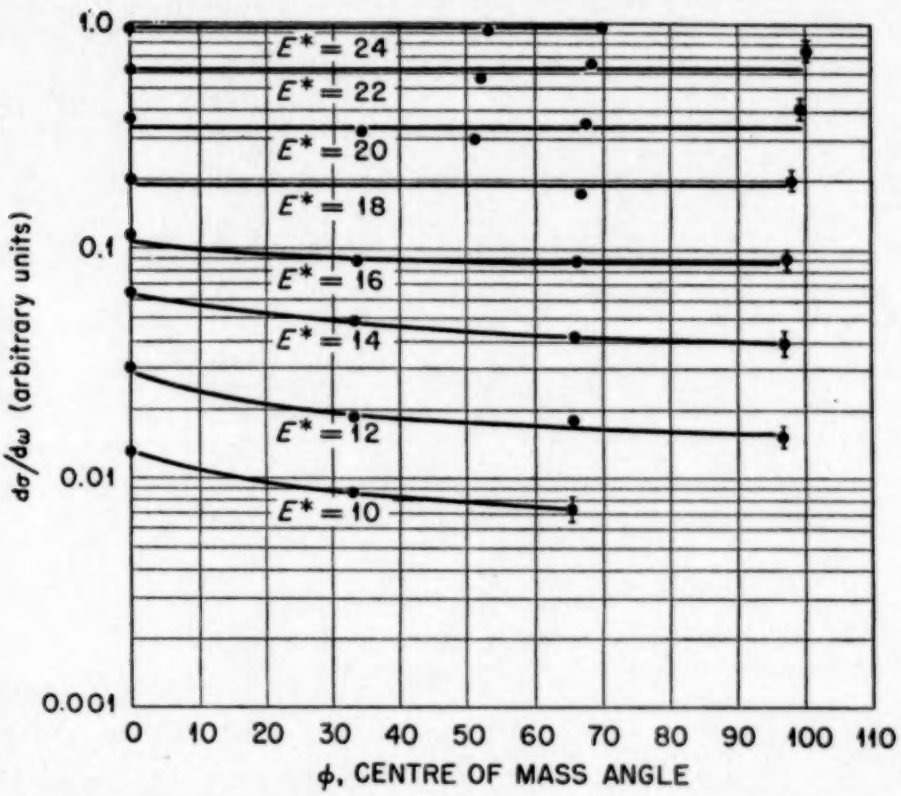


Fig. 4. Angular distribution of protons from the nitrogen bombardment of aluminium. Absolute errors, indicated for the last point, apply for all points on that curve. The relative intensities of the various curves are correctly represented by the ordinate.

of the beam integrator, the variation in target thickness, and statistical errors. At 0°, background counts from impurities deposited on the nickel beam stop were subtracted. The beam stop was changed frequently and the background, which was measured with the target withdrawn, did not exceed 10 % of the true counting rate.

One may see from these angular distributions that protons are emitted isotropically, except that at high proton energies (low $E^*$) there is a forward

peak with a maximum peak-to-valley ratio of about two. The $\cos \frac{1}{2}\theta$ correction for target thickness tends to produce a peak in the forward direction. As the angle $\theta$ increases, the target thickness increases also. Since the cross sections are smaller at lower nitrogen energies, the increase in target thickness does not produce a corresponding increase in counting rate. This effect would produce, at most, a decrease of 20 % from 0° to 90°. However, the largest anisotropy is to be found between 0° to 30° and this cannot be ascribed to the thickness of the target.

The alpha-particle angular distributions are similar to the proton curves, except that here the forward peaks are more pronounced and there seems to be a trough at 60°. Again, the anistropy is greater at higher alpha energies but it persists even at lower energies where the proton spectra appear flat.

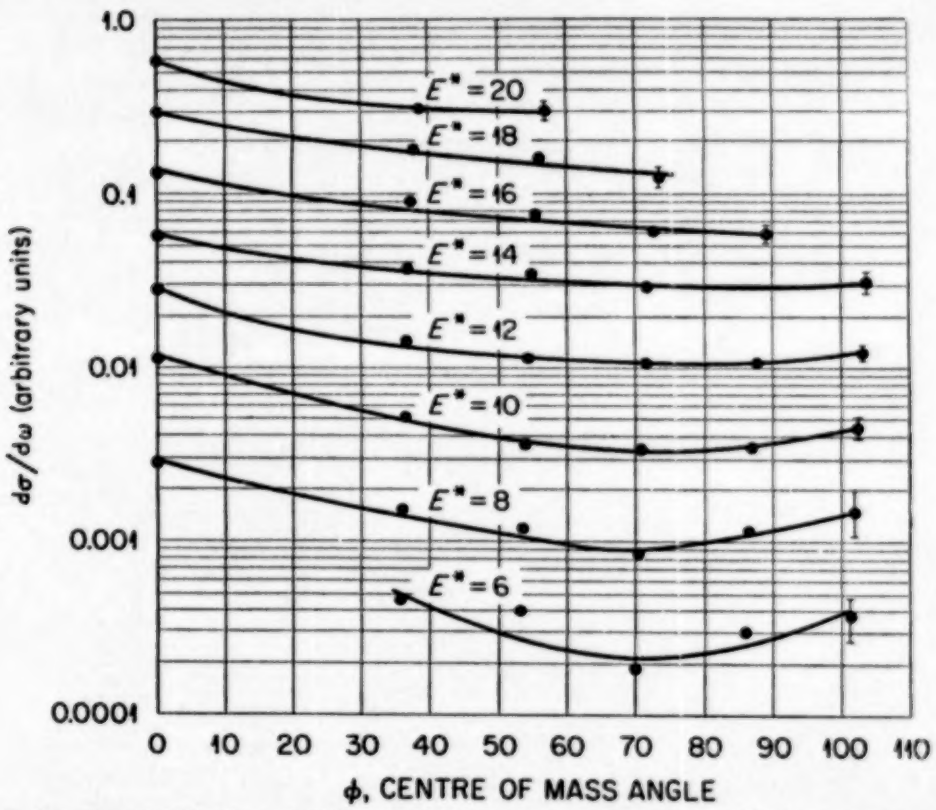


Fig. 5. Angular distribution of alpha-particles from the nitrogen bombardment of aluminium. Probable errors, indicated for the last point, apply for all points on that curve. The relative intensities of the various curves are correctly represented by the ordinate.

### 4.2. ENERGY DISTRIBUTIONS

One may plot the energy distribution of light particles in many ways; the one chosen here is designed to show the fit of the data to the simplest evaporation theory based on the statistical model as described by Blatt and Weisskopf [8]). The energy dependence of evaporated particles is given by

$$N(\varepsilon)\mathrm{d}\varepsilon = \mathrm{Const}\ \varepsilon\sigma_c(\varepsilon)w\mathrm{d}\varepsilon. \qquad (1)$$

Here $\varepsilon$ is the channel energy, $\sigma_c$ is the capture cross section of the particle of energy $\varepsilon$ on the residual nucleus, $w$ is the level density of the residual nucleus at an excitation energy $E^*$ corresponding to the channel energy $\varepsilon$, where $\varepsilon = E^*_{max} - E^*$. The level density $w$ is given in a simple form as

$$w = C \exp [2\sqrt{aE^*}]. \tag{2}$$

From eqs. (1) and (2) one can see that log $(N/\varepsilon\,\sigma_c)$ plotted as a function of $\sqrt{E^*}$ should result in a straight line and from the slope of this line one may obtain the value of the constant $a$. The constant $C$ does not affect the energy distribution, but is related to shell effects and the even-odd character of the residual nucleus.

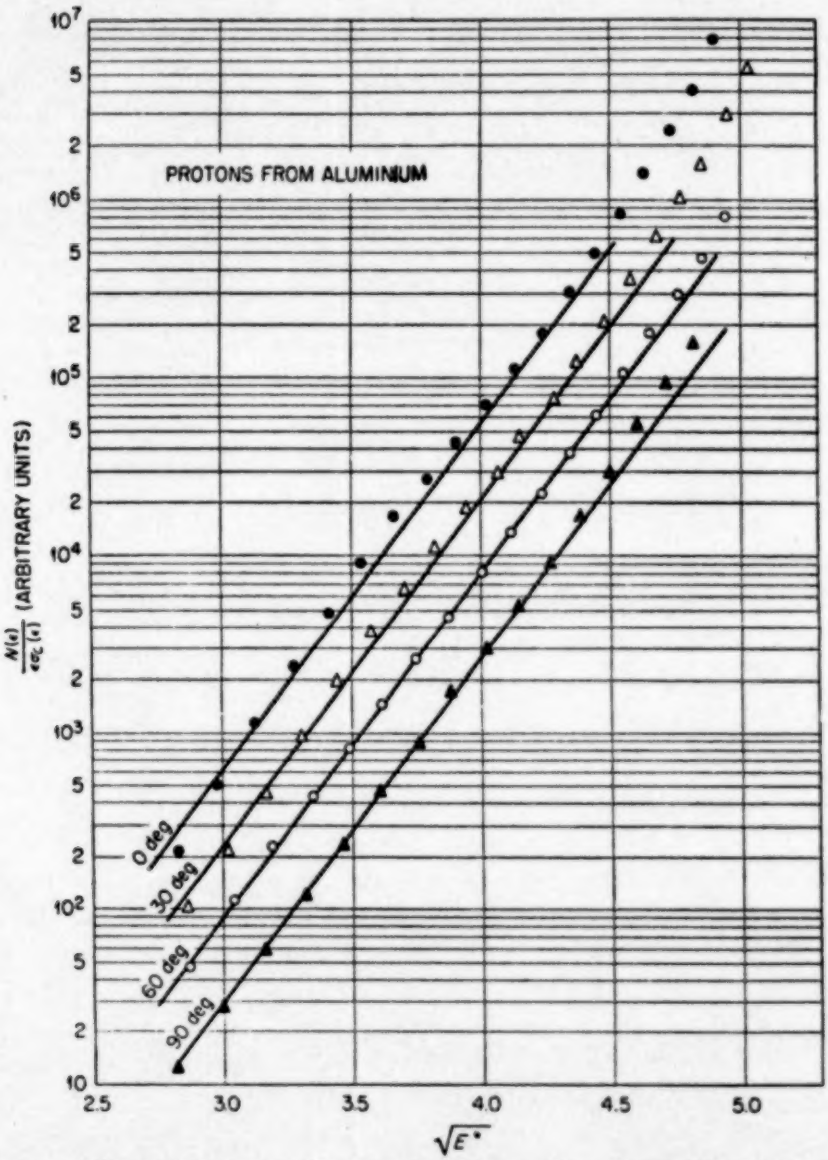


Fig. 6. The logarithm of the normalized energy distribution of protons plotted as a function of the square root of the excitation energy of the residual nucleus. The various angles are displaced arbitrarily to avoid overlapping.

Figs. 6 and 7 show such plots for four angles for protons and for six angles for alpha-particles. The points, shown in these figures were obtained from the smoothed energy spectra, read at 1 MeV intervals. The spread in $E^*$, due to the target thickness, is not shown in figs. 6 and 7. The values of $\sigma_c$ were obtained from the work of Shapiro [9]), using $r_0 = 1.5 \times 10^{-13}$ cm, and by linear interpolation for the desired value of $Z$. The tables of Shapiro do not extend to sufficiently high energies. In those regions an asymptotic formula was used:

$$\sigma_c = \pi(R+\lambda)^2 \left[1 - \frac{Z_1 Z_2 e^2}{\varepsilon(R+\lambda)}\right]. \tag{3}$$

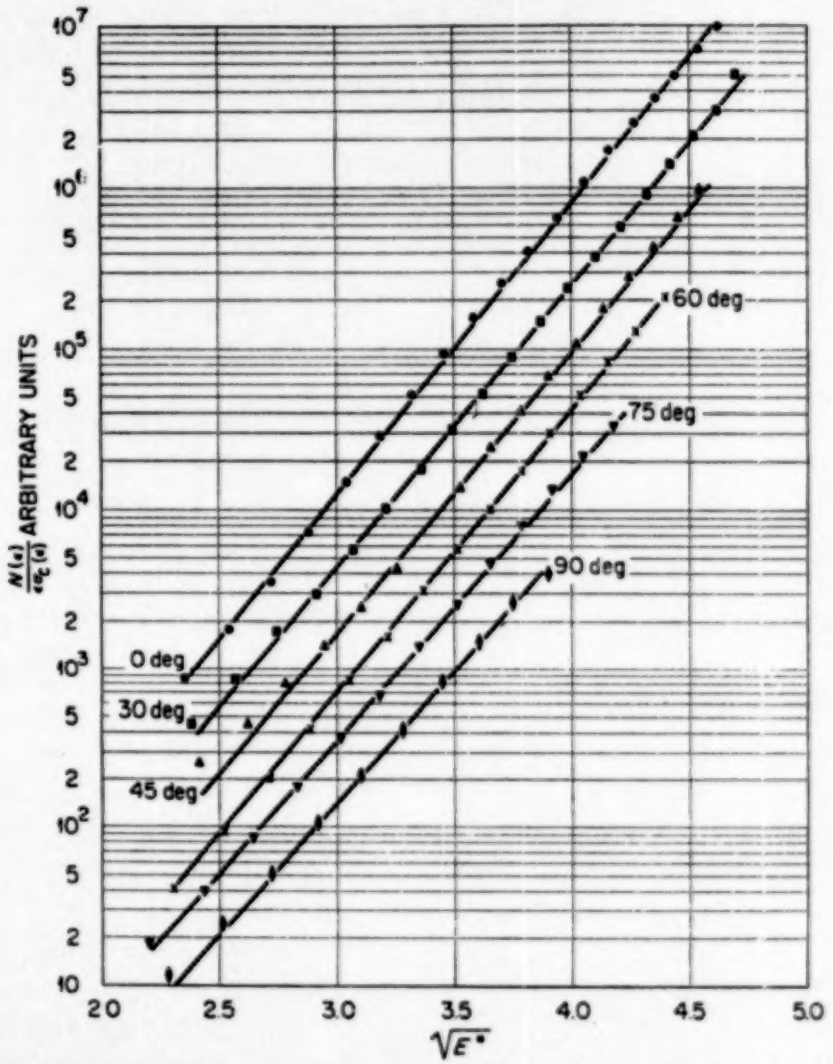


Fig. 7. The logarithm of the normalized energy distribution of alpha-particles plotted as a function of the square root of the excitation energy of the residual nucleus. The various angles are displaced arbitrarily to avoid overlapping.

All counting rates were corrected for solid angle and channel width. Wapstra's tables [10]) were used for all mass values necessary to calculate reaction energies.

It can be seen that in figs. 6 and 7, the data fall on straight lines which bear out the applicability of the relation given in eq. (2) for this type of nuclear evaporation. The question of the so-called second particle arises naturally at this point. All protons above 5 MeV are counted and it is probable that many of them will have been emitted after one or even two particles have already left the compound nucleus. However, it can be shown [11]) that second particle emission will not seriously distort the shape of the straight lines until one gets to very low particle energies, of the order of 6 or 7 MeV for protons. This will affect only the points of fig. 6 which lie above $\sqrt{E^*} = 4.5$ MeV$^{\frac{1}{2}}$. At low particle energies, it is therefore not surprising to find the data curving upwards from the straight lines, i.e. there is an excess of low energy protons. The above discussion applies to alpha-particles as well as to protons. For both, there appears to be a deviation from pure exponential behavior at forward angles, and best agreement at 90°. All kinematic calculations, such as solid angle corrections and the evaluation of $E^*$, were based on the assumption that the particle counted was the first one emitted.

## 5. Conclusions

The values of $a$ which are deduced from the slopes of the lines in figs. 6 and 7 are $a = 5.0 \pm 0.2$ for protons at all four angles. For alpha-particles $a = 4.37 \pm 0.3$ for $\theta = 0°$, $a = 4.25 \pm 0.3$ for $\theta = 30°$, 45°, 60° and $a = 3.80 \pm 0.3$ for $\theta = 75°$ and 90°. While all these values agree with an average $a = 4.1 \pm 0.3$ to within the estimated error, there does seem to be a systematic drop in $a$ at larger angles. It is not obvious whether there is any connection between the variation of $a$ with angle and the anisotropy in the angular distribution. The error in $a$ of $\pm 0.2$ for protons and $\pm 0.3$ for the alpha-particles is an estimate arrived at by drawing lines of various slopes through the points.

Lang and Le Couteur [12]) have summarized some experimental results concerning the magnitude of $a$ and its dependence on the atomic number $A$. They show that a function $a = A/10.5$ fits the values of $a$ obtained by Gugelot [13, 14]) from (p, n) and (p, p') reactions, and by Skyrme and Williams [15]) from 150 MeV proton bombardment. A theoretical fit of the statistical model to experimental determinations of excitation functions has been used by Porges [14]), Brolley, Fowler and Schlacks [15]) and Bleuler, Stebbins and Tendam [16]). In these cases, high energy alpha-particles or neutrons were used to produce the reactions and the values of $a$ are invariably smaller ($a = 2.2$ for Cu targets, or $a = 2.5$ for Ag targets) than the ones cited by Lang and Le Couteur, and they do not exhibit any strong dependence on $A$ as would be expected from a Fermi gas model of the nucleus. Ex-

periments by Eisberg, Igo and Wegner [19]) show that the energy distribution of protons from bombardment with 40 MeV alpha- particles of Cu, Ag and Au, gives a value of $a$ which varies from 1.2 to 1.4 and again does not show the characteristic $A$-dependence. Halbert *et al.* [3]) have shown that $a = 3.6$ gives a fair fit (within a factor of 2) for the observed ratio of the cross-section of two nitrogen-induced reactions in Na. They show that the value of $a$ should be considerably higher than those determined from alpha or neutron-induced reactions. On the other hand, the Saclay group [6]) has achieved the best fit for nitrogen and oxygen-induced reactions in Cu by using $a = 2$. Goodman and Need [4, 5]) have found that particle spectra, from nitrogen reactions on Be and Li, give a value for $a$ between 1 and 1.5, where the residual nucleus has a mass around 18. This is not inconsistent with $A/10.5$. It may be argued that in this case the nuclei are too light for the statistical model to apply.

Inspection of figs. 6 and 7 will show that even a small amount of direct interaction leading to an excess of high-energy particles may serve to lower the value of $a$ drastically. For example, increasing by an order of magnitude the number of high-energy particles (low values of $E^*$) will reduce $a$ for protons from $a = 5$ to $a = 2$, meanwhile increasing the total cross section by only 5 %. This shows that extreme care must be used in interpreting data on the basis of the statistical model, for reactions where direct interaction may play even a small part.

An attempt was made to fit the proton data at $0^0$ to a more detailed level density formula proposed by Newton [20]). The data, suitably divided by the channel energy and the barrier correction, are normalized to the theoretical curve at $U = 15$ MeV. The fit of the experimental points with the level density given in equation 32 of Newton's paper is shown in fig. 8. It is not too good at high particle energies, and it is certainly worse than the fit to the pure exponential level density. It must be pointed out that Newton's formula contains the level density for zero spin only. The spin dependence $(2J+1)$ was not included here because it is not clear where the particular $J$-values have their lowest state. Also, the total angular momentum in the compound nucleus has a range of values over which one must average. In any event, any added $(2J+1)$ dependence would produce better agreement between theory and experiment since it serves to raise the high-energy portion of the theoretical curve.

The relative probability of proton emission compared to alpha-particle emission can also be deduced from the present work. This probability is

$$P = \frac{[M\varepsilon\sigma_c w(E^*)]_p}{[M\varepsilon\sigma_c w(E^*)]_\alpha}(2s+1). \qquad (4)$$

Here $M$ is the reduced mass of the outgoing particle and $s$ is its spin. The

other terms have been defined before. The expression assumes that the statistical process averages, over all momentum variables except $s$. The ratio of protons to alpha-particles evaluated at the same $E^*$ and corrected by the known factors in eq. (4), then gives the ratio of level densities in the residual nuclei $K^{40}$ and $A^{37}$. The difference in level densities is due to the odd-even nature of the nuclei and its effect on the level density, and to differences caused by shell structure. The ratio $R$ as determined from experimental data and eq. (4) is $R = 2.5 \pm 0.2$. This value holds for most of the data. $R$ may get as large as 3.5 or 4 at low values of $E^*$ when second protons become important, and where, as we have seen before, there

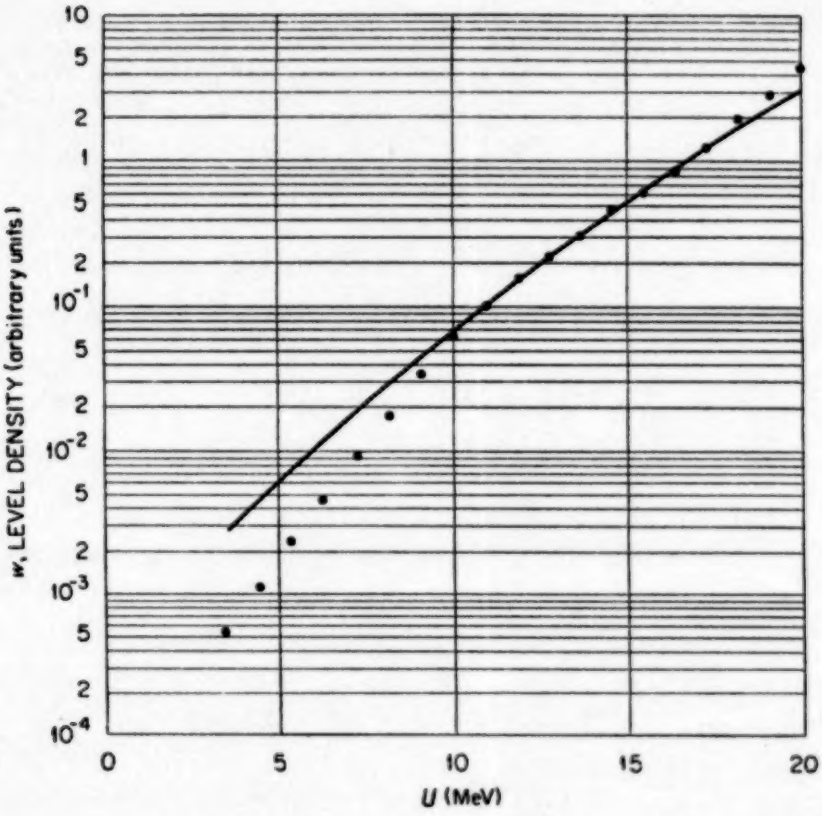


Fig. 8. Proton energy distribution compared to Newton's theoretical prediction for $J = 0$. The dots are experimental points, the solid line is the theoretical curve. The two are normalized at 15 MeV.

is excess of low-energy protons. Alpha-particles are not as likely to be emitted as second particles because the Coulomb barrier for them is much higher. The more pronounced forward peak of the alpha-particles serves to lower the value of $R$ at $0^0$ to $R = 2.3 \pm 0.3$, except at very high excitations, $E^* > 20$ MeV, when it drops even further to about 1.3. This can be seen qualitatively, from the angular distribution curves, and is due

to an excess of low-energy alphas at $0^0$. Over the greatest portion of the entire angular and energy region $R = 2.5 \pm 0.3$ is a good representation of the experimental data. Indeed $K^{40}$, being an odd nucleus (of even mass), should have a greater level density than $A^{37}$ which is an odd mass nucleus. This is borne out by the present experiment. In fact, from the work of Newton [20]), one obtains a value of $R = 2.13$ which is in good agreement with the results of this experiment.

It may be concluded that nitrogen-induced nuclear reactions in aluminium proceed mostly through a true compound nucleus which decays by particle emission, largely in accord with the predictions of the statistical theory. The absolute values of $a$ agree reasonably well with the theory [12]), the level density increases exponentially with the square root of the energy, the angular distributions are nearly isotropic, and the relative number of protons and alpha-particles also agrees with theoretical predictions.

The author is indebted to C. D. Goodman and M. L. Halbert for many discussions, to L. D. Wyly whose help was invaluable during one series of runs, to J. G. Harris who constructed the apparatus and to G. A. Palmer for help in the later runs. The cyclotron crew, A. W. Riikola and H. L. Dickerson, deserves thanks for providing steady beams over long periods of time.

## References

1) N. Bohr, Naturw. **24** (1936) 241
2) V. F. Weisskopf, Phys. Rev. **52** (1937) 295
3) M. L. Halbert, T. H. Handley and A. Zucker, Phys. Rev. **104** (1956) 115
4) C. D. Goodman and J. L. Need, Phys. Rev. (in press)
5) C. D. Goodman (in preparation)
6) J. Beydon, R. Chaminade, M. Crut, H. Faraggi, T. Olkowsky and A. Papineau, Nuclear Physics **2** (1956/57) 593
7) D. M. Parfanovich, N. V. Rabin and A. M. Semchinova, J. Exptl. Theoret. Phys. (U.S.S.R.) **31** (1956) 188
8) J. M. Blatt and V. F. Weisskopf, Theoretical Nuclear Physics (J. Wiley and Sons, New York, 1952) Ch. VIII
9) M. M. Shapiro, Phys. Rev. **90** (1953) 171
10) A. H. Wapstra, Physica **21** (1955) 367
11) H. R. Brewer, private communication
12) J. M. B. Lang and K. J. LeCouteur, Proc. Phys. Soc. A **67** (1954) 586
13) P. C. Gugelot, Phys. Rev. **81** (1951) 51
14) P. C. Gugelot, Phys. Rev. **93** (1954) 425
15) D. M. Skyrme and W. S. C. Williams, Phil. Mag. **42** (1951) 1187
16) K. G. Porges, Phys. Rev. **101** (1956) 225
17) J. E. Brolley, Jr., J. L. Fowler and L. K. Schlacks, Phys. Rev. **88** (1952) 618
18) E. Bleuler, A. K. Stebbins and D. J. Tendam, Phys. Rev. **90** (1953) 460
19) R. M. Eisberg, G. Igo and H. E. Wegner, Phys. Rev. **100** (1955) 1309
20) T. D. Newton, Can. Jour. Phys. **34** (1956) 804

*Nuclear Physics* **6** (1958) 434—439; © *North-Holland Publishing Co., Amsterdam*

Not to be reproduced by photoprint or microfilm without written permission from the publisher

# INELASTIC DEUTERON SCATTERING FROM CHROMIUM AND COBALT

F. A. EL BEDEWI and S. TADROS

*Faculty of Science, University of Alexandria*

Received 7 January 1958

**Abstract:** A magnetic spectrograph with photographic detection is used to study the angular distribution of some deuteron groups inelastically scattered from chromium and cobalt. The incident deuterons have an energy of about 8.7 MeV.

An observed level in $Cr^{52}$ at $1.44 \pm 0.02$ MeV is found to have spin $2^+$ supporting the recent theoretical prediction of Lawson and Uretsky [12]). Three levels in $Co^{59}$ at 1.27 MeV, 1.54 MeV and 1.75 MeV, with errors of 0.02 MeV, are observed. The angular momentum transferred to this nucleus at the 1.27 MeV level is found to be 2 units.

## 1. Introduction

In deuteron induced reactions, information about the nuclear properties of excited levels in residual nuclei have been successfully obtained when the angular distributions of the outgoing particles are compared with theoretical curves based on deuteron stripping mechanism. In the case of inelastic deuteron scattering, the theory proposed by Huby and Newns [1]) assumes that one of the nucleons of the incident deuteron interacts with the target nucleus but instead of being captured, it bounces off and rejoins its partner in the deuteron. Although this theory allows a determination of the value of the orbital angular momentum transferred to the target nucleus, the broadening in the experimental curves observed by El Bedewi [2]) and Hinds and Middleton [3]) requires some modifications to the approximations introduced in the theory. For this purpose, more experimental results concerning different target nuclei are needed.

In the course of studying the (d, p) reactions on some medium heavy nuclei [4]) some deuteron groups have been observed. In this paper we report the results obtained from the deuteron bombardment of $Cr^{52}$ and $Co^{59}$. Up to now, no inelastically scattered deuteron groups had been observed from either nucleus.

## 2. Procedure

Thin targets of chromium (0.5 mg/cm$^2$) and cobalt (1.5 mg/cm$^2$) were bombarded by deuterons accelerated by the Liverpool 37-inch cyclotron. The outgoing particles were analysed, at each angle of observation, by a heavy particle magnetic spectrograph [5]) and detected by Ilford $C_2 - 100\,\mu$ photographic plates. At Alexandria University, a binocular microscope was used in scanning a strip of width 8 mm centred about the axis of each plate.

Each point on the deuteron spectra will thus represent the number of deuterons counted in an area of $0.8 \times 8$ mm$^2$. Discrimination between deuterons and other particles was done on the basis of their differences in track lengths. The energy of each deuteron group was obtained from range measurements and applying the range-energy curve of El Bedewi[6]). For determining the energy of the incident deuterons, the mean value was derived from the elastically scattered deuteron groups, at various angles of observation, from the target nuclei as well as from the oxygen and carbon contamination. In the case of chromium, the mean value is found to be $8.67 \pm 0.02$ MeV while for the cobalt experiment it is equal to $8.70 \pm 0.02$ MeV. The relative beam intensities, at exposures performed at different angles of observation, were monitored by small photographic plates placed near the target and making an angle of 90° with respect to the direction of the incident deuteron beam. Detailed description of the experimental arrangement and procedure have been reported by Green and Middleton [5]) and El Bedewi [2]).

## 3. Results and Discussion

### 3.1. CHROMIUM

A typical deuteron spectrum at an angle of observation 57° is shown in fig. 1. Groups denoted by Cr, O and C are attributed to the elastically scatter-

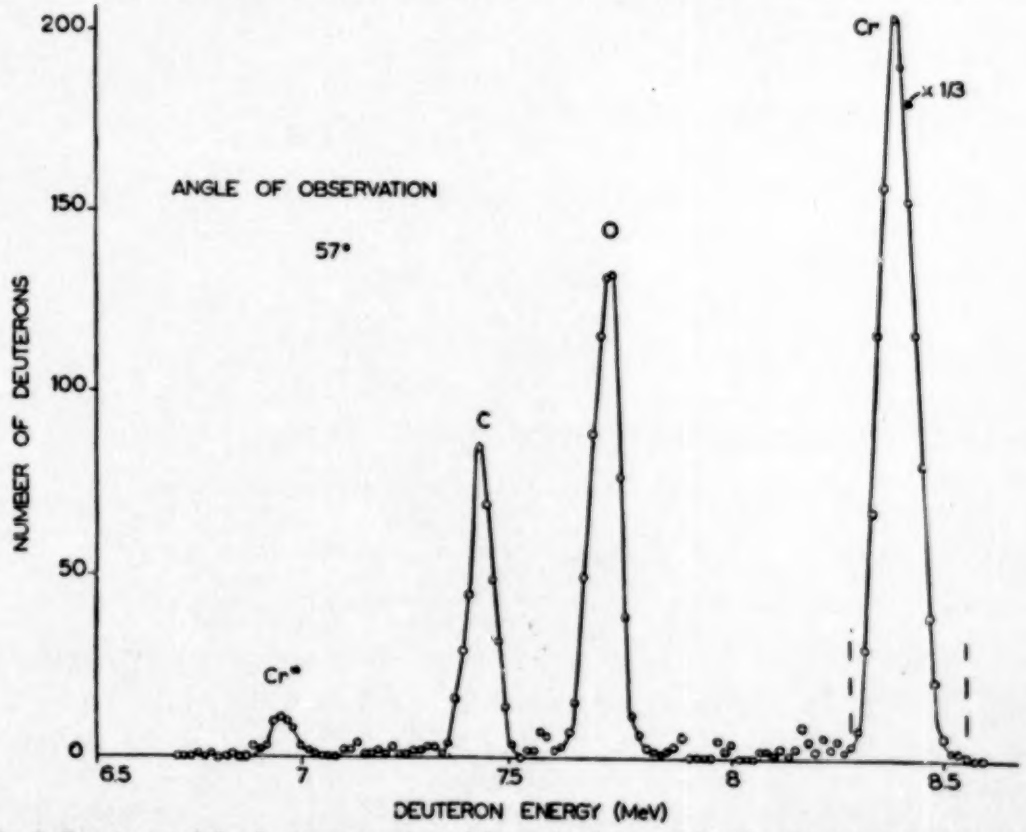


Fig. 1. Spectrum of the deuterons scattered from the deuteron bombardment of the chromium target.

ed deuteron groups from the chromium isotopes, oxygen and carbon. The weak group labelled Cr* was assumed to correspond to deuterons inelastically scattered from the most abundant isotope 52 of chromium. The mean value of the corresponding level in $Cr^{52}$ is found to be $1.44 \pm 0.02$ MeV, in excellent agreement with those determined from other reactions as shown in the following table.

| Reaction | Energy level in $Cr^{52}$ (MeV) | Reference |
|---|---|---|
| (d, d′) | $1.44 \pm 0.02$ | Present |
| (p, p′) | $1.45 \pm 0.02$ | Hausman *et al.* [7]) |
| (n, n′) | $1.44 \pm 0.05$ | Beghian *et al.* [8]) |
| $Mn^{52}$ ($\beta^+$) | 1.46 | Peacock and Deutsch [9]) |
| $V^{52}$ ($\beta^-$) | $1.44 \pm 0.02$ | Leblanc *et al.* [10]) |
| $Mn^{53}$ (p, α) | $1.434 \pm 0.016$ | Mazari *et al.* [11]) |
| Theoretical | 1.41 | Lawson and Uretsky [12]) |

The angular distribution of this deuteron group is plotted in the centre of mass system as shown in fig. 2. At each angle of observation the number of

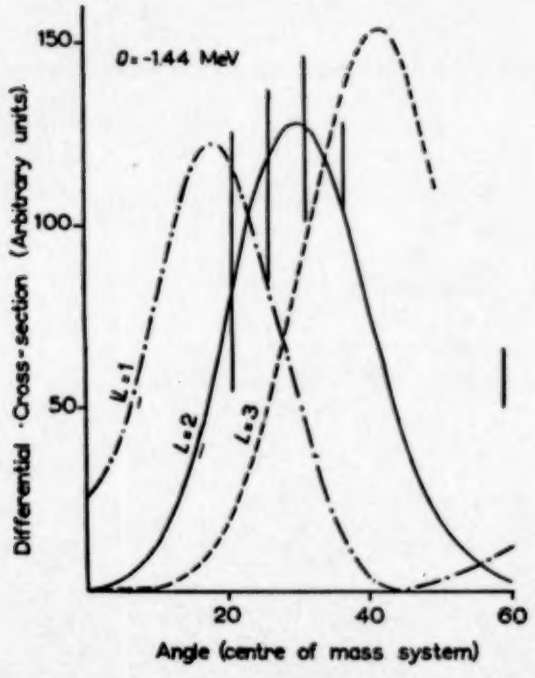


Fig. 2. Angular distribution of the inelastically scattered deuteron group Cr*.

tracks corresponding to this group was carefully estimated by taking in consideration the general deuteron background and the variation of the intensity of the incident beam with angle. Also represented in this figure, are some curves, calculated from the theory of Huby and Newns [1]), characterized by $L = 1, 2$ and 3. The radius of interaction was taken as $7.25 \times 10^{-13}$ cm, i.e. the Gamow radius plus $1 \times 10^{-13}$ cm. As seen, the best fitting between

the experimental and theoretical distributions is obtained when the orbital angular momentum $L = 2$. Since ${}_{24}Cr^{52}_{28}$, being an even nucleus, has a spin $0^+$ for its ground level, then, according to selection rules, the level at 1.44 MeV must have even parity and spin 1, 2 or 3. Odd values for the spin of that level may be excluded on the basis of Glaubsman's rule [13]) which states that for even nuclei, low lying levels of even parity should have even spin. Hence it follows that the spin of the 1.44 MeV level in $Cr^{52}$ should be $2^+$, which supports the value predicted by the theoretical calculation of Lawson and Uretsky [12]).

### 3.2. COBALT

A typical deuteron spectrum at an angle of observation 50° is shown in fig. 3. Groups denoted by Co, O and C are due to elastically scattered deuter-

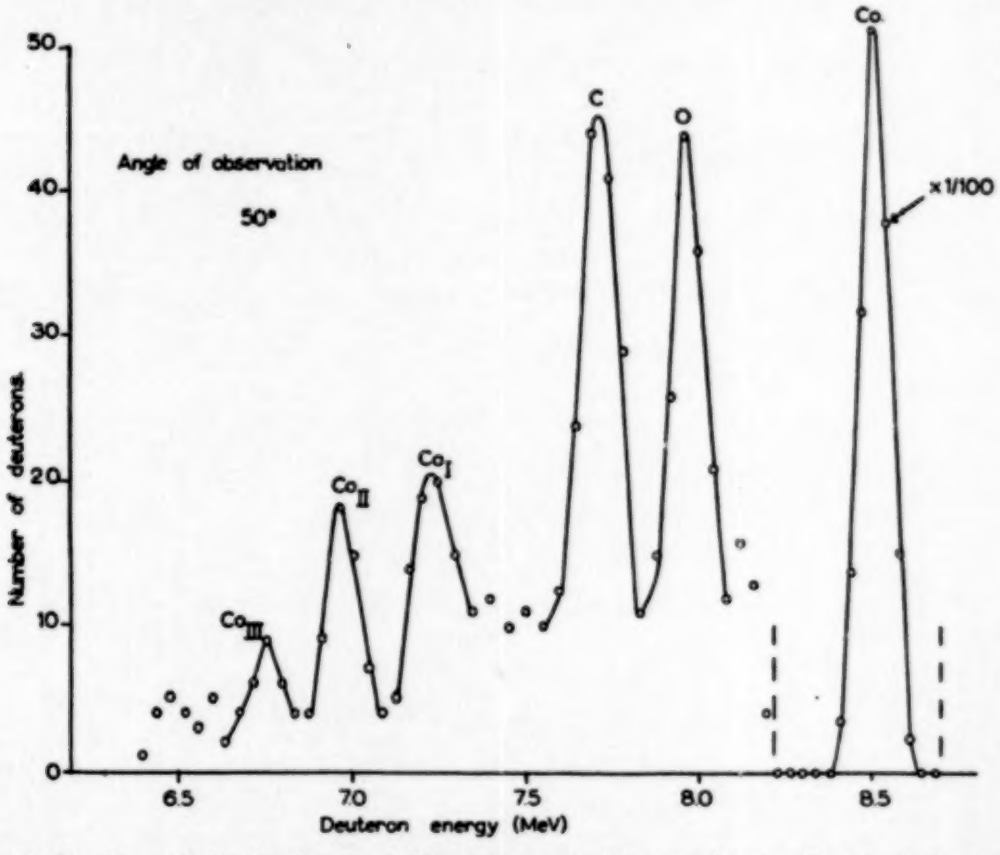


Fig. 3. Spectrum of the deuterons scattered from the deuteron bombardment of the cobalt target.

ons from cobalt, oxygen and carbon. From the general agreement of the $Q$-values calculated from spectra at different angles of observation, the groups labelled $Co_I$, $Co_{II}$ and $Co_{III}$ are attributed to deuterons inelastically scattered from cobalt. The mean values of the corresponding energy levels in $C^{59}$ are found to be 1.27, 1.54 and 1.75 MeV with errors of 0.02 MeV. The level at 1.27 agrees well with the value of 1.289 MeV reported by Metzger [14])

from the $\beta$-activity of iron or by Mazari *et al.* [15]) from the inelastically scattered protons from cobalt. The latter authors have used a magnetic spectrograph together with an electrostatic generator and were able to analyse 40 energy levels in $Co^{59}$. In the present region of investigation they have reported levels at 1.097, 1.189, 1.289, 1.432, 1.458, 1.479 and 1.743 MeV. The absence of some of these levels in the present experiment could be explained, if they do at all exist, by the fact that their intensity may be too low to allow them to be distinguished from the deuteron background.

The angular distributions of the groups $Co_I$ and $Co_{II}$ are represented in the centre of mass system as shown in fig. 4. The latter distribution is nearly isotropic, but the former could be fitted by a theoretical curve characterized by $L = 2$. The radius of interaction used in the formula of Huby and

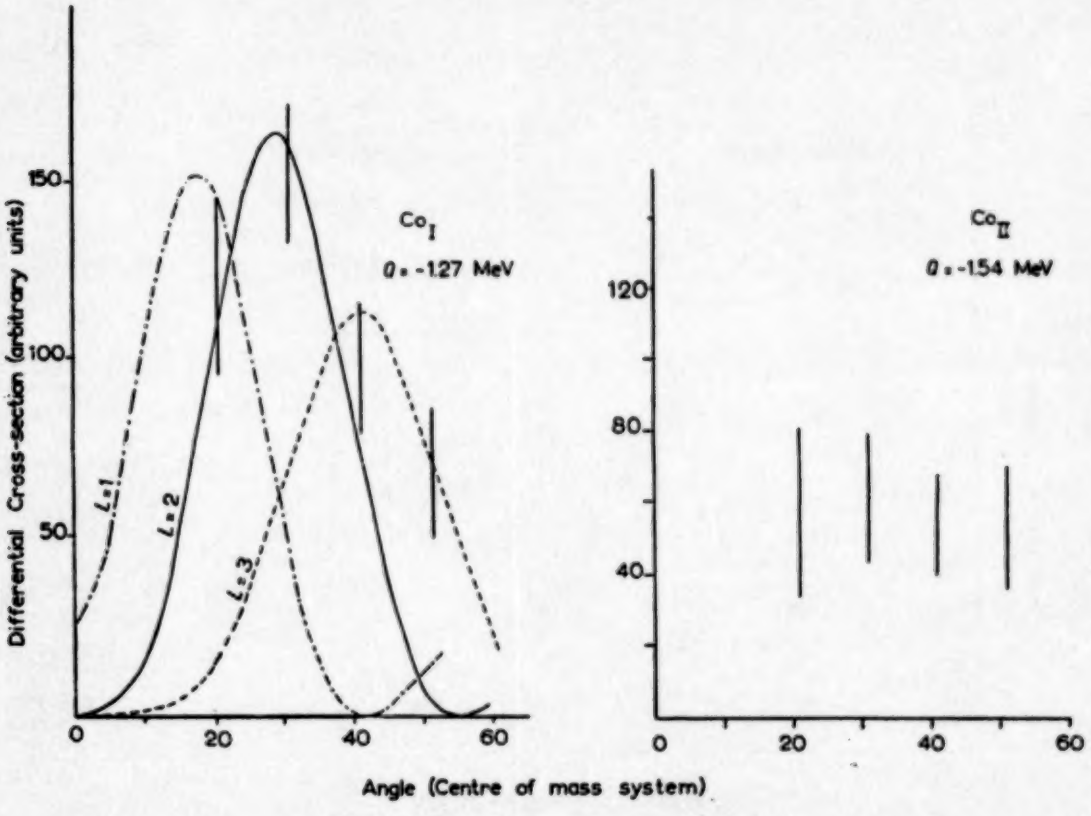


Fig. 4. Angular distribution of the inelastically scattered deuteron groups $Co_I$ and $Co_{II}$.

Newns [1]) is $7.5 \times 10^{-13}$ cm. Assuming the ground level of $Co^{59}$ to have spin $7/2^-$ as predicted by the shell model, the level at 1.27 MeV must have odd parity and a half integer spin lying between $\frac{1}{2}$ and 13/2. Metzger [14]) has suggested a spin $\frac{3}{2}$ for this level, which is compatible with the present investigation.

One of the authors (F. B.) is grateful to Professor H. W. B. Skinner for

his encouragement and advice during the performance of this experiment at the Nuclear Physics Research Laboratory, Liverpool.

The authors would also like to express their gratitude to Professor M. A. El Sherbini for his interest and discussion of the problem.

## References

1) R. Huby and H. C. Newns, Phil. Mag. **42** (1951) 1442
2) F. A. El Bedewi, Proc. Phys. Soc. A **69** (1956) 321
3) S. Hinds and R. Middleton, Proc. Phys. Soc. A **69** (1956) 347
4) F. A. El Bedewi and S. Tadros, to be published
5) T. Green and R. Middleton, Proc. Phys. Soc. A **69** (1956) 16
6) F. A. El Bedewi, Proc. Phys. Soc. A **64** (1951) 1079
7) H. J. Hausman, A. J. Allen, J. S. Arthur, R. S. Bender and C. J. Mcdole, Phys. Rev. **88** (1952) 1296
8) L. E. Beghian, D. Hicks and B. Milman, Phil. Mag. **1** (1956) 261
9) W. C. Peacock and M. Deutsch, Phys. Rev. **69** (1946) 306
10) J. M. Leblanc, J. M. Cork, S. B. Burson and W. C. Jordan, Phys. Rev. **93** (1954) 1124
11) M. Mazari, W. W. Buechner and A. Sperduto, Phys. Rev. **107** (1957) 1383
12) R. D. Lawson and J. L. Uretsky, Phys. Rev. **106** (1957) 1369
13) M. J. Glaubman, Phys. Rev. **90** (1953) 1000
14) F. R. Metzger, Phys. Rev. **88** (1952) 1360
15) M. Mazari, A. Sperduto and W. W. Buechner, Phys. Rev. **107** (1957) 365

*Nuclear Physics* **6** (1958) 440—442; © *North-Holland Publishing Co., Amsterdam*
Not to be reproduced by photoprint or microfilm without written permission from the publisher

# SIMPLE EXPANSION FOR THE REGULAR COULOMB WAVE FUNCTION

A. S. MELIGY
*Faculty of Science, University of Alexandria*

Received 7 January 1958

**Abstract:** The procedure employed by Shepanski and Butler [1]) for the expansion of the regular radial Coulomb wave function has been modified, leading to a simple expansion of the same rapidity of convergence.

## 1. Introduction

The Coulomb wave functions have been recently given much attention owing to their importance in nuclear scattering problems. Among various attempts to develop convenient formulae Shepanski and Butler [1]) reported an expansion for the regular radial Coulomb wave function as suggested by an iteration procedure on the wave equation. Although this expansion is more rapidly convergent than the usual expansion given by Yost, Wheeler and Breit [2]) yet it is more laborious in the evaluation of its terms. The object of this communication is to present an equally rapidly convergent expansion characterized by a simpler recurrence relationship between its terms.

## 2. Regular Solution of the Wave Equation

The regular radial Coulomb wave function, in standard notation [3]), is represented as follows:

$$F_L(\eta,\ \varrho) = C_L(\eta)\varrho^{L+1}\Phi_L(\eta,\ \varrho), \tag{1}$$

where

$$C_L(\eta) = \frac{2^L}{(2L+1)!}\left\{(1^2+\eta^2)(2^2+\eta^2)\ldots(L^2+\eta^2)\,\frac{2\pi\eta}{e^{2\pi\eta}-1}\right\}^{\frac{1}{2}}$$

and $\Phi_L(\eta,\ \varrho)$ is the regular solution of the differential equation

$$\varrho\frac{d^2\Phi_L}{d\varrho^2} + (2L+2)\frac{d\Phi_L}{d\varrho} + (\varrho-2\eta)\Phi_L = 0. \tag{2}$$

According to Yost, Wheeler and Breit, the power series solution of (2) is given as

$$\Phi_L(\eta,\ \varrho) = 1 + \frac{\eta\varrho}{L+1} + \frac{2\eta^2-L-1}{2(L+1)(2L+3)}\varrho^2 + \ldots. \tag{3}$$

It can be seen from (3) that, for small values of $\varrho$, the terms $\varrho d^2\Phi_L/d\varrho^2$ and $\varrho\Phi_L$ could be neglected in solving (2) for the first approximation. Thus,

$$\Phi_L^{(1)}(\eta, \varrho) = \exp\left(\frac{\eta\varrho}{L+1}\right). \tag{4}$$

This result and approximations of higher orders suggest an exact solution of (2) in the form

$$\Phi_L(\eta, \varrho) = e^{\eta\rho/(L+1)} \sum_{n=0}^{\infty} a_n \varrho^n. \tag{5}$$

On substituting (5) in (2), we find

$$a_0 = 1, \qquad a_2 = -\frac{\eta^2+(L+1)^2}{2(L+1)^2(2L+3)},$$

$$a_1 = 0, \qquad a_3 = \frac{\eta[\eta^2+(L+1)^2]}{3(L+1)^3(L+2)(2L+3)},$$

and in general, for $n \geqq 2$,

$$n(n+2L+1)a_n = -\frac{2\eta(n-1)}{L+1}a_{n-1} - \left[1+\left(\frac{\eta}{L+1}\right)^2\right]a_{n-2}. \tag{6}$$

It is evident that the present three-term recurrence relation, given in (6), is simpler than the five-term recurrence relation of the expansion of Shepanski and Butler. This was only a consequence of neglecting, in the first approximation, the term $\varrho\Phi_L$ in (2), which has been included in the work of the above mentioned authors. It should be noted that the present procedure does not spoil the rapidity of convergence of the resulting expansion. A comparison between the number of terms required in each expansion to evaluate $\Phi_L(\eta, \varrho)$ for different values of $L$ and $\eta$ is given in the following table; $\varrho$ is chosen as unity to reduce the expansions to their coefficients.

| $L$ | $\eta$ | $\Phi_L(\eta, 1)$ | No. of Terms | |
|---|---|---|---|---|
| | | | Present | S. and B. |
| 0 | 0 | 0.8415 | 4 | 4 |
| 2 | 0 | 0.9305 | 3 | 3 |
| 5 | 0 | 0.9622 | 3 | 3 |
| 0 | 1 | 2.0985 | 7 | 9 |
| 2 | 1 | 1.2937 | 5 | 5 |
| 5 | 1 | 1.1362 | 4 | 4 |
| 0 | 2 | 4.3653 | 10 | 12 |
| 2 | 2 | 1.7735 | 5 | 5 |
| 5 | 2 | 1.3388 | 5 | 4 |
| 2 | 3 | 2.4015 | 7 | 8 |
| 3 | 4 | 2.4624 | 6 | 6 |
| 4 | 5 | 2.5035 | 6 | 6 |
| 5 | 6 | 2.5331 | 5 | 5 |

From the table it is seen that both expansions have practically the same rapidity of convergence, which increases with increasing $L$. It should also be mentioned that for $\eta \leqq L+1$ the convergence is rapid, whereas it becomes slower as $\eta$ have values greater than $L+1$. In order to explain this behaviour mathematically, let eq. (5) be expressed in the following form:

$$\Phi_L(\eta, \varrho) = e^{\eta\rho/(L+1)} \sum_{n=0}^{\infty} c_n \left[1 + \left(\frac{\eta}{L+1}\right)^2\right]^{\frac{n}{2}} \varrho^n \tag{7}$$

where

$$c_0 = 1, \quad c_1 = 0, \quad c_2 = -1/2(2L+3),$$

and in general

$$n(n+2L+1)c_n = -\alpha(n-1)c_{n-1} - c_{n-2}, \tag{8}$$

where

$$\alpha = 2 \Big/ \left[1 + \left(\frac{L+1}{\eta}\right)^2\right]^{\frac{1}{2}}.$$

Since $0 \leqq \alpha \leqq 2$, for any value of $L$ and $\eta$, it follows that the rate of convergence of (7) is practically independent of the value of $\alpha$. Hence it is obvious from (7) that the expansion can be conveniently used when $\eta$ is not large with respect to $L$.

The writer would like to thank Professor Z. Morsi and Professor F. El Bedewi for their interest and discussion of the problem.

## References

1) J. R. Shepanski and S. T. Butler, Nuclear Physics **1** (1956) 313
2) Yost, Wheeler and Breit, Phys. Rev. **49** (1936) 174
3) M. Abramowitz, Tables of Coulomb Wave Functions, N.B.S. Applied Mathematics Series No. 17 (U.S. Government Printing Office, Washington, D.C., 1952)

*Nuclear Physics* **6** (1958) 443—445; © *North-Holland Publishing Co., Amsterdam*
Not to be reproduced by photoprint or microfilm without written permission from the publisher

# POLARIZATION OF PROTONS FROM THE d-d REACTION AT 1.2 MeV

BOGDAN MAGLIĆ † and JOVAN VUKOVIĆ
*Institute for Nuclear Sciences "Boris Kidrič", Belgrade, Yugoslavia*

Received 9 December 1957

## 1. Introduction

Polarization of d—d protons has been investigated at 0.3 MeV [1]) and at 0.65 MeV [2]). From the theoretical analysis of the d—d reaction [3]) the coefficient $B$ of the angular distribution becomes dominant only in the energy region above about 0.7 MeV, hence we thought it would be worthwhile to investigate whether there is an essential change of the magnitude or sign of polarization at the energies above 1 MeV, available with the Cockroft-Walton accelerator of the Institute.

## 2. Experimental Arrangement and Procedure

The deuteron beam was magnetically analyzed through 30° and the energy at the target was measured to be $1.2 \pm 0.05$ MeV. Thick heavy ice target, translatory moving and continuously refreshed by $D_2O$ vapour, described previously [4]), was used; a liquid air trap above the target assembly was applied to prevent carbon contamination.

The scattering on helium, known to give a 100 % polarization at 2 MeV and 90° cm[5], was used as an analyzer.

The protons emitted at 135° in the laboratory system, supposed to be polarized, enter the helium scattering chamber, after passing through a 23 cm long brass tube. A thin (6 fr) mica window, 2 cm in diameter, separated scattering chamber from the vacuum system. Helium of 99 % purity was at 2 atmospheres pressure, controlled by a **U**-manometer. A special precaution was taken in making the thin mica windows for such a pressure difference.

To measure the asymmetry of the protons scattered in He, two pairs of plates (Ilford C—2, 50 microns) were placed at each of the two positions: "right", $\phi = 0°$ and "left", $\phi = 180°$, where $\phi$ is azimutal angle. One of

† Present address: Laboratory for Nuclear Science, Massachusetts Institute of Technology, Cambridge 39, Massachusetts.

the two plates at each position was covered by a 30 micron Pb-foil to stop the recoil protons from the scattering chamber; the other was open to the scattered protons. The covered plates were to measure the background; although the whole system was in paraffin which slowed the fast D+D neutrons down, we were finding a very high recoil proton background, which looked to the scanners like the genuine protons from the reaction and so smeared the asymmetry considerably out. This is why we decided to cover one of the plates at each position. Then the spectra of protons in each of the two plates were taken and were subtracted from each other; only those protons in a narrow range region around the peak were taken, on both plates. The difference of the two plates: (true+background)—(background) was taken at both positions "right" and "left", as given in the table.

The energy of the protons before scattering was measured by a plate placed at the end of the scattering chamber, with He taken out during the run, so that we checked the position of the beam every 15 minutes of the run and also the spectrum of the protons after passing through helium. In a later set of experiments we used a fluorescent screen with a sensitive film, and in this way checked the geometry every 5 minutes. All these precautions were taken because any deviation of the beam from the centre of the scattering chamber could produce a false asymmetry and thus lead to a false polarization.

The experiment consisted of three separate exposures; the first two were to check the geometry: (1) without He in the scattering chamber: this gave an account of the neutron background and protons scattered on the walls of the chamber; (2) with argon in the scattering chamber; (3) with helium; this was the main experiment, whose data are given in this paper. Each of the exposures was about 300 $\mu$Ah.

A strong criterium for the consideration of the origin of every track was given to the scanners. Only those protons scattered within a solid angle defined by a half angle of 15° were counted. Also, only those tracks which originate at the surface of the emulsion, e.g. whose grain density was smaller at the surface, have been counted.

Constancy of the proton production was controlled by a helium ionization chamber, used as a monitor neutron detector, at a distance of 6 feet from the target.

## 3. Results and Conclusion

Proton energy at the moment of scattering was measured to be $2.05 \pm 0.05$ MeV. Numbers of protons in both "right" and "left" positions are shown in the table. Clearly, too high a background in the

plates in position "left" prevents us from obtaining better statistics.

| Position | "Right" | "Left" |
|---|---|---|
| Open plate | 483 | 427 |
| Covered plate | 183 | 244 |
| Difference | 300±26 | 181±26 |

These data, together with the error of the geometry, give for polarization

$$P = 0.24 \pm 0.08.$$

This result should be compared with that of Bishop *et al.*, giving $+30 \pm 6$ % for the polarization at 0.3 MeV and that of Segel and Hanna, who obtained $-17 \pm 7$ % at 0.65 MeV; the latter result has the negative sign because it was obtained at a forward angle and the identity of colliding particles requires the polarization to be antisymmetrical about 90° (c.m.). We can conclude from our result, which within the limits of statistical error essentially agrees with the two results obtained at lower energy and also with five other measurements on the d—d neutrons polarization (see table in ref. [2])), that both magnitude and sign of the polarization in the d—d reaction is nearly independent of the energy in the region between 0.3 and 1.2 MeV. As the most likely magnitude of the polarization in that region one should probably take that of Segel and Hanna, $17 \pm 7$ %, not only because we can obtain exactly their value by averaging all d—d polarization data, but also because their experimental setup was the one most capable of eliminating the effect of the neutron background.

The authors are indebted to Dr. R. J. Walen and Professor P. Savić.

## References

1) Bishop, Preston, Westhead and Halban, Nature **170** (1952) 113
2) Segel and Hanna, Phys. Rev. **106** (1957) 536
3) Beiduk, Pruett and Konopinsky, Phys. Rev. **77** (1950) 622
4) Maglić, Atomics **5** (1954) 85
5) Heusinkveld and Freier, Phys. Rev. **85** (1952) 80; M. J. Scott, to be published in Phys. Rev.

*Nuclear Physics* 6 (1958) 446—450; © *North-Holland Publishing Co., Amsterdam*
Not to be reproduced by photoprint or microfilm without written permission from the publisher

# INELASTIC SCATTERING OF 185 MeV PROTONS ON NUCLEI WITH MASSES FROM FLUORINE TO POTASSIUM

H. TYRÉN and TH. A. J. MARIS
*The Gustaf Werner Institute for Nuclear Chemistry, University of Uppsala, Uppsala, Sweden*

Received 9 January 1958

**Abstract:** Inelastic spectra of 185 MeV protons scattered at two different angles on nuclei from fluorine to potassium are reported.

In this paper energy spectra of high energy protons scattered on the natural elements from fluorine to potassium, neon excepted, are reported. The measurements were done with a magnetic analyser as described in ref. [1]). The average scattering energy varied from target to target between 179 and 184 MeV. Except for chlorine measurements were made at one small angle to show the forward peaked excitations, and at a larger angle, at which the forward dipped cross sections are more pronounced. The measured spectra are shown in figs. 1—3.

The measurements of chlorine and fluorine were made with LiCl and LiF targets. The parts of the spectra which are uncertain because of the subtraction of the lithium spectrum are dashed in the figures, as is also the region of the phosphorus spectrum which is influenced by the proton spectrum from water in the target. The absolute values of the phosphorus cross section were not measured directly, but the spectrum was normalized by comparison with neighbouring elements. Except for these cases, the absolute cross sections are thought to be good to 20 per cent. The ratios of the cross sections for distant parts of one single spectrum are estimated to be in error by not more than 10 per cent. For a more detailed description of these errors see ref. [1]). The statistical errors are indicated near the left margin of each spectrum.

We do not intend to discuss the results at present, but only to point out some of their systematics. Fig. 4 shows the cross sections of the broad, forward peaked, level structures around 20 MeV excitation energy for a number of different elements, the satellite peaks, of the same angular distribution but at somewhat lower energies, are included. In fig. 5 some energies of strongly excited levels have been plotted. The lengths of the vertical lines indicate upper limits for the widths of the levels or level groups. The lines corresponding to forward dipped levels are connected

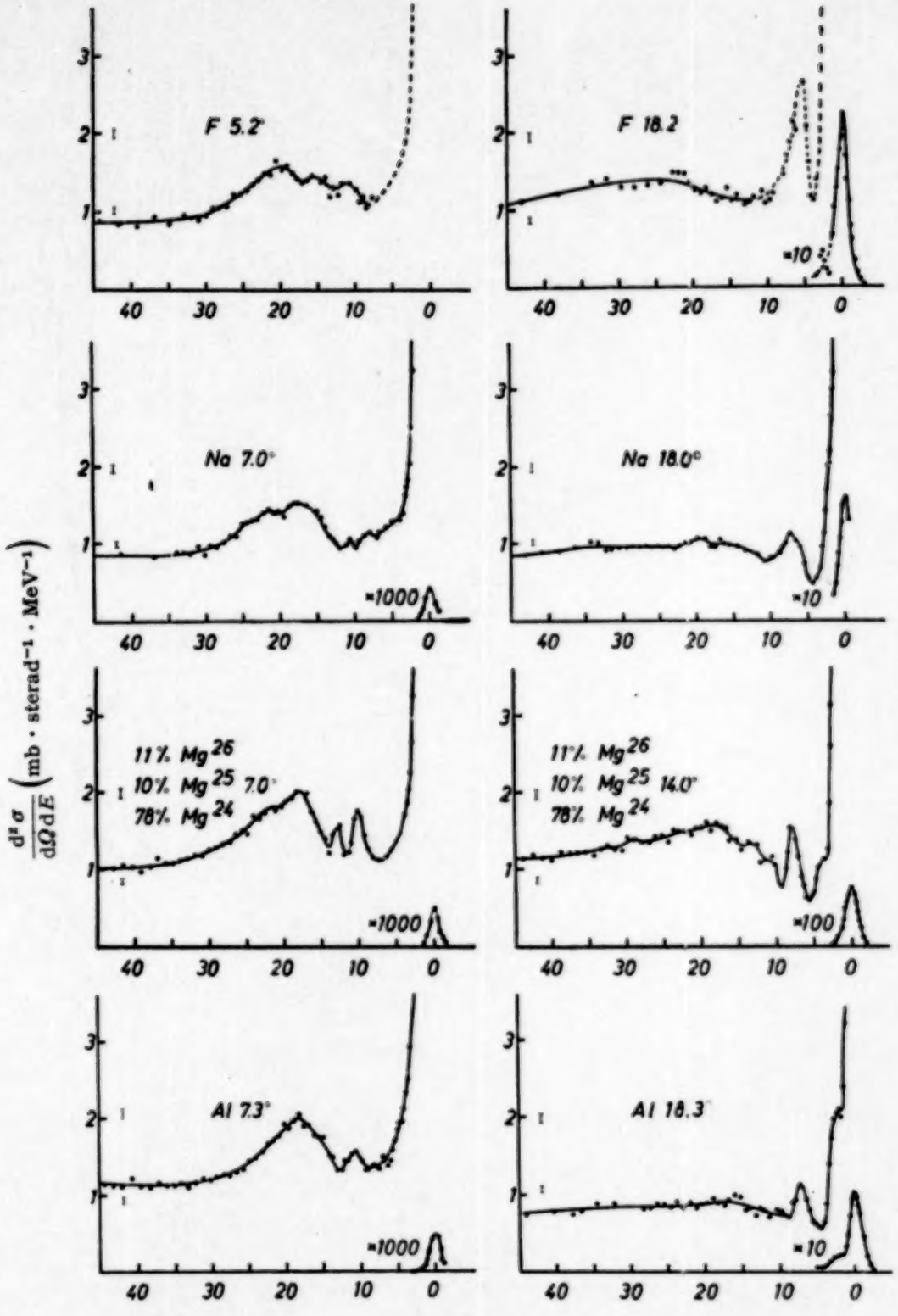


Fig. 1. Energy spectra for inelastic scattering of 185 MeV protons on natural F, Na, Mg and Al. Typical statistical errors are indicated near the left margin of the figures.

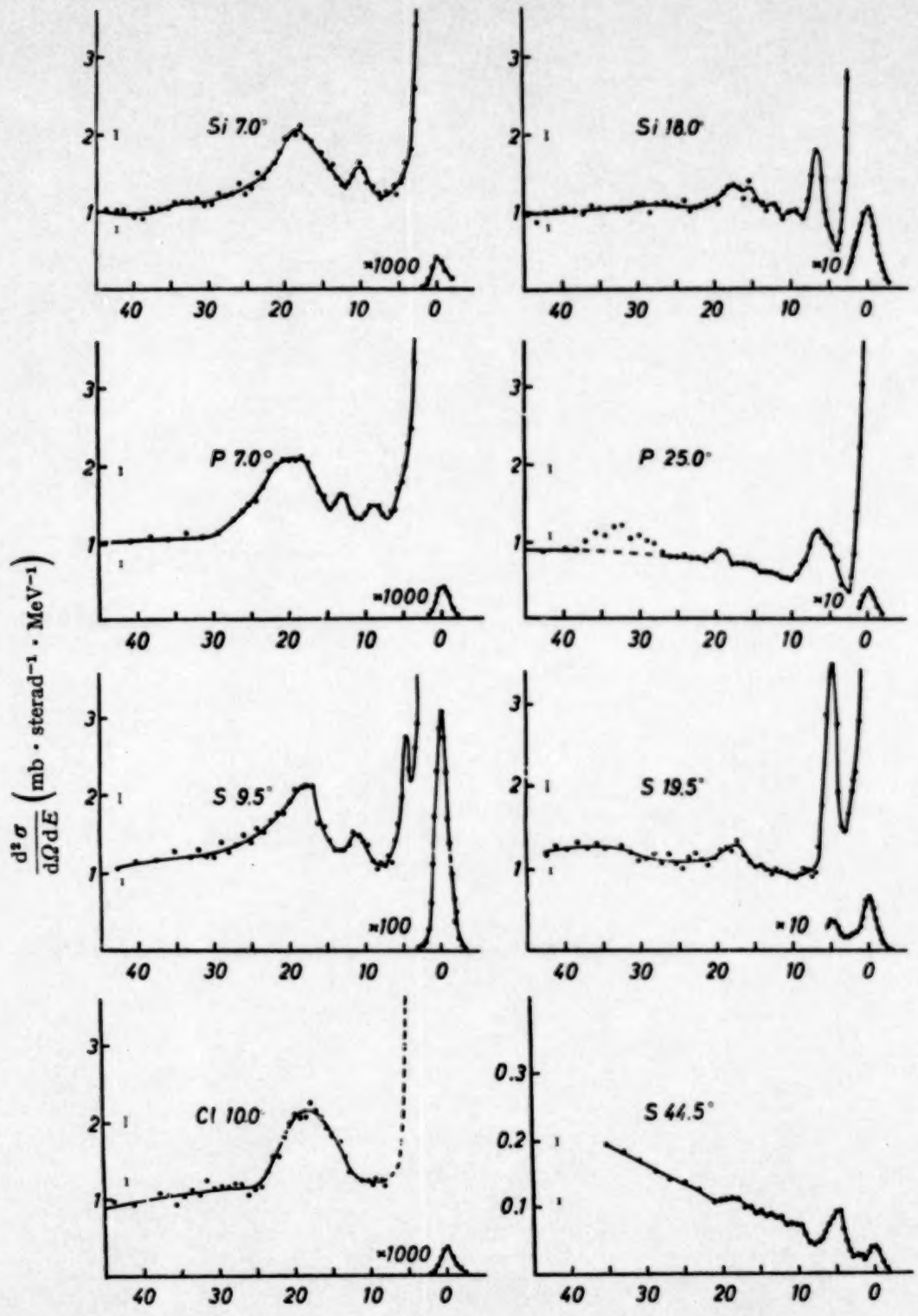


Fig. 2. Energy spectra for inelastic scattering of 185 MeV protons on natural Si, P, S and Cl.

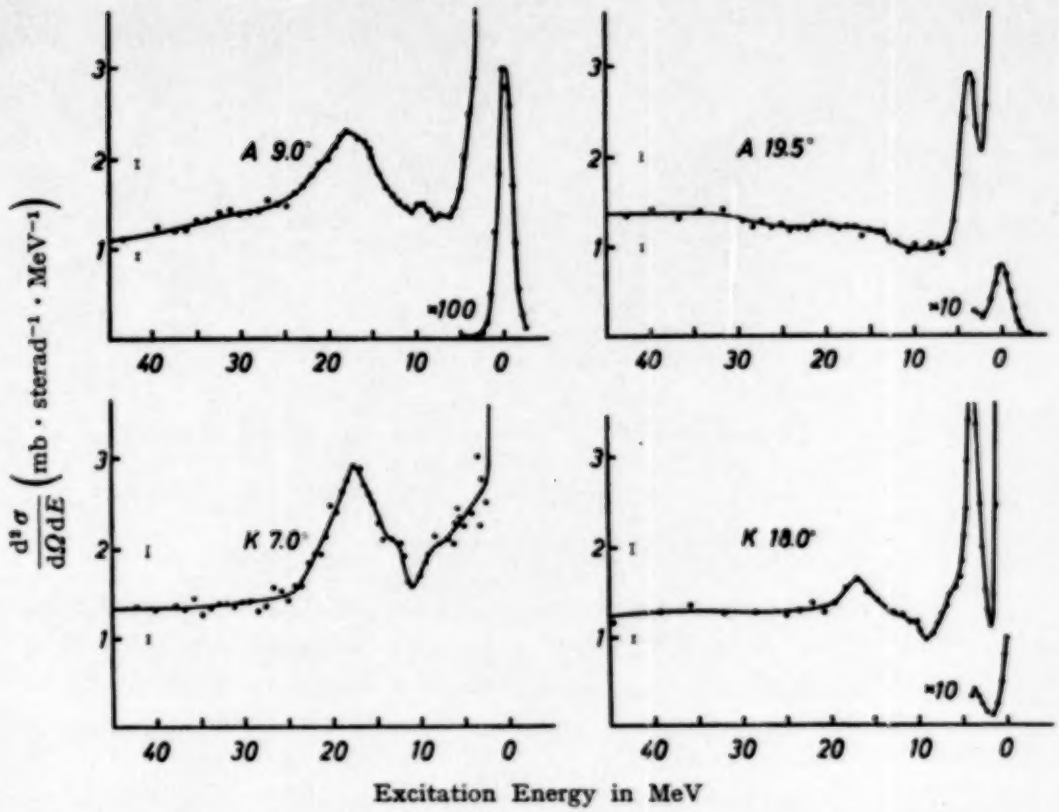


Fig. 3. Energy spectra for inelastic scattering of 185 MeV protons on natural A and K.

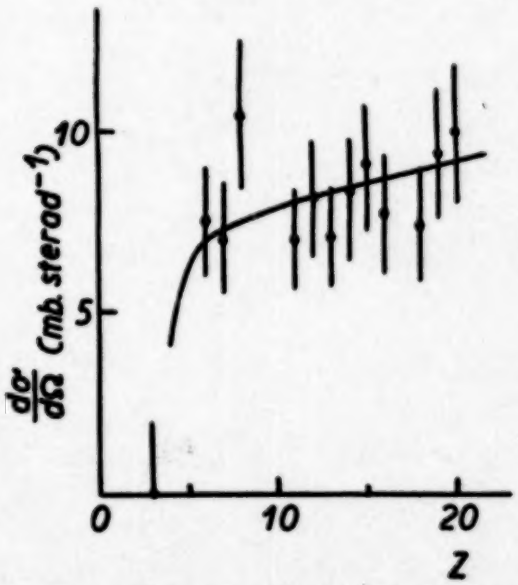


Fig. 4. Integrated small angle cross sections of the excitations around 20 MeV with forward peaked angular distributions, versus nuclear charge number. Some of our previous measurements are included. Estimated maximum errors are shown.

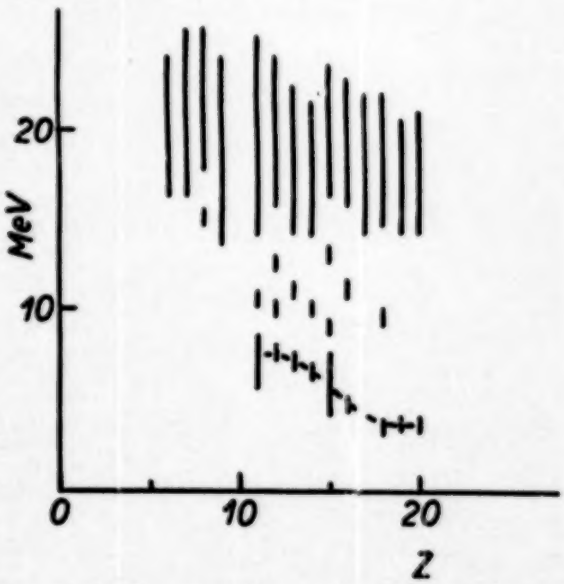


Fig. 5. Energies of strongly excited levels and level groups versus nuclear charge number. Upper limits for their widths are indicated. Levels with forward dipped angular distributions are connected by a dashed curve. Some low lying levels which are not satisfactory resolved are omitted. Some of our previous measurements are included.

by a dashed curve. In table 1 the energies of some sharp maxima are listed.

TABLE 1

| Nucleus | Energy (MeV) |
|---|---|
| Mg | 7.7±0.3 |
| Al | 7.0±0.3 |
| Si | 6.5±0.3 |
| S | 4.7±0.2 |
| A | 3.5±0.2 |
| K | 3.7±0.4 |

We thank Professor Svedberg for his interest. As always Dr. Peter Hillman and our other colleagues of the high energy group have been helpful. We thank Åke Svanheden and his cyclotron crew for their cooperation.

## Reference

1) H. Tyrén and Th. A. J. Maris, Nuclear Physics 4 (1957) 637

*Nuclear Physics* **6** (1958) 451—459; © *North-Holland Publishing Co., Amsterdam*
Not to be reproduced by photoprint or microfilm without written permission from the publisher

# COULOMB EXCITATION CROSS SECTIONS OF GADOLINIUM ISOTOPES FROM INELASTIC SCATTERING MEASUREMENTS

V. RAMŠAK†, M. C. OLESEN and B. ELBEK

*Institute for Theoretical Physics, University of Copenhagen*

Received 8 November 1957

**Abstract:** The cross sections for Coulomb excitation and the energies of the accessible low-lying rotational states in the six most abundant isotopes of gadolinium have been determined from measurements on the corresponding groups of inelastically scattered protons and deuterons. The projectiles were accelerated in an electrostatic generator to energies around 4 MeV. Particles scattered from isotopically pure targets prepared in an isotope separator were observed at an angle of 145° with respect to the beam by means of a magnetic spectrometer of high resolution. The lifetimes for the first excited states in $Gd^{154}$ and $Gd^{158}$ derived from the measured cross sections are in good agreement with the reported directly measured lifetimes of these states.

## 1. Introduction

The measurement of the cross section for Coulomb excitation of a nuclear state is equivalent to the determination of the lifetime of this state, since for a given multipole order the transition probability for excitation is the same as that for decay times a spin weight factor [1]). It is worth noting that the determination of the transition probability from the Coulomb excitation cross section is independent of details of the nuclear model and depends only on the description of the excitation mechanism.

The reduced transition probability contains important information about the excited state, and its accurate determination deserves considerable attention. It is also interesting to study the systematic variation of the transition probabilities through a whole region of the periodic table.

The region of the rare earths has been extensively studied in this respect. Direct measurements of the lifetimes have been carried out in some cases, but most information on transition probabilities originates in measurements of the absolute cross section for Coulomb excitation. Several difficulties, such as determination of the target thickness, detector efficiency and the absolute beam current are inherent in such measurements when based on observation of the radiation emitted during the decay of the excited state. Also the reduction of the observed transition probability to the nuclear transition probability demands a knowledge of the proper conversion

† On leave from the Josef Stefan Institute, Ljubljana, Yugoslavia.

coefficients and, in the case of odd nuclei, of branching ratios and M1—E2 mixing ratios.

If one determines the Coulomb excitation cross section of a nuclear level from measurements of the intensity of the corresponding group of inelastically scattered particles, these difficulties are avoided. The absolute inelastic scattering cross section can then easily be determined from a comparison with the simultaneously recorded group of elastically scattered particles, the cross section of which is given by the Rutherford scattering law.

Gadolinium has seven stable isotopes: $Gd^{152}$ (0.20 % abundance), $Gd^{154}$ (2.15 %), $Gd^{155}$ (14.73 %), $Gd^{156}$ (20.47 %), $Gd^{157}$ (15.68 %), $Gd^{158}$ (24.87 %) and $Gd^{160}$ (21.90 %). The Coulomb excitation of these isotopes, except $Gd^{152}$ the excitation of which has never been observed, has been studied by several authors using detection of gamma rays [2, 3]) or conversion electrons [4, 5, 6]). The energies determined in these investigations fit well into the systematics of the rotational description of low lying levels, but in view of the above-mentioned difficulties in the measurements of the absolute cross sections, it is not surprising that the transition probabilities reported scatter almost within a factor of two. In this experiment, therefore, all isotopes except $Gd^{152}$ have been reinvestigated by the method of inelastic scattering. These measurements are part of a systematic survey of the transition probabilities in the mass region 150—200.

## 2. Experimental Arrangement

The apparatus and the experimental procedure were essentially the same as described in a previous paper [7]). Protons or deuterons were accelerated in a 4-MV electrostatic generator. A 90° analysing magnet was used for deflection and energy selection of the beam. The defining slits of the analyser were adjusted to give a resolution corresponding to the target thickness, the latter being the limiting factor in the resolution obtainable.

After energy analysis the beam impinged on the target in the heavy particle spectrometer used for analysis of the scattered particles, which were recorded on Ilford C2 plates with an emulsion thickness of 25 or 50 microns. The thicker emulsion was used in exposures with deuterons to distinguish deuterons from protons of the same momentum originating in (d, p) reactions in the target backing. To obtain a larger range difference between these two kinds of particles in the emulsion, it was found advantageous to cover the photographic plate with a 5 mg/cm² aluminium foil, which, due to the oblique incidence of the particles on the plate, corresponds to an effective layer of about 9 mg/cm². By shifting the plateholder laterally in the spectrograph, three different exposures could be made on the same set of plates. To reduce the intensity of the very strong elastic group to a countable level, a short exposure was given before and after a long exposure

and recorded on the same plate. The relative intensity of the exposures was determined by means of the beam integrator.

The targets for the investigation were prepared in the electromagnetic isotope separator of the Institute in a way similar to that described earlier [7]). The charging material for the ion source was water-free gadolinium chloride which had been irradiated in a nuclear reactor to produce the 18-hour radioactive isotope $Gd^{159}$, which was needed for a $\beta$-spectroscopic investigation. The collector arrangement was made so that it was possible to collect the stable isotopes for this experiment at the same time that $Gd^{159}$ was collected for the $\beta$-source. Every separation gave two targets of each isotope: one on a thick aluminium backing on which the beam impinged directly, one on a formvar foil used for catching the atoms sputtered from the directly bombarded target.

An investigation of the penetration of heavy atoms from the 50 keV beam in the isotope separator into the bombarded aluminium surface is presently being undertaken [8]). The amount of heavy atoms and their distribution are determined from the line profile of elastically scattered 3.5-MeV $\alpha$-particles recorded in the heavy particle spectrometer. A few preliminary results of interest in connection with the targets used in the present experiment will be mentioned. The amount of gadolinium was normally about 30 $\mu g/cm^2$. The penetration depth in Al is about 15 $\mu g$ Al/$cm^2$, the width of the distribution being 45 $\mu g/cm^2$ of a mixture of approximately 3 Al atoms per Gd atom. The sputtered targets contain about 5 Al atoms per Gd atom. As in this experiment the scattered particles were observed in a backward direction and thus had to pass through the target twice, the broadening of the groups due to the target thickness was about 5 keV for protons of 4 MeV energy.

## 3. Results

The cross section for inelastic scattering was determined from the ratio between the inelastic and the elastic group together with the Rutherford scattering law, which can be expressed conveniently as

$$\frac{d\sigma_R}{d\omega} = 1.295 \cdot Z_1^2 \left(\frac{Z_2}{E}\right)^2 \frac{1}{\sin^4 \frac{\theta}{2}} \text{ mb/sterad.}$$

Here $d\sigma_R/d\omega$ is the differential cross section for scattering through the angle $\theta$, $Z_1$ and $Z_2$ are the atomic numbers of the incoming particle and nucleus, respectively, and $E$ is the bombarding energy in MeV. The equation is valid in the centre of mass system, but can for this purpose also be used in the laboratory system, as the correction is only of the order of $(A_1/A_2)^2 \approx 10^{-4}$, where $A_1$ and $A_2$ are the atomic numbers of the projectile and nucleus, respectively.

In these experiments both protons and deuterons were used as projectiles. We therefore thought it of interest to check whether the elastic scattering cross sections are equal for these two particles under otherwise identical conditions. For this purpose, a target of $Gd^{158}$ was bombarded successively with protons and deuterons of the same energy. Care was taken to reduce the content of molecular hydrogen ions in the deuteron beam to an insignificant amount by running the ion source of the generator with deuterium for 1/2 hour before exposure. Repeated measurements showed that the intensity of the elastic scattering was the same within 2 % for deuterons and protons. It was, therefore, concluded that, e.g., the polarization of the deuteron does not markedly affect the elastic cross section.

Having determined the inelastic scattering cross section, the reduced transition probability $B(E2)$ for E2 excitation was readily obtained from the expression for the differential cross section for Coulomb excitation [1]:

$$\frac{d\sigma(E2)}{d\omega} = \frac{4819}{Z_2^2} \frac{A_1(E-\Delta E')}{(1+(A_1/A_2))^2} \frac{B(E2)}{e^2} \cdot f(\xi, \theta) \text{ mb/sterad.}$$

Here $\Delta E'$ is the effective excitation energy in MeV related to the actual excitation energy $\Delta E$ through $\Delta E' = \Delta E[1+(A_1/A_2)]$, $B(E2)/e^2$ is the reduced transition probability expressed in units of $10^{-48}$ cm$^4$. In the following $B(E2)/e^2$ will be denoted as $B(E2)$ only. The function $f_{E2}(\xi, \theta)$ is tabulated in ref. [1]).

In all cases investigated there was good agreement between the values of $B(E2)$ determined with protons and those determined with deuterons. The E2 description is, therefore, adequate for these excitations.

For comparison of the determined transition probabilities with the results of previous determinations, we have in some cases recalculated the reduced transition probabilities from the measured transition probabilities, using the latest conversion coefficients of Sliv and Band [9]) together with those of Rose [10]). Such a revision sometimes changes the originally reported values of $B(E2)$ by 10—30 %, but nevertheless the transition probabilities measured by inelastic scattering often deviate by 20—30 % from those derived from other Coulomb excitation measurements. It is, therefore, satisfactory from our point of view that measurements of lifetimes for the first excited states in $Gd^{154}$ and $Gd^{156}$ have yielded $B(E2)$-values which are in good agreement with our values (see § 4). The results of earlier Coulomb excitation measurements on Gd-isotopes are given in table 2.

From our measured transition probabilities, given in table 1, the intrinsic quadrupole moment $Q_0$ was calculated according to the theory of Bohr and Mottelson [1]). The $Q_0$-values are given in table 1 and plotted in fig. 2.

TABLE 1

Measured excitation energies, electric quadrupole transition probabilities and intrinsic quadrupole moments

| Nucleus | $I_0$ | $E_1$ | $E_2$ | $E_2/E_1$ | $B_1$(E2) | $B_2$(E2) | $B_2/B_1$ | $Q_0$ |
|---|---|---|---|---|---|---|---|---|
| $Gd^{154}$ | 0 | 123 | — | — | $3.38^{+0.50}_{-0.30}$ | — | — | 5.8 |
| $Gd^{155}$ | 3/2 | 60 | 145 | 2.42 | $2.15 \pm 0.10$ | $1.12 \pm 0.15$ | 0.52 | 6.5 |
| $Gd^{156}$ | 0 | 89 | — | — | $4.50 \pm 0.25$ | — | — | 6.7 |
| $Gd^{157}$ | 3/2 | 54 | 131 | 2.42 | $2.21 \pm 0.10$ | $1.21 \pm 0.10$ | 0.55 | 6.6 |
| $Gd^{158}$ | 0 | 79 | — | — | $5.36 \pm 0.25$ | — | — | 7.3 |
| $Gd^{160}$ | 0 | 75 | — | — | $5.71 \pm 0.25$ | — | — | 7.6 |

$I_0$ is the ground state spin, $E_1$ and $E_2$ are the excitation energies of the first and second rotational state, respectively, given in keV. $B_1$ and $B_2$ are the corresponding reduced transition probabilities in units of $e^2 \times 10^{-48}$ cm$^4$. $Q_0$ denotes the intrinsic quadrupole moment derived from the transition probability $B_1$, the unit being $10^{-24}$ cm$^2$. The errors given for the $B$-values are standard errors on the mean. The errors in the excitation energies are estimated to be $\pm$ 1 keV.

TABLE 2

Survey of earlier determinations of excitation energies and transition probabilities for gadolinium isotopes. The values of $B_1$ and $B_2$ have been recalculated by means of the new conversion coefficients [9, 10]).

| Nucleus | $E_1$ | $E_2$ | $B_1$ | $B_2$ | Ref. |
|---|---|---|---|---|---|
| $Gd^{154}$ | 123 | | 4.46 | | [2] |
| | 123 | | 2.3 | | [3] |
| | 124 | | 3.7 | | [4] |
| | 123.2 | | 3.61 | | [11] |
| mean | 123.3 | | 3.52 | | |
| $Gd^{155}$ | 61 | 145 | | 1.3 | [2] |
| | | 140 | | | [3] |
| | 60.2 | 146 | 2.97† | | [5] |
| | 61 | | | | [6] |
| mean | 60.7 | 144 | 2.97 | 1.3 | |
| $Gd^{156}$ | 88 | | 4.44 | | [2] |
| | 89 | | 3.7 | | [3] |
| | 90 | | 7.4 | | [4] |
| mean | 89 | | 5.18 | | |
| $Gd^{157}$ | 55 | 131 | | 1.1 | [2] |
| | | 127 | | | [3] |
| | 54.6 | 132 | 3.38† | | [5] |
| | 56 | | | | [6] |
| mean | 55.2 | 130 | 3.38 | 1.1 | |
| $Gd^{158}$ | 78 | | 4.59 | | [2] |
| | 80 | | 4.6 | | [3] |
| | 80 | | 7.8 | | [4] |
| mean | 79 | | 5.66 | | |
| $Gd^{160}$ | 73 | | 4.41 | | [2] |
| | 76 | | 6.4 | | [3] |
| | 76 | | 7.4 | | [4] |
| mean | 75 | | 6.07 | | |

† These values are those originally reported.

## 4. Discussion of Individual Nuclei

### 4.1. $Gd^{154}$

The only group observed corresponds to the well-known first excited state at 123 keV. Three exposures with protons and, as a check on impurities, one exposure with deuterons were made using three different targets. The targets were prepared under different conditions during the isotope separation. A special problem arose in the determination of the proper elastic scattering intensity, in view of the possible presence of the isobar $Sm^{154}$ in the target, which would increase the elastic group. Because of the low abundance of $Gd^{154}$ only a small amount of Sm in the charging material of the isotope separator would cause a significant contamination. A careful search was made for an inelastic group corresponding to the 83-keV first excited state in $Sm^{154}$, which is well known from Coulomb excitation. No such group was found, but due to a somewhat fluctuating background we can only give an upper limit of 10 %. In this case atoms scattered in the isotope separator could also cause a small correction to the $Gd^{154}$ content in the target derived from elastic scattering. For a general discussion of background problems in the isotope separator see ref. [11]).

The mean value of the transition probabilities obtained was $3.4^{+0.5}_{-0.3}$. The individual determinations were in agreement within 7 %, the stated error being mostly due to the unknown contamination.

The transition probability has also been directly measured in the decay of $Eu^{154}$ [12]), yielding a half-life of $1.2 \times 10^{-9}$ sec. This corresponds to a value of $B(E2) = 3.6$. The agreement with our value is satisfactory.

### 4.2. $Gd^{155}$

The two well-known levels at 60 and 146 keV were excited. The determination of the inelastic scattering cross section was somewhat complicated by contaminations probably from tin and brass. In the deuteron exposures tin contamination gave rise to a small elastic group coinciding with the inelastic group belonging to the first excited state, and in the proton exposures another weak elastic group belonging to mass numbers about 64 (brass) was found at nearly the same place as the second inelastic group. Tin contamination in the target could be expected as tin compounds had been used earlier in the ion source of the isotope separator. $Sn^{120}$ (abundance 29 %) can combine with $Cl^{35}$ (75 %) and form an $SnCl^+$ ion with mass 155. The same can happen with $Sn^{118}$ (23 %) and $Cl^{37}$ (25 %). Ions of the neighbouring mass numbers can be formed with the other Sn isotopes, but because of the lower abundance, the Sn contamination has been of minor importance for the targets of the other Gd isotopes.

Eleven exposures were made with protons and deuterons at various

energies on different targets. From these exposures we have determined the $B(E2)$ values for the first and second excited state as 2.15 and 1.12, respectively.

The ratio between the $B(E2)$ for the second and the first excited state is 0.52, which is in agreement with the rotational prediction 0.55 for a nucleus with ground state spin 3/2.

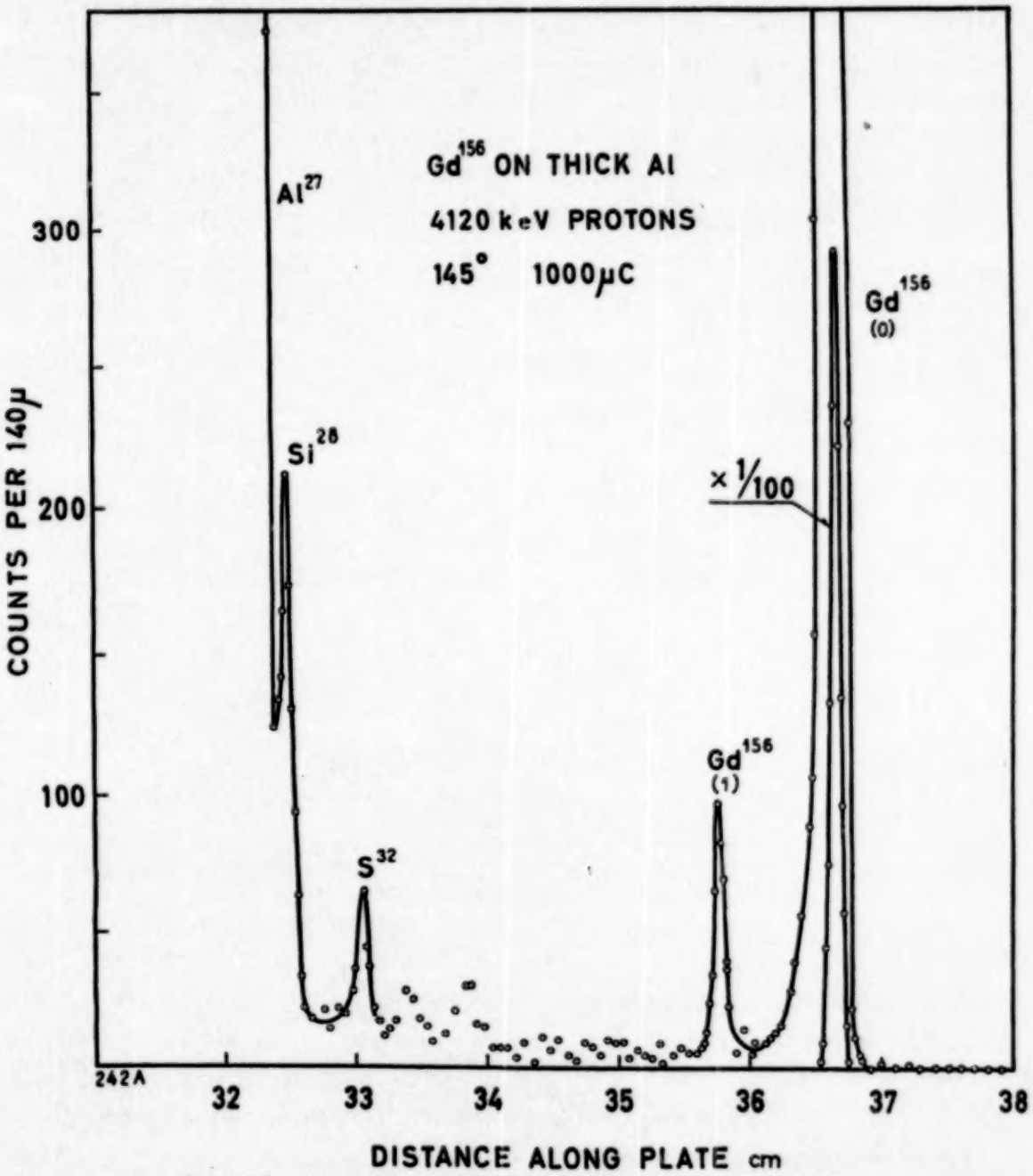


Fig. 1. Spectrum of protons scattered from a target of $Gd^{156}$.

4.3. $Gd^{156}$

Two exposures were made with protons, both yielding exactly the same transition probability $B(E2) = 4.50 \pm 0.25$ for the 89-keV state, which was the only state excited.

A recent determination of the lifetime of the same state, which is populated in the decay of $Tb^{156}$, has yielded $B(E2) = 5.1 \pm 0.3$ [13]), in good agreement with our result.

### 4.4. $Gd^{157}$

The excitation spectrum of the other odd Gd isotope, $Gd^{157}$, is very similar to that of $Gd^{155}$. The first two excited states at 54 and 130 keV were observed in nine exposures with protons as well as deuterons of different energies, three different targets being used. The ratio between the transition probabilities $B_2/B_1$ equals 0.55, in agreement with the rotational prediction. The intrinsic quadrupole moment determined from $B_1(E2)$ seems to be a little too low to fit smoothly into the systematics of the other quadrupole moments.

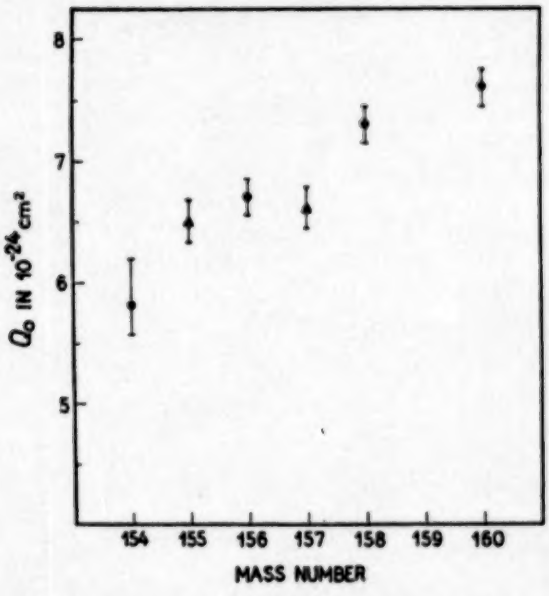


Fig. 2. Intrinsic quadrupole moments of gadolinium isotopes determined from the transition probabilities of the first excited states measured by inelastic particle scattering. In evaluating $Q_0$, the formulae of the rotational theory were used [1]).

### 4.5. $Gd^{158}$

Two exposures were made with protons of various energies on two different targets. The transition probabilities determined for the 79-keV excited state agreed within 3 %. The quadrupole moment determined is larger than that of the two preceding even isotopes, in agreement with the increasing deformation expected.

### 4.6. $Gd^{160}$

Two exposures with protons of different energies on the same target gave transition probabilities for the 75-keV state that agreed within 2 %. The quadrupole moment is again larger than that of the preceding even nucleus.

The authors wish to thank Professor Niels Bohr for the excellent working conditions at the Institute and for the hospitality extended to one of us (V.R.). We are greatly indebted to O. Skilbreid who has prepared the numerous targets in the isotope separator. The plates were counted by Miss Bente Klinken, Miss Ruth Bastiansen and Miss Helle Hansen, whom we wish to thank for the interest they have shown in obtaining accurate counts. One of us (V.R.) is indebted to the Josef Stefan Institute, Ljubljana, for financial support during his stay in Copenhagen.

## References

1) K. Alder, A. Bohr, T. Huus, B. Mottelson and A. Winther, Revs. Mod. Phys. **28** (1956) 432
2) N. P. Heydenburg and G. M. Temmer, Phys. Rev. **104** (1956) 981
3) H. Mark and G. T. Paulissen, Phys. Rev. **100** (1955) 813
4) T. Huus, J. H. Bjerregaard and B. Elbek, Mat. Fys. Medd. Dan. Vid. Selsk. **30** (1956) no. 17
5) J. H. Bjerregaard and U. Meyer-Berkhout, Z. Naturforsch. **11a** (1956) 273
6) E. M. Bernstein and H. W. Lewis, Phys. Rev. **105** (1957) 1524
7) B. Elbek, K. O. Nielsen and M. C. Olesen, Phys. Rev. **108** (1956) 406
8) K. O. Nielsen and M. C. Olesen, to be published
9) L. A. Sliv and J. H. Band, Tables of Gamma-Ray Internal Conversion Coefficients, Part 1 (Izdatelstvo Akademii Nauk SSSR, Moscow and Leningrad, 1956)
10) M. E. Rose, in Beta and Gamma-Ray Spectroscopy, edited by K. Siegbahn (North Holland Publishing Company, Amsterdam, 1955);
M. E. Rose, G. M. Goertzel and C. J. Swift, privately circulated tables of L-conversion coefficients
11) K. O. Nielsen and Ottar Skilbreid, Nuclear Instruments **2** (1958) 15
12) A. W. Sunyar, Phys. Rev. **98** (1955) 653
13) O. Nathan, Nuclear Physics **5** (1958) 401

*Nuclear Physics* **6** (1958) 460—463; © *North-Holland Publishing Co., Amsterdam*
Not to be reproduced by photoprint or microfilm without written permission from the publisher

# POLARIZATION OF X-RAY QUANTA AND NON-CONSERVATION OF PARITY IN K-CAPTURE

A. Z. DOLGINOV
*Physico-Technical Institute of the USSR Academy of Sciences, Leningrad*

Received 4 November 1957

**Abstract:** The effect of parity non-conservation in $\beta$-interaction on the correlation between circular polarization of X-ray quanta emitted by an atom after K-capture and polarization of nuclear spins or of subsequent nuclear quanta is considered. L-capture is examined and it is shown that in capture from the $L_{III}$ shell the angular distribution of X-ray quanta is anisotropic.

A number of investigations [1, 2]) carried out recently have confirmed Lee and Yang's hypothesis [3]) of parity non-conservation in $\beta$-interactions. This compels one to re-examine the previous results pertaining to $\beta$-processes. In an earlier paper [4]) the author suggested that correlation be studied between circular polarization of X-ray quanta emitted when a vacancy formed after allowed K-capture is filled up and the orientation of nuclear spins or polarization of the subsequent nuclear radiation. It was shown that such a study should yield information on the relative sign of the scalar and tensor $\beta$-interaction constants.

In the present work we shall generalize the results obtained in ref. [4]) by taking into account parity non-conservation. It will be shown that the qualitative predictions of ref. [4]) are valid but that the formulae are somewhat different. It will also be shown that in $L_{III}$ electron capture the angular distribution of the X-rays becomes anisotropic.

Since the calculations are not essentially different from those presented in ref. [4, 5]) we shall not develop them but simply give the final results.

The first case to be considered will be that in which the nucleus was oriented by an external field before K-capture and the direction and polarization of the nuclear quantum which may be emitted after K-capture is not studied. If the X-ray is emitted in an electron transition from a level with a momentum $I = \frac{1}{2}$ (e.g. $L_{II}$) to a vacant K-level, the correlation between circular polarization of this quantum and the direction of the nuclear spins will have the form

$$W_{j_0 \mathrm{X}}(\theta) = a+b+\sigma\varrho\{\tfrac{1}{2}[j_0(j_0+1)-j_1(j_1+1)+2]\,b-d\sqrt{j_0(j_0+1)}\}\cos\theta, \quad (1)$$

with

$$
\begin{aligned}
a &= (|C_S|^2+|C'_S|^2)|K_S|^2+(|C_V|^2+|C'_V|^2)|K_V|^2 \\
&\quad -2\,\mathrm{Re}(C_S C_V^*-C'_S C'^*_V)K_S K_V^*, \\
b &= (|C_T|^2+|C'_T|^2)|K_T|^2+(|C_A|^2+|C'_A|^2)|K_A|^2 \\
&\quad -2\,\mathrm{Re}\,(C_T C_A^*-C'_T C'^*_A)K_T K_A^*, \\
d &= 2\,\mathrm{Re}\,[(C_S C_T^*+C'_S C'^*_T)K_S K_T^*-(C_V C_T^*-C_V' C'^*_T)K_V K_T^* \\
&\quad -(C_S C_A^*-C'_S C'^*_A)K_S K_A^*+(C_V C_A^*+C'_V C'^*_A)K_V K_A^*], \\
\varrho &= \sum_{\mu_0} \mu_0 W(\mu_0)/j_0(j_0+1);
\end{aligned}
\tag{2}
$$

$\theta$ denotes the angle between the X-ray direction and that of predominant orientation of the nuclear spins, $j_0$ is the nuclear momentum in the initial state and $\mu_0$ is its projection in the $Z$-axis; $W(\mu_0)$ is the probability for a given value of $\mu_0$; $\varrho$ determines the degree of polarization of the nuclear spins; $\sigma = 1$ or $-1$ for right and left-handed polarization of the X-ray quanta respectively; $C_S$, $C_V$, $C_T$ and $C_A$ are the scalar, vector, tensor and axial-vector interaction constants; $C'_S$, $C'_V$ etc., are analogous constants in those terms which are permissible only in the case of parity non-conservation (that is, in those terms which contain an additional $\gamma_5 = \gamma_1\gamma_2\gamma_3\gamma_4$ where $\gamma_4 = -\beta$ and $\gamma_i$, $\gamma_5$ and $\beta$ are Dirac matrices). In calculating (1) we used the general form of $\beta$-interaction proposed by Lee and Yang [3]). $K_S$ and $K_T$ are nuclear matrix elements for scalar and tensor, and $K_V$ and $K_A$ for vector and axial-vector $\beta$-interaction. In the non-relativistic approximation for nucleons $K_S = -K_V$, $K_T = -K_A$. The correlation expression does not depend separately upon $K_S$ and $K_T$ but only on $K_S/K_T$. One has

$$
\begin{aligned}
K_S &= \int \psi^*_{j_1\mu_1}\beta\psi_{j_0\mu_0}\,\mathrm{d}\mathbf{r}, \\
C^{j_0\mu_0}_{1\Lambda j_1\mu_1}K_T &= (-1)^{1+\Lambda}\int \psi^*_{j_1\mu_1}\beta\sigma_{-\Lambda}\psi_{j_0\mu_0}\,\mathrm{d}\mathbf{r};
\end{aligned}
\tag{4}
$$

$\psi_{j_0\mu_0}$ and $\psi_{j_1\mu_1}$ are nuclear wave functions before and after electron capture; $\sigma_0 = \sigma_z$, $\sigma_{\pm1} = \pm\sqrt{(\frac{1}{2})}(\sigma_x \pm i\sigma_y)$; $\sigma_x$, $\sigma_y$, $\sigma_z$ are Pauli matrices. $C^{j_0\mu_0}_{1\Lambda j_1\mu_1}$ is a Clebsch-Gordan coefficient; $j_1$ and $\mu_1$ are the nuclear angular momentum and its projection after K-capture. Matrix elements $K_S$ and $K_T$ do not depend on the magnetic quantum numbers $\mu_0$, $\mu$ and $\Lambda$.

If a $\gamma$-quantum is emitted by a nucleus after K-capture the values of $a$, $b$ and $d$ can be determined by studying the correlation between the circular polarizations of X-ray and nuclear quanta. In this case it is not necessary to use oriented nuclei. If the X-ray quantum is emitted in an electron transition from a level with a momentum $I = \frac{1}{2}$ to the K-shell and the $\gamma$-quantum multipolarity is $2^L$, the correlation will have the form

$$W_{\gamma X}(\theta) = a+b-\sigma\sigma_\gamma[4j_1(j_1+1)L(L+1)]^{-1} \times [j_1(j_1+1)-j_2(j_2+1)+L(L+1)]\{[j_1(j_1+1)-j_0(j_0+1)+2]b +2d\sqrt{j_1(j_1+1)}\}\cos\theta. \quad (5)$$

Here $\theta$ is the angle between the directions of the X-ray and nuclear quanta, $\sigma_\gamma = 1$ or $-1$ for right or left hand polarization of the nuclear quantum.

If the electron which fills the K-shell vacancy comes from a level with a momentum $I = 3/2$ (e.g. $L_{III}$) a factor $-\frac{1}{2}$ should be introduced before $\sigma$ in eqs. (1) and (5). Since the probability of a transition from a level $I=3/2$ is almost twice that from a level $I = \frac{1}{2}$, the total correlation will be very small. Therefore in determining the polarization of X-ray quanta emitted from the $I = 3/2$ and $I = \frac{1}{2}$ levels the quanta should be separated in accord with their energy. The $K_{\alpha_1}$ and $K_{\alpha_2}$ lines are the most convenient for this purpose.

If allowed electron capture takes place from the $L_I$ or $L_{II}$ shells for which $I = \frac{1}{2}$ and $l = 0$ or 1 the correlation will be of the same nature as that for K-capture. In this case, however, complete compensation of right and left hand correlation in the total radiation, $L_{\beta_1}$, $L_\gamma$ etc., will not occur. It is difficult to compute theoretically the remaining fraction of polarization since a good knowledge of the electron wave functions is required.

Correlations (1) and (5) exist in the case of K, $L_I$ or $L_{II}$ capture only if the nuclei are dipolarly polarized. Correlations (1) or (5) are absent in the case of aligned nuclei. Aligned nuclei may be employed to study the angular distribution of X-ray quanta after $L_{III}$ capture. In this case $I = 3/2$, $l = 1$ and the angular distribution of X-ray quanta with respect to the direction of the aligned nuclei will be anisotropic. If the nuclei are not oriented but after $L_{III}$ capture they emit $\gamma$-quanta, an angular correlation will exist between the X-ray and nuclear quanta. Only tensor and pseudovector interactions contribute to the allowed $L_{III}$ capture. In this case the angular distribution of the X-ray quanta has the form

$$W(\theta) = 1+\sqrt{15(2j_0+1)/8}A_1 W(j_1 1 j_0 2;\ j_0 1)(3\cos^2\theta-1)R_j \quad (6)$$

where $W(abcd;\ ef)$ are Racah functions.

The $A_I$ depend only on the momentum $I$ of the electron which fills the vacancy in the $L_{III}$ shell: $A_{\frac{1}{2}} = 1$, $A_{3/2} = -4/5$, $A_{5/2} = 1/5$. If the nuclei are aligned and possible nuclear $\gamma$-quanta are not studied, one gets

$$R_j = \sum_{\mu_0}[3\mu_0^2-j_0(j_0+1)]W(\mu_0)[(2j_0-1)j_0(j_0+1)(2j_0+3)]^{-\frac{1}{2}}. \quad (7)$$

For angular correlation between X-ray and nuclear quanta from non-oriented nuclei one gets

$$R_j = \sqrt{(2j_1+1)(2L+1)}\left[1-\frac{3}{L(L+1)}\right]W(j_2 L j_1 2;\ j_1 L)C^{L0}_{L020}. \quad (8)$$

Expression (6) does not contain the L-capture nuclear matrix elements or constants $C$ and $C'$. They enter as a common factor which does not affect the form of angular correlation (6) and hence has been omitted.

The formulae for forbidden capture from K- or L-shells are more complex. Forbidden transitions are considered in another paper of the author [6]).

Investigation of correlation (6) does not yield information on $\beta$-interaction; however it can be used to determine the momenta of nuclear levels.

Available experimental data yield some information on $C$ and $C'$. These data are not complete and from the standpoint of present day theory they seem to be contradictory. Determination of such combinations of $C$ and $C'$ which have not been studied up to now would therefore seem to be of special interest. Quantities $a$, $b$ and $d$ which enter (1) and (5) are combinations of this type.

Hence it should be interesting to investigate (1) and (5) with the purpose of elucidating the nature of $\beta$-interaction.

## References

1) E. Ambler, R. Hayward, D. Hoppes, R. Hudson and C. Wu, Phys. Rev. **105** (1957) 1413; **106** (1957) 1361
2) R. L. Garwin, L. M. Lederman and M. Weinrich, Phys. Rev. **105** (1957) 1416
3) T. D. Lee and C. N. Yang, Phys. Rev. **104** (1956) 254
4) A. Z. Dolginov, Nuclear Physics **2** (1956/57) 723
5) A. Z. Dolginov, Nuclear Physics **5** (1958) 512
6) A. Z. Dolginov, JETP (in print)

*Nuclear Physics* **6** (1958) 464—476; © *North-Holland Publishing Co., Amsterdam*
Not to be reproduced by photoprint or microfilm without written permission from the publisher

# THE ENERGY AND ANGULAR DISTRIBUTION OF PROTONS FROM 14 MeV NEUTRON REACTIONS WITH Cu

D. L. ALLAN

*Atomic Energy Research Establishment, Harwell Didcot, Berks*

Received 29 January 1958

**Abstract:** The energy and angular distributions of protons from the reactions $Cu^{63, 65}$ (n, p) and $Cu^{63}$ (n, np) at 14 MeV have been determined. The energy distributions in the forward direction exhibit peaks spaced many times the known level spacing of the residual nuclei. The angular distributions are symmetrical about 90° only for protons in the energy interval 2—3 MeV; the angular distributions for other energy intervals show a forward asymmetry which increases progressively with proton energy.

## 1. Introduction

During the past few years evidence has been accumulating that nuclear reactions induced by particles having energies in the region 10—20 MeV cannot be completely described in terms of the formation and independent decay of a compound nucleus. According to the statistical theory [1]), the particles emitted as a result of compound nucleus decay have a characteristic low average energy and an angular distribution which exhibits forward and backward symmetry. Several experiments, particularly those of Graves and Rosen [2]) on the inelastic scattering of 14 MeV neutrons by nuclei from C to Bi, have shown that the energies of the particles emitted are low and, in the case of Bi, the angular distribution is essentially isotropic. [3]) However, there was a small yield of neutrons inelastically scattered from Bi with energies between 4 MeV and 12 MeV which were emitted preferentially in the forward direction. It is now believed that the emission of energetic particles in the forward direction is a characteristic of direct interactions.

Anisotropic angular distributions have also been observed in 14 MeV (n, p) reactions [4–7, 14]). In these reactions, the emission of protons by the compound nucleus process is somewhat inhibited by the presence of the Coulomb barrier. In some earlier work [4]), the energy distribution of the protons from the reactions $Cu^{63}$ (n, p) and $Cu^{63}$ (n, np) at 14 MeV was studied. It was estimated that compound nucleus processes contributed a total of 230 mb to the observed cross section for proton production in these two reactions. This is less than 20 % of a typical non-elastic 14 MeV neutron cross section ((n, n′)+(n, 2n)). This paper presents the results

of a study of the angular distribution of protons emitted in the reactions Cu (n, p) and Cu (n, np) as a function of proton energy. The experiment provides an opportunity for studying the anisotropic effects caused by direct interactions in reactions in which the contribution of compound nucleus processes is relatively small.

## 2. Apparatus

In this work a photographic plate camera of novel design was used in which the disposition of the target and the plate was the reverse of that usually employed for the determination of angular distributions. A single 1 in. × 1 in., 300 $\mu$, Ilford $C_2$ photographic plate was surrounded by a cylindrical Cu target (fig. 1), all parts of which were exposed to the neutron source. The tracks of protons from neutron induced reactions in Cu therefore approached the plate from all directions $\alpha = 0°-360°$ (see fig. 1),

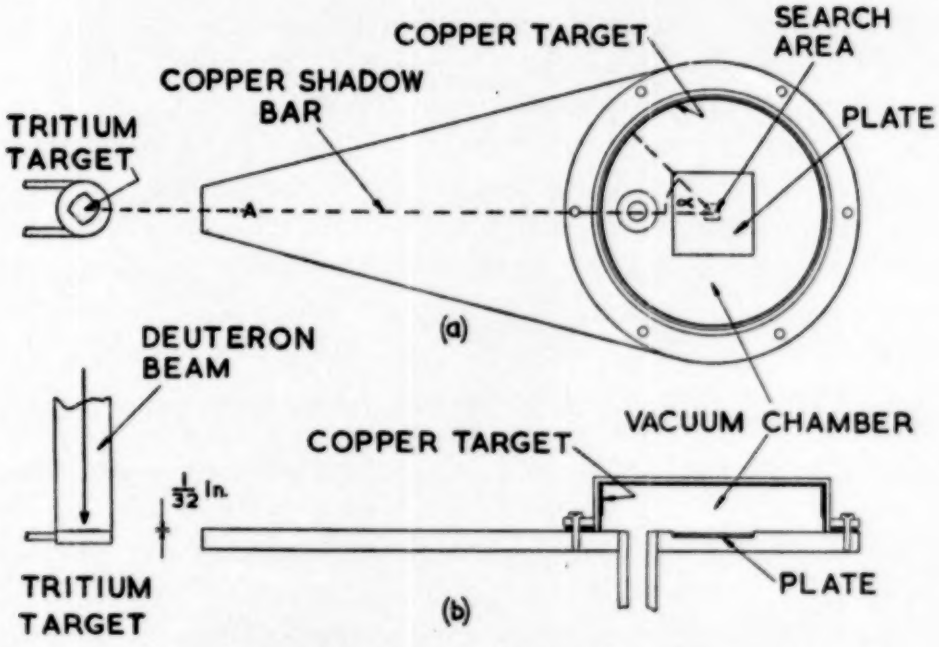


Fig. 1. Apparatus: (a) plan; (b) section.

corresponding to a wide range of angles between the incident neutrons and the emitted protons. The advantages of the method are the following:

(i) The density of tracks in the plates is high because protons from a large area of target are recorded in a small area of emulsion.

(ii) All the measurements required for the determination of the energy and angular distributions of the protons are made by scanning a single plate. The results are not sensitive to small variations in the track selection criteria applied by the scanner, nor are they sensitive to the number of tracks which are missed.

(iii) Background tracks can be easily allowed for.

The target was formed from a strip of 25 mg · cm$^{-2}$ Cu foil, 1.05 cm wide, which was clamped between grooves in a gold lined vacuum chamber to form a cylinder, radius 3.75 cm, about the centre of the plate. The height of the cylindrical target above the emulsion surface was such that protons from it entered the plate at an angle $15° \pm 8°$ to the emulsion surface.

A source of 14 MeV neutrons was provided by bombarding a zirconium tritide target with 250—300 keV deuterons. The photographic plate was screened from neutrons arriving directly from the source by a copper plate, $\frac{1}{4}$ in. thick, in which it was embedded (fig. 1b). The surface of the emulsion lay 1/32 in. below the upper surface of the copper plate.

During an exposure to neutrons, the apparatus was placed so that the zirconium tritide deposit in the neutron target assembly was also 1/32 in. below the upper surface of the copper plate and the centre of the deposit was 5 cm from its narrow end.

The photographic emulsion was therefore screened from the neutron source by the whole length of the plate. A particular advantage of the photographic plate as a detector is that it can be very effectively screened by a thin copper plate, because even a neutron which is scattered elastically through a small angle is unlikely to pass through the emulsion. The thickness of the copper plate we used was determined by the necessity of screening all parts of the neutron target assembly. For this reason, a specially shallow water-cooled target assembly was designed for use with the apparatus. Accurate alignment was facilitated by a light aluminium locating device.

## 3. Neutron Flux Determinations

The variation of neutron flux around the cylindrical target was determined by an activation method. Pieces of Cu foil were placed at eight different angles in the grooves normally occupied by the cylindrical target. After a series of short 14 MeV neutron irradiations with the apparatus in the usual position, the 10 min $\beta^+$ activity induced in the foils by the $Cu^{63}$ (n, 2n) $Cu^{62}$ reaction (threshold 11 MeV) was determined. In this way, the neutron fluxes received by the foils at eight angles ($\alpha$) were determined relative to the flux at $\alpha = 0°$, with a statistical accuracy of $\pm 1$ %. The ratios agreed with the calculated neutron flux distribution within these limits.

A similar activation method was used to verify that the cylindrical Cu target foil was not partially shadowed by the copper plate. By cutting each foil into four strips and determining the activity induced in each strip, it was found that the neutron flux was uniform (within $\pm 2$ %) with height above the upper surface of the plate. (For this experiment foils were placed at $\alpha = 0°$, 90°, and 180°.)

The absolute integrated neutron flux during photographic plate ir-

radiations was calculated from the total neutron output. This was monitored during each irradiation by placing a Cu foil 10 cm from the neutron source. About 12 hours later the 12.8 h $\beta^-$ activity induced by the $Cu^{65}$ (n, 2n) $Cu^{64}$ reaction was determined. These activities were calibrated later by exposing a similar foil to neutrons produced in a different target assembly in which the $\alpha$-particles from the $H^3$ (d, n) $He^4$ reaction entering a known small solid angle were counted.

## 4. Neutrons Scattered by the Copper Plate

The good agreement between the calculated neutron flux distribution and that determined by the activity measurements shows that the contribution to the $Cu^{65}$ (n, 2n) reaction of neutrons scattered by the copper plate is very small. The contribution of the scattered neutrons to the (n, p) reactions is also small because (i) those scattered inelastically into the energy range 0.5—4.0 MeV have insufficient energy to contribute significantly, (ii) there are very few neutrons scattered into the energy range 4.0—14.0 MeV, and (iii) those scattered elastically represent only a weak source of 14 MeV neutrons near A (fig. 1a). It has been shown above by the activity measurements that the elastically scattered neutrons cannot greatly distort the observed angular distributions.

## 5. Experimental Procedure

Nine plates were separately exposed in the apparatus with the cylindrical Cu target in position. Five plates were exposed with the cylindrical target replaced by a 5 cm length of similar Cu foil occupying the angular position $\alpha = 80°—160°$. The second group of plates recorded the background tracks, the 5 cm foil being required for the background normalization procedure described in § 6. The exposure times for the average neutron output of $10^{10}$ neutrons per second were about one hour for each of the first group of plates and about three hours for each of the second group.

The plates were scanned for tracks entering the surface of the emulsion over a central area 0.5 cm $\times$ 0.5 cm. The scanning was restricted to this area in order to simplify the geometry. Tracks entering the surface from all directions ($\alpha = 0°$ to 360°) were accepted for measurement and the length, position co-ordinates, dip angle, and angle ($\alpha$) were recorded. The dip angle measurements were used to exclude the tracks of protons which could not have come from the Cu target foil.

## 6. Analysis of Track Measurements

About 20 000 tracks were measured in the 9 plates exposed to the cylindrical Cu target foil. These tracks were sorted into the 264 energy-angle

intervals $\Delta E \Delta\theta$ required for the presentation of the results (figs. 3, 4, 5). $E$ is the proton energy in MeV at the layer of the Cu foil one half thickness deep; $\theta$ is the angle between the protons and the incident neutrons.

The quantities actually measured were the ranges $R$ and the angles $\alpha$ of the tracks in the plates. Each interval $\Delta E \Delta\theta$ therefore corresponded to an interval $\Delta R \Delta\alpha$ which was the interval actually used for sorting the track measurements. The relation between $\alpha$ and $\theta$ was calculated from the geometry of the apparatus. It will be seen that the angles $\alpha = 0°-180°$ correspond to the same angles $\theta$ as the angles $180°-360°$. The relation between $R$ and $E$ was obtained using the range-energy data of Rotblat [8]) for Ilford C2 emulsion and the range-energy data of Ribakov [9]) for protons in Cu. A 2 % correction was applied to the range-energy relation to allow for the average angle of dip of the tracks in the plates.

The background was measured in the 5 plates exposed to the 5 cm Cu monitoring foil. A typical angular distribution (as a function of $\alpha$) of tracks measured in one of the background plates is given in fig. 2. The

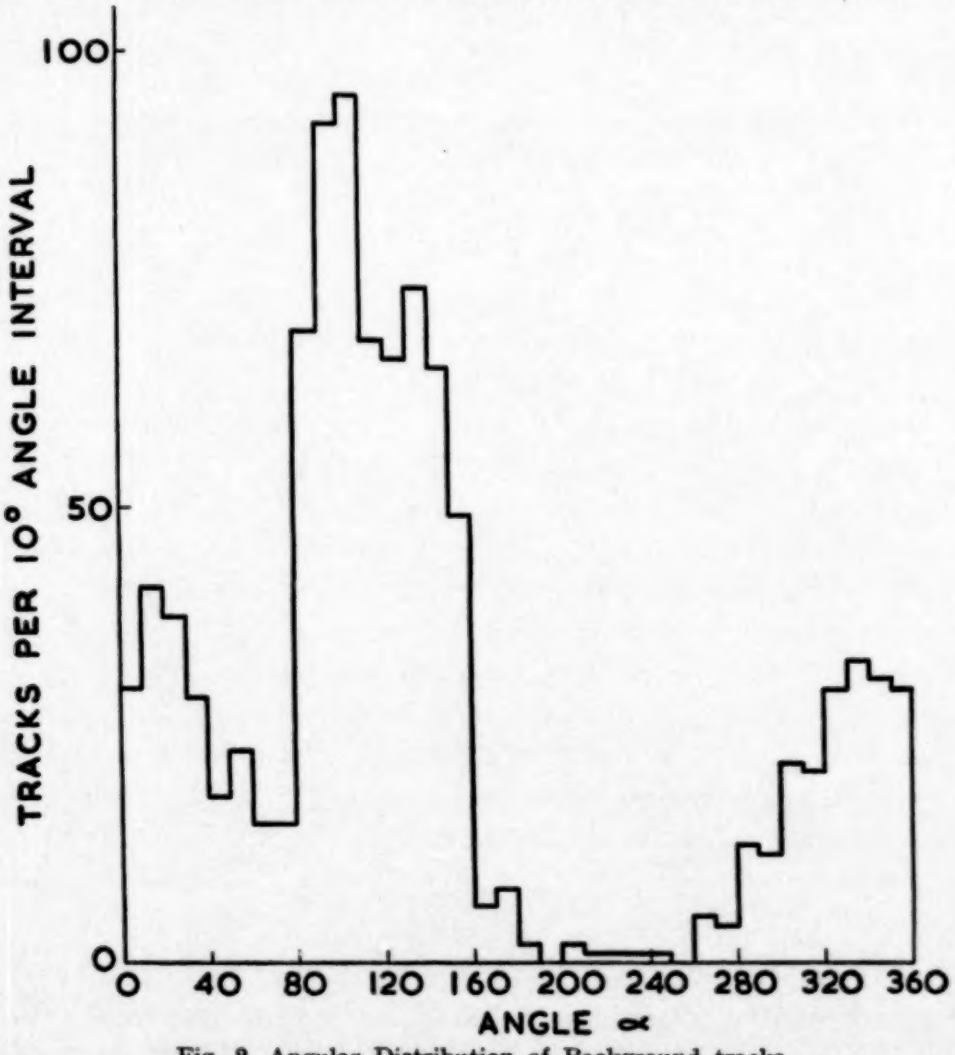


Fig. 2. Angular Distribution of Background tracks.

tracks between $\alpha = 80°$ and $160°$ are caused by protons from the 5 cm Cu foil; those at other angles are background. This histogram includes tracks of all lengths and most of the background shown corresponds to the more energetic protons. The background below 7 MeV is very small (see table 1). In order to be certain of excluding all tracks of protons from the Cu foil, only tracks in the angle ranges $0°-70°$ and $170°-360°$ were regarded as background. Since the background distributions in the two equivalent angle ranges $0°-180°$ and $180°-360°$ were found to be identical, it was assumed that the background in the region $70°-170°$ was the same as that found in the region $190°-290°$. The total background tracks from the 5 plates were sorted into the same 264 intervals referred to above.

The principle of background normalization which was used depended on the fact that, over the angle region $70°-170°$, the plates exposed to both the cylindrical Cu target foil and the 5 cm foil were recording the same events. The total numbers of tracks found in the two sets of plates in this angle region were therefore used to normalize the background. In practice, a more restricted interval corresponding to $\Delta E = 3-5$ MeV, and $\Delta\alpha = 100°-140°$ was used. A narrower angle interval was chosen in order to avoid errors caused by the limited resolution of the angle measurements ($\pm 3$ %). The restriction of the energy to 3–5 MeV was applied because the yield of tracks in this energy region is large and it is relatively insensitive to the angle $\alpha$ in the region $120°$.

Finally, for the angular distributions (figs. 4 and 5), the yield per interval was corrected for the variation of neutron flux around the target foil and for the fact that the intervals $\Delta\alpha$, corresponding to equal intervals $\Delta\theta = 10°$, were unequal.

## 7. Tests for Bias amongst the Scanners

A number of tests were applied to ensure that the angular distributions were not affected by observer angle bias. The results of some of these tests are given below:

(i) $90°$ and $270°$. The number of tracks between $0°$ and $180°$ was equal, within the statistical errors, to the number between $180°$ and $360°$ for all the energy ranges.

(ii) $0°$ and $180°$. The nine plates were placed on the microscope stage at three different angular orientations so that the scanners measured track angles $\alpha_1 = \alpha$, $\alpha+90°$, or $\alpha+270°$. No differences were found between the results from the three sets of plates.

(iii) Maximum Yield. There might have been a tendency for the scanners to favour those angles ($\alpha$) corresponding to the maximum yield of tracks. Five plates were re-scanned several times each by different scanners and

the angular distributions of the tracks missed by each scanner (10—15%) were compared with the final results. Within the statistical errors, the angular distributions were identical. The tracks missed by the scanners were therefore a random sample of those present in the plates.

## 8. The Determination of Cross Sections

The angular distributions presented in figs. 4 and 5 give the proton yield at the centre of the plate as a function of $\theta$, relative to the yield at 20°. In order to provide an absolute cross section scale it was necessary to determine three quantities:

(i) The integrated neutron flux during each irradiation over the region of Cu target foil at $\alpha = 0°$.

(ii) The number of tracks per cm² at the centre of the plate.

(iii) The solid angle subtended at the centre of the plate by the length of foil corresponding to the interval $\Delta\theta = 10°$.

The determination of neutron flux (i) was discussed in § 3. The number of tracks per cm² (ii) was obtained by re-scanning the plates a number of times, as mentioned in § 7 (iii). The solid angle subtended by $\Delta\theta$ (iii) was determined by placing a uniform deposit of Pu 239 of known activity in the target position and counting the number of $\alpha$-tracks recorded in a 0.26 cm² area of the plate.

## 9. Results

### 9.1. ENERGY DISTRIBUTIONS

The proton energy distributions at six angles of observation are given in fig. 3. The ordinates give the proton yield per 0.5 MeV energy interval in arbitrary units. The angle range is $\pm 10°$ for the spectra at 25° and 45° and $\pm 15°$ for the other spectra. The spectra are very similar apart from the presence of broad groups and a high energy tail in the spectrum at 25°.

### 9.2. ANGULAR DISTRIBUTIONS

The angular distribution (figs. 4 and 5) give the differential cross sections for eight different energy ranges. The angular distribution of the 2—3 MeV protons is approximately isotropic but shows a small dip in the region of 90°. The other distributions show a progressive increase in forward asymmetry as the proton energy increases. It should be pointed out that 2 MeV protons lose 1 MeV in traversing a half-thickness of the Cu target foil and therefore the proton energies for the first two or three energy intervals is not very precisely determined. At higher energies the energy loss is 0.3 MeV.

The energy intervals chosen for the angular distributions of fig. 5 correspond to the energies of the proton groups observed in the spectrum at

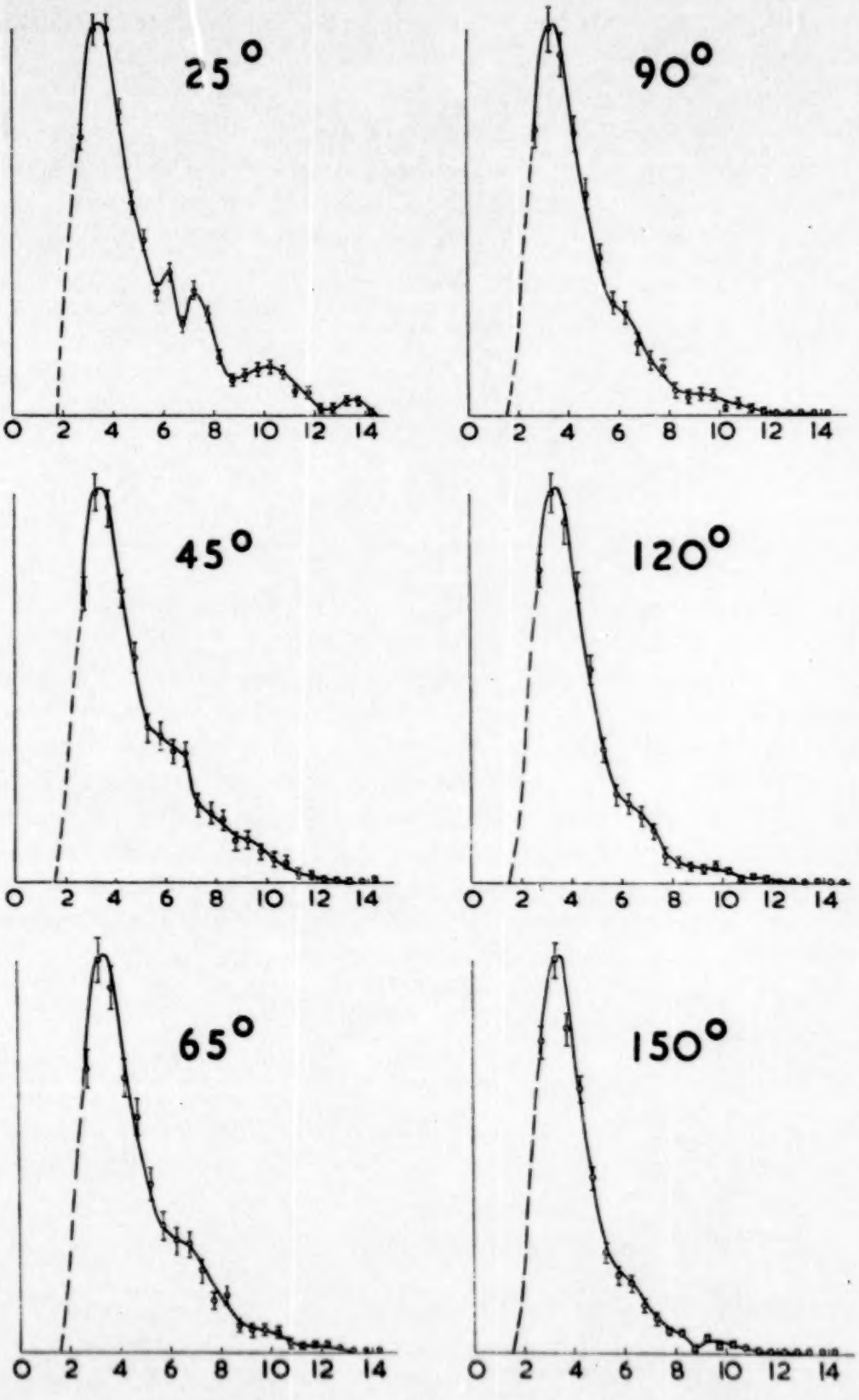


Fig. 3. Proton energy distributions. Ordinate: relative yield of protons (tracks/0.5 MeV energy interval). Abscissa: Proton energy (MeV).

25°. These angular distributions are all peaked strongly in the forward direction.

### 9.3. BACKGROUND INTENSITIES

The results given in figs. 3, 4, and 5 have been corrected for background. In order to illustrate the low intensity of the background in this work, the background as a percentage of the total number of tracks observed is given for some representative energies and angles in table 1.

TABLE 1
Background %

| $\theta$ \ $\Delta E$ (MeV) | 2–5 | 5–7 | 7–12 | 12–14 |
|---|---|---|---|---|
| 30° | 6 | 12 | 30 | 50 |
| 60° | 7 | 9 | 27 | 20 |
| 90° | 5 | 6 | 17 | 10 |
| 120° | 2 | 3 | 6 | 0 |
| 150° | 1 | 2 | 4 | 0 |

### 9.4. CROSS SECTIONS

The cross sections $\sigma(E)$, integrated over all angles are given in table 2 (column 2) for each of the energy intervals. Column 3 (table 2) gives the integrated cross section, $\sigma_s(E)$, per energy interval calculated from the 'symmetrical part' of the angular distribution. The 'symmetrical part' was defined as the angular distribution for 2–3 MeV protons between 90° and 180°, reflected about 90°. This symmetrical curve was normalized to the two highest angle points of each angular distribution. Column 4 gives the non-symmetrical part of the cross section, $\sigma_{ns}(E) = \sigma(E) - \sigma_s(E)$. Column 5 gives the rations $R = \sigma_{ns}/\sigma$, expressed as a percentage. The three cross sections, $\sigma$, $\sigma_s$ and $\sigma_{ns}$, integrated over energy are given in the bottom row of the table.

TABLE 2
Cross sections (natural Cu)

| $E$ (MeV) | $\sigma(E)$ (mb) | $\sigma_s(E)$ (mb) | $\sigma_{ns}(E)$ (mb) | $R$ (%) |
|---|---|---|---|---|
| 2–3 | 29 | 28 | 1 | 3 |
| 3–4 | 53 | 48 | 5 | 9 |
| 4–5 | 38 | 32 | 6 | 16 |
| 5–6 | 19 | 14 | 5 | 26 |
| 6–7 | 13 | 7 | 6 | 46 |
| 7–9 | 14 | 5 | 9 | 64 |
| 9–12 | 6 | 1 | 5 | 83 |
| 12–14.5 | 1 | 0 | 1 | 100 |
| $\Sigma\sigma(E)$ | 173 | 135 | 38 | |

## 10. Discussion

In the earlier work [4]), the high yield of low energy protons (2—4 MeV) was attributed to the reaction $Cu^{63}$ (n, np) $Ni^{62}$. In this reaction it was assumed that neutron emission occurred first, leaving the $Cu^{63}$ nucleus in states of excitation energy between the proton and neutron binding energies. The protons therefore penetrate the Coulomb barrier (7 MeV) because they are in competition only with $\gamma$-ray emission. Such an explanation

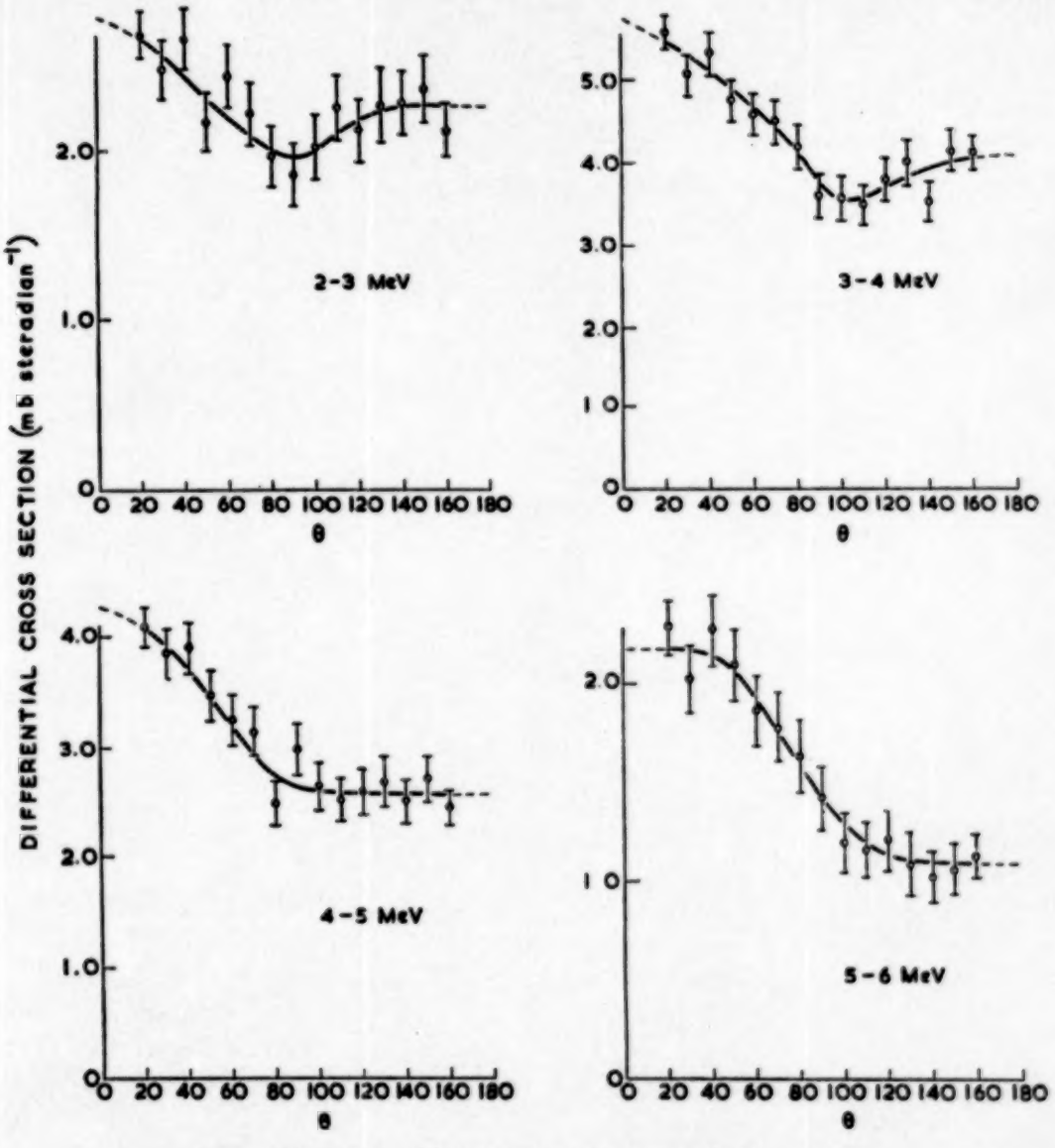


Fig. 4. Angular distribution of protons 2 MeV—6 MeV.

in terms of competitive compound nucleus decay is supported by the approximately isotropic angular distribution observed for 2—4 MeV protons.

The groups observed in the proton energy spectrum at 25° (fig. 3) correspond to excitation energies of the residual nucleus in the reaction

$Cu^{63}$ (n, p) $Ni^{63}$ of from 0 to 8 MeV. It is reasonable to assume that only the $Cu^{63}$ isotope is involved because the cross section of the $Cu^{65}$ (n, p) $Ni^{65}$ reaction is small (19 mb [10]); $< 40$ mb [4])). Two of the groups (proton energies 7.5 MeV and 10.2 MeV) were observed in the earlier work. The spacing of these groups (1—3 MeV) is very much greater than the expected spacing of the levels in $Ni^{63}$ at excitation energies of the order of several MeV. According to the semi-empirical level density formula of Lang and Le Couteur [11]), the level densities in a nucleus, $A = 60$, in states of excitation

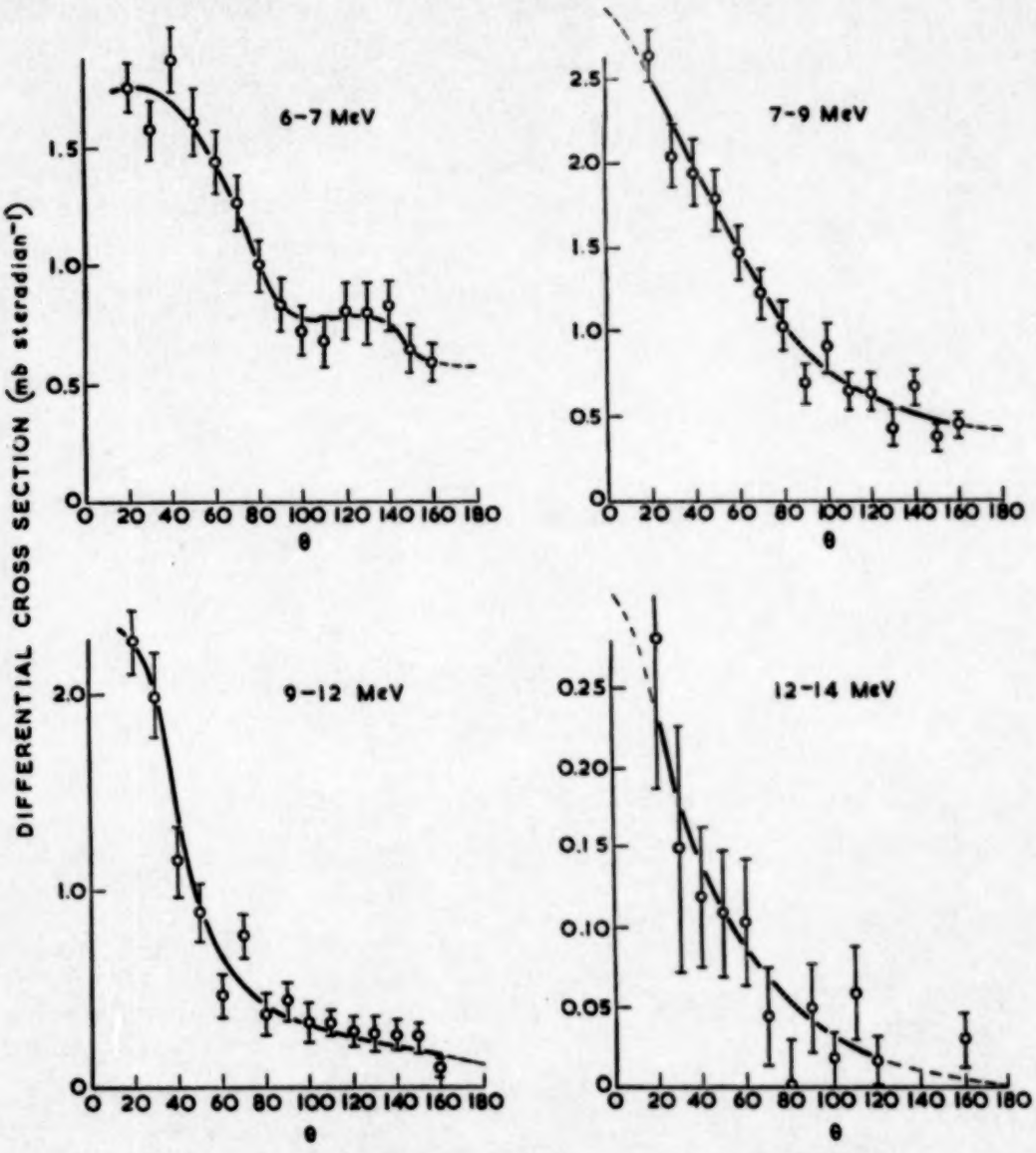


Fig. 5. Angular distribution of protons 6 MeV—14 MeV.

with energies 3—7 MeV, is of the order of tens to hundreds of levels per MeV. In the statistical theory it is supposed that, on the average, these levels compete equally in the decay of the compound nucleus. Therefore, the effects of individual levels should have been smoothed out in this experiment.

The observation of well spaced groups indicates that the levels do not compete equally in this region of excitation energy. This fact, and the pronounced forward anisotropy of the angular distributions (fig. 5), suggest that some of the protons are emitted as a result of direct interactions which leave the residual nucleus with an excitation corresponding to certain preferred groups of levels. Rather similar groups have been observed by Cohen [12]) in (p, p′) scattering experiments at 23 MeV for a wide range of target nuclei. Because of the rather poor energy resolution of the measurements reported here, it is not possible to make a reliable comparison between the (n, p) and (p, p′) proton spectra. However, the groups observed by Cohen for Ni at excitation energies 4.3 MeV and 7.0 MeV appear to correspond to the groups at proton energies 10.2 MeV and 7.5 MeV in fig. 3.

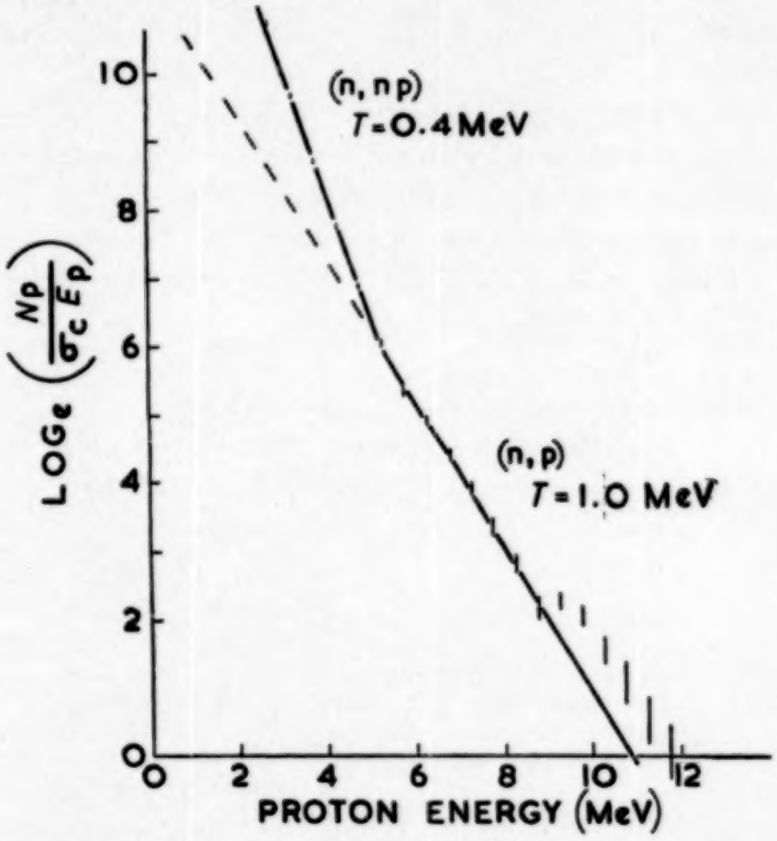


Fig. 6. Statistical theory plot for protons emitted at backward angles.

If these protons are derived from the reaction $Cu^{63}$ (n, p) $Ni^{63}$ ($Q = +0.72$ MeV), these groups correspond to excitation energies of the $Ni^{63}$ nucleus of 4.6 MeV and 7.3 MeV, respectively.

The division of the cross sections $\sigma(E)$ into symmetrical and non-symmetrical parts, $\sigma_s(E)$ and $\sigma_{ns}(E)$, is intended to show the size of the asymmetries in the angular distributions after the differential cross sections have been integrated over all angles. $\sigma_{ns}(E)$ can be identified with the cross

section for direct interaction provided there is no interference between the direct and compound nucleus reaction processes. The figures in table 2 show that the absolute magnitude of the asymmetry caused by direct interactions ($\sigma_{ns}$) per MeV is roughly constant over most of the spectrum, whereas the relative asymmetry ($R$) increases rapidly with proton energy.

The angular distributions are roughly isotropic for the backward angles over the whole spectrum. This suggests that the effect of direct interactions is small. Therefore, the spectra at backward angles provide an opportunity for comparing the results with the statistical theory. Fig. 6 gives a conventional statistical theory plot of the combined results from the 90°, 120° and 150° proton energy spectra. The ordinate is the logarithm of the proton yield divided by proton energy and the calculated cross section for compound nucleus formation by protons [13]). The points lie on two straight lines corresponding to the two reactions $Cu^{63}$ (n, np) $Ni^{62}$ and $Cu^{63}$ (n, p) $Ni^{63}$. The slopes of the lines give the temperature parameters, $T = 0.4$ MeV and $T = 1.0$ MeV, for the residual nuclei in these reactions, and their intersection (at an excitation energy for $Cu^{63}$ 0.6 MeV above the neutron binding energy) occurs at the point where competition from the $Cu^{63}$ (n, 2n) reaction becomes appreciable. These temperatures are in good agreement with the temperatures found by March and Morton [7]) for similar reactions induced by 13.5 MeV neutrons in $Fe^{54}$ and $Fe^{56}$.

The author wishes to thank Mrs. M. J. Bathe, Miss E. I. Harrison, and Mrs. A. S. Lane, for their patient work in scanning the plates. Thanks are also due to Dr. B. B. Kinsey and Dr. A. M. Lane for many helpful and stimulating discussions.

## References

1) V. F. Weisskopf and D. H. Ewing, Phys. Rev. **57** (1940) 472
2) E. R. Graves and L. Rosen, Phys. Rev. **89** (1953) 343
3) L. Rosen and L. Stewart, Phys. Rev. **99** (1955) 1052
4) D. L. Allan, Proc. Phys. Soc. A **70** (1957) 195
5) G. Brown, G. C. Morrison, H. Muirhead and W. T. Morton, Phil. Mag. **2** (1957) 785
6) R. K. Hailing, R. A. Peck Jr. and H. P. Eubank, Phys. Rev. **106** (1957) 971
7) P. March and W. T. Morton, Phil. Mag., to be published (1958)
8) J. Rotblat, Nature **167** (1951) 550
9) B. V. Ribakov, Zh. Ex. Teor. Fiz. **28** (1955) 651
10) S. G. Forbes, Phys. Rev. **88** (1952) 1309
11) J. M. B. Lang and K. J. Le Couteur, Proc. Phys. Soc. A **67** (1954) 586
12) B. L. Cohen, Phys. Rev. **105** (1957) 1549
13) J. M. Blatt and V. F. Weisskopf, Theoretical Nuclear Physics (Wiley, New York, 1952)
14) V. V. Verbinski, T. Hurliman, W. E. Stephens and E. J. Winhold, Phys. Rev. **108** (1957) 779

*Nuclear Physics* 6 (1958) 477—488; © *North-Holland Publishing Co., Amsterdam*

Not to be reproduced by photoprint or microfilm without written permission from the publisher

# SYMMETRICAL STRUCTURE AND CONSERVATION RELATIONS OF FOUR-COMPONENT NEUTRINO FIELD

TAKEHIKO TAKABAYASI
*Institut Henri Poincaré, Paris*

Received 24 January 1958

**Abstract:** A four-component spinor field with zero rest-mass $\psi$ is represented as the field defined by its modulus $\varrho$, an orthogonal frame in two-dimensional internal space, and a Lorentz frame in 4-dimensional internal space. This representation manifests the perfect isotropic property of the field in both internal spaces. In fact, the neutrino equation is invariant under arbitrary rotations in those internal spaces, which are conversely expressible by a certain four-component spinor $\zeta$. As the result of these new invariance properties the neutrino field is shown to satisfy several conservation relations that are vector or tensor equations with respect to both internal spaces. They contain, besides the conventional ones, a number of new conservation laws.

## 1. Introduction

It is well known that the free Dirac equation for zero rest-mass

$$\gamma_\mu \partial_\mu \psi = 0 \tag{1.1}$$

is invariant under certain particular kinds of transformations other than the usual Lorentz transformations; in particular, it is invariant under $\psi \to \gamma_5 \psi$ or $\psi \to \psi^C$ ($\psi^C$ denoting the charge conjugate). It has also been noticed occasionally that the field (1.1) satisfies some conservation relations over and above the usual conservation laws. Those problems, however, have not been treated systematically from a unifying standpoint.

In this paper we first show that the four-component neutrino field $\psi$ can kinematically be separated into its "modulus" $\varrho$, an orthogonal frame in two-dimensional internal space (called "$\omega$-space"), specified by a single quantity $\theta$, and a Lorentz frame in four-dimensional internal Lorentz space (called "$\xi$-space"), specified by mutually orthogonal four 4-vectors $a_\mu^\xi$. All of them are defined at each space-time point. The field equation is then expressed in terms of these quantities in a quite simple form, and it effects a dynamical coupling of both internal spaces. It is to be emphasized that the internal spaces are not spaces added to the original theory, but are already implied in the original spinor.

Now, this new formalism is clearly suitable to elucidate the above mentioned problems. The invariance properties, possessed by the neutrino field besides the customary Lorentz invariance, are there manifested simply as

those under arbitrary rotations in both internal spaces. The neutrino field thus forms a representation of a 6-dimensional Lorentz group (reducible to 2- and 4-dimensional spaces) besides that of the usual Lorentz group. We remark that the invariance properties considered by Pauli [1]) correspond exactly to the subgroup of *spatial* rotations in our $\xi$-space.

Now, such symmetry properties in the internal spaces tell us that the usual conservation relations as to probability, momentum-energy, and angular momentum can at once be generalized to relations for arbitrary directions of the internal space. This means that we get a number of new conservation relations for the neutrino field.

The correspondence between our theory and the usual $\psi$-formalism is exhibited at each stage of the argument. Moreover we shall introduce the grand wave function $\Psi = \begin{pmatrix} \psi \\ \gamma_5 \psi^C \end{pmatrix}$, which behaves as a spinor in $\xi$-space for spatial rotations in this space. Also we show that our transformations in internal spaces keeping the neutrino field invariant are themselves representable exactly by a certain 4-component spinor $\zeta$.

We consider in this paper the problem only in the simplest form, i.e., the c-number free neutrino field.

## 2. Basic Formalism and Invariance Properties

As we have shown in previous notes [2]) †, a Dirac spinor $\psi$ can be replaced equivalently in c-number theory by the following set of real scalar and vector quantities:

$$\psi \longleftrightarrow \{\Omega, \hat{\Omega}, \alpha_\mu{}^\xi\}, \tag{2.1}$$

where $\Omega$ and $\hat{\Omega}$ are scalar and pseudoscalar respectively, and $\alpha_\mu{}^\xi$ ($\xi = 1, 2, 3, 4$), are four mutually orthogonal 4-vectors ††, satisfying †††

$$\alpha_\mu{}^\xi \alpha_\mu{}^\eta = (\Omega^2 + \hat{\Omega}^2) \cdot \delta_{\xi\eta}. \tag{2.2}$$

The quantities (2.1) are related to $\psi$ through the following equations *:

$$\begin{aligned}
\Omega &= \bar{\psi}\psi, & \hat{\Omega} &= i\bar{\psi}\gamma_5\psi, \\
\alpha_\mu{}^4 &= \bar{\psi}\gamma_\mu\psi, & \alpha_\mu{}^3 &= i\bar{\psi}\gamma_5\gamma_\mu\psi, \\
\alpha_\mu{}^1 &= \tfrac{1}{2}(\bar{\psi}^C\gamma_\mu\psi - \bar{\psi}\gamma_\mu\psi^C), \\
\alpha_\mu{}^2 &= \frac{1}{2i}(\bar{\psi}^C\gamma_\mu\psi + \bar{\psi}\gamma_\mu\psi^C),
\end{aligned} \tag{2.3}$$

† The local Lorentz frame associated to a Dirac spinor was recently considered also by some authors independently [3]). In earlier times Weyl, Einstein and others introduced the so-called Beingrössen associated to the Dirac spinor at each point of space in the context of generalizing the spinor theory to general relativity, but they did not specify the explicit connection (2.3).

†† $\alpha_\mu{}^1$, $\alpha_\mu{}^2$, $\alpha_\mu{}^3$ and $i\alpha_\mu{}^4$ are real 4-vectors, i.e., their space-components are real and time-component pure imaginary. The former three are space-like while $i\alpha_\mu{}^4$ is time-like.

††† Greek subscripts or superscripts run from 1 to 4. Summation convention is applied to subscripts and also to superscripts, wherever repeated.

* The vector character of the quantities $\alpha_\mu{}^1$ and $\alpha_\mu{}^2$ for usual Lorentz transformations is noted in ref. [4]).

where the charge conjugate spinor $\psi^C$ is given by †

$$\psi^C = C\bar{\psi}^T$$

with

$$C^\dagger C = 1, \qquad C^T = -C, \qquad \gamma_\mu{}^T = -C^{-1}\gamma_\mu C. \tag{2.4}$$

The set of quantities (2.1) may further be replaced by the set of variables

$$\{\varrho, \theta, a_\mu{}^\xi\} \tag{2.5}$$

defined through

$$\Omega = \varrho \cos\theta, \qquad \hat{\Omega} = \varrho \sin\theta, \qquad \alpha_\mu{}^\xi = \varrho a_\mu{}^\xi. \tag{2.6}$$

Then $a_\mu{}^\xi$'s satisfy the conditions

$$a_\mu{}^\xi a_\mu{}^\eta = \delta_{\xi\eta}, \qquad a_\mu{}^\xi a_\nu{}^\xi = \delta_{\mu\nu}, \tag{2.7}$$

and thus define a local Lorentz frame at each point. The assignment of $\xi = 1, 2, 3, 4$ in (2.3) was made in such a way that $\{a_\mu{}^\xi\}$ be an orthochronous Lorentz transformation, thus

$$\det(a_\mu{}^\xi) = +1. \tag{2.8}$$

Now it can be shown that the Dirac equation for the free neutrino field (1.1) is equivalently replaced, in terms of our variables (2.5), by the following eight real (scalar and vector) equations:

$$\partial_\mu(\varrho a_\mu{}^\xi) = 0, \tag{2.9}$$

$$\partial_\mu\theta = -\frac{i}{2}\varepsilon_{\mu\alpha\beta\gamma}a_\alpha{}^\eta\partial_\beta a_\gamma{}^\eta, \tag{2.10}$$

where $\varepsilon_{\mu\alpha\beta\gamma}$ is the alternating symbol.

The above formalism manifests several remarkable features of the neutrino field. First it shows that the field has perfectly isotropic property in the $\xi$-space, i.e., the internal Lorentz space †† implied in the original spinor. In other words the field equations are invariant under an arbitrary 4-dimensional rotation in $\xi$-space:

$$a_\mu{}^\xi \to a_\mu{}^{\xi'} = A^{\xi\eta}a_\mu{}^\eta,$$

with

$$A^{\xi\zeta}A^{\eta\zeta} = \delta_{\xi\eta}, \tag{2.11}$$

($\varrho$, $\theta$ invariant),

where $A^{\xi\eta}$ denote the coefficients of the internal Lorentz transformation and do not depend on $x_\mu$. The invariance means that $a_\mu{}^\xi$ is not only a 4-vector in the usual Lorentz space *but also is a 4-vector in the internal Lorentz space* ($\xi$-*space*).

† In this paper * signifies complex conjugate, † Hermitian conjugate, $^T$ transposed and $\bar{\psi} = \psi^\dagger\gamma_4$.

†† It is to be noted that for this space directions only are defined but not the elongation.

Furthermore our field equations (2.9) and (2.10) are evidently invariant under simple transformations

$$\varrho \to R\varrho, \tag{2.12}$$

and

$$\theta \to \theta+\chi, \tag{2.13}$$

where $R$ and $\chi$ are arbitrary constants not depending on $x_\mu$.

Now we regard the variable $\theta$ as the specification of a direction in a two-dimensional internal space (called $\omega$-space), which is independent of the $\xi$-space. Then the invariance (2.13) simply means the invariance of the field equations to an arbitrary rotation in this $\omega$-space. It is convenient to express this fact in a similar manner just as was done for the $\xi$-space. To do so we note that $\theta$ defines a two-dimensional orthogonal frame in the $\omega$-space by the following two unit vectors in this space:

$$\omega^{(1)} = \begin{pmatrix}\omega_1{}^{(1)}\\ \omega_2{}^{(1)}\end{pmatrix} = \begin{pmatrix}\cos\theta\\ \sin\theta\end{pmatrix} = \begin{pmatrix}\Omega/\varrho\\ \hat{\Omega}/\varrho\end{pmatrix},$$

and (2.14)

$$\omega^{(2)} = \begin{pmatrix}\omega_1{}^{(2)}\\ \omega_2{}^{(2)}\end{pmatrix} = \begin{pmatrix}-\sin\theta\\ \cos\theta\end{pmatrix} = \begin{pmatrix}-\hat{\Omega}/\varrho\\ \Omega/\varrho\end{pmatrix},$$

satisfying

$$\omega_r{}^{(p)}\,\omega_r{}^{(q)} = \delta_{pq}, \qquad \omega_r{}^{(p)}\,\omega_s{}^{(p)} = \delta_{rs}, \tag{2.15}$$

where $p$, $q$, $r$, $s$ run over 1 and 2. The rotation (2.13) is expressed then by the following transformation of a vector, $\omega^{(1)}$ or $\omega^{(2)}$, in this space:

$$\omega_r{}^{(p)\prime} = \Lambda_{rs}\,\omega_s{}^{(p)},$$

with (2.16)

$$\Lambda_{rt}\Lambda_{st} = \delta_{rs},$$

where the matrix $\Lambda$ is written in terms of the angle of rotation $\chi$ such that

$$(\Lambda_{rs}) = \begin{pmatrix}\cos\chi & -\sin\chi\\ \sin\chi & \cos\chi\end{pmatrix}. \tag{2.19}$$

The invariance of the neutrino field under (2.13) is now expressed by the fact that the basic equations must be written as tensor equations in respect to $\omega$-space also. This is actually fulfilled because (2.10) is re-expressed as

$$\partial_\mu\,\omega^{(1)} = -\omega^{(2)}\,\frac{i}{2}\,\varepsilon_{\mu\alpha\beta\gamma}\,a_\alpha{}^\nu\,\partial_\beta\,a_{\gamma\nu}, \tag{2.18}$$†

i.e., a vector equation in $\omega$-space.

The most general transformation which keeps the neutrino equation invariant is obtained by combining the three kinds of transformations (2.11), (2.12), and (2.13):

† Note that $\partial_\mu\theta = \omega^{(2)}\,\partial_\mu\,\omega^{(1)}$.

$$\{R, \chi, A^{\xi\eta}\}. \tag{2.19}$$

This is, however, just the same kind of parameters as (2.5) apart from the fact that the former do not depend on $x_\mu$, involving eight independent parameters. This fact shows that in the first place the variables representing a state of the neutrino field can be altered, at one point of space-time, so as to have any arbitrary values; and that in the second place the transformation (2.19) must itself be representable by a certain 4-component spinor $\zeta$:

$$\{R, \chi, A^{\xi\eta}\} \longleftrightarrow \zeta, \tag{2.20}$$

just as (2.5) was representable by $\psi$ through the relations (2.3). We shall explicitly show this in sec. 4.

Next, it is evident that eq. (2.9) means a generalization of the equation of continuity. For $\xi = 4$ the equation is the usual equation of probability conservation, but (2.9) exhibits the existence of yet three other independent similar equations, together to form a vector equation in $\xi$-space. Thus each $Q^\xi = i\int \alpha_4{}^\xi \mathrm{d}^3x$ is scalar in usual space and is conserved: $\mathrm{d}Q^\xi/\mathrm{d}t = 0$.

Eq. (2.10) effects a dynamical coupling between the two-dimensional orthogonal frame and internal Lorentz frame which are kinematically independent of each other.

Finally we note that the scalar variables $\varrho$ and $\theta$ can be eliminated from the basic equations entirely, to obtain

$$\partial_\mu Z_{\rho[\nu\rho]} - \partial_\nu Z_{\rho[\mu\rho]} = 0, \tag{2.21}$$

$$\partial_\rho (Z_{\rho[\mu\nu]} - Z_{\mu[\rho\nu]} + Z_{\nu[\rho\mu]}) = 0, \tag{2.22}$$

with the abbreviation

$$Z_{\rho[\mu\nu]} = a_\mu{}^\eta \partial_\rho a_\nu{}^\eta,$$

which is antisymmetric in $\mu$ and $\nu$.

## 3. New Conservation Relations

In this section we shall study further consequences following from our basic equations. Since all the basic equations of our formalism are invariant under internal Lorentz transformations, any relation valid to the neutrino field must be written as a tensor equation with respect to the $\xi$-space (and also to $\omega$-space). For instance, corresponding to any usual conservation relation, we must have a certain tensor equation in $\xi$-space which includes that conservation relation as its specific component equation.

First, the energy-momentum tensor of the field is given by

$$\mathcal{T}_{\mu\nu} = \bar{\psi}\gamma_\nu \partial_\mu \psi - \partial_\mu \bar{\psi}\gamma_\nu \psi, \tag{3.1}$$

(apart from a constant coefficient $\hbar c/2$), and satisfies the relations

$$\partial_\nu \mathcal{T}_{\mu\nu} = 0, \qquad \partial_\mu \mathcal{T}_{\mu\nu} = 0, \tag{3.2}$$

$$\mathscr{T}_{\mu\nu}-\mathscr{T}_{\nu\mu}=-i\varepsilon_{\mu\nu\kappa\lambda}\partial_\kappa\alpha_\lambda{}^3. \tag{3.3}$$

The former is the conservation relation of energy-momentum, while the latter is that of angular momentum, since this is rewritten as

$$\partial_\rho(x_{[\mu}\mathscr{T}_{\nu]\rho}-i\varepsilon_{\mu\nu\rho\lambda}\alpha_\lambda{}^3)=0. \tag{3.4}$$

Now the quantity (3.1) is expressed in terms of our variables (2.5) as [5]

$$\mathscr{T}_{\mu\nu}=\varrho\left(\partial_\mu\theta\cdot a_\nu{}^3+\frac{i}{2}\varepsilon_{3\eta\zeta\iota}a_\rho{}^\eta\partial_\mu a_\rho{}^\zeta\cdot a_\nu{}^\iota\right), \tag{3.5}$$

which is, however, the third component of the following vector in $\xi$-space:

$$T^\xi_{\mu\nu}=\varrho\left(\partial_\mu\theta\cdot a_\nu{}^\xi+\frac{i}{2}\varepsilon_{\xi\eta\zeta\iota}a_\rho{}^\eta\partial_\mu a_\rho{}^\zeta\cdot a_\nu{}^\iota\right), \tag{3.6}$$

with

$$\mathscr{T}_{\mu\nu}=T^3_{\mu\nu}.$$

Thus the existence of the relations (3.2) and (3.3) indicates immediately that we must have more general relations,

$$\partial_\nu T^\xi_{\mu\nu}=0, \qquad \partial_\mu T^\xi_{\mu\nu}=0, \tag{3.7}$$

$$T^\xi_{\mu\nu}-T^\xi_{\nu\mu}=-i\varepsilon_{\mu\nu\kappa\lambda}\partial_\kappa(\varrho a_\lambda{}^\xi), \tag{3.8}$$

for any $\xi$. In fact these relations are directly verified as a consequence of our equations of motion (2.9) and (2.10).

On the other hand it can be shown † that the other components of $T^\xi_{\mu\nu}$ are identically written in $\psi$ as follows:

$$\begin{aligned} T^4_{\mu\nu}&=i(\partial_\mu\bar\psi\gamma_5\gamma_\nu\psi-\bar\psi\gamma_5\gamma_\nu\partial_\mu\psi),\\ T^1_{\mu\nu}+iT^2_{\mu\nu}&=i(\partial_\mu\bar\psi^{\mathrm{C}}\gamma_5\gamma_\nu\psi-\bar\psi^{\mathrm{C}}\gamma_5\gamma_\nu\partial_\mu\psi)=-2i\bar\psi^{\mathrm{C}}\gamma_5\gamma_\nu\partial_\mu\psi. \end{aligned} \tag{3.9}$$

The relations (3.7) and (3.8) may then be verified in the $\psi$-formalism also.

Due to (3.7), the quantity $P_\mu{}^\xi=-i\int T^\xi_{\mu 4}\mathrm{d}^3x$ is a vector both in the usual and in the $\xi$-spaces and is conserved: $\mathrm{d}P_\mu{}^\xi/\mathrm{d}t=0$. Eq. (3.8) represents the generalization of the conservation relation of angular momentum.

Incidentally we note the relation

$$T^\xi_{\mu\mu}=0, \tag{3.10}$$

which is simply equivalent to (2.10).

By quite similar procedures we can also obtain the following results. We introduce two antisymmetric tensors in $\xi$-space

$$M^{[\xi\eta]}_{\mu\nu}=\varrho(\sin\theta\cdot a^\xi_{[\mu}a^\eta_{\nu]}-i\cos\theta\cdot\varepsilon_{\mu\nu\kappa\lambda}a_\kappa{}^\xi a_\lambda{}^\eta), \tag{3.11}$$

† The expressions for $T^\xi{}_{\mu\nu}$ in $\psi$ given in (3.9) are kinematically identical with the expression (3.6); namely the identity is proved merely by the use of algebraic relations for $\gamma$-matrices but not of the equations of motion. The same applies to the identity between the expressions (3.11) and (3.17) or between (3.12) and (3.18).

$$J_\mu^{[\xi\eta]} = \varrho\left(\sin\theta \cdot a_\rho{}^\xi \partial_\mu a_\rho{}^\eta - \frac{i}{2}\cos\theta \cdot \varepsilon_{\xi\eta\zeta\iota} a_\rho{}^\zeta \partial_\mu a_\rho{}^\iota\right). \tag{3.12}$$

Then they satisfy the relations

$$\partial_\nu M_{\mu\nu}^{[\xi\eta]} = -J_\mu^{[\xi\eta]}, \tag{3.13}$$

$$\varepsilon_{\mu\nu\kappa\lambda}\partial_\nu M_{\kappa\lambda}^{[\xi\eta]} = -\varepsilon_{\xi\eta\zeta\iota} J_\mu^{[\zeta\iota]}, \tag{3.14}$$

$$\partial_\mu J_\mu^{[\xi\eta]} = 0, \tag{3.15}$$

due to the equations of motion.

$M_{\mu\nu}^{[\xi\eta]}$ is antisymmetric both in usual and in $\xi$-spaces, and so †

$$M_{\mu\nu}^{[\xi\eta]} = M_{\kappa\lambda}^{[\zeta\iota]}, \qquad (\xi\eta\zeta\iota) \sim (\mu\nu\varkappa\lambda) \sim (1234). \tag{3.16}$$

$M_{\mu\nu}^{[\xi\eta]}$ is expressed in $\psi$ as follows:

$$\begin{aligned} M_{\mu\nu}^{[34]} &= -\tfrac{1}{2}\bar\psi\gamma_{[\mu}\gamma_{\nu]}\psi, \\ M_{\mu\nu}^{[13]} + iM_{\mu\nu}^{[23]} &= \tfrac{1}{2}\bar\psi^{\mathrm{C}}\gamma_{[\mu}\gamma_{\nu]}\psi. \end{aligned} \tag{3.17}$$††

$M_{\mu\nu}^{[34]}$ is the so-called magnetic and electric moment density tensor.

On the other hand $J_\mu^{[\xi\eta]}$ is expressed in $\psi$ in the following way:

$$\begin{aligned} J_\mu^{[34]} &= -(\bar\psi\partial_\mu\psi - \partial_\mu\bar\psi\cdot\psi), \\ J_\mu^{[12]} &= \bar\psi\gamma_5\partial_\mu\psi - \partial_\mu\bar\psi\cdot\gamma_5\psi, \\ J_\mu^{[13]} + iJ_\mu^{[23]} &= \bar\psi^{\mathrm{C}}\partial_\mu\psi - \partial_\mu\bar\psi^{\mathrm{C}}\cdot\psi = 2\bar\psi^{\mathrm{C}}\partial_\mu\psi. \end{aligned} \tag{3.18}$$

$J_\mu^{[\xi\eta]}$ comprises the "convection current" of Gordon as its (34)-component, and the "magnetic current" of Proca as its (12)-component. Eq. (3.15) shows that the continuity equation for the convection current can be generalized into any plane of the $\xi$-space, and so it contains again new conservation relations.

To a rotation in $\omega$-space (2.13), $T_{\mu\nu}^{\xi}$ is invariant while eqs. (3.11)—(3.15) have not manifestly covariant forms. However, they can readily be combined into covariant forms as follows: First eq. (3.11) indicates that $M_{\mu\nu}^{[\xi\eta]}$ and its dual $-iM_{\mu\nu}^{[\zeta\iota]}$ form components of a vector in $\omega$-space, i.e.,

$$\mathscr{M}_{\mu\nu}^{[\xi\eta]} = \begin{pmatrix} M_{\mu\nu}^{[\xi\eta]} \\ -iM_{\mu\nu}^{[\zeta\iota]} \end{pmatrix} = -\varrho(\omega^{(2)}\cdot a_\mu{}^{[\xi} a_\nu{}^{\eta]} + i\omega^{(1)}\cdot a_\mu{}^{[\zeta} a_\nu{}^{\iota]}), \qquad (\xi\eta\zeta\iota) \sim (1234). \tag{3.19}$$

Similarly,

$$\mathscr{J}_\mu^{[\xi\eta]} = \begin{pmatrix} J_\mu^{[\xi\eta]} \\ -iJ_\mu^{[\zeta\iota]} \end{pmatrix} = -\varrho(\omega^{(2)}\cdot a_\rho{}^\xi \partial_\mu a_\rho{}^\eta + i\omega^{(1)}\cdot a_\rho{}^\zeta \partial_\mu a_\rho{}^\iota), \qquad (\xi\eta\zeta\iota) \sim (1234) \tag{3.20}$$

is a vector in $\omega$-space. Then (3.13) and (3.14) are combined into a vector

† $(\xi\eta\zeta\iota) \backsim (1234)$ signifies that $(\xi\eta\zeta\iota)$ is an even permutation of (1234).

†† Other components of $M_{\mu\nu}^{[\xi\eta]}$ are implied in (3.17) also, due to (3.16); e.g.,

$$M_{\mu\nu}^{[12]} = \tfrac{1}{2}\bar\psi\gamma_5\gamma_{[\mu}\gamma_{\nu]}\psi.$$

equation in this space:

$$\partial_\nu \mathscr{M}_{\mu\nu}^{[\xi\eta]} = -\mathscr{J}_\mu^{[\xi\eta]}, \tag{3.21}$$

and (3.15) is rewritten as

$$\partial_\mu \mathscr{J}_\mu^{[\xi\eta]} = 0. \tag{3.22}$$

These have the form explicitly covariant to the rotation (2.16).

## 4. Further Analysis of Transformation Character in Internal Spaces

As we have already seen in sec. 2, the neutrino field is invariant under transformation (2.19), i.e.,

$$\begin{aligned} &\varrho \to R\varrho \qquad && \theta \to \theta+\chi, \\ &a_\mu^{\xi'} = A^{\xi\eta} a_\mu^{\eta}, && (A^{\xi\zeta} A^{\eta\zeta} = \delta_{\xi\eta}). \end{aligned} \tag{4.1}$$

On the other hand the field equation in the $\psi$-formalism (1.1) is evidently invariant to the transformation

$$\psi \to \psi' = a\psi + a_1\gamma_5\psi + b\psi^C + b_1\gamma_5\psi^C, \tag{4.2}$$

characterized by a set of four arbitrary complex numbers $(a, a_1, b, b_1)$, involving again eight independent real parameters. Therefore, the transformation (4.1) in our representation must just correspond to the transformation (4.2) in the $\psi$-formalism, i.e.,

$$\{R, \chi, A^{\xi\eta}\} \longleftrightarrow \{a, a_1, b, b_1\}. \tag{4.3}$$

We can verify that this correspondence is explicitly given by the following:

$$R = (W^2+\hat{W}^2)^{\frac{1}{2}}, \qquad \tan\chi = \hat{W}/W, \tag{4.4}$$

with the abbreviations

$$\begin{aligned} W &= |a|^2-|a_1|^2-|b|^2+|b_1|^2, \\ \hat{W} &= -i(a^* a_1 - a a_1^* - b^* b_1 + b b_1^*), \end{aligned} \tag{4.5}$$

and

$$(A^{\xi\eta}) = \frac{1}{R}\begin{pmatrix} \frac{1}{2}(m-n+m^*-n^*) & \frac{i}{2}(m+n-m^*-n^*) & -i(l-l^*) & k-k^* \\ -\frac{i}{2}(m-n-m^*+n^*) & \frac{1}{2}(m+n+m^*+n^*) & -(l+l^*) & -i(k+k^*) \\ i(u-u^*) & u+u^* & p-q & -i(r+s) \\ -(t-t^*) & i(t+t^*) & i(r-s) & p+q \end{pmatrix} \tag{4.6}$$

with the abbreviations

$$\begin{aligned} m &= a^2-a_1^2, & n &= b^2-b_1^2, \\ k &= ab-a_1 b_1, & l &= ab_1-a_1 b, \\ t &= a^* b+a_1^* b_1, & u &= a^* b_1+a_1^* b, \end{aligned} \tag{4.7}$$

and

$$\begin{aligned} p &= |a|^2+|a_1|^2, & q &= |b|^2+|b_1|^2, \\ r &= a^* a_1+aa_1^*, & s &= b^* b_1+bb_1^*. \end{aligned} \tag{4.8}$$

One can really ascertain that the matrix (4.6) satisfies the condition $A^{\xi\zeta}A^{\eta\zeta}=\delta_{\xi\eta}$ for arbitrary values of $a$, $a_1$, $b$ and $b_1$, and also that $\det(A^{\xi\eta})=+1$.

Now, we regard the numbers $(a, a_1, b, b_1)$ as components of a 4-component spinor $\zeta$ in the following way:

$$\zeta=\begin{pmatrix} a \\ b_1 \\ a_1 \\ b \end{pmatrix}. \tag{4.9}$$

Then the above relations (4.4)—(4.8) are put in the following simple expressions:

$$\begin{aligned} &W=i\bar{\zeta}\gamma_5\zeta, \qquad \hat{W}=\bar{\zeta}\zeta, \\ &A^{1\mu}=\frac{1}{2R}(\bar{\zeta}^C\gamma_\mu\zeta-\bar{\zeta}\gamma_\mu\zeta^C), \\ &A^{2\mu}=\frac{1}{2iR}(\bar{\zeta}^C\gamma_\mu\zeta+\bar{\zeta}\gamma_\mu\zeta^C), \\ &A^{3\mu}=\frac{i}{R}\bar{\zeta}\gamma_5\gamma_\mu\zeta, \qquad A^{4\mu}=\frac{1}{R}\bar{\zeta}\gamma_\mu\zeta, \end{aligned} \tag{4.10}$$

in which, however, *we assume the following special representation of $\gamma$-matrices*†:

$$\gamma_1=\begin{pmatrix} -\sigma_2 & \cdot \\ \cdot & \sigma_2 \end{pmatrix}, \quad \gamma_2=\begin{pmatrix} \sigma_1 & \cdot \\ \cdot & -\sigma_1 \end{pmatrix}, \quad \gamma_3=\begin{pmatrix} \sigma_3 & \cdot \\ \cdot & -\sigma_3 \end{pmatrix}, \quad \gamma_4=\begin{pmatrix} \cdot & -i\sigma_0 \\ i\sigma_0 & \cdot \end{pmatrix}, \tag{4.11}$$

where the $\sigma_i$'s are Pauli matrices and $\sigma_0=\left(\begin{smallmatrix}1&0\\0&1\end{smallmatrix}\right)$. Eq. (4.10) shows that the relations between $\{R, \chi, A^{\xi\eta}\}$ and $\zeta$ are exactly the same with those between $\{\varrho, \theta, a_\mu^{\xi}\}$ and $\psi$ given in (2.3), with the following correspondence:

$$R\sim\varrho, \qquad \chi\sim\frac{\pi}{2}-\theta, \qquad A^{\xi\eta}\sim a_\eta^{\xi}. \tag{4.12}$$

Next, we remark that the correspondence between (4.1) and (4.2) breaks down in the special case where $R=0$, i.e.,

$$\begin{aligned} &|a|^2-|a_1|^2-|b|^2+|b_1|^2=0, \\ &a^* a_1-aa_1^*-b^* b_1+bb_1^*=0, \end{aligned} \tag{4.13}$$

† This representation of $\gamma$-matrices is different from any of the usually employed ones, but it is one satisfying $\gamma_\mu\gamma_\nu+\gamma_\nu\gamma_\mu=2\delta_{\mu\nu}$. In this representation

$$\gamma_5=\begin{pmatrix} \cdot & \sigma_0 \\ \sigma_0 & \cdot \end{pmatrix}, \qquad C=\begin{pmatrix} \cdot & -i\sigma_2 \\ i\sigma_2 & \cdot \end{pmatrix}.$$

because in this singular case we cannot define the corresponding transformation (4.1). The case represents the transformation which leads to a generalized Majorana field. Originally, our representation in the form stated in sec. 2 does not apply to Majorana field in which $\Omega$ and $\hat{\Omega}$ vanish identically.

In what follows we shall study various special cases of the transformation (4.1), i.e., (4.2). It is sufficient to normalize it such that

$$R = 1, \tag{4.14}$$

excepting the singular case (4.13).

(i) Pure Lorentz transformations in $\xi$-space (i.e., $\varrho, \theta$ invariant). Evidently this corresponds to the transformation in $\psi$-formalism (4.2) with the restrictions

$$\begin{aligned} |a|^2-|a_1|^2-|b|^2+|b_1|^2 &= 1, \\ a^* a_1-aa_1^*-b^* b_1+bb_1^* &= 0. \end{aligned} \tag{4.15}$$

(ii) Pure rotations in the $\omega$-space (2.13) correspond to

$$\psi \to \exp\left(\frac{i}{2}\chi\gamma_5\right)\cdot\psi, \tag{4.16}$$

i.e., the case in which $a = \cos(\chi/2)$, $a_1 = i\sin(\chi/2)$, $b = b_1 = 0$ in (4.2).

(iii) We now consider the case $a_1 = b = 0$, i.e.,

$$\psi \to \psi' = a\psi+b_1\gamma_5\psi^{\mathrm{C}}. \tag{4.17}$$

Then the condition (4.14) becomes

$$|a|^2+|b_1|^2 = 1, \tag{4.18}$$

and (4.6) simplifies to †

$$(A^{\xi\eta}) = \begin{pmatrix} \frac{1}{2}\{(a^2+b_1^2)+\text{c.c.}\} & \frac{i}{2}\{(a^2-b_1^2)-\text{c.c.}\} & -i(ab_1-\text{c.c.}) & 0 \\ -\frac{i}{2}\{(a^2+b_1^2)-\text{c.c.}\} & \frac{1}{2}\{(a^2-b_1^2)+\text{c.c.}\} & -(ab_1+\text{c.c.}) & 0 \\ -i(ab_1^*-\text{c.c.}) & ab_1^*+\text{c.c.} & |a|^2-|b_1|^2 & 0 \\ 0 & 0 & 0 & 1 \end{pmatrix}. \tag{4.19}$$

But (4.19) with (4.18) represents the general "spatial" rotation in $\xi$-space. The spatial part of (4.19) is exactly the relation between the matrix of spatial rotation $(A^{ij})$, $(i, j = 1, 2, 3)$, and the spinor parameters $(a, b_1)$ describing the same rotation.

To see this fact more simply, we regard $\psi$ and $\gamma_5\psi^{\mathrm{C}}$ as components of a spinor in $\xi$-space,

† c.c. signifies complex conjugate.

$$\Psi = \begin{pmatrix} \Psi^1 \\ \Psi^2 \end{pmatrix} = \begin{pmatrix} \psi \\ \gamma_5 \psi^C \end{pmatrix}, \tag{4.20}$$

which evidently satifies the field equation

$$\gamma_\mu \partial_\mu \Psi = 0. \tag{4.21}$$

It is readily observed that the transformation (4.17) of $\psi$ is then identical to the following transformation of $\Psi$:

$$\begin{pmatrix} \Psi^{1'} \\ \Psi^{2'} \end{pmatrix} = \begin{pmatrix} a & b_1 \\ -b^*_1 & a^* \end{pmatrix} \begin{pmatrix} \Psi^1 \\ \Psi^2 \end{pmatrix}. \tag{4.22}$$

Taking account of the condition (4.18), eq. (4.22) indicates that $\Psi$ transforms indeed as a spinor in $\xi$-space, when the "spatial" components of $\alpha_\mu{}^\xi$, (i.e., $\alpha_\mu{}^1, \alpha_\mu{}^2, \alpha_\mu{}^3$), transform as a vector in the same $\xi$-space.

The present transformation (4.17) with (4.18) is exactly the case considered by Pauli [1]), which is now grasped as the general spatial rotation in the internal Lorentz space.

(iv) Next special case is

$$\psi \to a\psi + b\,\psi^C, \tag{4.23}$$

where we have

$$W = |a|^2 - |b|^2, \qquad \hat{W} = 0.$$

The condition (4.14) then reduces to †

$$|a|^2 - |b|^2 = \pm 1, \tag{4.24}$$

and according as $\pm 1$ in (4.24), we have

$$\theta = \text{invariant} \qquad \text{or} \qquad \theta \to \theta + \pi.$$

The Lorentz transformation in $\xi$-space now becomes a general rotation around the third axis in $\xi$-space; the case $|a|^2 - |b|^2 = -1$ accompanies the reflection of this axis.

(v) A further special case is

$$\psi \to a\psi + a_1 \gamma_5 \psi. \tag{4.25}$$

The condition (4.14) takes the form

$$|a^2 - a_1{}^2|^2 = 1. \tag{4.26}$$

The rotation in $\xi$-space now separates into a rotation in the (12)-plane,

$$\begin{pmatrix} \frac{1}{2}\{(a^2 - a_1{}^2) + \text{c.c.}\} & \frac{i}{2}\{(a^2 - a_1{}^2) - \text{c.c.}\} \\ -\frac{i}{2}\{(a^2 - a_1{}^2) - \text{c.c.}\} & \frac{1}{2}\{(a^2 - a_1{}^2) + \text{c.c.}\} \end{pmatrix}, \tag{4.27}$$

and one in the (34)-plane,

† Besides (4.24) there exists the case $|a| = |b|$ for (4.23), but this falls within the singular case stated before, leading to a Majorana field $\psi' = a(\psi + \psi^C \cdot e^{i\delta})$.

$$\begin{pmatrix} |a|^2+|a_1|^2 & -i(a^*a_1+\text{c.c.}) \\ i(a^*a_1+\text{c.c.}) & |a|^2+|a_1|^2 \end{pmatrix}. \tag{4.28}$$

At the same time, $\omega$-space also rotates by

$$(\Lambda_{rs}) = \begin{pmatrix} |a|^2-|a_1|^2 & -i(a^*a_1-\text{c.c.}) \\ i(a^*a_1-\text{c.c.}) & |a|^2-|a_1|^2 \end{pmatrix}. \tag{4.29}$$

The transformation (ii) is a special case of the present one where (4.27) and (4.28) are diagonal. Also, the gauge-transformation, $\psi \to \psi e^{i\lambda}$ is another special case, in which (4.28) and (4.29) are diagonal, namely it is represented as a rotation in the (12)-plane of $\xi$-space by an angle $2\lambda$.

## 5. Conclusion

We have restricted the problem to c-number theory; similar treatment for the q-number case will become somewhat more complicated. In this case the range of the invariance of theory is diminished, as we must require the invariance of the anti-commutation relations besides that of the equations of motion.

Also, when interactions are introduced they will have the effect of reducing † the symmetry in the internal spaces. Consideration of the cases with interaction is, however, useful for clarifying further the physical meanings of the invariance properties and new conservation relations which we have obtained.

In our representation the Majorana field, which is equivalent to the two-component neutrino field, corresponds to a singular case. This field, however, can be treated by our general method using somewhat different representations. These problems will be studied in later papers.

† A finite rest-mass amounts to specializing the third axis in the $\xi$-space, and the electromagnetic interaction (this does not apply to the neutrino case) distinguishes between the (12) and (34) axes in the $\xi$-space (see ref. [2]).

## References

1) W. Pauli, Nuovo Cimento **6** (1957) 204
2) T. Takabayasi, Nuovo Cimento **7** (1958) 118; Comptes rendus Acad. Sci. **246** (1958) 64
3) F. Gürsey, Nuovo Cimento **5** (1957) 784;
A. Aymard, Comptes rendus Acad. Sci. **244** (1957) 3133;
B. C. Unal and J. P. Vigier, *ibid.* **245** (1957) 1785
4) R. H. Good, Jr., Revs. Mod. Phys. **27** (1955) 187;
J. M. Jauch and F. Rohrlich, The theory of Photons and Electrons (Addison-Wesley Pub. Cambridge, Mass. 1955) p. 54
5) T. Takabayasi, Suppl. Prog. Theor. Phys. (Japan) no. 4 (1957)

*Nuclear Physics* 6 (1958) 489—503; © *North-Holland Publishing Co., Amsterdam*
ot to be reproduced by photoprint or microfilm without written permission from the publisher

# NEW WAVE EQUATIONS FOR ELEMENTARY PARTICLES

YASUHISA MURAI

*Department of Theoretical Physics, University of Manchester* †

Received 17 January 1958

**Abstract:** The aim of this paper is to give an interpretation of the equation which was proposed by Umezawa and Visconti [3]) for isomerisation of particles of non-zero mass. The deduction of the equation is done by extending the definition of equivalent observers and introducing a new variable. The latter procedure is necessary to reconcile the extended definition of equivalent observers with the classical law of inertia, and it can be done in a unique way.

## 1. Introduction

The problem of parity, which stemmed from the $\theta-\tau$ puzzle, attracted the attention of all physicists when the violation of parity conservation in $\beta$- and $\mu$-decays was experimentally verified. But the original problem, the $\theta-\tau$ puzzle, has not been solved yet. Recently, it has become evident that in the decay of the $\Lambda$-particle, parity is not conserved [1, 2]). Hence it is very plausible that parity conservation is also violated in the decay of the $\theta$ and the $\tau$ and that they are actually a single-particle decaying into either $2\pi$'s or $3\pi$'s. We note that if the spin of this particle is zero there is no means of experimental verification of violation of parity conservation in these decay processes. In the present formalism, however, there is in any case no rule which tells us whether or not we have to disregard the conservation of parity in such cases. Only when a neutrino intervenes in the interaction can we get rid of the requirement of conservation of parity. This is because $\psi$ and $\gamma_5\psi$ can both be solutions of the Dirac equation, and we can impose a constraint on $\psi$ or we can permit generalized gauge transformations. But for the particles of non-zero mass there is no such situation. If, as Umezawa and Visconti [3]) have proposed, strange particles are described by an equation of the form

$$\left(\gamma_i \frac{\partial}{\partial x_i} + m\tau_1\right)\psi = 0$$

where $\tau$ denotes some new dichotomic variable, $\psi$ can be an eigenstate of an operator $\tau_3\gamma_5$ and if so, its eigenvalue changes under space reflection. (Here $\gamma_i$ means $1\times\gamma_i$ and $\tau_K$ means $\tau_K\times 1$, 1 denoting the two-by-two or

† On leave of absence from Saitama University, Japan

four-by-four unit matrix.) So if we assume that the $\Lambda$-particle is in an eigenstate of $\tau_3\gamma_5$, we need not consider parity conservation in the decay of the $\Lambda$-particle. Further, since the K-meson would decay via $\bar{\Lambda}+N \to \pi+\bar{N}+N$ into $2\pi$'s or $3\pi$'s, parity would not be conserved in the whole decay process. But to assume this equation for strange particles is not attractive, because there are already several variables which were introduced phenomenologically and have no clear physical foundation, e.g. strangeness and isobaric spin.

In this paper we attempt to obtain basic equations for "strange particles" which have the same form as the aforementioned one, starting from a fundamental principle. In the current theory of elementary particles we investigate the behaviour of particles in the framework of the Minkowski space and the Lorentz group. But insofar as we use this frame work there is no room for introducing other quantities than mass and spin to characterize particles. Nevertheless many particles are endowed with other characteristics, such as strangeness and isobaric spin. The shorthand way of incorporating these quantities in the theory is to form an abstract space and to assume the direct product of this space and the Minkowski space as a domain for particles. But the recent results of experiments suggest that these two spaces are not completely independent. The fact that we have two different attitudes to space reflection in the cases of strong and weak interactions exemplifies this. Moreover, there remain many unsolved problems concerning elementary particles — the relation between the strength of coupling and the violation of conservation laws, the foundation of strangeness, problems of divergence, etc. When we wish to investigate and solve any of these problems we have to reconsider carefully many concepts which we have been using up to now. They include space-time, Lorentz group, causality, locality, linearity, Hilbert space.

We try in this paper to change some features related to space-time and the Lorentz group. These stand on very firm foundations and we cannot change anything in a straightforward way. We use a five-dimensional formalism here, but there are many ways of introducing the fifth coordinate. In order to fix this new coordinate uniquely, we require that in the limiting case when it vanishes the set of equivalent observers is widened so as to include those in systems moving with uniform acceleration. The extension of the set of equivalent observers seems very plausible as long as we confine ourselves to domains of space-time with linear dimensions larger than $10^{-13}$ cm. But because it contradicts the classical law of inertia we cannot require it offhand; if, however, we require it as a limiting postulate, the way of introducing the new variable is fixed uniquely, and moreover after its introduction there remains no contradiction between the extension of equivalent observers and the classical law of inertia. In sections 2 and 3 we explain these points. In section 4 we construct equations which are to be satisfied by

particles of spins 0 and $\frac{1}{2}$. In section 5 we investigate the behaviour of $\psi$ under space reflection, particle-antiparticle conjugation and time-reversal. It will be shown that we can require the invariance under the product of space reflection and particle-antiparticle conjugation, but not under these transformations separately. As for time-reversal, the invariance under this transformation may be imposed. One might be worried if such assignment of internal structure would also cause parity violation in the case of strong interactions. But there appears automatically a clear distinction between particles being produced and particles decaying. These things will be explained briefly in the last section.

## 2. Extension of the Set of Equivalent Observers

It is usually believed that particles of spin $\frac{1}{2}$ obey the Dirac equation and those of spin 0 the Klein-Gordon equation. These equations are obtained if one assumes that the inhomogeneous Lorentz group is a fundamental group and wave functions form a substratum for an irreducible representation of this group. But when we are considering the behaviour of elementary particles, it is tacitly assumed that the equivalent observers are not necessarily to be connected only by inhomogeneous Lorentz transformations. Firstly we shall make this point clear.

For example, we use the Dirac equation to describe the motion of an electron which we observe in a laboratory on the earth. In such a case we never pay attention to the existing gravitational field. On account of the equivalence principle of Einstein this means that we are assuming the Dirac equation to be valid not only in the inertial system, but also in a system which is moving with a constant acceleration with respect to the inertial system. Then at once the allowable magnitude of acceleration will be asked. The effect of gravity would become most prominent in the vicinity of a particle, i.e., when we consider the renormalization of charge. According to Landau's argument [4]), the effect of gravity appears when $\varkappa\Lambda^2 \gtrsim 1$. Here $\Lambda$ is the magnitude of the cut-off momentum and $\varkappa$ is the constant of universal gravitation. With $\varkappa \approx 10^{-8}\,\mathrm{cm^3/g \cdot sec^2}$, the critical value of $\Lambda$ is $\Lambda \approx 10^{28}\,\mathrm{eV} \approx 10^{43}\,\mathrm{cm^{-1}}$. If on the other hand we take $\Lambda^{-1} \approx 10^{-13}$ cm, $\varkappa$ would have to be of the order of $10^{32}\,\mathrm{cm^3/g \cdot sec^2}$ to give rise to strong gravitational effects. Thus, if we give up the intention of investigating the ultramicroscopic world below $10^{-13}$ cm, it is not necessary to consider gravity unless the value of $\varkappa$ would be as much as $10^{40}$ times its actual value. However, when the magnitude of acceleration reaches $10^{33}\,\mathrm{cm/sec^2}$, the uniformly accelerated motion tends to the uniform motion of constant (light) velocity within $10^{-23}$ sec. Thus, we might safely extend the concept of equivalent observers so as to include those moving with a constant acceleration so long as we are treating

of elementary particles. However, there occurs a conflict between the extension of equivalent observers and the classical law of inertia. Actually, the classical equation of motion was a good tool for calculating approximate trajectories of electrons, protons, etc. Therefore we may not demand the extension of equivalent observers directly. We come back to this point in the next section. But before doing so, we shall introduce a convenient mathematical formalism, adapted to the extended equivalence of observers.

The transformation [5])

$$x^{1'} = \frac{x^1 + \frac{1}{2}\alpha x_k x^k}{1 + \alpha x^1 + \frac{1}{4}\alpha^2 x_k x^k}, \qquad x^{i'} = \frac{x^i}{1 + \alpha x^1 + \frac{1}{4}\alpha^2 x_k x^k} \qquad (i = 2, 3, 0)$$

which leads from an inertial system to a system moving with a constant acceleration $\alpha$, is not linear in the $x$'s but contains $x_i x^i$. Therefore, to make the transformation linear we first introduce an auxiliary variable $x^5$:

$$x^5 = x_i x^i = (x^1)^2 + (x^2)^2 + (x^3)^2 - (x^0)^2.$$

But this form cannot be regarded as a fundamental quadric. So we pass to homogeneous coordinates, and put

$$g_{\mu\nu} X^\mu X^\nu \equiv (X^1)^2 + (X^2)^2 + (X^3)^2 - (X^0)^2 - 2X^5 X^6 = 0. \qquad (2.1)$$

The relation between the coordinates $x^i$ in the Minkowski space and the homogeneous coordinates in the six-dimensional space is

$$x^i = \frac{X^i}{X^6}, \qquad \frac{1}{2} x_i x^i = \frac{X^5}{X^6}. \qquad (2.2)$$

Then the required transformations are those which leave (2.1) invariant. All the infinitesimal transformations of this type form a group of 15 parameters comprising the inhomogeneous Lorentz transformations (10 parameters), the above mentioned transformation (this has 3 parameters since the acceleration can be along the $x$, $y$ or $z$ axis), a transformation which corresponds to the temporal part of these spatial transformations, and a dilatation.

What we have done hitherto is rather trivial. Mathematically it is known that the group which includes the inhomogeneous Lorentz group and the transformations which lead from an inertial system to a uniformly accelerated system is a conformal group in the Minkowski space, and the conformal group in $n$-dimensional space is related to the rotation group in $(n+2)$-dimensional space [5, 6, 7]). It is a matter of course that the dilatation has been included on account of the relations (2.2). The physical meaning of the requirement of invariance of the dilatation was once studied by Hoffmann [8]). Indeed, if all the universe expands at the same rate, including measuring scales and clocks, there is no means to observe this expansion. Therefore, it seems reasonable to require invariance under the dilatation.

## 3. Introduction of the New Variable

As we mentioned in the previous section, we cannot extend the set of equivalent observers without conflicting with the classical law of inertia. But since we are using five coordinates (six homogeneous coordinates) there is room for introducing a new variable in order to circumvent these difficulties. In fact, everyone is aware that it is necessary to introduce new degrees of freedom to explain various characteristics of elementary particles. Now we demand that in the limiting case when this new variable tends to zero we really have an extended definition of equivalent observers. Further it would not seem far fetched to assume that the new variable has the dimension of length. This is, firstly, because, having now $h$ and $c$, there remains freedom only for quantities of dimension of length; secondly, future theory probably will contain some new feature concerned with a length, e.g. in a form of a universal length; and, thirdly, it seems very plausible that the new variable represents in some way a spatio-temporal extension of a particle. Then we can show that there is only one way of introducing a new variable $r$. Because of the transformation properties we can change only the second eq. (2.2); and we prove that the new variable $r$ should be introduced by

$$\tfrac{1}{2}(x_i x^i \pm r^2) = \frac{X^5}{X^6}.$$

At first we shall note that, because the transformations which leave $g_{\mu\nu}X^\mu X^\nu$ invariant contain a dilatation, we cannot arbitrarily use a constant of the dimension of a length. Therefore the most general possibility of introducing $r$, in such a way that when it vanishes $X^5/X^6$ becomes $\frac{1}{2}x_i x^i$, is

$$\frac{X^5}{X^6} = \tfrac{1}{2}x_i x^i \left(1+\mathrm{e}^{-a\frac{x_i x^i}{r^2}} F\left(\frac{x_i x^i}{r^2}\right)\right) + \tfrac{1}{2}r^2 \mathrm{e}^{-b\frac{x_i x^i}{r^2}} G\left(\frac{x_i x^i}{r^2}\right), \qquad (3.1)$$

where $a$ and $b$ are positive constants and $F$ and $G$ are arbitrary polynomials. Then

$$g_{\mu\nu}X^\mu X^\nu = -\tfrac{1}{2}x_i x^i \mathrm{e}^{-a\frac{x_i x^i}{r^2}} F\left(\frac{x_i x^i}{r^2}\right) - \tfrac{1}{2}r^2 \mathrm{e}^{-b\frac{x_i x^i}{r^2}} G\left(\frac{x_i x^i}{r^2}\right).$$

Now, because of the homogeneity of space-time, we require that $r$ does not change when the origin of coordinates is displaced. The infinitesimal translation of the origin is written as

$$X^i \to X^{i'} = X^i + \varepsilon^i X^6, \quad X^5 \to X^{5'} = X^5 + \varepsilon_i X^i, \quad X^6 \to X^{6'} = X^6,$$

which leaves $g_{\mu\nu}X^\mu X^\nu$ invariant and is equivalent to

$$x^i \to x^i + \varepsilon^i.$$

Then, from $g_{\mu\nu}X^\mu X^\nu = g_{\mu\nu}(X')^\mu (X')^\nu$, we get

$$e^{-a\xi}(F(\xi)-a\xi F(\xi)+\xi F'(\xi))+e^{-b\xi}(G'(\xi)-bG(\xi)) = 0,$$

where $\xi = x_i x^i/r^2$. Integrating this equation we have

$$e^{-a\xi}\xi F(\xi)+e^{-b\xi}G(\xi) = \text{const.} = C.$$

Thus (3.1) becomes

$$\frac{X^5}{X^6} = \tfrac{1}{2}(x_i x^i + Cr^2).$$

For a reason to be given later we take the positive sign before $r^2$; now we have in place of (2.2)

$$\frac{X^i}{X^6} = x^i, \qquad \frac{X^5}{X^6} = \tfrac{1}{2}(x_i x^i + r^2). \tag{3.3}$$

Then (2.1) becomes

$$g_{\mu\nu}X^\mu X^\nu \equiv (X^1)^2+(X^2)^2+(X^3)^2-(X^0)^2-2X^5X^6 = -(X^6)^2 r^2. \tag{3.4}$$

Geometrically the coordinates $X^\mu$ represent a time-like hyperboloid having a centre at $x^i$ and radius $r$. The hyperboloid is rep esented by

$$(\xi^i - x^i)(\xi_i - x_i) = -r^2,$$

which can be written as

$$X^6\xi_i\xi^i - 2\xi_i X^i + 2X^5 = 0. \tag{3.5}$$

But to consider $r$ in such a way requires some caution. This is because a point in the Minkowski space $(x^i)$ is transformed in different ways, according as we regard this point as the centre of a hyperboloid of radius $r$ or $r'$ ($r'$ may be zero: then we have a world point in the Minkowski space). Indeed, when we adopt the relation (3.3) the transformation which leads from an inertial system to a uniformly accelerated system becomes

$$x^1 \to (x')^1 = \frac{x^1 + \dfrac{\alpha}{2}(x_i x^i + r^2)}{1+\alpha x^1 + \dfrac{\alpha^2}{4}(x_i x^i + r^2)},$$

$$x^k \to (x')^k = \frac{x^k}{1+\alpha x^1 + \dfrac{\alpha^2}{4}(x_i x^i + r^2)} \qquad (k = 2, 3, 0), \tag{3.6}$$

$$r \to r' = \frac{r}{1+\alpha x^1 + \dfrac{\alpha^2}{4}(x_i x^i + r^2)}.$$

This transformation should be considered to be a coordinate transformation from a five-dimensional coordinate system $(x^i, r)$ to $((x')^i, r')$. If we interpret

this as a point transformation, it is a "sphere" transformation changing $(x^i, r)$ to $((x')^i, r')$.

The meaning of the transformation law (3.4) can be best seen when we consider the motion of a free particle. We get the line element of the five-dimensional space as follows. We cannot use $g_{\mu\nu}\mathrm{d}X^\mu \mathrm{d}X^\nu$ as a line element, since this is not invariant under $X^\mu \to \lambda X^\mu$. Instead we consider the angle

$$\cos\vartheta = -\frac{g_{\mu\nu}X^\mu X^\nu}{|X|\cdot|Y|}$$

from which we have

$$\mathrm{d}\vartheta^2 = (X_\mu X^\mu)^{-2}\{(X_\nu X^\nu)(\mathrm{d}X_\lambda \mathrm{d}X^\lambda) - (X_\nu \mathrm{d}X^\nu)^2\}.$$

In terms of the variables $x^i$ and $r$ this is

$$\mathrm{d}\vartheta^2 = -\frac{1}{r^2}(\mathrm{d}x^i \mathrm{d}x_i + dr^2),$$

and it gives as a geodesic line [9])

$$x^K = v^K t + x_0{}^K,$$

$$r = \frac{\lambda_0}{\sqrt{1-v^2}}\left\{1+\frac{(1-v^2)t^2}{\lambda_0{}^2}\right\}^{\frac{1}{2}} \quad (\lambda_0 \neq 0).$$

If we had a spatial hyperboloid ($r$ imaginary), $1-v^2$ would have to be negative. This is the reason why we took the positive sign before $r^2$ in (3.3).

Now this form of geodesic line holds for all equivalent observers. Therefore if we consider the centre of the hyperboloid to be the position of a particle, there occurs no contradiction with the classical law of inertia. It is interesting to compare the behaviour of $r$ with that of a wave packet. In fact, if we put $\lambda_0$ equal to the Compton wave length of a particle, the change of $r$ with time is the same as that of the width of a wave packet which has the Compton wave length initially as the width of a Gaussian distribution. Thus, insofar as we require an extension of the set of equivalent observers as a limiting postulate, we encounter no other curious result than a fact which is already common in quantum mechanics. The author feels that there is here something very akin to the situation in which the action quantum was first introduced, with the requirement that it should tend to zero in the classical limit.

## 4. Fundamental Equations

### 4.1. GENERAL METHOD

Now we are in a position to construct wave equations for particles with or without spin. A similar attempt was once made by Dirac in his investigation of various wave equations in conformal space [10]). He concluded that there would be no simple way of getting a wave equation in conformal space

corresponding to the ordinary wave equation for the electron. The coordinate system which he used was the $X$'s defined in (2.2). But from physical reasoning we have changed the definition of the $X$'s from (2.2) to (3.3); on account of the new variable we can get rid of the difficulty which Dirac came across.

The method of constructing wave equations is straightforward. The fifteen infinitesimal operators which we mentioned in section 2 are operators which leave $g_{\mu\nu}X^\mu X^\nu$ invariant. To make the expressions simpler we introduce $\xi_\mu$ related to $X^\mu$ by

$$\xi_K = X^K, \qquad \xi_4 = iX^0, \qquad \xi_5 = \frac{1}{\sqrt{2}}(X^6-X^5), \qquad \xi_6 = \frac{1}{i\sqrt{2}}(X^5+X^6).$$

The fundamental quadric is

$$\xi_1^2+\xi_2^2+\xi_3^2+\xi_4^2+\xi_5^2+\xi_6^2. \tag{4.1}$$

We denote the infinitesimal operators by $M_{\mu\nu}$, which satisfy

$$[M_{\mu\nu}, M_{\rho\sigma}] = i(\delta_{\mu\rho}M_{\nu\sigma}+\delta_{\nu\sigma}M_{\mu\rho}-\delta_{\mu\sigma}M_{\nu\rho}-\delta_{\nu\rho}M_{\mu\sigma}).$$

For example, $M_{\mu\nu}$ can be

$$M_{\mu\nu} = \overset{\circ}{M}_{\mu\nu} \equiv \frac{1}{i}\left(\xi_\mu\frac{\partial}{\partial\xi_\nu}-\xi_\nu\frac{\partial}{\partial\xi_\mu}\right). \tag{4.2}$$

There are three invariants which commute with every $M_{\mu\nu}$:

$$Q = \tfrac{1}{2}M_{\mu\nu}M_{\mu\nu}, \tag{4.3}$$

$$R = \tfrac{1}{2}M_{\mu\nu}\check{M}_{\mu\nu}, \tag{4.4}$$

$$W = \tfrac{1}{2}\check{M}_{\mu\nu}\check{M}_{\mu\nu}, \tag{4.5}$$

where $\check{M}_{\mu\nu}$ is defined by

$$\check{M}_{\mu\nu} = \tfrac{1}{8}\varepsilon_{\mu\nu\lambda\rho\sigma\tau}M_{\lambda\rho}M_{\sigma\tau}.$$

Hereafter we use $Q$, $R$ and $W$ as denoting eigenvalues of the operators $Q, R, W$.

### 4.2. EQUATION FOR SCALAR PARTICLE

If $M_{\mu\nu} = \overset{\circ}{M}_{\mu\nu}$, $R$ and $W$ are identically zero and we have only one non-trivial equation

$$(\tfrac{1}{2}\overset{\circ}{M}_{\mu\nu}\overset{\circ}{M}_{\mu\nu}-Q)\psi = 0. \tag{4.6}$$

This can be regarded as a generalized Klein-Gordon equation for scalar particles. In order to make it possible to transcribe it into an equation written in terms of the $x$'s and $r$, $\psi(X)$ must be homogeneous in the $X$'s. Because of (2.2) and (3.1), eq. (4.6) becomes

$$\left\{r^2\left[\Box+\frac{\partial^2}{\partial r^2}-\frac{2n+3}{r}\frac{\partial}{\partial r}\right]+n^2+4n-Q\right\}\phi = 0,$$

where $n$ is the degree of homogeneity of $\psi(X)$ and $\phi(x, r) = (X^6)^n\psi(X)$.

Separating variables we get

$$\phi(x, r) = r^{n+2} Z_{\pm\sqrt{Q+4}}(mr)\phi(x), \qquad Z_\rho = aJ_\rho + bY_\rho, \tag{4.7}$$

where $\phi(x)$ satisfies

$$(\Box - m^2)\phi(x) = 0.$$

### 4.3. EQUATION FOR SPIN-$\frac{1}{2}$ PARTICLE

To find out the wave equation for fermions of spin $\frac{1}{2}$, we follow the usual procedure and put

$$M_{\mu\nu} = \overset{\circ}{M}_{\mu\nu} + S_{\mu\nu}, \qquad S_{\mu\nu} = -\frac{i}{4}(\eta_\mu\eta_\nu - \eta_\nu\eta_\mu). \tag{4.8}$$

Here $\eta$'s are eight-by-eight matrices satisfying

$$\eta_\mu\eta_\nu + \eta_\nu\eta_\mu = 2\delta_{\mu\nu}. \tag{4.9}$$

In this case the expressions for the three invariants become

$$Q = \tfrac{1}{2}\overset{\circ}{M}_{\mu\nu}\overset{\circ}{M}_{\mu\nu} - \tfrac{1}{2}i\eta_\mu\eta_\nu\overset{\circ}{M}_{\mu\nu} + \tfrac{15}{4}, \tag{4.10}$$

$$R = \tfrac{9}{8}\eta_7(-i\eta_\mu\eta_\nu\overset{\circ}{M}_{\mu\nu} + 5), \tag{4.11}$$

$$W = \tfrac{3}{2}Q + \tfrac{45}{16}, \tag{4.12}$$

where $\eta_7$ is defined by

$$\eta_7 = i\eta_1\eta_2\eta_3\eta_4\eta_5\eta_6,$$

and satisfies

$$[\eta_7, \eta_\mu]_+ = 0, \qquad \eta_7^2 = 1.$$

Now we can form an equation for spin-$\frac{1}{2}$ particles. Using (4.11) we can write it as

$$[i\eta_\mu\eta_\nu\overset{\circ}{M}_{\mu\nu} - 5 + \tfrac{8}{9}\eta_7 R]\psi = 0. \tag{4.13}$$

To make the manipulation transparent we introduce another set of matrices, $\beta_\mu$, which are related to the $\eta_\mu$ as the $\xi_\mu$ are to the $X^\mu$.

$$\beta_K = \eta_K, \qquad \beta_0 = i\eta_4, \qquad \beta_5 = -\frac{1}{\sqrt{2}}(\eta_5 + i\eta_6), \qquad \beta_6 = \frac{1}{\sqrt{2}}(\eta_5 - i\eta_6),$$

$$\beta_7 = \beta^7 = \eta_7 = -\frac{i}{2}\beta_1\beta_2\beta_3\beta_0(\beta_5\beta_6 - \beta_6\beta_5),$$

$$\beta_\mu\beta_\nu + \beta_\nu\beta_\mu = 2g_{\mu\nu}, \qquad \beta_7\beta_\mu + \beta_\mu\beta_7 = 0, \quad \beta_7^2 = 1.$$

The suffixes may be raised by means of the $g^{\mu\nu}$. Through simple calculation (4.13) becomes

$$\left[2(\beta_\mu X^\mu)\left(\beta_\nu\frac{\partial}{\partial X_\nu}\right) - 2X^\mu\frac{\partial}{\partial X^\mu} - 5 + \tfrac{8}{9}\beta_7 R\right]\psi = 0. \tag{4.14}$$

The following relations can easily be proved:

$$\left[1+\frac{1}{2X^6}(\beta_i X^i)\beta_5\right](\beta_\mu X^\mu)\left[1-\frac{1}{2X^6}(\beta_i X^i)\beta_5\right]=X^6\left[\beta_6-\beta_5\frac{X_\mu X^\mu}{2(X^6)^2}\right],$$

$$\left[1+\frac{1}{2X^6}(\beta_i X^i)\beta_5\right]\left(\beta_\mu\frac{\partial}{\partial X_\mu}\right)\left[1-\frac{1}{2X^6}(\beta_i X^i)\beta_5\right] \tag{4.15}$$

$$=\frac{1}{X^6}\left[\beta_i\left(X^6\frac{\partial}{\partial X_i}-X^i\frac{\partial}{\partial X_6}\right)+\beta_6 X^6\frac{\partial}{\partial X_6}-\beta_5\left(X^\mu\frac{\partial}{\partial X^\mu}+2-\frac{X_\mu X^\mu}{2X^6}\frac{\partial}{\partial X_6}\right)\right].$$

By means of these relations we get for the transformed function $\psi'$

$$\psi'=\left[1+\frac{1}{2X^6}(\beta_i X^i)\beta_5\right]\psi, \tag{4.16}$$

an equation in which the variables $x$'s do not appear except in the form of a differential operator.

Now if the dimensions of all $X$'s are the same, the equation obtained is dimensionally correct. In our previous relations between the $X$'s and the $x$'s this was not the case. However, since $X^5$ and $X^6$ appear in the form of a product in the fundamental quadric, we may multiply $X^5$ by $l_0^{-1}$ and $X^6$ by $l_0$, $[l_0]=[L]$. Then the relations between the $X$'s and the $x$'s become

$$x^i=l_0\frac{X^i}{X^6},\qquad \tfrac{1}{2}(x_i x^i+r^2)=l_0^2\frac{X^5}{X^6}, \tag{4.17}$$

and we may consider the $X$'s dimensionless. As we have noticed in section 2, our group contains a dilatation. On account of (4.17) we may regard the dilatation as assigning a different value to $l_0$ and leaving the values of $x$'s and $r$ unaltered. Because of invariance under dilatation we may give an arbitrary value to $l_0$. We note that the introduction of $l_0$ does not affect the equation for spin-0 particles.

From (4.14), using (4.15), (4.16) and (4.17), we get

$$\left\{2\left(\beta_6 l_0+\beta_5\frac{r^2}{2l_0}\right)\left[\beta_i\frac{\partial}{\partial x_i}+\left(\beta_5\frac{r}{2l_0}-\beta_6\frac{l_0}{2r}\right)\frac{\partial}{\partial r}-\beta_5\frac{n+2}{l_0}\right]-2n-5+\tfrac{8}{9}\beta_7 R\right\}\varphi=0, \tag{4.18}$$

where

$$\varphi(x,r)=(X^6)^n\psi'(X).$$

We separate $\varphi$ into two parts:

$$\varphi=\varphi_1+\varphi_2=-\tfrac{1}{2}\beta_6\beta_5\varphi-\tfrac{1}{2}\beta_5\beta_6\varphi,$$

where $-\frac{1}{2}\beta_6\beta_5$ and $-\frac{1}{2}\beta_5\beta_6$ are projection operators and are orthogonal to each other. By multiplying $-\frac{1}{2}\beta_6\beta_5$ and $-\frac{1}{2}\beta_5\beta_6$ from the left into (4.18) we get

$$\frac{r^2}{2l_0}\beta_5\beta_i\frac{\partial\varphi_1}{\partial x_i}+\left(r\frac{\partial}{\partial r}-n-\tfrac{5}{2}+\tfrac{4}{9}\beta_7 R\right)\varphi_2=0, \tag{4.19}$$

$$l_0 \beta_6 \beta_i \frac{\partial \varphi_2}{\partial x_i} - \left( r \frac{\partial}{\partial r} - n - \tfrac{3}{2} - \tfrac{4}{9} \beta_7 R \right) \varphi_1 = 0. \tag{4.20}$$

We can solve these equations by iterating and separating variables. The solutions are

$$\varphi_1(x, r) = r^{n+2} Z_{\pm(4/9\beta_7 R - \frac{1}{2})}(mr) \varphi_1(x), \tag{4.21}$$

$$\varphi_2(x, r) = \frac{r^{n+3}}{\sqrt{2} l_0} Z_{\pm(4/9\beta_7 R + \frac{1}{2})}(mr) \varphi_2(x), \tag{4.22}$$

where

$$Z_{\pm(4/9\beta_7 R - \frac{1}{2})} \equiv \frac{1+\beta_7}{2} Z_{\pm(4/9R - \frac{1}{2})} + \frac{1-\beta_7}{2} Z_{\mp(4/9R + \frac{1}{2})}.$$

Substituting these solutions into (4.19) and (4.20) we get a pair of equations for $\varphi_i(x)$:

$$\beta_5 \beta_i \frac{\partial \varphi_1(x)}{\partial x_i} + \sqrt{2} m \varphi_2(x) = 0,$$

$$\beta_6 \beta_i \frac{\partial \varphi_2(x)}{\partial x_i} + \sqrt{2} m \varphi_1(x) = 0.$$

These can be combined into a single equation

$$\left\{ \beta_i \frac{\partial}{\partial x_i} - \frac{m}{\sqrt{2}} (\beta_5 + \beta_6) \right\} \varphi(x) = 0 \tag{4.23}$$

or

$$\left( \eta_i \frac{\partial}{\partial x_i} + im\eta_6 \right) \varphi(x) = 0. \tag{4.23'}$$

This is equivalent to the equation mentioned in section 2. Both $\varphi(x)$ and $\eta_7 \varphi(x)$ can be solutions of this equation.

To make the situation concrete we shall give an example of a representation of the $\eta$'s. To represent six $\eta$'s we need three sets of dichotomic matrices. They are

$$\varrho_K = 1 \times \sigma_K \times 1, \qquad \sigma_K = 1 \times 1 \times \sigma_K, \qquad \tau_K = \sigma_K \times 1 \times 1.$$

We can represent the $\eta$'s as follows:

$$\eta_i = \tau_3 \gamma_i (= \tau_3 \varrho_2 \sigma_K, \tau_3 \varrho_3), \quad \eta_5 = \tau_1, \quad \eta_6 = \tau_2, \quad \eta_7 = -\tau_3 \gamma_5. \tag{4.24}$$

Then the equation (4.23') can be written as

$$\left( \gamma_i \frac{\partial}{\partial x_i} + m\tau_1 \right) \varphi(x) = 0. \tag{4.25}$$

The projection operators $-\frac{1}{2}\beta_6\beta_5$ and $-\frac{1}{2}\beta_5\beta_6$ are represented by

$$-\tfrac{1}{2}\beta_6\beta_5 = \tfrac{1}{2}(1 + i\eta_5\eta_6) = \tfrac{1}{2}(1 - \tau_3),$$
$$-\tfrac{1}{2}\beta_5\beta_6 = \tfrac{1}{2}(1 - i\eta_5\eta_6) = \tfrac{1}{2}(1 + \tau_3).$$

If $\varphi(x)$ is constrained by a condition $\frac{1}{2}(1+\eta_7)\varphi = \varphi$, this means

$$\varphi = \begin{pmatrix}\varphi_1\\ \varphi_2\end{pmatrix} \quad \text{with} \quad \begin{matrix}\frac{1}{2}(1-\gamma_5)\varphi_1 = \varphi_1,\\ \frac{1}{2}(1+\gamma_5)\varphi_2 = \varphi_2.\end{matrix}$$

Furthermore, if $m = 0$, $\varphi$ can be an eigenstate of $\tau_3$ too and $\varphi$ may be

$$\varphi = \begin{pmatrix}\varphi_1\\ 0\end{pmatrix} \quad \text{with} \quad \tfrac{1}{2}(1-\gamma_5)\varphi_1 = \varphi_1.$$

When eq. (4.12) holds, the equation for $\psi$ which is inferred from eq. (4.9) requires the following relation between $Q$ and $R$:

$$Q = (\tfrac{4}{9}R)^2 - \tfrac{5}{2}. \tag{4.26}$$

We note that among the irreducible representations of the Lie group [11] † $\{M_{\mu\nu}\}$, those which satisfy (4.12) and (4.26) have $\pm 9/8$ and $\pm 27/8$ as the values of $R$.

## 5. Transformation Properties of $\psi$ for Spin $\frac{1}{2}$ Particles

Now we shall investigate the transformation properties of the wave function $\psi$. At first we introduce the adjoint $\psi^\dagger$ by

$$\psi^\dagger = i\psi^* \eta_4 \eta_6.$$

It satisfies the equation

$$\psi^\dagger [i\overleftarrow{M}_{\mu\nu}\eta_\mu\eta_\nu - 5 + \tfrac{8}{9}\eta_7 R] = 0.$$

Corresponding to the transformation

$$\xi'_\mu = a_{\mu\nu}\xi_\nu, \qquad a_{\mu\nu}a_{\mu\rho} = \delta_{\nu\rho},$$

$\psi$ and $\psi^\dagger$ are transformed into

$$\Lambda\psi \quad \text{and} \quad \pm\psi^\dagger\Lambda^{-1},$$

respectively. Here $\Lambda$ is determined through the conditions

$$\Lambda^{-1}\eta_\mu\Lambda = a_{\mu\nu}\eta_\nu, \qquad \eta_6\eta_4\Lambda^*\eta_4\eta_6 = \pm\Lambda^{-1}.$$

For the infinitesimal transformation $\xi'_\mu = \xi_\mu + \varepsilon_{\mu\nu}\xi_\nu$, $\Lambda$ is given by

$$\Lambda = 1 + \tfrac{1}{8}(\eta_\mu\eta_\nu - \eta_\nu\eta_\mu)\varepsilon_{\mu\nu}. \tag{5.1}$$

Using these $\Lambda$'s we can investigate the transformation properties of various bilinear forms and find out the relation between tensors in six-dimensional space and those in the Minkowski space.

The most interesting things may be the behaviour of $\psi$ under space reflection, time-reversal and particle-antiparticle conjugation.

We shall begin with space reflection. In terms of the $\xi$'s this transforma-

† Unfortunately, the irreducible representations obtained in ref. [11] were not complete, and the present definition of $R$ is different from the previous one by a factor 3.

tion is written as

$$\xi_K \to -\xi_K, \qquad \xi_\mu \to \xi_\mu \qquad (k = 1, 2, 3;\ \mu = 4, 5, 6)$$

and $\psi$ undergoes the transformation

$$\psi \to \eta_7 \eta_1 \eta_2 \eta_3 \psi.$$

But, moreover, $\psi$ has to move into the space of a different irreducible representation: in order that eq. (4.12) be invariant $R$ is to be replaced by $-R$. So, if we assign a definite representation to each particle, there is no reason to require parity-conservation in our formalism. From (4.15) we can easily see that $\phi$ is transformed in the same way under space reflection

$$\phi \to \eta_7 \eta_1 \eta_2 \eta_3 \phi.$$

Since $\eta_7 \eta_1 \eta_2 \eta_3$ anticommutes with $\eta_7$, if $\phi$ is in a definite eigenstate of $\eta_7$ the transformed $\phi$ belongs to a different eigenstate of $\eta_7$. We note that the internal wave function, which is a function of $r$ and $\eta_7 R$, does not change.

Next we shall consider particle-antiparticle conjugation. In this case $\psi$ is transformed in the following way:

$$\psi \to C\psi^{\dagger T}, \qquad R \to -R,$$

where $C$ is defined by

$$C\eta_\mu{}^T C^{-1} = \eta_\mu \quad \text{or} \quad -\eta_\mu, \qquad (C\eta_7{}^T C^{-1} = -\eta_7).$$

$\phi$ is transformed in the same way and in this case too, if $\phi$ is in a definite eigenstate of $\eta_7$, the conjugate $\phi$ belongs to a different eigenstate of $\eta_7$. Here we have also to change the sign of $R$, so we can safely require invariance under the product of space reflection and particle-antiparticle conjugation. On the contrary, in the case of time-reversal $\psi$ need not be moved into the space of a different irreducible representation, and it is permissible to require invariance under time-reversal. Under time-reversal $\psi$ is transformed into $\eta_6 C\psi^*$.

## 6. Concluding Remarks

We summarize the procedure we followed for obtaining the proposed equations for elementary particles. We have used a five-dimensional theory. The fifth coordinate was introduced in such a way that when the five-dimensional space reduces to the Minkowski space, the set of equivalent observers turns out to be extended so as to include those using a reference system moving with a constant acceleration. We have shown why we would like to extend the definition of equivalent observers in this way. It was only to reconcile a conflict between this extension and the law of inertia that we augmented the dimensionality of space from four to five. We should like to stress that we could introduce the new variable in a unique way.

After our postulate had thus been somewhat altered it provided a straightforward method to obtain wave equations for elementary particles. But what we have done contains more than the justification of the proposed wave equations. It shows automatically why it is legitimate to require invariance under T and CP. And further, though we got a definite form for the internal wave function, it disappeared from the final equation for the free particle. It might play a distinctive role when we consider the interactions between particles.

Now we shall briefly indicate some general aspects of interactions between particles which satisfy our equations. At first we require that all fermions of spin-$\frac{1}{2}$ satisfy the equations (4.13). We do not wish to distinguish between nucleons and strange particles. The former have qualities similar to those possessed by the latter. The only difference is that the nucleon has the smallest mass among particles of the nucleon family. We always start from the six-dimensional formalism; then we can obtain the Lagrangian density corresponding to that in the present formalism by integrating $L(x^i, r)$ with respect to $r$. We characterize each particle by a value of $R$ and one eigenvalue of $\eta_7$. (We note that because of the condition of convergence only discrete values of $R$ are permitted.) We do not assume any particular requirement of invariance which is valid only for weak interactions but not for strong interactions. We cannot say yet whether we can explain the difference between the coupling constants characterizing strong and weak interactions, but it is certain that the handedness of particles appears only when they decay. In general, every particle is represented by two four-component spinors $\varphi_{1,2}$ (cf. section 4), which belong to eigenvalues $\pm 1$ of $\gamma_5$. In the case of a strong interaction, both $\varphi_1$ and $\varphi_2$ appear in the interaction. But when a particle A decays into B and C, it turns out that only one part of $\varphi_i$, $\varphi_1$ or $\varphi_2$, is relevant to the decaying process, and real handedness appears. This is because the coupling constant contains

$$\int J_\lambda(M_A r) J_\mu(M_B r) J_\nu(M_C r) r^\alpha \, dr$$

and, subject to certain conditions on $\lambda$, $\mu$, $\nu$, it is very small or it vanishes when $M_A > M_B + M_C$. (We have to put $Z_\rho = J_\rho$ because of convergence.) In Fermi interactions too, we have integrals of triple products of $J$'s, since for the neutrino it is only allowed to use $J_0$, and $J_0(0) = 1$. The details of the interaction formalism will be given in a following paper.

The author has greatly benefited from the interest and kind criticism of Professor L. Rosenfeld. It is a great pleasure to thank Professor Rosenfeld and also the British Council, which awarded the author a scholarship for research at the University of Manchester.

## References

1) B. T. Feld, Padua-Venice Conference (September 1957)
2) T. D. Lee *et al.*, Phys. Rev. **106** (1957) 1367
3) H. Umezawa and A. Visconti, Nuclear Physics **4** (1957) 224
4) L. Landau in Niels Bohr and the Development of Physics (Pergamon Press, London, 1955)
5) J. Haantjes, Proc. Ned. Akad. Wetenschappen **43** (1940) 1288
6) R. L. Ingraham, Nuovo Cimento **9** (1952) 886
7) Y. Murai, Prog. Theor. Phys. **11** (1954) 441
8) B. Hoffmann, Phys. Rev. **89** (1953) 49
9) R. L. Ingraham, Nuovo Cimento **12** (1954) 825
10) P. A. M. Dirac, Ann. of Math. **37** (1936) 427
11) Y. Murai, Prog. Theor. Phys. **9** (1953) 147

*Nuclear Physics* **6** (1958) 504—516; © *North-Holland Publishing Co., Amsterdam*
Not to be reproduced by photoprint or microfilm without written permission from the publisher

# THE INELASTIC SCATTERING OF PROTONS BY $C^{12}$

E. J. SQUIRES

*Atomic Energy Research Establishment, Harwell, Didcot, Berks*

Received 17 January 1958

**Abstract:** The differential cross-section and polarization for the inelastic scattering of 180 MeV protons by $C^{12}$ leaving the nucleus in the 4.43 MeV state are calculated, using shell model wavefunctions in the *L-S* and *j-j* coupling extremes and nucleon-nucleon phase shifts taken from an analysis of free nucleon-nucleon scattering, and taking the absorption part of the optical model potential into account. Good agreement is found when *L-S* coupling is used, especially when use is made of information obtained from inelastic electron scattering to obtain a correction to the nuclear matrix elements calculated with the crude shell model wavefunctions. Some discussion is given of the difference between polarization and asymmetry in inelastic scattering and it is shown that this difference is likely to be small.

## 1. Introduction

Recently several measurements [1]) have been made of the differential cross-sections and polarizations in the inelastic scattering of protons by $C^{12}$ in the 150—200 MeV region. General considerations regarding the interpretation of the experiments have been given by Maris and Tyrén [2]) and by Benoist, Marty and Meyer [3]). The polarization to be expected on the collective model description of the excited states has been calculated by Maris [4]) and by Nishimura and Ruderman [5]) who both assume a phenomenological potential chosen to fit the elastic scattering data. The purpose of the present work is to see if one can obtain reasonable agreement with the differential cross-section and polarization for scattering to the 4.43 MeV level of $C^{12}$, using the known facts about free nucleon-nucleon scattering and the nuclear shell model in either its *L-S* or *j-j* coupling extreme [3]). No attempt is made to consider the case of intermediate coupling. The central absorption part of the optical model potential is taken into account in the calculations. In section 5 some comments are made on the difference between polarization and asymmetry in inelastic scattering.

## 2. Single Collision Description

The transition from the nuclear ground state $\Phi$ to the excited state $\Psi$ is assumed to be brought about by a single nucleon-nucleon collision inside the nucleus, which is described by means of the *t*-matrix appropriate to a free nucleon-nucleon collision. Only the coherent part of the scattering by

the rest of the nucleus is taken into account. In principle this can be done by replacing the incident proton wave $e^{i\mathbf{k}_0\cdot\mathbf{r}}$ and the final proton wave $e^{i\mathbf{k}_f\cdot\mathbf{r}}$ by "outgoing" and "incoming" solutions [6]), respectively, of the optical model potential of the nucleus. These are denoted by $\chi^{(+)}_{\mathbf{k}_0}(\mathbf{r})$ and $\chi^{(-)}_{\mathbf{k}_f}(\mathbf{r})$, respectively. In the present work, however, only the central absorption part of the optical model potential is taken into account. Reasons for believing that the real central part and the spin-orbit part will not seriously alter the results are given at the end of section 3. The approximation of replacing the $t$-matrix inside the nucleus by that obtained from free nucleon-nucleon scattering should be reasonable at this energy. The nucleus is assumed to be infinitely heavy.

If the matrix element for the transition considered is denoted by $T_\Psi$ we have

$$T_\Psi(\theta) = \sum_i < \Psi \chi^{(-)}_{\mathbf{k}_f} | t(i) | \chi^{(+)}_{\mathbf{k}_0} \Phi >, \tag{1}$$

where $\theta$ is the angle between $\mathbf{k}_0$ and $\mathbf{k}_f$, $t(i)$ is the operator for a free collision between the incident proton and the $i$th nucleon in the nucleus and where the sum over $i$ goes over all such nucleons.

The operator $t(i)$ is known (at least in principle) for energy conserving collisions, from free nucleon-nucleon scattering experiments, as a function of the relative momenta of the two nucleons before and after the collision. In the region of relative momenta associated with any given nucleon-nucleus scattering it will be assumed that $t$ can be considered as a function of the momentum transfer only, thus eliminating the effect of the momentum distribution of the nucleons in the nucleus, and, since the optical potential scattering is mainly through small angles, this momentum transfer will be taken to be $|\mathbf{k}_0 - \mathbf{k}_f|$. Thus the operator $t(i)$ can be written, in the $r$-representation,

$$t(i) = \delta(\mathbf{r} - \mathbf{r}_i) t_i(\theta) \tag{2}$$

where $t_i(\theta)$ is a matrix in the spin space of the two nucleons and is defined so that the free nucleon-nucleon differential cross-section in the centre of mass system is given by

$$\frac{d\sigma^F(\theta)}{d\Omega} = \frac{1}{4} \operatorname{tr} [t_i(2\theta)^+ t_i(2\theta)]. \tag{3}$$

With this definition the differential cross-section for the inelastic scattering considered is given by

$$\frac{d\sigma^\Psi(\theta)}{d\Omega} = 4 \sum_\Psi^1 \tfrac{1}{2} \operatorname{tr} [T_\Psi(\theta)^+ T_\Psi(\theta)] \tag{4}$$

where $\sum^1_\Psi$ means the sum over all final sub-states with the same energy and where the factor 4 arises from the fact that a factor $\frac{1}{2}$ has been incorporated

in the $t_i$ to take account of the reduced mass of the nucleons in free nucleon-nucleon scattering. The spin in eq. (4) refers to the spin space of the incident and final proton. Except for small corrections the effects of nuclear exchange are automatically taken into account by the use of the $t$-matrix [7]).

It is convenient to write the $t$-matrix in the form [8])

$$t_i = a_i + c_i(\boldsymbol{\sigma}_i+\boldsymbol{\sigma})\cdot\mathbf{n} + b_i\boldsymbol{\sigma}_i\cdot\mathbf{n}\boldsymbol{\sigma}\cdot\mathbf{n} + \mathbf{d}_i\boldsymbol{\sigma}_i\cdot\hat{\mathbf{K}}\boldsymbol{\sigma}\cdot\hat{\mathbf{K}} + e_i\boldsymbol{\sigma}_i\cdot\mathbf{P}\boldsymbol{\sigma}\cdot\mathbf{P} \quad (5)$$

where the set of mutually orthogonal unit vectors $\mathbf{n}$, $\hat{\mathbf{K}}$, $\mathbf{P}$ are defined by

$$\mathbf{n} = \frac{\mathbf{k}_0\wedge\mathbf{k}_f}{|\mathbf{k}_0-\mathbf{k}_f|}, \quad (6a)$$

$$\hat{\mathbf{K}} = \frac{\mathbf{k}_0-\mathbf{k}_f}{|\mathbf{k}_0-\mathbf{k}_f|}, \quad (6b)$$

$$\mathbf{P} = \frac{\mathbf{n}\wedge\mathbf{K}}{|\mathbf{n}\wedge\mathbf{K}|} \approx \frac{\mathbf{k}_0+\mathbf{k}_f}{|\mathbf{k}_0+\mathbf{k}_f|}. \quad (6c)$$

The momentum transfer vector defined by

$$\mathbf{K} = \mathbf{k}_0-\mathbf{k}_f \quad (6d)$$

will be used later.

The parameters $a_i, \ldots e_i$ are functions of the angle $\theta$. Their values have been obtained from the phase shifts of Gammel and Thaler [9]) for p-p and n-p scattering, by using the expressions given by Stapp and Ypsilantis [10]) for the p-p case and similar ones for the n-p case. These values are shown in tables 1 and 2. The phase shifts of Gammel and Thaler are derived from a mainly phenomenological potential chosen to give reasonable agreement with all known nucleon-nucleon scattering data. It is not possible to obtain a unique set of phase shifts by an analysis of the experimental results at present available.

TABLE 1

Some values of the $t$-matrix parameters for p-p scattering at 180 MeV

| Angle in c. of m. system | 0° | 30° | 45° | 60° | 90° |
|---|---|---|---|---|---|
| $ik\,a_{pp}$ | −0.525+0.788i | −0.416+0.508i | −0.306+0.272i | −0.185+0.076i | 0.033−0.131i |
| $ik\,b_{pp}$ | 0.036−0.369i | 0.016−0.358i | −0.010−0.259i | −0.026−0.037i | −0.033+0.131i |
| $ik\,c_{pp}$ | 0 | −0.359+0.001i | −0.458−0.002i | −0.503−0.007i | −0.519−0.009i |
| $ik\,d_{pp}$ | 0.038−0.372i | 0.005+0.141i | −0.015+0.451i | −0.029+0.499i | 0.009+0.467i |
| $ik\,e_{pp}$ | −0.236−0.812i | −0.205−0.627i | −0.175−0.465i | −0.145−0.385i | −0.065−0.205i |

The phase shifts of Gammel and Thaler referred to in the text have been used. The quantity $k$ is the relative momentum in the centre of mass system, divided by $\hbar$.

TABLE 2

Some values of the $t$-matrix parameters for n-p scattering at 180 MeV

| Angle in c. of m. system | 0° | 30° | 45° | 60° | 90° |
|---|---|---|---|---|---|
| $ik\,a_{pn}$ | −0.748+0.568i | −0.532+0.406i | −0.311+0.230i | −0.082+0.036i | +0.217−0.189i |
| $ik\,b_{pn}$ | 0.049+0.313i | 0.038+0.311i | 0.026+0.340i | 0.021+0.409i | −0.017+0.558i |
| $ik\,c_{pn}$ | 0 | −0.309+0.106i | −0.380+0.112i | −0.383+0.090i | −0.259−0.005i |
| $ik\,d_{pn}$ | 0.039+0.139i | +0.067+0.061i | 0.104−0.005i | 0.128−0.054i | 0.103−0.037i |
| $ik\,e_{pn}$ | −0.301+0.476i | −0.223+0.316i | −0.154+0.147i | −0.072−0.040i | +0.063−0.397i |

The phase shifts of Gammel and Thaler referred to in the text have been used. The quantity $k$ is the relative momentum in the centre of mass system divided by $\hbar$.

## 3. The Effect of Absorption

The imaginary part of the optical model potential at any point is proportional to the probability of a particle making a collision, allowed by the exclusion principle, at that point. Thus it is roughly proportional to the nucleon density in the nucleus. The exact shape should not matter greatly, since the required excitation of the nucleus can take place throughout its volume, and so the simple gaussian form is assumed

$$V(r) = -iV\mathrm{e}^{-\beta r^2}. \tag{7}$$

The value of $\beta$ is chosen so that the r.m.s. radius of this potential fits that of the charge distribution, as determined by electron scattering, which is $2.4 \times 10^{-13}$ cm [11]). $V$ has been estimated from the expressions for the absorption coefficient in terms of n-p and p-p cross-sections given by Cassels and Lawson [12]). A value of 60 MeV has been obtained for protons with incident energy 180 MeV.

Use of the above potential together with the W.K.B. approximation leads to the following expression for $\chi^{(+)}_{\mathbf{k}_0}$:

$$\chi^{(+)}_{\mathbf{k}_0}(\mathbf{r}) = \mathrm{e}^{i\mathbf{k}_0\cdot\mathbf{r}+iS} \tag{8}$$

with

$$S = \frac{ik_0V}{2E}\int_{-\infty}^{z}\mathrm{e}^{-\beta r^2}\mathrm{d}z \tag{9}$$

where the $z$ axis is taken to be along $\mathbf{k}_0$ and where $E$ is the energy of the incident proton. Similar expressions hold for $\chi^{(-)}_{\mathbf{k}_f}(\mathbf{r})$ except that the limits of integration must be replaced by $z$ to $\infty$ and the $z$ axis must be taken along $\mathbf{k}_f$.

If scattering in the forward direction, $\mathbf{k}_0 \approx \mathbf{k}_f$, is considered then the factor in the integral of (1) is

$$\exp -\frac{k_0 V}{2E}\left[\int_{-\infty}^{z} e^{-\beta r^2}\,dz+\int_{z}^{\infty} e^{-\beta r^2}\,dz\right]=\exp\left[-\frac{k_0 V}{2E}\left(\frac{\pi}{\beta}\right)^{\frac{1}{2}} e^{-\beta\rho^2}\right] \quad (10)$$

where $\varrho^2 = x^2+y^2$ and where use has been made of the fact that the final energy of the proton does not differ greatly from its initial energy. In order to simplify the final integral this function is represented approximately by one of a simpler form. For the above values of the parameters we put

$$\exp\left[-\frac{k_0 V}{2E}\left(\frac{\pi}{\beta}\right)^{\frac{1}{2}} e^{-\beta\rho^2}\right]\approx 1-0.9\, e^{-0.765\beta\rho^2}. \quad (11)$$

The error introduced by this approximation is certainly less than 10 %.

For scattering not in the forward direction the expression (11) is still used for the absorption factor but the $z$ axis is taken to be along $\mathbf{k}_0+\mathbf{k}_f$. The error in this procedure can be shown to be of the order of $\sin^2 \frac{1}{2}\theta$ and so will be small for the angles considered in this work. Thus we have

$$\chi^{(-)*}_{\mathbf{k}_f}(\mathbf{r})\chi^{(+)}_{\mathbf{k}_0}(\mathbf{r}) \approx e^{i\mathbf{K}\cdot\mathbf{r}}[1-0.9\, e^{-0.765\beta\rho^2}] \quad (12)$$

where $\varrho$ is the distance from the axis along $\mathbf{k}_0+\mathbf{k}_f$ passing through the centre of the nucleus.

Together with the imaginary central potential dealt with above, the optical potential contains a real central potential and a complex spin-orbit potential. It is not possible to assign unambiguous values to these quantities as no sufficiently complete analysis of the elastic scattering and total cross-sections are available. This is particularly true of the spin-orbit potential which has usually been treated as real [13]) although the analysis of small angle scattering of 300 MeV protons by $C^{12}$ carried out by Heckrotte [14]) shows that the real and imaginary parts are of approximately equal magnitude. This difficulty, and the fact that the inclusion of the extra term complicates the analysis and increases the numerical integrations required by at least an order of magnitude, are the reasons for ignoring these terms in this work. The neglect of the real central potential, at least for the region where the scattering is large, may be justified by noting that its value is around one half of the value of the imaginary at this energy [13, 15]) and that it only contributes to the cross-section and polarization in second order. An estimate of the effect of the spin orbit potential has been made by taking the value of the potential from the work of Levintov [16]) and assuming that it is real. In the region where the cross-section is maximum it increases it by about 20 %. The presence of an imaginary part of the spin-orbit potential will decrease this effect. The approximation of neglecting all but the imaginary part of the optical potential in the expression for the distorted waves has been used by Nishimura and Ruderman [5]).

## 4. The Nuclear States and Evaluation of $T_\psi$

At this stage it is necessary to specify a particular final state. The $2^+$ level of $C^{12}$ at 4.43 MeV will be considered here. The states are assumed to be described by the nuclear shell model in either the $L$-$S$ or $j$-$j$ coupling extreme. In the former case the ground and excited states are in the $(S^4\,P^8)$ configurations coupled to the most symmetrical states with spins 0 and 2 respectively. In the latter case the ground state is the $S^4_{\frac{1}{2}}\,P^8_{3/2}$ configuration and the excited state is a $S^4_{\frac{1}{2}}\,P^7_{3/2}\,P_{\frac{1}{2}}$ configuration.

The expressions (2), (5), (12) are inserted into eq. (1) and $T_\psi$ can be calculated for the $L$-$S$ and $j$-$j$ coupling cases. The results are simplest if the magnetic quantum number $M$ of the final state is measured along the $K$ axis. Some straightforward algebra leads to the following equations †:

*L-S coupling*

$$T_M = \tfrac{4}{3}(\tfrac{7}{5})^{\frac{1}{2}}(a+c\boldsymbol{\sigma}\cdot\mathbf{n})\{(I_0-I_1)\delta_{M,0}-(\tfrac{3}{2})^{\frac{1}{2}}J_1(\delta_{M,2}+\delta_{M,-2})\}, \tag{13}$$

*j-j coupling*

$$\begin{aligned} T_M = &-\frac{2\sqrt{2}}{3}(a+c\boldsymbol{\sigma}\cdot\mathbf{n})(I_0-I_1)\delta_{M,0} \\ &+\frac{2}{\sqrt{3}}[(a+c\boldsymbol{\sigma}\cdot\mathbf{n})(\delta_{M,2}+\delta_{M,-2})-d\boldsymbol{\sigma}\cdot\hat{\mathbf{K}}(\delta_{M,2}-\delta_{M,-2})]J_1 \\ &+\frac{1}{\sqrt{3}}(c+b\boldsymbol{\sigma}\cdot\mathbf{n})(\delta_{M,1}+\delta_{M,-1})(I_0-I_1+J_1) \\ &+\frac{1}{\sqrt{3}}ie\boldsymbol{\sigma}\cdot\mathbf{P}(\delta_{M,1}-\delta_{M,-1})(I_0-I_1-J_1), \end{aligned} \tag{14}$$

with

$$I_0 = \langle Y_{10}(\mathbf{r})|e^{i\mathbf{K}\cdot\mathbf{r}}|Y_{10}(\mathbf{r})\rangle-\langle Y_{11}(\mathbf{r})|e^{i\mathbf{K}\cdot\mathbf{r}}|Y_{11}(\mathbf{r})\rangle \tag{15}$$

$$\begin{aligned} I_1 = &\langle Y_{10}(\mathbf{r})|0.9\,e^{-0.765\beta\rho^2}\,e^{i\mathbf{K}\cdot\mathbf{r}}|Y_{10}(\mathbf{r})\rangle \\ &-\langle Y_{11}(\mathbf{r})|0.9\,e^{-0.765\beta\rho^2}\,e^{i\mathbf{K}\cdot\mathbf{r}}|Y_{11}(r)\rangle \end{aligned} \tag{16}$$

$$J_1 = \langle Y_{11}(\mathbf{r})|0.9\,e^{-0.765\beta\rho^2}\,e^{i\mathbf{K}\cdot\mathbf{r}}|Y_{1,-1}(\mathbf{r})\rangle. \tag{17}$$

In eqs. (13) and (14) the suffix $M$ signifies one of the 5 values of the nuclear spin orientation, and the parameters $a, \ldots e$ are the mean values of the $a_i, \ldots e_i$ for the p-p and p-n scattering. The term $I_0$ gives the effect of the undistorted plane waves and the terms $I_1$ and $J_1$ give the effect of the absorption. The $Y_{1M}(\mathbf{r})$ of eqs. (14), (15) and (16) are the complete spatial wave-functions of the p-state nucleons, including the radial part. For the latter we take harmonic oscillator wave-functions. Thus

† The term in these equations coming from the undistorted incident and final waves and from the terms in $t$ not containing $\sigma_1$ have previously been evaluated by Morpurgo [17]) in calculations on electron inelastic scattering.

$$Y_{1M}(\mathbf{r}) = \left[\frac{8\alpha^{5/2}}{3\pi^{\frac{1}{2}}}\right]^{\frac{1}{2}} r e^{-\frac{1}{2}\alpha r^2} Y_{1M}(\theta,\ \phi). \tag{18}$$

The value of $\alpha$ is fixed by the requirement that the r.m.s. radius of the nucleus should be equal to $2.4 \times 10^{-13}$ cm [11]). This leads to

$$\alpha = 0.376. \tag{19}$$

The density distribution given by harmonic oscillator wave-functions gives good agreement with the results of elastic electron scattering [18]).

The integral $J_1$, corresponding to the terms involving a change of 2 in the $z$ component of the orbital angular momentum of the struck particle, turns out to be very much smaller than the other integrals and its effect is therefore ignored in the results which follow. Its inclusion would increase the differential cross section by about 5 % in the region of the maximum for both $L$-$S$ and $j$-$j$ cases and would make an even smaller difference to the polarisation. The integral $I_0$ can be calculated simply and we get

$$I_0 = -\frac{K^2}{2\alpha} e^{-K^2/4\alpha}.$$

The integral $I_1$ has been evaluated by first doing the integral over $r$ analytically and then carrying out the two dimensional angular integral numerically.

## 5. Results and Comparison with Experiment

The cross-section is obtained from eq. (4) and the polarization from the eq. [8])

$$P(\theta)\frac{d\sigma(\theta)}{d\Omega} = 4\sum_{\psi}^{1} \tfrac{1}{2}(T_{\psi}^{+}\boldsymbol{\sigma}\cdot\mathbf{n}\,T_{\psi}). \tag{21}$$

Note that, with the approximations which have been made, the polarization and asymmetry are equal. This point is further discussed in section 5.

In terms of the $I_0$ and $I_1$ integrals the cross-sections and polarizations can be written down for the two cases. For $L$-$S$ coupling we have

$$\frac{d\sigma(\theta)}{d\Omega} = \frac{32.14}{45}[|a|^2+|c|^2](I_0-I_1)^2 \tag{22}$$

$$P(\theta) = \frac{2\,\mathrm{Re}\,a^*c}{|a|^2+|c|^2} \tag{23}$$

and for $j$-$j$ coupling

$$\frac{d\sigma(\theta)}{d\Omega} = \frac{32}{9}[|a|^2+|c|^2+\tfrac{3}{4}(|c|^2+|b|^2+|e|^2)](I_0-I_1)^2 \tag{24}$$

$$P(\theta) = \frac{2\,\mathrm{Re}\,(a^*c+\frac{3}{4}b^*c)}{|a|^2+|c|^2+\frac{3}{4}[|c|^2+|b|^2+|e|^2]}. \tag{25}$$

It can be seen from these equations that the constant ratio of 14/5 between the differential cross-sections for electron scattering in the $L$-$S$ and $j$-$j$ coupling limits [17]) does not apply here. This is because of the parts of $t_i$ containing $\sigma_i$ which have no analogue in the electron scattering case, and which give rise to the terms preceded by a factor 3/4 in eqs. (24) and (25).

Fig. 1 shows the values of $I_0$ and $I_0-I_1$ for 180 MeV incident protons plotted against the angle of scattering. It will be seen that the effect of the

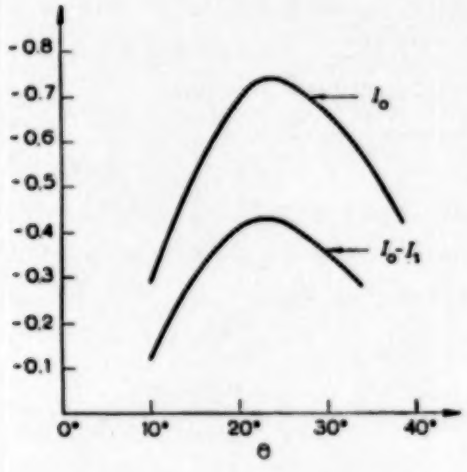


Fig. 1. The integrals $I_0$ and $I_0-I_1$.

absorption is to decrease the scattering amplitude by about one half in the region around the maximum.

The cross-sections and polarizations obtained from fig. 1 and the values of $a, \ldots e$ given by the phase shifts mentioned in section 2 are shown in figs. 2 and 3. It will be seen that the results favour the $L$-$S$ coupling case. This is especially so for the polarization which ought to be predicted more accurately than the cross-section since it is independent of the quantity $I_0-I_1$. In fact eq. (23) should be a good approximation to the polarization for a wide variety of nuclear models and final states for which the $\sigma_i$ terms in $t_i$ approximately reduce to zero. On the $L$-$S$ coupling model this is the case for all states which have total spin given by $S = 0$. In $C^{12}$ these include the ground state and the 4.43 and 9.6 MeV levels which should therefore have polarizations which are approximately equal. This is in fact the case except for large angles where they differ widely, as would be expected since the effect of the neglected part of the optical potential will be important here. The other levels which have been investigated for $C^{12}$ have cross-sections with forward maxima and thus are not states with $S = 0$. Similar results hold when inelastic scattering by $O^{16}$ and $Ca^{40}$ are compared with that for $C^{12}$. These equalities would not necessarily hold if the $\sigma_i$ terms contributed to the polarization, as for example on the $j$-$j$ coupling model.

It will be seen that the differential cross-sections on both models are too small to fit the experimental results. This is in agreement with what one would expect from the electron scattering data [18]) where the same effect occurs. It is due to the fact that the shell model wave-functions which have been used ignore all collective phenomena (e.g. $\alpha$-clusters, collective oscillations) inside the nucleus, which will certainly play some part in this process. Ferrel and Visscher [18]) have in fact shown that the introduction of from 10 to 50 % of collective oscillation into the $L$-$S$ description of the excited state gives good agreement with the experiments on electron scattering to the 4.43 MeV state. No agreement can be obtained in this way when $j$-$j$ coupled wave-functions are used.

If it is assumed that the $\sigma_i$ terms give no contribution and that the process can be considered as a single particle collision, then the nuclear matrix element for the term with undistorted waves can be obtained directly from the electron scattering data, and a result thus obtained which is independent of the nuclear model (except for the conditions above). In fact we have

$$|I_0|^2 = \frac{15.54}{z^2} |F_{\text{in}}|^2 \tag{26}$$

where $F_{\text{in}}$ is given by Morpurgo [17]) in eqs. (3) and (4) of his paper. The correction factor which has to be introduced due to departure from the shell model to make $|F_{\text{in}}|^2$ agree with the electron scattering experiments can then be applied to $|I_0|^2$. There is no analogue in the electron scattering case to the effect of absorption (Born approximation is used) and so it is not possible to obtain a similar correction factor for $(I_0 - I_1)^2$. As a rough guide, however, we can use the same factor as for $I_0^2$. Thus we can obtain roughly corrected values for the cross-section using only the above two assumptions. These values are shown in fig. 2 and the agreement is satisfactory. A correction of this type does not affect the polarization which is independent of $(I_0 - I_1)^2$.

A similar procedure to the above can be used to "correct" the values obtained using the $j$-$j$ coupling model but the agreement is much less satisfactory, values about 50 % too large near the maximum being obtained.

## 5. The Polarization - Asymmetry Difference

As has been pointed out several times, the equality of the polarization ($P$) produced by scattering an unpolarized beam and the azimuthal asymmetry ($A$) produced by scattering a completely polarized beam, which holds for elastic scattering [8]) does not hold in general for inelastic scattering. This is because the equivalence in the case of elastic scattering depends

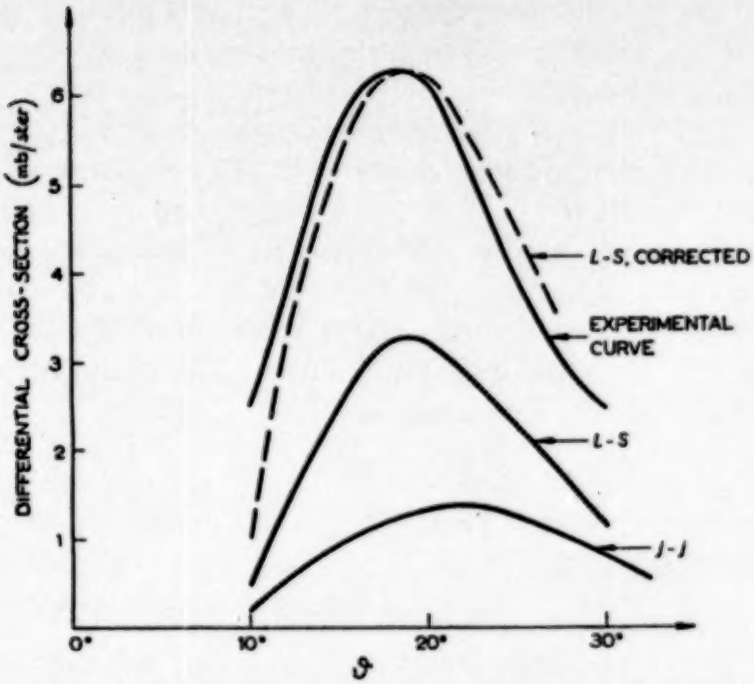


Fig. 2. The experimental differential cross-section for inelastic scattering of 180 MeV protons by $C^{12}$ leaving the nucleus in the 4.43 MeV level, and the values calculated using the *L-S* and *j-j* coupling extremes of the shell model. Also shown, by the broken line, is the value corrected for nuclear correlations as explained in the text.

on the fact that the two processes are time reversals of each other, which is not true for inelastic scattering.

The difference between $A$ and $P$ is given in terms of $T_\Psi$ by [8])

$$A-P=\sum_{\Psi}{}' \operatorname{tr}\left[T_\Psi\,\boldsymbol{\sigma}\cdot\mathbf{n}\,T_\Psi^{+}-T_\Psi^{+}\,\boldsymbol{\sigma}\cdot\mathbf{n}\,T_\Psi\right]. \tag{35}$$

It follows immediately from eqs. (13) and (14) that, with the approximations made previously (see below), $P\equiv A$.

To study the more general case it is convenient to write $T_\Psi$ in the form

$$T_\Psi=A_\Psi+B_\Psi\,\boldsymbol{\sigma}\cdot\mathbf{n}+D_\Psi\boldsymbol{\sigma}\cdot\hat{\mathbf{K}}+E_\Psi\,\boldsymbol{\sigma}\cdot\mathbf{P} \tag{36}$$

from which follows

$$A-P=8\,\operatorname{Im}\{\sum_{\Psi}{}' D_\Psi\,E_\Psi{}^{*}\}. \tag{37}$$

We then have the following two results.

1. If the approximation that $t$ depends only on the momentum transfer is made then $P=A$. To see this we insert eqs. (2), (5) and (12) into eq. (1) and consider the terms $D_\Psi$ and $E_\Psi$ of eq. (36). $D_\Psi$ contains the matrix element $\langle\Psi|e^{i\mathbf{K}\cdot\mathbf{r}}\,\boldsymbol{\sigma}\cdot\hat{\mathbf{K}}|\Phi\rangle$ and $E_\Psi$ contains $\langle\Psi|e^{i\mathbf{K}\cdot\mathbf{r}}\,\boldsymbol{\sigma}\cdot\mathbf{P}|\Phi\rangle$. If the axis along which spins are projected is taken along $\mathbf{K}$ it follows that $D_\Psi$ and $E_\Psi$ can only have non-zero components with states $\Psi$ having spin components 0 and $\pm1$ respectively. Thus there can be no cross-terms between them,

which proves the result. Note that the use of this approximation is the reason why, in the treatment given in the previous sections, the polarization and asymmetry are equal.

2. If all the terms in $t_i$ containing $\boldsymbol{\sigma}_i$ cancel out in eq. (1) (e.g. in the $L$-$S$ coupling shell model), then again $P \equiv A$. To prove this we first define the set of unit vectors $\mathbf{n}^{(r)}$, $\hat{\mathbf{K}}^{(r)}$, $\mathbf{P}^{(r)}$ which are similar to those of eq. (6) except that the vectors $\mathbf{k}_0$ and $\mathbf{k}_f$ are replaced by the relative momentum vectors $\mathbf{k}_0-\mathbf{k}_0$ (i) and $\mathbf{k}_f-\mathbf{k}_f$ (i) respectively, where $\mathbf{k}_0$ (i) and $\mathbf{k}_f$ (i) are the momenta of the struck nucleon before and after the collision. Then $t_i$ can be written in the form of eq. (5) with the $a_i, \ldots e_i$ now being functions of $\mathbf{k}_0-\mathbf{k}_0$ (i) and $\mathbf{k}_f-\mathbf{k}_f$ (i) separately. Thus

$$t_i = a_i+c_i(\boldsymbol{\sigma}_i+\boldsymbol{\sigma})\cdot\mathbf{n}^{(r)}+b_i\,\boldsymbol{\sigma}_i\cdot\mathbf{n}^{(r)}\boldsymbol{\sigma}\cdot\mathbf{n}^{(r)} + d_i\boldsymbol{\sigma}_i\cdot\hat{\mathbf{K}}^{(r)}\boldsymbol{\sigma}\cdot\hat{\mathbf{K}}^{(r)}+e_i\boldsymbol{\sigma}_i\cdot\mathbf{P}^{(r)}\boldsymbol{\sigma}\cdot\,.\,\mathbf{P}^{(r)} \quad (38)$$

We make the substitution

$$\mathbf{k}_0\ (\mathrm{i}) = \tfrac{1}{2}\mathbf{K}+\mathbf{s} \quad (39)$$

which leads by means of the momentum conservation equation to

$$\mathbf{k}_f\ (\mathrm{i}) = -\tfrac{1}{2}\mathbf{K}+\mathbf{s}. \quad (40)$$

Then

$$\mathbf{n}^{(r)} = \frac{\mathbf{n}+\mathbf{s}\wedge\mathbf{K}}{|\mathbf{n}+\mathbf{s}\wedge\mathbf{K}|} \quad (41a)$$

$$\hat{\mathbf{K}}^{(r)} = \frac{\mathbf{K}}{|\mathbf{K}|} \quad (41b)$$

$$\mathbf{P}^{(r)} = \frac{\mathbf{n}^{(r)}\wedge\mathbf{K}}{|\mathbf{n}^{(r)}\wedge\mathbf{K}|}. \quad (41c)$$

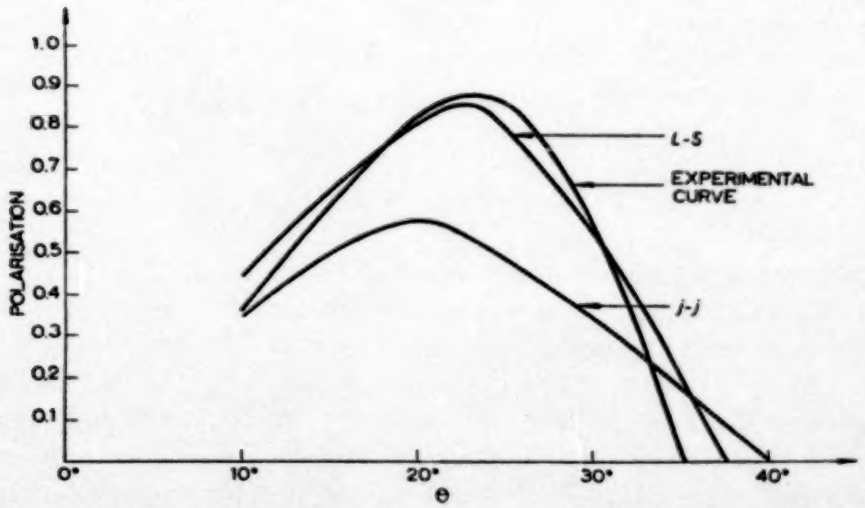


Fig. 3. The experimental and theoretical polarizations, corresponding to fig. 2.

Of these three vectors only $\mathbf{K}^{(r)}$ contains components along $\mathbf{K}$ so that only the term containing $\boldsymbol{\sigma}_i \cdot \mathbf{K}^{(r)}$ in (38) contributed to $D_\psi$. However such a term we have assumed to give zero; so the result follows.

From the above two sets of conditions we see that any $P$-$A$ difference depends upon the finite momentum distribution of the nucleons in the nucleus, upon the departure from momentum transfer dependence of the $t$-matrix and upon the degree of spin orbit coupling in the nucleus. All these effects are likely to combine to make the effect small, which is in agreement with the experimental evidence of Tyrén, Hillman and Johansson [1]). Some calculations have been made using the phase shifts of Feshbach and Lomon[19]) and the extreme $j$-$j$ coupling shell model. The largest effects occur at scattering angles of about 40° where the value of $P-A$ is about 20 %.

## 6. Conclusions

It is concluded that the description in terms of a single quasi free collision gives agreement with the experimental values of the differential cross-section and the polarization for the inelastic scattering of protons to the $2^+$ level of $C^{12}$, when the Gammel and Thaler phase shifts are used to describe the nucleon-nucleon collision. This agreement only holds when the absorption due to the imaginary part of the optical model potential is taken into account. Shell model wave functions with $L$-$S$ coupling give good agreement to the observed polarization but rather too small values for the differential cross-section as would be expected. By applying a crude correction, obtained by analysis of electron scattering experiments, to take account of collective effects in the nucleus the agreement is improved. The experimentally observed agreement between polarization and asymmetry is shown to be reasonable and reasons are given for believing that any difference between these quantities are likely to be small.

I wish to thank Dr. R. J. N. Phillips for advice concerning phase shifts, Dr. P. Hillman for communicating experimental results before publication and for discussions, Dr. B. H. Flowers for advice on presentation and Dr. T. H. R. Skyrme for many discussions throughout the course of this work.

## References

1) H. Tyrén, P. Hillman and A. Johansson, Nuclear Physics **3** (1957) 336; and private communication from P. Hillman;
H. Tyrén and Th. A. J. Maris, Nuclear Physics **2** (1956) 52;
R. Alphonce, A. Johansson and G. Tibell, Nuclear Physics **3** (1957) 185;
W. G. Chesnut, E. M. Haffner and A. Roberts, Phys. Rev. **104** (1956) 449
2) Th. A. J. Maris and H. Tyrén, Nuclear Physics **2** (1956) 35

3) P. Benoist, C. Marty and P. Meyer, Compt. rend. **244** (1957) 1893
4) Th. A. J. Maris, Nuclear Physics **3** (1957) 213
5) K. Nishimura and M. Ruderman, Phys. Rev. **106** (1957) 558
6) M. Gell-Mann and M. L. Goldberger, Phys. Rev. **91** (1953) 389
7) G. Takeda and K. M. Watson, Phys. Rev. **97** (1954) 1336
8) L. Wolfenstein and J. Ashkin, Phys. Rev. **85** (1952) 947
9) J. M. Gammel and R. M. Thaler, Phys. Rev. **107** (1957) 29; and additional paper to be published
10) H. P. Stapp and T. J. Ypsilantis, Phys. Rev. **105** (1957) 302
11) J. H. Fregau and R. Hofstadter, Phys. Rev. **99** (1955) 1503
12) J. M. Cassels and J. D. Lawson, Proc. Phys. Soc. A **67** (1954) 125
13) R. M. Sternheimer, Phys. Rev. **100** (1955) 886
14) W. Heckrotte, Phys. Rev. **101** (1956) 1406
15) R. Wilson, Phil. Mag. **1** (1956) 1013;
S. Fernbach, W. Heckrotte and J. V. Lepore, Phys. Rev. **97** (1955) 1059
16) I. I. Levintov, J. Exptl. Theoret. Phys. (U.S.S.R.) **30** (1956) 987
17) G. Morpurgo, Nuovo Cimento **3** (1956) 430
18) R. A. Ferrell and W. M. Visscher, Phys. Rev. **104** (1956) 475
19) H. Feshbach and E. Lomon, Phys. Rev. **102** (1956) 871

*Nuclear Physics* **6** (1958) 517—524; © *North-Holland Publishing Co., Amsterdam*
Not to be reproduced by photoprint or microfilm without written permission from the publisher

# CORRÉLATION ANGULAIRE ($\gamma$, $\gamma$) DANS LA RÉACTION $^{14}$N (p, $\gamma$) $^{15}$O

S. GORODETZKY, A. GALLMANN, M. CROISSIAUX et R. ARMBRUSTER
*Institut de Recherches Nucléaires de Strasbourg*

Reçu le 14 octobre 1957

**Abstract:** We have measured, in two different planes, the $\gamma-\gamma$ angular correlation in the cascade 8.34 MeV → 5.27 MeV → 0 of $^{15}$O through the $^{14}$N (p, $\gamma$) $^{15}$O reaction, at its resonance at 1.060 MeV. The experimental results agree with the value $J = 3/2$ for the angular momentum of the 5.27 MeV level. The computations we have made do not allow us to exclude the value $J = 5/2+$.

## 1. Introduction

La réaction $^{14}$N (p, $\gamma$) $^{15}$O présente plusieurs résonances. Celle de 1.060 MeV aboutit au niveau excité de 8.34 MeV dans $^{15}$O. Ce niveau peut se désexciter par rayonnement gamma soit directement vers le niveau fondamental, soit par l'intermédiaire des niveaux de 6.82 MeV et 5.27 MeV [1]. Nous avons étudié des corrélations angulaires ($\gamma$, $\gamma$) par le niveau de 5.27 MeV.

On sait que dans le cas d'une cascade double la corrélation angulaire ne dépend que de l'angle formé par les deux rayonnements. Elle est indépendante du plan de détection choisi. En général, il n'en est plus de même pour une cascade triple, par exemple une réaction p-$\gamma$-$\gamma$. En choisissant comme axe de quantification la direction du premier rayonnement (dans notre cas la direction du faisceau de protons incidents), la corrélation angulaire $\gamma_1-\gamma_2$ dépend du plan de détection choisi.

Dans le cas d'un plan perpendiculaire au faisceau, la corrélation angulaire $W_H$ sera la même qu'on détecte le premier rayonnement $\gamma$ dans un compteur ou dans l'autre. Il n'en est pas de même si on mesure la corrélation angulaire dans un plan contenant le faisceau. En choisissant par exemple comme direction du compteur fixe la direction du faisceau de protons incidents, on obtiendra des résultats différents, suivant qu'on mesure

(a) la corrélation angulaire $W_{\gamma_1}$ en détectant le premier rayonnement $\gamma$ de la cascade (celui de 3.07 MeV) parallèlement au faisceau, le compteur mobile détectant alors le deuxième rayonnement $\gamma$ (celui de 5.27 MeV), ou

(b) la corrélation angulaire $W_{\gamma_2}$ en détectant le deuxième rayonnement $\gamma$

de la cascade parallèlement au faisceau, le compteur mobile détectant alors le rayonnement de 3.07 MeV.

Les fonctions $W_H$, $W_{\gamma_1}$ et $W_{\gamma_2}$ peuvent toujours être exprimées sous la forme

$$W(\theta) = 1 + AP_2(\cos\theta) + BP_4(\cos\theta) + \ldots$$

où $\theta$ est l'angle que forment entre elles les directions dans lesquelles sont détectés les deux rayonnements gamma.

## 2. Dispositif expérimental

Pour la réaction en question nous avons effectivement mesuré ces trois corrélations à l'aide d'un spectromètre à coïncidences du type rapide — lent [2]).

La cible de NTa était la même que celle utilisée précédemment [3]).

Le compteur fixe était un photomultiplicateur Dumont 6 364 monté d'un cristal de NaI(Tl) de 4″ × 4″, le compteur mobile un photomultiplicateur RCA 6 342 monté d'un cristal de NaI(Tl) de 2″ × 2″. Les analyseurs d'impulsions des canaux latéraux étaient montés en discriminateurs.

Pour la corrélation angulaire dans un plan perpendiculaire au faisceau, seules passaient dans les deux canaux latéraux les impulsions correspondant à des énergies supérieures à 1.8 MeV. On ne détectait ainsi que la cascade 3.07 MeV—5.27 MeV. Les coïncidences triples déclenchaient un analyseur d'impulsions à vingt canaux branché sur une des dernières dynodes d'un des deux photomultiplicateurs. L'ensemble du spectre supérieur à 1.8 MeV était étalé dans la bande des vingt canaux. On pouvait ainsi enregistrer simultanément les coïncidences pour lesquelles un des deux compteurs comptait seulement les rayonnements $\gamma$ de 5.27 MeV, et celles pour lesquelles il comptait aussi bien les rayonnements $\gamma$ de 5.27 MeV et ceux de 3.07 MeV. Comme prévu, les corrélations dans les deux cas étaient les mêmes.

La corrélation angulaire dans le plan du faisceau a été mesurée en détectant le rayonnement $\gamma_1$ (3.07 MeV) parallèlement au faisceau ($W_{\gamma_1}$) puis le rayonnement $\gamma_2$ (5.27 MeV) parallèlement au faisceau ($W_{\gamma_2}$).

Dans le premier cas le canal 1 (compteur fixe) admettait les impulsions correspondant à une énergie supérieure à 1.8 MeV, et le canal 2 celles correspondant à une énergie supérieure à 3.30 MeV. L'analyseur d'impulsions mesurait alors le spectre soit du rayonnement $\gamma$ de 3.07 MeV quand il était branché sur le canal 1, soit de celui de 5.27 MeV quand il était branché sur le canal 2. Les deux corrélations angulaires ainsi obtenues qui correspondent au rayonnement $\gamma_1$ toujours détecté dans le même canal, doivent être les mêmes. Effectivement nous les avons trouvées égales.

Dans le deuxième cas c'était le canal 2 qui admettait les impulsions correspondant à des énergies supérieures à 1.8 MeV, tandis que le canal 1

discriminait à 3.30 MeV. On enregistrait alors à l'analyseur d'impulsions soit le spectre du rayonnement $\gamma$ de 5.27 MeV soit celui de 3.07 MeV, suivant qu'on était branché sur le canal 1 ou sur le canal 2. Là encore les corrélations angulaires obtenues étaient les mêmes.

## 3. Résultats

La figure 1 montre les points expérimentaux pour les trois corrélations angulaires. Les courbes en plein sont obtenues à partir des points expéri-

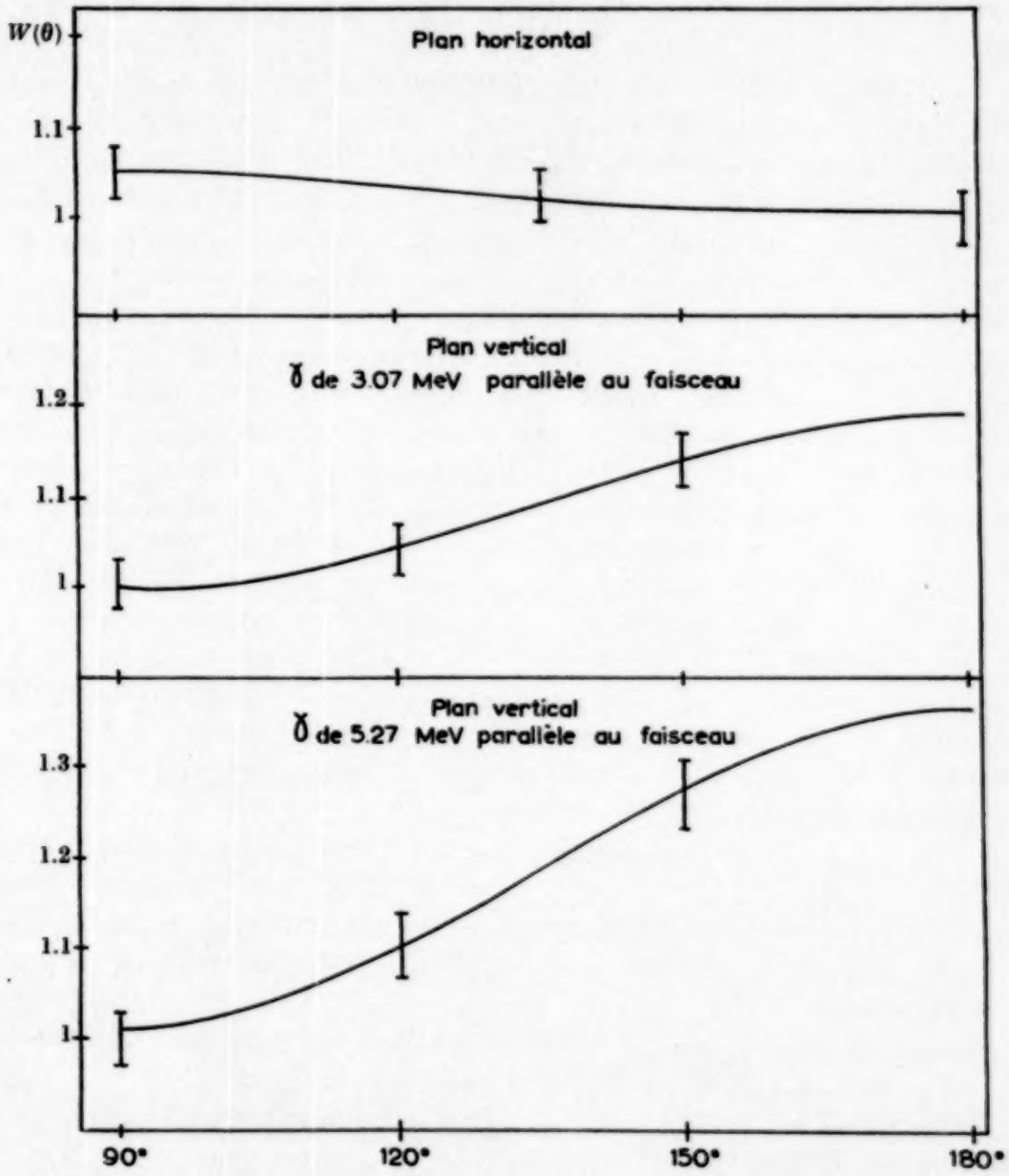


Fig. 1. Réaction $^{14}N(p\gamma)^{15}O$, $E_p$ = 1060 keV.
Corrélation angulaire par le niveau de 5.27 MeV

mentaux par la méthode des moindres carrés. Toutes corrections faites les corrélations angulaires peuvent s'exprimer par

$$W_H = (1\pm0.003)-(0.03\pm0.03)P_2(\cos\theta)-(0.006\pm0.050)P_4(\cos\theta),$$
$$W_{\gamma_1} = (1\pm0.003)+(0.13\pm0.03)P_2(\cos\theta)+(0.015\pm0.066)P_4(\cos\theta),$$
$$W_{\gamma_2} = (1\pm0.003)+(0.23\pm0.04)P_2(\cos\theta)-(0.026\pm0.080)P_4(\cos\theta).$$

On voit que dans les trois cas les termes en $P_4(\cos\theta)$ peuvent être considérés comme nuls.

## 4. Discussion

On connaît le moment angulaire du niveau fondamental de $^{14}$N: $I_1 = 1^+$ et celui du niveau de 8.34 MeV de $^{15}$O: $J_a = 3/2^+$. On admet pour le moment angulaire du niveau fondamental de $^{15}$O la valeur $I_2 = 1/2^-$ (la même que celle du noyau miroir $^{15}$N). Pour le niveau de 5.27 MeV de $^{15}$O Evans *et al.* [4]) ont indiqué $J_b \leqq 7/2^+$. En tenant compte pourtant du travail sur les intensités relatives des rayonnements $\gamma$ émis par ce niveau [1]) on peut réduire la valeur du moment angulaire du niveau de 5.27 MeV à $J_b \leqq 5/2$. Pour les calculs nous nous limitons ainsi aux valeurs $J_b \leqq 5/2$. Tautfest et Rubin [5]) d'une part, Hagedorn *et al.* [6]) d'autre part, indiquent, par l'étude de la diffusion élastique des protons, que le niveau de 8.34 MeV de $^{15}$O est formé par onde s. Dans nos calculs nous ne pouvons pas prendre pour les protons incidents une onde s pure. En effet, nous savons que si $l_p = l'_p = 0$, les trois corrélations angulaires $W_H$, $W_{\gamma_1}$ et $W_{\gamma_2}$ sont identiques. Or nos mesures montrent (fig. 1) que ceci n'est pas le cas. D'autre part, dans une étude antérieure [3]) nous avions mesuré la distribution angulaire du rayonnement $\gamma$ de 8.34 MeV et avons montré qu'elle pouvait être expliquée, entre autre, par une contribution égale ou supérieure à 0.25 % d'onde d à l'onde s prédominante. Nous supposons ainsi que lors de la formation du niveau de 8.34 MeV, intervient un mélange d'ondes s et d pour les protons incidents. On appellera $\varepsilon^2$ le rapport de l'intensité de l'onde d par rapport à celle de l'onde s et on donnera plus de poids aux résultats pour lesquels $\varepsilon$ est petit, pour tenir compte du résultat des auteurs cités ci-dessus[5,6]).

Les calculs ont été faits dans la notation du channel spin; $t$ étant la proportion de "channel spin" $s = \frac{1}{2}$, celle du "channel spin" $s = 3/2$ est alors $(1-t)$.

Nous avons calculé les fonctions de corrélation angulaire $W_H$, $W_{\gamma_1}$ et $W_{\gamma_2}$ correspondant à chacune des valeurs possibles de $J_b$.

Pour $J_b = 3/2^-$, $3/2^+$ et $5/2^-$, ces calculs ont été faits dans le cas le plus général. En tenant compte

1) des résultats obtenus dans la distribution angulaire du rayonnement $\gamma$ de 8.34 MeV de $^{15}$O qui nous donnait une relation entre $t$ et $\varepsilon$,

$$t = \frac{0.05\,\varepsilon^2+\varepsilon+0.05}{-0.5\,\varepsilon^2+\varepsilon+0.05}; \qquad (1)$$

2) des mélanges possibles de multipolarités $L_1$ ou $L_2$ des rayonnements $\gamma_1$ (3.07 MeV) ou $\gamma_2$ (5.27 MeV).
Ainsi pour

$J_b = 3/2^-$: on prendra pour $\gamma_1$ un rayonnement E1 et pour $\gamma_2$ un mélange M1+E2 ($\delta_2$),

$J_b = 3/2^+$: on prendra pour $\gamma_1$ un mélange M1+E2 ($\delta_1$) et pour $\gamma_2$ un rayonnement E1,

$J_b = 5/2^-$: on prendra pour $\gamma_1$ un rayonnement E1 et pour $\gamma_2$ un rayonnement E2.

Ces calculs sont complexes; nous résumons leurs résultats dans le tableau ci-après. La mention „oui" veut dire que le résultat expérimental peut être expliqué par la valeur du moment angulaire $J_b$ présumé, pour certaines valeurs de $\delta$. La mention „non", au contraire, signifie qu'aucun mélange de rayonnements $\gamma$ ne peut expliquer le résultat expérimental, quelle que soit la valeur de $\varepsilon$ satisfaisant à la relation (1) entre $t$ et $\varepsilon$.

Pour $J_b = \frac{1}{2}$ il n'est pas nécessaire de faire des calculs. On sait en effet que dans ce cas la corrélation angulaire est isotrope dans n'importe quel plan, quelles que soient les valeurs de $t$, $\varepsilon$ et $\delta$.

| $J_b$ | $W_\pi$ | $W_{\gamma_1}$ | $W_{\gamma_2}$ |
|---|---|---|---|
| $1/2^-$ | oui | non | non |
| $1/2^+$ | oui | non | non |
| $3/2^-$ | oui | oui | oui |
| $3/2^+$ | oui | oui | oui |
| $5/2^-$ | non | oui | non |

On voit que seulement dans le cas $J_b = 3/2$, les trois corrélations angulaires mesurées peuvent être expliquées. Pour chacune d'elles les calculs donnent une relation entre $\delta_1$ ($\delta_2$), $t$ et $\varepsilon$. A chaque couple de valeurs de $t$ et $\varepsilon$ donné par la relation (1) correspond une valeur de $\delta_1$ ($\delta_2$). Pour $\varepsilon = -0.2$, par exemple, c'est à dire pour une contribution de 4 % d'onde d à l'onde s prédominante, on trouve:

| | $J = 3/2^+$ | $J = 3/2^-$ |
|---|---|---|
| pour $W_H$, | $\delta_1 = +0.23 \pm 0.10$, | $\delta_2 = -0.25 \pm 0.10$ |
| pour $W_{\gamma_1}$, | $\delta_1 = +0.47 \pm 0.10$, | $\delta_2 = -0.44 \pm 0.10$ |
| pour $W_{\gamma_2}$, | $\delta_1 = +1.14 \pm 0.10$, | $\delta_2 = -0.65 \pm 0.10$. |

L'accord entre les valeurs de $\delta$ n'est pas parfait. (A noter pourtant que théoriquement $\delta$ peut varier entre $-\infty$ et $+\infty$.)

Pour la valeur $J_b = 5/2^+$ le rayonnement $\gamma_1$ peut être un mélange M1+E2 ($\delta_1$) et le rayonnement $\gamma_2$ un mélange M2+E3 ($\delta_2$). La corrélation angulaire devient ainsi fonction, dans le cas le plus général, des quatres paramètres $t$, $\varepsilon$, $\delta_1$ et $\delta_2$. Les calculs n'ont pas pu être faits d'une façon générale. Nous nous sommes limités au cas où le rayonnement $\gamma_2$ (5.27 MeV) est pur ($\delta_2 = 0$) et avons calculé les corrélations angulaires théoriques pour plusieurs valeurs de $\varepsilon$, en fonction du coefficient de mélange $\delta_1$ pour le rayonnement $\gamma_1$. Ainsi, pour une valeur de $\varepsilon = -0.05$, par exemple, toute valeur de $\delta_1$ comprise entre $-0.03$ et $-0.1$ conduit, pour le plan horizontal, à une fonction de corrélation quasi isotrope. Dans le plan vertical par contre, aussi bien pour $W_{\gamma_1}$ que pour $W_{\gamma_2}$, le coefficient $A_4$ de $P_4(\cos\theta)$ reste très grand pour la valeur de $\delta_1$ qui donne un coefficient $A_2$ de $P_2(\cos\theta)$ égal respectivement à 0.13 et 0.23. Or expérimentalement on trouve que $A_4$ est nul ou très faible. La valeur $J_b = 5/2^+$ ne convient donc pas pour les cas envisagés ci-dessus, mais, à priori, nous ne pouvons éliminer cette valeur.

## 5. Conclusion

Nous avons vu qu'il n'existait pas un accord parfait entre les résultats expérimentaux et théoriques des corrélations angulaires. En plus de la valeur $5/2^+$ que nous ne pouvons éliminer, la valeur $J_b = 3/2^-$ pour le moment angulaire du niveau de 5.27 MeV pourrait expliquer le mieux les trois corrélations angulaires trouvées. Dans ce dernier cas, le rayonnement $\gamma$ de 3.07 MeV serait E1 et celui de 5.27 MeV un mélange de M1 et E2. Il faut également supposer que le moment orbital des protons soit $l_p = 0$, $l'_p = 2$. La figure 2 montre le schéma des niveaux de $^{15}O$ qui nous intéressent dans ce travail (à gauche les valeurs des moments angulaires proposées par Evans *et al.*). La valeur $J_b = 3/2^-$, qui concorde le mieux avec nos résultats expérimentaux, expliquerait aussi le mieux les intensités relatives trouvées par Li [1]), qui indique des rayonnements gamma intenses de 8.34, 5.27 et 3.07 MeV et des rayonnements gamma de faible intensité de 6.82 et 1.50 MeV.

Signalons aussi un travail de Halbert et French [7]) qui calculent les moments angulaires des niveaux excités de $^{15}N$ (miroir de $^{15}O$) en supposant que leur parité soit paire. Ils indiquent ainsi les valeurs 5/2 et $\frac{1}{2}$ pour les

moments angulaires des niveaux respectivement de 5.28 MeV et 5.31 MeV. Ils indiquent également que Butler suggère un grand moment angulaire pour le niveau de 5.31 MeV, alors que Lane pense que ce moment angulaire est $\frac{1}{2}^+$. Dans un travail plus ancien Stanley [8]) étudie la corrélation angulaire p—$\gamma$ dans la réaction $^{14}$N (d, p) $^{15}$N pour l'ensemble des deux

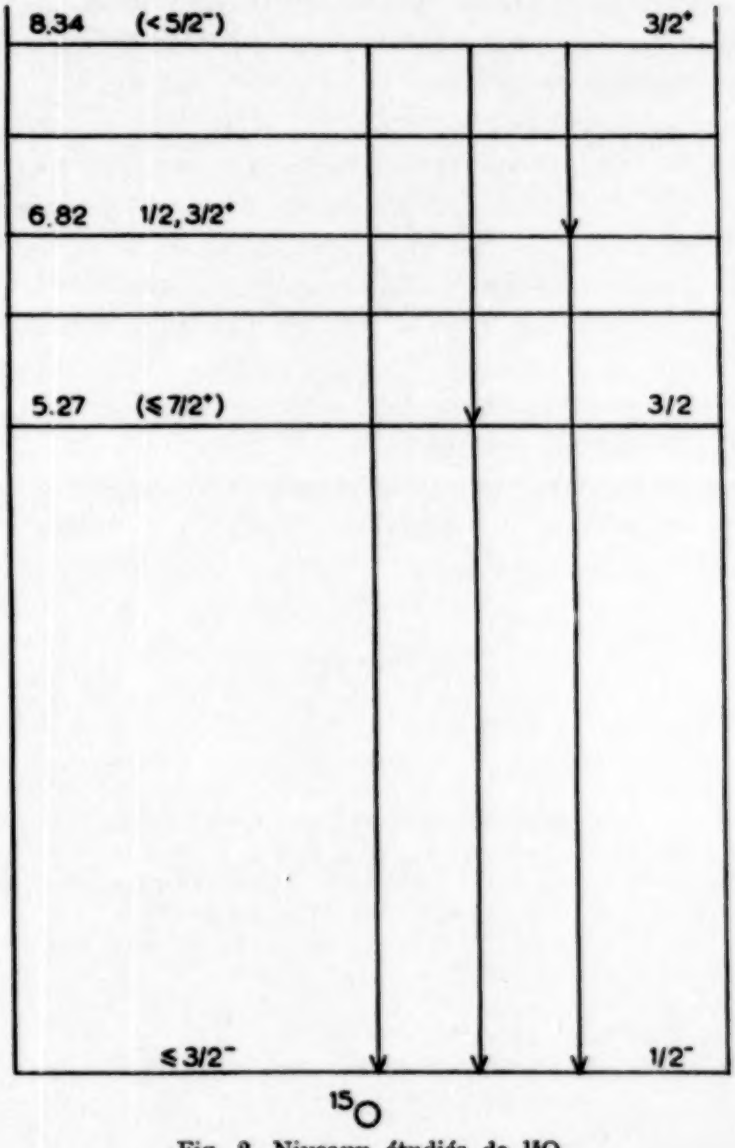


Fig. 2. Niveaux étudiés de $^{15}$O.

niveaux et indique $J_b = \frac{1}{2}$ ou 3/2 pour le moment angulaire des niveaux à 5.3 MeV.

J. P. Elliott et B. H. Flowers [9]) annoncent des calculs des spins et parités des niveaux de $^{15}$O et $^{15}$N.

Toutes ces discussions ont été faites en supposant que le niveau de 5.27 MeV de $^{15}$O est simple. Or le noyau miroir $^{15}$N présente dans cette région d'énergie deux niveaux séparés de 30 keV [10]). On peut ainsi admettre

que dans $^{15}O$ il y a également deux niveaux rapprochés vers 5.27 MeV et que par conséquent nous avons mesuré la somme de deux corrélations angulaires. Dans ces conditions plusieurs cas sont possibles:

(1) Les deux niveaux ont des parités différentes. La cascade passant par le niveau pair est alors défavorisée par rapport à celle passant par le niveau impair. On est ramené au cas d'un seul niveau.

(2) Les deux niveaux ont le même moment angulaire et la même parité. Toute la discussion reste valable.

(3) Les deux niveaux ont la même parité: un des niveaux a un moment angulaire $\frac{1}{2}$. Les corrélations angulaires proviennent de l'autre niveau qui est forcément différent de $\frac{1}{2}$. Les effets angulaires mesurés sont atténués.

(4) Les deux niveaux ont la même parité, mais des moments angulaires différents. Il est alors difficile, sinon impossible, d'analyser les corrélations angulaires trouvées, surtout si on ne connaît pas les intensités relatives des deux cascades.

L'accord plus ou moins bon des résultats expérimentaux peut alors provenir de la présence du doublet.

On voit que les valeurs attribuées aux moments angulaires des niveaux à 5.3 MeV de $^{15}N$ ne sont pas concordantes et que d'autres études sur ce noyau s'imposent, ainsi que sur $^{15}O$.

## Bibliographie

1) C. W. Li, Phys. Rev. **92** (1953) 1084 A
2) S. Gorodetzky, A. Gallmann, M. Croissiaux et R. Armbruster, C.R. Acad. Sciences **244** (1957) 62
3) S. Gorodetzky, A. Gallmann, M. Croissiaux et R. Armbruster, C.R. Acad. Sciences **244** (1957) 1759; Nuclear Physics **4** (1957) 112
4) W. H. Evans, T. S. Green and R. Middleton, Proc. Phys. Soc. A **66** (1953) 108
5) G. W. Tautfest and S. Rubin, Phys. Rev. **103** (1956) 196
6) F. B. Hagedorn, F. S. Mozer, T. S. Webb, W. A. Fowler and C. C. Lauritsen, Phys. Rev. **105** (1957) 219
7) E. C. Halbert and J. B. French, Phys. Rev. **105** (1957) 1563
8) A. G. Stanley, Phil. Mag. **45** (1954) 807
9) J. P. Elliott and G. W. Flowers, Proc. Roy. Soc. A **242** (1957) 57
10) R. Malm and W. W. Buechner, Phys. Rev. **80** (1950) 771

*Nuclear Physics* **6** (1958) 525—530; © *North-Holland Publishing Co., Amsterdam*
Not to be reproduced by photoprint or microfilm without written permission from the publisher

# UNIFIED NUCLEAR MODEL AND DIRECT NUCLEAR PHOTOEFFECT

## I. WEAK COUPLING EFFECTS

J. SAWICKI
*Palmer Physical Laboratory, Princeton University*†

Received 5 February 1958

**Abstract:** A contribution to the direct E1 nuclear photoeffect coming from the indirect interaction via the electric quadrupole moment of the core is discussed. The oscillating core absorbs the incoming $\gamma$-ray and emits a surfon which is subsequently reabsorbed with the emission of the proton. The interference term between this two-stage mechanism contribution and the usual E1-amplitude in the angular distribution is estimated in two particular cases to amount to a large fraction of the usual E1 term.

### 1. Introduction

It is well-known (compare e.g. ref. [1])) that for a number of nuclei of $A \approx 100$ the relative cross sections for ($\gamma$, p) and ($\gamma$, n) reactions are 20—1000 times larger than predicted by the statistical theory. Similar effects were observed also in the region of $A \approx 25$ (in particular for Mg and Si isotopes: see ref. [2]). The angular distributions of fast protons from ($\gamma$, p) reactions have been found to deviate from spherical symmetry in contradiction to the prediction of the statistical theory [3, 4]). Courant [5]) proposed that the direct photonuclear effect, in which the photon interacts directly with one of the nuclear protons should give an important contribution in addition to the compound nucleus mechanism. Katz *et al.* [2]) pointed out that the process proposed by Courant may play a dominant role in photonuclear reactions on Mg and Si isotopes and that its assumption is not necessarily contradictory to any previous experimental results.

Akhiezer and Sitenko point out in a recent paper [6]) the existence of a contribution to the Courant process due to the interaction of the quadrupole moment of a non-spherical deformed nucleus with the electromagnetic radiation. Their mechanism is essentially a two-stage process: the $\gamma$-ray interacts with the surface oscillations of the nucleus; a proton bound to the residual nucleus interacts with the oscillating core and is emitted. These authors estimated the ratio of the total cross section for this process

† This work was supported by the U. S. Atomic Energy Commission and the Higgins Scientific Trust Fund.

to the cross section for the direct electric dipole photoeffect to be $\sigma^q/\sigma^d \approx 0.1-00.5$ for $A \approx 100$, a surfon energy $\hbar\omega_s \approx 2-3$ MeV and an incident proton energy $\hbar\omega = 17.5$ MeV.

The aim of the present note is a more complete derivation of the two-stage processes of the described type and the indication of their possible importance for the angular distribution of the photoprotons.

The complete interaction Hamiltonian between a nucleon and the $\gamma$-ray has the form

$$H' = H'_{\mathrm{elm}}(p)+\Delta H' \tag{1}$$

where

$$H'_{\mathrm{elm}}(p) = e'\,\mathbf{e}\cdot\mathbf{r}+\Delta(\mathrm{M1})+\Delta(\mathrm{E2})+\ldots \tag{2}$$

with $e' = e[1-(Z/A)]$ for protons, $e' = -eZ/A$ for neutrons; $\mathbf{e}$ being the photon polarization unit vector. The magnetic dipole and the electric quadrupole terms $\Delta(\mathrm{M1})$, $\Delta(\mathrm{E2})$ are well-known (see e.g. ref. [7])) to give only rather small contributions at non-relativistic energies. The term $\Delta H'$ may be written

$$\Delta H' = \hat{Q}+H_{\mathrm{int}} \tag{3}$$

with

$$\hat{Q} = -\frac{i\omega}{6c}\,e\sum_{i,j} Q_{ij}\,\mathbf{e}_i\cdot\boldsymbol{\varkappa}_j, \tag{4}$$

where $(\omega/c)\boldsymbol{\varkappa} = \mathbf{k}_0$ is the momentum of the photon; $\hat{Q}$ represents the inter-

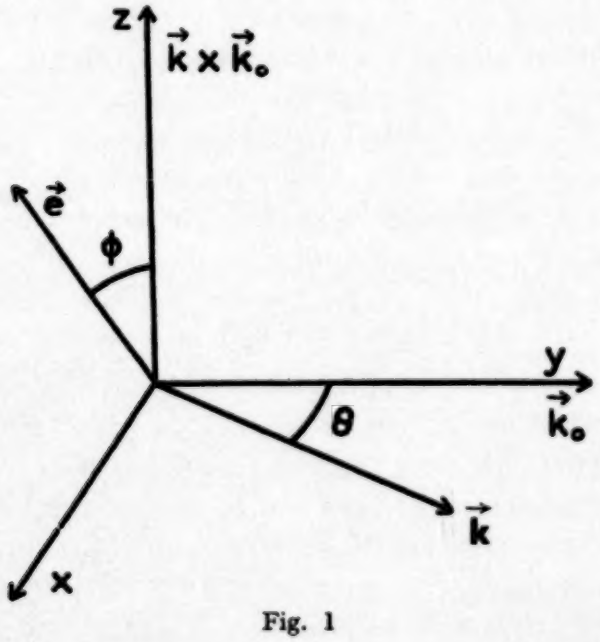


Fig. 1

action between the $\gamma$-ray and the quadrupole moment of the nucleus $eQ_{ij} = \int \rho_0(3x_i x_j - r^2\delta_{ij})\mathrm{d}v$; the charge density $\rho_0$ corresponds to the uniform distribution over the deformed core. A convenient space-fixed

frame of reference for calculating angular distributions and polarizations is that of ref. [8]) with the quantization axis $Oz$ parallel to $\mathbf{k}\times\mathbf{k}_0$, $\mathbf{k}$ being the momentum of the outgoing photoproton, and $Oy$ parallel to $\mathbf{k}_0$, as shown in fig. 1. In this frame,

$$e'\,\mathbf{e}\cdot\mathbf{r} = e'(z\cos\phi + x\sin\phi), \tag{5a}$$

$$\hat{Q} = -\frac{i\omega}{6c}e(Q_{zy}\cos\phi + Q_{xy}\sin\phi), \tag{5b}$$

$\phi$ being the angle between the directions of $\mathbf{e}$ and $\mathbf{k}\times\mathbf{k}_0$. One can easily express (5b) in terms of the surfon creation and annihilation operators using Kerman's method [9]). This gives

$$\hat{Q} = \frac{\omega}{c}\frac{Zer_0^2}{4\sqrt{5\pi}}\sqrt{\frac{3}{2}}\,e_2[(b_1 - b_1^+ - b_{-1}^+ + b_{-1})\cos\phi + (b_2^+ + b_{-2} - b_2 - b_{-2}^+)\sin\phi] \tag{6}$$

where

$$e_2 = \sqrt{\frac{4\pi}{3A}\frac{\hbar}{Mr_0^2\omega_2}}$$

and $b_\mu$ is an annihilation operator corresponding to the surfon angular momentum projection $\mu$ along the quantization axis $\mathbf{k}\times\mathbf{k}_0$; $r_0$ is the nuclear radius. The particle-surface interaction is

$$H_{\text{int}} = -r_0 V_0\,\delta(r - r_0)\sum e_2\{(-1)^\mu b_{-\mu}Y_{2\mu}(\omega) + \text{c.c.}\} \tag{7}$$

where $V_0$ is the depth of the nuclear well.

One can apply the Dirac perturbation theory to the full $H'$ by the method of Bethe [10]): $\Delta H'$ contributes only in the second and higher orders. The asymptotic form of the wave function of the total system can be rewritten as

$$\Psi \sim r^{-1}\,e^{ikr - iE_f t/\hbar}\left\{\langle E_1 + \hbar\omega|H'_{\text{elm}}(p)|E_f\rangle - \left(\sum_{E'} + \int dE'\right)\frac{\langle E_1+\hbar\omega|\Delta H'|E'\rangle\langle E'|\Delta H'|E_f\rangle}{E' - E_1 - \hbar\omega}|E_f\rangle\right\}\delta(E_f - E_1 - \hbar\omega), \tag{8}$$

where $\langle E_A|O|E_B\rangle$ stands for the matrix element of the operator $O$ for the transition between the states of the total energy $E_A$ and $E_B$ of the system.

Using all the involved orthogonality properties we may rewrite the complete reaction amplitude in the form

$$\begin{aligned} f(0) \propto \{&\langle E_1+\hbar\omega|H'_{\text{elm}}(p)|E_f\rangle - \hbar^{-1}(\omega_2-\omega)^{-1}\langle E_1+\hbar\omega|\hat{Q}|E_1+\hbar\omega_2\rangle \\ &\times\langle E_1+\hbar\omega_2|H_{\text{int}}|E_f\rangle - \hbar^{-1}(\omega_2+\omega)^{-1}\langle E_1+\hbar\omega|H_{\text{int}}|E_f+\hbar\omega+\hbar\omega_2\rangle \\ &\times\langle E_f+\hbar\omega+\hbar\omega_2|\hat{Q}|E_f\rangle\}\,|E_f\rangle_\infty\,\delta(E_f - E_1 - \hbar\omega), \end{aligned} \tag{9}$$

where $|E_f\rangle_\infty$ stands for the coefficient of $r^{-1}\,e^{(ikr-iE_ft/\hbar}$ in the asymptotic form of the state vector $|E_f\rangle$.

Akhiezer and Sitenko [6]), by a different method, only obtained a term equivalent to our last term in addition to the usual first one. However, the second term $\propto \hbar^{-1}(\omega_2-\omega)^{-1}$ produces an even larger contribution. This corresponds to first absorbing the photon by the core with emission of a virtual surfon, which is subsequently reabsorbed with emission of the proton.

For the sake of simplicity let us neglect the spin-orbit coupling. In this case we can expand the reaction amplitude corresponding to an initial state orbital $(l,\ m_l)$ in the explicit form

$$f_{lm_l}(\theta) \propto \sum_{LM_L} i^{-L} e^{i\delta_L} Y_{LM_L}(\Omega_k) \{\langle lm_l;\ (0)00|e'\,\mathbf{e}\cdot\mathbf{r}|LM_L;\ (0)\ 00\rangle$$
$$- \sum_{l'm'_l\nu} \left\{ \frac{\langle lm_l;\ (0)\ 00|\hat{Q}|l'm'_l;\ (1)\ 2\nu\rangle\langle l'm'_l;\ (1)\ 2\nu|H_{\text{int}}|LM_L;\ (0)\ 00\rangle}{\hbar(\omega_2-\omega)} \right. \tag{10}$$
$$\left. + \frac{\langle lm_l;\ (0)\ 00|H_{\text{int}}|l'm'_l;\ (1)\ 2\nu\rangle\langle l'm'_l;\ (1)\ 2\nu|\hat{Q}|LM_L;\ (0)\ 00\rangle}{\hbar(\omega_2+\omega)} \right\}.$$

The $\delta_L$'s are the elastic nuclear phase shifts of the proton interacting with the core; the quantum numbers of the form $(N)Rm_R$ following $lm_l(l'm'_l)$ in the symbols of the state vectors denote the number of surfons, their angular momentum and projection. The final result takes the following form:

$$f_{lm_l}(\theta) \propto \sum_{LM_L} i^{-L} e^{i\delta_L} Y_{LM_L}(\Omega_k) e' \left[\cos\phi\cdot z_{lm_l}^{LM_L} + \sin\phi\cdot x_{lm_l}^{LM_L}\right]$$
$$+ \sum_L i^{-L} e^{i\delta_L} \frac{2\omega_2}{\hbar(\omega^2-\omega_2{}^2)} (-\bar{V}_0 r_0{}^3 R_l(r_0) R_{\lambda f}(r_0) e_2{}^2)(L2;\ 00|l0)$$
$$\times \frac{\omega}{c}\,\frac{Zer_0{}^2}{4\sqrt{5\pi}} \sqrt{\frac{3}{2}} \sqrt{\frac{5(2L+1)}{4\pi(2l+1)}} \{-\cos\phi[(L2;\ m_l-1,\ 1|lm_l) Y_{L,m_l-1}(\Omega_k) \tag{11}$$
$$+ (L2;\ m_l+1,\ -1|lm_l) Y_{L,m_l+1}(\Omega_k) + \sin\phi (L2;\ m_l-2,\ 2|lm_l) Y_{L,m_l-2}(\Omega_k)$$
$$- (L2;\ m_l+2,\ -2|lm_l) Y_{L,m_l+2}(\Omega_k),$$

where the $R_{\lambda f}(r)$'s are the proton radial wave functions and $(L2;\ M_L\mu|lm_l)$ denotes a vector addition coefficient. The first sum refers to the usual Courant theory, while the term proportional to $2\omega_2/\hbar(\omega^2-\omega_2{}^2)$ is the collective motion contribution.

For the simple example of photoejection of 3s-state nuclear protons, the complete angular distribution takes the form

$$\sigma(\theta) \propto \sin^2\theta\ (\alpha+2\beta\cos\theta+\gamma\cos^2\theta) \tag{12}$$

where $\alpha = e'^2|(0|r|1)|^2$, $(0|r|L)$ denoting the E1 radial integral, and

$$\beta = \frac{3}{4\pi} Zee' r_0^5 e_2^2 \frac{\omega}{c} \frac{\omega_2}{\hbar(\omega^2-\omega_2^2)} \bar{V}_0 R_0(r_0) R_{2f}(r_0) (0|r|1) \cos(\delta_1-\delta_2), \quad (12a)$$

$$\gamma = \left(\frac{3}{4\pi}\right)^2 Z^2 e^2 r_0^{10} e_2^4 \left(\frac{\omega}{c}\right)^2 \frac{\omega_2^2}{\hbar^2(\omega^2-\omega_2^2)^2} \bar{V}_0^2 R_0^2(r_0) R_{2f}^2(r_0). \quad (12b)$$

The term $\propto \alpha$ corresponds to Courant's theory, the term $\propto 2\beta$ is the interference term and that $\propto \gamma$ is the quadratic term of the surface interaction amplitude. In general, if a spin-orbit coupling is included, producing a splitting of the final states ($p_{\frac{1}{2}}$ and $p_{3/2}$), we have in $\sigma(\theta)$ an isotropic term in addition, as given by eq. (11) of ref. [8]). The Coulomb barrier penetration factor for protons is assumed to be common to all the terms $\sigma(\theta)$, and as such unessential.

The validity of the perturbation expansion requires that $\hbar\omega_2 \gg (\hbar_2/AMr_0^2)$. A numerical estimate was made for $A = 150$, $Z = 65$, $r_0 = 1.45\, A^{1/3} \times 10^{-13}$ cm, $\hbar\omega_2 = 2.5$ MeV, $\hbar\omega = 17.5$ MeV and a binding energy of 8 MeV. The ratio of the interference term, proportional to $2\beta$, to the usual direct terms $\propto \alpha$ is $2\beta/\alpha \approx -0.35 \cos(\delta_1-\delta_2)$ and the ratio $\gamma/\alpha \approx 0.03$. If the surface effects described here are really present, they would show up in this particular case as a drop of $\sigma(\theta)$ at small angles and an increase of $\sigma(\theta)$ at large angles due to the interference effect †.

The case $l = 1$ is much more complicated. In this case the differential cross section has the following form:

$$\sigma(\theta) \propto a + b \sin^2\theta + A \cos\theta\, (C_1 + C_2 \cos^2\theta - 3C_2 \sin^2\theta), \quad (13)$$

where the small quadratic terms of the pure collective contributions are omitted. The term $a + b \sin^2\theta$ refers to the usual Courant theory, the remaining terms are the interference effect. On setting $\delta_L = 0$ the coefficients take on the form

$$a = e'^2 \tfrac{2}{9} [(1|r|0)^2 + (1|r|2)^2 + 2(1|r|0)(1|r|2)], \quad (13a)$$

$$b = e'^2 \tfrac{1}{3} [(1|r|2)^2 - 2(1|r|0)(1|r|2)], \quad (13b)$$

$$A = -\frac{1}{48\pi} \sqrt{\tfrac{3}{10}}\, Zee' r_0^5 e_2^2 \frac{\omega}{c} \frac{\omega_2}{\hbar(\omega^2-\omega_2^2)} \bar{V}_0 R_1(r_0), \quad (13c)$$

$$C_1 = -8\sqrt{\tfrac{6}{5}}\,(1|r|0) R_{1f}(r_0) + 9\sqrt{\tfrac{3}{10}}\,(1|r|0) R_{3f}(r_0) - 2\sqrt{\tfrac{6}{5}}(1|r|2) R_{1f}(r_0) + 18\sqrt{\tfrac{6}{5}}\,(1|r|2) R_{3f}(r_0), \quad (13d)$$

$$C_2 = 3\sqrt{\tfrac{15}{2}}\,(1|r|0) R_{3f}(r_0) + \tfrac{3}{2}\sqrt{\tfrac{15}{2}}\,(1|r|2)\, R_{3f}(r_0) - 6\sqrt{\tfrac{6}{5}}(1|r|2) R_{1f}(r_0) - \tfrac{9}{2}\sqrt{\tfrac{3}{10}}\,(1|r|2) R_{3f}(r_0). \quad (13e)$$

† *Note added in proof:* It should be noted that in general the interference term between the E1 and the direct E2 transition for protons has just the opposite sign to that of $\beta$. This term could thus act destructively on the $2\beta$-term. The author is indebted to Dr. J. S. Blair for this comment.

For the physical conditions described in the case $l = 0$ the order of magnitude of $C_1 A/a$, $C_2 A/a$, $C_1 A/b$, $C_2 A/b$ is the same as that of $2\beta/\alpha$ for $l = 0$. The interference term $\propto A$ is important at small angles, where it contributes appreciably to the usual "isotropic" term $a$.

The author feels greatly indebted to Dr. Carl A. Levinson for several illuminating discussions of this problem and to Dr. Sitenko for supplying him with a reprint of his paper.

## References

1) O. Hirzel and H. Waeffler, Helv. Phys. Acta **20** (1947) 373
2) L. Katz *et al.*, Can. Journ. Phys. **32** (1954) 580
3) N. Curtis *et al.*, Phys. Rev. **77** (1950) 290
4) B. Diven and G. Almy, Phys. Rev. **80** (1950) 407
5) E. Courant, Phys. Rev. **82** (1951) 703
6) A. I. Akhiezer and A. G. Sitenko, Kharkov University Reports **6** (1955)
7) D. H. Wilkinson, Proc. Int. Conf. Nucl. Reactions, Amsterdam (July 2—7, 1956) p. 103
8) W. Czyż and J. Sawicki, Nuovo Cimento **3** (1956) 864
9) A. Kerman, Phys. Rev. **92** (1953) 1176
10) H. A. Bethe, Ann. d. Phys. **4** (1930) 443

*Nuclear Physics* **5** (1958) 531—538; © *North-Holland Publishing Co., Amsterdam*
Not to be reproduced by photoprint or microfilm without written permission from the publisher

# A TENTATIVE UNIFIED CLASSIFICATION OF ELEMENTARY PARTICLES, INCLUDING LEPTONS

V. I. GOLDANSKI
*P.N. Lebedev Physical Institute of the USSR Academy of Sciences, Moscow*

Received 11 November 1957

**Abstract:** A unified classification of all families of elementary particles, that is, of baryons, Bose mesons and light fermions (leptons: $\mu$, e, $\nu$) is proposed.

The classification is based on extension of the isobaric multiplet principle to leptons. One of the corollaries of the scheme is that the six leptons known at present are the only ones that may exist. In weak interactions leading to the production of leptons the change of the 3-projection of the isobaric spin is $\Delta T_3 = 0, \pm\frac{1}{2}$. When viewed from this angle the values of the $\Delta T_3$ in various ways of hyperon $\beta$-decay indicate that many different modes of decay are possible, excepting a few cases that are specially mentioned.

The selection rules for $T_3$ are not sufficient to explain the absence of weak interactions involving formation of various electrically neutral lepton pairs. The absence of such interactions can be explained by introducing for leptons a certain number $N = Q - \frac{1}{2}m$ ($Q$ = electric charge, $m$ = neutrino charge) and postulating the selection rule $\Delta N = \pm 1$ for weak interactions involving lepton production.

## 1. The Proposed Scheme

The experimental data on hyperon and K-meson production and decay obtained during the last few years have considerably extended the region of applicability on the isobaric spin concept and underly the isobaric multiplet classification proposed by Gell-Mann [1]) and Nishijima [2]) and discussed in detail in ref. [3]). However, this classification does not apply to light spin-$\frac{1}{2}$ fermions (leptons), that is to $\mu$-mesons, electrons and neutrinos.

A tentative unified classification of all elementary particles is proposed in the present paper which is based on an extension of the isobaric multiplet principle to leptons.

As is well known, besides leptons there are three other classes of fundamental particles, namely, heavy fermions, baryons and antibaryons, and Bose mesons. Each of these classes is characterized by a definite value of the nuclear charge [4]) $n$, which is defined for any system as the difference between the numbers of baryons and antibaryons it contains. One has $n = +1$ for baryons, $n = -1$ for antibaryons and $n = 0$ for Bose mesons (as well as leptons).

We shall assume that the electric charge of a fundamental particle can

## Table of Elementary Particles (Including Leptons)

### I. Baryons (Fermions)

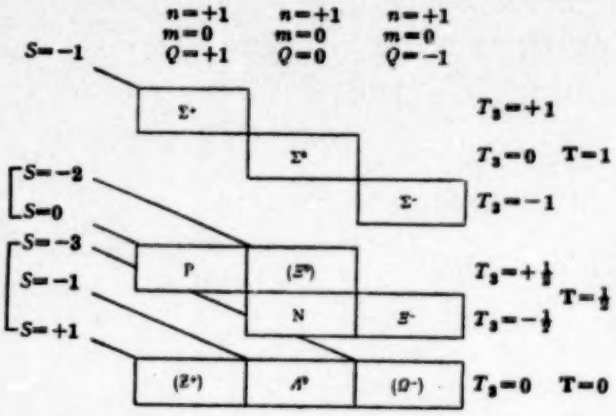


### II. Antibaryons (Fermions)

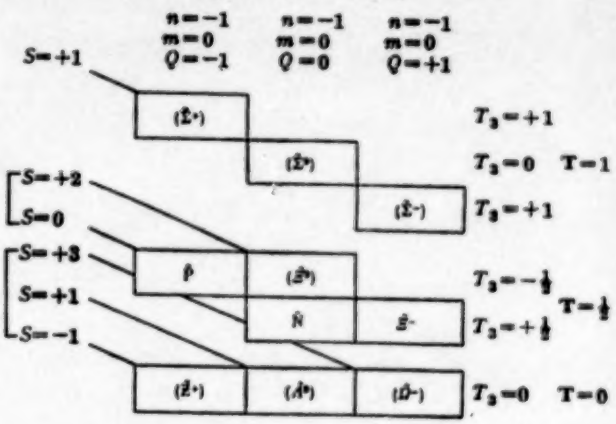


### III. Mesons and Antimesons (Bosons)

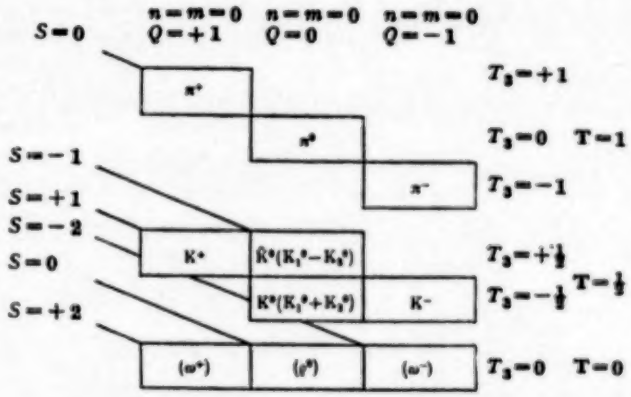


### IV. Leptons and Antileptons (Fermions)

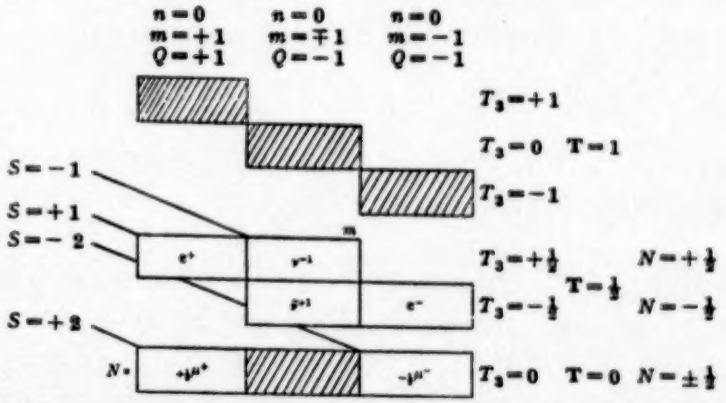


Symbols: $Q$ — electric charge, $n$ — nuclear charge, $T$ — isobaric spin, $S$ — strangeness $S = 2\,(Q - T_3 - \frac{1}{2}n)$, $m$ — neutrino charge, $N = Q - \frac{1}{2}m$ (for leptons).

have only three values $Q = 1, 0, -1$, or, in other words, that doubly or multiply charged fundamental particles do not exist. From the isobaric multiplet scheme it then follows that the isobaric spin can also assume only three values $T = 1, \frac{1}{2}, 0$. We shall further suppose that in each given class of elementary particles (that is, for a given $n$) there cannot be two or more particles with identical values of $Q$, $T$ and $T_3$ (3-projection of the isobaric spin). Evidently in this case there cannot be more than one isobaric triplet ($T = 1$; $T_3 = +1, 0, -1$) in a given elementary particle class, not more than two isobaric doublets ($T = \frac{1}{2}$, $T_3 = +\frac{1}{2}, -\frac{1}{2}$) and not more than three isobaric singlets ($T = 0$, $T_3 = 0$). Altogether therefore there cannot be more than 10 types of particles. The elementary particles (baryons, antibaryons and Bose mesons) which are permissible from this viewpoint are enumerated in table 1. Particles with equal values of $Q$ are arranged in vertical columns and particles with equal values of $T$ and $T_3$ in horizontal rows.

Symbols of hitherto undetected particles are enclosed between brackets in the table. Besides all possible types of antibaryons (excluding antinucleons), the three baryons $\Xi^0$, $Z^+$, $\Omega^-$ and three Bose mesons $\varrho^0$, $\omega^+$, $\omega^-$ predicted by Gell-Mann also await detection †. The diagonal lines in the table unite particles with equal values of the new quantum number $S$ (strangeness) introduced by Gell-Mann, which by definition is $S = 2(Q - T_3 - \frac{1}{2}n)$. If the table is constructed in the manner chosen here, the introduction of strangeness does not seem to make the classification easier for visualization. Moreover, as far as the selection rules are concerned, it may be recalled that consideration of $\frac{1}{2}\Delta S$ is equivalent to consideration of $-\Delta T_3$.

It should be noted that our elementary particle scheme (like most of such schemes) is of course completely symmetrical with respect to particles and antiparticles. Heavy fermions and their antiparticles differ with respect to the signs of their nuclear and electric charges and of the 3-projection of their isobaric spins. For mesons and antimesons $n = 0$ and therefore in this case the only difference between particles and antiparticles is that the signs of $Q$ and $T_3$ are opposite.

## 2. Classification of Leptons

Consider now the classification of leptons. Various ways of classifying these particles have repeatedly been discussed, the use of isobaric spins as well as introduction of new parameters having been suggested [5–8]). In

† The postulate that multiply charged elementary particles do not exist (i.e., are unstable) does not at all imply that all ten possible particles ($Q = 0, \pm 1$) in each of the three classes are stable, i.e., exist for a prolonged time on a nuclear scale. It is not excluded that some of them (e.g. $Z^+$, $\Omega^-$, $\omega^+$, $\omega^-$) may decay without change of strangeness into lighter particles and hence are unstable.

distinction to previous proposals we shall endeavour to attain complete similarity between the lepton classification and that of other elementary particles presented in table 1. Although the lepton nuclear charge is zero, a neutrino (or lepton) charge [9, 10]) $m$ can be assigned to these particles, $m$ being defined for any system as the difference between the numbers of leptons and antileptons contained in it.

One way of setting up a lepton classification would be to postulate the existence of two lepton-antilepton groups ($m = +1$ and $m = -1$) in analogy with the case of baryons and antibaryons. It is necessary to assume in this case that $\mu^+$, $\nu$ and $e^-$ (as well as $\mu^-$, $\tilde{\nu}$ and $e^+$) are triplets similar to $\Sigma$ and anti-$\Sigma$ particles. Fourteen vacancies in the scheme will then await occupation by future leptons and antileptons (two doublets and three singlets for $m = +1$ and for $m = -1$). This scheme, however, does not appear to be satisfactory, as the components of the $\mu\nu e$ triplets differ too strongly in respect of mass and lifetime. From this viewpoint inclusion of $\mu$-mesons in the same group as that containing electrons and neutrinos seems to be too artificial. It should furthermore be noted that the neutrino charges of $\mu^+$ and positon should apparently be assumed to be the same as those of $\mu^-$ and negaton rather than opposite to them.Thus, for example, according to the two-component neutrino theory [11–13]) the Michel parameter for $\mu$—e-decay should be 0.75 in the $\mu \rightarrow e+\nu+\tilde{\nu}$ decay (identical signs of $m$ for $\mu^\pm$ and $e^\pm$) and zero in the $\mu \rightarrow e+2\nu$ decay (opposite signs of $m$ for $\mu^\pm$ and $e^\pm$). Experiments [14]) yield the value $0.72 \pm 0.04$.

The foregoing remarks remain as an objection against a classification in which $\mu^+$, $\nu$ and $e^-$ (and, respectively, $\mu^-$, $\tilde{\nu}$ and $e^+$) are arranged in three singlets just as $Z^+$, $\Lambda^0$ and $\Omega^-$ and their antiparticles.

If one drops the idea of classifying leptons in analogy with heavy fermions and attempts to arrange them on the basis of an analogy with Bose mesons, the only possibility which arises is that presented in table 1. In order to explain this scheme it should be noted that a particle with $m = 0$ and also $n = 0$ is a Bose particle. Thus in the light fermion (lepton) class $m$ can assume only two values, $m = +1, -1$. This, however, implies that in the lepton classification under consideration the isobaric triplet ($T = 1$, $T_3 = +1, 0, -1$) and one (electrically neutral) isobaric singlet ($T = 0$, $T_3 = 0$) should drop out, since by assigning a definite sign of $m$ to the middle member of the triplet or middle member of the singlet we would violate the symmetry between particles and anti-particles. This type of symmetry is not violated only if two electrically neutral particles are present in two isobaric doublets since the neutrino charge of one of these particles is positive and that of the other is negative. The foregoing discussion is sufficient to understand the proposed lepton scheme based in isobaric multiplets, shown in the lower part of table 1.

The following results immediately follow from this scheme:

1. No leptons beyond those known at present ($\mu^{\pm}$, $e^{\pm}$, $\nu$ and $\tilde{\nu}$) can exist. In contrast to other classes of fundamental particles, for which one may expect to discover new particles, the classification proposed here shows that the discovery of light fermions is excluded.

2. Two types of neutrinos should exist, a neutrino ($\nu$) and antineutrino ($\tilde{\nu}$); the position of these particles in the fundamental particle scheme is similar to that of $\tilde{K}^0$ and $K^0$-mesons. Until recently the truth of this conclusion was not questioned, as it was supported by the fact of non-occurrence of double $\beta$-decay and by the negative results of the first experiments of Davis [15]) on transmutation of chlorine 37 into argon 37 under the action of neutrinos emitted from a nuclear reactor. Davis' latest data [16]) seem to indicate that the neutrino and antineutrino are identical but neither the experimental results nor even more their interpretation can be held as unimpeachable †.

The existence of two types of neutrinos does not necessarily imply that each of them is characterized by a definite direction of polarization as postulated in the two-component neutrino theory. For the following it does not matter whether each type of neutrino possesses one or two polarization components.

### 3. Selection Rules for Weak Interactions

A survey of all currently known types of weak interactions involving $\mu$-neutrino or electron-neutrino combinations indicates that such weak interactions are characterized by the following selection rules for the 3-projection of the isobaric spin: $\Delta T_3 = 0, \pm\frac{1}{2}$.

Besides the two general conclusions drawn above (concerning the absence of new leptons and the existence of two types of neutrinos) the selection rules just mentioned permit one to make some predictions of a more restricted nature if it be assumed that these selection rules are the same for all weak interactions involving leptons.

1. For the $\omega$-mesons with strangeness $S = \pm 2$ predicted by Gell-Mann the $\omega \to \mu + \nu$ and $\omega \to \pi^0 + \mu + \nu$ decay should be allowed, whereas the $\omega \to e + \nu$ and $\omega \to \pi^0 + e + \nu$ decays should be forbidden. For $\omega^+$ mesons

† It should be kept in mind that the use of the neutrino charge $m$ for the classification of leptons does not in the least imply that it is rigorously conserved: $m$ can be looked upon as an approximately conservative quantum number, which would express an approximation to the two-component neutrino. Proceeding from this interpretation of $m$ one finds that each type of neutrino can change into an equilibrium mixture of the two types just as is the case with $K^0$-mesons, which are the analogues of the neutrinos in the elementary particle table. B. M. Pontecorvo [17]), from another standpoint, arrived at the same conclusions concerning the possibility of lepton transformations involving non-conservation of the neutrino charge.

the decay $\omega^+ \to K^0+e^+(\mu^+)+\nu$ and for $\omega^-$ mesons the decay $\omega^- \to \tilde{K}^0+\tilde{e}(\mu^-)+\tilde{\nu}$ should also be allowed †.

2. $\mu$-meson and electron $\beta$-decay is possible for all types of hyperons, excluding a very few cases which will be discussed below. For example, the following decays are possible:

$$\Lambda^0 \to p+e^-+\tilde{\nu};\quad p+\mu^-+\tilde{\nu}$$
$$\Sigma^- \to n+e^-+\tilde{\nu};\quad \Lambda^0+e^-+\tilde{\nu};\quad n+\mu^-+\tilde{\nu}$$
$$\Sigma^+ \to n+e^++\nu;\quad \Lambda^0+e^++\nu$$
$$\Xi^- \to n+\mu^-+\tilde{\nu};\quad \Lambda^0+e^-+\tilde{\nu};\quad \Lambda^0+\mu^-+\tilde{\nu};\quad \Sigma^0+e^-+\tilde{\nu};\quad \Sigma^0+\mu^-+\tilde{\nu}$$
$$\Xi^0 \to p+\mu^-+\tilde{\nu};\quad \Sigma^++e^-+\tilde{\nu};\quad \Sigma^++\mu^-+\tilde{\nu};\quad \Sigma^-+e^++\nu.$$

On the other hand, the following decays are forbidden:

$$\Sigma^+ \to n+\mu^++\nu \qquad (\Delta T_3 = -1)$$
$$\Xi^- \to n+e^-+\tilde{\nu} \qquad (\Delta T_3 = -1)$$
$$\Xi^0 \to p+e^-+\tilde{\nu} \qquad (\Delta T_3 = -1)$$
$$\Xi^0 \to \Sigma^-+\mu^++\nu \qquad (\Delta T_3 = -1).$$

The mean hyperon lifetime against $\beta$-decay can be approximately estimated on the basis of data pertaining to $\beta$-decay of the neutron. The estimations show that the probability of decay of $\Lambda^0$ and $\Sigma^\pm$ hyperons amounts to 1 to 10 % of the probabilities of other decay modes, whereas for $\Xi^-$ and $\Xi^0$ hyperons the probabilities of $\beta$-decay and of other decay modes are of the same order of magnitude. The fraction of the forbidden decay mode is about 1/3 that of all decay modes of the $\Sigma^+$-hyperon; the fraction of forbidden decay modes of $\Xi^-$ and $\Xi^0$-hyperons is considerably greater than 1/2. We thus conclude that if the statistics of observations of various hyperon decays is sufficiently good (special attention being paid to various types of anomalous decay) it should not be difficult to check this prediction of our classification.

It would be especially interesting to verify whether the decays $\bar{\Xi}^0 \to n(p)+e^-+\tilde{\nu}$ occur in the absence of $\bar{\Xi}^0 \to n(p)+\mu^-+\tilde{\nu}$ decays. In all these decays the baryon strangeness changes by two units, and therefore, if one assumes that the participation of leptons does not affect the strangeness (i.e., $T_3$) selection rules, the various modes of cascade hyperon $\beta$-decay involving nucleon formation should be forbidden.

3. Both modes of $K_{e3}$ decay involving positon as well as negaton produc-

† The well known facts that $\pi_{e3}$ and $K_{e3}$ decays do not occur whereas the corresponding $\mu$-decays of these particles do occur, and that there also exists an equivalence between $K_{e3}$ and $K_{\mu 3}$ decays and electron or $\mu$-meson capture by K-mesons, remain inexplicable within the framework of the classification proposed here. Their explanation cannot be based on the general selection rules for $T_3$ and in this respect it must differ in principle from the explanation of forbiddenness of any of the $\omega$-meson decay modes discussed here.

tion are allowed for $K^0$ as well as $\tilde{K}^0$-mesons. However, $K_{\mu 3}$ decays with production of $\mu^-$-mesons are forbidden for $K^0$ and $K_{\mu 3}$ decays with $\mu^+$-meson production are forbidden for $\tilde{K}^0$. The ratio of $\mu^+$-decays to $\mu^-$-decays in a meson beam should therefore vary with time (or with the distance from the beam origin) in accord with the law presented in ref. [18]), whereas according to the selection rules presented above the ratio of $e^+$-decays to $e^-$-decays in a $K^0$ -meson beam should remain constant.

Among other corollaries of our lepton classification, one may mention forbiddenness of the $\mu^\pm \to e^\pm + \gamma$ decay. The explanation offered in ref. [9]) was that the neutrino charges of $\mu^\pm$ and $e^\pm$ were opposite in sign. In our case this transformation is forbidden by the condition $\Delta T_3 = \pm\frac{1}{2}$, since $T_3$ does not change during emission or absorption of $\gamma$-quanta.

## 4. Forbiddenness of Neutral Lepton Pair Decays

A number of processes are conceivable which, although not observed in reality, are not forbidden by the $T_3$ selection rules. As an example, it may be mentioned that meson or baryon decays involving production of electrically neutral lepton pairs such as $e^+e^-$, $\mu^+\mu^-$, $e^\pm\mu^\mp$ and $\nu\bar{\nu}$, are unknown at present.

In order to express the empirically indicated forbiddenness of such processes an additional lepton characteristic $N$ may be introduced which is related to the electric and neutrino charges by the equation $N = Q - \frac{1}{2}m$. After introduction of $N$ the selection rules for various interactions can be formulated as follows:

I. Strong interactions: $\Delta T_3 = \Delta N = 0$; $\Delta T = 0$.

II. Electromagnetic interactions: $\Delta T_3 = \Delta N = 0$; $\Delta T \neq 0$.

III. Weak interactions:

a) "Pure" interactions (not involving leptons at all or involving only leptons): $\Delta T_3 = \pm\frac{1}{2}$, $\Delta N = 0$.

b) "Mixed" interactions (involving leptons ($\mu\nu$, $e\nu$) as well as other particles): $\Delta T_3 = 0, \pm\frac{1}{2}$, $\Delta N = \pm 1$.

The selection rules for weak interactions given above are purely empirical and no attempt is made here to give them any theoretical foundation.

In conclusion it should be noted that the unified classification permits one to extend to leptons the concept of a compound or complex structure of most "elementary" particles [19–24]) and the concept of the existence of a comparatively small number of "basic" particles.

The author expresses his sincere thanks to Ya. B. Zeldovich, M. A. Markov and M. I. Podgoretsky for interest in this work and for valuable remarks.

## References


1) M. Gell-Mann, Phys. Rev. **92** (1953) 833
2) K. Nishijima, Progr. Theor. Phys. **12** (1954) 107
3) L. B. Okun, Uspekhi Fiz. Nauk **61** (1957) 535
4) Ya. B. Zeldovich, Doklady AN SSSR **86** (1952) 505
5) M. Cini and A. Gamba, Nuovo Cimento **10** (1953) 1040
6) R. Sachs, Phys. Rev. **99** (1956) 1573
7) S. Goto, Progr. Theor. Phys. **17** (1957) 107
8) M. A. Markov, Hyperons and K-Mesons, Part III (Joint Institute of Nuclear Research, 1956)
9) Ya. B. Zeldovich, Doklady AN SSSR **91** (1953) 1317
10) G. Marx, Acta Physica Hung. **3** (1953) 55; E. Konopinski and H. Mahmoud, Phys. Rev. **92** (1953) 1045
11) T. D. Lee and C. N. Yang, Phys. Rev. **105** (1957) 1671
12) L. D. Landau, Nuclear Physics **3** (1957) 127
13) A. Salam, Nuovo Cimento **5** (1957) 299
14) W. Dudziak and Sagani (Communication of W. Barkas at the VIIth Rochester Conference on High Energy Physics, 1957)
15) R. Davis Jr., Bull. Amer. Phys. Soc. **1** (1956) 219
16) R. Davis Jr., Report at Paris Conference on Radio-isotopes (1957)
17) B. M. Pontecorvo, Inverse $\beta$-Processes and Non-Conservation of Neutrino Charge, JINR (1957)
18) L. B. Okun, JETP **32** (1957) 400
19) M. A. Markov, On a Classification of Fundamental Particles (USSR Academy of Sciences, 1955)
20) S. Sakata, Progr. Theor. Phys. **16** (1956) 686
21) K. Matumoto, Progr. Theor. Phys. **16** (1956) 583
22) R. King and D. Peaslee, Phys. Rev. **106** (1957) 360
23) M. Goldhaber, Phys. Rev. **101** (1956) 433
24) G. Györgyi, JETP **32** (1957) 152

*Nuclear Physics* **6** (1958) 539—540; © *North-Holland Publishing Co., Amsterdam*
Not to be reproduced by photoprint or microfilm without written permission from the publisher

# PARITY NON-CONSERVATION AND TRANSVERSE POLARIZATION OF $\beta$-PARTICLES: ADDED REMARKS

G. GYÖRGYI
*Central Research Institute for Physics, Nuclear Physics Department, Budapest*
and
H. ÜBERALL
CERN, *Geneva*

Received 26 January 1958

In a recent elegant experiment, Goldhaber [1]) determined in a direct way the helicity of the neutrino emitted in K-capture. His method consists essentially in fixing the recoil direction by the requirement that a gamma ray emitted from the excited recoiling nucleus should produce resonance scattering, and by a simultaneous measurement of the gamma ray helicity.

We wish to point out here that the transverse $\beta$-polarization discussed by us [2]) can also be useful for a direct determination of the neutrino handedness, a principle which is related to Goldhaber's method insofar as it also requires a knowledge of the recoil, but the application of which is not limited to K-capture processes leading to an excited daughter nucleus. From the last table of ref. [2]), we note that the sign of $P_\perp$ depends, besides on electron charge and neutrino handedness, only on whether the transition is of F or GT type. This contrasts with longitudinal polarization, which can be used for a determination of neutrino helicity only if the exact type of transition — S or V, T or A — is known †. If we use the fact that $C = \overset{+}{(-)} C'$ or $\xi = \overset{+}{(-)}\ 1$ corresponds to the emission of a right (left) handed anti-neutrino, we arrive at the following table for the sign of the transverse polarization:

| $P_\perp$ | $\beta^- \bar{\nu}_R$ | $\beta^- \bar{\nu}_L$ | $\beta^+ \nu_L$ | $\beta^+ \nu_R$ |
|---|---|---|---|---|
| F | − | + | + | − |
| GT | + | − | − | + |

This sign is best established by observing an up-down asymmetry in Coulomb scattering of the electrons with respect to the decay plane. The

† This information was previously taken from angular correlation experiments, whose results are, however, not yet well established for the case of $\beta^-$-emitters.

recoil direction can be found either by a direct observation in cloud chambers, as discussed in ref. [2]), or using Goldhaber's method if the daughter nucleus is excited and decays by gamma emission, and performing the Mott scattering of the electrons in coincidence with a resonance scattering of these gamma rays.

Finally, we want to correct the sign in the second line of eq. (2) of ref. [2]), which should read $\pm$ instead of $+$. Furthermore, the statement after eq. (2) that the electron spin lies in the decay plane is correct only for pure transitions or if time reversal invariance holds, and eq. (3) represents therefore the component of $P_\perp$ in the decay plane ($\phi = 0$).

One of us (H. Ü.) would like to thank Dr. A. de-Shalit for discussions. The other author (G. Gy) is indebted to Prof. J. Werle for a critical remark.

## References

1) M. Goldhaber, L. Grodzins and A. W. Sunyar, Phys. Rev. (to be published)
2) G. Györgyi and H. Überall, Nuclear Physics 5 (1958) 405

*Nuclear Physics* **6** (1958) 541—542; © *North-Holland Publishing Co., Amsterdam*
Not to be reproduced by photoprint or microfilm without written permission from the publisher

# J. M. NUTTALL (1890—1958)

G. D. ROCHESTER

*Department of Physics, The Durham Colleges in the University of Durham*

Received 3 March 1958

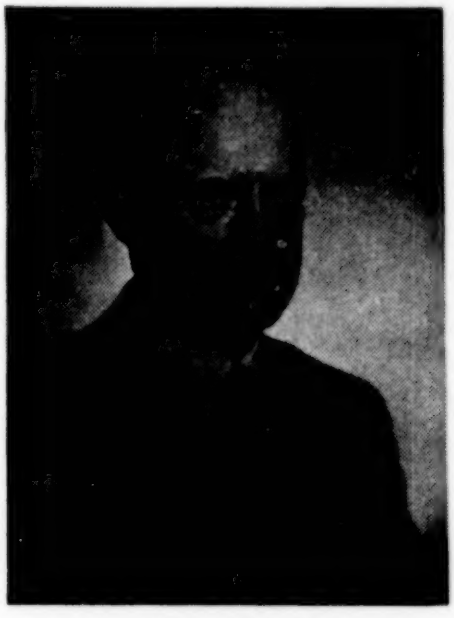

Dr. J. M. Nuttall, who was for many years a prominent member of the staff of the Physics Department of Manchester University, and had a direct person link with Rutherford's Manchester period, died on 28th January 1958.

John Mitchell Nuttall was born on 21st July 1890 at Todmorden in Yorkshire, England, and entered the Honours Physics School at Manchester in 1908. He graduated in 1911 with a First class degree in a brilliant year which included Sir James Chadwick and the late Professor Robinson, Vice-Chancellor of London University. Nuttall was awarded a Graduate Scholarship and began research with Geiger under the direction of Rutherford, who was then at the height of his powers, and had in his department, in addition to those already mentioned, Bohr, Darwin, Fajans, Marsden and Moseley. Nuttall's work with Geiger was very successful and resulted in the discovery of a relationship which later became known as the Geiger-Nuttall Law. After taking his M. Sc. degree he became a Junior Lecturer at Leeds University and at the outbreak of the first World War joined the Yorks. and Lancs. Infantry, but later transferred to the Field Survey Battalion of the Royal Engineers. He was promoted to the rank of Captain and was twice mentioned in despatches. In 1920 he returned to Manchester University as Senior Lecturer in Physics, and in the following year was made Assistant Director of the Physics Department. Professor (now Sir Lawrence) Bragg was Director of the Physical Laboratories at this time and although Nuttall continued to be active in research (his work with the late Professor E. J. Williams on the electrons ejected from atoms by X-rays is well known), he gradually assumed greater responsibility for the student teaching and the administrative work of the department.

Professor Blackett succeeded Bragg as Director of the Laboratories in 1938 and when he left for War service in 1939 Nuttall took charge and continued to act as Head until 1944. Throughout the second World War he was a prominent member of the University Civil Defence Corps. He retired in 1955.

Former colleagues and students, who remember Nuttall in his prime, will recall his nimbleness of mind, and his powers as a raconteur. His wit enlivened his lectures and made him popular with students. Many Manchester students will remember his oft-repeated and popular lecture on the history of the Manchester Physics School. He was keenly interested in sport, especially cricket.

The academic world has lost a man distinguished for his early work in radioactivity, and one who gave devoted service to Manchester University. His many friends have lost a man who will be remembered for his loyalty, integrity, generosity and native Yorkshire wit.

Dr. Nuttall is survived by his wife, who sustained and cheered him during some years of ill health, and by his son, Dr. Kenneth Nuttall.

*Nuclear Physics* **6** (1958) 543—544; © *North-Holland Publishing Co., Amsterdam*
Not to be reproduced by photoprint or microfilm without written permission from the publisher

# DEUTERON STRIPPING WITH POLARIZED DEUTERONS

G. R. SATCHLER
*Clarendon Laboratory, Oxford*

Received 8 February 1958

The angular distribution of nucleons from deuteron stripping reactions [1]) has proved a valuable source of information on nuclear structure, and measurements have recently been extended to the polarization of the outgoing nucleons [2]). While the angular distribution tells us only the orbital angular momentum $l$ with which a nucleon is captured into the target nucleus, the polarization measurement gives some measure of the relative amounts of *total* angular momentum $j = l \pm \frac{1}{2}$ that it carries [3]). In particular with a zero spin target only one $j$ value is involved, that equal to the spin of the residual nucleus. The sign of the polarization then distinguished between the two possibilities.

Equivalent information can be obtained by observing the left-right asymmetry in the angular distribution when polarized deuterons are used. In order to estimate this effect the 'distorted wave' Born approximation has been used. This approach has been discussed by many authors [4]), and recently it has received support from the formal theory of reactions [5]). We replace the plane waves of the ordinary Born approximation [1]) by waves distorted by scattering from appropriate optical potentials representing the target and residual nuclei. Without these interactions all polarization effects would vanish. The distortions can also have important effects on other measurements, such as the total cross section and nucleon—$\gamma$ angular correlation [4, 6]).

We speak of the (d, p) reaction for definiteness. If we neglect any spin dependence of the distorting optical potentials (including spin-orbit coupling) we find there is a simple relation between the proton polarization $\mathbf{P}_p$ produced when unpolarized deuterons are used, and the differential cross-section $(d\sigma/d\omega)_{pol.}$ when the incident deuterons have a polarization $\mathbf{P}_d$ [6]),

$$\left(\frac{d\sigma}{d\omega}\right)_{pol.} = \left(\frac{d\sigma}{d\omega}\right)_{unpol.} (1 - 3\mathbf{P}_p \cdot \mathbf{P}_d). \qquad (1)$$

In the usual way [7]), the polarization vectors are the average values of the particle spin vectors, $\mathbf{P} = \langle \mathbf{S} \rangle / S$, so the magnitude of $\mathbf{P}_d$ is

$$P_d = \frac{N(+1) - N(-1)}{N(+1) + N(0) + N(-1)}.$$

$N(\lambda)$ is the number of deuterons with spin component $\lambda$ along the direction

of $\mathbf{P}_d$. We note that any higher spin moments which may be present in the deuteron beam do not contribute to the reaction in this approximation. The proton polarization is perpendicular to the reaction plane, and chosen to be positive when $\mathbf{P}_p$ is directed along $\mathbf{n} = \mathbf{k}_p \times \mathbf{k}_d$. Clearly the asymmetry is greatest when $\mathbf{P}_d$ is also perpendicular to this plane.

On this model, when only one $l$ value contributes to the neutron capture, we can write the proton polarization [3])

$$P_p = \tfrac{1}{3}\left[\frac{\gamma^2_{l+\frac{1}{2}}}{l+1} - \frac{\gamma^2_{l-\frac{1}{2}}}{l}\right] \langle m \rangle (\gamma^2_{l+\frac{1}{2}} + \gamma^2_{l-\frac{1}{2}})^{-1},$$

which displays its dependence on the neutron capture probabilities or reduced widths $\gamma_j^2$ for the two values $j = l \pm \frac{1}{2}$. $\langle m \rangle$ is the average component along $\mathbf{n}$ of the orbital angular momentum $l$ of the captured neutron, and depends on the proton emission angle. In this case the maximum value $|P_p|$ can reach is 1/3 if $j = l - \frac{1}{2}$ and $1/3(l/l+1)$ if $j = l + \frac{1}{2}$. Experimentally [2]), $P_p$ is found to be $(\pm)$ as $j = l \mp \frac{1}{2}$, and on the stripping peak achieves a large fraction of the maximum permissible.

When using the relation (1) it is important that measurements should be made on the main stripping peak of the proton angular distribution. Off this peak there is the possibility of other competing processes (such as exchange stripping and compound nucleus formation) contributing in comparable intensity and completely destroying the simple relation.

A few words should be said about the neglect of spin-orbit coupling in the distorting optical potentials. While this is undoubtedly present, we argue that it is only a few MeV in a total potential of some 50 MeV, and thus plays a minor role. Its inclusion would modify somewhat the relation (1) (and allow higher deuteron spin moments to contribute). A simple semi-classical argument predicts the nucleon polarization produced by spin-orbit coupling alone to be negative for both $j = l \pm \frac{1}{2}$, contrary to experiment. This implies it cannot play more than a subsidiary role, merely enhancing the polarization for $j = l + \frac{1}{2}$ captures, and reducing it somewhat for $j = l - \frac{1}{2}$. More quantitative conclusions, however, must await numerical computation using the appropriate distorted waves.

## References


1) S. T. Butler, Phys. Rev. **106** (1957) 272
2) The experiments are summarized by J. C. Hensel and W. C. Parkinson, Phys. Rev. (1958) to be published
3) H. C. Newns, Proc. Phys. Soc. A **66** (1953) 477; J. Horowitz and A. M. L. Messiah, J. Phys. et Rad. **14** (1953) 731
4) J. Horowitz and A. M. L Messiah, J. Phys. et Rad. **14** (1953) 695; W. Tobocman, Phys. Rev. **94** (1954) 1655; W. Tobocman and M. H. Kalos, Phys. Rev. **97** (1955) 132
5) G. E. Brown and C. T. De Dominicis, Proc. Phys. Soc. A **70** (1957) 686
6) G. R. Satchler, Analysis of Deuteron Stripping Experiments (1958), unpublished
7) L. Wolfenstein, Ann. Rev. Nuclear Sci. **6** (1956) 43

*Nuclear Physics* **6** (1958) 545—546; © *North-Holland Publishing Co., Amsterdam*
Not to be reproduced by photoprint or microfilm without written permission from the publisher

# SCATTERING FUNCTIONS WITH CROSSING SYMMETRY: A CORRECTION

NING HU
*Joint Institute of Nuclear Research, Dubna, U.S.S.R.*

Received 10 January 1958

The conclusion reached in the last section of the paper with the above title [1]) cannot be upheld. It followed from an incorrect choice of Riemann sheet, due to overlooking the role of the neutral meson. To see this we consider the asymptotic wave function for scattering of negative meson by proton:

$$\psi = \{\chi_1(e^{-ik_1 r}+S_{11}e^{ik_1 r})+\chi_2 S_{21}e^{ik_2 r}\}e^{-i\omega t},$$

where $\chi_1$ and $\chi_2$ are, respectively, isobaric spin wave functions for $P\pi^-$ and $N\pi^0$ states; $k_1^2 = \omega^2-\mu_1^2$, $k_2^2 = \omega^2-\mu_2^2$, $\mu_1$ and $\mu_2$ being the rest masses of $\pi^-$ and $\pi^0$. Coulomb interaction has been included and cut off at large distances to ensure the above form of asymptotic solution. The mesic atom state is given by a pole of $S_{11}$ at $k_1 = -K_1+i\lambda_1$, $\omega = \omega_0-i\gamma$, where $K$, $\lambda$, $\omega_0$ and $\gamma$ are all positive and real. Since the capture of $\pi^-$ by the nucleon must be accompanied by an outgoing $\pi^0$ wave, we see that $S_{21}$ must also have a pole at $\omega = \omega_0-i\gamma$ and $k_2 = K_2-i\lambda_2$. Thus we have

$$\psi_{\text{K-capture}} = \left\{\chi_1 e^{-iK_1 r-\lambda_1 r}+\chi_2\frac{S_{21}}{S_{11}}e^{iK_2 r+\lambda_2 r}\right\}e^{-i\omega_0 t-\gamma t}.$$

Similarly we find that the reverse process of K-emission is given by a pole of $S_{11}$ and $S_{21}$ at $k_1 = K_1+i\lambda_1$, $\omega = \omega_0+i\gamma$ and $k_2 = -K_2-i\lambda_2$. The corresponding asymptotic wave function is

$$\psi_{\text{K-emission}} = \left\{\chi_1 e^{iK_1 r-\lambda_1 r}+\chi_2\frac{S_{21}}{S_{11}}e^{-iK_2 r+\lambda_2 r}\right\}e^{-i\omega_0 t+\gamma t}.$$

The above result shows that the poles of $S_{ij}$ representing K-capture and K-emission lie in the Riemann sheet Im $(k_1) > 0$, Im $(k_2) < 0$. (We have shown before that all other meta-stable states are represented by poles in the Riemann sheet Im $(k_1) < 0$.) A dispersion relation written for this Riemann sheet must therefore contain poles in the upper half $\omega$-plane as we have

stated in our paper. However, since the usual dispersion relation is derived for the Riemann sheet Im $(k_1) > 0$, Im $(k_2) > 0$, our consideration does not provide a case which would violate the dispersion relation.

*Note:*

We take this opportunity of pointing out a few misprints in our paper [1]):

(1) "$k^2$" in the first line below eq. (10) on p. 4 should be "$K^2$".

(2) "F-wave" in the first line of the last paragraph on p. 7 should read "P-wave".

(3) The equations at the bottom of p. 7 should be numbered (25).

(4) "(24)" in the fifth line from bottom on p. 8 should be "(23)".

## Reference

1) Ning Hu, Nuclear Physics **5** (1958) 1

*Nuclear Physics* **6** (1958) 547—560; © *North-Holland Publishing Co., Amsterdam*
Not to be reproduced by photoprint or microfilm without written permission from the publisher

# FISSION-FRAGMENT MASS SEPARATOR AND THE NUCLEAR CHARGE DISTRIBUTION OF FISSION FRAGMENTS OF A SINGLE MASS

BERNARD L. COHEN and CLYDE B. FULMER
*Oak Ridge National Laboratory* †, *Oak Ridge, Tennessee*

Received 3 January 1958

**Abstract:** An energetic fission fragment passing through a gas changes its charge frequently by electron capture and loss collisions with gas molecules. Its average charge $\bar{e}$ is found to be very nearly proportional to velocity, so that magnetic deflection depends only on the mass; thus, passing fission fragments through a gas-filled magnetic spectrograph gives mass separation. At low pressure the resolution is limited by the statistics of the electron capture and loss process; increasing the pressure to reduce this effect is eventually limited by energy loss and the resulting multiple scattering. However, before this occurs there is a pressure range where the resolution is limited by the nuclear charge distribution of fragments of a single mass. All of these effects were studied experimentally. The best resolution obtained for mass-97 fragments was 3.5 % full width at half maximum (with 20 mm-Hg of helium), of which 2.2 % is due to the width of the nuclear charge distribution. Combining this with the results of a study of the dependence of $\bar{e}$ on nuclear charge, gives the width of the nuclear charge distribution for mass-97 fragments as $2.4 \pm 0.5$ units. This is in agreement with determinations from yields of shielded isotopes, but is in disagreement with the predictions of most theories.

The best obtainable resolution from the mass separator is 4.5 mass units for light fragments. Several applications of the separator are described and others are suggested.

## 1. Introduction and Operating Principles

The properties of a wedge-magnet spectrograph [1]) are such that energetic ions originating at the source are focused to a position on the focal plane which is a function only of their radius of curvature $\varrho$ in the magnetic field $H$. From the Lorentz Law, $\varrho$ is determined by

$$H\varrho = \frac{mvc}{e}, \tag{1}$$

where $m$, $v$ and $e$ are the mass, velocity and charge of the ion, respectively, and $c$ is the velocity of light. If $e$ is much larger than one electron charge, and if the system contains an appreciable quantity of gas, the charge of the ions may change frequently due to electron capture and loss collisions with the gas molecules. In this case, the focal position is still determined by (1) but with $e$ replaced by $\bar{e}$, the time-average of the charge while the

† Operated for the USAEC by Union Carbide Nuclear Company.

particle is in the magnetic field. In general, $\bar{e}$ is a function of the velocity, the nuclear charge $Z$ of the ion, the type of gas in the system, and the pressure. It has been predicted theoretically [2]) and demonstrated experimentally [3]) that $\bar{e}$ is roughly proportional to velocity (see § 3.3), and Bohr and Lindhard have shown [2]) that to some approximation, $\bar{e}$ is proportional to $Z^{1/3}$ (see § 4). Thus, for given conditions of gas filling,

$$\bar{e} \propto Z^{1/3} v. \tag{2}$$

Inserting (2) in (1) then gives

$$H\varrho \propto \frac{m}{Z^{1/3}}. \tag{3}$$

Taking $m$ proportional to $Z$, (3) gives

$$H\varrho \propto m^{2/3}. \tag{4}$$

Thus, by simply passing fission fragments through a magnetic spectrograph which is filled with gas, mass separation of the fragments is achieved, independent of their energy and their direction of motion (within the acceptance angle of the spectrograph), and with a reasonably good dispersion, 0.7 % and 0.4 % per mass unit of light and heavy fragments, respectively. This separation, which ideally would be at least equivalent and usually superior to the results achieved by chemical procedures, is accomplished in a time lapse of the order of one microsecond; therefore, it allows the fragments to be separated and studied before any beta decay (or delayed-neutron emission) has taken place. Some of the many applications of such an instrument are discussed in § 5.

The principal difficulty with the instrument is its lack of resolution. This arises from several sources. In the first place, it must be noted that the process of charge changing by electron capture and loss collisions with gas molecules is a statistical one, so that the average charge $\bar{e}$, for different fragments of the same mass, velocity and initial charge † is subject to statistical fluctuation. From usual statistical considerations, this fluctuation varies inversely as the square root of the number of charge changing collisions. Since the latter is just proportional to the density of gas molecules, and hence to the gas pressure $p$, we have, from (1),

$$W = \frac{K}{\sqrt{p}}, \tag{5}$$

where the width $W$ is defined as $\Delta(H\varrho)/H\varrho$, and $K$ is a constant. In principle, then, this spreading of the resolution can be reduced indefinitely by in-

† Actually the initial charge is of negligible importance if the total number of charge changing collisions is much larger than the number of charge states that can be reached by charge changing collisions with reasonable probability ($\approx 5$). This condition is fulfilled for all cases of interest here. For example, at the most favorable pressures, the number of charge changing collisions is about $10^5$.

creasing the pressure. However, this also causes the fragments to lose energy and thus suffer strong multiple scattering, so that a resolution limit is set by the ratio of the electron capture and loss cross sections to the energy-loss cross section. Before this limit is reached, however, another factor — the nuclear charge distribution of fission fragments of a single mass — comes into predominance. Observation of the manner in which this factor limits the resolution is used to determine the width of this charge distribution.

Previous experimental studies [4, 5, 6]) of the nuclear charge distribution of fission fragments of a given mass have been achieved by determination of the independent yields of a few shielded isotopes. These data alone do not determine the nuclear charge distribution, since the centre of the charge distribution (most probable charge) is not known. This latter quantity is conventionally determined by the postulate of equal chain lengths, which has no basis in theory or experiment. Only points far down on one wing of the curve are determined. These do not determine the width at half maximum which is the important quantity for the theory of nuclear fission. The very low yields of the shielded isotopes (typically $10^{-5}$ per fission) can be influenced by any of a number of small effects, e.g., the details of the distribution of number of neutrons per fission, nuclear structure anomalies, isomeric states, etc. Shielded isotopes must necessarily occur near the minima of beta stability curves and, therefore, are not typical fission fragments. The paucity of data and the relatively tenuous treatment of it leave these determinations somewhat in doubt. For instance, Brunton's [7]) attempt to explain the energy distribution of fission fragments on the basis of nuclear charge distribution gives a width more than three times larger than was previously determined by shielded isotope data; he did not consider the latter results sufficiently convincing to contradict his theory.

In any case, the method of studying the nuclear charge distribution reported here is completely different from previously used techniques; an independent determination of a physical quantity by a different method is always desirable:

In outline, the procedure is as follows:

(a) Measurements were made of intensity of mass-97 fission fragments vs. $H\varrho$ for various pressures of helium gas. The widths of the distributions were thus determined.

(b) The contribution to the width from charge-change statistics was determined from the measurements at low pressures, where this effect is predominent. It was then extrapolated to higher pressures from (5). Corrections for dependence of the charge-change cross section on pressure and velocity were applied, although the results are relatively insensitive to these.

(c) The contribution to the width from multiple scattering was calculated theoretically. Some check on it is obtained from data at high pressures where it is predominant.

(d) Contributions from other experimental sources were examined. All were found to be negligible except those from source and detector size.

(e) The difference between the measured width and the width due to the above causes is thus due to the nuclear charge distribution. This is thus determined.

(f) In order to determine the width of the nuclear charge distribution from this width, it is necessary to determine the explicit dependence of atomic charge on nuclear charge. This was done by measuring the value of $H\rho$ for different mass fragments. Checks were made at various pressures.

## 2. Experimental

The fission fragment spectrograph was originally constructed to measure the energy distribution of fission fragments of a single mass, and it has been described in the report of that experiment [8]). To recapitulate briefly, it consists of a 40-degree, single-focusing wedge magnet mounted just outside the ORNL Graphite Reactor, and its entrance and exit arms. The entrance arm is a 16-ft long tube placed in a reactor hole with its far end

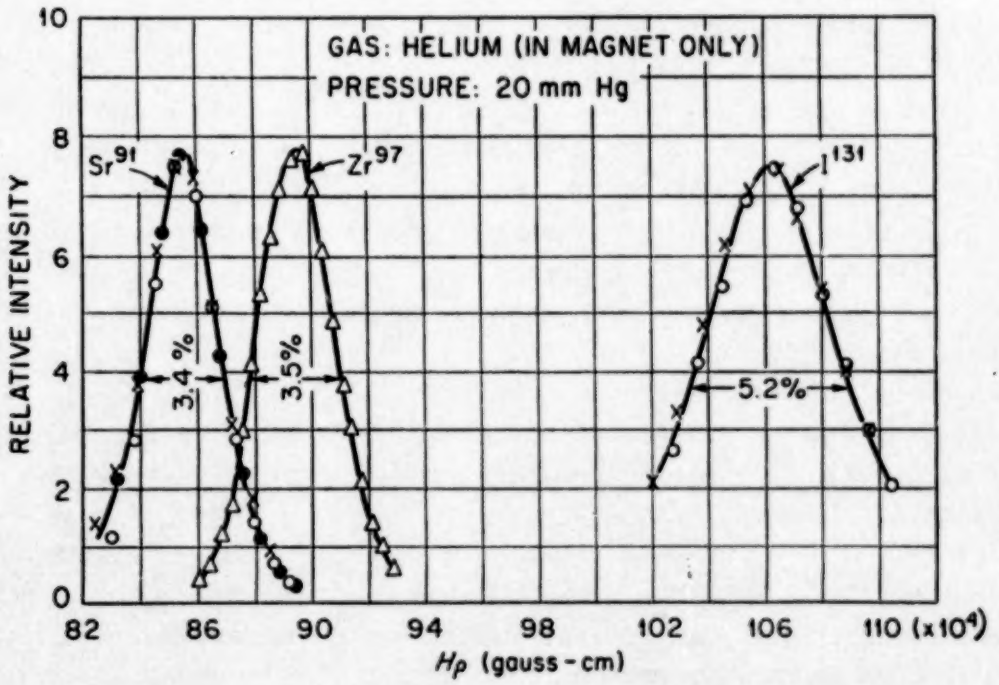


Fig. 1. $H\rho$ distributions of mass-91, -97 and -133 fission fragments with 20 mm-Hg of helium in the part of the system which passes through the magnetic field.

extending nearly to the centre of the reactor core. Mounted in that end is a thin plating of $U^{235}$ which, in the high neutron flux, provides an abundant source of fission fragments, and a thin plating of $Po^{210}$ which is used for calibration. The exit arm is a 6-ft tube at the end of which access to the focal plane of the system is provided. An aluminium foil is mounted on the focal plane so that the fission fragments lodge in it. After a suitable exposure, the foil is removed, and cut into strips — each strip corresponding to a given $H\varrho$. These are then radiochemically processed for the desired element — $Zr^{97}$, $Sr^{91}$ and $I^{133}$ were used in this work — and the activities were measured by Geiger counting.

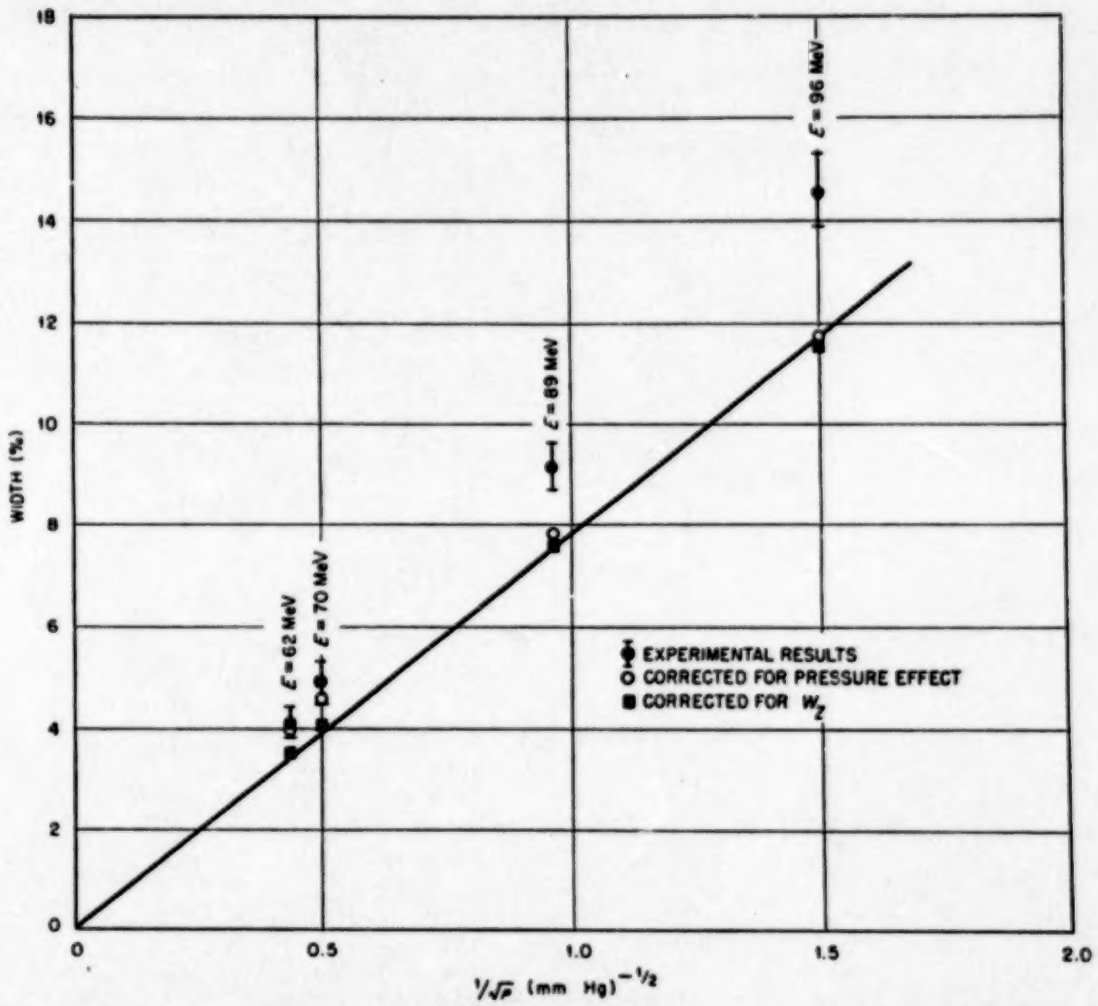


Fig. 2. Width of the $H\varrho$ distribution of mass-97 fragments for various pressures of helium gas filling the entire vacuum system. Energies are calculated at the centre of the magnetic field. These data determine the width due to charge-change statistics.

Gas is bled into the system through a needle valve, and the desired pressures are achieved as a dynamic equilibrium between bleed-in and pump-out. Pressures below 6 mm-Hg are measured with a McLeod gauge; higher pressures are measured with a U-tube manometer filled with King's

red indicator fluid (density 2.94). In some experiments it is desired to fill only the part of the system in the magnetic field with gas (this situation will be referred to as "gas in the magnet"). This is accomplished by mounting 100 $\mu g/cm^2$ formvar windows supported by 50 % transparent nickel grids between the part of the system in the magnetic field, and the entrance and exit arms. A separate pump is provided to establish the dynamic equilibrium with gas bleed-in, while the regular pumping system evacuates the entrance and exit arms. The pressure in the magnet is measured with U-tube manometers leading to each side of the windows.

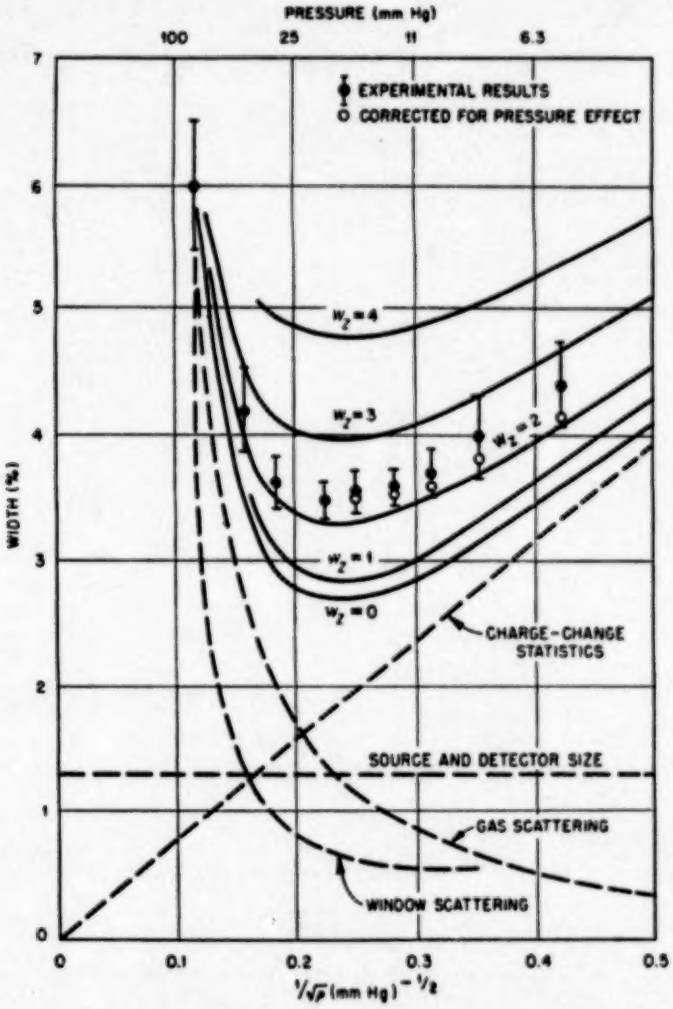


Fig. 3. Width of $H\varrho$ distribution of mass-97 fragments for various pressures of helium gas in the part of the system which passes through the magnetic field. The various curves are explained in the text.

Some typical $H\varrho$ distributions obtained with helium as the gas are shown in fig. 1. The principal information obtained from these data is the width of the distribution, defined here as the full width at half maximum, and the most probable value of $H\varrho$. The widths for masss-97 fission fragments as a function of pressure are plotted in fig. 2 for helium gas in the entire system,

and in fig. 3 for helium gas in the magnet only†. The energies shown are the energies at the centre of the magnet as calculated from range-energy data. The most probable values of $H\varrho$ in a few cases of interest are listed in table 1.

## 3. Factors Affecting Resolution

### 3.1. CHARGE-CHANGING STATISTICS

The contribution to the resolution width from the statistics of the charge-changing process is governed essentially by (5); thus the principal problem is to determine $K$. This is done by making measurements at low pressures where the contribution of other factors is small. The process for mass-97 fragments in helium is shown in fig. 2 where the measured width for some low pressure points is plotted vs. $p^{-\frac{1}{2}}$. According to (5), $K$ is determined from the slope of a straight line from the origin through these points; however, before this is done, three corrections must be applied to the data.

(a) A correction for the dependence of the cross section for charge-changing collisions on pressure. This arises from the fact that, at higher pressures, the fragment undergoes charge-changing collisions more frequently, so that there is a better chance that it will not undergo radiative de-excitation between collisions; its cross section for electron loss $\sigma_L$ will thus be increased. This phenomenon gives rise to the well-known dependence of equilibrium charge $\bar{e}$ on pressure [2]) which was studied experimentally in ref.[9]). The shift in equilibrium charge may be used to estimate the increase in the charge-changing cross section $\Omega$ if the dependence of the electron-capture cross section $\sigma_c$ on charge is known††. According to Bohr and Lindhard [2]), this last is given by

$$\sigma_c \propto e^3 \tag{6}$$

Since $\Omega$ must always be equal to $\sigma_c$ at equilibrium,

$$\Omega \propto \bar{e}^3. \tag{7}$$

From statistical considerations, the width of the $H\varrho$ distribution depends on $\Omega$ as

$$W \propto \Omega^{-\frac{1}{2}} \tag{8}$$

Whence, combining (7) (8),

$$W \propto \bar{e}^{-3/2}.$$

Values of $\bar{e}$ as a function of pressure can be obtained from ref. [9]), so that the data can be corrected. In figs. 2 and 3 the open circles show the correction to the pressure effect at 20 mm-Hg pressure, which is used as a standard.

† Ideally, it would have been preferable to make all measurements with gas in the magnet only; however, the data of fig. 2 were already available and repeating it with gas in the magnet only would have been very laborious, and would have added little to the experiment.

†† The notation used here is that of ref. [2]): $\Omega$ is the cross section for capture or loss at the equilibrium charge, that is where $\sigma_c = \sigma_L$; at this charge, $\Omega = \sigma_c = \sigma_L$.

In this derivation, we have assumed that $\sigma_c$ is unaffected by the state of excitation of the fragment. If it were affected, it would be reduced by the fact that the fragment is excited; this would cause the correction to be reduced.

(b) A correction for the dependence of the cross section for charge-changing collisions on energy. According to Bohr and Lindhard [2],

$$\Omega \propto E^{-\frac{1}{2}}, \tag{10}$$

whence, from (8)

$$W \propto E^{1/4}. \tag{11}$$

Since this is a relatively slow dependence, and since the energy range employed in this experiment is not large, this correction is generally quite small. In figs. 2 and 3 it has been included in the pressure effect correction.

(c) A correction for the width due to the nuclear charge distribution $W_Z$. Since $W_Z$ is obtained as a result of the experiment, this correction is, in principle, an iteration procedure. However, it is a very rapidly converging one. The squares in fig. 2 show this correction for $W_Z = 2.2$ %.

### 3.2. MULTIPLE SCATTERING

The width due to multiple scattering in the gas and in the windows was calculated from standard multiple scattering theory†, and the results are shown in fig. 3. The dependence of the window scattering on pressure arises from the fact that the latter determines the energy which strongly affects the former. The energy also has a strong effect on the gas scattering.

In order to minimize multiple scattering in the metal walls of the apparatus, an elaborate slit system was used. Inside of the 16-ft long, 3-in., ID, tube leading from the source to the magnet, aluminium foil diaphragms with $2\frac{1}{8}$-in. diameter openings were located at 30-in. intervals. Also, aluminium foil slits were inserted at each end of the magnet vacuum chamber. According to calculations, this system is more than adequate to eliminate any broadening of the distribution from multiple scattering from walls. The slits were made of 0.001-in. aluminium foil, which, although opaque to fission fragments, is tnin enough to avoid troubles from slit scattering.

No effects of wall scattering were found in measurements with polonium alpha particles, although calculations indicate that these should be more strongly multiple scattered than fission fragments.

### 3.3. VELOCITY DEPENDENCE OF THE QUANTITY $\bar{\varepsilon}/v$, AND SOURCE THICKNESS

Since fission fragments have a relatively wide velocity distribution the resolution would be adversely affected if the equilibrium charge were not strictly a linear function of velocity as was assumed above. This was studied in detail elsewhere [9], where it was found that approximating the

† Energies for use in the calculations were obtained from ref. [11]).

dependence of $\bar{e}$ on $v$ by

$$\bar{e} \propto v^{(1-x)}, \tag{12}$$

for the pressures of interest here

$$x = 0.015 \pm 0.01. \tag{13}$$

The fact that $x \ll 1$ indicates that $H\varrho$ is very nearly independent of velocity. Thus, the spread in velocity is not a significant contributor to the resolution; in fact, numerical calculations indicate that the thickness of the uranium source can be increased to nearly the full range of fission fragments without serious effect. This was done in some later experiments where greatly increased intensity was required; no loss of resolution was observed.

In addition to the effects of gross variation of $\bar{e}/v$, a loss of resolution would also be introduced if this quantity should undergo strong fluctuations as a function of velocity. This effect was also studied in detail in ref.[9]). No fluctuations of this sort were found; a liberal estimate of their upper limit would give a width to the $H\varrho$ distribution of less than 1 %.

### 3.4. ION OPTICS OF THE FOCUSING SYSTEM

The ion optics of the focusing system were studied by measuring the $H\varrho$ distribution of the alpha particles from a polonium plating mounted adjacent to the uranium source. The contribution to the width of the $H\varrho$ distribution from imperfections in the ion optics is less than 0.2 %.

### 3.5. SOURCE AND DETECTOR SIZE

The width of the uranium source contributes a width of 0.8 % to the resolution, and the width of the strips into which the detector foil is cut contributes a width of 0.9 %. These widths could easily be reduced at the price of intensity. The contribution of these effects plus those discussed in the preceding two subsections is shown by the horizontal line at $W = 1.3$ % in fig. 3.

### 3.6. NUCLEAR CHARGE DISTRIBUTION

The effect on the resolution of the width of the nuclear charge distribution is, for present purposes, considered as an unknown to be determined from the experiment. The combined contributions to the width from all other sources are shown by the line labelled $W_Z = 0$ in fig. 3, and the other lines show the net resolution expected for $W_Z = 1$, 2, 3 and 4 %. Comparing the observed resolution with these curves indicates $W_Z = 2.2 \pm 0.2$ percent.

The error assigned assumes no uncertainly in the other factors affecting resolution. The principle other factors that must be considered are the contributions of charge-change statistics and multiple scattering. The estimate of the former would seem to be especially unreliable because of the rather uncertain correction for the pressure effect. However, the determination of

$W_Z$ is surprisingly insensitive to this; for example, if this correction were entirely neglected, $W_Z$ would be decreased by only 10 %. This is because at low pressures, the pressure effect corrections on fig. 2 are largely cancelled by those on fig. 3, and at higher pressures, the contribution to the width from charge-change statistics is relatively not very large. It thus seems reasonable to take the error from this as $\pm$ 0.2 % in the width.

The contribution to the width from multiple scattering shown in fig. 3 was calculated under the assumption that the full nuclear charge of the fission fragment is effective, whereas electron screening might somewhat reduce this. Such a reduction in multiple scattering would destroy the agreement with the high pressure points in fig. 3, but these are also quite sensitive to the range-energy relations assumed, which are themselves somewhat uncertain. However, in the most extreme case where the multiple scattering is assumed to be negligible, $W_Z$ is increased by only 20 % at 20 mm-Hg, 7 % at 11 mm-Hg, and even less at lower pressures, so that this is not a large source of error. The error from this source is, therefore, estimated as $\pm$ 0.3 % in $W_Z$. It should be noted that the most probable directions of the errors from charge-change statistics and multiple scattering are opposite; they would thus tend to cancel. Taking all of these effects into account increases the error on $W_Z$ to

$$W_Z = 2.2 \pm 0.4\ \%. \tag{14}$$

## 4. Nuclear Charge Distribution of Single Mass Fission Fragments

In order to interpret the result for $W_Z$, it is necessary to determine the dependence of $H\varrho$, or equivalently of $\bar{e}$, on $Z$. If we take

$$\bar{e} \propto Z^n \tag{15}$$

differentiation gives

$$W_Z = \frac{\Delta\bar{e}}{\bar{e}} = n\frac{\Delta Z}{Z}. \tag{16}$$

Since $Z$ is known and $W_Z$ has been determined, $\Delta Z$, the width of the nuclear charge distribution of single mass fragments, can be calculated if $n$ is known.

In order to determine $n$, we assume that the dependence of $\bar{e}$ on $v$ and $Z$ is strictly separable, and that $\bar{e}$ is independent of $m$ (this last is essentially equivalent to assuming that outer electron configurations are isotope independent). From (1), (12) and (15)

$$\frac{H\varrho v^{-x}}{m} Z^n = \text{constant}, \tag{17}$$

where the constant is independent of mass, nuclear charge and velocity. The most probable value of $H\varrho$ for different mass fragments ($Sr^{91}$, $Zr^{97}$ and

$I^{133}$) was measured, and $n$ was then determined from (17). The results are given in table 1; the errors shown are from the uncertainty in the $H\varrho$ determinations only. The nuclear charges were calculated on the hypothesis of equal chain lengths [4]) using the Fermi empirical mass formula [12]). For the pressures of most concern here (10—20 mm-Hg), table 1 gives $n = 0.32$ from comparison of the two light fragments, and $n = 0.46$ from comparison of the light with the heavy fragments. The lack of agreement between the two types of determination is far outside of the limits of experimental error. It is very insensitive to the exponent of $v$ in (17) and relatively insensitive to assumptions about most probable nuclear charge vs. mass; it would not be changed by a possible explicit dependence of $\bar{\varepsilon}$ on mass. The only reasonable explanation is that (15) is not valid for large differences in $Z$. If this is the case, the determination of $n$ from the mass-91 vs. mass-97 data is appropriate for use in (16), since the difference in $Z$ is approximately the same as occurs in the nuclear charge distribution of single mass fragments. From this

TABLE 1

Most probable values of $H\varrho$ for mass-91, -97 and -133 fission fragments in helium gas at various pressures, and the corresponding values of $n$ that satisfy eq. (17).

| Pressure (mm-Hg) | $H\varrho$ (kG · cm) | | | $n$ | |
|---|---|---|---|---|---|
| | $Sr^{91}$ | $Zr^{97}$ | $I^{133}$ | 91 vs. 97 | 94 vs. 133 |
| 5 | 899 | 935 | 1099 | $0.37\pm0.05$ | $0.50\pm0.02$ |
| 10 | 880 | 917 | 1075 | $0.36\pm0.05$ | $0.51\pm0.02$ |
| 20 | 856 | 896 | 1065 | $0.29\pm0.04$ | $0.45\pm0.02$ |
| 30 | 845 | 885 | 1062 | $0.28\pm0.05$ | $0.43\pm0.02$ |

Gas was in magnet only; "94" in last column represents an average between 91 and 97.

point of view, table 1 gives $n = 0.32\pm0.03$. This is in good agreement with the Bohr and Lindhard [2]) estimate of $n = 1/3$. Inserting this value into (16), taking $W_Z$ from (14), and using $Z = 38$ for mass-97 fragments, gives $\Delta Z = 2.6\pm0.45$.

Two sources of error have not yet been considered. One is that due to the uncertainty in the difference between the most probable nuclear charges for masses 91 and 97. This enters in the determination of $n$, and $\Delta Z$ is approximately proportional to this difference. In the calculation, it was taken as 2.35 units, which is obtained either from the hypothesis of equal chain lengths using the Fermi formula, or from the hypothesis of unchanged charge distribution [4]). This introduces an uncertainty in $\Delta Z$ estimated from the calculation to be about $\pm$ 0.2.

Another source of error is the uncertainty in the exponent of $v$ in (17). According to the estimate from § 3.3, this introduces an uncertainty in $\Delta Z$

of less than $\pm 0.1$. To take these factors into account, the estimated uncertainty in $\Delta Z$ is increased to $\pm 0.5$.

One correction must still be applied to our result, namely the effect of the spread in masses being studied due to the variation in the number of neutrons per fission. This may be calculated as $(\partial Z/\partial m)\,\Delta m = 0.39\,\Delta m$. The width of the distribution of number of neutrons per fission is 2.5 [13]; when this is inserted for $\Delta m$, the contribution to the width is 1.0 charge units. Use of this correction gives our final result

$$\Delta Z = 2.4 \pm 0.5 \tag{18}$$

for the full width at half maximum of the nuclear charge distribution of mass-97 fission fragments. Although the data are somewhat less complete, it is clear from fig. 1 that approximately the same result would be obtained for mass-91 fragments.

The best estimate of the width from the treatment of shielded isotope data [4]) is $\Delta Z \approx 2.1$. This is in good agreement with the result obtained here; it is quite satisfying that two completely different approaches to the problem give similar results.

The agreement with theoretical predictions is somewhat less satisfying. Fong's analysis of the statistical theory [14]) predicts $\Delta Z = 1.2$, while Present's calculation based on the nuclear dynamics of the fission process [15]) gives $\Delta Z = 1.7$. Certainly the first is too small; the latter is slightly outside of our limit of error. On the other hand, Brunton's attempt to explain the energy distribution of the fragments on the basis of the nuclear charge distributions [7]) gives $\Delta Z \approx 7$, which is definitely much too large. It is noteworthy that Brunton's theory was proposed after publication of the shielded isotope and gas sweeping results; he did not consider those data sufficiently convincing to contradict his theory. However, his objections would not apply to the method used here.

## 5. Performance and Applications of the Fission-Fragment Mass Separator

In addition to the work described above with helium gas, measurements were also made with hydrogen, air and argon. Hydrogen seemed to be slightly less favorable than helium, and air and argon were considerably worse. It thus seems that the performance with helium at about 20 mm-Hg pressure is about optimum for light fragments. With source and detector size, and windows optimized, this should give a resolution near mass 97 of about 3.3 %, which corresponds to about 4.5 mass units. While this falls somewhat short of what one might wish for, it is still very useful for a wide variety of experiments.

Among the experiments that have already been carried out are studies of equilibrium charge of fission fragments as a function of velocity, pressure and type of gas, measurements of the response of scintillators to fission fragments, and various other atomic physics studies. From measurement of the ratio of beta counting rates to fission fragment counting rate, the lengths of the various fission decay chains can be determined which in turn give the average nuclear charge distribution between the two fragments in fission. This quantity, which is very important in fission theory, is only very pooly known.

Mass identification problems may be resolved in a very simple manner with this separator. Additional masses of delayed neutron emitters could also be determined, and for the first time, the various ones could be separated and studied individually. By use of time-of-flight techniques, the neutron energies could be accurately determined.

This technique should open up many new possibilities in the study of decay chains. Prominent beta and gamma rays can be detected with greatly reduced background and their grow-in and decay can by followed. Short-lived isomers can be detected, identified and studied. It would seem to be quite interesting to investigate some of these possibilities.

It also seems quite probable that a separator based on these principles will find application in the newly developing field of heavy ion nuclear physics. The higher energies and lighter masses used in this field would reduce the resolution limitation from charge-change statistics, but the proportionality of $\bar{\varepsilon}$ to velocity would have to be investigated.

The authors are greatly indebted to A. Foner Cohen, C. D. Coley, L. R. Hall and S. S. Hale for help in various phases of the experiments, to A. Zucker for valuable discussion, to S. Bernstein for a critical review of the experiment, and to R. S. Livingston and A. M. Weinberg for their support and encouragement.

## References

1) K. T. Bainbridge, Experimental Nuclear Physics, edited by E. Segre (John Wiley and Sons, 1953)

2) N. Bohr and J. Lindhard, Mat. Fys. Medd. Dan. Vid. Selsk. **28** (1954) no. 7

3) N. O. Lassen, Phys. Rev. **69** (1946) 137

4) L. E. Glendenin, C. D. Coryell and R. R. Edwards, Radiochemical Studies: The Fission Products, edited by C. D. Coryell and N. Sugarmann (McGraw-Hill Book Company, New York, 1951) paper 52, based on Clinton Laboratories Memorandum CL-LEG-1 (July 25, 1946) and unpublished data

5) A. C. Pappas, Technical Report No. 63, Laboratory for Nuclear Science and Engineering, Mass. Inst. of Tech. (1953) (unpublished)

6) T. J. Kennett and H. G. Thode, Phys. Rev. **103** (1956) 323

7) D. C. Brunton, Phys. Rev. **76** (1949) 1798

8) B. L. Cohen, A. Foner Cohen and C. D. Coley, Phys. Rev. **104** (1956) 1046
9) C. B. Fulmer and B. L. Cohen, Phys. Rev. **109** (1958) 94
10) N. F. Mott and H. S. W. Massey, Theory of Atomic Collisions (Clarendon Press, Oxford 1949) p. 278
11) C. B. Fulmer, Phys. Rev. **108** (1957) 1113
12) E. Fermi, Lectures on Nuclear Physics, edited by Orear, Rosenfeld and Schluter (University of Chicago Press, 1950)
13) Diven, Martin, Taschek and Terrell, Phys. Rev. **101** (1956) 2011
14) P. Fong, Phys. Rev. **102** (1956) 434
15) R D. Present, Phys. Rev. **72** (1947) 7

*Nuclear Physics* **6** (1958) 561—574; © *North-Holland Publishing Co., Amsterdam*
Not to be reproduced by photoprint or microfilm without written permission from the publisher

# INVESTIGATION OF NUCLEAR ISOMERISM IN $Hf^{180m}$

V. S. GVOZDEV, L. I. RUSINOV, YU. I. FILIMONOV and YU. L. KHAZOV
*Physico-Technical Institute of the USSR Academy of Sciences, Leningrad*

Received 29 October 1957

**Abstract:** The coefficient of internal conversion of the 57.6 keV transition in the L-shell of $Hf^{180m}$ was measured and found to be $\alpha_L = 0.33 \pm 0.10$. The $\gamma$-transition is shown to be of the E1 type. A 501.2 keV $\gamma$-transition has been detected; measurements of the internal conversion coefficient yield $\alpha_K = 0.035 \pm 0.014$. The 501.2 keV $\gamma$-transition is of the E3 type. The level with an excitation energy 1 142.9 keV was found to possess a spin 9 and negative parity. The experimental lifetimes for the 57.6 keV and 501.2 keV $\gamma$-transitions exceed those predicted by the single particle model by respectively $10^{14}$ and $10^9$ times. This large discrepancy is due to the high forbiddenness of the $\gamma$-transitions with respect to the quantum number $K$.

Internal conversion coefficients have also been measured for $\gamma$-transitions of 93.3 keV, 216 keV, 332.4 keV and 443.6 keV energy. The transitions were all found to be of the E2 type. The cross section for production of $Hf^{180m}$ in the (n, $\gamma$) reaction has been determined and found to equal $\sigma = 0.18 \pm 0.07$ barns.

## 1. Introduction

The $Hf^{180}$ nucleus has a rotational level system with excitation energies at 93.3 keV, 309.3 keV, 641.7 keV and 1 085.3 keV and spins of $0^+$ (ground state), $2^+$, $4^+$, $6^+$ and $8^+$.

The 93.3 keV excited level has been detected in Coulomb excitation experiments in which either $\alpha$-particles [1]) or protons [2]) were employed.

According to the data obtained in the second of these two investigations (in which separated isotopes were used) the K shell internal conversion coefficient of this $\gamma$-transition is 1.0 which corresponds to an E2 transition. The lifetime of the 93.3 keV excited state [3]) was found to be smaller than that predicted by the single-particle model [4]) by approximately 100 times and this likewise confirms the collective nature of this level.

Investigation of the internal conversion electron spectrum and of the relation between the intensities of unconverted $\gamma$-rays [5]) indicates the presence of 4 E2 transitions in the $Hf^{180m}$ decay scheme.

A metastable level with an energy of 1 142.9 keV and half life of 5.5 hours lies above the 1 085.3 keV excited level. The transition from the metastable level to the 1 085.3 keV excited level ($E_\gamma = 57.6$ keV) has been identified on basis of lifetime and internal conversion coefficient data as an M3 transition [5]). However, there are facts which seem to indicate that this

assignment is wrong since the 57.6 keV transition is highly $K$-forbidden. The necessity of more precise determinations of the multipolarity of this transition was mentioned in ref. [6]).

In the present paper the internal conversion electron and $\gamma$-ray spectra of $Hf^{180m}$ were investigated with the purpose of determining the multipolarity of the 57.6 keV $\gamma$-transition. Some preliminary results have been published previously [7]).

## 2. Experimental Method

### 2.1. $\beta$-SPECTROMETER

A $\beta$-spectrometer with $\pi\sqrt{2}$ electron focusing and a resolving power of 0.3 % for the ThB-line was employed to measure the internal conversion electron spectrum.

Electrons were recorded with a G—M counter of 11 mm internal diameter; the entrance slit of the counter was 1 mm wide and directed along the counter axis. The window was covered with a collodian film of about 25 $\mu g/cm^2$ thickness.

To facilitate rapid change of the sources required for measurement of the spectra of short-lived isotopes, the spectrometer was supplied with a vacuum lock.

### 2.2. $\gamma$-SPECTROMETER

A NaI(Tl) crystal and FEU-29 photomultiplier were used to record $\gamma$-quanta. The amplitude analyzer contained 128 channels and permitted simultaneous measurement of the pulses in 32 channels. The block diagram of the apparatus contains the following parts:

1. A two-stage cathode follower.
2. Linear amplifier with gain of 50 and passband of about 4 megacycles.
3. Linear time selector possessing a risetime $(1 \div 2) \times 10^{-7}$ sec and a linear characteristic up to 100 volt; it was employed to block the circuit during a period required for transformation of the input pulse into a signal in the respective channel of the information block.
4. Block of linear transformation of the input pulse into a number of standard electric pulses; the mean resolving time of the block was 100 $\mu$sec.
5. Circuit of distribution of pulses in the channels of the recording device; it was a 32 channel coincidence circuit consisting of a matrix of 192 germanium diodes. By aid of this device the number of electron tubes in the analyser could be considerably reduced.
6. The information block was a 32 channel binary adding circuit consisting of cold cathode tubes of the MTX-90 type. The capacity of each channel was 16 383 pulses. Its resolving power was 1 000 c.p.s. Information was drawn off by an octupole system.

In the analyser under discussion "expansion" of the spectrum was performed in the time part of the circuit and this improved the linearity of the circuit. The resolution of the spectrometer was 9 % for the $Cs^{137}$ line.

### 2.3. PREPARATION OF SOURCES

The sources employed in the $\beta$-spectrometer measurements were prepared by evaportaing hafnium fluoride in vacuum. A natural mixture of hafnium isotopes was used in the measurements. An aluminium foil $4\mu$ thick was used as a backing of the sources. The source length was 15 mm, width 1 mm.

In order to avoid contamination of the source, the hafnium fluoride which was evaporated was mounted on the surface of a graphite prism in the inner part of which an incandescent tantalum wire was placed.

From 1 to 2 mg of powdered hafnium fluoride was used in the $\gamma$-ray spectrum measurements.

The sources were irradiated 18 hours with a flux of thermal neutrons.

## 3. Measurements

### 3.1. MEASUREMENT OF COEFFICIENT OF INTERNAL CONVERSION OF 57.6 keV TRANSITION IN L-SHELL

The conversion coefficient for this transition was measured by two independent methods. In the first method use was made of the fact that decay of the $Hf^{180m}$ nucleus proceeds in accord with a cascade scheme. Therefore the intensities of all transitions are equal. The internal conversion coefficient for the 57.6 keV transition can thus be determined by measuring the ratio of the electron conversion line intensity associated with this transition to that of some other transition in $Hf^{180m}$ for which the conversion coefficient has been measured. Only the conversion coefficient of the 93.3 keV transition is known at present [2]). This transition was therefore chosen for determination of the conversion coefficient of the 57.6 keV transition.

The spectrum of the conversion electrons from $Hf^{180m}$ was measured with the $\beta$-spectrometer from 20 to 50 keV. The thickness of the source used in these measurements was 0.2 mg/cm$^2$. The spectrum is shown in fig. 1. The ratio of the intensities of lines L 57.6 and K 93.3 were determined from this spectrum. Corrections were applied for self-absorption of the electrons in the source, absorption in the counter window, decay and energy interval. The corrected ratio of the line intensities was $0.58 \pm 0.14$. The conversion coefficient for the 57.6 keV transition was derived from this ratio and found to equal $\alpha_L = 0.18 \pm 0.05$.

The relative internal conversion coefficient for the 57.6 keV transition was also derived from the spectrum shown in fig. 1 and found to equal $(L_I + L_{II})/L_{III} \approx 4$.

To check the value of the conversion coefficient cited above it was measured by a different method. A natural mixture of hafnium isotopes contains the $Hf^{180}$ isotope. Irradiation of $Hf^{180}$ with slow neutrons yields $Hf^{181}$ in the (n, $\gamma$) reaction; the isotope changes into $Ta^{181}$ by $\beta$-decay ($T_{\frac{1}{2}} = 46$ days). The decay scheme of $Hf^{181}$ has been studied in great detail and the internal conversion coefficients for $\gamma$-transitions in $Ta^{181}$ have been measured with sufficient accuracy [8]). By simultaneously measuring the internal conversion electron spectrum and $\gamma$-ray spectrum of $Hf^{180m}$ and $Ta^{181}$ one may determine the internal conversion coefficients for $\gamma$-transitions in $Hf^{180m}$ providing that the internal conversion coefficients of the $Ta^{181}$ $\gamma$-transition are known.

For determination of the internal conversion coefficient of the 57.6 keV $\gamma$-transition in $Hf^{180m}$, the 133 keV $\gamma$-transition in $Ta^{181}$ was chosen. This transition is the most intense one in the $Hf^{181}$ decay scheme and has a large K-shell internal conversion coefficient $\alpha_K = 0.49$ [8]).

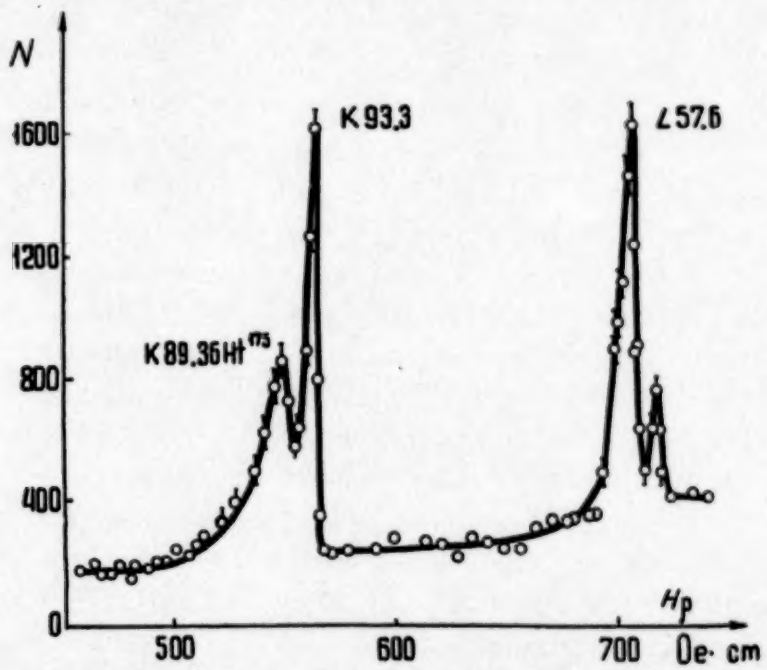


Fig 1. Section of internal conversion electron spectrum of $Hf^{175}$ and $Hf^{180m}$.

Moreover, the energy at the K-conversion electrons of this $\gamma$-transition ($E_e = 65.6$ keV) is close to that of the L-conversion electrons associated with the 57.6 keV $\gamma$-transition in $Hf^{180m}$ ($E_e \approx 47$ keV). This reduces the magnitude of the corrections which should be applied.

A section of the internal conversion electron spectrum, including the L-line of the 57.6 keV $\gamma$-transition in $Hf^{180m}$ and the K-line of the 133 keV $\gamma$-transition in $Ta^{181}$ is shown in fig. 2. The source employed in these measurements was 0.8 mg/cm$^2$ thick. The ratio of the K 133 keV and

L 57.6 keV line intensities was determined from the spectrum presented in the figure.

Corrections were applied to account for decay, energy interval, self absorption of electrons in the source and absorption in the counter window. A value $0.42 \pm 0.14$ was obtained for the coefficient $a$ defined by

$$N_{eL\,57.6} = aN_{eK133}. \tag{1}$$

The $\gamma$-ray spectrum measured with the scintillation spectrometer is shown in fig. 3. The first measurement (curve a in fig. 3) yielded the total spectrum for $Hf^{180m}$ and $Ta^{181}$. After decay of $Hf^{180m}$ the $Ta^{181}$ $\gamma$-ray spectrum was measured (curve b, fig. 3). The $Hf^{180m}$ $\gamma$-ray spectrum (curve c) was obtained by subtracting the $Ta^{181}$ spectrum from the $Hf^{180m} + Ta^{181}$ spectrum.

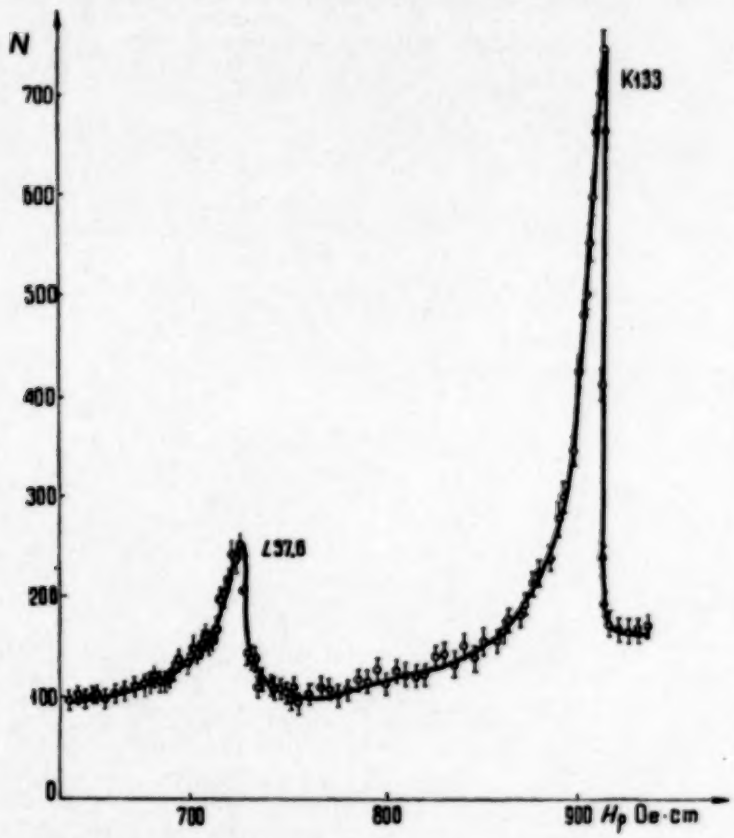


Fig. 2. Section of internal conversion electron spectrum of $Hf^{180m}$ and $Ta^{181}$.

A characteristic X-ray line associated with internal conversion of all E2 transitions in the K-shell of $Hf^{180m}$ is superimposed on the $\gamma$-line in the $Hf^{180m}$ spectrum. In order to take into account this circumstance the internal conversion coefficients for these transitions and the fluorescence yield in hafnium must be known. The K-shell internal conversion coefficients were taken from ref. [9]) and the L-shell coefficients from the tables presented in ref. [6]). Conversion in M, N and other shells was considered to comprise

0.3 of that in the L-shell. The fluorescence yield was assumed to equal 0.94 [6]).

The ratio of the intensity of the 57.6 keV line + X-ray line to that of the 133 keV line was derived from the $Ta^{181}$ and $Hf^{180m}$ $\gamma$-ray spectra:

$$N_{\gamma\,57.6}+\text{X-ray} = bN_{\gamma 133}. \qquad (2)$$

In determining this ratio the difference in the efficiency of the NaI crystal for 57.6 keV and 133 keV $\gamma$-rays was taken into account. 136.2 keV and 136.8 keV energy $\gamma$-rays from $Ta^{181}$ [8]) and 89.4 keV, 113.8 keV and 161.3 keV $\gamma$-rays from $Lu^{175}$ (which is produced by electron capture in $Hf^{175}$) are also confined in this part of the spectrum. A correction was introduced to account for these $\gamma$-rays. A value of $0.72\pm0.06$ was obtained for coefficient $b$. This value was determined simultaneously with that for $a$ in eq. (1). The coefficient for conversion of $\gamma$-rays in the L-shell was determined from eqs. (1) and (2): $\alpha_L = 0.47\pm0.18$.

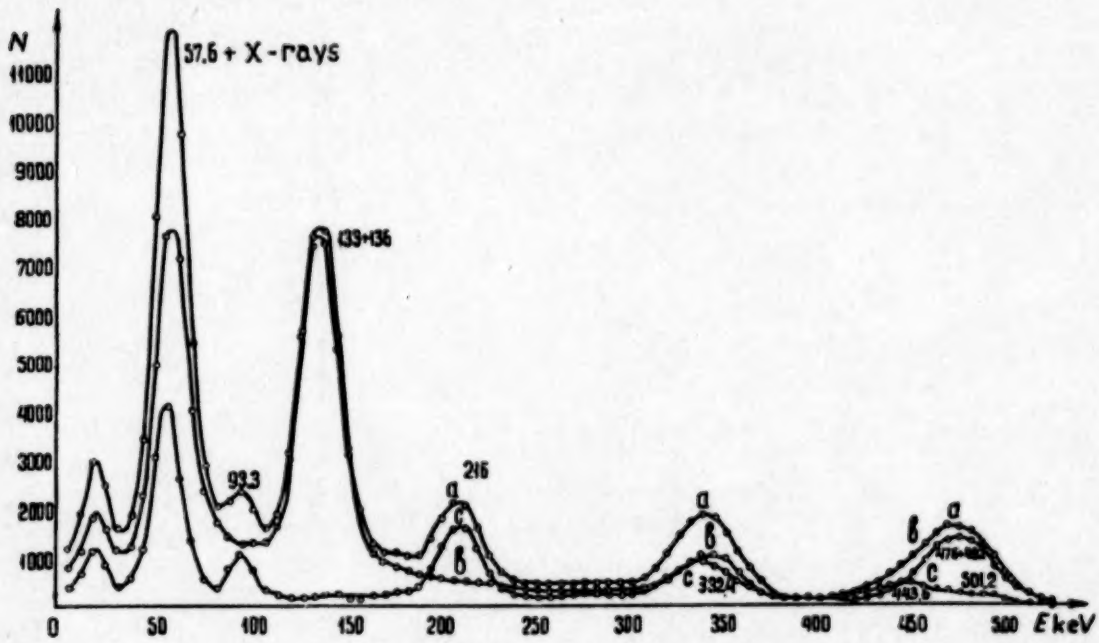


Fig. 3. $\gamma$-ray spectrum of $Hf^{180m}$ and $Ta^{181}$.

A mean value of $\alpha_L$ for this $\gamma$-transition will be presented after the additional experimental data presented below on the $Hf^{180m}$ decay scheme are taken into account.

### 3.2. THE 501.2 keV $\gamma$-TRANSITION

An experimental search of a $\gamma$-transition from the 1 142.9 keV excited level to the 641.7 keV excited level was carried out with the purpose of making a more detailed study of the $Hf^{180m}$ decay scheme. The energy of this $\gamma$-transition should be 501.2 keV.

A scintillation spectrometer with a NaI(Tl) crystal and a photomultiplier of the Khlebnikov design was used in the search of the 501.2 keV $\gamma$-transition. The diameter of the crystal was 29 mm and its height 11 mm. The diameter of the photocathode of the multiplier was 40 mm. Resolution of the spectrum with respect to the $Cs^{137}$ line was 8 %. The spectrum of the pulses from the photomultiplier was recorded by a 20 channel pulse height analyser with a resolving time of 10 $\mu$sec.

Special attention was directed to stability of the apparatus during prolonged operation and also to removal of shifts of the spectrum as a result of variation of the $\gamma$-ray source activity.

Since with aid of the scintillation spectrometer it is difficult to resolve the 476 keV and 482 keV $Ta^{181}$ and 443.6 keV and 501.2 keV $Hf^{180m}$ $\gamma$-lines

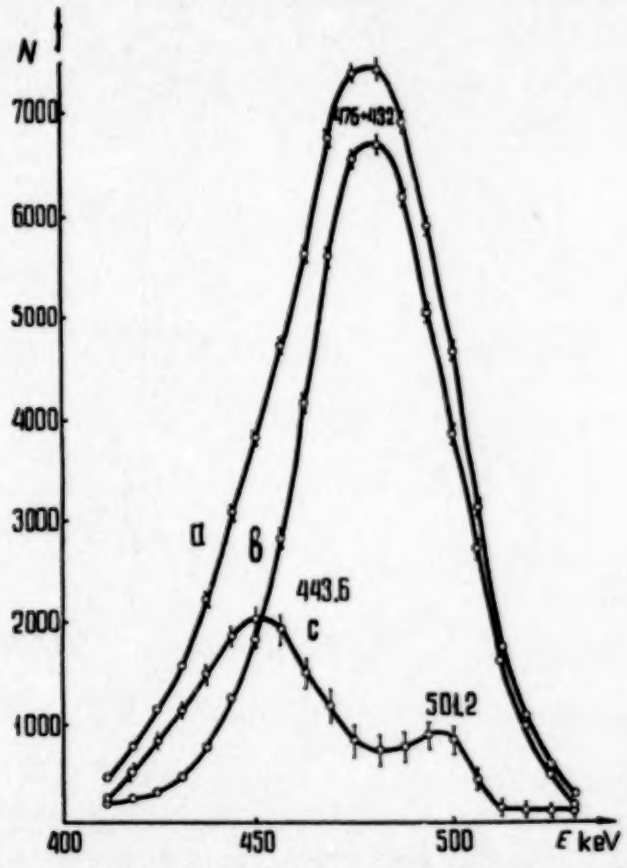


Fig. 4. Section of $\gamma$-ray spectrum of $Hf^{180m}$ and $Ta^{181}$.

from their mixed spectrum, measurements were made every hour during two $Hf^{180m}$ half life periods on the $\gamma$-spectrum of a sample containing $Hf^{180m}$ and $Hf^{181}$.

From the difference spectra (between the initial and each following measurement) the half life associated with each transition could be determined and the $Hf^{180m}$ spectrum could thus be separated from the $Ta^{181}$ $\gamma$-spectrum.

In order to check the stability of the spectrometer, each measurement was preceded by a measurement of the $\gamma$-ray spectrum of the reference ($Ta^{181}$).

The $\gamma$-spectrum measured between 415 and 535 keV is shown in fig. 4. Curve a in this fig. is the $\gamma$-spectrum of $Hf^{180m}$ and $Ta^{181}$. Curve b obtained after decay of $Hf^{180m}$ yields the $\gamma$-ray spectrum of $Hf^{180m}$. Curve c which is the difference between the first two curves is the spectrum of $Hf^{180m}$.

Besides the 443.6 keV $\gamma$-line, a line of about 500 keV energy was detected in the spectrum. The energy of these rays as well as the time variation of their intensity indicated that they were associated with a 501.2 keV transition.

In order to determine the relative intensity of this $\gamma$-transition with respect to the 57.6 keV transition it was sufficient to measure its intensity relative to the 443.6 keV $\gamma$-transition as the intensity of the latter is equal to that of the 57.6 keV $\gamma$-transition. In order to do this the internal con-

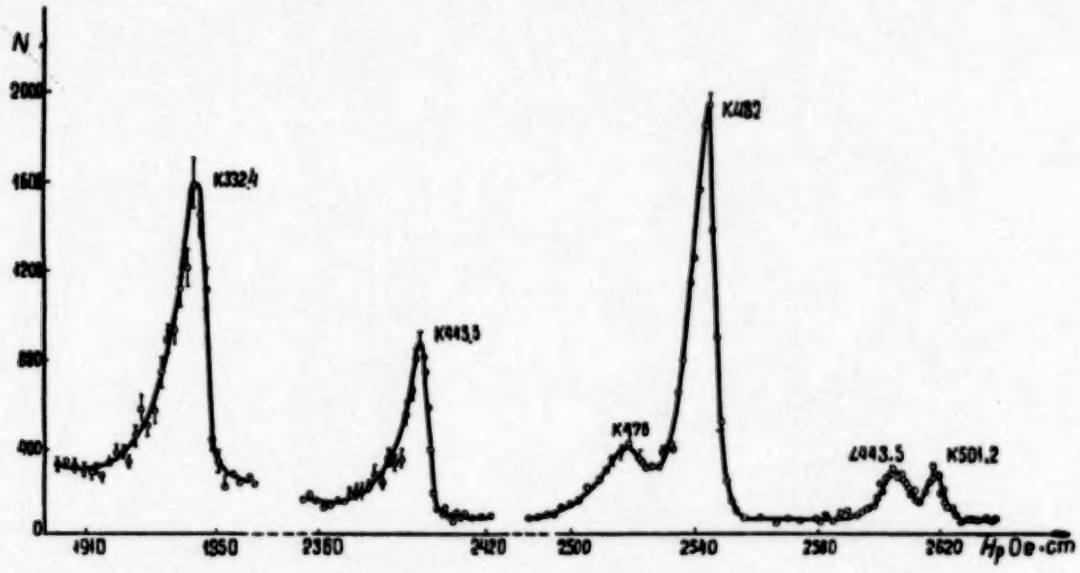


Fig. 5. Section of internal electron spectrum of $Hf^{180m}$ and $Ta^{181}$.

version coefficients for the 443.6 keV and 501.2 keV transitions should be known. Calculated values of the internal conversion coefficients [9, 6]) corresponding to E2 transitions were employed for the 443.6 keV transition.

The K-shell internal conversion coefficient for the 501.2 keV $\gamma$-transition was determined experimentally. For this purpose a part of the internal conversion electron spectrum of $Hf^{180m}$ and $Ta^{181}$ (fig. 5) was measured. The source was 2.0 mg/cm$^2$ thick. An internal conversion K-electron line associated with the 501.2 keV $\gamma$-transition was detected. After introduction of relevant corrections the ratio of the intensities of the K 501.2 $Hf^{180m}$ and K 482 $Ta^{181}$ lines was determined from the data of this spectrum. The ratio of the intensities of the 501.2 keV and 482 keV $\gamma$-lines was deter-

mined from the spectrum in fig. 4 simultaneously with the ratio of the intensities of the internal conversion electrons associated with these two transitions. Account was made of the existence of 476 keV $\gamma$-rays in the $Hf^{181}$ decay scheme and of 433 keV $\gamma$-rays in the $Hf^{175}$ decay scheme.

A correction was also applied to account for the difference in the efficiency of the NaI crystal for 482 keV and 501.2 keV $\gamma$-rays.

The internal conversion coefficient for the 501.2 keV transition in $Hf^{180m}$ was determined from the ratio of the intensities of the $\gamma$-rays and internal conversion electrons associated with the 501.2 keV and 482 keV transitions. A value $\alpha_K = 0.035 \pm 0.014$ was obtained. For the internal conversion coefficient of the 482 keV transition in $Ta^{181}$ the value 0.027 [8]) was accepted.

As will be seen from the following the 501.2 keV transition is of the E3 type.

The ratio of the intensities of the 501.2 keV and 443.6 keV $\gamma$-rays was determined from the data of fig. 4 after making the relevant corrections. With account of the internal conversion coefficients of these two transitions the value $0.15 \pm 0.05$ was obtained for the relative intensity of the 501.2 keV transition.

Due to the presence of the 501.2 keV $\gamma$-transition the intensity of the 57.6 keV $\gamma$-transition is lower than that of the other $\gamma$-transitions in $Hf^{180m}$. Therefore a correction must be introduced in the internal conversion coefficient of this $\gamma$-transition. The corrected internal conversion coefficient (mean weighted of the two measurements) was $0.33 \pm 0.10$.

### 3.3. MEASUREMENT OF INTERNAL CONVERSION COEFFICIENTS FOR 93.3 keV, 216 keV, 332.4 keV AND 443.6 keV $\gamma$-TRANSITIONS IN $Hf^{180m}$

The internal conversion coefficients for these $\gamma$-transitions were determined in the same way as that for the 501.2 keV $\gamma$-transition.

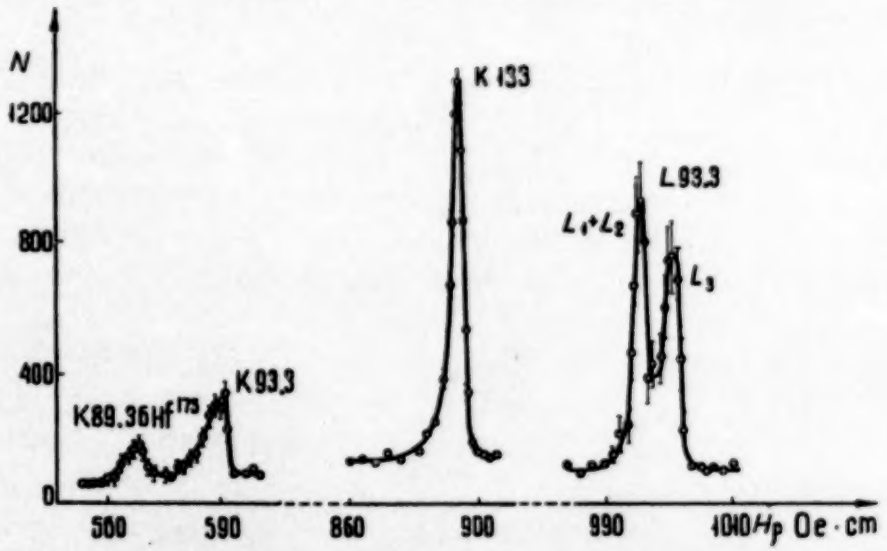


Fig. 6. Section of internal conversion electron spectrum of $Hf^{180m}$ and $Ta^{181}$.

For this purpose the total $\gamma$-ray spectrum of $Hf^{180m}$ and $Ta^{181}$ and the total internal conversion electron spectrum were measured. Separate intervals of the conversion electron spectrum were measured, sources of a definite thickness being used for each interval. The spectrum measured with a source 0.15 mg/cm² thick is shown in fig. 6; the spectrum obtained with a 0.56 mg/cm² source is shown in fig. 7.

The $\gamma$-ray spectrum is shown in fig 3.

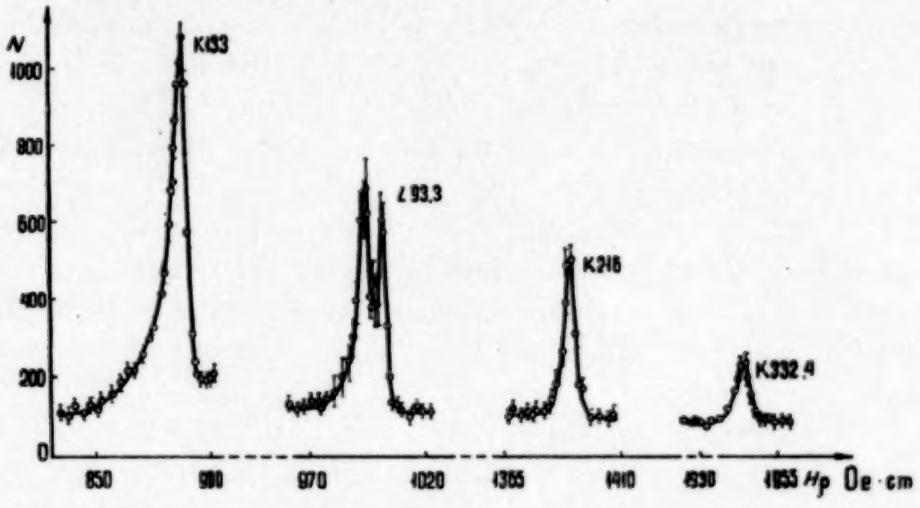


Fig. 7. Section of internal conversion electron spectrum of $Hf^{180m}$ and $Ta^{181}$.

### 3.4. DETERMINATION OF THE CROSS SECTION FOR PRODUCTION OF $Hf^{180m}$ IN THE (n, $\gamma$) REACTION

The results of measurement of the internal conversion electron and $\gamma$-ray spectra of $Hf^{180m}$ and $Ta^{181}$ permit one to determine the cross section for production of $Hf^{180m}$ in the (n, $\gamma$) reaction on $Hf^{179}$. The cross section for production of $Hf^{181}$ from $Hf^{180}$ in the (n, $\gamma$) reaction is known and equals $10\pm3$ barns [10]).

For determination of the cross section one must know the natural isotopic composition ($Hf^{179}$—13.8 %, $Hf^{180}$—35.4 %), irradiation time (18 hours), time between end of irradiation and beginning of measurements (8 hours), internal conversion coefficients for all $\gamma$-transitions in $Hf^{180m}$ and for those $\gamma$-transitions in $Ta^{181}$ which were chosen as references (133 keV and 482 keV) and also the intensities of these transitions in the decay scheme of the corresponding isotope.

The values of the internal conversion coefficients obtained in the present paper for the 57.6 keV and 501.2 keV $\gamma$-transitions in $Hf^{180m}$ were employed. For the remaining $\gamma$-transitions in $Hf^{180m}$ computed values [9, 6]) of the conversion coefficients were used. The data presented in ref. [8]) for the internal conversion coefficients and intensities of the 133 keV and 482 keV $\gamma$-transitions in $Ta^{181}$ were used. The cross section for production of $Hf^{180m}$

was calculated on basis of the $Hf^{180m}$ and $Ta^{181}$ internal conversion electron line intensities as well as on basis of the ratio of the $\gamma$-line intensities. A value of $0.18 \pm 0.07$ barns was obtained for $\sigma$ $Hf^{180m}$.

## 4. Discussion of Results

Results of measurement of the internal conversion coefficients for $\gamma$-transitions in $Hf^{180m}$ are collected in the table. For comparison, the computed values for conversion coefficients of E1, E2, E3, M1, M2, M3 transitions presented in ref. [9]) and [6]) are also given in the table.

TABLE

| Transition type | E1 | E2 | E3 | M1 | M2 | M3 | Experiment |
|---|---|---|---|---|---|---|---|
| $E_\gamma = 57.6$ keV | | | | | | | |
| $\alpha_L$ | 0.203 | 8.02 | 393 | 2.75 | 76.8 | 1591 | $0.33 \pm 0.10$ |
| $\frac{L_I + L_{II}}{L_{III}}$ | 3.1 | 1.26 | 1.98 | 300 | 8.6 | 1.51 | $\approx 4$ |
| Transition type | | | | | | | E1 |
| $E_\gamma = 93.3$ keV | | | | | | | |
| $\alpha_K$ | 0.338 | 1.0 | 2.14 | 3.98 | 33.1 | 115 | $1.3 \pm 0.4$ |
| $\alpha_L$ | 0.0572 | 1.59 | 24.4 | 0.661 | 9.59 | 120.2 | $2.7 \pm 0.8$ |
| $\alpha_K/\alpha_L$ | 5.9 | 0.63 | 0.088 | 6.02 | 3.46 | 0.96 | $0.48 \pm 0.15$ |
| $\frac{L_I + L_{II}}{L_{III}}$ | 3.77 | 1.4 | 2.21 | 219 | 12.2 | 2.31 | $1.4 \pm 0.3$ |
| Transition type | | | | | | | E2 |
| $E_\gamma = 216$ keV | | | | | | | |
| $\alpha_K$ | 0.0394 | 0·132 | 0.407 | 0.38 | 1.78 | 6.3 | $0.15 \pm 0.05$ |
| Transition type | | | | | | | E2 |
| $E_\gamma = 332.4$ keV | | | | | | | |
| $\alpha_K$ | 0.014 | 0.0417 | 0.119 | 0.118 | 0.432 | 1.29 | $0.055 \pm 0.014$ |
| Transition type | | | | | | | E2 |
| $E_\gamma = 443.6$ keV | | | | | | | |
| $\alpha_K$ | 0.0073 | 0.0204 | 0.0525 | 0.0537 | 0.178 | 0.452 | $0.026 \pm 0.007$ |
| $\alpha_L$ | $9.52 \times 10^{-4}$ | 0.0049 | 0.0144 | 0.00878 | 0.0306 | 0.0875 | $0.0063 \pm 0.0016$ |
| $\alpha_K/\alpha_L$ | 7.67 | 4.16 | 3.65 | 6.12 | 5.82 | 5.17 | $4.1 \pm 1.3$ |
| Transition type | | | | | | | E2 |
| $E_\gamma = 501.2$ keV | | | | | | | |
| $\alpha_K$ | 0.00543 | 0.0144 | 0.0372 | 0.0398 | 0.119 | 0.295 | $0.035 \pm 0.014$ |
| Transition type | | | | | | | E3 |

Comparison of the experimental and calculated internal conversion coefficients for 93.3 keV, 216 keV, 332.4 keV and 443.6 keV $\gamma$-transitions indicates that the transitions are of the E2 type. These experimental data confirm the rotational nature of the energy levels in the $Hf^{180}$ nucleus.

Comparison of the experimental and calculated internal conversion coefficients for the 57.6 keV $\gamma$-transition indicate that this transition is of the E1 type.

Thus the 1 142.9 keV excited level should have a spin of 7 or 9 and negative parity.

Judging from the magnitude of the internal conversion coefficient, the 501.2 keV transition should be either M1 or E3. A M1 type transition does not satisfy the parity selection rule as the parities of the 1 142.9 keV and 641.7 keV excited levels are different.

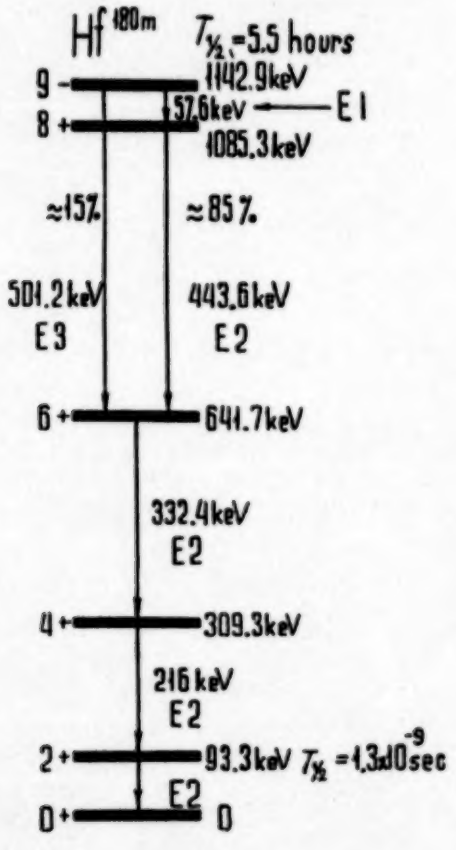


Fig. 8. Decay scheme of $Hf^{180m}$.

Thus the 501.2 keV transition should be of the E3 type and a spin 9 should be assigned to the 1142.9 keV excited level.

The $Hf^{180m}$ decay scheme which takes into account the new data is shown in fig. 8.

After completion of this work some results pertaining to the isomerism of $Hf^{180m}$ were published [11]). The data on the 57.6 keV and 501.2 keV transitions are identical with the results obtained in the present paper.

The lifetime calculated from formulae for single-particle transitions [4]) is of the order of $10^{-12}$ sec for the 57.6 keV dipole electric transition. This value is about $10^{16}$ times smaller than the experimentally observed lifetime of the $Hf^{180m}$ nucleus. The calculated lifetime for an octupole electric transition of 501.2 keV energy is of the order of $10^{-4}$ sec; this differs from the experimental value by $10^{9}$ times.

A possible explanation of the large discrepancy between the calculated and experimental lifetimes is that the $Hf^{180m}$ decay scheme has not been sufficiently investigated. Thus a weakly excited level with a half life of 5.5 hours may be located above the 1 142.9 keV excited level and the 57.6 and 501.2 keV $\gamma$-transitions may be in cascade with a $\gamma$-transition from the weakly excited level to the 1142.9 keV level. In this case the half-life of the 1 142.9 keV excited level would be less and the discrepancy between the computed and experimental lifetime values would become smaller.

The transition from the weakly excited level to the 1 142.9 keV level should be strongly converted. Preliminary experiments were carried out in an effort to detect this transition. The search was carried out by recording $\gamma$-rays with a proportional counter and pulse height analyser and by measuring internal conversion electrons with a $\beta$-spectrometer. However, neither $\gamma$-rays nor conversion electrons which could be attributed to the unknown transition were detected.

Comparison of the experimental $\tau_\gamma$ and theoretical $\tau_\gamma$ for a large number of isomeric nuclei yields a value of $\tau_{\gamma\,\mathrm{exp}}/\tau_{\gamma\,\mathrm{theor}}$, which does not exceed $10^{3}$ [12]). For $Hf^{180m}$ the ratio $\tau_{\gamma\,\mathrm{exp}}/\tau_{\gamma\,\mathrm{theor}}$ is anomalously large and this indicates some additional prohibition with respect to the probabilities of the 57.6 keV and 501.2 keV isomeric transitions. This additional prohibition is related to the circumstance that the 1 142.9 keV and spin $9^-$ excited level is probably the first level of a new system of rotational levels. Transitions from this level with a quantum number $K = 9$ to levels with spins $8^+$ or $6^+$ and quantum number $K = 0$, involve large changes of the quantum number $K(\Delta K = 9)$. For the 57.6 keV $\gamma$-transition the degree of forbiddenness is $\nu = \Delta K - l = 9 - 1 = 8$. For the 501.2 keV $\gamma$-transition the degree of forbiddenness is $\nu = 6$. A consequence of such a high degree of forbiddenness of these $\gamma$-transitions is the anomalously large lifetime of the 1 142.9 keV excited level in $Hf^{180m}$.

In conclusion the authors take the opportunity to express their sincere thanks to L. A. Sliv for discussion of this work and to I. A. Kondurov, E. P. Mazets, V. B. Chernyaev for help in the work.

*Note added in proof:* The life-time of the $Hf^{180m}$ E1 transition with $E_\gamma = 57.6$ keV has been calculated by V. V. Anisovich, using perturbation theory, and found to be $\approx 10^3$ h (JETP, in print).

## References

1) N. P. Heydenburg and G. M. Temmer, Phys. Rev. **100** (1955) 150
2) C. McClelland, H. Mark and C. Goodman, Phys. Rev. **97** (1955) 119
3) A. W. Sunyar, Phys. Rev. **95** (1954) 626
4) S. A. Moszkowsky, Phys. Rev. **89** (1953) 474
5) J. W. Mihelich, G. Scharff-Goldhaber and M. McKeown, Phys. Rev. **94** (1954) 794
6) K. Siegbahn, Beta- and Gamma-Ray Spectroscopy (Amsterdam, 1955)
7) V. S. Gvozdev and L. I. Rusinov, Doklady AN SSSR **112** (1957) 401
8) F. Boehm and P. Marmier, Phys. Rev. **103** (1956) 342
9) L. A. Sliv and I. M. Band, Tables of Coefficients of Internal Conversion of $\gamma$-Radiation (Moscow-Leningrad, 1956) p. 1 (K-Shell)
10) Donald J. Hughes, Pile Neutron Research (Cambridge, Mass. 1953)
11) G. Scharff-Goldhaber, M. McKeown and J. W. Mihelich, Bull. Am. Phys. Soc. **1** (1956) 206
12) E. P. Mazets and L. I. Rusinov, Doklady AN SSSR **101** (1955) 253

*Nuclear Physics* **6** (1958) 575—584; © *North-Holland Publishing Co., Amsterdam*
Not to be reproduced by photoprint or microfilm without written permission from the publisher

# DEUTERON STRIPPING ON SPHEROIDAL NUCLEI

J. SAWICKI
*Institute of Theoretical Physics, Warsaw University* †

Received 15 December 1957

**Abstract:** An explanation is proposed of the effect of mixtures of two or more $l$-values in (d, p) stripping angular distributions from the point of view of the spheroidal nuclear model. S. G. Nilsson's wave functions are employed to represent the captured neutron. General properties of the cross-sections and selection rules are discussed. Qualitative agreement is obtained in a number of examples. Angular $\gamma-$p correlations are discussed of $\gamma$-rays following (d, p) stripping reactions. Polarization of the outgoing protons is calculated.

## 1. Introduction

The deuteron stripping effect is well known as one of the best tools of the modern nuclear spectroscopy. Hitherto the analysis of this effect has been confined to the application of the nuclear shell model, either or taking into account the configuration mixing of different shells. In the latter case only perturbation methods have been used. The collective aspects were taken into account only by Satchler [1]) who discussed reduced widths for capture to vibrational and rotational states using the theory of perturbations. The configuration mixing effect (two or more $l$-values effective in stripping angular distributions) has been explained for medium heavy and light nuclei in terms of perturbation methods using two-body $L-S$ or intermediate couplings [see Bethe and Butler [4]), Okai and Sano [3]); for relative reduced widths Auerbach and French [2]); for angular correlations with $\gamma$'s following stripping or pick-up reactions Satchler [5]), Hittmair [6])]. The perturbation theory of the configuration mixing coefficients seems neither consistent with the basic (shell) model assumed nor does its validity seem obvious.

The best known target nuclei are rather strongly deformed as they belong to the 8—20 region. It seems, therefore, that the spheroidal nuclear model, which is able to represent the shell configuration mixing consistently, would be suitable to explain the effects in question. The directly calculated mixing coefficients are perfectly consistent with those automatically following from this model (mixing effects of the pairing energy type being neglected). S. G. Nilsson [7]) has worked out energy spectra and one-particle wave functions for a simple spheroidal harmonic oscillator well. In the

† Present address: Palmer Physical Laboratory, Princeton University.

present paper S. G. Nilsson's wave functions are employed, but the modification for the perhaps more realistic case of Gottfried's [8]) ellipsoidal model is straightforward.

In § 2.1 general expressions for the angular distributions and the relative differential cross-sections for transitions to different final states are given. Numerical examples are discussed in § 2.2. In § 3 angular correlations with $\gamma$-rays following a stripping reaction are discussed. In § 4 a formula is given for the polarization of the outgoing protons.

## 2. Angular Distributions

### 2.1. GENERAL THEORY

Let the symmetrized wave function of the ground state of the target nucleus of spin $I_1$ [its projection on the (intrinsic nuclear) symmetry axis $z'$ is $K_1$, its projection on the $z$-axis $M_1$] be in the usual notation [7])

$$\Psi_1 = \sqrt{\frac{2I_1+1}{16\pi^2}}\,\phi_0(\xi)\,[\chi_{\Omega_1}(i')\mathscr{D}^{I_1}_{M_1K_1}(\theta_1)+(-)^{I_1-\Sigma j_1}\chi_{-\Omega_1}(i')\mathscr{D}^{I_1}_{M_1,-K_1}(\theta_1)] \quad (1)$$

where $\phi_0(\xi)$ is the spinless core wave-function of the vibrational ground state, $\chi_{\Omega_1}(i')$ the wave-function of the particles outside the core, being in general a product of S. G. Nilsson's one-particle solutions; $i'$ denotes the coordinates of these particles in the intrinsic system; $\mathscr{D}^{I}_{MK}(\theta_1)$ are the usual rotational matrices depending on the Eulerian angles $\theta_1$. Let us consider a (d, p) reaction for definiteness. Let the function of the final nucleus of spin $I_f$ and projections $K_f$ and $M_f$ be

$$\Psi_f = \sqrt{\frac{2I_f+1}{16\pi^2}}\,\phi_0(\xi)[\chi_{\Omega_f}(i',\ n'_f)\mathscr{D}^{I_f}_{M_fK_f}(\theta_1)+(-)^{I_f-\Sigma(j_1+j_n)}\chi_{-\Omega_f}(i',n'_f)\mathscr{D}^{I_f}_{M_f,-K_f}(\theta_1)]; \quad (2)$$

$n'_f$ denotes all the coordinates of the captured neutron.

The parity and $j_z = l_z+s_z$ are the operators commuting with the total Hamiltonian; the $j_z$ quantum number is denoted, as usual, by $\Omega$. No vibrational excited states are considered. Let us now make the usual simplifying assumption of neglecting antisymmetrization of protons in target and deuteron, and further assume

$$\chi_{\Omega_f}(i',\ n'_f) \equiv \chi_{\Omega_1}(i')\chi_{\Omega_n}(n'_f).$$

The $\Omega$-value of the captured neutron $\Omega_n = \Omega_f-\Omega_1$. Using the orthonormality of $\phi_0$ and $\chi_\Omega$ one can obtain for the overlap integral

$$\int d\xi di'\,\Psi_f^*\,\Psi_1 = \sqrt{\frac{(2I_1+1)(2I_f+1)}{(16\pi^2)^2}}\,\{\chi^*_{\Omega_n}(n'_f)\mathscr{D}^{I_f*}_{M_fK_f}(\theta_1)\mathscr{D}^{I_1}_{M_1K_1}(\theta_1)$$
$$+(-)^{I_f-I_1-\Sigma j}\chi^*_{-\Omega_n}(n'_f)\mathscr{D}^{I_f*}_{M_f,-K_f}(\theta_1)\mathscr{D}^{I_1}_{M_1,-K_1}(\theta)\}. \quad (3)$$

In S. G. Nilsson's $(l, \Lambda)$-representation the symmetrization operator $(-)^{I_f-I_i-\Sigma j}$ can be symbolically rewritten as $(-)^{I_f-I_i-\frac{1}{2}+l}$, $l$ being the neutron orbital angular momentum.

For the sake of simplicity we shall first calculate the Butler type (d, p) matrix element, i.e. we shall replace the final state proton wave by $e^{i\mathbf{k}_p\cdot\mathbf{r}_p}\chi_{\mu_p}(\sigma_p)$ and the incident deuteron wave by $e^{i\mathbf{k}_d\cdot\mathbf{r}_d}S_{\mu_d}(\sigma_n,\sigma_p)\varphi(|\mathbf{r}_n-\mathbf{r}_p|)$, $\chi$ and $S$ being the usual spin functions; $\varphi(\varrho)$ is the deuteron internal function. The "distorted wave" generalization is straightforward in the zero range approximation. The matrix element is then in the usual notation

$$I^{K_1}_{\Omega_n}(M_1,\ \mu_d;\ M_f,\ \mu_p)$$
$$= \int d\xi d\mathbf{i}' \int d\theta_1 \int_{r_n\geq r_0} d\mathbf{r}_p d\mathbf{r}_n d\sigma_p d\sigma_n \Psi_f^* e^{-i\mathbf{k}_p\cdot\mathbf{r}'_p}\chi^*_{\mu_p}(\sigma_p)V_{np}(|\mathbf{r}_n-\mathbf{r}_p|) \quad (4)$$
$$\times\ \Psi_1 e^{i\mathbf{k}_d\cdot\mathbf{r}_d}S_{\mu_d}(\sigma_n,\ \sigma_p)\varphi(|\mathbf{r}_n-\mathbf{r}_p|),$$

$V_{np}$ being the usual transition operator and $r_0$ the Butler nuclear radius. We can now transform the captured neutron function from the intrinsic nuclear system to the fixed system:

$$\chi_{\Omega_n}(n'_f) \to \chi_{\Omega_n}(n_f)$$
$$= \sum_{l,\Sigma} A_{l,\Omega_n-\Sigma}\ R_{Nl}(r_n) \sum_{j\mu} (l,\ \tfrac{1}{2};\ \Omega_n-\Sigma,\ \Sigma|j\Omega_n)\mathscr{Y}^{j*}_{\mu\Omega_n}(\theta_1)\mathscr{Y}^{\mu}_{jl\frac{1}{2}}(\Omega_n,\ \sigma_n). \quad (5)$$

If $\Gamma=M\omega_0(\delta)/\hbar$ (see ref. [7]), we have $R_{Nl}(r_n)=\mathscr{N}_{Nl}r_n^{\,l}\,e^{-\frac{1}{2}\Gamma r_n^2}L_n^{l+\frac{1}{2}}(\Gamma r_n^2)$ (cf. ref. [22]), p. 1662); the principal quantum number $N=2n+l$ is, as in ref. [7]), practically a constant of the motion (we should write $\chi_{\Omega_n N}(n'_f)$ rather than $\chi_{\Omega_n}(n'_f)$ and sum over $N$). It is unlikely that more than one $N$, in general, contribute for a given $\Omega_n$. $(j_1j_2;\ m_1m_2/jm)$ denotes a vector addition coefficient and $\mathscr{Y}^m_{jls}$ a usual $j$-eigenfunction. The final result becomes

$$I^{K_1}_{\Omega_n}(M_1\mu_d;\ M_f\mu_p) \propto (\tfrac{1}{2}\tfrac{1}{2};\ \mu_p\mu_d-\mu_p/1\mu_d)\sum\{lj\mu\}\sum_{\Sigma}$$
$$\times (l\tfrac{1}{2};\ \mu-\mu_d+\mu_p,\ \mu_d-\mu_p|j\mu)(I_1j;\ M_1\mu|I_fM_f)B_{I_f}(lj;\ \Sigma|\Omega_nK_1) \quad (6)$$
$$\times\ S(l\mu-\mu_d+\mu_p)\int d\varrho\, e^{i\mathbf{K}\cdot\varrho}V_{np}(\varrho)\varphi(\varrho)$$

where $\mathbf{K}=\frac{1}{2}\mathbf{k}_d-\mathbf{k}_p$, $S(l,\ m)=\int_{r_n\geq r_0}d\mathbf{r}_n\ e^{i\mathbf{x}\cdot\mathbf{r}_n}R_{Nl}(r_n)\,Y^*_{lm}(\omega_n)$, $\mathbf{x}=\mathbf{k}_d-(M_1/M_f)\mathbf{k}_p$, $M_1$ and $M_f$ being the masses of the initial and final nuclei;

$$B_{I_f}(lj;\Sigma|\Omega_nK_1)=\{(l\tfrac{1}{2};\ \Omega_n-\Sigma\Sigma|j\Omega_n)(I_1j;\ K_1\Omega_n|I_fK_f)A_{l\Omega_n-\Sigma}$$
$$+(-)^{I_f-I_i-\frac{1}{2}+l}(l\tfrac{1}{2};\ -\Omega_n+\Sigma-\Sigma|j-\Omega_n)(I_1j;\ -K_1-\Omega_n|I_f-K_f) \quad (7)$$
$$\times\ A_{l-\Omega_n+\Sigma}\}=2A_{l\Omega_n-\Sigma}(l\tfrac{1}{2};\ \Omega_n-\Sigma\Sigma|j\Omega_n)(I_1j;\ K_1\Omega_n|I_fK_f).$$

Then the differential cross-section can be shown to be †

$$\sigma(\theta) \propto \sum_{lj} (2l+1)^{-1} P_{I_f}(lj|\Omega_n K_i) \sum_m |S(lm)|^2 G(K),$$
$$P_{I_f}(lj|\Omega_n K_i) = \sum_{\Sigma\Sigma'} B_{I_f}(lj;\ \Sigma|\Omega_n K_i) B_{I_f}(lj;\ \Sigma'|\Omega_n K_i). \tag{8}$$

If now the quantization axis is chosen along the vector $\mathbf{x}$, we get the selection rule $\mu = \mu_d - \mu_p$. Now $S(l,\ m) = \delta_{0m}(2l+1)^{\frac{1}{2}} i^l \mathscr{R}_{Nl}(x)$, where $\mathscr{R}_{Nl}(x) = \int_{r_0}^{\infty} j_l(|\mathbf{x}|r) R_{Nl}(r) r^2 \mathrm{d}r$, $j_l(x)$ being a spherical Bessel function. Now we have

$$\sigma(\theta) \propto \sum_{lj} P_{I_f}(lj|\Omega_n K_i) |\mathscr{R}_{Nl}(x)|^2 G(K). \tag{8a}$$

If $\varphi(\varrho)$ be a Hulthén function of the parameters $\alpha_d$ and $\beta_d$, we have $G(K) = [1-(K^2+\alpha_d^2)/(K+\beta_d^2)]$ (see e.g. Tobocman [9]). The factor $G(K)$ does not appear in the zero range approximation (becomes unity for $\beta_d \to \infty$). The functions $|\mathscr{R}_{Nl}(x)|^2$ give the characteristic stripping peaks of angular distributions for various $l$. Different $l$ contribute incoherently to $\sigma(\theta)$ as in the usual theory.

An alternative derivation of eqs. (6)–(8) can be easily performed by using the intrinsic nucleai system rather than the fixed one (i.e. by transforming all the functions excepting $\Psi_i$ and $\Psi_f$ to the intrinsic system).

We observe the following selection rules: $K_f = K_i + \Omega_n$ and $j \geqq |\Omega_n|$ together with $|I_f - I_i| \leqq j \leqq I_f + I_i$. If one $I_i$ or $I_f$ is zero, then only one value of $l$ contributes i.e. we have no mixing effect. This is the case for even-target nuclei with $I_i = K_i = \Omega_i = 0$ or for even-final nuclei in their ground states with $I_f = K_f = \Omega_f = 0$ (i.e. $\Omega_n = -\Omega_i$). It should be noted here that the known (d, p) reactions with two or more $l$'s effective involve odd mass target nuclei and odd final nuclei (or even in excited states) in agreement with the selection rule stated above. The examples are ${}_{12}Mg^{25}(d, p)_{12}Mg^{26}$ (first excited state), ${}_{13}Al^{27}(d, p)_{13}Al^{28}$ (third excited state), ${}_{15}P^{31}(d, p)_{15}P^{32}$, ${}_{17}Cl^{35}(d, p)_{17}Cl^{36}$, ${}_{19}K^{41}(d, p)_{19}K^{42}$, ${}_{21}Sc^{45}(d, p)_{21}Sc^{46}$.

The mixing coefficients $P_{I_f}(lj|\Omega_n K_i)$ depend on the particular spheroidal model properties assumed via the $A_{lA}$ coefficients being rather sensitive functions of the deformation parameter $\delta$, particularly around $A \approx 25$. These coefficients and the geometrical factors appearing in $P$ should, in general, explain why only one $l$ contributes effectively in one case and more $l$'s in another case. In particular, they should predict why a transition takes place to one final state with purely one $l$ (or "almost purely" one $l$),

† In the $j$-representation one should have

$$P_{I_f}(lj|\Omega_n K_i) = 4(I_i j;\ K_i \Omega_n | I_f K_f)^2 C_{jl}(\Omega_n)^2 \underset{(I_i, I_f \neq 0)}{=} 4\left(\frac{2I_f+1}{2I_i+1}\right) \beta_{jl}(K_i \Omega_n)^2,$$

where $C_{jl}(\Omega_n) = \Sigma_\Sigma (l\tfrac{1}{2};\ \Omega_n - \Sigma\Sigma | j\Omega_n) A_{l\Omega_n - \Sigma}$; $\beta_{jl}(K_i, \Omega_n)$ is a reduced width provided $C$'s and $A$'s are properly normalized ($\Sigma_{lA} A^2_{lA} = 1$).

while another final state of the same nucleus for the same reaction involves two $l$'s or more. Because of the sensitiveness of $A$'s to $\delta$ for $A \approx 25$, the $P$-coefficients might provide a useful tool of examining the spheroidal model parameters.

The relative values of $\sigma(\theta)$'s corresponding to different final states "1" and "2" for the same (d, p) reaction at their respective maximum values (branching ratios) can be written as

$$\frac{(\mathrm{d}\sigma_1)_{\max}}{(\mathrm{d}\sigma_2)_{\max}} = \frac{(k_\mathrm{p})_1}{(k_\mathrm{p})_2} \frac{\sum_{lj} P_{I_{f(1)}}(lj|\Omega_{\mathrm{n}(1)}K_1)\{|\mathscr{R}_{Nl}(x_{(1)})|^2 G(K_{(1)})\}_{\max}}{\sum_{lj} P_{I_{f(2)}}(lj|\Omega_{\mathrm{n}(2)}K_1)\{|\mathscr{R}_{Nl}(x_{(2)})|^2 G(K_{(2)})\}_{\max}}. \tag{9}$$

These relative cross-sections can be useful in the analysis of model similarly to analogous expressions in the theory of Auerbach and French [4]).

### 2.2. EXAMPLES

Let us consider several examples of (d, p) reactions on nuclei of $A \approx 25-28$. It is well known that in this $A$-region and at the incident deuteron energy considered below = 8 MeV the Coulomb effects do not affect the angular distributions much and may be neglected. On the other hand, however, S. G. Nilsson's spectra and wave functions require modification in this $A$-region and the nuclear deformations are not well known. In particular, the most important in this $A$-region $s_{\frac{1}{2}}$ orbital should be raised relative to its neighbouring orbitals [10]). Furthermore, as mentioned above, the $A_{lA}$-coefficients are rather sensitive to $\delta$ for $A \approx 25$. These and other well known shortcomings of this theory confuse the situation. One should, however, obtain qualitative and not bad quantitative agreement with the data and derive conclusions not only as to the assignments of spins and $\Omega_\mathrm{n}$-values of the final nuclear states, but also as to the possible modifications of the model wave functions.

Let us consider (d, p) reactions on the $Al^{27}$ target. The two most important proton groups correspond to the ground state ($Q = 5.494$ MeV) and to the 1.015 MeV level ($Q = 4.479$ MeV) of $Al^{28}$. According to Sheline [11]) the spin assignment should be: $I_f = 3+$, $K_f = 3$ and $I_f = 3+$, $K_f = 2$, respectively. This is consistent with the neutron configuration: $\nu[_8O^{16}, \mathrm{d}_{5/2}(\frac{1}{2}+^2, \frac{3}{2}+^2, \frac{5}{2}+^2), \mathrm{s}_{\frac{1}{2}}(\frac{1}{2}+^1)]$ in both the cases in question. Using eq. (8) one finds for the ground state

$$P_3(0\tfrac{1}{2}|\tfrac{1}{2}\,\tfrac{5}{2}) = 4A_{00}^2,\ \sum_j P_3(2j|\tfrac{1}{2}\,\tfrac{5}{2}) = \tfrac{5}{3}A_{20}^2 + \tfrac{35}{18}A_{21}^2 - \frac{5\sqrt{6}}{9}A_{20}A_{21} \tag{10a}$$

and for the excited state

$$P_3(0\tfrac{1}{2}|-\tfrac{1}{2}\,\tfrac{5}{2}) = \tfrac{2}{3}A_{00}^2,\ \sum_j P_3(2j|-\tfrac{1}{2}\,\tfrac{5}{2}) = \tfrac{5}{3}(A_{20}^2 + A_{2-1}^2). \tag{10b}$$

The most realistic deformation value of $Al^{28}$ seems to be $\beta \approx 0.20$ [12]). If one uses C. G. Nilsson's functions for $\eta = 4$, one has

$$\alpha_g = \frac{P_3(0\ \frac{1}{2}|\frac{1}{2}\ \frac{5}{2})}{\sum_j P_3(2j|\frac{1}{2}\ \frac{5}{2})} \approx 0.78$$

and

$$\alpha_c = \frac{P_3(0\ \frac{1}{2}|-\frac{1}{2}\ \frac{5}{2})}{\sum_j P_3(2j\ |-\frac{1}{2}\ \frac{5}{2})} \approx 0.155.$$

In the first (ground state) case one can then obtain an excellent fit to the data of Holt and Marsham [13]) using $r_0 = 6.15 \times 10^{-13}$ cm. The resulting angular distribution is very similar to theirs of their fig. 7. With $\alpha_g \approx 0.78$ the $l = 2$ contribution is almost completely masked and the case is almost pure $l = 0$. As to the excited state, the $l = 2$ peak is very distinct. However, an excellent fit to the data (a curve closely similar to that Holt and Marsham's of their fig. 8) would require $\alpha_e \approx 0.09$ rather than 0.155. A modification of $A$'s for the $s_{\frac{1}{2}}$ shell should probably account for the discrepancy (e.g. according to ref. [10]) with $\varkappa \approx \delta/\eta = 0.08$ one should employ $\eta \approx 2.3$ rather than $\eta \approx 4$).

In the case of the 32 keV-level of $Al^{28}$ we should have an admixture of $l = 2$ to $l = 0$ according to our model and Sheline's spin assignment. The 2.198 MeV-level is a pure $l = 2$ case in agreement with the assumed $I_f = 2+$, $K = 0$. However, the 2.137 MeV level with its $l = 0$ cannot be $I_f = 2+$, $K_f = 1$, as proposed by Sheline. Furthermore, if the 2.268 MeV-level is $I_f = 4+$, $K_f = 2$, it should be pure $l = 2$. More accurate experiments would be desirable.

Consider now the $Mg^{25}$ target with $I_i = K_i = 5/2$. Consider two proton groups corresponding to the ground and the 1.825 MeV first excited levels of $Mg^{26}$. The ground state is $I_f = 0+$, $K_f = 0$ (even-even nucleus). This makes pure $l = 2$ in agreement with the data [14]) with $\Omega_n = -5/2$ S. G. Nilsson's wave function. The 1.825 MeV state is $I_f = 2+$. One could explain a strong $l = 0$ admixture [14]) with $\Omega_n = -\frac{1}{2}$ and $K_f = 2$. However, on the other hand, according to the collective model this level should be not a particle level, but the first member of the rotational band based on the ground state. To account for the $l = 0$ admixture in this case one has to introduce a configuration mixing involving both the rotation — particle coupling and the interparticle forces. A detailed discussion of this reaction will be the subject of a separate publication.

### 3. Angular Correlations with $\gamma$-Rays

It is well known that angular correlations with $\gamma$-rays following a deuteron stripping reaction with the particle capture to an excited state of the final

nucleus provide useful tools in nuclear spectroscopy (they are sensitive to various coupling schemes — see e.g. ref. [5,6]) and also [15,16])). In particular, it is well known that such correlations are especially useful in determining nuclear spins which, in general, can be hardly determined by angular distributions only.

It is well known that, if the neutron in a (d, p) reaction is captured with a definite orbital angular momentum $l$ and a definite total angular momentum $j$, then the angular correlation function is just the product of the stripping cross-section with a factor depending on the angle of emission of the $\gamma$-ray provided there is no distortion of the deuteron or/and proton wave. On the other hand, if two or more $l$'s and $j$'s are involved, there are, in general, not only mixtures of different factors, but also interference terms between the contributions of different $l$'s and $j$'s in the correlation function. This occurs even if no distortion of the deuteron and proton waves is assumed. Since in our theory mixtures of $l$'s are of greatest interest, the angular correlations with $\gamma$'s are the more interesting.

The statistical matrix for the emission of $2^L$-pole radiation in the direction of propagation $\gamma$ from a nucleus making a transtition from a state of spin $I_t$ to one of spin $I'_t$ is proportional to

$$W_{M_t M'_t} = \sum_{\lambda\nu} (2\lambda I_t;\ \nu M_t | I_t M'_t)(LL;\ 1-1|2\lambda 0) \times W(I_t I_t LL;\ 2\lambda I'_t) Y_{2\lambda\nu}(\gamma)^* \qquad (11)$$

where $W(j_1 j_2 j_3 j_4;\ J_1 J_2)$ is a usual Racah coefficient. If $U_{M_t M'_t}$ is the statistical matrix for the orientation of the residual nucleus in a stripping reaction, the correlation function is given, as usually, by

$$\phi(\mathbf{k}_d,\ \mathbf{k}_p,\ \gamma) = \sum_{M_t M'_t} U_{M_t M'_t}(\mathbf{k}_d,\ \mathbf{k}_p) W_{M_t M'_t}(\gamma). \qquad (12)$$

Using the usual Racah sum rule techniques one can arrive at the following final result:

$$\phi \propto \sum_{\lambda\nu} Y_{2\lambda\nu}(\gamma) \sum \{ll' jj' mm'\}\, \xi_{jj'}^{lml'm'}(\Omega_n K_1 I_t) \times (-)^l \sqrt{\frac{(2j+1)(2j'+1)}{2l+1}}\, (2\lambda l';\ \nu m' | lm) F_{2\lambda}(LI'_t I_t) \times W(I_t I_t jj';\ 2\lambda I_1) W(ll' jj';\ 2\lambda \tfrac{1}{2}) \qquad (13)$$

where

$$F_{2\lambda}(LI'_t I_t) = (-)^{I_t - I'_t + 1} (2I_t+1)^{\frac{1}{2}} (2L+1)(LL;\ 1-1|2\lambda 0) W(I_t I_t LL;\ 2\lambda I'_t),$$

(tabulated in ref. [17])) and

$$\xi_{jj'}^{lml'm'}(\Omega_n K_1 I_t) = P_{I_t}(ll' jj' | \Omega_n K_1) S(lm) S(l'm')^*,$$

$$P_{I_t}(\ldots) = 4 \sum_{\Sigma\Sigma'} (l\tfrac{1}{2};\ \Omega_n - \Sigma\Sigma | j\Omega_n)(l'\tfrac{1}{2};\ \Omega_n - \Sigma'\Sigma' | j'\Omega_n) \times (I_1 j;\ K_1 \Omega_n | I_t K_t)(I_1 j';\ K_1 \Omega_n | I_t K_t) A_{l\Omega_n - \Sigma} A_{l'\Omega_n - \Sigma}. \qquad (14)$$

The factor $(-)^l$ may be omitted in (13) due to the parity conservation †. The integrals $S(l, m)$ can be written, in general, in the zero range approximation as

$$S(lm) = \int_{r \geq r_0} \mathrm{d}\mathbf{r} F^*_{\mathbf{k}_p}(\mathbf{r}) F_{\mathbf{k}_d}(\mathbf{r}) R_{Nl}(r) Y^*_{lm}(\omega), \tag{15}$$

$F_{\mathbf{k}_d}$ and $F_{\mathbf{k}_p}$ being the deuteron and proton waves distorted by a non-spin dependent potential (the most realistic distortion potential for the proton would be probably a spheroidal optical model well as given in refs. [18, 19]) — this would require a reformulation of the present theory). If the quantization axis is chosen along the vector $\mathbf{k}_d$ and the $x$-axis lies in the reaction plane, we can write

$$S(lm) \propto \sum_{L_p L_d} P^m_{L_p}(\cos\theta_{\mathbf{k}_p}) i^{L_d - L_p} \frac{(2L_p+1)(2L_d+1)}{\sqrt{2l+1}} \sqrt{\frac{(L_p-|m|)!}{(L_p+|m|)!}} \times (L_p L_d;\ 00|l0)(L_p L_d;\ m0|lm) \mathscr{R}_{Nl}(L_p L_d), \tag{16}$$

where

$$\mathscr{R}_{Nl}(L_p L_d) = \int_{r_0}^{\infty} r^2 \mathrm{d}r\, \mathrm{e}^{i\sigma_{L_p}(\eta_p) + i\sigma_{L_d}(\eta_d)} R_{Nl}(r)[F_{L_d} - \delta_{L_d} H_{L_d}][F_{L_p} - \beta_{L_p} H_{L_p}]$$

in Tobocman's notation [20]). If now all the distortion effects are neglected i.e. $\delta_\lambda = \beta_\lambda = \sigma_\lambda = 0$ — then $F_L = j_L(kr)$, we can quantize along $\mathbf{x}$ as in § 2 with $S(l, m) = \delta_{0m}(2l+1)^{\frac{1}{2}} i^l \mathscr{R}_{Nl}(x)$. The unimportant finite range factor $G(K)$ being independent of all the quantum numbers involved can be omitted throughout. Then we have

$$\phi \propto \sum_{\lambda} Y_{2\lambda 0}(\theta_\gamma) \sum \{ll' jj''\} \xi^{10l'0}_{jj'}(\Omega_n K_1 I_f) \times \sqrt{\frac{(2j+1)(2j'+1)}{2l+1}} (2\lambda l';\ 00|l0) F_{2\lambda}(LI'_f I_f) W(I_f I_f jj';\ 2\lambda I_1) \times W(ll' jj';\ 2\lambda \tfrac{1}{2}). \tag{17}$$

It is seen from (17) that in this case the emitted $\gamma$-rays are azimuthally symmetrical about the axis of quantization.

## 4. Proton Polarization

The polarization of protons from (d, p) reactions has been the subject of a number of papers (see e.g. ref. [9])). It is interesting to see how the mixing of $l$'s and $j$'s affects the polarization of protons in the case of spheroidal nuclei. For the sake of simplicity assume no spin-orbit distortion of the

† In the $j$-representation one has

$$P_{I_f}(\ldots) = 4(I_1 j;\ K_1 \Omega_n | I_f K_f)(I_1 j';\ K_1 \Omega_n | I_f K_f) C_{jl}(\Omega_n) C_{j'l'}(\Omega_n) = \sum_{(I_1, I_f \neq 0)} 4(2I_f+1/2I_1+1)\beta_{jl}(K_1\Omega_n)\beta_{j'l'}(K_1\Omega_n),$$

$\beta'_{jl}$s being the reduced stripping widths.

outgoing proton wave. The quantization axis $z$ be along the vector $\mathbf{k}_d$, and the $x$-axis in the reaction plane. The polarization pseudovector $\mathbf{P}$ is then easily calculated using standard techniques. One can show that the components of $\mathbf{P}$ in the reaction plane vanish and the degree of polarization is:

$$P \equiv P_y = \tfrac{4}{3}\Big\{\sum_l (2l+1)^{-1} \sum_{\mu_l=-\frac{1}{2}}^{l+\frac{1}{2}} \sqrt{(l+\tfrac{1}{2})^2-\mu_l^2}\ \mathrm{Im}\,[S(l\mu_l+\tfrac{1}{2}) \times S(l\mu_l-\tfrac{1}{2})^*] \sum_{j=l-\frac{1}{2}}^{l+\frac{1}{2}} (-)^{l+\frac{1}{2}-j}(2j+1)^{-1} P_{I_t}(lj|\Omega_n K_1)\Big\} \times \Big\{\sum_{lj} (2l+1)^{-1} P_{I_t}(lj|\Omega_n K_1) \sum_m |S(lm)|^2\Big\}^{-1} \qquad (18)$$

where $S(l, m)$ is given by eqs. (15)—(16). If no distortion effects are assumed (Butler (Born) approximation), $S(l, m) = \delta_{0m} S(l, m = 0)$ with $Oz \uparrow\uparrow \mathbf{x}$ we have no polarization as in the usual Butler (Born) theory. Eq. (18) becomes identical with eq. (21) of Grant [21]) provided only one $l$ and one $j$ contribute.

The author feels much indebted to Dr. R. K. Sheline and to Professor B. Mottelson for a helpful correspondence on deformed nuclei. He wishes to acknowledge a helpful discussion with Dr. Z. Szymański.

*Note added in proof:* After this work was completed, the author received a preprint of an excellent paper by G. R. Satchler on the same problem. Most of Satchler's results are essentially the same as ours. The author is greatly indebted to Dr. G. R. Satchler for sending him his preprint and for his criticism of the present paper.

## References

1) G. R. Satchler, Phys. Rev. **97** (1955) 1416
2) H. A. Bethe and S. T. Butler, Phys. Rev. **85** (1952) 1045
3) S. Okai and M. Sano, Prog. Theor. Phys. **15** (1956) 203
4) T. Auerbach and J. B. French, Phys. Rev. **98** (1955) 1276
5) G. R. Satchler, Proc. Phys. Soc. A **66** (1953) 1081
6) O. Hittmair, Zs. f. Phys. **143** (1955) 465
7) S. G. Nilsson, Mat. Fys. Medd. Dan. Vid. Selsk. **29** (1955) no. 16
8) K. Gottfried, Phys. Rev. **103** (1956) 1017
9) W. Tobocman, Technical report no. 29, Nucl. Phys. Lab., Case Institute of Technology (1956)
10) S. G. Nilsson's and B. Mottelson's private communication to R. K. Sheline and B. Mottelson's private communication to D. Chlebowska; cf. also fig. 5 of ref. [7])
11) R. K. Sheline, Nuclear Physics **2** (1956) 382
12) Private communication from R. K. Sheline
13) J. R. Holt and T. N. Marsham, Proc. Phys. Soc. A **66** (1955) 249
14) J. R. Holt and T. N. Marsham, Proc. Phys. Soc. A **66** (1953) 258
15) L. C. Biedenharn, Boyer and Charpie, Phys. Rev. **88** (1952) 517
16) J. Horowitz and A. M. L. Messiah, J. Phys. Rad. **15** (1954) 142
17) L. C. Biedenharn and M. E. Rose, Revs. Mod. Phys. **25** (1953) 729

18) B. Margolis and E. S. Traubetzkoy, Phys. Rev. **106** (1957) 105
19) W. N. Gribov, Zurn. Exper. Teor. Fiz. **32** (1957) 842
20) W. Tobocman, Phys. Rev. **94** (1954) 1655
21) I. P. Grant, Proc. Phys. Soc. A **68** (1955) 244
22) P. M. Morse and H. Feshbach, Methods of Mathematical Physics (McGraw-Hill, New York, 1953)

*Nuclear Physics* **6** (1958) 585—595; © *North-Holland Publishing Co., Amsterdam*
Not to be reproduced by photoprint or microfilm without written permission from the publisher

# A VARIATIONAL APPROACH TO THE NUCLEAR MANY-BODY PROBLEM

V. J. EMERY
*Cavendish Laboratory, Cambridge* †

Received 23 January 1958

**Abstract:** Jastrow's variation method is applied to the nuclear many-body problem. It is found that it is necessary to restrict the variation of the trial function in order to obtain reasonable results from the approximation used. Calculations of the properties of nuclear matter are used to investigate the effects of two possible restrictions. The physical justification of the restrictions is discussed and a method of generalizing the trial wave function is given.

## 1. Introduction

A variational approach to the many-body problem in quantum theory has been suggested by Jastrow [1]) and discussed further by Iwamoto and Yamada [2]). The method was devised to deal with problems in which the inter-particle forces were strong and of short range and it has been used by Iwamoto and Yamada [3]) to calculate the binding energy per particle and density of nuclear matter.

In this paper we consider a further application of the method to the nuclear many-body problem. It is found that it is necessary to impose restrictions on the choice of trial wave function in order that useful results may be obtained.

Section 2 gives a brief account of Jastrow's approach to the nuclear many-body problem and in section 3 the choice of a trial wave function is considered. In section 4, the method is used to calculate the binding energy per particle and density of nuclear matter and section 5 is devoted to a discussion of the results.

## 2. The Variational Approximation for Nuclear Matter

Suppose we have $A$ nucleons of mass $m$ and number density $\varrho$, there being equal numbers of protons and neutrons. Let $\mathbf{r}_i$ be the position vector of the $i$th particle and let $\mathbf{r}_{ij} = \mathbf{r}_i - \mathbf{r}_j$. It is assumed, for the moment, that the potential $v(r_{ij})$ between particles $i$ and $j$ is a central potential independent

† This work was commenced at the Dept. of Theoretical Physics, Manchester University and part of it was included in a Ph. D. thesis submitted to that University.

of spin and parity and has an infinite repulsive core of radius $r_0$. We shall take $A$ to be very large so that the Coulomb potential is omitted.

Jastrow [1]) suggested that the binding energy of such a system of particles should be calculated by the variation method using a trial wave function defined by

$$\Psi = FS \tag{1}$$

where $S$ is a Slater determinant of plane wave functions, spin functions and isobaric spin functions. $F$ is defined by

$$F = \prod_{i<j}^{A} f(r_{ij})$$

the product being taken over all pairs of particles. In order that the expectation value of the potential energy per particle should be finite we must insist that the "correlation function" $f(r)$ should vanish for $r \leqq r_0$. For $r > r_0$, the form of $f(r)$ is to be varied subject to the condition that $f(r)$ approaches unity for large $r$. The radial distribution function of the system is defined to be

$$g(r_{12}) = \frac{A(A-1)}{\varrho^2} \frac{\int |\Psi|^2 \mathrm{d}\mathbf{r}_3 \ldots \mathrm{d}\mathbf{r}_A}{\int |\Psi|^2 \mathrm{d}\mathbf{r}_1 \ldots \mathrm{d}\mathbf{r}_A}, \tag{2}$$

$\mathrm{d}\mathbf{r}_i$ being the volume element in the configuration space of particle $i$ and the integrals being taken over the volume of definition $A/\varrho$ of $\Psi$. Summation over spin and isobaric spin states is implied.

Denoting the gradient operator for particle $i$ by $\nabla_i$, we also define the distribution function

$$\mathbf{G}(r_{12}) = \frac{A(A-1)}{\varrho^2} \frac{\int |F|^2 \nabla_1 |S|^2 \mathrm{d}\mathbf{r}_3 \ldots \mathrm{d}\mathbf{r}_A}{\int |\Psi|^2 \mathrm{d}\mathbf{r}_1 \ldots \mathrm{d}\mathbf{r}_A} \tag{3}$$

With $\hbar = 1$, the kinetic energy operator acting on $\Psi$ gives

$$\frac{-1}{2m} \sum_{i=1}^{A} \nabla_i^2 \Psi = \frac{-1}{2m} \sum_{i=1}^{A} F \nabla_i^2 S - \frac{1}{m} \sum_{i=1}^{A} \nabla_i F \cdot \nabla_i S - \frac{1}{2m} \sum_{i=1}^{A} S \nabla_i^2 F; \tag{4}$$

$S$ is an eigenfunction of the kinetic energy operator so that the first term on the right hand side of eq. (4) gives a contribution

$$T_{\mathrm{F}} = \frac{1}{2m} \frac{3}{5} k_{\mathrm{F}}^2 \tag{5}$$

to the expectation value $T$ of the kinetic energy per particle; $k_{\mathrm{F}}$ is the Fermi momentum, $T_{\mathrm{F}}$ is simply the well known expression for the mean kinetic energy of a particle in the ground state of a Fermi gas.

If we assume that $[f(r)-1]$ approaches zero more rapidly than $1/r$ when $r$ is large and increasing and if we let the number of particles become

infinite, it can be shown that the remaining terms on the right hand side of eq. (4) give the following contribution $T_c$ to $T$:

$$T_c = \frac{-1}{2m}\frac{\varrho}{2}\int\left\{\left[\frac{\nabla_1^2 f(r_{12})}{f(r_{12})} - \frac{[\nabla_1 f(r_{12})]^2}{f^2(r_{12})}\right] g(r_{12}) + \frac{\nabla_1 f(r_{12})}{f(r_{12})}\cdot \mathbf{G}(r_{12})\right\} \mathrm{d}\mathbf{r}_{12}. \quad (6)$$

The expectation value $V$ of the potential energy per particle is given by

$$V = \frac{\varrho}{2}\int v(r_{12}) g(r_{12}) \mathrm{d}\mathbf{r}_{12}. \quad (7)$$

Jastrow [1]) suggested that the distribution functions $g(r_{12})$ and $\mathbf{G}(r_{12})$ should be expressed as cluster series in powers of the number density $\varrho$ and that a good approximation to the energy might be obtained by retaining only the first term in each series and substituting the results into eqs. (6) and (7).

In this approximation it is found that

$$g(r_{12}) = f^2(r_{12}) L(k_F r_{12}) \quad (8)$$

$$\mathbf{G}(r_{12}) = f^2(r_{12}) \nabla_1 L(k_F r_{12}) \quad (9)$$

where

$$L(X) = 1 - \tfrac{1}{4} p^2(X) \quad (10)$$

$$p(X) = \frac{3}{X^3}[\sin X - X\cos X]; \quad (11)$$

$L(k_F r_{12})$ is simply the radial distribution function for the ground state of a Fermi gas.

If we put (8) and (9) into (6) and (7), the expectation value of the energy per particle becomes

$$\begin{aligned} E = \frac{1}{2m}\tfrac{3}{5}k_F^2 &- \frac{1}{2m}\frac{\varrho}{2}\int\{f(r_{12})\nabla_1^2 f(r_{12}) - [\nabla_1 f(r_{12})]^2\} L(k_F r_{12}) \mathrm{d}\mathbf{r}_{12} \\ &- \frac{1}{2m}\frac{\varrho}{2}\int f(r_{12})\nabla_1 f(r_{12})\cdot\nabla_1 L(k_F r_{12}) \mathrm{d}\mathbf{r}_{12} \\ &+ \frac{\varrho}{2}\int v(r_{12}) f^2(r_{12}) L(k_F r_{12}) \mathrm{d}\mathbf{r}_{12}. \end{aligned} \quad (12)$$

This expression is to be minimized with respect to variations of $f(r)$ and of $\varrho$ or $k_F$ (since $\varrho = 2/3\pi^2) k_F^3$).

The terms which are neglected in the approximations (8) and (9) are given by Jastrow [1]) and by Iwamoto and Yamada [2]). These terms contain cluster integrals over the configuration spaces of three or more particles. In order to see if the cluster series is likely to converge rapidly, we shall evaluate the first correction term (three-body cluster) using the function $f(r)$ which makes $E$ a minimum. The largest contribution to the three-

body term is obtained by multiplying the integrands on the right hand side of eq. (12) by

$$I(r_{12}) = \varrho \int h(r_{13})h(r_{23})\mathrm{d}\mathbf{r}_3 \tag{13}$$

where

$$h(r) = f^2(r)-1.$$

Introducing bipolar coordinates we may rewrite

$$I(r_{12}) = \frac{2\pi\varrho}{r_{12}} \int_0^\infty \int_{|r_{12}-r|}^{r_{12}+r} rh(r)sh(s)\mathrm{d}s\mathrm{d}r. \tag{14}$$

This form for $I(r_{12})$ will be required later.

Eq. (12) is easily generalized to include spin dependent forces. A particular form of spin dependence to be used in the next section is that in which $v(r_{ij})$ acts in even states only and is given by $v_1(r_{ij})$ in singlet states and by $v_3(r_{ij})$ in triplet states. In this case, the appropriate expression for the expectation value of the energy per particle is

$$\begin{aligned} E = {} & \frac{1}{2m}\tfrac{3}{5}k_F^2 + \frac{1}{2m}\varrho\int [\nabla_1 f(r_{12})]^2 L(k_F r_{12})\mathrm{d}\mathbf{r}_{12} \\ & + \frac{\varrho}{2}\int [v_1(r_{12})+v_3(r_{12})]f^2(r_{12})H(k_F r_{12})\mathrm{d}\mathbf{r}_{12} \end{aligned} \tag{15}$$

where $H(k_F r_{12}) = (3/16)[1+p^2(k_F r_{12})]$, $p(X)$ being defined in eq. (11).

Eq. (15) would be obtained by using a Hartree-Fock approximation to calculate the binding energy of a system of particles in which the potential between particles $i$ and $j$ was given by

$$K_{ij} = \frac{1}{2m}\{[\nabla_i f(r_{ij})]^2+[\nabla_j f(r_{ij})]^2\}+v(r_{ij})f^2(r_{ij}), \tag{16}$$

$v(r_{ij})$ having the appropriate spin dependence. Thus $K_{ij}$ may be regarded as the "effective potential", between two nucleons in the nucleus. The single-particle potential which arises in the usual way in the Hartree-Fock method is, in this instance, dependent on momentum only and it corresponds to the single-particle potential of the Shell Model.

## 3. The Choice of a Trial Wave Function

Consider a trial wave function of the form

$$f(r) = \phi_1(r)+\alpha\phi_2(r) \tag{17}$$

where $\phi_1(r) = 0 = \phi_2(r)$, $r \leqq r_0$; $\phi_1(r) \to 1$ for large $r$ while $\phi_2(r) \to 0$ for large $r$ so that $f(r)$ satisfies the required boundary conditions. Substitution of (17) into (15) gives an expression of the form

$$E = E_1+2\alpha E_2+\alpha^2 E_3 \tag{18}$$

where $E_3$ is obtained by replacing $f(r)$ by $\phi_2(r)$ in eq. (15). Thus, if $E_3 < 0$ and $E_1$ and $E_2$ are finite, $E$ decreases without bound when $\alpha$ is large and increasing and there is no mimimum energy. Now it is easy to show that, since the forces are of short range, a function $f(r)$, which approaches unity for large $r$ without oscillating rapidly, can be modified to give a new function $\phi(r)$ which approaches zero for large $r$ and the modification can be made in such a way that the change in the energy given by eq. (15) is arbitrarily small. It follows that, if a trial correlation function can be found which gives a negative energy, then one can be found which gives an arbitrarily large negative energy.

This result is a consequence of the absence of a normalization term in eq. (15). The normalization appears in the neglected terms of the cluster series.

Moreover, since a finite binding energy per particle would be obtained if the variation were carried out using the exact expression for the expectation value of the energy, it is clear that a large binding energy obtained in the first approximation will be accompanied by correspondingly large correction terms. It follows that it is necessary to restrict the variation of $f(r)$ if useful results are to be obtained from the first approximation. If the restrictions are chosen in such a way that the correction terms are small, then, by the Variation Principle, the calculated energy is greater than the "true" energy. It is necessary to establish by calculation that it is possible to impose restrictions which lead to small correction terms and also give a good approximation to the energy.

Three possible restrictions suggest themselves immediately. They are chosen for mathematical convenience and their physical justification will be discussed in section 5.

We may

A) use the trial form of $f(r)$ given in eq. (17) but choose $\phi_2(r)$ so that $E_3 > 0$ in eq. (18),

B) insist that $f(r)$ satisfies

$$0 \leqq f(r) \leqq 1, \tag{19}$$

C) solve the Euler equation for variation of $E$ subject to a subsidiary condition on $f(r)$.

The last possibility has been considered by Jastrow [4]) with a subsidiary condition of the type

$$\int [f(r)-1]^2 L(k_F r)\mathrm{d}\mathbf{r} = \text{constant}$$

and will not be pursued further here.

In the next section we calculate the properties of nuclear matter to determine the effects of restrictions A and B.

## 4. Application to Nuclear Matter

For a trial function satisfying condition A we take

$$f(r) = \begin{cases} 0 & \text{for } r \leqq r_0, \\ \left[1 - \frac{r_0}{r} e^{-\lambda(r-r_0)}\right][1+\alpha e^{-\beta r}] & \text{for } r > r_0. \end{cases} \tag{20}$$

We shall see that this does in fact give a minimum energy.

The nucleon-nucleon potential to be used was determined phenomenologically from two body data by Gammel, Christian and Thaler [5]). The odd state potentials which they obtained were unreliable and may not give a large contribution to the binding energy, so they are omitted. The even state potentials have a common core radius $r_0 = 0.5 \times 10^{-13}$ cm and outside the core they take the form

$$v(r_{ij}) = -V_c \frac{\exp(-\mu_c r_{ij})}{\mu_c r_{ij}} - S_{ij} V_T \frac{\exp(-\mu_T r_{ij})}{\mu_T r_{ij}};$$

$S_{ij}$ is the tensor operator and $V_c$ and $\mu_c$ are spin dependent, $V_T = 45$ MeV and $\mu_T = 0.73 \times 10^{13}$ cm$^{-1}$. In triplet states, $V_c = V_c^3 = 6395$ MeV and $\mu_c = \mu_c^3 = 2.936 \times 10^{13}$ cm$^{-1}$, while in singlet states $V_c = V_c^1 = 905.6$ MeV and $\mu_c = \mu_c^1 = 1.7 \times 10^{13}$ cm$^{-1}$.

The function $f(r)$ in eq. (20) is spherically symmetric and so, since the angular average of the tensor operator is zero, the tensor force gives no contribution. Thus the expression for $E$ given in eq. (15) is suitable for the potential used. A method of choosing a more general correlation function which takes account of tensor forces is given in the appendix.

The integrations and variations were carried out numerically using the Manchester University Electronic Computer. The resulting binding energy per particle was 16.6 MeV at a density equivalent to a nuclear radius of $0.93\ A^{1/3} \times 10^{-13}$ cm. These results may be compared with 12.5 MeV and $0.95\ A^{1/3} \times 10^{-13}$ cm respectively obtained by Brueckner and Gammel [6]) who used the same potential to calculate the properties of nuclear matter by means of Brueckner's approach to the nuclear many-body problem. They obtained a total binding energy per particle of 18.5 MeV of which 6 MeV was contributed by the tensor force.

The values of the variation parameters of $f(r)$ in eq. (20) were $\alpha = 1.92$, $\beta = 0.95 \times 10^{13}$ cm$^{-1}$ and $\lambda = 1.0 \times 10^{13}$ cm$^{-1}$. The resulting form of $f^2(r)$ is shown by curve I in fig. 1. The individual contributions to the binding energy per particle were $V = -165.6$ MeV, $T_c = 115.1$ MeV and $T_F = 33.9$ MeV. These values are somewhat larger in absolute magnitude than one would expect to find at the experimental nuclear density which corresponds to a nuclear radius of $1.1\ A^{1/3} \times 10^{-13}$ cm.

The comparison of our results with those of Brueckner and Gammel [6])

suggests that we have obtained too great a binding energy. Moreover, in view of the generalization of $f(r)$ suggested in the appendix, the condition A allows a much wider choice of correlation function than the one which we have adopted here. Consequently, it is to be expected that the correction terms will be large. In fact an estimate of the three-body cluster terms shows that they give an additional binding energy of about 20 MeV per particle. This figure is a difference of corrections of the order of 800 MeV to $T_c$ and to $V$. The numerical evaluation of the four body cluster integrals would take an unreasonable length of time but it is evident that they would be small only in virtue of a fortuitous cancellation of large corrections to $T_c$ and $V$.

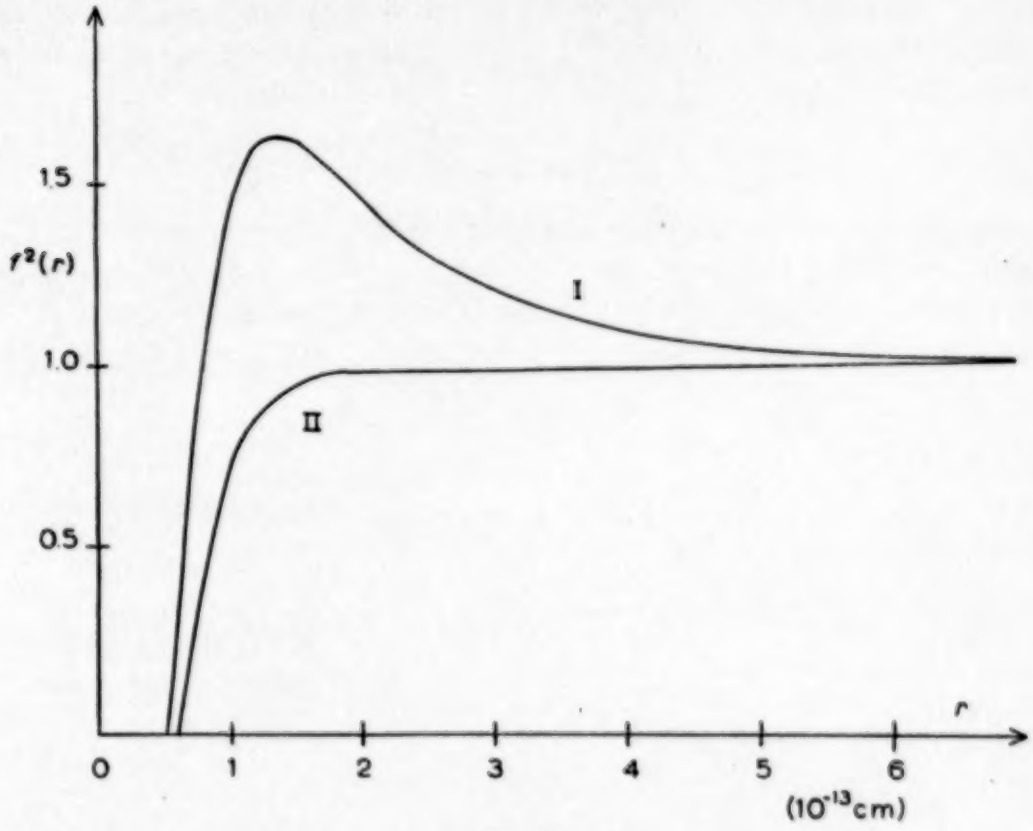


Fig. 1

An example of the use of condition B is provided by the calculation of Iwamoto and Yamada [3]), since the trial form of correlation function which they used satisfies the inequality (19). The assumed form of $f(r)$ was

$$f(r) = \begin{cases} 0 & \text{for } r \leqq r_0, \\ 1-e^{-\beta(r-r_0)} & \text{for } r > r_0. \end{cases} \tag{21}$$

They used a nucleon-nucleon potential given by

$$v(r) = -A\,\frac{1+P_M}{2}\exp\{-\alpha(r-r_0)\} \quad \text{for} \quad r > r_0;$$

$P_M$ is the Majorana operator and the potential has an infinite repulsive core of radius $r_0 = 0.6 \times 10^{-13}$ cm; $A = 397.3$ MeV and $\alpha = 2.627 \times 10^{13}$ cm$^{-1}$.

The resulting binding energy was 5.2 MeV per particle at a density corresponding to a nuclear radius of $1.1\, A^{1/3} \times 10^{-13}$ cm. At minimum it was found that $\mu = 5.0 \times 10^{13}$ cm$^{-1}$ and the three body clusters gave an additional binding energy of 0.6 MeV per particle, which was a difference of corrections of the order of 10 MeV to $T_c$ and $V$. The form of $f^2(r)$ is shown by curve II in fig. 1.

We see then that condition A can lead to large correction terms while condition B can lead to small correction terms. In the next section we consider the reasons for these results to see if they are a feature of the special cases considered or if they are typical consequences of the assumed conditions.

## 5. Discussion

In section 2, we saw that the size of the three body correction terms is largely determined by the integral $I(r_{12})$ given in eq. (14). $I(r_{12})$ in turn depends upon the function $rh(r)$. In fig. 2 we compare the functions $rh(r)$ arising from the trial forms of $f(r)$ given in eqs. (20) (curve I) and (21)

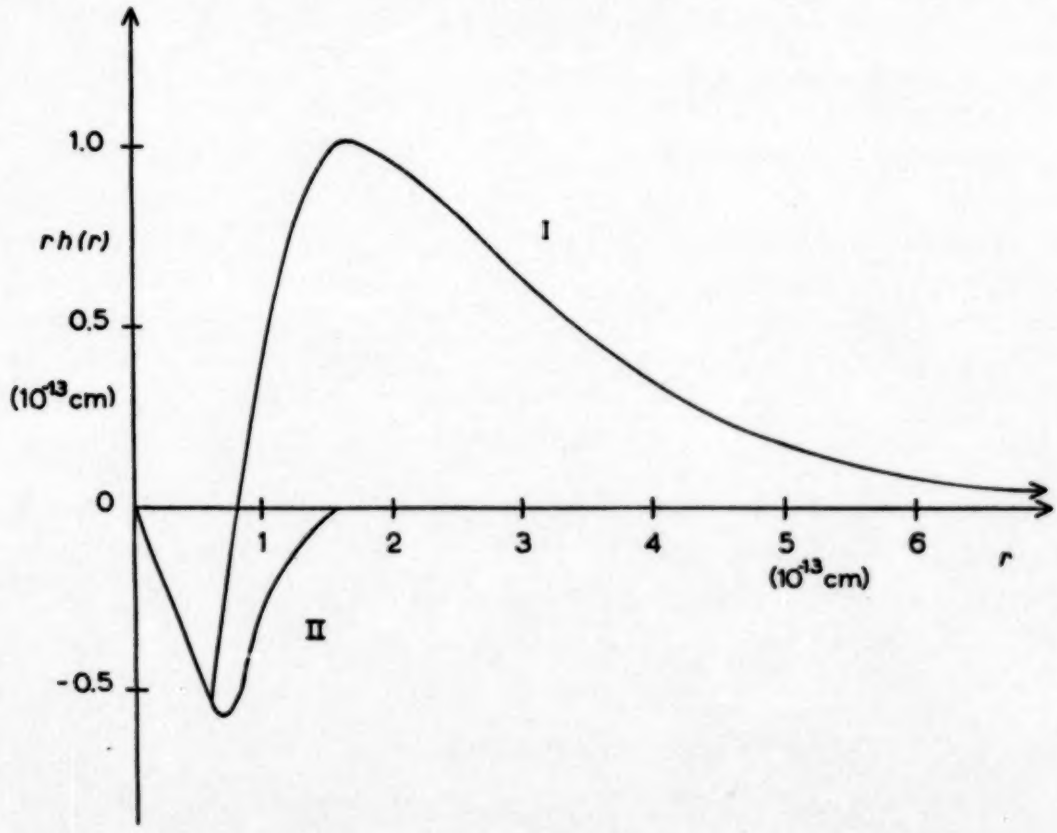


Fig. 2

(curve II). It is clear that the large correction terms arising from eq. (20) are due to the long range and broad peak of the correlation function. Such a shape is energetically favourable for correlation functions satisfying the restriction A. On the other hand, a short range correlation function gives the lowest energy if condition B is used, and this gives rise to small correction terms.

To see if these results are physically reasonable we consider the radial distribution function $g(r_{12})$. If particle 1 is at $\mathbf{r}_1$, the probability that there is another particle in the volume element $\mathrm{d}\mathbf{r}_2$ about $\mathbf{r}_2$ is given by $\varrho g(r_{12})\mathrm{d}\mathbf{r}_2$. Thus a measure of two particle correlations in the nucleus is given by $g(r_{12})$ and, in the approximation of eq. (8), by $f^2(r_{12})$. Since $f(r) = 0$ for $r < r_0$, there is a strong short-ranged anti-correlation. For $r > r_0$, we have seen that a long ranged positive correlation gives rise to large correction terms (see fig. 1). Thus, if the Jastrow method is to give a good approximation to both energy and wave function, any positive two-particle correlations must be weak or of extremely short range.

The experimental evidence for two-particle correlations in the nucleus has been reviewed by Brueckner, Eden and Francis [7]). High energy experiments indicate the presence of high momentum components in the nuclear wave function. However, such high momentum components could arise from the short-ranged anti-correlation with or without the longer ranged positive correlation. At the moment, the theoretical analyses of the experiments do not allow us to make an unequivocal choice between the two possibilities.

A more direct comparison with experiment could be obtained by applying the Jastrow method to a system of $He^3$ molecules. Here the radial distribution function can be inferred from X-ray scattering experiments. Unfortunately, at the present time, there appears to be insufficient experimental information for any conclusions to be drawn.

It may be argued that it is not necessary to seek a physical justification for a restriction such as (19), since, in practice, a variation method can give a good value for the energy with a poor approximation to the wave function. Thus it may be that we can work with a poor approxmation to $f(r)$ and to $g(r_{12})$ or that eq. (8) gives a poor approximation to $g(r_{12})$ but a good approximation to the energy.

At present, it seems that the inequality (19) is the best working restriction for $f(r)$. Its usefulness for calculating the energy should be judged by results but the wave functions obtained should be treated with reserve.

I wish to thank Dr. R. J. Eden for suggesting the problem and for his constant advice and encouragement.

This work was carried out during the tenure of first a maintenance grant

and then a research assistantship from the Department of Scientific and Industrial Research.

## Appendix

We wish to find a more general form of correlation function which will take account of tensor forces.

$F$ is required to satisfy the following conditions:

(i) $F$ commutes with the total angular momentum,

(ii) $F$ is invariant under exchange of pairs of particles,

(iii) $F$ is invariant under spatial inversion.

Condition (i) ensures that the total angular momentum of $\Psi$ is the same as that of $S$, as required by the Shell Model. Condition (ii) ensures that $\Psi$ is an antisymmetric wave function. Condition (iii) ensures that the parity of $\Psi$ is the same as that of $S$.

Unless we include spin functions, condition (i) implies that $f(r)$ is a function of $r$ only, so that the tensor force would give no contribution. Let $\sigma_i$, $\tau_i$; $\sigma_j$, $\tau_j$ be the spin and isobaric spin operators of particles $i$ and $j$ respectively. Then, putting $r_{ij} = r$, the most general scalar correlation function satisfying (i), (ii) and (iii) is

$$f(\mathbf{r}, \sigma_i, \sigma_j; \tau_i, \tau_j) = f_1(r)+f_2(r)(\sigma_i \cdot \sigma_j)+f_3(r)(\tau_i \cdot \tau_j) \\ +f_4(r)(\sigma_i \cdot \mathbf{r})(\sigma_j \cdot \mathbf{r})+f_5(r)(\tau_i \cdot \tau_j)(\sigma_j \cdot \sigma_i)+f_6(r)(\sigma_i \cdot \mathbf{r})(\sigma_j \cdot \mathbf{r})(\tau_i \cdot \tau_j).$$

By means of a non-singular linear transformation we can rewrite

$$f(\mathbf{r}, \sigma_i, \sigma_j; \tau_i, \tau_j) = E[\phi_1(r)\Omega_1+\phi_2(r)\Omega_3+\phi_3(r)S_{ij}] \\ +O[\phi_4(r)\Omega_1+\phi_5(r)\Omega_3+\phi_6(r)S_{ij}]. \qquad \text{(A1)}$$

Here $S_{ij}$ is the tensor operator and $E$, $O$, $\Omega_1$ and $\Omega_3$ are operators which, when acting on an antisymmetric wave function project into even, odd, singlet and triplet states respectively.

Since $\nabla_i^2 S_{ij} = -6(1/r_{ij}^2)S_{ij}$, we must have $\phi_3(r) \to 0$ and $\phi_6(r) \to 0$ for large $r$ in order to obtain a finite expectation value for the kinetic energy. The boundary conditions on the remaining $\phi_i(r)$ are $\phi_i(r) \to a_i$ for large $r$, subject to

$$3a_1^2+3a_2^2+a_4^2+9a_5^2 = 16 \qquad \text{(A2)}$$

so that $g(r) \to 1$ for large $r$.

(A1) and (A2) give a general extension of the correlation function which takes account of tensor forces and which allows an increased binding energy to be obtained when the form of the radial distribution function is restricted.

## References

1) R. Jastrow, Phys. Rev. **98** (1955) 1479
2) F. Iwamoto and M. Yamada, Prog. Theor. Phys. **17** (1957) 543
3) F. Iwamoto and M. Yamada, Prog. Theor. Phys. **18** (1957) 345
4) R. Jastrow, private communication
5) J. L. Gammel, R. S. Christian and R. M. Thaler, Phys. Rev. **105** (1957) 311
6) K. A. Brueckner and J. L. Gammel, Phys. Rev. **105** (1957) 1679; and correction to be published
7) K. A. Brueckner, R. J. Eden and N. C. Francis, Phys. Rev. **98** (1955) 1445

*Nuclear Physics* **6** (1958) 596—612; © *North-Holland Publishing Co., Amsterdam*
Not to be reproduced by photoprint or microfilm without written permission from the publisher

# A TENTATIVE GENERAL SCHEME FOR WEAK INTERACTIONS

B. D'ESPAGNAT and J. PRENTKI
CERN, *Geneva*

Received 8 February 1958

**Abstract:** A generalized isobaric spin formalism (*M* space formalism) that automatically conserves charge and can be extended to leptonic interactions was suggested by A. Salam and the authors in a previous article. The detailed application of this formalism to the whole set of presently known decays is here investigated. It is shown that within the framework of this theory there exists at least one choice of weak interactions that does not contradict any known experimental data on hyperon, K mesons, pion and muon decays, or on ordinary $\beta$ decays inasmuch as these are compatible with a V−A coupling. In relation to possible modifications of this choice one or two decay modes are mentioned, which might up to now have escaped detection.

## 1. Introduction

The search for the form of weak interactions proceeds along two parallel lines which are: a) the determination of their spatial properties (types of interaction and kinds of coupling), b) attempts at understanding their isospace properties, which would eventually give some relations between different coupling constants for a given type of coupling. As regards the problems connected with a), some very substantial advances have been made recently. It seems to us, however, that point b) also has its importance and that theoretical views on this subject may be useful. In fact data such as branching ratios between different modes of decay (e.g. $\Lambda \to p+\pi^-/\Lambda \to n+\pi^0$) can hardly be accounted for if one does not explicitly make use of some isobaric properties †.

An example of such consideration is the $|\Delta \mathbf{I}| = \frac{1}{2}$ rule [1]). Another one is the **M** conservation recently suggested by Salam and the authors [2]).

It seems perhaps appropriate to make some remarks about these theories. First of all some serious criticisms can be made of the $|\Delta \mathbf{I}| = \frac{1}{2}$, $\Delta U = \pm 1$ rule.

a) It can be applied only to processes involving "heavy particles" (baryons, $\pi$ and K mesons) for which isobaric spin and strangeness are defined. It seems worthwhile to point out in this connection that even the milder $\Delta U = \pm 1$ rule seems to have no meaning for decays involving leptons and that in fact all attempts directed at extending to leptons the concept of

† Even within the frame of e.g. a Fermi interaction theory they do not come out automatically, except in some cases to lowest order in the strong interaction coupling constants.

strangeness have sooner or later proved unsuccessful. It now looks as if this very concept of strangeness made no sense for leptons (this, of course, is not equivalent to saying that their strangeness is zero!); the same is *a fortiori* true for isobaric spin.

b) Recent experiments ($K^0 \to 2\pi^0/K^0 \to \pi^+ + \pi^-$ ratio) are a direct support to older arguments by Dalitz [3]) which show that $|\Delta \mathbf{I}| = \frac{1}{2}$ is too strict a rule and that some admixture of $|\Delta \mathbf{I}| = 3/2$ is necessary. The amount of this admixture has then to be taken as purely empirical.

c) It is a "violation" rule. Its precise statement, that the weak interaction Lagrangian $L_w$ is an isospinor, has a rather artificial look.

In view of these facts it seemed worthwhile to look for a completely different approach and it was suggested [4]) to formulate the weak interaction theory not as a violation law, but as a conservation law. The E.P.S. approach [2]) is built along this line. The violation of $|\Delta \mathbf{I}| = \frac{1}{2}$ rule can, moreover, be introduced into it in a very natural way and the amount of the $|\Delta \mathbf{I}| = 3/2$ admixture could thus *in principle* be calculated. It also turns out that it is able to treat leptons and baryons more or less on the same footing without involving, however, any of the difficulties inherent in the concept of leptonic strangeness.

The starting point of the E.P.S. theory is the [4] space of Salam-Polkinghorne [5]). Four kinds of interactions are then introduced (cf. also ref. [6]):

a) the very strong interactions (coupling constants $G_i$; see appendix): they are invariant for all rotations in this [4] space which is the direct product of two [3] spaces $I^+$ and $I^-$ ($\mathbf{I}^+$ and $\mathbf{I}^-$ separately conserved);

b) the intermediary strong interactions (coupling constants $\varepsilon_i$; for more details see appendix) invariant in $I^+$ space and also under rotations around the third axis in $I^-$ space ($\mathbf{I}^+$ = ordinary isospin conserved; $I_3^-$, related to strangeness, conserved);

c) the electromagnetic interactions which conserve $I_3^+$ and $I_3^-$;

d) the weak interactions which are invariant for rotations in another [3] subspace of the [4] space, the $M$ space, which is orthogonal to the fourth axis of the [4] space (weak interactions are invariant for rotations which conserve the fourth axis in the [4] space).

From the representations of the Salam-Polkinghorne theory the representations of particles in $M$ space can be obtained. The weak Hamiltonian is a sum of scalars which can be formed with these quantities.

In spite of the fact that the strong interactions (more precisely speaking, the intermediate strong interactions) completely destroy some of the symmetries that weak interactions would possess in their absence — and these symmetries therefore do not have any physical significance — it should be stressed that such an approach is indeed quite a consistent one. This is due to the fact that some *other* symmetries induced by the invariance

postulate either are not altered or are altered in a predictable way (see e.g. § 3 and § 4).

Although the $M$ space formalism [2]) gives some quite definite prescriptions (isospin and $M$-spin attributions, etc.) it has still the appearance of a general frame which, as regards the precise forms of Lagrangians, leaves very many possibilities open. Therefore no attempt was made in ref. [2]) to compare theoretical predictions with experimental results. The question, however, arises whether among these many possibilities there is at least one which can fit the numerous data now available. It is the aim of the present paper to show that indeed such a possibility exists and to describe it with some detail. It is *not* claimed, however, that this possibility is unique, nor even that it will ultimately prove to be the more appropriate one to use, even in the frame of the $M$ space formalism.

## 2. Pure Leptonic Interactions ($\mu$-decay)

The case of pure leptonic interactions is, in a way, the simplest that we have to consider since the strong interactions do not enter the picture. Definite experimental results can, moreover, be used as a guide: it is known in particular that Michel's parameter $\rho$ is nearly 3/4. As is well-known, this is compatible with an interaction Lagrangian for $\mu$ decay of the form

$$\overline{\mu^+}\gamma_\mu(1+\gamma_5)\nu \cdot \bar{\nu}\gamma_\mu(1+\gamma_5)\mathrm{e}^+. \tag{1}$$

The problem is to incorporate this interaction into the $M$ space scheme. In ref. [2]) the leptons were described by means of a vector $\mathbf{L}$ and a scalar $L_s$ in $M$ space with components † $\mathbf{L} = (\mu^+, \nu_3, \mathrm{e}^-)$, $L_s = \nu_s$. As the interaction should be invariant in $M$ space the first idea that comes to mind is to choose one of the many scalars that can be formed with four $\mathbf{L}$ or $L_s$, simply introducing a space-time operator $O = \gamma_\mu(1+\gamma_5)$ at the proper places. This would e.g. give

$$(\bar{\mathbf{L}}\times O\mathbf{L}) \cdot (\bar{\mathbf{L}}\times O\mathbf{L}), \qquad (\bar{L}_s O\mathbf{L}) \cdot (\bar{L}_s O\mathbf{L}), \qquad \text{etc.} \tag{2}$$

It turns out, however, that such a procedure cannot lead to the correct result (1). Instead it leads in a straight-forward way to terms of the general form

$$\bar{\nu}\gamma_\mu(1+\gamma_5)\mu^+ \cdot \bar{\nu}\gamma_\mu(1+\gamma_5)\mathrm{e}^-. \tag{1'}$$

Such an expression clearly embodies the Konopinski-Mahmoud [7]) hypothesis that $\mu^+$, $\mathrm{e}^-$, $\nu$ are the "particles". As Lee and Yang [8]) pointed out, it should be discarded because with this kind of coupling it leads to $\rho = 0$. It may, moreover, easily be shown that changing one of the $O$ to e.g. $O' = \gamma_\mu(1-\gamma_5)$ in any expression (2) is not a solution to this difficulty.

† Notations: Let $\mathbf{A}$ be a vector in $M$ space with components $A_1$, $A_2$, $A_3$. We define $A_+ = (A_1 - iA_2)/\sqrt{2}$, $A_- = (A_1 + iA_2)/\sqrt{2}$, and write $\mathbf{A}$ as $(A_+, A_3, A_-)$.

Fortunately, a very elegant way of introducing the $\gamma_\mu(1+\gamma_5)$ interaction was recently pointed out by Feynman [9, 10]), the principle of which is to describe a fermion field not by a 4-spinor $\psi$ but by either one of two 2-component spinors

$$\chi = a\psi \quad , \quad \xi = \bar{a}\psi$$

with

$$a = \tfrac{1}{2}(1+\gamma_5) \quad , \quad \bar{a} = \tfrac{1}{2}(1-\gamma_5).$$

In order to make use of this technique, we should redefine our **L** and $L_s$, in terms not of $\psi$ fields, but of $\chi$ or $\xi$ fields. Two possibilities must *a priori* be considered: either we choose only $\chi$ fields, $a\mu^+$ and $ae^-$ as components of the **L** vector: this, however, leads to (1′) again and therefore to the same difficulty as before ($\rho = 0$); or we choose a $\chi$ and a $\xi$ field, e.g. $a\mu^+$ and $\bar{a}e^-$ as components of **L**, i.e. we define

$$\mathbf{L} = (a\mu^+,\ \nu_3,\ \bar{a}e^-),\ L_s = \nu_s. \tag{3}$$

Substituting (3) in any Lagrangian (2), where now $O$ is defined as $\gamma_\mu$, one is clearly led to a Lagrangian where $\mu^+$ and $e^-$ always appear in products $a\mu^+$ and $\bar{a}e^-$, respectively. This also means that if in the Lagrangian thus obtained, use is made of the charge conjugate $e^+$ field to describe the negatons, this field will only appear in a product $ae^+$. It is now obvious that the $\mu$—e interaction terms in Lagrangians (2) are of the type (1). The fit is complete if $\nu_3$ and $\nu_s$ in (3) are replaced by

$$\begin{aligned} \nu_3 &= \frac{1}{\sqrt{2}}(\bar{a}\nu^c - a\nu) \\ \nu_s &= \frac{1}{\sqrt{2}}(\bar{a}\nu^c + a\nu), \end{aligned} \tag{4}$$

where $\nu$ is a 4-component neutrino field, $\nu^c$ its charge conjugate. The two-component neutrino theory can of course be used here, i.e.

$$\begin{aligned} &a\nu = \nu \quad , \quad \bar{a}\nu^c = \nu^c, \\ &\bar{a}\nu = a\nu^c = 0. \end{aligned} \tag{5}$$

This will be done in what follows.

*Remark 1*

The choice $\mathbf{L} = (a\mu^+, \nu_3, \bar{a}e^-)$ instead of $(\bar{a}\mu^+, \nu_3, ae^-)$ is of course arbitrary and of no importance; it corresponds to the arbitrary assumption that $\mu^+$, $e^+$ are particles and $e^-$, $\mu^-$ antiparticles and not the reverse, which is clearly a pure convention at this stage. Similarly the choice of **L** instead of

$$\mathbf{L}' = (ae^+,\ \nu_3,\ \bar{a}\mu^-) \tag{6}$$

is here of no importance: in fact **L** and **L'** are just, up to trivial factors, PC conjugates to each other. The situation is, however, slightly different when baryons are introduced.

*Remark* 2

The detailed form of the interaction Lagrangian (i.e. the choice between the different expressions (2)) could not yet be made in this section: in $M$ space still very many possibilities are left open.

## 3. Weak Interactions involving Baryons

Weak interactions involving nucleons (and $\Xi$) were described in ref. [2]) using a 3-vector **B** and a scalar $B_s$ in $M$ space:

$$\mathbf{B} = (\mathrm{p},\ (\Xi^0-\mathrm{n})/\sqrt{2},\ \Xi^-),\quad B_s = (\Xi^0+\mathrm{n})/\sqrt{2}.$$

Similarly, weak interactions involving $\Lambda$ and $\Sigma$ particles were described using the 3-vector $\boldsymbol{\Sigma}$ and the scalar $\Lambda$. Now a natural requirement [9, 10]) is that, also in the non-leptonic case, P and C non-conservation should be introduced by the Feynman procedure. Just as in § 2, this leads to a new definition of **B**, $B_s$, $\boldsymbol{\Sigma}$, $\Lambda$ such as, e.g.

$$\begin{aligned} &B_+ = a\mathrm{p},\quad B_3 = a\frac{\Xi^0-\mathrm{n}}{\sqrt{2}},\quad B_- = a\Xi^-; \\ &B_s = a\frac{\Xi^0+\mathrm{n}}{\sqrt{2}}; \\ &\boldsymbol{\Sigma} = a\boldsymbol{\Sigma}';\quad \Lambda = a\Lambda', \end{aligned} \tag{7}$$

where $\boldsymbol{\Sigma}'$, $\Lambda'$ are $\psi$-fields, $\boldsymbol{\Sigma}$, $\Lambda$, **B**, $B_s$ are $\chi$-fields. On the ground that $\mathrm{p}, \mathrm{n}, \Xi^0, \Xi^-, \Sigma^+, \Sigma^0, \Sigma^-, \Lambda$ are "particles" it seems natural to take the same projection operator, here $a$, for all of them †.

On the basis of a strict analogy with the pure leptonic interaction (§ 2) we build up the interaction Lagrangians according to the following prescriptions:

Interaction Lagrangians are of the form

$$\mathbf{V} = (\bar{X}_i,\ X_j)\cdot\mathbf{V}(\bar{X}_k,\ X_m) \tag{8}$$

† It must be stressed, however, that this is by no means necessary. It would also be possible to attribute to baryons the "antiparticle" character, i.e to define the fundamental fields which enter in the Hamiltonians with the $\bar{a}$ projection operator ($\mathbf{B} = \bar{a}\mathbf{B}'$, $\boldsymbol{\Sigma} = \bar{a}\boldsymbol{\Sigma}'$, $\Lambda = \bar{a}\Lambda'$). Both choices are equally legitimate. They correspond, however, to different physical situations: the first to $g_V = -g_A$, the second to $g_V = +g_A$, in the conventional notations. Other choices are also possible. See in this connection some remarks in § 4. The final decision in this respect is, of course, a matter of experiment.

where the $X_i$, $X_j$, ... stand for any quantity $B = \mathbf{B}$ or $B_s$; $\Sigma = \mathbf{\Sigma}$ or $\Lambda$; $L = \mathbf{L}$ or $L_s$, and where the bilinear form $\mathbf{V}(\bar{X}_i, X_j)$ is a vector both in space-time and in $M$ space.

Examples of possible $\mathbf{V}$'s are

$$\bar{B}_s\gamma_\mu\mathbf{B}, \quad \bar{B}_s\gamma_\mu\mathbf{L}, \quad \bar{\mathbf{B}}\times\gamma_\mu\mathbf{B}, \quad \bar{\mathbf{\Sigma}}\gamma_\mu L_s. \tag{9}$$

A supplementary requirement to be imposed on the interaction is, of course, that it conserves the number of baryons †.

Let us now try to account, at least qualitatively, for all known decays using the minimum number of terms in the Lagrangian.

### 3.1. INTERACTIONS INVOLVING BARYONS AND LEPTONS

The $\mu$ decay as seen in § 2, can be described through

$$\mathbf{V}(\bar{L}, L)\cdot\mathbf{V}(\bar{L}, L) \tag{10}$$

where the detailed form of $\mathbf{V}$ need not be specified further.

The $\beta$ radioactivity and $\pi\to\mu+\nu$ decay can be accounted for through

$$\mathbf{V}(\bar{L}, L)\cdot\mathbf{V}(\bar{B}, B). \tag{11}$$

Here the $\pi\to\mu+\nu$ decay takes place through one of the two intermediary steps

$$\pi\to \mathrm{N}+\bar{\mathrm{N}}\to\mu+\nu, \quad \pi\to\Xi+\bar{\Xi}\to\mu+\nu.$$

For most forms of $\mathbf{V}$ the $\pi\to \mathrm{e}+\nu/\pi\to\mu+\nu$ branching ratio is $\approx 10^{-4}$ (owing to the $\gamma_\mu$ coupling). This is, however, too large to fit the recent experimental data. A special choice for $\mathbf{V}$, discussed in § 4, offers a means to solve this well-known puzzle. The interaction (11) predicts also $\Xi\to \mathrm{N}+\mathrm{e}+\nu$ and $\Xi\to \mathrm{N}+\mu+\nu$ ††. The partial lifetime for $\Xi\to \mathrm{N}+\mathrm{e}+\nu$ can be easily calculated by phase-space considerations [11]) from the knowledge of the neutron lifetime (in fact (11) implies the same coupling constant and the same form of the Hamiltonian for both processes). It is found that this partial lifetime is of the order of $10^{-10}$ sec, i.e. more or less of the same order as the total $\Xi$ lifetime. The processes $\Xi\to \mathrm{N}+\mathrm{e}(\mu)+\nu$ should then be quite frequent. In other words, the branching ratio $\Xi\to \mathrm{N}+\mathrm{e}+\nu/\Xi\to\Lambda+\pi$ should be quite appreciable. This is a rather stringent prediction of the $M$ space formalism. It should be added that (11) does not predict any experimentally disproved process such as $\mu^-+\mathrm{N}\to \mathrm{N}+\mathrm{e}^-$ (in spite of the fact that $\mu^+$ and $\mathrm{e}^+$ are both "particles").

The $\mathrm{K}\to\mu+\nu$, $\mathrm{K}\to\pi+\mu+\nu$, $\mathrm{K}\to\pi+\mathrm{e}+\nu$ decays must be accounted for by using

† The $\mathbf{M}$ invariance automatically guarantees the conservation of charge.

†† It should be remembered that strangeness has no meaning for leptons and that therefore the $|\Delta U| = 1$ rule has anyhow no validity in this case.

$$\mathbf{V}(\bar{B}, \Sigma) \cdot \mathbf{V}(\bar{L}, L). \tag{12}$$

They happen through the graphs (fig. 1).

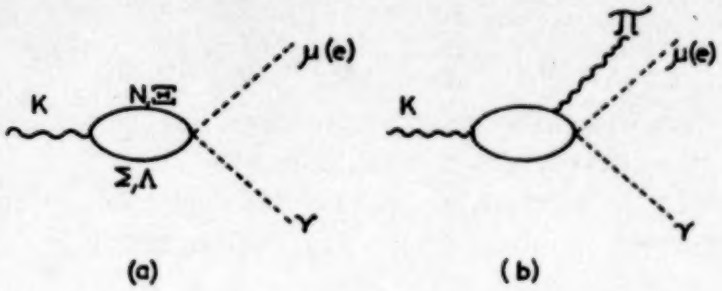


Fig. 1

The $(K \to e+\nu)/(K \to \mu+\nu)$ branching ratio is here again predicted to be $\approx 10^{-4}$. The $(K \to \pi+e+\nu)/(K \to \pi+\mu+\nu)$ branching ratio has, however, no particular reason to be small: this is in agreement with experiment.

It may be recalled in this connection that a *Fermi type* interaction between a baryon with $U = 0$, a baryon with $U = \pm 1$ and leptons is absolutely necessary (if no new particles are to be introduced). It was proved[12]) that a direct weak Yukawa interaction is unable to account for the existence of $K_{\mu 3}$ and $K_{e3}$ decay modes if the spin of K is zero. (Clearly this property is quite strong evidence against the Goldhaber [13]) composite model †.)

The interaction (12) also predicts some amount of

$$\Sigma \text{ or } \Lambda \to N+e(\mu)+\nu.$$

If, however, the coupling constants of (11) and (12) are taken equal, these decay modes should not exceed a few percent of the normal ones [11]).

### 3.2. INTERACTIONS INVOLVING BARYONS ONLY; $|\Delta I| = 3/2$ ADMIXTURE

Interactions involving baryons only should be responsible for the normal (non-leptonic) decays of hyperons and K mesons. This is a domain, however, where the strong interactions of the fields under consideration may very seriously upset the deductions that are drawn from the weak interaction Lagrangian $L_w$ alone. This is particularly true because of the fact [2]) that the "intermediate" or "medium" strong interactions are not invariant in $M$ space. Therefore, as mentioned in the introduction, the theory will here make sense only if consequences of $L_w$ can be derived which either (a) remain exactly true also in the presence of $L_{V.S.}$ and $L_{I.S.}$, or (b) remain exactly true in the presence of $L_{V.S.}$ and are modified in some predictable way by the introduction of $L_{I.S.}$.

† This became clear to us during a private discussion with Drs. Kamefuchi and Oneda.

That consequences of these kinds indeed exist is easily seen. An example of consequence of type (a) is the following theorem (which is just a special case of Lemma 1 of the appendix):

*Theorem* 1. *If* $L_w$ *involves only one* B *and no* K *field, or one* K *and no* B, *then the* $|\Delta \mathbf{I}| = \frac{1}{2}$ *rule is strictly valid.*

An example of consequence of type (b) is:

*Theorem* 2. *Whatever* $L_w$ *may be, for any real decay process the* $|\Delta \mathbf{I}| = 3/2$ *admixture necessarily goes to zero if the* $L_{\text{I.S.}}$ *coupling constants* $\varepsilon_i$ *tend to zero.*

This is a consequence of Lemma 2 (appendix) and of the fact that real decay processes never involve simultaneously more than one N, $\Xi$ or K.

As some $|\Delta \mathbf{I}| = 3/2$ admixture is experimentally known to exist the first theorem above can serve as a guide for the choice of $L_w$. For example,we see immediately that $\mathbf{V}(\bar{\Sigma}, \Sigma) \cdot \mathbf{V}(\bar{B}, \Sigma)$ would not account for this admixture whereas

$$\mathbf{V}(\bar{B}, B) \cdot \mathbf{V}(\bar{B}, \Sigma) \tag{13}$$

can do it †. Theorem 2 then shows that the $|\Delta \mathbf{I}| = 3/2$ admixture is proportional to some power of $\varepsilon$. Lemma 3 (appendix) further tells us in some cases what the minimum power of $\varepsilon$ is: for example the matrix element for $K_s$ giving $2\pi$ in a $I = 2$ state necessarily contains $\varepsilon^2$ as a factor, whereas the matrix element for **K** giving $2\pi$ in $I = 2$ state can be of the order $\varepsilon$ only.

The interaction (13) together with $L_{\text{V.S.}}$ and $L_{\text{I.S.}}$ accounts for $\Sigma$, $\Lambda \to \mathrm{N}+\pi$, $\Xi \to \Lambda+\pi$ with some $|\Delta \mathbf{I}| = 3/2$ admixture (proportional to $\varepsilon$ in the matrix element) which we would like to consider as responsible — partly at least — for the observed ratios †† $\Sigma^+ \to \mathrm{n}\pi^+ : \Sigma^+ \to \mathrm{p}\pi^0 : \Sigma^- \to \mathrm{n}\pi^- \approx 1 : 1 : 1$.

The interaction (13) also accounts for $K^+$, $K^- \to 2\pi$ via the $|\Delta \mathbf{I}| = 3/2$ admixture and therefore with a larger lifetime that $K_s \to 2\pi$. As regards this last phenomenon the discrepancy between $\frac{1}{2}$ and the observed $(\mathrm{K}^0 \to 2\pi^0)/(\mathrm{K}^0 \to \pi^+ + \pi^-)$ branching ratio should also be attributed primarily to the $|\Delta \mathbf{I}| = 3/2$ admixture (also partly to the difference between $\pi^+$ and $\pi^0$ masses [2]). The question whether a $|\Delta \mathbf{I}| = 5/2$ admixture is also needed, as suggested by Dalitz [3], is, of course, rather crucial in this context because (see Lemma 1, appendix) this admixture is not predicted by (13),

† Theorem 1 also shows that among all *a priori* possible Yukawa weak interactions, only those involving one K and two B fields can produce a $|\Delta \mathbf{I}| = 3/2$ admixture. This should be kept in mind in any attempt to construct a theory where non-leptonic decays are described through direct baryon meson weak interactions. Here, however, we stick to the generalized use of Fermi interactions.

†† The introduction of P and C violation by means of the projection operators $a$ and $\bar{a}$ seems to make it unlikely that these ratios can be fitted to a strict $|\Delta \mathbf{I}| = \frac{1}{2}$ rule, as is possible [14, 15]) when P and C violation are introduced with a greater freedom in the choice of the couplings.

nor indeed by any Fermi type interaction. As a result of some rough numerical calculations the opinion was reached, however, that, if the present experimental uncertainties on the $K_s$ branching ratio are duly taken into account, no conclusive answer can as yet be given to this problem.

Gathering the Lagrangians (10), (11), (12), (13) into a single formula, we may say that the Lagrangian

$$L_w = g[\mathbf{V}(\bar{L}, L)+\mathbf{V}(\bar{B}, \Sigma)] \cdot [\mathbf{V}(\bar{L}, L)+\mathbf{V}(\bar{B}, B)] \qquad (14)$$

where the detailed form of **V** can be left open (subject, however, to the restrictions above), accounts qualitatively — and, whenever estimation can be made, also in a very rough quantitative way — for the known experimental decay data of mesons and baryons.

## 4. Tentative Solution of the $\pi e\nu$—$\pi\mu\nu$ Puzzle

The universal Fermi interaction hypothesis in the usual sense (a modification of it is proposed below) leads to $\pi \to e+\nu/\pi \to \mu+\nu \approx 10^{-4}$ in the most favourable case (vector and pseudovector couplings). The assumption here is that the $\mu$—$\nu$—baryon—baryon and the e—$\nu$—baryon—baryon interactions are, term by term, exactly similar (same coupling constant and same structure). If a ratio smaller than $10^{-4}$ is desired, a modification has clearly to be made in the assumption stated above. This, in the usual theories, is extremely difficult for a dissymmetry has to be brought in somewhere between e and $\mu$ interactions and then there does not remain much of the original hypothesis.

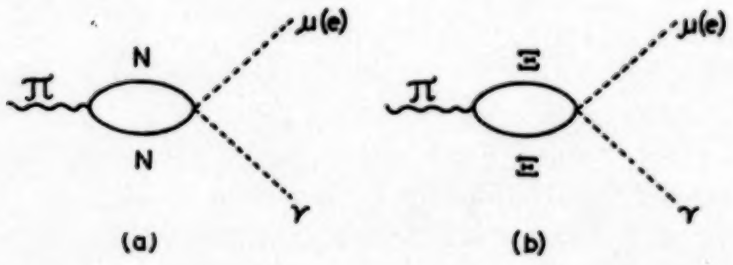


Fig. 2

As an example of such a procedure, let us consider the case when the interactions under consideration involve N and $\Xi$ baryons only. The decay graphs of lowest order are those of fig. 2. The $\pi \to \mu+\nu(\pi \to e+\nu)$ matrix element is, to this order, roughly proportional to $g_{N\mu}+g_{\Xi\mu}$ (to $g_{Ne}+g_{\Xi e}$) where the $g$'s are here the weak interaction coupling constants. A (partial) cancellation that is effective only for $\pi \to e+\nu$ and not for $\pi \to \mu+\nu$ is

achieved if e.g. $g_{N\mu} = g_{\Xi\mu} = g_{Ne} = -g_{\Xi e}$. Such an assumption may, for all we know, correspond to the truth but, because of the difference in signs, clearly cannot be associated with the concept of "universality" of the interactions.

The $M$ space formalism makes it possible to follow a somewhat more attractive procedure. It still uses the concept of an interaction that is both of the Fermi type and universal, in the sense that the interaction terms all have formally the same structure and the same coupling constant including sign. The difference with the usual universal Fermi interaction hypothesis is essentially that these interaction terms are not constructed using each particle field directly — subject only to charge conservation — but are built up with the entities that have a fundamental significance in $M$ space, i.e. $\mathbf{B}$, $B_s$; $\mathbf{L}$, $L_s$; etc., charge conservation being then automatic.

In order to preserve the previous agreement with experimental data concerning $\mu$ decay, $\beta$ decay and so on, the general form (14) of the Lagrangians should clearly be kept here. It shall, however, be specified further in such a way as to introduce a difference in sign between the (N, e) and ($\Xi$, e) interactions. This can be achieved by setting

$$\mathbf{V}(\bar{X},\ Y) = \bar{X}_s \gamma_\mu \mathbf{Y} - \bar{\mathbf{X}} \gamma_\mu Y_s \tag{15}$$

(as is easily checked by writing $\mathbf{V}(\bar{B},\ B)$ explicitly; see appendix). In the approximation in which intermediary strong interactions are neglected ($\varepsilon_i = 0$) a cancellation then occurs between the matrix elements of graphs (a) and (b) in fig. 2. Assumption (15) has thus the consequence that it slows down both $\pi \to e+\nu$ and $\pi \to \mu+\nu$, making their matrix element proportional — in the first approximation — to the coupling constant of *intermediary* strong interactions. Apart from this, nothing is changed in the results of the previous sections: $\beta$ decay, in particular, takes place as before.

At this stage the $\pi$ branching ratio is still roughly $10^{-4}$. The next step is to introduce a new interaction term, also of the general form (8) but which should be effective only for muons. This is indeed possible because of the projection operators $a$, $\bar{a}$ in (3) which, in any expression $\mathbf{V}(\bar{B},\ L)$, effectively eliminate the electron field. Let us therefore introduce the supplementary interaction term

$$\mathbf{V}(\bar{B},\ L) \cdot \mathbf{V}(\bar{L},\ B) \tag{16}$$

with $\mathbf{V}$ given by (15). Then in (16) the V.S. interactions become effective again in $\pi \to \mu+\nu$ decay: it turns out, in fact, that (16) couples $\mu$ only to $\Xi$, not to N. As a result, the $\pi$ branching ratio is now of the order

$$\left(\frac{\varepsilon}{G}\right)^2 \times 10^{-4} \tag{17}$$

where $10^{-4}$ comes from the $\gamma_\mu$ coupling and $(\varepsilon/G)^2$ comes from (14), (15) and (16). If the ratio $\varepsilon/G$ of intermediary strong to very strong interactions is $\lesssim 10^{-\frac{1}{2}}$ this branching ratio is compatible with present experimental data. As is easily shown, this result holds true to any order in the strong interaction coupling constants: this is essentially due to the fact that any modification of the lowest order graph (fig. 2) can be interpreted as a renormalization of the strong interaction constants.

The method used here is by no means unique [17]) and quite possibly it is not even the simplest possible one. We have given here only *one example* of possible schemes, which, whenever estimations can be made, accounts in a semi-quantitative way for all known data in the field of weak interactions.

It may perhaps be stressed that the choice of Hamiltonians (14) and (16) with (15) accounts not only for the numerous decays that have been observed, but also — and this is perhaps somewhat more remarkable — for the non-existence of many decays and reactions which are known not to take place. For example, it gives no reactions such as

$$\mu^- + \mathrm{p} \to \mathrm{p} + \mathrm{e}^- \tag{18}$$

(in spite of the fact that $\mu^-$ and $\mathrm{e}^-$ are both anti-particles) and also no decays of such types as

$$\Sigma(\Lambda) \to \mathrm{N} + \nu + \nu, \tag{19}$$

$$\mathrm{K}^\pm \to \mathrm{e}^\pm + \mathrm{e}^\mp + \pi^\pm,$$

$$\mathrm{K}^0 \not\to \begin{matrix} \mathrm{e}^+ + \mathrm{e}^- \\ \mathrm{e}^+ + \mathrm{e}^- + \pi^0 \end{matrix}. \tag{20}$$

The branching ratio given by this choice for $\mathrm{K}^\pm \to \mathrm{e}^\pm + \nu / \mathrm{K}^\pm \to \mu^\pm + \nu$ is, on the other hand, quite acceptable ($\approx 10^{-4}$) and so is the branching ratio $\mathrm{K} \to \pi + \mathrm{e} + \nu / \mathrm{K} \to \pi + \mu + \nu$ (which has no reason of differing from unity by any such large factor [16])).

## 5. Summary and conclusions

The results of the foregoing sections are here summarized.

a) As regards $\mu$ decay and $\beta$ radioactivity, it has been shown that all the results of a universal Fermi interaction of the V—A type can be obtained in the frame of the $M$ space formalism, combined with the formalism of ref. [9, 10]).

b) A $\Lambda(\Sigma)$, N, $\mu(\mathrm{e})\nu$ interaction is necessary [12]) to account for the $\mathrm{K}_{\mu 3}$ and $\mathrm{K}_{\mathrm{e}3}$ decay modes. It leads of course to $\beta$ decays of the $\Lambda$, $\Sigma$ and $\Xi$ particles. Such decays as $\Sigma^+ \to \mathrm{p} + \nu + \nu$ etc. are *a priori* also possible: our final choice of Lagrangians (i.e. expressions (14) and (16) with V given

by (15)) leads, however, to selection rules forbidding such processes. In fact, the only possible leptonic decays of baryons are of the type

$$\text{Baryon} \to \text{Baryon} + e(\mu) + \nu.$$

The partial decay rates for these processes may be easily estimated [11]) from the knowledge of the neutron lifetime. It may be pointed out in particular as a rather striking fact that, with our final choice of Lagrangians, the $\Xi \to N + e + \nu$ decay should occur with a decay rate $\approx 10^{10}$ sec$^{-1}$, presumably of the same order of magnitude as the total decay rate of the cascade particle.

c) The K mesons decays have the following properties: The V—A coupling makes $K \to e + \nu / K \to \mu + \nu \ll 1$; a similar inequality, however, does *not* hold [16]) for $K_{\mu 3}$ and $K_{e3}$, which can be of roughly the same order. Again the choice of Lagrangians (14) and (16) with (15) leads to selection rules: all leptonic decays of K mesons necessarily involve (e, $\nu$) or ($\mu$, $\nu$) pairs: in other words, combinations of the types ($e^+$, $e^-$), ($\mu^+$, $\mu^-$), ($\mu^\pm$, $e^\mp$) never occur. At the time of writing this seems rather satisfactory; it should, however, be mentioned that some terms could be added to the Lagrangian that would alter this conclusion. For instance a $K_0 \to \mu^+ + \mu^-$ decay mode (which, as a rare phenomenon, might up to now have escaped detection) could very naturally be accounted for [17]).

d) As mentioned in § 4, the choice of Lagrangians (14) and (16) with (15) is needed to explain the $\pi e \nu$, $\pi \mu \nu$ puzzle: the $\pi \to e + \nu$ decay is then proportional to $\varepsilon$ while the $\pi \to \mu + \nu$ decay is proportional to $G$. The $\pi e \nu / \pi \mu \nu$ branching ratio is then of the order $(\varepsilon/G)^2 \times 10^{-4}$ where the $10^{-4}$ factor comes from the V—A coupling, and the $(\varepsilon/G)^2$ factor from the structure of the Lagrangian. This ratio can be of the order of, or less than, $10^{-5}$ in agreement with present experimental data. It was stressed in the text that here such a rough quantitative estimation could be made because it is valid to all orders in the very strong interaction coupling constants.

e) Other problems discussed in this paper are connected with the $|\Delta \mathbf{I}| = \frac{1}{2}$ rule for non-leptonic processes. It has been shown that a violation of this rule occurs very naturally if elementary weak interactions between baryons are of the Fermi type. In particular the choice of Lagrangians (14) and (16) with (15) does allow for a $|\Delta \mathbf{I}| = 3/2$ admixture. According to lemma 2 in the appendix, this admixture is, however, strictly connected with intermediary strong interactions as far as real processes involving known particles are concerned. If $\varepsilon \ll G$ this admixture is thus rather small, of the order of $(\varepsilon/G)^2$. It can reasonably be hoped that it is sufficient to solve the $K^0 \to 2\pi^0 / K^0 \to \pi^+ + \pi^-$ problem and to account for the observed ratios $\Sigma^+$, $n\pi^+ : \Sigma^+$, $p\pi^0 : \Sigma^-$, $n\pi^- \approx 1 : 1 : 1$ although all interactions are here in $\gamma_\mu(1+\gamma_\mu)$.

According to lemma 1 in the appendix no $|\Delta \mathbf{I}| = 5/2$ admixture is possible with our choice of Lagrangians, nor indeed with any four-fermion elementary weak interaction in the frame of the $M$ space theory (except of course for admixtures of electromagnetic origin). This is also independent of any approximation on the strong interaction mechanism. A detailed calculation of the branching ratios mentioned above is on the contrary very much dependent, with present techniques, on such approximations: it was therefore not attempted.

f) It should be added that a supplementary interaction term is available which would induce $\Xi \to \mathrm{N}+\pi$; the decay rate, however, for the same reasons as in e), could not be estimated. A search for this decay mode would be interesting; it is not, however, (unlike the $\Xi \to \mathrm{N}+\mathrm{e}+\nu$ decay mentioned in b)) implied by our particular choice of Lagrangians (14) and (16) with (15).

While dealing with subjects of this kind, we would like to stress that care was exercised throughout this paper to describe the presently known facts with the minimum possible number of $M$-invariant terms in the Lagrangian. Other terms, however, might well coexist. We mention briefly[17]) the $\mathbf{V}(\bar{B}, B) \cdot \mathbf{V}(\bar{B}, B)$ term, which is the one that would induce $\Xi \to \mathrm{N}+\pi$, and the $\mathbf{V}(\bar{B}, L) \cdot \mathbf{V}(\bar{L}, \Sigma)$ term which would induce $\mathrm{K}_0 \to \mu^+ + \mu^-$.

As is always the case with theories involving Fermi interactions, the problem of handling the actual calculations is here a very serious one. The present theory even raises a calculation problem which, apparently, is a new one, namely, when, in the absence of intermediary strong interactions, a quantity such as, e.g., a branching ratio is determined by some general theorem, how do the intermediary strong interactions, viewed as a perturbation, modify the result? Up to now, only the qualitative results of lemma 3 in the appendix are available in this connection and a more refined approach would be highly desirable.

Our purpose, however, in the present paper was only to point out that in the frame of the $M$ space formalism and of a theory of universal Fermi weak interactions suitably adapted to this formalism — and if, let this be stressed, one excludes some questionable data on $\beta$ decays which disagree with the V—A scheme — it is possible to account in a qualitative, or even semi-quantitative, way for all experimental data available at the present time.

Our best thanks are due to members of CERN Theoretical Group, and particularly to Professor B. Ferretti and to Dr. R. Omnès, for some very interesting discussions during the elaboration of this paper.

## Appendix

### STRONG INTERACTION LAGRANGIAN

The strong interaction Lagrangian is

$$\begin{aligned} L = {} & (G_1+\varepsilon_1)\bar{\mathrm{N}}i\gamma_5\boldsymbol{\tau}\cdot\mathrm{N}\boldsymbol{\pi}+(G_1-\varepsilon_1)\bar{\Xi}i\gamma_5\boldsymbol{\tau}\cdot\Xi\boldsymbol{\pi} \\ & +G_2\bar{\Lambda}i\gamma_5\boldsymbol{\Sigma}\cdot\boldsymbol{\pi}+G_3 i\bar{\boldsymbol{\Sigma}}(i\gamma_5)\times\boldsymbol{\Sigma}\cdot\boldsymbol{\pi} \\ & +(G_5+\varepsilon_5)\bar{\Lambda}i\gamma_5\,\mathrm{K}^*\,\mathrm{N}+(G_5-\varepsilon_5)\bar{\Lambda}i\gamma_5\,\dot{\mathrm{K}}^*\,\Xi \\ & +(G_6+\varepsilon_6)\bar{\Sigma}i\gamma_5\,\mathrm{K}^*\cdot\boldsymbol{\tau}\mathrm{N}+(G_6-\varepsilon_6)\bar{\Sigma}i\gamma_5\,\dot{\mathrm{K}}^*\cdot\boldsymbol{\tau}\Xi \\ & +\text{h.c.}\equiv L_{\text{V.S.}}+L_{\text{I.S.}} \end{aligned} \tag{A1}$$

where $L_{\text{V.S.}}$ is the sum of the terms with $G$'s, $L_{\text{I.S.}}$ is the sum of the terms with $\varepsilon$'s, and where

$$\dot{\mathrm{K}} = i\tau_2\mathrm{K}^*.$$

In a 4-dimensional Euclidian space $L_{\text{V.S.}}$ is 4-invariant with the Salam and Polkinghorne attributions

$$(\mathrm{N},\ \Xi),\ (\mathrm{K},\ \dot{\mathrm{K}})\in\mathscr{D}(\tfrac{1}{2}\tfrac{1}{2});\quad \Sigma,\ \pi\in\mathscr{D}(1\,0);\quad \Lambda\in\mathscr{D}(0\,0).$$

(A1) is just the ordinary Lagrangian of ref [18]).

The 4-dimensional invariance character of $L_{\text{V.S.}}$ is easily exhibited as follows:

Write the 4-vectors $(\mathrm{N}\Xi)$ and $(\mathrm{K}\dot{\mathrm{K}})$ as

$$(B_k{}^i) = \begin{pmatrix} \Xi^0, & \mathrm{p} \\ \Xi^-, & \mathrm{n} \end{pmatrix},\quad (K_k{}^i) = \begin{pmatrix} \dot{\mathrm{K}}^0, & \mathrm{K}^+ \\ \dot{\mathrm{K}}^-, & \mathrm{K}^0 \end{pmatrix},$$

the antisymmetric self dual tensors $\Sigma$, $\pi$ and the scalar $\Lambda$ as

$$(\Sigma_k{}^i) = \begin{pmatrix} \dfrac{1}{\sqrt{2}}\Sigma^0, & \Sigma^+ \\ \Sigma^-, & -\dfrac{1}{\sqrt{2}}\Sigma^0 \end{pmatrix},\quad (\pi_k{}^i) = \begin{pmatrix} \dfrac{1}{\sqrt{2}}\pi^0, & \pi^+ \\ \pi^-, & -\dfrac{1}{\sqrt{2}}\pi^0 \end{pmatrix},$$

$$\Lambda_k{}^i = \frac{1}{\sqrt{2}}\delta_{kl}\Lambda.$$

Then ($\gamma$ matrices being omitted)

$$\begin{aligned} \frac{1}{\sqrt{2}}L_{\text{V.S.}} = {} & G_1 B_k{}^{i*}\pi_k{}^m B_m{}^i+G_2\Lambda_k{}^{l*}\pi_k{}^m\Sigma_m{}^l-G_3\Sigma_k{}^{l*}\pi_k{}^m\Sigma_m{}^l \\ & +G_5 B_k{}^{i*}\Lambda_k{}^m K_m{}^i+G_6 B_k{}^{i*}\Sigma_k{}^m K_m{}^i+\text{h.c.} \end{aligned} \tag{A1'}$$

The 4-invariance of each term is then evident. The $L_{\text{I.S.}}$ Lagrangian (invariant in the [3] space$I^+$) can be derived from (A1') by the following substitutions:

$$G_{1,5,6}\to(-)^i\varepsilon_{1,5,6}.$$

## THREE LEMMATA RELATIVE TO NON-LEPTONIC WEAK INTERACTIONS

We represent the K mesons in $M$ space by the vector

$$\mathbf{K} = (\mathrm{K}^+,\ (\dot{\mathrm{K}}_0 - \mathrm{K}_0)/\sqrt{2},\ \dot{\mathrm{K}}^-)$$

and the scalar $K_s = (\dot{\mathrm{K}}_0 + \mathrm{K}_0)/\sqrt{2}$.

*Lemma 1*

In an elementary weak interaction Lagrangian term, let $p$ be the total number of $\mathbf{B}$, $\overline{\mathbf{B}}$, $B_s$, $\bar{B}_s$, $\mathbf{K}$, $\overline{\mathbf{K}}$, $K_s$ and $\bar{K}_s$ factors. Then the change $\Delta\mathbf{I}$ in isobaric spin induced by this term satisfies $|\Delta\mathbf{I}| \leqq \frac{1}{2}p$. This result is not affected by the presence of V.S. and I.S. interactions.

*Proof*

Let $x = \binom{0}{1}$, $y = i\tau_2 x^* = \binom{1}{0}$ (spurions of 1st and 2nd kind). Then

$$\begin{aligned} \mathbf{B} &= x^* \boldsymbol{\tau} \mathrm{N} + y^* \boldsymbol{\tau}\, \Xi; & \mathbf{K} &= x^* \boldsymbol{\tau} \mathrm{K} + y^* \boldsymbol{\tau} \dot{\mathrm{K}}; \\ B_s &= x^* \mathrm{N} + y^* \Xi; & K_s &= x^* \mathrm{K} + y^* \dot{\mathrm{K}}. \end{aligned} \tag{A2}$$

If these formulae are used, the weak interaction term under consideration becomes a scalar in $I^+$ space, containing $p$ factors $x$ or $y$ which may be interpreted as the "emission" of $p$ spurions. If now we go from this process with bare fields to the process involving physical particles and a physical coupling constant, i.e. if we dress both the particle propagators and the weak interaction vertex by means of V.S. and I.S. interactions, the interaction matrix element we are dealing with still remains a scalar in $I^+$ space (because both V.S. *and* I.S. interactions are invariant in that space), account being taken of the $p$ spurions of $I^+$-spin $\frac{1}{2}$. Dropping the spurion factor, one is led to lemma 1.

*Lemma 2*

Let us consider a real process in which the total number of N, $\Xi$, K and $\overline{\mathrm{K}}$ particles involved is $q$ (counting both the particles in the initial and the final state) and let us consider the approximation in which the intermediary strong interactions are neglected (V.S. interactions are taken to all orders). Then the isobaric spin change $\Delta\mathbf{I}$ in the reaction satisfies $|\Delta\mathbf{I}| \leqq \frac{1}{2}q$.

*Proof*

Let us describe the reaction (which is usually a product of several elementary interactions) by means of a phenomenological interaction term: as both V.S. and weak interactions are invariant in $M$ space, this phenomenological interaction term is, to the approximation stated, also a scalar in $M$ space. The rest of the proof is as in lemma 1.

Lemma 2 is a particular case of

*Lemma* 3

The number $q$ being defined as in lemma 2, let us consider an expansion of the matrix element for the reaction in terms of the intermediary strong coupling constants $\varepsilon$. The $n^{\text{th}}$ term of this expansion induces an isobaric spin change $\Delta\mathbf{I}$ which satisfies $|\Delta\mathbf{I}| \leqq \frac{1}{2}q+n$.

*Proof*

It was shown by Polkinghorne [6]) that also the I.S. interactions (as written above in this appendix) can be made 4-dimensional invariants provided a new kind of spurion, $X$, is introduced, which is a vector in $I^-$ space and a scalar in $I^+$ space ($\mathscr{D}$ (0 1)) and whose only non-zero component is $X_3$: the I.S. elementary interactions are then linear in $X$. It should be stressed that the Polkinghorne approach in no way implies a new hypothesis about strong interactions: $X$ is purely a mathematical artifice by means of which the usual $\mathbf{I}$ and $U$ conserving Lagrangian [18]) can be conveniently split.

Let us now consider a complicated graph containing one weak interaction vertex, $n$ intermediary strong interaction vertices and an arbitary number of very strong interaction vertices. The associated matrix element can be made a scalar in $M$ space by introducing $n$ $X$-spurion lines. A phenomenological interaction term that describes the process is therefore necessarily a scalar in $M$ space with at most $n$ factors $X$. The rest of the proof is but a trivial generalization of that of lemma 2.

When applying lemmas 2 and 3, it should be noticed that $q = 1$ for all known decays.

EXPLICIT EXPRESSIONS FOR $\mathbf{V}(\bar{X}, Y)$

The expression $\mathbf{V}(\bar{X}, Y)$ given by (15) can be expanded ($\gamma_\mu$ factors being omitted) as follows:

$$\mathbf{V}(\bar{B}, B) = \begin{cases} [(\Xi^{0*}+n^*)\mathrm{p}-\Xi^{-*}(\Xi^0+n)]/\sqrt{2} \\ \mathrm{n}^*\Xi^0-\Xi^{0*}\mathrm{n} \\ [(\Xi^{0*}+\mathrm{n}^*)\Xi^- - \mathrm{p}^*(\Xi^0+\mathrm{n})]/\sqrt{2}, \end{cases}$$

$$\mathbf{V}(\bar{L}, L) = \begin{cases} [\nu^*\mu^+ - \mathrm{e}^{-*}\nu^c]/\sqrt{2} \\ 0 \\ [\nu^{c*}\mathrm{e}^- - \mu^{+*}\nu]/\sqrt{2}, \end{cases}$$

$$\mathbf{V}(\bar{B}, \Sigma) = \begin{cases} (\Xi^{0*}+\mathrm{n}^*)\Sigma^+/\sqrt{2} - \Xi^{-*}\Lambda \\ [(\Xi^{0*}+\mathrm{n}^*)\Sigma^0 - (\Xi^{0*}-\mathrm{n}^*)\Lambda]/\sqrt{2} \\ (\Xi^{0*}+\mathrm{n}^*)\Sigma^-/\sqrt{2} - \mathrm{p}^*\Lambda, \end{cases}$$

$$\mathbf{V}(\bar{L}, B) = \begin{cases} \nu^*\mathrm{p}/\sqrt{2} \\ \nu^*\Xi^0 \\ [\nu^*\Xi^- - \mu^{+*}(\Xi^0+\mathrm{n})]/\sqrt{2}. \end{cases}$$

## References

1) G. Wentzel, Phys. Rev. **101** (1956) 1215;
R. Gatto, Nuovo Cimento **3** (1956) 318;
B. d'Espagnat and J. Prentki, Nuovo Cimento **3** (1956) 1045;
G. Takeda, Phys. Rev. **101** (1956) 1547;
M. Kawaguchi and K. Nishijima, Prog. Theor. Phys. **15** (1956) 180, 182;
C. Iso and M. Kawaguchi, Prog. Theor. Phys. **16** (1956) 177
2) B. d'Espagnat, J. Prentki and A. Salam, Nuclear Physics **5** (1958) 447
3) R. H. Dalitz, Proc. Phys. Soc. A **69** (1956) 527
4) B. d'Espagnat, C. R. Acad. Sc. **245** (1957) 894
5) A. Salam and J. C. Polkinghorne, Nuovo Cimento **2** (1955) 685
6) J. C. Polkinghorne, Nuovo Cimento **6** (1957) 864
7) E. J. Konopinski and H. M. Mahmoud, Phys. Rev. **92** (1953) 1045
8) T. D. Lee and C. N. Yang, Phys. Rev. **105** (1957) 1671
9) R. P. Feynman, Rochester Conference (1957)
10) R. P. Feynman and M. Gell-Mann, Phys. Rev. **109** (1958) 193
11) R. H. Behrends and C. Fronsdal, Phys. Rev. **106** (1957) 345
12) B. d'Espagnat, R. Omnès and J. Prentki, Nuclear Physics **3** (1957) 471
13) S. Goldhaber, Phys. Rev. **101** (1956) 433
14) B. T. Feld, Nuovo Cimento **6** (1957) 650
15) Y. Yamaguchi, Prog. Theor. Phys.
16) J. J. Sakurai, Phys. Rev.
17) B. d'Espagnat and J. Prentki, C. R. Acad. Sc. **246** (1958)
18) B. d'Espagnat and J. Prentki, Nuclear Physics **1** (1956) 33;
A. Salam, Nuclear Physics **2** (1956/57) 173

*Nuclear Physics* **6** (1958) 613—617; © *North-Holland Publishing Co., Amsterdam*

Not to be reproduced by photoprint or microfilm without written permission from the publisher

# INELASTIC SCATTERING OF DEUTERONS FROM SPHEROIDAL NUCLEI

J. SAWICKI

*Institute for Nuclear Research, Theoretical Physics, Warsaw*†

Received 12 December 1957

**Abstract:** A direct interaction theory of (d, d') reactions is proposed for strongly deformed nuclei of mass number $A \approx 24$. Strong coupling approximation of the unified nuclear model is employed to represent the nucleus and the differential cross-section is calculated in Born approximation for rotational excitations up to the fourth power of the deformation parameter $\beta$. The theory is applied to the $Mg^{24}$ (d, d') $Mg^{24}$ (1.37 MeV) reaction. Agreement with experiment is obtained both for the angular distribution (except for $\theta \lesssim 20°$) and for the total cross-section. Further extensions of the model are indicated.

## 1. Introduction

The important effect of the inelastic scattering of medium energy deuterons from nuclei has been little investigated theoretically so far. In contrast to the inelastic scattering of nucleons from nuclei, the contribution of the compound nucleus formation mechanism in (d, d') reactions is extremely improbable, because of the low binding energy of deuteron. Both the strongly anisotropic (peaked) angular distributions and high cross-section values contradict the latter mechanism. It has therefore been proposed to explain these reactions using either a direct interaction mechanism [1, 2]) or an electric interaction theory [3]). A recent analysis [4]) provides comparison between these two mechanisms as applied to the angular distribution and cross-section data on $Li^6$, $Li^7$, $Be^9$, $C^{12}$, $Mg^{24}$, $Al^{27}$. Both the angular distributions (particularly for angles $\theta \gtrsim 20°$) and the cross-section data fit much better the nuclear interaction theory. The multipole moments required to fit the cross-section data in terms of the electric interaction theory are higher by 1—2 orders of magnitude than expected theoretically. On the other hand, however, the old nuclear interaction theory [1, 2]) is extremely crude and can be trusted at most only qualitatively. Among its obvious shortcomings the most doubtful points are the neglect of all Coulomb effects (plane waves replace the true Coulomb analogues) and Bhatia's stripping assumption that the interaction operates only over the surface of a sphere of radius $a$ (a delta function potential

† Present address: Palmer Physical Laboratory, Princeton University, Princeton, N.J.

for the neutron transition operator). The nucleus has been assumed spherical. The latter assumption makes it unreasonable to apply this theory to strongly deformed nuclei, in particular when rotational excitations are involved. Unfortunately, the classical example of the $Mg^{24}$(d, d')$Mg^{24}$ (1.37 MeV level) reaction involves the well known first 2+ member of the rotational band based on the ground state of an even spheroidal nucleus ($K_i = K_f = 0$). The theory of refs. [1, 2]) must not be employed here. The apparently successful fits to the data [1, 2, 4]) should therefore, be, regarded in this case as rather accidental. It seems necessary to construct a theory free from the assumption of sphericity and employing the unified nuclear model, so as to allow collective excitations. A simple outline of such a theory is the aim of the present work.

## 2. Calculations

A first order distorted wave perturbation theory gives the matrix element for a (d, d') process, when the incident and final deuteron momenta are $\mathbf{k}_i$ and $\mathbf{k}_f$, respectively, in the form

$$I \propto \int \mathrm{d}\xi \, \mathrm{d}\tau_n \, \mathrm{d}\tau_p \, \Psi_f^*[M_f] \Psi_{\mathbf{k}_f}[\mu'_d] (V_n + V_p) \Psi_i[M_i] \Psi_{\mathbf{k}_i}[\mu_d]; \qquad (1)$$

$\xi$ denotes all the target nuclear coordinates lumped together; $\Psi_i[M_i]$, $\Psi_f[M_f]$ are the initial and final nuclear states of spin $I_i$ (projection $M_i$) and $I_f$ (projection $M_f$), respectively; $\Psi_{\mathbf{k}}[\mu]$ represent the deuteron; $V_n$ and $V_p$ are the interaction potentials of the neutron and the proton with the target.

By properly antisymmetrizing e.g. the initial state of the total system, one gets an exchange amplitude in addition to the direct one. This exchange amplitude should not, however, contribute appreciably, in analogy to the heavy particle stripping [5, 6]) especially for small scattering angles, and in particular for even-nuclei, when rotational levels are excited. We shall, therefore, omit this contribution in the present treatment. Let us next assume that only one nucleon of the incident deuteron, in fact the neutron (the proton being repulsed by the Coulomb field), interacts strongly with the target. We shall, therefore, omit $V_p$ in eq. (1) (the neglect of one $V$ could be justified by a Tobocman type theory) †. Assuming $\Psi_{\mathbf{k}}[\mu]$ in the form $S_\mu(\sigma_n, \sigma_p)\chi(\varrho)\Psi_{\mathbf{k}}(\mathbf{r}_d)$ in the usual notation ($\varrho \equiv |\mathbf{r}_p - \mathbf{r}_n|$, $\chi(\varrho)$ is the S-state internal function) one may write

$$I(M_i\mu_d;\ M_f\mu'_d) \propto \delta_{\mu_d \mu'_d} \int \mathrm{d}\xi \int \mathrm{d}\varrho \, \mathrm{d}\mathbf{r}_n \, |\chi(\varrho)|^2 \Psi_f^*[M_f] \Psi_{\mathbf{k}_f}{}^*(\mathbf{r}_d) V_n \Psi_i[M_i] \Psi_{\mathbf{k}_i}(\mathbf{r}_d) \qquad (2)$$

where

† *Note added in proof:* Neglecting Coulomb repulsion and assuming equal contributions from $V_n$ and $V_p$ would give an additional factor 4 in the cross-section; the true factor will be between 1 and 4.

$$\Psi_1[M_1] = \sqrt{\frac{2I_1+1}{16\pi^2}}\,\phi_1^{\text{vib}}[\mathscr{D}^{I_1}_{M_1K_1}(\theta_1)\chi_{\Omega_1}+(-)^{I_1-\Sigma j_1}\mathscr{D}^{I_1}_{M_1-K_1}(\theta_1)\chi_{-\Omega_1}],$$
$$\Psi_f[M_f] = \sqrt{\frac{2I_f+1}{16\pi^2}}\,\phi_f^{\text{vib}}[\mathscr{D}^{I_f}_{M_fK_f}(\theta_1)\chi_{\Omega_f}+(-)^{I_f-\Sigma j_f}\mathscr{D}^{I_f}_{M_f-K_f}(\theta_1)\chi_{-\Omega_f}] \tag{3}$$

in the usual notation of the unified model. Let now $V_n$ be assumed to depend on the neutron solid angle $\omega_n$ in the fixed coordinate system and on $\theta_1$ implicitly. We assume $V_n = V_n\,[\hat{r}_n(r_n, \omega_n, \theta_1)]$, where $\hat{r}_n = r_n(1+\zeta)$, and $\zeta = \beta Y_{20}(\omega'_n) = \beta\sum_\nu \mathscr{D}^{2*}_{\nu 0}(\theta_1)\,Y_{2\nu}(\omega_n)$, $\beta$ being the nuclear deformation parameter and $\omega'_n$ referring to the intrinsic nuclear system. Assume now $\Psi_k(\mathbf{r}_d)$ in the form of plane waves (the Coulomb effect will probably not be very important at $E_d \approx 15$ MeV — see the example below). Let then the axis of quantization $Oz$ be chosen along $\mathbf{k} = \mathbf{k}_1 - \mathbf{k}_f$. Consistently to the assumption $V_n = V_n(\hat{r}_n)$ we put $\Omega_1 = \Omega_f$ and get

$$I(M_1\mu_d;\ M_f\mu'_d) \propto \delta_{\mu_d\mu'_d}\int d\xi\,\Psi_f^*[M_f]\Psi_1[M_1]\sum_l \sqrt{4\pi(2l+1)}\,i^l$$
$$\times \int d\omega_n\,Y_{l0}(\omega_n)\int dr_n\,r_n^2\,j_l(kr_n)V_n(\hat{r}_n(r_n, \omega_n, \theta_1))\cdot g(k) \tag{4}$$

where

$$g(k) = \int d\varrho\,e^{-i\frac{1}{2}\mathbf{k}\varrho}|\chi(\varrho)|^2$$
$$= \frac{4}{k}\,\frac{\alpha\Gamma(\alpha+\Gamma)}{(\alpha-\Gamma)^2}\left\{\operatorname{arc\,tg}\frac{k}{4\alpha} - 2\operatorname{arc\,tg}\frac{k}{2(\alpha+\Gamma)} + \operatorname{arc\,tg}\frac{k}{4\Gamma}\right\} \tag{5}$$

for a Hulthén function $\chi(\varrho) = N_H\,(e^{-\alpha\rho}-e^{-\Gamma\rho})/\varrho$.

For the sake of simplicity assume now $V_n$ to be

$$V_n = \begin{cases} -V_0 & \text{for } r_n \leqq R_0(1+\zeta) \\ 0 & \text{for } r_n > R_0(1+\zeta). \end{cases} \tag{6}$$

The $r_n$-integrals become now

$$-V_0\int_0^{R_0(1+\zeta)} r_n^2\,dr_n\,j_l(kr_n),$$

the $j_l$ being spherical Bessel functions. The scattering amplitude can be now expanded in powers of $\beta$. (In the case of a general form of $V_n$ different from (6) one should more conveniently first use the transformation of variables $(r_n, \omega_n) \to (\hat{r}_n = r_n(1+\zeta), \omega_n)$ with Jacobian $= (1+\zeta)^{-1}$.) Let us first confine ourselves to the term proportional to $\beta$ (the quadrupole excitation). Provided $I_f \neq I_1$ the final result is

$$I(M_1\mu_d;\ M_f\mu'_d) \propto \delta_{\mu_d\mu'_d}\delta_{M_fM_1}\sqrt{\frac{2I_1+1}{2I_f+1}}\,(I_1 2;\ M_1 0|I_f M_f)\,(I_1 2;\ K_1 0|I_f K_f)\bar{\beta}$$
$$\times\, g(k)\sqrt{20\pi}\,V_0 R_0^3\,j_2(kR_0) = O(\beta^2) \tag{7}$$

where $\bar{\beta} = \langle \phi_f^{\text{vib}} | \beta | \phi_1^{\text{vib}} \rangle \approx \beta$. The selection rules are $K_1 = K_f$ and $|I_1 - 2| \leqq I_f \leqq I_1 + 2$. The result (7) is similar to that of Brink [7]) or Hayakawa and Yoshida [8]) for the inelastic scattering of nucleons. In fact, if one writes $V_n = V_n$ (spherical square well) $+(-V_0 R_0 \zeta)\delta(r_n - R_0) + O(\beta^2)$ one readily obtains (7). The term of $V_n$ proportional to $\beta$ is just the familiar $H_{\text{int}}$ $(\beta, r_n, \omega'_n)$ of Bohr and Mottelson.

The $K$-selection rule is due to the form of $V_n$ appropriate only to collective excitations. In general, one should have $V_n = V_n(\mathbf{r}_n, \xi)$ containing e.g. the sum of individual particle forces $\sum_i^A V_{ni}(|\mathbf{r}_n - \mathbf{r}_i|)$. This would be able to produce individual particle excitations with $K$-selection rules relating $K$ and $\Omega$-numbers.

According to (7) the differential cross-section can be shown to be

$$\sigma(\theta) = \frac{k_f}{k_1} \frac{m_d^{*2}}{(2\pi\hbar^2)^2} g(k)^2 (I_1 2;\ K_1 0 | I_f K_f)^2 4\pi \bar{\beta}^2 \bar{V}_0^2 R_0^6 |j_2(kR_0)|^2 + O(\beta^3) \tag{8}$$

if $I_1 \neq 0$, and

$$\sigma(\theta) = \frac{k_f}{k_1} \frac{m_d^{*2}}{(2\pi\hbar^2)^2} g(k)^2 4\pi \bar{\beta}^2 \bar{V}_0^2 R_0^6 |j_2(kR_0)|^2 + O(\beta^3) \tag{8a}$$

if $I_1 = 0$ $(I_f = 2)$, $m_d^*$ being the deuteron reduced mass. The corrections proportional to $\beta^3$ and $\beta^4$ can be shown to be, if $I_1 \neq 0$,

$$\begin{aligned} \Delta\sigma(\theta) = \frac{k_f}{k_1} \frac{m_d^{*2}}{(2\pi\hbar^2)^2} g(k)^2 \bar{V}_0^2 R_0^6 \Big\{ & (I_1 2;\ K_1 0 | I_f K_f)^2 \tfrac{4}{7} \sqrt{20\pi}\, \bar{\beta}^2 \bar{\beta} \\ & \times \left[ j_2(kR_0) \left( j_2(kR_0) + \frac{kR_0}{2} j'_2(kR_0) \right) \right] \\ + \sum_{l=0,2,4} & (2l+1)^{-1} (22;\ 00 | l0)^4 (I_1 l;\ K_1 0 | I_f K_f)^2 \\ & \times 25 (\bar{\beta}^2)^2 \left[ j_l(kR_0) + \frac{kR_0}{2} j'_l(kR_0) \right]^2 \Big\} + O(\beta^5) \end{aligned} \tag{9}$$

and if $I_1 = 0$ (with $I_f = 2$),

$$\begin{aligned} & \Delta\sigma(\theta) \\ & = \frac{k_f}{k_1} \frac{m_d^{*2}}{(2\pi\hbar^2)^2} g(k)^2 \bar{V}_0^2 R_0^6 \left\{ \tfrac{4}{7} \sqrt{20\pi} \bar{\beta}^2 \bar{\beta} \left[ j_2(kR_0) \left( j_2(kR_0) + \frac{kR_0}{2} j'_2(kR_0) \right) \right] \right. \\ & \left. + \tfrac{20}{49} (\bar{\beta}^2)^2 \left[ j_2(kR_0) + \frac{kR_0}{2} j'_2(kR_0) \right]^2 \right\} + O(\beta^5). \end{aligned} \tag{9a}$$

It should be noted that $j'_2(kR_0) = \frac{1}{5}[2j_1(kR_0) - 3j_3(kR_0)]$.

## 3. Numerical Example and Discussion

Consider now the $Mg^{24}$(d, d') $Mg^{24}$ ($Q = -1.37$ MeV) reaction. The angular distribution $\sigma(\theta) + \Delta\sigma(\theta)$ was calculated using eqs. (8a), (9a) for

the incident deuteron energy 15.1 MeV. It was assumed that $\bar{\beta} \approx \beta \approx 0.42$ (see ref. [9])) and $\bar{\beta}^2 \approx \beta^2$; the value $\Gamma = 7\alpha$ was employed; $R_0$ was assumed to be $6.2 \times 10^{-13}$ cm after Haffner [4]). The resulting curve appears to be very much similar to that of Haffner's fig. 13. The contribution of $\Delta\sigma(\theta)$ is rather small; its only importance is filling in zeros of $\sigma(\theta)$. The only disagreement with experiment lies in the region $0 \leqq \theta \lesssim 20°$. The use of true Coulomb wave functions and the electric interaction could probably account for the discrepancy.

The total cross-section was computed by graphical integration to give 46.5 mb with $V_0 = 40$ MeV. The experimental value [4]) is 88 mb (to a factor of 2). This nice agreement with the data can be, of course, accidental with so many rather arbitrary assumptions. However, in any case the order of magnitude should remain the same in a more refined theory.

It would be interesting to extend this theory to take into account also individual particle excitations by interparticle forces between the projectile and the nucleons of the target. It seems that (d, d') reactions in analogy to the deuteron stripping can be helpful in many cases as tools of nuclear spectroscopy in providing supplementary information on nuclear structure.

## References

1) R. Huby and H. C. Newns, Phil. Mag. **42** (1951) 1442
2) Fairbairn, Proc. Roy. Soc. A **238** (1956) 448
3) C. J. Mullin and E. Guth, Phys. Rev. **82** (1951) 141
4) J. W. Haffner, Phys. Rev. **103** (1956) 1398
5) G. E. Owen and L. Madansky, Phys. Rev. **105** (1957) 1766
6) A. P. French, Phys. Rev. (to be published)
7) D. M. Brink, Proc. Phys. Soc. A **68** (1955) 994
8) S. Hayakawa and S. Yoshida, Proc. Phys. Soc. A **68** (1955) 656
9) R. K. Sheline, Nuclear Physics **2** (1956) 382

*Nuclear Physics* **6** (1958) 618—624; © *North-Holland Publishing Co., Amsterdam*

Not to be reproduced by photoprint or microfilm without written permission from the publisher

# THE HYPOTHESIS OF CONSERVATION OF COMBINED PARITY ONLY IN STRONG, ELECTROMAGNETIC AND WEAK INTERACTIONS

V. G. SOLOVIEV

*Laboratory of Theoretical Physics, Joint Institute of Nuclear Research, Dubna, U.S.S.R.*

Received 12 October 1957

**Abstract:** The hypothesis is considered that only combined parity IC is conserved in strong, electromagnetic and weak interactions. It is demonstrated that the hypothesis is not inconsistent with available experimental data. However, more precise polarization experiments are required for a proof that the hypothesis is correct. It is shown that gauge invariance in quantum electrodynamics and isobaric invariance in pseudoscalar meson theory lead to invariance of renormalizable interaction Lagrangians under space reflection I. Renormalizable and isobarically-invariant Lagrangians for the interaction between K-mesons and baryons are obtained which are invariant under the operation IC but not under the operation I.

## 1. Introduction

The fundamental properties of space-time impose definite limitations on Lagrangians, scattering amplitudes, equations of motion, etc.; examples are invariance under proper Lorentz transformations or under time reversal, etc. It is evident that restrictions of the theory conditioned by the very general properties of space-time and charge should be the same for the various types of interactions. Since non-conservation of space parity I has been experimentally proved for weak interactions, a hypothesis was proposed [1]) which is based on the requirement that the same unified conditions should hold for the various types of interactions. The hypothesis states that only the law of conservation of combined parity IC should hold in strong, electromagnetic and weak interactions between elementary particles involved in local and non-local theories. IC transformations were first considered by L. D. Landau [2]) and Lee and Yang [3]). It should be noted that in some interactions conservation of combined parity due to auxiliary invariance requirements leads to conservation of space parity, whereas in other interactions space parity is not conserved.

Consequences of the hypothesis formulated above are considered in the present paper and interactions in which supplementary (with respect to IC) invariance conditions lead to conservation of space parity I are also investigated.

## 2. Transformation of Field Operators

The transformation IC consists in reflection of space coordinates $x'_k = -x_k$ $(k = 1, 2, 3)$ and transformation of particles into antiparticles Under an operation IC the field operators shoul'. transform as follows:

a) spinor field (nucleons, hyperons)

$$\psi'(x) = S^{-1}\psi^+(-\mathbf{x}, x_4), \quad \psi^{+\prime}(x) = \psi(-\mathbf{x}, x_4)S, \tag{1}$$

where

$$S\gamma_\mu S^{-1} = -\gamma_\mu^{\mathrm{T}}, \qquad \gamma_4 = \beta, \qquad \gamma_k = \beta\alpha_k, \qquad (\mu = 1, 2, 3, 4);$$

b) pseudoscalar field ($\pi$-mesons)

$$\phi'_0(x) = -\phi_0(-\mathbf{x}, x_4), \qquad \phi'(x) = -\phi^*(-\mathbf{x}, x_4); \tag{2}$$

c) pseudoscalar field (K-mesons)

$$\mathrm{K}'_0(x) = -\mathrm{K}_0{}^*(-\mathbf{x}, x_4), \qquad K'(x) = -K^*(-\mathbf{x}, x_4); \tag{3}$$

d) electromagnetic field

$$A'_k(x) = A_k(-\mathbf{x}, x_4), \quad A'_4(x) = -A_4(-\mathbf{x}, x_4). \tag{4}$$

Under the operation IC the scalar field operators transform as follows: $\varphi'_0(x) = \varphi_0(-\mathbf{x}, x_4)$, $\varphi'(x) = \varphi^*(-\mathbf{x}, x_4)$. Thus, two types of bosons also exist with respect to the operation IC: one of these types is multiplied by $(-1)$ under IC while the other is not. Thus by a scalar or pseudoscalar we shall understand quantities which differ with respect to the IC transformation.

In the following, the relation between spin and statistics will be considered established and the kinematically independent spinor field operators will be assumed to be anticommutative.

## 3. Free Spinor Field

Consider the Lagrangian of a free spinor field which is invariant with respect to the operation IC. It may be written as follows:

$$\begin{aligned} L_0(x) = {} & \frac{i}{\sqrt{2}}\left(\bar\psi(x)\gamma_\mu\frac{\partial\psi(x)}{\partial x_\mu} - \frac{\partial\bar\psi(x)}{\partial x_\mu}\gamma_\mu\psi(x)\right) \\ & + \tfrac{1}{2}\left(\bar\psi(x)\gamma_5\gamma_\mu\frac{\partial\psi(x)}{\partial x_\mu} - \frac{\partial\bar\psi(x)}{\partial x_\mu}\gamma_5\gamma_\mu\psi(x)\right) - m\bar\psi(x)\psi(x). \end{aligned} \tag{5}$$

The numerical coefficients in (5) are chosen so that operators $\psi$ and $\bar\psi$ satisfy the equations

$$(\Box - m^2)\psi = 0, \qquad (\Box - m^2)\bar\psi = 0.$$

It should be noted that the term in (5) containing the matrix $\gamma_5$ is not

invariant with respect to the space reflection I. The equations for the field operators have the form

$$\left(-i\Gamma_\mu \frac{\partial}{\partial x_\mu} + m\right)\psi(x) = 0,$$
$$\bar{\psi}(x)\left(i\Gamma_\mu \frac{\partial}{\partial x_\mu} + m\right) = 0, \tag{6}$$

where $\Gamma_\mu = (\sqrt{2} - i\gamma_5)\gamma_\mu$. Since the matrices $\Gamma_\mu$ satisfy the relation

$$\Gamma_\mu\Gamma_\nu + \Gamma_\nu\Gamma_\mu = \delta_{\mu\nu}, \tag{7}$$

it follows that eqs. (6) are Dirac equations with a different representation of the $\gamma_\mu$ matrices. Indeed, this can easily be verified by performing the transformation

$$\psi' = S\psi, \qquad S\Gamma_\mu S^{-1} = \gamma_\mu$$

where

$$S = \tfrac{1}{2}\left\{\left(\sqrt{\sqrt{2}+1} + \sqrt{\sqrt{2}-i}\right) + i\gamma_5\left(\sqrt{\sqrt{2}+1} - \sqrt{\sqrt{2}-1}\right)\right\}. \tag{8}$$

Thus our hypothesis that only combined parity is conserved does not involve any changes in the Dirac equation for particles with non-vanishing mass $m$ and, as was previously shown, for $m = 0$ it makes the two-component neutrino theory possible.

## 4. Quantum Electrodynamics and Pseudoscalar Meson Theory

For a spinor field interacting with an electromagnetic field the Lagrangian which is invariant under the operation IC can be expressed as follows:

$$L = \bar{\psi}(x)\left[-i\gamma_\mu\left(\frac{\partial}{\partial x_\mu} - ieA_\mu\right) + m - e'\gamma_5\gamma_\mu A_\mu\right]\psi(x) + \text{H.c.} \tag{9}$$

The additional interaction term in $e'$ is responsible for non-conservation of space parity I. However, this term in $e'$ is not gauge invariant and hence must be discarded.

Thus in quantum electrodynamics, as a consequence of the gauge invariance condition, the requirement of invariance with respect to the IC operation automatically leads to invariance under the space reflection operation I.

The renormalized nucleon–$\pi$-meson field interaction Lagrangian which is invariant under the operation IC can be expressed in the following form:

$$\begin{aligned} L = {} & g(\bar{\psi}_p\gamma_5\psi_n\phi + \bar{\psi}_n\gamma_5\psi_p\phi^*) + g'_0\bar{\psi}_p\gamma_5\psi_p\phi_0 \\ & + g''_0\bar{\psi}_n\gamma_5\psi_n\phi_0 + ig'(\bar{\psi}_p\psi_n\phi - \bar{\psi}_n\psi_p\phi^*), \end{aligned} \tag{10}$$

where $g$, $g_0'$, $g_0''$, $g'$ are real quantities. The last term, $g'$, is not invariant under space reflection and permits one in principle to check the hypothesis proposed by us. It is well known that $\pi$-meson-nucleon interaction involving conservation of parity I can be written down in an isobarically invariant form. From (10) it can be seen that the term $g'$ cannot be written in such a form. If one requires that isobaric invariance be rigorously obeyed it would be necessary to discard $g'$.

Thus in renormalizable pseudoscalar meson theory a consequence of the isobaric invariance condition is that invariance under the operation IC leads to invariance under the operation I.

The results of our investigations can be summarized as follows: *a consequence of the conditions of gauge invariance in quantum electrodynamics and of isobaric invariance in pseudoscalar meson theory is that renormalized interaction Lagrangians invariant under the operation of combined inversion IC also become invariant under space reflection I.*

## 5. K-Mesons and Hyperons

The hypothesis of conservation of combined parity alone in all types of interactions offers a simple explanation of the decay of K-mesons into two as well as three $\pi$-mesons.

To explain the experimental data J. Schwinger [4]) has moreover assumed the existence of a strong K$-\pi$ interaction. He set up the Lagrangian of this interaction by assuming that K-mesons do not possess a definite parity. The hypothesis of conservation of only combined parity permits one to write the Lagrangian for strong K$-\pi$ interaction as follows:

$$L_{K\pi} = ig_{K\pi}\{K^* K_0 \phi - K K_0^* \phi^*\}. \tag{11}$$

This Lagrangian is not invariant under rotation in the isobaric spin space. Thus for direct K$-\pi$ interaction a local Lagrangian which is invariant under the operation IC cannot be written down in an isobarically invariant form.

A. Salam [5]) found a Lagrangian for strong interaction between nucleons and hyperons on the one hand and K and $\pi$-mesons on the other, which is invariant under the operations I, C and T. To this Lagrangian we shall add a term $L'$ which is invariant under an IC operation but in which I and C are not conserved separately. Employing with slight modifications the notations used in ref. [5]) and assuming that under IC the operators $K, K_0$ transform as those of a scalar field,

$$K_0'(x) = K_0^*(-\mathbf{x}, x_4), \quad K'(x) = K^*(-\mathbf{x}, x_4),$$

we obtain $L'$ in the following form [6]):

$$
\begin{aligned}
L' = {} & ig'_1(\bar{\psi}_p \psi_n \phi - \bar{\psi}_n \psi_p \phi^*) \\
& + ig'_2(\bar{\Lambda}\phi^\lambda \Sigma^\lambda - \bar{\Sigma}^\lambda \phi^\lambda \Lambda) \\
& + g'_3 (1/2i)\ \mathrm{tr}\ (\tau^\lambda \tau^{\lambda'} \tau^{\lambda''}) \bar{\Sigma}^\lambda \phi^{\lambda'} \Sigma^{\lambda''} \\
& + ig'_4(\bar{\Xi}^- \Xi^0 \phi^* - \bar{\Xi}^0 \Xi^- \phi) \\
& + ig'_5(\bar{N}\gamma_5 \Lambda\theta - \bar{\Lambda}\theta^* \gamma_5 N) \\
& + ig'_6(\bar{N}\gamma_5 \tau^\lambda \Sigma^\lambda \theta - \theta^* \bar{\Sigma}^\lambda \gamma_5 \tau^\lambda N) \\
& + g'_7(\bar{\Xi}\gamma_5 \tau^2 \theta^* \Lambda + \bar{\Lambda}\theta \gamma_5 \tau^2 \Xi) \\
& + g'_8(\bar{\Xi}\gamma_5 \tau^2 \tau^\lambda \Sigma^\lambda \theta^* + \theta \tau^\lambda \bar{\Sigma}^\lambda \tau^2 \gamma_5 \Xi),
\end{aligned}
\tag{12}
$$

where $g'_1, g'_2 \ldots g'_8$ are real quantities. If the operators K, $K_0$ transform according to (3) (pseudoscalar), the matrix $\gamma_5$, in the terms in $g'_5$, $g'_6$, $g'_7$, $g'_8$ should be replaced by $I$. It can be seen from (12) that besides the nucleon $\pi$-meson and cascade hyperon-$\pi$-meson interaction terms, all the remaining interactions can be written in a form which is invariant under rotation in isobaric spin space.

Thus renormalized interactions in which I and C are not conserved separately can be expressed in an isobarically invariant form, providing that they contain only such vertices at which at least one characteristic of a fermion, such as mass, electric charge, strangeness, is changed. This refers to K-meson-baryon interaction as well as to that between $\pi$-mesons and $\Lambda$ and $\Sigma$ hyperons. However, that part of the interaction Lagrangian which contains vertices at which only the momenta of the initial and final fermions differ, cannot be written in an isobarically invariant form. This is true for nucleon-$\pi$-meson, and cascade hyperon-$\pi$-meson interactions.

It should be noted that interactions which are invariant under IC conserve the $\mathcal{J}_z$ isobaric spin component and also the relation between $\mathcal{J}_z$, the number of nucleons minus number of antinucleons $n$, strangeness $S$ and electric charge, that is

$$\frac{Q}{e} = \mathcal{J}_z + \frac{n+S'}{2}.$$

We have restricted our considerations to renormalizable interaction Lagrangians. It may be noted that splitting of the interaction Lagrangian into renormalizable and non-renormalizable parts was carried out on the basis of an expansion of the $S$-matrix into a power series in the coupling constant. However, as was shown in ref. [7]), there is a significant physical difference between the renormalizable and non-renormalizable theories because in non-renormalizable theories the interaction Lagrangians are "debris" of non-localized interactions represented, as it were, in a localized form.

## 6. Relation to Experiment

The experimental verification of our hypothesis will be the next question to consider.

As shown in ref. [2]), if combined parity is conserved the particles cannot possess electric dipole moments. Therefore, the very precise experiments in which the upper limit of the electric dipole moment (say, of a neutron) was established, are not inconsistent with our hypothesis.

As is well known, parity selection rules are accurately obeyed in atomic spectroscopy. However, as shown above, in electrodynamics the gauge invariance condition leads to the result that conservation of combined parity IC automatically yields conservation of I and C separately. Therefore, atomic spectroscopy data are also compatible with our hypothesis.

Likewise, the data of nuclear spectroscopy and polarization experiments indicate conservation of parity I in strong interactions, providing that combined parity IC is assumed to be conserved in all interactions. The experiments described in ref. [8]) indicate that at energies of the order of several hundred MeV the contribution of terms responsible for parity violation is apparently not large.

More precise experiments to detect any asymmetry of second scattering with respect to the first scattering plane in nucleon-nucleon or nucleon-nuclear interactions should be performed to test our hypothesis.

Consider, for example, double elastic scattering of a spin $\frac{1}{2}$ particle on a particle of spin 0. The matrix element which is invariant under IC can be written as follows:

$$M_i = a_i + b_i \boldsymbol{\sigma} \cdot \mathbf{n}_i + c_i \boldsymbol{\sigma} \cdot \mathbf{p}_i. \tag{13}$$

Here $\mathbf{k}_1$ and $\mathbf{k}'_1$ are the momenta of the particle before and after scattering; $i = 1$ refers to the first scattering and $i = 2$ to the second,

$$\mathbf{n}_i = \mathbf{k}_i \wedge \mathbf{k}'_i, \qquad \mathbf{p}_i = \mathbf{k}_i + \mathbf{k}'_i, \qquad \mathbf{q}_i = \mathbf{k}_i - \mathbf{k}'_i.$$

The term $C_i \boldsymbol{\sigma} \cdot \mathbf{p}_i$ is responsible for non-conservation of space parity I. After the first scattering the beam becomes polarized. The polarization $\mathbf{P}_1$ can be expressed as

$$\mathbf{P}_1 = \mathbf{n}_1 A_1 + \mathbf{p}_1 B_1 + \mathbf{q}_1 (k_1^2 - k_1'^2) C_1. \tag{14}$$

The second scattering cross section will be written in the form

$$\sigma_2 = \sigma_2^0 \{1 + (\mathbf{P}_1 \cdot \mathbf{n}_2) F_2 + (\mathbf{P}_1 \cdot \mathbf{p}_2) L_2 + (\mathbf{P}_1 \cdot \mathbf{q}_2)(k_2^2 - k_2'^2) N_2\}, \tag{15}$$

where $\sigma_2^0 = \frac{1}{2} \operatorname{tr} M_2 M_2^+$. Inserting $\mathbf{P}_1$ expressed by (14) we obtain

$$\begin{aligned} \sigma_2 = \sigma_2^0 \{ & 1 + A_1 F_2 (\mathbf{n}_1 \cdot \mathbf{n}_2) + B_1 F_2 (\mathbf{p}_1 \cdot \mathbf{n}_2) + C_1 F_2 (k_1^2 - k_1'^2)(\mathbf{q}_1 \cdot \mathbf{n}_2) \\ & + A_1 L_2 (\mathbf{n}_1 \cdot \mathbf{p}_2) + B_1 L_2 (\mathbf{p}_1 \cdot \mathbf{p}_2) + C_1 L_2 (k_1^2 - k_1'^2)(\mathbf{q}_1 \cdot \mathbf{p}_2) \\ & + A_1 N_2 (k_2^2 - k_2'^2)(\mathbf{n}_1 \cdot \mathbf{q}_2) + B_1 N_2 (k_2^2 - k_2'^2)(\mathbf{p}_1 \cdot \mathbf{q}_2) \\ & + C_1 N_2 (k_1^2 - k_1'^2)(k_2^2 - k_2'^2)(\mathbf{q}_1 \cdot \mathbf{q}_2) \}. \end{aligned} \tag{15a}$$

The terms

$$\begin{aligned} &B_1 F_2(\mathbf{p}_1 \cdot \mathbf{n}_2), \quad C_1 F_2(k_1^2 - k_1'^2)(\mathbf{q}_1 \cdot \mathbf{n}_2), \\ &A_1 L_2(\mathbf{n}_1 \cdot \mathbf{p}_2), \quad A_1 N_2(k_2^2 - k_2'^2)(\mathbf{n}_1 \cdot \mathbf{q}_2) \end{aligned} \tag{16}$$

produce after second scattering an asymmetry with respect to the first scattering plane. The Lagrangian (12) is responsible for the appearance of these terms, since they arise as a result of interactions in which space parity I is not conserved. It should be noted that (12) contains isobarically invariant terms as well as isobarically non-invariant terms.

If one assumes all strong interactions to be isobarically invariant, similar expressions should appear as a result of participation of virtual K-mesons and hyperons as well as of non-local interactions. In this case $\pi$-meson-nucleon interaction will not contribute and hence the asymmetry effect of second scattering with respect to the first scattering plane should only appear at sufficiently high energies.

In conclusion I express my deep appreciation to N. N. Bogolubov, A. A. Logunov, M. A. Markov and I. S. Shapiro for fruitful discussions.

*Note added in proof:* The objection in ref. [2]), as the author himself now acknowledges, is based on a misunderstanding since the statement (expressed in ref. [1]) and in the present paper) that combined inversion and gauge invariance lead to conservation of parity in electrodynamics, refers only to renormalizable interactions.

In ref. [9]) an example of non-renormalizable interaction is given:

$$\bar{\psi}\gamma_5\gamma_\mu\psi\,\Box A_\mu .$$

Note that the hypothesis suggested by us would be trivial if parity non-conservation in the interactions were considered (as is the case in ref. [9])) to be a result of virtual weak interactions.

## References

1) V. G. Soloviev, JETP **33** (1957) 537
2) L. D. Landau, Nuclear Physics **3** (1957) 127
3) T. D. Lee and C. N. Yang, Phys. Rev. **105** (1957) 1671
4) J. Schwinger, Phys. Rev. **104** (1956) 1164
5) A. Salam, Nuclear Physics **2** (1956) 173
6) V. G. Soloviev, JETP **33** (1957) 796
7) N. N. Bogolubov and D. V. Shirkov, Uspekhi Fiz. Nauk **57** (1955) 3
8) O. Chamberlain, E. Segrè, R. Tripp, C. Wiegand and T. Ypsilantis, Phys. Rev. **93** (1954) 1430
9) Ya. B. Zeldovich, JETP **33** (1957) 1531

*Nuclear Physics* **6** (1958) 625—627; © *North-Holland Publishing Co., Amsterdam*
Not to be reproduced by photoprint or microfilm without written permission from the publisher

# ANGULAR CORRELATION BETWEEN RECOIL NUCLEUS AND GAMMA QUANTUM IN ELECTRON CAPTURE

J. ZIMÁNYI
*Dept. of Atomic Physics, Central Research Institute of Physics, Budapest*

Received 19 February 1958

**Abstract:** The $\nu-\gamma$ angular correlation is obtained for allowed K capture. For a Fermi transition there is no correlation, for a Gamow-Teller transition the correlation is given in the present paper and it is found to be the same for T and A coupling, depending only on the polarization of the neutrino.

## 1. Introduction

The angular and polarization correlations between the particles emitted by a nucleus in various nuclear transformations have been extensively studied. Similarly, several authors have treated the effect of the interactions violating parity on the different correlations ($\beta-\nu$, $\beta-\gamma$). However, the $\nu-\gamma$ correlation in electron capture has not yet been dealt with either in the former (conserving parity) or in the recent (violating parity) theory. The reason for this is probably that until recently it has not been possible to carry out experiments of this type. However, owing to the development of ion multiplier technique such experiments can now be carried out — although this is not a simple task.

## 2. Discussion

In the following we shall consider the $\nu-\gamma$ correlation in the *allowed* K captures. The process under consideration is illustrated schematically in figs. 1 and 2.

Let us find the correlation between the gamma quantum of multipolarity $L$, polarization $P_\gamma$ and the neutrino with polarization $P_\nu$. For the left-handed or right-handed circularly polarized gamma quantum $P_\gamma = +1$ and $P_\gamma = -1$ respectively, for the neutrino with spin parallel or antiparallel with the direction of its motion $P_\nu = +1$ and $P_\nu = -1$, respectively.

We shall calculate the transition probability of the process which leads from the initial state $j_1$, $m_1$ to state $j_2$, $m_2$ by K capture and successively from here to state $j_3$, $m_3$ by emission of a gamma quantum, released with polarization $P_\gamma$, at an angle $\varphi$ with respect to the direction of the emission



May 1958

of the neutrino. Thereupon we shall suitably sum with respect to the magnetic quantum numbers.

The relative probability can be obtained by a second order perturbation calculation in the well-known manner [1]). The factors which are independent

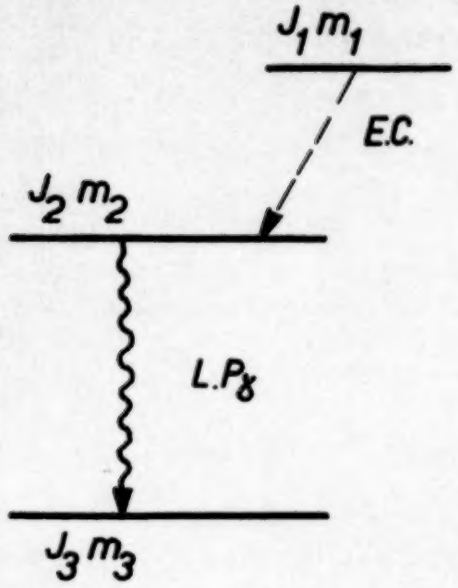


Fig. 1. A typical decay scheme of electron capture. $j_i, m_i$ are the respective angular momenta and their projections on the quantization axis.

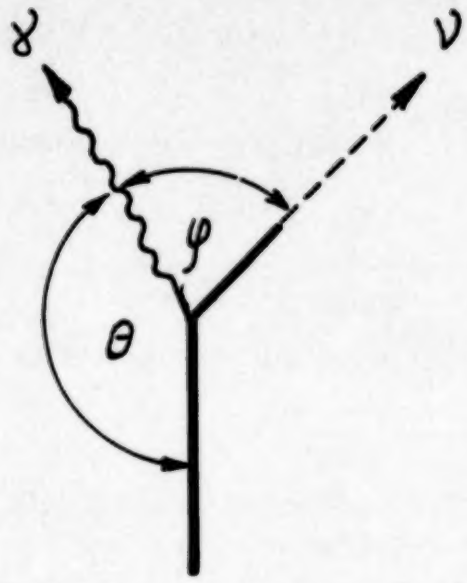


Fig. 2. Schematic picture representing the particles taking part in the process of electron capture. The thickened line marks the path of the recoil nucleus.

of angles and polarization, and thus do not affect the correlation in question, will be omitted. One finds

$$W(\varphi;\, P_\gamma P_\nu) = \sum_{m_1}\sum_{m_e}\sum_{m_3}\Big|\sum_{m_2}\langle j_3 m_3;\, \alpha''|H(\mathbf{k}_\gamma,\, P_\gamma)|j_2 m_2;\, \alpha'\rangle \langle j_2 m_2;\, \alpha'|H(\mathbf{k}_\nu,\, P_\nu)|j_1 m_1 m_e;\, \alpha\rangle\Big|^2,$$

where $\mathbf{k}_\gamma$, $\mathbf{k}_\nu$ are the wave vectors of the gamma quantum and the neutrino, respectively, with $\mathbf{k}_\gamma \cdot \mathbf{k}_\nu = |\mathbf{k}_\gamma||\mathbf{k}_\nu| \cos\varphi$, and $\alpha$, $\alpha'$, $\alpha''$ denote all the other quantum numbers, which are not indicated explicitly.

The summations can be performed by means of the Wigner-Eckart theorem [2]) and the Racah technique [3]). As in the gamma emission only pure transitions are considered, the reduced matrix elements can also be omitted. Thus we find that for Fermi transitions there is no correlation, and for Gamow-Teller transitions the correlation is given in the form

$$W(\varphi;\; P_\gamma P_\nu) = 1 + P_\gamma P_\nu b \cos\varphi. \tag{2}$$

Using explicit formulae for the Racah and Clebsch-Gordan coefficients, we find

$$b = \tfrac{1}{4}\frac{[2+j_2(j_2+1)-j_1(j_1+1)][L(L+1)+j_2(j_2+1)-j_3(j_3+1)]}{j_2(j_2+1)L(L+1)} \qquad (j_2 \neq 0),$$

$$b = 0 \qquad (j_2 = 0)$$

$$|j_2-1| \leqq j_1 \leqq j_2+1, \qquad |j_3-L| \leqq j_2 \leqq j_3+L.$$

The correlation is the same for T and A coupling, and depends only on the polarization of the neutrino.

As to the comparison with the experiment we remark that experimentally the polarization of the gamma radiation can be measured only as a function of the angle $\theta$, whereas in the above calculation the polarization is given in terms of the angle $\varphi$. A simple relation between the two angles can, however, be given taking into account the law of the conservation of momentum.

We may add that the calculation can be extended to the case of forbidden transitions as well as to that of mixed gamma transitions. In that case experiments investigating the direction correlation between the recoil nucleus and the gamma ray may be useful in nuclear spectroscopy. In such experiments the determination of the polarization of gamma rays — which is very tedious — is not necessary.

Finally I wish to express my thanks to Dr. L. Keszthelyi for suggesting this problem and to Dr. G. Marx and G. Györgyi for valuable advice in connection with the calculations.

## References

1) See e.g. L. C. Biedenharn and M. E. Rose, Revs. Mod. Phys. **25** (1953) 729
2) E. P. Wigner, Gruppentheorie (Friedrich Vieweg and Sohn, Braunschweig)
3) L. C. Biedenharn, J. M. Blatt and M. E. Rose, Revs. Mod. Phys. **24** (1952) 249

*Nuclear Physics* **6** (1958) 628—629; © *North-Holland Publishing Co., Amsterdam*
Not to be reproduced by photoprint or microfilm without written permission from the publisher

# ANALYTICAL PROPERTIES OF THE SOLUTIONS OF THE CHEW-LOW EQUATIONS

M. FROISSART † and R. OMNÈS
CERN, *Geneva*

Received 10 January 1958

**Abstract:** It is shown that the solutions of the Chew-Low equations can be continued analytically. In a few simple cases, this continuation leads to a finite Riemann surface with two sheets. In the general case, however, the number of sheets is infinite.

In a recent paper [1]) Ning Hu has attempted to construct solutions of the Chew-Low equations on the basis of an ansatz on the analytical properties of the matrix elements $S(k)$. He assumed that this function would be analytical on a Riemann surface with two sheets, which is precisely the same as that of the function $\omega(k) = \sqrt{(k^2+1)}$.

This procedure is perfectly justified in the case of the scalar meson, either neutral or charged and gives directly solutions in the form of finite products of algebraic functions. It would be interesting to see if this method can be extended to more complicated theories; this would be the case if the complete Riemann surface of $S(k)$ would be finite.

We have studied this question in detail [2]) for the case of the P waves in the symmetrical pseudoscalar meson theory. The main lines of our argument are the following. We consider the functions

$$S_\alpha(\omega) = 1+2iq^3v^2(q)h_\alpha(\omega)$$

where $h_\alpha$ is the solution of the Chew-Low equations [3]). These functions $S$ must be the same as those of Ning Hu, but are defined in the complex plane cut by two lines: (A) $(+1, +\infty)$ and (B) $(-1, -\infty)$. They satisfy the crossing relation

$$AS(\omega) = S(-\omega)$$

where $A$ is the crossing matrix. We seek to identify them to those of Ning Hu by analytic continuation. On the cut (A) each of the $S_\alpha$ is unitary and can be continued by Schwartz' lemma by

$$S_{\alpha 1}(\omega) = \frac{1}{\bar{S}_\alpha(\bar{\omega})} \equiv IS_\alpha(\omega).$$

† On leave of absence from the École Nationale Supérieure des Mines de Paris.

We prove easily that the continuation through (B) is given by

$$S_{-1}(\omega) = AIAS(\omega)$$

and that we can obtain further determinations of the analytic continuation of $S$ by the formulae

$$S_{p+2}(\omega) = (IA)^2 S_p(\omega), \qquad S_{p-2}(\omega) = (AI)^2 S_p(\omega),$$

taking $S_0 = S$.

If any $S_p$ coincides with $S$, the number of sheets of the Riemann surface of $S$ is finite. In this case $S$ can be put into the form of a finite and somewhat arbitrary product, following the method of Ning Hu. This is true for neutral or charged scalar theory where $(AI)^2 = 1$.

It is not true, however, for the symmetrical pseudoscalar theory. We have proved [2]) that no $S_p$ can coincide with $S$. This shows that the Riemann surface of $S$ has an infinite number of sheets. The proof is easily extended to the case of the symmetrical theory of S waves considered by Ning Hu. In fact, if we exclude the few theories † in which the crossing relations are simple (e.g. the neutral or charged scalar theories, for which the solution has been given by Castillejo, Dalitz and Dyson [4]), the method of Ning Hu would have to be extended to include an infinite number of sheets of the Riemann surface: it then appears that to each pole of $S$ there will correspond a pole on each of the even sheets of the Riemann surface, and we cannot express $S$ as a finite product such as those found by Ning Hu for the case of the simplest theories, even if we use functions which have the same infinite Riemann surface, such as $\arcsin \omega$.

† *Note added in proof:* We are indebted to Dr. Ning Hu for having informed us that these theories form the first class he mentions in his paper.

## References

1) Ning Hu, Nuclear Physics **5** (1958) 1
2) M. Froissart and R. Omnès, Comptes Rendus Acad. Sci. **245** (1957) 2203
3) G. F. Chew and F. E. Low, Phys. Rev. **101** (1956) 1570
4) L. Castillejo, R. H. Dalitz and F. J. Dyson, Phys. Rev. **101** (1956) 453

*Editor's Note:* In a letter to the Editor, Dr. Ning Hu points out that in the general case the $S$-function is an analytic function on a Riemann surface of two sheets except for a cut (or a line of discontinuity) from $k = -i$ to $k = -i\infty$. This means that if one continues analytically the $S$-function through the cut one will pass to new Riemann sheets, and finally get an infinite number of them, in agreement with the authors' conclusion. However, he thinks it would be more practical to consider $S$ as an analytic function on the original Riemann surface of two sheets with a line of discontinuity from $k = -i$ to $k = -i\,\infty$, than to use an infinite number of Riemann sheets.

*Nuclear Physics* **6** (1958) 630—644; © *North-Holland Publishing Co., Amsterdam*
Not to be reproduced by photoprint or microfilm without written permission from the publisher

# LEVELS IN $Dy^{161}$

## I. Experimental Investigation of the Decay of $Tb^{161}$

P. GREGERS HANSEN†, O. NATHAN, O. B. NIELSEN and R. K. SHELINE††
*Institute for Theoretical Physics, University of Copenhagen*

Received 3 February 1958

**Abstract:** The decay of $Tb^{161}$ has been reinvestigated by means of scintillation spectrometers, a six-gap $\beta$-ray spectrometer, and coincidence techniques. The following transitions were observed (energies in keV): 25.6 (E1), 28.7, 48.9 (M1), 57.1 (M1), 74.5 (E1), 77.6, 106 (M1 or E2), 132 (tentative). Lifetime measurements and coincidence experiments show unambiguously the existence of levels in $Dy^{161}$ with energies of 25.6, 74.5 and 132 keV. A level has tentatively been placed at 103.3 keV. The half lives of the 25.6 and 74.5 keV states are $(2.8\pm0.2)\times10^{-8}$ sec and $(3.0\pm0.3)\times10^{-9}$ sec. The $\beta$-spectrum contains a ground state transition with end point at $(610\pm15)$ keV and groups of $(525\pm15)$ and $(460\pm15)$ keV to the 74.5 and 132 keV levels.

## 1. Introduction

The levels observed in spheroidal odd-mass nuclei can in general be successfully interpreted as rotational bands based on single particle states in the deformed nuclear field[1–4]). In the case of $Dy^{161}$, the levels excited in the $\beta$-decay of $Tb^{161}$ have been studied by several investigators [5–10]), but the decay schemes proposed still disagree on important points. Thus, the first excited state has been given as 25.6 keV [9]) and 48.9 keV [10]). Also the intensities and energies of the $\beta$-ray groups reported differ significantly.

In view of the considerable interest attached to the study of the deformed odd-mass nuclei, it was decided to reinvestigate the $Tb^{161}$ decay. The results obtained confirm the main features of the decay scheme suggested by Cork *et al.* [9]).

## 2. Experimental

Two milligrams of isotopically enriched $Gd^{160}$ (supplied by the Oak Ridge National Laboratory) were irradiated for two weeks in the reactor at Saclay. The 3.7 min $Gd^{161}$ formed by neutron capture decayed into $Tb^{161}$, which was obtained carrier-free by ion exchange separation [11–13])

† Permanent address: Danish Atomic Energy Commission, Risø pr. Roskilde, Denmark.
†† Guggenheim and Fulbright research scholar on leave of absence from Florida State University, Florida.

from Gd. The resin was Dowex 50 with α-hydroxy isobutyric acid as the eluant. A β-ray source was prepared by a microchemical technique [14]) and mounted on a 150 $\mu g/cm^2$ aluminium backing.

The β-ray spectrum and the internal conversion lines were investigated in a six-gap β-ray spectrometer [15]). Only two gaps were used in order to obtain sufficient resolution ($\approx 0.9$ %). Coincidences between γ-rays and internal conversion electrons or β-particles were studied with a $1.5'' \times 1.5''$ NaI crystal placed above the source in the spectrometer. The resolving time of the coincidence circuit used was $\approx 2 \times 10^{-7}$ sec. A 36 channel analyser was used for recording the coincident γ-ray spectra.

The γ-ray spectrum was studied by means of a $1\frac{1}{4}'' \times 1\frac{1}{4}''$ NaI crystal and a single channel analyser.

A conventional fast-slow coincidence circuit [16]) utilizing RCA 6342 photomultipliers, followed by Hewlett-Packard amplifiers, was used for $\gamma-\gamma$ coincidence and lifetime measurements. The overall fast-slow resolving time varied from $8 \times 10^{-9}$ to $4 \times 10^{-8}$ sec, depending on the energy of the radiation.

## 3. The Decay Scheme

### 3.1. CONVERSION LINES AND γ-RAYS

Only the region from 10 to 200 keV was scanned for conversion lines, since there are no lines outside this energy region in the γ-ray spectrum of $Tb^{161}$. Fig. 1 shows the spectrum from 50 to 80 keV electron energy. A total of 22 conversion lines was observed, 21 of which were assigned to 7 transitions in $Tb^{161}$ (table 1). The shell binding energies make these assignments unambiguous.

The γ-ray spectrum (fig. 2) shows three strong photopeaks of 25, 50 and 75 keV. The peak at 50 keV is supposed to contain contributions from K X-rays as well as from transitions of 48.9 and 57.1 keV. A weak γ-ray corresponds to the conversion lines of the 106 keV transition.

Finally, a weak γ-ray of approximately 132 keV was observed. Although an electron line of 78.1 keV was found at the position of the K conversion line of this transition, the main part of this conversion line had to be interpreted as the L line of an 87 keV transition from the decay of $Tb^{160}$. The presence of a $Tb^{160}$ impurity in the source was confirmed by the observation of a weak 300 keV γ-ray. Independent estimates of the amount of $Tb^{160}$ activity, based on the conversion line and the γ-ray intensity, respectively, both indicated about 0.2 %. With the high neutron capture cross section of $Tb^{159}$ relative to $Gd^{160}$, it is likely that this activity had been formed from the amount of $Tb^{159}$ present in the $Gd^{160}$.

The transitions and energies observed correspond closely to those reported by Cork *et al.* [9]).

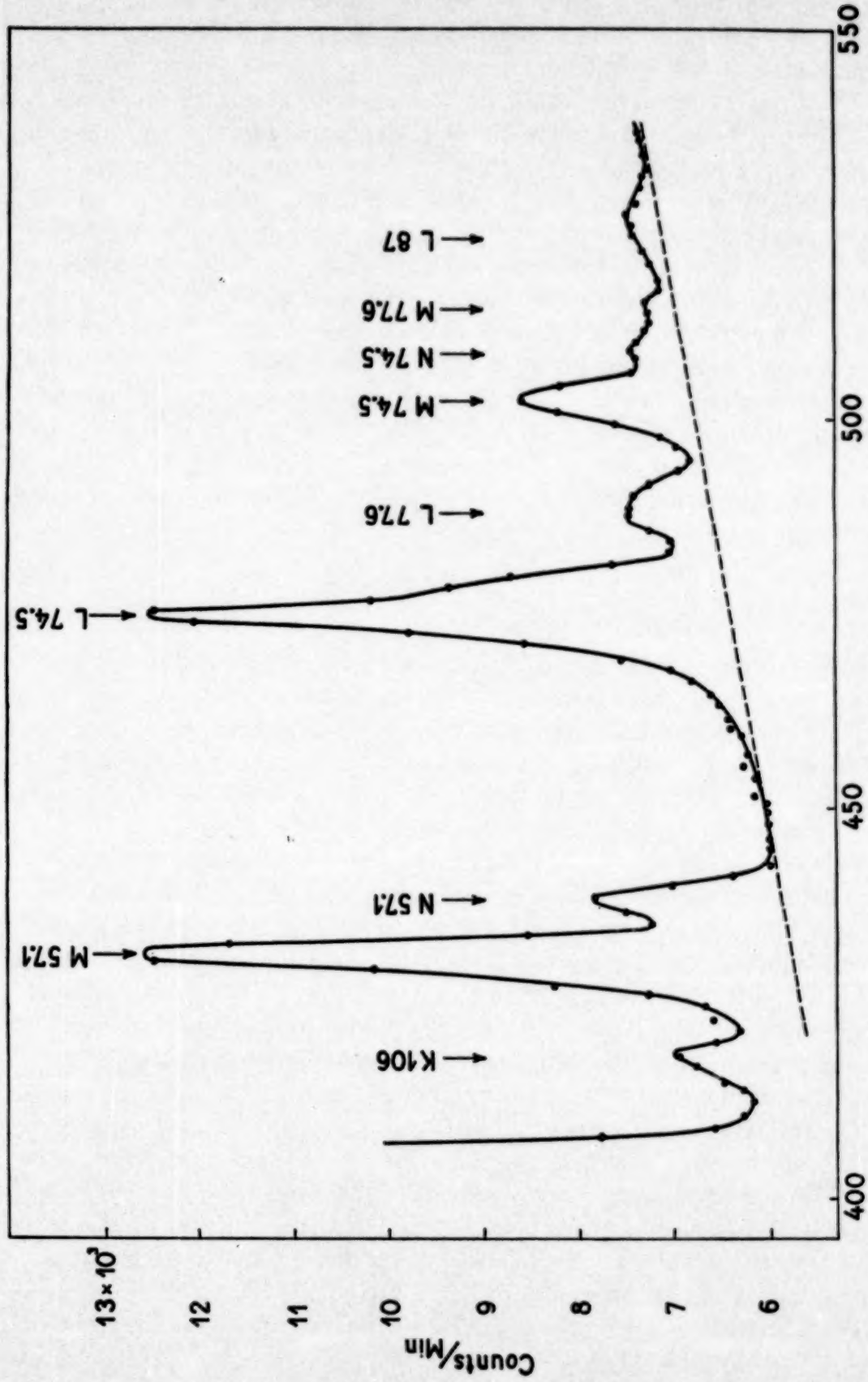


Fig. 1. Part of the internal conversion line spectrum of $Tb^{161}$. Not corrected for decay.

TABLE 1

Internal Conversion Lines

| Transition energy | Assignment | Conversion line | Intensity |
|---|---|---|---|
| 25.6 | E1 | $L_I+L_{II}+L_{III}$<br>M+N | 41 ±8<br>12 ±2 |
| 28.7 | | $L_I$<br>M | 1 ±0.5<br>(a) |
| 48.9 | M1 | L<br>M+N | 44 ±4<br>(b) |
| 57.1 | M1 | M+N | 1.1 ±0.2 |
| 74.5 | E1 | K<br>L<br>M+N | 4.4 ±0.8<br>0.84 ±0.15 |
| 77.6 | | K<br>L<br>M | (c)<br>0.13 ±0.05 |
| 106 | M1 or E2 | K<br>L | 0.11 ±0.05<br>0.05 ±0.02 |
| 87 | E2 | L | 0.046±0.02<br>(d) |

Intensities quoted in per cent of the total $\beta$-spectrum intensity.
(a) Weak line.
(b) N 48.9 containing L 57.1
(c) Line unresolved from M 25.6 and N 25.6.
(d) Line due to $Tb^{160}$ impurity.

### 3.2. e–$\gamma$ AND $\gamma$–$\gamma$ COINCIDENCE MEASUREMENTS

Table 2 summarizes the results of internal conversion line $\gamma$-ray coincidence experiments. The 25.6 and the 48.9 keV transitions are coincident

TABLE 2

Results of Internal Conversion Line–$\gamma$-ray Coincidences

| Selected event | Coincident $\gamma$-rays |
|---|---|
| L 25.6 | 50 keV |
| M 57.1 | 25,50,75 keV |
| L 48.9 | 25,50 keV [a]) |
| K 74.5 | 50 keV [a]) |

[a]) Unsymmetrical shape of 50 keV line indicates components K X-ray+57 keV $\gamma$-ray. See fig. 8.

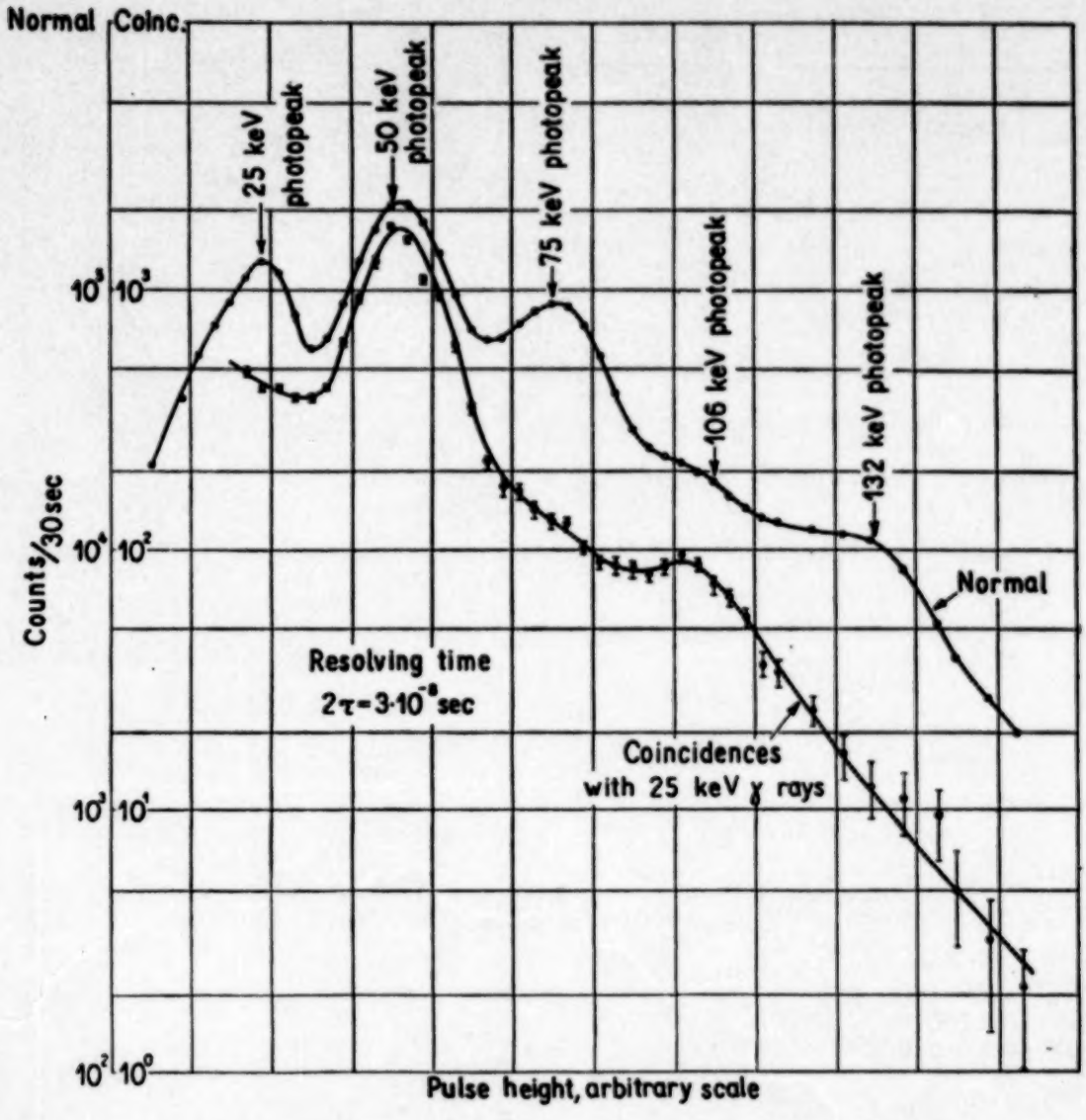


Fig. 2. The gamma ray spectrum of $Tb^{161}$ in coincidence with the 25 keV photons, and the normal gamma ray spectrum. Source-detector distance about 1 mm. The coincidence counts are corrected for random coincidences.

with each other, but not with the 74.5 keV transition. All three lines appear in coincidence with the 57.1 keV transition. This confirms the fact that the 25.6 and 48.9 keV transitions form a cascade with the 74.5 keV transition as a cross-over, as suggested by the energy relations. The smaller intensity of the 57.1 keV transition indicates that this is the upper member in the 57.1—74.5 keV cascade.

These relations establish levels at 74.5 and 132 keV. The $\approx$ 132 keV $\gamma$-ray possibly represents a transition from the 132 keV level to the ground state. The order of the 25.6 and 48.9 keV transitions cannot be inferred from their intensities, which are identical within the experimental uncertainties (fig. 3).

Fig. 2 gives the spectrum of $\gamma$-rays coincident with the 25 keV $\gamma$-rays obtained in a $\gamma-\gamma$ coincidence experiment with two NaI crystals. The observed coincidences between $\gamma$-rays of 25 keV and 106 keV may possibly

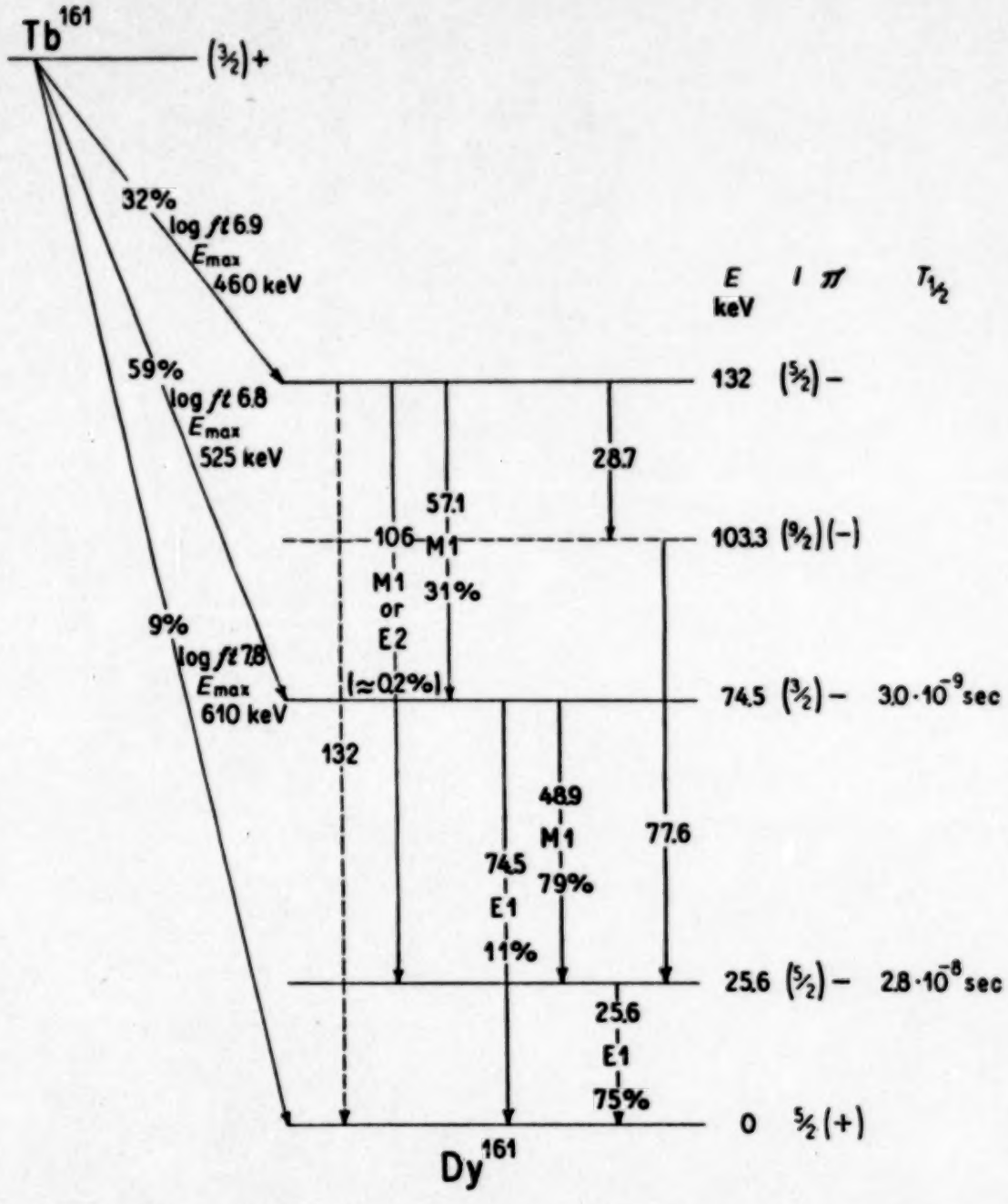


Fig. 3. The decay scheme of $Tb^{161}$. The intensities quoted are absolute intensities in per cent of the total $\beta$-spectrum.

be interpreted as indicating a 132—25.6—0 keV cascade; this experiment, however, cannot be taken as a definite proof of the existence of a 25.6 keV level.

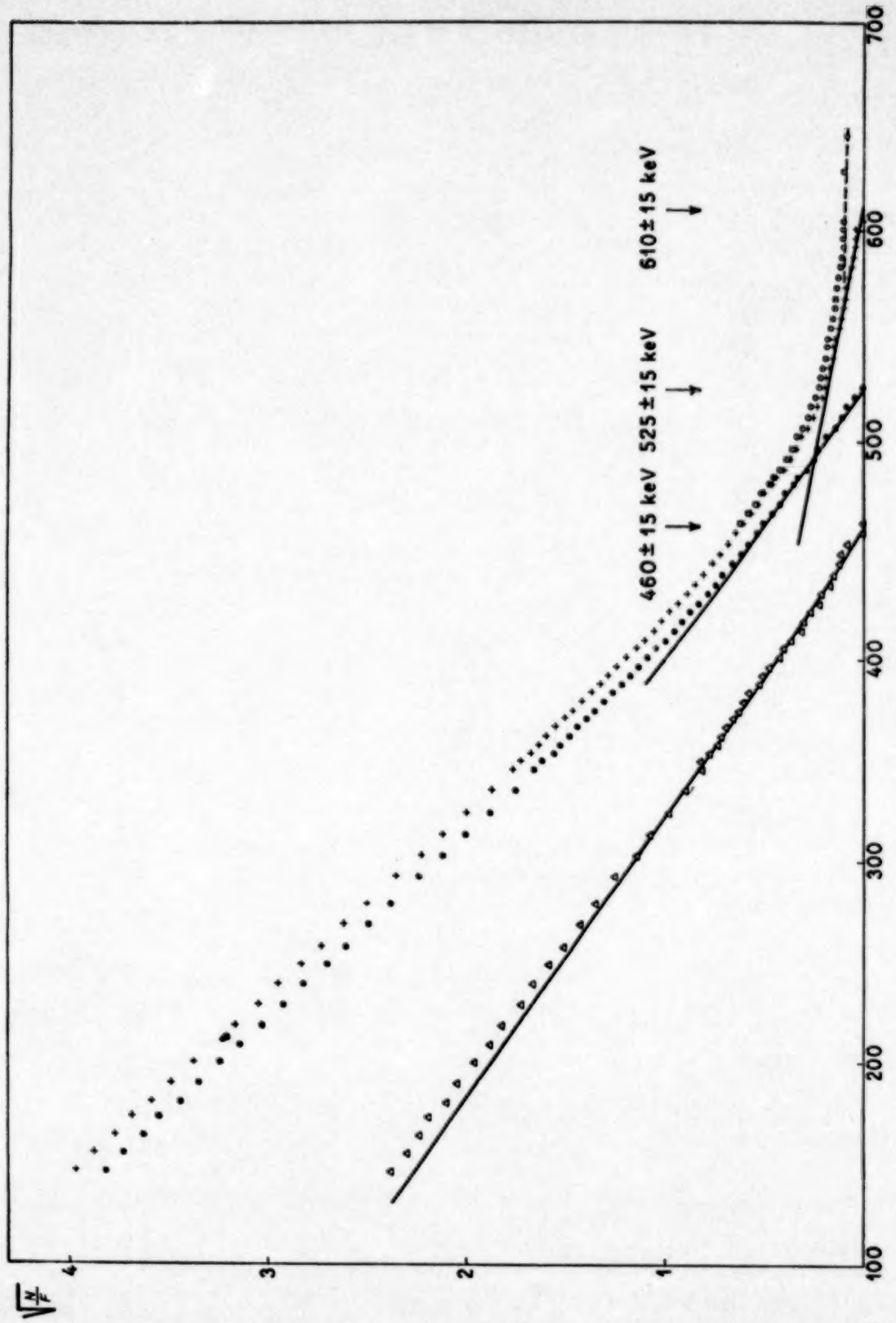


Fig. 4. Fermi plot for $Tb^{161}$. The very weak high energy group may be regarded as an arbitrary correction for an unidentified high energy background.

### 3.3. $\beta$-RAY MEASUREMENTS

The $\beta$-ray spectrum was measured with a statistical accuracy of 0.25 % (standard error) at the maximum. Energy calibration was performed with a source of $Cs^{137}$ in the same geometry as the $Tb^{161}$ source. A Fermi analysis, after subtraction of background, is shown in fig. 4. The upper part of this plot indicates a weak group ($\approx$ 0.5 %) with end point apparently not lower than 900 keV. For energy reasons this group cannot belong to the $Tb^{161}$ decay. However, the amount of $Tb^{160}$ known to be present is far too small to account for the intensity. Correction was made for this component, assuming a single group of allowed shape. It should be noted that the correction was so small that other reasonable assumptions about the type of contamination would not affect the results of the Fermi analysis for the $Tb^{161}$ groups.

When the high energy group was subtracted, the $\beta$-ray spectrum was clearly resolvable into three groups with end points at $610\pm15$, $525\pm15$ and $460\pm15$ keV.

An investigation of the coincidences between $\beta$-particles and $\gamma$-rays showed that the upper part of the $\beta$-spectrum was not coincident with $\gamma$-rays, and the 610 keV component is thus a ground state transition. The energy differences suggest that the two other groups feed the 74.5 and 132 keV levels. These results are qualitatively in accordance with Cork *et al.* [9]), who reported $\beta$-groups of 531, 447 and 405 keV feeding the ground state and levels at 74.8 and 132 keV.

$\beta$-group intensities and log *ft* values are given in fig. 3 together with the total transition intensities calculated from the conversion line intensities and the theoretical conversion coefficients. (For assignment of multipole orders see section 4.) The fact that the intensity values for the $\beta$- and $\gamma$-transitions were obtained independently allows a check on the consistency of the decay scheme. The result that the intensities of the 25.6 and 48.9 keV transitions were found to be the same within the experimental errors agrees with the finding that no $\beta$-group to levels between 0 and 74.5 keV was observed.

### 3.4. LIFETIME MEASUREMENTS

Lifetime measurements were carried out mainly in order to establish the position of the intermediate level in the 25.6—48.9 keV cascade, which could not be decided with certainty from the data presented above.

Delayed $\beta$—$\gamma$ coincidence measurements were first performed with two $2''\times2''$ plastic scintillators (supplied by Nuclear Enterprises Ltd). These made it possible to use short resolving times in spite of the low $\gamma$-ray energies, but the energy resolution was poor (fig. 5). All $\beta$-particles were stopped in front of the $\gamma$-ray crystal by a 5 mm lucite absorber. Coinci-

dences due to the $\gamma$-sensitivity of the $\beta$-counter were eliminated by selection of events of energies above 150 keV.

Two $\gamma$-ray components of measurable lifetime were observed. A transition of half life $2.8\times10^{-8}$ sec, corresponding to the low energy part of the $\gamma$-ray spectrum, is revealed in fig. 5a, which was obtained with a resolving time of $4\times10^{-8}$ sec.

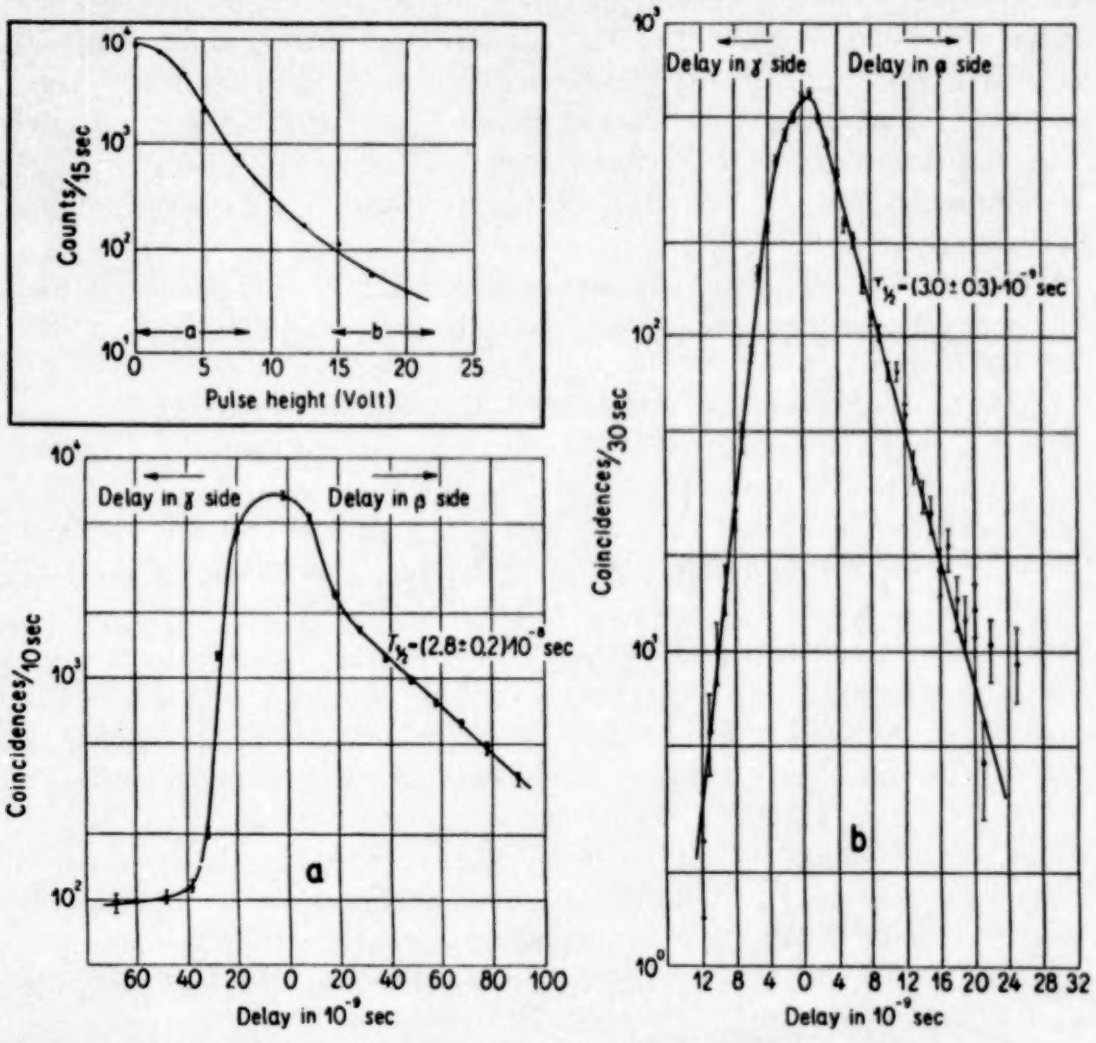


Fig. 5. Delayed beta-gamma coincidences, using 2″×2″ plastic scintillators. One counter was covered with 5 mm lucite (the gamma counter), the other used no absorber and counted both beta and gamma rays. The insert shows the pulse height spectrum of the gamma counter and the parts selected by the single channel analyser in this side for the two runs a and b. In both cases the beta counter was set to accept only events above 150 keV.

For the more energetic $\gamma$-rays ($\approx$ 75 keV), the delay curve fig. 5b could be measured with a resolving time $8\times10^{-9}$ sec. The long lived component was largely suppressed, but a $3\times10^{-9}$ sec half life appeared.

More accurate data on the energies of the $\gamma$-rays involved and on the positions of the two metastable states were obtained from measurements

with thin NaI crystals. When the 25 and 50 keV peaks were selected in the two channels, the resulting delay curve (fig. 6) showed that the 25 keV photon, in agreement with the previous measurement, is associated with the

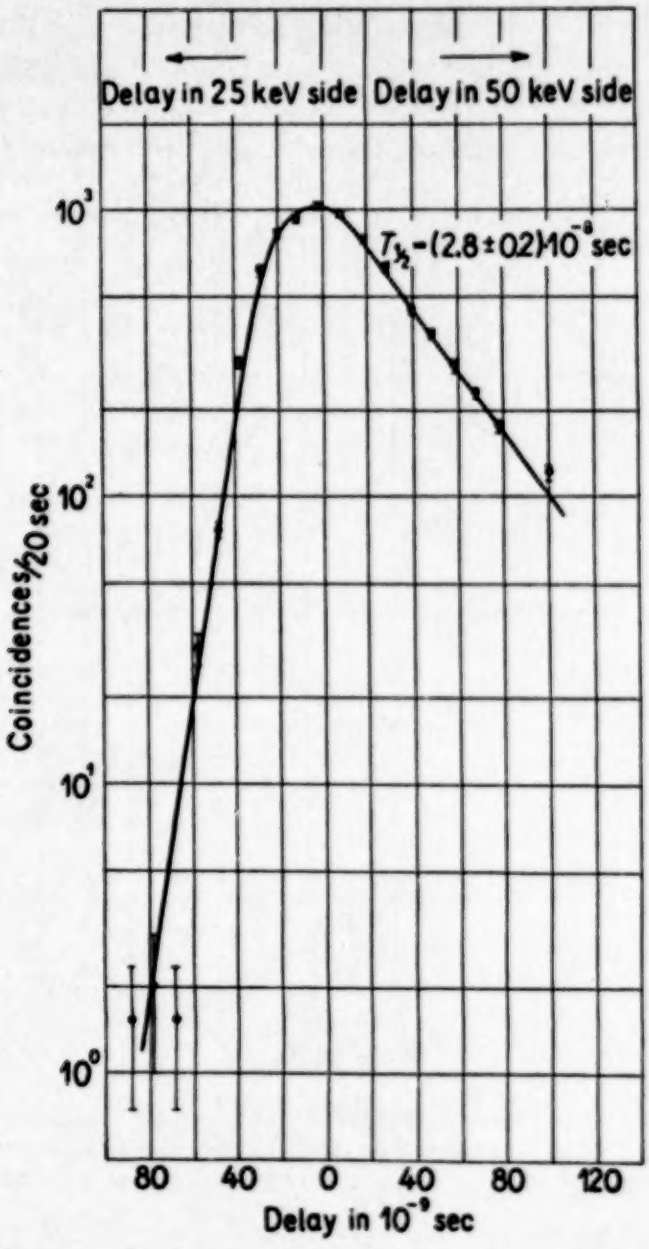


Fig. 6. Delayed gamma-gamma coincidences using NaI crystals ($\frac{1}{4}'' \times 1\frac{1}{2}''$ and $\frac{1}{2}'' \times 1\frac{1}{4}''$). The single channel analysers were set to accept the 25 keV and 50 keV peaks, respectively.

lifetime of $2.8 \times 10^{-8}$ sec and that it is preceded by radiation contained in the 50 keV peak.

With both channels selecting the 50 keV peak, the long lived component disappeared. This peak consists mainly of contributions from the 48.9 and 57.1 keV transitions, and consequently the 74.5 keV level cannot be the

origin of the slow component. The $2.8\times10^{-8}$ sec state must then be situated at 25.6 keV.

Finally, the 75 keV peak was selected by a NaI crystal, whereas $\beta$-particles with energy above 150 keV were selected by a plastic scintillator in the other channel. From the resulting delay curve (fig. 7) it can be seen that the 75 keV $\gamma$-ray is delayed by $(4\pm1)\times10^{-9}$ sec relative to the $\beta$-particles, in accordance with the curve in fig. 5b. The 74.5 keV level is excited directly by $\beta$-decay and also by the 57.1 keV transition. It seems most

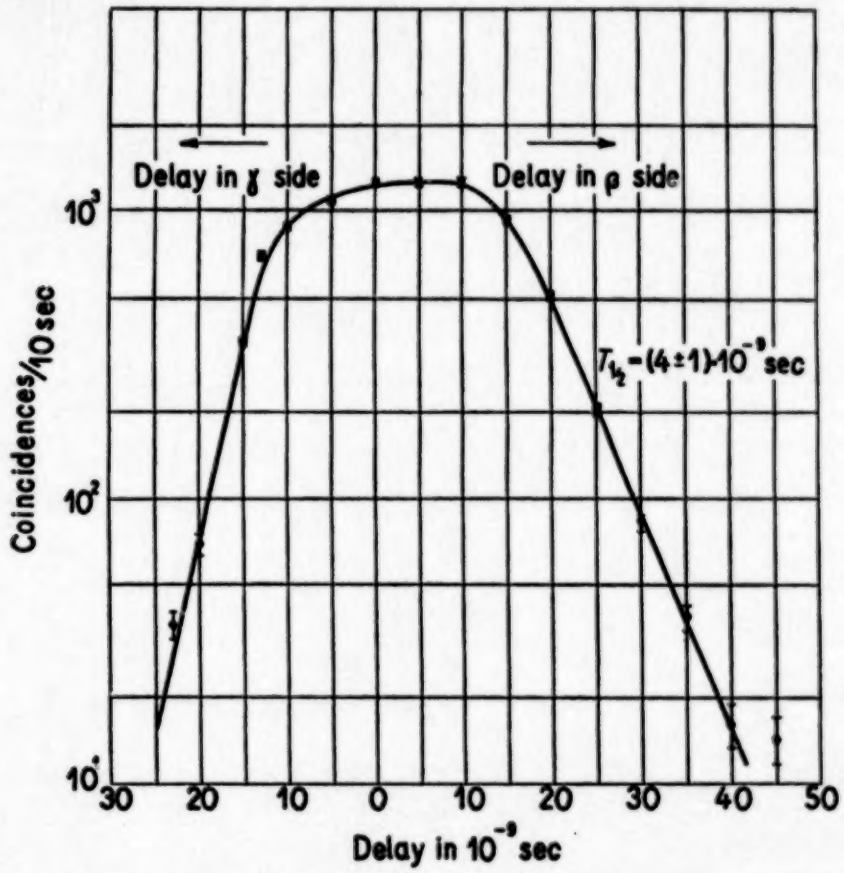


Fig. 7. Delayed beta-gamma coincidences with a $2''\times2''$ plastic scintillator in the beta side and a $\frac{1}{4}''\times1\frac{1}{2}''$ NaI crystal in the gamma side. The single channel analysers were set to accept events above 150 keV in the beta counter, and the 75 keV peak in the NaI crystal.

probable, however, that the 74.5 keV level rather than the 132 keV level has the $3\times10^{-9}$ sec half life, since no prompt coincidences are indicated on fig. 5b. On the lifetime of the 132 keV level, an upper limit only of about $3\times10^{-9}$ sec can be placed.

After these experiments were completed Vergnes [22]) reported the 25.6 and the 74.5 keV levels to have half lives of $(2.7\pm0.2)\times10^{-8}$ sec and $(2.3\pm0.7)\times10^{-9}$ sec, respectively. The results of the two half life investigations thus agree within the experimental error.

## 4. Assignment of Multipole Orders

E1 multipole nature has previously been reported for the 25.6 and 74.5 keV transitions [5, 10]), and M1 with less than 1 % E2 admixture for the 48.9 keV transition [10]). Also the 57.1 keV transition has tentatively been interpreted as E1 [10]).

The experimental results obtained in the present investigation are in substantial agreement with these assignments, except for the 57.1 keV transition. The E1 nature for the 25.6 keV transition is confirmed by the experimental $L_I : L_{II} : L_{III}$ ratio of 1 : 0.8 : 1.1 (theoretical E1 value 1 : 0.67 : 1.03). The 48.9 keV $\gamma$-ray converts mainly in the $L_I$ subshell with a $(L_I+L_{II})/L_{III}$ ratio of about 20 (theoretical ratios: M1 71, E1 2.7 and E2 0.9). This is consistent only with an assignment as M1 with $0.4\pm0.2\%$ E2 admixture.

The K/L ratio for the 74.5 keV transition is $5\pm1.5$. From fig. 1 the $(L_I+L_{II})/L_{III}$ ratio can be estimated to be of the order of 3. For E1, E2, and M1 radiation the theoretical values are for the K/L ratio 6, 0.45 and 6.80, and for the $(L_I+L_{II})/L_{III}$ ratio 3.7, 1.03 and 89. The experimental evidence is thus consistent only with an E1 assignment for this $\gamma$-ray.

The multipole order of the 57.1 keV transition presents a special problem, since only the M and N conversion lines were seen resolved. As the energy is above the K-binding energy of Dy (53.8 keV), conversion in the K shell must also be assumed to take place. Information about the K conversion coefficient of the 57.1 keV transition can therefore be obtained from the ratio of K X-rays to the 57.1 keV $\gamma$-ray in a coincidence spectrum, where the coincidence conditions eliminate contributions to the 50 keV peak from other transitions. The $\gamma$-ray spectrum coincident with the L conversion line of the 48.9 keV transition fulfills this condition. This spectrum (fig. 8) shows a strong line at 50 keV, and a weaker (unresolved) component of somewhat higher energy, which can be interpreted only as the 57.1 keV $\gamma$-ray. The ratio of K X-rays to $\gamma$-rays corrected for the fluorescence yield [19]) corresponds to a K conversion coefficient of about 6. The extrapolated theoretical values [18]) are E1 : 1, E2 : 3, and M1 : 8, thus suggesting M1 character. The pronounced difference at low energies between the K/L ratios for dipoles and for higher multipoles provides a valuable check on this assignment. Taking the L/(M+N) ratio as three, and using the theoretical K/L and $\alpha_K$ values for M1 transitions [17, 18]), the total transition intensity for the 57.1 keV transition calculated from the intensities of the observed M and N conversion lines is in good agreement with the intensity of the $\beta$-group feeding the 132 keV level. If the intensity is calculated from the assumption of pure E2 radiation, the low K/L ratio in this case makes the estimate a factor of 5 too low.

A determination of the intensities of the weak 106 and 132 keV $\gamma$-rays (fig. 2) was difficult due to the background conditions. Conservative limits on the intensities of the two $\gamma$-rays found by comparison with the known

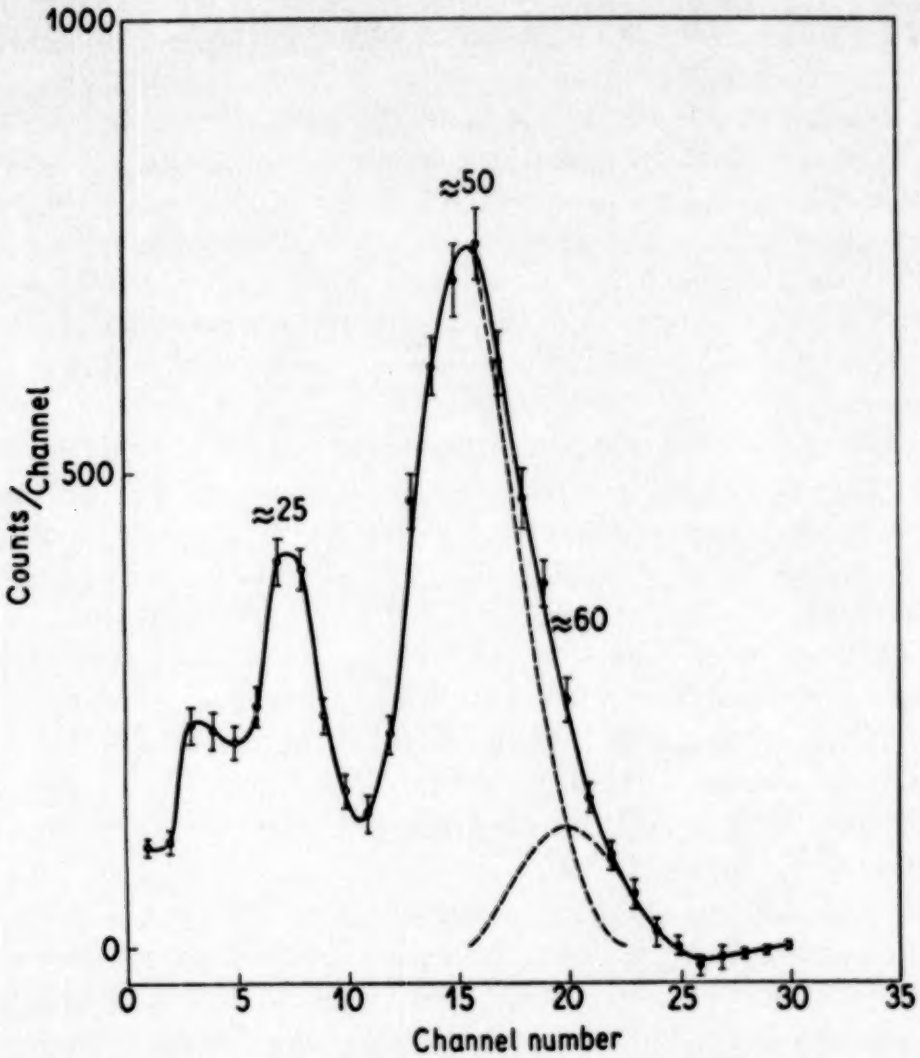


Fig. 8. Gamma spectrum coincident with the L conversion line of the 48.9 keV transition. Coincidences with the $\beta$-spectrum and random coincidences have been subtracted. The strong $\approx$ 50 keV peak is the K X-ray due to internal conversion of the 57.1 ($\approx$ 60) keV transition.

74.5 keV $\gamma$-ray are $0.05 < I_{106} < 0.2$ and $0.004 < I_{132} < 0.04$ per cent of the total number of disintegrations. For the 106 keV transition, the corresponding $\alpha_K$ is between 0.6 and 2.2. The theoretical values are E1 : 0.22, E2 : 0.98, E3 : 3.3, M1 : 1.75 and M2 : 14. The multipole order thus seems to be M1 or E2, confirming that no parity change takes place between the 132 and the 25.6 keV levels.

## 5. Discussion

The decay scheme presented in fig. 3 explains satisfactorily the present data as well as the majority of the measurements reported in earlier works.

The level tentatively placed at 103 keV is based mainly on the energy fit of the 28.7 and 77.6 keV $\gamma$-rays which also were reported by Cork [5]). Some evidence on the order of the two $\gamma$-rays comes from the decay of $Ho^{161}$ [20]) where only the 77.6 keV $\gamma$-ray is seen, thus making it most likely that this $\gamma$-ray has the lowest position in the level scheme.

The ground state spin of $Dy^{161}$ is probably 5/2 [23]). However, the experimental data do not allow an unambiguous determination of the spins and parities of the excited states. The values indicated in fig. 3 are consistent with the observed multipole orders and have been chosen according to the interpretation given by D. Bès [21]) on the basis of the unified model. Within the framework of this description, the $5/2^+$ ground state, the $5/2^-$ state at 25.6 keV and the $3/2^-$ state at 74.5 keV are intrinsic particle excitations, while the 103 keV state is a rotational state built on the 5/2 state and the 132 keV level likewise a rotational state associated with the $3/2^-$ state. A more detailed discussion of the level structure and of the transition intensities is given by D. Bès in the paper following this one [21]).

We are indebted to Professor Niels Bohr for the excellent working conditions in his Institute. During the investigation, close contact with Professor A. Bohr, Dr. D. Bès, and Dr. B. R. Mottelson has been of great help. One of us (P.G.H.) wishes to express his gratitude to the Danish Atomic Energy Commission, and especially to Dr. C. F. Jacobsen, for having given him the opportunity to participate in this work.

## References

1) S. G. Nilsson, Mat. Fys. Medd. Dan. Vid. Selsk. **29** (1955) no. 16
2) K. Gottfried, Phys. Rev. **103** (1956) 1017
3) B. R. Mottelson and S. G. Nilsson, Phys. Rev. **99** (1955) 1615
4) K. Alder, A. Bohr, T. Huus, B. Mottelson and A. Winther, Revs. Mod. Phys. **28** (1956) 432
5) J. M. Cork, J. M. LeBlanc, W. H. Nester and F. B. Stumpf, Phys. Rev. **88** (1952) 685
6) R. Barloutaud and R. Ballini, C. R. Acad. Sc. **241** (1955) 389
7) R. Ballini and R. Barloutaud, J. Phys. Rad. **7** (1956) 498
8) N. Bisi, S. Ferrani and L. Zappa, Nuclear Physics **1** (1956) 425
9) J. M. Cork, M. K. Brice, C. L. Schmid and R. G. Helmer, Phys. Rev. **104** (1956) 482
10) W. G. Smith, J. H. Hamilton, R. L. Robinson and L. M. Langer, Phys. Rev. **104** (1956) 1020
11) S. G. Thompson, B. G. Harvey, R. G. Choppin and G. T. Seaborg, J. Am. Chem. Soc. **76** (1954) 6229
12) G. R. Choppin and R. I. Silva, J. Inorg. and Nucl. Chem. **3** (1956) 153
13) P. Gregers Hansen and R. K. Sheline, Nuclear Instruments **2** (1958)
14) S. Bjørnholm, O. B. Nielsen and R. K. Sheline, Nature **178** (1956) 1110
15) O. B. Nielsen and O. Kofoed-Hansen, Mat. Fys. Medd. Dan. Vid. Selsk. **29** (1955) no. 6
16) O. Nathan, Nuclear Physics **4** (1957) 125
17) M. E. Rose, G. H. Goertzel and C. L. Perry, ORNL-1923 (1953);
M. E. Rose, G. H. Goertzel and C. Swift, L-shell internal conversion coefficients, privately distributed;
M. E. Rose, L-shell internal conversion coefficients with finite nuclear size included, privately distributed

18) L. Sliv and J. Band, Tables of Gamma-ray Internal Conversion Coefficients, Part I (Isdatelstvo Akademia Nauk SSSR, Moscow and Leningrad, 1956)
19) I. Bergstrøm in Beta and Gamma-Ray Spectroscopy, edited by K. Siegbahn (Amsterdam 1955)
20) J. W. Mihelich, B. Harmatz and T. H. Handley, Phys. Rev. **108** (1957) 989
21) D. Bès, Nuclear Physics **6** (1958) 645
22) M. Vergnes, J. Phys. Rad. **18** (1957) 579
23) A. H. Cook and J. G. Park, Proc. Phys. Soc. A **69** (1956) 282

*Nuclear Physics* **6** (1958) 645—654; © *North-Holland Publishing Co., Amsterdam*
Not to be reproduced by photoprint or microfilm without written permission from the publisher

# LEVELS IN $Dy^{161}$
## II. Theoretical

DANIEL R. BÈS
*Institute for Theoretical Physics, University of Copenhagen* †

Received 3 February 1958

**Abstract:** The experimental evidence on $Dy^{161}$ is shown to be in accord with the predictions of the unified model. Certain effects due to the Coriolis force are verified.

This paper attempts a theoretical interpretation of the experimental results concerning the levels in $Dy^{161}$. The data obtained in this Institute by P. Gregers Hansen, O. Nathan, O. B. Nielsen and R. K. Sheline [1]) will be used without further quotation. Whenever an experimental result, not found by them, is needed, the corresponding references will be given explicitly.

## 1. Single Particle Configurations and Level Scheme

The ground state spin of $Dy^{161}$ is 5/2 [2]). Those levels which may be unambiguously established from the decay of $Tb^{161}$ are shown in fig. 3 of ref. [1]). As is mentioned there, the results of Mihelich *et al.* on the decay of $Ho^{161}$ [3]) fix the position of the 77.6 keV gamma ray which depopulates a level at 103.2 keV. The 28.7 keV gamma ray probably goes from the 132 keV level to this last state. Coulomb excitation experiments determine the position of the levels corresponding to the ground state rotational band [4, 5, 6]). All the other observed levels have opposite parity relative to the ground state. The lifetime experiments reveal two intrinsic excitations at 25.6 and 74.5 keV.

Candidates for these three intrinsic states must be chosen from Nilsson's available single particle states for 95 nucleons [7]). Single particle states will be labelled by their "asymptotic" quantum numbers $(N, n_z, \Lambda, \Omega)$ : $N$ is the principal oscillator quantum number, $n_z$ the number of quanta along the symmetry axis; $\Lambda$ and $\Omega$ are the components, along the symmetry axis, of the orbital and total angular momenta, respectively. Using this notation, the empty states available are (642 5/2) and (523 5/2) and the possible hole states (521 3/2) and (505 11/2). The state (531 3/2) is the odd particle ground state in $Gd^{155}$ and $Gd^{157}$.

† Permanent address: Comisión Nacional de Energía Atómica, Buenos Aires, Argentina.

From the fact that the 25.6 and 74.5 keV gamma radiations are E1 it can be concluded that neither of the two intrinsic excited states is the (505 11/2) and that (642 5/2) represents the ground state.

The most probable configuration for $Tb^{161}$ is (411 3/2), as in $Tb^{157}$ and $Tb^{159}$. According to Alaga's selection rules [8]), the beta transitions from this level to the (521 3/2) states are unhindered, whereas those to (523 5/2) states are hindered. Most of the beta decay goes to the 74.5 and 132 keV levels; thus, these are probably the intrinsic excited state and first rotational state of the (521 3/2) band. The energy difference between these levels agrees very well with the energy of the first rotational states in $Gd^{155}$ and $Gd^{157}$ [9]).

The $Dy^{163}$ ground state spin is also 5/2 [2]). The very different moments of inertia of the first rotational bands in $Dy^{161}$ and $Dy^{163}$ suggest that the

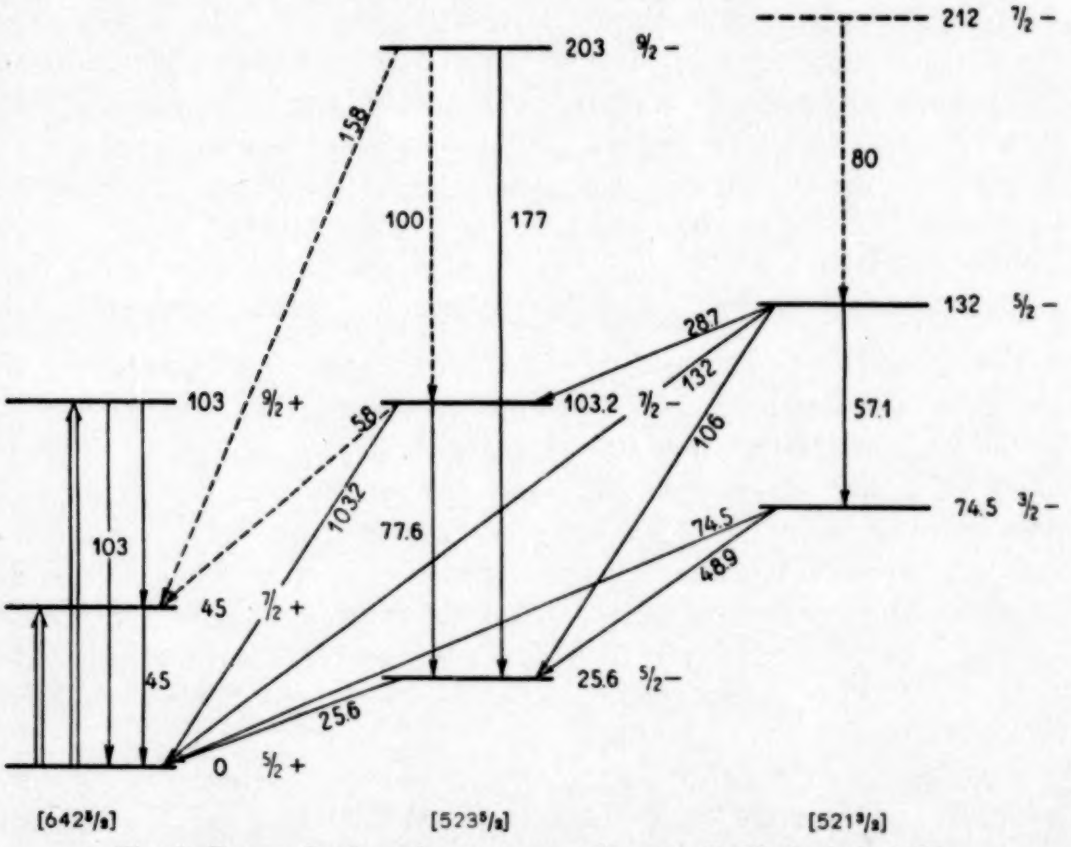


Fig. 1. Energy levels and gamma transitions in $Dy^{161}$ (both in keV).

ground state single particle configuration is not the same in both cases, and that therefore the one corresponding to $Dy^{163}$ ground state is (523 5/2). The first excited state in $Dy^{163}$ is at 75 keV [4, 5, 6, 10]). Therefore it seems very probable that the 77.6 keV gamma ray represents the deexcitation of the first rotational level of the $5/2^-$ band. In the decay of $Ho^{161}$ [3]), the second rotational level of the $5/2^-$ band is populated, and the previous assignments are confirmed, as will be shown below.

Consequenty, the level spectrum presents three intrinsic states with rotational bands built upon them (fig. 1).

## 2. Moments of Inertia

The rotational energy constants $3\hbar^2/\mathscr{I}$ of the $5/2^+$, $5/2^-$ and $3/2^-$ bands in $Dy^{161}$ are 39, 67 and 68 keV, respectively. The rotational constants of the ground state band in $Dy^{160}$ and $Dy^{162}$ are 86 and 82 keV, respectively. The differences between the moments of inertia of odd-mass and neighbouring even nuclei are associated with their different intrinsic excitations [9]). In order to understand these differences and, in particular, the large moment of inertia of the ground state band of $Dy^{161}$, it is convenient to use the "cranking" model. Inglis [11]) and Bohr and Mottelson [12]) have calculated moments of inertia by means of the formula

$$\mathscr{I} = 2\hbar^2 \sum_i \frac{|\langle \psi_0 | J_x | \psi_1 \rangle|^2}{E_i - E_0} \tag{1}$$

which takes into account the increase in energy of a nucleus due to its rotation; $J_x$ is the total angular momentum of the particles about an axis perpendicular to the symmetry axis. A simplified description of an odd-mass nucleus consists of an unpaired particle moving independently in the average field produced by the core. In the case of an odd-mass nucleus, the summation (1) may be split into two parts: $\mathscr{I} = \delta\mathscr{I} + \mathscr{I}_c$. The first part $\delta\mathscr{I}$ represents the contribution of the odd particle to the moment of inertia. The terms belonging to it correspond to transitions of the odd particle to unfilled levels and transitions of a particle of the core to the level of the odd particle. These terms have small energy denominators (they preserve the number of pairs). The second group of terms gives rise to $\mathscr{I}_c$. It is formed by transitions of a particle of the core to completely unfilled levels. The absence of low-lying states with $K = 1$ and positive parity in the spectrum of even nuclei shows that the energy denominators of the second group of terms are very large. The difference between $\mathscr{I}_c$ and the moment of inertia of neighbouring even nuclei is negligible with respect to $\mathscr{I}_c$, because it contains a much smaller number of terms with the same energy denominators. It is also a small quantity in comparison with $\delta\mathscr{I}$ because the energy denominators are much larger than those in $\delta\mathscr{I}$, although the number of terms is of the same order of magnitude.

Therefore, the contribution of an odd particle to the moment of inertia is given experimentally by the difference between the moment of inertia of the odd-mass and neighbouring even nuclei, and theoretically by the following expression:

$$\delta\mathscr{I} = 2\hbar^2 \sum_i \frac{|\langle 0 | j_x | i \rangle|^2}{|E_i - E_0|}, \tag{2}$$

where $\langle 0|j_x|i\rangle$ are the single particle matrix elements and the summation is to be extended to all single particle states. The same contribution from the odd particle to the effective moment of inertia is given in second order perturbation theory, if the unperturbed hamiltonian is that corresponding to particles with strong pairing interactions coupled to an axially symmetrical core by a potential, and the perturbing hamiltonian is the Coriolis force [13]).

The states $i$ that contribute the largest amount to (2) are $(N^i = N_0;\ n_z{}^i = n_z{}^0 \pm 1;\ \Lambda^i = \Lambda^0 \pm 1;\ \Omega^i = \Omega^0 \pm 1)$, which, according to Nilsson's energy diagram, are expected to lie between 1 and 2 MeV apart. Only in cases when $|E_i - E_0| \ll 1$ MeV is it expected that the contribution of other states may become important (e.g. $W^{183}$ [13])). If we average over the energy denominators and apply the closure property to (2) the contribution of the odd particle to the total moment of inertia is proportional to the expectation value [14]), i.e.

$$\delta\mathcal{I} \simeq \frac{2\hbar^2}{\overline{\Delta E}}\langle 0|j_x{}^2|0\rangle = \frac{\hbar^2}{\overline{\Delta E}}\langle 0|[j(j+1)-\Omega^2]|0\rangle. \tag{3}$$

The value of $\overline{\Delta E}$, as determined by the ratio of the experimental $\delta\mathcal{I}$ and the calculated $2\hbar^2\langle 0|j_x{}^2|0\rangle$, is found to be a fairly constant number along the deformed region. It is $1.7 \pm 0.4$ MeV for the rare earth region and $1.3 \pm 0.4$ MeV for the transuranic elements. This is a confirmation of the assumptions on which the calculation is based. The effect on the moment of inertia of the single particle of $Dy^{161}$ ($j = 13/2$, $\Omega = 5/2$) should thus be considerable.

In this particular case, it is interesting to compare the contributions of the odd particles in the different levels that correspond to the $i_{13/2}$ orbit

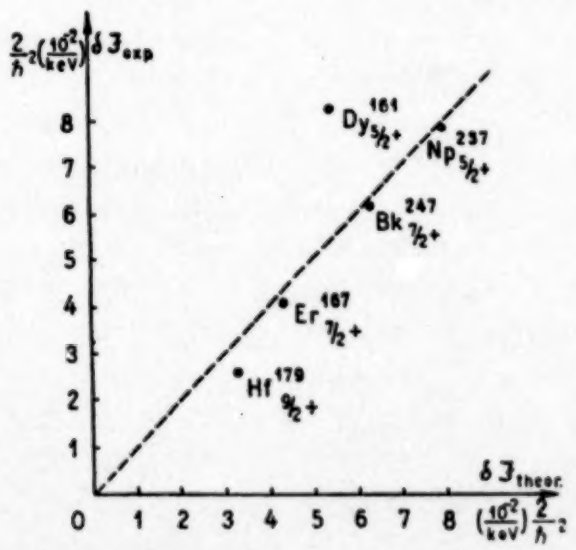


Fig. 2. Contribution of the unpaired $i_{13/2}$ particles to the moment of inertia (experimental versus theoretical values). The slope of the broken line is such as to give a best fit to the experimental points and corresponds to an average energy of 1.5 MeV for $Dy^{161}$.

in the limit of zero deformation, because they constitute an isolated set whose energy denominator differences are very close to an average. The results are represented in fig. 2. The theoretical dependence of the energy on $A$, $\Omega$ and the deformation have been taken from Nilsson's diagram [7]). One observes the expected increase in $\delta\mathscr{F}$ with decreasing $\Omega$, but a quantitative agreement is not obtained.

## 3. Beta Transitions

### 3.1. BETA TRANSITIONS IN THE DECAY OF $Tb^{161}$

The beta transition to the ground state of $Dy^{161}$ is allowed by both $I$ and $K$ selection rules, but is nevertheless retarded because the initial and final states differ by two in principal oscillator quantum number ($\log ft = 7.8$).

The upper limit of the beta intensity to the 25.6 keV level gives a $\log ft \geqq 8.1$. This is within the limits ($7.2 \leqq \log ft \leqq 8.3$) for first forbidden hindered transitions, as suggested by Alaga [8]).

The 212 keV level is the $I = 7/2$ state of the $3/2^-$ band and has not been found experimentally. It is fed by about 1 % of the $\beta$-decays, assuming a $\log ft = 8$ for this unique first forbidden transition. About one half of the transitions from this level goes by K conversion of an 80 keV gamma ray. The intensity of this line is then 0.5 in the units used in tables 2 and 3. This weak line, if present, would be hidden by the N conversion line of the 25.6 keV transition.

### 3.2. ELECTRON CAPTURE TRANSITIONS IN THE DECAY OF $Ho^{161}$

The half life of $Ho^{161}$ has been reported to be 2.5 h. No positons were observed [15, 3]). This implies $\log ft = 4.5$ for a decay energy of 1 MeV or $\log ft = 5.4$ for a decay energy of 2.5 MeV [16]). Thus, the decay is allowed unhindered. Accordingly, the ground state configuration of $Ho^{161}$ must be (523 7/2). This is also the ground state configuration of $Ho^{165}$, as expected. If the energy of the decay is around 1 MeV, the electron capture populates the 203, 103.2 and 25.6 keV levels in the ratios 2.5/25/100.

An electron capture transition to the 132 keV level implies an admixture of the $5/2^-$ band in the predominate $3/2^-$ band, since the single particle matrix element to the $3/2^-$ configuration is both $K$ forbidden and hindered. It should therefore be possible to measure the mixing between the bands by detecting the transitions which depopulate the 132 keV level in $Dy^{161}$. From the calculations of the Coriolis coupling (see section 4) it is possible to estimate the ratio of the electron capture to the 132 and 25.6 keV levels to be 2/100.

## 4. Gamma Ray Transitions

### 4.1. GAMMA TRANSITIONS IN THE DECAY OF $Tb^{161}$

Using the $(L_I+L_{II})/L_{III}$ ratios of Cork *et al.* [17]), it is possible to calculate the amount of E2 admixture in the 57.1 and 48.9 keV gamma rays as $\delta = 0.04$ and $\delta = 0.005$, respectively [18]). The latter value agrees very well with the result obtained in Copenhagen, viz. $\delta = 0.004 \pm 0.002$. The first value is in accordance with the E2 admixture in the 61 keV gamma ray of $Gd^{155}$ ($\delta = 0.05$) and 55 keV gamma ray of $Gd^{157}$ ($\delta = 0.04$) [9]).

The transition rates of several gamma rays occurring in the decay of $Tb^{161}$ are listed in table 1, together with theoretical estimates. The experimental values are determined using Rose's conversion coefficients, corrected for finite size effects [18]).

TABLE 1
Transition rates of some $Dy^{161}$ gamma rays

| Transition energy (keV) | Transition character | Moszkowski's estimate [19]) (1/s) | Nilsson's estimate (1/s) | Experimental value (1/s) |
|---|---|---|---|---|
| 25.6 | E1, h | $7.5\times10^{10}$ | $6.8\times10^{8}$ | $7.6\times10^{8}$ |
| 48.9 | M1, h | $3.2\times10^{9}$ | $1.4\times10^{8}$ | $4.8\times10^{7}$ |
| 48.9 | E2, h | $3.9\times10^{4}$ | $1.4\times10$ | $2.4\times10^{5}$ |
| 74.5 | E1, h | $1.8\times10^{12}$ | $3.9\times10^{8}$ | $2.1\times10^{7}$ |

h = hindered

Assuming that there is no coupling between the two odd bands, the ratio of the intensities of the 28.7 and 106 keV gamma rays depends only on geometrical factors. The calculated values for the ratios (28.7 keV, L)/(106 keV, K) and (28.7 keV, L)/(106 keV, L) are 0.26 and 1.8, respectively, while the measured ones are $9.2^{+15}_{-6}$ and $20^{+30}_{-13}$, respectively.

With the value of $g_\Omega - g_R = -0.85$ for the $3/2^-$ band, obtained from $Gd^{155}$ and $Gd^{157}$ [9]), it is possible to predict the relative intensities of all the transitions depopulating the 132 keV level. Theoretical intensities are normalized so that the experimental intensity of the L line of the 57.1 keV gamma ray coincides with its predicted value. The L/M ratio of this transition is assumed to be 3 (table 2).

TABLE 2
Intensity predictions for the transitions from the 132 keV level, assuming that the odd parity bands are pure rotational ones

| Transition (keV) | Predicted intensity | Measured intensity |
|---|---|---|
| 28.7 (L line) | 0.30 | 1 ±0.5 |
| 106 (K line) | 1.2 | 0.11 ±0.05 |
| 106 (L line) | 0.17 | 0.05 ±0.02 |
| 106 ($\gamma$-ray) | 0.65 | 0.12 ±0.08 |
| 132 ($\gamma$-ray) | 0.14 | 0.022±0.018 |

The most important disagreements between theory and experiment are the intensities of the 48.9 and 106 keV transitions. The latter discrepancy is that usually found for the strong forbidden transitions (see, for instance, $Lu^{175}$ [20]), $Hf^{177}$ [21]), $Np^{237}$ [22])). The rather extensive experimental material available concerning $Dy^{161}$ may permit, in this case, a better understanding of this discrepancy.

The simplest explanation for the enhancement of the 48.9 keV E2 gamma intensity is the existence of a coupling between the odd parity bands due to the Coriolis force. The matrix element of the Coriolis force between these two bands is expected to be small, since it vanishes in the limit of large deformations ($\Delta\Lambda = 2$). Moreover, it connects an empty state and a hole so there may be a further reduction in the coupling. Therefore, such coupling is expected to have little effect on the moment of inertia, where the matrix element enters quadratically, but to have a greater effect on the transitions between the two bands, because it enters linearly in the coefficients of the eigenfunctions. Accordingly, the momentum of inertia of the $5/2^-$ and $3/2^-$ bands in $Dy^{161}$ are in agreement with those in $Dy^{163}$, $Gd^{155}$ and $Gd^{157}$.

Assuming that all the E2 48.9 keV gamma ray transition comes from the mixing of the two bands, it is easy to calculate the admixture using first order perturbation theory. The eigenfunctions, with the same notation as in ref. [13]), are

$$\begin{aligned} \varphi^I_{\mathrm{L,H}} &= a^I_{\mathrm{L,H}}\, u^I_{5/2} + b^I_{\mathrm{L,H}}\, u^I_{3/2} \\ a^I_{\mathrm{L}} &= b^I_{\mathrm{H}} = 1 \\ a^I_{\mathrm{H}} &= -b^I_{\mathrm{L}} = -k\,(I+5/2)^{\frac{1}{2}}\,(I-3/2)^{\frac{1}{2}}. \end{aligned} \tag{4}$$

The experimental value of $k$ is $\pm 0.08$; the calculated one, assuming Nilsson's eigenfunctions, is $+0.10$. Therefore the $+$ sign has been chosen. The reduced transition probabilities between the mixed bands are derived in ref. [13]), section 3:

$$\begin{aligned} &B(\mathrm{M1}, I \to I') = \\ &\quad \frac{3}{4\pi}\left(\frac{e\hbar}{2Mc}\right)^2 \{a^{I'} a^I G^{5/2\ 5/2}_{\mathrm{M1}} \langle I1I'\tfrac{5}{2}|I\tfrac{5}{2}10\rangle + b^{I'} b^I G^{3/2\ 3/2}_{\mathrm{M1}} \langle I1I'\tfrac{3}{2}|I\tfrac{3}{2}10\rangle \\ &\quad + [a^{I'} b^I \langle I1I'\tfrac{5}{2}|I\tfrac{3}{2}11\rangle - b^{I'} a^I \langle I1I'\tfrac{3}{2}|I\tfrac{5}{2}1{-}1\rangle] G^{3/2\ 5/2}_{\mathrm{M1}}\}. \end{aligned} \tag{5}$$

From the gadolinium isotopes, $G^{3/2\ 3/2}_{\mathrm{M1}}$ has been determined as $-2.55$ [9]). $G^{3/2\ 5/2}_{\mathrm{M1}}$ may be derived by inserting in (5) the known half life of the 48.9 keV M1 transition and choosing the value with the same sign as that obtained from Nilsson's eigenfunctions: $G^{3/2\ 5/2}_{\mathrm{M1}} = -0.35$, $G^{3/2\ 5/2}_{\mathrm{M1\ (Nilsson)}} = -1.1$. Measurements of conversion coefficients, K/L and branching ratios, performed on $Dy^{163}$ by Temmer and Huus [10]), give an upper limit of $|g_\Omega - g_R|_{5/2^-} \leqq 0.05$. Using the values $(g_\Omega - g_R)_{5/2^-} = 0.05$, 0 and $-0.05$,

the intensities predicted in table 2 are replaced by those appearing in table 3. There is agreement between the measured and the predicted intensities, within the experimental accuracy, for the three assumed values of $(g_\Omega - g_R)_{5/2^-}$.

TABLE 3

Intensity predictions for the transitions between the odd parity bands, taking into account the mixing between the two bands.

| $(g_\Omega - g_R)_{5/2^-}$ | 28.7 keV (L line) | 106 keV (K line) | 106 keV (L line) | 106 keV ($\gamma$-ray) |
|---|---|---|---|---|
| 0.05 | 0.82 | 0.13 | 0.062 | 0.10 |
| 0 | 0.76 | 0.075 | 0.055 | 0.066 |
| −0.05 | 0.73 | 0.056 | 0.052 | 0.058 |

The corresponding calculations for the 132 keV gamma transition predict an intensity of $3 \times 10^{-3}$.

### 4.2. GAMMA TRANSITIONS IN THE DECAY OF $Ho^{161}$

With the previous estimates concerning the relative feeding of the 25.6, 103.2, 132 and 203 keV levels, and with the reduced gamma transition probabilities of the preceding section, it is a straight procedure to estimate the strongest lines in the $Ho^{161}$ decay. Table 4 shows these predictions for

TABLE 4

Transitions from the decay of $Ho^{161}$

| Predicted Intensities | | | | Measured Intensities† (Mihelich *et al.*[3]) | | |
|---|---|---|---|---|---|---|
| Transition energy (keV) | Gamma ray | K Line | L Line | Transition energy (keV) | K Line | L Line |
| 25.6 | | | $10^3$ | 25.65 | | $2 \times 10^2$ |
| 45 | | | 28 | | | |
| 48.9 | | | 13 | | | |
| 58 | 18 | | 5 | | | |
| 77.6 | 28 | 60 | 110 | 77.52 | unresolved | 110† |
| 100 | 2 | 2 | 2 | | | |
| 103.2 | 56 | 14 | 3 | 103.2 | 14 | 3 |
| 158 | 7 | 1 | | | | |
| 177 | 13 | 3 | | 175.4 | 3 | |

† The experimental intensities of Mihelich *et al.* are normalized so that the predicted intensity of the 77.6 keV L line coincides with the experimental value.

$(g_\Omega - g_R)_{5/2^-} = 0$. The 45, 58 and 158 keV intensities are calculated on the assumption that the 45 keV level is a pure rotational one.

Handley and Olson[15]) have found two gamma rays, by means of scintil-

lation spectrometer investigations: 90 keV and 170 keV (weak). The 90 keV transition is probably a mixture of 77.6 and 103.2 keV gamma rays; the 170 keV transition is a composite line of the 158 and 177 keV gamma transitions. The experimental results of Mihelich *et al.* [3]), who used a magnetic spectrograph, are included in table 4.

## 5. Conclusions

The unified model is able to interpret satisfactorily the levels in $Dy^{161}$. The intrinsic states are those predicted by theory. This nucleus provides several examples in which the validity of the "asymptotic" selection rules, characteristic of deformed nuclei, can be tested. The unified model does not predict a complete separation between rotational and intrinsic motions, because Coriolis' coupling is always present. Clear evidence of this force is to be found in the large moment of inertia of the ground state band. A second manifestation of the Coriolis coupling is the enhancement of the 49.8 keV E2 gamma ray transition rate. Other probable evidence lies in the fact that it is possible to predict an experimentally supported cancellation in the matrix element for the 106 keV gamma ray. In this last calculation, theoretical estimations have been used only for the choice between the positive and negative values of quantities whose absolute magnitudes were derived from experimental data.

The privilege of working in the Institute for Theoretical Physics, Copenhagen, provided by Professors Niels Bohr and Aage Bohr, is deeply appreciated and gratefully acknowledged. Sincere thanks are due to Dr. B. R. Mottelson for many suggestions offered during the course of this investigation. Moreover, contacts with Profs. Aa. Bohr and R. Sheline, and Civ. Engs. P. Gregers Hansen, O. Nathan and O. B. Nielsen have greatly stimulated this work. A scholarship from the Comisión Nacional de Energía Atómica, Buenos Aires, Argentina, is gratefully acknowledged.

## References

1) P. Gregers Hansen, O. Nathan, O. B. Nielsen and R. Sheline, Nuclear Physics **6** (1958) 630
2) A. H. Cooke and J. G. Park, Proc. Phys. Soc. A **69** (1956) 282
3) J. W. Mihelich, B. Harmatz and T. H. Handley, Phys. Rev. **108** (1957) 989
4) B. Elbek, K. O. Nielsen and M. C. Olesen, Phys. Rev. **108** (1957) 406
5) N. P. Heydenburg and G. F. Pieper, Phys. Rev. **107** (1957) 1297
6) E. M. Bernstein and S. Buccino, Bull. Am. Phys. Soc. **3** (1958) 55 U3
7) S. G. Nilsson, Mat. Fys. Medd. Dan. Vid. Selsk. **29** (1955) no. 16
8) G. Alaga, Phys. Rev. **100** (1955) 432
9) K. Alder, A. Bohr, T. Huus, B. R. Mottelson and A. Winther, Revs. Mod. Phys. **28** (1956) 432
10) G. Temmer and T. Huus, private communication
11) D. Inglis, Phys. Rev. **96** (1954) 1059; **97** (1955) 701

12) A. Bohr and B. R. Mottelson, Mat. Fys. Medd. Dan. Vid. Selsk. **30** (1955) no. 1
13) A. K. Kerman, Mat. Fys. Medd. Dan. Vid. Selsk. **30** (1955) no. 15
14) B. R. Mottelson and S. G. Nilsson, to be published
15) T. H. Handley and E. L. Olson, Phys. Rev. **93** (1954) 524; T. H. Handley, Phys. Rev. **94** (1954) 945
16) M. E. Rose, Chapter IX of Beta and Gamma Ray Spectroscopy, edited by K. Siegbahn (Amsterdam, 1955)
17) J. H. Cork, M. K. Brice, L. C. Schmid and R. G. Helmer, Phys. Rev. **104** (1956) 481
18) M. E. Rose, privately circulated tables no. 13, 14 and 15
19) S. A. Moszkowski, Chapter XIII of Beta and Gamma Ray Spectroscopy, edited by K. Siegbahn (Amsterdam, 1955)
20) D. M. Chase and L. Wilets, Phys. Rev. **101** (1956) 1038
21) S. Ofer, Nuclear Physics **3** (1957) 479
22) J. M. Hollander, W. G. Smith and J. O. Rasmussen, Phys. Rev. **102** (1956) 1372

*Nuclear Physics* **6** (1958) 655—668; © *North-Holland Publishing Co., Amsterdam*
Not to be reproduced by photoprint or microfilm without written permission from the publisher

# ON THE GAMMA SPECTRA OF $Ag^{110}$, $Sb^{124}$ AND $Eu^{152,154}$

B. S. DŽELEPOW and N. N. ZHUKOVSKY
*V. G. Khlopin Radium Institute, USSR Academy of Sciences, Leningrad*

Received 14 November 1957

**Abstract:** The elotron, a recoil electron gamma spectrometer with improved focusing properties, was used to study the gamma radiation from $Ag^{110}$, $Sb^{124}$ and $Eu^{152, 154}$.

## 1. Introduction

The measurements were carried out under conditions [1]) which were more favourable in respect to resolving power and efficiency than those encountered in ref. [2]). Coincidences were recorded with two air tight counters filled with a mixture of 60 % A and 40 % $CH_4$ at a total pressure of 10 cm Hg. During measurements the elotron chamber was continuously evacuated with a forevacuum pump. These improvements greatly lowered scattering of the recoil electrons and as a result the $\gamma$-line half-width at $h\nu = 1$ MeV decreased from 2.6 % to 1.7 % and the coincidence rate corresponding to the line peaks from a given source increased by 3 times.

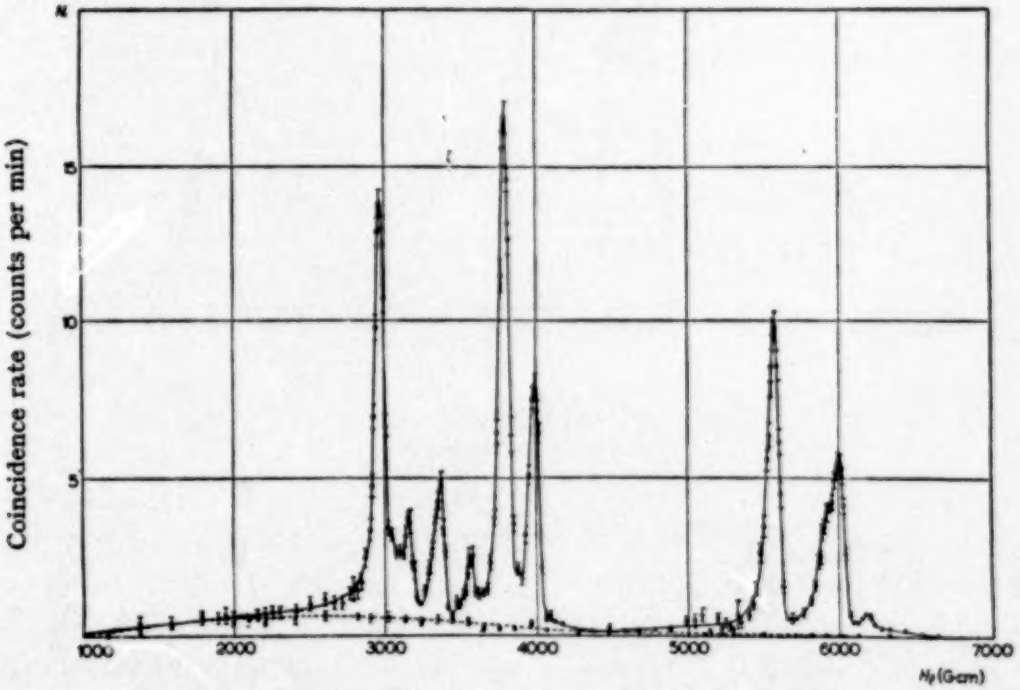


Fig. 1. Experimental gamma spectrum of $Ag^{110}$; $\overline{\phi}$–coincidence counting rate (counts/min) with target in gamma ray beam; $\overline{\cdot}$–background.

## 2. $Ag^{110}$

The $Ag^{110}$ source used was a 7.6 g silver shaving possessing an activity $\approx$ 700 mCu. The measurements were conducted three months after the source had been prepared. The experimental $Ag^{110}$ gamma spectrum is plotted in fig. 1. The circles refer to the coincidence rate with the target in the gamma ray beam; the points refer to the instrumental background. Decomposition of the $Ag^{110}$ gamma spectrum into its separate components with account of the instrumental shape of the lines is illustrated in figs. 2—4.

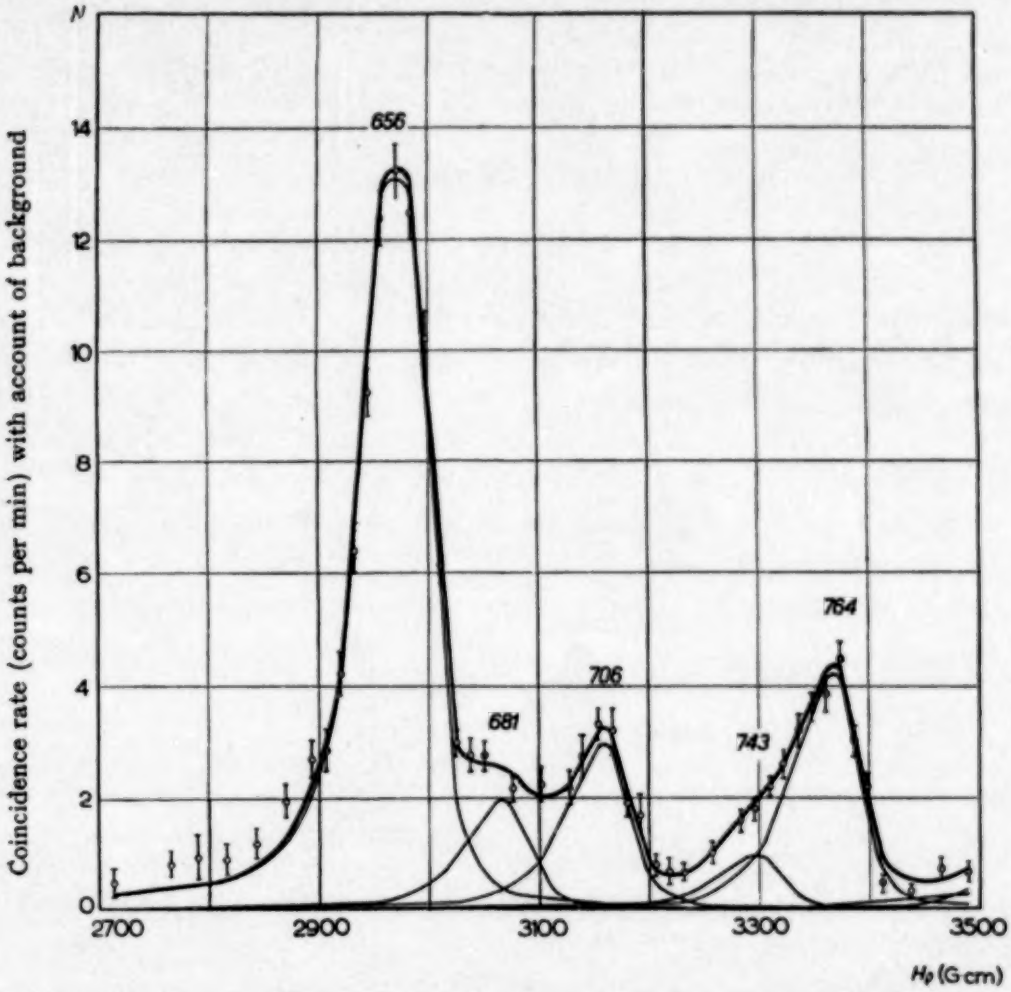


Fig. 2. Decomposition of region $H\varrho = 2700-3500$ G · cm of $Ag^{110}$ gamma spectrum into separate components.

Twelve gamma lines were detected. The 1560 keV gamma line has been observed for the first time; it was attributed to the $Ag^{110}$ gamma spectrum only on basis of the fact that its intensity during a three months period decayed with a half-life of $\approx$ 270 days. In table 1 are presented the gamma rays observed by us, their relative intensities and also the gamma transition multipolarities for which the relative intensities of the K-conversion lines were known from ref. [3]).

Our data confirm the existence of excited levels in $Cd^{110}$ with energies of 656, 1418, 1540, 2220, 2475 and 2924 keV (fig. 5). The sum of the energies of gamma transitions $h\nu = 740$ and 1480 keV is close to the energy of the excited level 2220 keV. This raises the question regarding the existence of

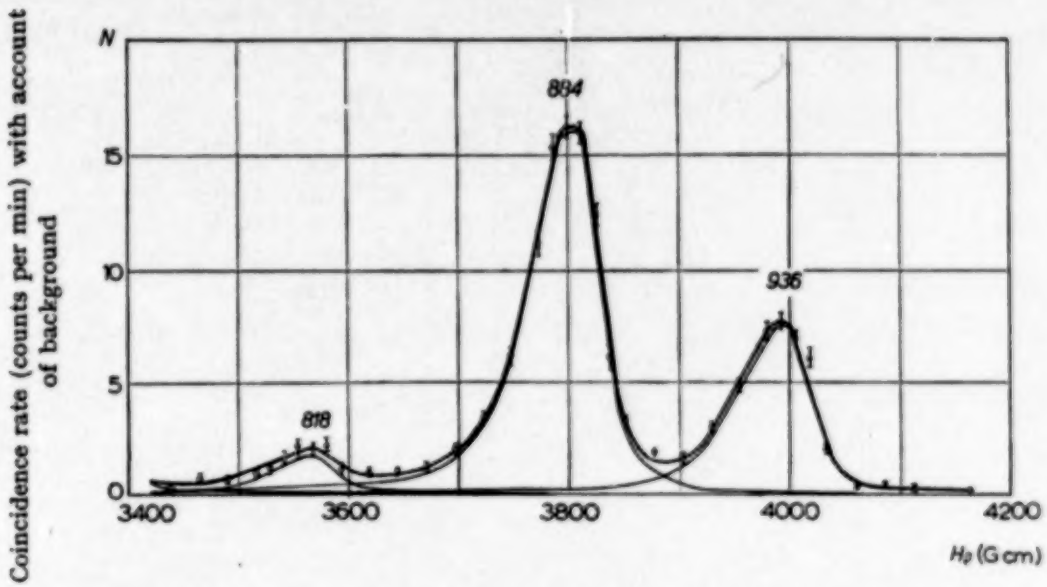


Fig. 3. Decomposition of region $H\varrho = 3400-4200$ G · cm of $Ag^{110}$ gamma spectrum into separate components.

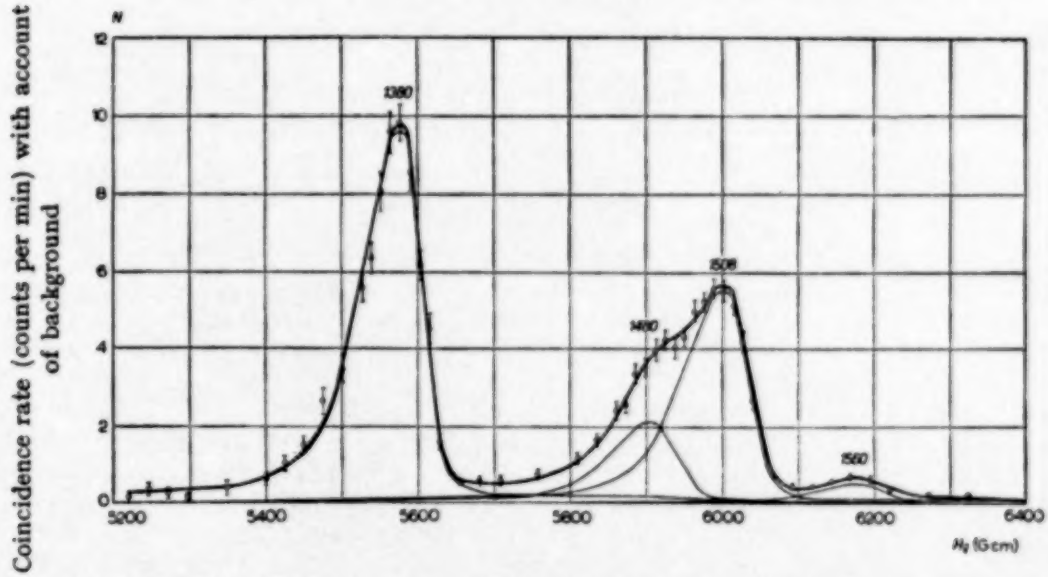


Fig. 4. Decomposition of region $H\varrho = 5200-6400$ G · cm of $Ag^{110}$ gamma spectrum into separate components.

an intermediate excited level in $Cd^{110}$ with an energy of either 740 or 1480 keV. We shall presume this energy to equal 1480 keV. Comparison with the level sequence in neighbouring even nuclei (e.g., $Mo^{96}$, $Pd^{104}$, $Pd^{108}$, $Cd^{114}$, etc.) seems to justify this assumption. According to the generalized nuclear

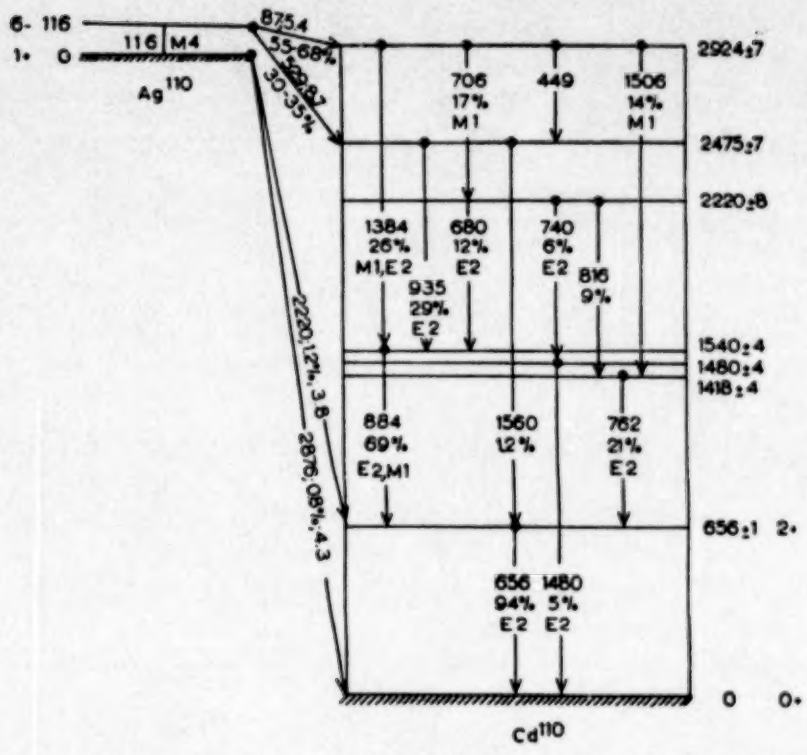


Fig. 5. Decay scheme of $Ag^{110}$ with account of our results on the gamma spectrum.

TABLE 1

Relative intensities and multipolarities of gamma transitions in $Cd^{110}$

| No. | Present data | | | Accepted energy values† $h\nu$ (keV) | Rel. intens. K-conv. line[3]) | Exper. value of $\alpha_K \times 10^3$ | Theoretical conversion coeff. $\alpha_K \times 10^3$[4]) | | | | | Assumed multi-polarity |
|---|---|---|---|---|---|---|---|---|---|---|---|---|
| | $h\nu$ (keV) | Rel. intens. | Number of $\gamma$-quanta per decay (%) | | | | E1 | E2 | E3 | M1 | M2 | |
| 1 | — | — | — | 116.1±0.1 | — | — | 97.8 | 832 | 3890 | 251 | 24600 | — |
| 2 | — | — | — | 446±1 | — | — | 2.45 | 7.94 | 23.4 | 7.38 | 25.7 | — |
| 3 | — | — | — | 575±1 | — | — | 1.33 | 3.89 | 10.0 | 4.08 | 12.0 | — |
| 4 | — | — | — | 619±2 | — | — | 1.12 | 3.16 | 7.75 | 3.39 | 9.55 | — |
| 5 | 656 | 100 | 94 | 656±1 | 100 | 2.76 | — | 2.76 | — | — | — | E2 |
| 6 | 681 | 13±2 | 12 | 680±2 | 8 | 1.7 | 0.93 | 2.51 | 6.89 | 2.76 | 7.59 | ? |
| 7 | 706 | 18±2 | 17 | 705±2 | 16 | 2.4 | 0.85 | 2.34 | 5.25 | 2.57 | 6.92 | E2, M1 |
| 8 | 743 | 6±2 | 5 | 741±3 | 3 | 1.5 | 0.78 | 2.04 | 4.57 | 2.34 | 6.02 | — |
| 9 | 764 | 23±2 | 21 | 762±3 | 16 | 1.9 | 0.73 | 1.95 | 4.26 | 2.19 | 5.62 | E2, M1 |
| 10 | 818 | 9±1 | 8 | 816±3 | 3.8 | 1.2 | 0.63 | 1.66 | 3.54 | 1.86 | 4.57 | ? |
| 11 | 884 | 75±4 | 69 | 884±3 | 32 | 1.2 | 0.59 | 1.38 | 2.88 | 1.55 | 3.71 | E2 |
| 12 | 936 | 32±2 | 29 | 935±3 | 13 | 1.1 | 0.48 | 1.20 | 2.46 | 1.35 | 3.24 | E2 |
| 13 | 1384 | 28±2 | 26 | 1384±4 | 6.5 | 0.65 | 0.23 | 0.52 | 0.96 | 0.56 | 1.23 | E2, M1 |
| 14 | 1484 | 6±1 | 5 | 1480±5 | 0.8 | 0.37 | 0.21 | 0.46 | 0.83 | 0.49 | 1.07 | E2, M1 |
| 15 | 1508 | 15±1 | 14 | 1506±5 | 2.5 | 0.46 | 0.20 | 0.44 | 0.80 | 0.48 | 1.02 | E2, M1 |
| 16 | 1560 | 1.3±0.2 | 1 | 1560±10 | — | — | 0.19 | 0.42 | 0.74 | 0.44 | 0.95 | — |

† Based on all available studies of $Ag^{110}$.

model of such nuclei (see for example the work of Scharf-Goldhaber and Weneser [5])) the first excited levels are collective vibrational levels, the energy of the second excitation level exceeding that of the first one by 2.0—2.4 times. In $Cd^{110}$ the energy of the first level is 656 keV and hence the second level may be expected to be located in the 1300—1570 keV region. It is possible that the 1418, 1480 and 1540 keV excitation levels comprise a triplet characteristic of double excitation of "round" even nuclei in the region $36 \leqq N \leqq 88$.

## 3. $Sb^{124}$

In the first elotron measurements of the relative $Sb^{124}$ gamma line intensities [2]) the errors were not smaller than $\approx$ 11—12 %. This was due to deficient knowledge of the spectral sensitivity and also to the low resolving

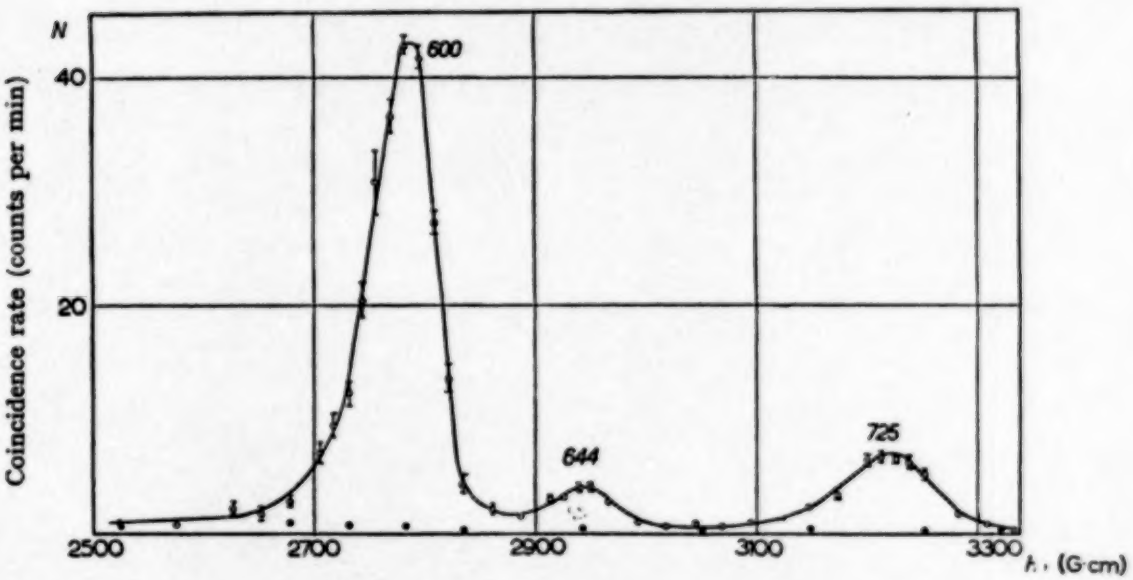


Fig. 6. Experimental gamma ray spectrum of $Sb^{124}$ in interval $H\varrho = 2500—3300$ G · cm.

power of the instrument in the soft region of the gamma spectrum caused by residual gas in the apparatus. In order to obtain more precise data we carefully studied under improved conditions the $H\varrho = 2500—3300$ and 4800—6300 G · cm sections of the $Sb^{124}$ gamma spectrum and also made new measurements on the peaks of the other gamma lines. Experimental curves obtained with a $\approx$ 1.5 Cu $Sb^{124}$ source are presented in figs. 6 and 7 (the general shape of the spectrum is given in ref. [2])). Decomposition into separate lines of the $H\varrho = 5200—6300$ G · cm section of the spectrum which corresponds to the left hand drop of the intense $h\nu = 1700$ keV gamma line is represented in fig. 8. The experimental curve with account of background

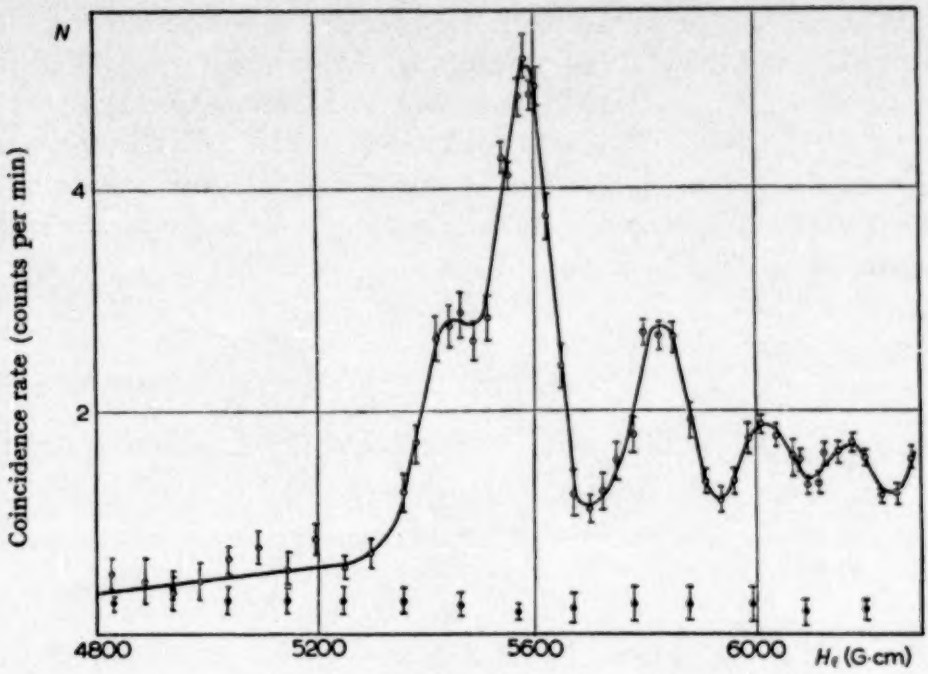


Fig. 7. Experimental gamma ray spectrum of $Sb^{124}$ in interval $H\varrho = 4800-6000$ G · cm.

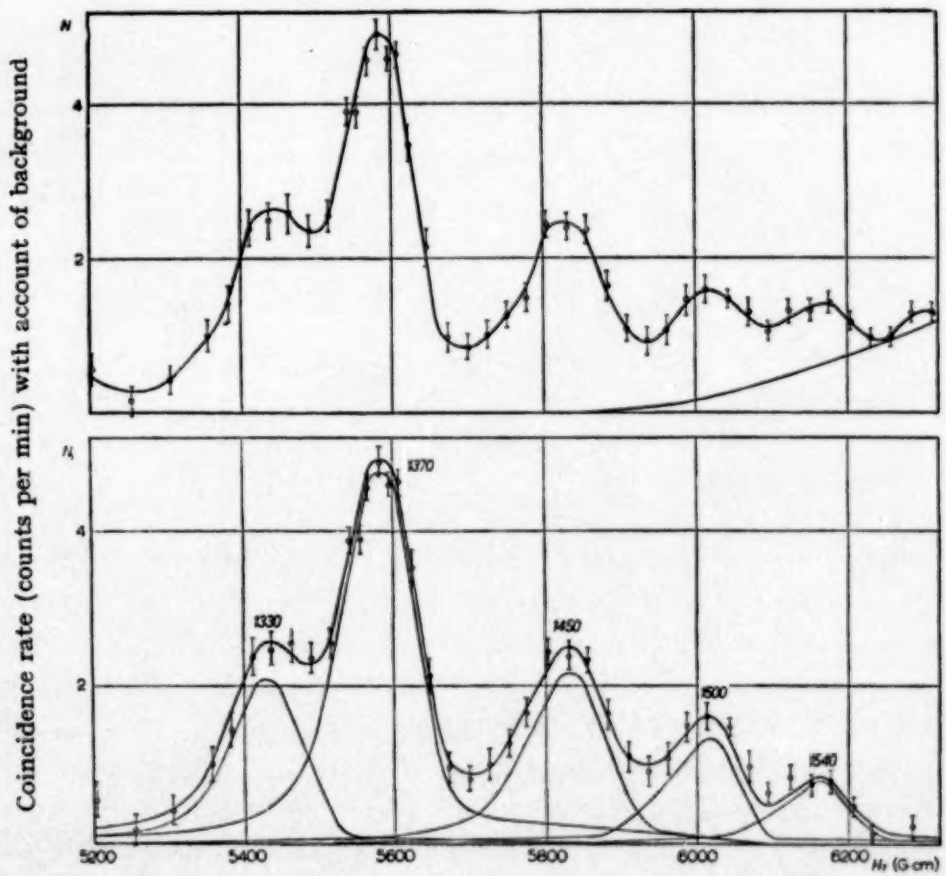


Fig. 8. Decomposition of region $H\varrho = 5200-6300$ G · cm of $Sb^{124}$ gamma spectrum into separate components.

is shown in the upper part of the fig. The thin line bounds that part of the spectrum which corresponds to the left hand drop of the $h\nu = 1700$ keV gamma line. The circles in the lower fig. refer to a section of the spectrum after exclusion of this drop. It should be noted that the half width of gamma lines $h\nu = 723$, 1330 and 1370 keV is much greater than the instrumental half width of the line in this region. The broadening is due to the fact that in reality we are dealing with doublets 714+723, 1298+1326 and 1361+1370 which are resolved only in conversion studies [6]).

In the $H\varrho = 5700-6300$ G · cm range, as in a previous work [2]), an appreciable excess over the background was observed which permitted us to identify the gamma-lines $h\nu = 1450$, 1500 and 1540 keV. A second measurement in this region performed $1\frac{1}{2}$ month later showed that the coincidence rate corresponding to the line peaks decreased with a half-life corresponding to that of $Sb^{124}$.

TABLE 2

Relative intensities and multipolarities of gamma transitions of $Te^{124}$

| No. | Accepted values $h\nu$ (keV) | Our data | | Rel. intens. of K-conv. line [3]) | Exp. value of $\alpha_K \times 10^3$ | Theoretical value of $\alpha_K \times 10^3$ | | | | | Assumed multi-polarity | Number of $\gamma$-quanta per decay (%) |
|---|---|---|---|---|---|---|---|---|---|---|---|---|
| | | $h\nu$ (keV) | Rel. intens. | | | E1 | E2 | E3 | M1 | M2 | | |
| 1 | 603±1 | 600 | 100 | 100 | 4.27 | — | 4.27 | — | — | — | E2 | 98.6 |
| 2 | 646±1 | 644 | 7.5±0.5 | 7.4 | 4.21 | 1.29 | 3.54 | 8.50 | 4.46 | 12.9 | M1 | 4.5 |
| 3 | 714±2 | 725 | 14±1 | 2.6 | 2.92 | 1.05 | 2.76 | 6.31 | 3.46 | 9.55 | E2;E2+M1 | 3.7 |
| 4 | 723±1 | | | 7.8 | 3.26 | 1.02 | 2.69 | 6.03 | 3.39 | 9.33 | M1 | 10.0 |
| 5 | 970±2 | 967 | 2.5±0.4 | ≈0.6 | ≈1.03 | 0.56 | 1.35 | 2.82 | 1.70 | 4.26 | ? | 2.5 |
| 6 | 1047±3 | 1048 | 2.4±0.4 | — | — | — | — | — | — | — | — | 2.4 |
| 7 | 1298±4 | 1330 | 2.3±0.3 | — | — | — | — | — | — | — | — | — |
| 8 | 1326±4 | | | — | — | — | — | — | — | — | — | 1.4 |
| 9 | 1361±4 | 1370 | 4.7±0.3 | — | — | — | — | — | — | — | — | — |
| 10 | 1370±4 | | | — | — | — | — | — | — | — | — | 4.6 |
| 11 | 1450±14 | 1450 | 2.1±0.2 | — | — | — | — | — | — | — | — | 21 |
| 12 | 1505±15 | 1505 | 1.1±0.2 | — | — | — | — | — | — | — | — | ≈ 0.1 |
| 13 | 1540±16 | 1540 | 0.6±0.2 | — | — | — | — | — | — | — | — | ≈ 0.6 |
| 14 | 1692±2 | 1700 | 51 ±3 | 2.9 | 0.24 | 0.21 | 0.42 | 0.80 | 0.49 | 1.05 | E1 | 50.0 |
| 15 | 2088±4 | 2090 | 6.6±1.0 | — | — | — | — | — | — | — | — | 6.5 |

In table 2 are presented the values of the relative intensities obtained by us and also the multipolarities of the gamma transitions in $Te^{124}$ computed on basis of these values and of those for the relative K-conversion line intensities obtained in ref. [6]) (the 603 keV transition being assumed to be a pure E2 transition).

Our data on the relative gamma line intensities confirm the existence of excitation levels in $Te^{124}$ with energies of 603, 1326, 1972, 2295 and 2691 keV (fig. 9). The existence of the $h\nu = 1450$ keV gamma line observed by us

apparently implies the existence of an excitation level in $Te^{124}$ at 1248 keV. Indeed, within the accuracy of the experiments the sums of the gamma line energies 1450+646 keV and 1047+646 keV are respectively equal to the

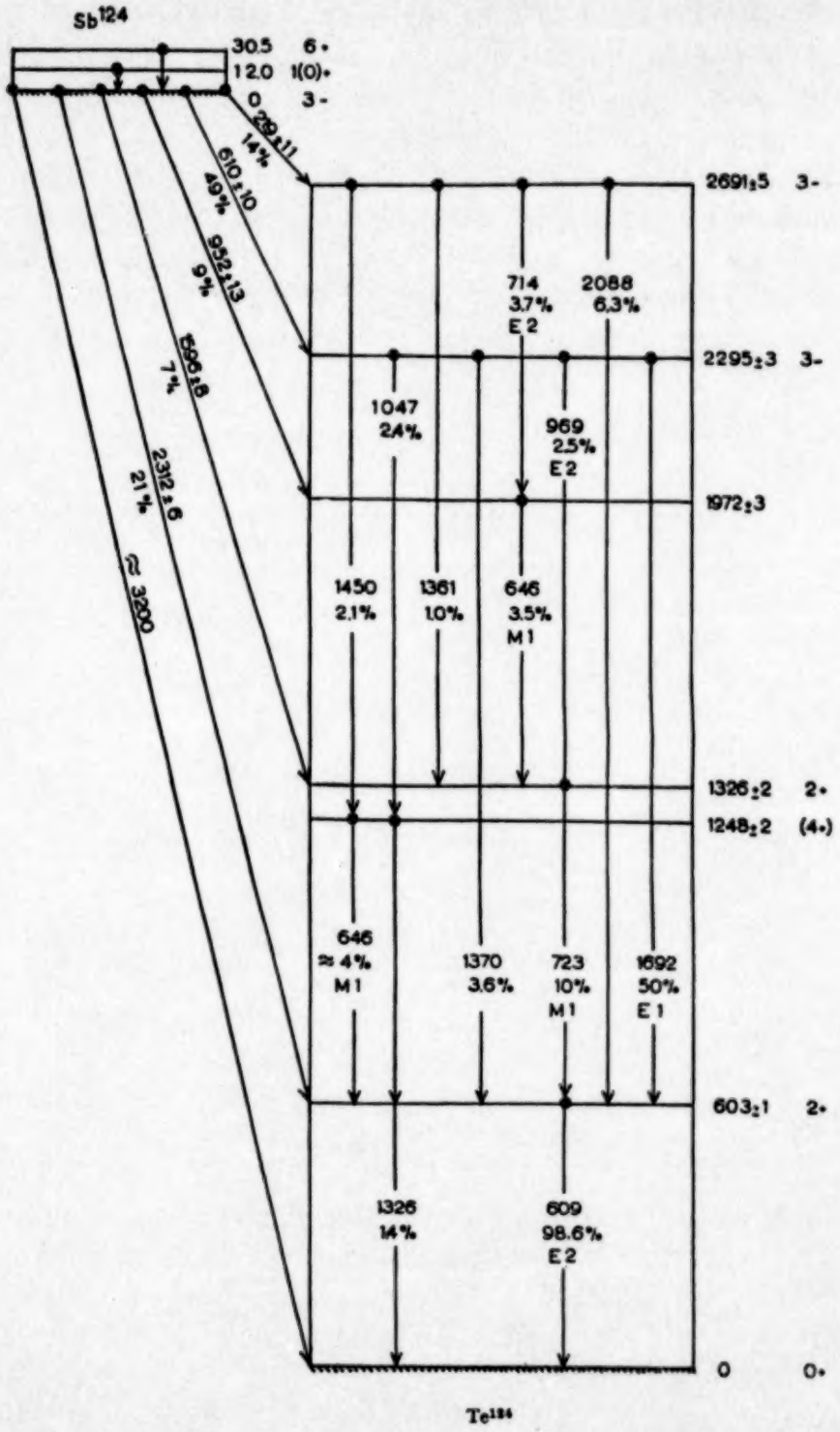


Fig. 9. Decay scheme of $Sb^{124}$ with account of our data on the relative intensities of the $Sb^{124}$ gamma lines.

energy differences between the 2691 and 603 keV levels and 2295 and 603 keV levels. The position of these lines in the $Sb^{124}$ decay scheme point definitely to the existence of a 1248 keV excitation level in $Te^{124}$. The 1248 and 1326 keV excitation levels should apparently be assigned to the doubly excited triplet predicted by the generalized model for collective vibrational states of undeformed nuclei.

Introduction of an excitation level in $Te^{124}$ at 1248 keV somewhat modifies the positions of the $h\nu = 646$ and 723 keV lines since

$$1972-1248 = 724 \text{ keV} \quad \text{and} \quad 1248-603 = 645 \text{ keV}.$$

The question regarding the doublet structure of these gamma lines can be solved by making a special study of the respective conversion lines with aid of a high resolution instrument.

## 4. $Eu^{152,154}$

The gamma spectrum of $Eu^{152, 154}$ was investigated by using a neutron activated oxide of a natural mixture of europium isotopes. The total weight

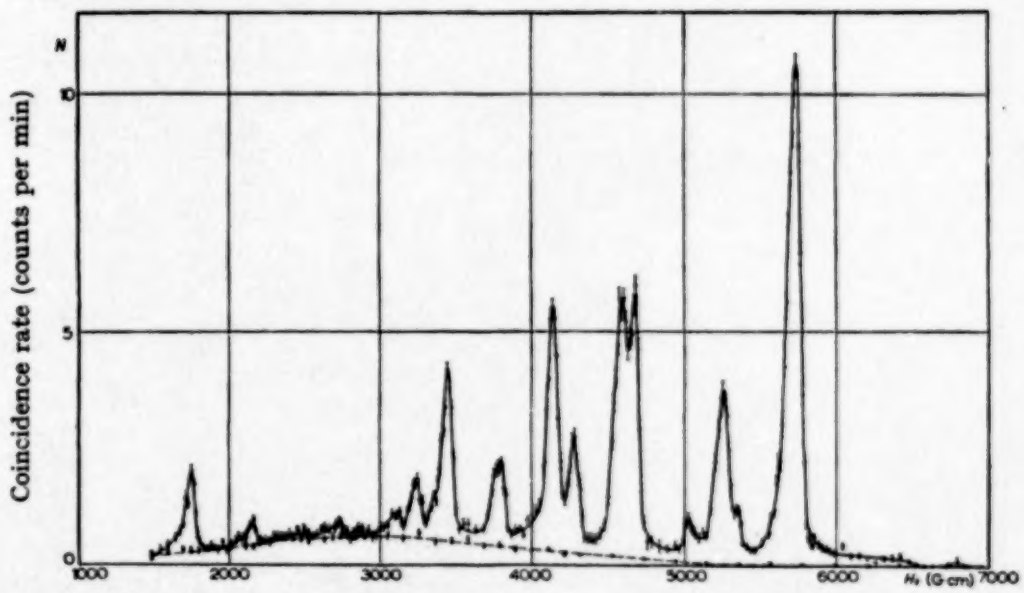


Fig. 10. Experimental gamma spectrum of $Eu^{152, 154}$.

of the source was 0.08 g and its activity $\approx$ 800 mCu. The experimental gamma spectrum of $Eu^{152, 154}$ is represented in fig. 10. Decomposition of the spectrum into its components is depicted in figs. 11—14. Seventeen gamma lines of appreciable intensity were observed. Because of the large statistical errors of our measurements we could not identify with sufficient certainty the weak gamma lines of $h\nu = 411$, 478, 550, 612 and 812 keV energy ob-

served by other authors but nevertheless a convincing indication that these lines really exist is that the coincidence rate definitely exceeds the background rate in those parts of the spectrum which correspond to these lines.

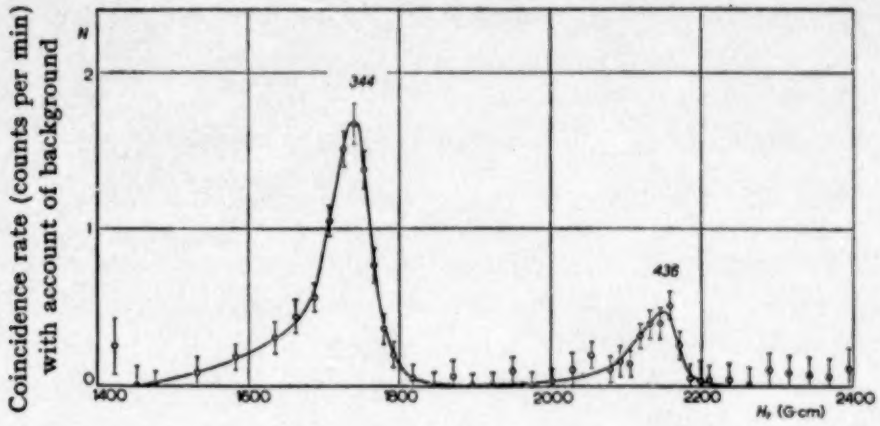


Fig. 11. Decomposition of interval $H\varrho = 1400-2300$ G · cm of $Eu^{152, 154}$ gamma ray spectrum into separate components.

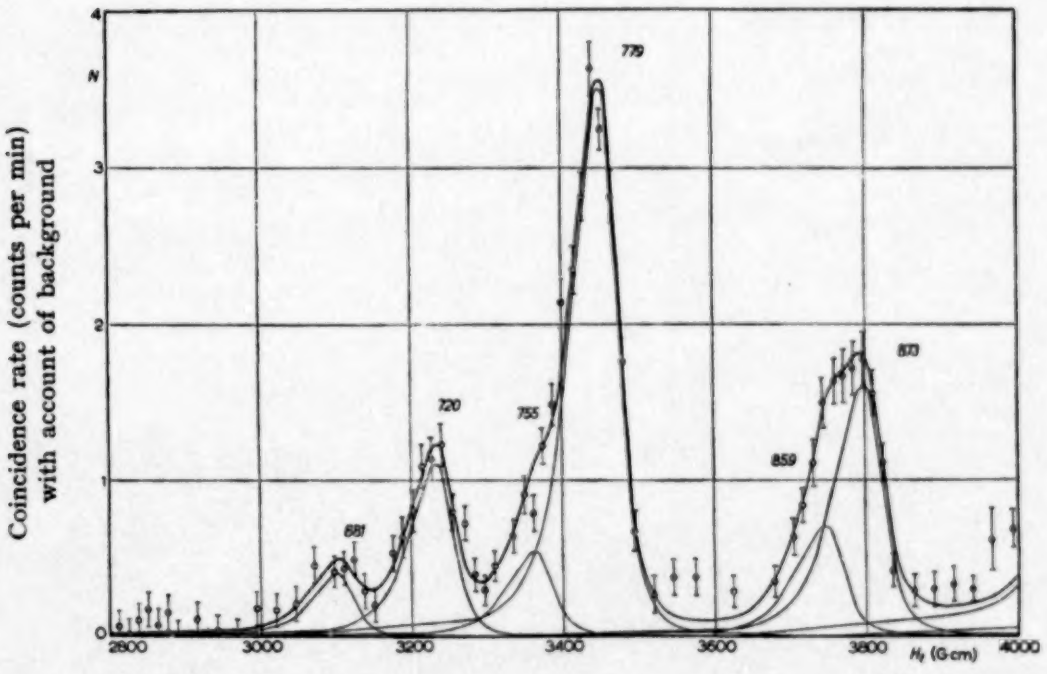


Fig. 12. Decomposition of interval $H\varrho = 2800-4000$ G · cm of $Eu^{152, 154}$ gamma ray spectrum into separate components.

The spectrum between $H\varrho = 3600$ and $H\varrho = 3900$ G · cm cannot be decomposed in a unique manner and the large discrepancy between the shape and half-width of the experimental curve and those of the expected instrumental line in this region confirm the existence of at least two gamma lines

$h\nu = 869$ and 874 keV observed by Bobykin and Novik [7]). In the paper of these authors there is also a definite indication that the gamma line which

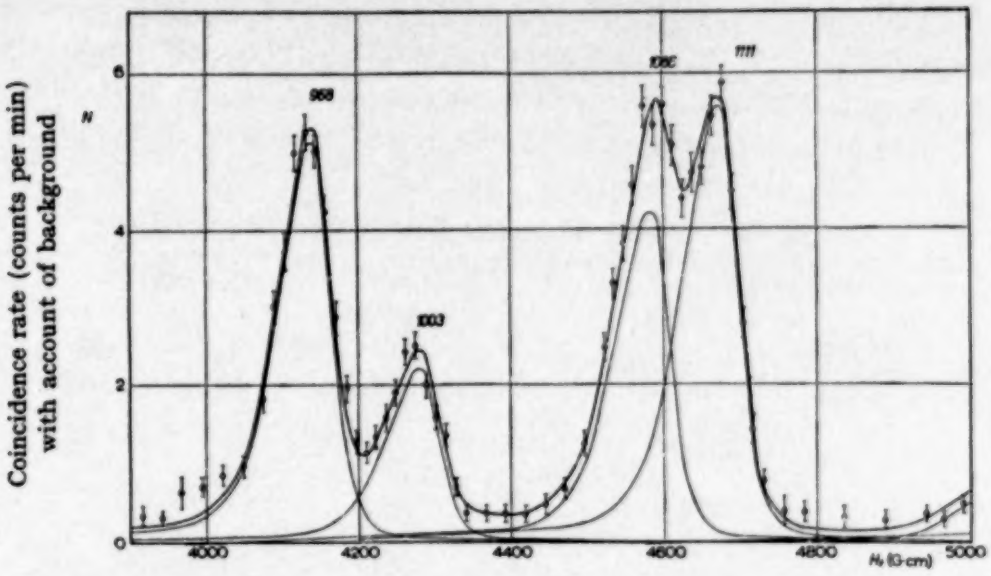


Fig. 13. Decomposition of interval $H\varrho = 3000-5000$ G · cm of $Eu^{152, 154}$ gamma ray spectrum into separate components.

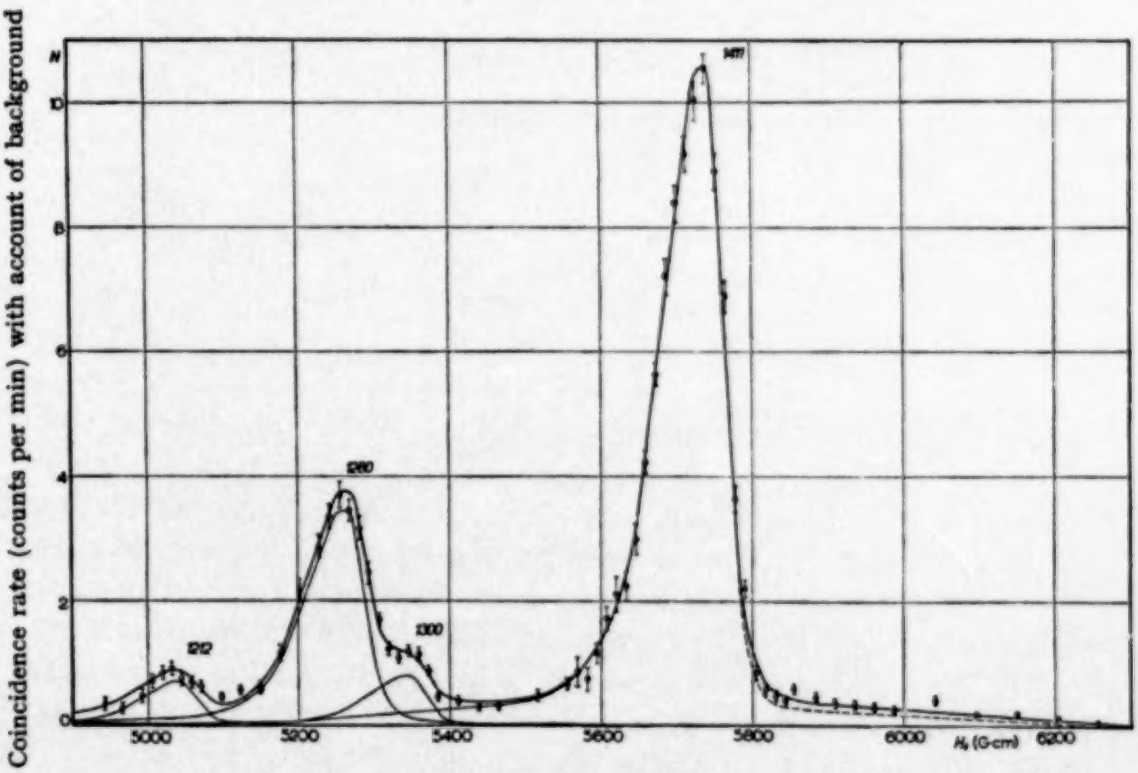


Fig. 14. Decomposition of interval $H\varrho = 4900-6300$ G · cm of $Eu^{152, 154}$ gamma ray spectrum into separate components.

we assigned the value $h\nu = 1003$ keV is a doublet consisting of the lines $h\nu = 997$ and 1003 keV. It should be noted that the right hand descending part of the line $h\nu = 1411$ keV passes above the line inscribed in the instrumental (dotted) line (fig. 14). Weak gamma lines apparently exist in this region ($h\nu \approx 1420-1500$ keV) but for their identification a more detailed investigation of this part of the spectrum would be required.

Our results and also those of other authors are presented in table 3.

TABLE 3

Relative intensities of gamma lines of $Eu^{152, 154}$

| No. | Dželepow *et al.* [8]) | | Grodzins and Kendall [9]) | | Nathan and Waggoner [10]) | | Data of present work | |
|---|---|---|---|---|---|---|---|---|
| | $h\nu$ (keV) | Rel. intens. | $h\nu$ (keV) | Rel. intens. | $h\nu$ (keV) | Rel. intens. | $h\nu$ (keV) | Rel. intens. |
| 1 | – | – | – | – | 41 | 367 | – | – |
| 2 | – | – | 122 | 236 | 122+123 | 167 | – | – |
| 3 | – | – | 244 | 36 | 244 | 44 | – | – |
| 4 | 341 | 86 | 344 | 108 | 344 | 111 | 344 | 118±7 |
| 5 | – | – | 408 | 10 | – | – | – | – |
| 6 | 427 | 14 | 442 | 20 | 420 | 4 | 436 | 23±6 |
| 7 | 593 | 7 | 550 | 2.0 | – | – | 583 | 8±6 |
| 8 | – | – | 690 | 1.2 | – | – | 681 | 8±2 |
| 9 | 717 | 14 | 720 | 4 | – | – | 720 | 21±2 |
| 10 | – | – | – | – | – | – | 755 | 10±4 |
| 11 | 779 | 43 | 778 | 36 | 775 | 44 | 779 | 61±4 |
| 12 | – | – | 866 | 24 | 860 | 14 | 859 | 11±2 |
| 13 | 871 | 25 | – | – | – | – | 873 | 24±2 |
| 14 | 958 | 73 | 963 | 56 | 965 | 67 | 968 | 61±4 |
| 15 | – | – | – | – | – | – | 1003 | 29±2 |
| 16 | | | 1085 | 52 | 1090 | 56 | 1086 | 50±7 |
| 17 | 1106 | 101 | 1100 | 6 | – | – | 1111 | 63±7 |
| 18 | | | 1110 | 48 | – | – | | |
| 19 | – | – | 1210 | 8 | 1200 | 22 | 1212 | 7±2 |
| 20 | 1281 | 41 | 1240 | 8 | 1280 | 13 | 1280 | 35±5 |
| 21 | | | – | – | – | – | 1300 | 8±3 |
| 22 | 1409 | 100 | 1410 | 100 | 1415 | 100 | 1411 | 100 |

Scintillation spectrometers were employed in ref. [9, 10]). As the authors of these investigations themselves note, the accuracy of estimation of the relative gamma line intensities in these studies was ≈ 30 %. The errors of our determinations of the relative intensity of completely resolved lines do not exceed 5—7 %. The accuracy of the determinations of the relative intensities of weak and unresolved gamma lines is smaller due to the statistical errors of the measurements and also to uncertainties arising in decomposition of the lines. Thus the total relative intensities of the gamma line pairs $h\nu = 755$ and 779, 859 and 873, 968 and 1003 and 1086 and 1111 keV are known with higher accuracy than the relative intensity of any of the lines separately.

Within the accuracy of the measurements our data on the relative gamma line intensities agree with the results obtained in ref. [10]) in which a $Eu^{152, 154}$ mixture was also employed. In ref. [9]) a source enriched with $Eu^{152}$ was used and hence gamma lines $h\nu = 583$, 681, 720, 755, 873, 1003 and 1280 keV which apparently are related (completely or partially) to the decay of $Eu^{154}$ were more intense in our work. The relative intensities of the remaining gamma lines satisfactorily agree with the results presented in ref. [9]).

TABLE 4

Multipolarities of gamma transitions of $Sm^{152}$ and $Gd^{152}$.

| No. | Accepted values $h\nu$ (keV) | Rel. intens. of $\gamma$-lines according to present data | Gamma transition assignment[7, 9-12]) | Relative intensity of K-conversion[10, 13]) line | $\alpha_K \times 10^3$ | Theoretical value of $\alpha_K \times 10^3$ [4]) | | | | | Assumed multipolarity |
|---|---|---|---|---|---|---|---|---|---|---|---|
| | | | | | | E1 | E2 | E3 | M1 | M2 | |
| 1 | 344 | 100 | $Gd^{152}$ | 100 | 30.9 | — | 30.9 | — | — | — | E2 |
| 2 | 444 | 20 | $Sm^{152}$ | 2.6 | 4.0 | 4.90 | 14.5 | 38.9 | 25.1 | 81.3 | E1 |
| 3 | 586 | 7 | $Gd^{154}$ | 1.3 | 5.8 | 2.76 | 7.50 | 18.2 | 14.2 | 42.6 | (E2) |
| 4 | 689 | 7 | $Sm^{152}$ | 5.7 | 25.1 | 1.86 | 4.68 | 10.9 | 7.95 | 22.9 | M2 |
| 5 | 720 | 18 | $Gd^{154}$ | 1.4 | 2.4 | 1.74 | 4.57 | 10.7 | 8.50 | 22.9 | (E1) |
| 6 | 757 | 8 | $Gd^{154}$ | 0.82 | 3.2 | 1.51 | 3.71 | 8.51 | 6.46 | 17.0 | E2 |
| 7 | 779 | 52 | $Gd^{152}$ | 1.5 | 8.9 | 1.51 | 3.89 | 8.70 | 7.07 | 18.2 | E3 |
| 8 | 864 | 9.2 | $Sm^{152}$ | 1.4 | 4.7 | 1.15 | 2.82 | 6.04 | 4.67 | 12.0 | (M1) |
| 9 | 874 | 21 | $Gd^{154}$ | 1.4 | 2.1 | 1.23 | 3.02 | 6.45 | 5.25 | 13.2 | — |
| 10 | 964 | 51 | $Sm^{152}$ | 3.7 | 2.2 | 0.93 | 2.24 | 4.68 | 3.72 | 9.34 | E2 |
| 11 | 997 | 24.1 | $Gd^{154}$ | 0.98 | 3.5 | 0.98 | 2.40 | 4.68 | 3.80 | 9.34 | M1 |
| 12 | 1005 | | $Gd^{154}$ | 1.7 | 3.4 | 0.96 | 2.34 | 4.68 | 3.80 | 9.34 | M1 |
| 13 | 1086 | 42 | $Sm^{152}$ | 2.8 | 2.1 | 0.76 | 1.78 | 3.72 | 2.88 | 7.09 | M1 |
| 14 | 1113 | 53 | $Sm^{152}$ | 2.5 | 1.5 | 0.73 | 1.70 | 3.55 | 2.70 | 6.60 | E2 |
| 15 | 1205 | 6 | $Sm^{152}$ | >0.3 | 1.5 | 0.63 | 1.48 | 2.95 | 2.24 | 5.37 | (E2) |
| 16 | 1273 | 29 | $Gd^{154}$ | 0.69 | 0.71 | 0.63 | 1.48 | 2.76 | 2.22 | 5.25 | E1 |
| 17 | 1411 | 84.5 | $Sm^{152}$ | 1.3 | 0.48 | 0.49 | 1.07 | 2.14 | 1.55 | 3.63 | E1 |

In table 4 are given $Z$ and $A$ assignments of the gamma transitions; they are based on the data contained in refs. [7, 9–12]) and also on the multipolarities of gamma transition for which the relative K-conversion lines intensities are known from ref. [10, 13]).

Our data on the relative gamma line intensities confirm on the whole the decay scheme of long lived $Eu^{152}$ proposed by Grodzins and Kendall [9]) and Nathan and Waggoner [10]). However it should be noted that the 1121 keV excitation level was assigned to $Sm^{152}$ in ref. [10]) without sufficient justification. Indeed the gamma line $h\nu = 1003$ keV consists of the two lines $h\nu =$ 997 and 1005 keV which refer to $Z = 64$ [7]). Moreover Grodzins and Kendall[9]) who used a $Eu^{152}$ enriched source did not detect gamma lines of appreciable intensity in this energy region. Thus it can be definitely asserted that these gamma lines accompany the beta decay of $Eu^{154}$.

The authors are grateful to V. G. Nedovesov, G. E. Shchukin and Yu. G. Kondakov for help in the measurements and treatment of the experimental results.

## References

1) B. S. Dželepow, N. N. Zhukovsky, V. G. Nedovesov and G. Shchukin, Izv. Akad. Nauk SSSR, ser. fiz. **21** (1957) 966
2) B. Dželepow, N. Zhukovsky, I. Uchevatkin, V. Nedovesov and V. Chumin, Nuclear Physics **2** (1956) 408
3) N. Antonieva, A. Bashilov and B. Dželepow, Doklady AN SSSR **77** (1951) 41
4) L. Sliv and I. Band, Tables of Internal Conversion Coefficients of Gamma Rays (Izd. Akad. Nauk 1956)
5) G. Schraf-Goldhaber and J. Weneser, Phys. Rev. **98** (1955) 212
6) A. Zolotavin, E. Grigoriev and M. Abroyan, Izv. Akad. Nauk SSSR, ser. fiz. **20** (1956) 289
7) B. Bobykin and K. Novik, Doklady AN SSSR **115** (1957) 202
8) B. Dželepow, N. Zhukovsky and B. Nedovesov, Izv. Akad. Nauk SSSR, ser. fiz. **19** (1955) 296
9) L. Grodzins and H. Kendall, Nucl. Sci. Abstr. **10** (1956) no. 12B 253
10) O. Nathan and M. Waggoner, Nuclear Physics **2** (1956/57) 548
11) J. Cork, M. Brice, R. Nelmer and D. Sarason, BAPS **2** (1957) 16 E3
12) F. Stephens, Jr., Thesis (1955) UCRL 2970; Nuclear Physics **2** (1956/57) 548
13) B. Bobykin and K. Novik, Izv. Akad. Nauk SSSR, ser. fiz. **21** (1957) 1556

*Nuclear Physics* **6** (1958) 669—671; © *North-Holland Publishing Co., Amsterdam*
Not to be reproduced by photoprint or microfilm without written permission from the publisher

# ON NON-UNIQUENESS OF NUCLEON-NUCLEON SCATTERING PHASE SHIFTS

L. G. ZASTAVENKO, R. M. RYNDIN and CHOU KUANG-CHAO
*Joint Institute of Nuclear Research, Laboratory of Theoretical Physics, Dubna, USSR*

Received 23 December 1957

The cross section for scattering of mesons by nucleons does not change upon application of the phase shift substitution proposed by Minami [1]). The two phase shift sets which are obtained from each other by means of this substitution can be differentiated either by carrying out polarization experiments [2, 3]) or by studying the energy dependence of the cross section at small energies. Below we derive similar transformations for nucleon-nucleon scattering.

Elastic nucleon-nucleon scattering can be completely described by the matrix $M(\mathbf{k}, \mathbf{k}_0; \boldsymbol{\sigma}_1, \boldsymbol{\sigma}_2)$ which defines the amplitude $\psi_f$ of the scattered wave in terms of the initial spin state $\psi_1$:

$$\psi_f = M(\mathbf{k}, \mathbf{k}_0; \boldsymbol{\sigma}_1, \boldsymbol{\sigma}_2)\psi_1. \tag{1}$$

Here $\boldsymbol{\sigma}_1$ and $\boldsymbol{\sigma}_2$ are Pauli matrices of the two nucleons and $\mathbf{k}_0$ and $\mathbf{k}$ denote unit vectors directed along the direction of motion of the incident and scattered nucleons.

In order to derive the transformations under consideration we note that the scattering cross section for unpolarized nucleons $\sigma_0 = \frac{1}{4}\,\mathrm{tr}\, MM^+$ is invariant with respect to replacement of $M(\mathbf{k}, \mathbf{k}_0; \boldsymbol{\sigma}_1, \boldsymbol{\sigma}_2)$ by any of the following matrices:

$$\begin{aligned} M_1 &= \boldsymbol{\sigma}_1 \cdot \mathbf{k} M \boldsymbol{\sigma}_1 \cdot \mathbf{k}_0, \\ M_2 &= \boldsymbol{\sigma}_2 \cdot \mathbf{k} M \boldsymbol{\sigma}_2 \cdot \mathbf{k}_0, \\ M_3 &= \boldsymbol{\sigma}_1 \cdot \mathbf{k} \boldsymbol{\sigma}_2 \cdot \mathbf{k} M \boldsymbol{\sigma}_1 \cdot \mathbf{k}_0 \boldsymbol{\sigma}_2 \cdot \mathbf{k}_0. \end{aligned} \tag{2}$$

Expanding $M$ in terms of the spherical functions $Y^{jm}_{ls}(\mathbf{k})$ which describe states with definite values of total angular momentum $j$, its projection $m$, orbital angular momentum $l$ and spin $s$, we get

$$M(\mathbf{k}, \mathbf{k}_0; \boldsymbol{\sigma}_1, \boldsymbol{\sigma}_2) = \sum_{j,m} \frac{2\pi}{ik} \sum_{l,s;\, l',s'} Y^{jm}_{ls}(\mathbf{k}) Y^{jm+}_{l's'}(\mathbf{k}_0) R^j_{ls;\, l's'}. \tag{3}$$

The values of $s$ and $l$ are determined by the summation rule for angular momenta as follows:

$$\text{for } s = 0 \text{ (singlet)}, \; l = j,$$

$$\text{for } s = 1 \text{ (triplet)}, \; l = j, \; j \pm 1.$$

For a given value of $j$ the $R^j_{ls;\,l's'}$, on account of the reversibility of motion, form a symmetrical four-row matrix $R^j$ which satisfies the condition

$$R^{j+} R^j = -R^j - R^{j+}; \tag{4}$$

this condition follows from the unitarity of the $S$-matrix.

Consider, for example, the first transformation (2). Since the operator $\boldsymbol{\sigma}_1 \cdot \mathbf{k}$ commutes with the total angular momentum operator we have

$$\boldsymbol{\sigma}_1 \cdot \mathbf{k} Y^{jm}_{ls}(\mathbf{k}) = \sum_{l_1 s_1} L^{(1)j}_{l_1 s_1,\, ls} Y^{jm}_{l_1 s_1}(\mathbf{k}), \tag{5}$$

where $L^{(1)j}$ is a unitary matrix. Thus

$$M_1(\mathbf{k}, \mathbf{k}_0; \boldsymbol{\sigma}_1, \boldsymbol{\sigma}_2) = \sum_{j,m} \frac{2\pi}{ik} \sum_{l,s;\, l',s'} Y^{jm}_{ls}(\mathbf{k}) Y^{jm+}_{l's'}(\mathbf{k}_0) R^{(1)j}_{ls;\, l's'} \tag{6}$$

where

$$R^{(1)j} = L^{(1)j} R^j L^{(1)j+}; \tag{7}$$

$R^{(1)j}$ therefore satisfies condition (4) and possesses the same symmetry properties as $R^j$. The elements of $R^{(1)j}$ can thus be considered as elements of a new scattering matrix which yields the same cross section as $M$. The same also applies to the matrices $R^{(2)j} = L^{(2)j} R^j L^{(2)j+}$ and $R^{(3)j} = L^{(3)j} R^j L^{(3)j+}$ corresponding to the second and third transformations in (2).

The matrices $L^{(i)j}$ have the form

$$L^{(1,2)j} = \frac{i}{\sqrt{2j+1}} \begin{pmatrix} 0 & 0 & \mp\sqrt{j+1} & \mp\sqrt{j} \\ 0 & 0 & \sqrt{j} & -\sqrt{j+1} \\ \pm\sqrt{j+1} & -\sqrt{j} & 0 & 0 \\ \pm\sqrt{j} & \sqrt{j+1} & 0 & 0 \end{pmatrix},$$

$$L^{(3)j} = \begin{pmatrix} -1 & 0 & 0 & 0 \\ 0 & 1 & 0 & 0 \\ 0 & 0 & -\dfrac{1}{2j+1} & -\dfrac{2\sqrt{j(j+1)}}{2j+1} \\ 0 & 0 & -\dfrac{2\sqrt{j(j+1)}}{2j+1} & \dfrac{1}{2j+1} \end{pmatrix}. \tag{8}$$

The first column (row) refers to a singlet and the remaining ones to a triplet with the following order of $l$ : $j$, $j+1$, $j-1$. The upper sign refers to index 1, the lower to index 2.

Since, in contrast to $\boldsymbol{\sigma}_1 \cdot \mathbf{k}\, \boldsymbol{\sigma}_2 \cdot \mathbf{k}$, the operators $\boldsymbol{\sigma}_{1,2} \cdot \mathbf{k}$ do not commute

with the operator of the square of total spin, $\frac{1}{4}(\sigma_1+\sigma_2)^2$, the matrices $M_1$ and $M_2$ lead to singlet-triplet transitions. The first two transformations therefore cannot be valid for collisions between identical nucleons for which singlet-triplet transitions are forbidden by the Pauli principle. This is also true for n—p scattering, providing that the hypothesis of isobaric invariance is correct.

The operators $\sigma_i \cdot \mathbf{q}$ are operators of rotation of the $i$th nucleon spin through an angle $\pi$ about the direction $\mathbf{q}$. This permits one to determine the transformation properties of various spin characteristics on replacement of $R^j$ by $R^{(3)j}$. A result of this substitution, for example, is a change in the sign of the polarization $P_0$ arising in collisions involving unpolarized nucleons.

In conclusion, it should be noted that the quantities measured in a complete set of experiments, sufficient for the construction of the nucleon-nucleon scattering matrix [4]), do not change if along with replacement of $R^j$ by $R^{(3)j}$ the signs of all phase shifts are reversed (complex conjugation of $R^j$). The non-uniqueness of the phase shifts which arises in this case can be removed by investigating the energy dependence of the cross section at low energies or by replacing one of the experiments of the complete set (e.g. $K_{nn}$) by a triple scattering experiment in mutually perpendicular planes.

## References

1) S. Minami, Progr. Theor. Phys. **11** (1954) 213
2) S. Hayakawa, M. Kawaguchi and S. Minami, Progr. Theor. Phys. **12** (1954) 355
3) R. Ryndin and Ya. Smorodinsky, Doklady AN SSSR **103** (1955) 69
4) L. Puzikov, R. Ryndin and Ya. Smorodinsky, Nuclear Physics **3** (1957) 436

*Nuclear Physics* **6** (1958) 672—685; © *North-Holland Publishing Co., Amsterdam*

Not to be reproduced by photoprint or microfilm without written permission from the publisher

# INVESTIGATION OF THE LIFE-TIMES OF LOWER NUCLEAR LEVELS EXCITED IN ELECTRON CAPTURE

E. Ye. BERLOVICH, K. GROTOVSKI†, M. BONITZ††, V. I. BRESLAV††† and
B K. PREOBRAZHENSKY††††

*Physico-Technical Institute of the USSR Academy of Sciences, Leningrad*

Received 9 September 1957

**Abstract:** On the basis of Xe and X$\gamma$ coincidence studies the following half-life values have been found for levels excited in electron capture:

264 keV level in $Er^{167}$: $T_{\frac{1}{2}} = (2.0 \pm 0.5) \times 10^{-9}$ sec,

121 keV level in $Sm^{147}$: $T_{\frac{1}{2}} \leq 2 \times 10^{-10}$ sec,

186 keV level in $Os^{190}$: $T_{\frac{1}{2}} = (5 \pm 2) \times 10^{-10}$ sec,

level of gadolinium (half-life 60 days): $T_{\frac{1}{2}} = (3.5 \pm 1.1) \times 10^{-10}$ sec.

Compared with predictions of the one-particle model, the investigated E2 transition in $Os^{190}$ and the partial E2 transition in $Er^{167}$ are accelerated respectively 50 and 300 times and the partial M1 transition is retarded 160 times. The intrinsic quadrupole moment of $Os^{190}$ is $Q_0 = (4.2 \pm 0.9) \times 10^{-24}$ cm$^2$.

## 1. Introduction

Experimental measurement of the life-time of excited nuclear states directly yields the transition probability between two levels and is an important method for the investigation of the structure of the nucleus [1, 2]).

The present work is devoted to a study of the life-time of the levels in some nuclei produced in the capture of orbital electrons.

All of the initial nuclei were neutron-deficient and were produced in deep disintegration reactions resulting from high energy proton bombardment.

The parent nuclei $Tu^{167}$, $Eu^{147}$ and $Gd^{145}$ were obtained by irradiating tantalum targets with 660 MeV protons from the synchrocyclotron of the Joint Institute of Nuclear Research. The thulium, europium and gadolinium sources were prepared chromatographically. The parent $Ir^{190}$ nuclei were prepared by irradiating a bismuth target and extracting with an iridium carrier.

## 2. Experimental Method

The life-time measurements were conducted by the delay coincidence method. The arrangement used for this purpose has been previously described

† On leave from the Institute of Nuclear Research, Polish Academy of Sciences, Cracow.

†† On leave from the Institute of Experimental Nuclear Research, Dresden, German Democratic Republic.

††† On leave from the Institute of Physics, Riga, Latvian S.S.R.

†††† On leave from the Khlopin Radium Institute of the USSR Academy of Sciences, Leningrad.

by one of the authors [2, 3, 4]). It consists of a "fast" coincidence circuit with a variable delay line of the spiral type and a "slow" triple coincidence circuit, and differs from that of Bell, Graham and Petch [5]) by the presence of differential pulse height analyzers in the lateral channels of the triple coincidence circuit. With the aid of these analyzers it is possible to select the coincidences in accord with the energy of the coinciding radiations.

It has been shown in ref. [2]) that differences in the fronts of pulses caused by the coinciding radiations may affect the shape and position of the coincidence curve, a result of this being distortion of the experimental values, especially for low life-times.

It was shown that in order to remove this effect it would be desirable to carry out the coincidence measurements in equivalent energy intervals for each of the coinciding radiations. If this requirement cannot be met one should measure the coincidence curves for the investigated transition and for the short lived transition (used as a reference) in the same intervals.

Coincidences between characteristic X-rays and $\gamma$-rays ($X\gamma$ and $\gamma X$ coincidences) or X-rays and internal conversion electrons (Xe and eX coincidences) were measured in the present work. It was not always possible to make the measurements in energy-equivalent intervals because of the great differences between the energies of the coinciding radiations.

In the $\beta\gamma$ (or e$\gamma$ or e$\beta$) coincidence measurements the "self comparison" method was applied [2]); this method essentially consists in comparison of coincidence curves obtained at two different positions of the $\beta$-ray (or conversion electron) filter; in coincidence measurements of electromagnetic radiations ($X\gamma$) the "self comparison" method was replaced by a different one which will be described below.

Another difficulty was due to the large amount of various coincidences which exist along with the investigated ones (e.g., coincidences between conversion electrons and the X-rays accompanying them, coincidences between X-rays from K-capture and, on the one hand, X-rays accompanying conversion or Auger electrons, on the other, etc.).

Type $1B$ photomultipliers were used in the measurements. It has 10 dynodes (made of an aluminium-magnesium alloy) arranged in a circle; the flat semi-transparent antimony-cesium photocathode was of the end window type. The rise time of these multipliers is $1-2\times10^{-9}$ sec [6]). The voltage applied to the photomultiplier tube was 2600—2700 V. With stilbene crystals the resolving time of the coincidence circuit was $2-3\times10^{-9}$ sec.

## 3. Measurements

### 3.1. $Tu^{167} \rightarrow Er^{167}$ TRANSITION

The source was prepared by drying on an aluminium foil a drop containing the thulium fraction from the chromatographic column.

The measurements were carried out one month after irradiation. This was sufficient for suppression of the 8-hour ($Tu^{166}$) and approximately 24-hour ($Tu^{165}$) activities, the remaining activity being practically due to the 9.6-day $Tu^{167}$ activity. The 100-day $Tu^{168}$ radioactivity was insignificant. A decay scheme for $Tu^{167}$ proposed in ref. [7]) and confirmed in ref. [8]) is represented in fig. 1. The 207 keV level is an isomer level. De-excitation of the upper level takes place via a 56.7 keV transition to the 207 keV level.

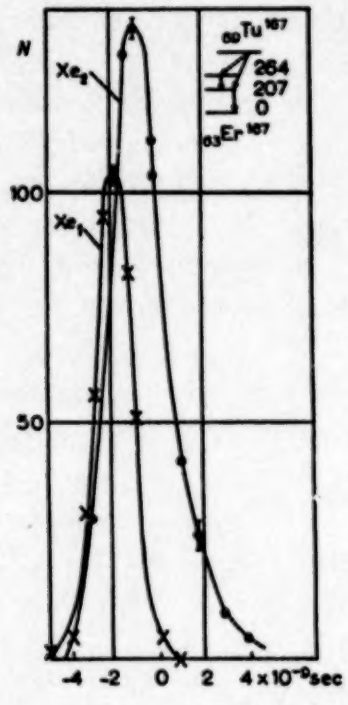


Fig. 1. $Tu^{167}$ coincidence curves: $Xe_2$ for 56.7 keV transition, $Xe_1$ for 207 keV transition. In this and the following figures the coincidence counting rate is plotted against the delay time in seconds.

Coincidences between the X-rays and conversion electrons (47 keV) from the L shell of $Er^{167}$ were measured for the 56.7 keV transition. A stilbene single crystal (diameter = 35 mm, height = 20 mm) covered by glass and a MgO reflector was employed to record the X-rays. The glass completely absorbed the conversion electrons and Auger electrons. Conversion electrons were recorded by a stilbene plate 5 mm thick covered by a 1$\mu$ aluminium foil reflector. Optical contact of the crystals with the photocathode surfaces was attained by using vaseline.

Differential pulse height analyzers were used to select the required energy intervals in each channel of the coincidence circuit.

Due to the high gain in the multipliers at the voltage employed the pulses from electrons produced in the stilbene crystal by X-rays were sufficiently large for cutting-off the limiting pentode.

The coincidence curve shown in fig. 1 was obtained by choosing in the electron amplitude spectrum an interval corresponding to conversion electrons from the 56.7 keV transition ($Xe_2$ curve); the right hand branch of this curve is of a pronounced exponential type. The exponential part of this curve was investigated with good statistical accuracy and is represented in a semilogarithmic scale in fig. 2. The half-life derived from this curve is $T_{\frac{1}{2}} = (2.0 \pm 0.5) \times 10^{-9}$ sec.

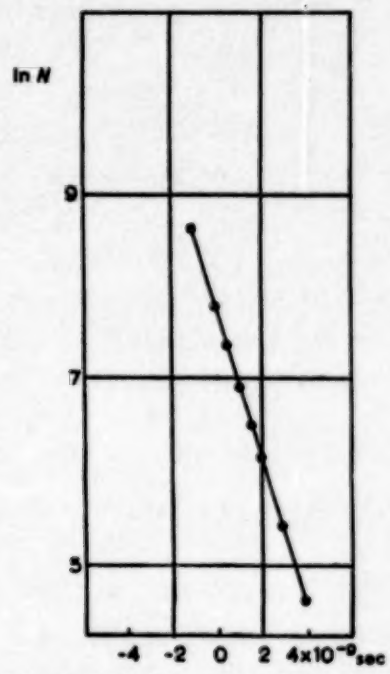


Fig. 2. $Tu^{167}$. Decreasing part of $Xe_2$ curve (fig. 1) in semilogarithmic scale.

The surplus "fast" coincidences mentioned at the end of section 2 correspond to small delay values near the peak in the curve in fig. 1.

As a check coincidences between X-rays and conversion electrons were measured for the 207 keV transition. Since the 207 keV level is an isomer level there could be no coincidences between the capture X-rays and conversion electrons from the 207 keV transition. However "fast" coincidences should exist between these electrons and X-rays accompanying the conversion process. In distinction to curve $Xe_2$ the coincidence curve for these electrons ($Xe_1$ curve) shown in fig. 1 has a symmetric shape.

Since determination of the life-time (which turned out to be relatively large) was performed not on the basis of displacement of the centre of gravity of the curve but by employing the exponential branch of the curve, the influence of the energy differences in the operating intervals of the two branches of the circuit was not significant.

### 3.2. $Gd^{145} \rightarrow Eu^{145}$ TRANSITION

Measurements with a gadolinium source possessing a 60-day half-period (ascribed by Murin and co-workers [10]) to the $Gd^{145}$ isotope) were carried

out three months after irradiation; this time was sufficient for disappearance of the $1\frac{1}{2}$-day ($Gd^{147}$) and 9-day ($Gd^{149}$) activities.

According to the measurements in ref. [10]) and those by Bashilov and co-workers [11]), two cascade $\gamma$-transitions of equal energy (115 keV) are produced in electron capture of $Gd^{145}$. The measurements are not affected by the high energy $\gamma$-ray admixture from the daughter $Eu^{145}$ nucleus. In the amplitude spectrum of the Compton distribution this admixture exhibits itself as a long low intensity tail which appears near the end of the main distribution produced by 115 keV $\gamma$-rays.

Coincidences of the X$\gamma$ and $\gamma$X type were measured with two large ($d = 35$ mm, $h = 20$ mm) packed stilbene crystals. The operating interval in the $\gamma$-ray channel of the pulse height analyzer in this case was fixed so that it corresponded to a certain part of the Compton distribution. In one set of measurements the $\gamma$-rays were recorded by the right hand counter (X$\gamma$ coincidences) and in a second set by the left counter ($\gamma$X coincidences).

The experimentally observed mutual shift of the two coincidence curves may be due to two causes: a) to differences in the pulse fronts resulting from the difference in the amplitude intervals in the two bias channels; the shift is in the direction of the X-ray detector since, as shown in ref. [2]), the instrumental shift always occurs in the direction of the detector recording the lower energy particles; b) to the appreciable life-time of the level (displacement in direction of $\gamma$-ray detector, since the delay is introduced in the channel of the radiation which precedes excitation of the level). In order to suppress the first, purely instrumental effect, along with measurements of the investigated source we also measured $\gamma-\gamma$ coincidences for the $Co^{60} \rightarrow Ni^{60}$ transition in the same operating intervals since, according to the $\gamma$-ray resonance scattering experiments of Metzger [12]), the life-time of the low lying level in the $Ni^{60}$ nucleus is very small ($\tau \approx 10^{-12}$ sec). Inasmuch as the end point in the Compton distribution for $Ni^{60}$ $\gamma$-rays exceeds by almost 30 times that of the Compton distribution for the investigated $\gamma$-rays and the height of the pulses (after amplification) entering the differential analyzers extends beyond the operating region of the analyzers, light absorption filters were placed between the phosphors and photocathode; these filters were chosen so that the length of the pulse height distribution for the $Ni^{60}$ $\gamma$-rays was close to the length of the pulse height distribution for the investigated $\gamma$-rays from $Eu^{145}$.

Results of measurements of the $Gd^{145} \rightarrow Eu^{145}$ and $Co^{60} \rightarrow Ni^{60}$ transitions are depicted in the figs. 3 and 4 respectively.

Mutual displacements of the centres of gravity were determined for each pair of curves [13]). They were found to equal $2\tau' = 2.1 \times 10^{-9}$ sec for the $Gd^{145} \rightarrow Eu^{145}$ transition and $2\tau'' = 3.1 \times 10^{-9}$ sec for the $Co^{60} \rightarrow Ni^{60}$ transition. The smaller displacement observed in the former case indicates

the existence of a measurable life-time of the $Eu^{145}$ level (the direction of the displacement due to the measurable life-time is opposite to that of the instrumental displacement). The difference between the two displacements yields a double value for the life-time $2\tau = 1.0 \times 10^{-9}$ sec.

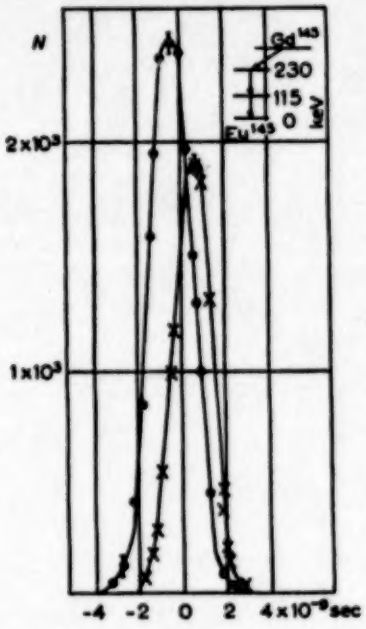


Fig. 3. $Gd^{145}$. Coincidence curves: $\cdot = X\gamma$, $\times = \gamma X$.

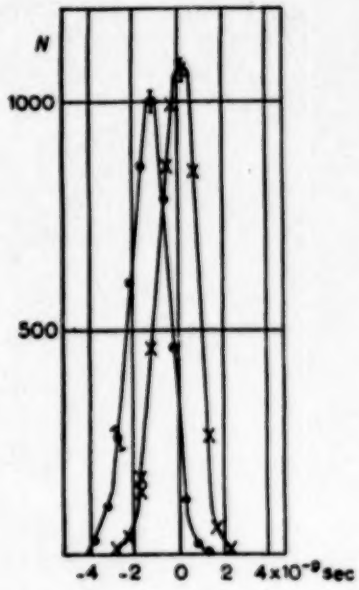


Fig. 4. $Co^{60}$ with filter. Coincidence curves.

The value of $\tau$ finally accepted by us was $\tau = (5.0 \pm 1.5) \times 10^{-10}$ sec. The correctness of this value was confirmed first of all by the fact that it could be repeatedly obtained and secondly by the fact that similar measurements performed with a europium source in the same operating intervals did not yield any displacement of the curves (see below).

An attempt was made to ascertain to which of the two $Eu^{145}$ levels the obtained life-time should be attributed. To this end a $\gamma-\gamma$ coincidence curve for this transition was measured in energy equivalent pulse height intervals located outside of the X-ray region. Descending parts of this curve were compared with those of the curve measured under identical conditions for the $Co^{60} \rightarrow Ni^{60}$ transition. No significant difference in the shapes of the descending parts of these curves were detected. However, in view of smallness of the life-time value obtained we cannot assert that this life-time is not related to the lower level.

### 3.3. $Eu^{147} \rightarrow Sm^{147}$ TRANSITION

The investigated europium fraction which was separated from the gadolinium fraction, contained only 24-day $Eu^{147}$ after decay of the 1.5-day $Gd^{147}$.

The decay scheme for $Eu^{147}$ established by Bashilov and co-workers and Murin and co-workers [10,11]) is presented in fig. 5. No transition between the 198 keV and 121 keV levels was observed.

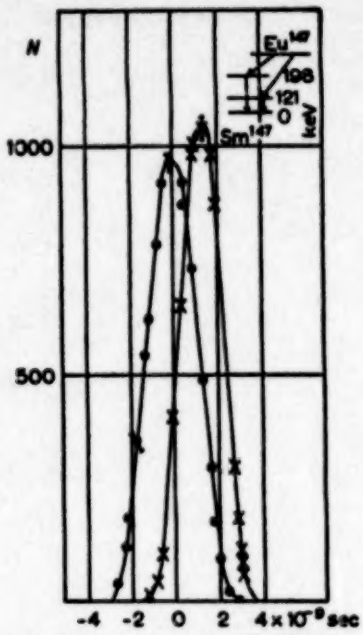


Fig. 5. $Eu^{147}$. Coincidence curves: · = Xγ, × = γX.

We measured the life-time of the lower 121 keV level; the energy of this level is very close to that of the γ-rays from the $Gd^{145} \rightarrow Eu^{145}$ transition (115 keV). Xγ and γX coincidences were measured, the operating interval in the γ-ray channel of the analyzer being chosen at a large distance from the 198 keV γ-ray Compton peak so that the effect of the upper transition on the experimental results was insignificant.

From the very start the $Eu^{147}$ and $Gd^{145}$ experiments were suitably matched: a) they were carried out in the same amplitude intervals and all the other conditions were identical; b) measurements with the $Co^{60}$ sources were always performed between the two isotope measurements. Thus in the life-time calculations for the europium source the same cobalt measurements were used as those that were employed in the case of a gadolinium source.

In contrast to the results obtained with the gadolinium source the displacement of the centres of gravity of the curves (Xγ and γX coincidences) obtained with a europium source (fig. 5) was practically identical with that for the cobalt source. These measurements, which may also serve as a check of correctness of the results for the $Eu^{145}$ levels, yield a value $\tau \leqq 2 \times 10^{-10}$ sec for the upper limit of the life-time of the 121 keV $Sm^{147}$ level.

### 3.4. $Ir^{190} \rightarrow Os^{190}$ TRANSITION

Electron capture by the $Ir^{190}$ nucleus leads to excitation of levels in the rotational band of the deformed $Os^{190}$ nucleus[14]).

In order to determine the intrinsic quadrupole moment of the $Os^{190}$ nucleus it seemed to be interesting to attempt to measure the life-time of the first, 186 keV excited state (fig. 6).

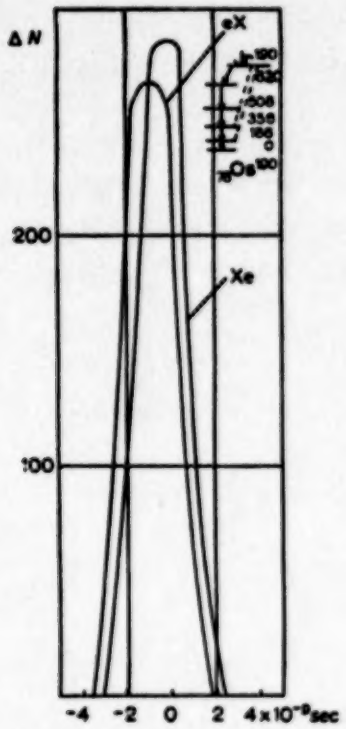


Fig. 6. $Ir^{190}$. eX and Xe coincidence curves obtained as differences of the experimental curves

$$(eX+\gamma X+X\gamma+\gamma\gamma)-(\gamma X+X\gamma+\gamma\gamma)$$

and

$$(Xe+X\gamma+\gamma X+\gamma\gamma)-(X\gamma+\gamma X+\gamma\gamma),$$

respectively. The averaged initial curves are used instead of the experimental points in plotting curves eX and Xe.

The iridium sample was deposited on filter paper which was cemented onto a 2 mm aluminium backing.

Xe and eX coincidence measurements seemed to be desirable for the following reasons. First of all the conversion coefficient of the lower transition was sufficiently large ($\approx 0.63$) and exceeded by an order of magnitude the sum of the conversion coefficients for all of the higher transitions. Furthermore, the fraction of conversion electrons from the upper transition whose pulses entered the operating interval of the analyzer (biased to measure electrons from the lower transition) was insignificant because of the large energy difference of the two aforementioned groups.

The conversion electron energy spectrum was smeared out as a result of multiple scattering in the relatively thick source and hence the measurements could be carried out in energy-equivalent intervals.

In the measurements two stilbene crystals without packing but with a re-

flector made of aluminium foil 1 micron thick were used. In addition to eX coincidences, $\gamma$X and $\gamma\gamma$ coincidences were also recorded and hence for each of the two orientations of the backed source the measurements were performed with no filter over the source or with a thin foil for absorption of conversion electrons produced in the investigated transition. Coincidences with electrons were derived from the difference of the counting rates in these two cases.

Results of measurement of Xe and eX coincidences are presented in fig. 6. From these data it can be deduced that the half value of the displacement of the centres of gravity of the curve is $(3.6\pm1.5)\times10^{-10}$ sec. However, it can be demonstrated that in order to evaluate the mean life-time this quantity should be multiplied by two.

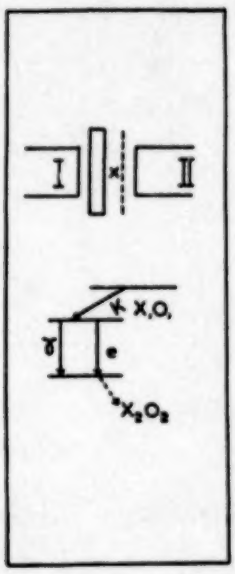


Fig. 7. $X_1$, $O_1$—X-rays and Auger electrons accompanying K-capture.
$X_2$, $O_2$—X-rays and Auger electrons accompanying internal conversion.

Consider the case when the thick backing of the source is directed to the left (fig. 7). Let $X_1$ and $O_1$ denote respectively X-rays and Auger electrons accompanying K-capture and $X_2$ and $O_2$ denote X-rays and Auger electrons accompanying internal conversion (fig. 7). Then under our conditions (after subtraction of the coincidence counting rate obtained with a thin foil at the right) the following types of coincidences will be measured:

$$\underrightarrow{X_1\,e};\quad \underrightarrow{X_1\,O_2};\quad \underleftrightarrow{X_2\,e};\quad \underleftarrow{X_2\,O_1}$$

the arrows below indicating the direction of displacement of a given type of coincidence curve; a double arrow signifies that there is no displacement.

Denoting the solid angles for the left and right counters by $\omega_1$ and $\omega_2$ respectively, the counting efficiency for X-rays by $\varepsilon$, the fraction of transitions occurring via conversion by $k=\alpha/(\alpha+1)$, where $\alpha$ is the conversion

coefficient, the luminescence yield by $W$ and the disintegration rate of the source by $N$ and assuming all radiations to be isotropic, the counting rates for each type of coincidence can be represented as follows:

1) $C(\overrightarrow{X_1 e}) = N\omega_1\omega_2 W\,\varepsilon\,k$

2) $C(\overrightarrow{X_1\ O_2}) = N\omega_1\,(1-\omega_2)\omega_2 W(1-W)\,\varepsilon\,k$

3) $C(\overleftrightarrow{X_2 e}) = N\omega_1\omega_2\,W\,\varepsilon\,k$

4) $C(\overleftarrow{X_2\ O_1}) = N\omega_1(1-\omega_2)\omega_2 W(1-W)\,\varepsilon\,k.$

The counting rates for coincidences of the second and fourth types are not large since for $Z = 76$, $1-W = 0.05$[15]); moreover, they are equal and lead to opposite shifts of the centres of gravity of the coincidence curves and hence do not affect their position. Coincidences of the third type are "fast"

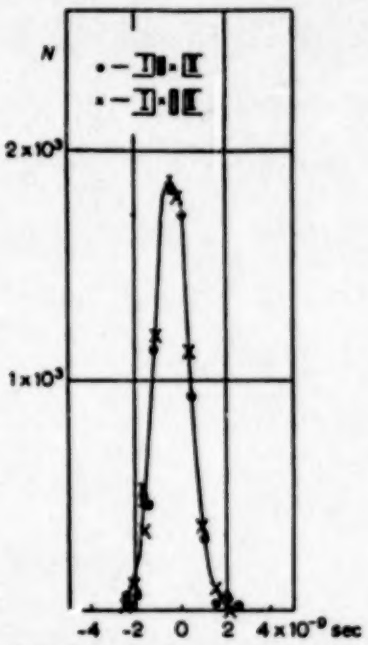


Fig. 8. $Co^{60}$ with a light filter. Coincidence curves. I and II are photomultipliers, x is the source, ▨ the thick backing.

and hence the centres of gravity of their coincidence curves are not displaced. They tend to decrease the displacement of the resultant coincidence curve. Since the counting rate for these coincidences is identical with that for the $X_1 e$ coincidences which are of interest for us, we find that the shift of the centre of gravity of the coincidence curve will be twice too small. Thus, the following values should be accepted as the experimental life-time for the first excited level of the $Os^{190}$ nucleus:

$$\tau = (7.2 \pm 3.0) \times 10^{-10} \text{ sec},$$

or

$$T_{\frac{1}{2}} = (5.0 \pm 2.1) \times 10^{-10} \text{ sec}.$$

Results of a control experiment with a $Co^{60}$ source performed in the same

equivalent operating intervals as in the $Ir^{190}$ case but with a light filter interposed are presented in fig. 8. It can be seen that the points referring to $\beta\gamma$ and $\gamma\beta$ coincidences satisfactorily lie on a single curve.

## 4. Discussion of Results

Diverse information regarding the structure of the nucleus can be derived from the experimental life-times of the levels in those cases when the transition multipolarities are known.

According to the data cited in ref. [7]), the 56.7 keV transition in the $Er^{167}$ nucleus is a mixed one and consists of 25 % E2 and 75 % M1. If the interpolation tables of G. F. Dranitsyna for L shell conversion coefficients based on Rose's work [17]) are used, we find that for our transition $\alpha_L = 5.05$ or $\alpha_{tot} = 6$. For the radiative half-life period we then get

$$T_\gamma = T_{exp}(1+\alpha) = 7\times 2.0\times 10^{-9}\ \text{sec} = 1.4\times 10^{-8}\ \text{sec}.$$

For the partial radiative half-lives we get

$$T_\gamma(\text{E2}) = 5.6\times 10^{-8}\ \text{sec and } T_\gamma(\text{M1}) = 1.87\times 10^{-8}\ \text{sec}.$$

Weisskopf's formulae [18]) based on the single particle model yield

$$T_{\gamma,W}(\text{E2}) = 1.73\times 10^{-5}\ \text{sec and } T_{\gamma,W}(\text{M1}) = 1.2\times 10^{-10}\ \text{sec}.$$

Thus the electrical quadrupole transition rate is greatly accelerated. The acceleration factor is

$$F = \frac{T_{\gamma,W}(\text{E2})}{T_\gamma(\text{E2})} = \frac{1.73\times 10^{-5}}{5.6\times 10^{-8}} = 310.$$

This circumstance is quite natural for the $Er^{167}$ nucleus which contains 17 neutrons in excess of the closed shell and is a highly deformed nucleus.

The magnetic dipole transition rate, in contrast, is appreciably retarded. The slowing-down factor is

$$F = \frac{T_{\gamma,W}(\text{M1})}{T_\gamma(\text{M1})} = \frac{1.2\times 10^{-10}}{1.87\times 10^{-8}} = 6.7\times 10^{-3} \approx \frac{1}{160}.$$

This transition evidently is of the slow magnetic dipole type [19]). This decrease of the transition rate is apparently connected with the collective nature of the magnetic transition.

In ref. [7]) a spin of $\frac{1}{2}$ is assigned to the 207 keV excited state and one of the values $\frac{1}{2}+$, $\frac{3}{2}+$, $\frac{3}{2}-$ to the 267 keV state. However in ref. [8]) the value $\frac{3}{2}-$ is considered to be the most probable one.

The assumption that in the highly deformed $Er^{167}$ nucleus (17 neutrons beyond the filled shell) the rotational band begins at the first excited

state and that the projection of the angular momentum on the nuclear symmetry axis is $\Omega = \frac{1}{2}$, yields the value $Q_0 = 17 \times 10^{-24}$ cm$^2$ for the intrinsic quadrupole moment. This value is considerably higher than that of the quadrupole moment in the mass number region under consideration ($Q_0 \approx 8.0 \times 10^{-24}$ cm$^2$) [20]).

A possible explanation of this discrepancy is that the values 25 % E2 and 75 % M1 given in ref. [7]) for the mixed transition are not correct, the real fraction of E2 transitions being much smaller.

Interpretation of the $Gd^{145} \rightarrow Eu^{145}$ transition is impossible not only because nothing is known about the multipolarity of this transition but also because there is uncertainty regarding identification of the investigated (115 keV) $\gamma$-rays. According to the data of A. A. Bashilov two 5-day europium activities exist; one of these is apparently due to $Eu^{145}$ whereas the other should also probably be ascribed to another europium isotope.

The upper limit for the life-time of the first excited state of $Sm^{147}$ obtained on the assumption that the transition is a mixed one (E2+M1) yields for the radiative life-time with account of conversion, an upper limiting value which is somewhat larger, $\tau_\gamma \leqq 5 \times 10^{-10}$ sec.

Calculations based on the Weisskopf formulae yield

$$T_{\gamma, W}(\mathrm{M1}) = 1.8 \times 10^{-11} \text{ sec and } T_{\gamma, W}(\mathrm{E2}) = 6.7 \times 10^{-7} \text{ sec.}$$

Since the $Sm^{147}$ nucleus which has only 3 neutrons beyond the filled shell is a spherical nucleus, the acceleration factor for E2 transitions should equal about 10. On the other hand the M1 transition rates, as a rule, should be smaller by two or more orders of magnitude. In this case our value for the upper limit of the life-time is evidently inconsistent with the assumption of a E2+M1 mixture.

Similar calculations carried out for E1 and M2 transitions showed that the measured life-time is consistent with the assumption of an almost pure E1 transition with $\tau_{\gamma, W}(\mathrm{E1}) \approx 2.6 \times 10^{-13}$ sec, account being taken of the fact that the transition rate may be retarded by three orders of magnitude compared to the 146 keV transition in the $Lu^{177}$ nucleus [22]). However, the assumption of a E1 transition does not agree well with the $\alpha_K/\alpha_L$ value which, according to the measurements of A. A. Bashilov, equals $\approx 3.5$[21]), whereas theoretically it should be somewhat higher.

A value $\tau_\gamma = 1.2 \times 10^{-9}$ sec is obtained from the observed value of the mean life-time of the first excited state in $_{76}Os^{190}$ by taking into account conversion in all the shells (K-shell conversion was computed from the tables in ref. [23])) and by assuming $\alpha = 0.71$. Calculations by Weisskopf's formula yield $T_{\gamma, W}(\mathrm{E2}) = 5.6 \times 10^{-8}$ sec and an acceleration factor $F \approx 47$. Using Bohr's formula [1]) for the reduced probability of even nuclei

$$B(\mathrm{E2}) = \frac{15}{32\pi} \cdot e^2 Q_0^2 \frac{(I+1)(I+2)}{(2I+3)(2I+5)}$$

we get $Q_0 = (4.2 \pm 0.9) \times 10^{-24}$ cm$^2$ and a deformation parameter

$$\frac{\Delta R}{R_0} = \frac{5Q_0}{4ZR_0^2} = 0.14$$

instead of 0.3 in the region of large deformations.

For the $_{76}Os^{186}$ and $_{76}Os^{188}$ isotopes which have 110 and 112 neutrons the intrinsic quadrupole moments are respectively $5.5 \cdot 10^{-24}$ cm$^2$ and $5.1 \times 10^{-24}$ cm$^2$ [20]). In this region the deformation of the nucleus decreases already as a result of the shell being filled; the two surplus neutrons in the $_{76}Os^{190}$ isotope should make it even smaller. Since transition from 114 neutrons ($_{76}Os^{190}$) to 116 neutrons ($_{76}Os^{192}$) involves a discontinuous decrease in the deformation, and the rotational level structure changes to a vibrational one, the decrease should be expected to be quite large and this is exactly what is observed experimentally.

The authors consider it a pleasant duty to express their thanks to B. S. Dželepow and co-workers, A. A. Bashilov and co-workers, and to A. N. Murin and his colleagues for making their experimental data on the investigated isotopes available prior to publication. We are very grateful to A. P. Dželepow and the synchrocyclotron team who made our investigations possible.

*Note added in the proof* It has been established by G. M. Gorodinsky, A. N. Murin, V. N. Pokrovsky and B. K. Preobrazhensky [25]) that the 115 keV $\gamma$-transition observed in gadolinium (50 day half-life) takes place in the $Eu^{148}$ nucleus. According to ref. [11]) the intensities of both $\gamma$-transitions are approximately equal. In this case it can readily be derived from the experimental life-time value $5 \times 10^{-10}$ sec, related to the first two excited levels in the $Eu^{148}$ nucleus, that the life-time of each of the levels is approximately $3.3 \times 10^{-10}$ sec ($T_{\frac{1}{2}} \approx 2.3 \times 10^{-10}$ sec).

## References

1) A. Bohr, Rotational States of Atomic Nuclei (Copenhagen, 1954)
2) E. Ye. Berlovich, Izv. Akad. Nauk SSSR, Ser. Fiz. **20** (1956) 1438
3) E. Ye. Berlovich, Izv. Akad. Nauk SSSR, Ser. Fiz. **19** (1955) 343
4) E. Ye. Berlovich, Prib. i Tekh. Eksp. (in press)
5) R. Bell, R. Graham and H. Petch, Can. J. Phys. **30** (1952) 35
6) E. Ye. Berlovich and B. K. Shilyayev, Prib. i Tekh. Eksp. (in press)
7) K. Ya. Gromov and B. S. Dželepow, Izv. Akad. Nauk, Ser. Fiz. (1957) (in press)
8) G. M. Gorodinsky, A. N. Murin, V. N. Pokrovsky and B. K. Preobrazhensky, Izv. Akad. Nauk SSSR, Ser. Fiz. 1957 (in press)
9) R. Bell, in Beta and Gamma Ray Spectroscopy, ed. K. Siegbahn (North Holland Publishing Company, Amsterdam, 1955) p. 132

10) G. M. Gorodinsky, A. N. Murin, V. N. Pokrovsky and B. K. Preobrazhensky, Report at VIIth All-Union Conference on Nuclear Spectroscopy, Leningrad (January 1957)
11) N. N. Antonyeva, A. A. Bashilov, B. S. Dżelepow and B. K. Preobrazhensky, Report at VIIth All-Union Conference on Nuclear Spectroscopy, Leningrad (January 1957)
12) F. R. Metzger, Phys. Rev. **103** (1956) 983
13) Z. Bay, Phys. Rev. **77** (1950) 419
14) A. H. W. Aten, G. D. de Feyfer, M. J. Sterk and A. H. Wapstra, Physica **21** (1955) 990; **21** (1955) 740
15) J. Bergström, in Beta and Gamma Ray Spectroscopy, ed. K. Siegbahn (North Holland Publishing Company, Amsterdam, 1955) p. 624
16) G. F. Dranitsyna, Internal Conversion Coefficients in $L_I-L_{II}-L_{III}$ Subshells (Izdat. Akad. Nauk SSSR, 1957)
17) M. E. Rose, in Beta and Gamma Ray Spectroscopy, ed. K. Siegbahn (North Holland Publishing Company, Amsterdam, 1955) p. 905
18) J. Blatt and V. Weisskopf, Theoretical Nuclear Physics (1952)
19) R. Graham and R. Bell, Can. J. Phys. **31** (1953) 377
20) K. Alder, A. Bohr, T. Huus, B. Mottelson and A. Winther, Revs. Mod. Phys. **28** (1956) 432
21) A. A. Bashilov, private communication
22) H. de Waard, Phil Mag. **46** (1955) 445
23) L. A. Sliv and I. M. Bard, Tables of Gamma Ray Internal Conversion Coefficients (1956) p. 1
24) L. K. Peker and L. A. Sliv, Report at VIIth All-Union Conference on Nuclear Spectroscopy, Leningrad (January, 1957)
25) G. M. Gorodinsky, A. N. Murin, V. N. Pokrovsky and B. K. Preobrazhensky, Programme and Abstracts of Reports at the VIIIth Annual Conference on Nuclear Spectroscopy in Leningrad, January 27—February 3, 1958 (Publishing House of the U.S.S.R. Academy of Sciences, Moscow—Leningrad, 1958)

*Nuclear Physics* **6** (1958) 686—690; © *North-Holland Publishing Co., Amsterdam*
Not to be reproduced by photoprint or microfilm without written permission from the publisher

# THE ENERGY DISTRIBUTION OF PROTONS EMITTED IN (n, p) REACTIONS

JUDIT NÉMETH
*Dept. of Atomic Physics, Central Research Institute of Physics, Budapest*

Received 19 February 1958

**Abstract:** If oscillation of the excited nucleus during evaporation is taken into account, the energy of the emitted protons is different in a system related to the nuclear surface from that in the laboratory system. The energy distribution of the emitted protons is qualitatively in good agreement with the experimental data. We studied the spectra of protons emitted in (n, p) reactions from Rh bombarded by 13.2 MeV neutrons.

It is known that when bombarding heavy nuclei by neutrons and considering the energy distribution of the escaping protons, a discrepancy is found between the earlier evaporation theory [1]) and the experimental data. The main differences are the following:

1) Low-energy particles are present in higher numbers than is to be expected.

2) The energy distribution curve is not as smooth as is to be expected theoretically but particularly in the case of heavier nuclei two or sometimes more peaks are observed.

3) The total cross section, specially for heavy nuclei, is found to be higher than predicted by the theory.

4) The angular distribution of the escaping protons is not isotropic.

Several attempts were made to improve the original evaporation theory in different ways. Recently, the theory of direct collisions [2]) seems to have become increasingly important. Brown *et al.* [3]) have shown that both the anisotropy of the angular distribution and the total cross section can be interpreted by the direct collision theory. It has been shown, however, by Elton [4]) that, if one takes into account the reflection on the nuclear surface, the total cross section for direct collision is reduced by a factor of ten. Another attempt was made by Kikuchi [5]) who calculated the effect of a diffuse nuclear boundary. In the case of a diffuse boundary the height of the Coulomb barrier is reduced; thus the total cross section will increase considerably and also a higher number of low-energy particles will be present.

It seems very probable, however, that the angular and energy distributions of the emitted protons are affected by a further phenomenon which has as yet not been considered, and with which we intend to deal in the

present paper. The phenomenon in question is the following: The excited nucleus is not at rest, but oscillates during evaporation. The radial velocity $v_S$ of the escaping protons in a system related to the nuclear surface will thus be different from their velocity $v_L$ in the laboratory system. One has $v_L = v_S + v$, where $v$ is the velocity of the oscillating nuclear surface. According to the theory of Weisskopf [1]), the energy spectrum of the emitted protons is, given by

$$w_\varepsilon = C\varepsilon\sigma(\varepsilon)\rho(E);$$

$\varepsilon$ is here the energy of the emitted proton and $\sigma(\varepsilon)$ the cross section of the inverse reaction, in which the residual nucleus is bombarded by protons of energy $\varepsilon$ and transformed into a compound nucleus; $\rho(E)$ is the level density of the residual nucleus (the energy of the residual nucleus being given by $E = \varepsilon_{max} - \varepsilon$, where $\varepsilon_{max}$ is the maximum possible energy of the protons); $w_\varepsilon$ is the probability that a particle of given energy $E$ escapes from the nucleus. In this formula, we must therefore take $\varepsilon = \frac{1}{2}m(v_S+v)^2$, and $v$ can be determined on the basis of the theory of the collective model. Considering even the simplest deformation, linear in the quadrupole deformation parameter $\alpha_2$, the oscillation velocity of the surface becomes:

$$v = R_0\dot{\alpha}_2 P_2(\cos\vartheta),$$

where $R_0$ is the radius of the nucleus in the equilibrium state. The time dependence of $\alpha_2$ is the following: $\alpha_2 = a_2 \sin \omega t$; $a_2$ can be determined by the oscillation energy. Thus $v$ is of the form $v_0 \cos \omega t \cdot P_2(\cos\vartheta)$; this has to be substituted into the evaporation formula and $w_\varepsilon$ averaged with respect to $\omega t$.

It is rather difficult to carry out quantitative calculations as various effects have to be taken into account, some of which are not even known exactly. It is not sufficient, for instance, to take into account only the $n = 1$ oscillations; on the other hand, if one wants to take into account oscillations of higher order, deformations of higher order have also to be considered. We do not know either the probability of proton emission by the excited nucleus for a given surface velocity. Further we do not know exactly the height of the Coulomb barrier if calculated with a diffuse nuclear boundary, nor the level density in a given nucleus. The accurate shape of the energy spectrum, however, strongly depends on these coefficients. All the same, it is obvious that by taking into account the oscillation and the diffuse nuclear boundary, the main characteristics described above of the experimental observations can be explained qualitatively.

1) The high number of low-energy particles can be explained by the two effects together in fairly good agreement with the experimental data. This is illustrated by the following example: Bombarding gold by 14 MeV neutrons, the energy of the emitted protons has been found [6]) to be between

5—14 MeV. The classical Coulomb barrier for gold is 14 MeV; thus, according to the statistical evaporation theory, particles cannot escape with lower energies. Taking into account the tunnel effect, even particles of 11 MeV energy are to be expected in considerable number. Calculating with a diffuse nuclear boundary, the minimum energy of the escaping protons will be about 7—8 MeV; and considering also the nuclear oscillation, the minimum energy will be reduced to 5—6 MeV. It is apparent that these values are in good agreement with the experimental data.

2) The fact that the energy distribution curve has more than one peak may also be explained by the oscillation. Taking into account $n = 1$ oscillations, the energy spectrum broadens, and if there was a peak at $\varepsilon_1 = \frac{1}{2}mv_1^2$ according to the evaporation theory, now two peaks can be expected approximately at the energies corresponding to velocities $v_1+\bar{v}$ and $v_1-\bar{v}$, where $\bar{v}$ is the mean velocity of the nuclear surface. Of course the nucleus oscillates only with a certain probability on the first level and there is also a certain probability of its being at rest or oscillating on higher levels. The total energy spectrum depends on the joint effect. If the energy of the bombarding neutron is about 10—20 MeV, the oscillation probability for light nuclei is very low, thus the nucleus is primarily at rest and there is a low probability of its oscillating on the first level. It can be expected, therefore, that the energy distribution curve for light nuclei has a large peak and to the right and left from this two smaller ones. For heavy nuclei, on the other hand, the oscillation probability is high, thus two almost equally large maxima are predicted. The effect of higher order oscillation levels may appear in further small irregularities of the spectrum †.

3) The total cross section is of the right order of magnitude if we calculate with a diffuse nuclear boundary.

4) The fact that the nucleus is in a state of deformation explains at the same time that the angular distribution of the escaping particles is not isotropic. As a matter of fact, considering the deformation of the nucleus and its angular momentum, the angular distribution observed experimentally is to be expected. Of course, particularly for heavy nuclei, the anisotropy is increased by direct collision too. The anisotropy in the angular distribution is not so large for light nuclei as for the heavy ones because in the former case oscillation occurs with less probability.

The above considerations do not necessarily postulate nuclear evaporation, it is enough to assume that part of the energy of the incident neutron is taken up by the collective motion and that particles are emitted from the oscillating nucleus.

In fig. 1 the theoretical energy distribution of protons emitted by rhodium

† Of course, irregularities of the spectrum may also be caused by protons emitted in (n, np) reactions or in direct collisions.

is shown. The measurement presented in fig. 2 has been carried out by Brown *et al.* [3]) with 13.2 MeV neutrons. It can be seen that there is good qualitative agreement between the theory and the experimental data. The calculations have been made for the simplest deformations neglecting the direct collisions. The height of the Coulomb barrier, calculated with a diffuse nuclear surface, is about 6 MeV; $\rho(E) \propto \exp 2\sqrt{aE}$, where $a \approx 6$ according to the calculations of Blatt and Weisskopf [7]). Brown *et al.* have obtained 25 mb for the total cross section while the cross section for evaporation calculated with a diffuse nuclear boundary is found to be 20 mb. The difference of 5 mb is probably due to direct collisions.

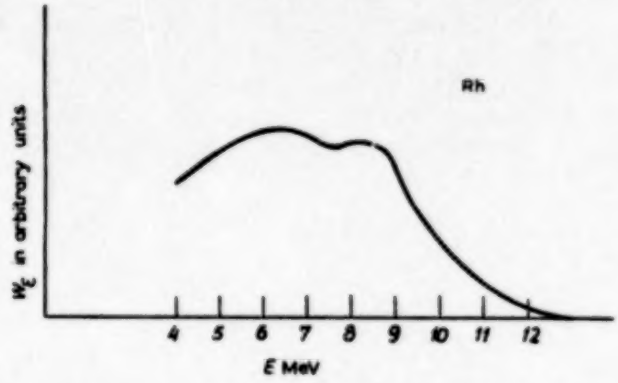


Fig. 1. Energy spectrum of protons from rhodium (theoretical).

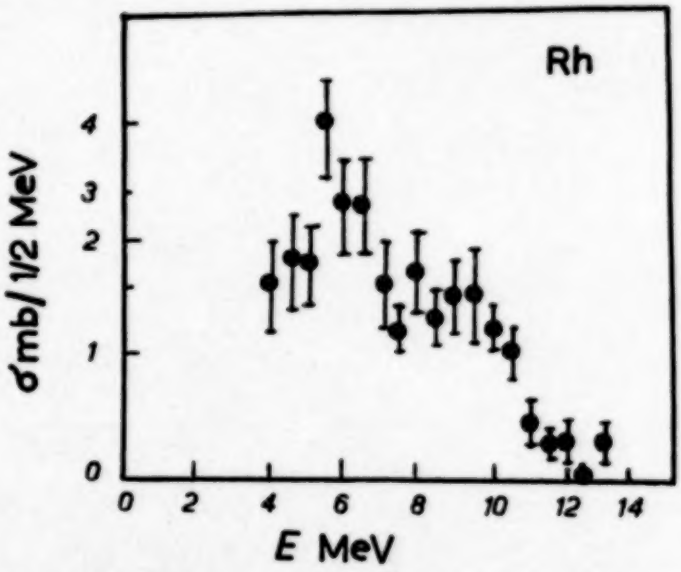


Fig. 2. Energy spectrum of protons from rhodium (experimental).

It is interesting to note that the position of the two peaks strongly depends on the height of the Coulomb barrier and the energy dependence of the level density; thus, sufficient experimental data being available, conclusions may be drawn as to the shape of the nuclear surface and level density by comparing the theoretical and experimental results.

I have to thank Professor G. Marx for his valuable observations and advice as well as Professor U. Facchini and Dr. L. Colli for their helpful comments.

## References

1) V. P. Weisskopf, Phys. Rev. **52** (1937) 295; V. P. Weisskopf and D. H. Ewing, Phys. Rev. **57** (1940) 472
2) R. M. Eisberg, Phys. Rev. **94** (1954) 293; H. McManus and W. T. Sharp, Phys. Rev. **87** (1952) 188; B. L. Cohen, E. Newman, G. A. Charpie and T. H. Handley, Phys. Rev. **94** (1954) 620; M. L. Goldberger, Phys. Rev. **74** (1948) 1269; S. Hayakawa, M. Kaway and K. Kikuchi, Progr. of Theor. Phys. **13** (1955) 413; G. Brown and H. Muirhead, Phil. Mag. **2** (1957) 473
3) G. Brown, G. C. Morrison, H. Muirhead and W. T. Morton, Phil. Mag. **2** (1957) 785
4) Elton and Gomez, Phys. Rev. **107** (1957) 1027
5) K. Kikuchi, Progr. Theor. Phys. **17** (1957) 643
6) R. A. Peck, Phys. Rev. **106** (1957) 965; L. Colli and U. Facchini, to be published
7) J. M. Blatt and V. P. Weisskopf, Theoretical Nuclear Physics (John Wiley and Sons, New York, 1952) p. 372

*Nuclear Physics* **6** (1958) 691—692; © *North-Holland Publishing Co., Amsterdam*

# NEWS ITEMS

## 1958 WAVERLEY GOLD MEDAL ESSAY COMPETITION

The essay competition was first organized by the Scientific Advisory Board of the journal *Research*, under the chairmanship of the late Lord Waverley, in 1953. It was designed to draw attention to the problem of communicating scientific information to the layman and also to scientists engaged in other fields. The writing of clear and concise reports is quite as important as carrying out the investigation which is the subject of the report.

The Waverley Gold Medal and £100 will be awarded for the best essay of about 3000 words based on some recent scientific research or new development (whether the author's work or not), giving some indication of the scientific background, the experimental results and its potential application in industry. The essay should be written in such a form that it is clearly intelligible to a scientist engaged in another field or a director of an industrial firm. The essays will be judged for technical content, by specialists in that field, for clarity of presentation and style.

A second prize of £50 will also be awarded and an additional prize, also of £50, for the best entry from a competitor under 30 years of age on the 31 July 1958. *The competition is only open to persons at present engaged in scientific work.*

### INSTRUCTIONS

1 All entries should be typewritten, double spaced, on one side of the paper only. Diagrams and photographs may be included. Entries by overseas competitors must be in English.
2 Entries shoud be marked "Under 30" if eligible for both sections of the competition.
3 Names should not be written on the essays as they must not be revealed to the judges. The name, present occupation, technical qualifications and age—in the case of entries qualifying for the under 30 prize only—of the author together with the *title of the paper* should be written on a separate sheet of paper and firmly attached to the essay. This information will, of course, be regarded as confidential.

### CONDITIONS

1 Entries will only be accepted if received by the editor on or before 31 July 1958. No responsibility can be accepted for entries delayed in the post or not received for any other reason.
2 Entrants may be required to prove to the satisfaction of the judges that they were actively engaged in scientific work in the period 1 January 1958 to 31 July 1958 and, where applicable, that they were under 30 years of age on 31 July 1958.
3 Manuscripts are the property of Butterworths Publications Ltd, and will not be returned. The rights of publication of all prize-winning entries rest with *Research* who also reserve the right to publish any other entry. The copyright of all published entries vests in the organizers. A fee will be paid for entries other than the prize-winning entries if they are published in *Research*.
4 Competitors are reminded that in their own interests it may be advisable for them to obtain prior permission and patent protection for any inventions described in their entries. The organizers can accept no responsibility in this matter.
5 If in the opinion of the judges no entry is of a sufficiently high standard, the judges reserve the right to award no prizes.
6 Joint entries by not more than two competitors may be submitted.
7 Entries are accepted only on the understanding that the entrant agrees to observe the conditions laid down by the organizers, Butterworths Publications Ltd, for the conduct of the competition.

### CLOSING DATE

Entries should be posted to reach The Editor, *Research*, 4/5 Bell Yard, London W.C.2, on or before 31 July 1958. *Entries can only be acknowledged if a stamped and addressed envelope for the purpose is enclosed.*

## COLLOQUE INTERNATIONAL „ELECTRONIQUE NUCLÉAIRE" (Paris, 16-20 Septembre 1958)

La Société des Radioélectriciens organise un Colloque International sur le sujet „Electronique Nucléaire" qui se tiendra à Paris du 16 au 20 Septembre 1958.

Pour tous renseignements s'adresser au Siège Administratif du Colloque: Colloque „Electronique Nucléaire", Société des Radioélectriciens, 10 Avenue Pierre Larousse, Malakoff (Seine), France.

## BOOK REVIEW

Concerning A. I. AKHIEZER and V. B. BERESTETSKY's *Quantum Electrodynamics* (this journal **6** (1957)135) a correspondent points out that another English translation of the same book is available as publication No. AEC-tr-2876 from the Office of Technical Services, United States Department of Commerce, Washington 25, D.C. for only 2.65 dollars.

## ERRATUM

M. Morita, Beta-Neutrino-Gamma Angular Correlation, Nuclear Physics **6** (1958) 132.

On p. 132, in the 4th line of eq. (1), the factor $\{12(j_1+1)\}^{-\frac{1}{2}}$ should be read $\{12j_1(j_1+1)\}^{-\frac{1}{2}}$.

# AUTHOR INDEX

ALAGA, G., L. ŠIPS and D. TADIĆ, Calculation of some relativistic corrections to the allowed and *l*-forbidden beta transitions . . 305
ALLAN, D. L., The energy and angular distribution of protons from 14 MeV neutron reactions with Cu. . . . . 464
ALMÉN, O., *see* Arnell
ARMBRUSTER, R., *see* Gorodetzky
ARNELL, S. E., J. DUBOIS and O. ALMÉN, Half-lives of the positon emitting mirror nucleides . . . . . 196
BARTON, G., Core effects in light nuclei . . . . . 100
BELL, J. S. and R. J. BLIN-STOYLE, Mesonic effects in beta-decay 87
BERKO, S., W. D. WHITEHEAD and B. C. GROSECLOSE, Angular distribution of elastically scattered 14.7 MeV neutrons . . . . . 210
BERLOVICH, E. YE., K. GROTOVSKI, M. BONITZ, V. I. BRESLAV and B. K. PREOBRAZHENSKY, Investigation of the life-times of lower nuclear levels excited in electron capture . . . . . 672
BÈS, D. R., Levels in $Dy^{161}$ II. Theoretical. . . . . 645
BIEDENHARN, L. C., J. M. BLATT and M. H. KALOS, Phenomenological neutron proton potentials . . . . . 359
BISI, A. and L. ZAPPA, Excited levels of $^{155}Gd$ . . . . . 252
BLAIR, J. S., Deuteron cross sections for high energy projectiles . . 348
BLATT, J. M., *see* Biedenharn
BLIN-STOYLE, R. J., *see* Bell
BLOCH, C., Sur la théorie des perturbations des états liés . . . . 329
BONITZ, M., *see* Berlovich
BORELI, F., *see* Clement
BRANSDEN, B. H. and R. G. MOORHOUSE, On the elastic scattering of pions by deuterons . . . . . 310
BRESLAV, V. I., *see* Berlovich
BUJDOSÓ, E., Investigation of the $B^{10}(n, \alpha)Li^7$ reaction by the photoemulsion method . . . . . 107
BUTCHER, J. C., B. A. CHARTRES and H. MESSEL, Tables of average numbers for electron-photon showers at small depths of absorber 271
CHARTRES, B. A., *see* Butcher
CHOU KUANG-CHAO and M. I. SHIROKOV, Spins and parities ${}_{\Lambda}H^4$ hyperfragment and K-meson. . . . . 10
CHOU KUANG-CHAO, *see* Zastavenko
CLEMENT, J. D., F. BORELI, S. E. DARDEN, W. HAEBERLI and H. R.

STRIEBEL, Polarization of neutrons scattered by intermediate and heavy nuclei . . . . . 177
COHEN, B. L. and C. B. FULMER, Fission-fragment mass separator and the nuclear charge distribution of fission fragments of a single mass 547
CROISSIAUX, M., *see* Gorodetzky
DARDEN, S. E., *see* Clement
DARDEN, S. E., *see* Striebel
DERRICK, G. H., A theorem on potentials with hard cores . . . . 287
D'ESPAGNAT, B. and J. PRENTKI, A tentative general scheme for weak interactions . . . . . 596
DIO, W. H. and E. SCHOPPER, Temperature dependence of the diffusion coefficient and the diffusion length of thermal neutrons in water . . . . . 175
DOLGINOV, A. Z., Polarization of X-ray quanta and non-conservation of parity in K-capture . . . . . 460
DUBOIS, J., *see* Arnell
DŽELEPOW, B. S. and N. N. ZHUKOVSKY, On the gamma spectra of $Ag^{110}$, $Sb^{124}$ and $Eu^{152,154}$ . . . . . 655
EDEN, R. J., *see* Hall
EL BEDEWI, F. A. and S. TADROS, Inelastic deuteron scattering from chromium and cobalt . . . . . 434
ELBEK, B., *see* Ramšak
EMERY, V. J., A variational approach to the nuclear many-body problem . . . . . 585
ERICSON, T., On the level density of deformed nuclei . . . . . 62
FILIMONOV, YU. I., *see* Gvozdev
FROISSART, M. and R. OMNÈS, Analytical properties of the solutions of the Chew-Low equations . . . . . 628
FULMER, C. B., *see* Cohen
FULTON, TH., Polarization of the recoil nucleus in $\mu^-$-capture . . 319
GALLMANN, A., *see* Gorodetzky
GALSTER, S., *see* H. Schopper
GOLDANSKI, V. I., A tentative unified classification of elementary particles, including leptons . . . . . 531
GORODETZKY, S., A. GALLMANN, M. CROISSIAUX et R. ARMBRUSTER, Corrélation angulaire $(\gamma, \gamma)$ dans la réaction $^{14}N(p, \gamma)^{15}O$ . . . . 517
GREGERS HANSEN, P., O. NATHAN, O. B. NIELSEN and R. K. SHELINE, Levels in $Dy^{161}$ I. Experimental investigation of the decay of $Tb^{161}$ 630
GROSECLOSE, B. C., *see* Berko
GROTOVSKI, K., *see* Berlovich
GVOZDEV, V. S., L. I. RUSINOV, YU. I. FILIMONOV and YU. L. KHAZOV, Investigation of nuclear isomerism in $Hf^{180m}$ . . . . . 561

GYÖRGYI, G. and H. ÜBERALL, Parity non-conservation and transverse polarization of $\beta$-particles: added remarks . . . . . 539
HALL, R. B. and R. J. EDEN, Momentum dependence of the nuclear shell model potential . . . . . 157
HAEBERLI, W., *see* Clement
HAEBERLI, W., *see* Striebel
ILYINA, I. L., *see* Vladimirsky
KALOS, M. H., *see* Biedenharn
KAMEFUCHI, S. and S. ONEDA, Decay interaction of the pi-meson 114
KHAZOV, YU. L., *see* Gvozdev
KÖHLER, H. S., Approximate optical model expressions for the elastic scattering and polarization of fast protons by nuclei in the forward scattering peak . . . . . 161
KONUMA, M., S. NAKAMURA and H. UMEZAWA, On the "neutrino charge" in weak and strong interactions . . . . . 282
MAGLIĆ, B. and J. VUKOVIĆ, Polarization of protons from the d—d reaction at 1.2 MeV . . . . . 443
MARIS, TH. A. J., *see* Tyrén
MARKLUND, I., *see* Nathan
MARTEGANI, A., *see* Vervier
MELIGY, A. S., Simple expansion for the regular Coulomb wave function . . . . . 440
MESSEL, H., *see* Butcher
MITRA, A. N., Role of pion-pion interaction in $\tau$-decay . . . . . 404
MITTELSTAEDT, P., Zur Streuung von K-Mesonen an Komplexen Kernen . . . . . 50
MOORHOUSE, R. G., *see* Brandsden
MORITA, M., Beta-neutrino-gamma angular correlation (see also Erratum p. 692) . . . . . 132
MURAI, Y., New wave equations for elementary particles . . . . 489
NAKAMURA, S., *see* Konuma
NATHAN, O. and I. MARKLUND, Rotational character of the transition from the 473 keV level in $Tm^{169}$ . . . . . 102
NATHAN, O., *see* Gregers Hansen
NÉMETH, JUDITH, The energy distribution of protons emitted in (n, p) reactions . . . . . 686
NIELSEN, O. B., *see* Gregers Hansen
NING HU, Scattering functions with crossing symmetry: a correction 545
OLESEN, M. C., *see* Ramšak
OMNÈS, R., *see* Froissart
ONEDA, S., *see* Kamefuchi
PASMA, P. J., Polarization measurements on D+D and T+D neutrons

generated by low energy deuterons . . . . . 141
PRENTKI, J., *see* d'Espagnat
PREOBRAZHENSKY, B. K., *see* Berlovich
RAMŠAK, V., M. C. OLESEN and B. ELBEK, Coulomb excitation cross sections of gadolinium isotopes from inelastic scattering measurements . . . . . 451
RIDLEY, B. W., The electron-neutrino angular correlation in decay of $Ne^{23}$ . . . . . 34
ROCHESTER, G. D., J. M. Nuttall (1890—1958) . . . . . 541
RUSINOV, L. I., *see* Gvozdev
RYNDIN, R. M., *see* Zastavenko
SANO, M., S. YOSHIDA and T. TERASAWA, Direct and compound processes in nuclear reactions . . . . . 20
SATCHLER, G. R., Deuteron stripping with polarized deuterons . . 543
SAWICKI, J., Unified nuclear model and direct nuclear photoeffect I. Weak coupling effects . . . . . 525
SAWICKI, J., Deuteron stripping on spheroidal nuclei . . . . . 575
SAWICKI, J., Inelastic scattering of deuterons from spheroidal nuclei 613
SCHINDEWOLD, U., *see* Wayne Swenson
SCHOPPER, H. and S. GALSTER, The circular polarization of internal and external bremsstrahlung. . . . . 125
SCHOPPER, E., *see* Dio
SHELINE, R. K., *see* Gregers Hansen
SHIROKOV, M. I., *see* Chou Kuang-Chao
ŠIPS, L., *see* Alaga
SOLNTSEFF, N., On the theory of scattering measurements in nuclear emulsion
II. The estimation of true scattering in the presence of distortion 222
SOLOVIEV, V. G., The hypothesis of conservation of combined parity only in strong, electromagnetic and weak interactions . . . . . 618
SQUIRES, E. J., The inelastic scattering of protons by $C^{12}$ . . . . 504
STORRUSTE, A. and P. O. TJÓM, Small angle scattering of 1.33 MeV and 1.17 MeV gamma rays . . . . . 151
STRIEBEL, H. R., S. E. DARDEN and W. HAEBERLI, Polarization of $Li^7(p, n)Be^7$ neutrons . . . . . 188
STRIEBEL, H. R., *see* Clement
TADIĆ, D., *see* Alaga
TADROS, S., *see* El Bedewi
TAKABAYASI, T., Symmetrical structure and conservation relations of four-component neutrino field . . . . . 477
TERASAWA, T., *see* Sano
TJÓM, P. O., *see* Storruste

TYRÉN, H. and TH. A. J. MARIS, Inelastic scattering of 185 MeV protons on lithium, beryllium, boron and nitrogen . . . . . 82
TYRÉN, H. and TH. A. J. MARIS, Inelastic scattering of 185 MeV protons on nuclei with masses from fluorine to potassium . . . 446
ÜBERALL, H., *see* Györgyi
UMEZAWA, H., *see* KONUMA
VAN HEERDEN, I. J., Angular distributions of elastically and inelastically scattered deuterons from neon . . . . . 55
VERVIER, J. F. et A. MARTEGANI, Sections efficaces totales pour des neutrons d'énergie voisine de 14 MeV . . . . . 260
VLADIMIRSKY, V. V. and I. L. ILYINA, Optical model calculation of the interaction of slow neutrons with prolate nuclei . . . . . 295
VUKOVIĆ, J., *see* Maglić
WALL, N. S., *see* Wayne Swenson
WAYNE SWENSON, L., U. SCHINDEWOLF and N. S. WALL, The elastic scattering of 30.5 MeV alpha-particles from Ni, Cu and Au . . 203
WERLE, J., Dependence of $\mu$-meson and electron polarization on correlation parameters in $K_{\mu 3}$ and $K_{e3}$ decay . . . . . 1
WHITEHEAD, W. D., *see* Berko
WILHELMSSON, H. and P. ZIELINSKI, Derivation of the $\Lambda^0$—$\alpha$ potential from the $^5He_\Lambda$ and $^9Be_\Lambda$ hyperfragment binding energies . . . . 219
YOSHIDA, S., *see* Sano
ZAPPA, L., *see* Bisi
ZASTAVENKO, L. G., R. M. RYNDIN and CHOU KUANG-CHAO, On non-uniqueness of nucleon-nucleon phase shifts scattering . . . . . 669
ZHUKOVSKY, N. N., *see* Dželepow
ZIELINSKI, P., *see* Wilhelmsson
ZIMÁNYI, J., Angular correlation between recoil nucleus and gamma quantum in electron capture . . . . . 625
ZUCKER, A., Protons and alpha-particles from the nitrogen bombardment of aluminium . . . . . 420

# SUBJECT INDEX

From now on the indexing of Nuclear Physics will be adapted to the system set up by the Nuclear Data Group of the National Research Council of the U.S.A. for their issue of Nuclear Theory Index Cards. With the kind authorization of Miss K. Way, it has been possible to take over the Nuclear Data Group's classification in its entirety, with only a few slight modifications (subdivisions 2.A.1, 2.A.2 instead of their 2.A; added class 2.L; subdivision and extension of class 6) and to extend it on the same principle to the domains outside its original scope.

## Indexing System

1. NUCLEAR STRUCTURE
   - 1.A General theory
   - 1.B Two- and three-body problems
   - 1.C Many-particle systems
   - 1.D Nuclear models
     - 1.D.1 Shell model
     - 1.D.2 Collective model
     - 1.D.3 Other models
     - 1.D.4 Relationship between different models
   - 1.E Properties of nuclei
     - 1.E.1 Energy levels
     - 1.E.2 Binding energies; masses
     - 1.E.3 Electric and magnetic moments
     - 1.E.4 Transition probabilities; Cross sections
     - 1.E.5 Nuclear radii; Matter distributions
     - 1.E.6 Nuclear moments of inertia
     - 1.E.7 Isobaric spin effects
     - 1.E.8 Other properties

2. NUCLEAR REACTIONS
   - 2.A General properties
     - 2.A.1 Cross-sections, energy relations
     - 2.A.2 General theory
   - 2.B Angular distributions, Correlations; Polarization
   - 2.C Resonance reactions; *R*-matrix theory
   - 2.D Statistical model
   - 2.E Optical model
   - 2.F Direct interaction (other than stripping)
   - 2.G Stripping and pick-up
   - 2.H Coulomb excitation
   - 2.I Photonuclear processes
   - 2.J Fission and spallation
   - 2.K Thermonuclear reactions
   - 2.L Scattering processes (except two-nucleon system and meson scattering)

3. ELECTROMAGNETIC RADIATION
   - 3.A Gamma radiation
   - 3.B Internal conversion
   - 3.C Extranuclear effects

4. BETA DECAY; PARITY

4.A General theory
4.B Formulation of Fermi theory
4.C Evaluation of matrix elements
4.D K-Capture
4.E Analysis of data

5. ALPHA DECAY

6. METHODS AND INSTRUMENTS

6A. Experimental
6.B Theoretical
6.C Constants, standards and units
6.D Tables and computational aids

7. QUANTUM FIELD THEORY

7.A General
7.B Quantum electrodynamics
7.C $\pi$-meson field (scattering and nuclear forces)

8. ELEMENTARY PARTICLES

8.A Experimental
8.B Theory: interactions, transformation properties
8.C Fundamental theory of matter

9. COSMIC RADIATION

9.A General
9.B Passage of particles through matter

10. NEWS ITEMS

10.A News items
10.B Reports on conferences and congresses
10.C Obituaries
10.D Book reviews

The index number of an article may refer to more than one class (e.g. 1.D.4: 1.E.4): the article is then listed under each of these classes.

# SUBJECT INDEX

## 1. Nuclear Structure

### 1.B *Two- and three-body problems*

Phenomenological neutron proton potentials, L. C. Biedenharn, J. M. Blatt and M. H. Kalos . . . . . 359
On non-uniqueness of nucleon-nucleon scattering phase shifts, L. G. Zastavenko, R. M. Ryndin and Chou Kuang-Chao . . . . . 669

### 1.C *Many-particle systems*

Momentum dependence of the nuclear shell model potential, R. B. Hall and R. J. Eden . . . . . 157
A theorem on potentials with hard cores, G. H. Derrick . . . . . 287
Sur la théorie des perturbations des états liés, C. Bloch . . . . . 329
A variational approach to the nuclear many-body problem, V. J. Emery . 585

### 1.D *Nuclear models*

#### 1.D.1 *Shell model*

The inelastic scattering of protons by $C^{12}$, E. J. Squires . . . . . 504

#### 1.D.2 *Collective model*

On the level density of deformed nuclei, T. Ericson . . . . . 62
Rotational character of the transition from the 473 keV level in $Tm^{169}$, O. Nathan and I. Marklund . . . . . 102
Optical model calculation of the interaction of slow neutrons with prolate nuclei, V. V. Vladimirsky and I. L. Ilyina . . . . . 295
Unified nuclear model and direct nuclear photoeffect: I. Weak coupling effects, J. Sawicki . . . . . 525
Deuteron stripping on spheroidal nuclei, J. Sawicki . . . . . 575
Inelastic scattering of deuterons from spheroidal nuclei, J. Sawicki . 613
Levels in $Dy^{161}$: II. Theoretical, D. R. Bès . . . . . 645
The energy distribution of protons emitted in (n, p) reactions, Judith Németh . . . . . 686

#### 1.D.4 *Relationship between different models*

Core effects in light nuclei, G. Barton . . . . . 100

### 1.E *Properties of nuclei*

#### 1.E.1 *Energy levels*

Rotational character of the transition from the 473 keV level in $Tm^{169}$, O. Nathan and I. Marklund . . . . . 102
Excited levels of $^{158}Gd$, A. Bisi and L. Zappa . . . . . 252
Inelastic deuteron scattering from chromium and cobalt, F. A. El Bedewi and S. Tadros . . . . . 434
Levels in $Dy^{161}$: I. Experimental investigation of the decay of $Tb^{161}$, P. Gregers Hansen, O. Nathan, O. B. Nielsen and R. K. Sheline . 630
Levels in $Dy^{161}$: II. Theoretical, D. R. Bès. . . . . 645

#### 1.E.2 *Binding Energies; Masses*

Half-lives of the positon emitting mirror nucleides, S. E. Arnell, J. Dubois and O. Almén . . . . . 196

#### 1.E.4 *Transition probabilities; Cross sections*

Core effects in light nuclei, G. Barton . . . . . 100
Coulomb excitation cross sections of gadolinium isotopes from inelastic scattering measurements, V. Ramšak, M. C. Olesen and B. Elbek . 451

## 2. Nuclear Reactions

### 2.A *General properties*

Direct and compound processes in nuclear reactions, M. Sano, S. Yoshida and T. Terasawa . . . . . 20

#### 2.A.1 *Cross-Sections. energy relations*

Investigation of the $B^{10}(n, \alpha)Li^7$ reaction by the photoemulsion method, E. Bujdosó . . . . . 107
The energy and angular distribution of protons from 14 MeV neutron reactions with Cu, D. L. Allan . . . . . 464
The energy distribution of protons emitted in (n, p) reactions, Judith Németh . . . . . 686

### 2.B *Angular distributions; Correlations; Polarization*

Polarization measurements on D+D and T+D neutrons generated by low energy deuterons, P. J. Pasma . . . . . 141
Polarization of neutrons scattered by intermediate and heavy nuclei, J. D. Clement F. Boreli, S. E. Darden, W. Haeberli and H. R. Striebel . . . 177
Polarization of $Li^7(p, n)Be^7$ neutrons, H. R. Striebel, S. E. Darden and W. Haeberli . . . . . 188
Polarization of protons from the d−d reaction at 1.2 MeV, B. Maglić and J. Vuković . . . . . 443
The energy and angular distribution of protons from 14 MeV neutron reactions with Cu, D. L. Allan . . . . . 464
Corrélation angulaire $(\gamma, \gamma)$ dans la réaction $^{14}N(p, \gamma)^{15}O$, S. Gorodetzky, A. Gallmann, M. Croissiaux et R. Armbruster . . . . . 517

### 2.D *Statistical model*

On the level density of deformed nuclei, T. Ericson. . . . . 62
Protons and alpha-particles from the nitrogen bombardment of aluminium, A. Zucker . . . . . 420

### 2.E *Optical model*

Approximate optical model expressions for the elastic scattering and polarization of fast protons by nuclei in the forward scattering peak, H. S. Könler . 161
Sections efficaces totales pour des neutrons d'énergie voisine de 14 MeV, J. F. Vervier et A. Martegani . . . . . 260
Optical model calculation of the interaction of slow neutrons with prolate nuclei, V. V. Vladimirsky and I. L. Ilyina . . . . . 295

### 2.F *Direct interaction (other than stripping)*

Deuteron cross sections for high energy projectiles, J. S. Blair . . . . . 348

### 2.G *Stripping and pick-up*

Deuteron stripping with polarized deuterons, G. R. Satchler . . . . . 543
Deuteron stripping on spheroidal nuclei, J. Sawicki . . . . . 575

### 2.H *Coulomb excitation*

Coulomb excitation cross sections of gadolinium isotopes from inelastic scattering measurements, V. Ramšak, M. C. Olesen and B. Elbek . . . . . 451

### 2.I *Photonuclear processes*

Unified nuclear model and direct nuclear photoeffect: I. Weak coupling effects, J. Sawicki . . . . . 525

### 2.J *Fission and spallation*

Fission-fragment mass separator and the nuclear charge distribution of fission fragments of a single mass, B. L. Cohen and C. B. Fulmer . . . . . 547

### 2.L *Scattering processes (except two-nucleon system and meson scattering)*

Angular distributions of elastically and inelastically scattered deuterons from neon: I. J. van Heerden . . . . . 55
Inelastic scattering of 185 MeV protons on lithium, beryllium, boron and nitrogen, H. Tyrén and Th. A. J. Maris . . . . . 82
Polarization measurements on D+D and T+D neutrons generated by low energy deuterons, P. J. Pasma. . . . . 141
Approximate optical model expressions for the elastic scattering and polarization of fast protons by nuclei in the forward scattering peak, H. S. Köhler 161
Temperature dependence of the diffusion coefficient and the diffusion length of thermal neutrons in water, W. H. Dio and E. Schopper. . . . . 175
Polarization of neutrons scattered by intermediate and heavy nuclei, J. D. Clement, F. Boreli, S. E. Darden, W. Haeberli and H. R. Striebel . . . 177
Polarization of $Li^7(p, n)Be^7$ neutrons, H. R. Striebel, S. E. Darden and W. Haeberli . . . . . 188
The elastic scattering of 30.5 MeV alpha-particles from Ni, Cu and Au, L. Wayne Swenson, U. Schindewolf and N. S. Wall . . . . . 203
Angular distribution of elastically scattered 14.7 MeV neutrons, S. Berko, W. D. Whitehead and B. C. Groseclose . . . . . 210
Inelastic deuteron scattering from chromium and cobalt, F. A. El Bedewi and S. Tadros . . . . . 434
Polarization of protons from the d−d reaction at 1.2 MeV, B. Maglić and J. Vuković . . . . . 443
Inelastic scattering of 185 MeV protons on nuclei with masses from fluorine to potassium, H. Tyrén and Th. A. J. Maris . . . . . 446
The inelastic scattering of protons by $C^{12}$, E. J. Squires . . . . . 504
Inelastic scattering of deuterons from spheroidal nuclei, J. Sawicki . . . 613

## 3. Electromagnetic Radiation

### 3.A *Gamma radiation*

Investigation of nuclear isomerism in $Hf^{180m}$, V. S. Gvozdev, L. I. Rusinov, Yu. I. Filimonov and Yu. L. Khazov . . . . . 561
On the gamma spectra of $A^{110}$, $Sb^{124}$ and $Eu^{152, 154}$, B. S. Dželepow and N. N. Zhukovsky. . . . . 655
Investigation of the life-times of lower nuclear levels excited in electron capture, E. Ye. Berlovich, K. Grotovski, M. Bonitz, V. I. Breslav and B. K. Preobrazhensky . . . . . 672

### 3.C *Extranuclear effects*

Small angle scattering of 1.33 MeV and 1.17 MeV gamma rays, A. Storruste and P. O. Tjøm . . . . . 151

## 4. Beta Decay: Parity

### 4.A *General theory*

Mesonic effects in beta-decay, J. S. Bell and R. J. Blin-Stoyle . . . . . 87
The circular polarization of internal and external bremsstrahlung, H. Schopper and S. Galster . . . . . 125
Beta-neutrino-gamma angular correlation, M. Morita (see also Erratum p. 692) 132
Parity non-conservation and transverse polarization of $\beta$-particles: added remarks, G. Györgyi and H. Überall . . . . . 539

### 4.C *Evaluation of matrix elements*

Calculation of some relativistic corrections to the allowed and *l*-forbidden beta transitions, G. Alaga, L. Šips and D. Tadić . . . . . 305

### 4.D K-*Capture*

Polarization of X-ray quanta and non-conservation of parity in K-capture, A. Z. Dolginov . . . . . 460

Angular correlation between recoil nucleus and gamma quantum in electron capture, J. Zimányi . . . . . 625

### 4.E *Analysis of data*

Half-lives of the positon emitting mirror nucleides, S. E. Arnell, J. Dubois and O. Almén . . . . . 196

Levels in $Dy^{161}$: I. Experimental investigation of the decay of $Tb^{161}$, P. Gregers Hansen, O. Nathan, O. B. Nielsen and R. K. Sheline . . . . . 630

## 6. Methods and Instruments

### 6.A *Experimental*

On the theory of scattering measurements in nuclear emulsion: II. The estimation of true scattering in the presence of distortion, N. Solntseff . . 222

Fission-fragment mass separator and the nuclear charge distribution of fission fragments of a single mass, B. L. Cohen and C. B. Fulmer . . . . . 547

### 6.B *Theoretical*

Simple expansion for the regular Coulomb wave function, A. S. Meligy. . 440

### 6.D *Tables and computational aids*

Tables of average numbers for electron-photon showers at small depths of absorber, J. C. Butcher, B. A. Chartres and H. Messel . . . . . 271

Phenomenological neutron proton potentials, L. C. Biedernharn, J. M. Blatt and M. H. Kalos. . . . . 359

## 7. Quantum Field Theory

### 7.A *General*

Scattering functions with crossing symmetry: a correction, Ning Hu . . . 545

Analytical properties of the solutions of the Chew-Low equations, M. Froissart and R. Omnès . . . . . 628

### 7.C *π-meson field (scattering and nuclear forces)*

On the elastic scattering of pions by deuterons, B. H. Bransden and R. G. Moorhouse . . . . . 310

## 8. Elementary Particles

### 8.A *Experimental*

The electron-neutrino angular correlation in decay of $Ne^{23}$, B. W. Ridley. . 34

### 8.B *Theory: interactions, transformation, properties*

Dependence of $\mu$-meson and electron polarization on correlation parameters in $K_{\mu 3}$ and $K_{e3}$ decays, J. Werle . . . . . 1

Spins and parities of the ${}_{\Lambda}H^{4}$ hyperfragment and K-meson, Chou Kuang-Chao and M. L. Shirokov. . . . . 10

Zur Streuung von K-Mesonen an Komplexen Kernen, P. Mittelstaedt . . . 50

Decay interaction of the pi-meson, S. Kamefuchi and S. Oneda . . . . . 114

The circular polarization of internal and external bremsstrahlung, H. Schopper and S. Galster . . . . . 125

Beta-neutrino-gamma angular correlation, M. Morita . . . . . 132

Derivation of the $\Lambda^0-\alpha$ potential from the ${}^{5}He_{\Lambda}$ and ${}^{9}Be_{\Lambda}$ hyperfragment binding energies, H. Wilhelmsson and P. Zielinski . . . . . 219

On the "neutrino charge" in weak and strong interactions, M. Konuma, S. Nakamura and H. Umezawa. . . . . 282

Polarization of the recoil nucleus in $\mu^-$-capture, T. Fulton . . . . . 319
Role of pion-pion interaction in $\tau$-decay, A. N. Mitra . . . . . 404
Polarization of X-ray quanta and non-conservation of parity in K-capture, A. Z. Dolginov . . . . . 460
Symmetrical structure and conservation relations of four-component neutrino field, T. Takabayasi . . . . . 477
New wave equations for elementary particles, Y. Murai . . . . . 489
A tentative unified classification of elementary particles, including leptons, V. I. Goldanski . . . . . 531
Parity non-conservation and transverse polarization of $\beta$-particles: added remarks, G. Györgyi and H. Überall . . . . . 539
A tentative general scheme for weak interactions, B. d'Espagnat and J. Prentki . . . . . 596
The hypothesis of conservation of combined parity only in strong, electromagnetic and weak interactions, V. G. Soloviev . . . . . 618
Angular correlation between recoil nucleus and gamma quantum in electron capture, J. Zimányi . . . . . 625

## 9. Cosmic Radiation

### 9.A *General*

Tables of average numbers for electron-photon showers at small depths of absorber, J. C. Butcher, B. A. Chartres and H. Messel . . . . . 271

### 9.B *Passage of particles through matter*

On the theory of scattering measurements in nuclear emulsion: II. The estimation of true scattering in the presence of distortion, N. Solntseff . 222

## 10. News Items

### 10.A *News items*

Nordic Institute for Theoretical Atomic Physics (NORDITA) . . . . . 137
International Congress on Nuclear Physics (Paris, 7—12 July, 1958) . . 138
Ninth Session of Council of CERN . . . . . 139
The 1958 Annual International Conference on High Energy Physics at CERN (Geneva, June 30—July 5, 1958) . . . . . 325
Electron Miscroscope Society of America . . . . . 328
1958 Waverly Gold Medal Essay Competition . . . . . 691
Colloque International „Electronique Nucléaire" (Paris, 16—20 Septembre 1958) . . . . . 692

### 10.B *Reports on conferences and congresses*

Nuclear Sizes and Density Distributions (Stanford University, 17—19 December, 1957) . . . . . 137

### 10.C *Obituaries*

J. M. Nuttall (1890—1958), G. D. Rochester . . . . . 541

### 10.D *Book Reviews*

Akhiezer, A. I. and V. B. Berestetsky, Quantum electrodynamics (L. R.) (see also p. 692) . . . . . 135
DePaul, D. J., editor, Corrosion and wear handbook for watercooled reactors (H. J. Axon) . . . . . 136
Frisch, O. R., editor, Progress in nuclear physics, volume 6 (L. R.) . . . 323
Hintenberger, H., editor, Nuclear masses and their determination (L. R.) 323
Series, G. W., Spectrum of atomic hydrogen (L. R.) . . . . . 135

### 10.E *Errata*

M. Morita, Nuclear Physics 6 (1958) 132 . . . . . 692